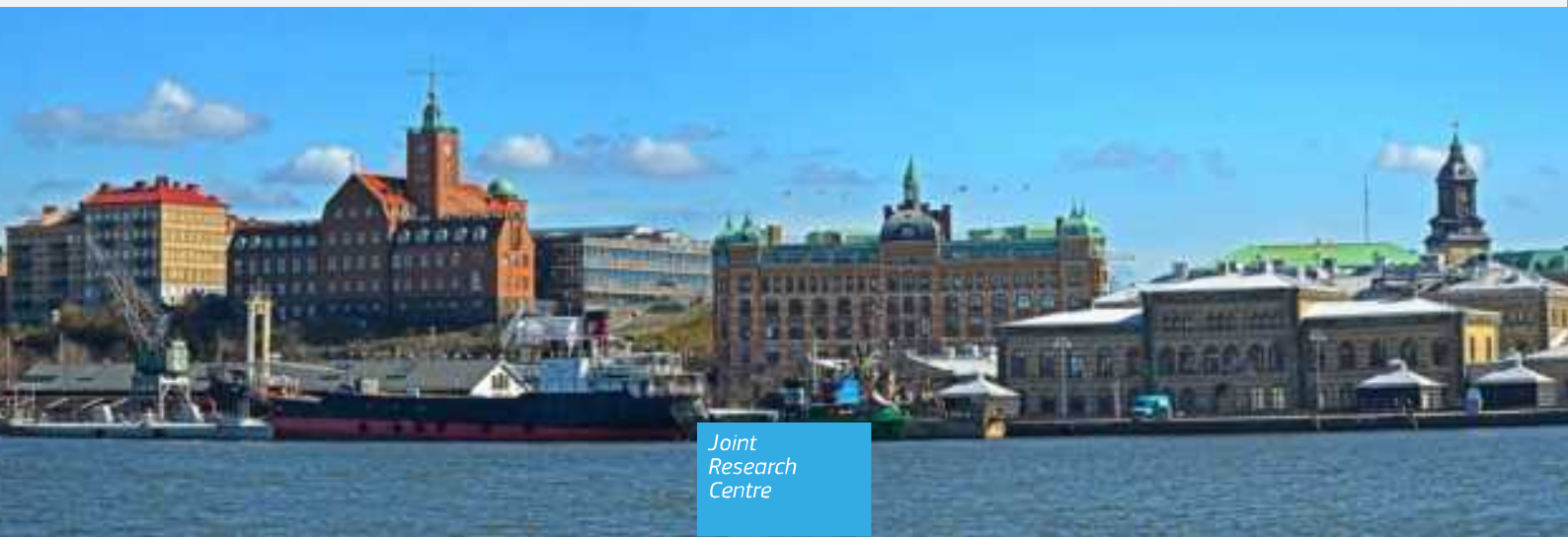




Proceedings of the 25th International Transport & Air Pollution (TAP) and the 3rd Shipping & Environment (S&E) Conference

Editors: Svetlana M. Molchanova, J. Laurén, M. Cha Y
Lundström, P. Santarosé G

2024



This document is a publication by the Joint Research Centre (JRC), the European Commission's science and knowledge service. It aims to provide evidence-based scientific support to the European policymaking process. The contents of this publication do not necessarily reflect the position or opinion of the European Commission. Neither the European Commission nor any person acting on behalf of the Commission is responsible for the use that might be made of the publication. For information on the methods, scope and quality underlying the data used in this publication for which the source is neither JRC nor other Commission services, users should contact the relevant JRC centre. The designations employed and the presentation of material on the maps do not imply the expression of any opinion whatsoever on the part of the European Union concerning the legal status of any country, territory, city or area or of its authorities, or concerning the delimitation of its frontiers or boundaries.

Contact Information

Contact Information

Name: Alice Smith

Email: alice.smith@ec.europa.eu

Name: George Edwards

Email: george.edwards@ec.europa.eu

EU Science Hub

<https://jrc-research-centre.ec.europa.eu>

JRC136825

PDF – ISBN 978-92-76-12810-7 – doi:10.2760/564701

E-12-24-2024-EN-N

Luxembourg: Publications Office of the European Union, 2024

European Union, 2024



The reuse policy of the European Commission documents is implemented by the Commission Decision 2011/833/EU of 12 December 2011 on the reuse of Commission documents (OJ L 330, 14.12.2011, p. 39). Unless otherwise noted, the reuse of this document is authorised under the Creative Commons Attribution 4.0 International (CC BY 4.0) licence (<https://creativecommons.org/licenses/by/4.0/>). This means that reuse is allowed provided appropriate credit is given and any changes are indicated.

For any use or reproduction of photos or other material that is not owned by the European Union permission must be sought directly from the copyright holders.

Cover photo by: Amjad Sheikh - Own work, CC BY 4.0, <https://commons.wikimedia.org/w/index.php?curid=57733344>

How to cite this report: European Commission, Joint Research Centre, *Proceedings of the 25th International Transport & Air Pollution (TAP) and the 3rd Shipping & Environment (S&E) Conference*, Sjödin, Å., Moldanova, J., Laurelin, M., Cha, Y., Lundström, H. and Fontaras, G. editors, Publications Office of the European Union, Luxembourg, 2024, <https://data.europa.eu/doi/10.2760/564701>, JRC136825.

Contents

Abstract	3
Acknowledgements	4
1 Introduction	5
1.1 Message of the Chairs	5
1.2 Organisation	7
1.2.1 General information	7
1.2.2 Local organisers	7
1.2.3 Collaborators	8
1.2.4 Funders/sponsors	8
1.2.5 Scientific Committees	9
1.2.6 Organising Committee	10
2 Conference Proceedings –Extended abstracts.....	11
2.1 TAP.01. New emission control concepts, testing conditions and pollutants, non-exhaust emission ...	15
2.2 TAP.02. On-board monitoring and diagnostics, emission tampering and deterioration.....	42
2.3 TAP.03. In-service conformity and new concepts for enhanced emission testing in PTI.	69
2.4 TAP.04. Remote sensing of vehicle emissions.....	94
2.5 TAP.05. Vehicle greenhouse gas emissions, energy consumption, vehicle and fuel life-cycle analysis.	
150	
2.6 TAP.06. Vehicle-emission modelling and measurements and impact assessment of emission regulations.....	201
2.7 TAP.07. Non-road emissions.....	254
2.8 JS.08. Air pollutant and GHG emissions, water contaminants, ambient and underwater noise and vessel-induced mixing.....	275
2.9 JS.09. Atmospheric processes and air quality impact studies: Modelling impacts of transport on air pollution, climate, health and ecosystems.....	343
2.10 JS.10. Compliance monitoring technological and legal frameworks; experimental studies; theoretical impact studies	442
2.11 JS.11. Reduction measures for GHG emissions – alternative fuels, electrification, energy use and optimization; inner-disciplinary and cross-sector studies.	469
2.12 JS.12. Scenarios and policy options for sustainable transport.....	477
2.13 SE.13. Marine processes – fate of pollution from shipping in the marine environment impact studies on ecotoxicology, eutrophication and acidification, energy pollution including underwater noise & induced mixing experimental work, modelling studies of dispersion, transport, and chemical and biological processes in marine waters.	483
2.14 SE.14. Holistic assessment of shipping impacts on the environment, shipping in the marine spatial planning	490
3 Conference Proceedings – Short abstracts.....	497
3.1 TAP.02. On-board monitoring and diagnostics, emission tampering and deterioration.....	502
3.2 TAP.03. In-service conformity and new concepts for enhanced emission testing in PTI.	505

3.3 TAP.04. Remote sensing of vehicle emissions.....	507
3.4 TAP.05. Vehicle greenhouse gas emissions, energy consumption, vehicle and fuel life-cycle analysis. 512	
3.5 TAP.06. Vehicle-emission modelling and measurements and impact assessment of emission regulations.....	514
3.6 TAP.07. Non-road emissions.....	517
3.7 JS.08. Air pollutant and GHG emissions, water contaminants, ambient and underwater noise and vessel-induced mixing.....	522
3.8 JS.09. Atmospheric processes and air quality impact studies: Modelling impacts of transport on air pollution, climate, health and ecosystems.....	529
3.9 JS.10. Compliance monitoring technological and legal frameworks; experimental studies; theoretical impact studies	534
3.10 JS.12. Scenarios and policy options for sustainable transport.....	538
3.11 SE.13 Marine processes – fate of pollutions from shipping in the marine environment: impact studies on ecotoxicology, eutrophication and acidification, energy pollution including underwater noise & induced mixing, experimental work, modelling studies of dispersion, transport, and chemical and biological processes in marine waters.	544
3.12 SE.14. Holistic assessment of shipping impacts on the environment, shipping in marine spatial planning.....	552
3.13 PS.1. Poster session 1 (TAP sessions)	557
3.14 PS.2. Poster session 2 (Joint and S&E sessions).....	575

Abstract

This publication contains the proceedings of the 25th International Transport & Air Pollution (TAP) and the 3rd Shipping & Environment (S&E) conference that took place in Gothenburg, Sweden, from the 25th to the 28th of September, 2023. The two joint conferences collected the main research developments and policy targets during 2020's in Europe, China and other parts of the world in the early 2020's in multiple transport areas. Topics covered research on air pollutant emissions and greenhouse gases from transport and clean shipping, emission measurements, remote sensing, emissions modelling and control, enhanced air quality modelling tools, and impacts of transport-related air pollution on health and ecosystems. Additional focus areas included reduction measures for emissions of GHGs and air pollutants such as electromobility, fuels and energy decarbonisation, low emission engines and vehicles, air pollution/climate change trade-offs, holistic assessment of shipping impacts including the marine environment, as well as scenarios, policy options for sustainable transport. The publication is addressed to researchers, engineers and policymakers, as well as to all those interested in developing more efficient and cleaner transportation systems.

Acknowledgements

We would like to thank all the people involved in the successful organisation of the 25th International Transport & Air Pollution and the 3rd Shipping & Environment conference, and in particular the members of the Scientific and Organizing Committees for their invaluable efforts. Above all we would like to thank all presenter and authors for their high-quality contributions to the conference and the conference proceedings.

1 Introduction

1.1 Message of the Chairs

The 25th International Transport and Air Pollution Conference (TAP) and the 3rd Shipping & Environment Conference (S&E) were jointly co-organized in Gothenburg, Sweden, from 25 to 28 September, 2023, by IVL Swedish Environmental Research Institute together with Chalmers University of Technology, University of Gothenburg and Swedish Institute for the Marine Environment, with financial support from the Swedish Transport Administration, the Swedish Environmental Protection Agency, the European Commission Joint Research Centre and Chalmers Area of Advance Transport.

The two joint conferences provided a forum to discuss a wide variety of questions related to the impacts of the transport sector on all parts of the environment, including atmosphere, climate, terrestrial ecosystems and the marine environment. At a time when a fast transition to carbon neutral transport is essential, this joint event facilitated along with the traditional areas of TAP and S&E conferences also holistic studies investigating multimodal transport and/or impacts on several areas of the environment.

For the TAP part of the conference the topics were: new emission control concepts, testing conditions and pollutants, non-exhaust emissions, onboard monitoring and diagnostics, emission tampering and deterioration, in-service conformity and new concepts for enhanced PTI emission testing, remote sensing of vehicle emissions, greenhouse gas emissions, energy use, fuel life cycle analysis, emission modelling and measurements and impact assessment of emission regulations, non-road emissions.

For the Joint TAP&SE part, focussing on shipping, the topics were: water contaminants, ambient and underwater noise and vessel-induced mixing, atmospheric processes and air quality impact studies, modelling impacts of transport on air pollution, climate, health and ecosystems, compliance monitoring: technological and legal frameworks; experimental studies; theoretical impact studies, reduction measures for GHG emissions - alternative fuels, electrification, energy use optimization; inter-disciplinary and cross-sector studies and scenarios and policy options for sustainable transport.

For the S&E part topics were: Marine processes - fate of pollution from shipping in the marine environment, impact studies on ecotoxicology, eutrophication and acidification, energy pollution including underwater noise & induced mixing; experimental work, modelling studies of dispersion, transport, and chemical and biological processes in marine waters, and holistic assessment of shipping impacts on the environment and marine spatial planning.

Taken together the two joint conferences were attended by close to 200 participants, to whom about 70 scientific papers were presented as oral presentations and about 90 as poster presentations.

The TAP part of the conference mirrored the increasing research interest in non-exhaust particle emissions and road vehicle CO₂ emissions, fuel consumption and energy use, the latter related to the growing fleet of battery electric vehicles in recent years. It also showed many new developments in the field of remote emission sensing techniques and their applications in the field of new emission legislation impacts, market surveillance and detection of high-emitters, due to e.g., deliberate tampering of the vehicle emission control systems. The needs and options to renew and improve inspection maintenance programs (PTIs) were also highlighted in several presentations.

The Joint TAP&SE part of the conference showed new developments in investigation of emissions from shipping and in compliance monitoring, where combustion of traditional and alternative fuels is expected to remain a significant source of air pollution affecting communities in coastal regions also in the future. Challenges of the current legislation targeting shipping in terms of enforcement, efficiency in emissions reduction, as well as trade-offs between impacts on different parts of the environment were discussed along with new developments in modelling tools for assessment of impact of transport sector on air quality. Several modelling studies showed potential of the mitigation options in road transport, shipping and the entire transport system to meet the air quality and GHG emission goals on different time horizons.

The marine part of the conference focused on impact of shipping on the marine environment and holistic studies taking all environmental impacts into consideration. Important topic of this part was impact of large increase of use of scrubbers, the exhaust gas aftertreatment enabling continuation of use of high-sulphur fuels containing metals and other toxic substances, which are transferring

emissions to the atmosphere targeted by IMO legislation, directly to the sea, bringing a serious threat to the marine environment.

The present report includes the proceedings of the joint 25th TAP and 3rd S&E conference (2023) and is divided into two parts: Volume 1 contains all extended abstracts submitted to the two conferences, whereas Volume 2 contains all the short (one page) abstracts that were not submitted as extended abstracts.

1.2 Organisation

1.2.1 General information

Conference Logo	
Conference Title	25th International Transport & Air Pollution and 3rd Shipping & Environment Conference
Date	25 -28 September 2023
Venue	Wallenberg Conference Centre, Gothenburg, Sweden

1.2.2 Local organisers



[IVL Swedish Environmental Research Institute](#)



[University of Gothenburg](#)



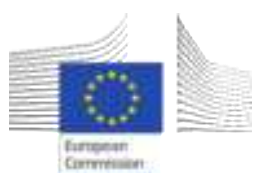
[Chalmers University of Technology](#)



Swedish Institute for
the Marine Environment

[Swedish Institute for the Marine Environment](#)

With the support of:



[European Commission Joint Research Centre](#)

1.2.3 Collaborators



[Laboratory of Applied Thermodynamics](#)
[Aristotle University of Thessaloniki](#)



[Graz University of Technology](#)



[EMPA Swiss Federal Laboratories for Materials Science & Technology](#)



[Université Gustave Eiffel](#)
[Institut Francilien des Sciences Appliquées](#)

1.2.4 Funders/sponsors



[Swedish Transport Administration](#)



[Swedish Environmental Protection Agency](#)



[Chalmers University of Technology](#)
[Area of Advance Transport](#)

1.2.5 Scientific Committees

1.2.5.1 *TAP Scientific Committee*

Miriam Elser	EMPA (CH)
Asif Faiz	Faiz&Assoc. LLC (US)
Salah Khardi	IFSA/University Eiffel (F)
Jens Borken-Kleefeld	IIASA/Technical University Dresden (AT/DE)
Benedikt Notter	INFRAS (CH)
James Tate	ITS/University of Leeds (UK)
Åke Sjödin	IVL (SE)
Georgios Fontaras	JRC (INT)
Gary Haq	JRC (INT)
Zisis Samaras	LAT/AUTh (GR)
Leonidas Ntziachristos	LHTEE/AUTh (GR)
Nicolas Moussiopoulos	LHTEE/AUTh (GR)
Jonathan Andersson	Ricardo (UK)
Nikolas Hill	Ricardo (UK)
Robin Smit	TEER (AU)
Norbert Ligterink	TNO (NL)
Robin Vermeulen	TNO (NL)
Ye Wu	Tsinghua University (CN)
Wen Yifan	Tsinghua University (CN)
Stefan Hausberger	IVT/TU Graz (AT)
Martin Rexeis	IVT/TU Graz (AT)

1.2.5.2 *S&E Scientific Committee*

Erik Fridell	IVL (SE)
Elisa Giubilato	Univ. of Venice (IT)
Julia Hansson	IVL (SE)
Lars Hole	Met Norway (NO)
Christa Maradino	Gemoar (DE)
Volker Matthias	Heron (DE)
Johan Mellqvist	Chalmers (SE)
Jana Moldanova	IVL (SE)
Leonidas Ntziachristos	AUTh (GR)
Danielle van Dinther	TNO (NL)

1.2.6 Organising Committee

The members of the Organising Committee (OC) of the conference undertook tasks related to the organisation of the conference, the reception, organisation and allocation of the scientific papers for review, the notification of authors, the identification of the thematic areas, the formulation of the program and the ~~in-situ organization of all conference's aspects~~. The members of the Organising Committee, as well as their affiliations are provided below:

- Åke Sjödin (TAP Chairman), IVL Swedish Environmental Research Institute (SE)
- Jana Moldanova (S&E Chairman), IVL Swedish Environmental Research Institute (SE)
- Yingying Cha (Conference Assistant), IVL Swedish Environmental Research Institute (SE)
- Helena Lundström (Conference Assistant), IVL Swedish Environmental Research Institute (SE)
- Ida-Maja Hassellöv (S&E Vice Chairman), Chalmers University of Technology (SE)
- Eva-Lotta Sundblad (S&E Conference Assistant), Swedish Institute for the Marine Environment (SE)

2 Conference Proceedings –Extended abstracts

The present chapter includes collection of all submitted extended abstracts that were presented during the conference. Short one-page abstracts of presentation for which the extended abstracts have not been prepared are available in Volume 2 of the Proceedings.

Papers of this section are:

- structured based on the thematic sessions of the TAP&SE 2023, as defined in the final program of the conference,
- listed in the order that were presented during the conference,
- included in the version that was submitted by authors to the conference's website before the implementation dates of TAP&SE 2023.

Table 1 lists the submitted extended abstracts by session/topic of TAP&SE 2023.

Table 1. Submitted extended abstracts by session/topic of TAP&SE 2023.
"PS" denotes poster presentations.

Session/Paper ID	Corresponding author, Title	
TAP.01	New emission control concepts, testing conditions and pollutants, non-exhaust emissions	
TAP.01.PS.1.5	Kulovuori, S.	Influence of vehicle weight on PM emissions from studded and studless winter tyres - laboratory and on-road results
TAP.01.PS.1.9	Colombo, A.	First application of a protocol for physico-chemical characterization of the nanoparticulate.
TAP.01.PS.1.13	Tsakonas, G.	Comparison of two Air Liquid Interface (ALI) systems: lung cells exposure to vehicle exhaust
TAP.01.PS.1.15	Dimaratos, A.	Design of a sampling system for brake particles on-road measurement – A computational preliminary study
TAP.02	On-board monitoring and diagnostics, emission tampering and deterioration	
TAP.02.3	Frateur, T.	Real world particle number emission factors from plume chasing data
TAP.02.PS.1.27	Svensson, N.	Effects of geofencing on exhaust emissions and noise: A combined test track and traffic simulation study
TAP.02.PS.1.31	Matzer, C.	Feasibility study for future on-board NOx monitoring of passenger cars
TAP.02.PS.1.33	Mehel, A.	Simultaneous in-cabin and on-road CO2 concentrations on-board measurements
TAP.03	In-service conformity and new concepts for enhanced emission testing in PTI's	
TAP.03.1	Melas, A.	Solid particle number (SPN) measurements during the periodic technical inspection (PTI) of vehicles
TAP.03.3	Wang, Y.	In-use NOx emission trends of diesel trucks in China informed by large-sized inspection data
TAP.03.PS.1.35	Franzetti, J.	Assessment of Hot Idling Test Procedure for NOx Measurement in Periodic Technical Inspection (PTI) of Vehicles
TAP.03.PS.1.48	Ktistakis, M.	Statistical evaluation of Conformity of Production of road vehicles
TAP.04	Remote sensing of vehicle emissions	
TAP.04.2	Yang, Z.	Single-blind test on the effectiveness of the Gumbel distribution method in detecting high-emitters in remote sensing data

TAP.04.6	Chu, M.	Applications of multi-sensor roadside networks for fleet emission source apportionment and single-vehicle EF determination
TAP.04.7	Buhigas, J.	Development and testing of a novelty Remote Sensing Device for the simultaneous measurement of vehicles' emissions & circulation in multilane roads
TAP.04.PS.1.43	Moroni, S.	Advanced Air quality sensors and Remote Sensing to investigate vehicular traffic emissions in Milan: CARES H2020 Project results
TAP.04.PS.1.47	Cha, Y.	Remote Sensing Measurements of Vehicle Emissions in Sarajevo
TAP.04.PS.1.49	Mahesh, S.	Emissions from in-use vehicles in Dublin using on-road remote sensing
TAP.04.PS.1.50	Piasecki, C.	Remote Sensing Emission Measurements on a German Motorway – Insights and initial Results
TAP.04.PS.1.51	Schaffer, P.	Simulations of a NIR TDLAS Sensor for Stand-Off Measurement of Carbon Dioxide for Remote Emission Sensing
TAP.04.PS.1.52	Rushton, C.	A modern, flexible cloud-based database and computing service for storing and analysing vehicle emission measurements
TAP.05	Vehicle greenhouse gas emissions, energy consumption, vehicle and fuel life cycle analysis	
TAP.05.1	Tansini, A.	From physical testing to on-board fuel consumption monitoring and telemetry: a pilot project for capturing the real-world fuel consumption of vehicles
TAP.05.2	Komnos, D.	CO2 emissions performance comparison of Australian and European SUVs
TAP.05.3	Hausberger, S.	Temperature Effects on Energy Consumption from Battery Electric Vehicles
TAP.05.5	Mellios, G.	Prediction of fuel consumption for truck planning based on VECTO simulations
TAP.05.6	Broekaert, S.	Experimental validation of battery electric truck simulation in VECTO
TAP.05.7	Frobert, A.	Emission Monitoring for used cars: Evaluation of On-Road Testing
TAP.05.PS.1.10	Wang, F.	Multi-sectoral drivers of decarbonizing battery electric vehicles in China
TAP.05.PS.1.18	Lejri, D.	Vehicle fleet electrification: electric energy consumption assessment at the scale of an urban area.
TAP.06	Vehicle emission modelling and measurements and impact assessment of emission regulations	
TAP.06.3	Tirico, M.	Assessing pollutant emissions on an urban area using different traffic simulation approaches: multi-agent modelling and microscopic modelling
TAP.06.4	Roldin, P.	Secondary aerosol formation from real vehicle exhausts – Development of an equivalent total particle emission index module for air quality modelling applications
TAP.06.5	Cox, B.	Emission savings potential of ecodriving based on over 1500 hours of driving data from 5 countries. Findings from the uCARe project
TAP.06.6	Johansson, E.	Impact of uCARe measures on air quality in selected cities
TAP.06.PS.1.22	Norman, M.	Nanoparticles in different environment in Stockholm, the nPETS project
TAP.06.PS.1.28	Wærsted, E.	Quantification of temperature dependence of NOx emissions from road traffic in Norway using air quality modelling and monitoring data
TAP.06.PS.1.30	Philips, I.	The impact of UK Clean Air Zones (CAZs) on the observed vehicle fleet

TAP.06.PS.1.34	Troncoso Lamaison, F.	Estimation of mobility and traffic emissions based on Cell Phone Data
TAP.06.PS.1.36	Quaassdorff, C.	Input requirements for modeling the microscale spatial distribution of emission hotspots based on real-world measured vehicle activity
TAP.07	Non-road emissions	
TAP.07.3	Demuynck, J.	Real-world NOx emissions of Stage IV and V machines
TAP.07.4	Gustafsson, M.	PM10 emissions and rubber content from different tyre types in relation to rubber hardness and road surface type
TAP.07.PS.1.38	Schmidt, C.	NRMM Real Operation NOx Emission Measurements with Plume Chasing
JS.08	Air pollutant and GHG emissions, water contaminants, ambient and underwater noise and vessel-induced mixing	
JS.08.2	Jalkanen, J.	Underwater noise emissions from ships during 2014-2020
JS.08.3	Weigelt, A.	Size resolved particle emission behaviour for different types of vessels
JS.08.9	Streibel, T.	Effects of sulfur scrubbers on particulate emissions from a marine diesel engine
JS.08.10	Kuittinen, N.	Methane slip from LNG engines - review and on-board study
JS.08.PS.2.1	Grigoriadis, A.	Particulate and gaseous emissions from a large 2-stroke slow speed marine engine equipped with open-loop scrubber under real sailing conditions
JS.08.PS.2.13	Grigoriadis, A.	A new set of Emission Factors for ships
JS.08.PS.2.17	Wang, G.	Automatic Classification of Aerosol Particles using Single-Particle Mass Spectrometry and Machine Learning
JS.08.PS.2.19	Heikkilä, M.	Gentlemen, do not start your engines: The association between vessel departures and air pollution in Helsinki port area 2016-2021
JS.08.PS.2.21	Krause, J.	Maritime Greenhouse Gas Emission Reduction Scenarios – Extension of DIONE model
JS.09	Atmospheric processes and air quality impact studies: Modelling impacts of transport on air pollution, climate, health and ecosystems	
JS.09.1	Uhrner, U.	Specification of Zero-Impact Vehicle Emissions & Demonstration of Zero Impact
JS.09.4	Megaritis, A.	The impact of shipping emissions to urban air quality in Europe - A port/city analysis
JS.09.6	Fink, L.	Potential impact of shipping on PM2.5 species in the Mediterranean region - a multi-model evaluation
JS.09.7	Ioannidis, G.	A numerical CFD model to quantify traffic-related pollutant concentrations in urban scale.
JS.09.8	Broman, L.	Health benefits if air pollution goals achieved along highways
JS.09.PS.1.46	Hafs, N.	Assessing the Impact of Car Cabin Filters mileage on In-Vehicle Air Quality: Results from Controlled Environment
JS.09.PS.1.57	Chekrouba, K.	A numerical study of particle dispersion in the wake of a static and rotating cylinder
JS.09.PS.2.29	Piccoli, A.	The assessment of a Zero Emission Zone air quality and human health impacts in the metropolitan city of Milan
JS.09.PS.2.31	Engardt, M.	Improving 3-day deterministic air pollution forecasts using machine learning algorithms
JS.09.PS.2.33	Schlesinger, D.	Effects of noise barriers on population exposure to and health impacts of air pollutants downwind of highways

JS.09.PS.2.39	Schwarzkopf, D.	Transition to cleaner and carbon-free marine fuels and their potential impacts on air quality in the North and Baltic Sea in the future
JS.09.PS.2.43	Kammerkar, A.	The impact of data splitting in air quality modelling on the possibilities of interpretation of the results
JS.09.PS.2.45	Toenges-Schuller, N.	Particle number box-model calculations in a street canyon and comparison to measurements
JS.09.PS.2.47	Toenges-Schuller, N.	Temporal distribution of national emission data for dispersion calculations with chemical transport models
JS.09.PS.2.50	Horváth, J.	Transport emission footprint in the Slovak economy
JS.10	Compliance monitoring: technological and legal frameworks; experimental studies; theoretical impact studies	
JS.10.1	Ntziachristos, L.	Shipping emissions monitoring with on-board and remote techniques and impacts on air quality: The SCIPPER project summary and results
JS.10.PS.2.2	Badeke, R.	Application of a 24-hour ship plume forecasting system
JS.10.PS.2.6	Rieker, M.	SEICOR - Ship Emission Inspection with Calibration-free Optical Remote sensing
JS.10.PS.2.8	Verbeek, R.	Experiences with sensor based continuous emission monitoring for demonstration of maritime emissions compliance
JS.11	Reduction measures for GHG emissions - alternative fuels, electrification, energy use optimization; inter-disciplinary and cross-sector studies	
JS.11.PS.2.48	Norman, M.	Active traffic management for improved air quality and reduced climate impact
JS.12	Scenarios and policy options for sustainable transport	
JS.12.PS.2.22	Pagels, J.	Solid Oxide Fuel Cells for Reduced Health and Climate Impact of Ship Emissions
SE.13	Marine processes - fate of pollution from shipping in the marine environment: impact studies on ecotoxicology, eutrophication and acidification, energy pollution including underwater noise & induced mixing; experimental work, modelling studies of dispersion, transport, and chemical and biological processes in marine waters	
SE.13.2	Picone, M.	Ecotoxicological effects of exhaust gas cleaning system (EGCS) discharge water on marine copepods
SE.14	Holistic assessment of shipping impacts on the environment, shipping in marine spatial planning	
SE.14.5	Johansson, T.	Financial incentives for ship underwater noise mitigation

2.1 TAP.01. New emission control concepts, testing conditions and pollutants, non-exhaust emission

Influence of vehicle weight on PM emissions from studded and studless winter tyres - laboratory and on-road results

S. Kulovuori¹ and M. Gustafsson²

¹Metropolia University of Applied Sciences, Department of Automotive and Mechanical Engineering, Vantaa, 00160, Finland, Sami.Kulovuori@metropolia.fi

²Swedish National Road and Transport Research Institute (VTI), Linköping, 581 95 Sweden.

Introduction

Automobiles are becoming progressively heavier, both as a result of customer preferences, such as the rise of SUVs, and the fact that electric vehicles are generally heavier than their fossil-fuel counterparts. There are also ongoing initiatives at the European level for longer and heavier heavy-duty vehicles motivated by lower emissions per ton of goods (e.g. (de Saxe et al., 2018)). Weight-dependent tyre and pavement deterioration (Beddows and Harrison, 2021; Low et al., 2023) and road dust resuspension pose a risk of heavier vehicles producing more non-exhaust emissions. In Nordic countries, where studded tyres are used, the risk of road deterioration and consequently PM emissions from roads is particularly high. In this study, the effects of weight on PM emissions in the laboratory and field were investigated.

Methods

The tests were carried out on the VTI road simulator (Figure 1A, (Gustafsson et al., 2009)) and on the road with an instrumented vehicle "sniffer" (Figure 1B, (Pirjola et al., 2009)). The VTI Road simulator is carousel-like equipment with four wheels that run on a circular pavement ring (Figure 1). Any type of pavement or light-duty vehicle tyres can be used. The tests can be run up to 70 km/h, and the hall is temperature-controlled. In the tests, studded tyres (two Nokian Hakkapeliitta 9 and two Kumho Wintercraft Ice) and the tests were performed at a start temperature of -5°C at 40 and 60 km/h on a mixed asphalt concrete pavement. Three different axle loads were used in the road simulator: 350, 450, and 550 kg/axle, resulting in total loads of 1400, 1800, and 2200 kg. Particle mass concentrations were measured using TEOM 1400a (Tapered Element Oscillating Microbalance, Rupprecht & Pataschnik Co.) and size distributions using APS 3321 (Aerodynamic Particle Sizer, TSI Inc.) and SMPS (Scanning Mobility Particle Sizer, TSI Inc.) PM10 concentrations were corrected for changes in stud protrusion during the tests.



Figure 1: A: The VTI road simulator. B: Sniffer vehicle. Photos by Mats Gustafsson, VTI, and Sami Kulovuori, Metropolia.

On-road measurements were performed on road number 130 in Nurmijärvi, Finland ($60^{\circ}28'26''N$, $21^{\circ}50'52''E$, where four different vehicle weights (3500, 4050, 4600, and 5150 kg) were evaluated at three different speeds (30, 50, and 70 km/h) using studded and friction tyres from the same manufacturer (Continental VanContact Ice and VanContact Viking). Tests were conducted in summer conditions, where the dust load on the road surface was low, and in spring conditions, where the dust load on the road surface was higher because of the use of winter tyres.

The ambient temperature and relative humidity were measured using temperature and humidity probes (Model HMP45A, Vaisala) during both campaigns. During spring measurements, ambient temperatures were between 7.4–15.5 °C and relative humidity was between 27 and 58 %, with a mean temperature and relative humidity of 12.3 °C and 41 %, respectively. In the summer measurements, the temperature and relative humidity were 16.1–26.7 °C and 28–63 %, respectively, and the mean temperature and relative humidity were 21.7 °C and 41 %, respectively. The road surface temperature and moisture were not measured; however, in both campaigns, the road surface was dry, and the ambient dew point temperature was lower than the measured ambient temperature. Changes in ambient temperature and relative humidity were not considered to significantly impact the results.

The tyre pressure for each weight/tire combination was set to 4.0 bar and the sample inlet height from the ground was adjusted with an air suspension of 8 cm, with each weight setting during the tests. The particle mass concentrations were measured behind the left rear wheel using a TEOM1405d (Tapered Element Oscillating Microbalance Thermo Scientific™ Direct-Link II; Model E530, TSI Inc.), and the particle size distribution using an OPS 3330 (Optical Particle Sizer, TSI Inc.).

The collected measurement data were divided into groups corresponding to each tyre, weight, speed, and test combination, resulting in 48 individual groups. For each group, stratified random sampling was applied (sample size: N = 300) to ensure an equal number of observations in each group. Each group was filtered by ± 3 km/h of the group target speed and inner quartile range (IQR) to remove possible outliers in each group. The normality of the observations was checked using the Shapiro-Wilk test (Shapiro and Wilk, 1965) and visually with Q-Q plots for each group. A nonparametric Kruskal-Wallis test (Kruskal and Wallis, 1952) was applied to the data to check if the median was equal between all groups. Dunn's test (Dunn, 1961) was performed to determine whether there was a statistically significant difference between the medians of the groups and which groups were in question in both the spring and summer measurements.

Results and discussion

Both test results showed an increase in PM₁₀ emissions with increasing speed and weight. In the simulator, the data reflected direct emissions, mainly from the road wear of studded tyres, whereas the on-road data reflected both direct and resuspended emissions.

The PM₁₀ emission factors from the road simulator showed a clear positive correlation with both load and speed, with a stronger load effect at higher speeds (Figure 2). The calculated emission factors are high compared to normal driving, which is normally of the order of a few hundred mg/vkm (for example, (Ferm and Sjöberg, 2015)). This is likely owing to the high turn-slip in the contact between the tyre and pavement in the simulator.

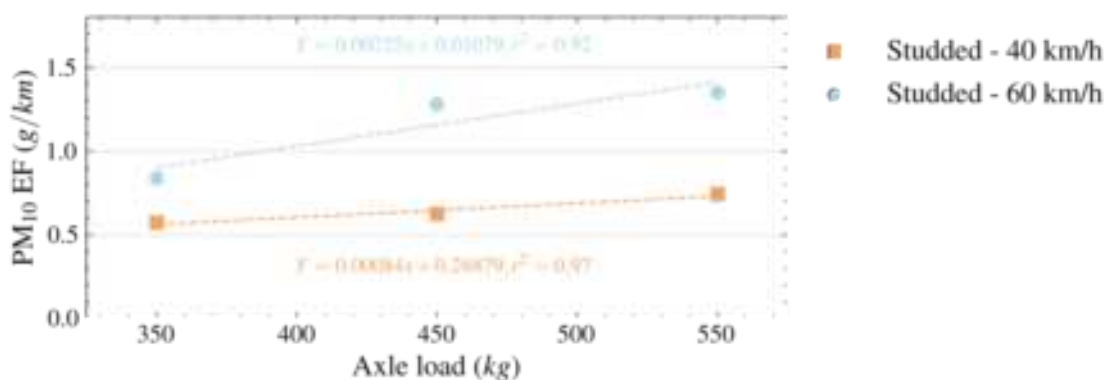


Figure 2: PM₁₀ emission factors for studded tyre tests as functions of axle load and speed.

The particle size distributions revealed a peak at approximately 20–30 nm for all the loads. The particle number concentration increased with the load (Figure 3A). The particle mass size distributions were bimodal with a preliminary peak at 2–3 μm and a secondary peak at 5 μm . The concentrations at 350 kg and 450 kg did not differ significantly in the APS data, whereas 550 kg generated considerably higher concentrations (Figure 3B).

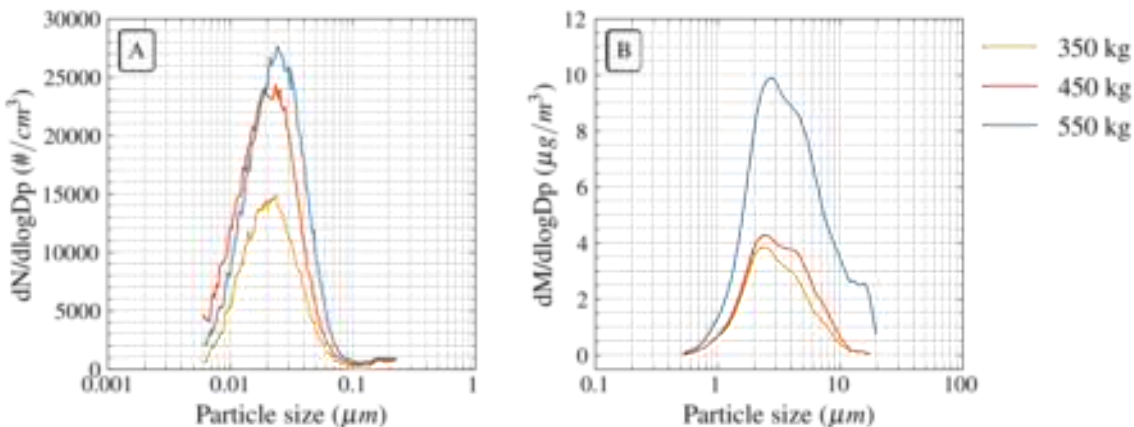


Figure 3: Particle number (A) and mass (B) size distributions at different loads measured using SMPS and APS at 60 km/h.

The road measurements in spring and summer showed increased measured PM_{10} concentrations with both tyres when vehicle weight and speed increased (Figure 4 A and B). In summer measurements, the behaviour of the measured PM_{10} concentration was as suspected, because the dust load on the road surface was lower than in spring measurements; therefore, the resuspension caused by vehicles was lower, making direct emissions from studded tyres the dominant factor compared to friction tyres.

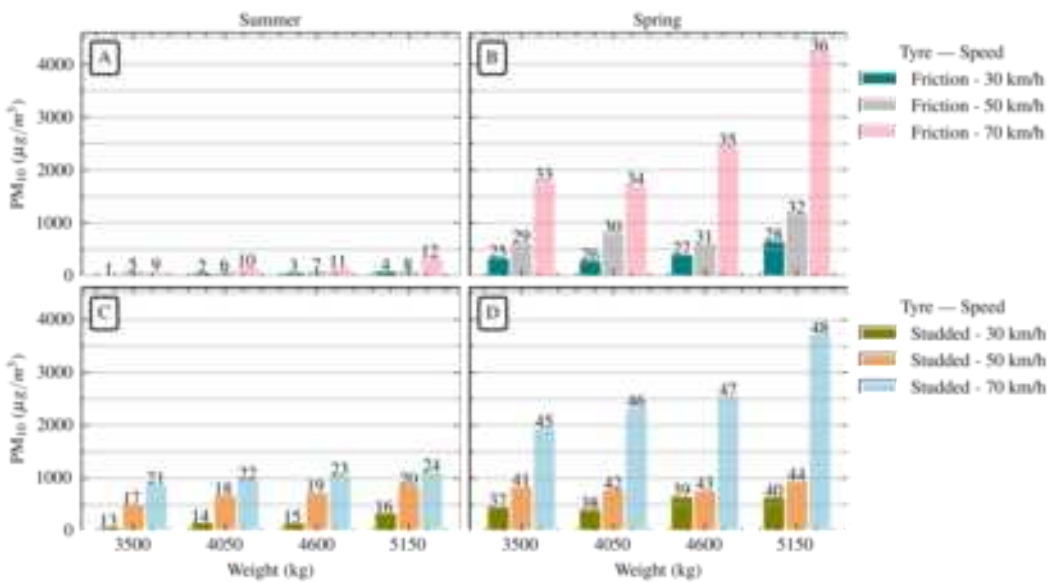


Figure 4: Mean measured PM_{10} concentrations of the Sniffer as a function of different weights, tyres, and speeds. (A = summer measurement with friction tyre, B = spring measurement with friction tyre, C = summer measurement with studded tyre, D = spring measurements with studded tyre; the number above bars = group number in the statistical tests).

In spring measurements, the dictating factor was resuspension, which was caused by the higher road surface dust load caused by studded tyre usage; therefore, the measured PM₁₀ concentrations were somewhat the same magnitude for both tyres. The mean concentrations of PM₁₀ in the spring measurements (Figure 4B and 4D) showed a clear increase when the speed of the vehicle increased from 30 or 50 km/h to 70 km/h for each weight class and tyre. The same effect was also observed with studded tyres in the summer measurements (Figure 4C) for each weight class.

The particle mass size distributions measured on-road (Figure 5) revealed similar observations as in the VTI road simulator (Figure 3B), where two peaks were observed. Figure 5 shows two distinctive peaks at 4-5 µm and 8-9 µm for both measurements and both tyres, which differ slightly from the VTI road simulator observations, although the peak at approximately 5 µm in the road simulator was also observed in Sniffer. Other tyre, weight, and speed combinations showed similar shapes, as shown in Figure 5. The effect of the road surface dust load on resuspension can be observed from the size distributions when summer measurements with a friction tyre were compared with spring measurements (Figure 5A and 5B).

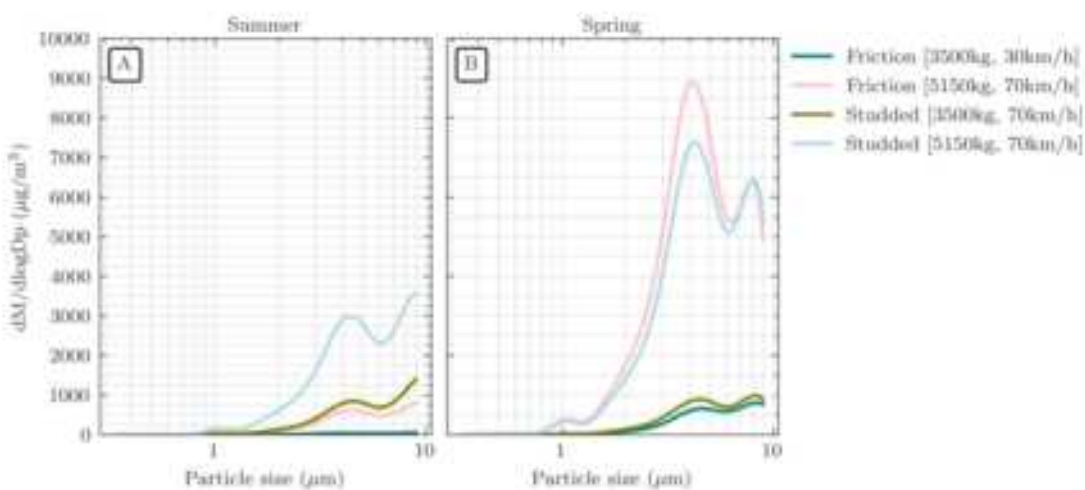


Figure 5: Mean particle mass size distributions with the lowest and highest vehicle weights and speeds for both tyres (A= summer measurements (low dust load) and B = spring measurements (high dust load)).

The statistical tests performed for the summer and spring measurements showed that the observations of the individual groups were not normally distributed, and the p-values of the Shapiro-Wilk test for each group were < 0.05. The Kruskal-Wallis test indicated that there were differences between the group medians (p-value < 0.05) for both summer and spring measurements. The Dunn test showed statistically significant differences between the groups, i.e., summer measurements with a friction tyre at speed of 30 km/h. There were no statistically significant differences in the group medians when vehicle weight was 4050 kg and compared to vehicle weight of 4600 kg (p-value:0.073). All the statistically insignificant comparisons are presented in Table 1.

Overall, statistical tests indicate that increasing vehicle weight and speed have statistical significance in measured PM₁₀ concentrations for both tyres, although 5.3 % and 1.5 % of the total amount of pairwise comparisons were not significant in summer and spring measurements, respectively. Similar observations of PM₁₀ concentrations were observed for all instruments, although some variations were observed in absolute PM₁₀ concentration values due to the different techniques used to measure PM₁₀ concentrations.

Table 1: Results of the Dunn test show instances in which statistical significance was not present (p-value > 0.05). (Group ID = where the groups are compared, speed = driven speed within groups, tyre = used tyre within groups, weight = vehicle weight assigned to the group).

Test	Groups	speed	tyre	weight	p-value
Summer	2-3	30	friction	4050-4600	0.073
Summer	5-6	50	friction	3500-4050	1.000
Summer	5-8	50	friction	3500-5150	1.000
Summer	6-8	50	friction	4050-5150	1.000
Summer	10-11	70	friction	4050-4600	0.613
Summer	14-15	30	studded	4050-4600	0.398
Summer	15-16	30	studded	4600-5150	0.051
Summer	17-18	50	studded	3500-4050	0.852
Summer	18-19	50	studded	4050-4600	0.852
Summer	18-20	50	studded	4050-5150	0.195
Summer	19-20	50	studded	4600-5150	1.000
Summer	22-23	70	studded	4050-4600	0.083
Summer	22-24	70	studded	4050-5150	0.074
Summer	23-24	70	studded	4600-5150	0.876
Spring	27-38	30	friction/studded	4050-4050	0.971
Spring	28-39	30	friction/studded	5150-4600	0.964
Spring	28-40	30	friction/studded	5150-5150	0.971
Spring	39-40	30	studded	4600-5150	0.365

Conclusions

The trend towards larger and heavier passenger and heavy-duty vehicles carries the risk of increasing road deterioration and PM emissions in Nordic countries, where winter maintenance and studded tyres are used during winter and spring. This study examined how an increase in vehicle weight affects PM emissions in the laboratory and field.

Laboratory and on-road measurements showed a clear correlation between weight, speed, and PM₁₀ emissions/concentrations in both the road simulator testing and on-road measurements. The particle mass size distribution was bimodal, with peaks around 2-3 µm and 5 µm in the simulator test and around 4-5 µm and 8-9 µm in on-road measurements. The particle number and mass concentrations increased with increasing axle load, indicating that heavier vehicles led to higher emissions.

On-road measurements revealed the seasonal effects of emissions. In summer, direct emissions from studded tyres dominated because of a lower road surface dust load, whereas in spring, resuspension from a higher road surface dust load was the primary factor of emissions from studded and friction

tyres. The statistical analysis identified statistically significant differences in PM₁₀ concentrations based on speed, tyres, and weight. This confirms the effect of increased vehicle weight and speed on PM₁₀ concentrations.

It is discerned that trends towards heavier vehicles could lead to higher emissions under the given conditions, presenting a concern, particularly for regions following similar winter maintenance practices and studded tyre usage.

Acknowledgements

This work was funded by the NordFoU project, *Nordic Road Dust Project Phase II (NorDust II)*. The authors are grateful to the ever-helpful technical staff Dennis Hydén and Tomas Halldin at the VTI road simulator facility and to staff members Harri Nordlund, Kari Heikkilä and Kari Leskinen from Metropolia University of Applied Sciences for giving a helping hand with the on-road measurements.

References

- Beddows, D.C.S., Harrison, R.M., 2021. PM10 and PM2.5 emission factors for non-exhaust particles from road vehicles: Dependence upon vehicle mass and implications for battery electric vehicles. *Atmospheric Environment* 244, 117886. <https://doi.org/10.1016/j.atmosenv.2020.117886>
- de Saxe, C., Kural, K., Kharrazi, S., Schmidt, F., Geem, C., Berman, R., Woodroffe, J., Cebon, D., 2018. FALCON III: Defining a Performance-Based Standards framework for high capacity vehicles in Europe.
- Dunn, O.J., 1961. Multiple Comparisons among Means. *Journal of the American Statistical Association* 56, 52–64. <https://doi.org/10.1080/01621459.1961.10482090>
- Ferm, M., Sjöberg, K., 2015. Concentrations and emission factors for PM2.5 and PM10 from road traffic in Sweden. *Atmospheric Environment* 119, 211–219. <https://doi.org/10.1016/j.atmosenv.2015.08.037>
- Gustafsson, M., Blomqvist, G., Gudmundsson, A., Dahl, A., Jonsson, P., Swietlicki, E., 2009. Factors influencing PM10 emissions from road pavement wear. *Atmospheric Environment* 43, 4699–4702. <https://doi.org/10.1016/j.atmosenv.2008.04.028>
- Kruskal, W.H., Wallis, W.A., 1952. Use of Ranks in One-Criterion Variance Analysis. *Journal of the American Statistical Association* 47, 583–621. <https://doi.org/10.1080/01621459.1952.10483441>
- Low, J.M., Haszeldine, R.S., Harrison, G.P., 2023. The hidden cost of road maintenance due to the increased weight of battery and hydrogen trucks and buses—a perspective. *Clean Technologies and Environmental Policy* 25, 757–770. <https://doi.org/10.1007/s10098-022-02433-8>
- Pirjola, L., Kupiainen, K.J., Perhoniemi, P., Tervahattu, H., Vesala, H., 2009. Non-exhaust emission measurement system of the mobile laboratory SNIFFER. *Atmospheric Environment* 43, 4703–4713. <https://doi.org/10.1016/j.atmosenv.2008.08.024>
- Shapiro, S.S., Wilk, M.B., 1965. An analysis of variance test for normality: Sampling distributions. *Biometrika* 52, 591–611. <https://doi.org/10.1093/biomet/52.3-4.591>

First application of a protocol for physico-chemical characterization of the nanoparticulate generated by brakes.

A. Colombo¹, C.E. Campiglio², S. Conti², A. Mancini³, B. Tsypa³, S. Petromelidou^{4,5,6}, A. Besis^{5,6}, D. Margaritis⁵ and D. Lambropoulou^{4,5}

¹Department of Environmental Sciences, University Research Center Mario Negri - IRCCS, Via Mario Negri 2, 20156 Milano, Italy, andrea.colombo@marionegri.it

²Int. Lab. de Ricerca e sviluppo Mario Negri - IRCCS, Via Stezzano 87, 24126 Bergamo, Italy

³Materials Engineering & Laboratories, Brembo Spa, Viale Europa 2, 24040 Stezzano (BG), Italy

⁴Aristotle University of Thessaloniki / School of Chemistry, Environmental Pollution Control Laboratory, University Campus, 54124, Thessaloniki, Greece

⁵Center for Interdisciplinary Research and Innovation (CIRI-AUTH), Balkan Center, Thessaloniki, GR-57001

⁶Centre for Research and Technology-Hellas (CERTH), Hellenic Institute of Transport (HIT), 6th km Charilaou-Thermi Rd, P.O. Box 60361, GR 57001 Thermi, Thessaloniki, Greece

1. Introduction

Although many efforts have been provided to monitor and reduce air pollutants in the last decades there still exists concern about air quality and adverse health consequences among the populations exposed [WHO, 2006, 2015, 2018, European Council, 2008, European Commission, 2012, European Environment Agency, 2021].

Many legislation activities were focused on particulate matter (PM), which adverse effects are related to their size and chemistry [WHO, 2015m Pope et al., 2002, Pope and Dockery, 2002, Valavanidis et al 2008, Kim et al., 2015]. The major fraction of outdoor ultrafine particles is traffic generated from road, rail, air, and sea transportation, each one representing a transport source. For these reasons the chemical and morphological characterization of nano-particulates produced by different exhaust and non-exhaust emission sources related to the transport sector is one of the aims of the nanoParticle Emissions from the Transport Sector (nPETs) project.

Therefore, to better understand the mechanisms behind adverse risks posed by different types and sources of the identified sub 100 nm particles, a reliable procedure for physico-chemical characterization of the sub 100 nm emissions was developed. In this paper, the results from the investigation of nanoparticle emissions generated by brakes are reported as example. More in detail, the investigated nano-particulate has been sampled in controlled environment involving a friction couple composed by a gray cast-iron (GCI) braking disc and an ECE R90 Copper-free friction material, representative of a standard original equipment for European automotive market.

2. Experimental

2.1 Materials & NanoParticulate Collection

Brake-related nanoparticle emissions are generated by a friction pair composed by a fully pearlitic gray cast iron braking disc (BD) coupled against an ECE R90 Copper-free friction material (FM). The nominal elemental composition of the materials involved in the study is reported in Table 1 for reference.

Table 1: Nominal composition of BD and FM. Only elements with concentration higher than 0.1 wt% are reported for brevity.

BD		FM	
Element	[wt%]	Element	[wt%]
C	3.8	C	31.5
Si	1.9	Fe	23.8
Mn	0.5	O	14.8
Cu	0.2	Zn	6.1
Cr	0.1	Mg	5.5
Fe	<i>balance</i>	Al	4.1
Others	<i>traces</i>	Sn	3.9
		S	3.0
		Cr	2.3
		Si	2.2
		K	2.0
		Ca	0.4
		Cu	0.3
		Mn	0.1
		Others	<i>traces</i>

The generated nanoparticulate sample is collected at a dyno-bench designed for emissions tests performed in controlled conditions [Perricone et al., 2015, 2016]. The procedure used to collect the particulates is the WLTP-Brake Cycle [Mathissen et al., 2018]: the PM material is collected both during the bedding cycles (5 WLTP-Brake repetitions) and during the cycle typically used for the evaluation of the emissions (*i.e.*, the 6th WLTP-Brake cycle repetition) to maximize the amount of collected nanoparticles. For all the tests, the braking corner is composed by: *i*) a four pistons fixed Aluminum caliper with pistons diameter of 44 mm; *ii*) a vented braking disc with a diameter of 342 mm and a thickness of 32 mm; and *iii*) a couple of pads with a surface of 89.1 cm². During the emission test, a controlled particle-free air flux of 245 m³ h⁻¹ enters the brake enclosure to match the temperature targets as suggested by the most recent guidelines from the Particle Measurement Programme (PMP) Informal Working Group and the United Nations Global Technical Regulation (UN GTR) on Laboratory Measurement of Brake Emissions for Light-Duty Vehicles [UN GRPE, 2020, 2023]. The entering air flux is filtered through a HEPA-H13 filter, which ensures an filtration efficiency higher than 99.95%. The collection of the PM emissions is carried out by an isokinetic sampling-probe, equipped with sharp-ended nozzles to ensure a high efficiency sampling. The nano-particulate is sampled through a Dekati Gravimetric Impactor (DGI), able to collect particles in size fractions below 25 µm. The instrument is used at the flow rate of 155 L min⁻¹ and a cyclone with a 2.5 µm cut-off is placed before the inlet to provide the first dimensional cut. Greased Aluminum substrates are used for the upper four stages, while a Teflon filter (pores diameter of 3 µm) is used as backup. In this paper, the material collected on the first collection substrate (S1: 130 < d₅₀ < 150 nm) represents the target sample for the study.

2.2. Organic Chemical Characterization

Organic chemical characterization protocol was developed according to the different EPA methods [USEPA, 1994, 2010], to obtain from a single extraction multiple runs by high-resolution mass spectrometry (HRGC–HRMS) [Mariani et al., 2009].

Briefly, samples were spiked with ¹³C-labelled standard (PCDD/Fs, PCBs, BDEs and PCNs) obtained from Wellington Laboratories (Canada) and deuterated PAHs, NPAHs and OPHAs obtained from Dr. Ehrenstorfer (Augsburg, Germany). After spiking samples were submitted to a single extraction, carried out by Pressurized Liquid Extraction (PLE), using an accelerated solvent extraction instrument (ASE 350, Dionex, Sunnyvale, CA, USA) with dichloromethane followed by a second extraction with acetone-dichloromethane for more polar chemicals. PLE conditions encompass a 5 min preheat time, followed by three static cycles of 15 min at 1500 psi. The flush volume is 60%, followed by a purge with gaseous nitrogen during 100 s. Finally, the two extracts were combined and concentrated to 5 ml and injected into a 5ml loop of an automated Gel Permeation Cromatography (GPC) system (AccuPrep MPSTM, J2 Scientific). The GPC column was 2.5 cm x 43 cm filled with 40 g of BioBeads SX-3 resin working at a flow rate of 5 ml/min using dichloromethane.

The 20% of the sample collected (1 ml) was concentrated to the final volume of 50 µl and submitted to PAH, OPAH and NPAH instrumental analysis. The 80% of the sample (4 ml) was concentrated until 0.5 ml and diluted with hexane to 4 ml. These 4 ml were submitted to an automated clean-up system (Dioxin/SPE module) using acid silica/neutral silica (Si/5G-44%H₂SO₄/Si, Supelco, USA) and basic alumina cartridges (manually packed with 7 g of active Aluminium oxide 90 basic, Supelco USA). The sample is loaded on an acid silica/neutral silica cartridge connected to a basic alumina cartridge and eluted with 75 ml of n-hexane. This fraction was discarded. The basic alumina column is eluted with 60 ml of 98/2 n-hexane/dichloromethane, and this fraction was collected for PCBs and PCNs analysis. Then the basic alumina is eluted with 120 ml of a 50/50 n-hexane/dichloromethane mixture, collected for non-ortho PCBs, PCDDs/Fs, and PBDE analysis.

The quantitative determination was performed by a TRACE GC 2000, Thermo Finnigan (Thermo Fisher Scientific), coupled with a high resolution Mat 95 XP Mass Spectrometer, operating in the electron impact ionization (EI+) mode at 48 eV with a resolution >10,000 and a temperature source of 280 °C. The MS is operated in Selected Ion Monitoring mode (SIM) for all compounds. For PCDD/Fs, PCBs, PCNs, PAHs, NPAHs and OPAHs, the capillary column was a BPX-DXN (60 m length, 0.25 mm i.d., 0.25 film thickness), while for PBDEs the capillary column was a Rtx-1614 (15 m length, 0.10 mm i.d., 0.10 film thickness). Compound identification was performed by comparison with the chromatographic retention time and mass spectra of authentic standards, reported mass spectra and the mass spectral library of the GC/MS data system. Moreover, for halogenated compounds peaks were accepted if the isotopic ratio was within 15% of the corresponding internal standard (IS) ratio. LODs were calculated individually for each sample on the basis of a 3:1 signal-to-noise ratio, while LOQs were calculated for each sample on the basis of a 10:1 signal-to-noise ratio.

2.3 Inorganic Chemical Characterization

The inorganic fraction is characterized by the combination of the Energy Dispersive Spectroscopy (EDS) and the Raman Spectroscopy (RS) to investigate both the elemental and the phase composition of the collected nanoparticulate. Scanning Electron Microscopy (SEM) imaging is used in order to verify qualitatively the granulometric profile of the collected material, while the Energy Dispersive Spectroscopy (EDS) analysis is used to unveil the elemental composition of the sample. The analysis is carried out by means of a Zeiss MA EVO10 scanning electron microscope, equipped with a 10 mm² active area INCA X-act silicon-drift detector (Oxford Instruments). The investigated sample is stripped from the collection substrates after dissolution of the collection grease in acetone and following sonication in 1 mL of isopropyl alcohol at 35 kHz for 2 minutes. The suspended particles are then recollected by centrifugation at 3000 rpm for 5 minutes and dried overnight in mild vacuum conditions (20 mbar) before the chemical analysis. The obtained powder is deposited onto an Aluminum stub for electron microscopy, previously covered with conductive carbon tape. The particulate is always manipulated with a small metallic yet non-magnetic spatula and stocked or deposited in glass containers in order to minimize the potential loss of sample. ~~1 square of approximately 500 x 200 µm are analyzed on the stub with an acquisition time of 500 s and a beam intensity of 300 pA. The elemental concentrations obtained in each region of interest are statistically averaged in order to obtain final compositional results. The experimental spectra are acquired at the instrument's ideal working distance of 8.5 mm (5 µm to sample surface).~~ The elemental composition is probed by back-scattered electrons (BSE) to maximize the interaction volume of the incident beam with the sample.

Raman Spectroscopy (RS) is used to unveil information on the phase composition of the collected nanoparticulate, *i.e.* on the main compounds composing the nano-powders. Raman analysis is carried out by the mean of the Horiba LabRAM HR, equipped with a solid-state laser source (473 nm). The laser power is set nominally to 12.5 mW, since higher power values were found to damage the sample, leaving burnt micro-areas after the measurement. All the spectra are acquired with 50x objective, which was found to be best compromise to balance magnification, resolution and signal/noise ratio. The acquisition range is set in the range of 50-2000 cm⁻¹, while high intensity grating (600 gr mm⁻¹) is used to maximize the collected signal. For each spectrum, five acquisition integrations of 10 sec are merged along the whole investigated frequency range.

2.4 Particle Size Distribution and Morphological Characterization

Dimensional and morphological characterization of nanoparticle emissions is carried out by means of Scanning Electron Microscopy (SEM – GEMINI column Cross-Beam 1540EsB Carl Zeiss GmbH). Samples collected were marked on stubs and coated with a deposition of a thin layer of gold (1 minute, 15 mA) in a sputter coater (Agar Scientific Ltd, Stansted, England). To visualize nanoparticles, samples have been observed using backscattered electrons detector. Particle size distribution was analysed using the plugin Trainable Weka Segmentation of ImageJ software.

3. Results

3.1 Organic Chemical Characterization

The above-described procedure has been used for the analysis of the organic chemicals in nanoparticulate samples collected from laboratory environment conditions. on the DGI Stage 1 (S1) collection substrate ($d_{50} < 150$ nm). Table 2 summarizes PAHs and OPAHs concentrations obtained for the nanoparticle emission collected on the DGI S1 collection substrate PAHs and OPAHs concentrations were 186.8 and 37.4 $\mu\text{g g}^{-1}$ respectively, while NPAHs and halogenated chemical concentrations were lower than the LOQ (data not reported).

Table 2: PAH and OPAH concentration values obtained for the nanoparticle emission collected on the DGI S1 collection substrate.

Compound	Abbreviation	Concentration ($\mu\text{g g}^{-1}$)
Naphthalene	Np	41.8
Acenaphthylene	Acy	5.1
Acenaphtene	Ace	4.4
Fluorene	F	2.6
Phenanthrene	Ph	32.8
Anthracene	An	<0.2
1-mPhenanthrene	1-MEPH	<0.2
2-mPhenanthrene	3-MEPH	<0.2
3-mPhenanthrene	2-MEPH	4.7
9-mPhenanthrene	9-MEPH	3.0
Fluoranthene	Fl	33.7
Pyrene	Py	26.9
Benz[a]anthracene	B[a]An	1.3
Triphenylene	TP	2.1
Chrysene	Chr	3.7
Benzo[b]fluoranthene	B[b]Fl	2.5
Benzo[k]fluoranthene	B[k]Fl	0.7
Benzo[j]fluoranthene	B[j]Fl	1.5
Benzo[e]pyrene	B[e]Py	1.7
Benzo[a]pyrene	B[a]Py	<0.1
Indeno[1.2.3-cd]pyrene	I[1.2.3-cd]Py	2.2
Benzo[ghi]perylene	B[ghi]Pe	7.6
Dibenz[a.h]anthracene	dB[a.h]An	0.3
Coronene	COR	7.6
Polycyclic Aromatic Hydrocarbons	PAHs	186.8
1,4-naphtoquinone	(1.4)O2NAP	1.0
9-fluorenone	9-OFLN	35.8
Acenaphtoquinone	AceNQ	<0.1
Antraquinone	(9.10)O2ANT	<0.1
2-nitrofluorenone	2-N-9-OFLN	<0.1
Benzo(a)fluorenone	BaOFLN	<0.1
Benzo(a)anthrone	BAN	<0.1
1,2 benzoantraquinone	O2BAA	<0.1
Oxygenated Polycyclic Aromatic Hydrocarbons	OPAHs	37.4

Figure 1 reports the distribution of PAHs and OPAHs for the material collected on the DGI S1 collection substrate, showing that the composition of the investigated nanoparticle emission is dominated Naphthalene, Acenaphtoquinone, Fluoranthene, Phenanthrene, Pyrene, Benzo[ghi]perylene and Coronene.

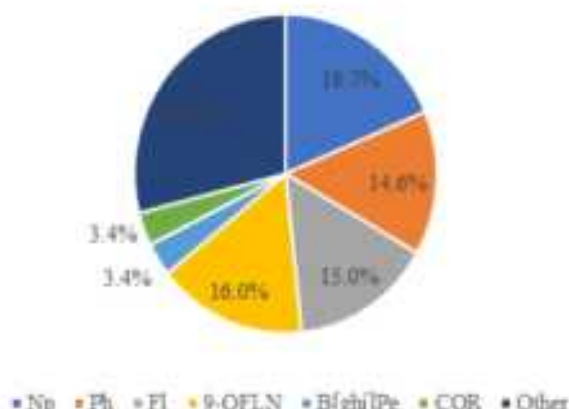


Figure 1: Distribution of PAHs and OPAHs for the material collected on the DGI S1 collection substrate.

3.2 Inorganic Chemical Characterization

The elemental composition of the nanoparticle emission, in the form of the material collected on the DGI Stage 1 (S1) collection substrate ($d_{50} < 150$ nm), is investigated by means of the EDS probe. Average elemental concentration values are reported in Table 3, together with the corresponding standard deviations. Figure 1 shows the elemental distributions over five different measurements, together with the average elemental composition.

Table 3: Average elemental concentration values obtained for the nanoparticle emission collected on the DGI S1 collection substrate. The standard deviation (SD) over five independent observations is reported for each element. Elements with concentrations lower than 0.1 wt% are not reported for brevity.

S1: $130 < d_{50} < 150$ nm		
Element	[wt%]	SD
Fe	37.9	1.7
C	25.5	0.7
O	24.7	1.0
Sn	2.6	0.2
Zn	2.1	< 0.1
S	1.6	0.1
Mg	1.5	0.1
Si	1.4	< 0.1
Al	1.3	< 0.1
K	0.3	< 0.1
Mn	0.3	< 0.1
Cr	0.3	< 0.1
Cu	0.3	< 0.1
Others	traces	-

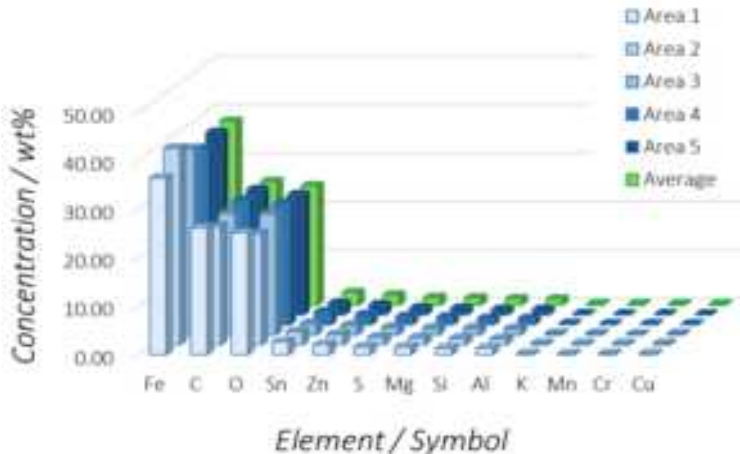


Figure 2: Distribution of elements as measured for the material collected on the DGI S1 collection substrate: in the five independent observations (blue histograms) and averaged results (green histograms).

The results reported in Table 3 and Figure 2 show that the elemental composition of the investigated nanoparticle emission is dominated by the presence of three main elements, namely Iron, Carbon and Oxygen. They account together for more than 85 wt% of the total particulate mass. Iron is an unspecific proxy for the wear of both sides of the tribological interface, *i.e.* it can arise from the wear and tribo-oxidation of both the cast iron brake disc and from the Iron-based compounds contained inside the friction mix of the brake pads. In turn, Carbon is a more specific marker for the consumption of the friction material, since several Carbon-based compounds are commonly used in friction composites, such for example organic resins as binders, graphite and cokes as solid lubricants, inorganic carbides and carbonates as abrasives and fillers [Dante. 2015]. Similarly to Iron, Oxygen arises from both sides of the friction couple: it is indeed a marker for both the oxidation of brake disc Iron and material from the friction composite, since several inorganic oxides, carbonates and silicates are commonly used in brake pads as abrasives and fillers [Dante. 2015]. Finally, the nanoparticle emission features the minor presence of several secondary and trace elements, which are typically found in concentrations lower than 5 wt%. Together, these elements account for slightly more than 10 wt% of the total nanoparticulate mass. The presence of these elements relates closely to the specific friction material formulation and, secondary, to alloying elements from the worn cast iron.

Phase composition of the collected nanoparticle emissions is investigated via Raman Spectroscopy. Figure 3 shows the Raman spectrum acquired directly from the particulate obtained from the DGI S1 collection substrate. As can be observed, some characteristic features are detected. In particular, two characteristic frequency ranges host Raman peaks: *i)* the low frequencies, from 50 to 700 cm⁻¹, hosting signals from Iron oxides; and *ii)* the high frequencies, from 1200 to 2000 cm⁻¹, where signals from elemental Carbon typically reside. In detail, the collected spectrum exhibits two peaks at about 215 and 280 cm⁻¹, which are associated with the Hematite (Fe₂O₃) phase. In addition, it is also possible to recognize two additional broad features at about 380 and 590 cm⁻¹, which are also coherent with the Hematite identification. Moving towards the higher frequencies, two peaks at about 1355 and 1570 cm⁻¹ can be observed, which testify the presence of elemental Carbon (*i.e.*, graphites and cokes) inside the investigated sample. All the described peaks are extremely broad and characterized by low intensities: this observation suggests an overall low degree of crystallinity of the identified compounds, which is coherent with the nature of the sample. Notably, the evaluation of the phase composition is in excellent agreement with observations from the elemental composition analysis.

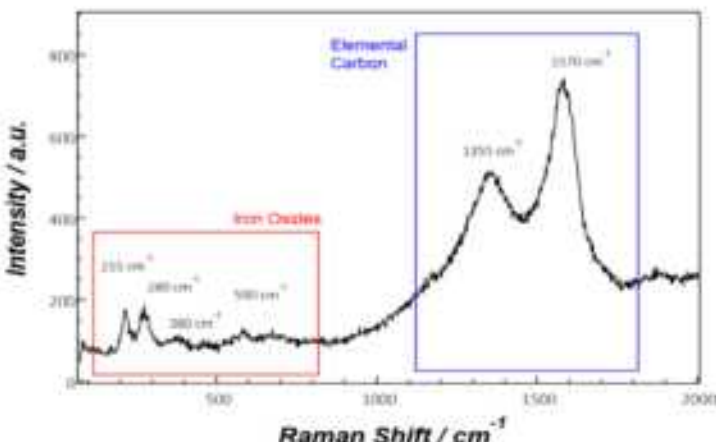


Figure 3 : Raman spectrum of the collected nanoparticulates.

3.3 Particle Size Distribution and Morphological Characterization

By SEM observation, we observed that the particles are homogenously distributed onto substrate (Figure 4a). They present irregular shapes and most of them appears agglomerated into nonhomogeneous structures.

The particle size distribution analysis allowed to identify major and minor axis size (Figure 4b). We can appreciate that most of the particles show a dimension included in the range 100 – 300 nm. The presence of numerous agglomerates could affect the measurement.

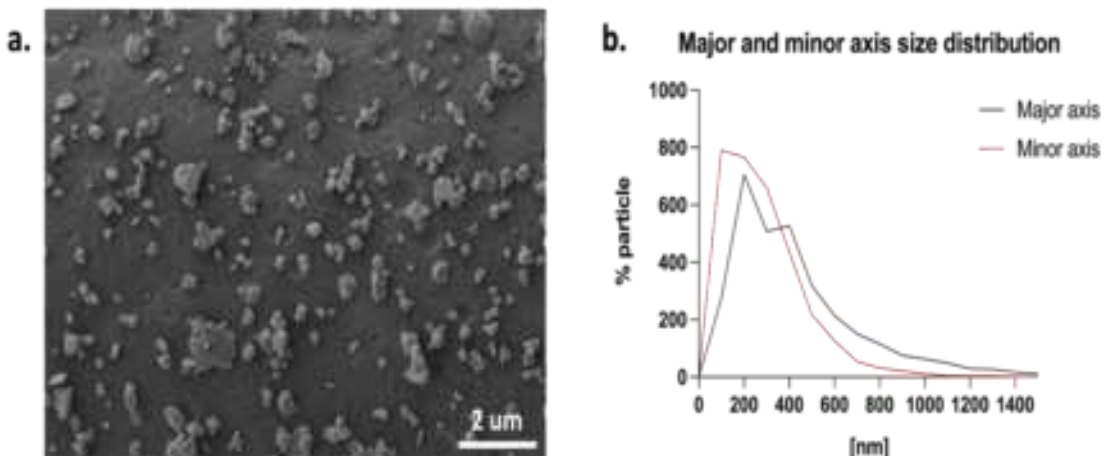


Figure 4 – (a) SEM micrograph of nanoparticles collected. (b) Major and minor axis size distribution in nm.

Acknowledgements

This work was supported by the European Union's Horizon 2020 research and innovation program under grant agreement No 954377.

References

- Campbell, K.: "Handbook of Friction Materials and their Applications". 1st Ed. London: The Woodhead Publishing, 2003.
- European Council. "Directive 2008/68/EC". Brussels, 2008.
- European Commission. "Commission Regulation (EU) 2019/2022". Brussels, 2022.
- European Environment Agency. "Air Quality in Europe - 2021 Report." Luxembourg, 2021.
- Fan, R.-J., Kabir, E., and Kabir, S.: "A Review on the Human Health Impact of Aeromobile Particulate Matter". Environ. Int. 74 (2015): 136-143.
- Mariani G., Amalfitano L., Manni A., Mueller A., Skejo H., Umlauf G. (2009) Organohalogen Compd. 71: 2796-2801.
- Mathissen, M., Grochowicz, J., Schmidt, C., Vogt, R., et al., "A novel Real-World Braking Cycle for Studying Brake Wear Emissions". wear 414-415, 219-226. 2018.
- Particle Measurement Programme Informal Working Group. Informal document GRPE_81_12. 81st GRPE. 9-11 June 2020. Agenda Item 7.
- Perricone, G., Wahlstrom, T., Gethin, D., "Procedure for Standardized Measurements of the Brake Emissions". Proc. I Mech E, Part E: Automobile Engineering, 1-8.2015.
- Perricone, G., Alemani, M., Metinoz, I., Matejka, V., et al., "Towards the Standardization of Aeromobile Particle Emissions from car Brakes – a System Approach". Proc. I Mech E, Part E: Automobile Engineering, 1-17. 2016.
- Pope, C. A., Burnett, R. T., Thun, M. J., Calle, E. L., et al., "Longitudinal Cohort Study of Mortality and Long-Term Exposure to Fine Particulate Air Pollution". Am. Med. Assoc. 287 (2002): 1132-1141.
- Pope, C. A., and Dockery, D. W.: "Health Effects of Fine Particulate Air Pollution: A Review of the Evidence". Air Water. Mater. Assoc. 56 (2002): 709-742.
- U.S. EPA. "Proposal for a New AP-42 on Laboratory Measurement of Brake Emissions for Light-Duty Vehicles". GRPE/87/Add.3. 2023. Geneva.
- USEPA 1613: Tetra- through Octa-Chlorinated Dioxins and Furans by Isotope Dilution HRGC/HRMS. 1994.
- USEPA 1614: Brominated Diphenyl Ethers in Water, Soil, Sediment, and Tissue by HRGC/HRMS. 2010.
- USEPA 1668c: Chlorinated Biphenyl Congeners in Water, Soil, Sediment, Biosolids, and Tissue by HRGC/HRMS. 2010.
- USEPA 3640A: Gel Permeation Clean-up. 1994.
- Valestin, J., Tardieu, R., and Vautour, E.: "Aeromobile Particulate Matter and Human Health: Toxicological Assessment and Importance of Size and Composition of Particles for Oxidative Damage and Carcinogenic Mechanisms". Environ. Int. 26 (2000): 351-362.
- World Health Organization. "WHO Air Quality Guidelines for Particulate Matter, Ozone, Nitrogen Dioxide and Sulfur Dioxide - Global Update 2005". Geneva, 2005.
- World Health Organization. "Economic Cost of the Health Impact of Air Pollution in Europe: Clean Air, Health and Wealth". WHO, Geneva, 2015.
- World Health Organization. "Assessment of Disease from the Joint Effects of Household and Ambient Air Pollution for 2010s". WHO, Geneva, 2018.

Comparison of two Air Liquid Interface (ALI) systems: lung cells exposure to vehicle exhaust

Tsakonas, G.¹, Stamatou, R.², Kontses, A.¹, Baltzopoulou, P.³, Papaioannou, E.³, Deloglou D.³, Lazou, A.² and Samaras, Z.¹

¹Aristotle University, Laboratory of Applied Thermodynamics, GR-54124, Thessaloniki, Greece

² Physiology Laboratory, School of Biology, Aristotle University of Thessaloniki, Thessaloniki, Greece

³Chemical Process and Energy Resources Institute (CPERI), Centre for Research and Technology Hellas (CERTH), 57001, Thessaloniki, Greece

Introduction

Air pollution is a major public health concern worldwide, with studies linking it to numerous premature deaths and adverse health effects (European Environment Agency, 2020). One significant source of air pollution is road traffic, which generates large amounts of emissions from exhaust fumes. Several researchers carried out extensive characterizations including toxicity analysis of particles emitted from gasoline engines (e.g., Durga et al., 2014, Bisig et al., 2018). Although their toxic effects, especially those of GDI engines, are not yet well understood, their mutagenicity cannot be overlooked. To better understand the impact of vehicle emissions on human health, researchers have utilized a method of exposing airway cells to diluted exhaust via Air Liquid Interface (ALI) (Asimakopoulou et al., 2013). This method has been shown to be a valid research technique for studying the harmful effects of vehicle emissions on human health (Paur et al., 2011). Cell exposure to a known concentration of pollutants can provide information about the way cells respond and even have quantification of this the effect.

In 2023, Lau et al aimed to investigate the effect on human cells of different vehicle emission standards under various driving conditions utilizing an ALI system. They specifically examined the vehicles' performance using the New European Driving Cycle (NEDC), idle cycle, and steady state cycle. The researchers observed that as the emission standards became stricter, the impact on cell viability was decreased. In another study (Bisig et al., 2018), gasoline passenger cars with Euro5b and Euro6b gasoline direct injection (GDI) were tested using the Worldwide harmonized Light vehicles Test Cycle (WLTC). The purpose was to assess the potential induction of oxidative stress and activation of pro-inflammatory pathways. The study did not find any statistically significant increase in oxidative stress markers or activation of pro-inflammatory pathways, indicating that the specific vehicle technologies did not affect these cellular responses, under the tested conditions. Studies such as the above mentioned provide valuable insights regarding the effect of emission standards and specific vehicle technologies on cellular health, under controlled test conditions. However, the relationship between toxicity, real-world driving conditions and driving dynamics still needs to be scrutinized. It is important to examine further aspects of emission effects in order to have a more comprehensive view of their potential correlation to cell toxicity.

In this context, the present study aims to assess the cell toxicity of exhaust emissions of a state-of-the-art vehicle utilizing two different air liquid interface (ALI) systems. The vehicle was tested on the chassis dynamometer using two driving cycles, a mild and a more dynamic one. To assess the cellular toxicity due to emissions, human epithelial A549 cells were used. Cells were exposed to diluted exhaust gases and cell viability was measured using the ALAMAR blue method. The particles that the cells were exposed were equivalent to normal air inhalation in an urban environment.

Methodology

In the experiments a gasoline port fuel injection (PFI) hybrid vehicle Euro 6d compliant was tested on a chassis dynamometer. Chassis dynamometer offers a controlled driving environment, allowing the performance of vehicles to be monitored and evaluated in various operating conditions, incl. Real driving, in a fully repeatable way. The vehicle exhaust pipe was connected to a constant volume sampling system

(CVS). The gaseous emissions were monitored with a portable gas emission measurement system (AVL M.O.V.E gas PEMS). Throughout the driving cycles, two cell exposure to gaseous and particulate pollutants systems were sampling through the CVS from sampling points 1 and 2. Sampling point 1 was free of particles larger than 450nm; with these particles being removed using a cyclone (for pre-removal of particles $>2.5 \mu\text{m}$) and an impactor (cut-off 450 nm at 1.5 l/min). At the same sampling point (after the impactor), a condensation particle counter (CPC) recorded total (solid and volatile) particle number emissions with a cut-off at 10 nm. Since the particle size recorded at the entrance of the exposure system is limited to the range of 10-450 nm, we will hereafter refer to these recordings as nTPN10 and the particles to which the cells were exposed as nanoparticles. The measurement set-up is shown in figure 1.

Table 1 Vehicle characteristics

	Manufacturer	Model	Technology	Engine displacement	Euro	Aftertreatment	Mileage [km]
Vehicle	Toyota	CH-R	Gasoline Hybrid-PFI	1800	6d	TWC	23000

The driving cycles used in this test campaign are presented in Figure 2. These test cycles were derived from on-road tests under real-world operation conditions and were designed in order to combine different driving characteristics (e.g., in terms of percentage of urban, rural, and motorway parts and driving dynamics). All tests have a duration of 2h. The target for the temperature in the engine test cell was to remain below 37°C during all testing.

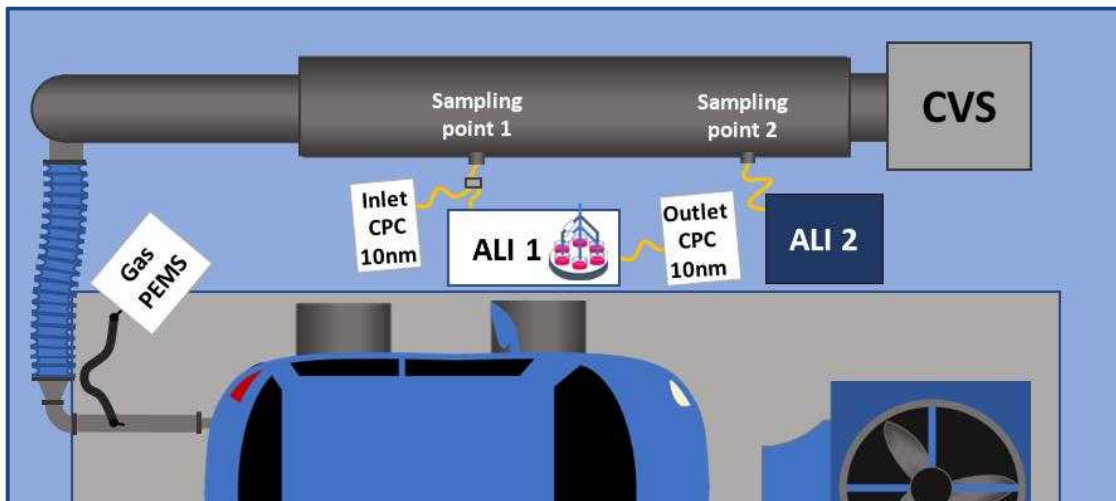


Figure 1 Measurement set-up

The main characteristics of the test cycles are as follows:

- mRDE (moderate real driving emissions) test: This test comprises an urban, rural and motorway part following the current RDE regulation. It is characterized by mild driving dynamics. This test ran twice in a row in each measurement to fulfil the 2-h duration.
- Combined: This is a combination of smaller cycles (or parts of cycles) to reach the two-hour target. It contains longer high-speed sections compared to the mRDE, while urban parts between the high-speed parts were used to maintain the test cell temperature at the target levels.

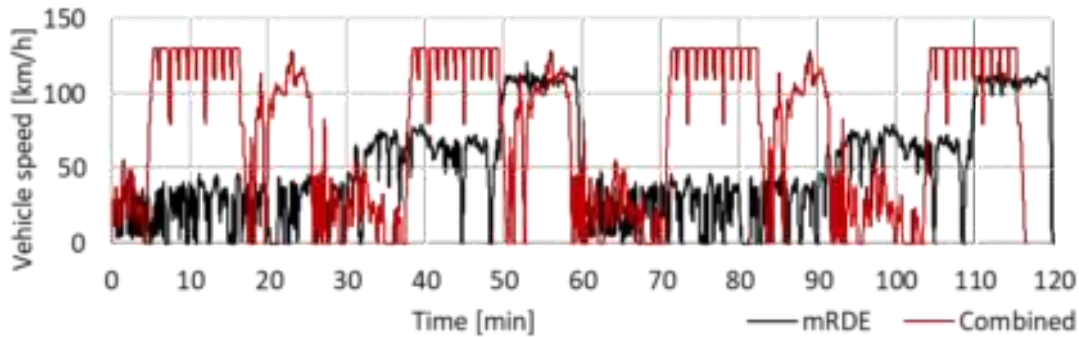


Figure 2 Test driving cycles

The most important difference between the two ALI systems used is the direction of aerosol flow towards the cells. The first ALI system (ALI 1) has six cell exposure chambers, four of which are used for cell exposure to both particulates and gaseous emissions while the other two filter out the particulates, thus allowing only gaseous pollutants to reach the cells. The particle deposition was monitored with two CPCs. CPC 3750 was recording the inlet particle concentration and CPC 3776 (set at a 10 µm cut-off) was sampling at the outlet of the exposure chambers. Thus, the particles were charged with a radioactive source (TSI 3077.5) and an electrostatic field was provided to the exposure chambers, in order to increase deposition efficiency through electrostatic precipitation (Brown, et al., 2005). To simulate the conditions inside the human lungs the aerosol was tempered (37°C) and humidified (about 90% RH), before entering the cellular chambers. In the second ALI system (ALI 2) – namely, Multiculture in-vitro Cell exposure Chamber (MEC) (Asimakopoulou et al., 2013) - the flow is parallel to the biological samples and allows diffusional deposition of fine particulate matter. The chamber was designed with a geometrical arrangement of exposed cell cultures to accommodate uniform testing of up to six identical positions for culture plates (each one able to hold up to 6 exposure inserts).

A549 human epithelial cells were used for testing, since the assessment of this cell-line viability is a well characterized model to assess nanoparticle-induced toxicity (Croasdell et al., 2021). Furthermore, the airway epithelial cells are actually both a barrier preventing microorganisms from invading the respiratory system and a key-player in lung homoeostasis. Reduced viability of lung epithelial cells can lead to decreased inflammation resolution and impaired tissue repair due to exposure to acids, hypoxia, or chronic irritants (Schroeter et al., 2006).

The cells were cultured to approximately 80% confluence. Then, they were recultivated on inserts suitable for 6-well plates (Falcon) at a concentration of 2×10^5 cells/well and incubated for 24 hours at 37°C with 5% CO₂ in Dulbecco's Modified Eagle Medium (DMEM)- High glucose supplemented with 10% Fetal Bovine Serum (FBS), 5% penicillin-streptomycin (PS) (100 U/ml, 100 µg/ml), and 1 mM Sodium pyruvate (complete medium). The medium from the upper side of the insert was removed, and inserts were transferred and placed at each ALI system, while a control experiment remaining in incubation, unexposed each time. Among the inserts of ALI 1, two were exposed only to gaseous emissions, wherein the emission sample passed through a HEPA filter, while the remaining four inserts were exposed to unfiltered sample that also contained nanoparticles. In ALI 2 the inserts were divided into two triads each placed in a different exposure position (A and B). Following a 2-hour exposure, the cells were incubated overnight in complete medium and then underwent a 3-hour incubation with Alamar blue stain. The number of cells was estimated by photometrical evaluation of the Alamar Blue assay is based on fluorometric detection of metabolic mitochondrial activity of cells. The results are presented as percentages of the control experiments that were not exposed to emissions, and comparisons were made between cells exposed under different conditions and unexposed control cells.

The formula that was applied to calculate the dose D in particles deposited per cell per hour was:

$$D = \frac{c_{TWA} \times Q_{exp}}{\text{Cell density} \times \text{Deposited surface}} \times \text{Deposition Efficiency} \quad (1)$$

$$c_{TWA} = \frac{\int_{t=1s}^{t=end\ of\ cycle} c_i}{t_{cycle}} \quad (2)$$

Where: C=particle concentration in the diluted exhaust [p/cm³], TWA=Time Weighted Average and Q_{exp}=supply of diluted exhaust for exposure [cm³/s]

Results

Cell exposures to both ALI systems were performed at realistic particle concentrations (realistic dose: 2-300 p/cell/h according to Paur et al, 2011) and in both ALI systems a decrease in cell viability compared to control was observed. Experimental data from ALI 1 confirm that part of the reduction in cell viability is due to nanoparticle emissions since there is a statistically significant difference between cell viability of particle and non-particle exposures. In ALI 2 no statistical difference was detected between the two exposure positions, verifying repeatability. In addition, the data show that an increase in driving dynamics leads to a further decrease in cell viability due to the particles (Figure 3).

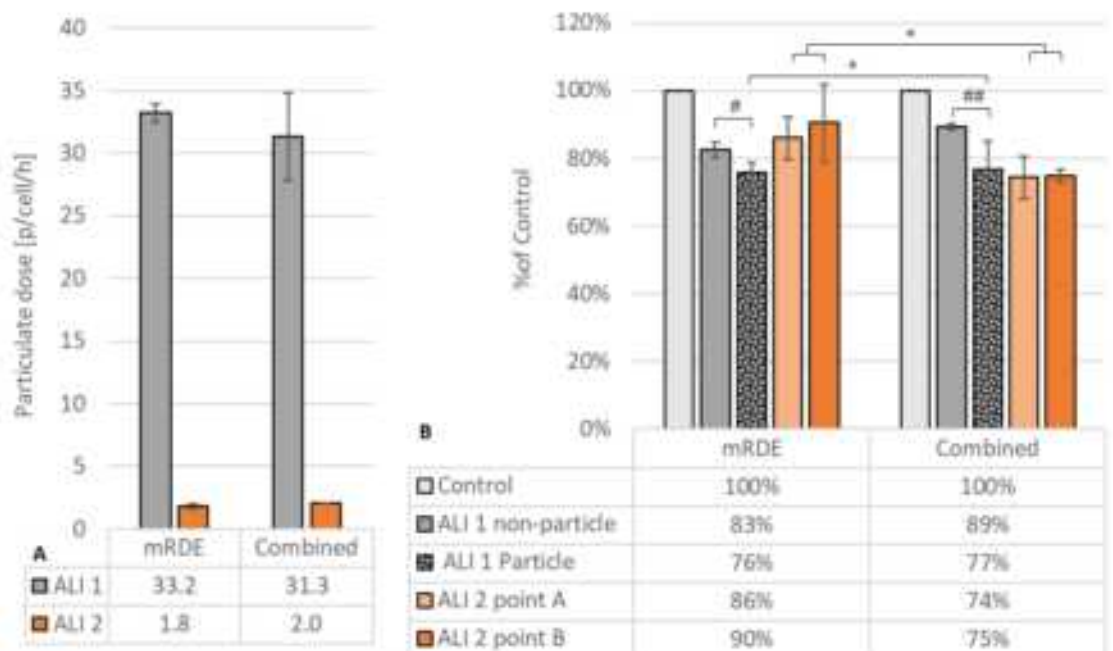


Figure 3 A. Particle dosage B. cell viability estimated after Alamar Blue staining presented as a percentage of control cell viability, Mann Whitney test statistical significance (p-value):

#p<0.05, ##p<0.01 particle exposure compared to non-particle exposure

*p<0.05 compared to the same exposure type in different driving dynamics

The toxicological effects presented using the methods and systems employed in this study should be interpreted as indicative of the potential effects of exposure to exhaust in controlled experimental conditions.

Summary/Conclusions

Two ALI systems were used to assess the toxicological effects of a modern gasoline car exhaust. ALI 1 provided the possibility to identify the effect on cell viability due to gaseous emissions alone or the effect induced by the total exhaust fumes. On the other hand, the second ALI, equipped with multiple exposure chambers, allowed to replicate the experiment several times at the same cycle. In both exposure systems a statistically significant reduction of cell viability was observed, due to emissions exposure. The presented results could indicate that the exhaust fumes can have a negative effect on human lung cells, while showing some dynamic driving-cell viability correlation. The possibility that particles deriving from modern gasoline exhaust can be harmful to the human respiratory system needs to be further evaluated.

References

1. Asimakopoulou, A., Daskalos, E., Lewinski, N., Riediker et al., Development of a dose-controlled multiculture cell exposure chamber for efficient delivery of airborne and engineered nanoparticles. *Journal of Physics: Conference Series*, 429, 012023, 2013, <https://doi.org/10.1088/1742-6596/429/1/012023>
2. Bisig, C., Comte, P., Güdel, M., Czerwinski, J., et al., Assessment of lung cell toxicity of various gasoline engine exhausts using a versatile in vitro exposure system. *Environmental Pollution*, 235, 263–271, 2018, <https://doi.org/10.1016/j.envpol.2017.12.061>
3. Brown, J. S., Wilson, W. E., & Grant, L. D., Dosimetric comparisons of particle deposition and retention in rats and humans. *Inhalation Toxicology*, 17(7–8), 355–385, 2005, <https://doi.org/10.1080/08958370590929475>
4. Croasdell Lucchini A, Gachanja NN, Rossi AG, Dorward DA, Lucas CD. Epithelial Cells and Inflammation in Pulmonary Wound Repair, *Cells*, 2021 Feb 5;10(2):339, 2021, doi: 10.3390/cells10020339
5. Durga, M., Soundararajan N., Rajasekar A., Thiagarajan D., Effects of ultrafine petrol exhaust particles on cytotoxicity, oxidative stress generation, DNA damage and inflammation in human A549 lung cells and murine RAW 264.7 macrophages, *Environmental Toxicology and Pharmacology*, 38, 2, 2014, <https://doi.org/10.1016/j.etap.2014.08.003>
6. European Environment Agency (2023). Road transport. <https://www.eea.europa.eu/en/topics/in-depth/road-transport>
7. Lau, Y.-S., Poon, H.-Y., Organ, B., Chuang, H.-C., et al., Toxicological effects of fresh and aged gasoline exhaust particles in Hong Kong. *Journal of Hazardous Materials*, 441(441, preprint no. 129846.), 2023, <https://doi.org/10.1016/j.jhazmat.2022.129846>
8. Paur, H.-R., Cassee, F. R., Teeguarden, J., Fissan, H., Diabate, S., Aufderheide, M., Kreyling, W. G., Hänninen, O., Kasper, G., Riediker, M., Rothen-Rutishauser, B., & Schmid, O. (2011). In-vitro cell exposure studies for the assessment of nanoparticle toxicity in the lung—A dialog between aerosol science and biology. *Journal of Aerosol Science*, 42(10), 668–692. <https://doi.org/10.1016/j.jaerosci.2011.06.005>
9. Schroeter, J. D., Kimbell, J. S., Bonner, A. M., Roberts, et al., Incorporation of tissue reaction kinetics in a computational fluid dynamics model for nasal extraction of inhaled hydrogen sulfide in rats. *Toxicological Sciences: An Official Journal of the Society of Toxicology*, 90(1), 198–207, 2006, <https://doi.org/10.1093/toxsci/kfj072>

Contact Information

Name: Samaras Zisis

Email address: zisis@auth.gr

Telephone: 0030 2310996014

Acknowledgments

This work was supported by the Horizon 2020 project nPETS, under grant agreement No 954377.

Design of a Sampling System for Brake Particles On-Road Measurement – A Computational Preliminary Study

A. Katsinos¹, A. Dimaratos¹, A. Kontses¹, V. Noutsou¹, G. Christou¹, A. Tomboulides¹, Z. Samaras^{1*}

¹ Laboratory of Applied Thermodynamics, Department of Mechanical Engineering, Aristotle University of Thessaloniki, Thessaloniki, 54124, Greece, zisis@auth.gr

Introduction

Brake wear particles are currently a major source of particle emissions, especially in urban environments. Their relative contribution is continuously increasing due to the great improvement of the emission control systems of combustion engines (thus, reduction of exhaust particles) and the penetration of electric vehicles in the fleet (Grigoratos and Martini, 2015; Air Quality Expert Group, 2019). The latter account for 13% of new registrations in the EU during the first half of 2023, versus almost 10% in the same period of 2022 (ACEA, 2023) and have great potential to reduce brake particle emissions owing to their regenerative braking function (Hicks et al., 2023).

In this context, brake wear emissions attract increased interest from all the relevant stakeholders, including regulatory authorities, the industry and the scientific community, around the globe (EuroBrake, 2021; Vanherle et. al., 2021; Wang et al., 2022). This is highlighted in the most explicit way by the inclusion of emission limits for brake particle emissions (together with another source of non-exhaust particles, i.e., tyres) in the proposed Euro 7 regulation for the first time ever (European Commission, 2022).

Therefore, the detailed characterisation of brake particle emissions is a very important topic. A brake particle measuring system needs to address various challenges, with the most important being the ~~absence of a common gas that could be the particles, as is the case with the exhaust gas of the combustion engine~~. The brake components on a vehicle form a system open to the environment and the sampling system needs to ensure separation of brake particles from other sources, such as tyres, resuspension of road particles etc. As summarised by Wang et al. (2022), six methods can be identified for sampling and measuring brake particles, ranging from simple laboratory test stands to highly sophisticated systems for real-world on-road measurements.

For regulatory purposes, a measurement methodology and protocol for particle emissions from brake systems in laboratory conditions was developed by the Particle Measurement Programme, which defined the exact test stand specifications and measuring procedure (PMP, 2021). In parallel, a number of prototype systems have been developed for sampling and measuring brake particles under real-world driving conditions and can be differentiated by the level of isolation of the brake system from the external environment. In this context, there are the open systems, using sampling hoses close to the brakes (e.g., Oroumiyah and Zhu, 2021), the semi-enclosed systems that isolate only partially the brakes from the environment, still sucking ambient air (e.g., Farwick Zum Hagen et al., 2019) and the fully-enclosed systems that encapsulate the brake components and apply a forced flow of conditioned air through the capsule (e.g., Feißel et al., 2020). Each system is characterised by particular advantages and disadvantages, in terms of particle separation from different sources, particle transport efficiency, effect on the temperature of the brake system components etc (Wang et al., 2022).

The current work makes a preliminary study of one semi-enclosed sampling concept with a cone-type sampler (Farwick Zum Hagen et al., 2019). To that aim, CFD calculations are performed, in order to examine a braking event of a mid-sized (segment C) passenger car running at 60 km/h. The overall target at this stage is to setup a computational tool for the simulation of the relevant phenomena in the brake particle sampling system and run a preliminary sensitivity analysis. At the next step, experimental data will be produced with a system that is currently being manufactured and the tool will be validated and further developed for more extended parametric analyses towards the optimisation of the brake particle sampling system.

Methodology – Simulation setup

The developed CFD tool uses the commercial solver STAR-CCM+ for the simulation of the flow and other relevant phenomena in the brake particle sampling system. Figure 1 shows the control volume, that consists of the full wheel assembly (power shaft, brake disc and pads, calliper etc.) and the particle collection cone, which is then connected to the pipe of the sampling system. The calculation domain is defined by the cavity enclosed by the wheel and the cone, while the flow enters from the inner side of the wheel and exits the domain at the cone outlet (Figure 1). Only the area which is in contact with the airflow is meshed, so no conjugate heat transfer is considered between the air and the solid parts. The mesh consists of around 2 million polyhedral cells, after a grid independence study that was performed. The inlet boundary condition is set to constant velocity with a uniform profile and the outlet as a pressure boundary equal to the ambient. The volumetric flow rate of the system is controlled by the magnitude of the inlet velocity and varies for the different cases of the sensitivity analysis, as shown and discussed in the results section. During the actual measurements, these operational parameters will be controlled with the blower of the sampling system.

A surface heat flux is introduced at the brake disc and the pads to account for the heat generated during the brake event. The magnitude of this heat flux is calibrated so that the predicted temperature matches the measured one on the brake disc. This was done by estimating the kinetic energy dissipation during braking and thus the actual heat generated during the brake event at 60km/h. Based on an order of magnitude analysis, the heat flux applied to match the measured temperature is about two to four times lower than the total kinetic energy dissipation estimated during braking, which given the uncertainties of the approach is deemed satisfactory. The temperature at the outer surface of the cone is set equal to the ambient. The standard k- ϵ -layer RANS turbulence model is used to simulate the flow turbulence. A moving reference frame is used to account for the rotating wheel and the rate of rotation imposed corresponds to the angular velocity of the wheel at 60 km/h, as mentioned earlier. Lagrangian particles are injected tangentially through line injectors lying on the pad-disc interface (produced by their friction), for both pads (one per each side of the disc). At this first setup phase, particles of constant diameter are considered, with only a one-way coupling with the flow. At a later development stage, particle size distributions will also be considered. Steady-state simulations, including a turbulent particle dispersion model are performed in a full three-dimensional setup.

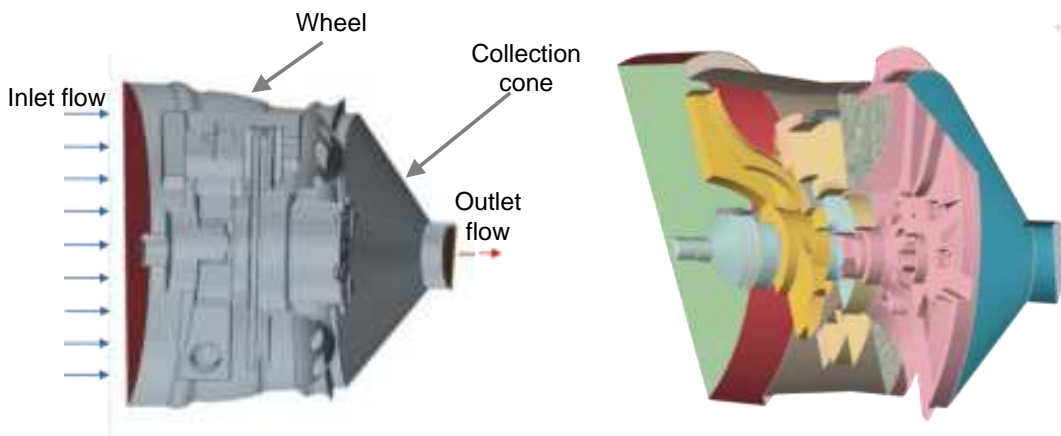


Figure 1: Left: Control volume for the CFD calculations. Right: Section cut of the wheel-cone assembly.

Methodology – Testing

As mentioned above, a system with a cone sampler is considered and simulated. Figure 2 (top) illustrates the layout of the complete system, which will measure brake particle number, mass and size distribution. Ambient particle concentration will be also measured as background and in order to estimate the number of particles coming solely from the brakes. The air flow will be adjusted with the blower and will be kept constant through a closed-loop control with a flow sensor. Additional measurements will include the temperature of the brake components (disc and pads), the pressure of the brake fluid and vehicle OBD data. A first experimental setup comprising the latter set of parameters has been already developed and brake disc temperature measurement has been conducted, as shown in Figure 2 (bottom-left). Consecutive braking events from 60km/h to complete stop were performed, until reaching a constant

temperature profile of the system during braking, allowing thus for steady-state simulations. The recorded temperature value at the end of the braking event is used for the calibration of the surface heat flux magnitude on the disc. Figure 2 (bottom-right) illustrates the evolution of disc temperature during these consecutive events, along with the brake pressure and the brake light voltage signals. The temperature drop around 1050 s results from the longer stop between two consecutive braking events.

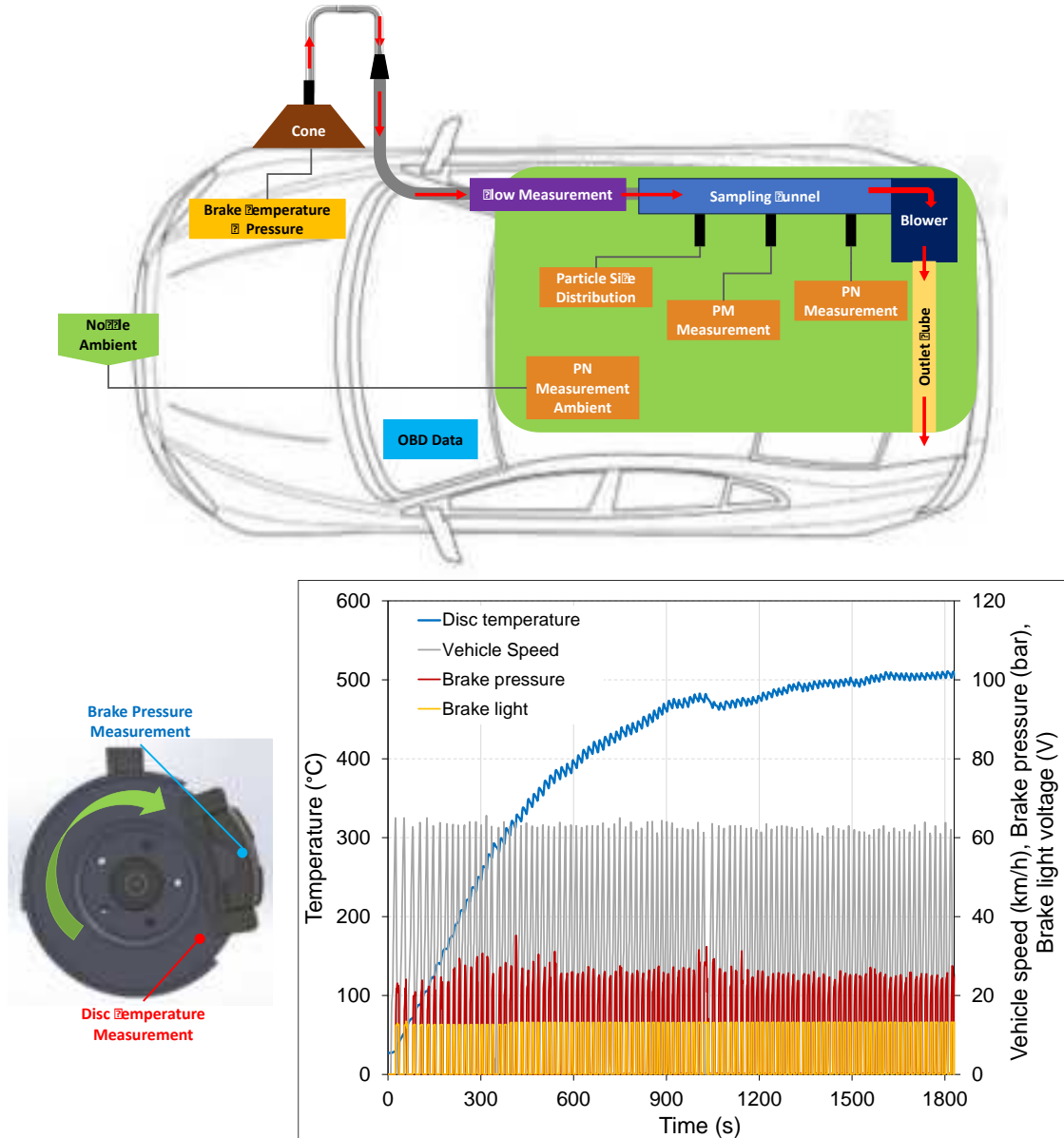


Figure 2: Top: Schematic layout of the brake particle sampling and measuring system. Bottom-left: Brake disc temperature and brake pressure measurement. Bottom-right: Disc temperature evolution consecutive braking events at 60 km/h.

Results

In the context of this preliminary study, a sensitivity analysis is performed in order to evaluate the computational tool's capability to capture changes in the operational characteristics of the sampling system.

For the base case of this sensitivity analysis, the volumetric airflow rate of the sampling system is equal to 100 m³/h. As the work done in each braking event (deceleration from 60km/h until complete stop in 6 seconds) is the same, independently of the presence of the cone or the volumetric flow rate of the sampling system, the boundary condition for the brake disc and pads is set to a constant surface heat flux. As explained above, the heat flux was calibrated so that the disc temperature matches the experimental one, for this base case. This way, the temperature of the disc is obtained as a solution by the CFD calculations.

Three sensitivity cases were examined with varying volumetric airflow rate by +30% and +50% around the base case to investigate its effect on the disc temperature. Figure 3 presents the variation of the disc temperature with the volumetric flow rate of the sampling system. As expected, the increase of the airflow rate leads to a temperature drop, due to the more intense heat transfer. However, as can be observed in Figure 3, a 50% increase in the flow rate causes only a moderate decrease of the disc temperature from 510 to 490 °C, i.e., less than 5%.

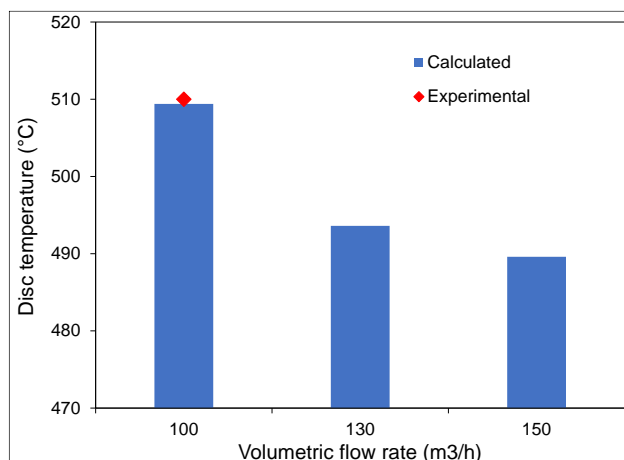


Figure 3: Effect of volumetric airflow rate on disc temperature.

At a next step, particles were introduced to the flow as described in the methodology section, at a mass flow rate of 0.167 mg/s. First the effect of particle diameter (in the range of 1 nm to 10 µm) was investigated on total particle mass flow rate collected by the sampling system at the cone outlet compared to the particle mass flow injected. For the examined range of volumetric airflow rates, the ~~mass outflow of particles larger than 10 µm is almost zero~~, i.e., large particles are stuck inside the cone or other internal surfaces of the system (e.g., wheel). For volumetric airflow rates lower than 120 m³/h, the particle mass flow rate at the outlet of the cone reaches a constant value for all particles with ~~diameter lower than 1 µm~~ ~~at this way down to 1 nm~~ ~~for greater volumetric airflow rates this plateau is reached for diameters lower than 2 µm~~ as shown in Figure 4. As the outlet mass flow rate is a combination of the number of particles that flow through the exit of the domain and of their mass (or diameter for the case of constant density), this value peaks at 3 µm and 2 µm for of 120 m³/h and 150 m³/h airflow, respectively. For larger particles, although the mass per particle increases, the total outlet mass flow rate decreases, as less particles follow the trajectory of the flow, and finally reaches zero at around 10µm. As particle size decreases below the diameter where the peaks are observed, the mass flow rate varies until it finally reaches a constant value, as the trajectory of the particles is not altered any further.

~~Since there is a significant part of particles emitted during the braking event below 1 µm (e.g., Nosko and Olofsson, 2017), the subsequent runs, aimed at investigating the effect of volumetric airflow rate on particle mass flow rate at the cone outlet, were all performed with 10 nm particles. Because the flow is confined, the behaviour of the particles as they reach the solid surfaces is critical. If all particles rebound, then the mass flow rate at the cone outlet is significantly increased, as shown in Figure 5, i.e., more particles are collected. With the increase of the air flow, the percentage of collected particles further increases. However, it does not reach 100% as the number of the particle tracking steps in the calculation is finite. This limit is therefore exceeded either by some particles that are trapped into vortices from where they never escape or by some particles that follow unrealistically long trajectories due to the rebound boundary condition that was set.~~

In the case that all particles stick on the solid surfaces, the percentage of collected particles at the outlet of the cone is as low as 1%. It is important to mention that if turbulent dispersion is deactivated, the percentage of particle mass collected increases even for sticking solid surfaces above 80%, for the range of the volumetric airflow rate examined here. This is due to the stochastic gas velocity components that are added to the flow-particle interaction by the turbulent particle dispersion model and which may drive them towards solid surfaces where they stick, instead of following the flow streamlines as indicatively shown in Figure 6.

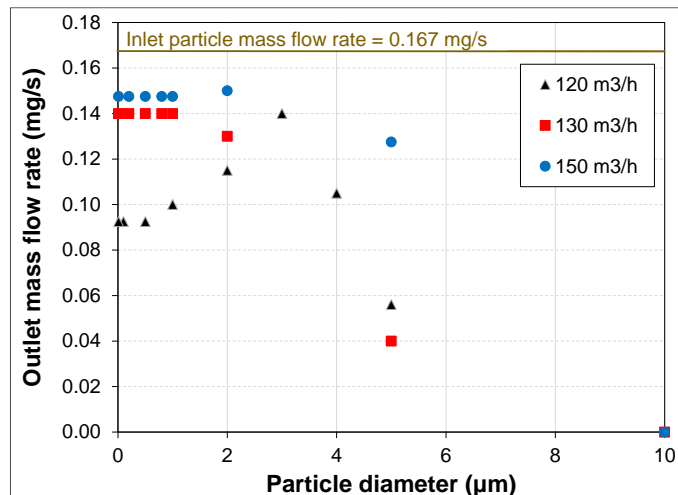


Figure 4: Effect of particle size on the mass flow rate at the cone outlet.

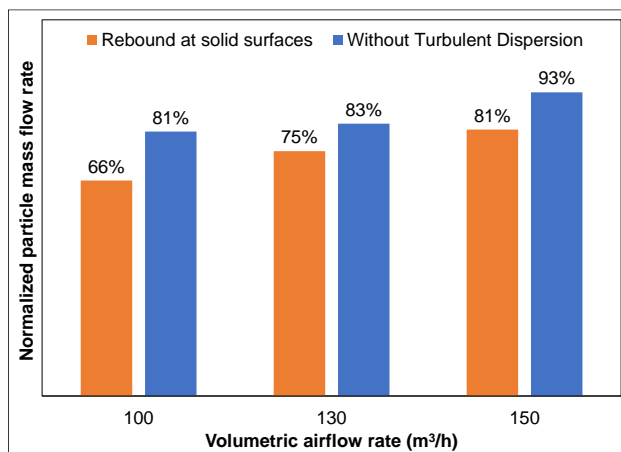


Figure 5: Percentage of particle mass collected at the outlet of the cone (particle diameter 10 nm).

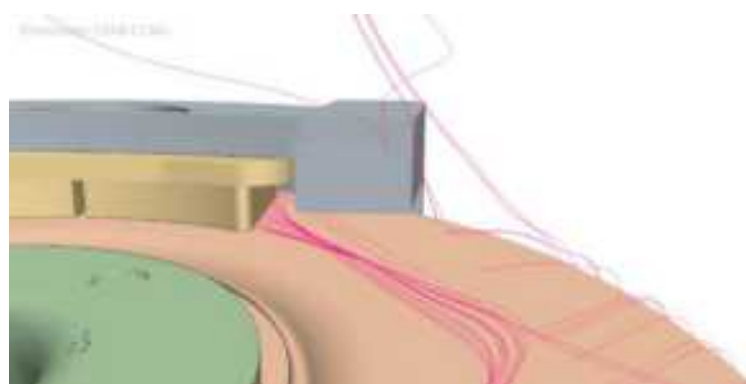


Figure 6: Indicative illustration of the streamlines followed by particles.

Summary & Next Steps

In the context of the present work, a brake particle collection system is examined, which is aimed for use in real-world on-road measurements on light-duty vehicles. A semi-enclosed sampling concept is considered with a cone-type particle collector. At this first phase, a computational tool was set up for the simulation of the relevant phenomena and a sensitivity analysis was conducted. A braking event of a mid-sized (segment C) passenger car from 60 km/h to complete stop was examined. Experimental data concerning brake disc temperature are produced with a targeted test campaign. The energy model was calibrated in order to match the measured disc temperature and the effect of the airflow rate was examined. At the next step, particles, generated by the friction between brake disc and pad, are introduced at a constant mass rate in the flow. The computational tool was used to examine the behaviour of particles under different assumptions. With the current setup (cone and wheel design) and in the range of examined air flow rates, particles larger than 10 μm are not captured at all while the percentage of particle mass collected at the cone outlet (compared to the inlet mass) stabilizes for diameters less than 1-2 μm at about 50 to 80%. Depending on the assumptions on particle behavior at solid surfaces, the collected particle mass percentage at the cone outlet varies from practically zero, if particles are sticking to solid surfaces, to 66%-81% if particles rebound on solid surfaces. In case that turbulent dispersion is deactivated, the percentage of particle mass collected increases even for sticking solid surfaces above 80%.

The computational tool will be further developed in the next phases, including the implementation of more realistic boundary conditions for the interaction of particles with solid surfaces, making a probabilistic selection between sticking and rebound. On the experimental side, next activities include the finalization of manufacturing of the sampling system and the execution of measurements of particle mass, number and size distribution. Using the so produced experimental data, the computational tool will be further developed and validated. It will then be further applied for the deeper investigation of the relevant phenomena in the system, particularly as concerns particle flow, as well as for the optimisation of the particle sampling system.

References

- ACEA, 2023. Press releases – New car registrations. <https://www.acea.auto/pc-registrations/new-car-registrations-15-2-in-july-battery-electric-13-6-market-share/>
- Air Quality Expert Group, 2019. Non-Exhaust Emissions from Road Traffic. DEFRA.
- EuroBrake 2021: Brake emissions regulation imminent as non-exhaust emissions surge. <https://www.fisita.com/post/eurobrake-2021-brakeemissions-regulation-imminent-as-non-exhaust-emissions-surge>
- European Commission, Internal Market, Industry, Entrepreneurship and SMEs, Euro 7 standard proposal, November 2022, https://single-market-economy.ec.europa.eu/publications/euro-7-standard-proposal_en
- Farwick Zum Hagen F.H., Mathissen, M., Grabiec, T., Hennicke, T., Rettig, M., Grochowicz, J., Vogt, R., Benter, T. (2019) On-road vehicle measurements of brake wear particle emissions. *Atmos Environ* 217, 116943.
- Feißel, T., Hesse, D., Augsburg, K., Gramstat, S. (2020). Measurement of Vehicle Related Non-Exhaust Particle Emissions Under Real Driving Conditions. EuroBrake 2020.
- Grigoratos, T., Martini, G. (2015) Brake wear particle emissions: a review. *Environ Sci Pollut R* 22, 2491-2504.
- Hicks, W., Green, D.C., Beevers, S. (2023) Quantifying the change of brake wear particulate matter emissions through powertrain electrification in passenger vehicles. *Environ Pollut* 336, 122400.
- Nosko, O., Olofsson, U. (2017) Effective density of airborne particles from car brake materials. *J Aerosol Sci* 107, 94-106.
- Oroumiyah, F., Zhu, Y. (2021) Brake and tire particles measured from on-road vehicles: Effects of vehicle mass and braking intensity *Atmos Environ X* 12, 100121.
- PMP IWG, Brake Emissions Task Force 2 (TF2). Minimum specifications for measuring and characterizing brake emissions. July 2021.
- Vanherle, K., Lopez-Aparicio, S., Grythe, H., Lukewille, A., Unterstaller, A., Mayeres, I., Eionet Report – ETC/ATNI 2020/5, March 2021. Transport Non-exhaust PM-emissions – An overview of emission estimates, relevance, trends and policies.
- Wang, Y., Yin, H., Yang, Z., Su, S., Hao, L., Tan, J., Wang, X., Niu, Z., Ge, Y. (2022) Assessing the brake particle emissions for sustainable transport: a review. *Renew Sust Energ Rev* 167, 112737

2.2 TAP.02. On-board monitoring and diagnostics, emission tampering and deterioration.

Real world particle number emission factors from plume chasing data

T. Frateur^{1*}, N.E. Lijsterink¹, J.P. Lollinga², D. Pöhler^{3,4}, C. Schmidt^{3,4}, M. Knoll⁵ and M. Vojtěch⁶

¹ Department of Sustainable Transport and Logistics, TNO, The Hague, South Holland, 2595 DA, NL,
thomas.frateur@tno.nl

² Department of Environmental Modelling, Sensing & Analysis, TNO, Utrecht, Utrecht, 3584 CB, NL

³ Airyx GmbH, Justus-von-Liebig-Straße 14, Eppelheim, 69214, Germany

⁴ Institute of Environmental Physics , University of Heidelberg, INF 229, Heidelberg, 69120, Germany

⁵ Institute of Electrical Measurement and Sensor Systems, Graz University of Technology, 8010 Graz, Austria

⁶ CVUT, Czech Technical University Prague, Praha, 166 07, Czech Republic

Introduction

Modern diesel vehicles are equipped with diesel particulate filters (DPF) to reduce particle emissions on the road. DPFs can crack or be removed from vehicles causing very high particle emissions and the associated health effects. Remote sensing techniques enable measuring a high volume of vehicles to gain statistical information and aid authorities in targeted inspections (Borken-Kleefeld, 2018). There are different measurement techniques to detect particle emissions. Commercial light-based RES systems are capable of determining statistically acceptable emission factors of gases, but they lack accuracy measuring particles. A more direct measurement technique is therefore preferred. Plume chasing is a remote sensing technique where a measurement vehicle, following vehicles, is equipped to analyse the exhaust plume of a chased subject vehicle. The technique is already well described in i.a. (Pöhler, 2021). Most of the existing knowledge on plume chasing concerns NO_x emission factors. Only a few studies are available which investigate particle number (PN) emission measurements for plume chasing (i.a. Järvinen et al., (2019), Leinonen et al., (2023) and Ježek et al. (2016), Ježek et al. 2018) introduce a PN application of plume chasing in a controlled test environment. They show PN emission factors correlate well with PEMS tests under controlled conditions. However, the second-by-second variation of PN/CO₂ ratios is typically larger than for NO_x/CO₂ due to other sources polluting the signal, requiring more data for a robust evaluation of the vehicle emission performance. On the other hand, differences between high and low emitters should be more pronounced for PN emissions.

Figure 1: CARES experimental plume chase vehicle.



Real world PN plume chase measurements of approximately 220 Euro VI heavy duty vehicles are used to show the validity of this technique on the road by determining the PN emission factor distribution of these vehicles and comparing different PN instrument results. Measurement data is obtained with an experimental TNO plume chase vehicle measuring HDV highway traffic in the Czech Republic in the CARES research program. Among other instruments, the measurement data used here are from a TEN AEM particle counter as a low-cost PN measurement device, a TSI SMPS+CPC combination as state of the art PN reference instruments, and an Airyx ICAD for CO₂ data.

Averaged PN emission factors (PN divided by CO₂ concentration) are calculated per vehicle. The different particle instruments result in different mean PN measurements due to differences in particle size ranges measured and measurement principles. They are however found to generate very similar emission distribution results with only marginal differences in the relative measurement variation. Results from the TEN AEM particle counter are used as leading factors to enable comparison with PTI-PN results.

CARES campaigns

CARES is a European Union sponsored research project aimed at investigating contactless measurement of vehicle exhaust emissions. During several CARES campaigns throughout Europe, several contactless measurement methods were used to measure the exhaust emissions from passing or followed vehicles to validate their suitability for monitoring pollutant emissions and improving city air quality. During a testing campaign in Prague, among other measurement methods, the plume chasing method was demonstrated for both NO_x and particle number emissions in an experimental plume chase vehicle. NO_x plume chasing was also performed in a market ready measurement setup by Airyx.

Method

Real world data acquisition

Particle number (PN) emission data is gathered from vehicles using plume chasing techniques. In plume chasing, a chase vehicle is equipped with a front mounted sampling system, exhaust gas analysing instruments and a data acquisition system. Vehicles are chased by the chase vehicle at a normal driving distance to position the sampling system in the exhaust plume of the followed vehicle. Exhaust gas is sampled and routed through the analysers in the back of the vehicle for analysis. Unprocessed measurement results are shown directly to the vehicle operators on a screen for vehicle selection and plume alignment. A schematic representation of the instrumentation setup used for this analysis is shown in Figure 2.

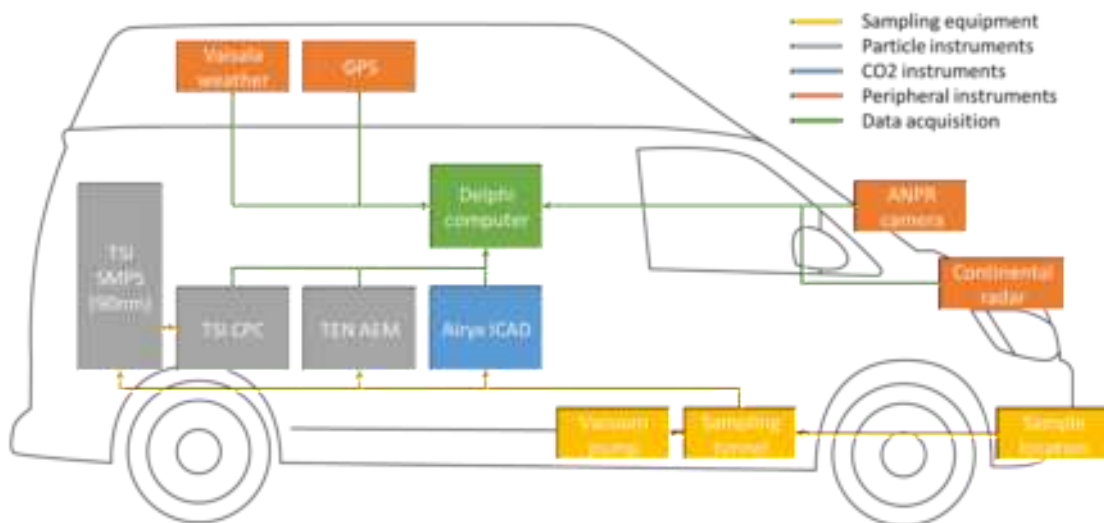


Figure 2: Schematic representation of instrument and data acquisition connections.

The relevant emission measurement instruments used for this analysis are listed in Table 1. Additional emission measurement instruments were present in the experimental vehicle but are not used in this work. Note that the TEN AEM particle counter device is originally designed for PTI checks of diesel particulate filters (DPF), in the Netherlands. The device is used here as a cheap PN instrument alternative and to enable linking of plume chase results to PTI measurements, focussing at 90 nm particle sizes. Instruments used to monitor measurement conditions are listed in Table 2.

Table 1: Exhaust gas plume chase instruments

Instrument name	Measurement parameters	Units	Comments
Airyx ICAD	NO _x / CO ₂	ppb / ppm	A secondary ICAD was used on some occasions for background measurements
TEN AEM	PN	k#/cm ³	PTI particle device used as a cheap alternative for real world PN measurements.
TSI SMPS + CPC	PN	#/cm ³	State of the art PN reference instrument with SMPS size selection of 90nm.

Table 2: Additional plume chase instruments

Instrument name	Measurement parameters	Comments
GPS	Position, velocity	
ANPR camera	License plates	Used to couple vehicle properties to measurement data.
Continental radar	Relative position and velocity of the chased vehicle	
Vaisala weather station	Relative windspeed, pressure, temperature & humidity	

All the relevant instruments were logged on a Delphi computer to enable aligned logger files with a static delay. Measurement of individual vehicles is manually started and stopped by the operator through an Airyx user interface to enable measurement ID assignment to the different chased vehicles.

During the CARES campaign, approximately 220 heavy duty Euro VI vehicles were successfully chased by the experimental plume chase vehicle to obtain measurement data on particle number emissions. Measurement data is saved to measurement logs for all instruments per measurement day.

Signal postprocessing

Background signals for all measured signals are determined on the bulk dataset of each measurement day. The background level is determined by taking the lower bound of each signal in 60 second windows and smoothing the resulting datapoints. The datasets are then split to vehicle specific datasets based on the measurement ID's assigned to the data during the chase drives. Subsequent operations are performed on each vehicle dataset separately.

Measured PN concentrations are normalised with a reference gas concentration. Similar to emission factor calculations of NO_x measurements (Pöhler, 2021), CO₂ is used as the reference gas for PN plume chasing. Different methodologies are used in calculating emission factors from measurement data. However, most methods such as total peak surface integration discard a lot of information about the quality and consistency of the signal. Instantaneous emission factor calculation attains this detail in the results. To ensure accurate results, the peaks of the particle and CO₂ measurements should however be properly aligned with this method. Due to noise in the signal, conventional peak alignment is hard to implement robustly, as multiple peaks may occur during measurements. A rising edge alignment method

is used to cope with variability and noise in the signals, during the measurement period for a single vehicle. As the rising edge of PN and CO₂ measurements of high emitters is observed to be steep, this method should result in good alignment between measurements.

A schematic example of the rising edge alignment is shown in Figure 3. Only data where CO₂ concentrations are well above the background value are used in the calculations. The reference threshold for CO₂ is therefore defined at 50 ppm above the background. For other measurement, the threshold is defined with the threshold ratio between the CO₂ maximum peak value (p_{max}) and the reference threshold (Tr_{ref}).

$$\text{Threshold ratio} = \frac{p_{max}}{Tr_{ref}}$$

Peaks are aligned on the t_1 line (Figure 3) of each signal. If a t_1 line is not available, e.g., due to noise, peaks can be aligned on the t_2 line (falling edge alignment).

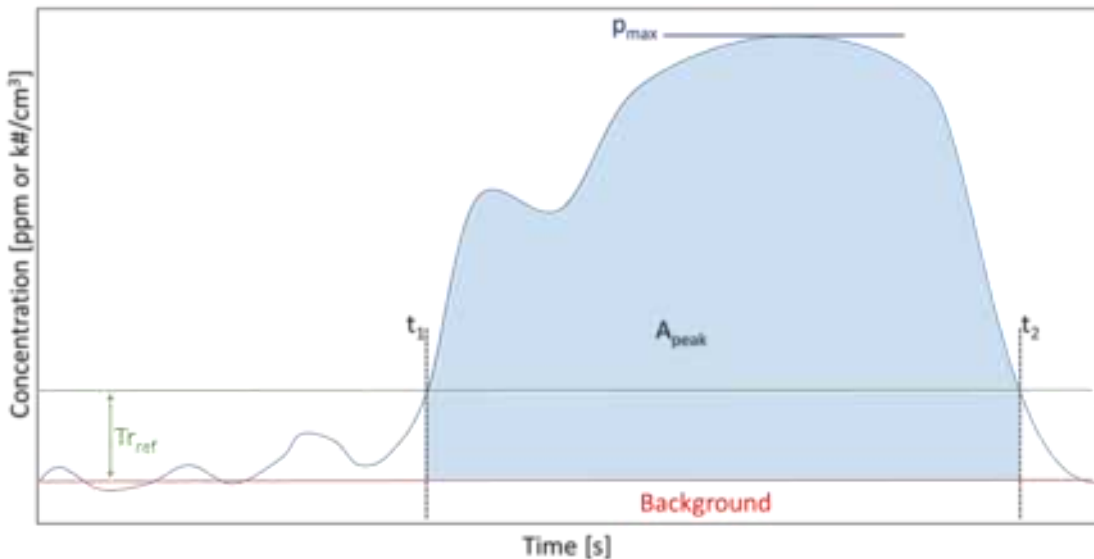


Figure 3: Schematic example of rising edge peak selection.

For all measurement points where the CO₂ signal is larger than the reference threshold above the background, the instantaneous particle number emission factor is calculated according to the carbon mass balance method (Hansen and Rosen, 1990) and as shown by the equation below.

$$PN_{ef} \left[\frac{k\#}{kg} \right] = 10^{12} \cdot \frac{PN \left[\frac{k\#}{cm^3} \right]}{CO_2 [ppm] \cdot \rho_{CO_2} \left[\frac{kg}{m^3} \right]}$$

Here the density of CO₂ is taken to be constant, in ambient conditions¹, with $\rho_{CO_2} = 1.84 \left[\frac{kg}{m^3} \right]$. The particle number emission factor for the vehicle is calculated as the average over the instantaneous emission factors of all valid measurements (CO₂ above threshold). In addition, the standard deviation in these instantaneous results is calculated. These steps are performed for both, the particle number measurements of the TEN AEM instrument and the CPC measurements of 90 nm size-selected particles.

¹ At 15 degree Celsius and 1 atmosphere pressure

Results

TEN AEM particle number emission factors

Approximately 220 Euro VI HD vehicles are measured with the experimental plume chase vehicle during the 2023 CARES Prague campaign. The PN emission factors from these vehicles as measured with the TEN AEM particle counter are shown in Figure 4 (left) as a histogram. Approximately 74.5% of the measured vehicles fall below the average PN measurement result of 2.76×10^{11} [k#/kgCO₂], indicating a clear right skew distribution in the measured emission factors. This distribution form is expected under the assumption that the majority of vehicles is compliant with the imposed emission regulation. The tail to the right of the distribution accounts for vehicles with smaller or larger defects in the aftertreatment system or tampered vehicles.

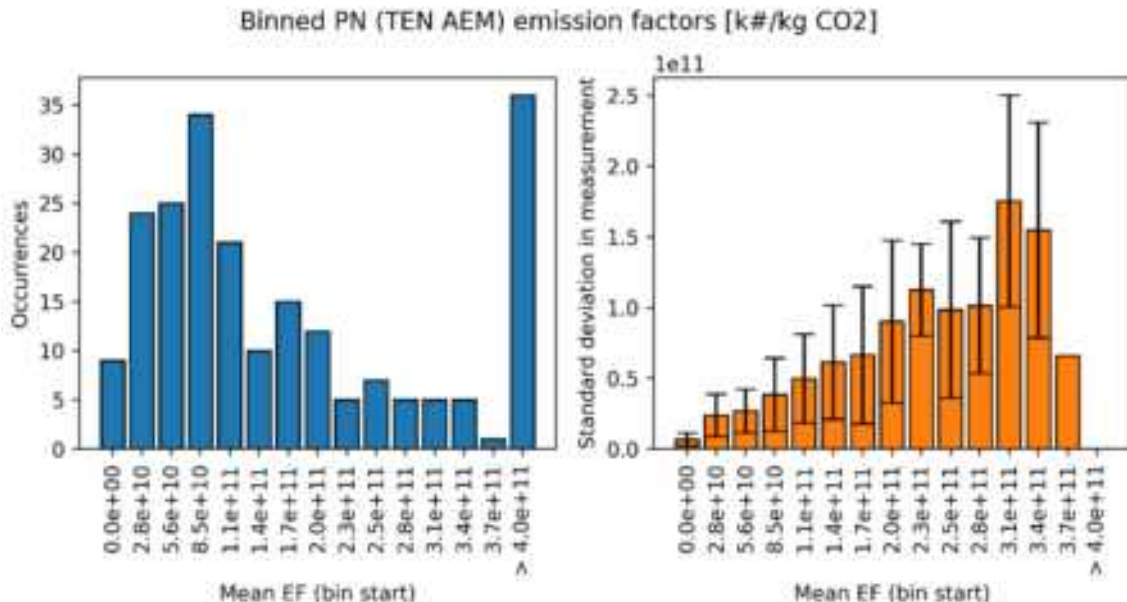


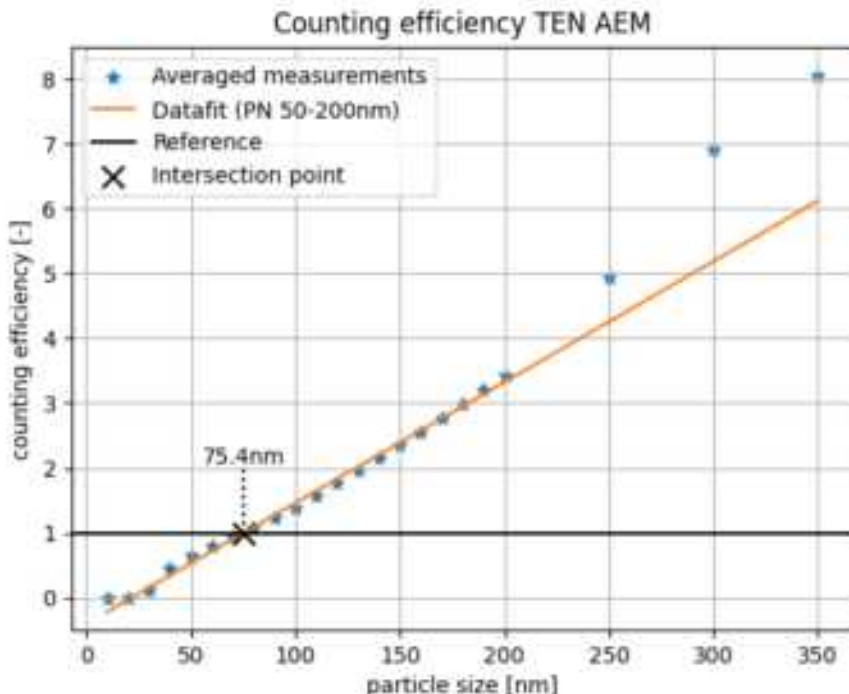
Figure 4: Binned PN emission factors (left) and mean standard deviations of individual measurements (right) from approximately 220 HD vehicles (Euro VI) using a PTI particle counter. Measurements above 4×10^{11} [k#/kgCO₂] are grouped to the right of the histogram, the average of this bin is 9.45×10^{11} [k#/kgCO₂].

In normal use, PN emission factors vary substantially during driving with variation increasing for high emitters. This is shown in the standard deviation ranges for individual measurements (Figure 1, right) which indicates the standard deviation in instantaneous emission factors obtained for each measured vehicle. Large variation in PN/CO₂, per vehicle, is consistent with similar findings in emission testing. The absolute emission values measured with the TEN AEM particle counter are however very high for Euro VI HD vehicles. The PN limit imposed on these vehicles in Euro VI legislation of 9.78×10^{11} [#/kWh] is equivalent to approximately 14.4×10^8 [k#/kgCO₂]². The high measurements of the TEN AEM particle counter can most likely be explained by the non-linearity of particle measurements with this device, based on the diffusion charging principle. Especially larger particles are overcounted significantly as can be seen in Figure 5. It is likely that concentrations of larger particles increase with distance from the source as particle number and particle sizes are not conserved quantities over time. Note that also differences in

² Assuming a typical HD highway CO₂ per kWh ratio of 680 [g/kWh]

background estimation for both CO₂ and PN have a large influence on the absolute values of the calculated emission factors.

Figure 5: TEN AEM PN validation results with TSI CPC on size selected exhaust samples from a diesel generator set. Averaged measurements are obtained by averaging stabilised PN results of 5 minute



measurements on the selected particle size and normalising TEN AEM results with TSI CPC results.

The validation measurements of the TEN AEM shown in Figure 5 are obtained from measurements on a diesel generator set with both a TEN AEM PTI particle counter and a TSI CPC connected to a TSI SMPS. The measurement results in the figure are the average rates between both instruments on several particle size selections. The data fit shown in this figure indicates the particle counter is only accurate in a limited range around the calibration particle size of the device. Some smaller deviations between the instruments with absolute particle concentrations levels is noted. This is not investigated further. Future work will look at the possibility of removing larger particles from the sample flow before the measurement to obtain more accurate PN results, for exhaust emissions in ambient conditions, with the TEN AEM device.

CPC particle number emission factors

The same emission factor distribution as shown above is made using 90 nm size selected particle measurements from a TSI SMPS+CPC combination. Note that size selection drastically limits the specific particle concentration in the sample. As such, much lower emission factors are expected with this approach. The calculated emission factor distribution of these measurements is shown in Figure 6. A similar right skew distribution is found in the emission factors as seen in the emission factors from the TEN AEM data. Also similar behaviour in the standard deviation of the measurements is found with standard deviations remaining at the same order of magnitude as the mean emission factor. It can also be observed that the standard deviation increases with higher emission factor measurements, note however that this effect might also be due to a different sample size of the bin. Future work could possibly look into this effect by analysing similar sized bins for all emission factors.

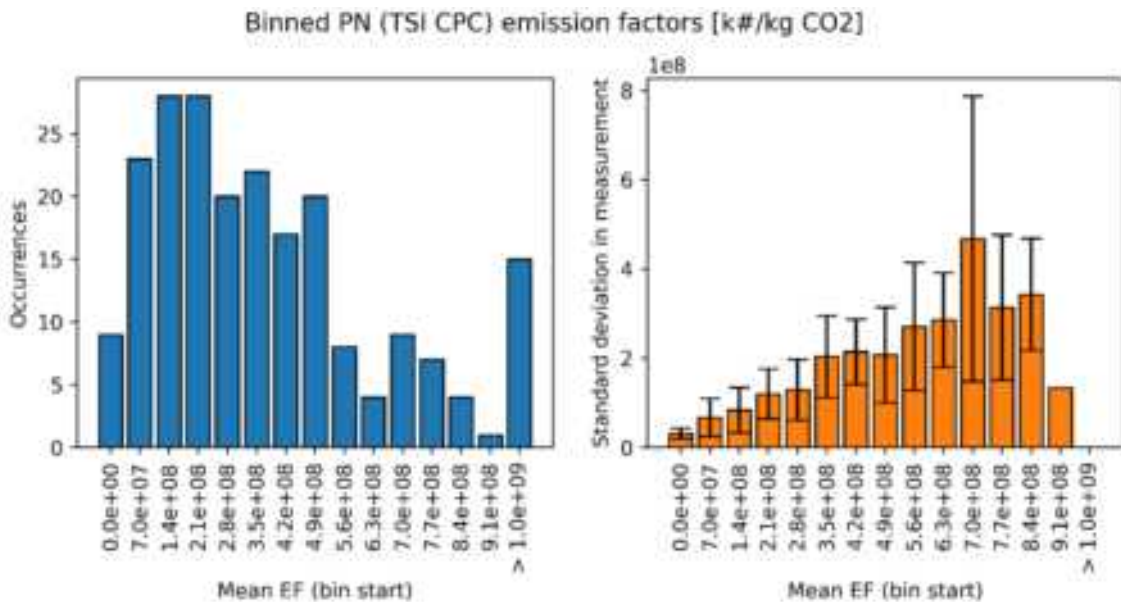


Figure 6: Binned PN emission factors (left) and mean standard deviations of individual measurements (right) from approximately 220 HD vehicles (Euro VI) of 90nm size selected particles. Measurements above 1e9 [k#/kgCO₂] are grouped to the right of the histogram, the average of this bin is 1.58e9 [k#/kgCO₂].

Discussion

Similar to remote emission factor measurements for NO_x emissions in real world conditions, PN emission factors can be measured on-road using plume chase techniques. From data analysis on 220 HD Euro VI vehicles in highway conditions, a clear right skew PN emission distribution is found. A right skew distribution is expected when the majority of vehicles complies with the legislative limits with a lower fraction of vehicles showing small to larger defects or tampering of the DPF. The similar right skew trend found in the data from two separate instruments used in this analysis indicates the distributions found are not influenced significantly by different instrument techniques. Both measurement methods can be used in detecting PN emissions under real world conditions.

While emission factor distributions are largely similar, emission factor magnitudes differ significantly between the two measurement methods. While the magnitude difference between total particle count and size selected count is to be expected, the magnitudes found using the TEN AEM PTI counter are higher than expected. From testing performed on the PTI instrument after the plume chase measurement campaign, an overestimation of PN, up to a factor 3.5 on large exhaust particles of 200 nm, is found. It can be assumed the higher PN magnitudes in the plume chase results are a result of this overestimation. As larger particles are not necessarily originating from exhaust emissions only, future work should look into the possibilities to separate these larger particles from the sample before the measurement as to prevent false positive high emitter identification under dusty road conditions.

Moreover, particle numbers and particle sizes are not conserved quantities over time. Measurements earlier and closer to the engine find more and smaller particles than measurements further away. A problem that led to a distance specification in the official PMP method. In plume chasing the distance is substantially larger and may lead to an increased particle size, possibly affected by volatiles.

No definitive threshold for high emitter detection is determined from this analysis. From the observed measurement results, direct correlation to the legislative PN limit is not representative. This is partially explained from the large particle sensitivity explained above, however, PN emission factor results are also heavily influenced by background determination and possibly weather effects. To enable classification, proper PN bandwidths for high emitters should be determined from comparison between TEN AEM data and PEMS PN data in future work.

Acknowledgements

This work was supported by the EU H2020 CARES Project No. 814966 and TNO research funds.

References

- Borken-Kleefeld, J., Dallmann, T. (2018). Remote Sensing of Motor Vehicle Exhaust Emissions. *White Paper*.
- Hansen, A. D. and Rosen, H. Individual measurements of the emission factor of aerosol black carbon in automobile plumes, *Journal of the Air and Waste Management Association*, 40, 1654–1657.
- Järvinen, A., Timonen, H., Karjalainen, P., Bloss, M., Simonen, P., Saarikoski, A., Kuuluvainen, H., Kalliokoski, J., Dal Maso, Mikkka, Niemi, J.V., Keskinen, J., Rönkkö, T. (2019). Particle emissions of Euro VI, EEV and retrofitted EEV city buses in real traffic. *Environmental Pollution*, 250, 708-716.
- Izquierdo, I., Díaz-García, I., Fernández, C., Martínez, M., & Vázquez, G. (2019). Determination of on-road black carbon and particle number emission factors and comparison between mobile and stationary measurements, *Atmospheric Measurement Techniques*, 14.
- Knoll, M., Lang, B., & Bergmann, A. (2021). Performance of Black Carbon Instruments for Extractive Remote Emission Sensing, *AAAR 39th Annual Conference*.
- Leinonen, V., Olin, M., Martikainen, S., Karjalainen, P., Mikkonen, S. (2023). Challenges and solutions in determining dilution ratios and emission factors from chase measurements of passenger vehicles, *Athmospheric Measurement Techniques*, 26
- Pöhler, D. (2021). Heavy Duty Vehicle (HDV) NOx emission measurement with mobile remote sensing (Plume Chasing) and subsequent inspection of high emitters, *Ribe: Danish Road traffic Authority*

Effects of Geofencing on Exhaust Emissions and Noise: A combined Test Track and Traffic Simulation Study

Nina Svensson¹, Anders Genell¹, Mats Gustafsson¹, Johan Olstam¹, Rihanna Gebrehiwot¹, Kinjal Bhattacharyya¹, Jonas Sjöblom²

¹VTI (Swedish National Road and Transport Research Institute), 583 30, Linköping, Sweden,

² Department of Mechanics and Maritime Sciences, Chalmers University of Technology, 412 96, Gothenburg, Sweden

*corresponding author: Nina Svensson, nina.svensson@vti.se

Introduction

Speed-limiting geofencing has been suggested as a mean to improve both traffic safety and to reduce emissions from road transport. However, there is limited knowledge of the effect of geo-fencing on air quality and noise. In this project we have performed a combined measurement and modelling study to evaluate the effects of geofencing on traffic performance, traffic safety (described elsewhere), exhaust and noise emissions.

Method

The study consists of a combination of measurements on a single car and modelling of a typical car fleet for the same case. The case is based on trajectory measurements using video from a real urban street with speed limit of 50 km/h with a ~200 meter long local speed limit section of 30 km/h. From the video measurements, typical driving behaviours were extracted corresponding to a median driver and an aggressive driver. In addition, a geofenced driving style was defined, where the driver assist system was assumed to keep all the speed limits and ensure a moderate acceleration.

Measurements of exhaust emissions (CO, CO₂, NO_x, PN) using a PEMS (Portable Emissions Measurement System, Figure 1) from AVL (AVL 492 Gas PEMS iS, AVL 496 PN PEMS and AVL 495 EFM) and noise emissions using stationary microphones were performed using a diesel-powered passenger car (Volvo V60, Figure 1) on a test track, which was set up to resemble the real site. The microphones were placed on the 50 km/h section, 100 m before the 30 km/h traffic sign, and 80 m into the 30 km/h section (see Figure 2). The microphones were placed 7.5 m from the centre of the driving lane at a height of 1.2 m above the road surface. The test driver conducted 10–18 repetitions for each driving style.



Figure 1. PEMS system and test car. Photo: Mats Gustafsson, VTI

A microscopic traffic simulation model (using PTV Vissim) was developed for the road stretch in the scenario. The simulated road stretch consisted of a two-lane arterial with three segments with speed limits of 50 km/h, 30 km/h, and 50 km/h, respectively. Calibration of the model was performed using the trajectory data from the video-based traffic measurements. Two scenarios were explored: one with and one without the presence of a signalized pedestrian crosswalk. Apart from this, the experiment design considered different acceleration and deceleration behavior of non-geofenced vehicles in response to the speed limit sign, different total demand levels (number of vehicles in one direction), and different penetration rates (0-100 %) of geofenced vehicles. Each combination was replicated 10 times in simulations with different random seeds to account for stochasticity. The tailpipe emissions (CO, CO₂, NO_x, HC and PM) were estimated by feeding the trajectories from the traffic simulation into the microscopic emission model PHEM (Hausberger et al. 2019) using a mix of emission legislative classes representative for Sweden, extracted from HBEFA (Hausberger et al. 2009). In order to avoid overestimation of the tailpipe emissions due to unrealistically quick changes in acceleration in the simulated trajectories, the trajectories were first treated with the smoothing function T4235H (Velleman, 1980) which have been applied in the work with development of the new WLTP driving cycles (UNECE, 2009). The average emissions per vehicle were measured in terms of g/h and g/km.

Results

Emission measurements

Figure 2 shows the vehicle speed and emissions of CO₂, NO_x and PN along the route for the three driving styles. The left column shows the instantaneous emissions along the route and the right column shows the total emissions in the different sections of the route and the whole route. The aggressive and median driver both drove faster than the speed limit and accelerated more often compared to the geofenced driver. NO_x and PN emissions were clearly lowest for the geofenced driver. The median value was reduced by 44 % and 59 % respectively compared to the median driver and 62 % and 68 % compared to the aggressive driver. A large emission reduction of NO_x and PN was seen in section 2 and 3 of the route, where only the median and aggressive drivers were accelerating, showing the benefit of keeping a constant speed to reduce emissions. For CO₂, there was a reduction compared to the aggressive driver of 16 %, while no reduction compared to the median driver.

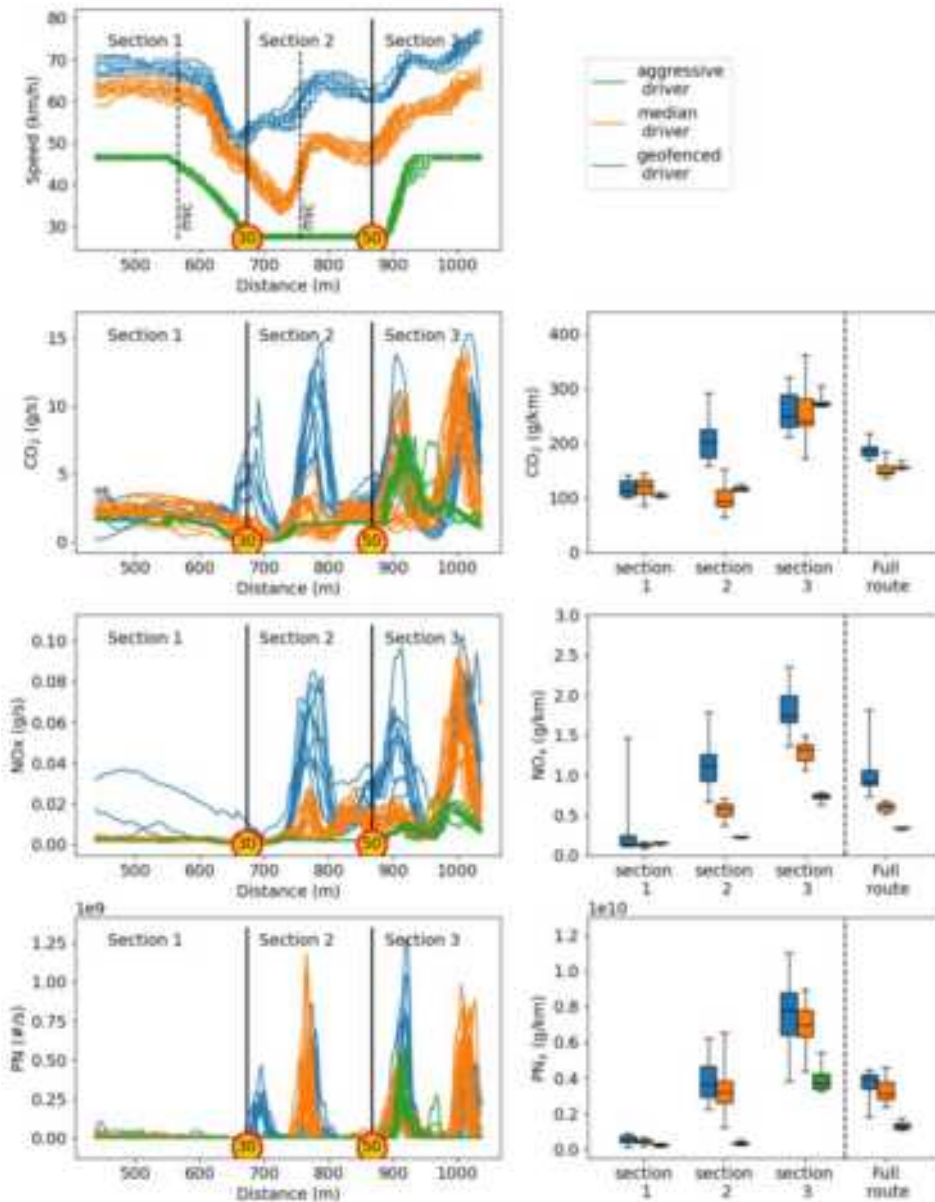


Figure 2: Speed and emissions from PEMS measurements along the route. The location of the microphones for noise measurements are shown in the speed figure.

Noise measurements

The noise measurements show a strong potential for reducing noise emission because of the lower vehicle speed. Figure 3 shows momentary (timestep 125 ms) a-weighted sound pressure level (SPL) for the two microphone positions along the road sections (marked in Figure 2). The black curve represents the 50 km/h section and the red curve represents the 30 km/h section. The LAFmax (maximum a-weighted sound level) values represent the highest momentary level for each microphone and the area under the curve above the background level, which is about 40 dB(A), represents the sound energy level LAE. When considering LAFmax, the difference between geofenced vehicles and non-geofenced vehicles is 5.6–10.6 dB(A) depending on the driving style and speed limit. As can be seen in the left half of Figure 4, LAFmax for the median driver is slightly lower than for the aggressive driver, and the level difference between the 30 km/h and 50 km/h sections is slightly larger than the corresponding level difference for the extreme driver. The geofenced driver scenario shows significantly lower maximum level for both sections and also a significantly increased level reduction for the 30 km/h section compared to the 50 km/h section. The difference in sound energy level (LAE) between geofenced and non-geofenced vehicles

is correspondingly 4.2–7.9 dB(A) depending on driving style and speed limit. The right half of Figure 4 shows how the different driver categories affect LAE for the two road sections. For the extreme driver there is little difference in sound energy level between the 30 km/h section and the 50 km/h section. For the median driver the difference between 30 km/h and 50 km/h sections is also small but clearly present. The geofenced driver scenario shows both significantly reduced overall sound energy level, and also that physically limiting the vehicle speed to the current speed limit greatly increases the sound energy level reduction for low-speed road sections.

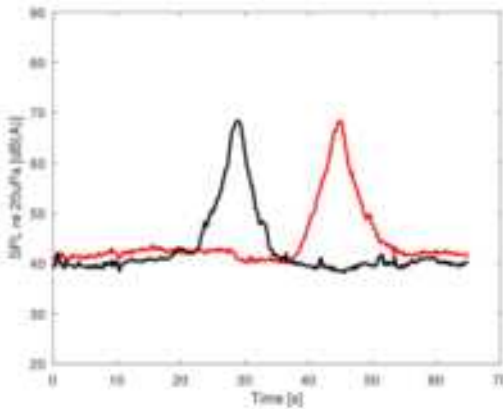


Figure 3: Momentary a-weighted sound pressure level vs time. Red curve represents the 30 km/h section and the black curve represents the 50 km/h section.

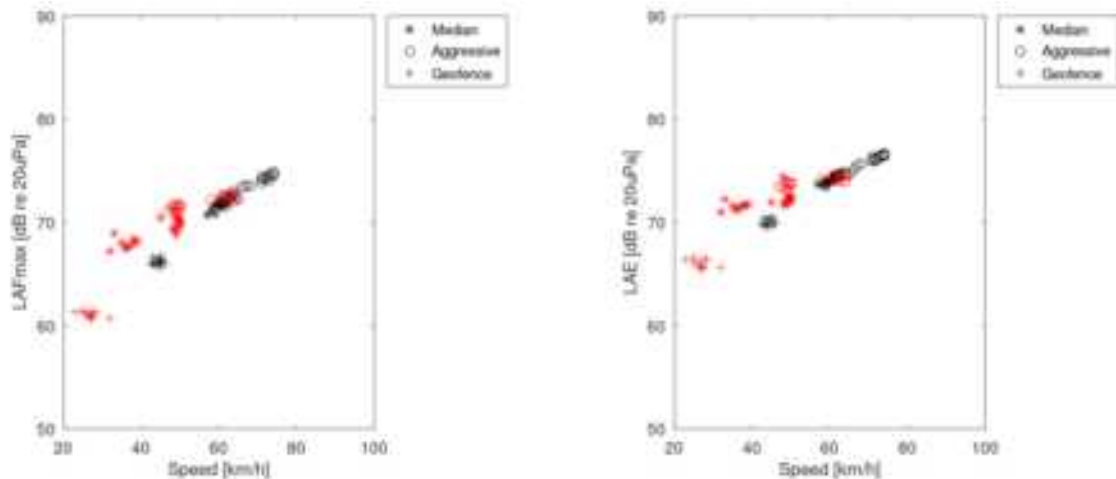


Figure 4: Maximum sound level and total sound energy level as a function of vehicle speed for the different driving styles. Red markers represent the 30 km/h section and black markers represent the 50 km/h section.

When studying the effect of vehicle acceleration (Figure 5), no effect could be identified for any driver or any scenario, indicating that the engine noise does not contribute much to the overall noise level in the current study. One reason might be that the a-weighting underestimates the low frequency sound from the diesel engine. Another reason may be that the mounted PEMS equipment reduced the exhaust noise significantly during measurements.

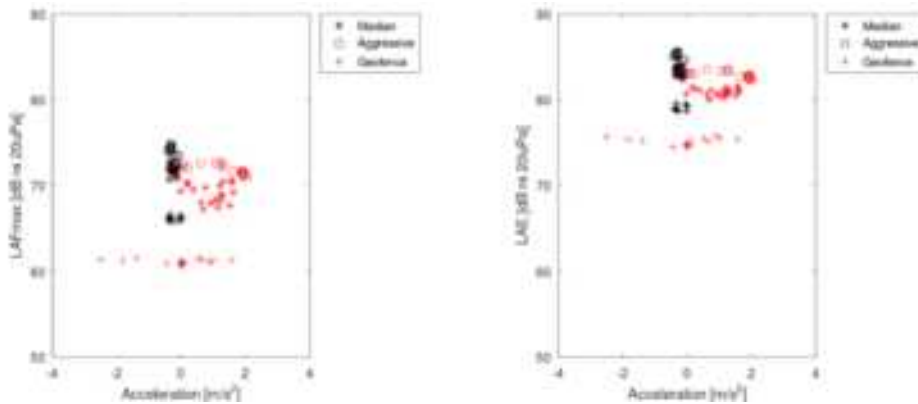


Figure 5: Maximum sound level and total sound energy level as a function of vehicle acceleration for the different driving styles. Red markers represent the 30 km/h section and black markers represent the 50 km/h section.

Traffic and emission simulation

The results from the combined traffic and emission simulations show a clear lowering effect on the cumulative speed distribution, mean speed and 85-percentile speed when introducing geofenced vehicles. As expected, a higher penetration rate of geofenced vehicles is required at lower traffic flows to reach a substantial effect on the total traffic. On the other hand, high penetration rates (70–80 %) are required to get the 85-percentile close to the speed limit. The analysis also revealed a clear reduction in tailpipe emissions per unit time (g/h), which improved with increasing penetration levels. However, an increase in emissions per unit distance (g/km) was observed when no signalized pedestrian crosswalk is present, while there was no change in the presence of the signalized crosswalk. CO₂ emission performances for the scenario without a signalized pedestrian crosswalk and with different penetration rates of geofenced vehicles are illustrated in Figure 6. The results for NO_x, PM and PN follow a similar trend as the results for CO₂. The reason for the increased emissions per unit distance may be attributed to a combination of two aspects: one, since the geofenced vehicles were more compliant to the speed limits, they accelerated from 30 km/h to 50 km/h once the speed restrictions were relaxed while the non-geofenced vehicles, being less compliant to the 30 km/h rule, accelerated (in average) only from 40 km/h to 50 km/h; secondly, the "slower" geo-fenced vehicles need longer travel time for each km, i.e. gains in emissions per time unit were lost due to longer travel time. On the other hand, introducing a signalised pedestrian crossing forces the vehicles to decelerate or accelerate depending on the traffic light. Thus, the acceleration behaviour of geo-fenced and non-geo-fenced vehicles become similar which has led to similar level of emission per unit distance regardless of the penetration rate of geo-fenced vehicles.

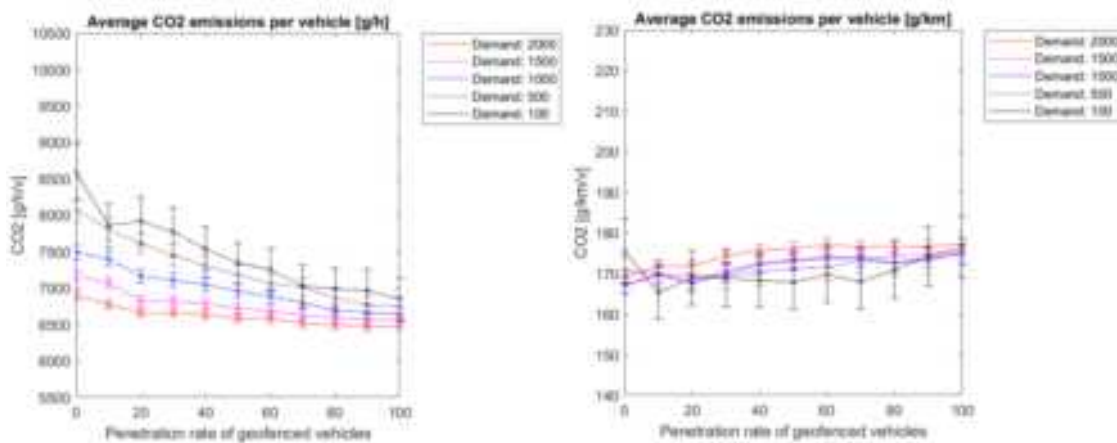


Figure 6: Average CO₂ emissions (g/h and g/km) per vehicle along the route with confidence interval as a function of penetration rates of geofenced vehicles (without signalized pedestrian crossing)

Discussion and conclusions

The emission and noise measurements both show a clear reduction for the geofenced driver compared to the other driving styles. The emission reduction is mainly due to decreased acceleration of the geofenced vehicles, while the noise reduction is mainly due to the decreased speed of the geofenced vehicles. Noise mapping is often used as a tool for investigating road traffic noise exposure, and mostly the noise emission is calculated based on posted speed limit. This study indicates that to evaluate effects on noise from countermeasures such as geofencing, the vehicle speed distribution should be taken into account.

The simulation results show a clear improvement in speed compliance with increased penetration of geo-fenced vehicles but there is no decrease in total emissions along the route. The main reason for this may be attributed to the perfect speed compliances of geofenced vehicles, in comparison to reduced speed compliances of non-geofenced vehicles, resulting in increased acceleration duration for the geofenced vehicles at speed transition zones. In contrast, the emission measurements from the test track study show high emissions even during the small speed changes of the aggressive and median driver, resulting in higher total emissions.

While, the field measurements only covered one specific car, the simulations covered a fleet representative for Sweden, which may account for the differences. The driving behaviour of each vehicle in the simulations was also stochastic in nature and not exactly the same as the three specific driving styles defined for the test track study. Thus, the present study shows that it can be important to use both field measurements and simulations to comprehensively assess the traffic and environmental impacts of a new strategy, such as speed geofencing in this case.

Acknowledgements

This work was funded by The Swedish Transport Administration (TRV dnr 2021/52944). The authors are grateful to Robert Buadu at Chalmers University of Technology who managed the PEMS measurements and to Henrik Biswanger at ASTA ZERO proving ground for valuable assistance during the track tests.

References

- Hausberger, S., Rexeis, M., Dippold, M. (2019). PHEM User guide for Version 13. TU Graz.
- Hausberger, S., Rexeis, M., Zallinger, M., & Luz, R. (2009). Emission Factors from the Model PHEM for the HBEFA Version 3. TU Graz institute for combustion engines and thermodynamics. https://www.hbefa.net/e/documents/HBEFA_31_Docu_hot_emissionfactors_PC_LCV_HDV.pdf
- PTV, PTV VISSIM 2022 user manual. PTV AG: Karlsruhe, Germany, 2022.
- UNECE. (2009). Experience of the Development of a Test Cycle - Data Collection, Processing and Assessment. Working paper No. WLTP-02-12. GRPE Informal Group WLTP. URL: <https://unece.org/DAM/trans/doc/2009/wp29grpe/WLTP-02-12e.pdf>
- Velleman, P. F. (1980). Definition and comparison of robust nonlinear data smoothing algorithms. Journal of the American Statistical Association, 75(371), 609-615.
- World Health Organization. (WHO, 2018). Environmental noise guidelines for the European region. World Health Organization. Regional Office for Europe.

Feasibility study for future on-board NO_x monitoring of passenger cars

C. Matzer¹, S. Hausberger¹, S. Lipp¹, U. Ellmers², J. Blassnegger³, A. Prosenc⁴

¹ Forschungsgesellschaft für Verbrennungskraftmaschinen und Thermodynamik (FVT), Graz, 8010, Austria

² Federal Highway Research Institute (BASt), Bergisch Gladbach, 51427, Germany

³ Technisches Büro Blassnegger (TBB), Wolfsberg, 9400, Austria

⁴ Austrian Automobile, Motorcycle and Touring Club (ÖAMTC), Vienna, 1030, Austria

Presenting author email: matzer@fvt.tugraz.at

Introduction

Due to the high efficiency of modern emission control systems, the identification of malfunctions and tampering is gaining high importance. On-board emission monitoring can support this target and is planned to be introduced with Euro 7. On-board fuel consumption monitoring (OBFCM) is already mandatory for all new passenger cars from 2021. FVT, TBB und ÖAMTC have conducted a feasibility study on how NO_x emissions of passenger cars can be monitored in real vehicle operation in future. The study 'On-board diagnostics (OBD): Analysis of the OBD with regard to emission data available in future for the Periodic Technical Inspection (PTI)' was carried out by FVT as part of a research contract. In this feasibility study, a method was developed to monitor NO_x emissions in real-world operation in the future. For the method development, a total of around 4,500 vehicle kilometres of measurement data were collected with different driving situations, which were recorded with a data logger. The tests were carried out both on the chassis dynamometer and on the road. Tests with specially generated faulty exhaust emission control system were also recorded. The measurement campaign, method development and application of the proposed method are described in the following chapters.

The Measurement Campaign

The measurement campaign formed the basis for the development of the method. The tests were carried out with a modern Euro 6d diesel passenger car. The exhaust gas aftertreatment system of the test vehicle consists of exhaust gas recirculation, an oxidation catalytic converter, a particulate filter (DPF) and two SCR catalytic converters including ammonium slip catalyst (Figure 1). Three NO_x sensors are also installed in the test vehicle as standard. One NO_x sensor is installed at the end of the exhaust line and can therefore detect whether the NO_x exhaust gas aftertreatment system is working properly.

Measurements were carried out with the test vehicle on the chassis dynamometer and on the road. A

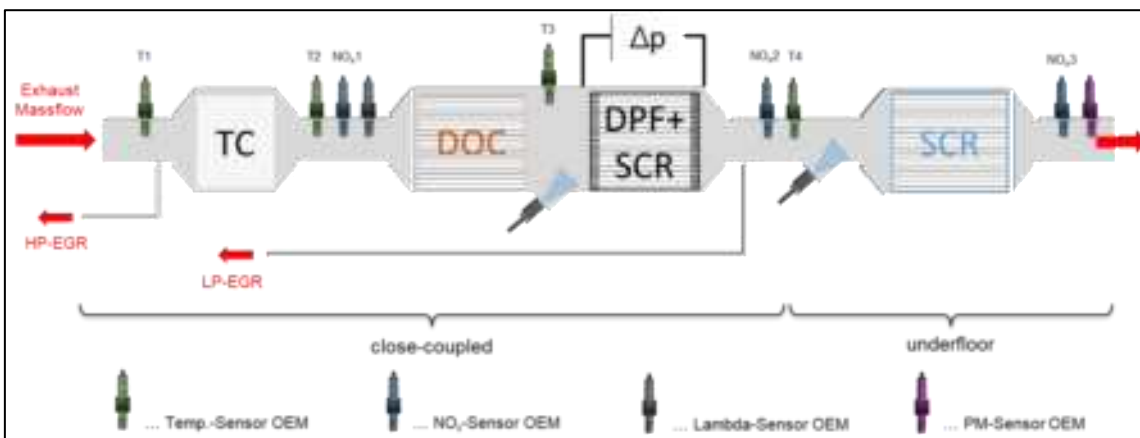


Figure 2: Schematic illustration of the exhaust gas aftertreatment system of the test vehicle

total of around 4,500 vehicle kilometres of measurement data were collected and recorded using a data logger. For the most part, the data includes conventional driving on the road (approx. 3,500 vehicle kilometres). However, it also includes measurement data in which the exhaust emission control system was modified (a total of approx. 450 vehicle kilometres) in order to be able to test the method for future NO_x monitoring. For this purpose, the following modifications were made to simulate a defect exhaust emission control system:

- AdBlue feed lines to the dosing valves disconnected and AdBlue fed into collection tank
- AdBlue tank emptied
- AdBlue tank filled with distilled water
- Exhaust gas recirculation valve unplugged

Measurement data was also collected for driving situations that are challenging for the exhaust emission control system (approx. 250 vehicle kilometres). Driving uphill and downhill with and without load as well as long traffic jams were classified as challenging driving situations. Figure 2 shows the NO_x emissions of the NO_x sensor installed by the vehicle manufacturer (OEM NO_x sensor) end-of-tailpipe of the individual tests, which are sorted in ascending order in the figure. The NO_x measurement data for the 110 tests range from 1 mg/km to 150 mg/km. The data also includes tests where periodic particulate filter regenerations happened, which can lead to higher NO_x emissions. Changes to the exhaust emission control system and challenging driving situations also lead to higher NO_x emissions. The tests were carried out between -15 °C and 35 °C ambient temperature. The average speed of the tests was 58 km/h, the maximum speed 170 km/h.

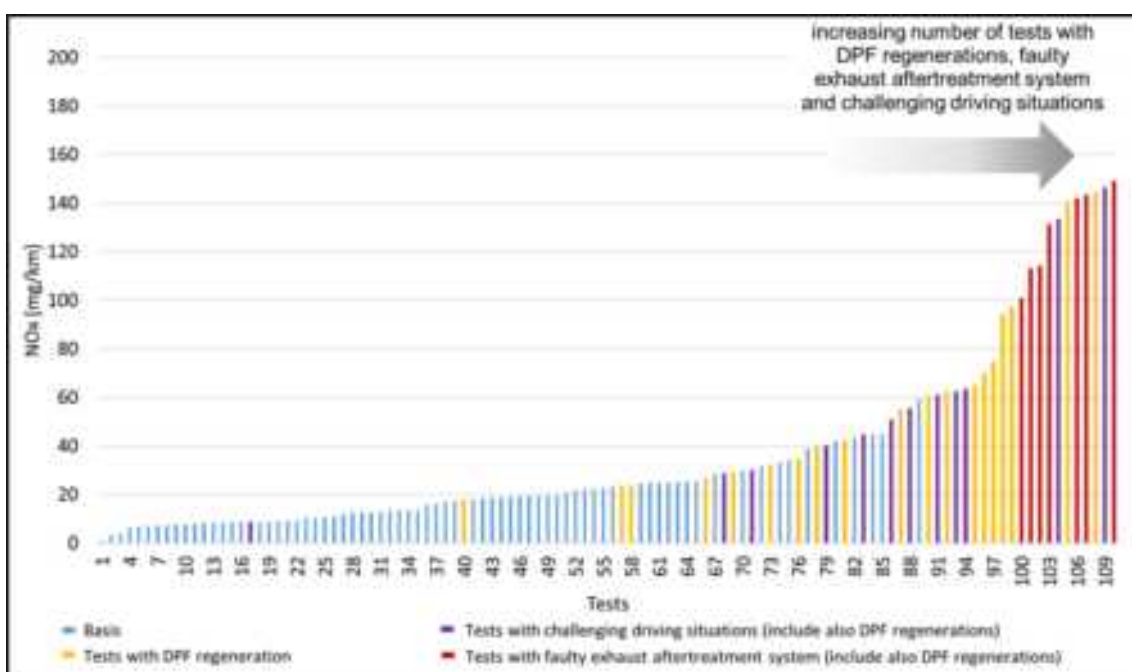


Figure 3: NO_x measurement data of the test vehicle of the individual tests arranged in ascending order (measurement data from each point in time from which the OEM NO_x sensor was active)

The OEM NO_x sensor data was also compared to the chassis dynamometer measurement data. The comparison showed that the NO_x sensor data matched that of the chassis dynamometer, taking into account sensor tolerances in the range of +/- 10 to 12 ppm for NO_x < 100 ppm.

Method development for future NO_x monitoring

All measurement data were used for development of the method. The following boundary conditions were taken into account when developing the method for future NO_x monitoring in real vehicle operation:

- The method should be able to detect faults in the NO_x exhaust emission control system. For this purpose, signals can be used which are already available in modern passenger cars with sufficient accuracy via the OBD interface of the vehicle.
- The application of the method should be possible for diesel as well as gasoline passenger cars. In the course of this project, the focus was on diesel passenger cars.

- It should be taken into account that higher NO_x emissions in certain driving situations, which are challenging for the exhaust emission control system, shall not be identified as a fault, provided that the exhaust emission control system is working properly.

When developing the method, a reference of the NO_x emissions to the kilometres driven (g/km) did not appear to be useful, since driving situations (e.g. with very high engine power) can lead to higher NO_x emissions in g/km, even if there is no fault in the exhaust emission control system (Notter et al. 2021). A reference of NO_x emissions to engine power therefore seems to be more appropriate. In many cases engine power is not available as a standard signal or is not available with sufficient accuracy via the OBD interface. However, since engine power is directly related to fuel mass flow (the relationship is also known as the Willans line), fuel consumption can also be used as a reference. The NO_x sensor and fuel consumption signal could be retrieved from the test vehicle via the OBD interface with appropriate accuracy. It is assumed that these signals are also available in modern passenger cars from other manufacturers. In future emission regulations, access to the relevant OBD signals can be defined as mandatory and checks for function and accuracy in the course of vehicle tests can be introduced to ensure the validity of these OBD signals. The following method proposal was derived from these considerations:

- Assessment of NO_x exhaust emission control system by the ratio g_{NO_x}/kg_{Fuel} . If the calculated ratio is above a threshold, there is a high probability for a fault in the NO_x exhaust emission control system (Figure 3). The g_{NO_x}/kg_{Fuel} ratio, if above the threshold, could lead to an "occasion-based" PTI or be indicated as a fault with the Malfunction Indicator Light (MIL) in the driver information display or be read out during the regular PTI. It would then make sense for the OBD system to also be able to define a source of error to enable efficient repairs.

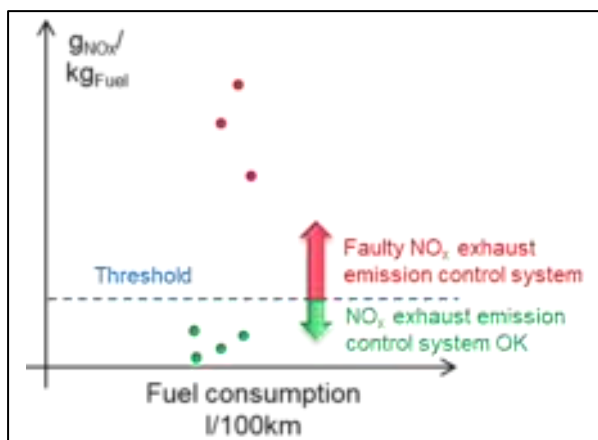


Figure 4: Schematic illustration of the proposal

Application of the proposed method

The method was applied to the measured data. In a first step, the ratio g_{NO_x}/kg_{Fuel} was calculated for each trip from which OEM NO_x sensor data were available at end-of-tailpipe. Figure 4 shows the result for the individual tests with the test vehicle plotted over the fuel consumption in l/100 km. Each data point represents the average value of a trip, calculated from the time when the OEM NO_x sensor was active. Data points outlined in red are those tests in which the exhaust emission control system was modified. Data points that are outlined in black are those tests in which DPF regeneration took place during the test. Tests with driving situations that are challenging for the exhaust emission control system are outlined in yellow. It can be clearly seen that tests with a faulty exhaust emission control system have a higher g_{NO_x}/kg_{Fuel} ratio than normal tests without DPF regeneration. It can also be seen that tests with DPF regeneration and tests with challenging driving situations can have higher g_{NO_x}/kg_{Fuel} ratios. The challenging driving situations included several uphill and downhill trips. During the uphill runs, high NO_x emissions but also high fuel consumption were present, which is why the g_{NO_x}/kg_{Fuel} ratio can again be classified as non-critical. During downhill runs, fuel consumption can be very low due to the longer drag phases, so that even with low NO_x emissions per kilometre, the g_{NO_x}/kg_{Fuel} ratio can be in the range of a faulty exhaust emission control system (e.g. the three data points outlined in yellow shown in the left area in Figure 4).

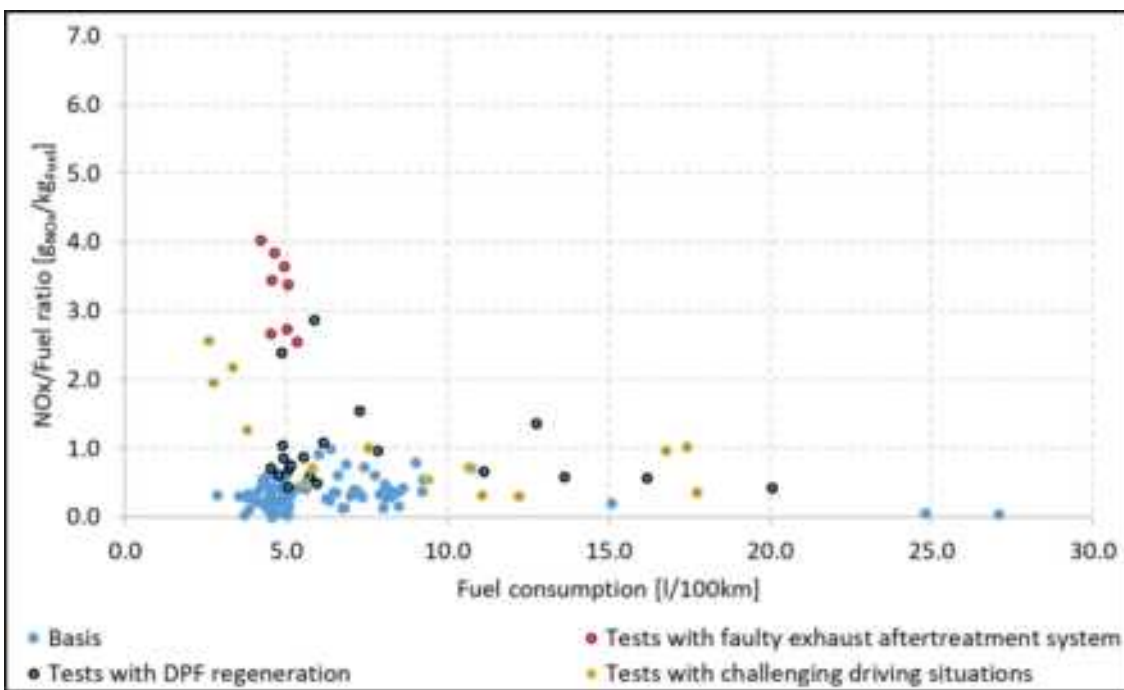


Figure 5: Application of the proposed method to the measurement data of the test vehicle

Applying the method to longer distances can compensate for possible uncertainties that may lead to higher g_{NOx}/kg_{Fuel} ratios for short tests, but where there is no fault in the exhaust emission control system. The investigations were carried out for 100 km sections. For this purpose, the measurement data of the test vehicle, which were recorded from the OEM NO_x sensor on the road, were strung together and evaluations were performed over 100 km sections. Figure 5 shows the calculated ratios plotted against l/100 km fuel consumption. Each data point represents the ratio over a 100 km section. In the course of the evaluation, it was found that tests with DPF regeneration phases can still lie in the areas of trips with faulty exhaust emission control system. Therefore, route sections with DPF regeneration phases were filtered out before calculating the g_{NOx}/kg_{Fuel} ratios on 100 km sections. It can be clearly seen that the tests made with properly working exhaust emission control system and without DPF regeneration phases are below a g_{NOx}/kg_{Fuel} ratio of 1. This also includes tests with challenging driving situations, such as uphill and downhill driving. In contrast to Figure 4, the challenging driving situations do not show conspicuous emission levels, since the downhill tests compensate with other tests over 100 km sections. However, should a downhill drive over 100 km take place, the g_{NOx}/kg_{Fuel} ratio could lie in a range in which values from faulty exhaust emission control system also lie. To prevent this, a filter excluding long phases with low fuel flow was also developed as part of the project. In summary, it can be recommended that the g_{NOx}/kg_{Fuel} ratios should not be considered on a cycle-specific basis, but rather over sections in the range of 100 km or longer.

Based on the measurement data of the test vehicle, a possible threshold value was also derived and plotted in Figure 5. Below this threshold value, a properly working exhaust emission control system can be assumed, at least for the test vehicle analysed in this study. If the g_{NOx}/kg_{Fuel} ratio is above the threshold value, a fault in the exhaust emission control system is very likely. This can also be confirmed with the 3-times standard-deviation from the test data using a log-normal distribution. If phases with DPF regeneration are not taken into account and evaluations are performed over 100 km sections as proposed, the measured values of tests with properly working exhaust emission control system are 99.7 % below 1.3 g_{NOx}/kg_{Fuel} (compared to the individual tests with properly working exhaust emission control system, 99.7 % are below 4.5 g_{NOx}/kg_{Fuel}). Therefore, a g_{NOx}/kg_{Fuel} ratio of 2 was derived as the threshold value in order to have also an additional margin against false detections. The data point at which a relevant defect first occurred during the 100 km interval would not yet be detected with a g_{NOx}/kg_{Fuel} ratio of just under 2, but if the error persisted, the error would become visible in the next 100 km interval. One may also apply 100 km moving average windows for monitoring for an earlier detection. With a faulty exhaust emission control system over 100 km, the g_{NOx}/kg_{Fuel} ratio for the test vehicle is around 3, meaning that clear identification is possible. The extent to which this threshold value is also valid for other vehicle models would still have to be validated with measurement data from other vehicle models.

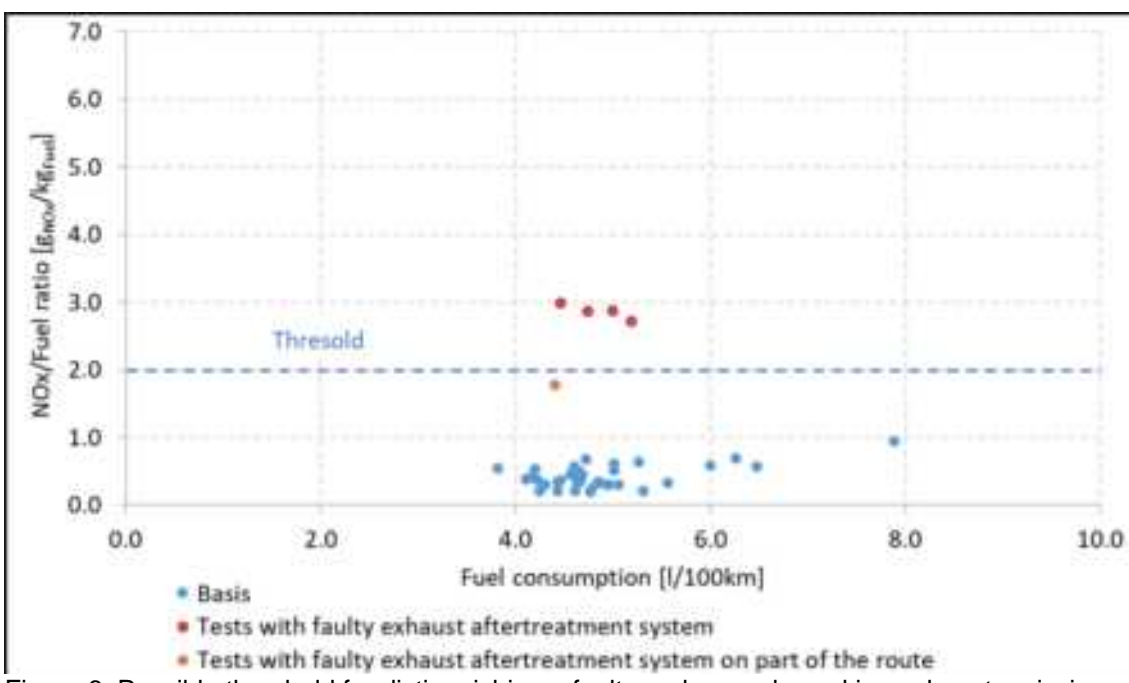


Figure 6: Possible threshold for distinguishing a faulty and properly working exhaust emission control system for Euro 6d vehicle emission levels

In the course of drafting the Euro 7 implementing acts, discussions are currently ongoing about whether vehicles need to comply NO_x limits at operating points under most driving situations in the planned Euro 7 legislation. Such a proposal was published by the EU Commission during the work on this project (EU COMMISSION 2022). This means that NO_x emissions would have to be below the limit values at almost all driving conditions, which is why NO_x emissions in real-world operation could also be monitored via g/km. Just a filter for the valid temperature and altitude ranges and possible additional boundaries for valid Euro 7 Real Driving Emissions (RDE) tests would be needed³. The NO_x emission limit in g/km with a safety margin for NO_x sensor uncertainty could then be used as the threshold value. However, the application of the developed method with g_{NO_x}/kg_{Fuel} would of course still be possible. It is therefore recommended to validate the proposed method with g_{NO_x}/kg_{Fuel} after the relevant boundary conditions of the Euro 7 legislation are decided and to optimize the best fitting method if necessary.

³ With more than 40 parameters the boundary conditions for valid Euro 6 RDE tests are rather too complicated and too selective to be applied in the Engine Control Units (ECUs) as filters.

Conclusion

In developing the method for future NO_x monitoring in real vehicle operation, consideration was given to the fact that higher NO_x emissions in certain driving situations, which are challenging for the exhaust emission control system, shall not be identified as a fault, provided that the exhaust emission control system is working properly. The developed method assesses the functionality of NO_x emission control systems by the ratio g_{NO_x}/kg_{Fuel}. The NO_x sensor and fuel consumption signals could be retrieved from the OBD interface on the test vehicle with appropriate accuracy. It is assumed that these signals are also available in modern passenger cars from other manufacturers. If the determined ratio is above a threshold value, there is a high probability that there is a fault in the NO_x exhaust emission control system. If the ratio is below the threshold value, it can be assumed that there is no fault. The g_{NO_x}/kg_{Fuel} ratio, if calculated above the threshold, could lead to an "occasion-based" PTI or be indicated as a fault with the MIL in the driver information display or be read out during the regular PTI. The method was tested using measurement data from 4,500 vehicle kilometers of a modern Euro 6d diesel passenger car. Tests with faulty exhaust emission control system could be clearly identified. Longer evaluation distances, e.g. 100 km sections, lead to a better differentiation of tests with and without malfunctions compared to shorter evaluation distances.

In course of drafting Euro 7 implementing acts, it is currently being discussed whether vehicles will have to comply with NO_x limits at operating points under almost any driving situations in the planned Euro 7 legislation. Monitoring in real operation could then also be carried out via g/km as alternative. However, the application of the developed method with g_{NO_x}/kg_{Fuel} would still be possible. It is therefore recommended to validate and optimize the most suitable method with g_{NO_x}/kg_{Fuel} after the boundary condition of the Euro 7 RDE test conditions are defined.

Acknowledgements

The study presented in this paper was designed and funded by BAST as part of the research contract "On-board diagnostics (OBD): Analysis of the OBD with regard to emission data available in future for the Euro 7 technical inspection (PTI)" ~~We would like to thank BAST for the excellent cooperation during the project and for the opportunity to make the results of the study available for this paper.~~

References

- EU COMMISSION (2022). *Proposal for a Regulation of the European Parliament and the Council on type approval of motor vehicles and engines and of systems, components and separate technical units for such vehicles with respect to their emissions and battery durability (Euro 7)*, COM (2022) 586final; Brussels, 10.11.2022.
- Notter B., Cox B., Hausberger S., Matzer C., Weller K., Dippold M., Poltschnig N., Lipp S., et al. (2021). HBEFA 4.2 - Documentation of updates, I-36/21/Wel EM Inst-21/04/20-670.

Simultaneous In-cabin and On-road CO₂ Concentrations On-board Measurements

A. Mehel ^{1*} and N. Hafs ¹

¹ ESTACA - Paris-Saclay, F-78180 Montigny-le-Bretonneux, France
* amine.mehel@estaca.fr

Introduction

Vehicle in-cabin could be subject of high pollution depending on external parameters such as road type, traffic condition (Hudda et al., 2012), the weather or even the distance with upstream vehicles (Mehel et al., 2023). But also on vehicle internal parameters such as its speed, age or ventilation settings (Knibbs et al., 2010; Hudda et al., 2012). The pollutants infiltrate vehicle in-cabin through the air intake and hence the Heating, ventilation and Air Conditioning (HVAC) system, but also from different leakages (Lee et al., 2015). Under certain situations, gaseous and particulates concentrations are higher in the car cabin in comparison to the on-road concentrations (Mehel et al., 2023).

In this situation, the passengers could be exposed to high in-cabin concentrations which could induce health risks. Indeed, several toxicological and epidemiological studies have associated the exposure to high levels of such toxic pollutants to the enhancement of respiratory inflammation, allergy and Asthma (Li et al., 2003) and numerous long-term health problems including lung cancer and cardiovascular diseases (Delfino et al., 2005; Silverman et al., 2012) and could even alter the placental function with a possible intergenerational effect (Valentino et al., 2016)

The most used solutions to reduce the in-cabin pollutants are on one hand the use of specific filters as the active carbon and/or High Efficiency Particulate Air (HEPA) filters (Xu et al., 2010). On the other hand, the use of the recirculated air ventilation mode (RC) allows reducing the infiltration of on-road pollutants into car-cabin however it induces CO₂ concentration accumulation inside the car cabin (Grady et al., 2013, Mehel et al., 2023).

This accumulation of CO₂ in the car cabin under RC ventilation is the result of passengers exhalation. When the ventilation is switched to outdoor air mode (OA), on-road CO₂ could infiltrate the car-cabin. We need to assess then what is its contribution to the global in-cabin CO₂, that is the objective of the present study.

In the present study, we conducted simultaneous in-cabin and on-road CO₂ concentration measurements during mobile on-board campaign around and in Paris.

2. Methodology

2.1 Car model and instrumentation

A diesel-powered SUV-type vehicle model with 28000 km mileage was used for the on-board measurement campaign. The HVAC system is equipped with new OEM filters including a High Efficiency filter and an activated carbon filter of 0 km.

Concerning the instrumentation, we used two TSI IAQ-Calc 7525 allowing for the measurement of CO₂ concentration, temperature, and Relative Humidity. The CO₂ concentration range allowed was 0-5000ppm, while the resolution was 1ppm with an accuracy of 3% of reading. The internal measurements probe was positioned between the front headrests (Figure 1a), while the external probe was positioned in the rear right passenger window (Figure 1b).



Figure 1: CO₂ concentration measurements probe positioning in (a) In-cabin and (b) On-road.

2.2 Ventilation settings

In the present study we wanted to investigate the on-road contribution of CO₂ to the in-cabin global CO₂ concentration. Hence, the ventilation mode was set to outdoor air (OA) for all the tests. The temperature was set to 22° and the air-conditioning was off. The fan speed was set to medium (4/8) or high (8/8).

2.3 Route type and test conditions

The route that was mainly used was of RDE-type with urban and freeways parts of the road. It included tunnels and ring road for a total length of 27.5 km. The test consisted of a round-trip with a stop in the centre of Paris with a complete aeration of the in-cabin at the arrival place for around 10 min. Average duration of the global journey was about 150 min for 55 km distance.

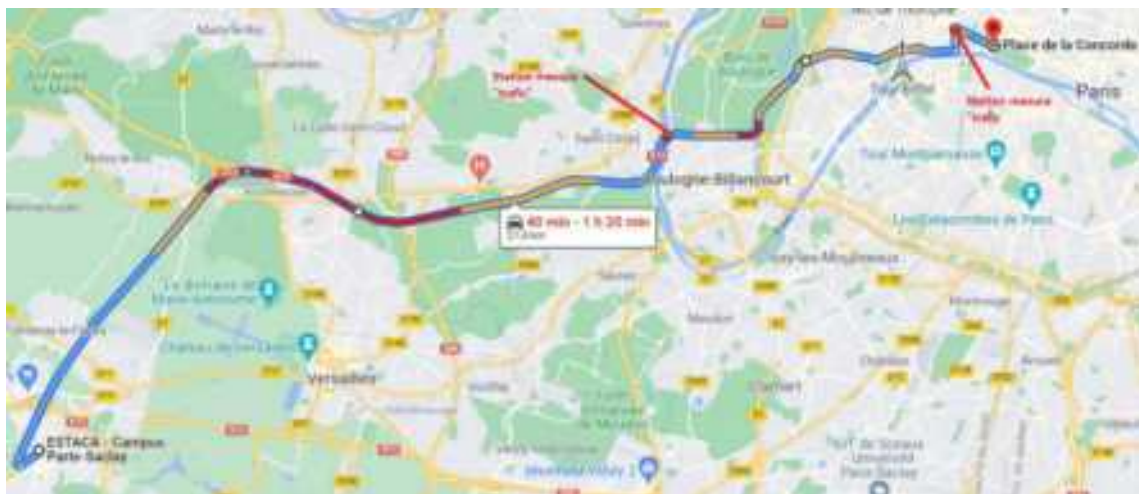


Figure 2: the used route for simultaneous in-cabin and on-road CO₂ concentrations, measurements.

During the test, only the driver is in the vehicle for the entire test duration.

3. Results and discussion

First, we conducted one-off test that showed the fast increase of the in-cabin CO₂ concentration when using the recirculated air (RC) ventilation mode (Figure 3). Indeed, when switching on the RC ventilation mode, we could notice in-cabin CO₂ concentration accumulation due to the driver exhalation. Hence, in RC ventilation mode, the contribution of on-road CO₂ to the in-cabin CO₂ is negligible.

Next tests were conducted both in static and driving modes. To compare the on-road and in-cabin concentrations, we calculated the ratio of the averaged In-cabin to On-road (I/O) concentrations:

$$R_{\bar{I}/\bar{O}} = \frac{\bar{C}_{in}}{\bar{C}_{out}} \quad (1)$$

Static measurements were achieved without passengers under OA ventilation and medium fan speed (4/8) at Estaca outdoor parking next an intersection. The results are presented in Figure 4. We could notice that both curves of the time evolution of the CO₂ concentration on-road and in the car-cabin show similar trends with less intensity of the in-cabin concentration peaks. This similar trend is not surprising since there is no passenger in the car cabin, the on-road CO₂ infiltrates the cabin and constitutes the main source. But it reveals that the active carbon has a negligible effect on CO₂ filtration.

The average in-cabin and on-road concentrations and the ratio of the average in-cabin to on-road concentrations are given in Table 1. The ratio is approximately equal to one which means that there is no buffering effect of the car cabin (ratio not larger than one). And inversely the on-road CO₂ infiltrates entirely the car cabin.(the ratio not smaller than one).

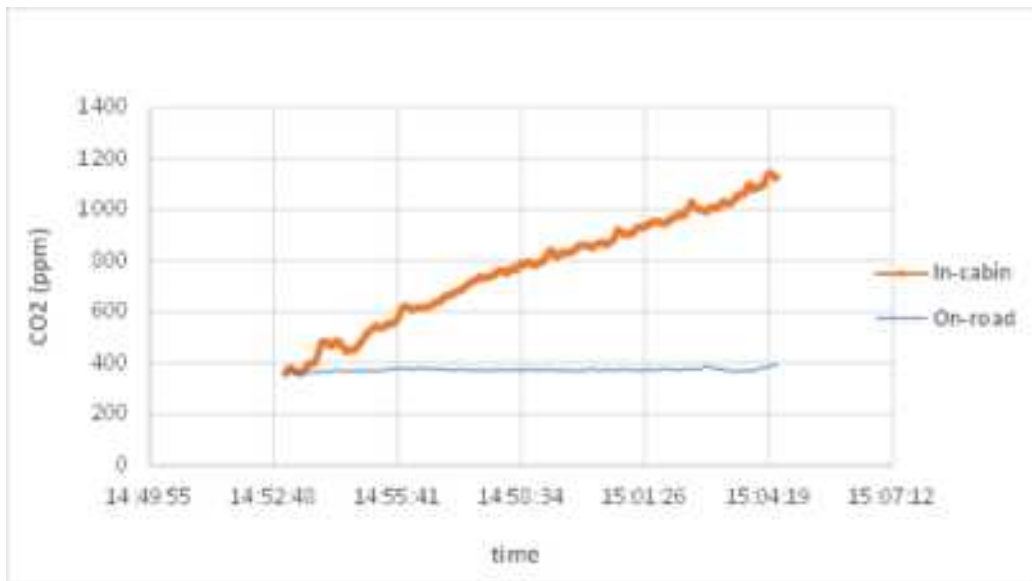


Figure 3 : In-cabin vs on-road CO₂ concentrations under RC ventilation mode with fan speed 4/8.

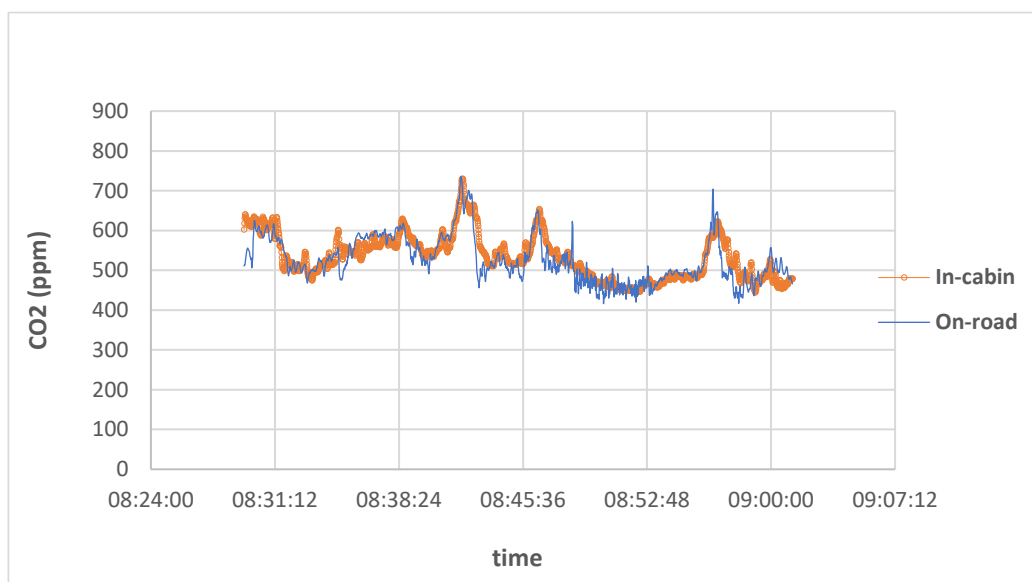


Figure 4 Time evolution of in-cabin and on-road CO₂ concentrations under OA ventilation with fan speed 4/8 during static measurements.

Table 1: In-cabin and on-road CO₂ mean concentrations and the ratio of the average concentrations:

\bar{C}_{in} (ppm)	\bar{C}_{out} (ppm)	$R_{\bar{I}/\bar{O}}$
534	526	1,01

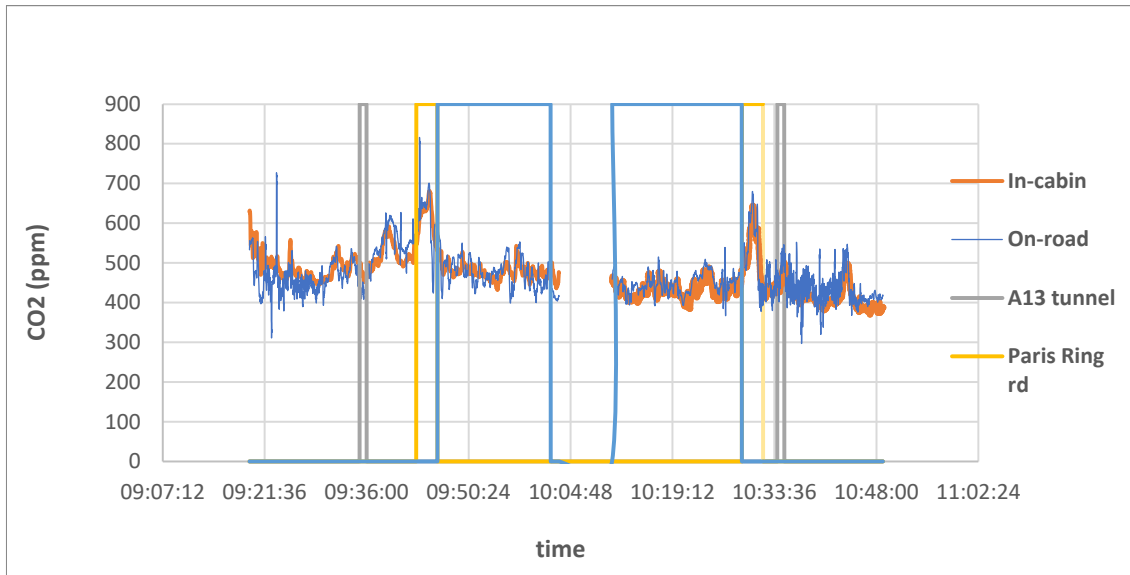


Figure 5 Time evolution of in-cabin and on-road CO₂ concentrations under OA ventilation with fan speed 4/8 outward and 8/8 during the return (Morning measurements).

The results obtained during mobile measurements following the route presented in Figure 2 are displayed in Figure 5. The curves are partitioned into two parts, the first one corresponds to the outward, followed by the stop stage in Paris center with a complete aeration of the car cabin by opening the doors (between 10H03 and 10H10). The final stage corresponds to the return trip. The gray boxes correspond to the road sections and tunnels. Where the yellow boxes correspond to Paris's ring road sections.

We could notice that in-cabin and on-road CO₂ concentrations curves measured during mobile test have similar trends with more dynamics for the on-road curve. As for static measurements, the same conclusion could be drawn, that is, when the OA ventilation mode was selected and one passenger was onboard, the main contributor to in-cabin CO₂ was from on-road sources. Indeed, among points that illustrate this behavior are the peaks that appeared in ring road where important traffic were found. These peaks are enclosed in the yellow boxes, during the outward at 9H45, while it is found at 10H30 during the return. These peaks were found simultaneously on-road and in the car cabin.

The ratio of the in-cabin to on road average concentrations $R_{\bar{I}/\bar{o}}$ were about 1.09 during the outward (OA, fan speed 4/8), while it was about 1.04 during the return stage (OA, fan speed 8/8). These ratios were obtained from numerous test repetitions. They show that, the on-road CO₂ infiltrated completely the in-cabin and depending on fan speed, the passenger exhalation could contribute to the increase of the global CO₂ concentration.

Conclusion

In this study we investigated the relevance of conducting simultaneous in-cabin and on-road CO₂ concentration measurements during on-board tests. The results showed that the ratio is greater than one for all cases, i.e., OA and RC ventilation mode and for all-fan speed, even the higher speed where the contribution of outdoor fresh air is introduced. It is also indicated that the OEM active carbon filters are not designed to filter the CO₂. This investigation could be used from a practical point of view of conducting on-board mobile measurements. Indeed, the question that arose was if it is necessary to conduct simultaneous on-road to in-cabin concentration measurements. It seems that, even if the on-road CO₂ infiltrates entirely the car cabin, its contribution to the global in-cabin concentrations is of the level of background pollution. Even in road sections with important pollution concentration, such tunnels or ring roads, the CO₂ concentration is below 1000 ppm which is the average recommended threshold for indoor air in numerous countries. Consequently, the contribution of on-road CO₂ is limited.

Acknowledgements

We are grateful to the French Environmental and Energy Management Agency (ADEME) for providing financial support for the present research.

References

- Delfino, R.J., Malik, S., and Sioutas, C., 2005. Potential role of ultrafine particles in associations between airborne particle mass and cardiovascular health. *Environmental Health Perspectives* 113, 934-946.
- Grady, M., Jung, H., Kim, Y., Park, J. et al. (2013). SAE Technical Paper, 2013-01-1494.
- Hudda, N., Eckel, S. P., Knibbs, L. D., Sioutas, C., Delfino, R. J., and Fruin, S. A. (2012). Linking in-vehicle ultrafine particle exposures to on-road concentrations. *Atmospheric Environment* 59, pp. 578-586.
- Lee ES, Stenstrom MK and Zhu YF. (2015). Ultrafine particle infiltration into passenger vehicles, Part I: Experimental evidence. *Transport Research D*, 38, pp. 156–165.
- Li, N.; Hao, M.Q.; Phalen, R. F.; Hinds, W.C.; Nel, A. E. (2003). Particulate air pollutants and asthmas A paradigm for the role of oxidative stress in PM-induced adverse health effects. *Clinical Immunology*, 109, pp. 250-265.
- Mehel, A., Deville-Cavellin, L., Joly, F., Sioutas, C., Murzyn, F., Cuvelier, Ph and Baudic, A. (2023). *Atmospheric Pollution Research*, 14 (2), 101673.
- Silverman, D.T., Samanic, C.M., Lubin, J.H., Blair A.E., Stewart, P.A., Vermeulen, R., Coble J.B., Rothman, N., Schleiff P.L., Travis, W.D., Ziegler, R.G., Wacholder, S. and Attfield M.D (2012). The Diesel Exhaust in Miners study: a nested case-control study of lung cancer and diesel exhaust. *Journal of the National Cancer Institute*:104 (11), pp. 55-68.
- Valentino, S.A., Tarrade, A., Aioun, J., Mourier, E., Richard, C., Dahirel, M., Rousseau-Ralliard, D., Fournier, N., Aubrière, M.-C., Lallemand, M.-S., Camous, S., Guinot, M., Charlier, M., Aujean, E., Al Adhami, H., Fokkens, P.H., Agier, L., Boere, J.A., Cassee, F.R., Slama, R., Chavatte-Palmer, P. (2016). Maternal exposure to diluted diesel engine exhaust alters placental function and induces intergenerational effects in rabbits. *Particle Fibre Toxicology*, 13 (39).
- Xu, B., Liu, S., Liu, J. and Zhu, Y. (2010). Effects of cabin filter on in-cabin to on-roadway ultrafine particle ratios. *Aerosol Science and Technology*, Aerosol Science and Technology, 45, pp. 215–224.

2.3 TAP.03. In-service conformity and new concepts for enhanced emission testing in PTI.

Solid particle number (SPN) measurements during the periodic technical inspection (PTI) of vehicles

A. Melas^{1*}, R. Suarez-Berto^a and B. Giechaskiel^{1*}

¹ Joint Research Centre, European Commission, 21027, Ispra, Italy

Anastasio.Melas@ec.europa.eu; Barouch.Giechaskiel@ec.europa.eu

Introduction

In the European Union (EU), after the introduction of a vehicle in the market, its roadworthiness is checked at authorized testing centers via a mandatory periodic technical inspection (PTI) that promotes road safety and environmental protection (Directive 2014/45/EU). In respect to the environment, the proper operation of the engine and after-treatment devices are checked with simplified tests. PTI emission tests can identify high polluting vehicles and potentially improve air quality. Particulate emissions of Diesel vehicles are checked with an opacity test.

Modern Diesel vehicles are equipped with particulate filters in order to comply with solid particle number (SPN) limits imposed during their type-approval. Several studies questioned the efficiency of opacity tests to identify malfunctioning or even manipulated Diesel particulate filters (DPFs) (Boveroux et al., 2019; Yamada, 2019). Considering that a small fraction of vehicles with malfunctioning or severely damaged DPFs may dominate the SPN emissions of the fleet (Burtscher et al., 2019), there is an emerging necessity of introducing a new particle test. On account of the doubts on the opacity measurement efficiency, several European member states apply or are planning to introduce a new methodology in their PTI for Diesel vehicles; the measurement of SPN concentration of particles with diameter approximately larger than 23 nm particle size, at low idling (herein after called SPN-PTI) (Bainschab et al., 2020; Vasilatou et al., 2022).

The Netherlands, Belgium, and Switzerland currently apply a SPN-PTI test at their PTI while Germany will soon introduce it. National regulations differ on several aspects like the applicability (homologation standard), the limit, the procedure, and the metrological requirements of the respective SPN measurement instrumentation. Table 1 presents measurement procedure requirements in different regulations/recommendations.

Table 1: SPN-PTI measurement procedures in different regulations/recommendations

Country	Engine conditions	Test duration (s)	Limit (#/cm ³)	Application
Netherlands, Belgium	Cold ^a or hot	15	10 ⁶	Euro 5 and Euro 6 ^b
Germany	Hot (Engine coolant >60 °C)	30 (x 3 repetitions)	2.5 x 10 ⁵	Euro 6
Switzerland	Hot	5 (x 3 repetitions)	10 ⁵ or 2.5 x 10 ⁵	DPF-equipped
EU recommendation	Cold ^a or hot (Engine coolant >60 °C)	At least 15 s total duration	2.5 x 10 ⁵	Euro 5b and Euro 6

^a *Very cold case of power demand* ^b Depending on the region, also vehicles equipped with DPF and homologated before Euro 5 can be tested

European Commission recently published a recommendation for SPN measurements during PTI that harmonizes the different approaches proposing some minimum requirements that ensure the robustness of the methodology. Moreover, in the upcoming revision of the Directive 2014/45/EU, the SPN-PTI test will be considered.

In this work, we present an overview of the main experimental results obtained by JRC at different experimental campaigns performed from 2021 to 2023 with the participation of different companies producing SPN-PTI instruments. The experimental campaigns aimed to establish the correlation between low idling concentrations and type-approval emissions and define metrological-procedural requirements that guarantee accurate SPN measurements (Melas et al., 2023, 2022, 2021; Vasilatou et al., 2023) considering the uncertainty of the methodology as well as the challenges that arise from the place of testing (garage).

Experimental

The experimental campaigns performed by JRC involved seven different instruments used for SPN-PTI tests. These instruments are typically composed of a sampling line, a pre-conditioning unit that removes volatiles and/or dilutes exhaust particles, and a particle detector. The entire instrument has a cut-off size at approximately 23 nm, similarly to particle number counters used for vehicle type-approval testing in EU (Giechaskiel et al., 2021). Table 2 presents the PTI instruments that were tested. The manufacturers that provided the PTI devices were in alphabetical order: CAPELEC (Montpellier, France) and PEGASOR (Tampere, Finland), DEKATI (Kangasala, Finland), MAHLE (Stuttgart, Germany), SENSORS (Erkath, Germany), TEN (Baambrugge, The Netherlands), and TSI (Aachen, Germany). The SPN-PTI instrument #6 was owned by JRC and it was the NPET of TSI.

Table 2: Sampling and measurement technologies used by the PTI instruments.

PTI ₂₃ instrument code	Sampling line	Dilution	Volatile particle remover	Particle detector
#1	Heated	No	Thermal denuder *	Diffusion charger
#2	Heated	Venturi	Evaporation tube	Diffusion charger
#3	Heated	No	Evaporation tube	Diffusion charger
#4	Heated	200:1	Evaporation tube	Condensation Particle Counter
#5	Not heated	20:1	Catalytic stripper	Condensation Particle Counter
#6	Not heated	10:1	Catalytic stripper	Condensation Particle Counter
#7	Heated	10:1	Evaporation tube	Condensation Particle Counter

* in some tests catalytic stripper

In total, 11 vehicles were used in this study; 9 Diesel- and 2 gasoline-fueled. For all of them, SPN emissions were measured at low idling while V1, V3, V7, V8, V9, V10 were also tested according to type-approval driving cycles. Table 3 lists information on the vehicles.

Table 3: Main characteristics of tested vehicles.

Code	Euro	Fuel	Mileage (km)	Engine displacement (cm ³)	Power (kW)	Particulate filter
V1	6b	Diesel	23 800	1560	88	Yes
V2	6b	Gasoline PFI	20 000	1400	70	No
V3	4	Diesel	211 000	1997	100	Yes
V4	6d	Diesel	5 000	1968	110	Yes*
V5	5b	Gasoline DI	158 800	1197	77	No
V6	3	Diesel	286 000	2933	150	No
V7	6d	Diesel	26 700	2933	210	Yes
V8	6c	Diesel	125 500	1968	110	Yes
V9	6d-TEMP	Diesel	11 600	1997	107	Yes
V10	6d	Diesel	5 000	1950	143	Yes
V11	6d	Diesel	4 100	1999	132	Yes

* For this vehicle the DOC and the DPF were bypassed and a DPF efficiency of 90% was simulated.

Two reference systems were used in the testing campaigns: a solid particle number measurement system down to 23 nm (SPN₂₃) and down to 10 nm (SPN₁₀). A total particle number system (both solid and volatile) down to 10 nm (TPN₁₀) was also used. Solid particle number measurements were performed with the Advanced Particle Counter (APC) (AVL, Graz, Austria). APC removed volatile particles using a catalytic stripper. The reference instrumentation was calibrated less than one year from the tests. Total particle measurements were done with two cold dilution stages and a CPC 3792 (TSI, Shoreview, MN, USA) with cut-off size at 10 nm.

Cold vs. hot idling concentrations

The low idling SPN₂₃ emissions of vehicles V1 to V5 were measured with PTI instruments #1 to #7. Tests were performed both with cold (engine coolant <25°C) and hot (engine coolant >60°C) engine in a room conditioned at approximately 23°C. The measurement duration varied from 15 to 90 s according to the different measurement protocols of European countries, i.e. 15 s in the Netherlands and Belgium, 90 s in Germany.

Figure 1a plots the relative (%) increase of SPN emissions when sub-23 nm particles are considered (i.e. the contribution of sub-23 nm particles to the final concentration) while Figure 1b, the relative increase when volatile particles are considered (i.e. the contribution of volatile particles to the total concentration).

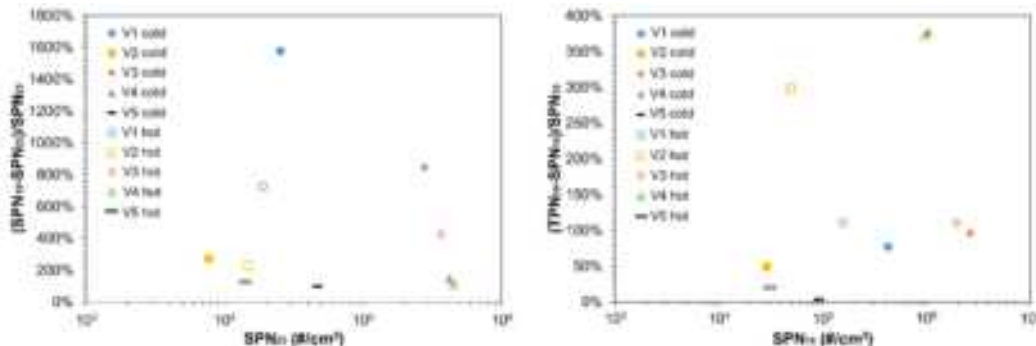


Figure 1: (a) Relative increase of SPN₂₃ when sub-23 nm particles are considered (from Melas et al., 2022), (b) Relative increase of SPN₁₀ when volatile particles are considered (from Melas et al., 2022).

Vehicles V1 and V3 presented very high sub-23 nm particle concentrations (Figure 1a). At cold conditions the relative increase was 1580 % for V1 and 845 % for V3 which at hot engine conditions sub-23 nm decreased to 725 % and 430 %, respectively. For V3 the sub-23 nm fraction at a type-approval cycle

(worldwide harmonized light vehicles test cycle - WLTC) was much lower, ~20 %. High sub-23 nm solid particle emissions at low idling were observed also in previous studies and have been attributed to polyaromatic hydrocarbons (PAHs) that do not evaporate at 350°C or to lubrication oil particles (De Filippo and Maricq, 2008; Lähde et al., 2014).

The highest volatile particle concentrations were observed for V4 (~370 % more than SPN₁₀) while the engine temperature did not influence the volatile particles formation. A possible reason for high volatile particles emissions for V4 was that DOC was bypassed.

Figure 2 summarizes the cold (Figure 2a) and hot (Figure 2b) engine low idling measurements performed with PTI instruments against the reference instrumentation SPN₂₃. The red dashed lines indicate the SPN-PTI in Germany, 250,000 #/cm³, and divide the graphs in four rectangles. Points in the up and left rectangle are higher than the limit when measured with a PTI instrument but lower when measured with reference instrumentation. These points would be "false low" instead points in the down and right rectangle would be a "false high". Additionally, the purple dash dotted lines show values ± 25 %, or 2.5 x 10⁴ #/cm³ (whichever is greater) according to the maximum permissible error in the NL regulation. The green dotted lines indicate the DE maximum permissible error, i.e., ± 50 % but at least 5 x 10³ #/cm³. In Figure 2a and 2b we also plot a linear fit (black solid line) by setting the intercept zero and we also report the slope and the R².

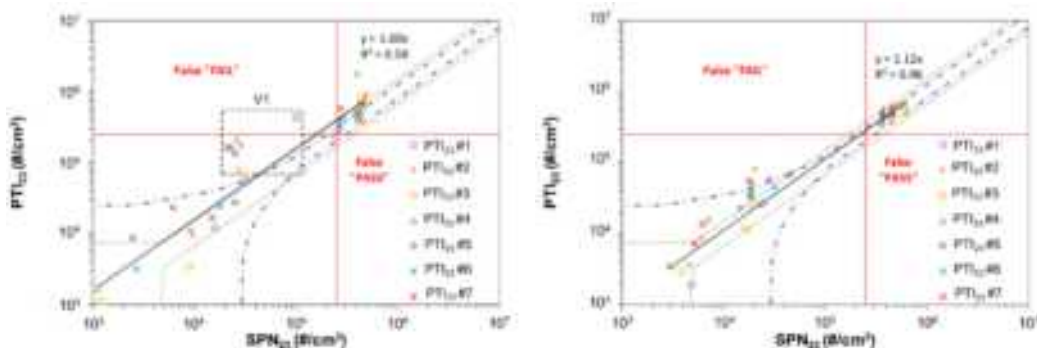


Figure 2: SPN concentrations down to 23 nm of 5 vehicles at low idling measured with seven PTI₂₃ instruments and compared to a reference system (SPN₂₃) (from Melas et al., 2022): (a) cold engine, (b) hot engine. The red dashed lines indicate the German SPN-PTI limit, the purple dash dotted lines the NL maximum permissible error, the green dotted lines the DE regulation and the black solid line is a linear fit with intercept set at zero.

Linearity between PTI instruments and reference instrumentation was not good when the engine was cold. Specifically, the slope was 1.6 and R²=0.58. In most cases the PTI instruments overestimated SPN concentrations. The highest differences were observed for V1 and V3 which also had the highest nucleation particles concentrations. Note that for V1 one PTI instrument reported a "false low". This result shows the importance of these nucleation particles in PTI instruments deviations. Instead, for V4, with high volatile particles concentrations, the agreement was good and specifically ± 40 %.

When the engine was hot, the agreement between PTI instruments and reference instruments was very good, the slope being 1.12 and R² = 0.98. No "false low" or "false high" was observed. A possible reason for the better agreement is the reduction of sub-23 nm particles.

Correlation of type-approval SPN emissions with SPN concentrations during PTI

Figure 3 plots the SPN emissions down to 23 nm of different Diesel vehicles at type-approval tests against hot low idle SPN concentrations. The horizontal dashed line indicates the Euro 5b and Euro 6 limit of 6 x 10¹¹ #/km. The dotted line is a linear fit of the results obtained in this and previous studies. Specifically, TNO study results were presented in (Kadijk et al., 2017) and previous JRC results in (Giechaskiel et al., 2020). Dashed yellow lines are a ± 65% which include all measurements near the limit 6 x 10¹¹ #/km. The correlation factor between PTI and type-approval was found to be 8.2 x 10⁶ (km/cm³) and R²=0.90. By applying the 65% uncertainty for values near the type-approval limit, we obtain that a PTI limit of ~1 x 10⁵ #/cm³ would include a procedure correlation uncertainty to add due to the "Procedure correlation" uncertainty also the PTI instruments should be added.

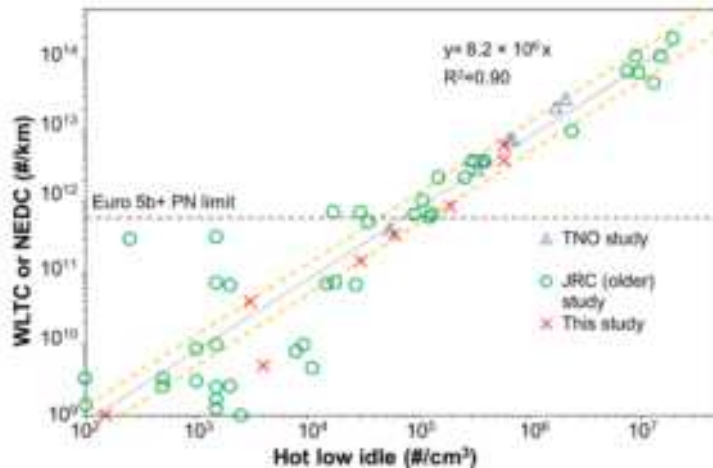


Figure 3: Solid particle number emissions at type-approval driving cycle against hot low idling emissions. Dashed lines are a $\pm 65\%$ uncertainty (from Melas et al., 2022).

Conclusions

This study examined the accuracy of instruments designed for SPN-PTI measurements as well as the correlation of the SPN-PTI methodology with the vehicle type-approval testing. When vehicle engine was cold, we obtained high differences between PTI_{23} and SPN_{23} . The agreement was much better when the vehicle was warm. Future SPN-PTI tests are recommended to be performed with an engine coolant temperature of at least $60^\circ C$. Finally, a very good correlation between SPN-PTI and type-approval SPN_{23} emissions were observed showing that the SPN-PTI methodology can detect high SPN emitters.

Acknowledgements

Authors would like to thank T. Selleri, F. Forloni, V. Valverde, C. Gruening for the discussions and D. Luseur, P. Le Lijour, A. Migneco, J. Franzetti, L. Bigozzi, F. Forni, P. Canevari for the experimental support.

References

- Bainschab, M., Schriefl, M.A., Bergmann, A., 2020. Particle number measurements within periodic technical inspections: A first quantitative assessment of the influence of size distributions and the fleet emission reduction. *Atmospheric Environment*: X 8, 100095. <https://doi.org/10.1016/j.aeaoa.2020.100095>
- Boveroux, F., Cassiers, S., Buekenhoudt, P., Chavatte, L., De Meyer, P., Jeanmart, H., Verhelst, S., Contino, F., 2019. Feasibility study of a new test procedure to identify high emitters of particulate matter during periodical technical inspection. *SAE Technical Paper* 2019-01-1190. <https://doi.org/10.4271/2019-01-1190>
- Burtscher, H., Lutz, Th., Mayer, A., 2019. A new periodic technical inspection for particle emissions of vehicles. *Emiss. Control Sci. Technol.* 5, 279–287. <https://doi.org/10.4236/escit.201905028>
- De Filippo, A., Maricq, M.M., 2008. Diesel nucleation mode particles: Semivolatile or solid? *Environ. Sci. Technol.* 42, 7957–7962. <https://doi.org/10.1021/es8010332>
- Giechaskiel, B., Lähde, T., Suarez-Bertoa, R., Valverde, V., Clairotte, M., 2020. Comparisons of laboratory and on-road type-approval cycles with idling emissions. Implications for periodical technical inspection (PTI) sensors. *Sensors* 20, 5790. <https://doi.org/10.3390/s20205790>
- Giechaskiel, B., Melas, A., Martini, G., Dilara, P., 2021. Overview of vehicle exhaust particle number regulations. *Processes* 9, 2216. <https://doi.org/10.3390/pr9122216>
- Kadijk, G., Elstgeest, M., Ligterink, N.E., Van der Mark, P.J., 2017. Investigation into a Periodic Technical Inspection (PTI) test method to check for presence and proper functioning of Diesel Particulate Filters in light-duty diesel vehicles – part 2. TNO report TNO 2017 R10530.

Lähde, T., Virtanen, A., Happonen, M., Söderström, C., Kytö, M., Keskinen, J., 2014. Heavy-duty, off-road diesel engine low-load particle number emissions and particle control. *J. Air Waste Manag. Assoc.* 64, 1186–1194. <https://doi.org/10.1080/10962247.2014.936985>

Melas, A., Selleri, T., Suarez-Bertoa, R., Giechaskiel, B., 2022. Evaluation of measurement procedures for solid particle number (SPN) measurements during the periodic technical inspection (PTI) of vehicles. *Int. J. Environ. Res. Public Health* 19, 7602. <https://doi.org/10.3390/ijerph19137602>

Melas, A., Selleri, T., Suarez-Bertoa, R., Giechaskiel, B., 2021. Evaluation of solid particle number sensors for periodic technical inspection of passenger cars. *Sensors* 21, 8325. <https://doi.org/10.3390/s21248325>

Melas, A., Vasilatou, K., Suarez-Bertoa, R., Giechaskiel, B., 2023. Laboratory measurements with solid particle number instruments designed for periodic technical inspection (PTI) of vehicles. *Measurement* 215, 112389. <https://doi.org/10.1016/j.measurement.2023.112839>

Vasilatou, K., Kok, P., Pratzler, S., Nowak, A., Waheed, A., Buekenhoudt, P., Auderset, K., Andres, H., 2022. New periodic technical inspection of diesel engines based on particle number concentration measurements. *OIML Bulletin LXIII*.

Vasilatou, K., Wälchli, C., Auderset, K., Burtscher, H., Hammer, T., Giechaskiel, B., Melas, A., 2023. Effects of the test aerosol on the performance of periodic technical inspection particle counters. *J. Aerosol Sci.* 172, 106182. <https://doi.org/10.1016/j.jaerosci.2023.106182>

Yamada, H., 2019. Improving methodology of particulate measurement in periodic technical inspection with high-sensitivity techniques: laser light scattering photometry and particle number method. *Emiss. Control Sci. Technol.* 5, 37–44. <https://doi.org/10.1007/s40825-019-0108-z>

In-use NO_x emission trends of diesel trucks in China informed by large-sized inspection data

Y.Wang², H.Cheng², S.Zhang^{1*}, Y.Wu¹ and Z.Ran²

¹ School of Environment, Tsinghua University, Beijing, China, zhsjun@tsinghua.edu.cn

² Clean Air Asia China Office, Beijing, China

Introduction

With the advancement of economic and social development, as well as the prominence of air pollution, Nitrogen Oxides (NO_x) emissions from anthropogenic sources have become a matter of great concern. As critical precursors of ozone (O₃) and fine particulate matter (PM_{2.5}), NO_x (mainly NO₂ and NO) emissions may cause severe environmental issues such as photochemical smog and acid rain and pose a high risk to human health (Chen et al., 2012; Li et al., 2019; Pye et al., 2022; Richter et al., 2005; Shaw and Van Heyst, 2022; Wei et al., 2019). Among the anthropogenic sources of NO_x emissions, on-road vehicles are the largest contributor. Specifically, diesel trucks account for more than 80% of the NO_x emissions from on-road vehicles, although they account for only 11% of the on-road vehicle stock, highlighting the importance of controlling NO_x emissions from diesel trucks (Li et al., 2023; Ministry of Ecology and Environment, 2022).

Since the 11th Five-Year Plan, China has adopted robust regulations and policies to control NO_x emissions from in-use diesel trucks. On the one hand, China has been progressively improving its emission standards for new diesel trucks, known as China IV, China V, and China VI. Especially, the implementation of China VI standard, *Limits and measurement methods for emissions from diesel fueled heavy-duty vehicles (GB 17691-2018)*, which requires diesel trucks to be equipped with remote on-board diagnostic (OBD) system to ensure that NO_x emissions satisfy stringent criteria, has pushed the emission control of new vehicles to an international level (Zhang et al., 2020). On the other hand, since the launch of *Action Plan for Diesel Truck Pollution Control* in 2018, China has gradually developed a Sky-Ground-Vehicle-Personnel (SGVP) integrated emission control system that integrates multiple emission monitoring tools, such as roadside remote sensing, on-board monitoring, and periodic emission inspection (Hao et al., 2022; MEE et al., 2018). Required by the active regulations, diesel trucks must undergo periodic emission inspections at least once a year. Inspections should be conducted based on the *Limits and measurement methods for emissions from diesel vehicles under free acceleration and lugdown cycle (GB 3847-2018)*, and non-compliant trucks must be repaired or scrapped according to the Inspection and Maintenance (I/M) program.

NO_x emission concentration data of lug-down test in emission inspections can provide comprehensive coverage of diesel trucks with various emission standards, vehicle types, and vehicle weights. However, only a few studies have focused on NO_x emission analysis using inspection data. This study utilized representative and high-quality inspections data, which was validated using multi-source test data, to analyze the effectiveness of current emission control programs in reducing NO_x emissions from diesel trucks. Additionally, this study presents the emission reduction effects of a scenario implementing stricter NO_x emission limits in the lug-down test. The findings will provide valuable recommendations for the formulation and implementation of relevant policies aiming to reduce O₃ and PM_{2.5} emission synergistically and lower their harmful impacts on the environment and public health.

Data and methods

Owing to the heterogeneity in emission performance, diesel trucks with varying emission standards, gross vehicle weight (GVW), and vehicle types were included in this study. In terms of emission standards, China III, IV, V, and VI diesel trucks are chosen and further classified into four GVW categories: mini trucks (GVW ≤ 1800 kg), light-duty trucks (LDTs) (1800 kg < GVW < 4500 kg), medium-duty trucks (MDTs) (4500 kg ≤ GVW < 12000 kg), and heavy-duty trucks (HDTs: GVW ≥ 12000 kg). Straight, dump, public service, refrigerated, and tractor trucks, the most prevalent vehicle types in the Chinese market, were included in this study.

Although various emission monitoring techniques exist for diesel trucks, including the lug-down test used for periodic emission inspection, portable emission measurement system (PEMS), OBD, plume-chasing measurement, and remote sensing, most monitoring techniques either lack large samples or lack data reliability. However, periodic emission inspections cover a high proportion of diesel truck fleets while ensuring good data reliability and accuracy, which has been validated in the consistency analysis section. The *Regulations of the People's Republic of China on the Implementation of the Road Traffic Safety Law* mandates that trucks registered for less than 10 years must undergo an annual inspection and those registered for more than 10 years must undergo a twice-yearly inspection. Periodic emission inspection, a mandatory program for annual truck inspection, covers representative and large in-use diesel trucks that can be analyzed to evaluate the NO_x emission performance over many years, providing excellent data for assessing the effectiveness of diesel truck emission reduction strategies.

This study assessed the NO_x emission performance of in-use diesel trucks during periodic emission inspections from 2019 to 2021 in a systematic and comprehensive manner using valid lug-down test data. In the selection of vehicle samples, this study used a random sampling method to select truck samples that underwent their first emission inspection of the year, using the sampling parameters listed in Table 1. The sample size for each vehicle model was determined using Eq. (1), and the vehicles models covered in this study accounted for more than 90% of the in-use truck models.

$$n \approx \frac{\left(\frac{Z_{\alpha}}{2}\right)^2 \sigma^2}{E^2} \quad (1)$$

where n is the sample size for each vehicle model, σ^2 is the variance of the observed NO_x emission concentrations for each vehicle model, E is the sampling error, and $Z_{\alpha}/2$ is the reliability factor that indicates the confidence interval, with 1.96 used for the 95% confidence interval and 1.645 used for the 90% confidence interval.

Table 1: Summary of sample size and sampling parameters in this study

Year	2019	2020	2021
Emission Standard	China III; China IV; China V; China VI	China V; China VI	China IV; China V; China VI
Sampling Error (lug-down test)	10%	5%	10% (China IV; China V) 5% (China VI)
Confidence Level (lug-down test)	95%	95%	90% (China IV; China V) 95% (China VI)
Number of models (lug-down test)	5,683	2,827	5,996
Number of vehicles (lug-down test)	123,465	390,000	356,185
Number of vehicles (PEMS)	140	933	933
Number of vehicles (OBD)		6,503	6,262
Number of vehicles (plume-chasing)	800	3,070	1,791

The emission inspection standard, *GB 3847-2018*, set two NO_x limits for the lug-down test: limit A, 1500 ppm and limit B, 900 ppm. However, limit B has not been adopted in any province or city in China (MEE and SAMR, 2018). In this study, to avoid abnormal values caused by high-emission trucks, the NO_x emission control performance was assessed using the lug-down test data of diesel trucks compliant with limit A, if not specified.

This study also employed PEMS, OBD, and plume-chasing data from vehicle models covered by periodic emission inspections to validate the accuracy and reliability of the lug-down test data. The validity of the plume-chasing test on low- and high-emission vehicles has been demonstrated previously (Wang et al., 2020). In the consistency analysis of the multi-source test data, the units of NO_x emissions were all converted to ppm based on the relationship between NO_x (g/kg-fuel) and NO_x (ppm) built using the PEMS data, which validated the strong correlation with a correlation factor of 0.97 (R^2). The detailed test data sizes are presented in Table 1.

Results and discussions

NO_x emissions control effectiveness of new vehicle emission standards upgrade

Since the end of the 11th Five-Year Plan, China's new vehicle emission standards have been upgraded thrice, from China III to China VI, with a clear benefit to the reduction of NO_x emission from diesel trucks. Particularly, the NO_x emissions from diesel trucks were significantly reduced with the implementation of China VI standard. By comparing the NO_x concentrations of China IV, V, and VI diesel trucks tested in the emission inspections during 2019–2021, it was found that China IV trucks have comparable NO_x concentration levels to China III trucks, the NO_x concentration of China V trucks was at most 25% lower than that of China IV trucks, and the NO_x concentration of China VI trucks was more than 50% lower than that of China V trucks.

NO_x emissions control effectiveness of in-use vehicle emission control programs

To investigate the NO_x emission control effect of in-use vehicle emission control programs, we evaluated the variation in the NO_x concentration of China IV and China V diesel trucks tested from 2019 to 2021, which were grouped by registration year to limit the impact of deterioration. The NO_x concentrations in China IV diesel trucks increased yearly, significantly for those registered in the early years, with higher deterioration levels. Taking the China IV diesel trucks registered in 2015 as an example, the average NO_x concentration of trucks tested in 2021 was 9.6% higher than that of trucks tested in 2019. However, the NO_x emission trend of China V diesel trucks with varied registration years were opposite to that of China IV trucks. As shown in

Figure 1, there is a clear downward trend in the NO_x concentrations of the China V trucks tested from 2019 to 2021, regardless of the registration year. Considering the China V trucks registered in 2017 as an example, the NO_x concentration decreased on average annually from 1.7% to 10.5%, depending on the GVW categories and vehicle types, which could be explained by the retrofitting of remote OBD system on in-use China V trucks.

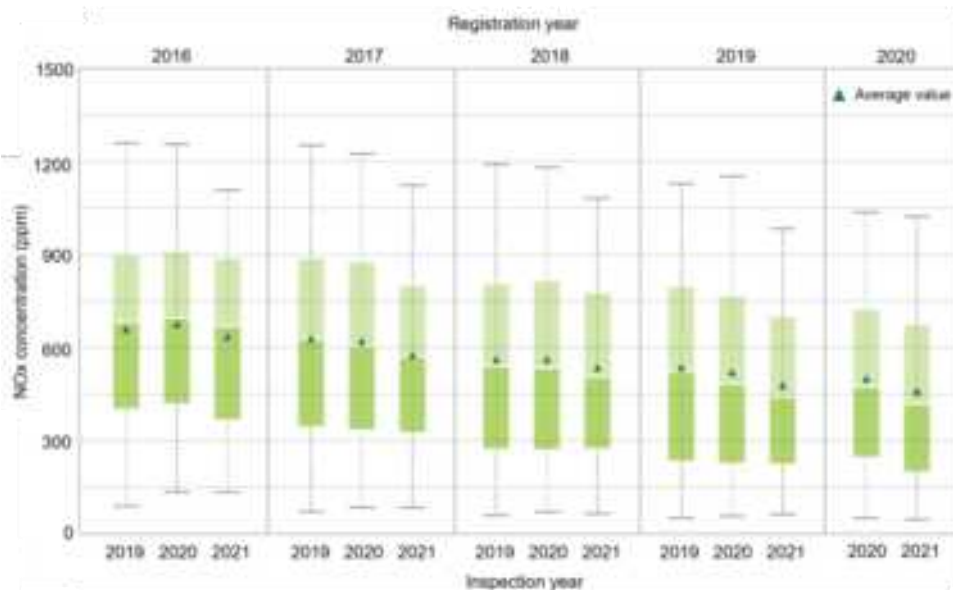


Figure 1: Distribution of NO_x concentrations in China V diesel trucks with varied registration years tested in emission inspections from 2019 to 2021.

Furthermore, we compared the NO_x concentrations of China V diesel trucks that were tested two years after registration but had various registration years. It was found that the NO_x emission control of China V trucks registered after 2018, the initial launch year of the *Action Plan for Diesel Truck Pollution Control*, outperformed trucks registered earlier. Considering HDTs as an example, the average NO_x concentrations of trucks registered in 2018 were 5.8% lower than those of trucks registered in 2017, whereas the average NO_x concentrations of trucks registered in 2019 were 12.1% lower than those of trucks registered in 2018. Therefore, in-use vehicle emission control programs are effective in controlling NO_x emissions from China V diesel trucks but have limit efficiency in controlling NO_x emissions from China IV diesel truck.

NO_x emissions control effectiveness of implementing lug-down test limit B

In the case of currently implemented limit A, less than 3% of the diesel trucks tested in the 2021 emission inspection were identified as high-emission vehicles, that is, non-compliant vehicles, regardless of the emission standard. This suggests that limit A was too lax for identifying high-emission diesel trucks. Limit B would have a higher efficacy in identifying high-emission vehicles, with 34% of China IV trucks, 18.5% of China V trucks, and 4.8% of China VI trucks screened as high-emission vehicles. The high-emission vehicle identification efficacy of limit B in lug-down test is consistent with that of plume-chasing test, which is illustrated in Figure 2. As more high-emission trucks were identified, more trucks must be repaired or scrapped according to the requirements of the I/M program, thus lowering the NO_x concentration level and total NO_x emissions of the diesel truck fleet. If the NO_x concentration in high-emission vehicles identified by limit B is lowered to the limit level (900 ppm) after repair, the average NO_x concentrations in China IV and China V diesel trucks will decrease by 9.6% and 5.8%, respectively. If the high-emission China IV vehicles identified by limit B were replaced by China VI vehicles or battery-electric vehicles, the total NO_x emissions of the diesel truck fleet in 2021 would be reduced by 5.3%–9.7%. Therefore, the implementation of limit B needs to be expedited because of its important role in optimizing truck fleet structure and minimizing NO_x emissions.

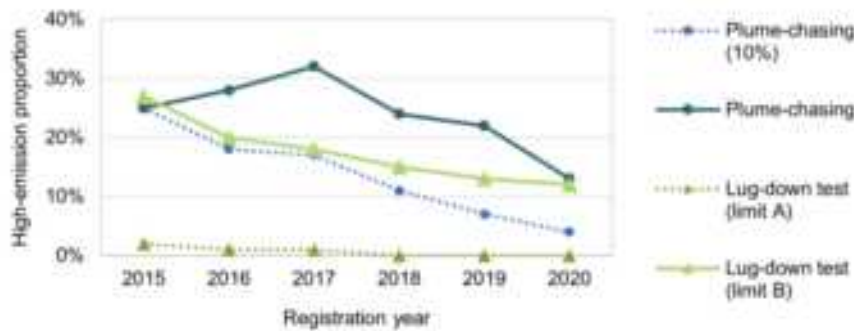


Figure 2: Identification efficacy in high-emission China V diesel trucks of lug-down and plume-chasing tests. There were two high-emission determination thresholds of plume-chasing test: plume-chasing and plume-chasing (10%), which were derived from full test data and the top 10% value, respectively, by balancing the accuracy and efficiency in identifying high-emission China V diesel trucks.

Consistency analysis

As demonstrated in Figure 3, there was good emission trend consistency among the multi-source test data, regardless of emission standards, GVW categories, or vehicle type. The average NO_x concentration of China VI vehicles was 56%–92% lower than that of China V trucks, the NO_x concentration of HDTs was 60%–246% higher than that of LDTs, and the NO_x concentration of tractor trucks was 30%–75% greater than that of straight trucks.

The NO_x concentration derived from the lug-down tests was consistently the highest across the datasets for both the China V and VI trucks. This is largely because of truck idling prior to emission inspection, where lower selective catalytic reduction (SCR) system temperatures are not conducive to emission control, as well as high-load conditions during test, which result in higher emissions. Additionally, compared with China V trucks, China VI trucks demonstrated a smaller gap between the NO_x concentrations of LDTs and HDTs, which could be attributed to distinct aftertreatment technology routes, with a portion of China V LDTs employing EGR and China V HDTs employing SCR, whereas China VI diesel trucks adopted the same SCR technology regardless of LDTs and HDTs, resulting in a smaller variance in emission performance. Furthermore, the average NO_x concentration of tractor trucks with the same emission standard was 30%–75% higher than that of straight trucks, which could be attributed to the comparably lower operating efficiency of SCR systems in tractor trucks.

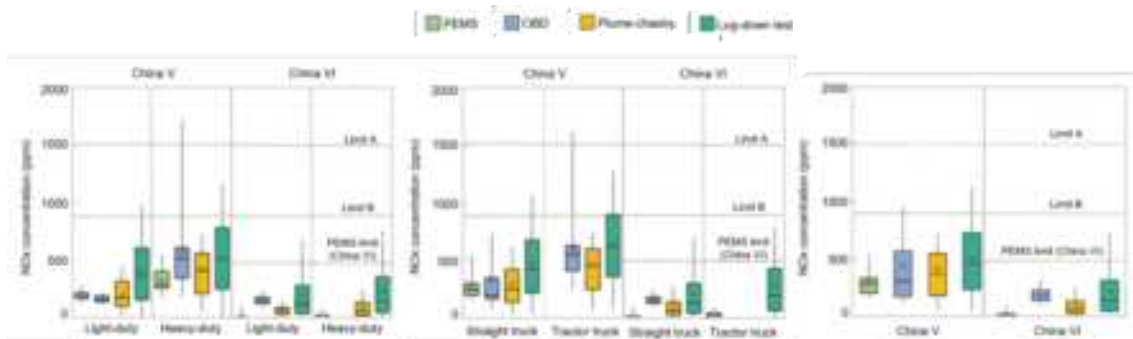


Figure 3: NO_x emissions trend from multi-source test data of diesel trucks grouped by emission standards, GVW categories, and vehicle types.

Conclusions

In this study, the NO_x data from the lug-down test were validated with good consistency across many data sources, including PEMS, OBD, and plume-chasing tests. Based on valid lug-down test data, adequate samples were selected to evaluate the effectiveness of NO_x emission control programs for diesel trucks, with a focus on two aspects: emission standard upgrades for new vehicles and the enhancement of in-use vehicle emission control programs.

New vehicles emission standards upgrade, particularly the implementation of the China VI standard, have resulted in a significant decrease in the NO_x emission concentrations of diesel trucks. The NO_x concentrations of China V diesel trucks are up to 25% lower than those of China VI trucks, whereas the concentrations of China VI trucks are more than 50% lower than those of China V trucks. In-use vehicle emission control programs have effectively reduced NO_x emissions from China V diesel trucks. Based on a time-series comparison, it was found that the average NO_x concentrations of China V diesel trucks decreased on average annually by 1.7%–10.5% across the different GVW categories and vehicle types. Furthermore, the NO_x concentrations in trucks registered after 2018 were significantly lower than those registered before 2018. However, the NO_x emissions from China IV diesel trucks are too challenging to regulate in the context of the current in-use vehicle emission control programs.

Limit A of the lug-down test in periodic emission inspections is deemed ineffective for controlling NO_x emissions, as less than 3% of diesel trucks with different emission standards are identified as high-emission vehicles. Limit B, however, identifies more high-emission vehicles, with a high-emission proportion of 34% for China IV trucks, 18.5% for China V trucks, and 4.8% for China VI trucks, implying that more vehicles would be repaired to be compliant or replaced with cleaner vehicles. If the high-emission vehicles identified by limit B were repaired to decrease the NO_x concentration to the limit of level B (900 ppm), the average NO_x concentrations of China IV and China V diesel trucks would decrease by 9.6% and 5.8%, respectively. If the high-emission trucks identified by limit B are replaced with China VI trucks or battery-electric trucks, the total NO_x emissions of diesel trucks in 2021 would be reduced by 5.3%–9.7%. Currently, several provinces and cities in China have issued plans to phase out in-use China IV vehicles. In these areas and others with large stocks of China IV diesel trucks, the implementation of limit B needs to be expedited to serve as an enabling tool to optimize the fleet structure and minimize NO_x emissions, thus further contributing to the synergistic reductions in PM_{2.5} and O₃ as well as the improvement of urban air quality in China.

In the future, the lug-down test in identifying high-emission vehicles in diesel trucks with gradually lower NO_x concentrations as the emission standards upgrade, should be continually validated using multi-source test data, to ensure the high-efficiency of in-use vehicle emission control programs in reducing NO_x emissions from diesel trucks.

References

- Chen R.J., Samoli E., Wong C.M., et al. (2012). Associations between short-term exposure to nitrogen dioxide and mortality in 17 Chinese cities: The China Air Pollution and Health Effects Study (CAPES), *Environment International*, 45, 32–38.
- Hao L.J., Yin H., Wang J. F., et al. (2022). Research on Analysis Method of Remote Sensing Results of NO Emission from Diesel Vehicles, *Atmosphere*, 13, 1100.
- Li K., Jacob D.J., Liao H., et al. (2019). A two-pollutant strategy for improving ozone and particulate air quality in China, *Nat. Geosci.*, 12, 906–910.
- Li S., Wang S.X., Wu Q.R., et al. (2023). Emission trends of air pollutants and CO₂ in China from 2005 to 2021, *Earth Syst. Sci. Data*, 15, 2279–2294.
- MEE (Ministry of Ecology and Environment, P.R.C.), NDRC (National Development and Reform Commission, P.R.C.), MIIT (Ministry of Industry and Information Technology, P.R.C.), et al. (2018). Action Plan for Diesel Truck Pollution Control (in Chinese).
- MEE (Ministry of Ecology and Environment, P.R.C.), SAMR (State Administration for Market Regulation, P.R.C.). (2018). Limits and measurement methods for emissions from diesel vehicles under free acceleration and lugdown cycle (GB 3847-2018) (in Chinese).

- MEE (Ministry of Ecology and Environment, P.R.C.), SAMR (State Administration for Market Regulation, P.R.C.). (2018). Limits and measurement methods for emissions from diesel fuelled heavy-duty vehicles (CHINA VI) (GB 17691-2018) (in Chinese).
- MEE (Ministry of Ecology and Environment, P.R.C.). (2022). China Mobile Source Environmental Management Annual Report 2022.
- Pye H.O.T., Appel K.W., Seltzer K.M., et al. (2022). Human-health impacts of controlling secondary air pollution precursors, *Environmental Science & Technology Letters*, 9(2), 96-101.
- Richter, A., Burrows, J., Nuß, H., et al. (2005). Increase in tropospheric nitrogen dioxide over China observed from space, *Nature*, 437, 129–132.
- Shaw S., Van Heyst B. (2022). An Evaluation of Risk Ratios on Physical and Mental Health Correlations due to Increases in Ambient Nitrogen Oxide (NO_x) Concentrations, *Atmosphere*, 13, 967.
- State Council (the State Council, P.R.C.). (2019). Regulations of the People's Republic of China on the Implementation of the Road Traffic Safety Law (in Chinese).
- Wang H., Wu Y., Zhang, K.M., et al. (2020). Evaluating mobile monitoring of on-road emission factors by comparing concurrent PEMS measurements, *Science of The Total Environment*, 736, 139507.
- Wei W., Li Y., Ren Y.T., et al. (2019). Sensitivity of summer ozone to precursor emission change over Beijing during 2010–2015: a WRF-Chem modeling study, *Atmospheric Environment*, 218, 116984.
- Wu Y., Zhang S.J., Hao J.M., et al. (2017). On-road vehicle emissions and their control in China: A review and outlook. *Science of the Total Environment*, 574, 332-349.
- Xu G.Y., Shan W.P., Yu Y.B., et al. (2023). Advances in emission control of diesel vehicles in China, *Journal of Environmental Sciences*, 123, 15-29.
- Zhang S.J., Zhao P., He L.Q., et al. (2020). On-board monitoring (OBM) for heavy-duty vehicle emissions in China: Regulations, early-stage evaluation and policy recommendations, *Science of The Total Environment*, 731, 139045.

Assessment of a NOx Measurement Procedure for Periodic Technical Inspection (PTI) of Light-Duty Diesel Vehicles

Jacopo Franzetti¹, Tommaso Selleri^{1,2,*}, Christian Ferrarese¹, Anastasios Melas¹, Dario Manara¹, Barouch Giechaskiel¹ and Ricardo Suarez-Bertoa^{1,*}

¹ Joint Research Centre (JRC), European Commission, 21027, Ispra, Italy

² European Environment Agency (EEA), 1050 Copenhagen, Denmark

ricardo.suarez-bertoa@ec.europa.eu; tommaso.selleri@eea.europa.eu

Introduction

Periodic technical inspection (PTI) of vehicles promotes road safety and environmental protection. Indeed, PTI is also used to verify the proper functioning of the vehicle aftertreatment system (ATS) over its lifetime. During PTI, the emissions of every vehicle circulating are checked for opacity (if it is a Diesel vehicle) or CO levels (in case of spark ignition engines). The compliance with PTI requirements are the responsibility of the car owner. While the current Directive 2014/45/EU, which covers the PTI, does not require NOx emissions measurement, the ongoing revision of the roadworthiness package aims at including new methods for measuring exhaust NOx and particle number (PN) emissions.

PTI tests are required to be simple, quick, inexpensive and effective. Due to the variety of de-NOx aftertreatment technologies (Selleri et al. 2021) in the current Diesel fleet, it becomes difficult to define a simple, quick, inexpensive and still robust technique able to verify proper functioning of the overall ATS.

Herein, a new procedure for the identification of selective catalytic reduction (SCR) unit malfunctioning in modern Diesel vehicles during PTI is assessed. The focus is on post-RDE (real-driving emissions) regulation light-duty Diesel vehicles (Euro 6d and 6d-TEMP) where SCR units are ubiquitous. The procedure is based on the functioning principles of the SCR and its capability to efficiently reduce NOx emissions at low idling when appropriately conditioned.

Experimental

Seven vehicles were tested at Vehicle Emissions Laboratories (VELA) of the Joint Research Centre (JRC) of the European Commission. All of them met post-RDE emission standards. Table 1 summarises the main characteristics of the vehicles tested. Vehicle #1 was tested a second time, at a later stage, with a malfunction in the urea injector (referred to as vehicle #1b). This condition was exploited to assess a real case of SCR system malfunctioning.

A summary of the NOx measurement equipment used and their working principle is presented in Table 2. Laboratory equipment included a MEXA 7400 bench analyser and a MEXA 7100 bench analyser (HORIBA, Kyoto, Japan), a MEXA ONE bench analyser (HORIBA, Kyoto, Japan) and an AMA i60 bench (AVL, Graz, Austria). All the analysers were equipped with a chemiluminescence detector (CLD). In addition to laboratory-grade equipment, Portable Emission Measuring Systems (PEMS) were also used, including: an AVL MOVE (AVL, Graz, Austria) PEMS with a non-dispersive ultra-violet sensor (NDUV) and an HORIBA OBS ONE PEMS equipped with a CLD.

Table 1: Summary of vehicles tested.

#	Fuel	Displacement (cm ³)	Registration	Emission control system	Vehicle category	Euro standard
1	B7	1968	2019	EGR, DOC, DPF, SCR	N1 Class III	Euro 6d-TEMP-EVAP-ISC
2	B7	1995	2021	EGR, DOC, DPF, SCR	N1 Class III	Euro 6d-ISC-FCM
3	B7	1997	2019	EGR, DOC, DPF, SCR	M1	Euro 6d-TEMP-EVAP-ISC
4	B7	2184	2021	EGR, DOC, DPF, SCR	N1 Class III	Euro 6d-ISC-FCM
5	B7	1968	2020	EGR, DOC, DPF, SCR	M1	Euro 6d-ISC-FCM
6	B7	1499	2020	EGR, DOC, DPF, LNT, pSCR	M1	Euro 6d-TEMP-EVAP-ISC
7	B7	1998	2020	EGR, DOC, DPF, LNT, SCR	M1	Euro 6d-ISC-FCM

EGR: exhaust gas recirculation, DOC: diesel oxidation catalyst, DPF: diesel particulate filter, SCR: selective catalytic reduction, LNT: lean NOx trap, pSCR: passive SCR.

Table 2: Summary of the measurement equipment used. On-vehicle NOx sensors were used when available from OBD port.

Vehicle #	1	2	3	4	5	6	7
Laboratory	HORIBA MEXA 7400 - CLD			HORIBA MEXA ONE - CLD	HORIBA MEXA 7400 - CLD	AVL AMA i60 - CLD	HORIBA MEXA ONE - CLD
PEMS	AVL MOVE - NDUV	AVL MOVE - NDUV	AVL MOVE - NDUV	HORIBA OBS ONE - CLD			
OBD NOx sensors	X	X		X			X

* CLD: chemiluminescence detector, OBD: On board diagnostics, NDUV: non-dispersive ultra-violet sensor.

Hot idling procedure

The procedure assessed in this work aims at identifying, during a PTI, modern Diesel vehicles that present a malfunctioning SCR unit and therefore excess emissions of NOx. A malfunctioning SCR system would result in undesired high NOx emissions. The test procedure is also presented schematically in Figure 1 for better understanding and it consists of two main phases:

- 1) vehicle warm-up phase, in order to ensure that SCR unit temperature is high enough to trigger NOx reduction activity;
- 2) hot idling phase, where NOx emissions are measured at tailpipe.

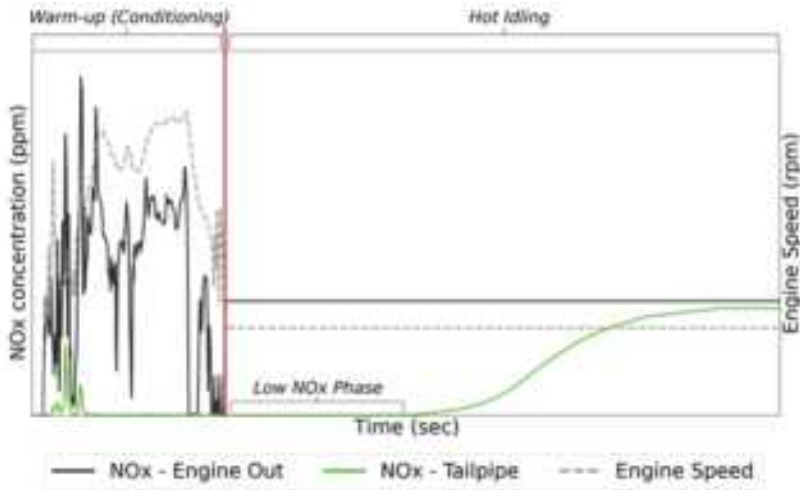


Figure 1: Simplified schematic representation of the hot idling procedure. NOx concentration and engine speed displayed are indicative.

During the hot idling phase, unless there is a SCR unit malfunction, NOx tailpipe level are expected to be low for few minutes where the SCR keeps reducing the NOx emissions (referred as low NOx phase – from hot idle start till tailpipe NOx concentration >1 ppm). During the low NOx phase, the NOx reduction takes place due to their reaction with NH₃, which is available because the urea injection continues during vehicle hot idling or because it remains stored on the catalyst during the warm-up phase (Czerwinski et al., 2019; Selleri et al., 2022; Giechaskiel et al., 2022). Both cases would suggest an SCR that is properly functioning, allowing to exclude a malfunctioning of the system. After the low NOx phase a gradual NOx increase at tailpipe is expected with time, since NH₃ stored previously in the SCR is progressively consumed and/or SCR unit temperature is not sufficiently high to have a reaction even though there is still stored NH₃.

Functioning vs. Malfunctioning SCR system

Figure 2 shows the NOx emission profiles of vehicles #1 and #1b during the hot idling test. Figure 2a shows NOx emission profile for vehicle #1, equipped with a well-functioning SCR unit: low NOx tailpipe concentration lasted ca. 81 sec. Then, NOx concentration gradually increased reaching values (~86 ppm) comparable with the levels observed at engine out steady state emission (99 ppm). Figure 2b plots NOx emission profile for vehicle #1b, with urea injection system not working: NOx concentration increased by more than 45 ppm right since the idling start, not following the pattern observed for the same vehicle with a properly functioning SCR.

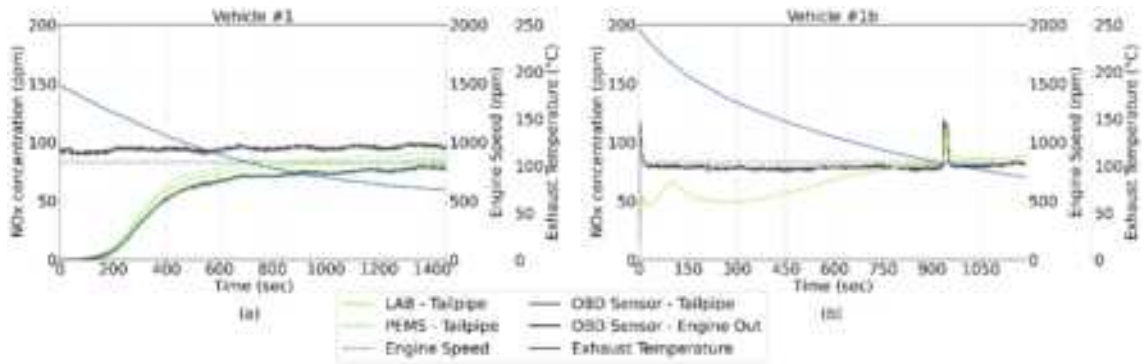


Figure 2: NOx emission profiles of vehicle #1 (a) and vehicle #1b – vehicle #1 with Diesel Exhaust Fluid (DEF) injector not working - (b) during the hot idling test. NOx tailpipe concentration measured by laboratory-grade CLD NOx analysers (solid light green line) and vehicle NOx engine out (solid dark green line) concentrations are displayed together with vehicle engine speed (dashed grey line) and exhaust temperature (solid blue line line) for both vehicles.

The average low NOx duration (<1 ppm) for all tests was 363 sec, ranging from 81 sec for vehicle #1 to 544 sec for vehicle #2 (see Table 3). To provide additional insight on the NOx increase time, Table 3 also presents the time required for the NOx tailpipe concentration to reach 10 ppm and 20 ppm from idle start. For all the vehicles the time needed increased. For example, for vehicle #1 it increased to 199 sec to reach 10 ppm of tailpipe NOx concentration and to 245 sec for 20 ppm.

The low NOx duration obtained from the tested vehicles (81 – 544 sec), together with the immediate increase of NOx at tailpipe for the malfunctioning vehicle #1b, suggest that a short measurement time span (e.g., between 15 and 45 seconds) would suffice to distinguish between a vehicle with a properly operating or a malfunctioning SCR. Such a short measurement time would support the PTI criteria of having a quick test.

Table 3: Low NOx phase duration, time required for NOx tailpipe concentration to reach 10 ppm and 20 ppm (except for vehicle #3 for which the test was stopped before those concentrations were reached) and NOx engine out average concentration measured during hot idling.

Vehicle	#1	#2		#3	#4		#5
	Test 1	Test 1	Test 2	Test 1	Test 1	Test 2	Test 1
Low NOx phase < 1 ppm (sec)	81	460	544	246	496	301	412
NOx < 10 ppm (sec)	199	591	709	598	573	421	571
NOx < 20 ppm (sec)	245	671	812		610	542	671
NOx Engine Out ave. conc. (ppm)*	99	118 (81)	135 (100)		187 (46)	224 (41)	96 (63)

* Engine out values were recorded at the OBD port for those vehicle where the NOx engine out sensor signal was available (except for vehicle #5 where NOx at engine out was measured with a laboratory analyser). For those vehicles where engine out concentration changed during the idle two values are reported: the maximum concentration period average and in brackets the lowest. When two tests were performed on the same vehicle the results were both reported.

Challenges

Figure 3 shows the NOx emission profiles of vehicles #6 and #7 during the hot idling test. In particular, Figure 3a shows vehicle #7 NOx tailpipe emission profile and engine speed, together with the NOx sensor signal at the LNT outlet and Figure 3b shows the NOx tailpipe emission profile and engine speed for vehicle #6 following the hot idling procedure. At a first glance, vehicle #7 NOx concentration profile at the LNT outlet is analogous to the one discussed above, low NOx values were observed at the hot idle start, <1 ppm for 340 sec. However, this behaviour is related to a different principle, namely NOx adsorption (Forzatti et al., 2015). The NOx increase at the LNT outlet is damped by the operation of the two SCRs and the effect is visible on the NOx concentration at the tailpipe only delayed in time. Vehicle #6 is equipped with an LNT and a passive SCR unit (pSCR), relying on the NH₃ emitted by the LNT during its regeneration (Hou et al., 2012). The trend illustrated in Figure 3b for vehicle #6 is analogous to the one presented above in case of active SCR unit (with DEF injection, commercially known in Europe as AdBlue). Also the NOx values observed are consistent with the ones described in Table 3: low NOx values were observed at the hot idle start, <1 ppm for 639 sec. NOx concentration then gradually increase up to ~148 ppm.

Finally, the presence of an LNT in the ATS could, under certain situations, limit determining whether or not the SCR unit has DEF dosing malfunction under the hot idling procedure studied for two main reasons: (i) LNT may adsorb NOx emissions during the length of the hot idle test keeping the concentrations low; (ii) even without DEF dosing the SCR unit could be active reducing NOx using the NH₃ released by LNT.

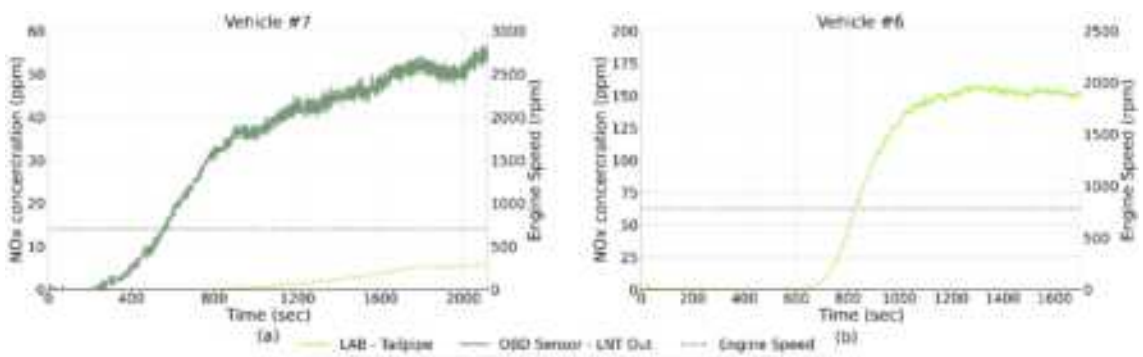


Figure 3: NOx concentration profiles at tailpipe (solid light green line) from vehicle #7 (a) and #6 (b) during hot idling test. (a) also includes NOx sensor signal at the LNT outlet (solid dark green line), available at the OBD port. Engine speed (dashed grey line) is reported on the secondary axis.

Conclusions

Seven light-duty vehicles fulfilling post-RDE Euro 6 requirements and equipped with selective catalytic reduction SCR unit/s were tested following a hot idling procedure designed for NOx Periodical Technical Inspections (PTI). The test consists of two phases: (i) a vehicle warm-up phase, ensuring that the SCR unit temperature is high enough to trigger NOx reduction activity and (ii) a hot idling phase where NOx emissions are measured at the tailpipe. The aim is to identify malfunctioning SCR units that would result in high NOx emitting vehicles. For well-functioning SCR units, a consistent NOx pattern was observed: low tailpipe NOx concentration at the hot idle start, then gradually increasing with time to values comparable to engine out levels. A well-functioning SCR unit will continue to reduce NOx as long as the temperature is high enough and that there is ammonia in the system to reduce them. Malfunctioning SCR unit resulted instead in high NOx tailpipe emissions, closer to engine out levels, from the idling phase start. This suggests that hot idling procedure could be effectively used to discriminate between functioning and malfunctioning SCR systems. Finally, the average low NOx concentration duration (<1 ppm) for all tests was 363 sec, the minimum 81 sec and the maximum 544 sec. Shorter time spans (e.g. from 15 to 45 sec) may also be used as PTI measurement period. Future steps will focus on: the investigation of the vehicle conditioning (warm-up phase definition), the detection of actual malfunctioning vehicles equipped with ATS including an LNT in their configuration and the definition of an effective and robust pass/fail criteria.

Acknowledgements

The authors would like to acknowledge the support and collaboration of JRC VELA technical staff.

References

- Czerwinski, J., Comte, P., Engelmann, D., Mayer, A. et al. (2019). Considerations of Periodical Technical Inspection of Vehicles with deNOx Systems, *SAE Technical Paper 2019-01-0744*.
- Forzatti, P., Lietti, L. & Castoldi, L. (2015). Storage and Reduction of NO_x Over LNT Catalysts. *Catal Lett*, 145, 483–504.
- Giechaskiel, B., Selleri, T., Gioria, R., Melas, A.D., Franzetti, J., Ferrarese, C., Suarez-Bertoa, R. (2022). Assessment of a Euro VI Step E Heavy-Duty Vehicle Lean Exhaust deNOx system. *Catalysts*, 12, 1230
- Hou, X., Schmieg, S. J., Li, W., & Epling, W. S. (2012). NH₃ pulsing adsorption and SCR reactions over a Cu-CHA SCR catalyst. *Catalysis today*, 197, 1, 9-17.
- Selleri, T., Melas, A.D., Joshi, A., Manara, D., Perujo, A., Suarez-Bertoa, R. (2021). An Overview of Lean Exhaust deNOx Aftertreatment Technologies and NOx Emission Regulations in the European Union. *Catalysts*, 11, 404.
- Selleri, T., Gioria, R., Melas, A.D., Giechaskiel, B., Forloni, F., Mendoza Villafuerte, P., Demuyck, J., Bosteels, D., Wilkes, T., Simons, O., et al. (2022). Measuring Emissions from a Demonstrator Heavy-Duty Diesel Vehicle under Real-World Conditions—Moving Forward to Euro VII. *Catalysts*, 12, 184.

Statistical evaluation of Conformity of Production of road vehicles⁴

M.A. Ktistakis¹, J. Suarez², J. Pavlovic¹, D. Komnos², B. Ciuffo², A. Marotta², and G. Fontaras^{2*}

¹ FINCONS Group, Vimercate, 20871, Italy

² European Commission, Joint Research Centre (JRC), Ispra, 21027, Italy, *georgios.fontaras@ec.europa.eu

Introduction

European Union (EU) requires that road vehicles are certified for their CO₂ emissions over a laboratory test cycle (a process that is part of vehicle type approval). The certified CO₂ emissions values are used for monitoring and emissions target compliance purposes in addition to user information, taxation and other purposes, hence they play an important role in the introduction of vehicle within the EU market (European Commission, 2023). The test was based on the New European Driving Cycle (NEDC) (European Commission, 2007) until 2020 and has since been replaced by the Worldwide Harmonized Light Vehicles Test Procedure (WLTP) (European Union, 2017). Initially, this approval process involves testing a limited number of vehicle prototypes. When a group of vehicles successfully meets the stipulated criteria, they are granted type approval, validating their compliance with EU regulations and allowing them to enter the market.

To ensure the accuracy and representativeness of certified CO₂ emissions and energy consumption data for EU vehicles, the European Commission has instituted validation mechanisms. Among them are the Conformity of Production (CoP) tests, an ongoing process ensuring quality and standards throughout the vehicle production lifecycle. A central objective of the CoP is to verify that the CO₂ emissions measured in production vehicles align with the values declared by the manufacturer for that specific vehicle in the vehicle's certificate of conformity (CoC). These values are interpolated from the type approval tests conducted on the best and worst case prototype vehicle of the same vehicle CO₂ family. Notably, manufacturers have the option to declare CO₂ emissions that exceed those measured in the type approval procedure. These declared emissions are every year reported to the Commission for each new vehicle registered in the EU and used to assess manufacturers' compliance with annual targets (European Union, 2019).

Until the end of 2022, the CO₂ emissions of Light-Duty Vehicles (LDVs) under the CoP framework have been evaluated using a sequential sampling schema. This method, while operational, exhibits an inherent flaw: the pass and fail thresholds almost coincide. As a result, pass or fail decisions are almost invariably determined with the minimum sample size of just 3 vehicles. This characteristic hinders the sample mean from effectively converging towards the population mean. Moreover, manufacturers have often opted to over-declare CO₂ emissions by up to 5% (Chatzipanagi et al., 2020), a strategy aimed at reducing the risk of CoP failure. This practice has cast a shadow on the efficacy of EC's annual targets, manifesting notably in an artificial increase in post-2020 CO₂ targets.

In view of these concerns, the Joint Research Centre (JRC) has formulated an enhanced sequential sampling schema to address the shortcomings identified in the statistical assessment of CoP tests. This advanced method has been formally incorporated into the Regulation and, has been in practice since 2023, endorsed by the authorities responsible for type approval to ensure manufacturers' adherence. The enhanced sampling schema is also being proposed for broader integration across various dimensions of the EU's regulatory framework, thereby establishing a comprehensive approach to CO₂ compliance. The scope of application encompasses both LDVs and Heavy-Duty Vehicles (HDVs). Certain proposals have already been embraced, exemplified by the CO₂ accuracy requirements of On-Board Fuel and Energy Consumption Monitoring (OBFCM) devices within LDV CoP. Other initiatives are progressing towards final implementation stages, notably including the validation of CO₂ emissions for in-service LDV vehicles. Furthermore, initial strides have been taken in other part of vehicle certification regulation such as the In-Service Verification (ISV) statistical evaluation for HDVs.. This study explores the application of the sequential sampling method in verifying CO₂ emissions during the CoP process for LDVs within the EU, highlighting its significance in improving CoP accuracy. By exploring the method's inception, evolution, and impact, a more comprehensive understanding of CO₂ compliance assessment is achieved.

⁴ The opinions expressed in the paper are purely those of the authors and shall not be considered an official European Commission position under any circumstance.

Methodology

The former problematic methodology utilised in the CoP for LDVs and the currently adopted approach both incorporate sequential sampling methods. Sequential sampling is distinct from conventional sampling methods due to its unique characteristic of not being reliant on a predetermined sample size. Instead of waiting for a fixed number of samples to accumulate, sequential sampling continuously evaluates emerging data, allowing for more efficient resource utilisation and heightened efficiency. This approach strikes a balance between statistical precision and practical efficiency, making it a valuable tool in decision-making processes and quality control. Furthermore, this dynamic approach allows for adjustments to sample size and decision-making criteria through ongoing data analysis, ensuring both efficiency and well-informed outcomes. Thresholds, depending on the sample size, are established to guide decision-making. If the data strongly support a particular decision, the sampling process concludes; otherwise, it continues until conclusive evidence is obtained. A predefined initial and maximum sample size provide flexibility within a structured framework.

The CoP procedure for LDVs operates at a group level, organised into CoP families that correspond to planned annual production volumes of over 1,000 vehicles. Furthermore, the flexibility to consolidate smaller families is permitted. The sampling frequency is tailored to production scale, a design ensuring a systematic and effective assessment of CO₂ emissions conformity. This approach guarantees a comprehensive evaluation, contributing to the overall quality and precision of CO₂ compliance verification within the LDV manufacturing process.

Previous statistical framework for CoP

For each family, the process started with an initial random sample of $N = 3$ vehicles selected from the production line. These vehicles underwent testing, where their CO₂ emissions and/or electric consumption were measured in a laboratory setting. Subsequently, these measured values underwent normalisation by dividing them by each vehicle's official/declared value. The decision-making criteria relied upon both the mean value (X_{tests}) and the sample variance (Var) of the normalised values. The outcomes encompassed three possibilities:

1. If $X_{tests} < A - Var$, the family passed.
2. If $X_{tests} > A - \frac{N-3}{13} \times Var$, the family failed.
3. Otherwise, another vehicle underwent testing, increasing the sample size by 1, and subsequently recalculating the mean and variance.

This iterative procedure continued until a conclusive pass or fail decision was reached. Notably, the maximum sample size was capped at 16 vehicles, beyond which the pass and fail boundaries aligned at A. Here, A was set at 1.01, serving as a safety margin to account for the measurement inaccuracies.

However, this method suffers from a significant drawback: the variance of the normalised values is notably small, typically ranging from 10^{-3} to 10^{-4} . As a result, the pass and fail boundaries nearly coincide, leading in an almost binary decision pattern involving just three vehicles. To elaborate, if the average ratio surpasses 1.01, the result is a fail, while a value below triggers a pass (as illustrated in Figure 1). Consequently, a decision is nearly always reached with only three vehicles. This scenario renders the adoption of a sequential sampling method unnecessary and prevents the sample mean from effectively converging to the population mean, given the consistent three-vehicle outcome. Moreover, a critical issue emerges: there exists a substantial likelihood that if the manufacturer truthfully declares the actual CO₂ emissions and adheres to EC regulations during the type approval procedure, the family of vehicles might fail. This predicament arises due to the error margin, denoted by the factor A, which is set at 1%, potentially falling short when compared to the often-higher variability observed in production lines.

Consequently, OEMs over-declared the CO₂ emissions during the type approval process, thereby minimising the chances of both a family's failure and the testing of more than three vehicles in the CO₂ emissions CoP procedure. The statistical limitations of the previous methodology are visually represented in Figure 1, where the pass and fail boundaries are illustrated. The blue line on the graph portrays the distribution of the sample mean of three vehicles from a simulated dataset. This dataset is assumed to follow a normal distribution with a mean equal to 0.95 and a standard deviation of 2%. The pass and fail boundaries are so close in the graph that the difference between them is not even visible, demonstrating the challenge of making decisions based on a small sample size and leading to an almost binary outcome in many cases.

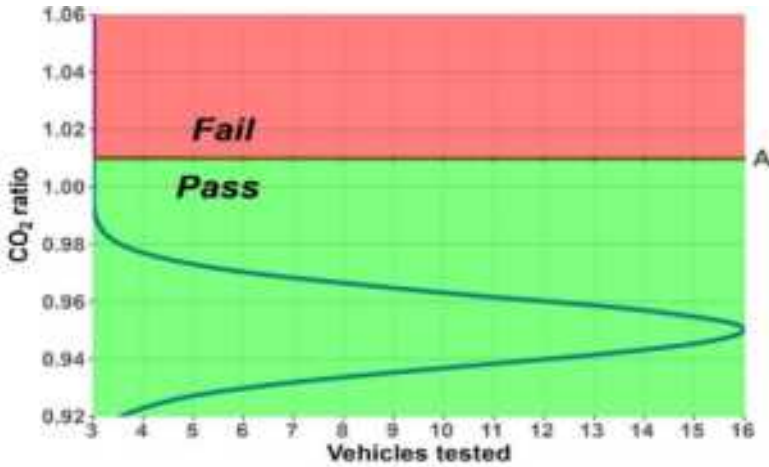


Figure 1: Illustration of the old method.

Innovative statistical framework for CoP

To overcome this, JRC has developed an improved sequential sampling approach that addresses the shortcomings identified in the CoP's statistical evaluation, while fulfilling the following essential criteria:

- Statistical Soundness: Pass and fail decisions are grounded in robust statistical criteria.
- Balanced Risk: Optimal balance between consumers' and manufacturers' risks is achieved by controlling false fail and false pass rates.
- Testing Efficiency: The testing burden is minimised by reducing the number of vehicles tested, while maintaining procedure robustness.
- Resilience against Excess CO₂: The method safeguards against scenarios where CO₂ emissions measured within CoP ($CO_{2,COP}$) significantly exceed the respective declared values ($CO_{2,DV}$): $If CO_{2,COP} \gg CO_{2,DV}$
 $CO_{2,DV} \text{ fail} \Leftrightarrow \text{if } \frac{CO_{2,COP}}{CO_{2,DV}} \gg 1 \text{ fail}$

The proposed validation criteria of this method are rooted in the expected statistical variability of a limited sample of observations' mean value, as it converges towards the population average with increasing tests. This decision procedure recognises the uniqueness of each family by demarcating distinct pass and fail regions, dependent on its variability, leading to diverse decisions. Similar to the previous method, the measured to declared CO₂ emissions ratio is examined, with vehicles categorised into CoP families. The family criteria for pass and fail are defined as follows:

The pass and family criteria are the following:

1. If $X_{tests} \leq A - (t_{P1,i} + t_{P2,i})$, then the family passes.
2. If $X_{tests} > A + (t_{F1,i} - t_{F2,i})$, then the family fails.
3. Otherwise, another vehicle undergoes testing, increasing the sample size by 1, followed by recalculating the sample mean (X_{tests}) and standard deviation (s).

Key factors influencing the pass and fail rates are:

- Maximum Number of Tested Vehicles: The maximum allowable sample size before a decision is reached significantly impacts the conclusion's speed, with lower limits accelerating decisions at the expense of reduced confidence and increased risk.
- A Factor: The A factor is crucial, accounting for uncertainties like measurement inaccuracies and the potential high costs of failure. It sets the pass/fail boundary after testing the maximum number of vehicles.
- Pass and fail coefficients ($t_{P1,i}$, $t_{P2,i}$, $t_{F1,i}$ and $t_{F2,i}$) play a pivotal role in determining the decision speed – the number of vehicles tested before a pass or fail decision.

- Family Mean Value (Bias): The average difference between CO₂ emissions measured within CoP and the official values, encompassing the average over-declaration.
- Family Standard Deviation: This factor reflects the variability of the ratio, influenced by measurement errors and repeatability.

Following an extensive cost-benefit analysis utilising data provided by type approval authorities and simulations, the following parameters were selected: a maximum allowable sample size of 16 vehicles, an A factor set at 1.01, and specific pass and fail coefficients detailed in Table 2 of the Annex. Furthermore, a minimum sample size of three was retained, as this represents the threshold for achieving a meaningful standard deviation.

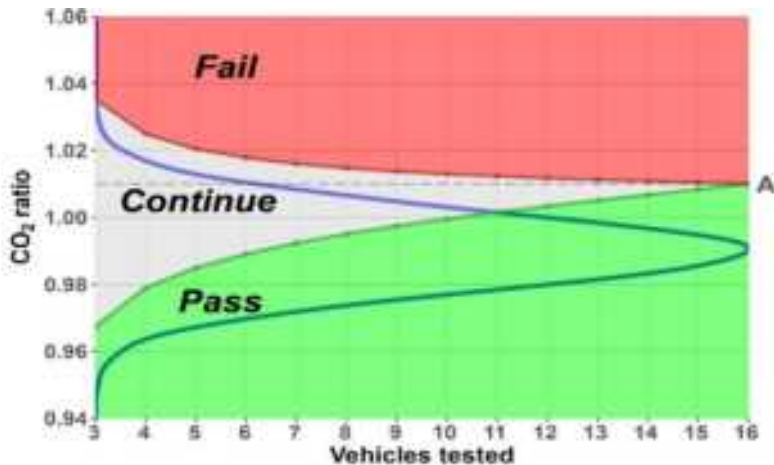


Figure 2: Illustration of the new method

The fail and pass thresholds are illustrated in Figure 2. If the calculated average falls below the pass threshold (denoted by the green region) or exceeds the fail threshold (indicated by the red region), the procedure concludes, resulting in a family pass or fail, respectively. Alternatively, if the calculated average falls within the grey region, an additional vehicle is incorporated into the sample, and the process continues until a conclusive pass or fail determination is reached. Figure 2 demonstrates the boundaries for a representative family with a population standard deviation of 2%. The boundaries are depicted for a theoretical example where the sample standard deviation is always 2%, which will not be exactly the case, however it should fluctuate around this variability. Conspicuously, greater variability expands the grey region, indicating a more prolonged decision-making process. Regardless of variability, the pass and fail boundaries converge to the A factor after 16 tests. The family's pass and fail rates depend on the ratio distribution (blue line) and the boundaries which in turn are dependent of the sampling standard deviation of the tested vehicles.

Table 1 presents the pass rates for both the previous methodology and the proposed one. Apparently, the former approach consistently rendered pass or fail verdicts with just three or four vehicles. This is evident from the fact that the cumulative pass rate achieved with four tests is equivalent to the overall pass rate obtained from 16 tests. For instance, under the assumption of a 1% over-declaration for a family with a 2% standard deviation, the old method yielded a total pass rate of 96% (which represents the pass rate after all vehicles are tested). Strikingly, this same pass rate of 96% is achieved even when testing only 3 or 4 vehicles using the previous approach. In contrast, the new proposal gradually escalates pass and fail outcomes. With a 1% over-declaration and reasonable variability, manufacturers have ensured passes (100% total pass rate). This strategy minimises the occurrence of false fails. Conversely, even a 1% under-declaration causes the total pass rate to drop below 50%, an unacceptable scenario for manufacturers. Consequently, the false pass rate is also managed, ensuring a low level of risk for consumers.

Table 1: Pass rates for a population with standard deviation of 2%

Mean (bias)	Cumulative vehicles	Old method	New method
0.95 (5% over-declaration)	4	100	98
	16	100	100
0.99 (1% over-declaration)	4	96	42
	16	96	100
1.00 (0% over-declaration)	4	80	16
	16	80	95
1.01 (1% under-declaration)	4	49	3
	16	49	38

Discussion

The sequential sampling approach introduces pass and fail criteria that effectively balance consumer and manufacturer risks, reducing false fail and false pass rates. This approach dynamically adjusts sample size through continuous data analysis, optimising resource utilisation while maintaining decision-making reliability.

The new methodology significantly enhances CO₂ compliance assessment across regulatory aspects, spanning both Light-Duty and Heavy-Duty Vehicles. The study lays the groundwork for addressing evolving challenges such as pollutant emissions and energy consumption. It is important to acknowledge that this overview captures key insights while omitting the intricate stages and complexities involved in the actual process. Furthermore, the extensive dataset provided by type approval authorities, which played a pivotal role in validating and refining the method, is not presented here.

The analysis of the new method reveals notable improvements over the previous approach. As elucidated in Table 1, even a 1% over-declaration leads to a total pass rate approaching 100%, showcasing a remarkable equilibrium between effective risk management and safeguarding consumer interests. Conversely, it is noteworthy that a minor 1% under-declaration can lead to considerably low pass rates, underscoring the fine line manufacturers tread in ensuring compliance. In conclusion, the advanced approach enhances CO₂ emissions compliance evaluation, benefiting both manufacturers and consumers, while acknowledging the need for ongoing refinement and validation processes.

References

- Chatzipanagi, A., Pavlovic, J., Fontaras, G., et al., (2020). Impact of WLTP introduction on CO₂ emissions from M1 and N1 vehicles : evidence from type-approval and 2018 EEA data, *Publications Office of the European Union*, Luxembourg.
- European Commission, (2007). Regulation (EC) No 715/2007 of the European Parliament and of the Council of 20 June 2007 on type approval of motor vehicles with respect to emissions from light passenger and commercial vehicles (Euro 5 and Euro 6) and on access to vehicle repair and maintenance information. *Official Journal of the European Union*
- European Union, (2017). Commission Regulation (EU) 2017/1151 of 1 June 2017 supplementing Regulation (EC) No 715/2007 of the European Parliament and of the Council on type-approval of motor vehicles with respect to emissions from light passenger and commercial vehicles (Euro 5 and Euro 6) and on access to vehicle repair and maintenance information, amending Directive 2007/46/EC of the European Parliament and of the Council, Commission Regulation (EC) No 692/2008 and Commission Regulation (EU) No 1230/2012 and repealing Commission Regulation (EC) No 692/2008. *Official Journal of the European Union*
- European Union, (2019). Regulation (EU) 2019/631 of the European Parliament and of the Council of 17 April 2019 setting CO₂ emission performance standards for new passenger cars and for new light commercial vehicles, and repealing Regulations (EC) No 443/2009 and (EU) No 510/2011. *Official Journal of the European Union*
- Suarez, J., Komnos, D., Ktistakis, M.A., Fontaras, G., (2023). 2025 and 2030 CO₂ emission targets for Light Duty Vehicles, *Publications Office of the European Union*, Luxembourg.

Annex

Table 2: Pass and fail coefficients.

Tests (i)	PASS		FAIL	
	$t_{P1,i}$	$t_{P2,i}$	$t_{F1,i}$	$t_{F2,i}$
3	1.686	0.438	1.686	0.438
4	1.125	0.425	1.177	0.438
5	0.850	0.401	0.953	0.438
6	0.673	0.370	0.823	0.438
7	0.544	0.335	0.734	0.438
8	0.443	0.299	0.670	0.438
9	0.361	0.263	0.620	0.438
10	0.292	0.226	0.580	0.438
11	0.232	0.190	0.546	0.438
12	0.178	0.153	0.518	0.438
13	0.129	0.116	0.494	0.438
14	0.083	0.078	0.473	0.438
15	0.040	0.038	0.455	0.438
16	0.000	0.000	0.438	0.438

2.4 TAP.04. Remote sensing of vehicle emissions.

Single-Blind Test on the Effectiveness of the Gumbel Distribution Method in Detecting High-Emitters in Remote Sensing Data

Z. Yang^{1*}, J.E. Tate², C.E. Rushton², J. Borken-Kleefeld³, M. Qiu⁴, Å. Sjödin⁵

¹School of Transportation and Logistics, Southwest Jiaotong University, Chengdu, 611756, China

²Institute for Transport Studies, University of Leeds, Leeds, West Yorkshire, LS2 9JT, England

³Transportation Ecology, Technische Universität Dresden, 01062 Dresden, Germany

⁴Department of Earth System Science, Stanford University, Stanford, CA 94305–2004, United States

⁵IVL Swedish Environmental Research Institute, Stockholm, SE-10031, Sweden

1. Introduction

Gumbel distribution has been used to find the cut-off point between normally-behaving vehicles and high-emitters (HEs) with faulty, deteriorated, or tampered emission after-treatment system based on remote sensing measurements (Rushton et al., 2021; Yang et al., 2022). Vehicles with extremely high emission values that do not follow the Gumbel distribution are often considered as candidate HEs. However, as remote sensing measurement units only capture a snapshot sample of emission rates, whether these vehicles are true HEs have not been validated. In this paper, a single-blind test was designed to investigate whether the Gumbel HE identification method applied only on instantaneous emission rates can effectively screen out vehicles whose average emission values are higher than a certain level.

2. Materials and Methods:

2.1 Data Preparation

Following Qiu and Borken-Kleefeld (2022), data sets of 25 fleets were prepared based on PEMS and Chassis measurements, with known HEs in the mix. Each set includes single/multiple sampled instantaneous NO_x emissions (g/kg) of 5,000 diesel cars as well as other information: fleet ID, vehicle ID, speed and acceleration, vehicle specific power (VSP), average NO_x emission rates (over a complete test cycle in the PEMS and Chassis measurements). The data are from tests under normal conditions with temperature between 20 and 25°C, and the quality of the measurements has been checked.

Data from three emission standards are prepared: Euro 5, Euro 6a/b and Euro 6d-temp. In this trial, a slightly-HE is defined as a vehicle whose average emission factor is 2 times above the limit value but 5 times below the limit value ($2 * \text{limit} < \text{slightly-HE} < 5 * \text{limit}$). And a super-HE is a vehicle with an average NO_x emission rate 5 times or more above the emission limit value ($\text{super-HE} \geq 5 * \text{limit}$). The emission limit value is the NEDC limit converted to the unit g/kg using an average (real world) fuel efficiency, arriving at 3.516 g (NO_x)/Kg (fuel) for Euro 5 diesel cars, and 1.563 g (NO_x)/Kg (fuel) for Euro 6a/b and Euro 6d-temp diesel cars.

2.2 Study Design

Researchers were divided into three groups in this trial. Group A prepared the data sets, they had the full information including which vehicles are HEs. Group B conducted the Gumbel HE identification method and screened out the "candidate" HEs. Group B were blind to which vehicles are "true" HEs. Group C were provided with the list of "true" HEs by Group A and the list of "candidate" HEs by Group B. Group C were an intermediary to check the effectiveness of the Gumbel distribution in detecting HEs. The detailed trial process is stated as follows:

Step 1: Group A prepared data sets of 25 fleets and each fleet includes full information of every record (fleet ID, vehicle ID, instantaneous NO_x emission rate, instantaneous speed and acceleration, vehicle specific power, average NO_x emission rates of the vehicle);

Step 2: Group A transmitted the data excluding average NO_x emission rates to Group B; Group A transmitted the list of true HEs (including slightly-HEs and super-HEs) and the corresponding average NO_x emission rates to Group C.

Step 3: Group B fitted the Gumbel distribution into each fleet, screened out candidate HEs, and passed the detailed list of candidate HEs to Group C.

Step 4: Group C compared the true HEs provided by group A with candidate HEs provided by Group B and calculated the accuracy rate of using the Gumbel distribution to identify HEs.

2.3 the Gumbel Distribution HE Identification Method

Rushton et al. (2021) proposes using the Gumbel distribution to identify HEs in passenger car emissions testing data. The probability density function (pdf) $f(x)$ and cumulative density function (cdf) $F(x)$ of a Gumbel distribution are given as:

$$f(x) = \frac{1}{b} e^{-(\frac{x-a}{b} + e^{-\frac{x-a}{b}})} \quad \text{Eq. 1}$$

$$F(x) = 1 - e^{-e^{\frac{x-a}{b}}} \quad \text{Eq. 2}$$

Where a is the location parameter and represents the highest observation frequency in a dataset; and b is the scale parameter and represents the spread of the dataset.

The Gumbel distribution identifies the candidate HEs by dynamic threshold (cut-off point based on the testing fleet's emission performance, meaning the candidate HEs identified by the Gumbel distribution are not above a fixed threshold but are abnormal outliers from the rest of the fleet, see Figure 1). However, when conducting the single-blind test, Group B with known HEs can only provide vehicles above a fixed threshold (i.e., 2 or 5 times above the NEDC emission limit value). As a result, the candidate HEs identified by the Gumbel distribution and HEs with average emission above a certain threshold are not directly comparable. This study therefore compares the percentage of true HEs (including slightly-HEs and super-HEs) with candidate HEs identified by the Gumbel distribution.

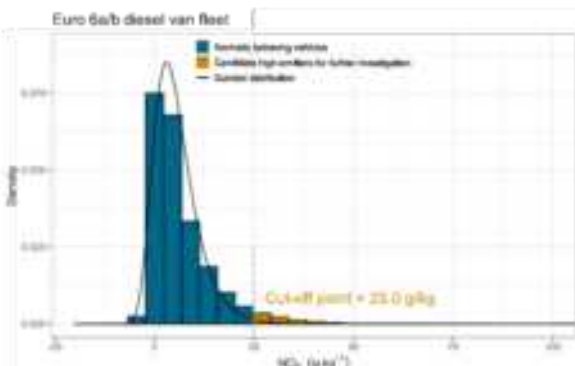


Figure 1: Using the Gumbel distribution to identify candidate HEs in Euro 6a/b van fleet (Yang et al., 2022)

3. Results

3.1 Results from Fleets with Single Records

- Percentage of slightly-HEs and super-HEs in every fleet

The prepared 25 fleets have increasing share of HEs (including slightly-HEs and super-HEs) from 0% to 100% (see left plot on Figure 2). The predicted HE shares by the Gumbel distribution is shown on the right plot of Figure 2. The predicted HE shares and true HE shares are more consistent when the fleets have more clean vehicles (share of true HEs below 50%). However, the Gumbel distribution estimates there is only 1% of HEs in every fleet while the share of true HEs accounts for 55%-100% of the fleet. Similar results have been found in Yang et al. (2022), where there are no or only 1% of model Euro 5 diesel vans identified even though that Euro 5 diesel vehicles are often considered to have lots of HEs (Carslaw et al., 2011). The assumption is that most Euro 5 diesel vans have high emissions, so the measurements are fitted to the Gumbel distributions with relatively high location and scale parameters and left very

few off-model vehicles that are assessed as candidate HEs. This indicates that the method failed to screen out the slightly-HEs and super-HEs within fleets that have a very high share (>50%) of true HEs.

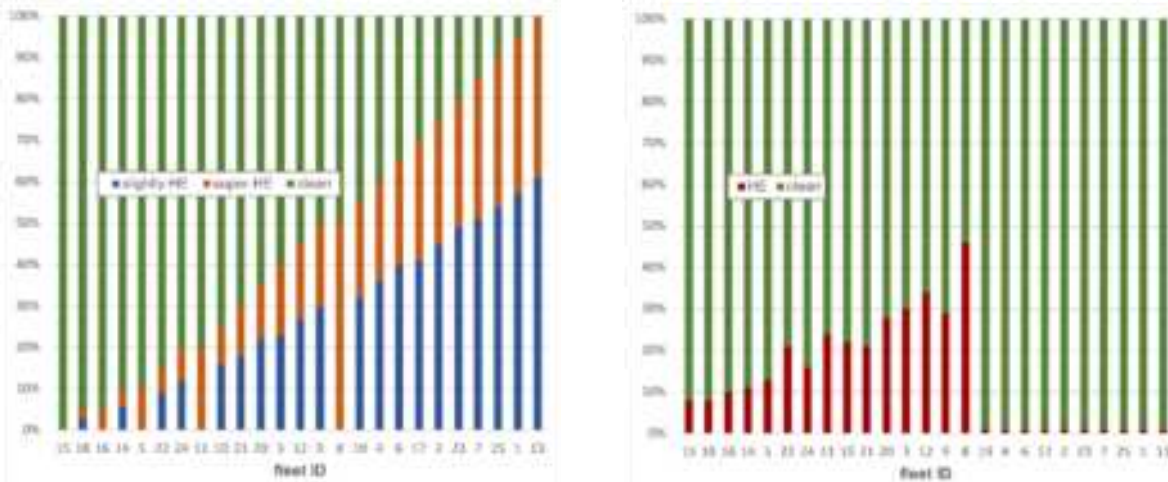


Figure 2: Share of true HEs and super-HEs in sampled Euro 5 fleets (left), share of predicted HEs identified by the Gumbel distribution (right)

In addition, the R² value (goodness-of-fit) of observed and theoretical quantiles of the Gumbel distribution is calculated for each fleet, fleets with R² values higher than 98% are considered as more reliable results, and these fleets are fleet 15, 18, 16, 2, 23, 7, 25, 1, 13, which are fleets with either the lowest or the highest share of true HEs. Whether fleets with higher R² value have more accurate prediction of true HEs is discussed as follows.

- Error of commission

Error of commission is the amount of vehicles that the Gumbel distribution identifies as HEs whereas they are actually clean vehicles. Within the 1% of candidate HEs identified in the Euro 5 fleets 2, 23, 7, 25, 1, 13 (these fleets are considered as a good fit of dirty fleets by the Gumbel), 99% are true HEs. In detail, 38% of vehicles are super-HEs ($\geq 5^{\text{th}}\text{ limit value}$) and 61% are slightly-HEs ($2^{\text{nd}}\text{ limit} < \text{slightly-HE} < 5^{\text{th}}\text{ limit}$). Within the 8%/10% of candidate HEs in fleet 15, 18, 16 (these fleets are considered as good fit of clean fleets by the Gumbel), 25% are true HEs. In detail, only 21% of the vehicles are super-HEs and 5% are slightly-HEs. This indicates that the error of commission in clean fleets are very high. For fleets with lower R² values, 77% of the candidate HEs are true HEs. In detail, 53% are super-HEs and 24% are slightly-HEs.

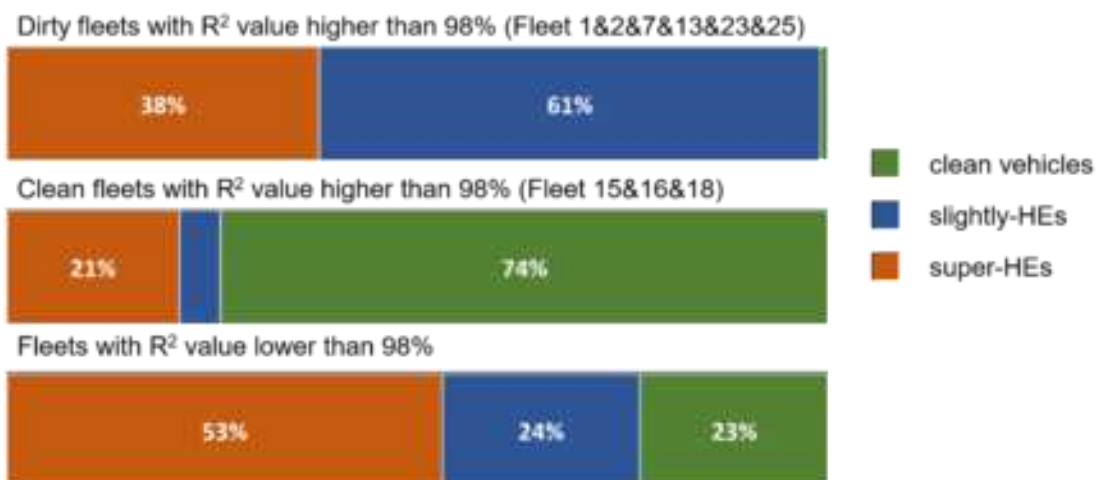


Figure 3: the share of super-HEs and slightly-HEs within the off-model vehicles identified by the Gumbel distribution

3.2 Results from Fleets with Multiple Records

This section analyses the effectiveness of the Gumbel distribution in detecting HEs by using multiple records fleets. Within each fleet, there are 5,000 vehicles in total and for each vehicle there are 7 random selected records based on PEMS and Chassis measurements. It is expected that multiple records fleets, the Gumbel HE identification method will have improved performance.

- Percentage of slightly-HEs and super-HEs in every fleet

(To follow)

- Error of commission

(To follow)

4 Summary and Conclusions

This is an area of ongoing research in Autumn 2023, repeating this analysis with fleets of Euro 6b and Euro 6d-temp diesel cars as well as multiple records fleets, following the same process as reported for the Euro 5 fleets. The full results will help to verify the effectiveness of the Gumbel distribution in detecting HEs.

Acknowledgements

We are grateful for the provision of RS data from the H2020 CARES project and for modal chassis and PEMS data from the ERMES dbEFA.

References

- Carslaw, D.C., Beevers, S.D., Tate, J.E., Westmoreland, E.J. and Williams, M.L. 2011. Recent evidence concerning higher NOx emissions from passenger cars and light duty vehicles. *Atmospheric Environment*. 45(39), pp.7053-7063. <https://doi.org/10.1016/j.atmosenv.2011.09.063>
- Qiu, M. and Borken-Kleefeld, J. 2022. Using snapshot measurements to identify high-emitting vehicles. *Environmental Research Letters*. 17(4), p044045
- Rushton, C.E., Tate, J.E. and Shepherd, S.P. 2021. A novel method for comparing passenger car fleets and identifying high-chance gross emitting vehicles using kerbside remote sensing data. *Science of The Total Environment*. 750, p142088. <https://doi.org/10.1016/j.scitotenv.2020.142088>
- Yang, Z., Tate, J.E., Rushton, C.E., Morganti, E. and Shepherd, S.P. 2022. Detecting candidate high NOx emitting light commercial vehicles using vehicle emission remote sensing. *Science of The Total Environment*. 823, p153699. <https://doi.org/10.1016/j.scitotenv.2022.153699>

Applications of multi-sensor roadside networks for fleet emission source apportionment and single-vehicle EF determination

Mengyuan CHU¹, Peter Brimblecombe², Dane Westerdahl¹, Ning Zhi^{*1}

¹ Division of Environment and Sustainability, The Hong Kong University of Science and Technology, Hong Kong, zhining@ust.hk

² Department of Marine Environment and Engineering, National Sun Yat-sen University, Kaohsiung, Taiwan

Introduction

Vehicular emissions make a significant contribution to air pollution in cities. Hong Kong is one of the most densely populated cities in the world, with many people living, working, and commuting in areas that are directly exposed to these emissions. These pollutants may harm people and more information is needed on these pollutants to assess and mitigate the sources (Sun et al., 2019). It is crucial to identify and quantify the emission of the wide range of vehicles, especially high emitters' emission factors (EFs) for urban air quality management (Huang et al., 2022).

Different methods have been applied to investigate in-use vehicle emissions. The Hong Kong Environmental Protection Department uses Remote Sensing (RS) as an enforcement tool for detecting high-emitting vehicles beginning in 2014. However, this RS driven enforcement program does not include diesel vehicles - a primary source of NOx emissions, which is problematic in Hong Kong (Huang et al., 2022). Portable emissions measurement system (PEMS) are also used to measure emissions from many types of vehicles, but measure only one vehicle at a time, making it less suitable to represent an in-use traffic fleet. Chasing methods have also been applied to assess emissions and estimate the EF of in-use vehicles but also require a considerable workforce and elaborate monitoring protocols. Further, PEMS and RS measurements do not provide actual concentration required for exposure estimation at the heavily occupied roadside in urban area. Our study extends and complements existing in-use emissions measurement methods. We used a high-time-resolution kerbside microsensor-based network, capturing plumes of passing vehicles to determine concentrations and calculate EFs of NOx and CO.

Method

Instrumentation

The sensor we used in the study was based on the High Speed Sensor system (HSS, Sapiens). It is a microsensor-based monitor customized for portable and continuous air pollution measurements. With a pump inside, it can actively sample and measure the concentration of NO, NO₂, CO and CO₂ with 1Hz time resolution. In addition to local storage (backup), real-time, direct output of pollutant concentrations and system status data were transmitted to a cloud server for online data processing. An automated plate capture and recognition system were developed and applied to obtain vehicle information. Supplementary measurements including temperature, relative humidity, wind speed and direction were conducted using a mini-meteorological station (Hongyue HY-WDC5).

Sites

We conducted two measurement campaigns. The first was over 4-days in a busy street canyon in Hennessy Road, Causeway Bay, with ~3300 vehicles/day (from 9am – 7pm). The site was within a street canyon, where buildings on either side of the roadway range between 20 and 40 storeys (~120–220 m) forming a relatively confined space. The impact of the opposite lanes was largely separated by the wall of the tram tracks station and the footbridge near the site (Figure 1a). Seven HSSs were positioned on both sides and top of the carriageway to capture the exhaust plume and at elevated locations to be more representative of air quality at the canyon bottom. The L1, L2, R1, R2 are sensors set at the kerb were ~40 cm above the ground, to be close to tailpipe height, which enable the sensors capture the fast changing vehicle plumes. The elevated sensor nodes were denoted H for high. The one on the lamp post on the left were named as LH. The one on the exterior of the overpass over the center of the carriageway was marked as CH. The one outside the stairway that provides access to the tram stop right (RH) was about 2m about the road. The set up can be found in Figure 1a (Brimblecombe, et al., 2021).



Figure 1. (a) Photograph illustrating the site on Hennessy Road, looking west (b) Photograph illustrating the site on Hiram's Highway, looking north (© Google, June 2023) (c) Layout of system.

A second monitoring campaign was conducted at the roadside of a rural highway (Hiram's Hwy) in Sai Kung, have been found around 1200 vehicle passed from 9am – 7pm in average in the 5 days of monitoring. The monitored section of the highway is characterized by its uphill gradient and its dual-lane, one-way configuration. The area is further distinguished by the presence of trees flanking both sides of the highway. We deployed 4 sensors on each side of the road, with R1, L1 closest to the tailpipe, ~40 cm above the ground, and R2, L2 1.5 m away from R1 and L1 with the same height. Like the Causeway site, the elevated sensor nodes were denoted H for ~ 1.5m high (Figure 1b).

Sensor Calibration

Laboratory calibration of the pollutant sensors took place before and after the measurements. Standard CO (100 ppm CO and 10% CO₂/N₂, Linde HKO Ltd., Hong Kong, China) concentrations came from a dynamic calibrator (T700U, Teledyne, Sauzend Oaks, CA, USA) combined with a zero-gas generator (701, Teledyne, Sauzend Oaks, CA, USA). The NO₂ and NO were generated with a NO₂/NO/O₃ calibration source (714, 2B Technology, Boulder, CO, USA). During calibration and linearity checks, the gas flow rate was constant at 0.6~0.8 L min⁻¹, which was validated by a flow meter (Defender 520, Mesa Labs, Lakewood, CO, USA). Prior to the calibrations, both the T700U and 2B 714 instruments were warmed up for 60 min, while the pollutant sensors were warmed up for 12h to ensure a steady state.

Data Analysis

The roadside environment can highly variable, thus short response time of sensors are required to track the fast-changing concentration fluctuations of observed plumes. Thus, a novel deconvolution algorithm was developed and applied. The algorithm reconstructed sensor output and improved their response time from 30–80 seconds to 5–15 seconds, allowing further analysis of the plume data (Chu et al., 2022; Brimblecombe et al., 2022) (Figure 2).

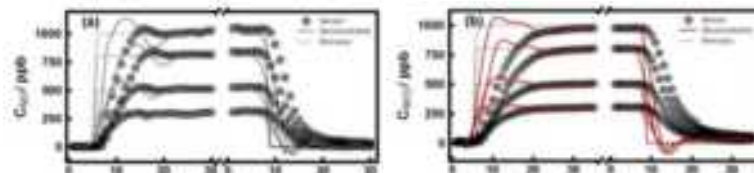


Figure 2. (a) Imposed changes in NO concentration in laboratory experiments (dotted line), concentration measurements as black dots and deconvoluted concentrations as gray line. (b) similar plots for NO₂. Adapted from: ... /NOx and primary NO₂ from individual vehicles. ... Atmospheric Environment, Volume (295), 295, 119562. Copyright (2023) by Elsevier.

Then the NO_x, CO, and CO₂ plumes selected with criteria were matched with specific vehicles based on the time the vehicle captured by our camera. Algorithms were developed to estimate the EFs of individual vehicles based on the carbon balance principle and identify high emitters among a fleet from the snapshot of vehicle emissions. The algorithm was written using python.

Results

Overview of concentrations

The sensor network as illustrated in Figure 1a offers an opportunity to delve into the intricate dispersion process within the urban street canyon of Causeway Bay. Prior to scrutinizing the EF of individual vehicles, we utilized a variety of

statistical tools including Fourier transforms, auto-correlation function, cross-correlation function, and non-parametric test to investigate the fluctuation of pollutant concentration in the street canyon micro-environment.

The kerbside concentrations showed cyclic changes that corresponded to passing traffic. To discern patterns at lower frequencies, we employed Fourier analysis for the examination, which revealed weak cycles at 60s and 110s (Figure 3 f-j) which matches with the traffic light interval. Generally, the vehicles from crossroad near the site wait 60-s for a green light, then go straight ahead or turn left and pass the site. The traffic flow along Hennessy Road followed another cycle of 110 s. These two cyclic periods were clearest in the data from node L1, which was close to the crossroad. (Brimblecombe et al., 2021).

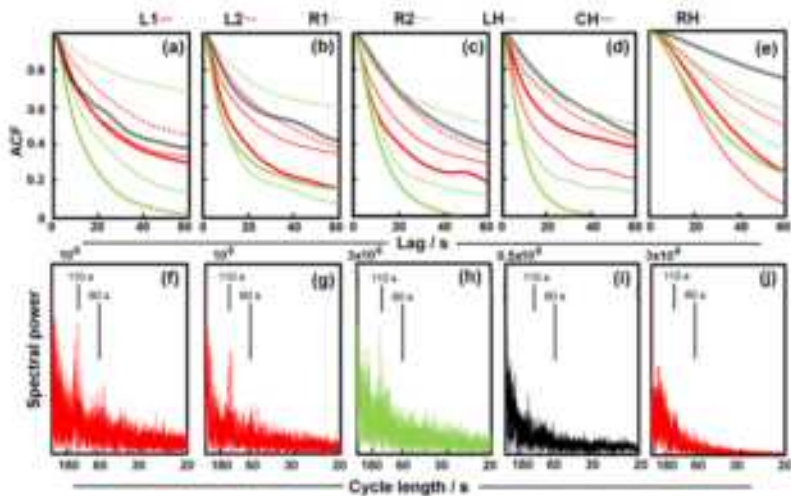


Figure 3. The autocorrelation function (ACF) of 1-s NO_x concentrations for the seven nodes for the four days: (a) 12–21, (b) 12–22, (c) 12–28 and (d) 12–29. (e) Average autocorrelation of 1-s CO across the four nodes for the entire campaign. Fourier transforms for NO_x on 12–21 at the kerbside nodes, (f) L1, (g) L2 and (h) R2, and the elevated node on the overhead walkway (i) CH, along with the transform for (j) kerbside CO at L1. Note the spectral power takes the units ppb² Hz⁻¹, with the quantity at the top of each figure (f–j) shown by the small numerals. *Adapted from Environments, Volume 8(12), 137.*

Autocorrelation is the correlation of a signal with a delayed copy of itself as a function of delay. It was used in previous study to examine the fluctuations of pollutant concentration in a street canyon. Researchers noted that autocorrelation persists in the stagnant zones of air that lie outside the vortices in urban canyons (Pavageau and Schatzmann, 1999). In our study, autocorrelation of 1-s NO_x concentrations at nodes R1 and R2, which were closest to the tailpipe and the turbulence caused by the passing vehicles, generally showed a rapid decline (Figure 3a–d). Node L2 on the less turbulent left-hand lane often showed a decline that was slower than that of nodes R1 and R2. The autocorrelation function at the more elevated nodes LH, CH and RH also decayed more slowly; this was probably associated with less turbulent air and less variation in pollutant concentrations. The average autocorrelation of 1-s CO concentrations across the four days is shown in Figure 3e. Similarly, it was more persistent at the elevated nodes on the walkway.

The application of cross-correlation analysis has been demonstrated to be instrumental in elucidating the variations in airflow between an enclosed street canyon and its intersections (Richmond-Bryant et al., 2009). In this study, we employed cross-correlation function to explore the lags between the appearance of pollutants at various locations, with node R1 taken as the reference. Across the entire campaign, the cross-correlation functions of NO_x were slightly delayed at the other nodes (Figure 4a). A similar picture emerged for CO (Figure 4b). The lag time was longer for the elevated nodes (Figure 4c), indicating that the pollutant signal moved more slowly in the vertical direction. The signals, and presumably the plumes of passing vehicles, moved more rapidly in the horizontal direction, as the kerbside nodes were separated by less than 10 m, representing just a few seconds of vehicles travel along Hennessy Road. However, it took slightly longer for the concentration signal to cross the carriageway from the right-hand kerb to that on the left (nodes L1 and L2). The signal took some tens of seconds to reach the elevated nodes, e.g., the signal observer on the walkway (CH) was often delayed by more than 20 s.

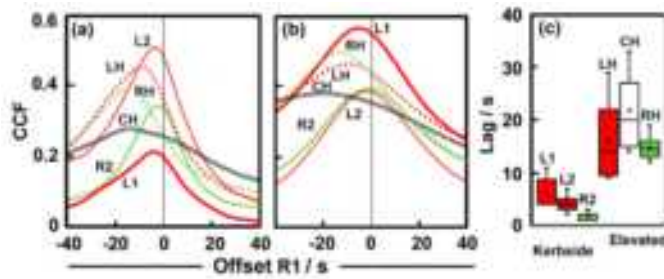


Figure 4. (a) The cross-correlation function (CCF) of 1-s NO_x concentrations from the other six nodes with R1 on 12–28 and (b) CO. (c) The lag of each node for both NO_x and CO with node R1 determined for the four days.
Environments, Volume 8(12), 137.

The 1-min average concentrations are compared with distinct vehicle flows in Figure 5 as box and whisker plots. The averaged kerbside NO_x related to double-decker bus frequency, indicating the main NO_x contributors were diesel-fueled double-decker buses (Figure 5a). The Kruskal-Wallis test suggested the concentrations at different flows of buses was not the same ($p < .0001$). While CO concentration increasing with the flow of EURO 4 or lower-emission standard vehicles (Figure 5b), most of which were private cars (PC) and taxis (Chu et al., 2022). This trend was significant (Kruskal-Wallis $p < .001$).

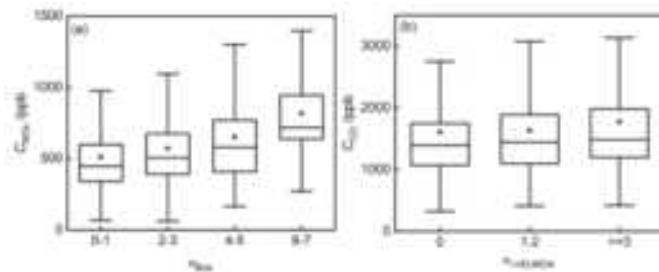


Figure 5. Box and whisker plots and mean values (triangles) for (a) 1-min averaged roadside NO_x concentration and number of double-decker buses per minute (n_{Bus}) and (b) 1-min averaged roadside CO concentration and number of EU4 ($n_{<=EURO4}$) and lower standard vehicles per minute. Note: measurements from node R2 omitted values during congestions. The box represents the interquartile range or IQR (25–75%) of the data. The horizontal line through the center of the box is the median. The whiskers represent $1.5 \times IQR$.
Wei, P., Liu, C. H., Du, X., & Ning, Z., 2022, Atmospheric Environment, Volume (271), 118878. Copyright (2023) by Elsevier.

Emission factors

We applied a carbon-balance, differential method to estimate the EF from clear isolated peaks of CO₂ and pollutants including NO_x and CO (Chu et al., 2022). After the alignment of plumes of different pollutants, The EF is determined from the best-fit to the slope of C_p against C_{CO2} :

$$EF_p = w_c dC_p/dC_{CO2}$$

Instead of using only the maximum and minimum points of the peak, the EF was estimated by all the points throughout the plume. The benefit of this method is it avoiding the error caused by the determination of the baseline which may cause big error in EF estimation (Georgopoulos & Seinfeld, 1986). The EFs extracted from the snapshot of the vehicles can be paired with a specific vehicle from information extracted from photo recognition of the vehicle registration plate and matched to non-private registration information including engine size, vehicle type, fuel used and registration year. Such information only available for the Causeway Bay project, therefore, all subsequent discussion will be limited to the Causeway Bay project.

The differences in EF_{NOx} from the five typical vehicle types are shown in Figure 6a, buses > middle goods vehicles (MGV) > private car (PC) > light good vehicles (LGV) > taxis, and the EFs appear not to be drawn from the same distribution ($p < 0.005$). It's worth mentioning that the buses in this project are diesel double-decker buses, and most LGV are diesel 5-seats vans. Further, there appears to be a slight increase in EF_{NOx} with diesel engine size (Figure 6b). The Kruskal-Wallis test reveals that the samples were not all drawn from the same distribution ($p < 0.05$). The fuel type (Figure 6cd) suggests the EF_{NOx} fall in the order diesel > petrol > LPG. The Kruskal-Wallis test suggests again that

these are not drawn from the same population ($p < 0.05$). For EF_{CO} , LPG vehicles, mainly mini-bus and taxis, had the highest value. Our EF estimates were in the range of previous studies (Chu et al., 2022).

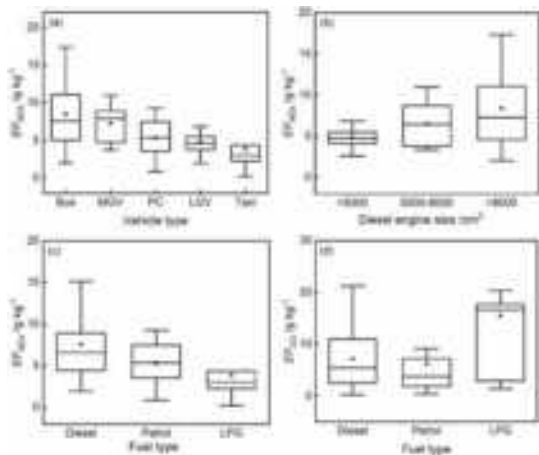


Figure 6. Emission factors calculated from individual plume segments for various elements of the fleet: Double Decker buses (Bus), medium goods vehicle (MGV), private car (PC), light goods vehicle (LGV) and taxi (a) EF_{NOx} for vehicle types (b) EF_{NOx} for various engine sizes (c) EF_{NOx} for individual vehicles using different fuels (diesel, petrol, and liquid petroleum gas: LPG) and (d) EF_{CO} for individual vehicles using different fuels.

Z., 2022, Atmospheric Environment, Volume (271), 118878. Copyright (2023) by Elsevier.

EF from different sensor nodes

The benefit of the multi-sensor network is we can measure the different part of the plume and estimate the EF accordingly. The Figure 7a shows a pair of typical plume segment detected using raw data from sensors L2 and LH. The Figure 7b compares the EF estimated from L2 and LH of the plumes in a scatter plot, the scatter shows a close to one slope (1.08 for NOx and 0.97 for CO) and R^2 (0.91 and 0.96 for NOx and CO respectively), indicating a consistence value of EF in the dispersion process of plumes.

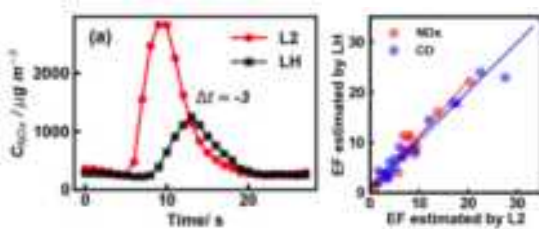


Figure 7. (a) A typical plume segment detected using raw data from sensors L2 and LH showing concentration peaks and time difference Δt . (b) EF_{NOx} and EF_{CO} determined from the plume segment detected at sensor LH compared with that determined from sensor L2.

Discussion

This study has demonstrated the feasibility of using roadside gas sensors to derive EFs from individual plume segments. We captured data from many vehicles and developed a database for real-world on-road EF. Importantly, this method is particularly effective in identifying high emitters, given that low emitters may not release sufficient quantities for detection by the sensors. This cost-effective approach could be particularly advantageous for developing countries. In fact, it has already been successfully implemented in India (Raparthi et al., 2023). While the method may have lower accuracy, this limitation can be mitigated through repeated measurements, which is an avenue for future research. The technique could also be extended to other pollutants such as PM, BC, or toxic organic substances and can readily be expanded into more sites.

Acknowledgements

This work was supported by European Union (EU) – Hong Kong Research and Innovation Cooperation Co-funding Mechanism by Research Grants Council (RGC) (Ref.: E-HKUST601/19), Collaborative Research Fund (CRF) for 2018/19 (Ref No. C7064-18G), Hong Kong Environment and Conservation Fund (ECF/21/2021).

References

- Brimblecombe, P., Chu, M. Y., Liu, C. H., & Ning, Z. (2021). NO_x and CO fluctuations in a busy street canyon. *Environments*, 8(12), 137.
- Brimblecombe, P., Chu, M., Liu, C. H., Fu, Y., Wei, P., & Ning, Z. (2023). Roadside NO₂/NO_x and primary NO₂ from individual vehicles. *Atmospheric Environment*, 295, 119562.
- Chu, M., Brimblecombe, P., Wei, P., Liu, C. H., Du, X., Sun, Y., & Ning, Z. (2022). Kerbside NO_x and CO concentrations and emission factors of vehicles on a busy road. *Atmospheric Environment*, 271, 118878.
- Georgopoulos, P. G., & Seinfeld, J. H. (1986). Instantaneous concentration fluctuations in point-source plumes. *AIChE journal*, 32(10), 1642-1654.
- Huang, Y., Lee, C. K., Yam, Y. S., Mok, W. C., Zhou, J. L., Zhuang, Y., & Chan, E. F. (2022). Rapid detection of high-emitting vehicles by on-road remote sensing technology improves urban air quality. *Science Advances*, 8(5), eabl7575.
- Pavageau, M., & Schatzmann, M. (1999). Wind tunnel measurements of concentration fluctuations in an urban street canyon. *Atmospheric environment*, 33(24-25), 3961-3971.
- Raparthi, N., Barudgar, A., Chu, M., Ning, Z., & Phuleria, H. C. (2023). Estimating individual vehicle emission factors from near-road measurements in India. *Atmospheric Environment*, 308, 119869.
- Richmond-Bryant, J., Eisner, A. D., Hahn, I., Fortune, C. R., Drake-Richman, Z. E., Brixey, L. A., & Ellenson, W. D. (2009). Time-series analysis to study the impact of an intersection on dispersion along a street canyon. *Journal of Environmental Monitoring*, 11(12), 2153-2162.
- Sun, S., Stewart, J. D., Eliot, M. N., Yanosky, J. D., Liao, D., Tinker, L. F., ... & Wellenius, G. A. (2019). Short-term exposure to air pollution and incidence of stroke in the Women's Health Initiative. *Environment international*, 132, 105065.

Development and testing of a novelty Remote Sensing Device for the simultaneous measurement of vehicles' emissions circulating in Multilane Roads

J. Buhigas¹ and J. Muñoz¹

¹Opus RS Europe SL, Madrid, 28015, Spain

Introduction

Remote Sensing (RS) plays a vital role in road traffic emissions monitoring, providing effective and efficient means of evaluating the real-world emissions of motor vehicles. Remote Sensing Devices (RSD) can remotely detect and measure ~~pollutant concentrations emitted by the vehicles, sample on an individual basis. This information is essential for market surveillance, air quality modelling and implementing targeted measures, such as emission reduction programs and enhanced vehicle inspection programs. Data from the RSDs helps policymakers to design fair and efficient policies and allocate resources effectively.~~ By monitoring traffic emissions, RSDs can also identify highly polluting vehicles (known as high-emitters, HE) for selective action. Most of the cases in the world use portable RSDs, capable of being easily placed on the sides of the road without complicated interventions or installations. In this way, the devices can be moved frequently to cover many points of a territory with few instruments. However, there are applications where a long-term measurement at a specific site might be desirable. Similarly, being able to measure more than one lane of the road at a time would increase the number of sites where these systems can be placed, and thus reduce operating cost in long-term programs. Thanks to the European Union's grant in the "2020 NEAR" project we have developed a new device, called LRSD, based on interband and quantum cascade lasers, with a modular architecture based on fibre optic for guiding the lasers radiation, with the intention of measuring at least 2 lanes simultaneously, using a single main system. This paper describes the instrument and evaluates this multilane capability, as well as its drawbacks and barriers identified during testing. In the last part of the paper, an alternative dual-lane system is evaluated by adapting a commercial RSD.

State of the art

Vehicle emissions RS has been used, validated and improved for decades and there is extensive literature on the subject. The classic RS approach employs infrared (IR) and ultraviolet (UV) radiation to quantify the presence of the targeted pollutants by measuring the amount of radiation that every single pollutant absorbs through the optical path. The amount of each pollutant is obtained by calculating the gas column density thought the Lamber-Beer law (equation 1).

$$-\ln\left(\frac{I(\lambda)}{I_0(\lambda)}\right) = k(\lambda) C \quad (1)$$

Where: I is the intensity of the received radiation as a lambda function; I_0 is the emitted intensity of the radiation as a lambda function; k is the absorption coefficient for a specific gas as a lambda function; and C is the column density (product of gas concentration and length of the gas column).

The principle of the vehicle emissions RS measurement is to calculate ratios of pollutants to CO₂ present in the exhaust gas plume of each analysed vehicle. The pollutant ratio is a good indicator of whether the vehicle is more or less polluting and can be transformed into fuel-specific emissions by applying the combustion equation, for further estimating the travelled-distance emissions of a vehicle and, for instance, comparing measured values to type-approval limits. The underlying principles are detailed and reviewed in the relevant literature (Bishop, B.A., 1996).

There are different technologies, architectures and providers, but portable or semi-fixed remote sensing devices (RSD) ~~that are placed on the side of the road for cross-road monitoring are the most widely used systems to date (Bemand et al., 2010).~~ Other systems are installed overhead on the road lanes to measure in a top-down manner the tailpipe emissions from the vehicles, but their high operating costs and installation complexity make them difficult to use. For a top-down RSD to be beneficial compared to a cross-road RSD, its installation and operation must be much simpler and they must provide multi-lane measurement capabilities.

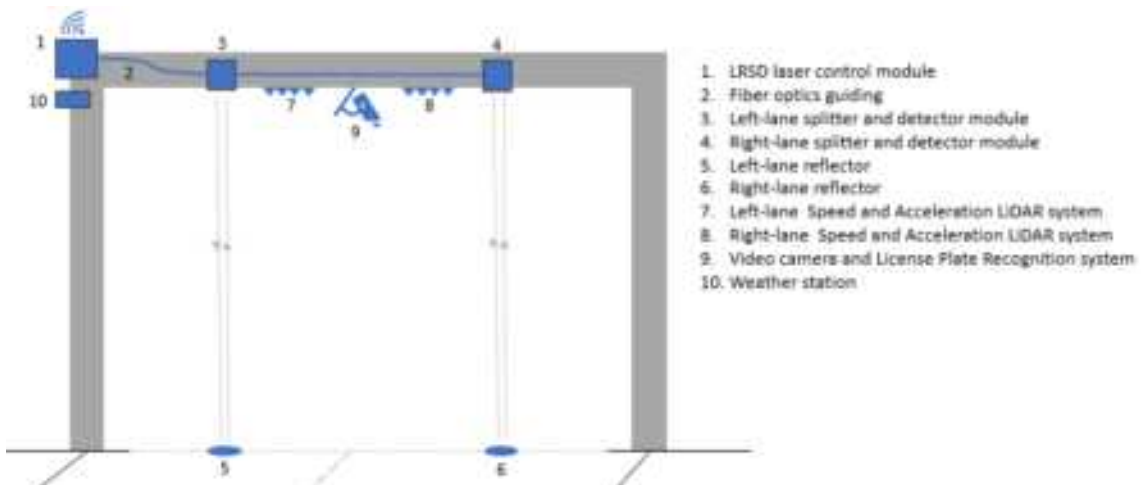
Description of the LRSD

The proposed Laser Remote Sensing Device (LRSD) applies Tuneable Diode Laser Absorption Spectroscopy (TDLAS) to measure CO₂, CO, NO, NO₂, NH₃ and HC (unburned hydrocarbons, typically specified as propane). The gas column density is calculated by a regression between the measured absorptance and the chemical model HITRAN (<https://hitran.org/>). Particulate matter (PM) is measured similarly to traditional RSDs, but it is measuring of plume's opacity in the UV range. When performing a measurement for a vehicle passage, the system sequentially activates each of the 5 lasers

to emit 5000 measurement profiles in 0.5 seconds. In other words, the device takes 1.5 million measurements in 0.5 seconds. The system takes both a "pre-plume" (ambient air) and a "post-plume" (exhaust plume) record. The subtraction of both measurements provides a value of the plume concentrations only.

The LRSD uses interband and quantum cascade lasers (ICL and QCL, respectively) for each of the targeted species (a total of 6 lasers). A QCL is a novelty technology that can be applied in infrared spectroscopy. It has layers of semiconductors forming a high quantum well, which transform the electronic energy into electromagnetic radiation (Chen and Furukawa, 2023). The QCL can emit in the spectral region from 4 to 10 microns. The ICL is a coherent optical source for the mid-wave infrared band (defined from 3 to 6 microns) (Graydon et al., 2018). ICL are less powerful, but ~~one laser is required to target the laser's temperature and current control~~. are two of the most difficult issues in this kind of systems, so all the lasers are grouped in the same module, and custom-made electronics have been developed to centralize the lasers temperature and current control, and to synchronize the emission of the lasers. The LRSD has been designed to be used in a cross-road configuration or in a top-down configuration. For the latest, the prototype has a modular architecture (Figure 1), with the intention of measuring more than 1 lane simultaneously. It is composed of a) a laser control and emission module, b) individual detector and processing modules (one for each lane), c) a splitter module, d) a fiber optic bundle for guiding the lasers radiation from the emission module to the detectors and e) processing units over each of the road lanes. With this design the LRSD can simultaneously measure several lanes, thus evaluating up 7000 vehicles per hour, increasing the capabilities of the RS technology to massively monitor real-world emission from road transport. Fiber optics make it possible to guide all the emitted radiation to the detector and processing units on the top of each lane. The detector and processing units have a collimation optics for sending each laser radiation to the road's embedded retroreflector, returning the light to the detector module on the gantry, once it has passed through the exhaust plume of the vehicle.

Figure 1: Schematic of LRSD for multilane vehicle emissions measurement.



System performance results

Prior to an evaluation of the system to measure multiple lanes, the prototype was sent to Ispra's Joint Research Centre (JRC) for an evaluation of its performance. The tests were conducted on May 10, 11 and 12, 2022. The LRSD system was placed on a quiet road, with light positive slope of approx. 1.3°, with the main module on one side of the track and the reflector module on the opposite side of the road. PEMS-equipped vehicles were used as "Reference" to check the emissions measurements of the LRSD against a known method. To obtain instantaneous vehicle emissions at the RSD location, a set of five reference vehicles were all equipped with PEMS. PEMS measure the gaseous concentrations in and the mass flow of the exhaust of the vehicles within a known uncertainty range and were considered as the reference within this study. Calibrated systems from AVL and Horiba were used during the campaign. Each vehicle had its PEMS installed and pre- and post-test checks following the RDE (Real Driving Emission) regulation were performed. The systems were recording measurement data continuously with 1 Hz while the vehicles were driving on the JRC site and through the E-RSD setup about 20 times each. Details on PEMS measurements as regularly performed at the JRC can be found in Bonnel P. et al. 2022. The characteristics of the tested vehicle are described in Table 1.

Table 1: PEMS-equipped vehicles.

Vehicle ID	Model	Brand	Engine type	Fuel type	Emissions std	Year
1	Forester	Subaru	ICE	Gasoline	Euro 6d	2021
2	Q3	Audi	OVC-HEV	Gasoline	Euro 6d	2021
3	F-Pace	Jaguar	ICE	Diesel	Euro 6d-temp	2019
4	Golf	VW	NOVC-HEV	Gasoline	Euro 6d-temp	2020
5	Boxer	Peugeot	ICE	Diesel	Euro 3	2006

The results were presented in TRA2022, Lisbon (Buhigas et al., 2022) and a summary is shown in Figure 2. Linear regression revealed very good agreement of LRSD with PEMS data: CO/CO₂ slope = 1.02, R² = 0.78; NO/CO₂ slope = 0.94, R² = 0.93 and NO₂/CO₂ slope = 0.82, R² = 0.95.

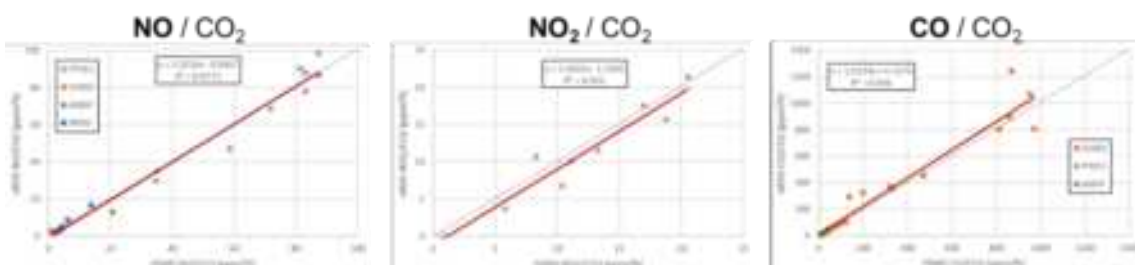


Figure 2: Scatter plots for NO, NO₂ and CO to CO₂ ratios (ppm/%) between PEMS (x-axis) and LRSD (y-axis) measurements for the different reference vehicles.

Top-down installation and performance assessment

After the JRC's evaluation the LRSD was tested in a top-down configuration in Madrid, Spain. The first test was done in October 2022, in a private test area of the company INDRA (www.indracompany.com), which collaborated in the project, installing the LRSD on a 1-lane gantry, with the reflector on the ground (Figure 3). The second test was done in December 2022, on a public 2-lane road, on a fully equipped gantry managed also by INDRA (Figure 4).



Figure 3: First deployment of the LRSD on a gantry in a test road. a) Retroreflector system installed on road. b) and c) System installed on the gantry.



Figure 4: Second deployment of the LRSD on a gantry in a public road. a) General overview. b) Detail on the laser module and one of the detectors over one lane.

The instrument alignment and measurement capabilities were tested in both top-down setups. Although there were no PEMS vehicles to repeat previous tests, there was a qualitative analysis on the measured concentrations. 24/7 uninterrupted monitoring was successfully tested too, with the system operating several days without interruption. The fibre optics for guiding the radiation from the laser module to the lane detectors worked well too. Fibre optics losses were measured, finding losses (including insertion losses and attenuation on the fibre optics), between 3.5 dB and 4.5 dB, depending on the wavelength and laser beam diameter for 2 m fibre length. The initial power output of the laser sources is between 20mW and 250mW. The system is capable to measure with signal around 3 mW per lane (in the worst cases). Therefore, considering also the splitting losses, at least two lanes can be measured with a single set of lasers, as tested in this experiment. A larger number of lanes could be measured if alternative laser radiation sources are found for those with lower output power or implementing more than one laser module.

However, although the experiment was successful, the researchers found several critical challenges for a top-down remote sensing system, which are described below:

- **Installation complexity:** The installation of a top-down system was found to be extremely challenging, especially for a multilane deployment. Installing equipment above the road requires complying with strict road safety rules. The reflector on the asphalt requires modifying the road itself, which is a separate and difficult procedure for road environment and road safety too. Additionally, a multilane deployment requires closing traffic lanes. All this makes the installation permits difficult and costly to get.
- **Equipment maintenance:** Any maintenance on the overhead modules requires overcoming stringent safety requirements, which is a barrier to establishing long-term, low-cost monitoring programs. Similarly, the road reflector has proven to be an even greater problem. The need for a clean reflector represents a critical problem due to dust and water accumulation, as well as durability issues caused by passing vehicles. These problems are more acute if the measurement site receives regular rainfall (as is the case in many parts of the world) and/or if the traffic intensity is high or with a high share of heavy vehicles passing by. Our findings suggest that any road reflector will need regular maintenance and sporadic replacement. This would require, again, solving challenging permitting and executing civil works, including closing lanes. These drawbacks increase the operational costs for a long-term monitoring.

Therefore, because of the shortcomings found above, a top-down measurement system may be less favourable than a cross-road system for continuous and long-term monitoring, which was precisely one of the objectives of this research."

Cross-road RSD adaptation for multilane measurement

In order to find a solution to the problems identified above, the RSD 5700 is adapted to measure on two-lane roads with a horizontal (cross-road) deployment. Although this type of setup has been tested in the past, it had never been implemented in a robust way. The system is upgraded with a double camera system, capable of identifying the passage of vehicles in the right and left lanes, reading their license plates associating them with each lane. The limitation of a dual-lane cross-road RSD is that if two vehicles pass parallel (or very close to each other) in the two lanes at the measurement point, the acquired column density refers to the sum of the pollutants emitted by the two vehicles. To

prevent this phenomenon, a logic is implemented that marks the measurements of events of this type as invalid. The software identifies the passage of each vehicle in each lane, with a timestamp and a vehicle speed. By applying a rule that leaves enough space between one vehicle and the next, the system can seamlessly identify isolated plumes of vehicles preventing cross-contamination, and flag passes from very close vehicles as invalid. With this methodology, considering typical traffic intensities on European roads, it is believed that these events would be very unusual in most locations. In other words, a dual-lane cross-road remote sensing approach can be efficient and trustworthy.

This new system has been tested in a two-lane test area. In this case the tests have been carried out in Teesdorf, Austria, in a test area of KAPSCH (www.kapsch.net) who is also a partner of the NEMO project. The tests were conducted in June 2023.

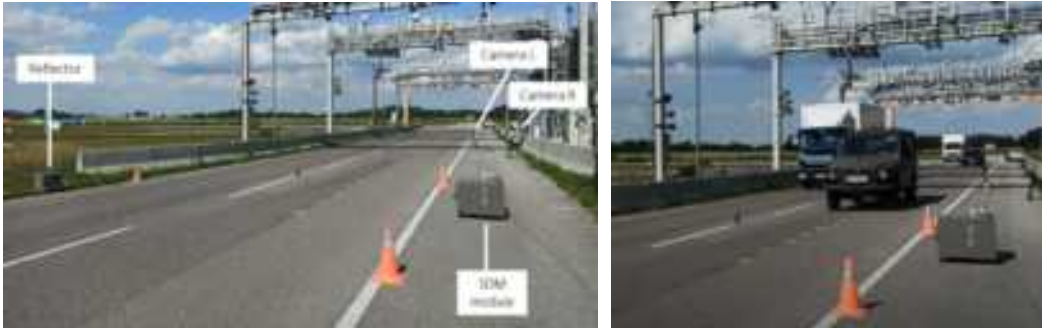


Figure
5:

Deployment of the RSD5700 on dual-lane road. Left: deployed components. Right: a photograph of four different vehicles circulating on both lanes.

A total of 2,202 records were collected over 3 days of measurements. 1,843 of those records were related to known vehicles (cars and trucks). Car drivers were instructed to circulate with and without acceleration, to capture small and large plumes. In all scenarios vehicles drove with a large or very close separation between them. Table 2 summarizes the percentage of valid measurements for the different tested scenarios. In the worst-case scenario (vehicle circulating in 2-lanes simultaneously and drivers were not accelerating at the measurement point) the validity rates are 49% and 76% for cars and trucks respectively, so there is still a high share of records with valid measurements even if vehicles drive very close on purpose.

Table 2: Valid measurement rates (% from total) in each tested scenario and vehicle type.

Scenarios	Validity rate for cars	Validity rate for trucks
1-lane driving no acceleration	71%	68%
1-lane driving with acceleration	98%	--
2-lane driving no acceleration	49%	76%
2-lane driving with acceleration	82%	--

The results are also analysed based on the vehicle-to-vehicle interval time, since it is the critical factor to ensure that the plumes can be measured in isolation. Figure 6 summarizes these results. Each bar shows the total valid measurements (in percentage) of each scenario, breaking down between passes of vehicles that are very close or separated. The results show that when vehicles are very close, the validity rates are 7% to 27%, as many of these events are discarded by the dual-lane algorithm. It is also observed that if vehicles pass by the system with some acceleration, the rates of vehicles with valid measurements are higher, whether the vehicles are closer together or further apart.

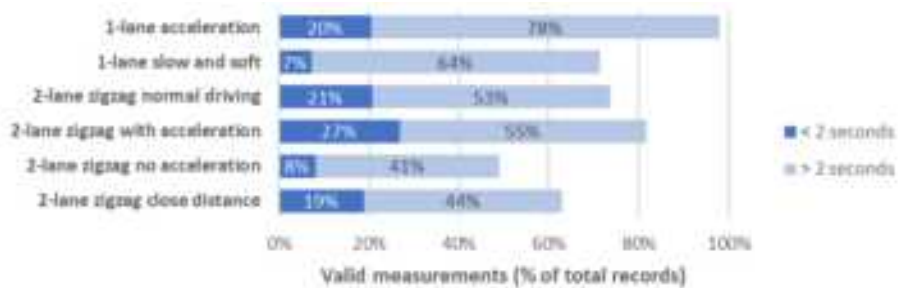


Figure 6: Valid measurement rates in each scenario and by vehicle-to-vehicle interval time. Dark blue: less than 2 seconds between one vehicle and the next. Light blue: more than two seconds.

Conclusions

- The developed LRSD system can measure vehicular pollutant emissions remotely and unassisted and can be installed in different road infrastructures to measure in a top-down manner the passing vehicles, but the technical and operational complexity of this configuration has proved to be very high. One of the reasons for considering a vertical approach is to facilitate unattended and cost-effective competitive monitoring in the long term, but the installation and maintenance costs of this deployment type can be insurmountable.
- The RSD 5700 in dual-lane mode can measure all types of vehicles traveling on dual-lane roads without installing any elements on the asphalt or over the lanes, which suggests that it can greatly facilitate both the installation and maintenance of the system, making it more viable than a vertical setup in the long-term. Thanks to the installation of internal cells in the RSD, the system can regularly self-audit itself, without the need for the use of any external gas cylinder, and therefore also operate 24/7 without any human assistance.
- Dual-lane measurements with a cross-road setup is feasible and reliable if the system marks as invalid records where there is an overlap of plumes (measured or potential). Taking into account that most of the kilometres of road built in the world are two-lane, this amplifies the possibilities for cross-road systems.

Acknowledgements

This project was funded by the European Commission within the H2020 programme in the NEMO project (ref. 860441). The authors thank the VELA team of the JRC for their work evaluating the system's performance and express their sincere thanks to the ITS companies INDRA and KAPSCH for their collaboration in the testing of the systems in Spain and Austria.

References

- Bernard Y., German J., Muncruief R. (2019). Worldwide use of remote sensing to measure motor vehicles emissions, *ICCT whitepaper*.
- Bishop, G.A.; Stedman, D.H. (1996). Measuring the Emissions of Passing Cars. *Accounts of Chemical Research*, 29: 489-495.
- Bonnel, P. et al. (2022). European market surveillance of motor vehicles - Results of the 2020-2021 European Commission Vehicle Emissions Testing programme, *EUR 31030 EN*, Publications Office of the European Union, doi:10.2760/59856, JRC128360.
- Buhigas et al. (2022). Performance of a remote sensing device based on a spectroscopic approach for the remote measurement of vehicle emissions, *Transport Research Arena (TRA) Conference*.
- Chen J., Furukawa H. (2023). Rapid and non-invasive detection of high-thickness glucose solutions concentrations using quantum cascade laser-based transmission infrared spectroscopy, *Infrared Physics & Technology*, volume 131.
- Graydon O. (2018). Interband cascade laser. *Nature Photon* 12, 568.

Advanced Air quality sensors and Remote Sensing to investigate vehicular traffic emissions in Milan: CARES H2020 Project results

S. Moroni^{1*}, F. Cruz Torres^{1,8}, R. Pedrini¹, P. Palomba¹, S. Belmuso¹, M. Bedogni¹, S. Casadei², T. Rossi², G. Migliavacca², M. Knoll³, C. Schmidt^{4,5}, H. Juchem⁴, D. Pöhler^{4,5}, Y. Bernard⁶ and A. Sjodin⁷

¹ AMAT Agenzia Mobilità Ambiente e Territorio s.r.l., Department of Environmental Transition, Milan, 20134, Italy

² Innovhub - Istituto Sperimentale per le Nuove Tecnologie dell'Industria Milano, 20134, Italy

³ Graz University of Technology, Institute of Electrical Measurement and Sensor Systems, Graz, 8010, Austria

⁴ University of Heidelberg, Institute of Environmental Physics, Heidelberg, 69120, Germany

⁵ Airyx GmbH, Eppelheim, 69214, Germany

⁶ ICCT International Council on Clean Transportation, Berlin, 10178, Germany

⁷ IVL Swedish Environmental Research Institute, Box 530 21, SE-400 14 Gothenburg, Sweden

⁸ Politecnico di Milano, Department of Energy, 20156 Milan, Italy

Corresponding author: silvia.moroni@amat-mi.it

Keywords: sensors, air quality, remote sensing, vehicular traffic emissions.

1. Introduction

To support urban air quality (AQ) policies, sensor technologies entailing lower costs than reference instruments have recently become available and may complement traditional AQ reference instruments (Kang et al., 2022). One of the cities currently equipped with such AQ sensors is the city of Milan, Italy. In particular, Milan is equipped with advanced, i.e., near-reference, AQ sensors through AMAT, an agency belonging entirely to the Municipality of Milan. Such technologies (Moroni et al., 2022) seamlessly collect information at vulnerable sites to support the implementation of the recently adopted local Air Quality and Climate Plan.

The City of Milan was involved in the EU funded Horizon 2020 project *City Air Pollution Emission Sensing*⁵ (CARES). Such project investigated real-world emissions to help improve urban AQ as well as enforce pollutants limits in three European cities, including Milan. Emissions from over 45,000 real-driving vehicles were monitored in Milan during the fall 2021. Measurements were carried out by means of remote emission sensing (RES) techniques, including commercial systems and an innovative, lower cost, point sampling (PS) system. The latter may constitute a more accessible system to detect emissions from high-polluting vehicles, which are targeted by Congestion Charge Zones and Low Emission Zones such as Milan's Area C and Area B. Additionally, advanced AQ sensors may provide an easily deployable system to determine airborne pollutant concentrations, thus providing city administrations with a more complete effectiveness evaluation of their AQ policies.

Assessments of advanced AQ sensors performance, which differ from low-cost sensors (cf. Castell et al., 2017), are still few to date (Karagulian et al., 2019) and the CARES project provided the unique opportunity to assess a subset of such advanced AQ sensors. In particular, in this paper the sensors' capability to detect exposure to vehicular traffic-related emissions, including from high polluting vehicles, was analysed.

2. Material and methods

For this research a measurement campaign was carried out during the fall of 2021 at the H2020 CARES Project RES location of Via Madre Cabrini (Milan, Italy). This street well exemplifies urban street canyons and develops along the south-west to north-east direction.

In the next sections the methodology followed by this research is outlined (Section 2.1) and the related instrumentation is described (Section 2.2).

2.1 Methodology

As a first step of the measurement campaign, the compact AQ station equipped with advanced (near-reference) sensors technology (Sun et al., 2016), deployed by AMAT, and a reference mobile AQ cabin, deployed by Innovhub-SSI, were collocated. The collocation enabled simultaneous, parallel measurements of the same set of pollutants. Such collocation made it possible to determine the accuracy of the advanced sensors compared to the reference instruments.

At this stage, observations were filtered so that data collected during precipitation events (> 0 mm), windy events (wind intensity > 1.5 m/s) and when wind comes through the street canyon opening (wind intensity > 0.2 m/s and

⁵ <https://cares-project.eu/>

direction from 303° to 346°) were excluded. The number of observations before weather-related filtering amounted to 25,688. Remaining datapoints after data filtering amounted to 22,335 (83%), whereby datapoints excluded are 2,315 (9%) for wind intensity and 1,038 (4%) for rainfall. This filtering operation made it possible to limit the undesired effect of the urban canyon opening and to only consider data during convenient weather conditions for AQ monitoring.

As a second step, the compact AQ station was deployed in combination with the RES systems in the typical urban street canyon of via Madre Cabrini for eleven days (from 27.09.2021 to 07.10.2021) to detect traffic-related air pollutant concentrations (e.g., NO₂, NO, CO, CO₂, PM₁₀, PM_{2.5}, PM₁, particle number (PN) and black carbon (BC)).

At this stage, AQ data were collected by means of the advanced AQ sensors at a 1-minute resolution and compared with measurements from the RES point sampling system deployed by Graz University of Technology and Airyx GmbH. Such RES point sampling measurements were gathered at a 1-second resolution and averaged over 1-minute intervals, so as to consistently compare them with 1-minute AQ data. Additionally, 5-minute running means were calculated to determine statistical correlation between the two data series.

Finally, an analysis of variance (ANOVA) test was performed to verify the hypothesis that advanced AQ sensors are capable of detecting ~~each individual transit of vehicles by the street location~~. Traffic data was used to categorize each minute with the number of vehicles that passed through the street in that time frame. Subsequently, an ANOVA was carried out to test whether the mean value of each advanced AQ sensor pollutant is different among the categories of vehicular transits.

2.2 Instrumentation

The advanced sensors compact station (Mod. MAS-AF300, Sapiens Env. Technology Co., Ltd) deployed by AMAT was calibrated with reference instruments and is equipped with:

- Electrochemical sensors for detection of gaseous pollutants (NO, NO₂, O₃, CO),
- Photoionization detector for Total Volatile Organic Carbon (TVOC),
- Non-Dispersive Infrared - NDIR detector for CO₂,
- Optical Particle Counter - OPC equipped with 50 channels with length between 0.3 μm and 10.0 μm for PM₁₀, PM_{2.5}, PM₁ and Particle Number (PN),
- A 5 wavelength aethalometer, including 880 nm and 375 nm absorption analysis for BC monitoring. The measurement of BC is referred to the PM_{2.5} fraction.

The reference AQ monitoring station deployed by Innovhub-SSI is a relocatable cabin equipped with:

- SO₂ and CO analyzers, HORIBA model APSA-360 and HORIBA model APMA-360, respectively,
- An NO_x analyzer, HORIBA model APNA-360, which uses cross-modulated chemiluminescence.
- An Ozone analyzer, a HORIBA model APOA-360, utilizing non-dispersive UV absorption with cross-modulated flow.
- A methane and non-methane hydrocarbons analyzer, a HORIBA model APHA-360, based on flame ionization with cross-modulated flow.
- An ammonia analyzer CNH3S2, which relies on the chemiluminescence principle and is equipped with an additional NH₃ to NO converter consisting in a quartz tube filled with quartz wool heated to 980°C.
- The Aethalometer® Model AE33 by MAGEE Scientific is the analyzer used for Black Carbon monitoring.

The instruments used in the reference Innovhub cabin for meteorological parameters detection are produced by MICROS. They are:

- a Relative humidity sensor MICROS model SRHS/C,
- an Atmospheric Pressure MICROS model SRHS/C SDVD.0/2,
- an Air temperature MICROS model STEP.0/2V,
- a Rain gauge MICROS model PLUV,
- a Total solar radiation sensor (pyranometer) MICROS PIR model,
- a Wind direction and speed sensor: MICROS model SDVD.0/2.

The sensors are fixed on top of an extensible pole by means of a support, consisting of a stainless-steel bar fitted with two collars.

Meteorological parameters (ambient temperature, pressure, precipitation, wind and speed direction) could both be monitored with compact sensors integrated in the AQ relocatable station and reference instruments. In the current analysis, however, only meteorological data measured by reference instruments were considered.

3. Results

A first indication of the level of agreement between the advanced AQ sensors and the reference instruments can be seen in Figure 1 for NO₂ and Figure 2 for BC. When considering a 1-minute time resolution, a good agreement between advanced AQ sensors and AQ reference instruments can be noticed, despite the different principles of measure.

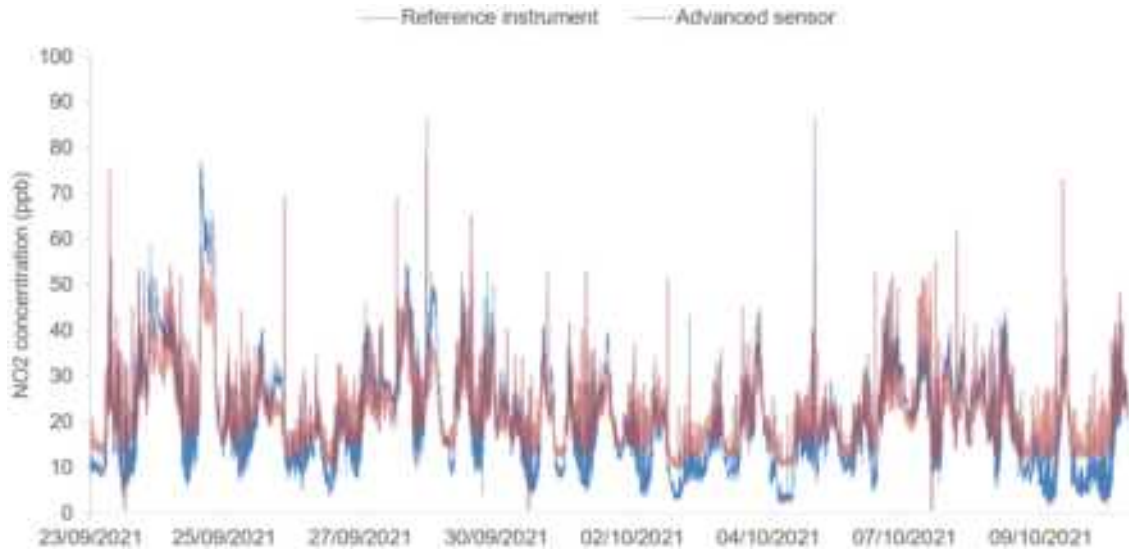


Figure 1. NO₂ concentration measurement collocation results.

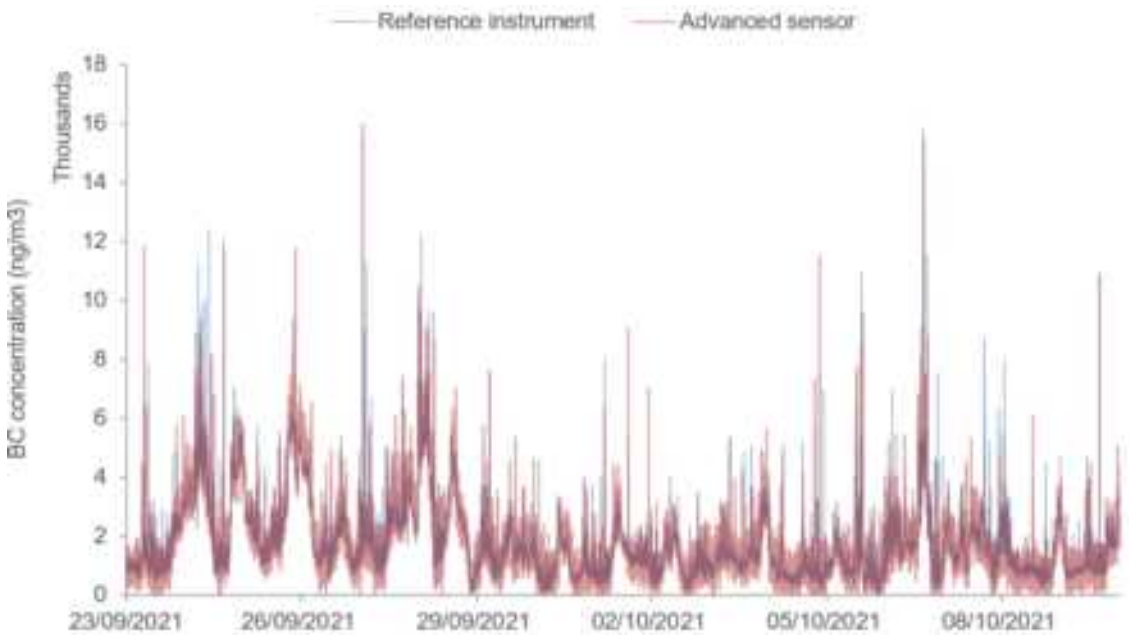


Figure 2. BC concentration measurement collocation results.

A more rigorous degree of agreement between advanced AQ sensors and the reference instruments was determined for each pollutant monitored via the coefficient of determination (R^2) and the regression model. The relative results (Figure 3) indicate that the advanced AQ sensors reach good agreement with the reference AQ instruments in detecting airborne traffic tracers such as NO₂ ($R^2 = 0.81$), NO ($R^2 = 0.74$) and Black Carbon ($R^2=0.79$) despite the different measuring principle. Also, Ozone (O₃), an important interfering pollutant for airborne NO₂ measurements, presents good agreement between AQ sensors and AQ reference instruments data ($R^2 = 0.80$). Carbon monoxide (CO) concentrations feature a lower correlation ($R^2=0.40$). This is probably due to the very low absolute airborne values near the lower detection limit, which leads to a higher noise variance in the data.

With regard to emissions, a significant positive correlation was observed between the advanced AQ sensors data and the RES Point sampling detections of gaseous traffic-related pollutants such as NO₂ ($R^2 > 0.60$) and CO₂ ($R^2 > 0.60$). Such results need to be viewed with due consideration of the existing distance (i.e., 15 m ca.) and height difference

between the RES system and the AQ monitoring site. Lower correlation coefficients are found for BC ($R^2 > 0.30$) probably due to the non-gaseous nature of the pollutant (gravity force, particle-particle interaction) (Figure 4).

The coefficient of determination R^2 relative to NO₂ measurements by advanced AQ sensors and by RES Point sampling system ranges between 0.6 and 0.8. In particular, the higher R^2 (0.8) is obtained when 5-minute average AQ concentrations are considered, instead of 1-minute ones. Moreover, as the level of NO₂ emission increases, as measured by the point sampling sensors, a less than proportional increase in the NO₂ concentration, as measured by the AQ sensors, can be expected. In particular, with the increase of 1 ppb (1.91 $\mu\text{g}/\text{m}^3$) of NO₂ measured by the RES Point sampling sensors, an increase of 0.5-0.6 ppb (0.96-1.15 $\mu\text{g}/\text{m}^3$) is observed on average in the measurements made by the AQ sensors.

The coefficient of determination R^2 relative to BC measurements by advanced AQ sensors and by RES Point sampling system ranges between 0.3 and 0.4. In particular, a higher R^2 is obtained when 5-minute average AQ concentrations are considered, instead of 1-minute ones. In addition, conversely to NO₂, as the level of BC emission increases, as measured by the RES Point sampling sensors, a less than proportional increase in the BC concentration, as measured by the AQ sensors, can be expected only when considering a 1-minute concentrations average.

The coefficient of determination R^2 relative to CO₂ measurements by advanced AQ and by RES point sampling sensors ranges between 0.7 and 0.8. In particular, the higher R^2 (0.8) is obtained when 5-minute average AQ concentrations are considered, instead of 1-minute ones. As a result, a clear agreement between the advanced AQ and RES point sampling sensors can be observed.

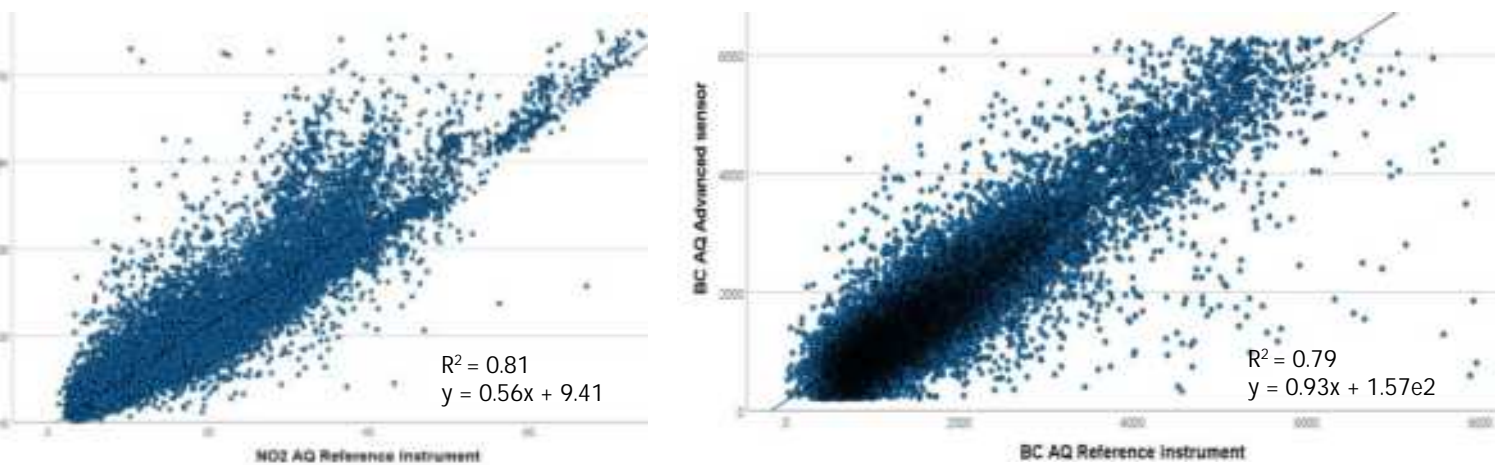
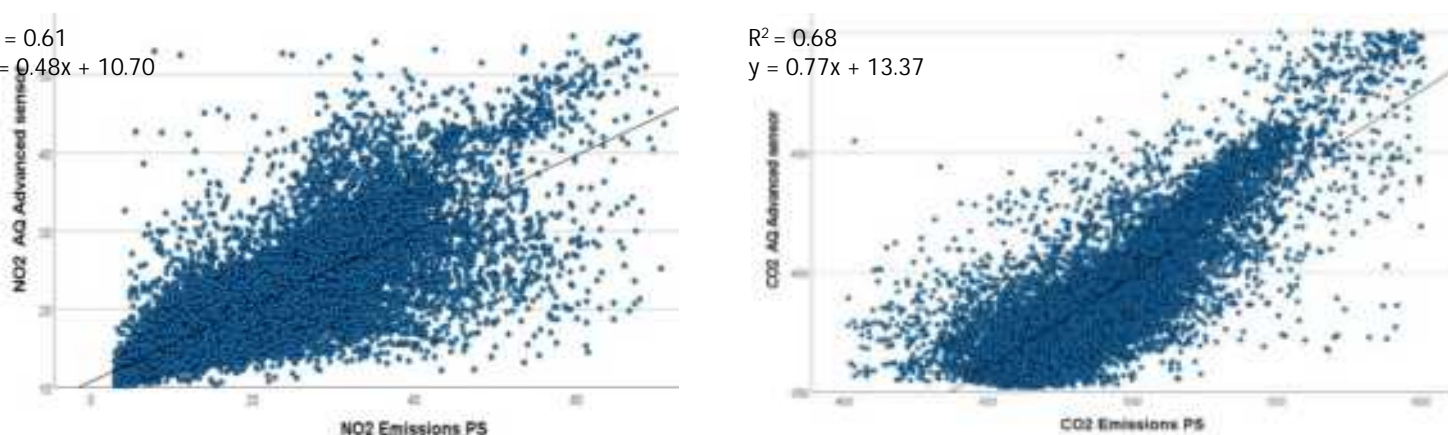


Figure 3. Agreement between advanced AQ sensors and reference instruments in the case of NO₂ [ppb] (left), and BC [ng/m³] (right).



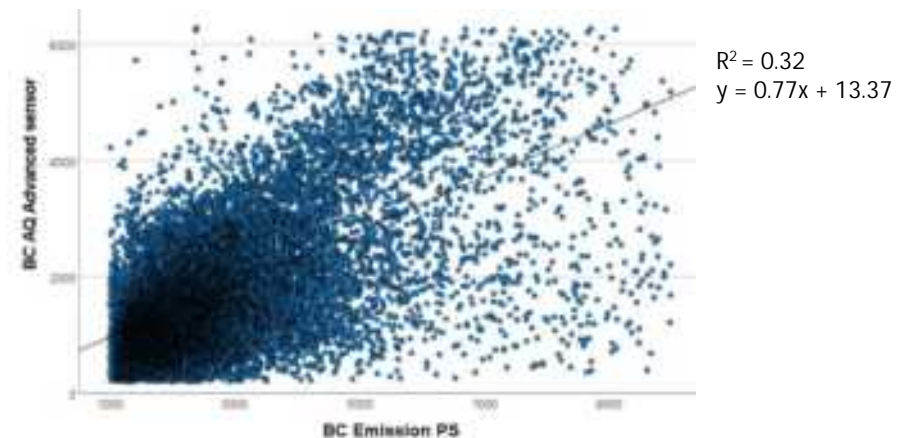


Figure 4. Relationship between advanced AQ sensors and RES Point Sampling measurements for NO₂ [ppb] (top left), CO₂ [ppm] (top right), and BC [ng/m³] (bottom).

With regard to traffic, ANOVA results show that advanced AQ sensors are capable of detecting incremental transits of vehicles (Figure 5). Indeed, as a consequence of an incremental vehicle transit, an increase in NO₂ concentration was observed. Such increase shows to be statistically significant for the incremental transit from zero to every other condition, also from one to two and from five to more than five.

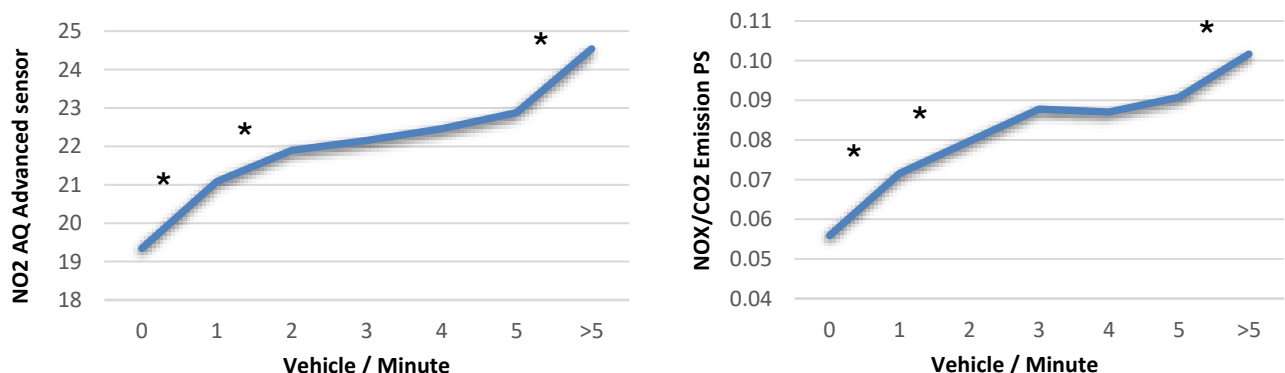


Figure 5. Impact of vehicle transits [Vehicle/Minute] on NO₂ concentrations [g/m³] as measured by the advanced AQ sensor (left) and NOx emission factor (NOx/CO₂) monitored by Point sampling (right) (statistically different means marked with *).

4. Conclusions

The H2020 CARES Project's Milan case study results demonstrate that advanced (near-reference) sensors technologies are capable of detecting exposure to traffic-related emissions (NO₂, BC, CO₂) in local environmental monitoring. Such sensors, recently available for AQ monitoring in the city of Milan, are able to detect exposure to high polluting vehicles as well. Moreover, the analysis of variance (ANOVA) test results show that advanced AQ sensors are capable to detect local traffic volume variations.

These results are important for the City of Milan and large European cities still not in compliance with the European Union's AQ limit values or breaching WHO AQ guidelines. For Milan, this means that advanced AQ sensors which continuously collect information at vulnerable sites, can support the Air Quality and Climate Plan recently adopted by the City Council, attempting to counteract vehicular traffic-related air pollution. For European large cities, these results suggest the adoption of lower cost technologies, both emission- (e.g., RES Point Sampling) and concentration-detecting, to better assess traffic policy effectiveness such as Limited Traffic Zones.

Acknowledgements

This project received funding from the EU Horizon 2020 research and innovation program under grant agreement No.814966 (CARES Project) and by the Agenzia Mobilità Ambiente e Territorio, a totally funded agency of the City of Milan.

References

- Castell, N., Dauge, F. R., Schneider, P., Vogt, M., Lerner, U., Fishbain, B., Broday, D., & Bartonova, A. (2017). Can commercial low-cost sensor platforms contribute to air quality monitoring and exposure estimates? *Environment International*, 99, 293–302. <https://doi.org/10.1016/j.envint.2016.12.007>
- Kang, Y., Aye, L., Ngo, T. D., & Zhou, J. (2022). Performance evaluation of low-cost air quality sensors: A review. *Science of The Total Environment*, 818, 151769. <https://doi.org/10.1016/j.scitotenv.2021.151769>
- Karagulian, F., Gerboles, M., Barbiere, M., Kotsev, M., Lagler, A., & Borowiak, A. (2019). *Review of sensors for air quality monitoring*. Publications Office. <https://data.europa.eu/doi/10.2760/568261>
- Moroni, S., Cruz Torres, F., Palomba, P., Santo, U. D., & Colombi, C. (2022). Near-Reference Air Quality Sensors Can Support Local Planning: A Performance Assessment in Milan, Italy. *Environmental Sciences Proceedings*, 19(1), Article 1. <https://doi.org/10.3390/ecas2022-12814>
- Sun, L., Wong, K., Wei, P., Ye, S., Huang, H., Yang, F., Westerdahl, D., Louie, P., Luk, C., & Ning, Z. (2016). Development and Application of a Next Generation Air Sensor Network for the Hong Kong Marathon 2015 Air Quality Monitoring. *Sensors*, 16(2), 211. <https://doi.org/10.3390/s16020211>

Remote Sensing Measurements of Vehicle Emissions in Sarajevo

Y. Cha and Å. Sjödin

IVL Swedish Environmental Research Institute, Stockholm, 10031, Sweden.

Yingying.cha@ivl.se

Introduction

Road traffic is often the main source of poor air quality in urban areas. Although stricter emission requirements and improved emission control technology in Europe have led to reduced emissions from petrol-powered vehicles, in particular since the early 1990s, problems with high emissions of nitrogen oxides (NO_x) and particulate matter (PM) from diesel vehicles remain. This is in part due to major shortcomings in EU exhaust legislation alongside historic deceptions perpetrated by car manufacturers (e.g. "dieselgate"). As a result, emissions during real-world driving in traffic are many times higher than in driving cycles used to set legal requirements. Consequently, air quality in European cities has not improved in proportion to increasingly toughened legal requirements. As a result, interest in measuring emissions in real traffic has increased sharply in recent years, both by national authorities and individual cities.

A comprehensive investigation of air pollutant emissions from traffic in real-world environments can help to better understand the impact of transport on urban air quality and to support regulations and techniques to mitigate future emissions. Remote sensing (RS) technology is a well-established technique to monitor real-driving traffic emissions and has been used extensively throughout the world. RS is well suited to measuring different types of pollutants, especially gaseous species. The data handling and processing of RS is also well-developed which makes it easy and efficient to apply for tests at different scales.

In this study, an intensive vehicle emission campaign was conducted with OPUS RS devices at four sites in Sarajevo, the capital of Bosnia and Herzegovina, in the summer of 2022 to measure air pollutant emissions from on-road traffic. The pollutants measured include gaseous species; oxides of nitrogen NO_x , nitrogen dioxide NO_2 , hydrocarbon HC, and carbon monoxide CO, as well as particulate matter PM. Around 25,000 vehicle passages were recorded of which approximately 14,000 vehicles were analysed. These covered passenger cars (PC), light commercial vehicles (LCV), buses, trucks, and motorcycles.

This report describes the Sarajevo measurement campaign and summarizes the main findings from the measurements. Emissions of NO_x , PM, CO, and HC from passenger cars were analysed in terms of the fuel-specific and distance-specific emissions. The emissions of NO_x and PM from the Sarajevo measurement campaign were compared with corresponding results derived from the CONOX database from measurements carried out in Switzerland (Sintermann et al., 2021) and Italy (Bernard et al., 2023) in the year of 2021.

In addition, distance-specific emissions were evaluated against the corresponding type-approved regulatory limits. Findings from the measurements of other type of vehicles, such as LCV, buses, trucks, and motorcycles are presented. The main findings are highlighted in the conclusion section and outlooks for future work are provided.

Overview of measurements

Measurement site

The measurement campaign was carried out at four sites in Sarajevo city: site KSL012 (Longitude 18.329452o, Latitude 43.840630o), located on Kurta Schorka and near the intersection of Kurta Schorka and Laticka; site KSL03 (Longitude 18.365916o, Latitude 43.851690o), located on street Radenka Abazovica between Safeta Zajke and Dzemala Bijedica; site KSL09 (Longitude 18.391150 Latitude 43.858410o), located on street Hamdije Cemerlica near the intersection of Hamdije Cemerlica and Put zivota; and site BETANIJA (Longitude 18.407006o, Latitude 43.87170o), located on street Betanija at the intersection of Alipasina and Betanija. (KSL012, KSL03, KSL09, and BETANIJA)

Distribution of samples

There were 25,079 vehicle passages recorded in total, of which 15,409 (61.4%) were identified as passenger cars (PC), 1,787 (7.1%) were light commercial vehicles (LCV), 197 (0.8%) were buses, 134 (0.5%) were trucks, and 80 (0.3%) were motorcycles. For 7,472 (29.8%) records, the vehicles could not be identified. The measurements comprised approximately 14,000 unique vehicles, as some vehicles were measured more than once. The fuel used for PC was 77.4% diesel and 22.6% petrol. For LCV it was 85.3% diesel and 14.7% petrol, for buses 59% diesel and 41% with other type of fuel (such as CNG and LPG), for trucks 98% diesel and 2% petrol, and motorcycles were all petrol-powered. The measurements of heavy-duty trucks were less successful due to less effective vehicle license plate identification.

Results

Passenger cars: fuel-specific emissions

Of the 15,409 remote sensing measurements recorded for passenger cars, 11,928 cars were diesel-powered and 3,477 were petrol-powered. In this section, the fuel-specific emissions of PM, NO_x, NO₂, HC and CO are presented. The NO_x emission results from the Sarajevo measurement were compared with corresponding data retrieved from the CONOX database. Distance-specific emissions of PM, NO_x, HC, and CO were also evaluated to compare to the legislative emission limits.

The valid numbers of remote sensing measurements for the emissions of PM, NO_x, NO₂, HC, and CO by fuel type and emission standard are summarized in Table 1. The most common vehicles were Euro 3, Euro 4, Euro 5 and Euro 6, and consisted of about 96% of all the diesel vehicles and 94% of all petrol vehicles. For PM, the average measured emission decreased from Euro 1 to Euro 6 for both diesel and petrol cars. The average PM emission for Euro 6 was 0.024 g/kg fuel for diesel vehicles, and -0.0005 g/kg fuel for petrol cars. Negative average values indicate the majority of the emissions measured were below the detection limit of the remote sensing instrument. Much lower PM emissions were observed for petrol cars compared to diesel cars for Euro 1-4, while for Euro 6 the difference between diesel and petrol vehicles was small. A large reduction can also be seen for NO_x emissions from Euro 2 (18 g/kg fuel) to Euro 6 (close to 0 g/kg fuel) for petrol vehicles, while for diesel vehicles the change is slower varying from around 17 g/kg fuel (Euro 2) to 8.5 g/kg fuel (Euro 6).

Higher emissions of HC and CO were measured for petrol cars compared to diesel cars. However, remarkable reductions were observed with increasing emission standard from Euro 1 to Euro 6 for petrol vehicles, with a reduction ratio of approximately 95% for CO and 96% for HC.

Table 1. Summary of the number of pollutant emission measurements for passenger cars by emission standard and fuel type (diesel and petrol).

Standard	Diesel counts (share)	Petrol counts (share)
Euro 1	73 (0.6%)	22 (0.6%)
Euro 2	217 (1.8%)	155 (4.5%)
Euro 3	2,459 (20.6%)	633 (18.2%)
Euro 4	3,661 (30.7%)	1,079 (31%)
Euro 5	3,516 (29.5%)	723 (20.8%)
Euro 6	1,831 (15.4%)	817 (23.5%)
Unknown --	171 (1.4%)	48 (1.4%)
Total	11,928 (100%)	3,477 (100%)

Figure 1 and Figure 2 show the average measured fuel-specific NO_x and PM emissions, respectively, of passenger cars in grams of pollutant emitted per kilogram of fuel burned (g/kg) by fuel type and emission standard. The emissions were compared with the CONOX database, which were included in these figures. In the CONOX datasets, Euro 6 includes Euro 6, Euro 6b, Euro 6c, and Euro 6d. Average emissions of NO_x for Euro 2, Euro 3, Euro 4 and Euro 5 petrol cars from the Sarajevo measurements were remarkably higher, by a factor of 1.5 - 3, compared to the CONOX data. For diesel cars, unlike for the petrol cars, the NO_x emissions measured in Sarajevo were about 20-30% lower than the average levels obtained from CONOX. This is true for most Euro standards (Euro 1-5), except for Euro 6, for which the average NO_x emission in Sarajevo was about 40% higher than according to the CONOX-2021 dataset.

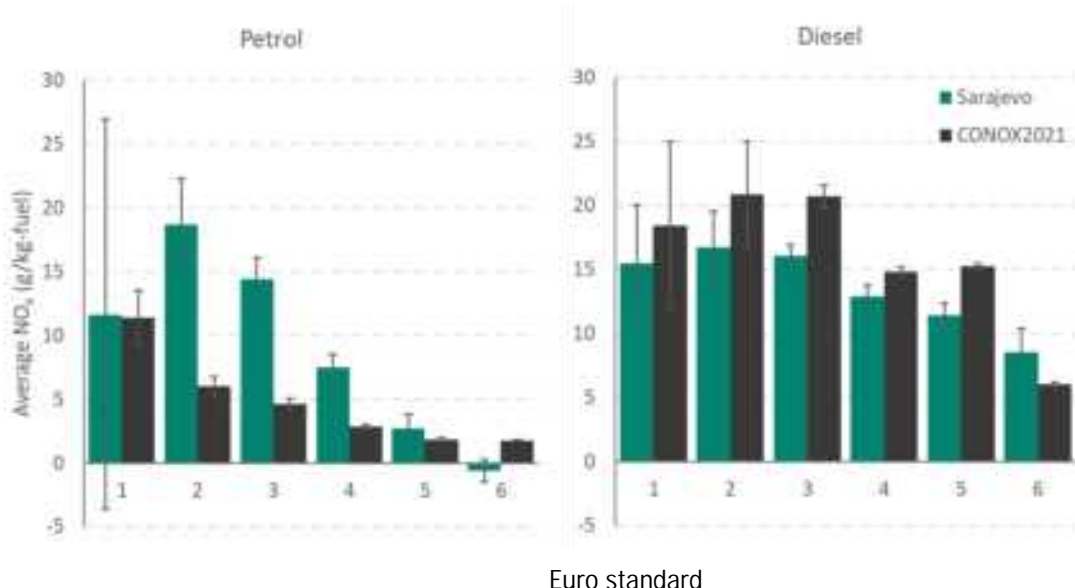


Figure 1. Average fuel-specific NO_x emissions from diesel and petrol passenger cars by emission standards for Sarajevo and CONOX database (2021). Whiskers represent the 95% confidence interval of the mean.

As can be seen in Figure 2, for petrol cars, PM emissions were substantially higher in Sarajevo compared to the CONOX data for all Euro standards, especially prior to Euro 5, except for Euro 6 in which case the average emissions of both datasets were close to 0 g/kg, i.e., below the detection limit of the RS instrument. The average PM emissions for diesel cars in Sarajevo were higher than those of the CONOX dataset for all Euro standards except for Euro 6, but the differences were not statistically significant.

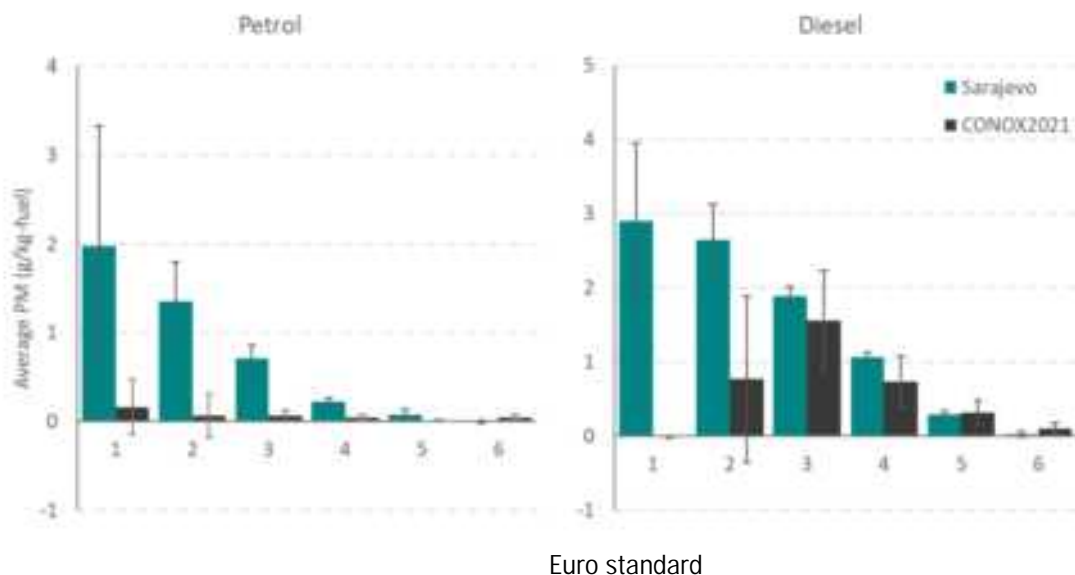


Figure 2. Average fuel-specific PM emissions from diesel and petrol passenger cars by emission standards for Sarajevo and CONOX database (measurements done in 2021). Whiskers represent the 95% confidence interval of the mean.

Passenger cars: distance-specific emissions

In addition to the fuel specific emissions of pollutants analysed above, the tailpipe pollutant concentration ratios were converted to distance-specific estimates in grams per kilometre (g/km), by combining the average pollutant emissions derived by RS with fuel consumption factors presented in Table 2.

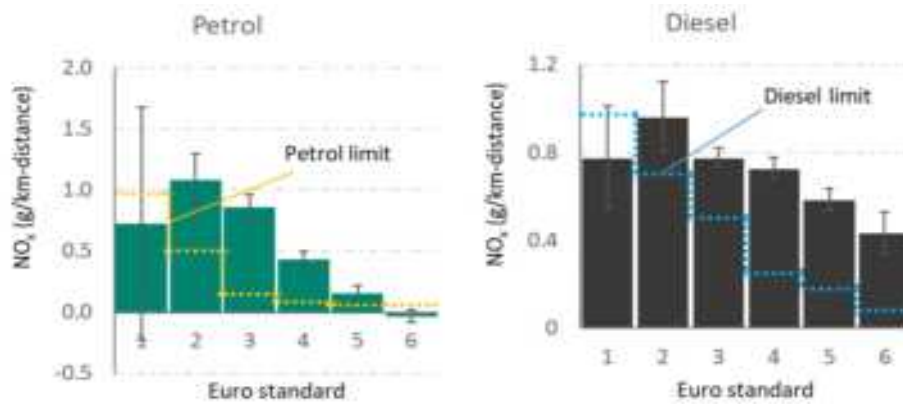
Table 2. Fuel consumption factors for passenger cars (Borken-Kleefeld et al., 2018)

	Diesel PC	Petrol PC
	FC kg/km	FC kg/km
Euro 1	0.0504	0.0622
Euro 2	0.0576	0.058
Euro 3	0.0485	0.0597
Euro 4	0.0565	0.0575

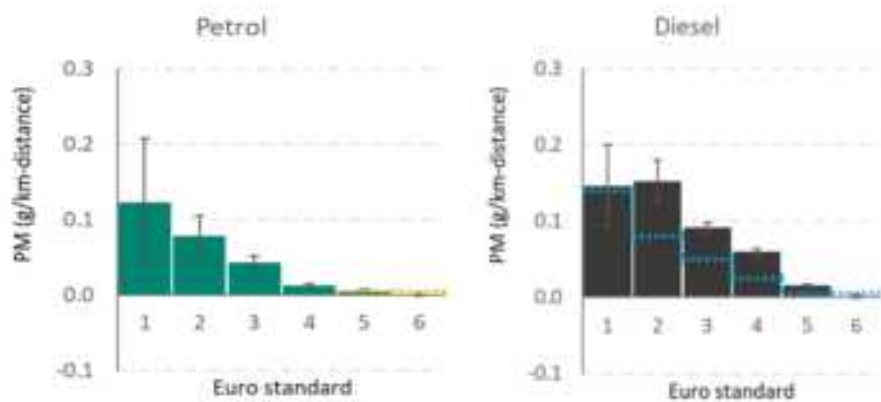
Figure 3 presents the average distance-specific NO_x, PM, CO and HC emissions by fuel type and emission standard for the Sarajevo measurements. The overall trend shows that the emissions of all pollutants (NO_x, PM, CO, and HC) have decreased with increasing emission standard for both petrol and diesel and cars. NO_x and PM emissions from petrol cars are lower than those from diesel cars, especially for the latest emission standards Euro 5 and Euro 6. This is contrary to the emissions of CO and HC which have reduced more slowly or levelled off. In comparison to the EU emission regulation limits for each stage, the real-world NO_x and PM emissions from diesel passenger cars greatly exceed the regulatory limits for vehicle groups including Euro 2-Euro 5, which were found to have real-world emissions of NO_x and PM about 40% to 220%, and about 80% to 200%, respectively, higher than the respective laboratory type-approval limits. For petrol vehicles with emission standards prior to Euro 6, the real-world measured values were 2-6 times higher for NO_x emissions (excluding Euro 1), 2-6 times higher for CO emissions, and 2-5 times higher for HC emissions, than the laboratory type-approval limits, respectively. CO and HC emissions from diesel cars were found to be lower than the limits for all emission standards, with only Euro 3 and Euro 4 found to have slightly higher CO emissions than the limits.

The share of NO_x and PM emissions (by g/km) from PCs and the share of measurements by fuel type and Euro standard were estimated. The results indicate that Euro 3, Euro 4, and Euro 5 diesel vehicles contribute the highest shares of total NO_x emissions from all passenger cars with a total share of about 74% for NOx emissions, which together account for about 63% of the total number of measurements. For petrol vehicles, Euro 3, Euro 4, and Euro 5 petrol vehicles make up 16% of the total measurements and they together only contribute 13% of the total NO_x. Similarly, Euro 3 and Euro 4 diesel vehicles together are responsible for the greatest share of total PM emissions from all passenger cars, which are responsible of 74% of total PM emissions, with a share of only 40% of total measurements.

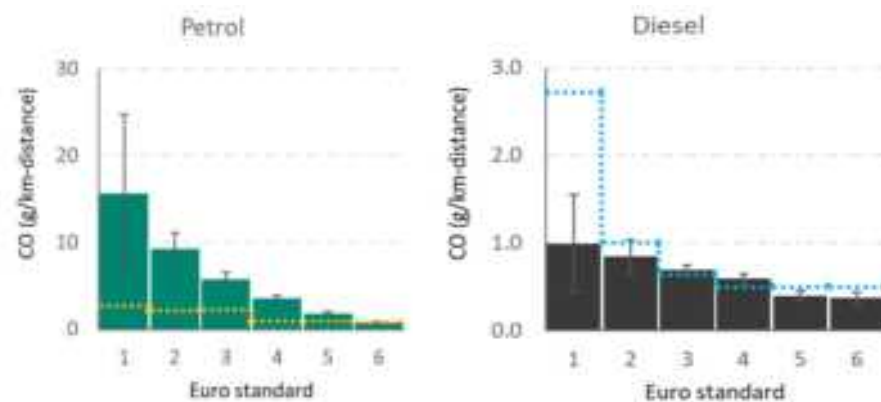
Euro 6 diesel and petrol cars were found to have lower real-world emissions of PM, CO, and HC than the regulation limits. For NOx emissions, Euro 6 petrol cars were measured with an average level lower than the limit, while Euro 6 diesel vehicles had approximately 5 times higher emissions of NOx than the regulation limit. This result indicates that the latest Euro 6 standard implementation step has significantly lowered real-world emissions of all regulated pollutants (NOx, PM, CO, and HC) for petrol cars and greatly reduced the emissions of the PM, CO and HC for diesel cars. NOx emissions are the only exception, which remain high for diesel cars. It should be noted that while Euro 6 petrol cars comprised 5% of all measurements, they produced negligible NOx and PM emissions (with both levels under the detection limit of the RSD). Euro 6 diesel cars contributed approximately 9% and 0.4% of total NO x and PM emissions, respectively, while comprising 12% of all measurements. Based on these findings, the replacement of previous Euro standard vehicles with Euro 6 vehicles will remarkably reduce the contribution of emissions from PCs to urban air pollution.



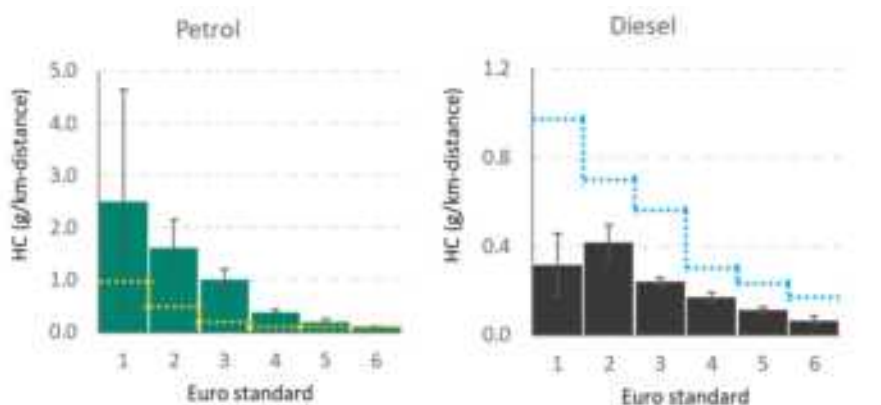
(a) NO_x emissions



(b) PM emissions



(c) CO emissions



(d) HC emissions

Figure 3. Average distance specific NO_x, PM, CO, and HC (gram per kilometre) emissions for diesel and petrol passenger cars by Euro standard. Whiskers represent the 95% confidence interval of the mean. Regulation limits for each emission substances are indicated with orange dash lines (petrol regulation limits) and blue dash lines (diesel regulation limits).

Emissions from LCVs, Buses, and Trucks

In total 1,787 measurements were obtained for LCV (7.1% of the total number of measurements), among which 1,524 (85%) were diesel-powered, 262 were petrol-powered, and one powered by other type of fuel. Around 90% of all diesel-powered LCVs were type-approved to Euro 4, Euro 5 and Euro 6. Of all petrol-powered LCVs, 57% were type-approved to Euro 6, with Euro 4 and Euro 5 constituting the remaining 42%. The average fuel-specific NO_x, PM, HC, and CO emissions were analysed. For petrol LCVs only Euro 4, Euro 5 and Euro 6 were detected in the Sarajevo campaign, and for diesel LCVs the total attempted measurements of Euro 1, Euro 2 and EEV was less than 20, which was considered too small to draw a representative conclusion. By looking at the results of Euro 4, Euro 5 and Euro 6 LCVs with both fuel types, decreasing trends were shown for NO_x, PM, HC and CO emissions as the emission standard increased, especially for petrol vehicles, although the average CO emission increased for diesel vehicles.

197 measurement records were identified as for buses (0.8% of total measurements), among which 116 (59%) buses were powered by diesel and 81 were powered by other types of fuel. For the diesel buses detected, the average fuel-specific emissions of NO_x and PM by emission standard were estimated. Approximately 49% of the diesel buses were Euro 2 and Euro 3, 33% were Euro 6, 7% were EEV, and the remaining were Euro 4 and Euro 5. The average NO_x emission of Euro 6 diesel bus was 13 g/kg fuel, which was slightly lower (around 10%-65%) than the buses with older Euro standards from Euro 3 to Euro 5. In comparison to other Euro standard stages, a significantly lower average PM emission (about 0.02 g/kg fuel) was found for Euro 6 buses, which was up to 30 times lower than Euro 2 buses.

There are in total 134 measurements (0.5% of total measurements) obtained for trucks, among which 131 (98%) were diesel-powered and 3 were petrol-powered. The measurements of heavy-duty trucks were less successful, due to vehicle license plate capture, as previously stated. By reviewing a random sample of 300 photographs where license plates were not identified, about 13% could be manually identified as trucks, indicating the proportion of trucks initially identified was heavily underestimated. Around 85% of all diesel trucks were Euro 3-6, with the remaining 15% made up of older emissions standards than Euro 3. Despite the small sample, a significant reduction in both NO_x and PM emissions, especially for PM emission, can be seen for the trucks with the latest Euro 6 emission standards.

Conclusions

The one-week remote sensing pilot study in Sarajevo successfully recorded around 25,000 vehicle passages from which emission measurements of PM, NO_x, HC and CO were made, split into different vehicle types (PC, LCV, trucks, buses and motorcycles), fuel types (mainly diesel and petrol) and Euro standards (Euro 1-6).

Data capture for heavy-duty trucks was less successful, due to less effective vehicle number plate identification, which is a well-known limitation of remote sensing in this context. A higher capture rate could be achieved with a different positioning of the video camera, but due to other problems (e.g., elevated tailpipes, connected trailers affecting the exhaust plume) associated with measuring exhaust plumes from trucks, capture rates will always be lower than for light-duty vehicles.

As observed in many other recent European remote sensing studies, the PM emissions from the Sarajevo vehicle fleet have reduced substantially for all vehicle types (on the order of 80-90%), as Euro standards increase from Euro 1 to Euro 6. In contrast, NO_x emissions from diesel vehicles have only reduced on the order of around 50%, despite the stricter Euro standards.

Euro 3 – 5 diesel passenger cars contributed 74% of all NO_x emissions from all passenger cars, while accounting for 63% of the number of all passenger cars measured. Similarly, Euro 3 and Euro 4 diesel cars together are responsible for 74% of total PM emissions from all passenger cars, while representing only 40% of all passenger cars measured.

The emission performance of the Sarajevo vehicle fleet deviates from that of other European fleets, mainly for petrol cars. Emissions of PM, NO_x, HC, and CO were substantially higher for pre-Euro 5 cars in Sarajevo, i.e., older cars, compared to those in other European cities where similar remote sensing measurements have also been performed. The main reason for this observation is the substantially higher share of high-emitting cars within the Sarajevo petrol car fleet.

The latter observation raises the question whether a lower quality of petrol fuel has been (and still is) used in Sarajevo than in the EU, e.g., with higher sulphur content poisoning the three-way catalyst, poor maintenance and/or tampering of the cars, possibly in combination with an inefficient inspection and maintenance program (PTI).

Based on the results from this study, the implementation of a low emission zone which impose restrictions on pre-Euro 6 diesel vehicles would significantly reduce the contribution of air pollution emissions from road traffic.

Future measurements should also consider a focus on heavy-duty, typically diesel fuelled, vehicles as their data capture were relatively low, while their relative contribution to NOX remains high.

Acknowledgements

We gratefully acknowledge the support of Opus RSE for both providing valuable input regarding the selection of measurement sites in Sarajevo and carrying out the remote sensing measurements. We gratefully acknowledge our colleagues at the Ministry of Traffic and the Ministry of Spatial Planning, Civil Engineering and Environment at the Canton of Sarajevo for investigating/assessing/documenting many different locations in Sarajevo allowing us to select the most appropriate measurement sites for this study. The support from IVL colleagues Helena Lundström, Anders Roth, and Tomas Wisell are highly appreciated.

References

- Borken-Kleefeld, J., Hausberger, S., McClintock, P., Tate, J., Carslaw, D., Bernard, Y., Sjödin, Å. (2018). Comparing emission rates derived from remote sensing with PEMS and chassis dynamometer tests - CONOX Task 1 report. IVL Report No. C 293. <https://www.ivl.se/english/ivl/publications/publications/comparing-emission-rates-derived-from-remote-sensing-with-pems-and-chassis-dynamometer-tests---conox-task-1-report.html>.
- J. Sintermann, G.-M. Alt, M. Götsch, F. Baum, V. Delb (2021) Langjährige Abgasmessungen im realen Fahrbetrieb mittels Remote Sensing https://www.zh.ch/content/dam/zhweb/bilder-dokumente/themen/umwelt-tiere/luft-strahlung/luftschadstoffquellen/verkehr/abgasmessungen-rsd/rsd_bericht_2021.pdf
- Bernard, Y. et al. (2021) Summary report on partner cities measurement campaigns. <https://cares-project.eu/wp-content/uploads/2023/06/CARES-814966-D3.4-Summary-report-on-partner-cities-measurement-campaigns.pdf>.

Emissions from In-use Vehicles in Dublin using On-road Remote Sensing

S. Mahesh^{1*}, B. Ghosh¹, A. McNabola¹, W. Smith², D. Timoney², B. Fowler³, and P. Willis³

¹Department of Civil, Structural and Environmental Engineering, School of Engineering, Trinity College Dublin, Dublin, Ireland,
Srinath.nda@gmail.com

²School of Mechanical and Materials Engineering, University College Dublin, Dublin, Ireland

³Ricardo Energy and Environment, Oxfordshire, United Kingdom

Introduction and background

Air pollution causes approximately 7 million deaths ~~per year worldwide and approximately 91% of world's population live in places where air quality exceeds World Health Organisation (WHO) guideline limits (WHO, 2016)~~. At present, it is the greatest environmental risk to our health and environment. In Europe, approximately 364,200 premature deaths annually are attributable to fine particulate matter ($PM_{2.5}$), ozone (O_3) and nitrogen dioxide (NO_2) exposure (EEA, 2021). The transport sector and more particularly road-transport emission is a major source of these key pollutants and greenhouse gases. In Ireland, the emission share from transport is about 20%, of which 95.8% is caused by on-road vehicles (EPA, 2018). Due to high density of on-road vehicles and due to proximity of pollutant generation to high density urban dwellings the impact of air pollution is higher in urban areas.

In Europe, air quality has been a priority and through policy development, legislation, standardisation and compliance, transport sector has successfully reduced emissions of some pollutants. However, reductions in emissions have been lower than originally anticipated over the last two decades. This is due to growth in road-transport, especially diesel vehicles, and the fact that the levels of 'real-world emissions' particularly from diesel passenger cars and vans, generally exceed the permitted European emission (Euro) standards, which define the limits for exhaust emissions of new vehicles sold in the EU Member States (EEA, 2019).

Since 1996, the introduction of European emission legislation, NEDC (New European Driving Cycle) has been used for vehicle type-approval tests in the EU. Several studies (Ntziachristos & Samaras, 2012; Dey et al., 2018) indicated that these laboratory tests using NEDC or similar cycles underestimate the exhaust emissions from in-use vehicles during real-world driving conditions due to low acceleration pattern, constant speed cruising and high number of idling events and other factors. The discrepancies between type approval and real-world emissions is significant.

In addition to the test cycle, laboratory tests are generally conducted using new and/or well-maintained engines/vehicles, which may not represent the conditions of a large proportion of most vehicle fleet. In reality, the level of vehicle maintenance has a significant effect on emissions (Bishop et al., 1996). The type of after-treatment used also affects the emission levels especially NO_x (Carslaw et al., 2011). The differences in emissions highlighted the need to include real-driving emission (RDE) testing to accurately estimate the emissions from in-use vehicles (Donateo and Giovinazzi, 2018; Carslaw et al., 2011). The main approaches used to measure emission rates from in-use vehicles under real-world conditions are principally Portable Emission Measurement Systems (PEMS) and vehicle emission Remote Sensing (RS). Typically, the PEMS is used in the RDE procedure and is the basis of the European RDE Regulations (European Commission, 2018). PEMS provides the advantage of providing detailed emissions information from individual vehicles over whole drive cycles in real conditions. Currently, PEMS is quite frequently used for generation of EFs (emissions factors) to models. It requires that individual vehicles to be instrumented which is costly and time consuming and can test only a small number of vehicles. The RS technology developed by Bishop and Stedman (Bishop and Stedman, 1996) utilises short-duration road-side measurement of individual vehicle plumes using IR long-path photometry. A large number of measurements are captured using RS to derive statistically significant measurements of emission estimates from different types of vehicles.

Remote sensing has been successfully used to distinguish between emission trends of petrol and diesel vehicles. In a study of light duty vehicles in Zurich during 2000–2012, it was seen that unlike petrol vehicles, the diesel NO_x emissions [g/kg fuel] had actually increased although emission limits had been progressively tightened (Chen and Borken-Kleefeld, 2014). Similarly, Carslaw et al. (2011) and Carslaw and Rhys-Tyler (2013) used RS in London and found that

only petrol vehicles showed a reduction in NO_x/CO₂ over the period of 1985–2012, while diesel vehicles, including those with after-treatment systems designed to reduce NO_x, showed little evidence of NO_x/CO₂ reduction.

Data collection and analysis

Remote sensing (RS) instruments measure tail-pipe emissions from passing vehicles under real-world driving conditions. RS instruments use an open-path optical measurement system that consists of ultra-violet (UV) and infrared (IR) light sources that are directed across a single lane carriageway to a mirror and then returned to the detection system within the remote sensing unit. The light is absorbed by pollutants as it passes through the exhaust plume and measured in relation to the absorption of carbon dioxide (CO₂) to provide pollutant emissions as ratios to CO₂ emissions. In conjunction with the vehicle emissions measurements, a camera records the number plates of passing vehicles, and a pair of light gates record the vehicle speed and acceleration. In this study, the camera was placed to capture the rear license plate of the vehicle. Vehicle details, such as make, model and fuel type, was later obtained from the number plate of each vehicle and merged to the emissions measurements for the vehicle.

In this study, a comprehensive remote sensing campaign spanning sixteen weeks was conducted. The campaign involved collection of real-world data in two phases: winter and summer across six different locations using Opus RSD 5000. The instrument is capable of measuring emissions of nitric oxide (NO), nitrogen dioxide (NO₂), particulate matter (PM), ammonia (NH₃), carbon monoxide (CO) and hydrocarbons. Emissions are measured as ratios to CO₂ and the analysis routine uses combustion equations to calculate fuel-specific emissions in units of grams of pollutant per kilogram of fuel (g/kg fuel). Distance specific emissions can be estimated from fuel-specific emissions by estimating the amount of fuel burnt per kilometre travelled (kg/km). The vehicle emissions presented in the subsequent section are in units of g/kg fuel. The number plate of each vehicle was matched to a set of vehicle details obtained from either the Department of Transport (Ireland), or derived from DVLA and SMMT databases in the UK, including, where available, vehicle type (i.e., car, van, bus, heavy goods vehicle (HGV)), fuel type, Euro standard, engine size, vehicle weight, date of registration, and the odometer reading at last mandatory vehicle testing.

The RSD 5000 is always calibrated internally prior to each data collection session, in a process that only takes a few minutes. During the session, the RSD 5000 was audited each hour, to verify the system is performing within specifications and does not need re-alignment and/or re-calibration. This process involves measurements of gases of known concentrations through the RSD5000. As data is collected, exhaust plume verification software reviews each measurement in real-time to ensure it is of adequate strength, that the exhaust plume decayed in a manner consistent with warm loaded-mode vehicle operations, and that the prevailing background levels are stable and can be accurately determined. Each session's dataset is compiled every day and put together into a database. Measurements were made at six locations with an aim to capture different vehicle types: (1) Southbound on Templeogue Road, directly after the traffic light-controlled crossroads, (2) Mayor Street Lower, a single lane road next to the tram lines, (3) College Green, on the bend of the R137 road, forking off the R138, (4) Southbound on Beach Road (Strand Road), directly after the junction with St John's Road (5) Southbound on Chapelizod Hill Road, underneath the Chapelizod Bypass bridge, and (6) Northbound on Richmond Street, next to the cycle lane. Sites at Mayor Street lower and Richmond Street were later omitted as they were found to be unsuitable due to less traffic or lack of acceleration when the vehicle passed the remote sensing setup.

In total, more than 136,000 emission tests were conducted which included cars, taxis, vans, and buses of different Euro emission standards and fuel types (predominantly diesel and petrol). The dataset included vehicles of five different fuel types with 59.1% diesel vehicles and 28,128 (29.2%) petrol vehicles. The share of hybrid and plug-in hybrid vehicles was 9.5% and the share of electric vehicles was 2.2%. This indicates that the vehicle fleet in Dublin is predominantly diesel fuelled and the share of hybrid / electric vehicles is low.

The vehicles were classified into different Euro classes based on their year of registration. Emission factors (in g/kg fuel) were determined for different Euro emission standards including Euro 6b, 6c, 6d-temp, and 6d.

Results and discussion

From Figure 1, we see that the CO emission factor decreases with evolution in the emission standard for all vehicle types. For cars, there is a significant reduction from Euro 4 to Euro 5 (28%), but a relatively smaller reduction from Euro 5 to Euro 6b (11.36%), and a decreasing trend is seen from Euro 6b to 6d(t). In the case of vans, the mean emission factor value reduces by 10.6% for Euro 5 compared to Euro 4 and by 16.6% for Euro 6b compared to Euro 5. A significant reduction (29.4%) is seen for Euro 6 buses compared to the Euro 5 buses. Comparing the different vehicle types with same emission standard, vans have the highest emission factors. Figure 2 shows the mean HC emission factors (g/kg fuel) for the different vehicle types and Euro classes within each vehicle type. Clearly, the HC emission factor decreases with improvement in the emission standard for all vehicle types. For cars, there is a significant reduction from Euro 4 to Euro 5 (35.7%), and a relatively smaller reduction from Euro 5 to Euro 6b (21.3%). In the case of taxis, a significant reduction is observed from Euro 4 to Euro 5 (35%) and also from Euro 5 to Euro 6b (22.5%). Comparing the different vehicle types with same emission standard, vans have the highest emission factor for Euro 4. Buses have the lowest HC emission factors among all the vehicle types.

The variation of the NO emission factors is shown in Figure 3. The trends are similar for cars, vans and taxis with Euro 6 having the lowest value and Euro 5 having the highest. Also, among the three vehicle types, taxis have slightly higher emission factor when compared to cars and vans of the same emission standard. This could be due to the relatively higher mileage and assertive driving style for taxis compared to cars and vans. In the case of buses, a significant reduction is observed for Euro 6 (0.5 g/kg fuel) compared to Euro 5 (25.6 g/kg fuel).

The variation of the NO₂ emission factors is shown in Figure 4. The trends are similar for cars and vans with Euro 6 having the lowest value and Euro 4 having the highest. In the case of taxis, the Euro 4 taxis had a significantly lower mean value (1.3 g/kg fuel) than Euro 5 taxis (2.1 g/kg fuel). Both Euro 5/6 buses have significantly low NO₂ emissions (< 1 g/kg fuel).

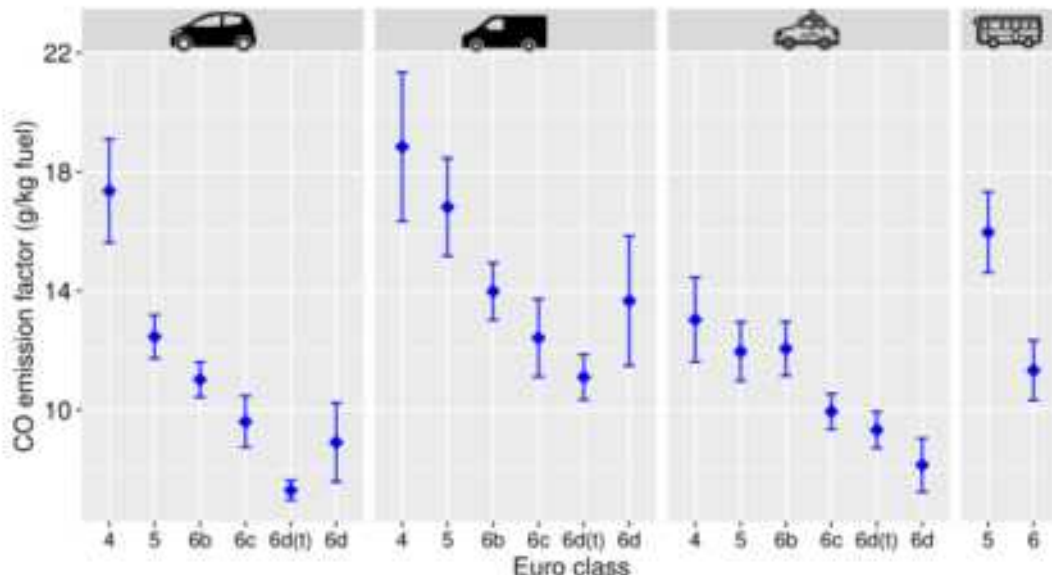


Figure 1: EF of CO (g/kg fuel) for different diesel vehicle types based on the Euro class. The point represents the mean and the error bars indicate one standard deviation on either side of the mean.

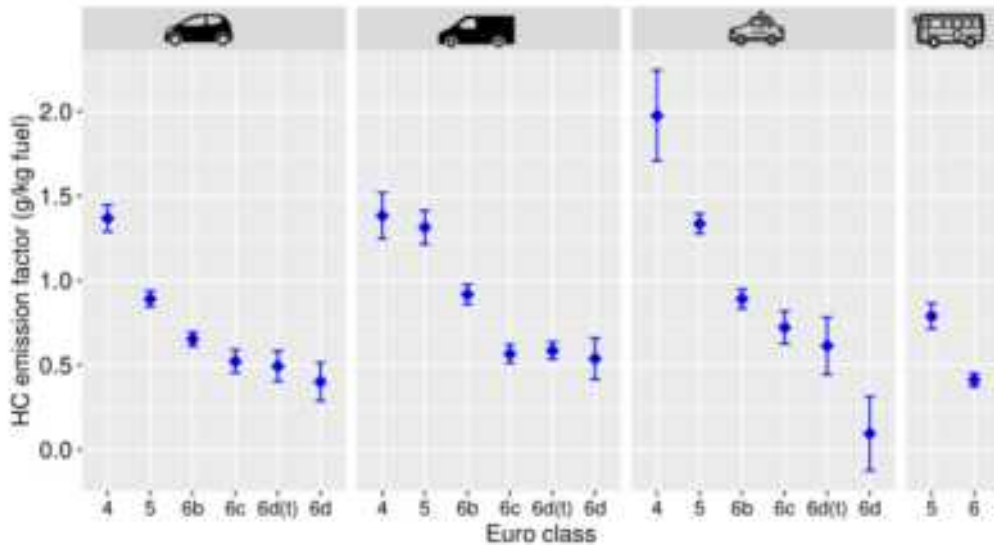


Figure 2: EF of HC (g/kg fuel) for different diesel vehicle types based on the Euro class. The point represents the mean and the error bars indicate one standard deviation on either side of the mean.

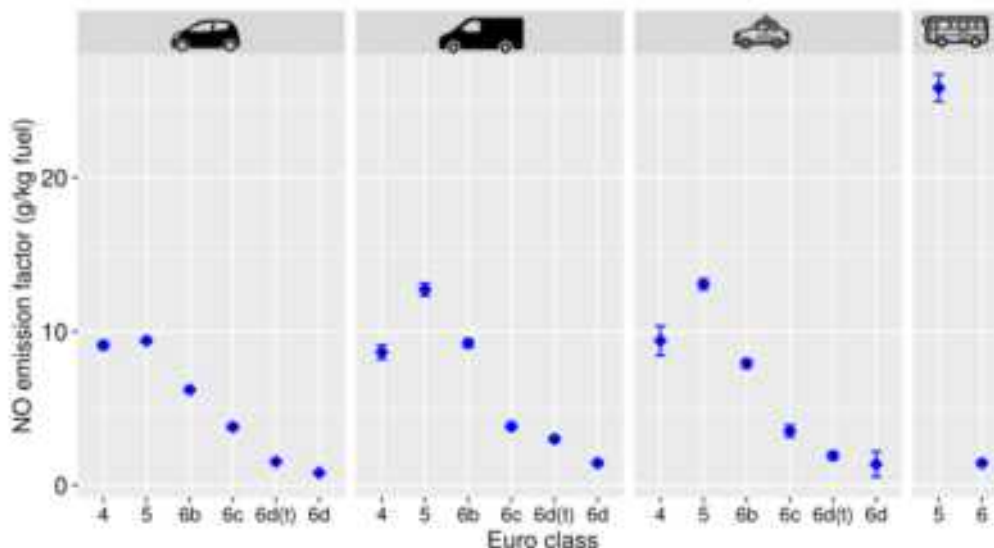


Figure 3. EF of NO (g/kg fuel) for different diesel vehicle types based on the Euro class. The point represents the mean and the error bars indicate one standard deviation on either side of the mean.

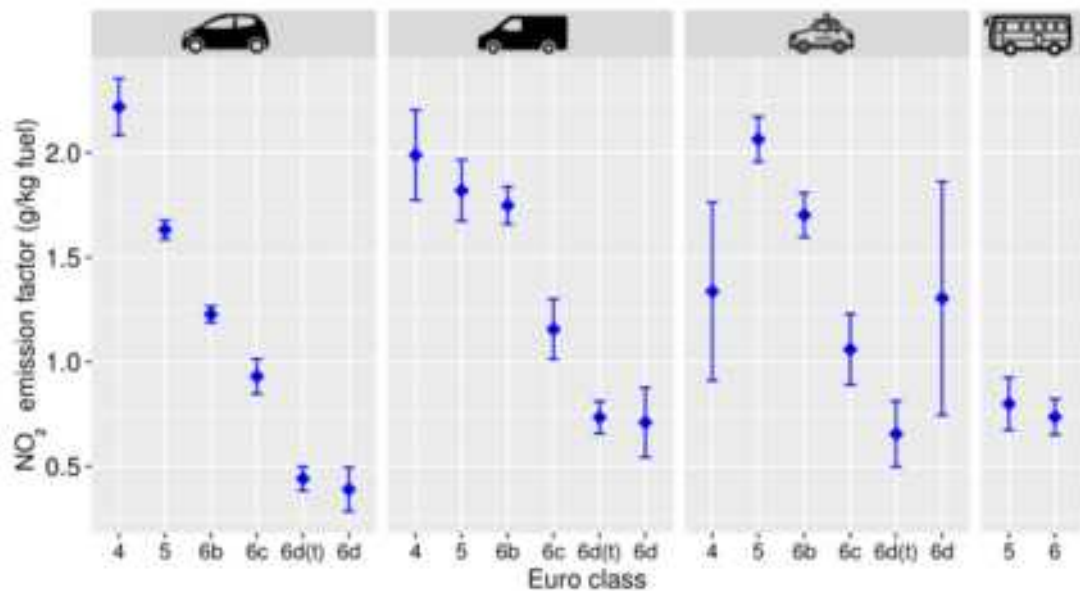


Figure 4: EF of NO₂ (g/kg fuel) for different diesel vehicle types based on the Euro class. The point represents the mean and the error bars indicate one standard deviation on either side of the mean.

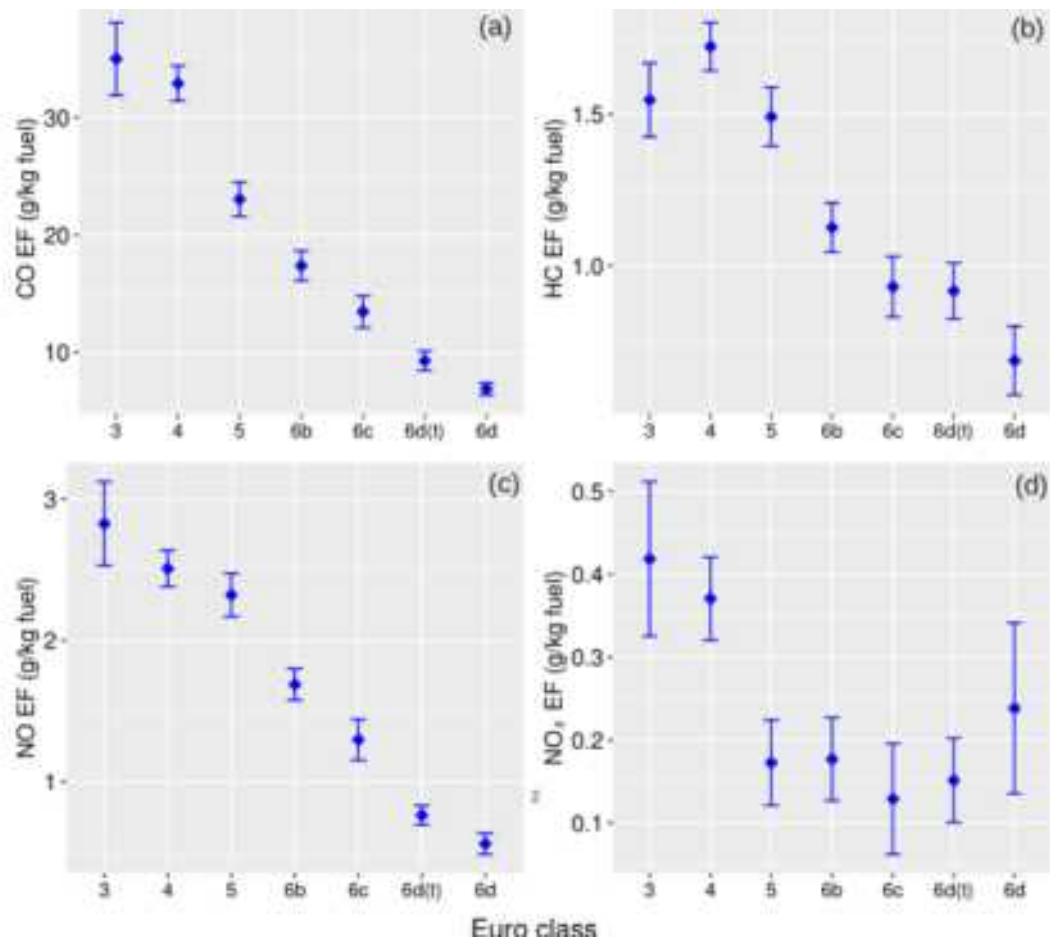


Figure 5: Emission factors (g/kg fuel) for petrol cars based on emission standards. The points represent the mean and the error bars indicate one standard deviation on either side of the mean.

The trends in NO EF with year of registration for petrol cars is shown in Figure 6. Similar trends are seen for both summer and winter plots. Comparing the winter and summer EFs for the same year of registration, the mean EF values are not significantly different. However, the variability is higher for the values before 2015 and lesser from 2016 onwards. The trends in NO₂ EFs are shown in Figure 7. The mean EF values are significantly lower in winter compared

to the summer values. The EFs in winter are less than 0.5 g/kg fuel for most of the vehicles and the values seem to have stabilized beyond 2015 in both summer and winter cases.

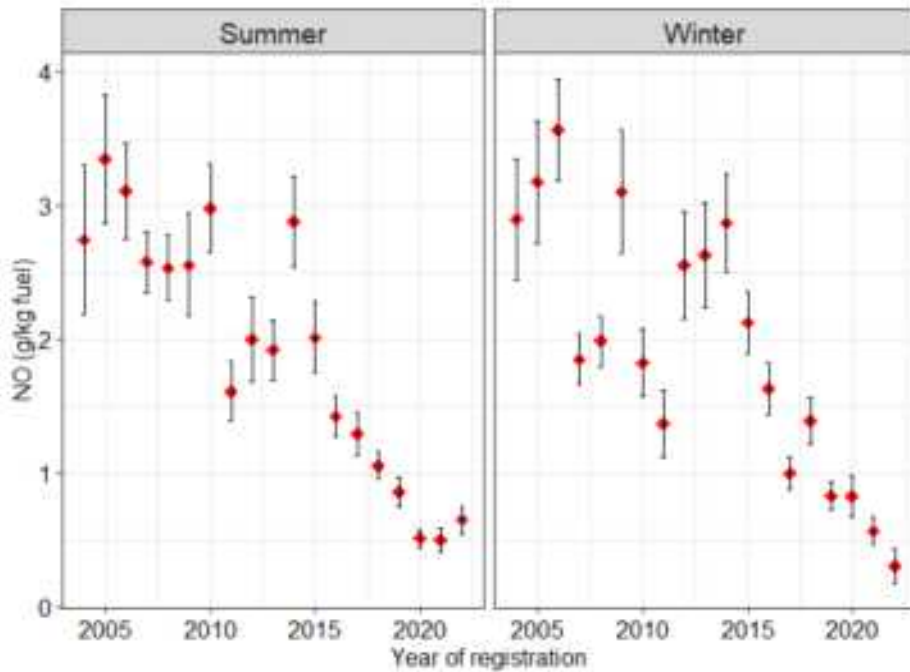


Figure 6: Trends in the NO EF with year of registration for summer and winter, petrol cars

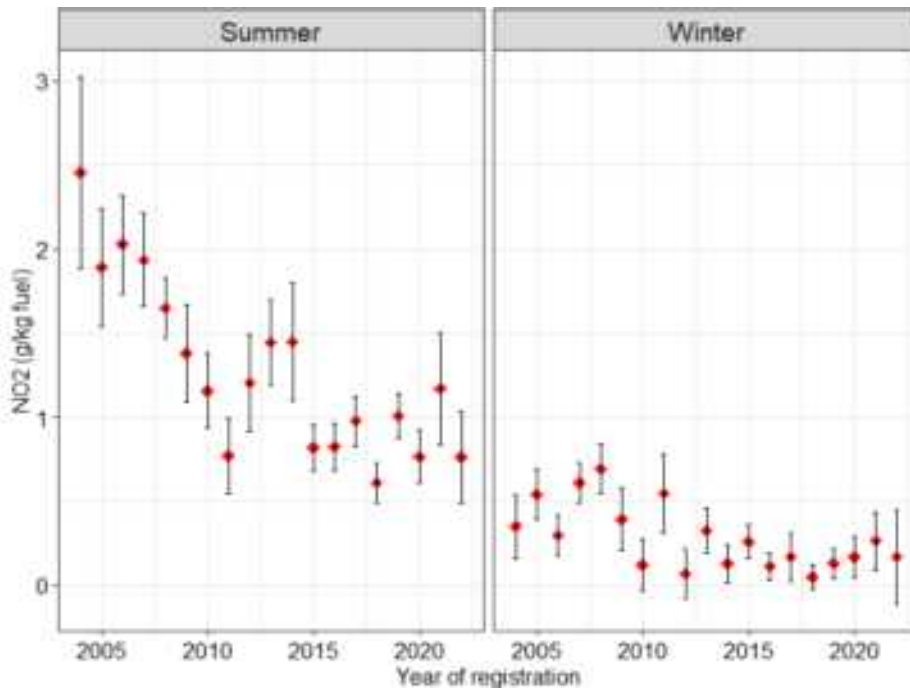


Figure 7: Trends in the NO₂ EF with year of registration for summer and winter, petrol cars

To summarize, the RS technique for measuring emissions of key pollutants (including NO, NO₂, and PM) from in-use vehicles was successfully applied for the first time in Dublin, Ireland. The data collection campaign, conducted in two phases, provided a comprehensive dataset comprising of different vehicle types (cars, taxis, vans, and buses) of varying makes, mileage, fuel type, and Euro classes. The dataset was used to determine the emission factors of CO, HC, NO, and NO₂ from the fleet of vehicles in Dublin. The Euro classes of the vehicles ranged from Euro 3 to Euro 6 with a large number of the latest Euro 6 vehicles in the dataset. Thus, the dataset can be considered to be representative of the current fleet of vehicles in Dublin, and the findings provide evidence for benefits of fleet renewal. However, since the study was restricted to Dublin, which may have a newer fleet of vehicles compared to other areas of Ireland, the

older vehicles may be underrepresented. Based on the findings from this study, it is recommended that similar remote sensing-based emission measurement studies should be carried out in other cities of Ireland, which would help in the quantification of emissions from in-use vehicles more accurately. This can form the basis for suitable emission mitigation measures for that particular city.

The trends in NO EFs were similar for diesel cars, vans, and taxis with Euro 6 having the lowest value and Euro 5 having the highest. Also, among the three vehicle types, taxis have slightly higher emission factor when compared to cars and vans of the same emission standard. This could be due to the relatively higher mileage and assertive driving style for taxis compared to cars and vans. In the case of buses, a significant reduction in NO EF was observed for Euro 6 (0.5 g/kg fuel) compared to Euro 5 (25.6 g/kg fuel). It is recommended that Euro 3 and Euro 4 compliant cars, and Euro 5 compliant buses are phased out as soon as possible. The NO emission factor reduced by 43.5% for Euro 6 relative to Euro 5. The HC emission factor increased from Euro 3 to Euro 4 and then decreased with a significantly low value for Euro 6 (1.0 g/kg fuel). The NO₂ emission factors were similar for Euro 5 and Euro 6 cars and significantly lower relative to Euro 3 and Euro 4. In general, an overall decreasing trend of emission factors was observed for NO and NO₂ with improving emission standards.

Conclusions

The analysis of the real-world emissions from different vehicle types using RS provided several important findings. A decreasing trend in the mean emission factor values of NO_x is seen for all the vehicle types. Decreasing trends were also observed for CO and HC with improvement in emission standards. The trends in EFs were compared for summer and winter and different trends were observed. The NO_x emissions from diesel cars decreased with registration year after 2015. This is likely a result of more stringent emissions limits for Euro 6 vehicles. The comparison of NO_x emissions for summer and winter campaign showed similar values with only slight increases for some registration years during the summer campaign. The NO_x emissions from buses dropped considerably after 2013, likely due to the introduction of Euro VI buses towards the end of 2013. In the case of petrol cars, the CO emission factor was similar for Euro 3 and Euro 4 cars and decreases significantly for Euro 5 and Euro 6 (41.3% less than Euro 5). A similar trend was observed for the NO emission factor with 43.5% reduction for Euro 6 relative to Euro 5. The HC emission factor increases from Euro 3 to Euro 4 and then decreases with a significantly low value for Euro 6 (1.0 g/kg fuel). The NO₂ emission factors were similar for Euro 5 and Euro 6 cars and significantly lower relative to Euro 3 and Euro 4. In general, an overall decreasing trend of emission factors was observed for CO, NO, and NO₂ with improving emission standards.

The findings from this study provide evidence that fleet renewal measures could lead to significant air quality benefits. The results also indicate the presence of a small number of vehicles which pollute significantly higher than others. Identifying and penalizing those vehicles would also impact the air pollution levels, especially along the major arterial roads. The results can also be useful for evaluating the effect of introducing low emission zones on local air quality.

Acknowledgements

This work was funded by the Environmental Protection Agency of Ireland and Department of Transport Ireland through the REDMAP project (No-209974/Award no-16217). The authors acknowledge Dublin City Council for providing permits for on-road data collection and Department of Transport for providing the vehicle registration data.

References

- Bishop, G. A., and D. H. Stedman. (1996). Measuring the emissions of passing cars. *Accounts of Chemical Research* 29.10: 489-495.
- Bishop, G. A., Stedman, D. H. and Ashbaugh, L. L. (1996). Motor vehicle emissions variability. *Journal of Air and Waste Management Association*, 46: 667–675.
- Carslaw, D. C., & Rhys-Tyler, G. (2013). New insights from comprehensive on-road measurements of NOx, NO2 and NH3 from vehicle emission remote sensing in London, UK. *Atmospheric Environment*, 81, 339-347.
- Carslaw, D. C., et al. (2011). Recent evidence concerning higher NOx emissions from passenger cars and light duty vehicles, *Atmospheric Environment* 45.39: 7053-7063.
- Chen, Y., & Borken-Kleefeld, J. (2014). Real-driving emissions from cars and light commercial vehicles—Results from 13 years remote sensing at Zurich/CH. *Atmospheric Environment*, 88, 157-164.
- Dey, S., Caulfield, B. and Ghosh, B. (2018). The potential health, financial and environmental impacts of dieselgate in Ireland, *Transportation Planning and Technology*, 41.1: 17-36.
- Donateo, T., and Giovinazzi, M. (2018). Some Repeatability and Reproducibility Issues in Real Driving Emission Tests. No. 2018-01-5020. SAE Technical Paper.
- EEA. (2021). Air quality in Europe – 2021 report. European Environment Agency, EEA Report No 15/2021.
- EEA. (2019) Progress of EU transport sector towards its environment and climate objectives
- EPA. (2018). Air Quality in Ireland 2017. Key Indicators of Ambient Air Quality. Environmental Protection Agency, Wexford, Ireland.
- European Commission. (2018). European Commission - Fact Sheet. Testing of emissions from cars. Brussels, 4 May 2018. Accessed on June 26, 2019. Accessed https://ec.europa.eu/growth/sectors/automotive/environment-protection/emissions_en on 09/07/2018
- Ntziachristos, L., Zissis, S., (2012). Exhaust emissions from road transport – EMEP/EEA Emission Inventory Guidebook 2009
- World Health Organization. (2016). Ambient air pollution: A global assessment of exposure and burden of disease.

Remote Sensing Emission Measurement on a German Motorway – Insights and initial Results

C. Piasecki^{1*},

¹ Federal Highway Research Institute (BASt), Brüderstrasse 53, 51427 Bergisch Gladbach, Germany, piasecki@bast.de

Introduction

The admission of motor vehicles to road traffic is regulated by the EU-wide type approval process. The effort linked with this permission is rather extensive and covers, among other things, the examination of the exhaust gas emissions under challenging conditions, laid down in EU Legislation (Reg. (EC) No 715/2007 and Reg. (EC) No 692/2008). Complex and standardized laboratory dynamometer test runs in defined driving cycles and on-road emission measurements with mobile measurement equipment (PEMS – Portable Emission measurement Systems) are carried out for this purpose. If the test results comply with the specified emission limit values under relevant driving conditions, the vehicle type is approved evidenced by a certain certificate. Besides the type approval procedure, there are different measures in operation to ensure that an approved vehicle meets the prescribed technical specifications over a defined period (usually defined as a specific lifetime durability or mileage requirements). Periodical technical inspections, market surveillance programs and roadside inspections should be mentioned here.

Independent emission measurements, however, installed along the roadside in running traffic have not been embedded in current regulations yet and have therefore only been carried out very occasionally and for research purposes (Ghaffarpasand et al., 2023). Due to partly supposed inconsistencies in the emission behavior of approved vehicles on the road compared to emission characteristics determined in the type approval procedure, such roadside measurements are becoming increasingly important. The project presented in this study is intended to use an overhead remote sensing measurement system "Emission Detection and Reporting" (EDAR) (Gruening et al., 2019), (Dallmann et al., (2019) from Hager Environmental and Atmospheric Technologies (HEAT) for measuring vehicles tailpipe emissions contactless on a federal motorway in Germany for the first time, see figure 1.



Figure 1: Emission Detection and Reporting System (EDAR) by HEAT (Hager Environmental & Atmospheric Technologies); roadside construction on German Motorway A61.

This procedure differs from the measurements applied in the type approval procedure in a way that it is only a selective and contactless measurement inside the exhaust plume of passing vehicles at a fixed location. The emissions are recorded in a specific vehicle operation point (with regard to e. g. vehicle speed, acceleration) and the measurement system is able to carry out a large sample of measurements within a comparatively short period of time. The data sets generated within this procedure can be used for in-depth emission analyzes and this large sample of data may represent a basis for initializing further emission investigations in future, if necessary.

Since the recording of exhaust emissions on a test bench or under real driving conditions (RDE) does not cover any vehicle operation points, the non-contact measurement of exhaust emissions in moving traffic is an additional instrument for getting insights into the real-world vehicle fleet emission characteristic. Due to the large number of vehicles recorded, the measurement method can, for example, discover aging effects of a specific engine and vehicle type. It is also possible to detect unusual emission characteristics or so called high-emitting vehicles. Measurements

with the EDAR system are – according to the current state of the art - no high-precision vehicle-individual measurements that would allow deriving expert statements on the individual vehicle emission behavior, however, such measurements are suitable for cluster formation of vehicle classes with similar technologies. So, initial statements regarding the fleet emissions and their changes over time can be derived. In addition to applications of remote sensing systems in the traffic sector, such data sets can also form a basis for analyzes and measures in the field of air quality issues, as ambient pollution concentrations are continuously recorded, too.

Project description and goal

In the framework of this project, a contactless emission measurement system for the recording of emissions in the exhaust plume of motor vehicles on public roads was installed and evaluated. The measurements were implemented in the moving traffic without affecting the traffic flow. Hereby, no adaption of the driving behavior in terms of artificial braking or changing lanes was provoked. The EDAR measuring system applied in this project recorded the relevant exhaust gas emission components on a German Autobahn spot (BAB) in a speed range between 80 km/h and 100 km/h. The location was selected by considering system-specific criteria, among others, vehicles had to drive under engine load at the measurement spot to generate specific exhaust gas flows that can be measured – realized by choosing a spot with a positive road gradient. An extensive approval process for setting up the measuring system including a test run was successfully completed before the measurements began. Measurements were then carried out on the BAB 61 in Rhineland Pfalz for twelve days in June 2022. The emission data measured were linked with relevant engine and vehicle specific characteristics (e. g. emission class, vehicle type, engine type, registration year etc.) from the official registration database of the Federal Motor Transport Authority (KBA). Therefore, a data protection concept was drawn up for this project, which focused primary on legal aspects like license plate detection and personnel data processing. Finally, the emission behavior of the vehicle fleet at the abovementioned spot was measured and analyzed regarding different criteria and vehicle characteristics like, among other things, vehicle category, emission classes as well as country of registration. As part of the research project, HEAT worked together with DTV-Verkehrsconsult GmbH and Prof. Borken-Kleefeld (Dresden University) in a consortium, who have already been active in this work area in several applications (Rauterberg-Wulff et al., 2021).

The overall goal of this research project presented here is to demonstrate the feasibility of a remote sensing emission measurement system on a federal motorway. Furthermore, the possibilities and limits of this measuring system for recording exhaust emissions in road traffic on motorways including legal and organizational aspects should also be shown. This includes, among other things, data protection requirements and the combination of emission data with vehicle features provided by the KBA. Even the main concern here was evaluating the feasibility and practicability of the measurement, the data obtained here should also be processed and analyzed in an exemplary evaluation. Hereby, it should become apparent in which specific areas remote sensing data might become a basis for dealing with environmental related questions and for deriving subsequent legal measures.

In addition, the interaction of the responsibilities for the process of a remote sensing measurement of different legal actors should be tested including the German Federal Office for Logistics and Mobility (BALM), the police and the Federal Motor Transport Authority (KBA). These three authorities are also responsible for market surveillance, roadside inspection and manipulation detection in the road traffic sector. It should be stated at this point that the project presented in the study focused explicitly on the goals outlined above and is not intended to uncover possible inconsistencies in the emission behavior of individual road users and their vehicles.

Location

Certain requirements have to be met for emission measurement with the EDAR system on public roads. These primarily include the general option of installing the system next to or above the motorway and access to the installation site, as well as the necessity for motor vehicles to be driven under engine load so that a relevant exhaust plume is generated at the measuring point. The mandatory specification in this project was the measurement on a federal highway. An extensive road selection process was carried out for this purpose. From the BISSTRA database (Federal street information system guidance by the Federal Highway Research Institute in Germany) some locations for the measuring system in the federal trunk road network were successfully determined.

System-related limitations occurred by the need for an electric power supply, the application and subsequent removal of a reflector strip on the road surface without leaving any residue, and the possibility of mounting the measuring system vibration-free. As a result, there were only very few locations on the motorways in North Rhine-Westphalia

and Rhineland-Pfalz declared as suitable in relation to the large number of kilometers of motorways in general. The traffic density at the measurement point also had to be considered to ensure that a sufficiently large sample of vehicle emission measurements could be collected. Opposed to motorways, finding a suitable location on rural or inner-city roads seems to be easier, as safety criteria and power supply issues can be enforced in a more manageable way. Finally, a location on the A 61 motorway was chosen for this project that suited best with abovementioned criteria. Here the measuring system was set up with a traverse system behind the crash barrier on an incline at operational kilometer 187,40 (see figure 2).



Figure 2: Location of BASt-coordinated emission measurement campaign via remote sensing technology (www.openstreetmap.org).

Data protection concept

The emission data recorded by the EDAR system need to be linked to technical specification of the measured vehicles in order to carry out a purposeful evaluation. These specifications include, among other things, criteria like vehicle class and -type, manufacturer, emission class, date of first registration, fuel type or energy source and unladen and maximum weight. This data is made available by the KBA. Therefore, it is necessary to record the license plates of the vehicles as a vehicle-unique feature and to match it with the centralized vehicle database. Even if number plates are recorded only for a short time, it is essential to create a comprehensive data protection concept due to the regulations laid down in the General Data Protection Regulation (GDPR, 2016). The creation of the concept in close cooperation with the Federal Commissioner for Data Protection and Freedom of Information (BfDI) was necessary in order to fulfill the high data protection requirements with regard to the protection of individual data of vehicle owners. Depending on the system and process, this has to be considered individually for each measuring system in which camera-based systems are applied. The creation process for the individual data protection concept used in this study was finally accepted by relevant authorities and can serve as a basis for further applications of the EDAR system in Germany. Depending on the location, however, the data protection concept must be individually adapted then.

Measurement

The measurement on the BAB A61 with the EDAR measurement setup on a specially designed traverse was successfully carried out in June 2022. The installation took a few hours with the appropriate preparation. However, the installation process on motorway is always associated with a lane closure, on the one hand for the application of the reflector strip on the road and on the other hand according to safety aspects. Once installed, the system works more or less autonomously, provided that a power supply is available. The measurements were carried out within the planned time slot without any interruptions. The weather conditions were favorable, there was no rain or strong winds during the measurement, that might affect the accuracy of the system. In total, approximately 124.000 vehicles were recorded within 12 days. The EDAR system was dismantled in the reverse order to the assembly. Here, too, the right lane had to be closed to remove the reflector strip and to uninstall the traverse mounting.

Results

Approximately 84% of the 124.000 recorded data sets contained all relevant information required for an in-depth emission evaluation. As already described, the focus of this pilot project was not the pure collection and evaluation of measurement data itself, instead, questions concerning the feasibility of remote sensing systems on German motorways in general including legal aspects were prioritized. Nevertheless, an initial evaluation of measured data sets was carried out of which selected results are presented in this study. Figure 3 allocates the measurements

according to EU-vehicle classes and, additionally, vehicles with non-German number plates are displayed. It is noticeable, that the share of foreign-registered vehicles is disproportionately high, accounting for almost one third of all valid measurements. The reason for this can be found in the commercial traffic (N3), which takes place particularly on the right-hand lane in Germany, which was the only lane measured here and contains a high share of foreign heavy-goods vehicles. By measuring the entire one-direction traffic an increase in passenger car data can be expected resulting in a reduced share of foreign registered vehicles.

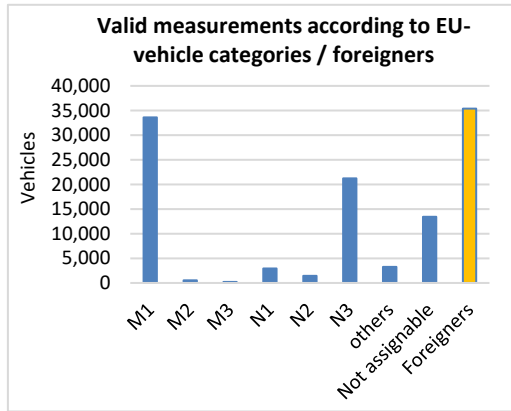


Figure 3: EDAR measurements differentiated according to EU-vehicle categories (Reg. (EC) No 2018/858) and by foreigner registrations.

With regard to the invalid measurements, it is assumed that either the measured pollutant concentration is too low, different exhaust gas plumes overlap and the measurement is therefore declared as invalid, or that the number plate was not recorded and assigned correctly. Concerning the emission behavior of the German passenger car vehicle fleet the following evaluation provides insights into the capabilities of the remote sensing system. The average nitrogen oxide (NO_x) emission values – indicated in grams / kg fuel – for Euro 6 approved diesel passenger cars with different registration years are shown, see fig. 4. For comparison purposes the type approval limit value of Euro 6 diesel passenger cars (80 mg / km, correspond to approximately 1.6 g/kg fuel) is displayed. A strong decrease of measured average NO_x values depending on the vehicles registration year and depending on the ongoing Euro 6 standard (from Euro 6b to Euro 6d) becomes apparent.

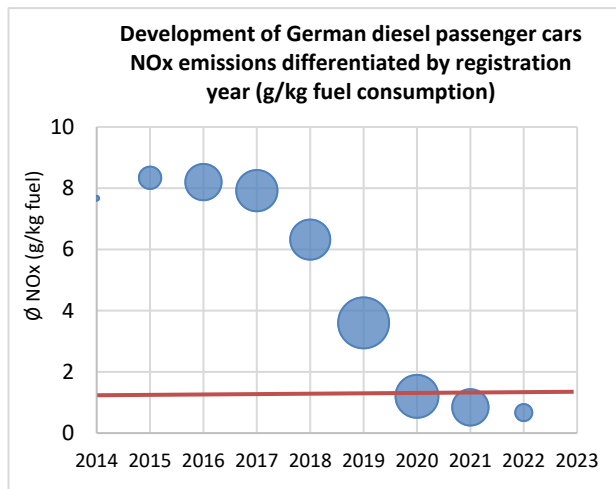


Figure 4: Development of German passenger cars (Euro 6, diesel) NOx emissions differentiated by registration year (in g/kg fuel consumption) and by record numbers (bubble size represents the number of vehicles measured).

One has to state out here, that the average emission values indicated in figure 4 comprise all different vehicle and exhaust after-treatment technologies of Euro 6 diesel passenger cars – a further distinction could be made by a detailed assignment of vehicle identification number to technology standard. The bubble size represents the number of records per registration year – ~~with a total of approximately 220 for 2014's vehicles and 1,850 for vehicles registered in 2019~~. Comparable statements regarding the average emission behavior could also be made for other pollutant components (such as, among others, carbon monoxide, particles or hydrocarbons) and – as far as enough data sets are available - for other vehicle categories. However, one has to state out that average fleet evaluations require an

adequate number of records per vehicle segment in order to generate robust and meaningful statements and to minimize the effects of major exceptions. In the powered two-wheeler segment, for instance, the data base does not provide an explicit picture. Approximately 90 records of the measured data sets are available and declared valid for motorcycles (L3e category), which in turn can be allocated to different Euro emission standards (mainly Euro 3 to Euro 5) and different technologies. In particular, the wide variation of vehicle and engine concepts in this vehicle category makes it difficult to derive clear statements concerning the emission behavior of certain segments. One can assume, that motorcycles are partly under-recorded in this campaign as they probably do not drive primarily on right lanes on motorways – this applies particularly for heavy machines. For vehicle segments representing a high share to total traffic – e. g. passenger cars and heavy-good vehicles - reliable results can be achieved with the system in question even with relatively short measurement periods. For other segments, either the measurement period should be extended or measurements should be taken on all road lanes.

Outlook and Conclusion

As part of this research project, a remote sensing emission measurement system was successfully used for the first time on a motorway in Germany. Emission measurements were carried out over a period of two weeks in the summer of 2022. Data protection issues were clarified in advance of the measurement and suitable locations for possible further measurements were identified. Depending on the share of the vehicle segment to the entire vehicle fleet the measurement data provide a very good snapshot of the fleet emission behavior. Detailed analyzes of the change in fleet emissions over time can be derived. In addition, particularly strong emitting vehicles could be identified. In order to be able to make reliable statements for less strongly represented vehicle segments such as motorcycles or historic vehicles, it is advisable either to extend the measurement period or to measure across all road lanes. Increasing costs, however, have to be considered in any case and weighted against possible benefits. The use of temporary remote sensing devices as a pre-selection of high emitting vehicles for subsequent technical inspections is conceivable.

References

Commission Regulation (EC) No 715/2007 of the European Parliament and of the Council of 20 June 2007 on type approval of motor vehicles with respect to emissions from light passenger and commercial vehicles (Euro 5 and Euro 6) and on access to vehicle repair and maintenance information, *Official Journal of the European Union L 171/1*, 2007.

Commission Regulation (EC) No 692/2008 of 18 July 2008 implementing and amending Regulation (EC) No 715/2007 of the European Parliament and of the Council on type-approval of motor vehicles with respect to emissions from light passenger and commercial vehicles (Euro 5 and Euro 6) and on access to vehicle repair and maintenance information, *Official Journal of the European Union L 199/1*, 2008

Commission Regulation (EU) 2018/858 of the European Parliament and of the Council of 30 May 2018 on the approval and market surveillance of motor vehicles and their trailers, and of systems, components and separate technical units intended for such vehicles, amending Regulations (EC) No 715/2007 and (EC) No 595/2009 and repealing Directive 2007/46/EC, *Official Journal of the European Union L 151/1*, 2018.

Dallmann, T., Bernard, Y., Tietge, U., Muncrief, R. (2019). Remote sensing of motor vehicle emissions in Paris, Final Report.

Ghaffarpasand, O., Ropkins, K., Beddows, David C. S., Pope, Francis D. (2023). Detecting high emitting vehicle subsets using emission remote sensing systems, *Science of The Total Environment*, Volume 858, Part 2, 159814.

Gruening, C., Bonnel, P., Clairotte, M., Giechaskiel, B., Valverde, V., Zardini, A., Carriero M. (2019). Potential of Remote Sensing Devices (RSDs) to screen vehicle emissions - Assessment of RSD measurement performance. EUR 29871 EN, *Publications Office of the European Union*, Luxembourg, ISBN 978-92-79-11820-6, doi:10.2760/277092, JRC117894.

Rauterberg-Wulff, A., Schmidt, W., Düring, I., Borken-Kleefeld, J., Laxenburg, A. (2021). Bestimmung der Real-Emissionen von Kraftfahrzeugen im Berliner Straßenverkehr mit Remote Sensing Detection und Vergleich mit den Emissionsfaktoren des HBEFA 4.1. *Immissionsschutz*, Volume 26, Issue Number: 3. pp 131-5. ISSN: 0039-2219.

<https://www.bast.de/DE/Verkehrstechnik/Fachthemen/v2-bisstra.html>

Map data copyrighted OpenStreetMap contributors and available from <https://www.openstreetmap.org>.

Datenschutz-Grundverordnung (DSGVO); EU) 2016/679; <https://dsgvo-gesetz.de/>

Simulations of a NIR TDLAS Sensor for Stand-Off Measurement of Carbon Dioxide for Remote Emission Sensing

Paul Schaffer¹, Hafiz Hashim Imtiaz¹, Benjamin Lang¹, Martin Kupper¹ and Alexander Bergmann¹

¹Institute of Electrical Measurement and Sensor Systems, University of Technology, Graz, Austria, paul.schaffer@tugraz.at

Introduction

Over the course of the last two decades emission limits for type approval of vehicles in the EU and worldwide have steadily tightened. This led to lower emissions in the whole on-road transport sector from compliant vehicles. Vehicles with damaged or inoperable exhaust aftertreatment systems do not comply with the imposed emission limits. Therefore, the challenge of measurement and identification of those high-emitting vehicles emerged. The impact of such high emitting vehicles to road pollution is substantial, as 15 % of vehicles on the road can be classified as high-emitters, causing over 90 % of total pollution (Bainschab et. al. (2020)).

Remote Emission Sensing (RES) has proven to be a promising emission measurement method for the on-road transport sector. The characteristics of RES systems is the measurement of passing vehicles by a measurement device installed directly at the roadside. By its non-invasive nature, a RES system can monitor the emissions of thousands of vehicles under real-world driving conditions. This allows for the identification of high-emitting vehicles and the transmission of the respective license plate to legislative authorities, which can impose further investigations, such as an inspection of the vehicle in a workshop. By design, RES systems are employed in unmanned 24/7 operation and allow the installation of the system in various locations, such as city center driveways, highways or other highly frequented roads.

RES systems commonly rely on spectroscopic methods for the determination of emission factors (gas concentrations relative to a stoichiometrically calculated CO₂ value) of passing vehicles, such as passenger cars, trucks, etc. With the increasing availability of diode lasers, Tunable diode laser absorption spectroscopy (TDLAS) has been shown as a promising approach also for direct emission measurement in RES systems (Lin et. al. (2023)), emission factors can be calculated. TDLAS offers high accuracy combined with fast sampling, making it an ideal method for RES. However, TDLAS measurements are currently employed only for the measurement of emission factors.

In this work we present a TDLAS based RES system that allows for a direct concentration measurement of CO₂ over an open path length of 10 m. The TDLAS system is combined with a gas imaging technique that enables the determination of the exhaust plume size at the moment of the spectroscopic measurement. The system design can easily be adapted to include more analytes, which allows the RES system to measure e.g. CO, NO, NO₂ or NH₃ in future applications.

The TDLAS measurement presented here targets the absorptions lines of CO₂ in the wavelength range between 1601.0 nm and 1601.6 nm. The targeted absorption lines in this wavelength range show several benefits over other commonly used absorption lines with similar line strengths. Interfering absorption lines from other, commonly encountered gases in RES, such as H₂O or CO show only minor influence on the CO₂ absorption, as the line strengths are much smaller. Furthermore, the shape of the absorption lines of CO₂ at 1601 nm can be considered to have a good temperature stability, as the line shape is well preserved even at elevated temperature of 300 °C.

The aforementioned gas imaging technique used to determine the size of the exhaust plume is based on schlieren imaging. Using a defined arrangement of the system setup therefore enables the calculation of the absorption pathlength in the exhaust plume.

The proposed TDLAS system design was evaluated using simulations with a numerical model for two different measurement approaches. The evaluation and validation of both approaches and the system design in the laboratory is ongoing. The simulations were used as an excellent starting point for the design of the spectroscopic setup.

Laser Absorption Spectroscopy

TDLAS as a spectroscopic measurement principle relies on the absorption of parts of the incident laser intensity by the targeted gaseous medium. The absorption of intensity is described by the Beer-Lambert law

$$I = I_0 e^{-\chi(\lambda) \cdot c \cdot L}. \quad (1)$$

The received laser intensity I is affected by the emitted laser intensity I_0 , the wavelength dependent absorption cross section χ , the number concentration of the absorbing gas species c and the absorption path length L .

When employing TDLAS to an open-path measurement, such as in setups used for RES, the targeted gas volume extends only over parts of the total measurement path. In the case of a roadside application of a RES system, the total pathlength would cover the full width of the road, but the targeted gas volume, in this case the exhaust plume, extends

only over a relatively small length. To measure the gas concentration in the exhaust plume, the knowledge of the size of the exhaust plume along the measurement path is necessary.

The TDLAS system design presented in this work is integrated in a RES system concept developed in the LASTRES-project which allows us to present a new solution to this challenge. The RES system employs Synthetic Schlieren Imaging to capture real-time images of the exhaust plume emitted by passing vehicles. In this technique a high-quality camera placed on one side of the road is focuses on a checker patter board situated on the opposite side of the road. The exhaust plume emitted by passing vehicles alters the refractive index in parts of the volume between camera and board, resulting in small distortions in the captured image of the board. By capturing and subtracting consecutive images the relative changes between the images are calculated, generating Synthetic Schlieren Images. Furthermore, advanced image processing techniques are applied to the images the highlight the exhaust plume against the background and eliminate displaced pixels. An object detection algorithm employing Convolutional Neural Networks (CNN) then identifies the exhaust plume. The extension of the exhaust plume is then determined by considering the plume size in pixels, the camera sensor size, the distance from the camera and the focal length, giving the absorption path length in the exhaust plume.

Tunable Diode Laser Absorption Spectroscopy

TDLAS relies on the wavelength tuning of a diode laser to scan the targeted absorption feature. This wavelength tuning is commonly realized by a periodic modulation of the injection current supplied to the laser diode, often also referred to as sweeping. Usually this modulation is applied as a triangular waveform, which is the approach followed in this work. Depending on the type of laser diode and driver the resulting tuning range can be up to several nm. The increase in injection current also results in an increase in optical power, leading to the so-called Residual Amplitude Modulation (RAM).

In addition to the direct absorption technique another method, called Wavelength Modulation Spectroscopy (WMS) can be applied. In this technique an additional sinusoidal modulation is superimpose onto the triangular sweep. This modulation is of much smaller amplitude, but higher frequency. Due to this modulation, the absorption modulation is encoded in an amplitude modulation at the modulation frequency f , decreasing the influence of many occurring noise sources. The detected amplitude modulated signal is then processed by Lock-In algorithms, extracting the absorption information at different harmonics of the modulation frequency f . In the presented application the first and second harmonic signals are extracted. The realization approach and the chosen components for this work are described below.

Simulations of the Direct Absorption Setup

As a starting point for the design of the spectroscopic setup of the RES system simulations of a direct absorption setup were done. In this simulation, critical components of the system, such as the laser diode and the photodetector were simulated using their real-world characteristics as reported by their corresponding datasheets. The gas specific parameters for absorption were considered by connecting the simulation with the HITRAN database (Gordon et. al. (2022)) through the RADIS python package (Pannier et. al. (2019)). By simulating the absorption process intensity spectra are recorded. The spectra are then analyzed using a multi component, multi variable least-squares fit to obtain both the gas concentration and the gas temperature.

The proposed signal analysis algorithm for the direct absorption spectroscopy was tested by simulating different gas compositions at different temperatures. Here we present exemplary results of 0.1 % CO₂ in ambient air, assuming an open absorption pathlength of 10 m at standard ambient conditions. The resulting baseline corrected intensity spectrum is displayed in Figure 1.

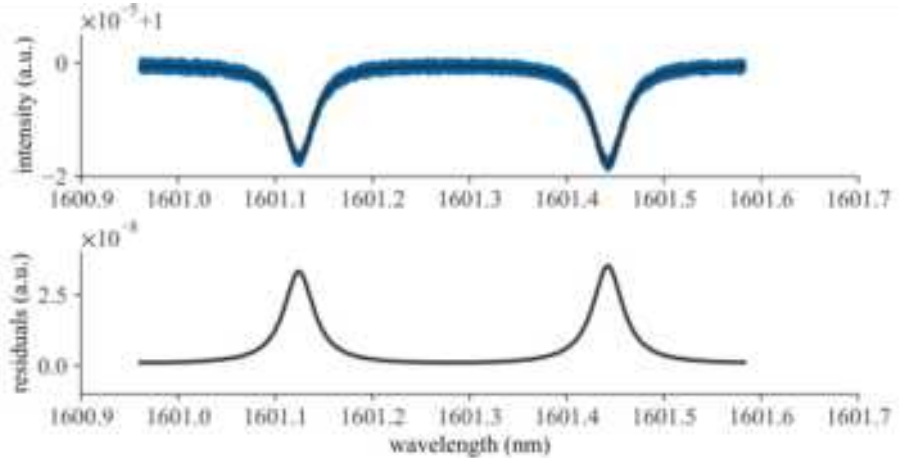


Figure 7: Simulated transmittance of a CO₂ measurement. A concentration of 0.1 % CO₂ was simulated in ambient air and ambient conditions. The top graph shows the simulated, baseline corrected intensity signal (blue) and the intensity profile calculated with the described fitting algorithm. The bottom graph shows the residual between the calculated and real intensity profile.

The simulated intensity spectrum is used to extract both temperature and concentration information. The calculated deviations between set and retrieved gas properties are below 5 % for the gas temperature and 2 % for the gas concentration.

Simulations of a Wavelength Modulation Spectroscopy Setup

The proposed TDLAS system design is simulated using a wavelength modulation approach to assess performance. The laser diode is wavelength tuned using a triangular modulation of the injection current between 32.518 mA and 74.686 mA at a frequency of 1 Hz. This modulation allows a sweep over the CO₂ absorption feature located at 1601.12 nm. Superimposed on this triangular modulation is a sinusoidal modulation at a frequency of 1 kHz with an amplitude of 2.588 mA.

Absorption is simulated in a similar way to the direct absorption case for two different detection schemes, to compare the system performance. The simulated intensity signal is then detected by two different types of amplified photodetectors: a single photodetector (PDA30B2, Thorlabs Inc., similar to the direct absorption simulation) and a

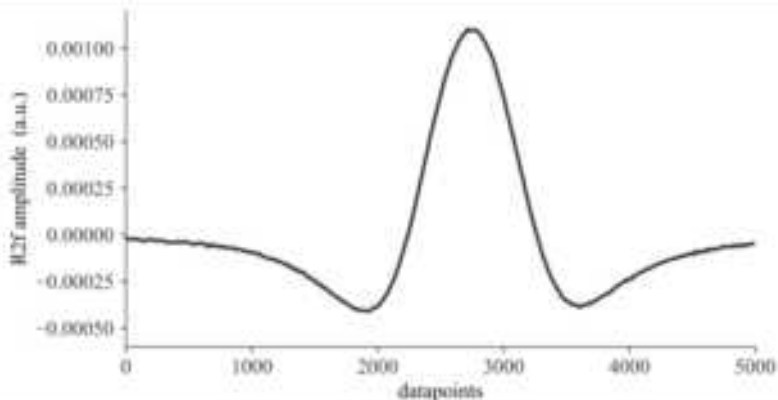


Figure 2: The simulated demodulated 2f-signal of the balanced detection scheme for a CO₂ concentration of 14000 ppm.

balanced photodetector (2017 Nirvana Auto-Balanced Optical Receiver, Newport Cooperation). To remove the residual amplitude modulation for the single photodetector a high-pass filter with a cut-off frequency of 500 Hz is simulated after signal detection on the photodetector. To simulate an ADC front end of a DAQ system the detected signal is then down sampled to 14-bit precision (ALPHA250, Koheron SAS). Further, the signal was demodulated at both $1f$ and $2f$ (1 kHz and 2 kHz respectively) using a digital Lock-In detector.

For assessing the system performance two edge cases are simulated, a low CO_2 concentration, similar to ambient background and a high CO_2 concentration, as expected in vehicle exhaust. The concentration used are 50 ppm for the low concentration case and 14000 ppm for the high concentration case respectively. The conditions are as stated above, 10 m absorption pathlength at ambient conditions. The simulation result for the high concentration case in the balanced detection scheme is depicted in Figure 2, while Figure 3 shows the low concentration case. The demodulated $2f$ -signal of the high concentration case is well resolved, whereas the $2f$ -signal in the low concentration case shows significant disturbances originating from quantification noise from the analog to digital conversion. However, further signal processing would be still possible in this case.

The results of the simulated case of a single photodetector are presented in Figure 4 for the high concentration and in Figure 5 for the low concentration. While the demodulation of the simulated signal in the high concentration case recovers the $2f$ -signal properly, the results of the low concentration case show no detectable signal. The characteristic $2f$ -signal vanishes in the noise background completely in this case and further signal processing would not be possible.

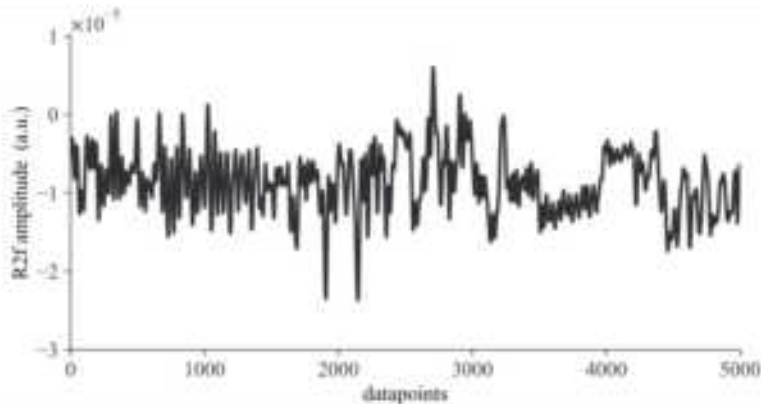


Figure 5: The simulated demodulated 2f-signal of the single photodetector for a CO_2 concentration of 50 ppm.
concentration of 14000 ppm.

In summary, both simulated detection schemes show equal performance at high target gas concentrations, making them both suited for an application in a RES system for high-emitter detection. When investigating lower concentrations in the simulation, the single photodetector setup is not able to recover the absorption signal from the simulated low concentration case. The balanced detection scheme shows a visible influence of noise on the signal while still allowing further signal processing to be done.

Preliminary Measurements in the Wavelength Modulation Setup

Using a setup similar to the simulated setup described in the previous section measurements to verify the operation of the system design are conducted in the laboratory. The laser diode (NLK1L5GAAA, NTT Electronics) is installed in a laser driver (CTL101-2-B-200, Koheron SAS). The modulation of the injection current is provided by the DAQ system (ALPHA250, Koheron SAS). The fiber coupled output of the laser diode is collimated using a mirror collimator (RCO2APC-P01 Thorlabs Inc.) and directed to the multi-pass gas cell (MGC1C/M-P01, 1 m pathlength, Thorlabs Inc.). After the gas cell the laser beam is focused and directed onto the photodetector (PDA30B2, Thorlabs Inc.) using an off-axis parabolic mirror (MDP129-M01, Thorlabs Inc.). The detected signal output from the photodetector is high-pass filtered using a custom made 1st order high-pass filter with a cut-off frequency of 4.98 kHz. Digitization of the signal is done using the RF front-end of the DAQ system.

For the validation of the system design the gas cell was filled with 100 % CO₂ at ambient pressure. The injection current is modulated at frequencies of 244.14 Hz for the triangular, and 105.05 kHz for the sinusoidal modulation. The triangular modulation was selected from 50 mA to 130 mA to sweep one absorption feature while the superimposed sinusoidal modulation was set to 20 mA to yield a high signal amplitude after high-pass filtering. The recorded signal is then demodulated using two digital Lock-In amplifiers detecting at the 1f and 2f frequencies (105.05 kHz and 210.10 kHz respectively).

In Figure 6 an exemplary measurement of the 2f amplitude is shown. The recovered shape of the 2f signal meets the expectation and thus proves the proper operation of the system design in the case of WMS with a single photodetector. Further investigations using varying gas concentrations as well as a balanced photodetector will be conducted in the future.

Summary

In this paper we present a system concept for a TDALS based CO₂ measurement for a RES system. The proposed setup was simulated for a direct absorption measurement to analyze the system components. A specially designed fitting algorithm for evaluating gas concentration and temperature from the recorded intensity spectra was tested. In the presented test conditions the algorithm was able to recover gas concentration and temperature within 2 % error for the concentration and 5 % error for the temperature respectively.

Further simulations were done to investigate the implementation of a wavelength modulation technique (WMS). Two different detection schemes, a single photodetector and an auto-balanced photodetector were simulated to assess their performance over the expected concentration range. While the balanced photodetector was able to recover the signal for both concentration cases, the single photodetector only provided reasonable output for the high concentration case. The setup was then realized in a laboratory setup to perform initial feasibility tests for a WMS approach. The recorded signals using a gas concentration of 100 % CO₂ show good agreement with the simulations.

Conclusion and Outlook

Based on the results from the preliminary laboratory measurements with the WMS setup further measurements will be done. The direct correlation between signal amplitude and CO₂ concentration will be evaluated. A setup using a balanced photodetector will be realized to further verify the simulation results.

The presented TDALS system will further be included into the mentioned RES system alongside the described gas imaging system to allow direct concentration measurements of pollutants of passing vehicles.

Acknowledgements

This work is funded by the Austrian Research Promotion Agency FFG (Fund Project 868105 - LADEN) and supported by AVL List GmbH.

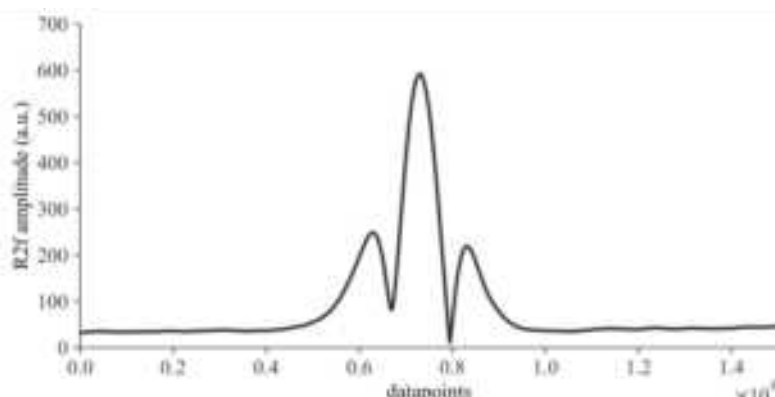


Figure 6: Recorded 2f-amplitude of a measurement with 100 % CO₂ at an absorption path length of 1 m.

References

- Bainschab M, Schriefl M. A., and Bergmann A. (2020). Particle number measurements within periodic technical inspections: A first quantitative assessment of the influence of size distributions and the fleet emission reduction. *Atmospheric Environment: X*, Volume 8, p. 100095, <https://doi.org/10.1016/j.aeaoa.2020.100095>
- Lin, H Wu, K Zhang T, Lai X, Mei L. (2023). Remote sensing of vehicle emitted carbon oxides employing wavelength modulation spectroscopy and a segment modulation method. *Microwave and Optical Technology Letters*. Volume 65, pp. 1162-1168, <https://doi.org/10.1002/mop.33214>
- Gordon I. E., et. al. (2022). The HITRAN2020 molecular spectroscopic database. *Journal of Quantitative Spectroscopy and Radiative Transfer*. Volume 277, pp. 107949, <https://doi.org/10.1016/j.jqsrt.2021.107949>
- Pannier E., Laux C. O. (2019). RADIS: A nonequilibrium line-by-line radiative code for CO₂ and HITRAN-like database species. *Journal of Quantitative Spectroscopy and Radiative Transfer*. Volumes 222–223, pp. 12-25, <https://doi.org/10.1016/j.jqsrt.2018.09.027>

A Modern, Flexible Cloud-Based Database and Computing Service for Storing and Analysing Vehicle Emission Measurements

C.E. Rushton^{*1}, J.E. Tate¹, M. Callaghan², M. Knoll³, and A. Sjodin⁴

¹ Institute for Transport Studies and ²School of Computing, University of Leeds, Leeds, LS2 9JT, UK

³ Institute of Electrical Measurement and Sensor Systems, Graz University of Technology, Inffeldgasse 33/I, 8010 Graz, Austria

⁴ IVL Swedish Environmental Research Institute Ltd. P.O Box 210 60, S-100 31 Stockholm, Sweden

Keywords: remote sensing, point sampling, data science, vehicle emissions.

Presenting author email: c.e.rushton@leeds.ac.uk

Introduction

Data dashboards (Sarikaya et al, 2018) offer an opportunity to streamline various processes associated with analysis of large and complicated data sets (Stadler et al, 2016). They are often deployed at city levels to aid data driven decision and policy making (Kourtit & Nijkamp, 2018). Dashboards offer advantages over traditional data presentation methods because they can be made more widely available, are interactive and engaging, present up-to-date and near real-time information, and can generate support the publication of evolving documents, unlike more traditional static papers and reports. Intelligently designed dashboards can improve user engagement and the accessibility of more advanced scientific methods and analysis techniques, whilst limiting the potential for unintentional or malicious misuse of data and statistics. Data sets can be updated and expanded, new algorithms can be added and existing algorithms can be improved in close to real time, meaning that the end user has access to the latest data, methodology and insights possible. The impact of this approach to this field is significant as air pollution is a quickly evolving topic and resources from a few years ago may be out of date relatively quickly. This is mitigated by a database that is frequently updated and a dashboard that gives most users some access to the most up to date data in a clear and approachable package.

The overarching objective of the CARES project was to remove or reduce barriers to implementation of remote sensing device (RSD) measurements. An online data dashboard coupled to a persistent database allows researchers and citizens alike the opportunity to access and interact with the data collected as part of the CARES project. A historical barrier to entry for RSD data analysis is cost. The devices are expensive to purchase, require complex installation and specialist expertise to analyze the data. The lower-cost point sampling (PS) devices advanced as part of the CARES project (described elsewhere by Knoll et al., 2023) has significantly helped make remote sensing vehicle emissions more accessible and affordable. The data dashboard has also helped, removing the barrier for specialist data analysis skills to extract relevant insights from measurement campaigns.

This research paper describes a modern, flexible cloud-based database and computing service for storing and analyzing vehicle emission measurements.

Methodology

There are two key strands to this work: a database and a web-app. The two work together to deliver reliable data in a data dashboard that is accessible to most users.

Database: The Microsoft CosmosDB database platform, part of the Azure cloud computing platform⁶ was chosen for this task as it provides an enterprise level suite of tools for data science, app deployment and database construction and maintenance. The Azure platform is used worldwide and across multiple sectors, with users including banks, energy firms and telecom businesses e.g. ABN-AMRO (<https://www.abnamro.com>), Centrica (<https://www.centrica.com/>),

⁶ <https://cosmos.azure.com/>

and Vodafone (<https://www.vodafone.co.uk/>). Azure provides Infrastructure as a Service through a range of virtual machine, storage and network offerings that allow a user to build and manage their own virtual infrastructure in the cloud. Azure's Platform as a Service (PaaS) allows a user to develop and deploy web-applications, mobile applications, and APIs without worrying about underlying infrastructure. PaaS is useful for building new applications quickly and without the need to worry about managing infrastructure. Data and analytics services include Cosmos DB and SQL Databases, Machine Learning etc. The analytics services are useful for building applications that can collect and analyse and process large volumes of data in the cloud which can be used to build intelligent applications that can make data-driven decisions and gain insight from large data sets. The CosmosDB database is a document style, NoSQL database that uses JavaScript Object Notation (JSON) style documents to store data. The documents are organized into containers and the containers are organized into databases. The containers are schema-agnostic, meaning that no standard schema is required or enforced by the database. The flexibility that a schema-agnostic system offers is of paramount importance to the data storage process and was a key factor in the decision to use this approach.

Each measurement is entered into the database in its own document. The document format consists of key: value pairs. A value may take on different data types: Boolean, numeric and character, as well as lists of data and dictionaries. The values used for remote sensing are typically single valued, but storing data in a key list may also be done for much longer time series data. More complex documents can be created such imported GeoJSON files.

The documents created for the CARES measurements use four keys to organize the data. These keys are required for most documents but not all. Meta-data documents do not require measurement data. The keys are capitalized to signify their necessity and are:

- `TIMESTAMP_MS`
- `MEASUREMENT_OBSERVED_VALUE`
- `MEASUREMENT_DESCRIPTION`
- `DB_DATA_TYPE`

`TIMESTAMP_MS` is an integer typed UNIX timestamp in milliseconds. This column indicates the time the measurement was taken. It is set to the hour of measurement (e.g., 23:45:59 would be set to 23:00:00) for GDPR⁷ compliance. This obscuration of time is considered adequate to meet GDPR compliance for studies less than two weeks in length, whilst still being adequate for most scientific analysis purposes in line with other related air quality and traffic flow data sets that typically aggregate to an hour-long time interval. A UNIX timestamp was chosen over a traditional YMD/HMS date format to make querying time intervals easier.

`MEASUREMENT_OBSERVED_VALUE`: is the measurement taken or the value observed. This is typically a floating point variable and corresponds to the thing of interest for this particular measurement.

`MEASUREMENT_DESCRIPTION`: is the description of the number in the previous key pair and usually includes the units if available. The format of these descriptions is {description}_{unit}.

`DB_DATA_TYPE`: is the data type being measured. For the CARES project this is typically the instrument type but can also include metadata such as site location.

A sample measurement document is shown below.

```
{
```

⁷ <https://gdpr-info.eu/>

```

"campaign_id": "PL_2021_1",
"measurement_id": *****,
"site_id": "JOSEFA",
"instrument_id": 5059,
"make_raw": "SKODA",
"model": "FABIA COMBI",
"build_year": 2007,
"eng_disp": 1896,
"eng_power": 74,
"co2_ta": 129,
"emission_standard_raw": null,
"fuel_type_1": "diesel",
"ptr_type": "ICEV",
"emission_standard_calc": "Euro 4",
"TIMESTAMP_MS": 166*****,
"DB_DATA_TYPE": "rsd_heat_data",
"MEASUREMENT_DESCRIPTION": "speed_kmh-1",
"MEASUREMENT_OBSERVED_VALUE": 63.3735802,
}

```

The database is queried using something resembling a SQL query. A query as simple as "SELECT * FROM rsd" will return the entire contents of the container it is directed to. But more targeted queries can also be built. For example "SELECT MEASUREMENT_OBSEVED_VALUE FROM rsd WHERE make_raw = 'SKODA' AND emission_standard_calc = 'Euro 4' AND fuel_type_1 = 'diesel'" and "DB_DATA_TYPE = 'rsd_heat_data'" would return emission rates only for all Euro 4 Skoda diesels measured by the RSD HEAT instrument in a given container. Well designed queries are more efficient than downloading the entire data set whenever a single calculation is required.

The schema-agnostic containers mean that different measurements do not require the same key and value structure. The flexibility to use different instruments that may have different output data structures is critical to the CARES project and the document style database allows for that. It is reasonable to store RS data in the same container as point sampling or other data sets from different instruments collected as part of the CARES project.

Web App: A suite of web applications were developed as front-ends to the database. The web apps were developed in Python using Streamlit⁸ as a front end, Altair as a data visualization package and a range of standard Python libraries for data analysis including NumPy⁹, SciPy¹⁰ and Pandas. A relatively user-friendly user interface allows more streamlined access to different areas of interest for different users without them having to have prior knowledge of the database, its structure, or querying with third party tools. The apps also do not require any analysis to be done on the part of the user as all figures are pre-developed and displayed within the app. Three apps were developed:

- CARES Public App
- CARES City App

⁸ <https://streamlit.io>

⁹ <https://numpy.org>

¹⁰ <https://scipy.org>

- CARES Science App

The CARES public app is available at <https://cares-public-app.azurewebsites.net> and was designed for the public. The data collected throughout the CARES project was funded by EU and UK taxpayers, so is made open and accessible. The City App presents the same figures as in the Public App, but with a wider population of cities that have remote sensing data available. Access to the city app is only available to registered users on a request basis. Neither the Public nor City apps reveal the raw data used to create the figures so reduce the risk of misuse of data. The Science App was designed for registered experienced remote sensing developers. Deeper analysis is available on all data sets and the raw, anonymised data is available to download.

Outputs

City / Public App: The three CARES cities included in the CARES Public-App are Milan, Prague and Krakow. A range of different figures may be created using the CARES Public and City App. These include:

- Fleet composition
 - Euro class
 - Vehicle type
 - Manufacturer
 - Euro class and fuel type
- Vehicle dynamics
 - Speed and acceleration
 - Vehicle specific power (VSP)
- Vehicle emissions
 - Euro class (Figure 1)
 - Year of registration
 - Manufacturer
 - Summary
- Weather
 - Temperature
 - Pressure
 - Humidity
 - Wind speed
 - Wind direction

CARES Science App: More detailed analysis can be performed using the Science App. These include:

- Point Sampling
 - Simple (single channel) point sampling
 - Complex (multi-channel) point sampling
 - Automatic triggered point sampling
- Remote Sensing
 - Remote sensing summary (Figure 2)
 - High emitter detection

Impact

The CARES app suite and in particular the public-App go some way to increasing the visibility and accessibility of remote sensing data, which was a key objective of the CARES project. It has also modernized and gone a long-way to future proofing the pan-European vehicle emission remote sensing database and data architecture initially created in the CONOX initiative (Sjödin et al, 2018).

More EU and UK citizens and other interested parties can now begin to understand the emissions of the vehicles in some EU cities and think about how they might best use the newly accessible information and resource to help design and realise their own air pollution mitigation policies. For example, the diesel facet of Figure 2 shows that there is an

improvement in overall emission factors for Euro 6d (yellow) and Euro 6d-temp (purple) vehicles compared to Euro 6 (a/b/c - orange). This suggests that policies that target diesel vehicles below these emission standards will be more impactful than policies that include non-d /d-temp Euro 6 vehicles. The information that backs up this claim is now publicly accessible and free to anyone who is interested in looking it up.



Figure 8: Vehicle emissions by Euro class for NO₂: CO₂ ratios for Milan from the CARES Public App

Future Work

The platform used for these apps was selected with the future in mind. Whilst the data presentation is an innovative step, the data collection and storage follow well-established processes that can reduce the immediacy of the impact of this work. Automating well understood processes on the cloud can lead to a quicker and more cost-effective turn-around of RS data and its insights from scientific experts to policy makers.

As more sensors become connected to the Internet of Things (IoT) then more real-time data dashboards may be developed. This work may serve as a basis for any future IoT enabled vehicle emission measurement systems. When deployed at scale, particularly the lower-cost point sampling devices tested during other phases of the CARES project, these devices connected to a real-time data platform will be able to provide a close to real-time picture of the status of vehicle emissions in the measurement region.

The real-time data stream could be integrated into machine learning algorithms to predict future trends and potentially identify areas of concern before they become problematic. This extra knowledge could help decision-making processes for city authorities tasked with reducing the exposure to air pollution of their citizens.

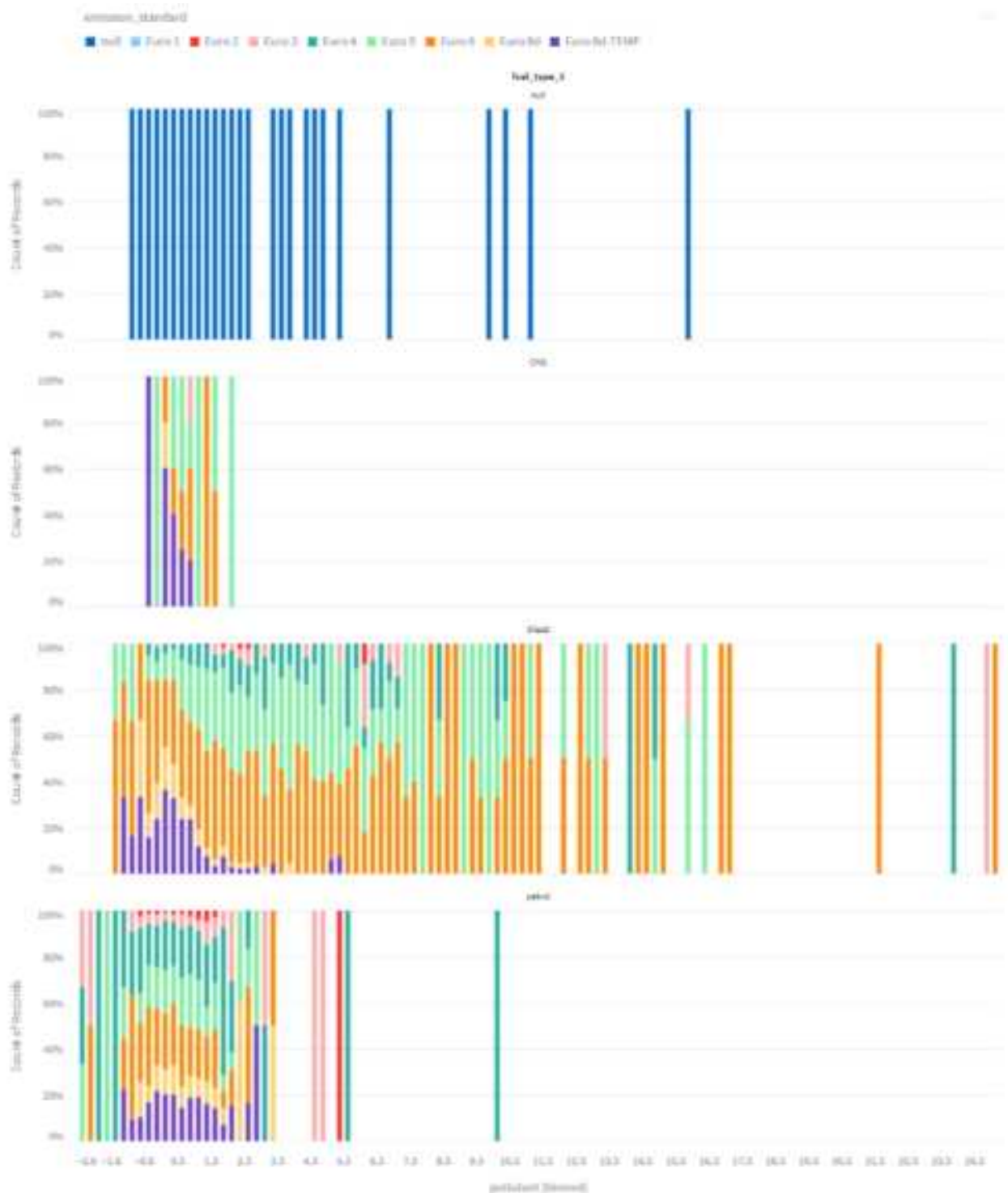


Figure 9: Normalized histogram of emission factors for NO₂ fuel mass measurements in Milan, faceted by fuel type and colored by Euro standard, taken from the CARES Science App.

Beyond air pollution there is a wealth of publicly available data that is often difficult to parse or analyze without specialist knowledge. The use of interactive dashboard type web applications to improve the visibility and accessibility of public health related data and other publicly available data remains a relatively untapped resource. It may be possible to apply the lessons learned through the CARES project to a wide range of useful and impactful data sources that are currently publicly available but not publicly accessible.

References

- Knoll, M., Penz, M., Juchem, H., Schmidt, C., Pöhler, D., & Bergmann, A. (2023). Large-scale automated emission measurement of individual vehicles with point sampling. *EGUsphere, 2023*, 1-46.
- Kourtit, K., & Nijkamp, P. (2018). Big data dashboards as smart decision support tools for i-cities—An experiment on stockholm. *Land use policy, 71*, 24-35.
- Sarikaya, A., Correll, M., Bartram, L., Tory, M., & Fisher, D. (2018). What do we talk about when we talk about dashboards?. *IEEE transactions on visualization and computer graphics, 25*(1), 682-692.
- Sjödin, Å., Borken-Kleefeld, J., Carslaw, D., Tate, J., Alt, G.-M., De la Fuente, J., Bernard, Y., Tietge, U., McClintock, P., Gentala, R., Vescio, N., Hausberger, S (2018) Real-driving emissions from diesel passenger cars measured by remote sensing and as compared with PEMS and chassis dynamometer measurements - CONOX Task 2 report. On behalf of the Federal Office of Environment, Switzerland, <https://www.bafu.admin.ch/bafu/en/home/topics/air/publications-studies/studies.html>
- Stadler, J. G., Donlon, K., Siewert, J. D., Franken, T., & Lewis, N. E. (2016). Improving the efficiency and ease of healthcare analysis through use of data visualization dashboards. *Big data, 4*(2), 129-135

2.5 TAP.05. Vehicle greenhouse gas emissions, energy consumption, vehicle and fuel life-cycle analysis.

From physical testing to on-board fuel consumption monitoring and telemetry: a pilot project for capturing the real-world fuel consumption of vehicles¹¹

*A. Tansini¹, J. Suarez¹, N. Aguirre², A. Laverde³ and G. Fontaras¹ **

¹Sustainable Transport and Sustainable Mobility Unit, European Commission's Joint Research Centre, Ispra, Italy

* georgios.fontaras@ec.europa.eu

²Nestor Aguirre, nfaguirrec@gmail.com

³Universitat Politècnica de València, VRAIN, València, Spain

Introduction

The European Union (EU) is committed to an ambitious strategy to reduce CO₂ emissions from various sectors including road transport. This commitment is deeply tied to international agreements, such as the Paris Agreement (Paris Agreement, 2015), and EU regulations, such as the climate law (EU Regulation 2021/1119), setting a comprehensive target to achieve carbon neutrality by 2050. Road transport sector is one of the main contributors to Greenhouse Gas (GhG) emissions and has come under increased scrutiny due to its substantial carbon footprint. In this context, monitoring and understanding real-world fuel consumption and CO₂ emissions from vehicles have emerged as a paramount objective. GhG emissions reduction measures need to be effective in real world operation that is continuously changing. For decades, the standard approach involved vehicle tests on a chassis dynamometer within controlled laboratory conditions. These tests quantified CO₂ emissions and fuel consumption over predefined drive cycles. Recent regulatory enhancements introduced with the Worldwide harmonised Light vehicles Test Procedure (WLTP) and EU Regulation 2017/1151 have refined these laboratory tests to more accurately mirror on-road scenarios, thereby narrowing the gap between laboratory and real-world emissions (Pavlovic, 2020). Despite these improvements, no laboratory test can always fully replicate the diversity of on-road operations (e.g. ambient conditions and vehicle usage pattern) and energy consumption demands (e.g. use of auxiliaries) (Fontaras, 2017). Acknowledging their limitations, data sourced from real-world contexts emerges as a method to grasp the full spectrum of fuel consumption variability (Pavlovic, 2018). This approach complements the standardised certification processes and enhances the understanding of road transport energy demand and carbon impact, ultimately favouring consumer awareness (EU Regulation 2019/631). As of January 2021, EU vehicles must incorporate On-Board Fuel Consumption Monitoring (OBFCM) devices to enable real-time readout and internal storage of fuel consumption metrics. These devices, among other things, accumulate distance and fuel consumption data over a vehicle's lifetime, offering a straightforward way to obtain real-world average fuel consumption. These values are subject to accuracy requirements and can be extracted from the vehicle's On-Board Diagnostics (OBD) system.

This paper describes a pilot project initiated by the European Commission's Joint Research Centre (JRC) aimed at collecting OBFCM and vehicle telemetry data from private and corporate vehicles across Europe using OBD-dongles with internet connectivity. Upon the beginning of a new trip, these devices automatically start recording instantaneous parameters such as speed, engine RPM, engine fuel rate and ambient temperature. Additionally, they gather OBFCM lifetime distance and fuel data, transmitting this comprehensive dataset to a centralised repository for storage and analysis. Vehicles are monitored for a long time, as much as the vehicle owner/driver agrees to, therefore supporting data collection throughout all seasons and driving conditions. This innovative approach enables a holistic understanding of real-world vehicle performance and fuel efficiency, empowering regulatory advancements and informed decision-making. This short scientific paper thus seeks to present the preliminary results obtained in this pilot project and the opportunities it brings to understand the interplay between real-world conditions, driving style, vehicle technology and environmental impact. By shedding light on these aspects, this study offers valuable insights into the ongoing efforts to reshape the landscape of sustainable mobility and drive the EU towards a greener future.

¹¹ The views expressed in this paper are purely those of the authors and shall not be interpreted as an official position of the European Commission under any circumstance

Materials and methods

The project collects real-world OBFCM from vehicles in use. It is composed of two main blocks: (a) production of vehicle data and transfer to central server (b) data storage and manipulation in the data centre.

Block (a) encompasses OBD-dongles preparation, testing, installation in vehicles and check of their correct operation. Installation requires that these devices are connected to the car's OBD port. Data production relies on collecting OBD data and other measurements from the dongle, an open-hardware and open-software device featured by an Arduino programmable board, OBD port and chip, GNSS, motion sensor and cellular module. A few upgrades were applied to the device under both hardware software perspectives, focusing on OBD and OBFCM data collection performance. OBD is a vehicle system to monitor and manage various aspects of their performance, emissions, and overall health. It consists of both hardware and software parts complying with the technical requirements and communication protocols defined by the Society of Automotive Engineering (SAE) and ISO standards. Initially introduced for emissions control, OBD has evolved into a comprehensive diagnostic tool integrated into modern vehicles. The hardware consists of sensors and Electronic Control Units (ECUs) distributed throughout the vehicle, collecting data from different components and devices. This data includes information about engine performance, emission levels, fuel efficiency, and operating parameters. ~~OBDS primary function is to identify and report malfunctions or nonfunctions in the vehicle's systems but it~~ also plays a role in real-time emissions monitoring, which is crucial for environmental regulations. OBD systems can detect anomalies in emissions control systems and alert the driver or technician if a potential problem could affect the vehicle's emissions performance. Building on OBD capabilities, EU Regulation 2017/1151 added the requirement for European vehicles to be fitted with OBFCM devices as of 1st January 2021 for new models and as of 1st January 2022 for all models. OBFCM data consists of both instantaneous and lifetime cumulative signals and is retrievable through OBD protocols (Society of Automotive Engineering, 2023). The list of instantaneous and lifetime signals covered by OBFCM is presented in Table 1.

Table 1: mandatory data on OBFCM-compliant vehicles

Instantaneous signals (all vehicles)	Lifetime signals (all vehicles)	Additional lifetime signals (OVC-HEVs only)
vehicle speed (km/h)	total distance travelled (km)	total distance travelled in charge depleting operation with engine off (km)
engine fuel rate (lt/hr)	total fuel consumed (lt)	total distance travelled in charge depleting operation with engine running (km)
engine fuel rate (gr/s)		total distance travelled in driver- selectable charge increasing operation (km)
vehicle fuel rate (gr/s)		total fuel consumed in charge depleting operation (lt) total fuel consumed in driver-selectable charge increasing operation (lt) total grid energy into the battery (kWh)

In addition to these signals, the following OBD data is collected within our project: accelerator pedal position, engine speed, engine load, engine coolant temperature, ambient temperature and vehicle odometer. The OBD-dongle collects instantaneous signals and internal measurements on a second-by-second basis, and lifetime

values every 30 seconds to limit the workload and network usage. Data is transmitted Over-The-Air (OTA) to a central server for convenient and robust data management (see Figure 1).

Block (b), on the other hand, encompasses all the operations required on the data centre side to secure and prepare the data for later analysis. The raw data, i.e. the trips timeseries collected by the OBD-dongles are stored in a non-relational MongoDB database to ensure scalability and flexibility of the data schema. In addition to the raw data from devices, the database also holds a table with vehicle specifications (powertrain type, fuel type, others) to enable deeper analysis per vehicle or group. The dataset enable analysis from different perspectives and with different level of complexity: simple assessment on the most recent lifetime values, inspection of the instantaneous and lifetime signals in a trip, analysis of the aggregation of data per trip or per other segment/group as defined by the data analyst: per season, per month, per vehicle, per powertrain type. An additional criteria for OVC-HEVs could be aggregating data between charging events (leveraging the total grid energy into the battery lifetime parameter).



Figure 1: over-the-air collection of vehicle data (OBFCM and telemetry) through OBD-dongles

A very insightful and simple way of analysing the data that was explored in this study is to aggregate data per trip, obtaining for each of them the total distance travelled, the total fuel consumed, the average fuel consumption in litres/100km together with context data to study its variability: average ambient temperature, average trip speed, share of urban, rural or motorway driving, trip dynamicity and other metrics. The numbers and plots presented in the next section are obtained by aggregatind data per trip. The results are to be considered preliminary since the data collection experienced some issues in these early stages of the project, with trips getting divided into two or more segments because of network, device or server problems. Ways to solve this problem are under investigation, raw data as received by the server shall be fixed and trips reconstructed as they took place in reality, identifying and concatenating in a robust way all their segments. Such a fix is going to be applied in follow-up investigations on the same data. For the time being, data are being processed and presented in a relatively independent way from the trips identification as it came in the raw data. The data processing aimed at calculating the travelled distance and the consumed fuel by computing deltas on the total distance and total fuel OBFCM lifetime parameters. It was impossible for some vehicles to read the lifetime parameters due to incompatibilities between the OBD-dongles pre-implemented OBD library and the CAN messages of the vehicles. Instead, depending on the OBD device, the OBD instantaneous values for these vehicles were used instead (vehicle speed to calculate total distance, fuel rates to calculate total consumed fuel).

Preliminary results

An overview of the data captured until the writing of the paper (August 2023) on OBFCM vehicles since the start of the project in late 2021 is provided in Table 2. The number of vehicles, the sum of distance and the sum of days per vehicle is presented for each powertrain technology covered (conventional, mild hybrid, full hybrid and plug-in hybrid). The distance here presented is calculated by considering only the trips where the OBD-dongles actively log data, therefore cumulating any trip it was possible to capture after the installation. Anyhow, the OBFCM lifetime parameters enable us to obtain the average fuel efficiency from the entire vehicle history, therefore also covering the travelled distance before this moment. This implies that from the captured data, it is possible to derive the average fuel efficiency for even longer total distances than the values reported in Table

2; this additional value is nevertheless missing the context data that telemetry could bring (vehicle speed, ambient temperature, engine load, etc.). The data aggregation process described in the materials and methods section generated a population of trip average fuel efficiencies expressed in litres per 100 kilometres. These results are presented in Figure 2 in the form of distributions complemented by median value, 5% and 95% percentiles. The subplots on the left show the simple distribution of trips average fuel consumption, wherein each trip counts the same regardless of the travelled distance. The subplots on the right show the same average fuel consumption values but after distanceweighting process to assign higher significance to longer trips (for their higher relevance in the vehicles lifetime). The distance-weighting is also to return the true value of average vehicles lifetime fuel efficiency through the median.

Table 2: Captured data overview (until Aug. 2023)

Type	Count (-)	Sum of distance (km)	Sum of days per vehicle (-)
Conventional	13	135602	1760
Mild hybrid	8	48548	832
Full hybrid	4	11379	303
Plug-in hybrid	7	53663	1169
All	32	249194	4064

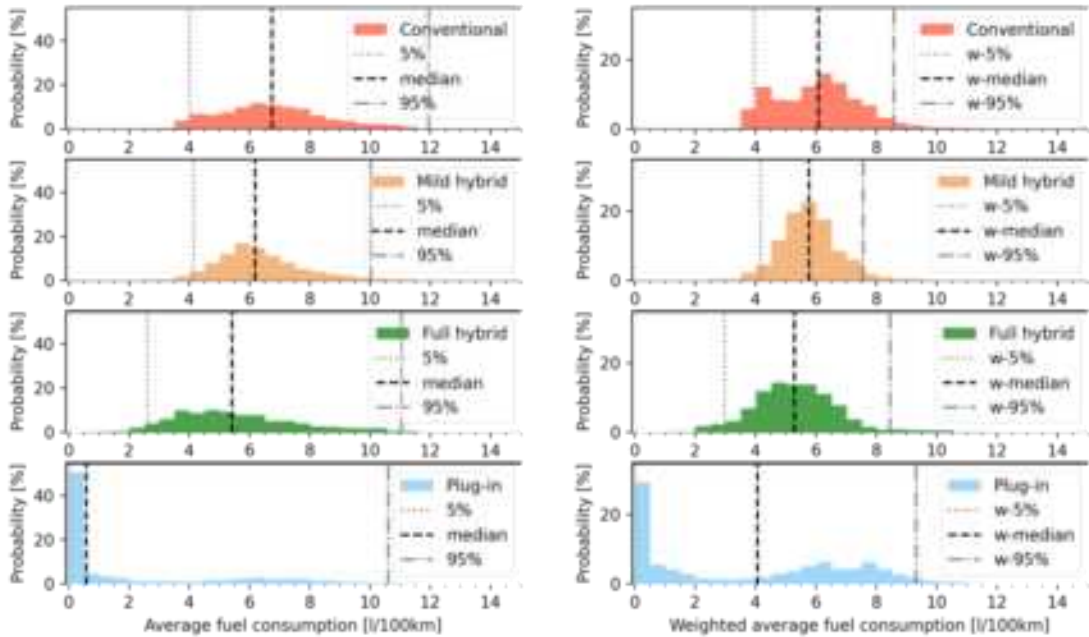


Figure 2: Per trip fuel consumption distributions (left) and distance-weighted fuel consumption distributions (right) per technology (conventional, mild, full and plug-in hybrid)

Different distributions are returned for the same technology from the two different representations, with different median values and percentiles. For plug-in hybrid in particular the difference is striking. The simple distribution returns a median trip average fuel consumption of about 0.6 litres/100km, which is unrealistically low, whereas the distance-weighted distribution returns more trustworthy values of about 4.0 litres/100km. The

explanation of the very different median value is found in the twofold nature of plug-in hybrids, which can drive trips in pure electric mode in addition to fuel-supported trips (as any other engine vehicle). From the captured data, it is clear that for plug-in hybrids pure electric trips outnumber the fuel-supported ones, bringing the median value of the simple distribution close to zero. These numerous purely electric trips are though cumulating a limited part of the vehicle lifetime distance and have limited significance when looking into the average fuel efficiency over a long period. The distance-weighting of trips is therefore highly significant to obtain the best representation of vehicles average fuel efficiency. In conclusion, focusing on the subplots on the right of the figure, a gradual decrease in fuel consumption is identified with increasing electrification degree (moving from top, conventional vehicles, to bottom, plug-in hybrids), as expected. By comparing the median values between the minimum and maximum electrification degree one can see that the average fuel consumption drops from 6.1 to 4.0 litres/100km. Nevertheless, these results largely depend on the vehicles and drivers in our sample, which is not big enough to generalise conclusions. Furthermore, the plug-in hybrids sample also covers some corporate users applying very little charging to their vehicles' batteries negatively impacting the average fuel consumption of the entire group. A much bigger sample, or more careful analysis and discussion of the results, is required to comment on plug-in hybrids' real-world fuel-saving potential.

To highlight the positive aspects of the project's methodology, Figure 3 presents an example of the data that is possible to produce through OBD and telemetry, which serves as invaluable context information to the fuel consumption values provided by OBFCM. More information could be produced based on the available OBD signals or the measurements that can be carried out and delivered by the OBD-dongles. From the figure, one can derive the trip average speed (subplots on the left) and the trip average ambient temperature (subplots on the right) to put the fuel efficiency data into perspective for each vehicle and usage condition.

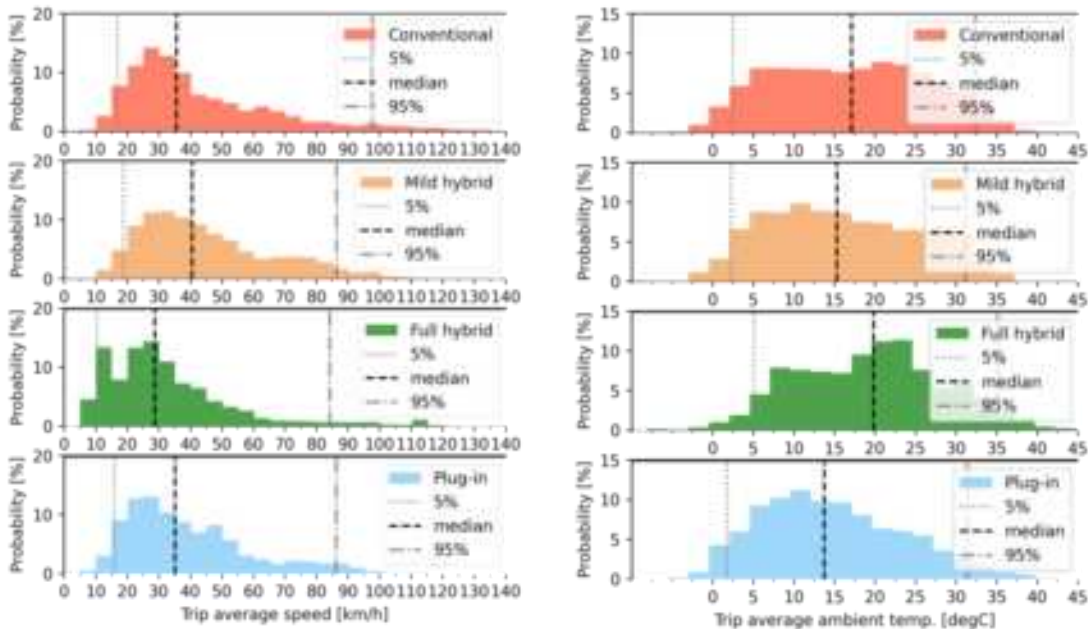


Figure 3: Distributions of trip average speed (left) and trip average ambient temperature (right) per technology (conventional, mild, full and plug-in hybrid)

The results in this section showcase how the methodology enables the collection of real-world fuel consumption data, complemented by context data, for different vehicle technologies, for a significant amount of distance and with relatively little effort. No laboratory, professional measurement instrument or trained technician/driver is involved in producing this data, which comes straight from the vehicle monitoring systems to our data centre, opening the road to the collection of very large amounts of driving and fuel consumption data from all Europe. The realworld vehicles usage patterns and efficiency can therefore be obtained and analysed considering the boundary conditions found in each region.

Acknowledgements

The authors acknowledge Fabrizio Forloni, Lorenzo Mainieri, Kostis Anagnostopoulos, Thomas Vliagkofotis, Athina Mitsiara for their invaluable help in kickstarting, upgrading and supporting the project. The authors are also grateful to the project volunteers who agreed in sharing their driving data and make our data collection campaign possible.

References

- COMMISSION REGULATION (EU) 2017/1151 of 1 June 2017 supplementing Regulation (EC) No 715/2007 of the European Parliament and of the Council on type-approval of motor vehicles with respect to emissions from light passenger and commercial vehicles (Euro 5 and Euro 6) and on access to vehicle repair and maintenance information, amending Directive 2007/46/EC of the European Parliament and of the Council, Commission Regulation (EC) No 692/2008 and Commission Regulation (EU) No 1230/2012 and repealing Commission Regulation (EC) No 692/2008. *Official Journal of The European Union*.
- Fontaras G., Zacharof N. G., Ciuffo B. (2017). Fuel consumption and CO₂ emissions from passenger cars in Europe - Laboratory versus real-world emissions, *Progress in Energy and Combustion Science*, 60, 97131.
- Pavlovic J., Anagnostopoulos K., Clairotte M. et al. (2018). Dealing with the Gap between Type-Approval and In-Use Light Duty Vehicles Fuel Consumption and CO₂ Emissions: Present Situation and Future Perspective, *Transportation Research Record*, 2672(2), 23–32.
- Pavlovic J., Fontaras G., Ktistakis M. et al. (2020) Understanding the origins and variability of the fuel consumption gap: lessons learned from laboratory tests and a real-driving campaign. *Environ Sci Eur* 32, 53.
- REGULATION (EU) 2019/631 OF THE EUROPEAN PARLIAMENT AND OF THE COUNCIL of 17 April 2019 setting CO₂ emission performance standards for new passenger cars and for new light commercial vehicles, and repealing Regulations (EC) No 443/2009 and (EU) No 510/2011. *Official Journal of The European Union*.
- REGULATION (EU) 2021/1119 OF THE EUROPEAN PARLIAMENT AND OF THE COUNCIL of 30 June 2021 establishing the framework for achieving climate neutrality and amending Regulations (EU) No 401/2009 and (EU) 2012/1994 – ~~Official Journal of The European Union~~. *Official Journal of The European Union*.
- Society of Automotive Engineering (2023). J1979-DA, Digital Annex of E/E Diagnostic Test Modes.
- UNFCCC, The Paris Agreement, Paris Climate Change Conference November 2015, COP 21.

CO₂ emissions of Australian and European Sport Utility Vehicles¹²

D. Komnos¹, J. J. Gómez Vilchez¹³, R. Smit³, L. Ntziachristos¹ and G. Fontaras^{2*2}

¹ Aristotle University, Thessaloniki, 54124, Greece

² European Commission, Joint Research Centre (JRC), Ispra, 21027, Italy

³ Transport Energy/Emission Research (TER), Launceston, Tasmania, 7249, Australia

Introduction

To address the increasing emissions from road transport and mitigate climate change, in 2009 the first CO₂ standards were adopted in European Union (EU), setting intermediate fleet-wide targets for the next decade – 130 g/km for 2015, and 95 g/km for 2020 – and providing time for the technology to mature and the car fleets to adapt (Regulation (EC) No 443/2009). Multiple studies indicated an increasing discrepancy between the officially reported CO₂ values and the ones realised under real-world (RW), reaching in 2017 a gap of 40% (Pavlovic et al., 2020; Tietge, 2019). The main reason was the flexible definition of the certification procedure used for efficiency benchmarking, the New European Driving Cycle (NEDC). Consequently, the NEDC-based CO₂ and fuel consumption values continuously decreased, but without improvement in RW conditions. They undermined the efforts to produce cleaner vehicles and reduce the CO₂ footprint of road transport. The EU regulators' reaction was to introduce a new certification procedure, the Worldwide Harmonised Light Vehicles Test Procedure (WLTP) to address the RW gap issue and to provide more detail in the manufacturers' CO₂ and fuel consumption data. The new test protocol corresponded better to RW conditions resulting to a substantial drop of the gap – to half – between certified and the RW values (Fontaras et al., 2017; Pavlovic et al., 2020; TER, 2019). In 2019, new regulations integrated the new protocol and created a path for CO₂ standards in the following decade, also putting in place provisions to ensure the CO₂ gap is not growing again (Regulation (EU) 2019/631).

The evolution of EU regulation increased confidence in the stability of the CO₂ framework, which aligned with a larger climate ambition in the EU (European Commission, 2019). In 2023 the EU voted for more ambitious CO₂ targets for 2030 and a reduction of 100% for 2035 (Regulation (EU) 2023/851). These actions intend to bring public attention and progressively decarbonise the sector. It is already visible that vehicle electrification is rapidly increasing, providing a cleaner and more efficient on-road fleet. However, this is not the case worldwide, even among developed countries. In Australia (AU) light-duty vehicles are still being certified using the NEDC, and the growth of the sales of electric vehicles is limited compared to EU (TER, 2019). Lacking CO₂ emissions standards, in parallel to continuous growth in the sales of heavier and more energyconsuming sport-utility vehicles (SUV) and utes, vehicle manufacturers have no incentive to introduce fuel-efficient vehicles into the AU fleet. Moreover, the vehicles are less fuel efficient than identical makes and models available overseas (Smit et al., 2022, 2021). As a result, the AU passenger vehicle fleet is moving towards higher absolute CO₂ emissions and a likely widening RW CO₂ gap. A recent study showed that the AU on-road fleet will only achieve a 35-45% reduction in (well-to-wheel) GHG emissions in road transport in 2050 compared to 2019 levels, even if a delayed and ambitious EU EV penetration scenario is followed (Smit, 2023).

The present paper shows the preliminary results of the simulations performed to analyse SUVs' RW consumption and CO₂ gap and provides insights by comparing a regulated (EU) versus a relatively non-regulated market (AU). The EU is the reference market where CO₂ targets have been established for over a decade and where up-to-date test procedures have been adopted, while the Australian market provides the unregulated example with the continued use of an outdated test protocol and a lack of (mandatory) CO₂ or fuel efficiency regulation.

Methodology

Overview. A schematic representation of the approach followed to simulate the annual CO₂ gap of the SUV fleet for EU and AU is shown in Figure 1. Technical characteristics of indicative SUVs from both regions were collected and combined with representative RW trips and representative ambient temperatures to build realistic RW scenarios. Combinations of all the different parameters, i.e., representative vehicles, trips, and temperatures,

¹² The views are purely those of the authors and should not be considered as an official EU Commission position

¹³ Corresponding author georgios.fontaras@ec.europa.eu

were simulated with a vehicle simulator to derive each individual vehicle's RW CO₂ gap from the certified values. For the present research, the study team has used the PyCSIS tool that is a light version of CO₂MPAS (Fontaras et al., 2018). PyCSIS performs detailed simulations because its physical models are sensitive to the individual vehicle characteristics and the environmental parameters used as inputs. It has proven its accuracy in simulating laboratory tests (following both NEDC and WLTP certifications) and RW driving in several studies, with the most recent assessing the EU fleet gap of 2018 and 2019 (Komnos et al., 2022). To derive the SUV fleet annual RW consumption and gap, the individual vehicle RW gaps simulated were then intersected with the below distributions:

1. Certified CO₂ distributions of SUVs of one registration year for both EU and AU.
2. RW trip distance distributions of annual usage.
3. Population-weighted average ambient temperature distributions.

For each of these distributions, 10,000 Monte Carlo simulations were performed following their characteristic shapes. Then, each Monte Carlo simulation was compared to the values previously selected as representatives. This procedure was followed to assign a percentage correspondence to the full distribution. For example, each vehicle selected reflects a specific percentage of vehicles in the fleet in CO₂ terms. For this purpose, the distance between each representative value and each Monte Carlo simulated value was calculated; then, every value of the 10,000 Monte Carlo is distributed to the representative value that their distance is the minimum.

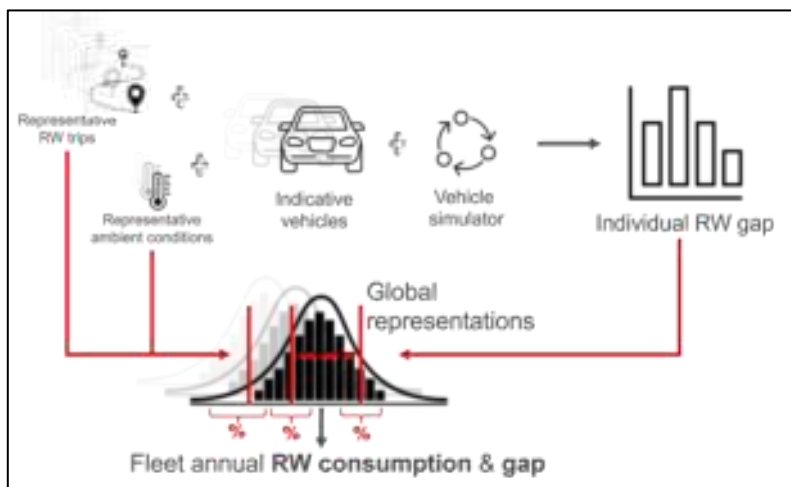


Figure 1: Schematic workflow of the process followed.

The following subparagraphs provide detailed explanations for distributions and the representative values used for the simulations.

EU and AU and representative SUVs and fleets. Finding representative EU and AU market data for SUVs was a crucial step. For the EU market, the Joint Research Centre (JRC) database that collects the vehicle technical characteristics of the vehicles tested each year for the EU Market Surveillance (Bonnel et al., 2022) was used, and four indicative vehicles were selected. Four SUVs tested under real-world conditions (PEMS) and representative of typical SUVs sold in AU (Smit et al., 2022) were selected for AU. In Table 1, essential characteristics for both vehicle sets are provided. Each set of vehicles is ordered by their certified CO₂ value. The AU vehicles are a mix of diesel and gasoline vehicles and have larger engine capacities and higher weights as compared with the EU SUVs. Altogether, the first indication is that the AU SUVs are bigger vehicles than the ones most frequently sold in EU. Regarding the SUV fleets of both regions, it was decided to study the registered vehicles in the year 2020. The 2020 EU registered SUVs were collected by combining the 2020 EU monitoring dataset for passenger vehicles reported by the European Environment Agency (European Environment Agency, 2023), with a database created by collecting data from online sources. This provided new vehicle sales numbers by make and model and with associated NEDC and WLTP-certified CO₂ values. The dataset was used to identify which vehicles are SUVs. In the EU 3,192,369 vehicles were identified as new SUVs sold in 2020.

Table 1: Characteristics of the sampled EU and AU representative SUVs. Gas: Gasoline; Dies: Diesel; T: Turbo engine; A: Naturally aspirated engine.

	EU				AU			
	Veh 1	Veh 2	Veh 3	Veh 4	Veh 1	Veh 2	Veh 3	Veh 4
Fuel	Gas T	Dies T	Gas T	Gas T	Gas N	Dies T	Dies T	Gas N
Gear box	Auto	Auto	Auto	Auto	Auto	Auto	Auto	Auto
Engine capacity	1.2	2.0	1.4	2.0	2.5	3.0	2.8	3.5
Rated power	96	110	110	141	126	130	130	218
Vehicle mass	1208	1728	1592	1645	1560	2142	2315	2045
Year	2021	2021	2017	2019	2020	2018	2019	2019

The AU Green Vehicle Guide (DITRDCA, 2020) was used collect the NEDC certified CO₂ values of all the SUVs present in the AU market for the period 2018-2021. AU sales data were retrieved from online sources for the 100 top sold vehicles in 2020. Combining the two sources 376,655 vehicles were identified as new SUVs in 2020 for AU, which is about 80% of total SUV sales in 2020 (TER, 2022). Figure 2 shows the CO₂ distributions for both regions and the two sets of representative vehicles. Distributions were produced by fitting the fleet data to lognormal and gamma distributions for EU and AU CO₂ values, respectively. The selected probability distributions for each fleet provided the best fit and lowest errors.

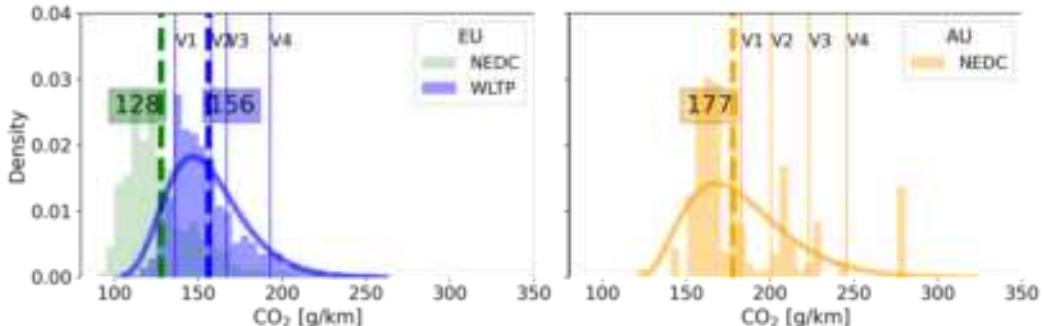


Figure 2: CO₂ certified values for EU (left) and for AU (right). The vertical lines indicate the certified CO₂ values of the representative vehicle selected. The thick lines correspond to the distributions fitted to the data.

In the Figure 2 (left), two distributions appear for the new EU SUVs because 2020 was the last year that regulation allowed for a smooth transition from NEDC to WLTP. Comparing the EU with the AU distributions and their average values (Figure 2), it is evident that even with the more representative protocol of WLTP, the EU SUV fleet is, on average, more efficient by 21 g/km of CO₂. The accuracy of the EU distributions is considered acceptable since they were produced using official information reported by the EU member states. This is not the case for the AU distributions. However, comparison with a detailed study of the 2018 AU sales and emissions data (TER, 2019) confirms good agreement and provides confidence in the initial results for AU.

Real-world set up. Previous studies (Fontaras et al., 2017) split the factors in vehicle-related factors, environmental factors and traffic/driving pattern related factors. Vehicle-related factors are reflected in the vehicle characteristics of the representative vehicles selected for the study. The impact of the road factors is introduced by utilising trips recorded in a one-year RW campaign (Pavlovic et al., 2020). To reduce the computational cost of the simulations, representative trips falling to similar average trip speeds as in the 4 phases of the WLTP cycle (Low – D1, Medium D2, High – D3, Extra-High – D4) were selected. For the Extra-High phase, two different speed profiles were used to understand the influence of the highway trips in the fuel consumption and the total annual milage driven (D4 case 1 and case 2). More details are shown in Table 2. For

this initial investigation, it has been assumed that RW driving conditions are comparable in the EU and AU, but future work will include AU driving behaviour in more detail.

Table 2: Distances of the trips selected for the simulations.

	D1	D2	D3	D4 case 1	D4 case 2
RW distances [km]	3	10	27	130	216

Annual average ambient temperatures were collected for all EU Member States and states and territories in AU via web scraping and combined with population figures. This showed that the two regions have different range of ambient temperatures that can impact the RW vehicle usage (e.g., need for heating, ventilation and air conditioning of the cabin), the vehicle efficiency (e.g., coldstart). To understand the variability, in addition to the population-weighted mean, also the temperatures corresponding to the 1st, 25th, 75th, and 99th percentiles of the distributions were simulated (hereafter referred to temperatures T1 to T5): 3°C (T1), 8°C (T2), 10.5°C (T3), 14°C (T4) and 17°C (T5) for EU, and 11°C (T1), 14°C (T2), 17°C (T3), 19°C (T4) and 22°C (T5) for AU. Besides the population weighted mean, another way to produce representative ambient temperatures is by applying vehicle-kilometres-travelled (VKT) weight average. Comparing the two methods we see that the population-weighted mean calculated for AU (17°C) is close to the VKT weighted temperature estimated in previous study, that was 18.2°C (Smit, 2014).

Results

Model validation. PyCSIS has been validated under different vehicle configurations and simulation environments, but validation was performed also for the indicative vehicles used for the present study. The validation included an assessment if the selected vehicles' certified values are reproduced and if their RW performance is replicated in the case of the AU representative vehicles. It should be noted the simulation of the certified values followed the respective test cycles, the initial vehicle conditions (e.g., initial engine temperatures) and test cell temperature. For the EU vehicles the official test mass and road load coefficients were used. For the AU vehicles, road load coefficients were obtained from coast-down tests (Smit et al., 2022) and were assumed to be WLTP representative. The translation to NEDC representative values followed the EU NEDC-WLTP correlation work (Regulation (EU) 2017/1153). Regarding the AU RW trips used for the validation, the PyCSIS simulated CO₂ signals and aggregated values were compared to measured emissions during on-road trips performed in Sydney using portable emissions measurement systems. Table 3 shows that all the simulated cases show acceptable accuracy, giving confidence for the next steps.

Table 3: Sampled vehicle validation.

	Veh 1	Veh 2	Veh 3	Veh 4	Average
Error [%]	AU certification (NEDC)	-3.1	-3.8	4.9	15.6
	AU RW trips	1.9	6.1	1.3	0.5
	EU certification (WLTP)	2.4	8.2	6.1	4.1
					5.2

Global representations and CO₂ gap. In this subparagraph using the global representations from the distributions derived from the SUV fleets, the annual trip distances, and average ambient temperatures, the previous results will be expanded to produce annual SUV fleet values. The fleet shares in Table 4 provide the share of each individual vehicle in the fleet. The shares sum up to the total number of SUVs registered in the two regions in 2020. The trip shares sum up to 10,671 km for case 1 and 11,770 km for case 2, with the half of them driven in the highway (trips D4). Regarding the temperatures selected, only the extremes appear to have lower contribution than the others. In further work, EU trip data will be compared with AU trip data to

further refine these initial estimates. To understand the possible influence of the vehicle to the CO₂ gap, Figure 3 shows the annual RW gap simulated for the four EU and four AU SUVs. The average annual CO₂ gap in EU (WLTP-based) ranges between 7 and 19%, showing a declining trend as SUV are getting bigger. Similar trends appear for AU when the estimated WLTP-based CO₂ values are examined. The NEDC-based gap is considerably larger, reaching values of up to 45%. The CO₂ gap ranges, either WLTP-based or NEDC-based are in line with the scientific literature (Ktistakis et al., 2021; TER, 2019).

Table 4: Global representations.

Fleet shares [%]		Trip shares [%]		Temperature shares [%]	
EU	AU	Case 1	Case 2	EU	AU
V1	40	66	D1	34	34
V2	26	17	D2	33	32
V3	19	10	D3	24	28
V4	15	7	D4	9	6
				T1	14
				T2	27
				T3	27
				T4	20
				T5	12
					25

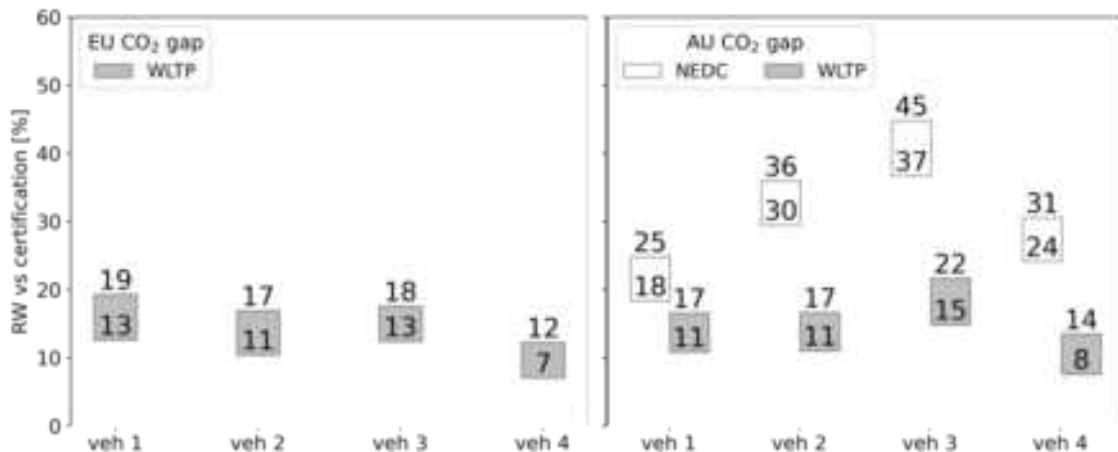


Figure 3: Individual vehicles CO₂ gaps. Left: EU; Right: AU. The bottom of each box represents the trips share case 2 and the top of the boxes are produced with the trips share case 1.

Combining the individual vehicles' annual gaps with the fleet shares data. The calculated EU SUV fleet CO₂ gap ranges between 12%-18% (WLTP). The calculated AU SUV fleet CO₂ gap ranges between 26%-32% (NEDC). Applying the WLTP certification procedure in AU, the certification values would be closer to the RW driving, thus the CO₂ gap would reduce to 11% to 17%.

Discussion and Conclusions

Two different markets were assessed for the year 2020: the EU market as the regulated market and AU as the unregulated market. Since there has been an upturn of SUVs worldwide the recent years, the study focused on these vehicles. A methodology is proposed to assess the two markets, combining representative vehicles, fleet data and environmental conditions from both regions with a simulation-based RW framework to perform a detailed analysis. The preliminary results quantify the performance of the SUVs in EU and AU, clearly showing a higher fuel efficiency of the EU vehicles. Using the simulation framework, the RW consumption was derived and also the CO₂ gap. The EU WLTP-based CO₂ gap is calculated to be around 18% and the AU NEDC-based CO₂ gap ranges up to 32%, with both figures being in line with existing literature. With the support of the

simulation tool, the WLTP-equivalent CO₂ values for AU were derived, and the annual SUV fleet CO₂ gap dropped considerably and in the same levels as in EU. It should be acknowledged that other factors than regulation will shape a countries on-road fleet, and this will be further explored in future work. Despite any fallbacks experienced in the last decade, the EU fleet is transforming fast, while the opposite appears to be the case for AU. Furthermore, the WLTP protocol provides more realistic CO₂ and consumption values and supports building public awareness and making better choices for private commuting.

References

- Bonnel, P., Clairotte, M., et al., 2022. European market surveillance of motor vehicles Results of the 20202021 European Commission Vehicle Emissions Testing Programme. <https://doi.org/10.2760/59856> DITRDCA, 2020. Green Vehicle Guide. URL <https://www.greenvehicleguide.gov.au/>.
- European Commission, 2019. EU climate action and the European Green Deal. Climate Action - European Commission. URL https://ec.europa.eu/clima/policies/eu-climate-action_en.
- European Environment Agency, 2023. Datasets — European Environment Agency. URL https://www.eea.europa.eu/data-and-maps/data/#c0=5&c11=l3fwryepgj&c5=all&b_start=0.
- Fontaras, G., Ciuffo, B., et al., 2017. The difference between reported and real-world CO₂ emissions: How much improvement can be expected by WLTP introduction? Transportation Research Procedia, World Conference on Transport Research - WCTR 2016 Shanghai. <https://doi.org/10.1016/j.trpro.2017.05.333>
- Fontaras, G., Valverde, V., et al., 2018. The development and validation of a vehicle simulator for the introduction of Worldwide Harmonized test protocol in the European light duty vehicle CO₂ certification process. Applied Energy 226, 784–796. <https://doi.org/10.1016/j.apenergy.2018.06.009>
- Komnos, D., Tsiakmakis, et al., 2022. Analysing the real-world fuel and energy consumption of conventional and electric cars in Europe. Energy Conversion and Management 270, 116161. <https://doi.org/10.1016/j.enconman.2022.116161>
- Ktistakis, M., Pavlovic, J., et al., 2021. Understanding the fuel consumption gap using self-reported user and smartphone application datasets. <https://doi.org/10.2760/019404>
- Pavlovic, J., Fontaras, G., et al., 2020. Understanding the origins and variability of the fuel consumption gap: lessons learned from laboratory tests and a real-driving campaign. Environmental Sciences Europe 32, 53. <https://doi.org/10.1186/s12302-020-00338-1>
- Smit, R., 2023. An independent and detailed assessment of greenhouse gas emissions, fuel use, electricity, and energy consumption from Australian road transport in 2019 and 2050. Air Quality and Climate Change. <https://www.transport-e-research.com/publications> (2023c)
- Smit, R., 2014. Australian Motor Vehicle Emission Inventory for the National Pollutant Inventory (NPI). C01772. <https://www.transport-e-research.com/publications> (2014b)
- Smit, R., Awadallah, M., et al., 2022. Real-world emission factors for SUVs using on-board emission testing and geo-computation. Transportation Research Part D: Transport and Environment 107, 103286. <https://doi.org/10.1016/j.trd.2022.103286>
- Smit, R., Bainbridge, S., et al., 2021. A decade of measuring on-road vehicle emissions with remote sensing in Australia. Atmospheric Environment 252, 118317. <https://doi.org/10.1016/j.atmosenv.2021.118317> Tietge, U., 2019. From laboratory to road: A 2018 update of fuel and real-world fuel consumption and CO₂ values for passenger cars in Europe
- TER, 2022. Australian Fleet Model (AFM). Transport Energy/Emission Research. URL <https://www.transport-e-research.com/software-afm>.
- TER, 2019. Real-World CO₂ Emissions Performance of the Australian New Passenger Vehicle Fleet 20082018 – Impacts of Trends in Vehicle/Engine Design. Transport Energy/Emission Research, Australia, <https://www.transport-e-research.com/publications> (2019a)

Temperature Effects on Energy Consumption from Battery Electric Vehicles

S. Hausberger¹, G. Silberholz¹, S. Lipp¹, M. Opetnik¹

¹ Institute for Thermodynamics and Sustainable Propulsion Systems, University of Technology, Graz, Styria, 8010, Austria

Introduction

Fuel consumption and CO₂-emissions per km from conventional cars proved to be on average much higher in real world driving than in type approval. Studies such as (Eisenmann, 2021) and (Weller, 2019) indicate for conventional cars ca. +10 to 20% compared to the WLTP (+35% to 40% compared to NEDC). Reasons are auxiliary power demands not considered in type approval, higher road loads due to side wind, wet road, roof racks, trailers etc. but also engines optimised for the load profiles of the type approval cycles. For PHEVs the ratio real world/type approval is even worse (Plötz, 2022). In a study for UBA Germany, (Helms, 2022)], we analysed the real world effects for the energy consumption of Battery Electric Vehicles (BEVs). Based on this study, the paper analyses following questions:

- What is the difference between real world and type approval energy consumption?
- What are the main parameters for possibly higher energy consumption in real world?
- Is there a need to adjust type approval testing?

Methods and data used for the study

The fleet average differences between real world and type approval energy consumption were analysed using real world energy consumption according to spritmonitor.de (data 2019 to 2022) with the type approval energy consumption for the same fleet. For detailed analysis of the parameters influencing the real world energy consumption we measured three BEVs, also referred to as pure electric vehicles (PEVs): a VW ID.3, a Renault Zoe and a Tesla Model Y. The tests were driven on the road but with different pre-conditioning on the temperature test stand of the University of Technology, Graz (TUG), with different real world routes and different settings of the heating, ventilation and air conditioning (HVAC) system. The test data was used to parametrise the vehicle emission and energy consumption model PHEM from TUG for each measured vehicle to meet the measured energy consumption values in all tests.

The energy consumption of the HVAC system and of other auxiliaries was simulated with the Software AuSyn from TUG, which considers inter alia sun radiation, ambient temperature, passenger heat release and a user-defined mix of fresh and recirculated air for an energy balance to calculate the cooling and heating energy demand for any ambient condition. To assess the related electric energy demand, a combined cooling circuit and heat pump is simulated. The model was applied for different temperatures and for the European average conditions (Table 1).

Table 1: Solar radiation in [W/m²] (left) and average temperature in [°C] (right) per month and time slots for Frankfurt

Month	23-5:00	5:00-11:00	11:00-17:00	17:00-23:00
1	0.00	37.72	160.34	0.01
2	0.00	90.30	305.15	1.46
3	0.00	168.53	431.52	18.04
4	0.00	317.89	581.28	48.51
5	0.28	445.05	730.48	94.28
6	1.26	471.06	733.06	101.50
7	0.35	451.45	776.92	114.97
8	0.00	387.56	673.34	65.98
9	0.00	238.69	484.31	23.90
10	0.00	132.96	320.20	1.63
11	0.00	67.66	162.98	0.00
12	0.00	34.65	114.44	0.00

Month	23-5:00	5:00-11:00	11:00-17:00	17:00-23:00
1	-0.80	-1.06	2.97	1.25
2	-0.51	-0.49	4.34	1.98
3	2.46	3.18	8.80	6.12
4	5.33	7.70	13.73	10.17
5	9.04	12.26	18.32	15.32
6	11.68	15.65	21.46	18.02
7	14.41	17.51	23.30	20.57
8	13.87	16.57	23.02	19.44
9	11.29	12.99	19.19	15.79
10	7.94	8.58	14.00	11.14
11	2.86	3.18	7.52	5.07
12	0.30	0.16	3.92	1.98

The average conditions in Table 1 are based on hourly weather data weighted according to traffic volumes over a year in Frankfurt. We also performed an extensive literature review on energy consumption from auxiliaries and of BEVs in general to support the simulation results. Finally we compared a model for a "typical compact BEV" from the single vehicle models supported by literature data.

Figure 1 shows a schematic picture of the vehicle emission model PHEM from TUG. PHEM calculates the power demand at the wheels for given driving cycles using the equations of longitudinal dynamics. The motor power demand and rotational speed is calculated from the transmission ratios and losses in the axle and gear box. For BEVs a battery model is implemented which simulates the charging and discharging losses from the resulting voltage and current with defined internal resistance values depending on the battery capacity and voltage. A simple map depictsures the electric power demand over mechanical power output and rpm of the electric motor. The auxiliary power demand is an input value, which was simulated here with the model AuSim as described before.

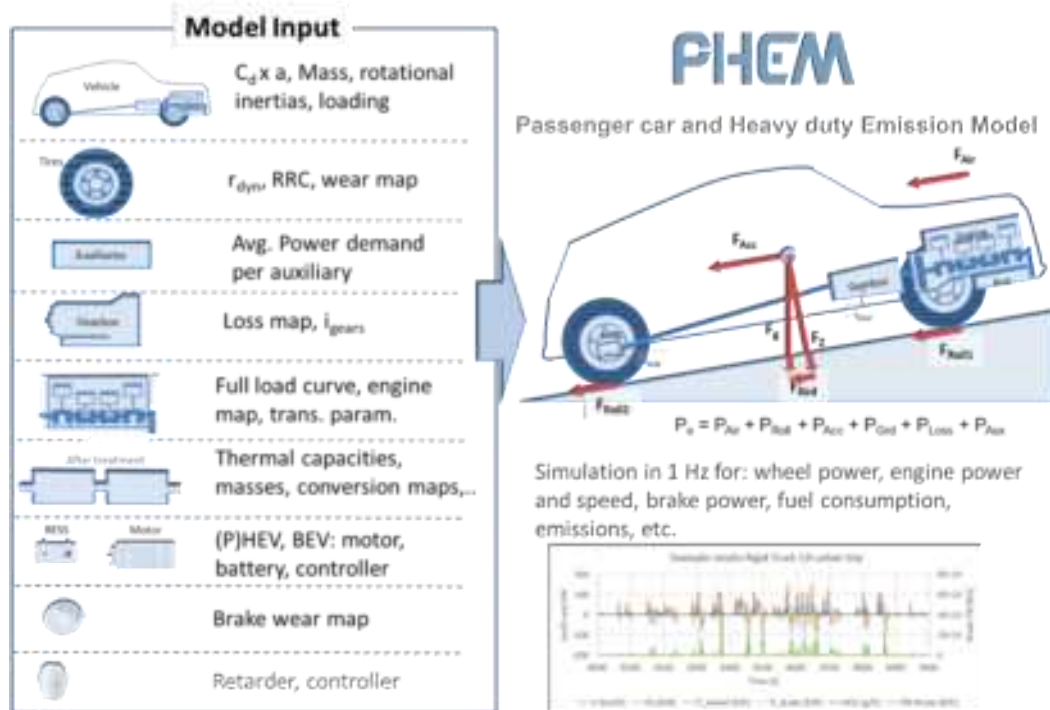


Figure 1: Schematic picture of the vehicle emission model PHEM from TUG

The model PHEM is also used to calculate exhaust gas emissions and energy consumption values for all vehicle categories in the Handbook on Emission Factors (HBEFA, www.hbefa.net). The BEV model used here however, is different to the HBEFA 4.2 model, since the HBEFA BEV car model was designed around 2018.

Type approval test procedure for BEVs

The type approval procedure to measure the energy consumption and the electric range of BEV cars is described in Regulation (EU) 2017/1151. BEVs are driven in a special test cycle starting with full battery (100% state of charge, SOC) on the chassis dynamometer until vehicle stops with 0% SOC. Constant speed phases (CSS) are used to discharge the battery over the entire test completely in a driver friendly manner. The net energy consumption from the battery is measured during the test. Then the battery is charged to 100% SOC with a charging method according to OEM choice. The ratio between recharged energy and consumed energy in the test provides the charging loss factor, which is considered in the type approval energy consumption values:

$$EC_{WLTP} [\text{Wh}/\text{km}] = EC_{(DS1 \& DS2)} \times \text{charging loss factor}$$

Where $EC_{(DS1 \& DS2)}$ is the net energy consumption in [Wh/km] measured at the battery during the two DS phases shown in Figure 2. The DS (dynamic segment) phases consist of the WLTC with a repetition of the two low speed phases and thus represent higher shares of urban driving (almost 50% of the distance) compared to the WLTC for conventional vehicles. In the type approval value for the electric range the charging losses are not considered since they do not influence the battery capacity if a trip is started with 100% SOC. The DS sub-cycle shows in the simulation a ca. 10% lower energy consumption than the WLTC due to the higher low speed shares. The entire test has typically even lower energy consumption due to the CSS phases.

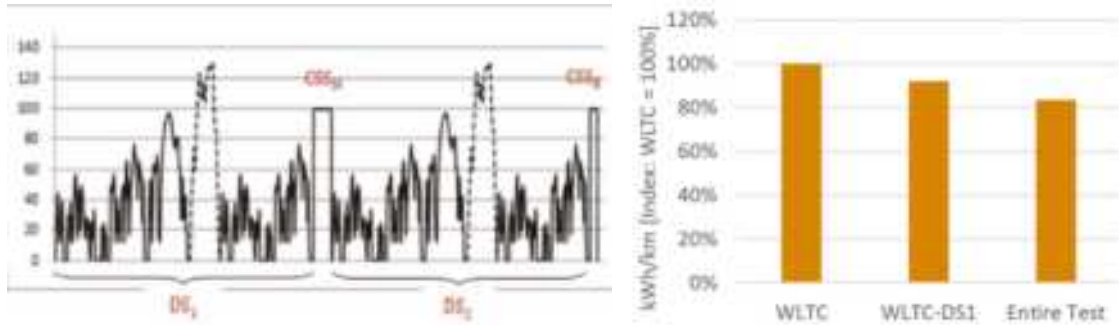


Figure 2: Schematic picture of the BEV type approval test (Regulation (EU) 2017/1151) and energy consumption simulated for the generic compact BEV car in the WLTC cycle, in the DS1 part and in the entire BEV type approval test

Deviation real world versus type approval

Figure 3 shows the results from the comparison of the average energy consumption recorded for BEVs in spritmonitor.de compared to the related type approval energy consumption values and the deviation between these values. The analysis included only the makes and models where type approval data was available (Helms, 2022). A main uncertainty in the spritmonitor.de data is the handling of charging losses since it is not defined if users fill in the energy consumption provided by the vehicle dash board or the one read from the charging station. Since type approval data includes charging losses, also the real world data should be based on the charged energy. We decided to assume, that ca. 50% of the real world data includes charging losses and thus corrected the spritmonitor.de values with a factor of 1.1. The average charging losses found in the study are ca. 17%, (Helms, 2022). The assumption, that 50% of the data include the charging losses may rather underestimate real world energy consumption since users may rather read the kWh/km from the vehicles dashboard than using the total charged energy which needs to be divided by the mileage driven since the last (full) charging. Consequently, the real world energy consumption of BEVs may currently be on average ca. 10 to 25% higher than the type approval values. Reasons for the higher deviation for the registration year 2021 were not identified. We found a tendency for higher deviations with increasing battery capacity but no significant correlation between deviation and rated power of the vehicles.



Figure 3: Average energy consumption recorded for BEVs in spritmonitor.de compared to the related type approval energy consumption values and deviation between these values

Since BEVs currently may be used more often for commuting and for urban trips than the average car, the real world energy consumption of BEVs may increase in future with increasing fleet penetration since then the relative share of leisure and holiday trips from BEVs may increase. The latter have more passengers and luggage in the vehicle, roof racks, more and faster highway driving etc.

Relevant parameters for higher real world energy consumption

Overall, the measurements and simulations for warm conditions, i.e. between ca. 20°C and 30°C indicated excellent energy efficient for the BEVs. While we had to increase real world rolling and air resistances as well as the average loading and auxiliary power demand to meet reported real world fuel consumptions of conventional cars in the simulations we performed in (Eisenmann, 2021), we had to reduce the generic parameters for the BEVs to meet the values measured at the three tested BEVs. Obviously, the target of sufficient electric range motivates to optimise the BEVs also in real world driving.

Beside the (unavoidable) extra driving resistances due to cross wind, wet road etc., the main parameters increasing the BEVs energy consumption compared to the type approval value are:

- Low temperature driving with a main parameter being the initial energy demand to heat the battery cells up to 15°C to 20°C
- Heating and cooling of the passenger compartment
- High speed driving due to exponential increase of air drag and dropping motor efficiency at high rpm (revolutions per minute)
- Charging losses possibly different to the ones with the charging system used in type approval.

We calibrated the AuSym model for the base auxiliary power demand from the BEVs with the test trips with deactivated HVAC system where also the blower was switched off. The model for the additional HVAC power demand was calibrated with tests with activated HVAC both in stand still and different driving conditions. Tests covered ambient conditions between 0°C and 26°C.

The left picture in Figure 4 shows the results for stationary thermal conditions, i.e. after the initial heating or cooling of the battery and of the passenger compartment. The square shows the result for the European temperature and sun radiation variation over a year with Frankfurt weather conditions, the circles show the results for constant temperature conditions with the corresponding average solar radiation. The initial heating energy for the battery was calculated for a target temperature of 20°C from the thermal capacity of the cells. Figure 4 shows the measured heating energy at a cold start at 4°C, which was used to calibrate the specific heat capacity value of the generic battery cells.

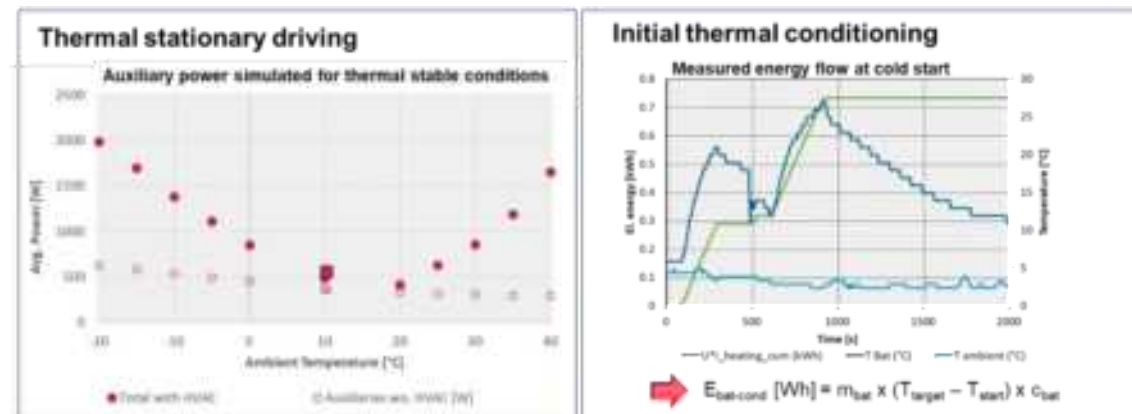


Figure 4: Auxiliary power demand with and without HVAC in thermal stationary driving conditions (left) and electric energy consumption for initial battery heating after cold start at 4°C (right)

Figure 5 shows the results from the simulation of a 36 km long urban trip with different start temperatures compared to the BEV-WLTP test for the full DS1 phase. Average urban driving at 20°C leads to even lower energy consumption compared to the type approval values. Towards low temperatures the energy demand for initial heating of the battery and the passenger compartment is getting more relevant. Due to the short distance, the initial heating energy per km is getting quite high. This can lead to more than double energy consumption per km compared to a similar trip at 20°C. The energy consumption for HVAC at thermal stable vehicle conditions after the initial heating has comparable lower impact. Since the driver does not see the charging losses on the dashboard while they are included in type approval values, drivers may recognize in urban driving between 10 and 30°C a similar or even lower energy consumption compared to the average value from type approval.

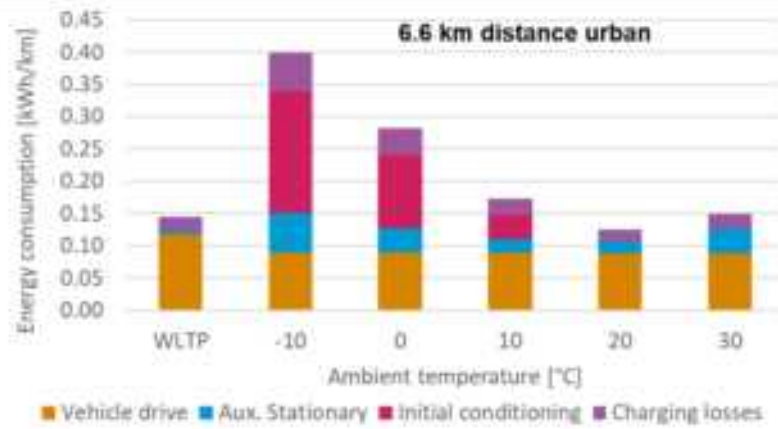


Figure 5: Energy consumption simulated for the generic medium size BEV for type approval (DS1 of WLTP) and for short distance urban driving

Figure 6 shows the results for long distance motorway driving with an average speed of 119 km/h. The initial heating of the battery needs the same absolute value in terms of kWh as in city driving but the division by the high number of km driven after the initial heating leads to a low contribution in the kWh/km result of the total trip. Due to the higher air resistance and the lower efficiency of the electric motor at higher rpm, the energy consumption of the electric motor is clearly higher in the motorway trip than in the WLTP-DS 1 sub-cycle. Lower speed on the motorway and a gear box with two or more gears would help to reduce the BEVs energy consumption on motorways.

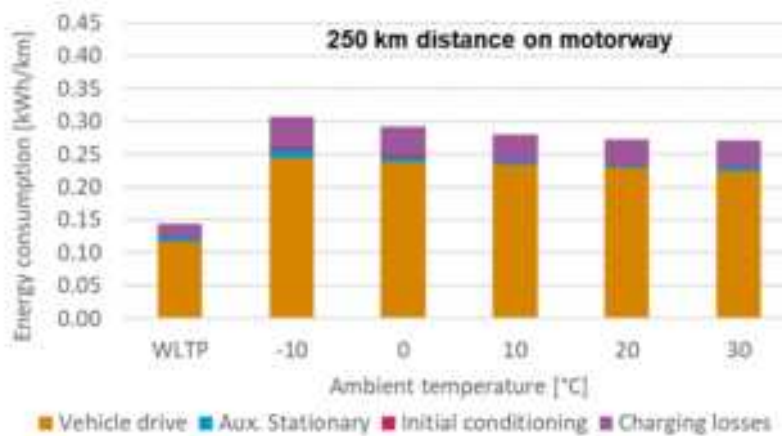


Figure 6: Energy consumption simulated for the generic medium size BEV for long distance highway driving and for type approval (DS1 of WLTP)

Today, BEVs may be used rather for urban trips and for commuting which can be used as argument for the higher share of urban driving in the BEV type approval compared to the WLTC for conventional cars. The average real world mix of driving situations from BEVs is unknown, also the entries in spritmonitor.de do not provide information on the typical vehicle use profile.

However, with sharply increasing shares of BEVs in new registrations, the usage of BEVs will most likely align with the current user profile of conventional passenger cars.

Summary

We have updated the simulation model for BEV cars in our software tool PHEM and calibrated the input data with measurements of three BEVs in various driving and ambient conditions. The simulation results indicate:

- Current BEVs have already a high energy efficiency in warm conditions.

- Average real world energy consumption for driving in central Europe is ca. 10 to 25% higher than the type approval value, depending on the driving mix. Both, colder or hotter climates increase the real world energy consumption.
- The BEV type approval cycle (DS phases) has higher urban shares than the WLTC cycle, which leads to a ca. 10% lower energy consumption compared to the conventional WLTC.
- Main reasons for higher real world energy consumption are:
 - Battery conditioning at temperatures below ca. 15° to 20°C to minimize deterioration is not relevant in type approval, which starts with 20°C,
 - HVAC and other auxiliaries are not engaged in the type approval test,
 - Effects of side wind, partly wet and snowy roads, small shares of roof boxes etc. and possibly also a different driving mix than the WLTP-DS phases for BEVs most likely also contribute to higher real world consumption values. A quantification of the average impacts was yet not possible.

From the results, some adjustments for the BEV type-approval test can be considered:

- A low temperature test (e.g. at 0°C) should be added in future type approval of BEVs to incentivize a low energy demand for initial battery conditioning. The type approval value may then be a weighted average of the 23°C and the low temperature test.
- The WLTP cycle for BEVs may be adjusted to the one for conventional cars, i.e. to eliminate the additional low speed phases in the evaluation since in the long term, BEVs will be used similar and instead of conventional cars.

References

Eisenmann C., Kuhnighof T., Tietge U., Dornoff J., Diaz S., Mock P., Allekotte M., Heidt C., Knörr W., Althaus H.-J., Notter B., Oberpriller O., Läderach A., Hausberger S., Matzer C. (2021): Erarbeitung einer Methode zur Ermittlung und Modellierung der CO₂-Emissionen des Kfz-Verkehrs, Forschungskennzahl 3716 58 180 0

Helms H., Bruch B., Räder D., Hausberger S., Lipp S., Matzer C. (2022): Energieverbrauch von Elektroautos (BEV), Projektnummer 1711964, UBA-Texte |160/2022

Plötz P., Link S., Ringelschwendner H., Keller M., Moll C., Bieker G., Dornoff J., Mock P. (2022): REAL-WORLD USAGE OF PLUG-IN HYBRID VEHICLES IN EUROPE A 2022 UPDATE ON FUEL CONSUMPTION, ELECTRIC DRIVING AND CO₂ EMISSIONS; Fraunhofer, ICCT; Berlin June 2022

Weller K., Lipp S., Röck M., Matzer C., Bittermann A., Hausberger S. (2019): Real World Fuel Consumption and Emissions From LDVs and HDVs; Engine and Automotive Engineering, Frontiers in Mechanical Engineering 5:45., doi: 10.3389/fmech.2019.00045

Prediction of fuel consumption for truck planning based on VECTO simulations

N. Kousias¹, F. Kyriakidis¹, K. Agavanakis², R. Quittard² and G. Mellios¹

¹Emisia SA, Thessaloniki, GR55535, Greece, Corresponding author email: nikos.kousias@emisia.com

²ADD, Avenir Développement Durable, Marseille, 13007, France

Introduction

Globally, emissions from freight transport account for 8-10% of Greenhouse Gases (GHG), with road transport being responsible for 62% of all freight emissions worldwide (Punte et al., 2022). In the EU, a similar pattern emerges, with road transport accounting for 75% of total freight transport, while Heavy-Duty Vehicles (HDVs) contribute to 25% of road transport GHG emissions and 5% of the EU's total CO₂ emissions (Eurostat, 2021). Beyond their environmental impact, these emissions directly influence fuel costs for carriers, establishing a clear industry-driven incentive to explore strategies for reducing carbon footprint.

Significant efforts are underway to enhance the reporting and reduction of GHG emissions from freight transport. However, addressing this challenge within the road transport sector proves particularly challenging due to its fragmentation, characterized by a multitude of small carriers. This inherent complexity impedes the monitoring and harmonization of practices. In an attempt to address this, initiatives like the GLEC Framework have emerged, aiming to include all transport modes (road, air, sea, rail) under a single methodology that remains feasible even with limited data (Punte et al., 2022). These simplified methodologies can be integrated into fleet management software to facilitate consumption calculations and promote harmonization. Nonetheless, these methodologies lack consideration for specific vehicle and route technicalities, thereby limiting the value of predictions, especially for the planning of new routes.

Modelling tools offer a promising way of generating digital twins that significantly enhance fuel consumption predictions (Agavanakis et al., 2022). Specifically, a digital twin for road transport emissions prediction can be constructed through vehicle modelling software. Various solutions, such as the GT-suite, AVL Boost, and VECTO, are available. Notably, the VECTO tool emerges as a good candidate for developing a digital twin for freight transport planning due to its demand for less extensive technical information compared to other tools. Additionally, it is tailored for simulating HDVs and holds official recognition from the EU for the type approval of new trucks. However, its complexity still presents a barrier for direct use by non-experts, especially in the context of accurate route planning. Consequently, a gap remains in achieving seamless integration of VECTO with limited truck data for effective route planning.

In this paper, we present a novel tool designed to predict fuel consumption for new routes. Our approach involves the generation of a VECTO digital twin model rooted in basic information and historical data from a specific truck. Subsequently, a routing tool is deployed to explore alternative routes between any given origin and destination points. Each alternative route is assessed using the digital twin model to calculate fuel consumption, facilitating the identification of the most fuel-efficient option. Central to our methodology is the utilization of historical data, which in this case study is harnessed by Fleetenergies (FE). As a provider of fleet management systems, FE possesses access to technical specifications and real-time data for numerous trucks, enriching the accuracy of our digital twin predictions.

Methodology

A VECTO-based model serves as a digital twin for a truck, drawing from three primary sources.

- Firstly, we leverage key truck parameters provided by FE. Table 1 summarizes the input parameters required, along with their corresponding values for six vehicles selected for the analysis. These inputs originate from the identification of the truck within the EEA database including all HDVs sold in the EU (Database, 2021).
- Secondly, we extract pertinent information concerning the truck from the EEA database that is not available from FE, such as air drag and gearbox data.
- Lastly, we calculate the truck engine's fuel consumption for each operational point by adopting the methodology in Zacharof et al., 2019.

Complementing the technical dataset provided by FE, we incorporate real-world historical timeseries data for each vehicle. Captured at a time resolution of at minimum 50 seconds, this data includes the truck's geolocation,

mileage, mean velocity, altitude, fuel consumption, and total weight (including payload). The truck's fuel consumption is derived from in-tank volume measurements, further refined using AI algorithms for increased accuracy. The utilization of such precise measurements contributes to the robust performance of our tool. The historical data is processed to extract short trips connecting consecutive stops, ensuring a constant payload throughout each trip, which can be seamlessly integrated into the VECTO model.

Table 1. Main vehicle data

Parameter	Model	Vehicle Type	Gross Vehicle Weight	Axes	Engine Rated Power
<i>Vehicle #1</i>	MAN TGS	Rigid	26 t	6x2	470 kW
<i>Vehicle #2</i>	DAF CF480	Tractor	44 t	4x2	483 kW
<i>Vehicle #3</i>	DAF CF480	Tractor	44 t	4x2	483 kW
<i>Vehicle #4</i>	MAN TGX	Tractor	44t	4x2	510 kW
<i>Vehicle #5</i>	Ford F-MAX	Tractor	44 t	4x2	500 kW
<i>Vehicle #6</i>	Volvo FM	Rigid	32 t	6x2	520 kW

The historical data play a key role in constructing and fine-tuning the digital twin's fuel consumption. This fine-tuning process involves adjusting the truck's engine map to increase or decrease fuel consumption. To ensure data integrity, a few trips characterized by significant variance in total truck weight were excluded from the analysis. Figure 1 illustrates the total weight timeseries for two trips – one included in the analysis and one excluded due to substantial weight fluctuation. Notably, a total of 677 routes were used in our analysis and the average trip distance across all routes for the six vehicles stands at 54 km.



Figure 1: Timeseries of the gross vehicle weight for Vehicle #1 including one trip that was used in the analysis and one that was excluded due to large variance of the weight measurement.

Subsequently, the digital twin is employed to replicate actual trips undertaken by the truck, utilizing the recorded speed and altitude profiles. Predicted fuel consumption (in liters) is then compared to actual consumption for each trip. Additionally, we assess the digital twin's fuel consumption (in liters per 100 km) against actual data for different truck weights, substantiating the twin's accuracy in forecasting fuel consumption for individual trips.

Following digital twin validation, we harness its capabilities for planning purposes. Leveraging the HERE API (HERE, 2023), we identify potential routes for specified origin and destination pairs. The API accommodates various parameters, including vehicle dimensions, and offers essential route information for conducting VECTO simulations, such as altitude and vehicle speed profiles. Importantly, we fine-tune the API's speed profile output, adjusting it for distinct road types (e.g. highway, residential). This fine-tuning, conducted across five road categories, ensures alignment between predicted mean speeds and actual mean speeds derived from historical

data. To validate HERE's speed profile accuracy, we force the API to replicate the actual route, comparing its average speed profile against measured data and plotting both profiles for a single trip.

Finally, building upon this evaluation, we employ the HERE API to generate alternative routes for the same origin and destination. Up to four alternative routes are identified for each trip of every vehicle, with truck dimension limits set at: length of 8 m or greater, width of 2.5 m or greater, height of 4 m or greater, and weight of 25 t or greater. These identified routes are subsequently subjected to the digital twin for fuel consumption calculation. The route with the lowest fuel consumption is then determined, compared against actual consumption, and used to quantify potential fuel savings. In Figure 2, the actual route and three alternatives identified by HERE for the mentioned trip in Figure 1 are depicted. Notably, the real route corresponds to alternative 3, exclusively utilizing the highway. Alternatives 1 and 2 encompass smaller roads for segments of the route and exhibit shorter distances.



Figure 2: Real route and HERE alternative routes for one trip of Vehicle #1.

Results

Digital twin performance

To assess the predictive capability of the digital twin, we start by demonstrating its performance in forecasting real fuel consumption in liters. Figure 3 provides a visual representation of the correlation between the actual measured and the VECTO simulated fuel consumption for each individual vehicle. Meanwhile, Figure 4 employs a bar plot to compare the actual measured and VECTO simulated fuel consumption in liters per 100 km across varying payload categories.

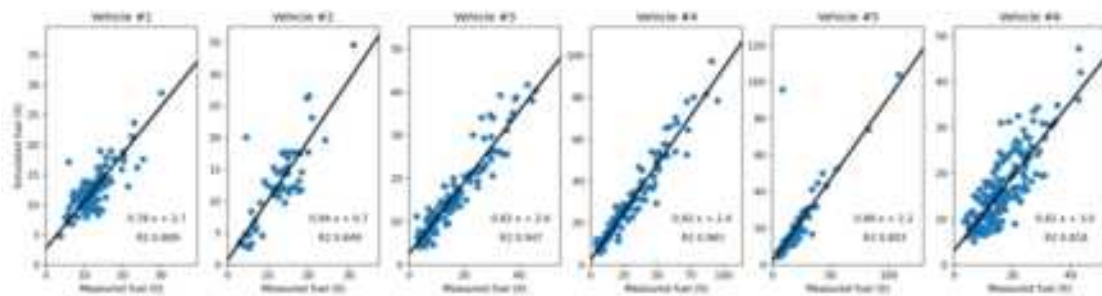


Figure 3: Correlation plots of the real and the digital twin consumed fuel in litres.

A good correlation is observed between the actual and predicted fuel consumption for individual trips across all vehicles. The digital twin of Tractors (Vehicles #2 to #5) outperforms Rigid trucks (Vehicles #1 and #6) in terms of predictive accuracy. Among these, Vehicle #4's digital twin stands out, with an exceptionally high R^2 value. It is noteworthy that Vehicle #4 undertook longer trips, averaging around 105 km, approximately twice the mean distance covered by all six vehicles combined. In contrast, Vehicle #6's digital twin exhibits the lowest R^2 values, displaying scattered data points around the linear fit. Vehicle #6's trips were notably shorter than the average (40 km), and it possessed the lowest payload-to-empty weight ratio. Vehicle #5's digital twin showcases a robust correlation across most data points, despite an outlier trip. This outlier's measured fuel consumption (9 liters for 250 km, with a total truck weight of 41 t) seems erroneous, as opposed to the VECTO prediction of

90.5 liters, which aligns coherently with the linear fit. While this case represents an extreme discrepancy, it underscores the potential for slight errors in measured fuel data across various trips, contributing to an enhanced R² value in the correlation analysis.

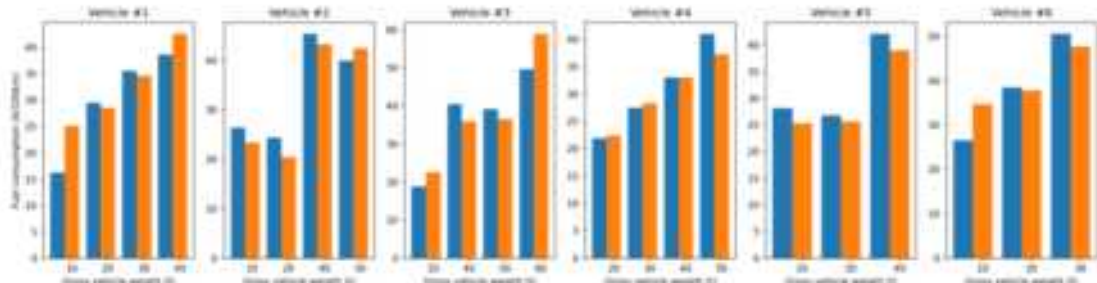


Figure 4: Bar plot of the real and digital twin fuel consumption in litres per 100 km for various truck weight classes for each one of the six simulated vehicles

Moving forward, Figure 4 compares the actual measured and VECTO simulated truck consumption in liters per 100 km, categorized by varying total truck weight classes. The anticipated trend of increasing consumption with increasing truck weight is evident across all vehicles. Importantly, any secondary impacts stemming from diverse speed or altitude profiles between distinct trips are mitigated through averaging, as each bar shows the average of several trips. This averaging effect substantiates the robust performance of the digital twins. Fuel consumption aligns closely with the measured values for nearly all vehicles and truck weights. An overprediction is noticeable for very heavy-loaded trucks in the case of Vehicle #3, albeit this anomaly is attributed to the small number of trips included in this bar. Another instance of overprediction appears during empty running of Rigid trucks (Vehicles #1 and #6). This discrepancy is attributed to these trucks exhibiting an empty weight lower than their technical specifications. Such deviations can be rectified through suitable modifications to the digital twin.

HERE Routing - Speed profile evaluation

To evaluate the performance of the HERE speed profile, we present the results in Table 2, showing the average speed in km/h for both the actual real routes, the HERE profiles based on the default speed table, and the HERE profiles based on the calibrated speed table. This identical table is applied across all six vehicles, with HERE constrained to replicate the precise routes undertaken by each truck.

Table 2: Comparison of the average speed for each vehicle based on the real speed profile, the HERE default speed profile, and the HERE calibrated speed profile.

	Vehicle #1	Vehicle #2	Vehicle #3	Vehicle #4	Vehicle #5	Vehicle #6
Real speed (km/h)	54.1	49.6	54.3	66.2	69.7	55.8
HERE – default (km/h)	35.0	34.9	37.1	53.9	55.5	37.7
HERE – calibrated (km/h)	48.7	46.6	49.2	65.1	66.6	50.2

Examination of the data reveals that the default speed table within HERE leads to a substantial underestimation of the truck's average speed. In contrast, the calibrated speed profile is significantly closer, particularly for Vehicles #4 and #5, which predominantly travel on highways, yielding higher average speeds. However, a minor underestimation of average speed is apparent for Vehicle #1, displaying the greatest deviation from real speed values. This divergence can be attributed to the calibrated speed table, primarily constructed based on larger tractors frequenting highways, whereas Vehicle #1 stands as the smallest in weight among the six vehicles.

Figure 5 shows the real measured speed, the HERE default speed profile, and the HERE calibrated speed profile for the retained trip highlighted in Figure 1. Both HERE profiles show a similar trend, with the default speed profile consistently lagging behind the calibrated counterpart across most of the route. Moreover, the default profile consistently maintains speeds below 70 km/h, an observation that appears relatively conservative even for a heavy-duty vehicle. The calibrated profile, by contrast, looks very similar to the real profile, although with a small divergence around the 40th km mark, where the calibrated profile somewhat underestimates the truck's speed. Additionally, it's evident that the real profile displays a smoother trend compared to the profiles generated by HERE. This distinction largely results from the interval between consecutive data points. While the real data points span between 1 and 2 km, the HERE-generated profiles show much shorter intervals, typically a few hundred meters at most.

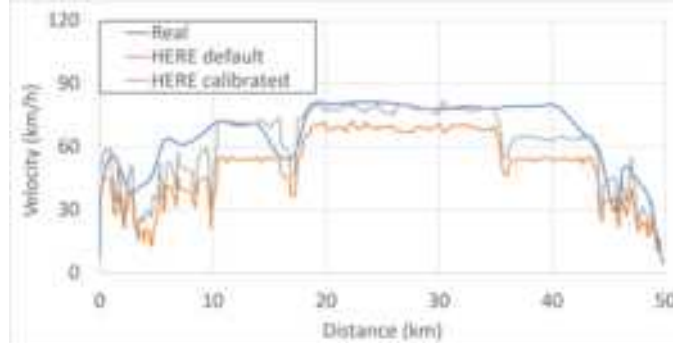


Figure 5. The real speed profile, the HERE speed profile for the default speed table and the HERE profile for the calibrated speed table for the first trip of Vehicle #1.

Figure 6 illustrates the measured fuel consumption alongside the predictions from the digital twin based on both the default and calibrated HERE speed profiles. Even with the provision of the exact truck route to HERE, minor deviations in travelled distances arise due to inherent errors in latitude and longitude coordinates within the recorded data. To ensure an equitable comparison of fuel consumption, we shift our analysis to liters per 100 km, accounting for these variations. Evidently, the default HERE speed profile leads to an underestimation of fuel consumption, while the calibrated speed profile aligns well with the actual consumption figures. This underprediction can be attributed to the lower velocity, acceleration, and deceleration inherent to the default profile. Only Vehicle #1 experiences a modest overprediction of 6.5% for the calibrated speed profile and 4.5% for the default speed profile.

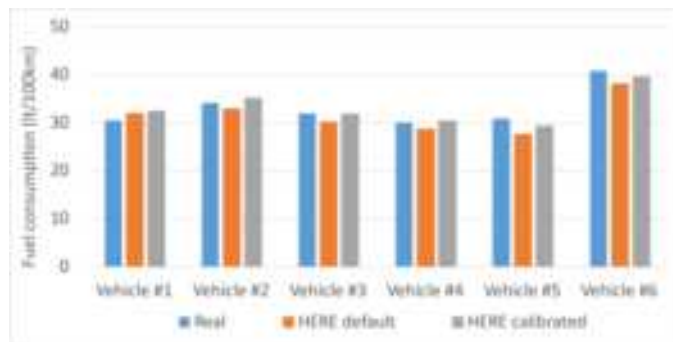


Figure 6. Fuel consumption for each vehicle based on the real data and the HERE speed profiles

HERE Routing – Identify the best route

The final phase of our investigation entails leveraging the HERE API to explore alternative routes for identical origin and destination points. The quantity of routes identified varies across trucks, with some having only one route, while others including up to four alternatives. In each instance, the most fuel-efficient route is selected. Subsequently, we compute the overall distance traveled and the aggregate fuel consumption for each vehicle based on these optimal routes. Table 3 summarizes the outcomes of this analysis, alongside the actual measured data for reference.

From this data, it's apparent that the total travel time estimated by HERE tends to be higher than the real values. This alignment with the mean velocities highlighted in Table 2 implies that while the projected travel

time might appear to increase, the actual impact might be negligible or only marginally increased. Fuel consumption, measured in liters per 100 km, shows a minor reduction across all vehicles, except for Vehicle #1. However, the total distance traveled along the optimal routes perfectly aligns with the actual distance. On the route level, we observe that shorter routes are generally favored as expected to reduce fuel consumption. Yet, there are instances where all alternatives are longer than real routes. This results from certain roads not being classified as suitable for trucks, prompting the routing tool to explore other (longer) alternatives.

The difference in the total consumed fuel for each vehicle ranges from 0 to 3.5 % with Vehicles #1 and #4 showing the highest potential for fuel savings. Vehicle #1 due to selection of shorter routes, and Vehicle #4 due to identification of more fuel-efficient ones. The total cumulative savings across all six vehicles are 140 liters, translating to a 1.2% reduction in fuel consumption.

Table 3: Comparison of main route data for the real and the HERE optimised alternative routes

	Real distance (km)	Real travel time (h)	Real fuel (lt/100km)	HERE distance (km)	HERE travel time (h)	HERE fuel (lt/100km)
Vehicle #1	4404	80.8	30.5	4069	86.4	31.9
Vehicle #2	2145	42.2	34.3	2138	43.4	33.7
Vehicle #3	6589	122.1	31.9	6705	127.5	30.8
Vehicle #4	10851	162.6	30.1	10839	160.8	30.1
Vehicle #5	4831	68.2	30.9	4947	74.9	29.2
Vehicle #6	7949	142.0	40.8	8075	161.1	40.2

Discussion

In this study, we have successfully demonstrated the creation and validation of VECTO-based digital twins using limited input data, that can be easily used even by non-experts. Through the generation of six digital twins, we showcased their robust performance against real-world data, establishing their potential as reliable predictive tools. Furthermore, we harnessed the HERE API to identify truck-suitable alternative routes and construct realistic speed profiles, thereby enabling accurate fuel consumption calculations for each route. This methodology led to the identification of more fuel-efficient routes, yielding potential fuel savings of up to 3.5% for specific vehicles.

The proposed approach exhibits flexibility and potential for refinement. Further optimization of the routing tool's calibration could address instances where routes are wrongly classified as unsuitable for trucks. It's important to acknowledge that the presented analysis is individualised for to a particular digital twin, implying that the optimal route may vary across different vehicles. The methodology, while demonstrated within the context of diesel trucks, can readily adapt to accommodate various powertrain configurations.

Importantly, while high-quality historical data undoubtedly enhances predictive accuracy, it is not an absolute prerequisite for the tool's functionality. Carriers lacking extensive or detailed data can still achieve good results using lower resolution data. For carriers without any data, generic vehicle profiles or non-fine-tuned VECTO models can be employed. Despite potential accuracy compromises, such models surpass methods relying on generic emission factors, exemplifying the tool's robustness in diverse data scenarios.

The tool's output, referred to as the "optimum" route in this context, can be further tailored to user requirements. For instance, if time-sensitive deliveries are important, additional criteria can be incorporated into the route suggestion process. With such refinements, our methodology extends beyond fuel savings.

In conclusion, our study introduces an innovative framework that combines digital twin technology, real-world data, and advanced routing capabilities to optimize freight transport fuel consumption. By enabling carriers, including non-experts, to enhance route selection and reduce environmental impact, this approach may significantly contribute to the broader sustainability goals of the freight industry. Further investigations and refinements have the potential to amplify the impact of this methodology across various freight transport scenarios and powertrain technologies.

Acknowledgements

The study was self-funded.

References

- Agavanakis, K., et al., 2022. "Telemetry transformation towards industry 4.0 convergence - A fuel management solution for the transportation sector based on digital twins", *AIP Conference Proceedings* 2437, 020083
- EEA Database, 2021, "Monitoring of CO₂ emissions from heavy-duty vehicles - Regulation (EU) 2018/956", Prod-ID: DAT-251-en
- Eurostat, 2021, "Freight transport statistics - modal split". Available online at: https://ec.europa.eu/eurostat/statistics-explained/index.php?title=Freight_transport_-_modal_split, Last accessed: 20th July 2023
- HERE, © 2023, 2023, Calculate Route Endpoint, <https://developer.here.com/>
- Punte, S., Greene S., Lewis A. et al., 2022. *GLECI Framework Version 2.0*
- Zacharias, V., Lutz, M., Pradella, G., Guglielmo, F., et al., 2019. A Generalized Component Efficiency and Input-Data Generation Model for Creating Fleet-Representative Vehicle Emission Classes in VECTO's GLECI Toolkit, Paper 2019-01-1280

Experimental Validation of Battery Electric Truck Simulation in VECTO¹⁴

S. Broekaert¹, E. Bitsanis¹ and G. Fontaras^{1*}

¹European Commission, Joint Research Centre, Directorate for Energy, Mobility and Climate, Ispra, Lombardy, 21027, Italy,
Georgios.Fontaras@ec.europa.eu

Introduction

The European Union (EU) aims for climate neutrality by 2050. This can be achieved by reducing greenhouse gas emissions in all sectors, including transport. Therefore, the EU has set CO₂ emission reduction targets for new heavy-duty vehicles (HDVs) (EU, 2019), requiring the reduction of the average CO₂ emissions by 15% and 30% for 2025 and 2030, respectively. A more ambitious proposal was put forward by the European Commission in 2023. It increases the CO₂ emission reduction target to 45% for 2030 and introduces reduction targets of 65% and 90% for 2035 and 2040, respectively. Moreover, it introduces a zero-emission vehicle target of 100% by 2030 for urban buses.

An increasing number of battery electric lorries and buses are being introduced to the market in recent years to gradually meet the CO₂ emission reduction targets. To inform the customer about the energy consumption and operating range of battery electric vehicles, these properties are to be determined as of 2024 as part of the vehicle type approval (EU, 2022). The approach is similar to the one for determining the CO₂ emissions and fuel consumption of HDVs powered by an internal combustion engine (EU, 2017). Each new vehicle is simulated over different mission profiles with the Vehicle Energy Consumption Calculation Tool (VECTO), a software tool developed by the European Commission (Fontaras, 2013). Component models and operating strategies are currently being added to the tool, to be able to accurately simulate the energy consumption of battery electric HDVs (Silberholz, 2022).

The Joint Research Centre has tested a battery-electric, rigid lorry on the road and on the chassis dyno. The vehicle was equipped with wheel torque transducers and current and voltage sensors in the powertrain to measure energy consumption. On the chassis dyno, the regional delivery VECTO mission profile was replicated under regulatory conditions to allow for a direct comparison to the VECTO declaration results. The on-road trip replicated typical vehicle operating conditions and allowed for validating the real world representativeness of VECTO. The positive electric work of the electric machine was simulated within 5 and 6% for the regional delivery and on-road cycle, respectively.

Methods

Test vehicle

The experiments were conducted with a 27 tonne gross vehicle weight rigid lorry. The vehicle powertrain consists of 2 electric machines (EM) combined with a 2-speed transmission. Table 1 summarises the main vehicle specifications.

The vehicle was instrumented with current and voltage sensors at the battery terminals and at the DC-side of the EMs to measure the energy demand in the powertrain. Wheel torque transducers were installed on the driven wheels to measure the instantaneous wheel torque. The wheels with the torque sensors were lifted from the ground so that the applied torque was zero, at the start and the end of each test. The transducers were zeroed at the start of each test, and the residual sensor drift was recorded at the end of each test. The recorded drift values were used to correct linearly for torque-drift. The sensor data and relevant operating parameters from the vehicle's Controller Area Network were logged at a sample rate of 100Hz and downsampled to 2Hz for the analysis.

¹⁴ The views expressed are purely those of the authors and shall not be considered as an official Commission position under any circumstance.

Table 1: Vehicle specifications.

Axle configuration	6 x 2
Chassis configuration	Rigid
TPMLM [tonnes]	27
Powertrain architecture	E2
Transmission	2-speed
Battery size [kWh]	448
Motor max. power [kW]	400

Laboratory tests

The regional delivery cycle was performed under regulatory conditions, with the reference payload, on the Vehicle Emissions Laboratory chassis dyno (VELA 7). The driving cycles prescribe speed as a function of distance. Therefore, a VECTO simulation was performed to obtain the speed as a function of time, taking into account the vehicle performance and the VECTO driver model and replicating that on the chassis dyno. The measured speed and slope profiles are shown in Fig. 1. The characteristics of the cycle are listed in Table 2. The cycle was repeated 3 times and the relative standard deviation (RSD) of the wheelwork and battery energy (Table 2) indicates a good repeatability of the experiments.

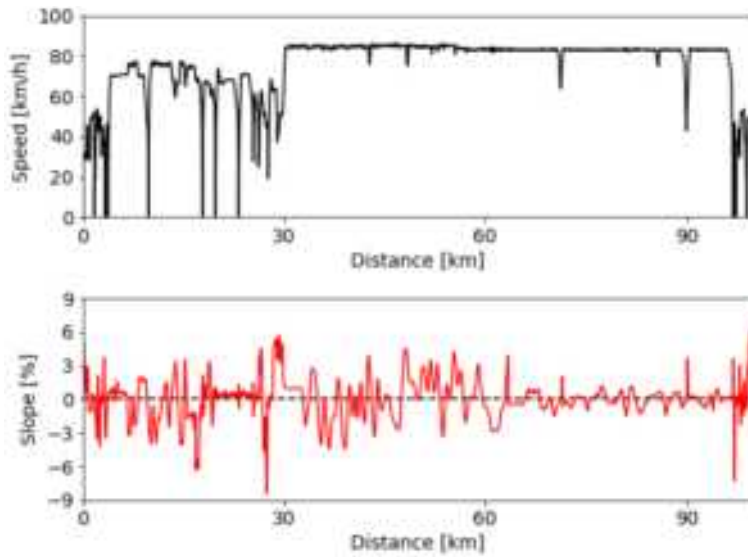


Figure 1: Speed and slope profile of the regional delivery cycle.

Table 2: Regional delivery properties.

Distance [km]	100
Urban distance share [%]	9
Rural distance share [%]	14
Motorway distance share [%]	77
Start SoC [%]	80
RSD wheel work [%]	0.6
RSD battery energy [%]	1.0

On-road tests

On-road tests were performed in the vicinity of the Joint Research Centre site in Ispra, Italy to obtain data of the vehicle under real world operating conditions. The vehicle was loaded to 90% of its maximum payload and a warm-up was conducted before the start of the test, compliant with the Verification Testing Procedure (EU, 2017). The measured speed and slope profile are shown in Fig. 2. The characteristics of the cycle are listed in Table 3. The cycle was repeated 3 times and the RSD of the wheel work and battery energy (Table 3) indicate a good repeatability of the experiments.

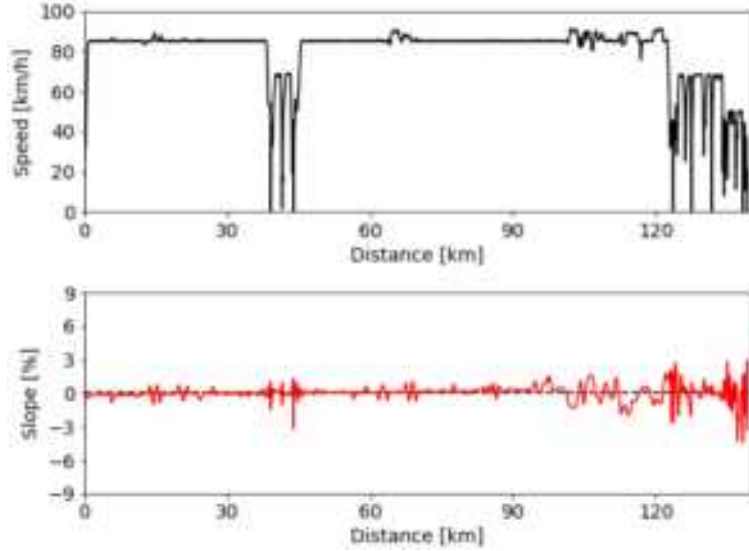


Figure 2: Speed and slope profile of the on-road trip.

Table 3: On-road trip properties.

Distance [km]	139
Urban distance share [%]	8
Rural distance share [%]	9
Motorway distance share [%]	83
Start SoC [%]	98
RSD wheel work [%]	0.7
RSD battery energy [%]	1.2

VECTO simulations

A model of the vehicle was created in VECTO, with the tyre rolling resistance and air drag properties determined according to (EU, 2017). The EM and transmission are integrated (Integrated Electric Powertrain Component), but were treated as separate components and their properties were characterised with available engineering data. The official regional delivery cycle, the measured speed trace during the regional delivery cycle and the measured speed trace during the on-road trip were simulated in VECTO version 0.7.7.2547. The measured speed traces were converted to cycles with the speed as a function of distance.

Results

The relative error of the simulation compared to the measurements is show in Figure 3, for the official regional delivery mission profile, the regional delivery cycle with a measured speed trace and the on-road trip with a measured speed trace. The wheel work is overestimated in the simulation for the laboratory tests. This can be attributed to the speed-dependent yaw angle correction of the air drag value that is applied in VECTO compared

to the fixed road load coefficients that the chassis dyno imposes. The opposite can be observed for the on-road trips, where the wheel work is underestimated. This discrepancy can originate from various sources where the idealized conditions in the simulation deviate from the real world, e.g. road surface friction or wind speed. The error of the wheel work results in a similar error of the mechanical and electrical work done by the EM for propulsion (positive). The recuperated energy by the EM (negative work), on the other hand, is underestimated by VECTO.

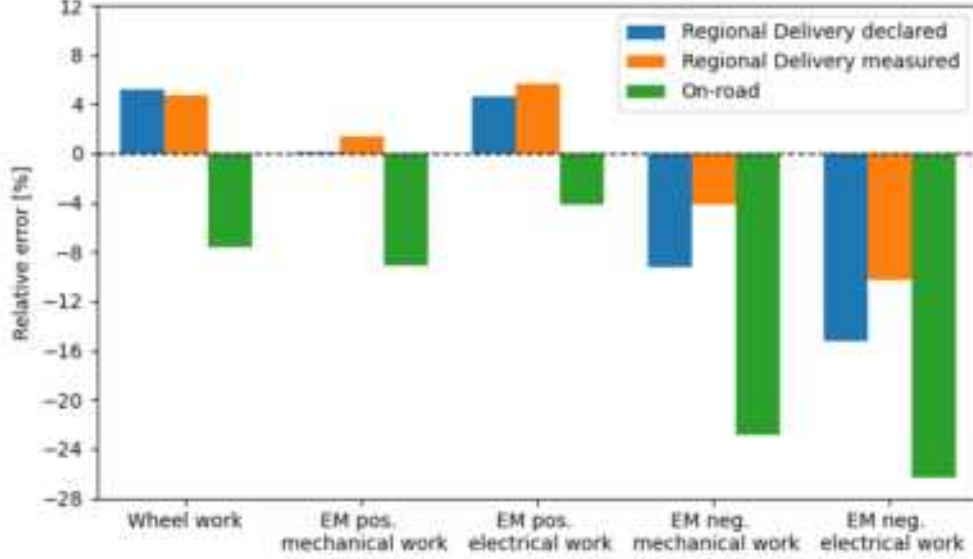


Figure 3: Relative error of the simulation.

The efficiency of the powertrain during propulsion and recuperation can be defined as follows:

$$\eta_{propulsion} = \frac{\text{wheel work}_{propulsion}}{\text{EM electrical work}_{propulsion}}$$

$$\eta_{recuperation} = \frac{\text{EM electrical work}_{recuperation}}{\text{wheel work}_{recuperation}}$$

The simulation error of both efficiencies is shown in Fig.4. Errors of 2 and 3% for the propulsion powertrain efficiency are found for the regional delivery and on-road trip (Table 4). Hence, VECTO is able to accurately simulate these events under the same simulated boundary conditions (wheel work). The powertrain efficiency during recuperation, on the other hand, is underestimated.

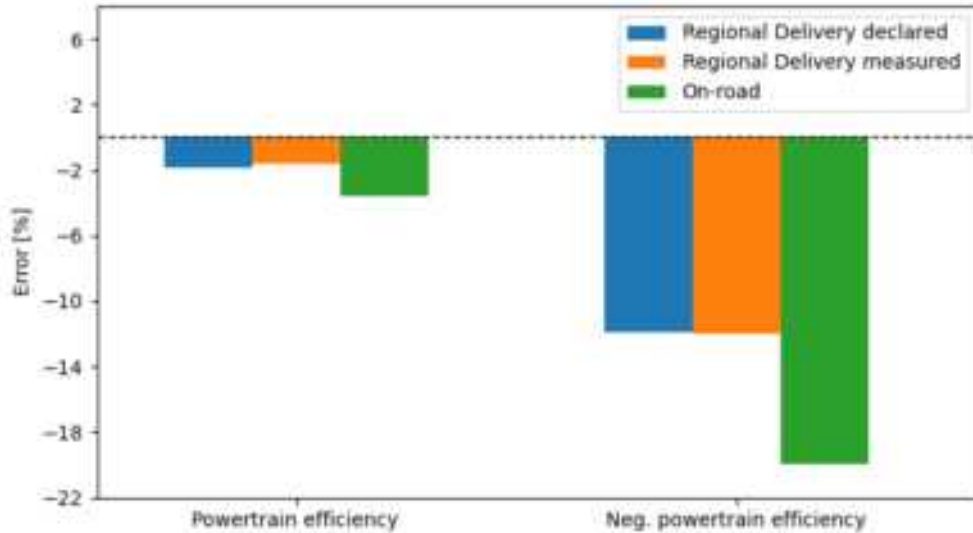


Figure 4: Error of the simulated error

Table 4: Relative error between simulation results and experimental measurements.

Cycle	EM positive electric work (%)	Powertrain efficiency (%)
Regional Delivery declaration	+4.7	-1.7
Regional Delivery measured	+5.7	-1.5
On-road	-4.2	-3.3

As the vehicle is equipped with a 2-speed transmission, the gearshift model in VECTO will select the most appropriate gear in every time step. The distance share where the simulation and the measurement have the same or a different gear is shown in Fig. 5. The gear is correctly simulated by VECTO.

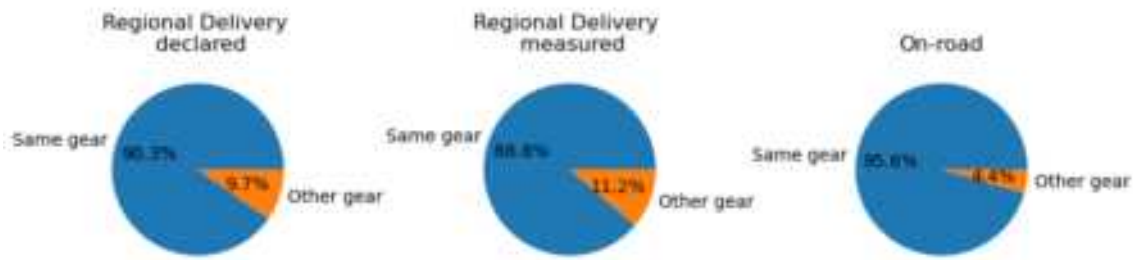


Figure 5: Error of the simulated gear

Conclusions

A test campaign was performed that allows the validation of VECTO under regulatory and real world operating conditions. It shows that VECTO is able to accurately simulate the energy consumption during propulsion. However, the simulation of brake energy recuperation needs to be improved further.

The next steps will be to repeat the validation with newer VECTO development versions and to simulate the cycles with the speed as a function of time and with the wheel power as input. The latter will remove errors introduced by the environment and will allow validating the vehicle powertrain by itself.

Acknowledgements

The authors like to acknowledge Daimler Truck for providing the vehicle, for technical support during the measurement campaign and for conducting the VECTO simulations. The authors greatly acknowledge the work done by the staff of the Vehicle Emissions Laboratory.

Disclaimer

The opinions expressed in this manuscript are those of the authors and should in no way be considered to represent an official opinion of the European Commission. The mentioning of trade names or commercial products does not constitute endorsement or recommendation by the authors or the European Commission.

References

- European Union. (2017). Commission Regulation (EU) 2017/2400 of 12 December 2017 implementing Regulation (EC) No 595/2009 of the European Parliament and of the Council as regards the determination of the CO₂ emissions and fuel consumption of heavy-duty vehicles and amending Directive 2007/46/EC of the European Parliament and of the Council and Commission Regulation (EU) No 582/2011.
- European Union. (2019). Regulation (EU) 2019/1242 of the European Parliament and of the Council of 20 June 2019 setting CO₂ emission performance standards for new heavy-duty vehicles and amending Regulations (EC) No 595/2009 and (EU) 2018/956 of the European Parliament and of the Council and Council Directive 96/53/EC.
- European Union. (2022). Commission Regulation (EU) 2022/1379 of 5 July 2022 amending Regulation (EU) 2017/2400 as regards the determination of the CO₂ emissions and fuel consumption of medium and heavy lorries and heavy buses and to introduce electric vehicles and other new technologies.
- Fontaras, G., Rexeis, M., Dilara, P., Hausberger, S. et al. (2013). The Development of a Simulation Tool for Monitoring Heavy-Duty Vehicle CO₂ Emissions and Fuel Consumption in Europe, *SAE Technical Paper 2013-24-0150*.
- Silberholz G., Rexeis M., Quaritsch M., Present S. (2022).VECTO: Extension to hybrids and further technical support, Final report for Service Contract Number 340201/2018/789690/SER/CLIMA.C.4.

Emission Monitoring for used cars: Evaluation of On-Road Testing

P. Dégeilh, J. Kermani, S. Rodriguez¹ and A. Frobert²

¹ IFP Energies nouvelles, Institut Carnot IFPEN TE, 1-4 avenue de Bois-Préau, 92852 Rueil-Malmaison, France

² IFP Energies nouvelles, Institut Carnot IFPEN TE, Echangeur de Solaize, 69360 Solaize, France

Keywords: Emissions, Used Cars, Embedded Measurement, On-Road, PTI.

Presenting author email: arnaud.frobert@ifpen.fr

Introduction

Air quality remains a major health issue. Road transport has an important contribution to the emissions of local pollutants as particulate matter (PM), nitrogen dioxide (NO_2), and ground-level ozone (O_3). These local pollutants have a significant impact on the health of the European population, particularly in urban areas (European Environment Agency, 2020). This point has been highlighted during the lockdown of spring 2020, when the traffic has been drastically reduced due to COVID-19 pandemic. That unprecedented situation led to a significant reduction of the local air pollutants in cities, in particular NO_2 (Donzelli et al., 2020 ; Fu et al., 2020 ; Kumari et al., 2020). For a more standard situation, among the road transport contributors, it has been proven that the fraction of the most polluting vehicles has a major contribution to the overall pollution. It is estimated from plume chasing measurements that only 10% of the vehicles are at the origin of respectively 38%, 69% and 54% of NOx, CO and PN emissions from the rolling stock (Wang et al., 2015). The Euro6d latest generation vehicles are cleaner even in severe condition (Dégeilh et al., 2020 ; Giechaskiel et al., 2021), notably thanks to the entry into force of the RDE standard and the growing electrification of the fleet. That status will even be improved with the future entry into force of Euro7 (European Commission, 2022), but as the renewal of the fleet remains a slow phenomenon, the current rolling stock must be closely considered. Acting effectively on the reduction of transport emissions over the next 15 years therefore involves monitoring actions for the current fleet to pinpoint and repair the most polluting vehicles.

For that, the two main levers currently available are In Service Conformity (ISC) and Periodical Technical Inspection (PTI). The latest is the more widespread one, as it concerns 100% of used cars (after 1 to 4 years, depending on the kind of vehicle and the local regulation). The emissions tests are currently performed in the workshop with a range from OBD-sensing only to (on some non-European countries) chassis-dyno testing. As an intermediate, most of emission tests are operated on steady-state conditions on some specific indicators (Opacity for Diesel cars, CO and A/F ratio for Gasoline cars). Even if that protocol is evolving, e.g. with the addition of a PN measurement in some European countries as Netherlands, Belgium, Germany (Netherlands Ministry of Infrastructure and Water Management, 2021), some pollutants as NOx are still not properly considered despite their impact on human health.

The NOx performance is something very difficult to assess in steady-state or low-load conditions, as it is strongly multi-factorial (engine speed, load, ambient temperature and pressure...) and it depends on numerous organs, especially for diesel (air loop, EGR, Turbocharger, Aftertreatment system). Information from the On-Board Diagnostics system can't be used safely as it is managed by OEMs. In that context, the best option is to drive the car on real street conditions. For that, the investment in a full-range chassis-dyno does not seem realistic. The other way is to drive the car outside of the PTI workshop to have a complete answer on the emission level of the vehicles on the roads. It raises numerous technical challenges as the measuring device must be cost-efficient, easy to handle and give an intelligible result in as-short-as-possible trip.

Based on these findings, that paper proposes an analysis of the current and potential future protocols for measuring vehicle emissions for large-scale monitoring, including on-road tests based on the in-house IFP Energies Nouvelles REAL-e solution.

Panel & Protocol

Vehicle Panel

The study is focused on passenger cars and the first challenge is to define and find a representative panel of the French fleet (French Ministry of the Ecological Transition, 2021). For that, a sample of 33 vehicles (Euro3 to Euro 6dTemp) are selected from about 54 personal vehicles of volunteer IFP Energies nouvelles employees (Figure 1).



- by standard:

- 1 Euro 1,
- 2 Euro 3,
- 6 Euro 4,
- 10 Euro 5 (Diesel-only),
- 14 Euro 6 (b, c and d-Temp).

- By fuel :

- 1 E85 (not presented),
- 1 GPL (not presented),
- 16 gasoline,
- 15 Diesel.

These vehicles are representative of numerous classes: urban car, sedan, 4WD, SUV, van. No distinction has been made between standard intermediate steps, to keep representative samples.

Figure 1: Panel of 33 vehicles tested, sorted by standard, Fuel, mileage and model-year

Test Protocol

Each vehicle is borrowed for 2 business days. It allows to perform during the first day: the devices setup, the steady tests and a first drive (hot conditions). The second day is devoted to a second drive with a cold start and the vehicle check-out. The different test performed are described hereafter:

Static Tests

Several tests are performed in steady state conditions, in a dedicated workshop. The gas measurement systems are stock devices, supplied by CAPELEC and described in Table 1.

Table 1: Devices for steady-state measurements

Device	Outputs	
CAPELEC CAP3600 – standard version	OBD, CO, CO ₂ , lambda (O ₂), opacity	
CAPELEC CAP3600 – additional features	HC (propane), NOx (NO)	

CAPELEC CAP3070	PN (+ 23 nm)	
-----------------	--------------	------------------------------------------------------------------------------------

The first protocol is the French PTI emission test, performed with a CAPELEC CAP3600 station, following the official guideline (lambda and CO for gasoline cars, opacity for diesel cars). OBD test is made as well. This non discriminating results will not be developed here.

The second protocol is named "enhanced static test" and has been designed with the ambition to calculate all available PTI emission measurements with an exhaustive protocol. The proposed protocol associates 7 low-idle phases, 3 accelerated idles (phase 2 – 1500 rpm, phase 4 – 2500 rpm and phase 6 – 3500 rpm) and 3 free accelerations for a total test duration of less than 10 minutes. An example is given in Figure 2.

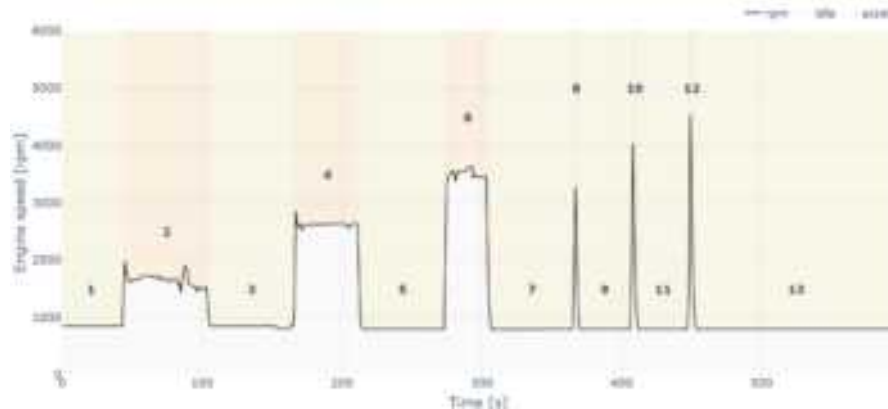


Figure 2: RPM vs Time for the "enhanced static test" protocol.

On-Road Tests

For on-road tests, the in-house embedded system REAL-e has been used (Dégeilh et al., 2019). It provides a raw measurement of:

- CO, CO₂, O₂, NO, NO₂, NH₃, PN, HC (propane)
- GPS (Speed, altitude, position)
- OBD (Vehicle speed, Engine speed, Coolant temperature, engine load)

Raw data are continuously stored on a cloud and treated at the end of the trip to obtain "TLEMS-like" results as the amounts of pollutants in mass per distance and RDE indicators.

Concerning the chosen trip, it has been designed to be short (30 min) but exhaustive. Main characteristics are summarized in Table 2. That drive is not compliant with the Euro 6d RDE package 4 (European Commission, 2018) because of its duration, its urban / rural / motorway share and its elevation. Nevertheless, the conditions meet the latest Euro 7 proposal (European Commission, 2022).

Table 2: Main characteristics of the chosen trip

Distance [km]	Duration [min]	Average Vehicle Speed [km/h]	Pos. Elevation [m]	Stop share [%]
23 Urban: 11,8 (51 %) Rural: 6,3 (28 %) Motorway: 4,8 (21%)	30 Urban: 22 (74 %) Rural: 5 (17 %) Motorway: 3 (9 %)	44	950	10

Results, Discussions & Analysis

Main results by protocol

French PTI Emission test

All the vehicles tested passed the emission part of the French PTI protocol, with a comfortable margin, for both diesel (opacity test) and gasoline cars (air-fuel ratio and CO emissions). This result is not surprising, as the selected vehicles own a valid PTI certificate – mandatory to borrow vehicle in a legal framework.

Enhanced static test

The following results are presented using boxplots, allowing a statistic representation of the results.

Figure 3 gives an overview of the raw NOx emissions by volume during the 13 phases of the proposed protocol. For diesel cars, no trend can be deducted whatever the test phase (low idle, accelerated idle, accelerations). Moreover, the results are very sensitive to the test conditions: accessory state (AC on / AC off), EGR shut-off for long low-idles, SCR and combustion chamber temperature (depending of the previous test or drive).

Concerning the gasoline cars, the average level is lower, except for some Euro 6 car during the acceleration phases, probably due to a poor transient air-fuel ratio management.

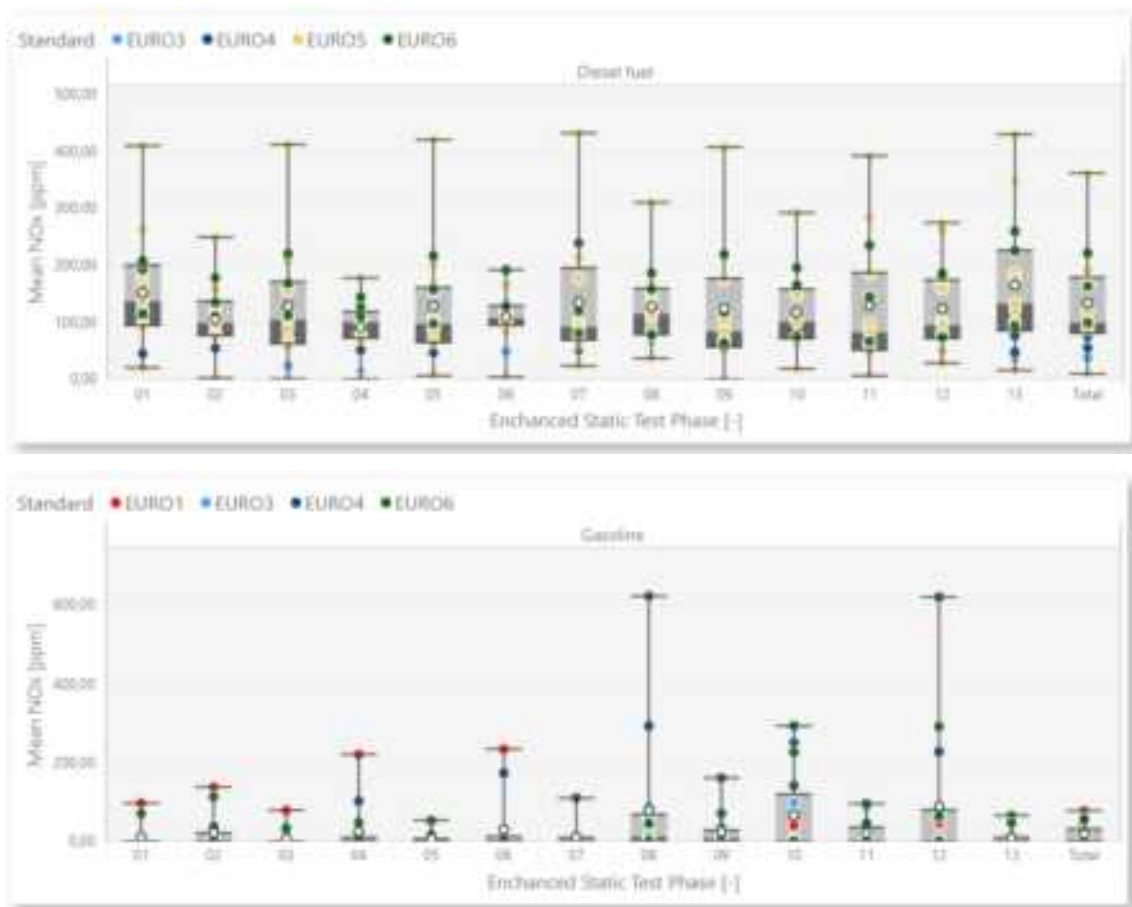


Figure 3: Raw NOx Emissions during the Enhanced static test – Up : Diesel cars, Down : Gasoline cars

Short On-Road tests

Concerning NOx, the average emissions of the diesel vehicles are of 975, 1012 and 747 mg/km, respectively for Euro 4, Euro 5, and Euro 6b/c/d vehicles. One can notice that the only post-RDE Euro 6d vehicle is the lower diesel emitter with 154 mg/km.

For gasoline cars, the average NOx results are 194, 423 and 100 mg/km, respectively for Euro 3, Euro 4 and Euro 6 vehicles (no Euro 5 gasoline car is available in our panel). The Euro 4 results, built from a reduced panel of 3 vehicles are upsized by a high-emitting vehicle, with results close to 1 g/km.

The cold start effect has been evaluated during that test campaign. For the complete panel, the impact is +21%: +15% for the diesel cars and +59% for the gasoline cars. This general trend is strongly variable between the vehicles, with even some inverted results.

The results are illustrated in Figure 4 hereunder, with a boxplot representation of the complete panel for diesel car on the left and gasoline cars on the right. The results are shared by standard; the red dots are used for warm tests and the blue dots for cold starts.

The results are in line with numerous studies, for instance ICCT 2014 (Posada, 2014) with a huge gap between the standard and the real-life measurement. The short track protocol leads to higher NOx levels compared to the RDE one, due to a high severity of the trip with short distance, high elevation, and a dynamic driving.

Concerning CO (Figure 5), the diesel results are very low with few exceptions. Gasoline engines are mainly represented by Euro 6 cars. For Euro 4 (1 car) and Euro 5 (3 cars), results are not statistically relevant. A huge disparity is demonstrated between Euro 6 cars, with CO emission up to 2 g/km, even for warm tests. These results must be moderated considering the severe test conditions.

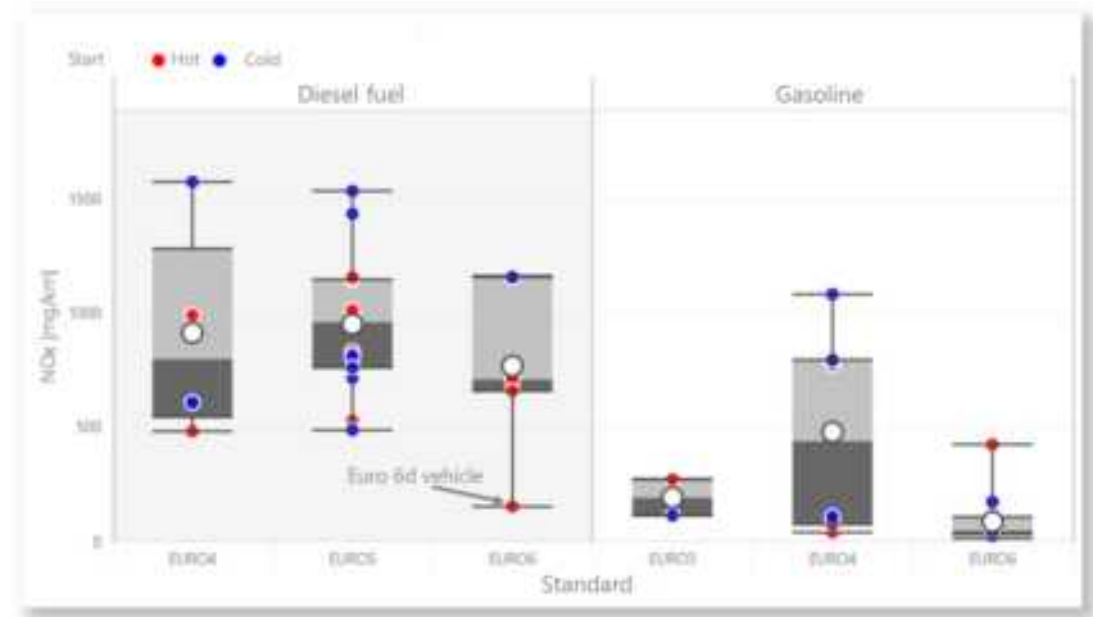


Figure 4: NOx mass emissions during the short drive test for Diesel (left) and Gasoline (right) cars, sorted by homologation standards.

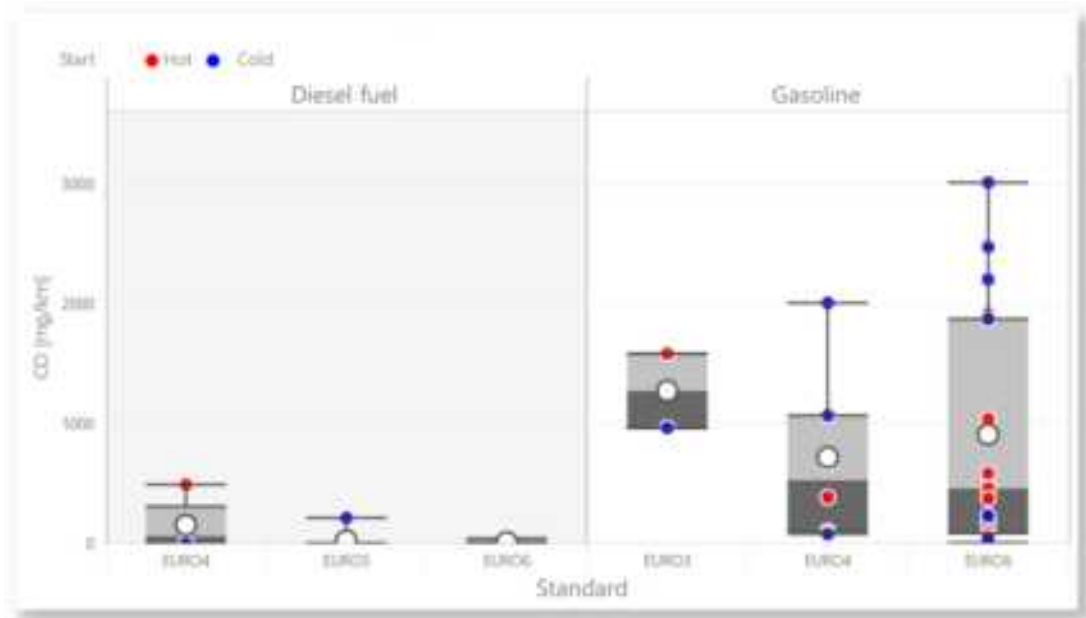


Figure 5:CO mass emissions during the short drive test for Diesel (left) and Gasoline (right) cars, sorted by homologation standards.

Protocols comparison & Impact of the trip duration

Due to the paper format, it's unfortunately not possible to give an exhaustive comparison of the protocols for each pollutant. The more important results concern the NOx status, as static tests are not able to give a proper answer. This is illustrated in Figure 6 where each dot represents one vehicle. The Euro 4 NOx limit (250 mg/km) is added for illustration. Low-idle static results have been kept for this illustration, but results are similar for accelerated idles or free acceleration: no clear correlation can be identified between static and road tests. Moreover, depending on the vehicle, huge errors can be made: for instance, the best diesel car on the road (the only Euro6d of the diesel panel) has one of the worst results during low-idle. It leads to a very damageable false positive result. On the contrary, several diesel and a gasoline vehicles have a poor test on the road (>1000 mg/km) and decent results during low-idle (<100ppm) (False negative).

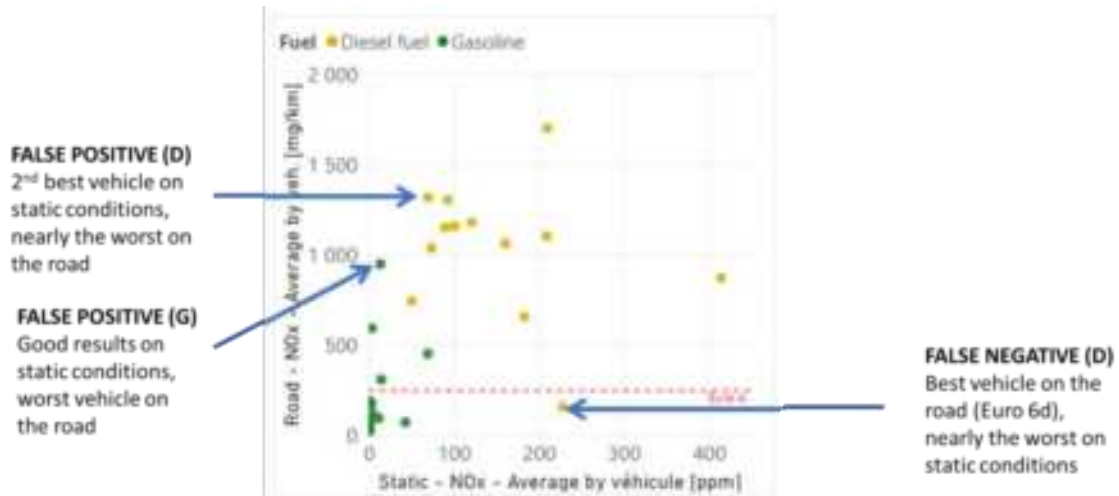


Figure 6: Comparison of static NOx results in ppm (during low idles) vs. on-road ones in mg/km for diesel (yellow) and gasoline (green) cars

As the road test appears to be a more discriminative test, a specific study has to be carried out to identify the shortest required trip.

The question of the minimum amount of data required for robust diagnostics arises, as it is not feasible to carry out large-scale tests lasting more than 90 min / 80 km, as specified for a valid RDE test.

Figure 7 provides an analysis of the effect of the amount of data available (trip distance) on diagnostic errors.

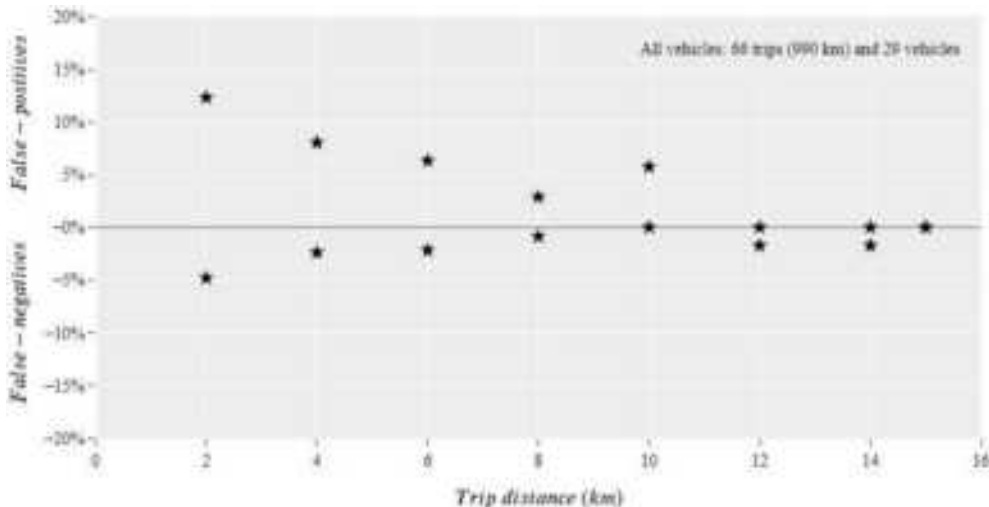


Figure 7: Error Rate (false positives and false negatives) due to the trip distance reduction – Defect threshold set at 5*CF (Conformity Factor)

To carry on the investigation, at first, a reference status is set for each vehicle (compliant or non-compliant) from the data over the entire trip (15 km). This is established by comparing the emissions level over the journey with the vehicle's normative emissions threshold multiplied by a compliance factor of 5. On Figure 7, no diagnostic errors (false positives or false negatives) are visible for 15km trips, as this distance was used to set the reference status.

A status is then computed with shorter sample runs: 10 km, then 8 km, 6 km 4 km and down to 2 km, using the same methodology, comparing the emission levels on these runs with the normative emission threshold.

Finally, the diagnostic error rate is established by comparing these statuses with the reference status:

- Carrying out 2 km trips results in a false positive rate (vehicle judged compliant when it failed the 15 km test) of 12%.
- Carrying out 2 km trips results in a false negative rate (vehicle judged to be faulty when it was compliant at the 15 km test) of 5%.

These error rates are significant, in order to keep the false positive and false negative rate low, the minimum distance should be magnified to at least 8km according to Figure 7. However, to compute the vehicle status, the test conditions are not considered: the tolerated threshold (5 times the standard) is constant whatever the experimental conditions. Taking into account the behavior of a nominal vehicle on this particular test, through modelling, could improve the status quality and help to lower the minimum distance.

Work is currently underway to propose a dynamic conformity factor that depends on the conditions (ambient temperature, engine temperature, driving style, gradient). It would be calibrated to represent the nominal behavior of vehicles (for example, it has been observed and therefore tolerated that Euro 6d diesel fueled vehicles nominally over-emit 4-5 times more than the norm after 2 km when starting from cold) (Dégeilh et al., 2020). This work should make it possible to maintain acceptable diagnostic error rates while reducing minimum test times, by taking test conditions into account.

Conclusions & Perspectives

That work gives an overview of different emission measurement protocols that could be operated during a PTI test, to better identify malfunctioning vehicles.

The French PTI protocol for emission has not been discriminating for our panel, as it has been designed to pinpoint heavy engine or aftertreatment failures. In the framework of this project, an enhanced static procedure has been developed. It provides a more detailed and exhaustive status for CO, PN or opacity but is not helpful to identify NOx issues.

It has also been proven that short trips (approximately 20min / 15km) on the road with a dedicated embedded measurement system are realistic and give a more reliable picture of the emissions performance. Nevertheless, the results are strongly influenced by the nature and the duration of the trip. The first sensitivity study shows that the error rate decreases when the trip duration increases, with a reasonable compromise found with a 8 km drive. The remaining challenge stands in the objectivization of the trip whatever the profile and the duration (with potential minimum requirements) and the determination of related alert and failure thresholds. For that, another experimental study with a larger panel of trips and vehicle is required to fit a more statistically representative digital model.

Acknowledgements

This work was supported by The French Agency for Ecological Transition (ADEME) in the framework of the SESAME project (2021-2022) – Agreement 2166D0010.

References

- Dégeilh P., Kermani J., Rodríguez S., Froberty A. et al. ; REAL-e: Robust and affordable IoT solution for market surveillance. *23rd Transport and Air Pollution Conference*, Thessaloniki, 2019
- Dégeilh P., Kermani J., Sery J., Michel P., Study of Euro 6d-TEMP emissions - IFPEN for DGEC: Summary report. [Research Report], *French Ministry of the Ecological Transition*, 2020. (hal-03632915)
- Donzelli, G.; Cioni, L.; Cancellieri, M.; Llopis Morales, A.; Morales Suárez-Varela, M. The Effect of the Covid-19 Lockdown on Air Quality in Three Italian Medium-Sized Cities. *Atmosphere* 2020, 11, 1118, doi:10.3390/atmos1101118.
- European Commission, *Commission Regulation (EU) 2018/1832 of 2 November 2018 Amending Directive 2017/1151 of the European Parliament and of the Council, Commission Regulation (EC) No 692/2008 and Commission Regulation (EU) 2017/1151 for the Purpose of Improving the Emission Type Approval Tests and Procedures for Light Passenger and Commercial Vehicles, Including Those for in-Service Conformity and Real-Driving Emissions and Introducing Devices for Monitoring the Consumption of Fuel and Electric Energy*, *Publ. L No. 301 I Sud* 27.11.2018, 1 (2018), <http://data.europa.eu/eli/reg/2018/1832/oj>
- European Environment Agency. Air Quality in Europe: 2020 Report; *Publication Office of the European Union: Luxembourg*, 2020; ISBN 978-92-9480-292-7.
- European commission, *Proposal 2022/0365 for a REGULATION OF THE EUROPEAN PARLIAMENT AND OF THE COUNCIL on type-approval of motor vehicles and engines and of systems, components and separate technical units intended for such vehicles, with respect to their emissions and battery durability (Euro 7) and repealing Regulations (EC) No 715/2007 and (EC) No 595/2009*, 10th November 2022
- French Ministry of the Ecological Transition, WebSite « Service des données et études statistiques (SDES) », « Données sur le parc automobile français au 1er janvier 2021 », 2021 : <https://www.statistiques.developpement-durable.gouv.fr/parc-et-immatriculations-des-vehicules-routiers>
- Fu, F.; Purvis-Roberts, K.L.; Williams, B. Impact of the Covid-19 Pandemic Lockdown on Air Pollution in 20 Major Cities around the World. *Atmosphere* 2020, 11, 1189, doi:10.3390/atmos11111189.
- Giechaskiel B et al., « Comparisons of Laboratory and On-Road Type-Approval Cycles with Idling Emissions. Implications for Periodical Technical Inspection (PTI) Sensors », *Sensors* 2020, 20, 5790; doi:10.3390/s20205790
- Giechaskiel, B.; Valverde, V.; Kontses, A.; Suarez-Bertoa, R.; Selleri, T.; Melas, A.; Otura, M.; Ferrarese, C.; Martini, G.; Balazs, A.; et al. Effect of Extreme Temperatures and Driving Conditions on Gaseous Pollutants of a Euro 6d-Temp Gasoline Vehicle. *Atmosphere* 2021, 12, 1011. <https://doi.org/10.3390/atmos12081011>
- Kumari, P.; Toshniwal, D. Impact of Lockdown on Air Quality over Major Cities across the Globe during Covid-19 Pandemic. *Urban Clim.* 2020, 34, 100719.
- Netherlands Ministry of Infrastructure and Water Management. *Regulation of the State Secretary for Infrastructure and Water Management*, of 12 January 2021 No. IENW / BSK-2020/125046, amending the Vehicle Regulation for the introduction of the PTI particulate filter check with particle counter, 12th January 2021
- Poole, M. et al. *On-Line On-Board Testing of Non-DPF Diesel Vehicle in the United States*; ICF International, 2014

Suarez Bertoa, R., Valverde Morales, V., Clairotte, M., Pavlovic, J., Giechaskiel, B., Franco, V., Kregar, Z. and Astorga-Llorens, M., On-road emissions of passenger cars beyond the boundary conditions of the real-driving emissions test, *ENVIRONMENTAL RESEARCH*, ISSN 0013-9351, 176, 2019, p. 108572, JRC114583.

Wang J.M. et al., « Plume-based analysis of vehicle fleet air pollutant emissions and the contribution from high emitters », *Atmos. Meas. Tech.*, 8, 3263–3275, 2015

Multisectoral drivers of decarbonizing battery electric vehicles in China

F. Wang^{1*}, S. Zhang¹ and Y. Wu¹

¹ School of Environment, Tsinghua University, 100084, Beijing, People's Republic of China, contact wangfang18@mails.tsinghua.edu.cn.

Introduction

As the end-use sector with the highest reliance on fossil fuels, the global transport sector (8.3 Gt) was responsible for ~23% of total combustion carbon dioxide (CO₂) emissions before the Covid-19 pandemic (IEA, 2021). Among all transport modes, light-duty vehicles, predominantly passenger cars, were the largest contributor to the total transport CO₂ emissions (IEA, 2021). Electrifying passenger cars are regarded as one predominant solution to deliver deep mitigation of their CO₂ emissions in the future. China has made great progress in the electrification of passenger cars, and the sales of battery electric vehicles (BEVs) have reached 20% (IEA, 2023).

The potential environmental and climate benefits of BEVs provide an important motivation for China's supportive policies in developing BEVs (Liang X. et al., 2019). However, considering the high reliance on coal-based electricity generation, there remains ongoing public debate on the actual impacts of BEVs on mitigating CO₂ emissions. Life-cycle assessment (LCA) methods then were developed to address this issue, which could be typically categorized into two types according to the boundary setting, well-to-wheels [WTW, only focusing on the fuel cycle; (Hu et al., 2010; Wu et al., 2012; Shen et al., 2019; Gan et al., 2021)] or cradle-to-grave [C2G, further including production and recycling processes of automotive components materials; (ICCT, 2021; Wu et al., 2019)].

The influence of multiple complex factors apart from the electricity mix not comprehensively analyzed. In this study, we emphasize that BEVs and internal combustion engine vehicles (ICEVs) at fleet level as compared components, and summarise their recent huge progress on C2G CO₂ emissions by dissecting multiple-sectoral drivers from electricity, vehicle fuel economy, Li-ion battery, and major automotive metals with real-world investigated data. Furthermore, we synthesized all the drivers to evaluate the potential C2G CO₂ emissions reduction in 2030 with each factors dissected.

Scope

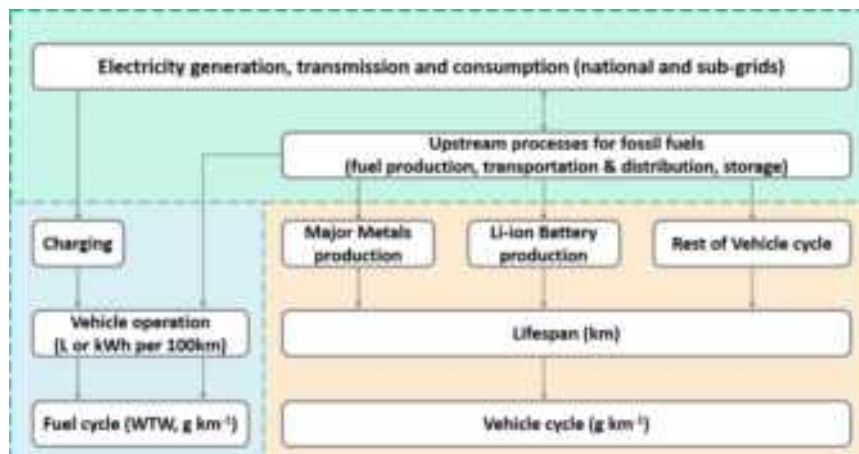


Figure 1: Scope of cradle-to-grave analysis of CO₂ emissions for BEVs in China

We selected model years (MY) of 2015, 2020, and 2030 as the past, present, and future study years to compare C2G CO₂ emissions between BEVs and ICEVs. C2G CO₂ emissions are expressed in the CO₂ emissions per unit distance traveled during the vehicle lifespan. The LCA study consists of two main aspects the fuel cycle (i.e. WTW) and the vehicle cycle and thus the C2G emissions are calculated as Eq. (1).

$$E_{C2G} = \frac{FC \times EF_{WTW} \div 100}{Eff_{charging}} + \frac{E_{major\ metals} + E_{battery} + E_{others}}{Lifespan} \quad (1)$$

Where FC refers to fuel consumption for ICEV and BEV in the unit of L 100 km⁻¹ and kWh 100 km⁻¹, respectively. EF_{WTW} is the CO₂ emission factor for gasoline (g L⁻¹) or electricity (g kWh⁻¹), and $Eff_{charging}$ represents the charging efficiency of chargers, which depicts the proportion available for batteries from the output of chargers (80% in 2015, 86% in 2020, and 92% in 2030).

Results and Discussion

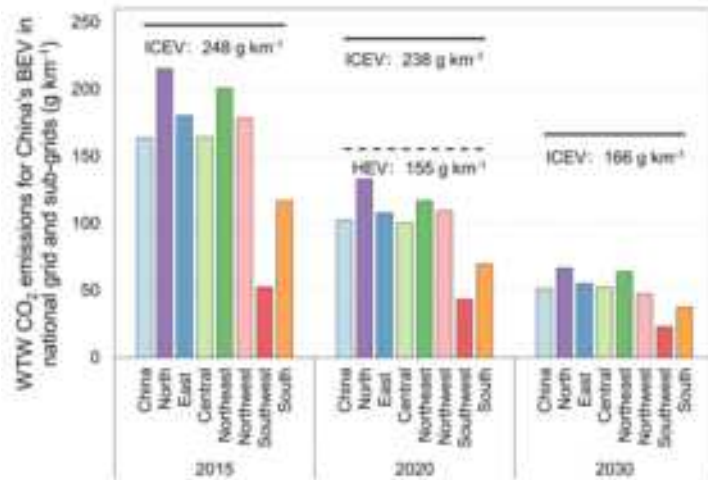


Figure 2: WTW CO₂ emissions for China's BEVs in national grid and sub-grids (2015, 2020, and 2030).

BEVs are estimated to mitigate WTW CO₂ emissions by 57% in 2020 with the national-average grid (102 g km⁻¹ for BEVs, 155 g km⁻¹ for HEVs, and 238 g km⁻¹ for ICEVs) and could deliver WTW CO₂ emission mitigations across all sub-grid regions. In the most coal-dependent region, the North sub-grid (a coal-based share of 79%), BEVs could still reduce 44% WTW CO₂ emissions compared with the ICEV counterparts there. In cleaner sub-grid regions, such as the South and Southwest, the mitigation percentages could be enlarged to 71% and 82%.

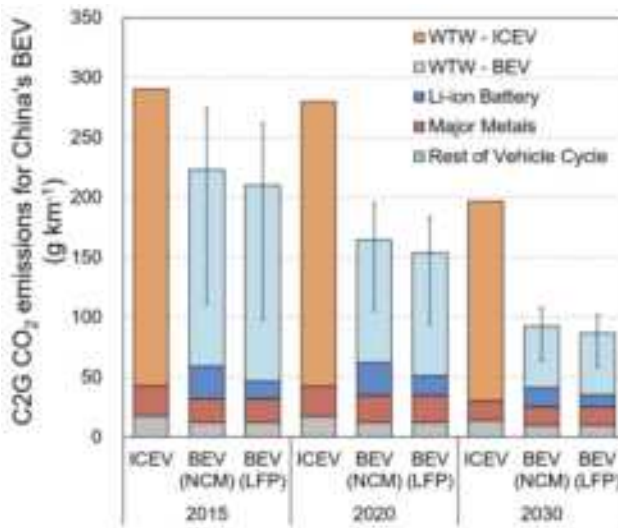


Figure 3: Cradle-to-grave CO₂ emissions of ICEV and BEV during 2015-2030 with the national-average electricity mixes. The error bars represent the variability of WTW CO₂ emissions due to the different electricity mixes across various sub-grids.

The estimated C2G CO₂ emissions of NCM-BEVs, LFP-BEVs and ICEVs in 2020 are 165 g km⁻¹, 153 g km⁻¹, and 280 g km⁻¹, respectively. According to the national-average electricity mix, BEVs have already shown approximately a 40% reduction in C2G CO₂ emissions compared with ICEVs in 2020 and the reduction would further increase to 53% in 2030, despite only a 23% reduction in 2015. As far as sub-grid regions are concerned, the C2G CO₂ mitigations of NCM-BEVs range between 30% and 62%. This indicates that even in the North grid still with a high proportion of coal-fired electricity, BEVs can achieve considerable emission reduction benefits.

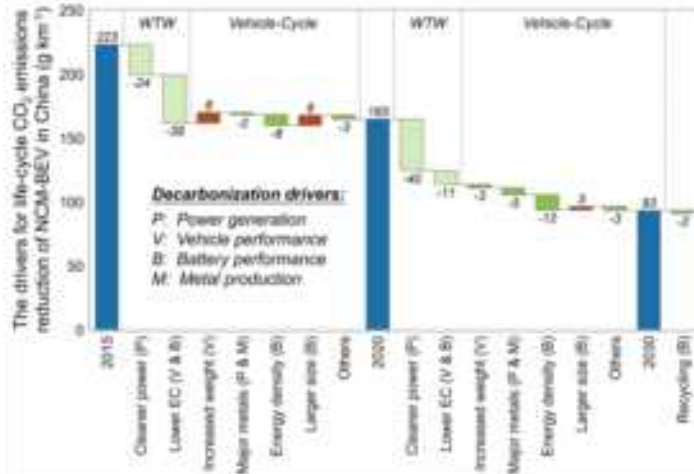


Figure 4: Drivers on decarbonizing NCM-BEVs from 2015 to 2030. The drivers are categorized into two phases (WTW and vehicle cycle) and four major parts: P: Power generation; V: Vehicle performance (e.g., vehicle weight, energy consumption (EC)); B: Battery performance (e.g. battery size, energy density); and M: Metal production. See Fig. S1 for the results of LFP-BEVs.

With the accelerated decarbonization of the power system during 2020-2030, we estimate that the future cleanliness of the electricity mix will be the major driver to reduce C2G CO₂ emissions for BEVs. The total reductions then will reach 43% (72 g km⁻¹ and 66 g km⁻¹) for the two types of BEVs. For NCM-BEVs, the cleaner electricity will lead to 40 g km⁻¹ of C2G CO₂ emission mitigation. The improved operating and charging efficiency would be other drivers to reduce WTW CO₂ emissions by 11 g km⁻¹ (thus jointly reducing the WTW CO₂ emissions by 51 g km⁻¹). The improvement in the energy density of the battery is still significant, resulting in 12 g km⁻¹ C2G CO₂ mitigation. The decarbonized production of metal materials can also contribute to emission mitigation by 5 g km⁻¹. Battery recycling can bring additional emissions mitigation of 2 g km⁻¹.

The European Union's (EU) proposed battery regulation aims to enhance sustainability across the battery value chain, including introducing a carbon footprint limit for electric vehicle (EV) batteries. This aligns with a growing trend emphasizing the pivotal role of life cycle assessment (LCA) in climate mitigation. Addressing data limitations, our study provides primary industry-based data from China's battery and automotive sectors, enhancing reliability in assessing carbon footprints. By incorporating real-world data, including China's carbon peaking and neutrality policies, we analyze key drivers for decarbonizing passenger vehicle emissions. This informs policymakers of the complexities in reducing EV emissions during electrification, emphasizing technology enhancement and supply chain decarbonization. Amid the global imperative to limit warming, our study demonstrates BEVs' potential to significantly reduce CO₂ emissions compared to ICEVs by 2030, supporting China's climate targets. While advanced strategies like smart charging and battery reuse can further amplify benefits, focusing on the entire BEV fleet underscores potential uncertainties. Improved battery life-cycle data, evolving smelting technologies, and renewable energy integration offer untapped mitigation avenues. Although plug-in hybrid electric vehicles are not considered here, broader decarbonization strategies hold promise for them as well. Harnessing these factors through a comprehensive supply-chain approach can enhance BEV carbon mitigation within future policy frameworks.

Acknowledgements

This work was sponsored by the National Key Research and Development Program of China (grant No. 2022YFC3703600) and the National Natural Science Foundation of China (grant No. 42261160645).

References

- Gan Y, et al. (2021). Provincial greenhouse gas emissions of gasoline and plug-in electric vehicles in China: comparison from the consumption-based electricity perspective. *Environ Sci Technol.* 55, 6944–6956.
- Huo H, Zhang Q, Wang MQ, Streets DG, He K. (2010). Environmental implication of electric vehicles in China. *Environ Sci Technol.* 44, 4856–4861.
- ICCT (2021). A global comparison of the life-cycle greenhouse gas emissions of combustion engine and electric passenger cars.
- IEA (2021). Net zero by 2050, IEA, Paris.
- IEA (2023). Global EV Outlook 2023, IEA, Paris.
- Liang X, et al. (2019). Air quality and health benefits from fleet electrification in China. *Nat Sustain.* 2, 962–971.
- Shen W, Han W, Wallington TJ, Winkler SL. (2019). China Electricity generation greenhouse gas emission intensity in 2030: implications for electric vehicles. *Environ Sci Technol.* 53, 6063–6072.
- Wu Y, et al. (2012). Energy consumption and CO₂ emission impacts of vehicle electrification in three developed regions of China. *Energy Policy.* 48, 537–550.
- Wu Z, et al. (2019). Assessing electric vehicle policy with region-specific carbon footprints. *Appl Energy.* 256, 113923.

Vehicle fleet electrification: electric energy consumption assessment at the scale of an urban area.

D. Lejri¹, B. Jeanneret², C. Bécarie² and R. Trigui²

¹LICIT-ECO7, Univ Lyon, Univ Eiffel, ENTPE, F-69675 Lyon, France, delphine.lejri@entpe.fr

²LICIT-ECO7, Univ Eiffel, Univ Lyon, ENTPE, F-69675 Lyon, France

Introduction

In the field of transportation, one of the European strategies being considered to mitigate climate change is the deployment of electric vehicles (EVs). In France, fleet electrification is rather slow, but it seems to be intensifying: EVs and Plug in HEV account for 22% of new car sales in France in 2022. Indeed, electric mobility has proven to be a powerful technology for decarbonization of the transportation sector (Kouridis, 2022). In comparison to conventional vehicles, EVs have either zero or lesser tailpipe greenhouse gas emissions. However, their carbon emissions are shifted from the exhaust pipe to the electric generators. Therefore, EVs are more eco-friendly the lower the carbon intensity of the electricity generation mix (De Angelis, 2020).

As more electric vehicles are introduced into the fleet, the consumption of electric energy increases. The amount of electric energy consumed is often simply assessed by considering that a typical personal electric car consumes 20kWh per 100km on average. However, some papers focus on the evaluation of EVs electric consumption (EC): (Zhang, 2015) proposes an estimate from driving cycles, (Al-Wreikat, 2021) analyses experimental data to understand the relevant factors that influence EC during operation, (Fiore, 2019) looks at impact of traffic conditions on fuel and electric consumption by modelling it from various speed profiles.

In this paper, the issue is to assess EC at the scale of an urban network with a fleet of vehicles including an increasing share of EV. Is a flat rate estimate sufficient? What is the appropriate description of traffic conditions in order to provide a more accurate estimate? Our objective is to compare on a large urban area, namely L63V (3 districts in the metropole of Lyon) (i) an estimate using detailed speed profiles directly derived from simulated trajectories and (iii) an estimate using average flow velocity per road section, (ii) an estimate using average flow velocity per Iris zone.

Case study: Lyon63V

The case study is the Lyon63V¹⁵ network, a 15 km² urban area divided into 75 sub-areas (fig.1). The supply specification covers the various transportation modes: light, heavy vehicles, and public transport (metro, tram and bus). The demand specifications are defined dynamically on morning peak hour (from 6.30 am to 10.30 am), for each vehicle category and each OD pair. This baseline demand profile has been calibrated on loop detectors measurements.



Figure 1. L63V network : road sections and 75 IRIS areas (uniform subdivision of the population for statistical purposes, INSEE¹⁶)

¹⁵ 3rd and 6th districts of Lyon and Villeurbanne

¹⁶ French national institute of statistics and economic studies

The traffic microsimulation was implemented in the SYMUVIA platform¹⁷. Vehicle movements at the microscopic scale are governed by a set of rules, including car-following modelling (Leclercq, 2007a, 2007b), lane-changes (Laval and Leclercq, 2008) and specific movements at intersections (Chevallier and Leclercq, 2007). The platform also copes with the cohabitation on the network of vehicles with different kinematics, including passenger cars, buses and heavy-duty vehicles.

In this first study, we have decided to focus on passenger cars. We will consider three levels of information in order to study the impact of traffic dynamics level of description on the evaluation of electricity consumption: (i) vehicle trajectories, (ii) traffic variables at link scale and (iii) at IRIS zone scale. In the first case, we consider each individual vehicle, so the output of the traffic simulation is characterized by its instantaneous speed profile. In the other cases, a spatio-temporal element is considered (i.e., the road section for 10min or the zone for 10min) and the micro-simulation outputs are aggregated to obtain the associated average speeds and distance travelled.

According to the fleet composition published by Citepa¹⁸ in December 2022, the share of electric vehicles is 0.64% of passenger cars in France. However, this share is constantly growing. In 2023, 23.5% of new vehicle registrations were for electric vehicles (European Alternative Fuels Observatory¹⁹). For the purposes of this study, we assume that all vehicles are electric, in order to avoid introducing biases by randomly selecting vehicles. We will therefore focus on the relative differences between the proposed options. The passenger car electric fleet considered is composed of Tesla model 3, Renault Zoe and Citroën C0, three EVs with different sizes and autonomy ranges. For more realistic case study, one must consider the actual French EVs share.

Finally, two different simulations are used to evaluate and compare the energy consumption of the EV fleet in the considered area. In the first option, accurate EV simulation energetic models are used based on VEHLIB software description and the different generated trajectories (Vinot, 2008), while for the second and the third options, a curve of EC in function of the average speed has been previously built using the same models and speed profiles databases.

Electrical consumption assessment

Energy consumption of electric vehicles depends on several internal (vehicle features) and external (environment) parameters. The most impacting vehicle characteristics are the weight, the aerodynamic drag, the frictions and the efficiency of the components such as the battery and the electric drive systems. The environment parameters that influence the energy consumption are related to the infrastructure (road type, slopes, lights), the traffic and the weather conditions. Consequently, a precise calculation of the consumed energy during a trip is a complex task.

The Accurate Dynamic Model (ADM)

For more than two decades, LICIT-ECO7 lab has been developing VEHLIB, an energy consumption software dedicated to all types of vehicles, including EVs. VEHLIB is now an open-source software available on the Gitlab platform (Jeanneret & al, 2021). Two types of simulation are possible, namely forward simulation and backward simulation. The first is based on Simulink blocks and allows to simulate in a causal way the power flow in each component of the vehicle using speed control and a driver model. The second uses Matlab scripts and an inverse causality, i.e upstream from the effect to the cause (e.g. from the speed to the forces that cause it). Both need the instantaneous speed profile as input and allow the calculation at each time of the power going through the different systems of the vehicle. As no driver model and control loop is needed in the backward model, this makes it faster and fairer for comparison as the speed profile is supposed to be exactly followed. The forward model is on the other hand more adapted to develop components and vehicle controls and is often used in real time experiments such as hardware in the loop tests. We suggest in this paper to use the backward model for the energy consumption simulation (first option) and this will be considered as the reference for the energy comparison of the different simulation options because of its proven validity when compared to vehicle test.

¹⁷ <https://github.com/licit-lab/Open-SymuVia>

¹⁸ <https://www.citepa.org/en/>

¹⁹ <https://alternative-fuels-observatory.ec.europa.eu>

The pre-processed interpolated model (PIM)

The previous model requires as input the instantaneous speed profile, at least second by second, and the detailed vehicle parameters data. For a global calculation of a whole fleet of vehicle in a given area and during significant period of time this imposes two constraints that are firstly the availability of the huge amount of instantaneous data and secondly the computation time that can exceed the capacity of standard computers.

Therefore, one solution to accelerate simulation, in order to consider larger spatial and time scales, could be the use of the accurate model to generate pre-processed consumption results for each vehicle. The approach is to use ADM VEHLIB based model of the EV and a representative set of speed profiles (here we considered data from Hyzem, Artemis and WLTC speed profiles). The speed data so gathered is divided into sequences, each one represents an elementary speed profile from the vehicle start until the next stop. The ADM model of the EV is then executed on each sequence to calculate the corresponding EC. In this paper, the described method is applied to the three electric vehicles considered (Tesla, Zoe and C0). The EC of each sequence is plotted in blue function of the average speed of the sequence for the three vehicles (fig 2). To obtain a mathematic function of the EC to be used in the aggregated options (option 2 and 3), we considered an exponential interpolation function plotted in red on the same figures.

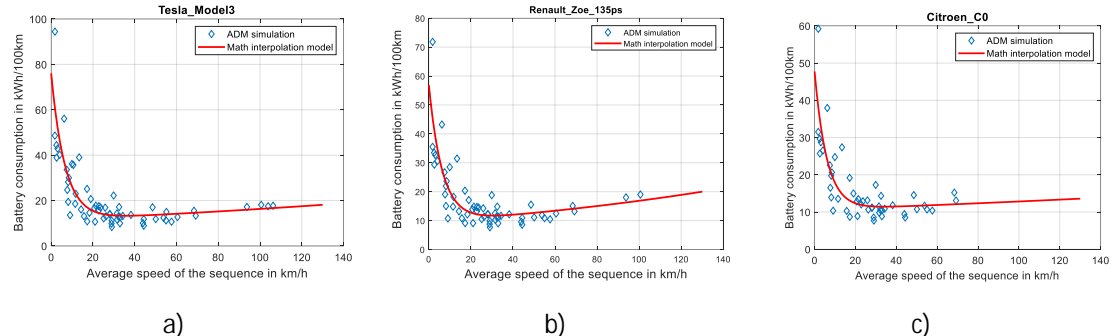


Figure 2. Energy consumption according to the average speed and the vehicle model: (a) Tesla model3, b) Renault Zoe, c) Citroen C0

Results and discussion

Global energy consumption

Using the traffic simulation software SYMUVIA and the two energy models (ADM for option1 and PIM for options 2 and 3) the total energy consumed during the simulation period (from 6.30 am to 10.30 am) is calculated for each vehicle then for the whole fleet. The vehicle fleet is supposed to be composed equally of Tesla, Renault Zoe and Citroen C0. The results are depicted in Table 1. As total energy consumption is the energy consumed by the battery, we add a column corresponding to the total energy need that includes the energy lost during charging with a charge efficiency value of 90%.

Table 1: Global Electric Energy Consumption of the three simulation options

[Simulation Options]	Distance (km)	Total EC (kWh)	Total Energy need (kWh)	Error in % Ref option1	Mean EC (kWh/100km)	Error in % Ref option1
Option 1	323202	47758	53 064	0	16.4	0
Option 2	326012	44742	49 713	-6	14.9	-9
Option 3	328754	42260	46 955	-11	14.3	-13

We can notice that the three options do not lead exactly to the same distance as this variable calculation method is different from an option to another (integral of speed for option 1 and sum of the length of different segments for option 2 and 3).

As shown in Table 1, options 2 and 3 underestimate the total energy requirement by 6 and 11% respectively. If we include the distance calculation effect, the average difference in energy consumption reaches 9 and 13% error compared to the reference option1.

In terms of computation time, option 1 runs in a parallel mode with 4 workers on a laptop I7-7820HQ CPU @ 2.90GHz processor and lasts almost 5 hours to achieve the whole simulation for the 3 vehicles. Options 2 and 3 need only one worker and last less than one second on the same computer.

As the PIM model is average speed dependant, and in order to understand the error origin for the options 2 and 3, we plotted in figure 3 the speed distribution according to the distance for the 3 options.

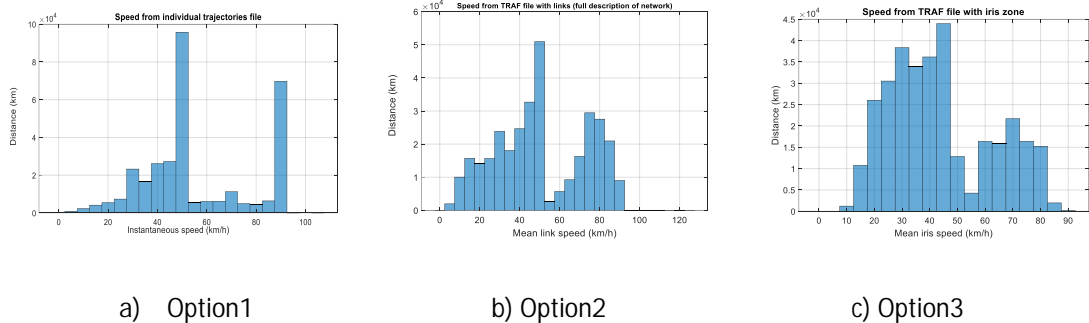


Figure 3. Speed distribution according to the distance for the three options of simulation

As shown in figure 3 a), the option 1 with instantaneous speed distribution includes two main classes around 50 and 90 km/h corresponding to the two speed limits encountered (urban and rapid loop speeds). These classes have less weight in option 2 and almost equal to the other classes in option 3. This is due to the average speed estimation on each link for the two options (full link and iris zone use respectively). As the PIM model uses these speeds to determine the energy consumption according to the mathematic model presented in figure 2, it seems coherent that EC is lower for option 2 and the lowest for option 3 (90 km/h has high EC).

Impact of the traffic

One advantage of the proposed model coupling (SYMUVIA+VEHLIB) is to evaluate the impact on the energy consumption of the traffic intensity according to the time of the day. Figure 4 presents a temporal simulation in the morning (from 6.30 am to 10.30 am) in the considered area (L63V) using option 2 methodology. Although the effect of a higher traffic density around the peak hours (8.40 to 9.40) is clearly registered on the energy consumption (without charging efficiency), the difference between the peak value and the lowest value of the consumed energy is only about 3 %.

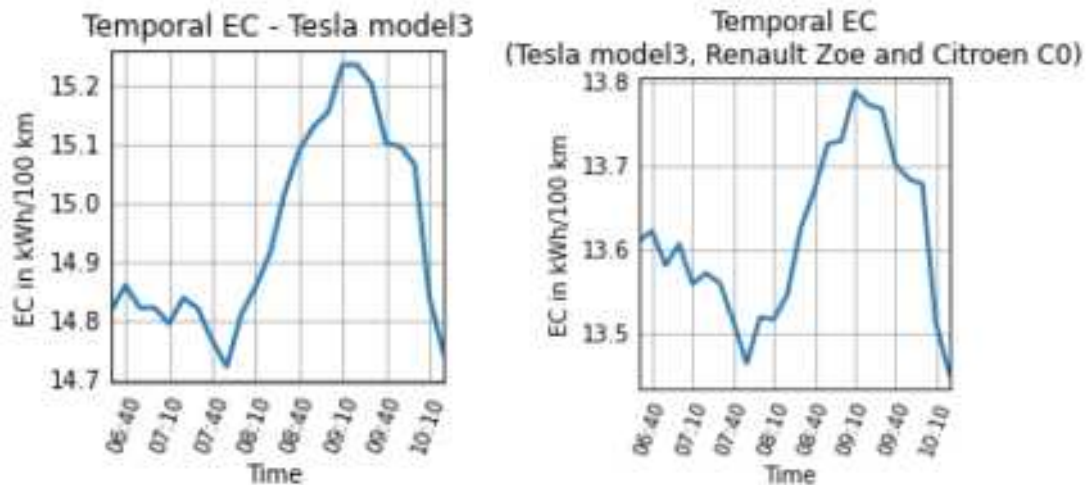


Figure 4. Electric Energy Consumption per vehicle and per 100km of the Evs fleet simulated on L63V according to the time. a) tesla model 3 vehicle b) average of the three vehicles

Conclusion

In order to assess energy consumption in a large urban area considered infrastructure network and traffic constraints a new methodology based on traffic simulation tool and energetic vehicle modeling coupling is presented. Three options using this coupling have been set and compared. The first one, taken as reference, uses instantaneous description of the speed profile and a high-fidelity energetic vehicle model. It gives in theory the most reliable results. The second and the third option are derived from the traffic description with mean speed values for each segment. The third option, compared to the second, is based on area subdivisions to further reduce spatial description. The simulation results showed a deviation from the baseline of the total energy consumed with options 2 and 3 of 6 and 11% respectively. Depending on the objective of the various studies, these values could be considered satisfactory or not because, on the other hand, options 2 and 3 allow a drastic reduction in the calculation time. This opens up prospects for assessing energy consumption on a large scale as:

- Enlarging the spatial area to cover a whole town or metropolitan area and further study the scale effect.
- Using large scale traffic simulations or real census data.

However, studying power constraints on components is important for EVs. For example, the battery is a key component and its thermal behavior during use impacts its lifetime. In this case the option 1 is the only alternative to highlight and further control these phenomena.

References

- Al-Wreikat, Y., Serrano C., Ricardo Sodré, J. (2021) *Applied Energy*, <https://doi.org/10.1016/j.apenergy.2021.117096>
- Chevallier, E., Leclercq, L. (2007). A macroscopic theory for unsignalized intersections, *Transp. Res. Part B Methodol.* 41, 1139–1150. <https://doi.org/10.1016/j.trb.2007.05.003>
- De Angelis, E., Turrini, E., Carnevale, C., Volta, M. (2020) *IFAC-PapersOnLine*, <https://doi.org/10.1016/j.ifacol.2020.12.784>
- Fiori, C., Arcidiacono, V., Fontaras, G., Makridis, M., Mattas, K., Marzano, Thiel, C., Ciuffo, B. (2019) *Transportation Research Part D*, <https://doi.org/10.1016/j.trd.2018.11.018>.
- Jeanneret, B., Kabalan, B., Redondo-Iglesias, E., Vinot, E., Trigu, R., VEHLIB2 software, 01/10/2021
<https://gitlab.univ-eiffel.fr/eco7/vehlib>
- Kouridis, C., Vlachokostas, C. (2022) *Renewable and Sustainable Energy Reviews*, <https://doi.org/10.1016/j.rser.2021.111775>
- Laval, J.A., Leclercq, L. (2008). Microscopic modeling of the relaxation phenomenon using a macroscopic lane-changing model, *Transp. Res. Part B Methodol.* 42, 511–522, <https://doi.org/10.1016/j.trb.2007.10.004>

Leclercq, L. (2007a) A hybrid approach to the solution of the Lighthill-Whitham-Richards model. *Transp. Res. Part B Methodol.* 41, 701–709, <https://doi.org/10.1016/j.trb.2006.11.004>

Leclercq, L. (2007b). Bounded acceleration close to fixed and moving bottlenecks, *Transp. Res. Part B Methodol.* 41, 309–319, <https://doi.org/10.1016/j.trb.2006.05.001>

Vinot, E., Scordia, J., Trigui, R., Jeanneret, B. and Badin, F. (2008) *International Journal of Vehicle Systems Modelling and Testing*, <https://doi.org/10.1504/IJVSMT.2008.023835>

Zhang, R., Yao, R. (2015) *Trans. Res. Part D*, <https://doi.org/10.1016/j.trd.2015.10.010>

2.6 TAP.06. Vehicle-emission modelling and measurements and impact assessment of emission regulations.

Assessing pollutant emissions on an urban area using different traffic simulation approaches: multi-agent modelling and microscopic modelling

M.Tirico¹, V. Le Bescond², D. Lejri¹, P. Gastineau², A. Can³

¹LICIT-ECO7, Univ Lyon, Univ Eiffel, ENTPE, F-69675 Lyon, France

²AME-SPLOTT, Université Gustave Eiffel, Bouguenais, 44344, France

³UMRAE, Université Gustave Eiffel, CEREMA, Bouguenais, 44344, France

Abstract

Human exposure to traffic-related air pollution is widely acknowledged as a major health hazard worldwide. Computational models are estimated to be valuable tools to assess the exposure of humans to pollutants in an urban context. Promising outputs have been obtained by modelling chain of traffic models, emission models, and dispersion models. In this paper, we focus on the impact of traffic models on the emissions obtained. We are coupling two traffic models, the agent-based MATSim and the microscopic simulator Symuvia, with the emission model HBEFA. Our analysis comprises three main comparisons: the traffic conditions, the statistical distribution of emission and the spatial distribution of the gaps between models. Although emissions computed with the multi-agent model are higher than emissions obtained with the microscopic model, we observed some correlations between total air pollutant emissions. A correlation can be found spatially. However, we observed some significant gaps that needed to be investigated in more depth. This preliminary work is the first step in assessing human exposure to traffic-related emissions using different modelling approaches.

Introduction

Exposure to traffic-related air pollution, such as the frequency of pollutant events that are dangerous to human health, is a significant risk to humans. According to the Air Quality in Europe report (European Environment Agency, 2022), 96% of the urban population is exposed to unaccepted levels of air pollutants. Evidence supports a causal relationship between traffic exposure and the exacerbation of asthma in children (Institute Health Effects, 2022), colon cancer (Roswal, 2023), and mortality (Beelen, 2008). Particulate matter (PM) inhalation induces respiratory and cardiovascular diseases (Apte, 2018). A correlation in terms of mortality has been shown between human home addresses and the proximity of congested roads (Beelen, 2008). High exposure is also a source of social inequalities and escalates urban segregation (Gurram, 2019). Emission abatement may decrease the impacts of pollutants on human health, but it often involves economic and social costs. Therefore, improving air quality in urban areas is a major challenge nowadays.

The contribution of traffic to individual exposure is difficult to quantify. Despite recent sensor improvements showing promise for measuring pollutant concentrations, detailed information about pollutant concentration cannot be obtained by interpolating data from sparsely distributed sensor measurements. The European Environment Agency report (2022) encourages the use of computational models to estimate air quality to support planners and policy makers. In this field, the combination of traffic, emission and dispersion models has become an extended practice to estimate human exposure. Predicting models have become an essential tool for human exposure from traffic-related assessment. Evaluating human exposure to traffic requires detailed information on the nature and distribution of pollutants' emissions and dispersion. To this end, we should look for the improvement of two aspects: (1) improving our understanding of complex interaction dynamics between traffic emission, air pollutant dispersion and human exposure, and (2) developing decision support tools to estimate exposure and reduce human nuisances via traffic mitigation strategies.

In this context, the Symexpo project (SYstemic approach for assessing the impact of urban Mobility on EXposures to environmental Pollutions) aims to investigate human exposure to traffic-related emissions in an urban context. The main expected output of the project is to formalize a framework for estimating traffic-related emissions, computing air diffusion of pollutants and estimating human exposure pollutants at different spatiotemporal scales. The developed modelling chain will also enable proposing and evaluating the benefit of mitigation strategies. To this end, this paper aims to set up preliminary bricks of the Symexpo project by investigating traffic air emission at two urban scales using two modelling chains.

Methodology

Traffic models

Estimating traffic-related air pollutant emissions is challenging. Generally speaking, a solid approach consists of coupling static or dynamic traffic models with emission models (Fallah, 2015). Despite their realistic macroscopic description of traffic conditions, static models do not provide a detailed spatio-temporal description of traffic conditions over the transportation network. For this reason, here we only consider dynamic traffic models.

A variety of dynamic models has been proposed. They can be resumed in three main classes: (1) in aggregated traffic models, based on the Macroscopic Fundamental Diagramm (Daganzo, 2007), traffic conditions are measured with fluid dynamics-inspired equations at the level of sub-urban areas (called reservoirs), (2) in microscopic models, the traffic condition is estimated by representing the vehicles' individuality and calculating the main vehicle kinematics such as speed and acceleration at second and (3) in mesoscopic models, the vehicles' kinematics are described without explicitly designing the vehicles' interactions.

An essential advantage of MFD models is the low computational cost, which allows the development of real-time network monitoring systems for traffic emissions. However, the definition of network partitioning might influence the total exhaust emissions of the network (Batista, 2022). Moreover, congestion conditions, which are supposed to be responsible for the most dangerous hot spot for human health, are aggregated at the reservoir level and do not emerge at the street level. Therefore, microscopic and mesoscopic models are more adapted for estimating human exposure. To quantitatively assess the impact of those models, we will compare emission rates obtained with the HBEFA model and traffic simulations, derived from the microscopic model Symuvia (Leclercq, 2007) and the mesoscopic model MATSim (Horni, 2016).

Several differences can be found between the microscopic model Symuvia and the mesoscopic model MATSim. Symuvia is a vehicle-centered model, where the route traffic choice is governed by a dynamic traffic assignment model that minimises the vehicles' travel time. A set of rules governs the vehicles' dynamics, including the laws of pursuit, lane change and intersection crossing. The main focus of this model is on understanding vehicles' interactions. Therefore, intermodality (the possibility of an individual changing his transportation mode along his trip) is not implemented. Due to the detailed modelling of vehicle interactions, the traffic situation can be measured by aggregating individual kinematics. Therefore, this approach is expensive regarding computational costs, limiting case studies on a few roads or neighbourhoods and for a few hours of a day simulation. On the other hand, MATSim is an individual-centered model where each agent of a synthetic population (representative of the real population) is associated with some daily activities. The route traffic choice is the result of the maximisation of each utility agent associated with different options, which aim to represent the profitability after each trip. Therefore, intermodality is a crucial feature of the MATSim approach. Outputs are aggregated at the level of links of the transportation network. In other words, we know the traffic condition at each link as a congestion level. The computational requirement of this approach is less than that of the Symuvia approach, allowing it to simulate the daily evolution of traffic conditions in wide urban areas.

Emission model

To estimate the real impact of the difference between these models on emissions, we coupled them with the same emission model HBEFA (Kickhöfer, 2016). This latter is a European database of emission factors for all current vehicle categories. The model is based on traffic situations: emission factors are associated with five traffic conditions (from free flow to congested) and the characteristics of the streets. Therefore, we obtained each link's traffic condition by measuring the average speed with the Symuvia and MATSim models, finding the related emission factor in the HBEFA model and computing the associated emissions for each link. We investigate the impacts of model mechanisms on emissions rates by comparing the outputs of each modelling chain.

Our modelling chains have been designed as independently as possible. Concerning the demand input, the origin-destination matrices were obtained from similar data (household and travel surveys, census data, etc.), but using different processing methods specific to each modelling approach. Furthermore, the transportation networks came from two different geographical datasets (from the French geographical dataset BDTOPO for Symuvia and from the open-access OpenStreetMap for MATSim). Due to those essential differences between modelling chains, we group our outputs by a spatial tessellation. Several kinds of tessellation can be proposed. In this paper, we start with an administrative tessellation.

Results

The study case of this paper is the L63V neighbourhood: this urban area covers the 1st, 3rd and 6th districts of Lyon and Villeurbanne urban area (France). The area covers 15 km² of the North-East Lyon metropolitan area, which covers 75 administrative subareas (IRIS). In the following, the IRIS tessellation will be used to investigate the spatial distribution of our outputs. While the MATSim simulation covers a day of simulation, the Symuvia simulation covers 4 hours (between 6:00 am and 10:00 am). Our analysis is over this last time range, and our results are aggregated for 15 min time slots.

Figure 1 depicts the traffic condition for each 15 minutes time slot. Although the total distance of vehicles at each time slot is similar (figure 1, left), the number of vehicles currently over the networks is 3 times more in MATSim simulation than in the Symuvia simulation (figure 1, middle). Intuitively, the average vehicle speed is less in MATSim (figure 1, right).

As expected, the different traffic patterns impact PM10, CO2 and NOx emissions (figure 2). The shape of the emission evolution obtained from the MATSim and Symuvia simulations are similar (Gaussian-like shape). However, for all pollutants, MATSim overestimates pollutant emissions compared with Symuvia.

Figure 3 depicts the correlation between the total emissions obtained from MATSim and Symuvia models, while Figure 4 depicts the spatial distribution of the total gap between emissions obtained from both models. As previously mentioned, the total emissions are overestimated by MATSim model compared to that of Symuvia. However, in Figure 3 we observe that low values are more correlated for the three pollutants than higher values.

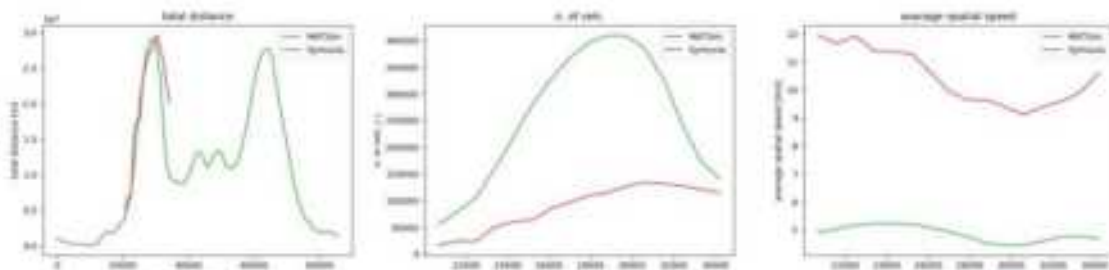


Figure 10: Traffic condition estimation: average speed (left), number of vehicles (middle) and total distance travelled by vehicles (right).

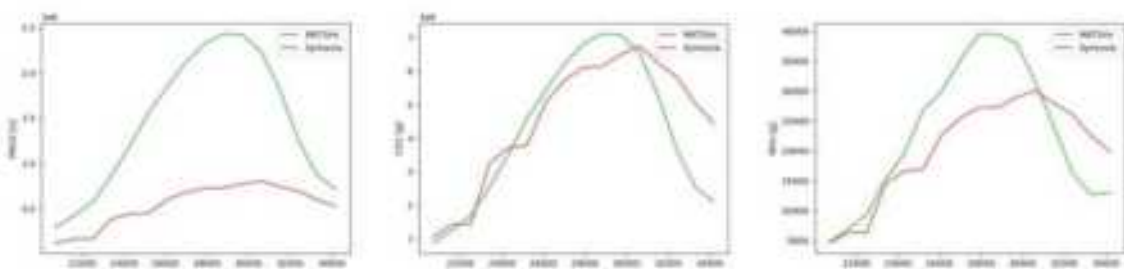


Figure 11: Total emission for 15 min slots of PM10 (left), NOx (middle) and CO2 (right).

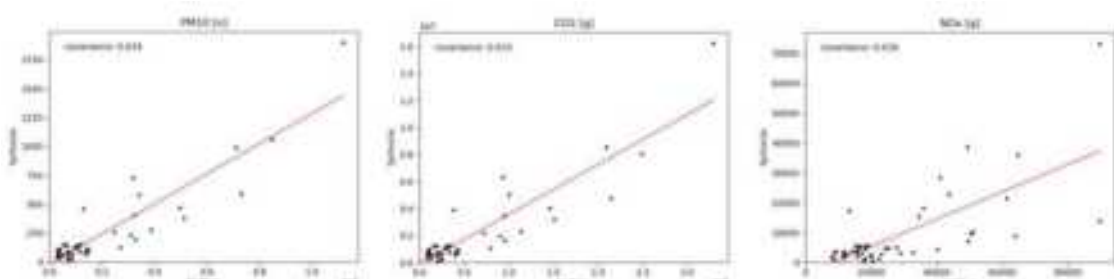


Figure 3: total emissions correlation between Symuvia and MATSim models for PM10 (left), NOx (middle) and CO2 (right).

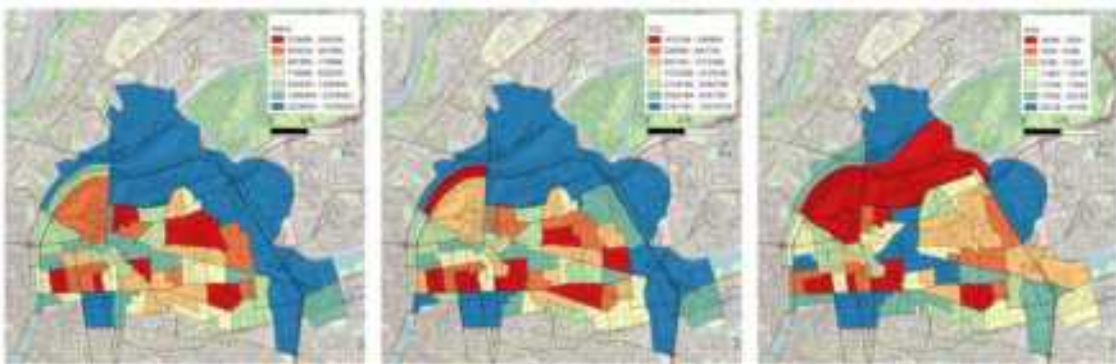


Figure 4: Spatial distribution of the gap of PM10 (left), CO2 (middle) and NOx (right) between the emissions computed from Symuvia and MATSim.

Discussion and conclusion

The first step to conceptualizing a modelling chain to investigate human exposure to traffic-related air pollution is coupling a traffic model with an emission model. Several kinds of models can be taken into consideration. Among the different aspects to consider, the traffic representation is a crucial feature. This paper compares traffic-related emissions computed from two completely independent models: the microscopic (Symuvia) and the mesoscopic (MATSim) traffic simulator. In order to avoid being affected by uncertainty due to emission models, we coupled both models with the emission model HBEFA, and we estimated the corresponding pollutant emissions.

First, we observe that traffic conditions are quite different between our models. The average speeds of vehicles are lower in Symuvia than in MATSim, and the number of vehicles over the network is higher in Symuvia than in MATSim. The total distance of vehicles for each 15 min time slot is similar. Those differences found reasons for the model concept of our models. In MATSim, each street is modelled as a queue in which vehicles must wait at least for the free travel time. The flow rate and storage capacity are limited to reproduce the congested behavior and therefore speeds are averaged over links. Otherwise, in Symuvia vehicles know at all times exactly designed. Average speeds are computed from instantaneous kinematics.

Statistical and spatial analyses show patterns and heterogeneities of total emission over the study area. Concerning the spatial distribution of pollutant emissions, we observe that the gap between our models differs for each pollutant. For example, in the north-east of our study area, we observe greater variation in PM10 and CO₂ emissions. This area represents the Lyon ring road, for which traffic behaviour is very different from that of the central zones. This area is also the limit of our study: that of the Symuvia simulation, but that of an extraction from the MATsim simulation. These two points need to be considered in greater detail to explain such differences. Pollutant emissions are higher for MATSim simulation and, for lower values, strongly correlated.

This work is based on a preliminary brick that assesses the impacts of traffic mitigation strategies on human exposure to traffic-related air emissions. Here our purpose is to explore the impact of two types of traffic models on emission rates. However, this work is open to plenty of perspectives. First, we want to improve our spatial analysis by testing different tessellations (e.g., regular grid and network-centered) to avoid spatial incoherencies. Second, in the following, we will consider time variations over the spatial tessellation to

understand the gap between models on the impact of different traffic conditions on emission rates. Finally, we will validate our results by comparing the completed modelling chain with empirical measurements.

Reference

- Apte, Joshua S., Michael Brauer, Aaron J. Cohen, Majid Ezzati, and C. Arden Lelieveld. 2018. "Ambient PM2.5 Reduces Global and Regional Life Expectancy." *Environmental Science & Technology Letters* 6: 50–51.
- Babbar, N. F., A. Gubria, T. Ig, and Monica Meneguzzi. 2022. "Exploring the Potential of Aggregated Traffic Models for Estimating Network-Wide Exposure." *Transportation Research Part D: Transport and Environment* 109.
- Beelen, Rob, Gerard Hoek, den Brandt Piet A. van, R. Alexandra Goldbohm, Paul Fischer, Leo J. Schouten, Michael Jerrett, Edward Hughes, Ben Armstrong, and Hedi Brunekreef. 2008. "Long-Term Effects of Traffic-Related Air Pollution on Mortality in a Dutch Cohort (NLCS-NL3 Study)." *Environmental Health Perspectives* 116 (2): 191–202.
- Castiglioni, Carlo. 2007. "Traffic Gridlock: Methodology, Modeling and Mitigation Approaches." *Transportation Research Part B: Methodological* 41 (1): 49–62.
- European Environmental Agency. 2022. "Air Quality in Europe 2022." *Hochburg*. <http://www.eea.europa.eu/publications/air-quality-in-europe-2022>.
- Fallah Shorshani, Masoud, Michel André, Céline Bonhomme, and Christian Seigneur. 2015. "Modeling Urban Air Pollution from Road Traffic: Air and Water Quality Techniques, Current Status and Future Prospects." *Environmental Modelling & Software* 64 (February): 102–23.
- Guttmann, Sascha, Arne Lyngfelt, Kai Nagel, and André Pyko. 2019. "Agent-Based Modeling to Estimate Exposures to Urban Air Pollution from Transportation: Exposure Disparities and Impacts of High-Resolution Data." *Computers, Environment and Urban Systems* 75 (May): 22–34.
- Horni, Andreas, Kai Nagel, and Kay W. Axhausen. 2016. *The Multi-Agent Transport Simulation MATSim*. Ubiquity Press. Ubiquity Press.
- Institute for Health Effects. 2022. "Health Effects Institute Annual Report 2022." <http://www.healtheffects.org/annual-report-2022>.
- Kuckelser, Benjamin. 2016. "Urban Model." In *The Multi-Agent Transport Simulation MATSim*.
- Leterrier, Ludovic. 2017. "Hybrid Approaches to the Selection of the Lightfoot–Whitham–Reimann Model." *Transportation Research Part B: Methodological* 41 (7): 701–9.
- Roswall, Nina, Jesse D. Thacher, Mikael Ögren, Andrei Pyko, Agneta Åkesson, Anna Oudin, Anne Tjønneland, et al. 2023. "Long-Term Exposure to Traffic Noise and Risk of Incident Colon Cancer: A Pooled Study of Eleven Nordic Cohorts." *Environmental Research* 224.

Primary and Secondary Aerosol Formation from Real Vehicle Exhausts – Development of an Equivalent Total Particle Emission Index Module for Air Quality Modelling Applications

P. Roldin^{1,2*}, M.P. Rissanen³, L. Pichelstorfer⁴, S. Iyer³, P. Karjalainen³, T. Olenius⁵, J. Pagels⁶, A. Oudin⁷, H. Timonen⁸, T. Rönkkö³, P. Aakko-Saksa⁹

¹Swedish Environmental Research Institute IVL, Malmö, 211 19, Sweden, pontus.roldin@ivl.se

²Department of Physics, Lund University, Lund, 221 00, Sweden

³Aerosol Physics Laboratory, Physics Unit, Tampere University, Tampere, 33720, Finland

⁴pi-numerics, Neumarkt am W., 5202, Austria

⁵ Swedish Meteorological and Hydrological Institute, Norrköping, 601 76, Sweden

⁶Ergonomics and Aerosol Technology, Department of Design Sciences, Lund University, Lund, 221 00, Sweden

⁷Planetary Health, Lund University, Lund, 221 00, Sweden

⁸Aerosol Composition Research, Finnish Meteorological Institute, Helsinki, 00101, Finland

⁹Emission Control and Sustainable Fuels Team, VTT Tech. Res. Centre of Finland Oy, Espoo, 02150, Finland

Introduction

In the Horizon Europe project PAREMPI (<https://parempi.eu/>) we will develop a vehicle emission equivalent total particle emission index module (ePMI). ePMI will be used for European and global scale chemistry transport model applications for improved air pollution population exposure and health impact assessments.

ePMI is intended to be a generally applicable module that can predict the atmospheric primary and secondary aerosol formation (number and mass concentrations) for a wide range of transport applications (road, marine, non-road, aviation), considering the ambient conditions, fuel and engine technologies.

This requires comprehensive knowledge about the tailpipe exhaust composition (primary particles and secondary aerosol precursors) during real driving conditions. In PAREMPI we are reviewing existing emission measurements and fill experimental gaps, especially for European wintertime conditions.

The real vehicle exhaust experiments are also complemented with molecular level oxidation flow-tube experiments for representative VOCs (e.g. benzene, toluene, xylene, naphthalene, dodecane, etc.) at high and low-NOx conditions.

Method

The development and evaluation of the ePMI module build on four connected modelling/experimental tasks:

1. Detailed molecular cluster dynamics and aerosol dynamics simulations of controlled exhaust dilution experiments. Vehicle exhaust particle toxicity have been linked to lung-deposited particle surface area, which is governed by the initial second to minute tailpipe to urban background primary particle number size distribution evolution.
2. Development of explicit gas-phase chemistry and secondary organic aerosol formation mechanisms for ~50 vehicle exhaust representative VOCs. This is based on dedicated laboratory oxidation flow-tube experiments and a theoretical framework for automated VOC oxidation mechanism generation (Pichelstorfer et al., 2023; Iyer et al., 2023).
3. Simulation of real vehicle exhaust oxidation flow reactor experiments, targeting the potential total aerosol mass formation for different vehicle/engine/fuel setups. This task relies on the experimental data and mechanisms developed in task 1 and 2.
4. Simulation of primary and secondary aerosol formation during real atmospheric conditions with a complex mixture of anthropogenic and biogenic aerosol precursors. The results are evaluated against atmospheric observations.

In the three first tasks the primary model tool used is the aerosol dynamics, gas- and particle-phase chemistry model for laboratory chamber experiments ADCHAM (Roldin et al., 2014; Roldin et al., 2019).

In task 1, we simulate of the molecular cluster dynamic ($\text{H}_2\text{SO}_4\text{-H}_2\text{O-NH}_3$) leading to new nanoparticles and aerosol dynamics (condensation, evaporation, coagulation) during the controlled vehicle exhaust dilution experiments (e.g. Karjalainen et al., 2016; Timonen et al., 2017). For this we use the novel cluster dynamics plugin module ClusterIn (Olenius and Roldin, 2022) in ADCHAM. The exhausts organic condensable vapor properties are constrained by comprehensive observations of gaseous compounds, semi-volatiles and non-volatiles, complemented by specific volatility basis set (VBS) distributions when needed, and optimized using ADCHAM to capture the full condensable primary organic aerosol dynamics (i.e. the semi-volatile primary particle formation, growth and evaporation dynamics during the complete exhaust dilution and cooling stages from the tailpipe to urban background conditions.

In task 2, explicit VOC gas-phase chemistry mechanisms are developed using the novel autoPRAM-fw mechanism generator (Pichelstorfer et al., 2023). AutoAPRAM-fw calculates the alkoxy/peroxy radical reaction pathways, rate coefficients and condensable vapor pure-liquid saturation vapor pressures using existing structural activity relationships. The generate alkoxy/peroxy radical autoxidation mechanisms (APRAM) are coupled to the Master Chemical Mechanism (MCM) (Jenkin et al., 1997; Saunders et al., 2003; Bloss et al., 2005; Jenkin et al., 2015) and evaluated using flow-tube and smog chamber experiments (Roldin et al., 2019; Iyer et al., 2023; Pichelstorfer et al., 2023). The complete APRAM+MCM schemes are then used in ADCHAM to reproduce the observed secondary organic aerosol formation (composition, number and mass concentrations) during existing and new VOC-oxidation experiments, in smog chambers and oxidation flow reactors (OFRs), covering a wide range of atmospheric relevant temperatures, UV-light intensities and NO_x levels.

In task 3 we will use the complete MCM-APRAM vehicle exhaust mechanism (> 50 secondary organic aerosol precursors) from task 2 in ADCHAM and simulate real vehicle exhaust OFR experiments. The aim is to close the gap between the observed and modelled secondary aerosol formation (organic and inorganic) formation in vehicle exhaust exposed to different stages of atmospheric ageing (cumulative OH exposure). The generate comprehensive model result datasets will be used to train a machine learning method to emulate the explicit model results on the time dependent formation of ultrafine primary and secondary aerosol particles and condensable vapors. The end product will be the equivalent total particle emission index module ePMI. ePMI will predict the secondary organic and inorganic PM_{2.5} and non-volatile and semi-volatile nano-particle formation rates based on a limited number of input variables ($[\text{NO}_x]$, $[\text{O}_3]$, temperature, UV-light, VOC mixtures, $[\text{NH}_3]$ etc.), which are standard variables provided by regional and global scale chemistry transport models (Figure 1).

In task 4 ePMI will be implemented and evaluated with the Lagrangian chemistry transport model ADCHEM (Roldin et al., 2011; Roldin et al., 2019). We will run ADCHEM both with the detailed near-explicit secondary aerosol formation chemistry schemes (MCM+APRAM) and with the simplified ePMI approach along air mass trajectories arriving at selected ACTRIS stations in Europe, covering the conditions during all seasons. The modelled secondary and primary aerosol particle mass and number concentrations will be evaluated with observations at the targeted stations. From this we will be able to judge the performance of ePMI against the benchmark MCM+APRAM secondary aerosol formation schemes, for realistic atmospheric conditions in Europe.

Finally, we will implement ePMI into the global chemistry transport model TM5 (Huijnen et al., 2010) and run the model for selected years, with and without emissions from road traffic, shipping, aviation and off-road vehicles. The modelled monthly average primary and secondary PM_{2.5}, PM₁₀ and particle number concentrations from the different model simulations will be used to estimate the vehicle fleet contribution to the PM and particle number concentration levels in Europe and globally. These results will also be used for health impact assessment and socio-economic cost analysis of PM_{2.5} originating from vehicle exhausts in Europe.

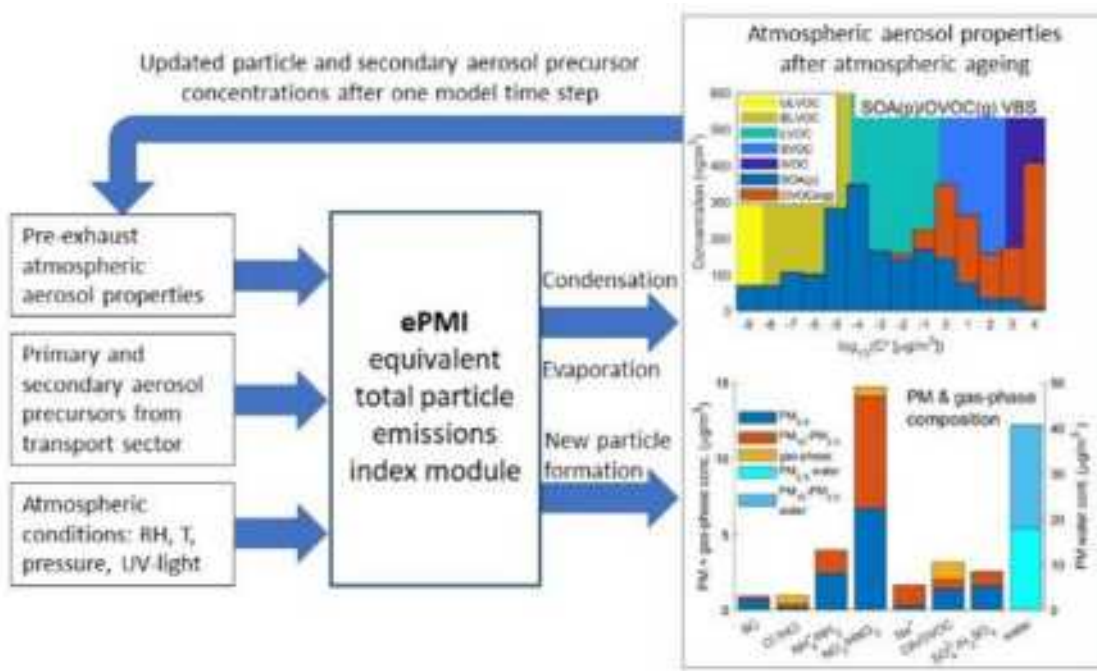


Figure 1: Illustration of the intended implementation of the equivalent total particle emission index module (ePMI) into a chemistry transport model.

Previous and initial results

Based on the methodology presented in task 2 and 4 we have previously developed near-explicit mechanism that are fully capable of capturing the observed highly oxygenated organic molecule (HOM) gas-phase mass spectrum and SOA formation for the monoterpenes α -pinene and β -caryene at a wide range of atmospheric conditions (temperatures, NO_x levels etc) (Roldin et al., 2019; Nie et al., 2023). In PAREMPI we are now focusing on the HOM and SOA potential of anthropogenic VOCs. The global emissions of the aromatic compounds benzene, toluene and xylenes account for >20 % of the total anthropogenic non-methane volatile organic compound (NMVOC) emissions (Yan et al., 2019). We have finalized a complete APRAM mechanism for benzene (Pichelstorfer et al., 2023). Based on flow reactor experiments, quantum chemical calculations and ADCHAM simulations we have recently shown that the molecular rearrangement of bicyclic peroxy radicals for aromatic compounds is a key route to HOM and secondary organic aerosol formation for toluene and that this likely also apply for many other aromatic compounds (Iyer et al., 2023). Including this new knowledge, APRAM mechanism for several aromatic compounds will be developed.

According to our simulations alkoxy/peroxy radical autoxidation can explain up to 100% of the benzene-SOA formed during the OH oxidation of benzene under low-NO_x conditions (Pichelstorfer et al., 2023) and for toluene at least 30-40 % of the observed SOA mass formation during OH oxidation of toluene can be explained by HOM formed rapidly after the molecular rearrangement of bicyclic peroxy radicals.

During the conference we will present the general methodology behind the ePMI module development and show preliminary results from simulations of SOA formation from representative aromatic VOCs (benzene, toluene) and molecular cluster dynamics and aerosol dynamics simulations of controlled exhaust dilution experiments from previous projects.

Acknowledgements

This work was supported by the European Union's Horizon Europe research and innovation program (EU) under grant agreement No 01096133 (PAREMPI: Particle emission prevention and impact: from real-world emissions of traffic to secondary PM of urban air).

References

- Bloss, C., Wagner, V., Jenkin, M. E., Volkamer, R., Bloss, W. J., Lee, J. D., Heard, D. E., Wirtz, K., Martin-Reviejo, M., Rea, G., Wenger, J. C., and Pilling, M. J. (2005). Development of a detailed chemical mechanism (MCMv3.1) for the atmospheric oxidation of aromatic hydrocarbons, *Atmos. Chem. Phys.*, 5, 641–664, <https://doi.org/10.5194/acp-5-641-2005>.
- Huijnen, V., Williams, J., van Weele, M., van Noije, T., Krol, M., Dentener, F., Segers, A., Houweling, S., Peters, W., de Laat, J., Boersma, F., Bergamaschi, P., van Velthoven, P., Le Sager, P., Eskes, H., Alkemade, F., Scheele, R., Nédélec, P., and Pätz, H.-W. (2010). The global chemistry transport model TM5: description and evaluation of the tropospheric chemistry version 3.0, *Geosci. Model Dev.*, 3, 445–473, <https://doi.org/10.5194/gmd-3-445-2010>.
- Iyer, S., Kumar, A., Savolainen, A., Barua, S., Daub, C., Pichelstorfer, L., Roldin, P., Garmash, O., Seal, P., Kurtén, T. and Rissanen, M. P. (2023). Molecular rearrangement of bicyclic peroxy radicals is a key route to aerosol from aromatics. *Nat Commun*, 14, <https://doi.org/10.1038/s41467-023-40675-2>.
- Jenkin, M. E., Saunders, S. M., and Pilling, M. J. (1997). The tropospheric degradation of volatile organic compounds: a protocol for mechanism development, *Atmospheric Environment*, 31, 81–104, [https://doi.org/10.1016/S1352-2310\(96\)00105-7](https://doi.org/10.1016/S1352-2310(96)00105-7).
- Jenkin, M. E., Young, J. C., and Rickard, A. R. (2015). The MCM v3.3.1 degradation scheme for isoprene, *Atmos. Chem. Phys.*, 15, 11433–11459, <https://doi.org/10.5194/acp-15-11433-2015>.
- Karjalainen, P., Timonen, H., Saukko, E., Kuuluvainen, H., Saarikoski, S., Aakko-Saksa, P., Murtonen, T., Bloss, M., Dal Maso, M., Simonen, P., Ahlberg, E., Svenningsson, B., Brune, W. H., Hillamo, R., Keskinen, J., and Rönkkö, T. (2016). Time-resolved characterization of primary particle emissions and secondary particle formation from a modern gasoline passenger car, *Atmos. Chem. Phys.*, 16, 8559–8570, <https://doi.org/10.5194/acp-16-8559-2016>.
- Nie, W., Yan, C., Yang, L., Roldin, P. et al. (2023). NO at low concentration can enhance the formation of highly oxygenated biogenic molecules in the atmosphere, *Nat Commun* 14, 3347 (2023). <https://doi.org/10.1038/s41467-023-39066-4>.
- Olenius, T., Roldin, P. (2022). Role of gas–molecular cluster–aerosol dynamics in atmospheric new-particle formation. *Sci Rep* 12, 10135, <https://doi.org/10.1038/s41598-022-14525-y>
- Pichelstorfer, L., Roldin, P., Rissanen, M., Hyttinen, N., Garmash, O., Xavier, C., Zhou, P., Clusius, P., Foreback, B., Golin Almeida, T., Deng, C., Baykara, M., Kurten, T., and Boy, M. (2023). Towards a mechanistic description of autoxidation chemistry: from precursors to atmospheric implications, *EGUsphere* [preprint], <https://doi.org/10.5194/egusphere-2023-1415>.
- Roldin, P., Swietlicki, E., Schurgers, G., Arneth, A., Lehtinen, K. E. J., Boy, M., and Kulmala, M. (2011). Development and evaluation of the aerosol dynamics and gas phase chemistry model ADCHEM, *Atmos. Chem. Phys.*, 11, 5867–5896, <https://doi.org/10.5194/acp-11-5867-2011>.
- Roldin, P., Eriksson, A. C., Nordin, E. Z., Hermansson, E., Mogensen, D., Rusanen, A., Boy, M., Swietlicki, E., Svenningsson, B., Zelenyuk, A., and Pagels, J. (2014). Modelling non-equilibrium secondary organic aerosol formation and evaporation with the aerosol dynamics, gas- and particle-phase chemistry kinetic multilayer model ADCHAM, *Atmos. Chem. Phys.*, 14, 7953–7993, <https://doi.org/10.5194/acp-14-7953-2014>.
- Roldin, P., Ehn, M., Kurtén, T., Olenius, T., Rissanen, M. P., Sarnela, N., Elm, J., Rantala, P., Hao, L., Hyttinen, N., Heikkilä, L., Worsnop, D. R., Pichelstorfer, L., Xavier, C., Clusius, P., Öström, E., Petäjä, T., Kulmala, M., Vehkamäki, H., Virtanen, A., Riipinen, I., and Boy, M (2019). The role of highly oxygenated organic molecules in the Boreal aerosol–cloud climate system, *Nat Commun*, 10, 4370, <https://doi.org/10.1038/s41467-019-12338-8>.
- Saunders, S. M., Jenkin, M. E., Derwent, R. G., and Pilling, M. J. (2003). Protocol for the development of the Master Chemical Mechanism, MCM v3 (Part A): tropospheric degradation of non-aromatic volatile organic compounds, *Atmos. Chem. Phys.*, 3, 161–180, <https://doi.org/10.5194/acp-3-161-2003>.
- Timonen, H., Karjalainen, P., Saukko, E., Saarikoski, S., Aakko-Saksa, P., Simonen, P., Murtonen, T., Dal Maso, M., Kuuluvainen, H., Bloss, M., Ahlberg, E., Svenningsson, B., Pagels, J., Brune, W. H., Keskinen, J., Worsnop, D. R., Hillamo, R., and Rönkkö, T. (2017). Influence of fuel ethanol content on primary emissions and secondary aerosol formation potential for a modern flex-fuel gasoline vehicle, *Atmos. Chem. Phys.*, 17, 5311–5329, <https://doi.org/10.5194/acp-17-5311-2017>.
- Yan, Y., Cabrera-Perez, D., Lin, J., Pozzer, A., Hu, L., Millet, D. B., Porter, W. C., and Lelieveld, J. (2019). Global tropospheric effects of aromatic chemistry with the SAPRC-11 mechanism implemented in GEOS-Chem version 9-02, *Geosci. Model Dev.*, 12, 111–130, <https://doi.org/10.5194/gmd-12-111-2019>.

Emission savings potential of ecodriving based on over 1500 hours of driving data from 5 countries. Findings from the uCARE project

Brian Cox^{1*}, Benedikt Notter¹, Martin Opetnik², Leo D'Amato³

*brian.cox@infras.ch

¹INFRAS, Bern, 3012, Switzerland

²Institute of Thermodynamics and Sustainable Propulsion Systems, TU Graz, Graz, 8010, Austria

³ETEC Department & MOBI Research Group, Vrije Universiteit Brussel, Brussels, 1050, Belgium

Introduction

Ecodriving training can be an effective way to achieve reductions in average driving emissions and energy consumption on a timescale much faster than fleet renewal. In this contribution, we estimate the potential emission savings achievable by large-scale training of European drivers in 10 different ecodriving interventions. This analysis is based on over 1500 hours of measured driving data from 5 countries, including measurements and surveys taken from the same drivers before and after ecodriving training. We examine the willingness and ability of drivers to implement ecodriving practices to reduce their emissions. We also use these inputs to generalise results to estimate best-case and most-likely emission savings potentials for average European vehicles and driving situations.

This work was done within work package 4 of the uCARE project, which was a Horizon 2020 project funded by the European Union that ran between 2019 and 2022 (www.project-ucare.eu).

Methods

Description of interventions

Table 1 lists the interventions included in the uCARE project. We refer to the implementation of these interventions as "ecodriving", which we characterize as changing driving behavior with the goal of reducing not only fuel consumption and CO₂ emissions, but also reducing pollutant emissions.

Table 1 Summary of individual interventions

Intervention	Description
Default	Normal or default driving by untrained drivers
Tire	Drivers are encouraged to monitor their tire inflation and to use winter tires only when appropriate. They are also asked to consider the most efficient tires possible when choosing replacements.
Load	Drivers are encouraged to remove unneeded roof boxes and bicycle racks etc. from their vehicles. Furthermore, drivers are asked to remove unneeded things from their vehicle, as they increase the mass that needs to be carried around, making the vehicle work harder.
AC	Drivers are asked to reduce their use of air conditioning and other auxiliary devices, such as seat heaters to only when they are really needed
Shift	Drivers are given tips on how to improve their shifting behavior to minimise fuel consumption and pollutant emissions.
Speed	Drivers are asked to keep their maximum speed below 120 km/h.
Acceleration	Drivers are encouraged to accelerate strongly (but not maximally) until speeds of around 50 km/h and to limit their acceleration above this speed.
Brake	Drivers are asked to brake gently and to use engine brakes where possible. Furthermore, drivers are asked to look ahead and try to avoid slowing down only to have to speed up again. For example, when approaching a red light that is expected to turn green such as better to slow down earlier and more gently so that breaking emissions are reduced and the need to reaccelerate is reduced.
Idling	Drivers are asked to turn their engines off when they expect to remain stopped for longer than 30 seconds.
Traffic	Drivers are encouraged to plan their routes considering how many other cars are on the road. Perhaps the trip can wait until the traffic is reduced, or perhaps a different route can be taken where traffic flows more smoothly.
Cold start	Drivers are asked to chain their trips together to reduce the number of cold starts that the vehicle makes.

Input from measured driver behaviour

To measure the ability of drivers to implement these interventions, pilots were run with a total of 72 drivers in Cyprus, Austria, Belgium, the Netherlands, and the UK, collecting over 1700 hours of second-by-second driving data²⁰. Before starting the pilots, drivers were first asked to fill out a survey to provide a baseline of their motivation and understanding of ecodriving. At this time a device was installed into their vehicle that measures their driving behavior. This device allowed 1 Hz resolution recording of driving parameters such as location, speed, acceleration, and gear choice, and uploaded the data to an online platform, the uCARE website. After this, drivers were recorded for a certain amount of time while behaving normally. This provides the baseline against which the drivers performance after ecodriving training can be compared.

At the end of the base period, the drivers were provided with training in the ecodriving interventions listed in Table 1. They were also given access to a cell phone application and the uCARE website, which showed them a log of all their trips and provided feedback on their driving style and how they could improve their driving to reduce emissions even further. After the ecodriving training the drivers were asked to implement the interventions listed in Table 1 while going about their daily driving and to regularly consult the website to monitor their progress in implementing the principles of ecodriving. After several weeks (or, in some pilots, much longer) the pilot ended, and the driver was given a final survey that asked them about their experiences. They were asked questions about how well they thought they implemented ecodriving as well as how difficult they found it to implement the interventions.

²⁰ Out of 72 total participants, 41 drivers completed both the before and after surveys. Driving data from both before and after driver training was successfully gathered for 45 drivers, totalling over 1500 hours of useable data.

For more information about the pilots, see uCARe deliverables 3.4 (Geivanidis, Jamson, & Forward, 2022), 3.5 (Geivanidis, Fragkiadoulakis, & Bidios, 2022), and 3.6 (Geivanidis, Jamson, & Forward, 2022) from the uCARe project (www.project-ucare.eu/).

Modelling potential emission savings from changes in driver behaviour

To be able to make the step from changes in driver behaviour to changes in driving emissions, the PHEM tool is used. The PHEM tool is a vehicle simulation tool developed by TU Graz. PHEM stands for Passenger car and Heavy-duty Emission Model and the tool has been in development since the late 1990s. In a nutshell, the PHEM tool takes information describing a vehicle (such as weight, rolling resistance, air resistance, and specific engine emission maps), and driving information (such as velocity, engine speed, road gradient) to calculate the fuel consumption and emissions associated with that trip as driven by that vehicle.

The main idea in this part of the uCARe project was to create the uCARe PHEM tool (Opetnik & Hausberger, 2022). This update to the tool allows calculation of emissions from trips as if they were driven by a professional driver practicing perfect ecodriving: the maximum acceleration is reduced, maximum speed is limited to 120 km/h, and braking behaviour and gear selection are optimised to reduce emissions and fuel consumption. Calculation input parameters such as vehicle weight, aerodynamic drag and tyre rolling resistance coefficients, start-stop behaviour, and auxiliary energy demand can also be modified to represent other ecodriving interventions.

The emissions savings potential of ecodriving interventions can be estimated by comparing the emissions results of the uCARe PHEM tool with default inputs to those calculated with input parameters modified to represent ecodriving interventions. For each intervention, we model both a best-case and a most-likely implementation of ecodriving. The best-case implementation is based on the upper limit of what is reasonably possible for a driver to implement. The most-likely case is based on experience gained from the pilots regarding how willing and successful drivers were in implementing each intervention.

Where possible, we use measured pilot data for the creation of the most-likely implementations²¹. For interventions where direct measurements were impossible (for example, we were unable to take daily tire pressure readings on the participants' vehicles), we relied on the survey results of the drivers to estimate their own compliance to the ecodriving protocols. In some cases, we also extended the pilot survey results with other surveys performed in the uCARe project (Geivanidis, Jamson, & Forward, 2022).

Interested readers are pointed to deliverable 4.2 from the uCARe project (D'Amore, Costa, Messagie, Cox, & Notter, 2022), which describes this methodology in much more detail.

Generalising results

To generalise the knowledge gained in the pilots, we used the uCARe PHEM tool to calculate emissions from representative driving cycles driven by a wide variety of passenger vehicle types with and without ecodriving interventions. For the calculations with ecodriving interventions we used both the best-case and the most-likely implementations as described above.

27 passenger car types (petrol, diesel, and CNG fuel types with emission standards ranging from pre-Euro to Euro 6d) were modelled in the uCARe PHEM tool for each intervention, as well as combinations of interventions. To ensure that a complete and representative set of driving situations were considered, all 2345 possible combinations of driving cycles and road gradients from the Handbook of Emission Factors for Road Transport (HBEFA) (INFRAS, TUG, ifeu, HSDAC, WSP, 2021) were used as the calculation basis in the uCARe PHEM tool. These vehicles and driving cycles are also used as the basis to calculate the emission factors for the HBEFA database. The driving cycles are used to represent different traffic situations, and these traffic situations are weighted for each country to represent average driving conditions.

We estimate the European average shares of driving on each road type, gradient, speed limit, and level of service²² based average traffic situation data from the Handbook for Emission Factors (HBEFA) version 4.2. This data source includes highly detailed information on the vehicle fleets and shares of traffic situations of

²¹ For example, the best-case implementation of the ecodriving intervention for the 120 km/h speed limit was based on the data from the pilot survey. We used the data from the pilot survey to create a new maximum acceleration curve for the PHEM Tool. For the most-likely implementation, we created a new maximum acceleration curve using the 90th percentile of what trained drivers were able to accomplish in the pilots.

²² Level of Service (LOS) defines the level of congestion on a road, which has a significant influence on driving behaviours such as average speed, average acceleration, and time spent idling. The LOS ranges from Freeflow, which represents low traffic volume and smoothly flowing traffic at speeds near the speed limit, to Stop+go_II, which represents gridlock conditions.

Germany, France, Austria, Sweden, Norway, and Switzerland. We assume that the weighted average shares of traffic situations of the six countries in HBEFA can be used as an approximation for the European average.

We also estimate the average shares in the total mileage of the European passenger car fleet using detailed information from the HBEFA version 4.2. This detailed fleet information is scaled to be more representative for Europe as a whole by using data from EuroStat (eurostat, 2022) to correct for the average age distribution of the fleet as well as shares of gasoline, CNG, and diesel vehicles across Europe.

Results

The overall relative emission savings potential of ecodriving compared to normal driving are shown in Figure 1. These results are for an average European car in the year 2020 under an average mix of driving conditions, with all ecodriving interventions applied. These results show that the most-likely implementation of ecodriving (orange bars) could lead to 10-20% savings for emissions of CO₂, NO_x, CO, and PM₁₀. In the best-case, the savings could be up to 30-40% for most pollutants, and over 50% for non-exhaust PM₁₀ emissions. We note that the uncertainty for non-exhaust PM₁₀ emissions is large as the method is still in development.

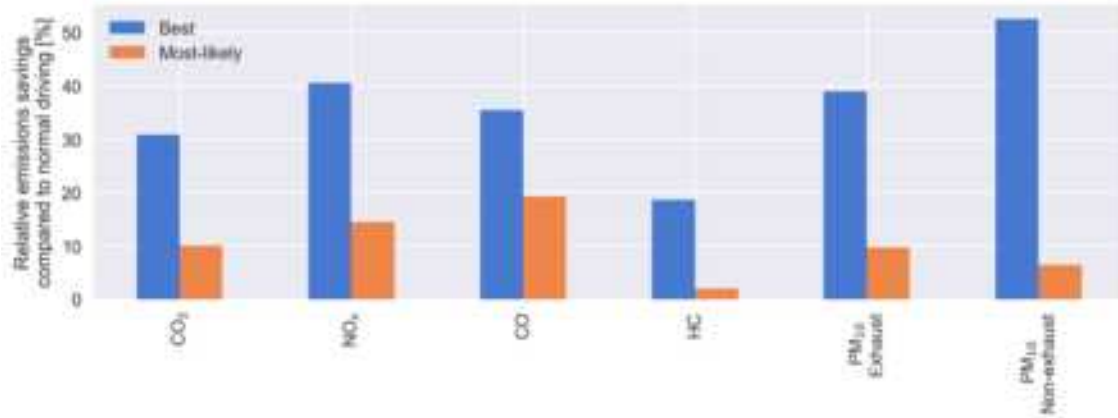


Figure 1 Relative emission savings potential of ecodriving compared to normal driving if all interventions are implemented. Results are for an average European vehicle in 2020 under average driving conditions.

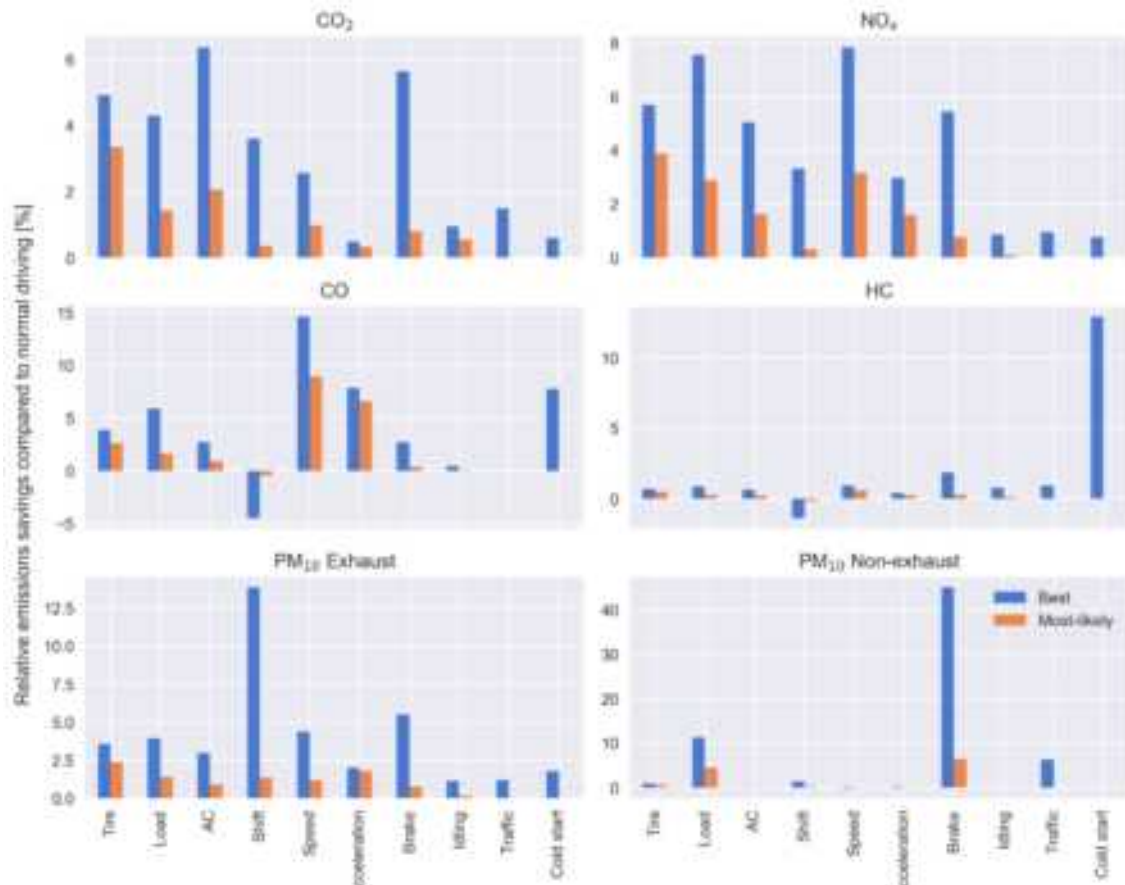
Figure 2 compares the relative emission savings potential of each intervention for an average European vehicle in 2020 under an average mix of driving conditions. Each panel shows results for a different substance. The first five panels show direct exhaust emissions from the vehicle, while the bottom right panel shows PM₁₀ non-exhaust emissions, which include emissions from both brake and tire wear. The y-axis represents the emission savings potential of each individual intervention relative to normal driving, with positive values indicating emission savings compared to untrained drivers. The blue and orange bars show the results for the best-case and most-likely implementations of each intervention respectively. The results for the implementation of all interventions simultaneously are shown in Figure 1²³. Results for different vehicle types are shown in Figure 3.

Reduction potential for CO₂ emissions and fuel consumption are found mostly for the interventions Tyre, AC²⁴, Load, and Speed. The Tyre and AC interventions contribute well over half of the improvements in the most-likely case. NO_x reductions are found to be largest for the interventions Tire, Speed, and Load, with contributions from Acceleration and AC. CO emission improvements come nearly exclusively from the interventions Speed and Acceleration. Reductions in HC emissions in the best-case are most affected by reducing the number of cold starts, but no changes in this driver behaviour were found in the pilots, so the most-likely improvements to HC emissions remain quite small. Reductions in PM₁₀ emissions are found to result from small improvements across seven out of the ten interventions examined, with the largest improvements coming from the Tyre intervention. Non-exhaust PM₁₀ emission reductions are found to come mostly from the Load and Brake interventions. In the best-case implementation, some improvements are also expected due to the intervention to avoid heavy traffic, as this reduces driving situations where lots of braking is required.

²³ We note that the overall improvement potential is slightly less than the sum of the relative improvements, as some effects overlap. For example, the improvement potential of removing roof racks is slightly reduced when drivers avoid driving at very high speeds and vice versa.

²⁴ The emissions savings potential for the best-case AC intervention for more recent Euro classes are very optimistic and should be considered an upper bound of potential savings.

Figure 2 Relative improvement of each intervention compared to normal driving for an average 2020 European



vehicle in average driving conditions. The blue and orange bars represent results for the best-case and most-likely implementations of each intervention respectively.

Figure 3 shows the absolute emissions in grams per kilometer for normal driving (bars) overlaid with results for the best-case (light dots) and most-likely (dark dots) implementation of all interventions applied together. The six panels show results for different pollutants, and the x-axis contains selected vehicle types and the fleet averages in 2020, 2025, and 2030. The blue colors represent average European vehicles in the years 2020, 2025, and 2030, while the orange and green colors represent diesel and gasoline vehicles, respectively.

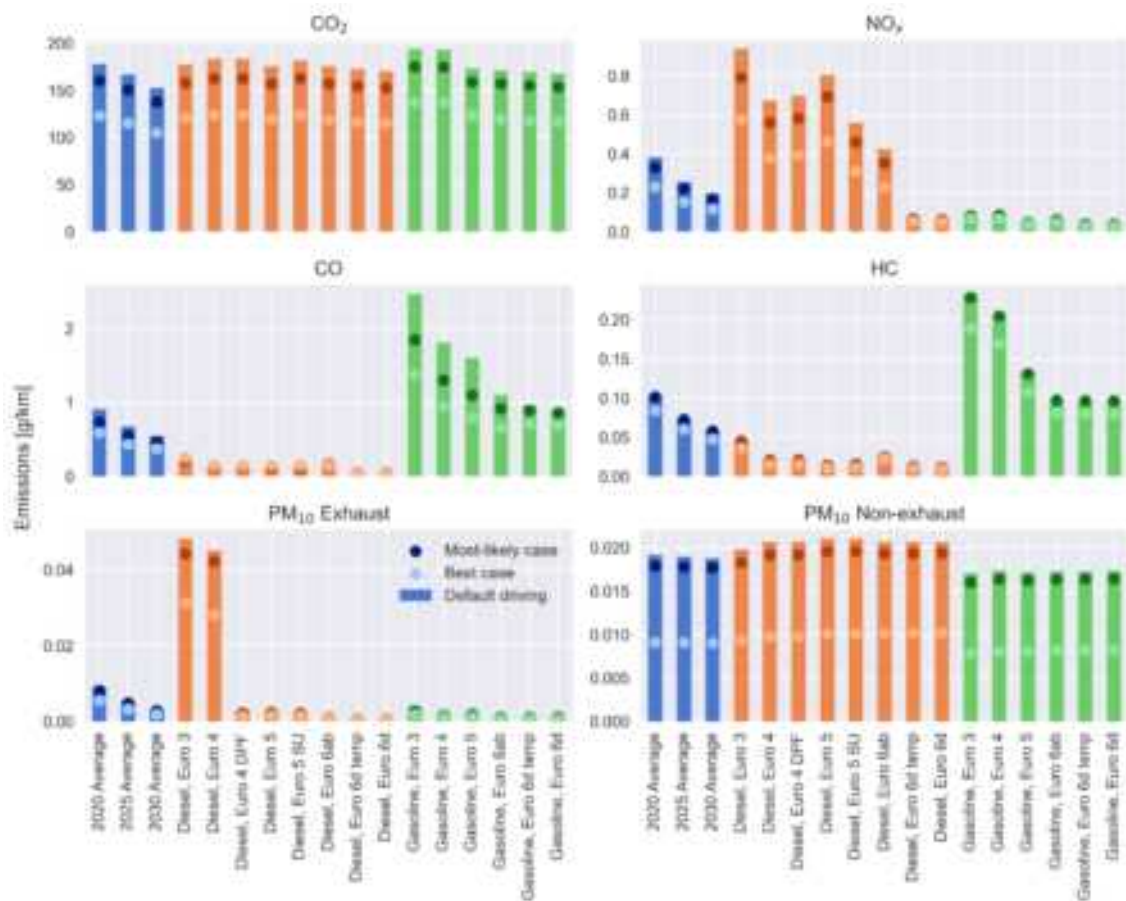


Figure 3 Emissions per kilometer in g/km if all interventions are applied concurrently. Bars represent default driving, while dots represent the best-case and most-likely implementation of each intervention.

The overall CO₂ emission improvement potentials are similar across vehicle types: around 50-60 g/km in the best-case, and 15-20 g/km in the most-likely case. The relative contribution of each intervention varies across vehicle types. For example, earlier vehicles generally show less benefit from reducing AC use (as air conditioning and other power consuming auxiliaries are less common among these vehicles) but show relatively greater potential improvements due to interventions that reduce maximum speed (due to generally higher aerodynamic drag coefficients) or improvement regarding acceleration and shifting. Complete results disaggregated by vehicle type, intervention, and traffic situation are available in Appendix C of uCARe deliverable 4.2 (D'Amore, Costa, Messagie, Cox, & Notter, 2022).

The improvement potential for pollutant emissions depends strongly on the vehicle fuel type, as well as the Euro class. For example, diesel vehicles with emission standards prior to Euro 6d-temp show the largest potential improvement for NO_x. The improvement potential for carbon monoxide (CO) and unburned hydrocarbons (HC) is largest for gasoline vehicles, especially earlier Euro classes. The largest driver in reducing carbon monoxide emissions is found to be the improvement in acceleration behaviour and reduction of maximum speed. For hydrocarbon emissions, the improvement potential is found to be overwhelmingly dominated by the potential to reduce the number of cold starts by trip chaining and other measures. The overall improvement potential for CO and HC emissions from diesel vehicles is found to be near zero or even slightly negative. This is because the ideal shifting intervention slightly increases the emissions of these two pollutants for diesel vehicles²⁵. While an increase in the emission of these pollutants is certainly not desirable, the modified shifting performance leads to significant reductions in CO₂, NO_x and PM₁₀ emissions for these vehicles at the expense of small increases in CO and HC emissions.

²⁵ The optimal shifting intervention is designed to seek out the optimum gear to minimize the sum of costs associated with fuel and the external costs of the emissions. See uCARe deliverable 2.2 for more information.

Absolute exhaust PM₁₀ emission reduction potential is dominated by earlier diesel vehicles without particle filters. The overall PM₁₀ emissions for all European passenger cars could have been reduced by over 15% by improving the shifting behaviour of only drivers of older diesel cars without particle filters in the best-case. However, drivers were found to have difficulty in meeting the ideal shifting criteria, so the overall improvement due to shifting behaviour was less than 2% in the most-likely case. This is still a significant improvement potential considering that the share of these vehicles in the overall fleet is comparatively small. Averaged over all vehicle types and considering all interventions, drivers are expected to be able to reduce their PM₁₀ emissions by about 10% on average in the most-likely case.

The improvement potential for PM₁₀ non-exhaust emissions is dominated by potential reductions in brake wear emissions due to improved braking performance. The best-case implementation of this intervention is very optimistic and assumes that all heavy braking events can be avoided, which is unlikely to be possible during real driving. In the pilots, real drivers were found to be able to achieve less than 15% of the ideal braking reduction potential, which explains the large difference between the results for the best-case and most-likely implementations of this intervention.

It is noted that the fleet average reduction potentials for all pollutants are found to decrease in the future. This is because, on the one hand, the future fleet has a higher share of more modern vehicles, which generally have lower improvement potentials, and, on the other hand, because the future fleet has a higher share of alternative powertrains, which have no improvement potential for exhaust pollutant and CO₂ emissions. However, the non-exhaust emissions and energy consumption (not calculated here) can still be improved by following these interventions with alternative drivetrain vehicles.

Discussion

While the method of modelling emission reductions using representative driving cycles provides an excellent way to estimate the best-case emission savings potential of ecodriving, we faced one major limitation in determining the most-likely implementations that should be discussed. This limitation is that the changes to the input parameters to the uCARe PHEM tool reflecting most-likely changes to driving style must be determined correctly. For interventions where driver performance can be directly calculated from driving data this is comparatively straight forward. However, for several interventions, we were forced to rely on self-assessments from the drivers, which were found in this project to be unreliable when these self-assessments could be verified with measured data. Not only were drivers unable to reliably determine if they had made positive improvements in their driver training, but it was also impossible to quantify the magnitude of this improvement. This forced us to rely heavily on expert judgement in determining the most-likely improvements to driving. This is one area where further research is needed. We further note that the two interventions that generally show the highest promise of emission savings in the most-likely case: Tire and AC, could not be quantified using the driving data from the pilots. Although we conducted an additional survey to try to get an accurate estimation of potential behavioural change for these interventions, uncertainty in the real-world behavioural change remains high, which means that the uncertainty of the most-likely emission savings potential also remains high.

Conclusions

In the best-case, ecodriving could reduce average emission factors of European passenger cars by 30-40% for most pollutants. However, in the most-likely case this improvement is expected to be only 10-20%. The potential emission savings in the most-likely case are lower than the best-case emission savings because of two main factors. The first is that not all drivers are willing to change their driving behavior. An example of this could be that some drivers really enjoy the feeling of hard accelerations and high engine speeds and are not *willing* to give up this driving experience in exchange for a reduction in fuel consumption and emissions. In general, we found that two-thirds to three-quarters of drivers in the pilots were willing to change their driving behavior and showed quantifiable performance improvements in most of the measured metrics. We note that the drivers willing to participate in the pilots probably show above average motivation to improve their driving behavior and that achieving this participation rate among all European drivers could be difficult. The second, and perhaps more important, reason that the most-likely savings are lower than the best-case is that drivers are not always *able* to reach the theoretical optimal performance of ecodriving. Examples of this could be that achieving the ideal shifting performance is too complex for some drivers or that it is very difficult to achieve optimal braking behaviour in the uncertain conditions of real driving and that some hard braking events are unavoidable. Moreover, the frequency of such events in real traffic conditions are unknown. We found that the drivers in the pilots often had great difficulty achieving the optimal driving styles that would be associated with best-case emission savings in real life driving situations. In many cases, drivers were able to achieve less than 10% of the improvements that would be associated with the theoretical ideal.

While the uCARe project provided many useful insights into the potential of ecodriving to reduce emissions, there is still much room for further research into how to make ecodriving training more effective to A) motivate

a greater share of drivers to implement ecodriving practices and B) to help drivers move their ecodriving performance closer to the theoretical ideal

Acknowledgements

This work was completed in the uCARe project (GA 815002). The co-authors would like to acknowledge the contribution of other participants in the uCARe project, especially: Stefan Hausberger, Martin Dippold, Savas Geivanidis, Pavlos Fragkiadoulakis, Samantha Jamson, Daniele Costa, Michal Vojtisek, Mats Gustafsson, Norbert Lijsterink, Geoff Holmes, and Paul Tilanus.

This extended abstract is adapted from Deliverable D4.4 from the uCARe project (Cox & Notter, 2022).

References

- Cox, B., & Notter, B. (2022). D4.4: Report targeted towards policy makers, on the impact of measures. Project uCARe.
- D'Amore, L., Costa, D., Messagie, M., Cox, B., & Notter, B. (2022). D4.2: Updated ranking of measures, reflecting likeliness of success. Project uCARe.
- eurostat. (2022). eurostat statistics database. (European Commission) Retrieved 2022, from <https://ec.europa.eu/eurostat/web/main/data/database>
- Geivanidis, S., Fragkiadoulakis, P., & Bidios, P. (2022). D3.5: Final results of the pilot projects in terms of achieved emission reduction. Project uCARe.
- Geivanidis, S., Jamson, S., & Forward, S. (2022). D3.4: Final description of intervention strategies and methodological details for implementation of measures. Project uCARe.
- Geivanidis, S., Jamson, S., & Forward, S. (2022). D3.6: Final results of the pilot projects in terms of user feedback and user awareness. Project uCARe.
- INFRAS, TUG, ifeu, HSDAC, WSP. (2021). HBEFA. Handbook of emission factors for road transport 4.2.
- Opelnik, M., & Hausberger, S. (2022). Deliverable D2.2: Software for online and for trip analysis in post-processing with car owner guidelines. Project uCARe.

Impact of uCARe measures on air quality in selected cities

E. Johansson^{1*}, R. van Gijlswijk², B. Schäppi³ and B. Notter³

¹ IVL Swedish Environmental Research Institute, Gothenburg, SE-41133, Sweden, emelie.mm.johansson@ivl.se

² Netherlands Organisation for Applied Scientific Research TNO, 2595DA The Hague, The Netherlands

³ INFRAS, Consulting, Analysis & Research, 8045 Zurich, Switzerland

Introduction

With approximately four million annual premature deaths due to outdoor pollution, improvement of air quality has become one of society's main challenges (World Health Organization, 2022). In Europe traffic and transport have a large effect on air quality, specifically passenger cars and commercial vehicles and to a lesser extent non-road mobile machinery. While technical improvements and more stringent legislation have led to a significant improvement of air quality, traffic and transport emissions are still a major contributor to air pollutant concentrations in cities, and air quality along roads with heavy traffic is still poor. Although the use of electric and other zero-emission propulsion technologies may drastically reduce the pollutant exhaust emissions from traffic, the slow introduction of such vehicles as well as the trend of increasing vehicle lifetimes means that vehicles with internal combustion engines are expected to dominate the fleet beyond 2030. In the uCARe project, opportunities are investigated to reduce emissions from vehicles, not by improving vehicle technology, but by actively involving vehicle users and enabling their contribution to clean driving by giving feedback on their driving style and vehicle use pattern. In this deliverable, the effect of these behavioural measures on local air quality in three different cities is quantified.

Study areas and scenarios

The three studied cities were Zurich, Gothenburg and Amsterdam. The number of inhabitants, and also the total number of vehicle kilometres, is largest in Amsterdam, then Gothenburg and Zurich. Large emission sources are for all three cities road transportation, industrial activities, and households. Gothenburg and Amsterdam also have large harbours, which contribute to the emissions. For each city, three different emission scenarios were investigated for two different years, resulting in six scenarios for each city. The studied years are 2019/2020 (2019 for Gothenburg and 2020 without the pandemic for the other cities) and 2030.

The emission scenarios consist of a baseline scenario (which assumes business as usual), a best-case scenario, which assumed an ideal implementation of the studied uCARe measures, and a most-likely scenario, which assumed a more likely implementation of the measures.

The studied pollutants were nitrogen dioxide (NO_2) and particulate matter (PM_{10} and $\text{PM}_{2.5}$). For Gothenburg, PM_{10} was not included, due to lack of emission factors. Therefore, NO_2 and $\text{PM}_{2.5}$ will be the focus here.

Models

For each city a different model has been applied. For Zurich the dispersion model "ReLuMep" (developed by INFRAS and Meteotest) was applied. The latest version stems from July 2020 (Heldstab et al., 2020). For Gothenburg, ADMS-Urban was used (Cambridge Environmental Research Consultants, 2020), and for Amsterdam, the air quality model applied was an interactive version of SRM-1 and SRM-2 (van der Velde and Wesseling, 2020). Since all the models are Gaussian/quasi-Gaussian, the emission dispersion was modelled in the same way for all cities.

For Gothenburg, the only emissions included were road transport emissions, while for Zurich and Amsterdam, other emission sources such as industrial processes and households were also accounted for. This could lead to an underestimation of the air pollutant concentration in Gothenburg, but the contribution of these other emissions is assumed to be relatively small along the road network. The road emissions are specified on a grid, and this grid has a finer resolution for Zurich and Amsterdam, than for Gothenburg. For Zurich, the resolution is 20 m for road transportation and 100 m for all other emission sources. For Amsterdam, the resolution is 10 m next to urban roads and larger in other areas, while the resolution is 50 m for Gothenburg. For Amsterdam, the effect of street canyons was included, meaning that emission dispersion could be limited by buildings.

All three models take roughly the same meteorological input data, and the chemistry scheme is the same (the photochemical reactions between NO , NO_2 and O_3).

Road transport input data

Two different road transport emission models were used to calculate the emission factors. For Gothenburg and Zurich, the Handbook of Emission Factors for Road Transport, Version 4.2 (Notter et al., 2022) was used. For Amsterdam, VERSIT+ was used, emission factors SRM version 2022-03-29, method description report version 2022 (Geilenkirchen et al., 2022).

~~For all case studies we calculated “Delta emission factors” (delta EF) were derived, where the relative improvements are expressed in % of the default average emission factors for passenger cars, for the two evaluated scenarios. These two scenarios are the ‘Best-case’ and the ‘Most-likely’ scenarios described above and correspond to those evaluated in Deliverable 4.2 (D4.2) of the uCARe research program (D’Amore et al., 2022). In Table 1, different interventions are listed. These interventions are implemented to a perfect extent in the ‘best-case’ scenario, and to a more likely extent in the ‘most-likely’ scenario. The extent is based on comparisons of driving patterns before and after training in the uCARe pilot studies and on surveys.~~

Emission factors from HBEFA 4.2 were corrected by considering effects from aging and temperature, and then the delta EFs were applied to these corrected emission factors for each road link, resulting in absolute emission factors for each road link.

Table 1: Summary of individual interventions and intervention groups.

Intervention	Abbreviation	Intervention group	Overall intervention
Default driving by untrained drivers	Default	Default	Default
Correct tire pressure/use most efficient tires	Tire	Maintenance	Best-case, Most-likely
Remove roof boxes, no extra load etc.	Load		Best-case, Most-likely
Reduce A/C use	AC	AC	Best-case, Most-likely
Optimal shifting	Shift	Ecodrive	Best-case, Most-likely
Avoid excessive speed	Speed		Best-case, Most-likely
Accelerate smoothly	Acceleration		Best-case, Most-likely
Brake gently/use engine brakes	Brake		Best-case, Most-likely
Do not idle more than 30 seconds	Idling	Idling	Best-case, Most-likely
Avoid heavy traffic	Traffic	Traffic	Best-case, Most-likely
Avoid cold starts	Cold start	Cold start	Best-case, Most-likely
Avoid unnecessary driving	Drive less		
Purchase new cleaner and more efficient car	New car		

Results

In Figure 1, a comparison of the relative reduction of NO_x and PM_{2.5} road transport emissions is shown. The reduction is largest for Zurich, followed by Gothenburg, and smallest in Amsterdam. The largest emission reductions are seen for the best-case scenario, with a -31% change in NO_x emissions in Zurich 2020 and a -49% change in PM_{2.5} emissions in 2030, also for Zurich.

The emission reductions also resulted in a reduction in air pollutant concentration, see Figure 2. The largest reductions are seen for Zurich and for the best-case scenario for 2020 (NO₂: -14% and PM_{2.5}: -7%) and the smallest differences are seen for Amsterdam.

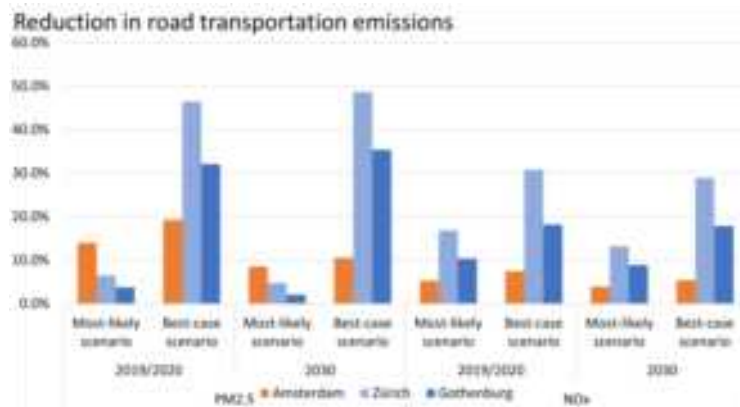


Figure 1: Comparison of reduction in road transport emissions in the three cities for different scenarios and years.

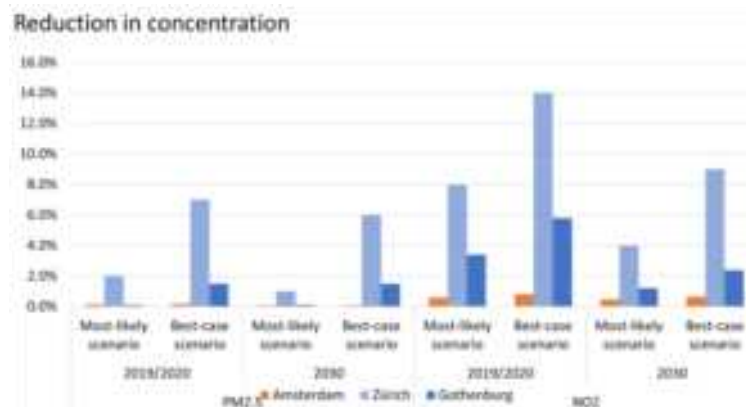
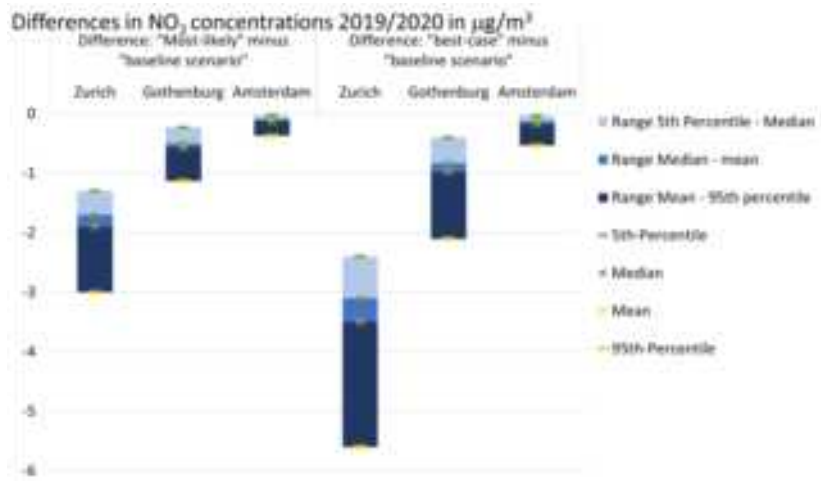


Figure 2: Comparison of reduction in average air pollutant concentration for three cities for different scenarios.

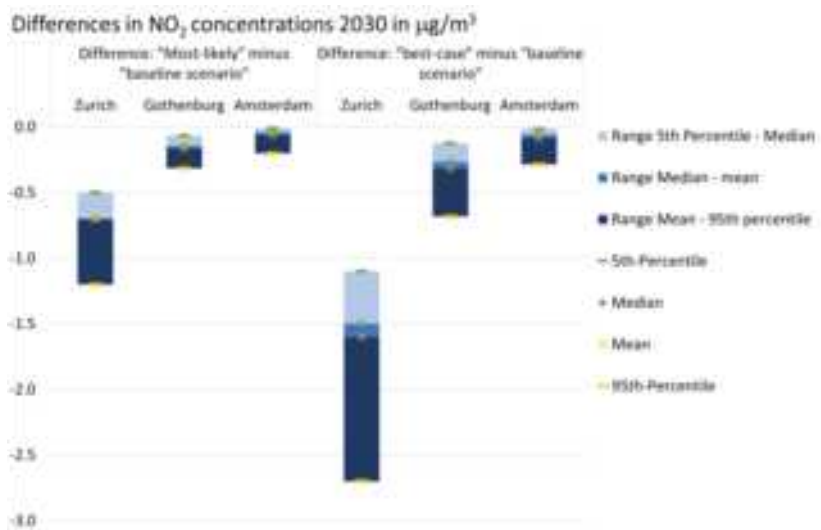
In the baseline scenario for 2019/2020, the annual average concentration exceeds the limit value for NO₂ (40 µg/m³, 30 µg/m³ in Switzerland) in some locations for all three cities (mostly near the road networks). The reductions that are observed for the other scenarios are most noticeable along the road networks and will prevent most of these occurrences. Regardless of limit values, any reduction of long-term average concentration levels of NO₂ and particulates is beneficial to human health.

The difference in air pollutant concentrations compared to the baseline scenario is visualised in Figure 3 for NO₂ and in Figure 4 for PM_{2.5}. Focusing on the 95th percentile, the maximum differences for NO₂ are 5.6 µg/m³ (Zurich), 2.1 µg/m³ (Gothenburg) and 0.53 µg/m³ (Amsterdam). For PM_{2.5}, the maximum differences are 1.2 µg/m³ (Zurich), 0.26 µg/m³ (Gothenburg) and 0.06 µg/m³ (Amsterdam). For both pollutants, the maximum differences are seen for scenario best-case minus baseline for 2019/2020.

The reductions are typically higher for Zurich than for the other cities. In the model for Zurich, the effect of measures on the background concentration is considered. This is believed to be one reason to the higher reduction in the Zurich case. As mentioned earlier is the effect of street canyons considered for Amsterdam. This could lead to a large reduction within the street canyon, while it is smaller in the surrounding area that is shielded by the buildings. In addition, the general air pollutant concentration levels are lower in Gothenburg than in Zurich. Therefore, an equal relative change will result in a smaller absolute change in Gothenburg.

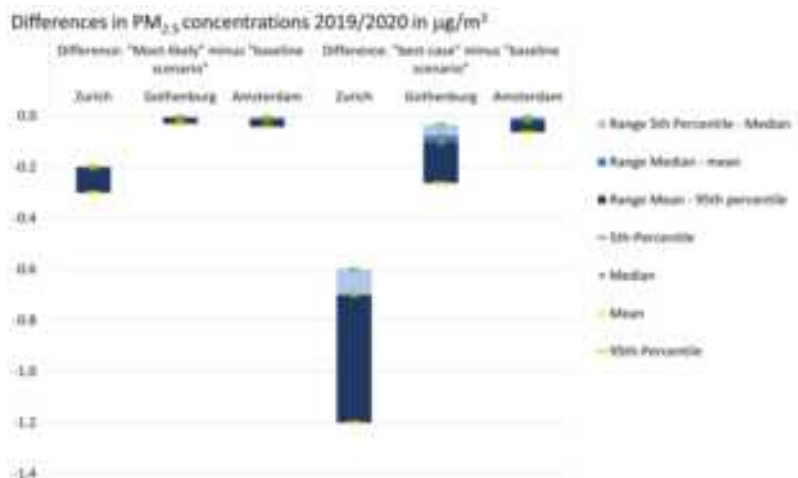


(a)

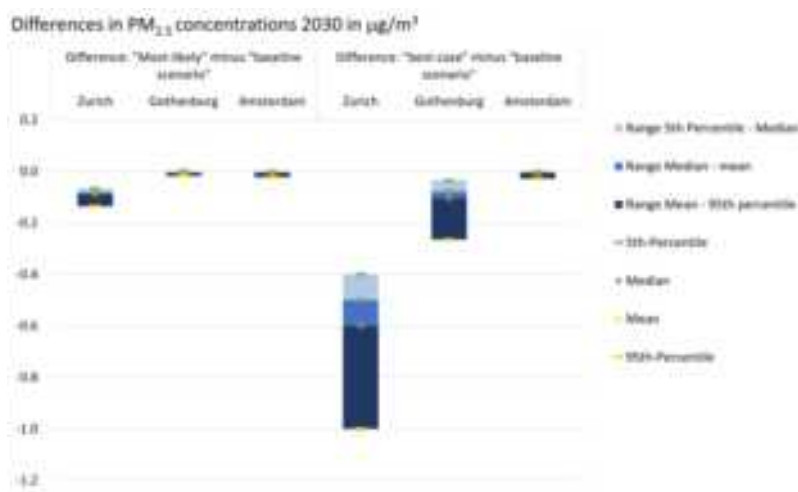


(b)

Figure 3: Differences in NO_x concentrations with respect to the baseline scenario for all three cities in 2019/2020 (a) and 2030 (b).



(a)



(b)

Figure 4: Differences in PM_{2.5} concentrations with respect to the baseline scenario for all three cities in 2019/2020 (a) and 2030 (b).

Discussion

The impact of the considered consumer behaviour measures on average annual air pollutant concentrations was modelled for the cities of Zurich, Gothenburg and Amsterdam. The results show varying effects for these cities and this variation can partially be accounted for by differences in the models used. The models differ primarily in the following aspects: the impact of interventions on background concentration and how street canyons are considered.

If measures are implemented in neighbouring cities and other countries, the measures will affect the background concentration as well. For Zurich, it is assumed that the share of road transportation in the background concentration is the same as the share of road transportation in the total direct emissions. This contribution is then taken into account when the new background concentration is calculated. This is a somewhat simplified assumption, which need to be assessed in more detail to better understand the effect of measures on background concentration and how imported air pollutants affect the background levels.

Street canyons generally trap air pollution at the street level, which leads to higher concentrations along the roads and lower concentrations further away. In the modelling for Amsterdam, this was included, and in a simplified way for Zurich by using three classes of building density. For Gothenburg, it was not included at all. In the results for Amsterdam, it could be seen that the effect of the measures is mainly visible along the main roads, since there is where the pollution concentration is highest.

Conclusions and recommendations

With the uCARe measures, the models show reductions along the road network of up to 5.6 µg NO₂/m³ and up to 1.2 µg PM_{2.5}/m³. Even the most-likely scenario shows substantial reductions along the main roads in all study areas. These study areas focus on the city centres of the three cities, which for all three cities is densely populated. This means that the achieved emission reductions therefore reduces the population's air pollutant exposure significantly.

By just comparing the baseline scenarios between 2019/2020 and 2030, a significant reduction of both NO₂ and PM_{2.5} is observed. The reason for that is the expected change in the vehicle fleet, to cars with lower emissions. This means that the uCARe measures will be more effective in the short term than in the long term.

This calls for a rapid implementation of the proposed measures and interventions. The idea of the uCARe project was to elaborate measures which can be implemented quickly, since new emission limits for cars, such as the expected EURO 7, take rather long to show full benefits due to the time needed for fleet renewal.

This study focused on potential changes in emissions due to reduction measures performed by the driver. Part of these reductions may also be achieved by traffic measures (such as enabling smoother driving with fewer stops at red lights).

Furthermore, this study shows the importance of applying different types of models. To accurately assess impacts of measures on air pollutant concentrations, the model needs to account for the effect of street canyons, and an accurate assessment of the impact on background concentrations is necessary.

Acknowledgements

This work was supported by the European Union, grant number (H2020 LC-MG-1-1-2018).

References

- Cambridge Environmental Research Consultants (2020). ADMS-Urban User Guide, Cambridge. [http://www.cerc.co.uk/environmental-software/assets/data/doc_userguides/CERC_ADMS-Urban5.0_User_Guide.pdf]
- Geilenkirchen G., Heldstab J., Schäppi B., Künzle T., Matzner M., Weller K. (2022). *Updated linking of methods reflecting the state of science*. Deliverable D4.2 of the uCARe EU research program, GA 815002. Vrije Universiteit Brussels (VUB), INFRAS, Brussels and Berne.
- Geilenkirchen G. et al. (2022): Methods for calculating the emissions of transport in The Netherlands., The Hague, PBL Netherlands Environmental Assessment. [https://www.pbl.nl/sites/default/files/downloads/pbl-2022-methods-for-calculating-the-emissions-of-transport-in-nl-4923_0.pdf]
- Heldstab J., Schäppi B., Künzle T. (2020). NO2-, PM10- und PM2.5-Immissionen Schweiz / Liechtenstein - Aktualisierung des PolluMap-Modells für 2015, 2020 und 2030, on behalf of the federal office for the environment of Switzerland. [https://www.bafu.admin.ch/dam/bafu/de/dokumente/luft/externe-studien-berichte/no2-pm10-pm2-5-immissionen-schweiz-liechtenstein-aktualisierung-des-pollumap-modells-fuer-2015-2020-und-2030.pdf.download.pdf/PolluMap_Technischer-Bericht.pdf]
- Notter B., Cox B., Hausberger S., Matzner C., Weller K., Dippold M., Politschnig N., Lipp S., Knörr W., Allekotte M., André M., Gagnepain M., Hult C., Jerksjö M (2022). HBEFA 4.2. Documentation of updates. Bundesamt für Umwelt BAFU (CH), Institut National de l'Environnement et de la Rénergie INERIS (FR), Trafikverket (SE), Miljødirektoratet (NO). [https://www.hbefa.net/e/documents/HBEFA42_Update_Documentation.pdf]
- Visser S. and Wesseling J. (2020). Actualisering en addenda SRM-1 en SRM-2, RIVM report 2020-0118. [<https://rivm.openrepository.com/handle/10029/624458>]
- World Health Organization (2022). Ambient (outdoor) air pollution. [[https://www.who.int/en/news-room/fact-sheets/detail/ambient-\(outdoor\)-air-quality-and-health](https://www.who.int/en/news-room/fact-sheets/detail/ambient-(outdoor)-air-quality-and-health)]

Nanoparticles in different environments in Stockholm, the nPETS project

M. Norman^{1*}, S. Silvergren¹, D. Schlesinger¹, M. Tu², U. Olofsson²

¹ SLB-analys, Environment and Health Administration, City of Stockholm, S-104 20, Sweden

² KTH Royal Institute of Technology, Industrial Technology and Management, S-100 44, Stockholm, Sweden

Presenting author email: michael.norman@slb.nu

Introduction

Nanoparticles has gained increased attention during recent years. The World Health Organization (WHO) summarized the knowledge of their health effects in the latest report (WHO, 2021). Several studies have documented short-term effects of exposure to nanoparticles, including mortality, respiratory symptoms and long-term effects on mortality and several types of morbidity. Based on this WHO suggests distinguishing between high and low particle number concentrations (PNC). Low PNC should be considered less than 1000 particles [N] per cm³ as 24-hour mean and high PNC as above 10 000 [N]/cm³ as 24-hour mean or above 20 000 [N]/cm³ as hourly mean. WHO also recommends more measurements of PNC as well as measurements of particle number size distribution (PNSD) in areas where people are expected to be exposed to high concentrations. In the new EU proposal there is also suggestion for mandatory measurement of PNC in larger cities across Europe (EU, 2022).

In Stockholm measurements of nanoparticles have been running for almost two decades, resulting in one of the longest available time series of ultrafine particles in Europe. The nPETS project (nanoparticles Emissions from the Transport Sector) aims to study the life of the sub 100 nm particles from emission to its path to humans. The nPETS project in Stockholm includes measurement of PNC, black carbon (BC), nitrogen oxides (NOx) and particle number size distribution (PNSD) among other component. Measurements of PNC and NOx were conducted in four different environments in Stockholm including a road tunnel (Söderledstunneln), a densely trafficked street (Sveavägen), a subway station (Tekniska högskolan) and urban background (roof top) during both summer and winter. In addition, BC and PNSD were measured at the roadtunnel, subway station and urban background.

Method

Measurements of nanoparticles in Stockholm has been carried out using condensation particle counters from TSI (model 3022, 3775, 3752). All measurements were carried out for total particle number meaning there were no upper size limit on the inlet. The measurement using the model 3022 has a lower cut-off 7 nm while the more modern models 3775 and 3752 has a lower cut-off 4 nm. All data from the 3022 has been recalculated to 4 nm using parallel measurements. BC was measured by using multiwavelength aethalometers (Magee Scientific, model AE31 and AE33). Particle number size distribution measurements was made by a home built differential particle sizer (DMPS) for particles with sizes between 10 and 450 nanometers. Additional PNSD was measured with an ELPI+ at the subway, road tunnel and urban background. NOx was measured using Environnement SA model AC32M.

Results

The trend of PNC in Stockholm, Figure 1, shows a clear decreasing trend, especially in road traffic environments. The decrease in PNC have been shown to closely correlate with change in vehicle fleet composition and their exhaust emissions (Krecl et al., 2017). A more recent study also shows the differences in PNC and BC in relation to gasoline or diesel car and light- and heavy-duty vehicles respectively (Krecl et al., 2023).

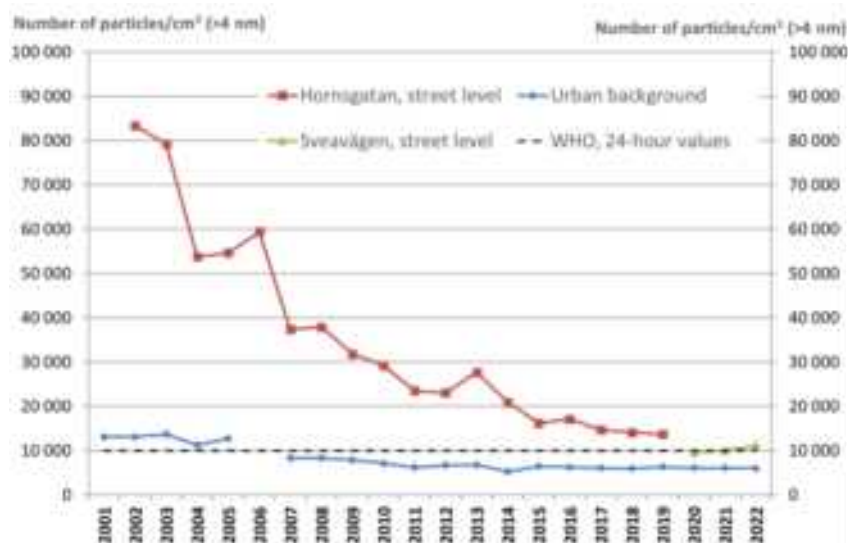


Figure 1. Trend in PNC in Stockholm

Despite the clear downward trend in PNC from Stockholm in Figure 1, concentrations above the WHO guideline values still occur for more than 12-hours per day as seen in Error! Reference source not found. This also highlights the importance of the traffic exhaust emission for the observed PNC concentrations in Stockholm. During year 2022 there were 142 days with average daily PNC that exceeded the WHO guideline for high particle number concentrations of $10\,000\text{ cm}^{-3}$. This shows the importance of monitoring the nanoparticle in several environments, including traffic.

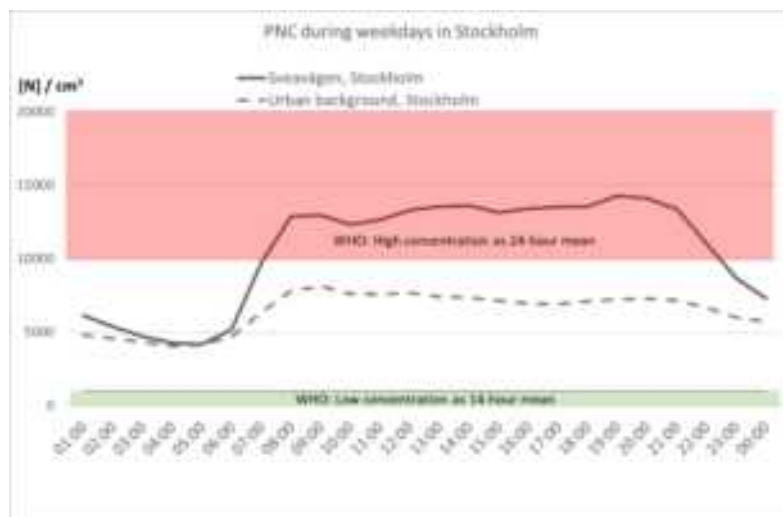


Figure 2: Average diurnal variation in PNC at an urban street (Sveavägen) in Stockholm in comparison to WHO guidelines.

Within the nPets project measurements were performed in different environments during both winter and summer. The PNC was more than an order of magnitude higher in the road tunnel compared to the subway and urban background environments, Figure 3. The urban street data was about twice as high as subway and urban background, Figure 3. This shows that road traffic is the most significant source of nanoparticles in Stockholm, which also is supported by the strong correlation between PNC and NOx in the road tunnel, the urban street and to some extent also at the urban background site. In both road tunnel and urban streets both the measured PNC and NOx concentrations were higher during winter compared to summer. This is probably due to meteorological situation with more stable conditions in winter. Higher PNC in winter could also be due to the higher particle number concentrations being produced from traffic exhaust at colder temperatures, which has been observed earlier in Stockholm (Olivares et al., 2007). The PNC in the subway was found to be similar to that in the urban background and significantly lower than road tunnel and urban street, indicating subway trains to be a less important source of nanoparticles than road traffic. Both the NOx and the BC (Figure 5) was higher

in winter than in summer. This is most likely due to the difference in ventilation at the subway station between summer and winter, with less ventilation in winter.

The PNC was higher in summer at the urban background, in contrast to the two traffic sites, this is discussed more below.

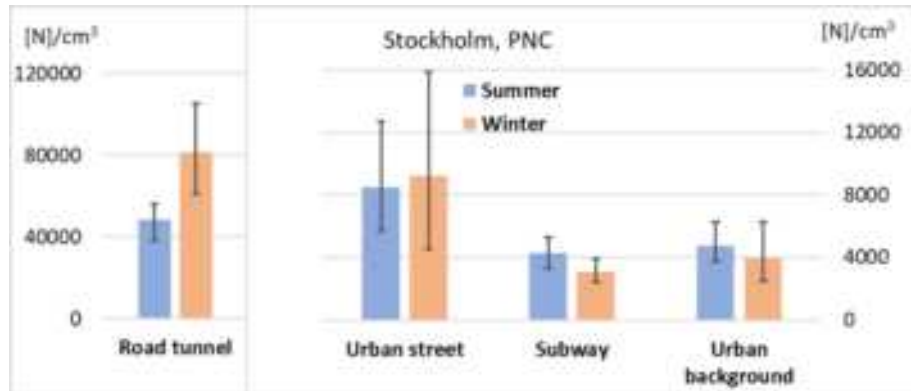


Figure 3. PNC (>4 nm) in four different environments in Stockholm. Median with 25 and 75 percentile.

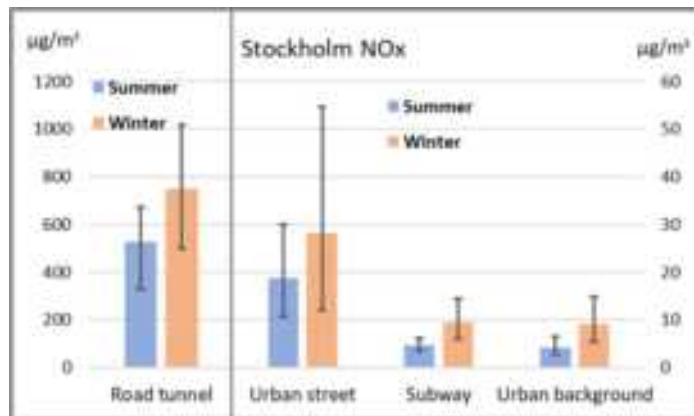


Figure 4. NOx in four different environments in Stockholm. Median with 25 and 75 percentile.

Black carbon (BC) measurements showed a different pattern, Figure 5, with high concentration in both road tunnel and subway and much lower concentrations in the urban background. The BC in the road tunnel is clearly from the road traffic due to the strong correlation with NOx (NOx shown in Figure 4, but the correlation is not shown). Traffic is probably also the dominating source for BC at the urban background site due to the correlation with NOx, but other sources are more important in the urban background. High concentration of BC is also found in the subway environment although the NOx there is low (Figure 4). This could be explained by dark mechanically generated particles in the subway that is measured by the Aethelometer as BC. The BC concentration was higher during winter for all environments.

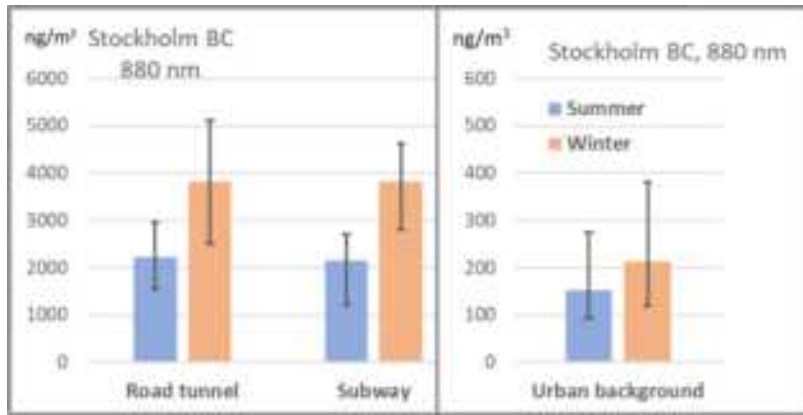


Figure 5. BC in three different environments in Stockholm. Median with 25 and 75 percentile.

The PNSD from a DMPS (differential mobility particle sizer) in the urban background environment, Figure 6, exhibits a difference between the summer and winter measurements. The maximum PN was found at sizes 50-60 nm during summer, while the winter maximum peak was found at 30-40 nm. Also the PNSD showed higher concentration in summer which is in line with PNC in Figure 3. The reason for the difference in median size distribution and the higher number in summer is not known. Some potential factors could be a larger influence from biogenic particles in summer at larger sizes than exhaust particles. Volatile organic carbons and photochemistry in summer could also influence as well as meteorological factors, such as relative humidity.

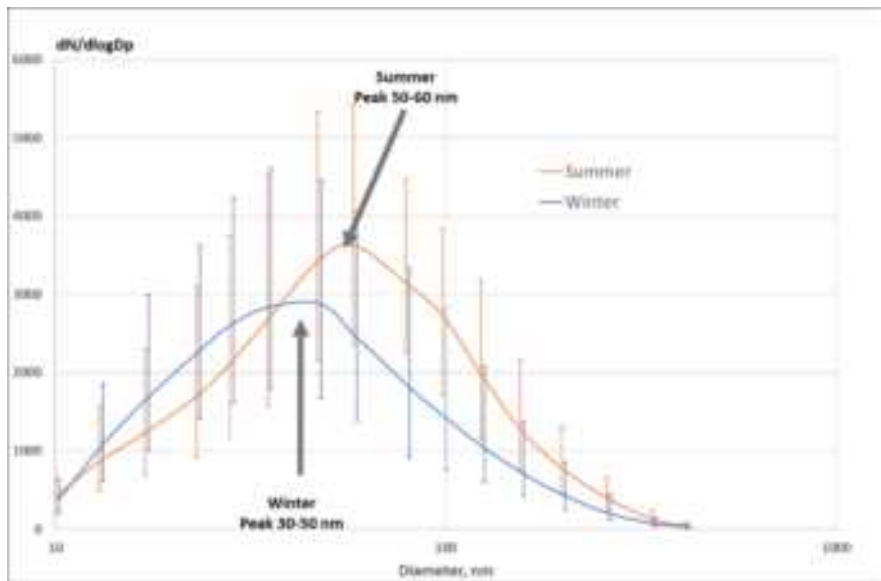


Figure 6. Particle number size distribution from DMPS at urban background in Stockholm. Median with 25 and 75 percentile.

The PNSD at the urban background occasionally show strong variability during short timescales. This is illustrated with the PNSD during two days in October in 2022 in Figure 7. Between those two days a strong decrease in particles was observed around 100 nm and instead a significant peak at smaller sizes around 30 nm occurs. During the 16th of October a heavy rainfall occurred which could be caused by a change in air mass. The >100 nm particles were either washed out by the rain or new air mass caused the decrease. When the >100 nm particles vanished the primary particles and gases from the local traffic likely produced particle that resulted in a peak at around 30 nm.

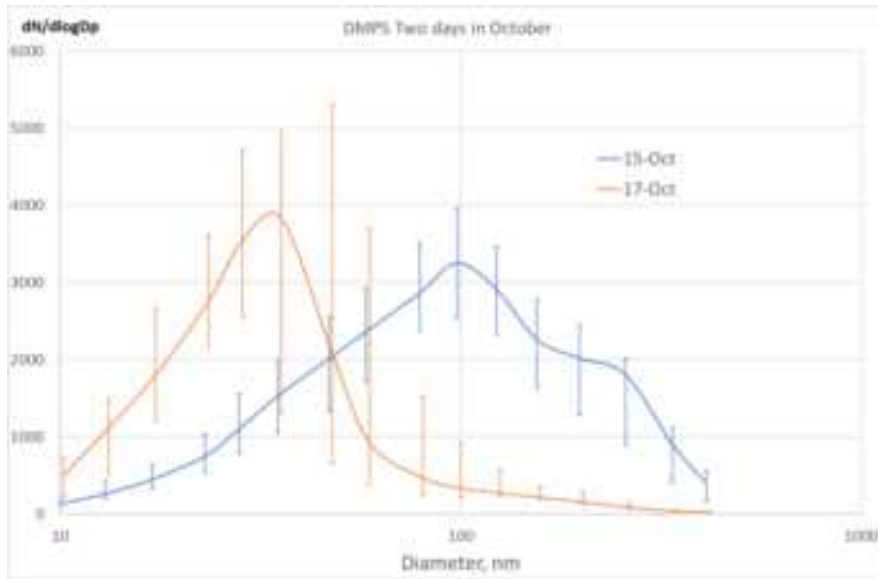


Figure 7. Particle number size distribution at urban background in Stockholm during 15th and 17th October 2022. Median with 25 and 75 percentile.

The PNSD at the urban background occasionally indicated new particle formation as shown in Figure 8. A sudden increase in particles around 10 nm occurs in the morning of the 3rd of May that is followed by an increase in both size and particle number during the day.

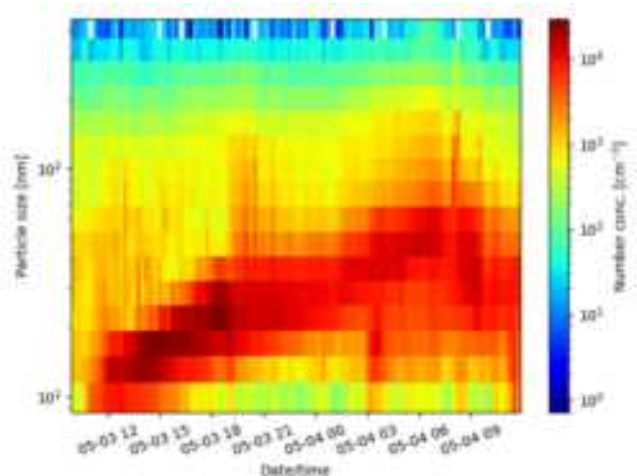


Figure 8. Evolution of the PNSD during the 3rd and 4th of May 2022 in urban background.

Additional PNSD was measured by an ELPI+ at the subway, the road tunnel and urban background during summertime. The PNSD obtained with the ELPI+ measured in the roadtunnels and in the urban background shows a peak around 15 nm. This indicates the same source and that the urban background to a large extent is influenced by road traffic. The size distribution from the subway shows much lower concentrations but also relatively larger fraction of particles larger than 100 nm compared to the other sites. The particles in the subway are mechanically generated in contrast to the particles in the exhaust from traffic which causes the PNSD to be shifted towards larger sizes (Tu, 2023).

The PNSD from the DMPS and the ELPI+ are slightly different from each other at the urban background were they measured in parallel. This difference is not analysed in detail, but the different measurement techniques of the instruments as well as different inlets could be some reasons.

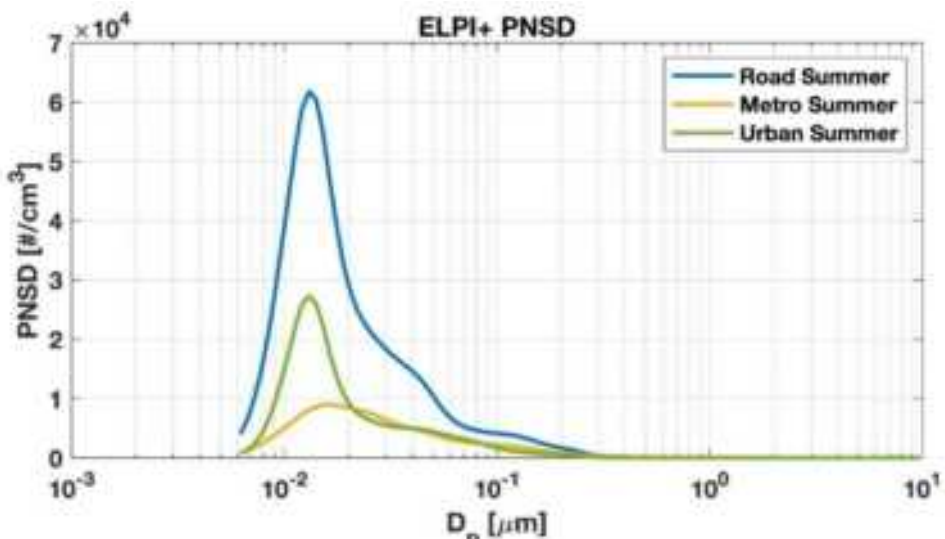


Figure 9. PNSD measured by the ELPI+ during summer at the road tunnel (Road), subway (Metro) and urban background.

Summary

Nanoparticles from the transport sector has been studied in Stockholm within the nPets project. The concentration of nanoparticle has decreased significantly in Stockholm the last 20 years. Despite this are concentrations above the WHO guidelines still common in Stockholm. The measurements showed that road traffic exhaust is the major source for nanoparticles in Stockholm and significantly higher particle number concentrations were measured in road traffic environments in comparison to for example subway and urban background. The nanoparticles in the subway also showed a different size distribution indication other major source. Black carbon and NOx are also emitted from road traffic exhaust and correlates with the particle numbers measured. High BC concentrations were measured in the subway and is explained by dark mechanically generated particles in the subway that is measured as BC.

Acknowledgements

The nPETs project is funded by the European Union's Horizon 2020 programme under grant No 954377.

References

- EU (2022). Proposal for a revision of the Ambient Air Quality Directive. https://environment.ec.europa.eu/publications/revision-eu-ambient-air-quality-legislation_en
- Krecl P., Johansson C., Creso A., Ström J., and Burman L. (2017). Trends in black carbon and size-resolved particle number concentrations and vehicle emission factors under real-world conditions. *Atmospheric Environment* 165 (155-168).
- Krecl P., Johansson C., Norman M., Silvergren S., and Burman L. (2023). Long-term trends of black carbon and particle number concentrations and vehicle emission factors in Stockholm. *Extended abstracts, Transport and Air pollution Conference*, Gothenburg 2023.
- nPets project, <https://www.npets-project.eu/>
- Olivares G., Johansson C., Ström J., and Hansson H.-C. (2007). The role of ambient temperature for particle number concentrations in a street canyon. *Atmospheric Environment* 41 (2145-2155).
- Tu M., and Olofsson U. (2023). Train type effect on nanoparticles on an underground metro platform in Stockholm. *Extended abstracts, Transport and Air pollution Conference*, Gothenburg 2023.
- WHO (2021). WHO global air quality guidelines. <https://www.who.int/publications/i/item/9789240034228>

Quantification of Temperature Dependence of NO_x emissions from road traffic in Norway using Air Quality Modelling and Monitoring data

E. G. Wærsted^{1*}, I. Sundvor², B. R. Denby¹ and Q. Mu¹⁺

¹ Norwegian Meteorological Institute, Henrik Mohns plass 1, 0313, Oslo, Norway, eivindgw@met.no

² Norwegian Institute of Transport Economics, Gaustadalléen 21, 0349, Oslo, Norway

+ Current address: Department of Health and Environmental Sciences, China Institute-Liverpool University, 215123, Suzhou, China

Introduction

This study investigates the temperature dependence of NO_x emissions from road traffic in Norway by comparing modelled and observed concentrations at roadside air quality monitoring stations in the period 2016–2019. The results suggest that the emissions are 3.3 times higher at temperatures below -13 °C than at high temperatures, and 2.7 times higher at -7 °C, with the increase starting at around +12 °C. The temperature range and magnitude of this temperature dependence are consistent with the existing literature on emission measurement experiments performed on various models of diesel vehicles. This extended abstract is an abbreviated version of the paper Wærsted et al. (2022) published in Atmospheric Environment X.

Emissions of nitrogen oxides (NO_x) from road traffic are dependent on a range of factors including vehicle type, speed, driving patterns and engine temperature (e.g. Söderena et al., 2021). Recently a number of studies have indicated that ambient air temperature plays an important role in vehicle NO_x emissions, mainly due to various technical challenges of exhaust after-treatment systems of diesel vehicles of Euro 4/IV and newer that occur at low ambient temperatures (e.g. Grange et al., 2019; Ko et al., 2017; Weber et al., 2019) (see Wærsted et al. (2022) for a more comprehensive discussion).

This study aims to derive a correction formula to account for this temperature dependence when calculating emissions from road traffic in Norway at hourly resolution. NO_x emissions from the Norwegian traffic fleet are dominated by diesel vehicles of Euro 4/IV and newer: we found they comprise ca. 82 % of the emissions even without accounting for an increase in low temperatures (see Wærsted et al. (2022) for details). Thus, based on the studies performed on such vehicles, we expect to see an increase in NO_x emissions of a factor 2–4 at -7 °C relative to high temperatures (23 °C). To find out if this occurs in practice, we study NO_x observations at traffic sites combined with an air quality model.

Methodology

To find empirical evidence for the temperature dependence of emissions from the whole vehicle fleet, we use measured hourly NO_x concentrations in the period 2016–2019 at 46 sites dominated by road traffic sources. We then compare with the NO_x concentrations calculated with a chemistry-transport model without any temperature dependence in its road traffic emissions and study the bias as function of temperature.

We use NO_x observations from the network of air quality monitoring stations in Norway, including all road traffic stations (39) and all urban background stations except two stations that are importantly influenced by shipping or industry (7 stations). Monitoring data have been quality controlled and aggregated to hourly mean concentrations by the Norwegian National Air Quality Reference Laboratory, and we obtained them through a public API (<https://api.nilu.no>).

NO_x concentrations are modelled for each hour at the location of each monitoring station using the EMEP/uEMEP modelling system. The model setup is similar to the one used in the Norwegian operational air quality forecasts, which is described in section 4 of Denby et al. (2020). In short, the concept is to use Gaussian plume modelling (uEMEP model) for nearby emission sources (within a 10 km x 10 km square around the station) and gridded concentrations from the EMEP MSC-W chemistry transport model (EMEP model) (Simpson et al., 2012) at 2.5 km resolution for sources further away. In this way, the model system can capture fine-scale hot-spots in concentrations around emission sources such as roads.

We apply detailed national datasets for four GNFR emission sectors: industry (B), residential combustion (C), road traffic (F) and shipping (G). Only the emissions from these sectors are included in the Gaussian plume modelling. Emissions from all other sectors are taken from the CAMS-REG-AP_v1.1 dataset. The road traffic

emissions are based on traffic volumes of light and heavy vehicles from the national road database (NVDB) and constant emission factors calculated for the whole country using the HBEFA emission model.

Hourly temperature is interpolated to each station from the gridded temperature analysis dataset of the Norwegian Meteorological Institute at 1 km resolution (Met Nordic analysis).

See Wærsted et al. (2022) for a more detailed presentation of the methodology and more references.

Results

Figure 1 compares modelled and observed concentrations of NO_x over the four years. The model underestimates NO_x concentrations significantly at most stations, particularly at the traffic stations. The bias has a clear seasonal cycle: the NO_x concentrations are higher in winter than in summer both in the model and in observations, but the magnitude of this seasonal cycle is much stronger in the observations. In summer there is only a weak negative bias, while this bias is about a factor two in winter.

Figure 1a also shows how much of the modelled NO_x is locally emitted (within 10 km x 10 km) by each emission sector. The majority comes from local road traffic exhaust (78 %), while local industry, shipping and wood-burning contribute very little. The category "EMEP non-local" is the second-most important contribution to NO_x (19 %) and comprises all emissions outside the 10 km x 10 km domain as well as GNFR sectors other than B, C, F and G.

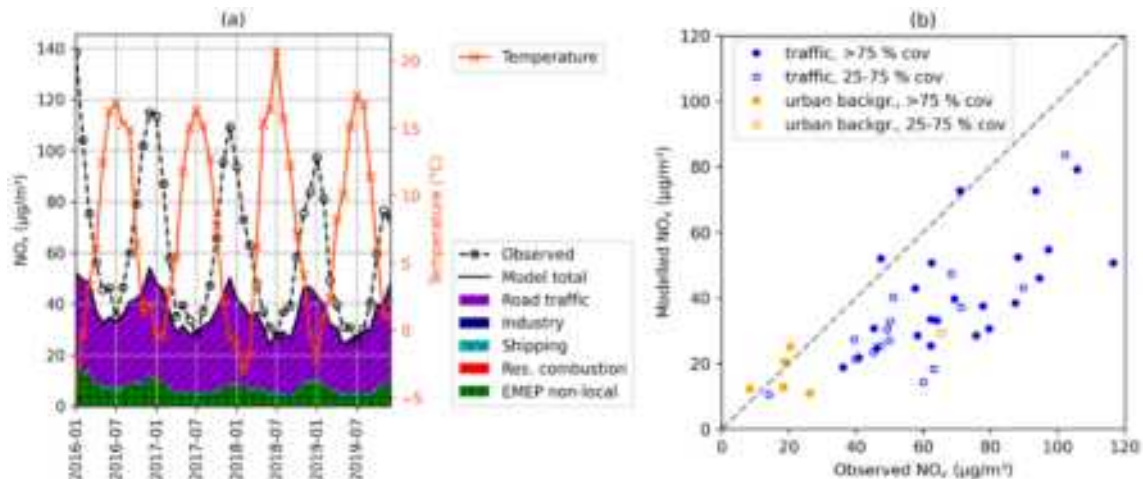


Figure 1: Statistics of observed and modelled NO_x concentrations in the period 2016–2019: Subplot a shows the monthly time series of observed concentration, and the modelled concentration, which is divided into sector contributions, and temperature from Met Nordic analysis. Data have been aggregated by averaging over all stations with available observations at each hour, and then taking the monthly mean. Subplot b shows the observed vs. modelled concentration averaged over the 4-year period at each station and indicating the type of station and data coverage (stations with less than 25 % coverage are not shown).

Figure 2a shows the NO_x concentration plotted against temperature in the model and observations, averaged over all data at all the stations. There is a clear temperature dependence in the observations in the range from about -10 °C to +10 °C. The modelled concentrations also have a temperature dependence in this range, but it is much weaker.

The ratio of observed to modelled mean concentration at each temperature is plotted in Figure 2b. Above ca. 15 °C this ratio is close to 1 and constant with temperature. Below 15 °C the ratio increases close to linearly with decreasing temperature until ca. -14 °C, below which the increase is much weaker. At the lowest temperatures the ratio is close to 3. An indication of the variability of the observed-to-modelled concentration ratio in the dataset within each temperature bin is also shown in Figure 2b. It confirms the gradual increase when temperatures decrease that is seen in the ratio of mean concentrations.

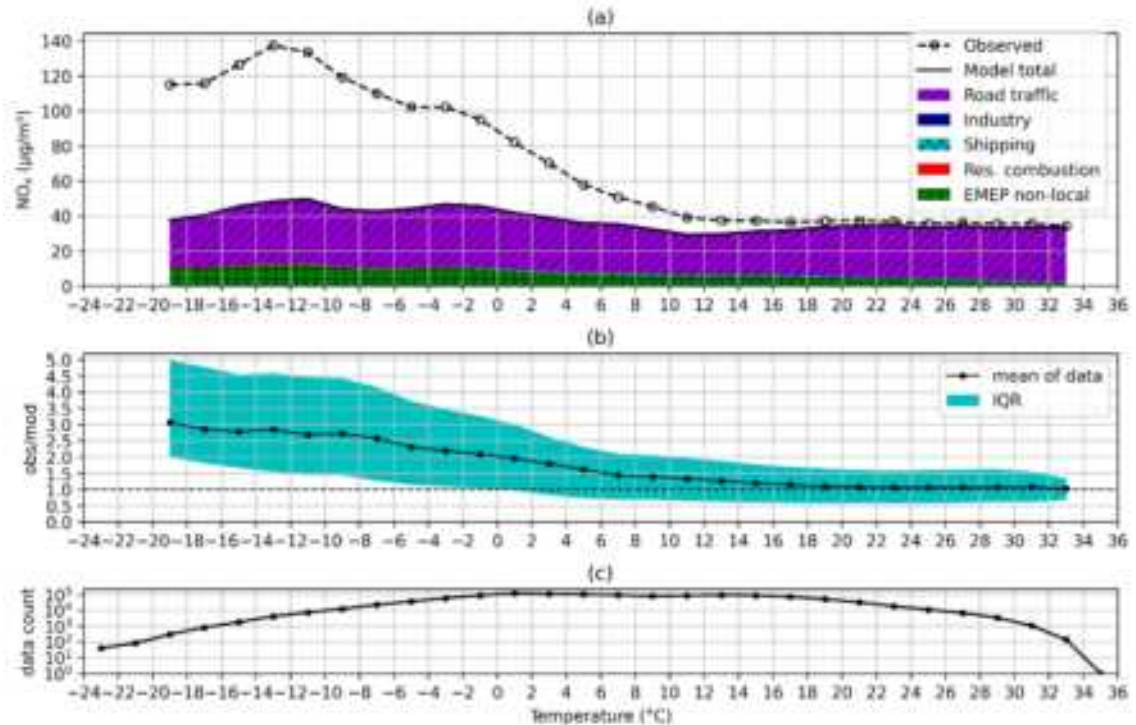


Figure 2: Statistics of observed and modelled NO_x concentration vs. analysis temperature in 2016–2019 at 46 monitoring stations: (a) For each 2 $^{\circ}\text{C}$ temperature interval ($[-20, -18]$, $[-18, -16]$, etc.), all data with analysis temperature within that range have been averaged, weighing each hour with data at each station equally. The average observed NO_x concentration is shown as a circle for each temperature bin. The mean modelled NO_x concentration in each bin is indicated with the solid line, under which the shaded areas indicate the sectoral contributions. (b) For each temperature bin, the black dot shows the ratio of the observed and modelled mean NO_x concentrations. The shaded area indicates the interquartile range (IQR) of observed-to-modelled ratio of single hourly data values in each bin. (c) The number of hourly data values contained in each temperature bin. Only bins with at least 100 data values are plotted in (a) and (b).

Discussion

The large deviation between modelled and observed NO_x concentrations at lower temperatures can be the result of a number of factors. If it is chiefly the result of increased road traffic emissions of NO_x at low temperatures, then the pattern in Figure 2b corresponds well with the effect of more and more vehicles having reduced efficiency of the exhaust aftertreatment system and driving more in cold-phase. The levelling-off at high temperature is interpreted to happen because the exhaust aftertreatment systems function well for all vehicles when it is sufficiently warm, and the levelling-off at low temperature because below a certain temperature all the vehicles will have reached the most sub-optimal situation.

We investigated the temporal and spatial variability of the temperature-dependent bias and found a similar pattern for different years, seasons and stations, although there is some variability (for details, see Wærsted et al., (2022)). We concluded that the temperature signal in NO_x bias is really related to temperature and not to spatial or temporal patterns that correlate with temperature.

An alternative explanation for the temperature-dependent bias is that the model systematically overestimates dilution at low temperature, leading to underestimated concentrations even with no bias in emissions. Dilution of pollutants can be reduced on cold days because low temperatures often occur as a result of high-pressure situations in the winter when clear skies and little wind lead to a stable boundary layer that inhibits turbulent mixing. In areas where pollution is emitted near the surface, both low wind speed and little vertical mixing will limit dilution and lead to elevated concentrations. Gryning et al. (1987) pointed out the difficulties in Gaussian plume modelling under stable conditions and this remains a problem for these types of models.

To check this hypothesis, we investigated the stability regime and the wind speed bias as alternative explanatory variables. In Figure 3, we have categorised the dataset into periods with stable, neutral and unstable conditions, using the modelled Obukhov length. Assuming that the stability regime is correctly modelled, we see that for temperatures below 6 °C, the underestimation of NO_x by the model is slightly larger in stable conditions than in neutral or unstable conditions. The occurrence of stable conditions also rises with decreasing temperature. This might indicate that some of the temperature-dependent bias stems from too much vertical mixing in stable conditions; however, it could also be that the model overestimates the vertical mixing in unstable conditions. It should also be noted that below -10 °C, the underestimation of the NO_x concentration is as strong in the unstable and neutral regimes as in the stable regime. By comparing the observed and modelled wind speed as function of temperature at synoptic stations near the air quality stations, we found there was no systematic bias in wind speed at low temperatures (see Wærsted et al. (2022) for details). These results indicate that overestimated dilution at low temperatures is not the main cause for the underestimation of NO_x concentrations, so most of the signal should come from temperature dependence in NO_x traffic emissions.

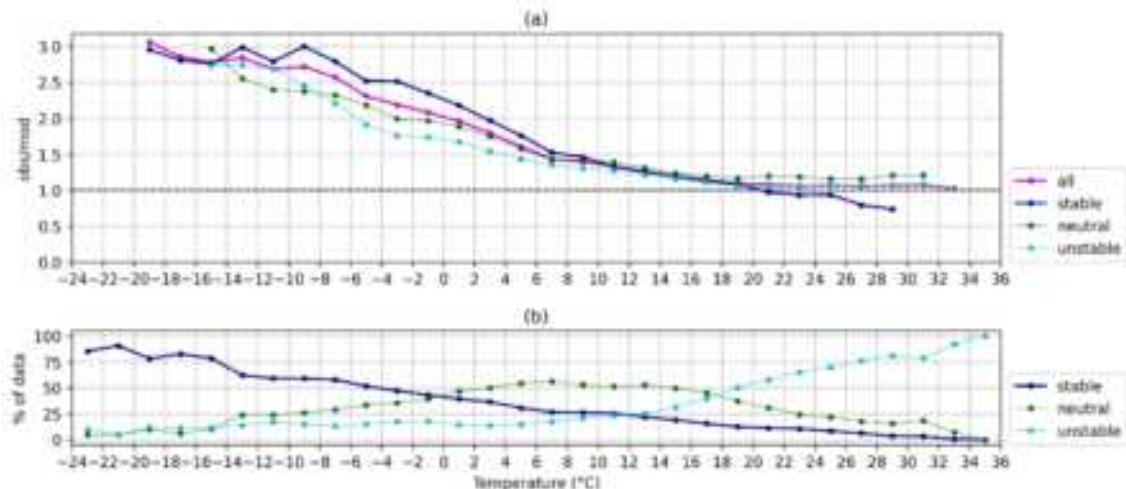


Figure 3: Same as Figure 2b-c, but plotted separately for different stability regimes, defined by the modelled Obukhov length L: Stable ($0 \text{ m} < L < 200 \text{ m}$), neutral ($|L| > 200 \text{ m}$), unstable ($-200 \text{ m} < L < 0 \text{ m}$).

Yet another way to check dilution vs. emissions as a cause for the bias is to consider the coarse particulate matter (sizes between 2.5 and 10 µm, PM_{co}). In Norway, road traffic non-exhaust particles are the most important local source for PM_{co}, particularly at traffic stations. We carried out a similar analysis for PM_{co} as for NO_x and found no temperature-dependent bias (see details in Wærsted et al. (2022)).

Temperature correction formula

If we attribute the temperature-dependent bias to increased road traffic emissions at low temperatures, we can derive a temperature-dependent correction factor to be applied to the road traffic emissions. Since not all the NO_x comes from road traffic, we first need to isolate the road traffic contribution. This contribution is the sum of the local traffic and the fraction of the LNEP non-local (see figure 1a-2a that disaggregates from road traffic).

In a separate model run where we studied contributions from abroad, we found that sources outside Norway contribute ca. 1 µg/m³ to NO_x on average (i.e. about 15 % of the non-local). In another run where we used a larger and more detailed source tracking area, we found that road traffic, shipping, industry and off-road machinery all give contributions of similar importance to the non-local contribution from within Norway. Based on these two runs, we estimate that about 20 % of the non-local contribution comes from road traffic in Norway.

The NO_x sources other than road traffic in Norway are assumed to have no temperature-dependent bias. We also neglect any road traffic contribution to the small negative bias that can be seen at high temperatures in Figure 2a. From these assumptions, we can calculate the observed (O_{tra}) and modelled (M_{tra}) total road traffic contributions to NO_x in each temperature interval in Figure 2:

$$M_{tra} = M_{tra,local} + f_{tra,nl} M_{nl}$$

$$O_{tra} = O_{tot} - (M_{tot} - M_{tra} - \varepsilon_{warm})$$

Where M_{tot} and O_{tot} are the total modelled and observed NO_x concentrations, respectively, $M_{tra,local}$ and M_{nl} are the modelled local road traffic and EMEP non-local contributions, respectively (shaded in Figure 2a), $f_{tra,nl} = 0.2$, and $\varepsilon_{warm} = -4.25 \mu\text{g}/\text{m}^3$ is the mean bias at temperatures above 14°C .

Figure 4 shows O_{tra} and M_{tra} plotted in each temperature interval and the ratio between them. We applied curve-fitting to the line in Figure 4b by imposing a linear decrease between two temperatures T_0 and T_1 , from a value f_0 for temperatures $T < T_0$ to exactly 1 for $T > T_1$. Optimized values for the parameters are $f_0 = 3.28$, $T_0 = -12.9^\circ\text{C}$, and $T_1 = 12.4^\circ\text{C}$. Road traffic NO_x emissions can be multiplied by this parametrization in order to correct for the temperature dependence.

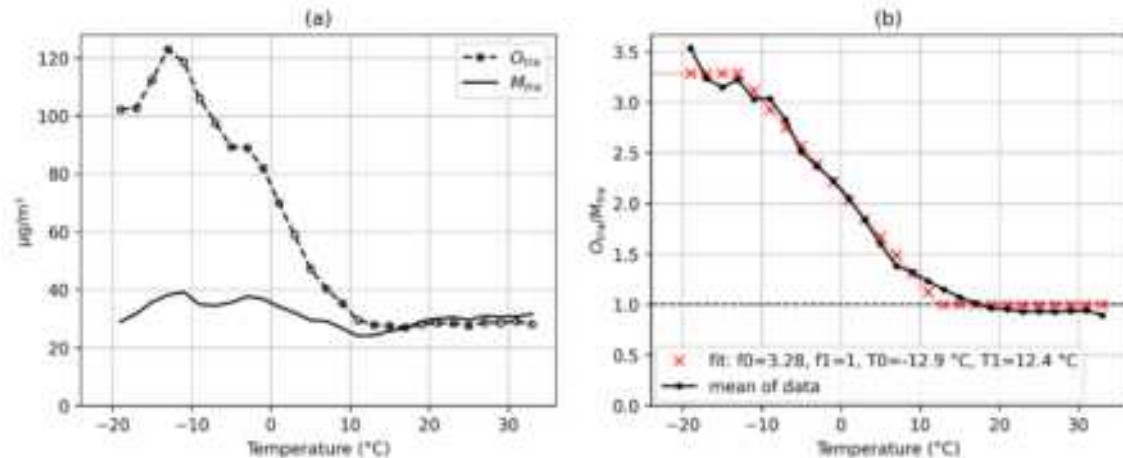


Figure 4: As Figure 2a-b, but plotting only the estimated road traffic contributions to NO_x (O_{tra} and M_{tra}) instead of the total observed and modelled concentrations.

The correction implies that road traffic emissions are 2.7 times higher at -7°C than at the highest temperatures. The correction is applied to the emissions from the vehicle fleet as a whole. If we included only the Euro 4/IV or newer vehicles, which contributes 82 % of road traffic emissions in warm conditions, then the increase in emissions at -7°C for these vehicles must be a factor 3.1 in order to produce the same effect. This increase is within the range of 2–4 that was expected based on the experimental studies.

Conclusion

By comparing observed and modelled NO_x concentrations over a 4-year period at 46 Norwegian monitoring stations, we found a clear temperature dependence in the bias. The average observed-to-modelled ratio of NO_x concentration increases with decreasing temperature, from 1.09 above $+14.0^\circ\text{C}$ to 2.90 below -13.4°C . Both below and above this range the ratio is approximately constant with temperature. This temperature dependence is quite similar between stations, seasons and years. Our analysis indicates that road traffic emissions must cause most of the temperature dependence, rather than dilution bias in the model.

Based on these results, a correction formula for the NO_x traffic emissions was derived. The correction factor is 1 at high temperatures and 3.28 at low temperatures, with a linear increase in the range from $+12.4^\circ\text{C}$ to -12.9°C . This implies that road traffic emissions are 2.7 times higher at -7°C than in warm conditions, and that the emissions continue to increase with decreasing temperature also below -7°C . Since the correction is derived empirically, it might not be directly transferable to other time periods or areas, but if the vehicle fleet is similar it is likely to be a good approximation.

Acknowledgements

This work was supported financially by the Norwegian Public Roads Administration (Statens Vegvesen).

References

- Denby, B.R., Gauss, M., Wind, P., Mu, Q., Wærsted, E.G., Fagerli, H., Valdebenito, A., Klein, H. (2020). Description of the uEMEP_v5 downscaling approach for the EMEP MSC-W chemistry transport model, *Geoscientific Model Development*, 13, 6303–6323, <https://doi.org/10.5194/gmd-13-6303-2020>
- Grange, S.K., Farren, N.J., Vaughan, A.R., Rose, R.A., Carslaw, D.C. (2019). Strong temperature dependence for light-duty diesel vehicle NO_x emissions, *Environmental Science & Technology*, 53, 6587–6596, <https://doi.org/10.1021/acs.est.9b01024>
- Gryning, S.E., Holtslag, A.M., Irwin, J.S., Sivertsen, B. (1987). Applied dispersion modelling based on meteorological scaling parameters, *Atmospheric Environment* (1967), 21, 79–89, [https://doi.org/10.1016/0004-6981\(87\)90273-3](https://doi.org/10.1016/0004-6981(87)90273-3)
- Ko, J., Jin, D., Jang, W., Myung, C.L., Kwon, S., Park, S. (2017). Comparative investigation of NO_x emission characteristics from a Euro 6-compliant diesel passenger car over the NEDC and WLTC at various ambient temperatures, *Applied Energy*, 187, 652–662, <https://doi.org/10.1016/j.apenergy.2016.11.105>
- Simpson, D., Benedictow, A., Berge, H., Bergström, R., Emberson, L.D., Fagerli, H., Flechard, C.R., Hayman, G.D., Gauss, M., Jonson, J.E., Jenkin, M.E., Nyiri, A., Richter, C., Semeena, V.S., Tsyró, S., Tuovinen, J.P., Valdebenito, A., Wind, P. (2012). The EMEP MSC-W chemical transport model – technical description, *Atmospheric Chemistry and Physics*, 12, 7825–7865, <https://doi.org/10.5194/acp-12-7825-2012>
- Söderena, P., Laurikko, J., Weber, C., Tilli, A., Kuikka, K., Kousa, A., Väkevä, O., Venho, A., Haaparanta, S., Nuottimäki, J. (2020). Monitoring Euro 6 diesel passenger cars NO_x emissions for one year in various ambient conditions with PEMS and NO_x sensors. *Science of the Total Environment*, 746, <https://doi.org/10.1016/j.scitotenv.2020.140971>
- Weber, C., Sundvor, I., Figenbaum, E. (2019). Comparison of regulated emission factors of Euro 6 LDV in Nordic temperatures and cold start conditions: diesel- and gasoline direct-injection, *Atmospheric Environment*, 206, 208–216, <https://doi.org/10.1016/j.atmosenv.2019.02.031>
- Wærsted, E.G., Sundvor, I., Denby, B.R., Mu, Q. (2022). Quantification of temperature dependence of NO_x emissions from road traffic in Norway using air quality modelling and monitoring data, *Atmospheric Environment: X*, 13, 100160, <https://doi.org/10.1016/j.aeaoa.2022.100160>

The impact of UK Clean Air Zones (CAZs) on the observed vehicle fleet.

Ian Philips¹; James Tate¹.

¹Institute for Transport Studies (ITS), University of Leeds, Leeds, West Yorkshire, LS2 9JT, England

Introduction

Local Authorities (LAs) in the UK with persistent exceedances of NO₂ (nitrogen dioxide) concentrations are required to develop and implement Local Plans to reduce these concentrations. Local Plans include charging measures in the form of Clean Air Zones (CAZs) of different classes covering different vehicle types. The classes being implemented are: 'A' - buses, coaches, taxis, private hire vehicles, 'B' - heavy goods vehicles (HGVs) and 'C' - vans, minibuses, light goods vehicles (LGVs) and 'D' - passenger cars and C1 commercial. CAZ standards are Euro 6/VI for diesel vehicles and Euro 4/IV petrol. Additionally non-charging policies such as support to upgrade vehicles and speed limit reductions are being implemented. A multi-year central evaluation of these local plans is being carried out (IPSO MORI and ITS Leeds, 2023). It includes before and after studies of air quality concentrations, traffic flow data, and fleet composition data. This paper presents the findings from the analysis of the fleet composition data derived from ANPR observations and changes over time to the end of September 2022. Newer vehicles with higher Euro standard have lower emissions. Changes in fleet composition are expected to be a factor in improved air quality, along with total flow.

Data and Methods

Each LA implementing a CAZ has to submit a 1-week sample of data from a representative subset of its ANPR cameras prior to the CAZ launch as a baseline sample. It then submits quarterly samples. LAs not implementing a CAZ are asked to submit a 1-week sample of data on an annual basis. The Department for Transport Vehicle Statistics Team join the ANPR sample data to the DVLA stock table database (Google Cloud Platform SQL database with R used as an interface) to which they have access, using the VRM (number plate) as the linking field. To establish the Eurostandard, they cross reference vehicle make and model from the DVLA database to other databases, firstly the Society of Motor Manufacturers and Traders (SMMT) dataset purchased under licence²⁶. The Allgemeiner Deutscher Automobil-Club (ADAC) vehicle classification database²⁷, which allows the specific Euro 6 designation of light-duty vehicles to be established (Euro 6a/b, Euro 6c, Euro 6dtemp and Euro 6d). In the event no matches are found on these databases, year of first registration and body type are used to infer Eurostandard. Some vehicles (Mainly Busses and HGVs) have been retrofitted to reduce tailpipe emissions. Retrofitted vehicles are classed as Euro 6/IV for CAZ compliance purposes. Retrofit status is established by referencing the Clean Vehicle Retrofit Accreditation Scheme (CVRAS)²⁸. LAs implementing a CAZ must also report vehicles registered as taxis or private hire vehicles²⁹.

Data is anonymised by replacing the VRM with a unique identifier for each 1-week sample, unique IDs are not carried over between quarterly samples. The data used in this paper are based on the anonymised fleet data (AFD) and not raw ANPR data. AFD data are processed using www.R-project.org. *tidyverse*, *data_table* and *ggplot2* are the principal packages used to process and visualise the changing trend in compliance.

The Emissions factor Toolkit (EFT) (DEFRA, 2021) used the observed fleet data, the AFD, as an input to estimate the relative change in traffic related emissions. In the absence of speed data for specific links the average 'Urban Road' speed of 27 km/h was used calculated from DfT statistics³⁰. Average emissions per vehicle km driven (Emission Factor, EF grams.km⁻¹) are calculated for weekdays and weekends and a weighted 7 day average calculated. Suitable data was available for Bath, Birmingham, Leeds and Portsmouth.

Results

²⁶ Further information at: www.smmt.co.uk/vehicle-data

²⁷ Further information at www.adac.de

²⁸ Further information at www.energysavingtrust.org.uk/service/clean-vehicle-retrofit-accreditation-scheme

²⁹ Local Authority Clean Air Zone Implementation Guidance (Department for Transport, Local Government and the Constitution, 2020) (available online at www.gov.uk) Regulation 2019: www.legislation.gov.uk (available online at www.gov.uk)

³⁰ 5 Department for Transport statistics, Table CGN0503a, Monthly and 12 month rolling average speeds on local 'A' roads in England, average of 'Urban roads' January to September 2022. https://assets.publishing.service.gov.uk/government/uploads/system/uploads/attachment_data/file/1123837/cgn0503.xls

The evolution of the vehicle fleets in Cities/Towns/Local Authorities of Bath (Bath and North East Somerset - BANES), Basildon, Birmingham, Bradford, Black Water Valley (BWV), Coventry, Farnham, Leeds, Portsmouth and Southampton are illustrated in Figure 1. The fleet changes are summarised as the % compliance with a Clean Air Zone (CAZ) policy, whether a CAZ is being implemented or not. The minimum CAZ standards are Euro 6/VI for diesel vehicles and Euro 4/IV for light-duty petrol vehicles (passenger cars and light-goods vehicles).

The Cities of Bath, Birmingham, Bradford, Bristol, Portsmouth and Southampton have introduced CAZs and have provided at least one sample of data post-launch.

The impact of the first CAZ launched in Bath (class C) in March 2021 is clear with a step increase in compliance rates across almost all vehicle types affected by the class C policy between the before sample in January 2021 and the first after data from June 2021 (Bus & Coach 73% to 94%, Taxi 55% to 85%, Articulated HGVs 82% to 95%, rigid HGVs 71% to 82%, LGVs 47% to 67%. Passenger car not impacted by the CAZ policy improved with in step with the UK average 67% to 71%. A broadly similar before/after response was observed when Birmingham launched its CAZ class D in June 2021 except with older passenger cars also brought up to the charging envelope, a step-change increase in their compliance rate was observed from 72% to 87%. Portsmouth then launched the CAZ class B in November 2021 seeing similar fleet step-changes across Heavy-duty vehicle classes and Taxies but not LGVs. These findings clearly illustrate CAZ policies of different classes are largely only impacting the respective vehicle types they are targeting. There is only one sample (baseline) sample available ahead of these CAZ launches. It is expected ahead of these first samples, fleet operators, businesses and the public were preparing their fleets for the imminent CAZ launch dates. The full impact of the CAZs is therefore expected to be greater than reported.

In the proceeding samples each quarter further behavioural responses in response to the CAZ policies and under-lying natural fleet turn-over are observed, with Bus and Coach compliance greater than 96% in the Bath, Birmingham and Portsmouth CAZ samples from late summer 2022, whereas Local Plan areas not/ not yet implementing a CAZ policy were in the 70 – 85% range. After the CAZ launches in Bath and Birmingham there was a strong, continued improvement in the LGV compliance rates from June/July 2021 to late summer 2022. In Bath for example LGV compliance rates post-CAZ launch rose from 67% to 79% over this period.

Leeds withdrew its plan to implement a CAZ in Autumn 2020 with a fall back in bus compliance from over 90% in May 2020 to less than 85% in June 2021. Articulated vehicles are used intensively and high levels of reliability are required and have a high level of compliance in the CAZ areas and non-CAZ Leeds (over 90%). Rigid HGV compliance has increased in the CAZ LAs since implementation (Over 90% in Bath Birmingham and Portsmouth). Compliance has increased at a similar rate in Southampton but from a lower base. In Leeds (non-CAZ) there has been an improvement in compliance to just under 90%. A strong increase in LGV compliance is seen in Bath and Birmingham (from around 50% pre-launch to over 75%). Leeds has a less dramatic increase in LGV compliance ~~than Bath or Birmingham, which are not subject to charges in Portsmouth and local implementation being CAZ B. In Portsmouth, improvement in LGV compliance has been modest and in Southampton it appears to have declined. Birmingham is the only LA where passenger cars are subject to charge. Birmingham has a much more dramatic increase in passenger car compliance than other LAS (72% in April 2021 – over 85% post launch). Cars which were not targeted by the CAZ improved compliance in line with the UK fleet average from 67% to 71%~~.

The EFT modelling of changes in average emission factor from vehicles are shown in the stacked area plots below (Figure 2). Emissions reductions are more noticeable in Bath (BANES Bath and North East Somerset Local Authority) and Birmingham. In Both LAs there was a clear fall in average emissions per vehicle km following launch in 2021, (-17.1% and -20.5% respectively in 2022. Bath's reduction stabilised at -22%, but, in Birmingham the fall continues (-28.3% in July 2022).

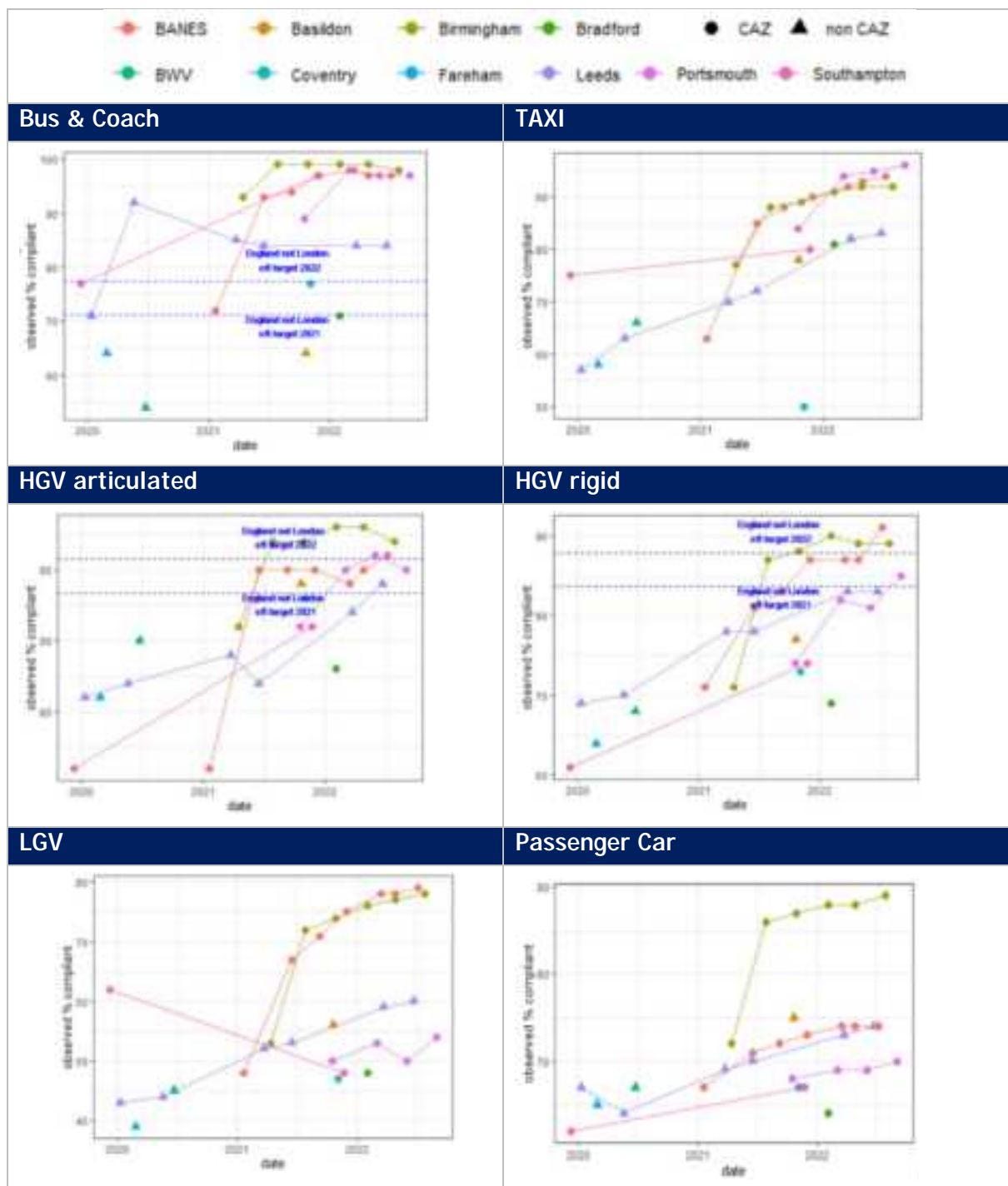


Figure 1: Graphical representation of the fleet composition changes, the % compliance with a CAZ policy across LAs by vehicle type from January 2020 to end of September 2022 (where data is available).

Note: Dashed blue lines horizontal lines annotate the EFT % compliance for end of calendar year 2021 and 2022. (Source IPSOS MORI and ITS Leeds, 2023)

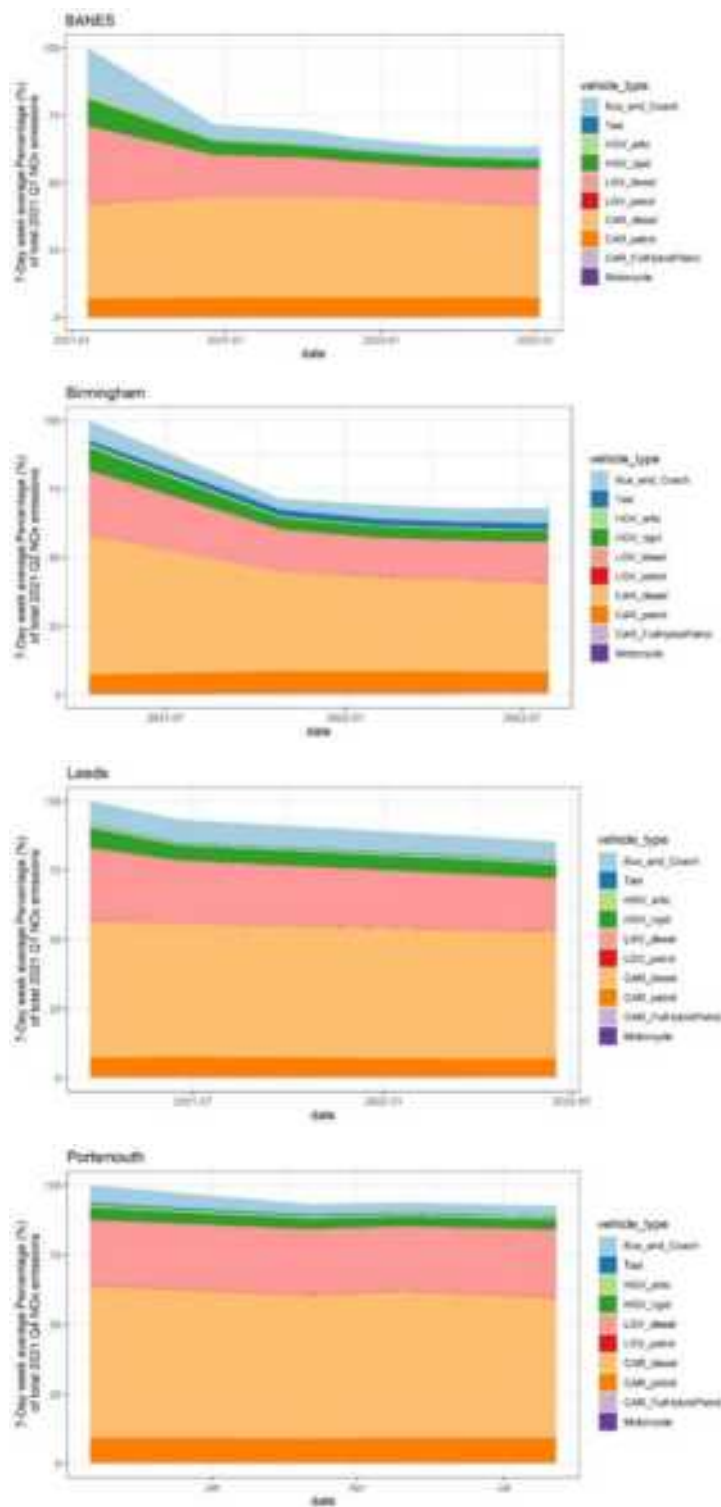


Figure 2: Stacked area plots showing change in weekly average (7-day) vehicle NOx emission factor (per vehicle.km⁻¹) from the first AFD sample (taken as the baseline) as a percentage (%), segregated by vehicle type. (Source IPSOS MORI and ITS Leeds, 2023)

Conclusion

CAZ implementation is associated with an improvement in vehicle fleet Euro standard for the vehicle types subject to the CAZ. Modelling using the EFT based on the observed fleet suggests a significant reduction in air quality emissions (NOx) due to CAZs. Baseline data may not have fully captured all fleet change that occurred in the lead up to CAZ implementation, so actual improvements in Eurostandard and air quality may be underestimated.

The scope of this evaluation is examining fleet composition within Local plan areas, so it would not be appropriate to extrapolate these findings to entire local authority districts. Covid may act as both a confounder on results but also offer insights to changes in air quality under disruption (e.g. Ropkins and Tate, 2021).

To further examine changing fleet composition trends at fine spatial scales not only within Local Plan Areas but more broadly may it may be useful make use of data products currently being developed, which make use of existing administrative data (DVLA and DVSA records) to provide spatio-temporal research ready data which can be used for evaluation purposes. (e.g. <https://environment.leeds.ac.uk/dir-record/research-projects/1794/cars-connecting-administrative-vehicle-data-for-research-on-sustainable-transport>).

Acknowledgements

We would like to acknowledge the support of colleagues in DEFRA / DfT working with the Joint Air Quality Unit particularly Anthony Walker, Thomas Parry and James Relph.

References

- DEFRA, 2021. Emissions Factors Toolkit v11.0 User Guide. Department for Environment Food and Rural Affairs, London.
- IPSOS MORI, ITS Leeds, 2023. Local NO₂ Plans Evaluation 2022 Annual Report. Ipsos / University of Leeds, London.
<https://randd.defra.gov.uk/ProjectDetails?ProjectID=20688&FromSearch=Y&Publisher=1&SearchText=AQ0851%20&SortString=ProjectCode&SortOrder=Asc&Paging=10#Description>
- Ropkins, K., Tate, J.E., 2021. Early observations on the impact of the COVID-19 lockdown on air quality trends across the UK. Sci. Total Environ. 754, 142374. <https://doi.org/10.1016/j.scitotenv.2020.142374>

Estimation of Mobility and Traffic Emissions Based on Cell Phone Data

F. Troncoso Lamaison^{1*}, T. Vieira da Rocha¹, D. Collet², G. De Nunzio², M. Seppecher³, J.M. André¹, S. Moukhtar¹ and J. Boutang¹

¹ Department of Atmospheric Pollution, Mobility & Territories, Citepa, Paris, 75 010, France

² IFP Energies nouvelles, Rond-point de l'échangeur de Solaize, BP 3, 69 360 Solaize, France

³ Université Gustave Eiffel, Université Lyon, ENTPE, LICIT, F-69 518, Lyon, France

Introduction

Urban air quality is a crucial environmental and health issue. This issue is also central in the fight against climate change and adapting cities to this change. Road traffic and chronic congestion contribute significantly to atmospheric emissions in urban areas. Therefore, joint monitoring of road traffic and related emissions is an essential support for urban public decision-making. Indeed, public authorities need methods for quickly evaluating transport policies according to environmental criteria.

Coupling dynamic traffic models with traffic-related emission estimation models is a suitable response to this need. However, integrating this solution into decision support tools requires characterizing urban mobility in near real-time. In the context of continuously increasing cell phone usage, the data they generate, and Call Detail Records (CDR), appear to be an interesting alternative to traditional data, such as origin/destination traffic survey. In fact, CDR data are rich, massive, with high penetration rates, in a universal format and available worldwide. They have already supported critical mobility analysis, such as origin-destination (OD) matrices estimations (Iqbal et al., 2014). However, their use for systematic traffic characterization has remained limited. It is mainly due to the low spatial resolution of these data and their temporal sampling rate, which is sensitive to communication behaviours.

The objective of this work is to develop a mobility modelling tool based upon CDR analysis. The aim is to predict the variation of air pollutants and GHG emissions realistically and quickly according to traffic variables. These traffic variables are necessary to capture specific events or transport regulation measures implemented by authorities. The tool will allow assessing ex-ante or explicit ex-post variation in emissions for each regulatory measure (temporary or structural) or disruptive event. The first results of the project have been successfully obtained for the city of Santiago de Cali (Colombia), using extensive and detailed CDR data provided by CLARO mobile provider. The methodological framework for estimating the traffic variables, needed to calculate emissions, OD matrix and total travel distances, is presented below. The CDR data have been anonymized to respect European Union Data Protection Rules (GDPR).

Methodology

This section presents the methodology to estimate air emissions related to road traffic from CDR data. The methodology is first based on the mobility reconstruction at city scale (Santiago de Cali), as detailed by Seppecher (2022). It describes the urban traffic according to dynamic OD matrices, as well as distances travelled by cell phone users. Then the flows of users from OD matrices are separated according to the means of transport they use, according to a methodology of Transport Mode Detection (TMD). Finally, the air emissions associated with road traffic from motorized mobility are estimated. These emissions are represented in a spatiotemporal resolution.

CDR data

The democratization of cell phone data has enabled mobility analysis based on communication data, particularly Call Detail Records (CDR) which collect communication events like calls, texts, or data connections. CDR data offers high representativity of population mobility patterns and spatial coverage due to widespread cell phone usage. CDR data is less intrusive from a privacy perspective compared to GPS data as for example it provides protective spatial resolution. In fact, CDR data is stored at the base station scale, which means the spatial resolution of the data depends on the density of the base station network. Another aspect of CDR data that makes it very interesting for air pollution is that the data collection ratio depends on users' communication behaviours.

Though some studies have analysed CDR data, reconstructing traffic variables from it remains limited due to spatial and temporal constraints. To address this, researchers have focused on estimating OD flows and users' distances travelled to explain traffic variables, mostly considering regular mobility patterns of residents and

commuters. However, to fully characterize mobility, non-regular users must also be included (Chen et al., 2019; Jiang et al., 2016; Zhao et al., 2021).

The proposed methodology aims to include non-regular users in reconstructing road traffic variables such as total travelled distances from CDR data at a city scale, with the modelled traffic used to estimate related air emissions. The methodology classifies users into residents, commuters, and visitors based on presence patterns. Scaling factors are estimated to represent the overall population for each category. Users are further classified into regular (residents and commuters) and irregular (visitors and occasional travellers) mobility patterns based on their entropy. The methodology is further developed in (Seppecher2022).

For regular users, their daily mobility footprint is enriched using activity-based representation (an activity corresponding to a period during which a user is identified at a specific position) and completed with missing activities using historical data. Trip map-matching and path assignment are then used to reconstruct spatial trips. For irregular users, a subsample of statistically representative users is selected based on daily completeness (minimum threshold above the collected mobility data from a user is considered complete over a day), and their travel distances are estimated using a hybrid distance approach with detour ratios. This particular methodology for irregular user is developed in (Seppecher et al., 2023).

This methodology provides insights into both regular and irregular users' mobility patterns, enabling a more comprehensive understanding of urban mobility and its environmental impact. In order to estimate the emissions generated from traffic variables, a transport mode detection combined with an air emissions model is necessary.

Transport Mode Identification

Transport Mode Detection (TMD) is a mandatory step to separate the observed flows of individuals according to the means of transport they use. In fact, this is crucial for an accurate estimation of the CO₂ and pollutant emissions of mobility on a territory because such emissions are very different from one transport mode to another. Errors in the modal share estimation for mobility flows may lead to significant errors in the mobility emissions estimation.

There is an extensive literature on Transport Mode Detection (TMD) with GPS data (Wu et al., 2016), which can be coupled with other data available from mobile phone sensors (such as inertial mass unit, magnetometer, gyroscope, or barometer), Geographic Information System (GIS) data, or based solely on the GPS trajectory containing information on the position, velocity, and acceleration of individuals throughout their trips. However, CDR data contain much less information than GPS data, because the raw information contained in CDR consists of highly uncertain asynchronous positions. Therefore, GIS data is an extra dataset easily available likely to be coupled with CDR data, in order to add precious geographical context information. The philosophy of this TMD algorithm is to find the most likely portion of the transport network used during a trip, and consequently the most likely associated means of transport. This is done by projecting (or map matching) the reconstructed CDR trips per user on the different transport networks, corresponding to the different transport modes available on the territory under study.

Once the trip has been map-matched over the networks for every transportation mode, it is possible to assess which one is the most likely to have been taken by the user. To assess this, a twofold cost function, denoted by J , is considered:

$$J = J_{spat} + J_{movement}$$

Where J_{spat} is a cost function assessing the similarity in space, which is small when the similarity in space between the trip measured and the trip mapmatched on GIS data is small, and $J_{movement}$ is a cost function assessing the similarity in the movement, which is small when the movement of the measured and map-matched trips are similar. In practice, for the CDR trips, a vector of time instants associated with each measured position is considered. Then, this is compared with time vectors estimated differently depending on the mode of transport, using for instance traffic information in the GIS data for personal transport modes (such as cars), and timetable data for public transport. Eventually, the TMD algorithm presented hereby aims at finding the transportation mode minimizing the cost function J when compared to the corresponding measured trip.

As already mentioned, TMD is of primal importance in the proposed pollutant estimation strategy because modal share per Origin-Destination (OD) flow is needed. To estimate the mode per OD pairs of zones, a sample

of N trips from an OD pair AB is considered, where the i -th trip considered is denoted by x_i^{AB} , with $1 \leq i \leq N$. The function $TMD(x)$ allows us to estimate the transport mode of the trip x . The modal part μ_M^{AB} of the OD AB for the transport mode M is thus the following:

$$\mu_M^{AB} = \frac{1}{N} \sum_{i=1}^N 1_{TMD(x_i^{AB})=M}$$

Where the function $1_{x=y}$ yields 1 when the Boolean expression $x = y$ is true and 0 otherwise.

Air emissions estimations

After estimating the traffic variables and the modal share per OD pairs of zones, air emissions are estimated based on the emissions factors used in the local inventory of Cali from (CVC, 2018). These emissions factors, expressed in g/km for different pollutants and transport modes are presented in the following table.

Table 1: Emission factors by air pollutant and transport mode from (CVC, 2018)

TM	CO (g/km)	VOC (g/km)	NO _x (g/km)	SO _x (g/km)	PM (g/km)
Vehicle	18,00	0,78	1,17	0,05	0,01
Bus	8,59	1,65	15,01	0,69	0,67
Truck	11,8	2,53	20,40	0,97	1,34
Motorcycle	16,00	5,00	0,99	0,02	0,21

The emissions are then calculated in two steps. First, we calculate the emissions of regular users as:

$$Emiss_{t,mode} = Flow_{ODT} \times Lengths_{OD} \times modal\ share_{OD,mode} \times FE_{mode}$$

Where:

- $Emiss_{t,mode}$: emissions by mode as a function of time t,
- $Flow_{ODT}$: ODT matrix from regular patterns, with T being the time,
- $Lengths_{OD}$: average OD distances resulting from the study of road network,
- $ratio_{mode}$: modal share per OD pair from the TMD,
- FE_{mode} : Emission factors by mode from the CVC.

The emissions of irregular users are then added to comparison with the local inventory:

$$Emiss_{t,mode} = TTD_{irreg} \times modal\ share_{OD,mode} \times FE_{mode}$$

Where TTD_{irreg} is the daily total travelled distance from irregular users.

Case study: City of Cali, Colombia

The CDR data applied in the case of this study was provided by the American communication provider CLARO. More than two years of data were collected but only two months' analysis of mobility and emissions are presented here. The historical data length is two months of the pre-COVID-19 period (January to February 2020) for irregular users. For regular users, whose mobility patterns allows a daily data reconstruction, traffic variables were estimated for three months (January to March 2020).

The data structure was compressed for privacy protection and transfer efficiency. The compression consisted of aggregating the event's consecutive communication events occurring at the same base station into a unique communication sequence entry. The final structure is then characterized by the user id, the base station (with the associated location provided on a different table), the timestamps of the first and last event occurred in the same sequence and the number of events occurred during the sequence, as described Table 1.

Table 2: Compressed data structure example

User ID	Base Station	First timestamp	Last timestamp	Nb of events
A	BS ₁	09:30	12:15	4
A	BS ₂	20:30	20:31	1

The data covers 22 economic urban districts and 15 corresponding rural districts of Cali and two neighbouring municipalities Yumbo in the north and Jamundi in the south. The number of base stations covering Cali, Yumbo and Jamundi is 1400 with an uneven density. The density of the base station network is higher in the centre of the city and decreases as moving away from the centre. In fact, the network density is 2.0 base stations per square kilometre in the centre whereas it is 0.16 outside of Cali, the centre covers during 70% of the base stations of the area of study. From a Voronoi tessellation is used to distribute base stations over an area. Each cell of the tessellation is the theoretical geographical area of a user's location assuming users' events are processed by the closest base station.

Results

- ✓ Origin-destination matrices

The regular mobility methodology allowed us to determine the daily trips for the period studied. The daily trips are then aggregated into OD matrices that can be spatially distributed on the region level (an aggregation of Voronoi cells according to a certain population density and area thresholds) as on a higher scale, at the *comuna* scale as illustrated Figure 1.

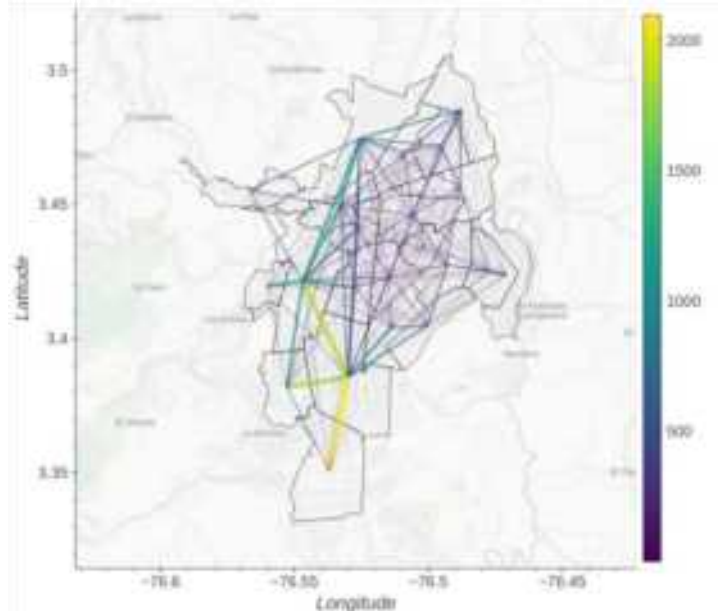


Figure 1: Daily Origin-Destination matrix obtained from the mobility estimation based on CDR data.

Daily trips can be temporally distributed as illustrated in Figure 2. One can observe the impact of COVID-19 lockdown, which started on March 23, 2020. The figure shows that there was probably some anticipation of the population before the first lockdown starts (from March 21).

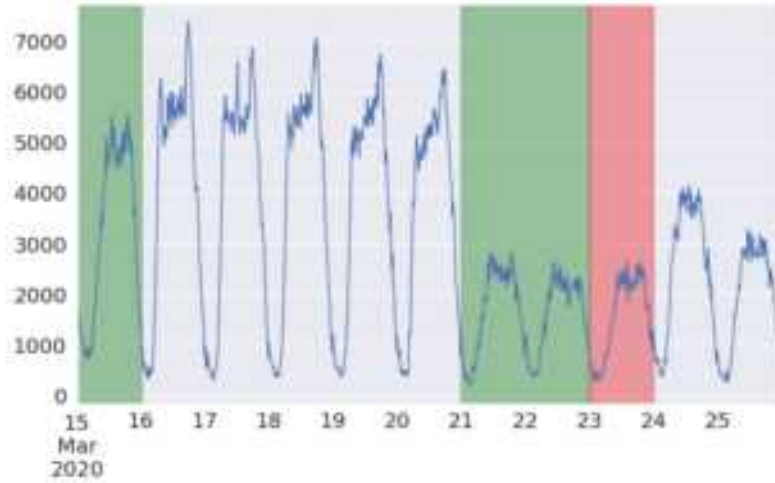


Figure 2: The number of trips per quarter-hour for the week before and after COVID-19 (15 March 2020 to 25 March 2020 included). Green band represents weekends and red band represents the beginning of the lockdown.

- ✓ Traffic variables by mode

In Figure 3, the modal share of the flow on one considered OD found by the TMD algorithm is illustrated.

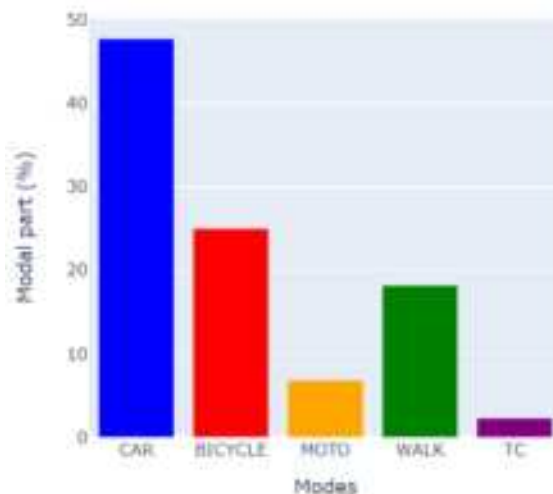


Figure 3: Illustration of the overall modal share in percent for one considered OD pair (between two *comunas*).

- ✓ Daily and annual emission estimation

The following figure shows the daily emissions per pollutant for the regular mobility only. The results presented here relate only to air pollutants. The finest granularity is 15 minutes. The CO emissions are found to be the highest followed by NOx emissions. This can be attributed to the high CO emission factors for motorcycles and vehicles, coupled with their significant modal share.

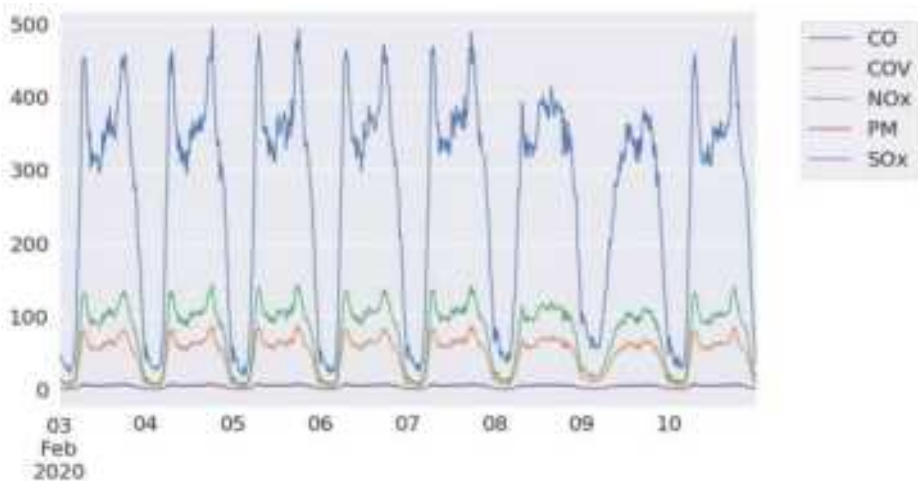


Figure 4: Illustration of the overall modal share in percent for one considered OD pair (between two *comunas*).

Total air emissions of regular and irregular users were then summed and extrapolated for the whole year by multiplying total emissions over a pre-COVID week by the number of weeks in a year. By comparing it with the local inventory (CVC, 2018), the following differences by pollutant are found:

Table 3: Comparison of annual emissions modelled with the local inventory.

CO (t/year)	COV (t/year)	NOx (t/year)	PM (t/year)	SOx (t/year)
-78%	-75%	-26%	-50%	-21%

References

- Chen, G., Viana, A. C., Fiore, M., & Sarraute, C. (2019). Complete trajectory reconstruction from sparse mobile phone data. *EPJ Data Science*, 8(1). <https://doi.org/10.1140/epjds/s13688-019-0206-8>
- CVC. (2018). *Actualizacion del inventario de emisiones de Santiago de Cali*.
- Iqbal, M. S., Choudhury, C. F., Wang, P., & González, M. C. (2014). Development of origin-destination matrices using mobile phone call data. *Transportation Research Part C: Emerging Technologies*, 40, 63–74. <https://doi.org/10.1016/j.trc.2014.01.002>
- Jiang, S., Ferreira, J., & Gonzalez, M. C. (2016). Activity-Based Human Mobility Patterns Inferred from Mobile Phone Data: A Case Study of Singapore. *IEEE Transactions on Big Data*, 3(2), 208–219. <https://doi.org/10.1109/tbdata.2016.2631141>
- Seppecher, M. (2022). *Mining call detail records to reconstruct global urban mobility patterns for large scale emissions calculation*. <https://theses.hal.science/tel-03703230>
- Seppecher, M., Leclercq, L., Furno, A., Rocha, T. V. da, André, J.-M., & Boutang, J. (2023). Identification of Aggregate Urban Mobility Patterns of Nonregular Travellers from Mobile Phone Data. *Future Transportation 2023, Vol. 3, Pages 254-273*, 3(1), 254–273. <https://doi.org/10.3390/FUTURETRANSP3010015>
- Wu, L., Yang, B., & Jing, P. (2016). Travel Mode Detection Based on GPS Raw Data Collected by Smartphones: A Systematic Review of the Existing Methodologies. *Information 2016, Vol. 7, Page 67, 7(4)*, 67. <https://doi.org/10.3390/INFO7040067>
- Zhao, Z., Koutsopoulos, H. N., & Zhao, J. (2021). *Identifying Hidden Visits from Sparse Call Detail Record Data*. <http://arxiv.org/abs/2106.12885>

Input Requirements for Modelling the Microscale Spatial Distribution of Emission Hotspots based on Real-World Measured Vehicle Activity

C. Quaassdorff^{1,2*}, L. Pillai¹, T. Khan¹, and H.C. Frey¹

¹ Department of Civil, Construction and Environmental Engineering, North Carolina State University, Raleigh, North Carolina 27606, United States of America.

² Escuela Técnica Superior de Ingenieros Industriales, Universidad Politécnica de Madrid. 28006 Madrid, Spain, c.quaassdorff@upm.es

Introduction

Quantification of spatial variability in on-road vehicle emission rates helps to identify locations of emission hotspots, which affect near-road air quality and human exposure. Quantification of the spatial distribution in vehicle emission rates is needed to identify emission hotspots (locations with higher pollutant emissions) and provide insight regarding why emission hotspots occur (Quaassdorff et al., 2022b). However, the spatial resolution of many traffic and emissions models is mesoscopic, based on road links between intersections or junctions. Link-based models lack resolution to accurately estimate emissions hotspots at specific locations such as near intersections. The aim of this work is to define the input requirements of a microscale vehicle tailpipe emissions model to support estimation of on-road emission rates at high spatial resolution. The specific objective of this work is to develop and demonstrate procedures for allocating measurements of second-by-second (1 Hz) vehicle activity to high resolution segments and prepare this information to estimate segment average emission rates by means of a microscale emission model.

Methods

One Hz data for a sample of 10 light duty gasoline vehicles are used to demonstrate a method for creating segment-by-segment trajectory data files for input to a vehicle emissions model.

Measurements

One Hz data were collected in previous work by North Carolina State University (NCSU) using an on-board diagnostic scantool, global positioning system receivers with in-built barometric altimeters and Portable Emission Measurement Systems (PEMS). From the measurements, 1 Hz (second-by-second) vehicle activity and emissions were quantified, including speed, acceleration, road grade, vehicle specific power (VSP), and emissions of carbon dioxide (CO_2), nitrogen oxides (NO_x), hydrocarbons (HC) and carbon monoxide (CO) (Khan et al., 2020).

Each vehicle was measured over 8 one-way designated study routes between NCSU, North Raleigh (NR), and Research Triangle Park (RTP), in North Carolina (NC) United States of America (USA) and divided into 4 out routes from NCSU to NR and from NR to RTP, and 4 in routes from RTP to NR and from NR to NCSU (Figure 1). The total length of the trip over the 8 routes is 177 km long. These routes have a broad coverage of road types, speed limits and road grades.

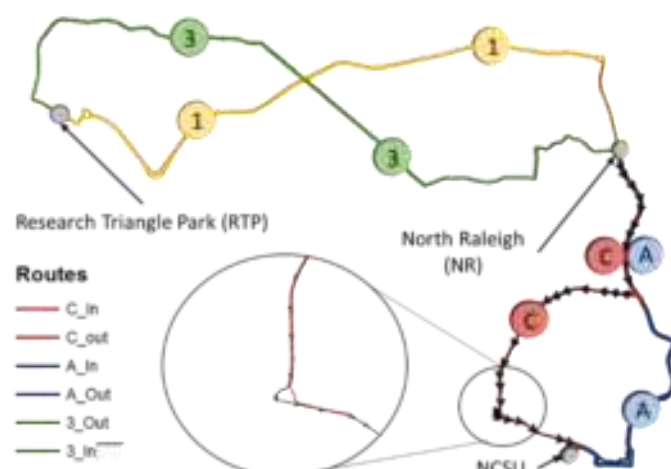


Figure 1. Measured 8 one-way routes between NCSU, North Raleigh (NR) and Research Triangle Park, NC.

This study illustrates the process for allocating measurements of second-by-second (1 Hz) vehicle activity to high resolution segments and prepare this information to estimate segment average emission rates for a set of selected 10 measured light duty gasoline vehicles (LDGV). These are Tier 2 gasoline passenger cars with sedan body type as detailed in Table 1. To model high resolution segments based on 1Hz vehicle activity the high resolution emission model MOVES3 has been selected (details in the Model section). There are some factors, such as the model year or age of the vehicle, that can be represented in MOVES3. Other factors such

as rated horse power, curb weight, rated fuel economy, and mileage, are not considered in the model but can influence variability in measured emission rates.

Table 1. Vehicle characteristics of ten selected Tier 2 gasoline passenger cars with sedan body type.

Vehicle	Model inputs		Vehicle characteristics that are not modelled			
	Model Year	Age when measured (years)	Rated Horse Power (hp)	Curb weight (kg)	Rated Fuel Economy (L/100 km)	Mileage (km*1000)
Toyota Camry	2005	7	160	1435	11.3	171
Toyota Camry	2012	0	178	1470	10.1	31
Kia Forte	2013	0	156	1266	9.7	14
Honda Accord	2012	2	185	1487	10.9	48
Ford Fusion	2016	0	175	1556	10.9	0
Toyota Corolla	2009	7	132	1245	9.4	280
Hyundai Elantra	2010	7	132	1246	9.7	119
Mazda 6	2006	12	160	1436	12.3	278
Honda Civic	2011	7	140	1284	9.7	101
Hyundai Sonata	2009	10	175	1481	11.3	230

Segmented trajectories

The 8 routes were previously divided into a total of 450 directional road segments that average 0.4 km in length. The segments were determined in previous work based on locations of intersections, entrance and exit points of ramps, and vertical curves, considering constant road grade, speed limits and road types (Khan et al., 2020). Dividing those routes into smaller segments provides the opportunity to consider variations of vehicle activity in small distances for the emission estimations. As an example of segmented data, Figure 2 includes the outbound trip segment average road grade. ArcGIS 10.3.1 is used to generate microscale maps of vehicle activity.

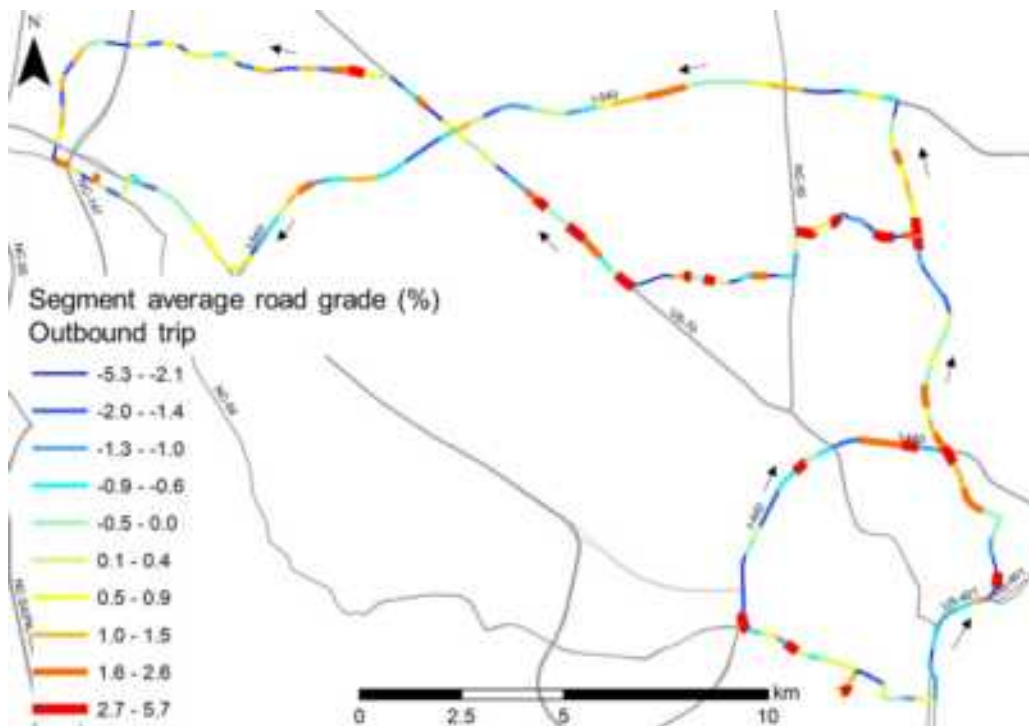


Figure 2. Segment average road grade (%) on outbound trips.

The second-by-second data from the measurements are spatially joined to the segments using ArcGIS so that each segment can be assigned the corresponding second-by-second data from the vehicle trajectory. For that, one single .csv file containing the trajectory data of each vehicle and route is created as input for ArcGIS. This file contains the second-by-second measured information for one vehicle over one route with location (latitude and longitude) of each measured second. Each of these second-by-second files for each of the 8 routes and for each of the 10 vehicles are uploaded into ArcGIS as dot layer to perform a spatial join with the line layer of the corresponding segmented route. The spatial join is based on proximity (type closest), which finds the closest segment in a route for each instantaneous measurement. Thus, each measured data is assigned to the closest segment.

Figure 3 is an example of segmentation of the second-by-second speed trajectory of one vehicle (blue line), in this example a Ford Fusion, over route A-out with 42 segments. Each of the high resolution microscale segments (numbers in the top of the figure) has been assigned constant road grade (dotted brown line) based on linear regression of elevation versus distance data from GPS measurements.

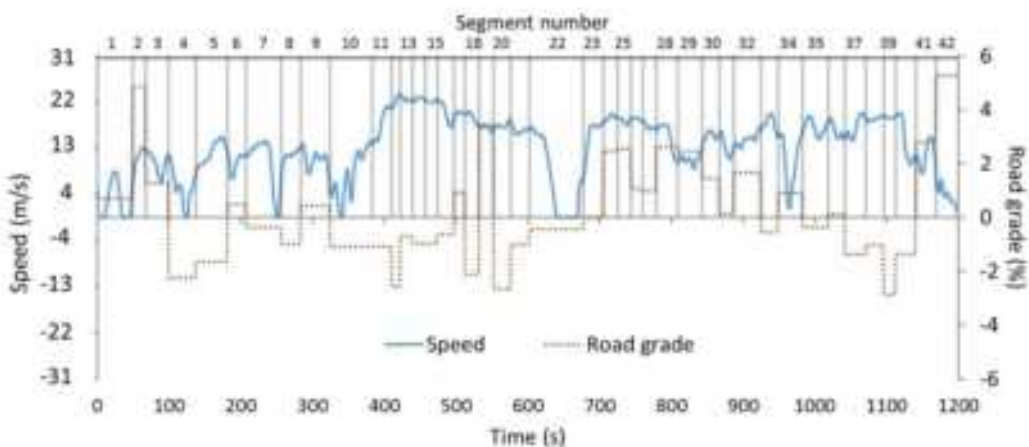


Figure 3. Second by second vehicle speed and segment average road grade for an example vehicle trajectory (Ford Fusion) over route A-out (42 segments).

Model

In this case, for the segmented trajectories, the U.S. E.P.A. Motor Vehicle Emission Simulator version 3 (MOVES3) is used. MOVES3 is widely used to characterize emissions for the U.S. vehicle fleet. The model does not calculate individual vehicles but a vehicle fleet based on the vehicle type, vehicle model year, ambient conditions on the day of the measurement, and second-by-second speed and road grade data from the measured segmented trajectories.

To run MOVES3, each vehicle requires a Run Specification (run spec), an input database and an output database. The run spec file contains information on spatial resolution (i.e. microscale), time of the day when the vehicle was measured, geographic bounds (state and county), type of vehicle (passenger car or passenger truck), pollutants, a link to vehicle-specific data, and the name of the output database where the model outcomes are stored. Vehicle-specific data include vehicle age, fuel type, ambient conditions, segmented 1Hz vehicle speed and road grade data, and segment details. Each of these vehicle-specific data are stored as single files in one input database. A description of the vehicle-specific data files included in the input database is given Table 2.

Table 2. MOVES emission model set of vehicle-specific data input files required for each vehicle input database.

Files required for MOVES input database	File description	File generation
age distribution	Defines the vehicle age	User defined
meteorology data	Contains information on the meteorology. Includes temperature and relative humidity.	User defined
fuel	Includes information on fuel used (supply, formulation, usage fraction, subtype).	Model default data based on user provided vehicle information
links	Contains an enumeration of all the links (segments) measured for a vehicle, and includes the info of county, zone, road type and segment length.	User defined
link drive schedule	Contains a second-by-second enumeration of the links the vehicle has been driven on, and the information on speed (mi/h) and road grade (%) for each second.	User defined
link source types	Contains a second-by-second enumeration of the links the vehicle has been driven on, vehicle type and fraction per vehicle type. The number of second-by-second links must match the link drive schedule.	User defined

To set up and run groups of run specs, MOVES batch mode was used. In the batch mode, a MOVES3 run for one vehicle with 450 segment trajectories takes 300 seconds. To simplify the input of data into the model and minimize potential human errors, a LabVIEW code was developed to run the model in batch calculation mode iterating the calculation process from vehicle to vehicle with the final aim of generating microscale segment average emission rates per distance (g/km) for each single vehicle. The use of the batch mode provides the opportunity to run groups of single vehicles at the same time in an automatic way. Five main steps for running the batch mode are specified in Figure 4.

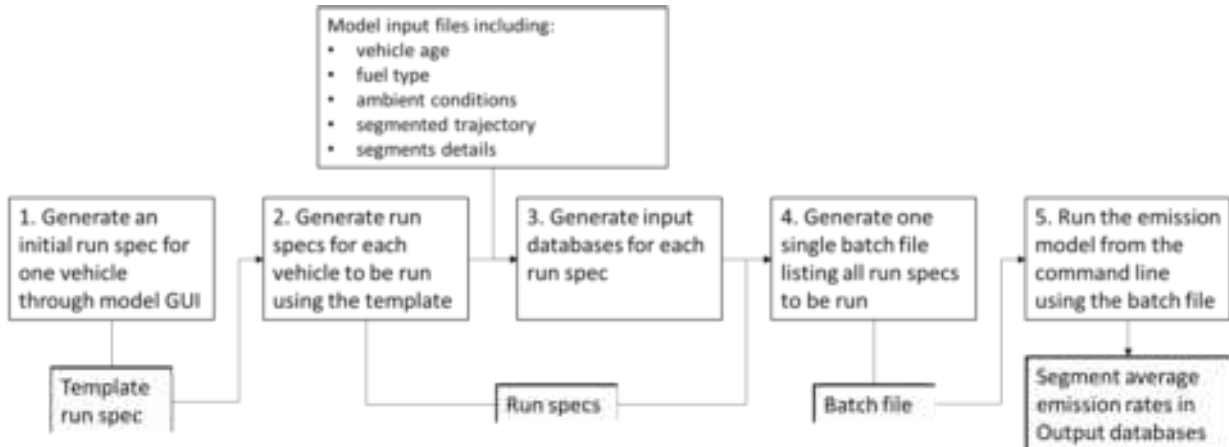


Figure 4. Flow diagram of the model batch calculation process.

Model outputs include fleet average segment based pollutant emission rates per distance (g/km) for CO₂, CO, NO_x, HC and Total Energy Consumption (g/J) corresponding to the model year and age of each vehicle, from Table 1, and segment. Those outputs are stored in an output database and are useful to identify potential emission hotspots (only those segments whose outputs are defined as segments within the top 10% to 90% percentile) of segments average emission rates for each pollutant. ArcGIS 10.3.1 is used to generate microscale maps of vehicle activity and segment fleet average emission rates.

Results and discussion

The outcomes of this methodology are segment average emission rates for each of the modelled vehicles and pollutants over the 450 segments. Quantification of spatial variability in segment average emission rates enables identification of potential emission hotspots. By aggregating and averaging the emission rate estimates for a fleet (in this case represented by 10 vehicles) hot-spot locations can be identified.

As example and due to health effects related to exposure to NO₂ (U.S. EPA, 2016), Figure 5 highlights the location of NO_x emission hotspots for the segment average emission rate of the ten selected vehicles. As highlighted in the black circles (a and b) in the figure, hotspot segments can be differentiated from lower emission segments that are spatially very close together. The location of the hotspots is influenced by the factors such as positive road grade change and red lights in Figure 2 which refers to the location of hotspot regions in Figure 5. However, not all the hotspots are explained by positive road grade change (E in Figure 5). Several factors, and interactions among them, can be involved in the generation of a hotspot (Khan, et al., 2020). Further analysis to depict the main factors involved in the spatial distribution of modelled emission rates is needed and is recommended for future work. This will help to provide detailed information on the location of hotspots and why those occur.

Modelled segment average emission rates are used as part of an ongoing project to assess the ability of a microscopic vehicle emissions model to accurately predict hotspots in comparison to high spatial resolution tailpipe exhaust measurements (Quaassdorff, et al., 2022a; Quaassdorff, et al., 2023).

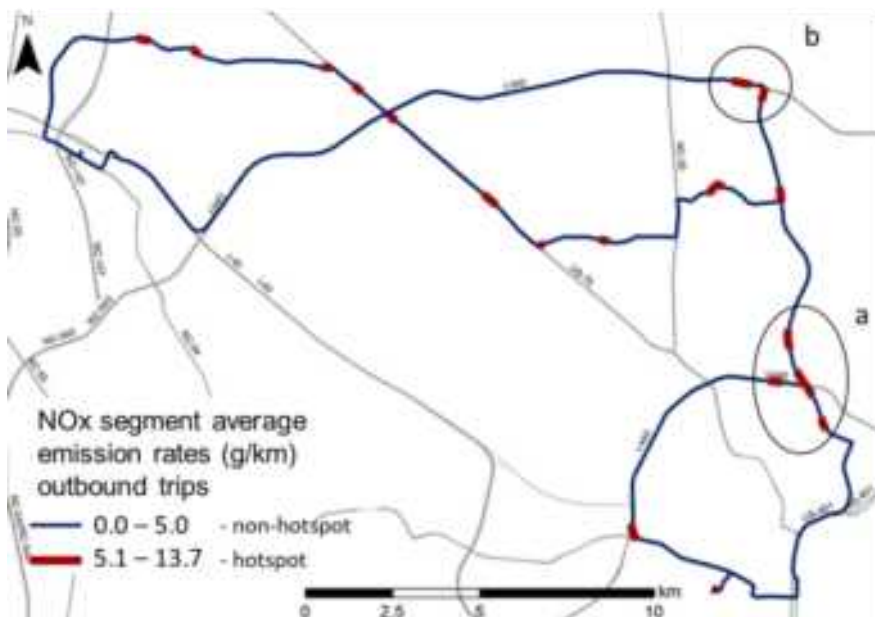


Figure 5. Ten-vehicle modelled segment average NOx emission rates (g/mi) for outbound trips, with hotspot (red thicker lines) areas highlighted in black circles (a and b).

Conclusions

Second-by-second (1 Hz) vehicle activity is a required input for microscale vehicle tailpipe emissions models to support estimation of on-road emission rates at high spatial resolution. In this work a procedure is given for allocating measurements of 1 Hz vehicle activity to high resolution segments. Estimation of segment average emission rates by means of a microscale emission model has been successfully demonstrated for a set of 10 vehicles. This methodology is useful to identify microscale emission hotspots locations at high spatial resolution, and will be applied to a larger dataset to support a more comprehensive assessment of spatial variability in real-world emissions and more robust identification of emissions hotspots.

Acknowledgements

This work was supported by the IRTEMS project (H2020-MSCA-IF-2019/896417/EU/IRTEMS) funded by the European Union's Horizon 2020 research and innovation programme under the Marie Skłodowska-Curie grant agreement No 896417; and the Glenn E. and Phyllis J. Futrell Distinguished University Professorship at North Carolina State University. Victor de la Cruz Salmerón helped developing the LabVIEW code. Disclaimer: The information here presented reflects the author(s) view and does not necessarily reflect the views or policy of the European Commission and REA, those of the NC State University nor those of any other sponsor which are not responsible for any use that may be made of the information it contains.

References

- Khan, T., Frey, H. C., Rastogi, N., Wei, T. (2020). Geospatial Variation of Real-World Tailpipe Emission Rates for Light-Duty Gasoline Vehicles. *Environ. Sci. Technol.* 54: 11111-11118.
- Quaassdorff, C., Khan, T., Frey, H. C. (2022a). Accuracy of the predictions of modeled emission hotspots based on real-world measured vehicle activity and emissions. *CRC Real-World Emission Workshop*. San Diego, California, USA. March 13-16, 2022.
- Quaassdorff, C., Smit, R., Borge, R., Hausberger, S. (2022b). Comparison of microscale traffic emission models for urban networks. *Environ. Res. Lett.* 17:094030.
- Quaassdorff, C., Khan, T., Pillai, L., Frey, H. C. (2023). Evaluation of model predictions of real-world emission hotspots based on measured vehicle activity and emissions. *CRC Real-World Emission Workshop*. Long Beach, California, USA. March 26-29, 2023.
- U.S. EPA. Integrated Science Assessment (ISA) for Oxides of Nitrogen – Health Criteria (Final Report, Jan 2016). U.S. Environmental Protection Agency, Washington, DC, EPA/600/R-15/068, 2016.

2.7 TAP.07. Non-road emissions.

Real-world NO_x emissions of Stage V NRMM

R. Vermeulen¹, J. Demuynck^{2*}, P. Paschinger¹, D. Bosteels²

¹TNO, The Hague, the Netherlands, robin.vermeulen@tno.nl

²Association for Emissions Control by Catalyst, AECC aisbl, Brussels, Belgium, joachim.demuynck@aecc.eu

Abstract

This work investigates the real-world NO_x emissions of stage V engines used in a variety of Non-Road Mobile Machinery (NRMM) applications. The purpose is to understand the real-world usage patterns in the fleet and resulting emissions under a variety of operating conditions. The monitoring data of thirteen Stage IV and V machines is analysed. NO_x emissions were measured during real-world operation with Smart Emissions Measurement Systems (SEMS).

It is observed that engine load patterns vary between machines, even when they are of the same type. In general, the average engine load is relatively low or can have intermittent periods of working and stand-by periods. A variety in average emissions performance can be observed. Several machines have average NO_x emissions below the limit, some around the limit and others are significantly above the limit. Impact on air quality is not only determined by the average emissions, as specific usages seems associated with higher emissions. The study therefore investigated the distribution of emissions as well, based on the Stage V In-Service Monitoring (ISM) post-processing procedures. In contrast to Euro 6/VI for on-road vehicles which has requirements for testing In-Service Conformity with PEMS, Stage V for NRMM includes testing with Portable Emissions Measurement Systems (PEMS) for monitoring purposes only, called In-Service Monitoring (ISM).

For five out of eight of the monitored Stage IV and V machines ($56 \leq P < 130$ kW and $130 \leq P \leq 560$ kW, respectively), real-world NO_x emissions are reasonably low, in the range of the limit value, due to the usage of Selective Catalytic Reduction (SCR) systems. There are, however, events with higher emissions, which are often categorised as non-working event or invalid window in the ISM procedures. For three of the eight machines of these categories higher emissions are observed during the monitoring programme, mainly due to insufficient thermal management under low-load operation. Real-world NO_x emissions of low powered (<56 kW) and high-powered (>560 kW) categories are high due to the higher NO_x limits, which do not require the use of SCR.

Introduction

NRMM (Non-Road Mobile Machinery) is a broad category of machinery which includes mobile machinery and transportable equipment which are not primarily used for transporting people or goods over the road and most of which are fitted with an internal combustion engine (diesel mainly). As such, the machinery is to be regarded as a source of pollutant and greenhouse gas emissions. For instance, NRMM in the construction sector can be a significant contributor to local air pollution (NO_x, PM), acidification and eutrophication of nearby nature reserves (NO_x, NH₃). EU regulation has become more stringent over time with the aim to reduce pollutant emissions of the engines for most power categories. The regulation uses standardized tests to verify the emissions under controlled laboratory conditions. In-service emissions are only checked by means of monitoring with PEMS (Portable Emissions Measurement System), but this is limited to a selective part of the operation of the machinery.

Objectives

The objectives of the study at hand were to increase the understanding of real-world NO_x of stage IV/V engines applied in NRMM. More specifically, their usage patterns, dependencies of the emissions, fleet composition and contributions to total emissions were investigated. Furthermore, possible opportunities for improving regulatory requirements were identified and emissions put in perspective with air quality contributions. Finally, hot spots (largest contributing categories) and possible white spots in knowledge and data were identified.

Approach

The approach taken was to collect and analyse the real-world emissions and usage data which was measured on a number of Stage IV and V certified NRMM in the testing programs conducted by TNO for the Dutch Ministry of Infrastructure and Water management.

NRMM

In the Netherlands

To be able to show the significance of emissions from NRMM and to get a view of the fleet of NRMM, the situation in the Netherlands was used as an example. In the Netherlands the EMMA model [6] is used to estimate annual emissions. Presently, 87 different types of machines are considered in the model, from chainsaws to pile drivers. Probably, there are still types in-use which are not identified and included. Regarding the fleet of NRMM in the Netherlands it should be noted that there are large uncertainties in terms of numbers and types of NRMM due to lack of registration, e.g., a large underestimation was unveiled by the mandatory registration of 350,000 agricultural tractors, which is almost five times the initially estimated number of 71,000. Also, there is a large uncertainty of the usage of the machinery.

Annual NO_x emissions [8] are at approximately the same level compared to inland shipping, somewhat higher than passenger cars, light-, or heavy-commercial vehicles and about 44 % of total traffic NO_x emissions. Annual PM₁₀ emissions of NRMM are as high as the total of road traffic. Annual NO_x emissions are estimated to decrease slightly from 2022 to 2030 due to the substantial increase of the share of stage V engines. This includes some growth of the fleet. The EMMA model estimates that the contribution to total NO_x emissions is highest for medium powered categories (75–560 kW). This may shift to the lower power category with less stringent emissions limits. This may account for particulate matter as well.

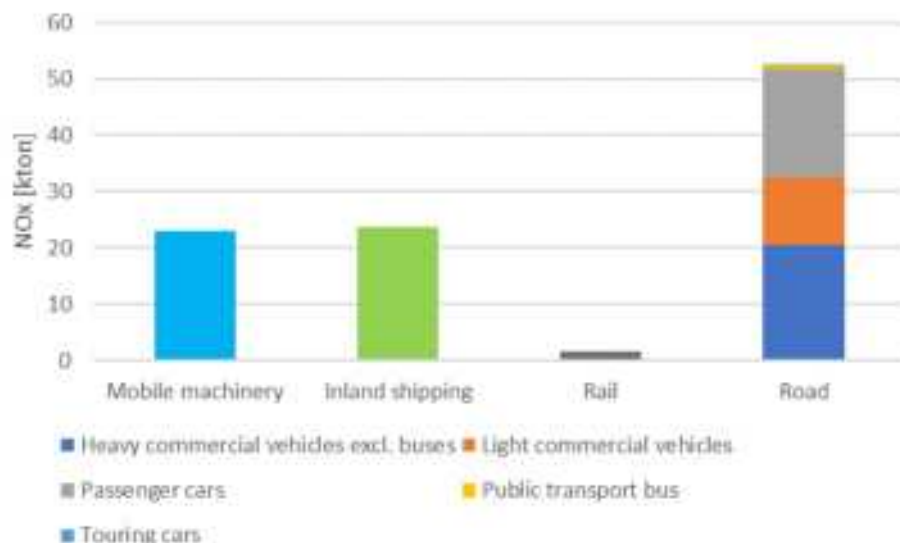


Figure 1: Total annual NO_x emissions in the Netherlands per sector for the year 2021.

EU Regulation

The EU NRMM Regulation [3] defines emission limits for NRMM for different power ranges and applications. It also lays down the procedures engine manufacturers must follow in order to obtain type-approval of their engines – which is a prerequisite for placing their engines on the EU market. The Regulation defines which applications fall under the scope. In scope are applications such as NRE (Non-Road Engines), NRG (Non-Road Gensets), IWP (Propulsion engines of Inland Waterway Vessels), RLL (Rail Locomotives) and RLR (Railcars). Test cycles for engine tests are to be conducted on an engine test bed. They consist of a transient test, the NRTC, and several steady-load tests, such as the NRSC (mode tests C1, E2, E3, etc). Emissions limits are differentiated by net power categories, with for each power category a different set of limits for the substances CO, HC, NO_x, PM (Particulate Matter) and PN (Particulate Number). For Stage V the power categories between 19 kW and 560 kW have more stringent PM and PN limits and the power categories between 56 and 560 kW also have a more stringent NO_x limit. In-service monitoring was initially applicable for NRE v > 5 and 6 > 56 < P < 150 kW and 130 < P < 560 kW, respectively) but is extended to lower and higher power categories as well, entering into force December 2022. For the power categories with more stringent limits the requirements lead to application of a DPF (Diesel Particle Filter) to comply to the respective PM and PN limits and SCR (Selective Catalytic Reduction) to comply to the NO_x limits.

Measuring real word emissions: method

To be able to determine real world emission levels of NRMM, the emissions and usage data of the NRMM were measured using a Smart Emissions Measurement System (SEMS). SEMS is a sensor-based system developed by TNO [4]. SEMS has been used in various programmes to measure and analyse the tailpipe NO_x, NH₃ and CO₂ emissions. Moreover, the fuel consumption during daily operation and a range of vehicle/engine parameters are monitored. The purpose is to characterize the typical operation of the vehicles or machinery. In this way, for the group of test subjects, weeks up to months of data were collected per subject. The SEMS uses a calibrated (periodically checked and adjusted) automotive NO_x sensor which is combined with an O₂ sensor, an ammonia sensor, GPS, and a data-acquisition system to record the sensor data and data from the vehicle and engine at a sample rate of 1 Hz.



Figure 12: Smart Emissions Measurement System (SEMS). Left, emissions sensors in the tail pipe of an NRMM. Right, data recorder and transmitter to read, store and transmit sensor data, engine data and GPS data to a central server.

Mass emissions and instantaneous engine power are calculated combining sensor data and engine and vehicle data, such as manifold air flow, fuel rate, engine torque, engine speed and sensor O₂ concentration where available. Depending on availability of signals, the best of the following methods is chosen in terms of expected accuracy: carbon-balance, mass air flow and fuel flow, speed density, emission-over-CO₂ ratio and estimate of specific fuel consumption.

Data from four projects was collected and reprocessed to calculate and depict emissions and usage parameters of thirteen NRMM used in real operation in their daily duty. In the programmes fifteen individual machines fulfilled the criterion of having either stage IV or V certification. Two machines were rejected from the sample because one ran only for a very short duration (3 h) during a long test period and another one had a faulty NO_x sensor signal. In Table 1 an overview is given of the machinery which was used in the analysis.

Table 1: Overview of measured Stage IV and V NRMM available for analysis.

Type	Brand	Type	Power [kW]	EU NRMM Stage	Machine running hours at beginning of test	Total test hours
Excavator	Kubota	KX027-4	18.5	V (IID)	1716	8
Excavator	Hitachi	ZX85US-6	42.4	V (NRE-v-4)	n.a.	83
Excavator	Takeuchi	TB290-2	51.6	V (NRE-v-4)	1648	163
Excavator	Takeuchi	TB 2150 R	85	V (NRE-v-5)	2322	53
Wheeled Excavator	Takeuchi	TB295W	85	V (NRE-v-5)	n.a.	45
Excavator	Caterpillar	326	152	IV (R)	n.a.	144
Wheel loader	Volvo	L70h	127	IV (R)	3635	211
Wheel loader	Caterpillar	950M	171	V (NRE-v-6)	405	468
Asphalt Roller	Bomag	174AP-4AM	55.4	V (NRE-v-4)	2665	587
Paver	Dynapac	SD2500C	129	V (NRE-v-5)	2096	275
Pile driving rig	ABI	TM18/22B	563	V (NRE-v-7)	888	516
Terminal Swap body transporter	Kamag	PM	115	V (NRE-v-5)	4390	1278
Tractor	Valtra	N4	114	IV (R)	n.a.	55.3



Figure 13: Pictures of the types of NRMM that were part of the analyses.

NO_x emissions of 13 Stage IV and V NRMM

EU emissions regulation aims to limit the brake specific emissions, but for air quality the time-based emissions are important. Therefore, for the thirteen NRMM both the average work specific as well as the average hourly mass emissions were determined, see Figure 4 and Figure 5, respectively. Real-world NO_x emissions of cat. NRE 5 and 6 ($56 \leq P < 560$ kW), which all use SCR, are reasonably low in most regular cases such as excavators and wheel loaders: 0.2 – 1.8 g/kWh, but are higher for some other regular cases, the wheeled excavator (2.4 g/kWh) and the tractor (IV, 1.7 g/kWh) and are high for a special case, the swap body transporter (6.7 g/kWh).

Real-world NO_x emissions of the monitored low powered cat. 2 – 3 ($P < 10$ kW) and cat. 4 – 5 ($P < 55$ kW) are high due to the higher NO_x limits which do not require the use of SCR. The same may apply for NRE-1 and 3 which have not been monitored. Real-world NO_x emissions of a category NRE-7 machine, the pile driving rig,

are very high (7.3 g/kWh) due to the higher NO_x limit which does not require the use of SCR and are also high in g/h due to the high power of the engine and running at low load.

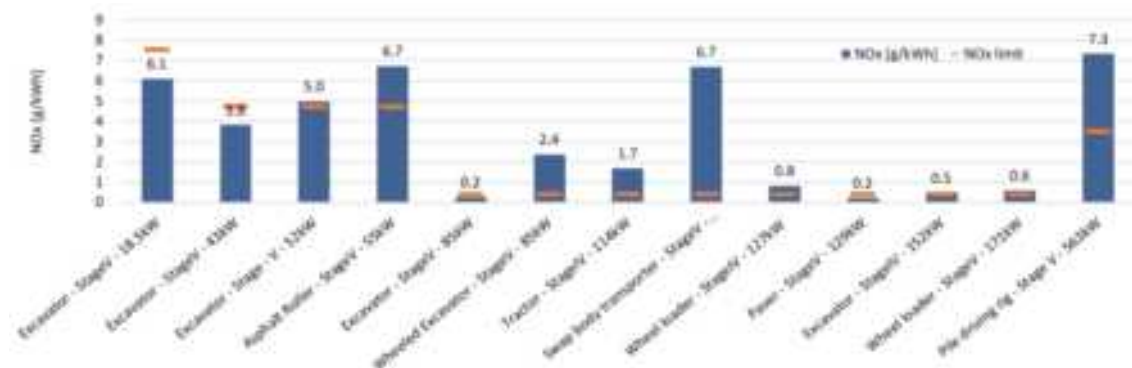


Figure 4: Average work specific NO_x emissions of 13 NRMM in real world operation and the NO_x limit according to the EU NRMM Regulation which applies for the prescribed laboratory test cycles.

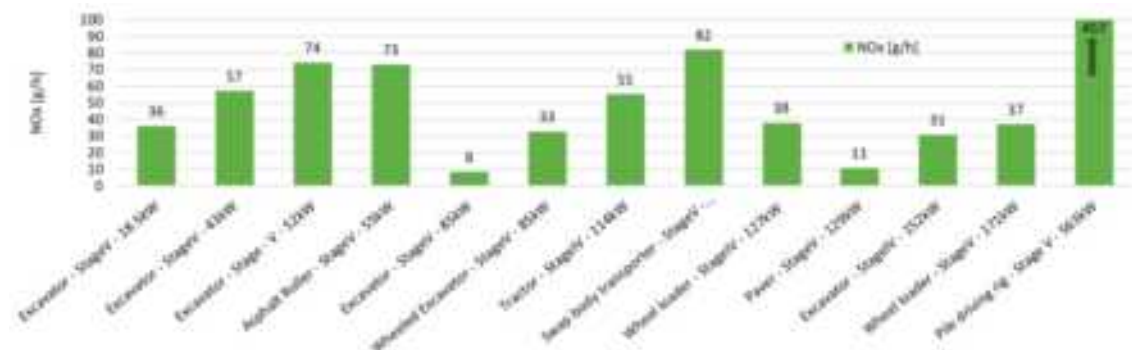


Figure 5: Average hourly NO_x emissions of 13 NRMM in real world operation.

Impact on local air quality is not only determined by the average emissions. The study at hand therefore looked into the distribution of emissions as well. The data is analysed according to the Stage V In-Service Monitoring (ISM) procedures, using the Moving Average Windows (MAW) methodology. This method averages emissions in a window with a fixed amount of engine work of which the duration is thus determined by the level of engine power. Criteria are defined to exclude MAW (invalid MAW, eg. average engine power <20%), short sequences and non-working events (eg. average engine power <10%, take off from the ISM evaluation. Figure 6 illustrates the frequency of the MAW NO_x values measured for the wheeled excavator of 85 kW and the swap body transporter. The blue bars represent the data which remains after applying the ISM procedure (containing working events and valid MAW), the orange bars show data which are excluded (non-working events and invalid MAW). The example of the wheeled excavator shows that 42 % of the MAWs are in the lowest NO_x bin. A long tail is however observed, with some MAWs going up to 10 g/kWh and where higher fractions of MAW are excluded. For the swap body transporter almost all MAW are excluded. The peak of the distribution lies around 7 g/kWh. Figure 7 shows that the ISM method leads to different shares of valid, invalid MAW and exclusions depending on the NRMM and its usage. The pile driving rig and swap body transporter have a low share of valid MAW. Both NRMM run at a very low power of about 11 % of maximum rated power on average. Also, the wheeled excavator which shows 48 % of valid MAW runs at a low average power of 16 %.

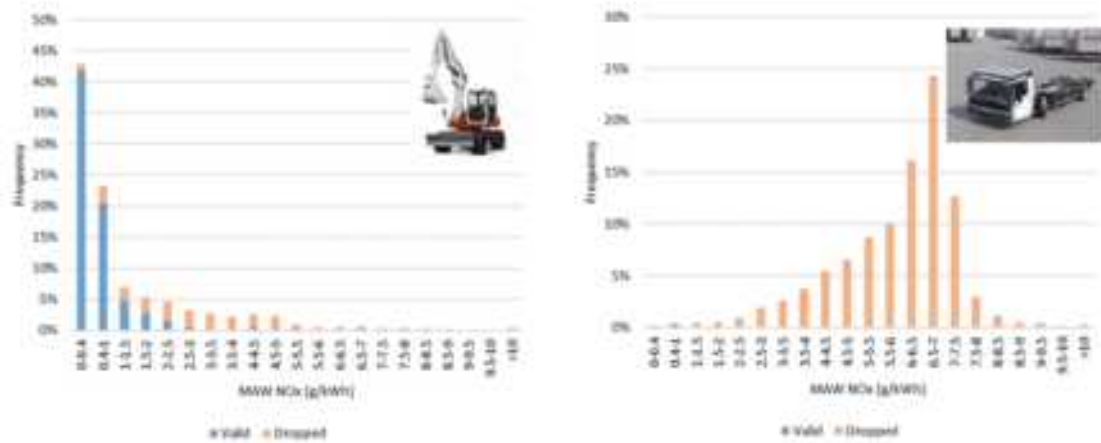


Figure 6: Examples of the distribution of work specific NO_x emissions in Moving Averaging Windows (MAW) of two NRMM. This for all valid MAW and MAW which are dropped (invalid and excluded) due to the in-service monitoring rules.

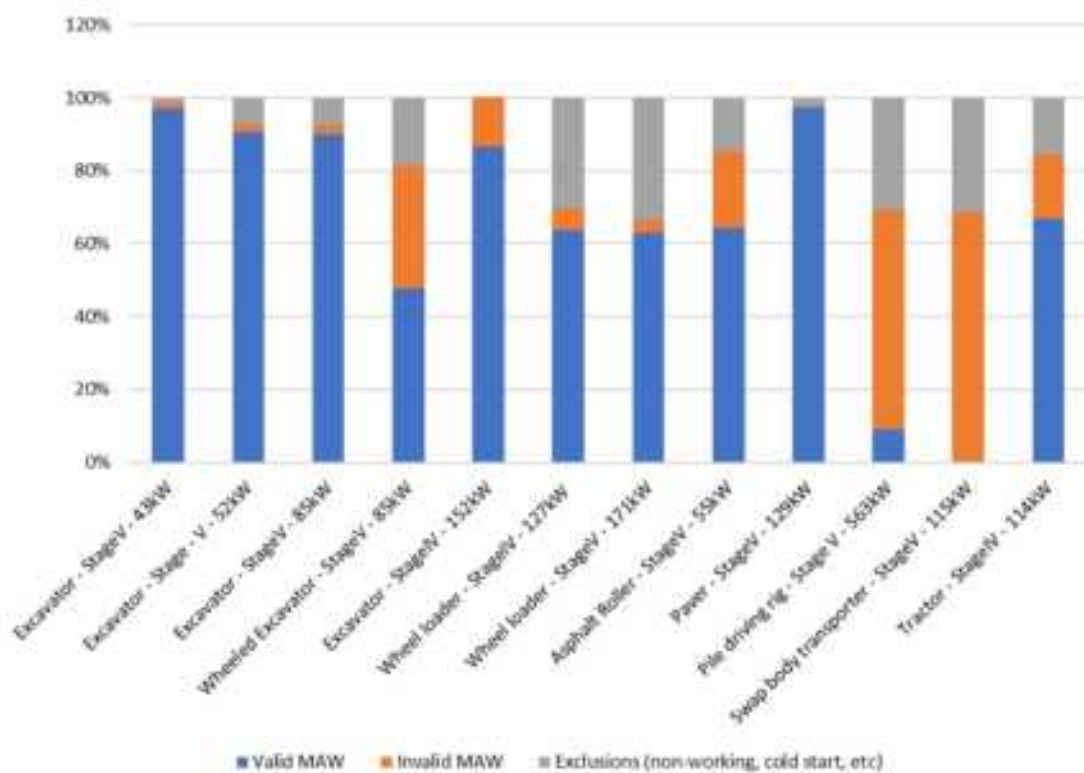


Figure 7: Shares of valid and invalid Moving Averaging Windows (MAW) and exclusions (non-working events, cold starts) after applying the calculation rules for in-service monitoring.

Analysis of the distribution of engine power reveals that for most machines the power distribution is on the low side, with a high share below 30 % of maximum engine power. With exception of four machines, most machines show a distribution of exhaust gas temperatures above 200°C which indicates that for those applications SCR working temperatures is reached most of the times, despite the in some cases lower loads below 30 %. The small excavator (18,5 kW, no SCR) shows larger shares of low exhaust gas temperatures, and so do the swap body transporter (115 kW, SCR) and the pile driving rig (563kW, Exhaust Gas Recirculation – EGR – only) which resulted in high NO_x emissions.

Figure 11 shows the percentage of total NO_x emissions that can be avoided by switching it off in idle. On average 18 % of total NO_x can be avoided by switching off the engine after 5 minutes of stand-by, with a variation being between 3–44 %.

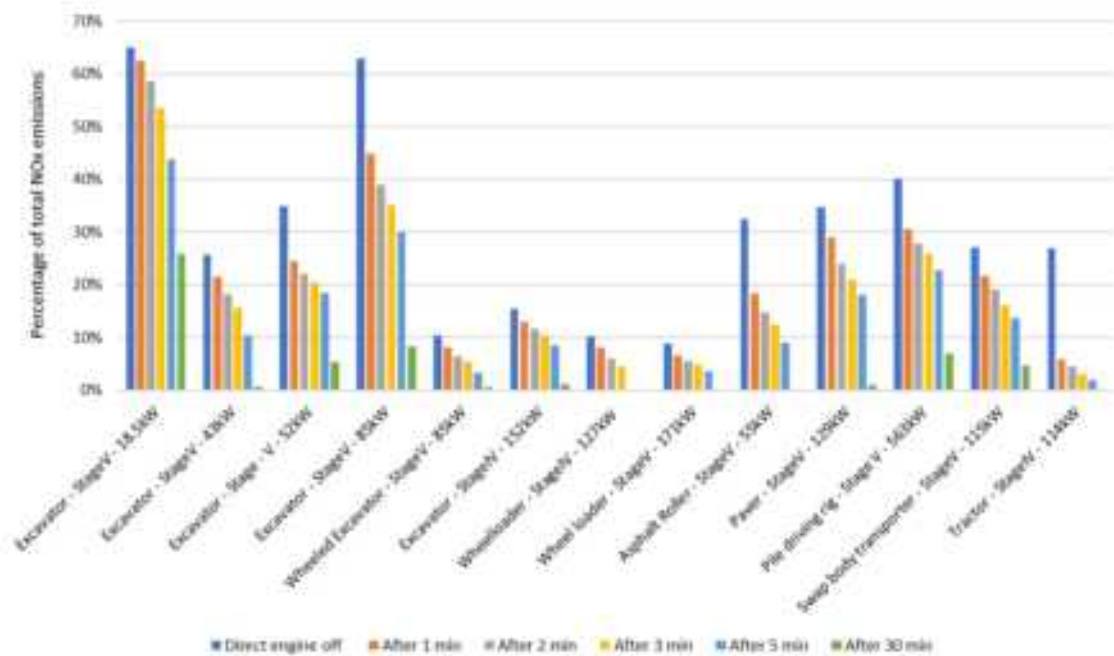


Figure 8: Percentage of total NO_x emissions which can be avoided when the engine is switched off at different times after a working event.

Discussion

Engine load patterns vary between machines of the same type and between different types of machines. In general, the average engine load is relatively low or can have intermittent periods of working and stand-by events. Despite the low power, with a few exceptions most tested NRMM are able to maintain sufficiently high SCR working temperatures to reduce engine out NO_x emissions for most of the running time, in the case NRMM are equipped with SCR. Generally, on average higher or temporarily higher NO_x emissions for these NRMM are caused by average low load operation, intermittent load operation and high stand-by shares of the usage, which are not controlled by NRMM test cycles.

NRMM in the low (<56 kW) and high-power (>560 kW) categories have less stringent NO_x limits, hence SCR is not needed to comply to the EU Regulation. This results in high absolute emissions for the low power categories (P<56 kW) and very high NO_x emissions for the high powered NRMM (>560 kW). No PN limit and a less stringent PM limit for the engine category 'P < 19 kW and P > 560 kW', might not require the use of a DPF which probably results in high PN and PM emissions. Engine power sizing is pushed to categories with less stringent NO_x and/or PN/PM limits, e.g., >560 or <19 kW/<56 kW where no emissions abatement is needed to achieve the test cycle emission limits. For example, several machines were identified with an engine power just outside the boundary (e.g., 18.5, 55 and 563 kW).

Representativeness of test cycles; test cycles do not cover the spread of usage in terms of engine load patterns observed. There is a lack of control of real-world emissions from normal (varying) usage with stand-by/idling, low load, intermittent loads, which are all not well-covered in test cycles. The high average load over the test cycle does not require low temperature SCR light off. The NRTC has higher speeds and loads than the WHTC test used for heavy-duty engines. For NRMM this results in faster reaching the operating temperatures for exhaust aftertreatment in the test cycle. The transient operation of NRTC does resemble the typical part of transient engine operation of certain construction machinery while working, such as wheel loaders and excavators. In real use, working events can however be followed or preceded by stand-by or non-working events, which are not included in test cycles and which according to SM rules are excluded from

monitoring. ISM is limited to conditions comparable to the NRTC, i.e., working events with well-functioning SCR and high load, excludes low load and idling and was only applicable for medium powered NRE, while stand-by NO_x emissions and NO_x from intermittent load cycles are significant. For multiple machines which were monitored, a substantial part of the real-world data needed to be excluded because it was considered as a non-working event or not valid. The absence of signals from on-board control units makes it difficult to calculate the engine load in some cases. Furthermore, the calculation method of engine power is not always clear due to lack of standardization.

Conclusions

NRMM contributes significantly to the total PM and NO_x emissions. Due to the lack of stringent emission limits for the low and high-powered engines, the incomplete coverage of normal operation of NRMM in test procedures and the use of older machinery with a long lifetime, the contribution of NRMM will remain significant in the upcoming years. In contrast, the emissions of road transport will decrease further due to the effective Euro VI- step E and Euro 6d and introduction of Euro 7.

There are many NRMM types. For the ones tested usage patterns vary.

For the latest generation of NRMM (Stage IV with SCR and stage V) real-world NO_x emissions vary from 0.2 to 7.3 g/kWh and depend on usage and the NRE power category. The large variation is caused by:

- The applicable type-approval test procedures which only partly covers normal conditions of use, but does not cover typical use such as stand-by, intermittent load and low load operation. As a result, NRMM regulation does not consider a substantial share of the real working conditions. The ISM evaluation also excludes substantial test data of normal use, such as low engine load conditions and stand-by/idle. This while NRMM often remain on one location to do their work for a period of time, hence all usage and related emissions matter for local air-quality and nitrogen deposition.
- The fact that higher NO_x emissions are allowed for Stage V NRE in the low and high-power categories. Similar issues for control of PM/PM emissions are expected for NRE in the low and high-power categories with absence of a PN and a stringent PM limit.

This can be tackled by more stringent NOx limits for P<56 kW and >560 kW, a PN limit for low (<19 kW) and high-powered engines (>560 kW), better coverage of real-world usage in tests and for ISM, extension of window of control, covering a larger part of real-world usage, including low load operation.

Technical solutions include automatic engine shut off, NO_x abatement for low and high-powered diesel engines (EGR, SCR), increasing low temperature SCR performance and DPF for low and high-powered diesel engines and electrification depending on the use case.

Acknowledgements

For this work data was used of projects funded by the Dutch Ministry of Infrastructure and Water management.

Sources and References

- [1] C.D. Desouza, D.J. Marsh, S.D. Beevers, N. Molden, D.C. Green, Real-world emissions from non-road mobile machinery in London, *Atmospheric Environment*, Volume 223, 15 February 2020
- [2] C.D. Desouza, D.J. Marsh, S.D. Beevers, N. Molden, D.C. Green, A spatial and fleet disaggregated approach to calculating the NOx emissions inventory for non-road mobile machinery in London, *Atmospheric Environment: X* Volume 12, December 2021, 100125
- [3] Regulation (EU) 2016/1628 of the European Parliament and of the Council of 14 September 2016, on requirements relating to gaseous and particulate pollutant emission limits and type-approval for internal combustion engines for non-road mobile machinery, amending Regulations (EU) No 1024/2012 and (EU) No 167/2013, and amending and repealing Directive 97/68/EC (Text with EEA relevance)
- [4] Heijne, V., Spreen, J., Smokers, R., Vermeulen, R., Ligterink, N., Stelwagen, U., Kadijk, G. (2016). Assessment of road vehicle emissions: methodology of the Dutch in-service testing programmes, TNO 2016 R11178, 20 October 2016.
- [5] Ligterink, N., Louman, R., Buskermolen, E., & Verbeek, R. (2018, October). Connekt Topsector logistiek, Use of construction machines and associated NOx and CO2 emissions.
- [6] Hulskotte, Ir. J.H.J., Verbeek, Ir. R.P., Emissiemodel Mobiele Machines gebaseerd op machineverkopen in combinatie met brandstof Afzet (EMMA), TNO rapport TNO-034-UT-2009-01782_RPT-ML, November 2009
- [7] Vermeulen, van Goethem, SEMS operating as a proven system for screening real-world NOx emissions, paper for the Transport and Air-Pollution Conference 2014, Graz, Austria
- [8] Vermeulen, R.J., Ligterink, N.E., van der Mark, P.J., Real-world emissions of non-road mobile machinery, TNO report TNO 2021 R10221, 11 February 2021
- [9] Vermeulen, Paschinger, NRMM stage IV/V real-world NOx emissions: status quo and perspectives, TNO 2023 P10252, 24 January 2023

PM10 emissions from, and rubber content in, different tyre types in relation to rubber hardness

M. Gustafsson¹, P. Tromp², N. Svensson¹

¹Swedish National Road and Transport Research Institute (VTI), Linköping, 581 95 Sweden. mats.gustafsson@vti.se

²TNO - Department EMSA, Utrecht, 3584 CB, The Netherlands

Introduction

Tyre wear particles (TWP) are a source to both air-borne particles and microplastic pollution of soil, water and sediments (Baensch-Baltruschat et al., 2020). The total wear of tyres in Europe has been estimated to 1.3 million tonnes/year (Wagner et al., 2018), making it one of the largest sources to microplastics. The tyre rubber mix consists of about 40–60% synthetic and/or natural rubber, depending on tyre type. The rest is reinforcing fillers (30–35 %), plasticizers (15 %), vulcanization agents (2–5 %) and other additives (5–10 %) (Wagner et al., 2018). Winter tyres need to have softer rubber mixes than summer tyres to maintain friction at low temperatures, when rubber gets stiffer. Therefore, winter tyres normally contain a higher share of natural rubber than summer tyres.

Except being an important source for general microplastics, defined as polymer containing particles smaller than 5 mm, tyre wear also contributes to airborne particles (e.g. Fussel et al., 2022). Since non-exhaust particles from tyres, brakes and road surface are not yet regulated, their emissions increase with increasing traffic amounts. Also, increasing emissions of tyre and road wear particles are promoted by vehicles continuously getting heavier as a result of trends (e.g. SUV:s) and vehicle propulsion developments (electrification) (e.g. Beddows and Harrison, 2021).

Information about tyre wear emissions and how their size and physico-chemical characteristics are affected by material properties and use is scarce, but highly relevant for future mitigation. In this paper, results from the Horizon Europe project Nº 955387 *Low particle Emissions and Low Noise Tyres (LEON-T)* are presented. In the project particle emissions from six sets of tyres (summer, all-season and winter) run in a road simulator have been investigated, characterized, and analysed in relation to tyre properties. Data from similar tests of summer and winter tyres in a governmental assignment (GA) at VTI are also presented.

Methods

The VTI Road simulator is a carousel-like equipment with 4 wheels running on a circular pavement ring (Figure 1). Any kind of pavement and light duty vehicle tyres can be used. The maximum speed is 70 km/h and the hall is temperature controlled.



Figure 1. The VTI road simulator

Tyres used in the LEON-T experiments were sets of three summer tyres, one 4-season tyre and one winter tyre. In the GA, four sets of summer tyres and four sets of winter tyres for Nordic conditions were used. All tyres in

LEON-T were tested on a cement concrete pavement in the same temperature conditions (15°C and 70 km/h). In the GA, tyres were tested on an asphalt concrete pavement in the same temperature but at a speed of 60 km/h. Axle load was 450 kg and inflation pressure 2.5 bars in both tests. PM and particle size distributions were measured using TEOM, FIDAS AQguard and Aerodynamic particle sizer (APS) and analysed in relation to tyre rubber hardness. Hardness was measured in Shore at room temperature (20°C).

To acquire the rubber content (SBR, NR) and total TWP content of PM, chemical analysis was performed using TED-GCMS following a similar approach as Eisentraut et al. (2019). The analysis is a two-step method: Thermo Extraction (step 1) and Desorption (step 2). In summary, a sample is first decomposed in a thermogravimetric analyzer (TGA) and the gaseous decomposition products are then trapped on a solid-phase adsorber. Subsequently, the solid-phase adsorber is analyzed with thermal desorption gas chromatography mass spectrometry. The instrument that was used is a TGA-TED-GCMSMS; decomposition products were sampled with Tenax-TA as a solid-phase adsorber at a temperature between 290–550°C. Dipentene and 4-phenylcyclohexene were used as markers for qualification and quantification of natural rubber (NR) and styrene-butadiene rubber (SBR). Two quantification techniques were used: (1) a direct calculation of TWP based on an average conversion factor from approximately 40 reference car and truck tyres and (2) an indirect method, based on the quantification of SBR and NR rubber and an estimation of the amount of rubber in car and truck tyres (appr. 50%).

Results and discussion

Despite lower speed, the resulting concentrations (and consequently emissions) are markedly higher in the GA project compared to the results in the LEON-T project (Figure 2). A probable reason for this is differences in road surface properties and how consecutive tests were run. In the GA project, every third test on the asphalt road surface was made with studded tyres, while studded tyres were not used in the LEON-T test sequence at all. Studded tyres will roughen the road surface. A rougher surface will both abrade the next set of studless tyres tested but also, the road surface itself will more easily emit mineral particles since tyre rubber will polish the aggregates in the surface. In LEON-T, the road surface is consistently being polished by summer and studless winter tyres, why emissions from both tyres and road surface are lower.

Therefore, for easier comparison between projects, in Figure 2, the normalised PM₁₀ emissions from both projects are shown. PM₁₀ emissions are negatively correlated to rubber hardness. As can be seen, winter tyres, which has softer rubber mixes, emit more PM₁₀ in both data sets, compared to summer tyres and the only 4-season tyre. The higher PM₁₀ levels in the normalised (to mean values of each data set) LEON-T data set are likely to be related to the higher speed used in tests. Cement concrete pavements have, exposed to studded tyre wear, been shown to emit more PM₁₀ due to the contribution from the cement matrix (Gustafsson et al., 2019). If this is a contributing factor also for studless tyres is not known.

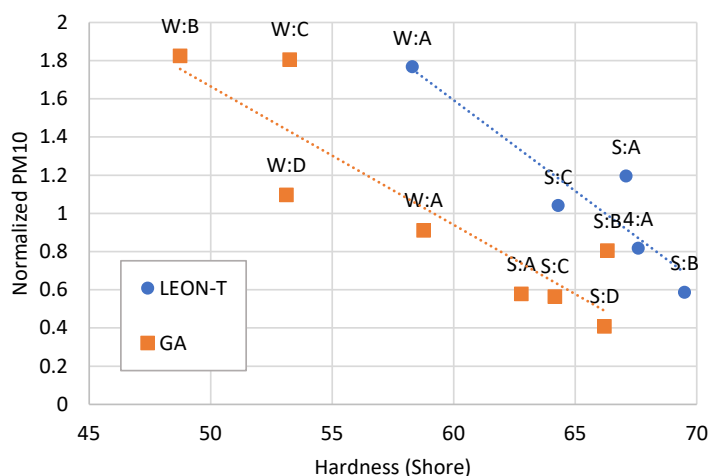


Figure 2. Relationship between rubber hardness and PM₁₀ emissions in LEON-T project and the governmental assignment (GA) project. S=summer tyre, W=winter tyre, 4=4-season tyre. Letters A-G represent different tyre brands.

Results from the rubber analyses of the LEON-T PM₁₀ samples, show that only a small fraction of PM₁₀ is TWP, the remaining PM most likely originates from the concrete pavement (Table 1 and Figure 3). Possibly also other emission mechanisms (evaporation & condensation of semi-volatile organic components in tyres) play a

role, as the carbonaceous content in PM, observed with electron microscope, seems higher than the analysed TWP concentrations. The winter tyre generates a five-fold TWP concentration in the PM10 (Table 1).

Table 1. Concentration SBR, NR, TWP in PM10 ($\mu\text{g}/\text{m}^3$) and percentage TWP in PM10

Tyre type	SBR	NR	%NR	TWP	%TWP
Winter	1,6	0,15	9%	3,5	4.9%
4 Season	0,26	0,02	6%	0,54	1.3%
Summer	0,14	0,02	10%	0,31	0.8%

Considering the low concentration of TWP in PM10, it can be concluded that the obvious correlation between PM10 emission and rubber hardness depends on higher tyre wear at lower hardness, but mostly in higher emissions of road wear. Since the road surface in the simulator do not accumulate dust being overrun very frequently, it can be argued that softer rubber may cause higher slip forces and thus generate higher wearing of the cement concrete as well. Note that the cement binder itself, which is softer and more brittle than the rock ballast aggregates, also is a possible source to PM10 in this pavement type (Gustafsson et al., 2019).

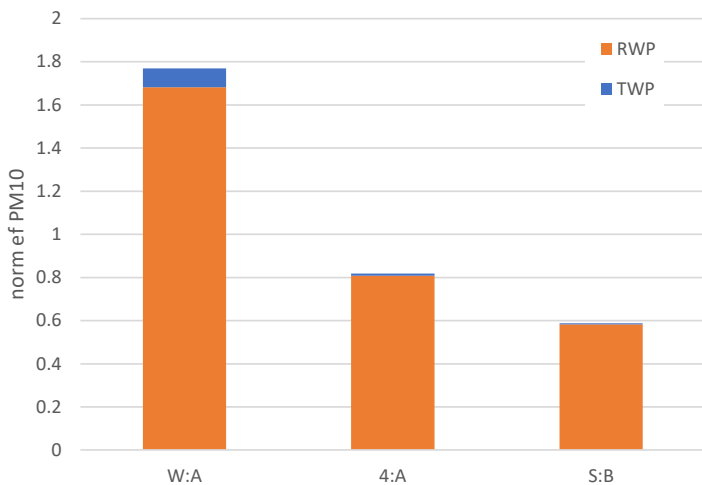


Figure 3. Shares of road and tyre wear particles in the normalized emission from the winter, 4-season and summer tyres analysed. S=summer tyre, W=winter tyre, 4=4-season tyre. Letters A and B represent different tyre brands.

In Figure 4, calculated emission factors for PM10 from the AQguard instrument and simultaneous gravimetical sampling as well as emission factor for TWP during the LEON-T experiments are shown as function of rubber hardness. The emission factors are very low compared to literature, which could be attributed to a high degree of polishing of the road surface.

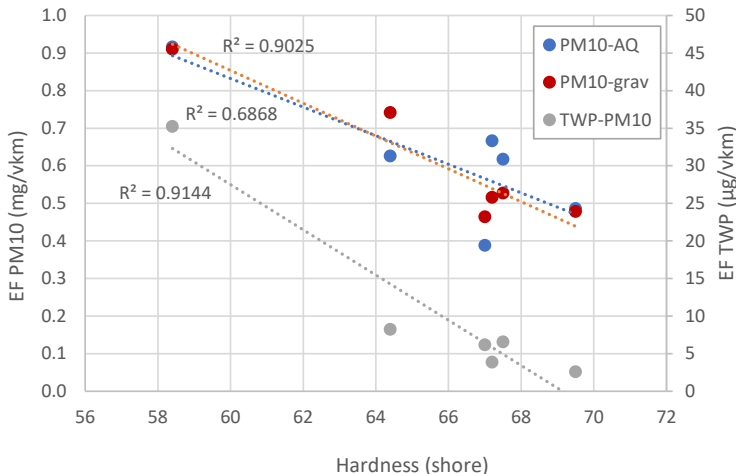


Figure 4. Emission factors for PM10 om mass per vehicle kilometre from AQguard instrument and gravimetric measurements and emission factor for TWP during the LEON-T experiments.

In Figure 5, PM10 size distributions as measured by APS of a winter, summer and 4-season tyre from the same manufacturer are shown. The mass size distributions reveal that the winter tyres have a markedly finer and more narrow mass peak at slightly below 2 μm compared to the other tyres' broader mass peaking at 2–5 μm . This is in agreement with the TED-GCMS analysis of PM10, PM2.5 and PM1.0. For winter tyres a higher percentage of TWP is in the smaller size fraction. For example, for winter tyres approximately 45% of TWP is in the PM2.5 fraction, while for the summer tyres this is approximately 20%.

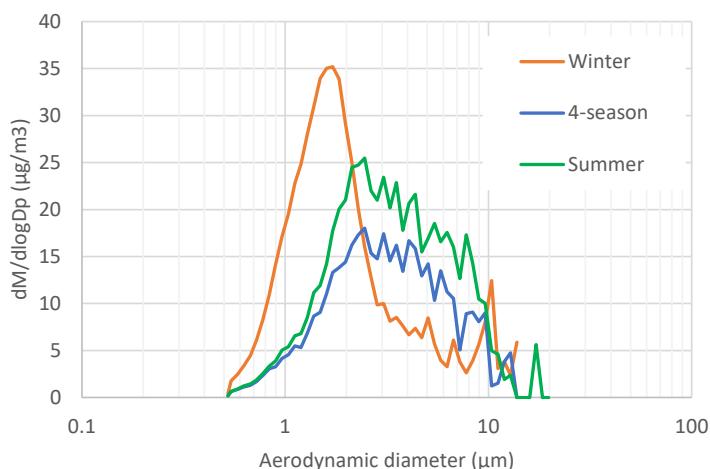


Figure 5. Particle number size distribution and mass size distribution of three tyre types from the same brand.

Conclusions

From this study it can be concluded that the tyres with lower hardness relates to higher yields of PM10. The winter tyres tested yields higher amounts of TWP content and a finer mass size distribution compared to the summer and 4-season tyres. The contribution of tyre wear to the PM10 produced is between 1–5%, while the dominant part is minerals. The higher PM10 emissions from the rougher asphalt may be a result of higher tyre wear as well as of higher wear of the pavements rougher surface.

Acknowledgements

This work was funded by the European Commission through the Horison Europe project N°955387 *Low particle Emissions and Low Noise Tyres (LEON-T)*. The authors are grateful to the ever-helpful technical staff Dennis Hydén and Tomas Halldin at the VTI road simulator facility and to Johan Esveld and Paul Fokkens for sampling set-up.

References

- Baensch-Baltruschat, B., Kocher, B., Stock, F., Reifferscheid, G., 2020. Tyre and road wear particles (TRWP) - A review of generation, properties, emissions, human health risk, ecotoxicity, and fate in the environment. *Sci Total Environ* 733, 137823, <https://doi.org/10.1016/j.scitotenv.2020.137823>.
- Beddows, D.C.S., Harrison, R.M., 2021. PM10 and PM2.5 emission factors for non-exhaust particles from road vehicles: Dependence upon vehicle mass and implications for battery electric vehicles. *Atmospheric Environment* 244, <https://doi.org/10.1016/j.atmosenv.2020.117886>.
- Dahl, A., Gharibi, A., Swietlicki, E., Gudmundsson, A., Bohgard, M., Ljungman, A., Blomqvist, G., Gustafsson, M., 2006. Traffic-generated emissions of ultrafine particles from pavement-tire interface. *Atmospheric Environment* 40, 1314-1323, <https://doi.org/10.1016/j.atmosenv.2005.10.029>.
- Eisentraut P, Dümichen E, Ruhl AS, et al. Two Birds with One Stone - Fast and Simultaneous Analysis of Microplastics: Microparticles Derived from Thermoplastics and Tire Wear. *Environ Sci Tech Lett*. 2018;5(10):608-613. <https://doi.org/10.1021/acs.estlett.8b00446>
- Gustafsson, M., Kraft, L., Olofsson, U., 2019, Moderna betongbeläggningar: utveckling mot mindre slitage och partikelemission, 03476030 (ISSN), Statens väg- och transportforskningsinstitut, <http://urn.kb.se/resolve?urn=urn:nbn:se:vti:diva-13697>
- Fussell, J.C., Franklin, M., Green, D.C., Gustafsson, M., Harrison, R.M., Hicks, W., Kelly, F.J., Kishta, F., Miller, M.R., Mudway, I.S., Oroumiyah, F., Selley, L., Wang, M., Zhu, Y., 2022. A Review of Road Traffic-Derived Non-Exhaust Particles: Emissions, Physicochemical Characteristics, Health Risks, and Mitigation Measures. *Environmental Science & Technology*, <https://doi.org/10.1021/acs.est.2c01072>.
- Mathissen, M., Scheer, V., Vogt, R., Benter, T., 2011. Investigation on the potential generation of ultrafine particles from the tire-road interface. *Atmospheric Environment* 45, 6172-6179.
- Wagner, S., Hüffer, T., Klöckner, P., Wehrhahn, M., Hofmann, T., Reemtsma, T., 2018. Tire wear particles in the aquatic environment - A review on generation, analysis, occurrence, fate and effects. *Water Res*. 139, 83-100, <https://doi.org/10.1016/j.watres.2018.03.051>.

NRMM Real Operation NO_x Emission Measurements with Plume Chasing

C. Schmidt^{1,2*}, D. Pöhler^{1,2}, S. Schmitt², C. Heidt³, F. Münch³, U. Platt^{1,2}

¹Institute of Environmental Physics, University of Heidelberg, Heidelberg, Germany,
cschmidt@iup.uni-heidelberg.de

²Airyx GmbH, Eppelheim, Germany

³ifeu – Institut für Energie- und Umweltforschung Heidelberg gGmbH, Heidelberg, Germany

Introduction

Non road mobile machinery (NRMM) contributes significantly to pollution (Helms and Heidt, 2014). The introduction of emission limits in Directive 97/68/EC for new engines (e.g., Stage II: 8000 mg/kWh and Stage IIIA: 7500 mg/kWh) has significantly reduced emissions in recent years. With the introduction of the EU Stage V emission standard (Regulation EU 2016/1628) in 2019, monitoring of real-world emissions during operation is carried out for the first time as part of an in-service monitoring (Regulation EU 2017/655). The current data on real-world emissions from NRMM is still incomplete and mostly based on PEMS measurements, which are rare and costly. To obtain a greater knowledge of the emissions of machines under different operating conditions, it is advisable to use a mobile device that can easily determine reliable emission values. A feasibility study applying Plume Chasing / Point Sampling for NO_x emissions using an ICAD-NO_x device (Horbansky et al., 2019) from Airyx GmbH was conducted. The real driving NO_x emissions from construction machinery were measured and compared with the NO_x limits for the investigated construction vehicles.

Methods

In this study, a combination of Plume Chasing and Point Sampling is used. Plume Chasing is an emission measurement method where the plume is traced, while Point Sampling is a stationary method which measures the exhaust plume when vehicles pass by. The measurements were conducted next to the construction site 2 – 8 m from the investigated vehicles. The exhaust plume was sampled at about 2 m above the ground with a tripod. The ICAD-NO_x measurement device was placed in a bicycle trailer. With this mobile device it was possible to change the measurement position easily depending on the wind conditions and the working position of the construction vehicle. The plume was measured several minutes per construction vehicle and operation condition. The measurement principle is shown in Figure 1.

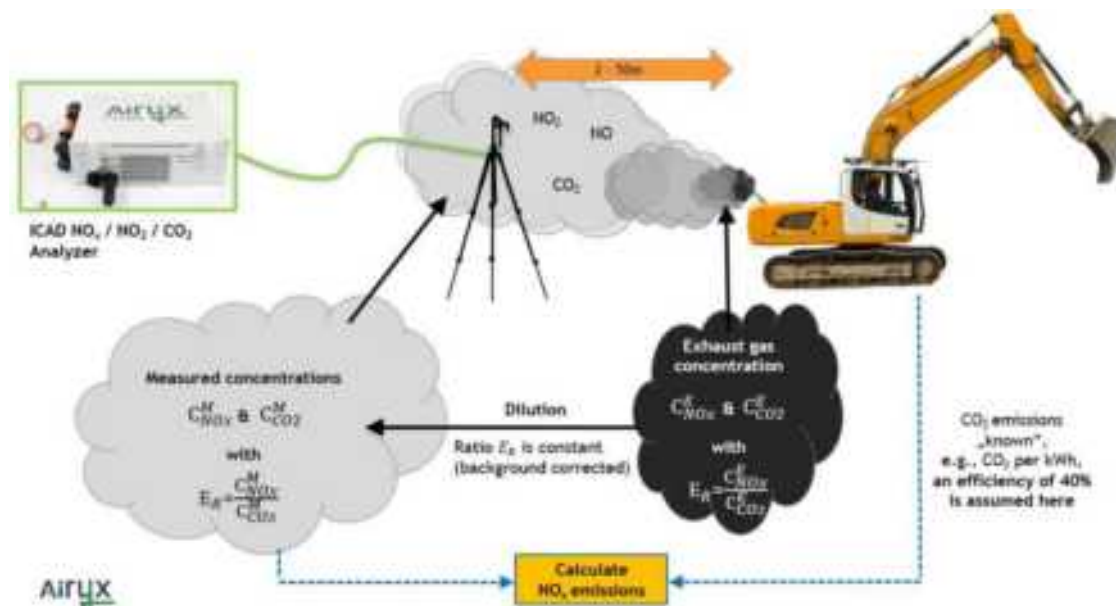


Figure 1: Measurement principle Plume Chasing of NRMM.

Assuming that the ratio E_R between NO_x and CO₂ concentrations remains the same as the gas becomes diluted after leaving the exhaust pipe (Eq. 1), the specific emissions in g/kWh can then be calculated from the NO_x to CO₂ ratio in the sampled air with the assumption of the CO₂ emissions of the vehicle C_E^ECO₂. A motor efficiency of 40% is assumed.

$$E_R = \frac{C_{NOx}^E}{C_{CO2}^E} = \frac{C_{NOx}^M - C_{NOx}^{BG}}{C_{CO2}^M - C_{CO2}^{BG}}$$

(1)

The background (BG) concentrations C_{CO2}^{BG} and C_{NOx}^{BG} of CO₂ and NO_x, respectively, are determined using a 5 s moving average of the time series of the measured signals. The BG values are determined as the lowest CO₂ value within a 120 s time interval prior to each individual measurement point, along with its corresponding NO_x value. To ensure that only emissions from the plume of the chased NRMM are considered, a threshold of 30 ppm was applied for CO₂. The measurement data point was considered valid only if the CO₂ concentration C_{CO2}^M exceeded the BG value by more than 30 ppm.

Investigated vehicles

Four different NRMM were investigated. Vehicle characteristics, including manufacturer, model, type, and Euro stage, are presented in Table 1. Among these NRMM, two are older construction vehicles of stage I and II (O&K L6.5 and Takeuchi TB135), measured at a rural location apart of other traffic (Figure 2, left). The investigations of the remaining two vehicles of stage IIIA (Gehl AL340, Takeuchi TB228) took place next to a busy road (Figure 2, right).

Table 1: Characteristics of investigated NRMM with time and location of measurements as well as weather conditions.

Manufacturer	O&K	Takeuchi	Gehl	Takeuchi
Model	L 6.5	TB135	AL 340	TB228
Type	Wheel loader	Mini-excavator	Wheel loader	Excavator
				
Motortype	Perkins 704.30	Vanmar 3TNV88-QTB	Yanmar 3TNV88 Interim Tier IV	3TNE82A
Fuel type	diesel	diesel	diesel	diesel
Euro stage	EU I	EU II	EU IIIA	EU IIIA
NO _x limit (g/kWh)	9.2	8	7.5	7.5
Day measurement of	03.03.21	03.03.21	24.03.21	24.03.21
Wind conditions	occasional light breeze from the south, south-west/east, ~2-4 m/s		from the south, ~0-2 m/s	
Measurement location	rural, country road (no traffic)		next to federal highway B3 (main traffic)	

Results and Discussion

Examples of the time series of the NO_x and CO₂ signal along with their respective determined BG (NO_x_BG) and BG-corrected time series (NO_x_BGcorr), are depicted in the upper two panels of Figure 3 and Figure 4. The concentrations in Figure 3 are declining from 14:11 onwards after the Takeuchi TB135 mini-excavator changed the working position. This movement occurred on the downwind side within a field as the excavator was engaged in digging a shaft, as illustrated in



Figure 15: Takeuchi TB135 mini-excavator with Plume Chasing setup at 03.03.2021 during digging a shaft (left) and Takeuchi TB228 excavator during idling at 24.03.2021 (right).

Figure 2 (left). While the measurement device and sampling position remained stationary in this situation, the mini-excavator moved further away. The concentrations dropped rapidly, leading to a situation where hardly any plume was detectable, and no data points exceeded the CO₂ threshold. This underscores the significance of a mobile measurement setup like the bicycle trailer, which can be easily relocated even in uneven terrain. This flexibility allows the setup to track the NRMM plume based on its work location and the prevailing wind conditions. For example, between 13:58 and 14:11 the measurement position was established at a distance of 6 to 8 m from the excavator in the northeast direction (measuring height ~2 m) resulting in good emission signal. Note that between 13:59:30 and 14:02, work operations were momentarily paused.

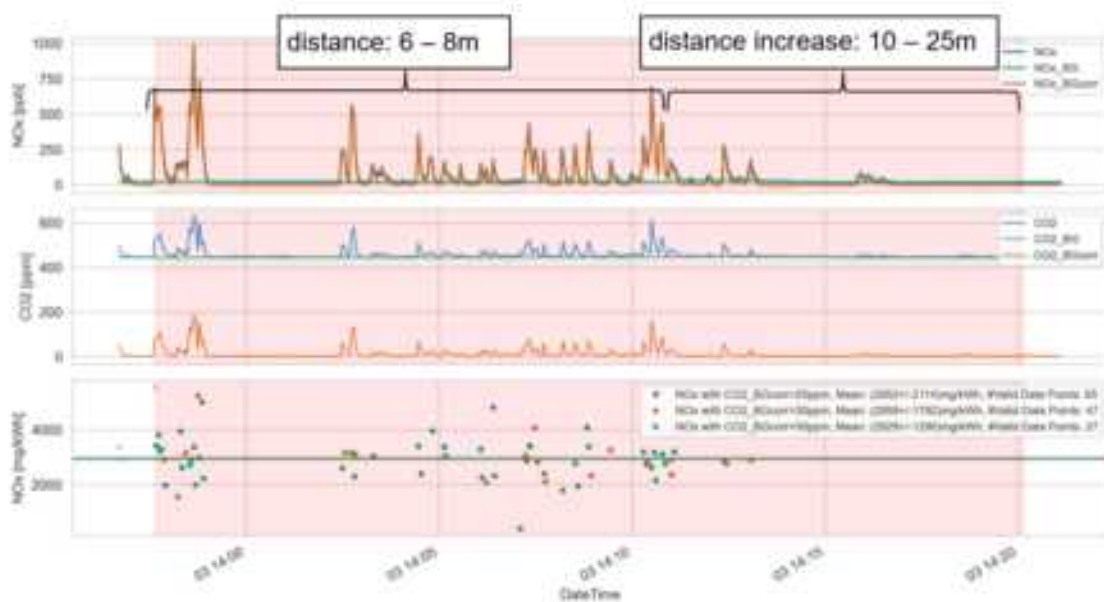


Figure 14: NO_x and CO₂ timeseries, 03.03.2021, Takeuchi TB135 mini-excavator (Stage II) digging a shaft; measuring height: ~2 m.

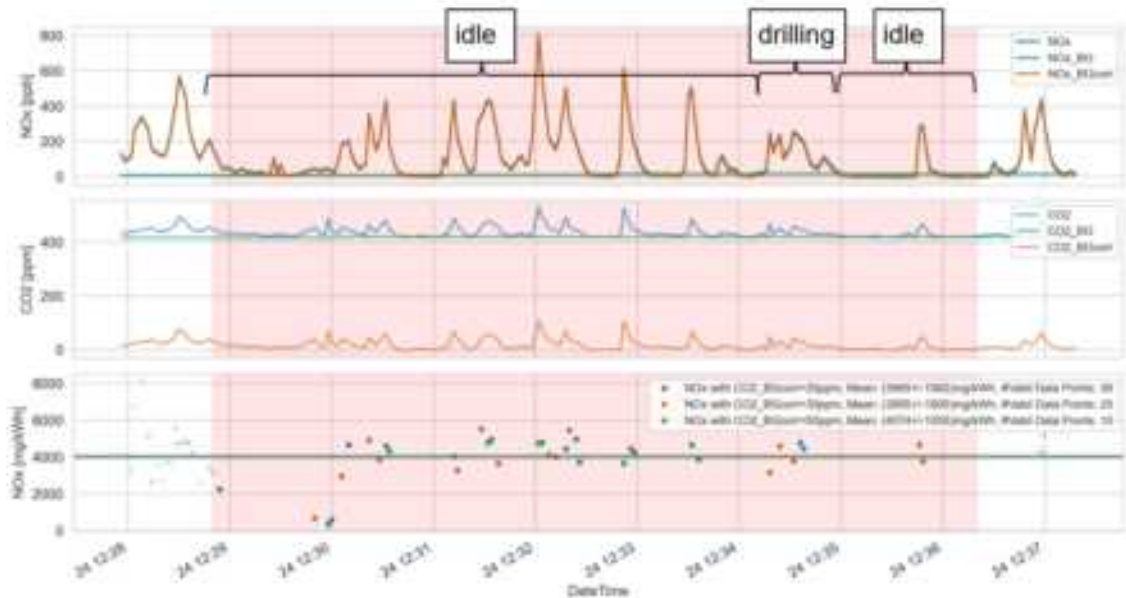


Figure 16: NO_x and CO₂ timeseries, 24.03.2021, Takeuchi TB228 excavator during idling and drilling; Measuring position: ~4 m behind the excavator, measuring height: 1.6 m.

In Figure 4, the emission measurements took place while idling of the Takeuchi TB228 excavator. Only from ~12:34 to 12:35 it was drilling. Due to the measurements being conducted near a busy road (see Figure 2, right), the road's impact on the background (BG) values was examined further. This investigation was carried out during timeframes when no plume was emitted from the construction vehicles, but significant traffic was present on the main road. Given that the wind direction aligned with the main road from the south, little variation in BG was observable in the concentrations at the measurement height of approximately 2 m, the plume CO₂ concentrations were most of the time below 10 ppm and always below 30 ppm. Nevertheless, it's important to recognize that at construction sites proximate to external emission sources, careful consideration of wind conditions and measurement positioning is crucial to ensure the correct plumes are detected. The lower panels in Figure 3 and Figure 4 illustrate the 2-second NO_x emission values computed using Eq. 1. These 2-second values are time-weighted and do not represent the Moving Average Windows Method³¹. Different colours show different CO₂ thresholds. The smaller the CO₂ threshold the more valid data points are captured. The mean NO_x values ($\bar{NO_x} \cdot BG_{corr} / CO_2 \cdot BG_{corr} \cdot C_{CO_2}^E$, power weighted, comparable to PEMS mean values) are indicated by a horizontal line.

The mean NO_x values and the median of the 2 s NO_x values are plotted in Figure 5 together with the distribution of the emission values for the different measured NRMM. The results show that the calculated emission values are consistent and plausible within the expected ranges. For the stage I (NO_x limit 9200 mg/kWh) wheel loader (Figure 5, top left) an average emission value of 8682 mg/kWh was determined during idling. The stage II mini-excavator (NO_x limit 8000 mg/kWh) displayed an average emission value of 3181 mg/kWh during earth removal (Figure 5, top right) and 2959 mg/kWh while shaft excavation (Figure 5, middle). The distributions show, that there is not a big difference between these two operation conditions. The two stage IIIA (NO_x limit 7500 mg/kWh) NRMM exhibited average emission values of 4394 mg/kWh and 8396 mg/kWh during idling, respectively, for the excavator (Figure 5, bottom left) and the wheel loader (Figure 5, bottom right).

³¹ <https://eur-lex.europa.eu/legal-content/DE/TXT/PDF/?uri=CELEX:32011R0582&from=ES>

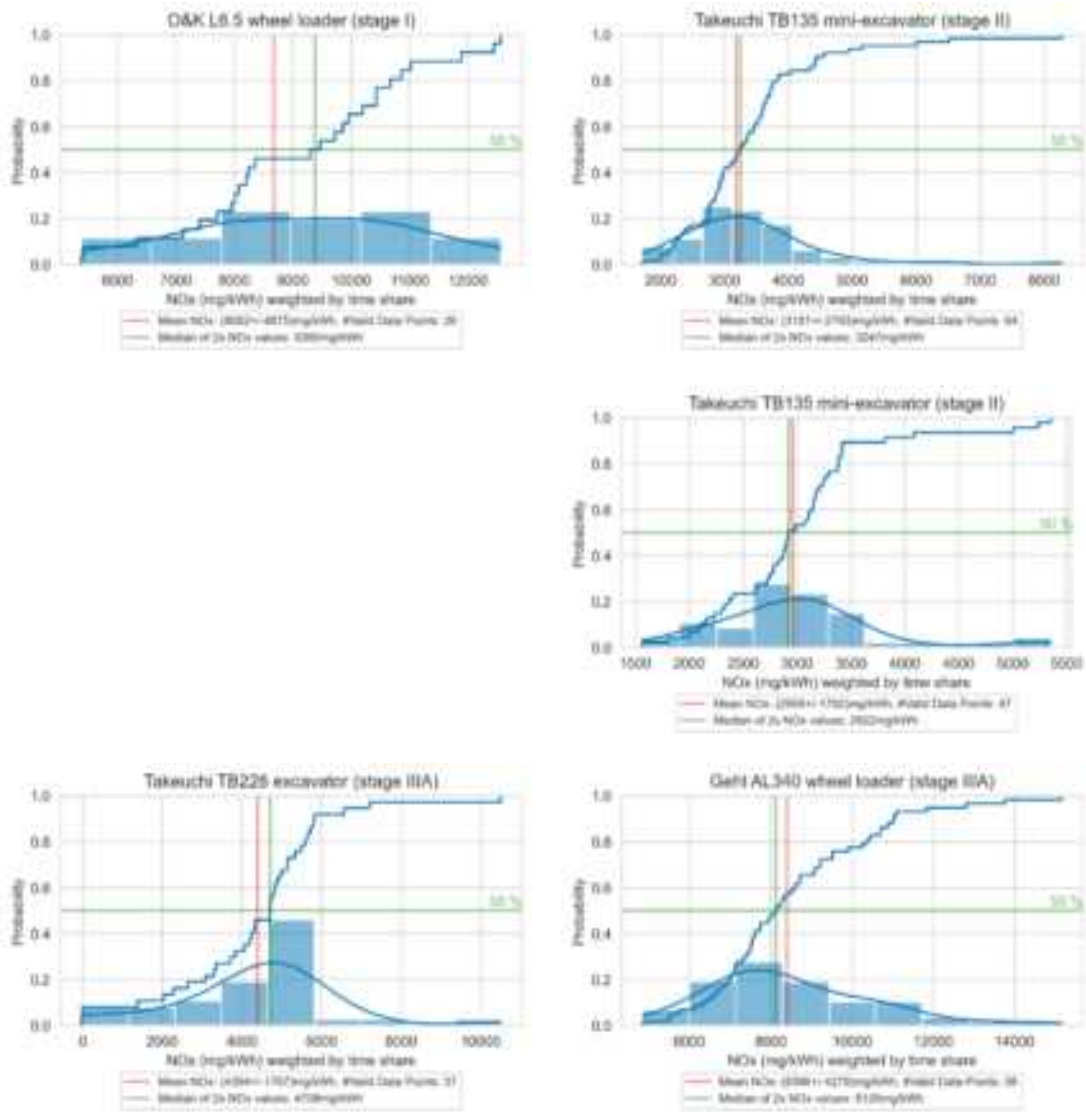


Figure 5: Emission measurements of O&K L6.5 wheel loader (stage I) idling (top, left), Takeuchi TB135 mini-excavator (stage II) during earth removal (top, right) and digging a shaft (middle), Takeuchi TB228 excavator (stage IIIA) idling (bottom, left) and Gehl AL340 wheel loader (stage IIIA) idling (bottom, right).

Conclusions

The optimal measurement position and distance is dependent on wind conditions and the specific NRMM being measured. For this study, the optimal measurement distance is greater than 3 m, ensuring that measurements are taken at a non-disturbing distance from the NRMM's work area. Direct measurements within 3 m of the machinery are not recommended due to difficulty in tracking exhaust plumes and disruption to NRMM operations. Emission signals could still be detected at 8 m with light wind. Despite potential disturbances, measurements close to roads with heavy traffic appear to work well. However, converting NO_x/CO_2 ratios to NO_x emissions using a 40% engine efficiency assumption can lead to underestimating NO_x emissions, particularly for smaller, older, or low-load machinery as a lower efficiency would lead to a higher calculated emission factor. So far, no ECU data was used. This data could be added in future measurements with the use of on-board diagnostics (OBD). To further enhance the understanding of NRMM emissions, measurements should also include particle emissions. Particle instruments could also be used to simplify the localization of the exhaust plume of the construction vehicles due to their high sensitivity. Within the EU CARES project (www.cares-project.eu), different particle instruments are tested for remote emission sensing techniques like plume chasing or point sampling which could probably also be used for NRMM measurements.

Acknowledgements

This work was supported by Beißwenger Garten- und Landschaftsbau GmbH.

References

Helms H., Heidt C. (2014). Erarbeitung eines Konzepts zur Minderung der Umweltbelastung aus NRMM (non-road mobile machinery) unter Berücksichtigung aktueller Emissionsfaktoren und Emissionsvermin-derungsoptionen für den Bestand, *Umweltbundesamt (Hrsg.)*.

Horbanski, M., Pöhler, D., Lampel, J., and Platt, U. (2019). The ICAD (iterative cavity-enhanced DOAS) method, *Atmospheric Measurement Techniques*, 12, 3365–3381

2.8 JS.08. Air pollutant and GHG emissions, water contaminants, ambient and underwater noise and vessel-induced mixing.

Underwater Noise Emissions From Ships During 2014-2020

Jukka-Pekka Jalkanen^{1,*}, Lasse Johansson¹, Mathias H. Andersson², Elisa Majamäki¹, Peter Sigray³

¹ Atmospheric Composition Research, Finnish Meteorological Institute, P.O. Box 503, FI-00110 Helsinki, Finland, jukka-pekkajalkanen@fmi.fi

² Underwater Technology, Division of Defence Technology, Swedish Defense Research Agency, Stockholm, Sweden

³ Marine Robotics Laboratory, Engineering Mechanics, Royal Institute of Technology, Stockholm, Sweden

Introduction

The disruption of shipping after the notorious September 11th attack on the World Trade Center in 2001 was followed by an unpredictable exposure and change during however due to the reaction to an unexpected terrorist event in North American sea regions (Rolland et al., 2012). In 2020, global COVID-19 pandemic brought with it a global disruption, which changed the traffic patterns of shipping and ground almost the whole cruise sector to a halt. It is expected that this global disruption of movement of goods and passengers have a widespread effect in the shipping sector. Regional lockdown periods and travel restrictions reflect strongly on ship movements, especially those concentrated on passenger traffic. While the Sep 11th 2001 events led to marine traffic restrictions mostly concentrated in North American coastal regions, the COVID-19 pandemic had global consequences. It is not currently known how marine life reacted to this unexpected change in shipping intensity of 2020, but it is widely recognized that noise impact on marine life ranges from masking of communication, stress to behavioral changes and may ultimately lead to adverse effects on population level (Duarte et al., 2021).

The current study was recently published (Jalkanen et al., 2022).

Materials and methods

The Ship Traffic Emission Abatement Model (STEAM) of Finnish Meteorological Institute (FMI) was used in this work (Jalkanen et al., 2012, 2018, 2009; Johansson et al., 2013, 2017). Input data for the model, the vessel activity and fleet description, were obtained from Automatic Identification System (AIS) data provided by Orbcomm Ltd. and IHS Markit, respectively. The STEAM model predicts instantaneous vessel power use, based on ship identity, vessel description and speed indicated by AIS position reports. The model describes the overall state of the vessels and their engines considering relevant environmental regulations. Previously, this approach has been used to estimate emissions to air, discharges to the sea and underwater noise emissions.

STEAM estimates vessel noise source levels using the Wittekind noise source model (Jalkanen et al., 2018; Wittekind, 2014) which describes low- and high frequency cavitation and machinery contributions separately. In the Wittekind model, vessel speed affects the noise source levels (in dB re 1 μPa² m⁻² s⁻¹) and the noise could show significant increase if cavitation inception speed (CIS) is exceeded. Throughout this paper, the noise source energy emitted by a ship to the sea is considered as noise emissions and are reported in energy units (Joules) because the duration of the noise signal is also considered. The key benefits of the used modeling approach include: a) the use of transponder data from AIS, which describes the ship activity as a function of time; b) updates of global underwater noise emission inventories, which can be reported annually; c) realistic description of noise as a function of vessel physical and technical description and d) construction of noise scenarios, which allow testing of vessel based mitigation options.

The source level is defined at 1 m distance the energy is calculated by integration of the source level on a sphere using the source level. Both the source level and the energy are thus hypothetically placed in an infinite uniform lossless ocean, following the definition in ISO18405 (2017). When instantaneous noise is integrated over time, a noise source energy map is obtained

(Jalkanen et al., 2018) which can be used to understand the geospatial distribution of vessel noise source energy. This is a cumulative noise source energy assessment with an integrating period of one year (total noise source energy) or one day. The work reported in this paper involves description of noise sources and their time integration as an anthropogenic environmental pressure, which can be used as a basis for further work but should not be taken as a description of environmental state.

Results and discussion

This work is based on the global modeling of noise source energy output of individual ships. In the results, the noise source energy is aggregated to daily grids with a resolution of 0.1° (WGS84 coordinate system). The noise emissions were calculated as Gigajoules (1E9) of total emitted acoustic energy over a year and a specified area, in a specified frequency band (Jalkanen et al., 2018). These gridded data were produced for 63, 125 and 2000 Hz center frequencies of 1/3 octave bands and the data generated are available for further study. All modeling was done at vessel level, which enabled studies of noise emissions by vessel type, age, flag state or size. In Figure 1, the geographical distribution of global underwater noise source energy emissions from ships (63 Hz 1/3 octave band) to the sea is presented. The main shipping lanes, e.g. the ones from China via the Malacca Strait and Red Sea to Europe, have the highest noise contributions from shipping.

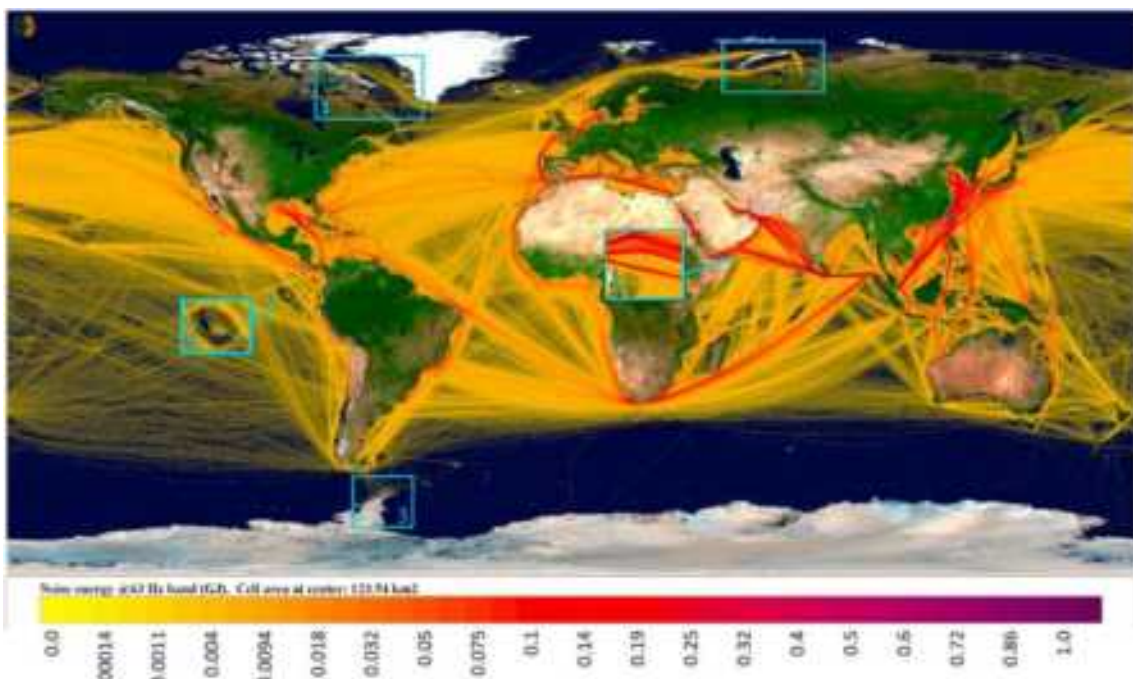


Figure 1 Global map of underwater noise emissions from ships in 2019 (63 Hz 1/3 octave band, in Gigajoules). The labeled areas are 1: Baffin Sea with Milnemining operations; 2: Kara Sea with Yamal gas fields; 3: Palmer basin research stations; 4: Galapagos Islands; 5: Socotra Island.

In Figure 2, the difference of annual total noise source energy from ships between years 2014 and 2019 is shown. This has been done simply by subtracting the annual totals of 2019 from the totals of 2014 (63Hz 1/3 octave band data). Therefore, negative values indicate a reduction of noise source energy and positive values an increase, respectively. It can be seen from Figure 2 that in most areas the annual shipping noise emissions have increased. An increase in emitted noise was predicted for the South China Sea, Yellow Sea, and the Mediterranean Sea. Despite some regional differences in underwater noise emission patterns, increased emissions were discovered in most sea areas from 2014 to 2019. At global level, the underwater noise emitted by ships has doubled in the period of 11.5 years for this frequency band, which is in line with the often quoted observations of +3 dB/decade rate, and corresponding to doubling of energy, for the

Northeast Pacific (McDonald et al., 2006). The observed +3 dB/decade rate is not directly associated with noise emissions, but our results indicate non-uniform regional development of noise emissions.

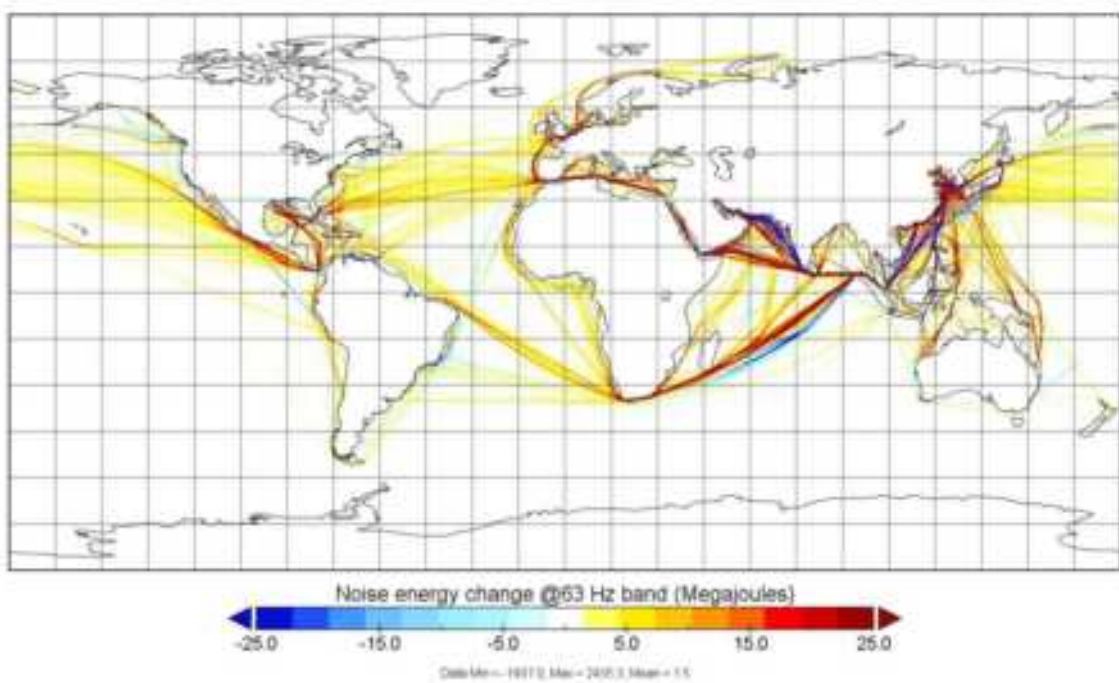


Figure 2 Changes in underwater noise source energy emissions, 2014–2019, at 63Hz 1/3 octave band (in Megajoules). This difference map illustrates the changes during this period. Red areas indicate increase in shipping noise and blue areas signal a decrease.

The increasing trend observed for the 2014–2019 period for the global domain was broken by the COVID-19 pandemic. This caused a disruption in shipping activities, which, in turn, resulted in reduced the noise emissions from ships nearly to 2017 levels. Recently, studies reporting decreased shipping noise in various areas have appeared (Cetinic et al., 2021; Thunell and Barlow, 2020) which could be used to understand changes the pandemic introduced to underwater noise in different areas. It is expected that this decrease of underwater noise is only temporary and upon the recovery of the world economy, noise emissions will be increased again. This is probable unless vessel operation and fleet size changes as a response to greenhouse gas (GHG) reduction efforts.

In Figure 3, the reduction of underwater noise emissions from ships (at 63Hz frequency of 1/3 octave band) is visible on major shipping lanes between China and the EU (Arabian Sea: -8%, Red Sea: -5%, Mediterranean Sea: -9%). The emissions of shipping noise on Eastern China Sea (-3%) were only slightly changed and in some sub-regions, like the Gulf of Thailand, noise emissions increased (+13%) despite the pandemic. The noise emissions from the Baltic Sea and the Mediterranean Sea shipping had a temporary increase in autumn 2020, after the June–July 2020 minimum, but decreased again towards the end of 2020. In the North Sea, a decreasing trend was predicted throughout the year 2020. The decrease in noise emissions towards the end of 2020 coincides with the start of the second wave of lockdowns in Europe (Looi, 2020).

2020-2019, Noise energy difference, Megajoules

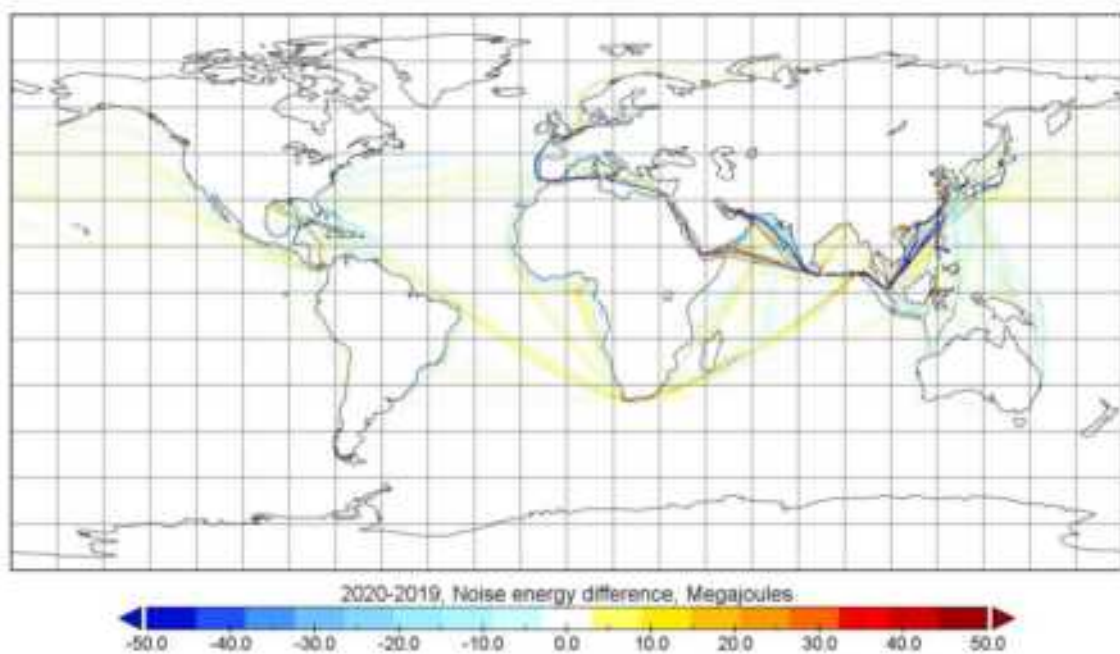


Figure 3 Changes in underwater noise source energy (63 Hz 1/3 octave band) emitted from ships in 2020–2019 (in Megajoules). This image is a difference plot of annual noise source energy emitted in 2020 and 2019. Noise source energy emissions are given in units of megajoules per grid cell. The COVID-19 pandemic decreased the underwater noise emissions significantly in major shipping routes.

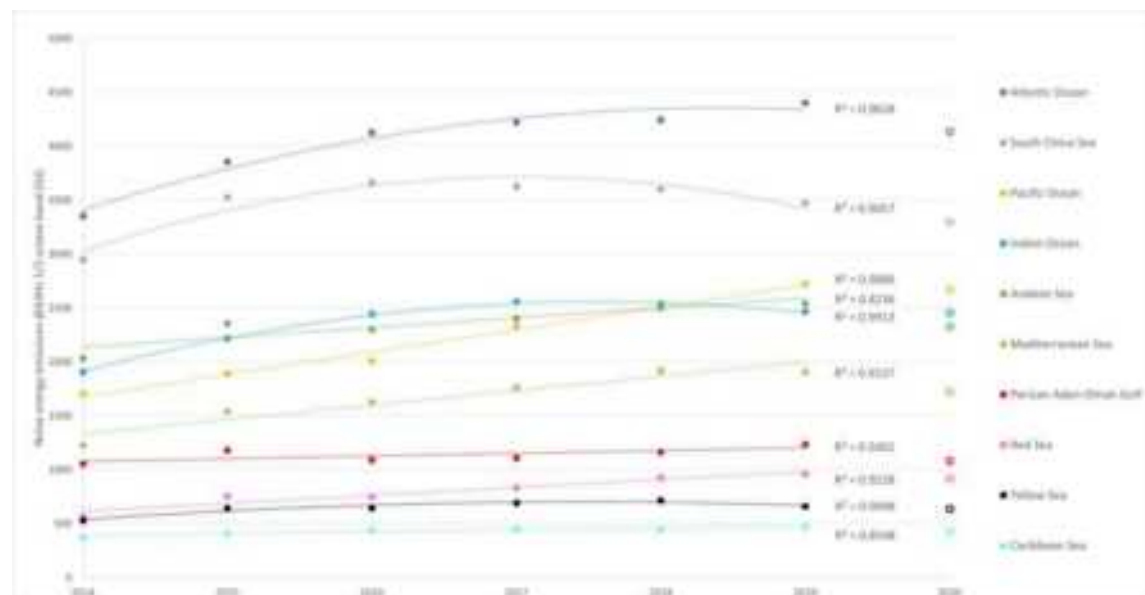


Figure 4 Regional trends of underwater noise source energy emitted by ships in 63Hz frequency at 1/3 octave band. Increasing noise emissions are observed in most sea areas. Open symbols are noise energies for same sea regions in 2020, but these have not been included in the estimation of the trend. Note, that a parabolic function leads to a better fit than a linear trendline in some cases.

Previous measurements in Northeast Pacific over four decades indicated an increasing 3 dB/decade trend (doubling of noise every ten years), which has been viewed as moderate growth of shipping noise (McDonald et al., 2006). For comparison, we have computed the annual noise source energy emitted from ships in selected sea regions – including the Pacific - during 2014– 2019 (Figure 4) using the sea area definitions from the International Hydrographic Organization (IHO). The long-term development of noise is different in various areas and a single number, like the 3dB/decade, does not describe the heterogeneous trends very well.

The increase of regional ship underwater noise emissions in the 2014–2019 period was found to be diverse in various parts of the world. Based on the global modeling of ship underwater noise emissions, the global trend from 2014 to 2019 indicates that noise emissions may double every 11.5 years, but regional variations of noise increase are large (Figure 4).

Based on the trends shown in Figure 4 it is possible to estimate the time which it takes to double the underwater noise source energy emissions. Investigation of slope of the trendline indicates the steepness of the change, and for some sea areas, doubling of shipping noise emissions may occur in a surprisingly short period. The regional differences in noise emission doubling are evident from *Figure 5*. The high latitudes clearly stand out, but also the Pacific Ocean and several European seas are areas of concern.

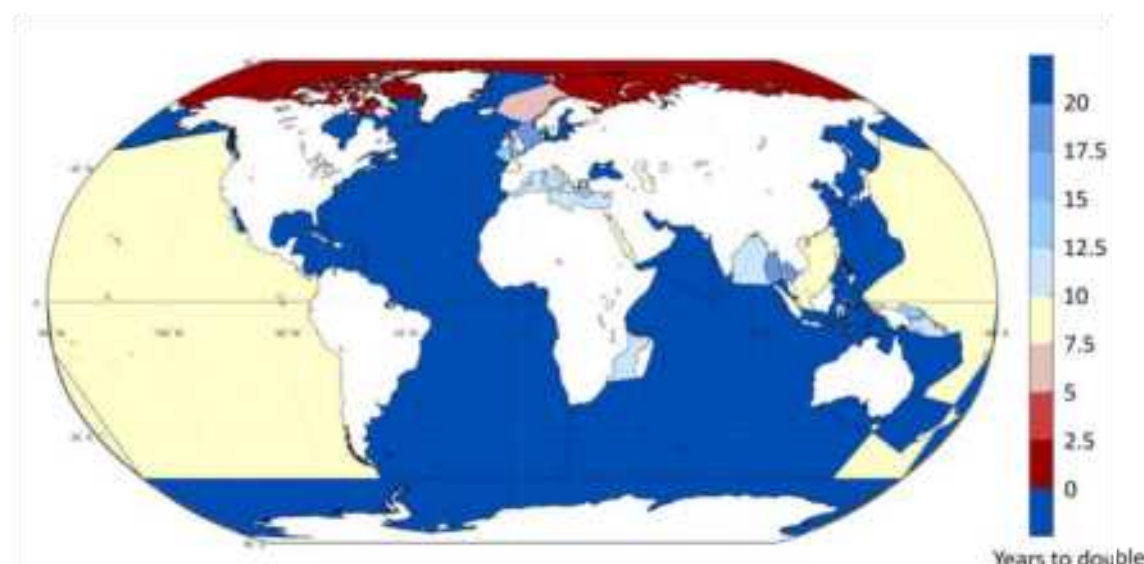


Figure 5 Underwater noise emissions trend in various sea areas. Shades of blue = Doubling of shipping noise emissions takes more than 10 years, or it has decreased over time; Light yellow = noise emissions double within 7.5–10 years; Light red = noise emission doubling within 5–7.5 years; Dark red = noise emissions doubling in less than 3 years; It should be noted that Arctic shipping noise emissions in 2014 started at a very low level and modest increase in Arctic shipping easily doubled the noise emissions from ships.

Conclusions

A major result of this modeling study is the quantified increase of underwater noise emissions from shipping and its regional heterogeneity. At the current rate, the global shipping noise emissions double every 11.5 years. The COVID-19 pandemic has temporarily disrupted this increasing trend, but it is expected that noise emissions will increase again once the world economy recovers. In this paper, a rapid increase of shipping noise emissions in near pristine areas, like the Arctic was found, but starting from a low level. Mining operations, oil/gas extraction and vessel routing through Arctic areas will lead to increased shipping noise in these regions.

Acknowledgements

This work has received support from the European Union's Horizon 2020 Research And Innovation Programme under grant agreement n° 754255 - AWARE project. This work reflects only the authors' view and NEA is not responsible for any use that may be made of the information it contains.

References

- Coutinho, J., Duarte, C. M., Munoz, L., Kukkonen, J., Brink, A. and Stipa, T.: Impact of COVID-19 on environmental noise emitted from the port, *Sci. Total Environ.*, 756, doi:10.1016/j.scitotenv.2020.144147, 2021.
- Duarte, C. M., Chapuis, L., Collin, S. P., Costa, D. P., Eguiluz, V., Erbe, C., Halpern, B. S., Havlik, M. N., Gordon, T. A. C., Merchant, N. D., Meekan, M., Miksis-Olds, J. L., Parsons, M., Predragovic, M., Radford, A. N., Radford, C. A., Simpson, S. D., Slabbekoorn, H., Staaterman, E., Opzeeland, I. C. Van, Winderen, J., Zhang, X. and Juanes, F.: The soundscape of the anthropocene ocean, *Science* (80-.), 371(eaba4658), 1–10, doi:10.1126/science.aba4658, 2021.
- Jalkanen, J.-P., Johansson, L., Kukkonen, J., Brink, A., Kalli, J. and Stipa, T.: Extension of an assessment model of ship traffic exhaust emissions for particulate matter and carbon monoxide, *Atmos. Chem. Phys.*, 12(5), 2641–2659, doi:10.5194/acp-12-2641-2012, 2012.
- Jalkanen, J.-P., Johansson, L., Liefvendahl, M., Bensow, R., Sigray, P., Östberg, M., Karasalo, I., Andersson, M., Peltonen, H. and Pajala, J.: Modelling of ships as a source of underwater noise, *Ocean Sci.*, 14(6), 1373–1383, doi:10.5194/os-14-1373-2018, 2018.
- Jalkanen, J.-P., Johansson, L., Andersson, M. H., Majamäki, E. and Sigray, P.: Underwater Noise Emissions from Ships During 2014–2020, *Environ. Pollut.*, 311, 119766, doi:<https://doi.org/10.1016/j.envpol.2022.119766>, 2022.
- Jalkanen, J. P., Brink, A., Kalli, J., Pettersson, H., Kukkonen, J. and Stipa, T.: A modelling system for the exhaust emissions of marine traffic and its application in the Baltic Sea area, *Atmos. Chem. Phys.*, 9(23), 9209–9223, doi:10.5194/acp-9-9209-2009, 2009.
- Johansson, L., Jalkanen, J.-P. P., Kalli, J. and Kukkonen, J.: The evolution of shipping emissions and the costs of regulation changes in the northern EU area, *Atmos. Chem. Phys.*, 13(22), 11375–11389, doi:10.5194/acp-13-11375-2013, 2013.
- Johansson, L., Jalkanen, J.-P. and Kukkonen, J.: Global assessment of shipping emissions in 2015 on a high spatial and temporal resolution, *Atmos. Environ.*, 167, 403–415, doi:10.1016/j.atmosenv.2017.08.042, 2017.
- Looi, M. K.: Covid-19: Is a second wave hitting Europe?, *BMJ*, 371, 4113, doi:10.1136/bmj.m4113, 2020.
- McDonald, M. A., Hildebrand, J. A. and Wiggins, S. M.: Increases in deep ocean ambient noise in the Northeast Pacific west of San Nicolas Island, California, *J. Acoust. Soc. Am.*, 120(2), 711–718, doi:10.1121/1.2216565, 2006.
- Rolland, R. M., Parks, S. E., Hunt, K. E., Castellote, M., Corkeron, P. J., Nowacek, D. P., Wasser, S. K. and Kraus, S. D.: Evidence that ship noise increases stress in right whales, *Proc. Biol. Sci.*, 279(1737), 2363–8, doi:10.1098/rspb.2011.2429, 2012.
- Thomson, D. J. M. and Barclay, D. R.: Real-time observations of the impact of COVID-19 on underwater noise, *J. Acoust. Soc. Am.*, 147(5), 3390–3396, doi:10.1121/10.0001271, 2020.
- Wittekind, D. K.: A simple model for the underwater noise source level of ships, *J. Sh. Prod. Des.*, 30(1), 1–8, doi:10.5957/JSPD.30.1.120052, 2014.

Size resolved particle emission characteristics for different types of vessels.

A. Weigelt¹, J. Beecken^{1,2}, D. van Dinther³, S. Griesel¹, J. Mellqvist⁴ and L. Ntziachristos⁵

¹Federal Maritime and Hydrographic Agency (BSH), Hamburg, Germany, Andreas.Weigelt@bsh.de

²now at Explicit ApS, Copenhagen, Denmark

³Netherlands Organisation for Applied Scientific Research (TNO), Petten, the Netherlands

⁴Chalmers University of Technology, Gothenburg, Sweden

⁵Aristotle University Thessaloniki, Thessaloniki, Greece

Introduction

In addition to various gaseous pollutants, vessels do emit a large number of exhaust aerosol particles (Beecken et al., 2015). This is a result of both high particle numbers per unit of fuel used as well as an overall high fuel consumption rate. Therefore, seagoing vessels are a very important anthropogenic source of atmospheric aerosols (e.g. Ausmeel et al., 2019) and do have a significant impact on public health and climate effects (Sofiev et al., 2018). Nevertheless, to date, there are no legal limits for particulate emissions from seagoing vessels. Moreover, the understanding of the particle emission characteristics of vessels under real-life conditions is limited, as only few data are available ~~to the EU Commission project SCIPPER of the European Union~~ to Inland Pollution Push for the Enforcement of Regulations (www.scipper-project.eu) long-term particle measurements were carried out to close this gap and to provide recommendations for future regulations and monitoring mechanisms. Thereby, for nearly two years the particle size distribution was measured in individual plumes of bypassing vessels. Within the present study the total particle emission, as well as the size resolved particle emission characteristics for different types of vessels are presented. A side-by-side comparison of different particle measurement methods was also carried out within SCIPPER but is presented separately by van Dinther et al (2023).

Measurement and analysis Method

In 2020 and 2021 the German Federal Maritime and Hydrographic Agency (BSH) installed two combined particle size spectrometers at their ship emission monitoring sites in Wedel (approach to Hamburg harbour) and the Kiel fjord (approach to Kiel and Kiel Canal). At both locations vessels pass the measurement sites in a distance of about 300 to 800 meter (cf. Fig.1). The measurements are ongoing. Both combined particle size spectrometers are composed of a TSI Fast Mobility Particle Sizer (FMPS, Model TSI 3091) and a TSI Optical Particle Sizer (OPS, Model TSI 3330). The FMPS measures the particle size distribution with 32 logarithmic equidistant size channels in the size range of $5.6 \text{ nm} < dp < 560 \text{ nm}$. The OPS measures the particle size distribution with 16 logarithmic equidistant size channels in the size range of $0.3 \mu\text{m} < dp < 10 \mu\text{m}$. Both systems can measure the full size range with a response time of 1s. This means every second from each combined system a particle size distribution from 5.6 nm to 10 μm with



Figure 1: Location of the measurement sites at the Elbe River in Wedel, about 10 km in front of the entrance to the port of Hamburg (left) and in the Kiel fjord north of the Kiel Canal lock (right). Satellite images were taken from Google maps.

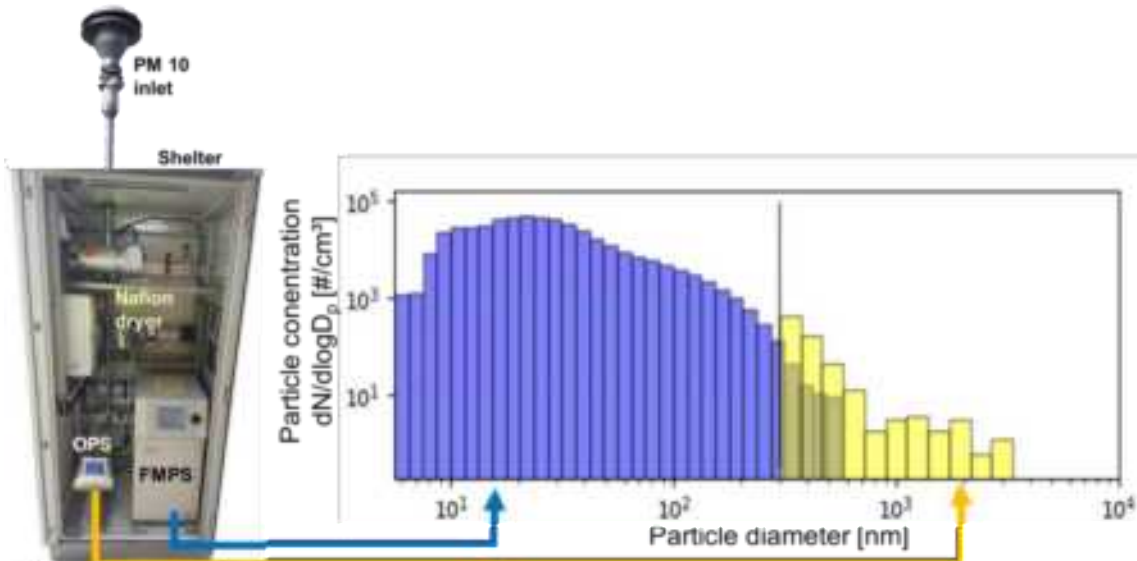


Figure 2: Combined particle size spectrometer (TSI FMPS 3091 + OPS 3330) installed into a climate-controlled shelter (left). Sample air is dried with a Nafion counter flow dryer. The PM-10 inlet prevents particles larger than 10 μm to enter the system. Particle size distribution (right) is measured with 1 Hz resolution with 32 (FMPS, blue) and 16 (OPS, yellow) size channels between 5.6 nm and 10 μm with an overlap between 300 and 500 nm.

a 48 size channel resolution is available. The setup is shown in Figure 2. The instruments are installed in air-conditioned shelters so that they can be operated at constant ambient conditions and independent of the weather. To ensure comparable measurements at low relative humidity, the sample air is dried by using Nafion counterflow dryers. The PM-10 inlet head removes particles with a diameter larger than 10 μm . As it can be seen in Fig. 2 on the right graph, there is an overlap between the size distributions measured by FMPS and OPS. Because the FMPS is known to be less accurate in the largest size channels (above 300 nm), from that size only the OPS data were used.

Besides the particle size distribution, at both sites the concentration of CO_2 , SO_2 and NO_x , as well as the meteorological conditions (T , p , RH, wind direction and speed, global radiation) are continuously measured with 0.1 Hz resolution. Additionally, the identity track and some operational details of bypassing vessels, the vessels Automated Identification Signals (AIS) are recorded. By combining the measured vessel plumes (identified peaks in the time series of trace gas and aerosol measurements) with the vessels positions (AIS) and wind data (calculation of trajectories between vessel and measurement station), the measured plumes can be automatically allocated to individual vessels. A Matlab algorithm was developed for this allocation.

Figure 3 gives an exemplary insight into the temporal development of the integral particle concentration (Fig. 3a) and the particle size distribution (Fig. 3b) at the Wedel station. Vessel plumes can be easily identified by the enormous peaks in both graphs. All peaks were assigned to passing vessels (vessel type indicated in Fig. 3b). It is obvious that the emission characteristics observed for various vessels differ, both in particle number concentration and particle size. This will be further investigated in the below results chapter. Furthermore, from Fig 2 and 3b it is apparent that the FMPS and the OPS measure similar particle number concentration at the crossover point between the instruments.

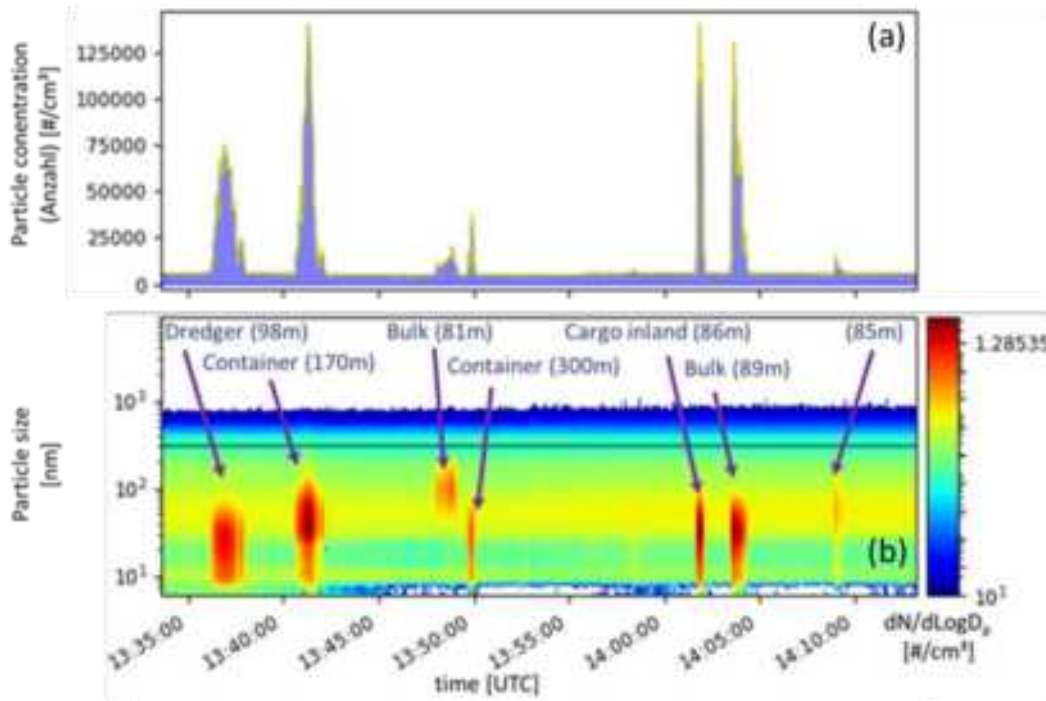


Figure 3: Time series of combined integral particle number concentration (a) and particle size distribution (b), measured in September 2020 at the BSH ship emission measurement site in Wedel/Hamburg. In Figure (a) the total particle concentration is indicated in blue (contribution by FMPS) and yellow (contribution by OPS). The crossover from FMPS to OPS is indicated in (b) as black line. Plume allocated vessel types and length are displayed in Fig. (b).

By subtracting the background concentration detected before and after a plume peak event from the concentration measured during the plume passage, the contribution from the vessel can be isolated. When normalizing the individual plume pollutant concentration with the plume CO₂ concentration and assuming the vessel's fuel conversion of 8.7% carbon which is completely converted to CO₂, pollutant individual emission factors in amount of pollutant per kg of burned fuel can be derived (Schlager et al., 2006; Agrawal et al., 2008; Moldanova et al., 2009; Balzani Lööv et al., 2014; Beecken et al., 2014, 2015; Kattner et al., 2015). This allows comparing, combining and statistically analysing size resolved particle emission factors from different measurements, regardless of the degree of dilution of the individual measurement. Similar methods are used for vessel's SO₂ and NOx emissions and are described in detail e.g. by Beecken et al., 2014, 2015, Kattner et al., 2015, van Roy et al., 2022a,b). For the present study, size resolved emission factors from more than 10.000 plumes have been analysed and allocated to individual vessels.

Results

On average, approximately 1.4·10¹⁶ particles per kg of burned fuel (#/kg fuel) are emitted to the atmosphere by seagoing vessels at the measurement sites in Wedel and Kiel. However, significant different emission characteristics were observed for different types of vessel, both in terms of number concentration (cf. Fig. 4) and particle size (cf. Fig. 5). For example, with 1.64·10¹⁶ #/kg fuel the mean emission factors of dredgers, small cargo vessels (< 100m) and medium-size tankers are found to be four times larger than that of inland vessels (1.51 and 5.07·10¹⁵ #/kg fuel). Furthermore, small cargo vessels were found to have an average particle emission factor 60% higher than the largest cargo vessels (>300m) and at the same time, however, the largest variability in the measured emission factors (difference between 10 and 90% percentile). Sea-going passenger vessels, i.e. ferries and cruise liners, show a relatively low total particle emission factor of 9.41·10¹⁵ #/kg fuel. However, this is still 3 times more than the average particle emission factor of inland vessels.

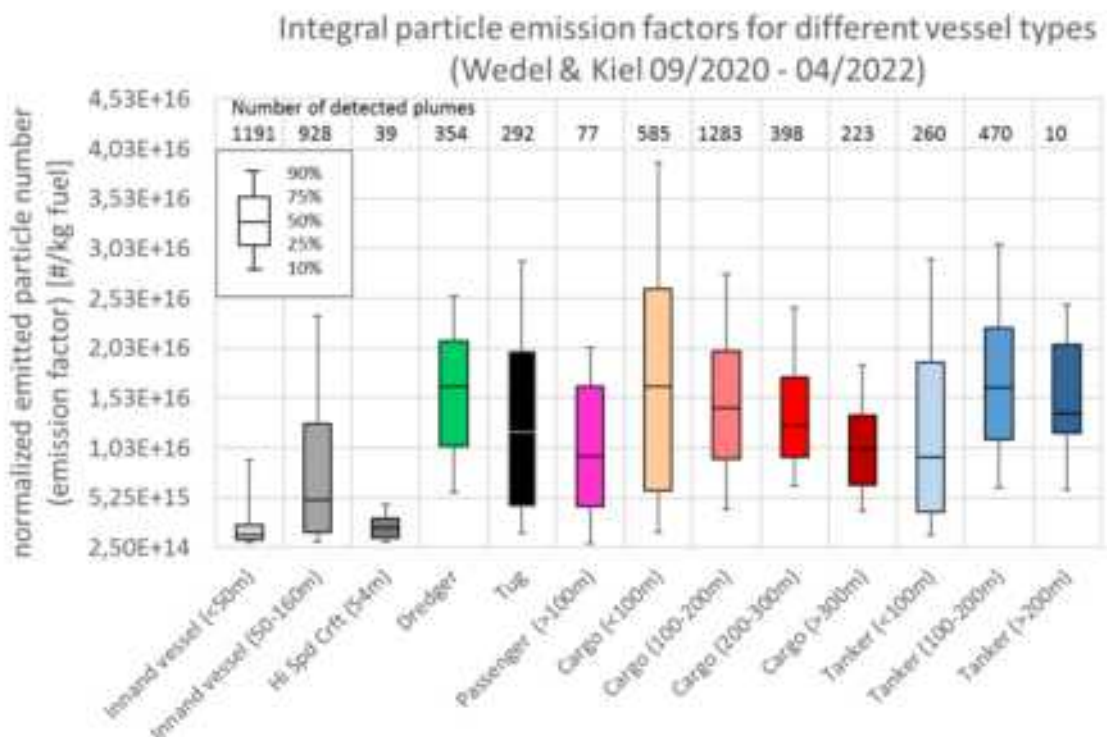


Figure 4: Integral particle emission factors for different vessel types, measured between September 2020 and April 2022 at the two BSH measurement sites in Wedel/Hamburg and the Kiel fjord. The numbers above the boxes indicate how many analysed plumes were used for the respective category to calculate the given median and percentiles.

As already indicated above, with the presented measurement and analysis method size resolved particle emission factors can be derived for different vessel types. Even though for particles larger than 200 nm the emission factors looks rather similar for the different vessel types (Fig. 5a), it was found that the emission of coarse mode particles ($d_p > 1000$ nm) is on average five orders of magnitude smaller than for particles in the ~~coarse mode ($d_p > 500$ nm)~~ for particles smaller than 200 nm, however significant differences in the size of the emitted particles become apparent (Fig. 5b). The majority of particles emitted by dredgers are on average 75% larger than particles emitted from all other types of investigated vessels ($d_{p,\max}=50$ nm). It is noticeable that for all other types of seagoing vessels the size of the emitted particles is very similar (distribution of the maxima of the curves on the X-axis), even if there are significant differences in the number of emitted particles per unit of burned fuel (height of the peaks on the Y-axis). Apart from the dredgers, the inland vessels show a different emission characteristic with regard to both, particle size and number by having lower emission factors for all size classes, except below 20 nm (grey lines Fig 5 a, b). This means that the majority of particles emitted by inland vessels is below 20 nm and therefore smaller than for all seagoing vessels.

The reasons for the different emission characteristics of the various vessel types probably lie in the difference of (I) installed engines, (II) fuels in use and (III) vessel operation modes and needs to be investigated further to obtain detailed particulate emission characteristics. The elapsed time between emission at the vessel's stack and measurement at the station (in this study mostly between 5 and 12 minutes) may also influence the determined emission factors and should be taken into account in future studies. As the measurements are ongoing at both locations, a unique dataset will be created to perform statistically sound analysis on the particle emission characteristics of vessels under real-life conditions.

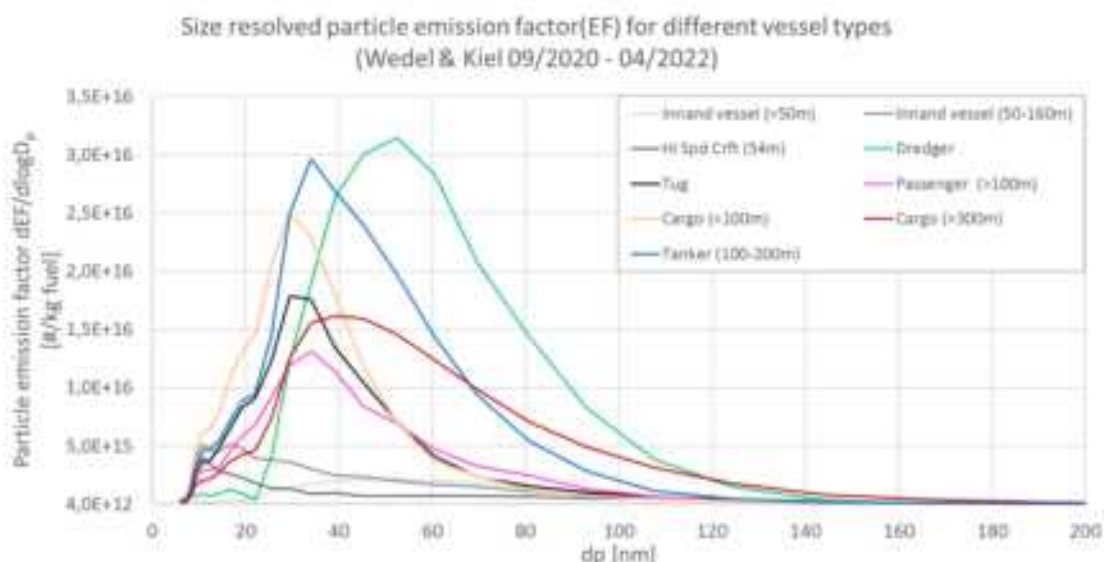
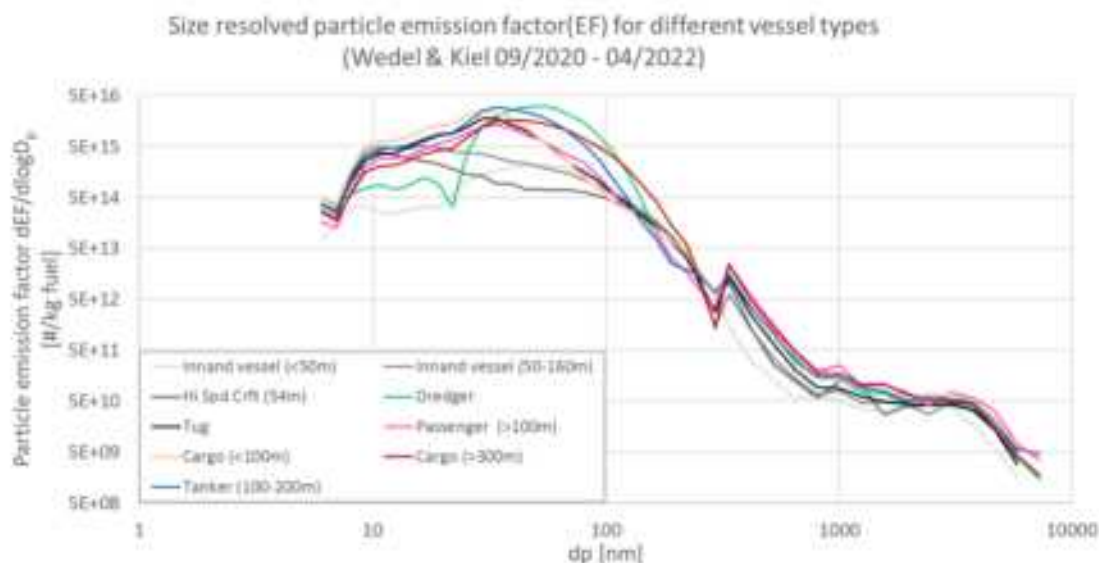


Figure 5: Integral particle emission factors for different vessel types, measured between September 2020 and April 2022 at the two BSH measurement sites in Wedel/Hamburg and the Kiel fjord. The Number of vessel plumes used for each vessel type is given in Fig. 4.

Acknowledgements

The SCUTTER project has received funding from the European Union's Horizon 2020 research and innovation programme under grant agreement Nr.814893.

References

- Agrawal, H., Eden, R., Zhang, X., Fine, P. M., Katzenstein, A., Miller, J. W., Ospital, J., Teffera, S., and Cocker, D. R. (2008). Primary Particulate Matter from Ocean-Going Engines in the Southern California Air Basin, *Environ. Sci. Technol.*, 43, 5398–5402
- Ausmeel, S., Eriksson, A., Ahlberg, E., and Kristensson, A. (2019). Methods for identifying aged ship plumes and estimating contribution to aerosol exposure downwind of shipping lanes, *Atmos. Meas. Tech.*, 12, 4479–4493, <https://doi.org/10.5194/amt-12-4479-2019>, 2019.
- Balzani Lööv, J. M., Alfoldy, B., Gast, L. F. L., Hjorth, J., Lagler, F., Mellqvist, J., Beecken, J., Berg, N., Duyzer, J., Westrate, H., Swart, D. P. J., Berkhout, A. J. C., Jalkanen, J.-P., Prata, A. J., van der Hoff, G. R., and Borowiak, A. (2014). Field test of available methods to measure remotely SO_x and NO_x emissions from ships, *Atmos. Meas. Tech.*, 7, 2597–2613, doi: 10.5194/amt-7-2597-2014
- Beecken, J. (2015) *Remote measurements of gas and particulate matter emissions from individual ships*, Dissertation, Chalmers University of Technology, ISBN 978-91-7597-141-4.
- Beecken, J., Mellqvist, J., Salo, K., Ekholm, J., and Jalkanen, J.-P. (2014). Airborne emission measurements of SO₂, NO_x and particles from individual ships using a sniffer technique, *Atmos. Meas. Tech.*, 7, 1957–1968, doi:10.5194/amt-7-1957-2014
- Beecken, J., Mellqvist, J., Salo, K., Ekholm, J., Jalkanen, J.-P., Johansson, L., Litvinenko, V., Volodin, K., and Frank-Kamenetsky, D. A. (2015). Emission factors of SO₂, NO_x and particles from ships in Neva Bay from ground-based and helicopter-borne measurements and AIS-based modeling, *Atmos. Chem. Phys.*, 15, 5229–5241, doi: 10.5194/acp-15-5229-2015
- Kattner, L., Mathieu-Üffing, B., Burrows, J. P., Richter, A., Schmolke, S., Seyler, A., and Wittrock, F. (2015). Monitoring compliance with sulfur content regulations of shipping fuel by in situ measurements of ship emissions, *Atmos. Chem. Phys.*, 15, 10087–10092, <https://doi.org/10.5194/acp-15-10087-2015>
- Moldanova, J., Fridell, E., Popovicheva, O., Demirdjian, B., Tishkova, V., Faccinetto, A., and Focsa, C. (2009). Characterisation of particulate matter and gaseous emissions from a large ship diesel engine, *Atmos. Environ.*, 43, 2632–2641,
- Schlager, H., Baumann, R., Lichtenstern, M., Petzold, A., Arnold, F., Speidel, M., Gurk, C., and Fischer, H. (2006). Aircraft-based Trace Gas Measurements in a Primary European Ship Corridor, proceedings TAC-Conference, 83–88
- Sofiev, M., Winebrake, J.J., Johansson, L., Carr, E.W., Prank, M., Soares, J., Vira, J., Kouznetsov, R., Jalkanen, J.P., Corbett, J.J (2018). Cleaner fuels for ships provide public health benefits with climate tradeoffs. *Nat Commun.*, 9, 406, <https://doi.org/10.1038/s41467-017-02774-9>.
- van Dinther, D., Weigelt, A., Beecken, J., Mellqvist, J., Conde Jacobo, V.A., Blom, M., and Duyzer, J. (2023). Comparison of particle emission factors from shipping using different instruments, *TAP and S&E conference 2023* oral presentation
- van Roy, W., Schallier, R., van Roozendael, B., Scheldeman, K., van Nieuwenhove, A., and Maes, F. (2022a). Airborne monitoring of compliance to sulfur emission regulations by ocean-going vessels in the Belgian North Sea area, *Atmospheric Pollution Research*, 13-6,<https://doi.org/10.1016/j.apr.2022.101445>.
- van Roy, W., Scheldeman, K., van Roozendael, B., van Nieuwenhove, A., Schallier, R., Vigin, and L., Maes, F. (2022b). Airborne monitoring of compliance to NO_x emission regulations from ocean-going vessels in the Belgian North Sea, *Atmospheric Pollution Research*, 13-9, <https://doi.org/10.1016/j.apr.2022.101518>.

Effects of Sulfur Scrubbers on Particulate Emissions from a Marine diesel engine

T. Streibel^{1,2*}, S. Jeong³, J. Bendl³, M. Saraji-Bozorgzad³, M. Sklorz¹, C. Gehm⁵, L. Anders¹, J. Passig^{1,2}, J. Schade³, U. Etzien⁴, T. Adam³, B. Buchholz⁴, Detlef E. Schulz-Bull⁵, and R.Zimmermann⁶

¹ Joint Mass Spectrometry Center (JMSC) at Comprehensive Molecular Analytics, Department Environmental Health, Helmholtz Zentrum München, Ingolstaedter Landstrasse 1, 85764, Neuherberg, Germany

² Joint Mass Spectrometry Center (JMSC) at Chair of Analytical Chemistry, Institute of Chemistry, University of Rostock, Albert-Einstein-Strasse 27, 18059, Rostock, Germany

³ University of the Bundeswehr Munich, Faculty for Mechanical Engineering, Institute of Chemical and Environmental Engineering, Werner-Heisenberg-Weg 39, 85577, Neubiberg, Germany

⁴ Chair of Piston Machines and Internal Combustion Engines, Faculty of Mechanical Engineering and Marine Technology, University of Rostock, Albert-Einstein-Strasse 2, 18059, Rostock, Germany

⁵ Leibniz Institute for Baltic Sea Research, Marine Chemistry, Seestrasse 15, 18119, Rostock, Germany

thorsten.streibel@uni-rostock.de

Introduction

The International Maritime Organization capped the fuel sulfur content of marine fuels outside ECA zones to 0.5 % in 2020. Consequently, either low-sulfur fuels or additional exhaust gas cleaning devices for the reduction in sulfur dioxide (SO_2) emissions became mandatory. Although a wet scrubber reduces the amount of SO_2 significantly, there is still a need to consider the reduction in particle emissions and organic pollutants.

When assessing potential damage to the environment due to emissions from shipping, the focus is mainly on sulfur oxides, nitrogen oxides, heavy metals and particle mass concentration. Particle number and particle size distributions are not considered. Particulate matter with sizes below 2.5 μm (PM2.5) contribute little to mass, but have very large number concentrations. In addition, organic pollutants are bound to the particles and enter the environment with the particles or are inhaled by humans. These organic components, which include, for example, polycyclic aromatic hydrocarbons (PAHs) with a large number of toxic and carcinogenic representatives, have also received little attention to date. A precise evaluation of the size distributions and number concentrations of the small particle fractions with scrubber operation has not yet taken place, nor has a comprehensive chemical characterization of the particulate phase. The effects on these physical and chemical parameters by the additional installation of particulate filter technologies in addition to the scrubber have also not yet been researched.

We present data on the particle removal efficiency of a scrubber regarding particle number and mass concentration with different marine fuel types, viz. marine gas oil and two heavy fuel oils (HFOs) with sulfur contents of 1.3 % and 2.4 %, respectively. An open-loop sulfur scrubber was installed in the exhaust line of a marine diesel test engine. Fine particulate matter with diameters below 2.5 μm (PM2.5) was comprehensively characterized in terms of its physical and chemical properties.

Influence of a sulfur scrubber system on the properties of emitted particles

Table 1: Exhaust PM mass in mg kWh^{-1} with 60 kW engine load before and after the sulfur scrubber (upstream and downstream)

	MGO	HFO 1.3	HFO 2.4
PM upstream mass	59±3	275±12	201±8
PM downstream mass	39±1	201±23	218±13

An important question was the effect of the use of a sulfur scrubber on the physical properties of the emitted particles, in particular their size distribution and mass concentration. The latter was determined for all particles, and the contents of sulfate particles and soot particles were also measured. With the engine operating at 75% of maximum power (60 kW) and the scrubber in open loop mode, the emitted particles were compared for MGO, HFO with 1.3% sulfur and HFO with 2.4% sulfur. The measured values are calculated as emission factors with reference to the energy output of the engine in kWh (Table 1). MGO exhibits much smaller numbers in comparison to the heavy fuel oils. The HFO with the lower sulfur content showed a slightly higher mass emission factor compared to the HFO with 2.4 % sulfur. Furthermore, it was revealed to contain a larger amount of PAHs

after analysis by two-dimensional gas chromatography/mass spectrometry. Consistently, in terms of total mass concentration, it can be observed that the reduction by the sulfur scrubber is relatively small (38% for MGO, 27% for HFO with 1.3% sulfur), and there is even a slight increase of 8% for HFO with 2.4% sulfur. This can be explained by the new formation of sulfate particles due to the high sulfur content in the exhaust gas, while the soot particles decrease to a comparable extent as the total concentration.

Another important parameter for the particles is the number concentration, which is determined together with the size distribution (Figure 1).

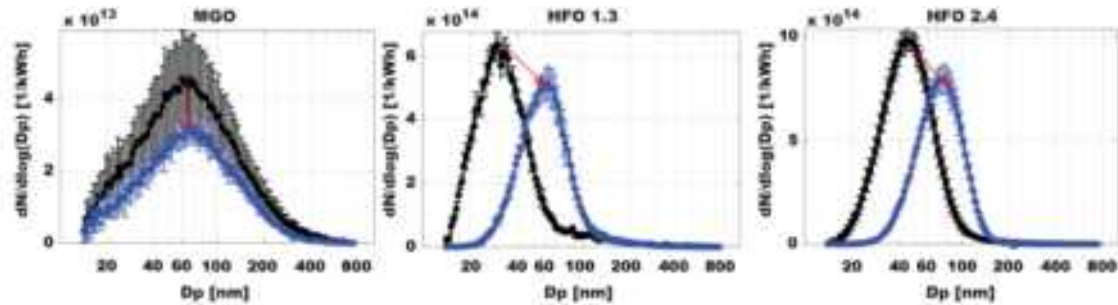


Figure 1: Particle size distributions referring to energy output at 60 kW load of the engine for MGO and the heavy fuel oils with 1.3 % and 2.4 % sulfur, respectively (after Jeong et al., Environmental Pollution 316 (2023) 120526)

Again, MGO shows much smaller numbers than the heavy fuel oils. A shift in the distribution towards larger particles is seen for the heavy fuel oils after the scrubber, while the shape of the curve remains the same for MGO. For all fuels, there is a reduction in the number concentration, but this is also relatively low, comparable to the mass concentrations (40% for MGO, 25% for HFO with 1.3% sulfur, 30% for HFO with 2.4% sulfur). Accordingly, the scrubber alone will not be sufficient to achieve future restrictions on particulate emissions in the nanoparticle range; additional downstream filter systems will be needed for this purpose.

The first test measurements with such particle filters were also carried out as part of the engine trials. It quickly became apparent that reliable and targeted operation in the exhaust gas of marine diesel engines poses a major challenge to the design and operation of the filters. Well-known concepts from the automotive industry cannot simply be transferred directly. Although a wet electrostatic precipitator achieved an almost complete reduction of the total particle concentration of 99 % with HFO 2.4 % sulfur and 60 kW, continuous operation was only possible for a short period of time. A lot of development and optimization work is still necessary here in the future.

In addition to the physical properties of the emitted particles, their chemical composition and its changes as the particles pass through the sulfur scrubber is also of interest. In this context, Polycyclic Aromatic Hydrocarbons (PAH) are of particular importance due to their health-damaging potential. Single particle mass spectrometry provides an insight into this. In a basic evaluation approach of the detected single particle mass spectra, the number of particles containing PAHs or no PAHs can be determined. This is shown in Figure 2.

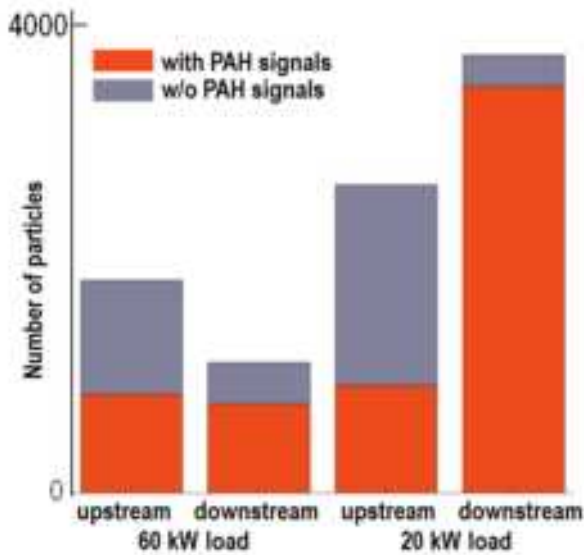


Figure 2: Number of PAH-containing particles in the exhaust before and after the Scrubber (Open Loop) when running with HFO 2.4 % sulfur.

The figure shows the number of particles detected in one hour for the two engine loads under investigation. Overall, about half of the particles emitted from the engine show clear PAH signals. The scrubber reduces the total particle count at 60 kW, but to a greater extent for the particles without PAHs. This is likely due to less effective collection for particles with non-polar compounds by the scrubber. For the 20 kW load condition, an increase in the total particle count can be seen due to smaller instabilities in the engine run. However, the decrease in the proportion of particles without PAHs with a simultaneous increase in particles containing PAHs is also clear here. When looking at the accompanying single mass spectra themselves, an important result is that the relatively strong signals of alkylated phenanthrenes, which actually always occur with PAH-containing particles, are only slightly influenced by the sulfur scrubber. The scrubber therefore does not ensure a significant reduction of these three-ring PAHs on the particles.

A quantitative approach to the changes in the concentration of larger PAHs (4-ring systems and above) on the particles by the scrubber is made possible by two-dimensional gas chromatography with mass spectrometry as a detector. For this, particles collected on filters were analysed. These quantitative measurements were performed for a selected number of major PAH compounds using the heavy fuel oils with high sulfur content. The first thing to notice from these measurements is an up to a factor of 10 higher PAH content in the raw exhaust gas for the HFO with 1.3% sulfur compared with the higher sulfur HFO. This reflects the results from the analyses of the fuels, where the HFO 1.3% sulfur stood out due to an exceptionally high aromatic content. Since a large proportion of the PAHs enters the exhaust gas as unburned fuel, and is subsequently adsorbed on the surface of the particles, this difference in PAH content can be explained.

Furthermore, it was found that the PAH concentrations were higher at 20 kW than at 60 kW load, a tendency that also holds for particle mass concentrations. Moreover, at 20 kW the emission factors of the PAHs increase after the scrubber, while they decrease at 60 kW. This result, also in conjunction with the results of the single particle mass spectrometry, indicates that it is not possible to make any sweeping statements that are generally valid for all conditions with regard to the changes in PAH content. In order to come to a final conclusion, further experiments are necessary.

An interesting question with respect to the operation of a wet sulfur scrubber is the transfer of gaseous exhaust constituents to the wash water of the scrubber. For the investigation of this problem, an online measurement technique capable of monitoring PAHs in aqueous systems was applied. For this purpose, a newly developed mass spectrometric detection method was used, in which the scrubbing water is continuously passed over a silicone membrane. PAHs (and also other organic compounds) can pass from the water through the membrane into a mass spectrometer, whereas the water itself is unable to do so.

Figure 3 shows the PAH pattern in the wash water during open-loop operation with an engine load of 20 kW. Two more fuels were used in this experiment for further comparison, a heavy fuel oil with 0.5 % sulfur (so called compliant fuel eligible for ship engine operation without a scrubber) and diesel fuel. For all fuels, naphthalenes and phenanthrenes are clearly detectable in the wash water. Naphthalene was quantified and found to be between 47 and 125 µg/l in the heavy fuel oils. Comparison with GC-MS measurements show a

slight overestimation of the concentration level, but it is clear that PAHs are transferred to the wash water in greater amounts for the heavy fuel oils, while the distillate fuels show only a minor transition.

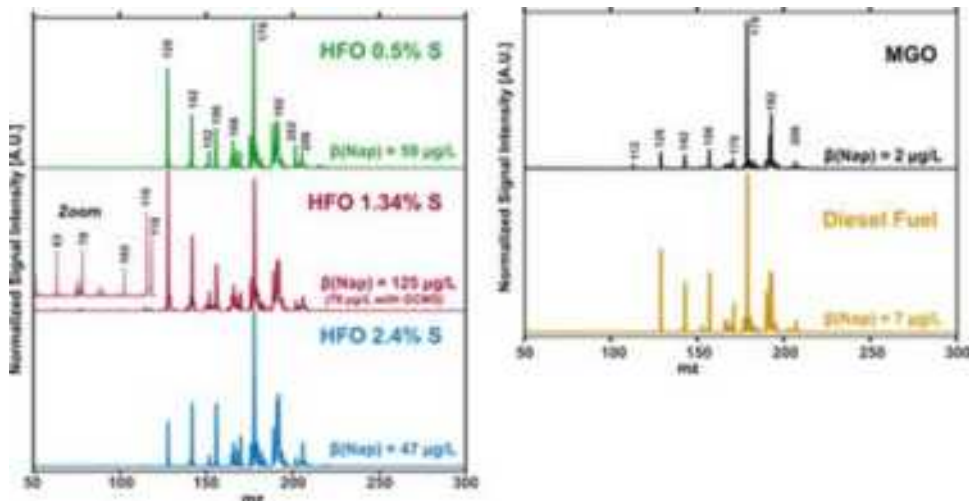


Figure 3: Real-time monitored PAHs in the discharged wash water of the scrubber in Open-Loop operation with five different fuels with 20 kW load point.

Conclusion

The sulfur scrubber leads to only a slight reduction of up to 30% in the number of particles and the emitted particulate mass in the ultrafine particle range; at some operating points, a slight increase in the particulate mass concentration was even recorded with higher-sulfur fuels due to the formation of sulfate-containing particles. The PAH concentrations emitted with the particles and their change due to the scrubber depend very much on the load points and can lead to both an increase and a decrease. No general conclusions can be drawn here. However, the number of PAH-containing particles is not reduced by the sulfur scrubber and may even get higher after passing the device. A further reduction of the total particle mass and the number of particles was only achieved with a particle filter downstream of the sulfur scrubber. Thus, complete removal of the particles from the exhaust gas is possible in principle with modern filter technology, but the relevant experiments have shown that additional research is required for stable long-term operation of such filter systems.

A transfer of PAHs from the exhaust gas into the scrubbing water of the sulfur scrubber could be observed in real time by online mass spectrometry. For open-loop operation of the scrubber that would lead to a transfer of PAHs into the seawater.

An unilateral focus on the removal of the sulfur-containing components of exhaust gas is not sufficient to minimize negative impacts of ship emissions on air quality, climate and health. In contrast, it is recommended to focus on a more complete reduction of particulate emissions.

Acknowledgements

This work was supported by the Federal Ministry for Economic Affairs and Climate Action by the project SAARUS (grant number 03SX483D). The research is also supported by dtec.bw – Digitalization and Technology Research Center of the Bundeswehr (project LUKAS and MORE). Dtec.bw is funded by the European Union – NextGenerationEU. Support by the companies Saacke, RVT, Gea, AVL, and Sult is gratefully acknowledged.

References

- Jeong, S., Bendl, J., Saraji-Bozorgzad, M., Käfer, U., Etzien, U., Schade, J., Bauer, M., Jakobi, G., Orasche, J., Fisch, K., Cwierz, P.P., Rüger, C.P., Czech, H., Karg, E., Heyen, G., Krausnick, M., Geissler, A., Geipel, C., Streibel, T., Schnelle-Kreis, J., Sklorz, M., Schulz-Bull, D.E., Buchholz, B., Adam, T., Zimmermann, R. (2023). Aerosol emissions from a marine diesel engine running on different fuels and effects of exhaust gas cleaning measures, *Environmental Pollution*, 316, 120526

Methane slip from LNG engines – review and on-board study

N. Kuittinen^{1*}, M. Heikkilä², H. Vesala¹, M. Karppanen¹, P. Koponen¹, P. Piimäkorpi¹, J.-P. Jalkanen² and K. Lehtoranta¹

¹ VTT Technical Research Centre of Finland, P.O. Box 1000, FI-02044, Finland, niina.kuittinen@vtt.fi

² Finnish Meteorological Institute, FI-00560 Helsinki, Finland

Introduction

Following the regulations set by the International Maritime Organization for emissions of nitrogen oxides (NO_x) and fuel sulphur content, the use of liquefied natural gas (LNG) as shipping fuel has increased in recent years. According to a recent report, about 20% of the total vessel orders in 2021 were LNG-fuelled (Plevrakis et al., 2022). Vessels using LNG as fuel enable one transition pathway from fossil to non-fossil fuels and utilization in dual-fuel engines fuel flexibility for the ship operators. Compared to conventional liquid fuels, LNG has direct effects, namely benefits, on air quality and human health. The use of LNG as marine fuel can also reduce the emissions of NO_x and particulate matter including black carbon, relative to operation on marine gas oil.

LNG is mainly composed of methane (CH_4) which has higher hydrogen-carbon ratio and energy content compared to liquid fuels, leading to lower emissions of carbon dioxide (CO_2). However, unburned methane is a greenhouse gas (GHG) with a global warming potential of 28–30 times higher than CO_2 . Thus, while the use of LNG has benefits in terms of CO_2 emissions and local air pollutants, slip of unburnt methane to atmosphere remains a concern. Currently, the European Union is in the process of issuing amendments for directives that regulate maritime transport as part of the Green Deal and Fitfor55 environmental packages. Two specific regulations will affect methane emissions from ships: the Emissions Trading System and the FuelEU Maritime, which both will include CO_2 , CH_4 , and nitrous oxide GHG emissions. Currently, the emission data of methane slip from vessels utilizing LNG is limited. In this study, results from a review considering methane slip and other emissions from LNG engines are presented, together with comparison to new results collected during on-board campaign on a modern RoPax ferry.

Methods

A literature review was conducted to collect emission factors of brake-specific methane slip and other emissions from LNG engines from published literature and from ship owner data for engines from recent years. From the literature, published methane emission results could be found for engines from years 2010 (and older / newer), 2012, 2013 (and newer), 2016, 2016 (retrofitted), and 2021. In addition, ship owner data was received, including results for engines designed and constructed in the recent years (2019–2022).

The LNG engines could be divided to four categories according to the engine technology they apply. Lean Burn Spark Ignited (LBSI) engines are typically 4-stroke (4-S) high or medium-speed engines which use only natural gas with spark plug ignition. Low Pressure Dual Fuel engines include both 4-stroke (4-S) and 2-stroke (2-S) engines, in which natural gas is injected in low pressure during compression stroke and injection of small quantity of pilot fuel is used for ignition. Fourth engine type are 2-S High Pressure Dual Fuel engines where natural gas is injected in high pressure at the end of the compression stroke, simultaneously with the liquid pilot fuel injection. The choice of engines for a vessel is dependent at least on the ship type, size, and operational parameters. Large container ships often use 2-stroke engines and mainly operate in deep-sea regions where they may apply constant engine load for long periods after exiting the harbour. On the other hand, ferries or cruise ships are typically equipped with 4-stroke engine and operate on coastal areas where engine load changes may be more frequent (Schuller et al., 2021). To consider these varying operational patterns with different engine types, the methane slip values are presented as function of engine load percentage.

To complement the review, emission measurements on a state-of-the-art LNG ferry were conducted on-board *Aurora Botnia*, Wärtsilä's Roll-on/Roll-off vessel operating on the route between Vaasa (Finland) and Umeå (Sweden). In December 2021, the vessel's construction was finalized in 2021 and its operation started in the autumn 2021. Aurora Botnia is equipped with four Wärtsilä 31DF 4-S medium-speed dual-fuel engines with 8 cylinders and power of 550 kW per cylinder. Exhaust was sampled from one of the engines with normal 31DF setup (ME4) and an engine which was piloting a new combustion concept (ME3). Both engines were operated at load points of 10%, 25%, 50%, 75% and 90% and the loadings were realized with the accuracy of $\pm 2\%$ -units. The engines used LNG with high methane content of 95.1% and marine diesel oil (MDO) with very low sulphur content of 0.01% was used as pilot fuel. The contribution of pilot fuel to the total fuel flow depended on the

engine (3-13% with ME4) and (10-28% with ME3) and load condition with higher shares of MDO utilization at the lowest load conditions.

On-board, raw exhaust gas sample was drawn through a sonde installed in the exhaust duct few meters downstream the engine and then divided to separate gaseous and particulate instruments applying different sample conditioning. A gas chromatograph (Agilent MicroGC) was applied to study methane concentrations. Additionally, methane was measured with Fourier transform infrared spectroscopy (FTIR, Gasmet DX4000) together with water, NO, NO₂, and formaldehyde. The FTIR as well as the sampling line and the filter prior to the FTIR spectrometer were heated to 180°C. NO_x was also measured by standard method with chemiluminescence detector (CLD). CO₂ and carbon monoxide (CO) were measured with a nondispersive infrared (NDIR) analyzer. For particle emissions, particle number (PN) was studied according to the procedure mandated by EU Stage V regulation for inland waterway vessels which considers non-volatile particles with a diameter greater than 23 nm (PN_{>23nm}). In addition, smaller particles with a diameter exceeding 10 nm (PN_{>10nm}) were studied with same methodology applying a Dekati Engine Exhaust Diluter (DEED) for sample conditioning. The system consists of two ejector diluters, providing a total dilution ratio of 1000:1. The temperature of the first ejector was ~200 °C, and the temperature at the outlet of the DEED unit was below 35 °C. Condensation particle counters (Airmodus A23 CPC and Airmodus A20 CPC) were used to determine PN_{>23nm} and PN_{>10nm} concentrations, respectively. Measurements were conducted similarly for both engines and carbon balance method (described e.g., in ISO 8178 and NOx technical code) was used to calculate emission factors in kWh⁻¹ basis. The fuel consumption measured during the onboard studies was provided by the vessel operator together with the engine loading data (power in kW) and LNG bunkering report including fuel composition. Pilot fuel sample was received from the vessel and was further analysed for C, H and N, to include in the calculation of the exhaust gas mass flow rate by the carbon balance method.

Results & discussion

The methane slip data regarding LNG engines is limited and relies largely on measurement data from test-bed (Lehtoranta et al., 2019; Ushakov et al., 2019) or data provided by engine manufacturers (Lindstad et al., 2020; Mærsk Mc-Kinney Møller Center for Zero Carbon Shipping, 2022; Pavlenko et al., 2020; Rolls-Royce, 2012; Schuller et al., 2021; Stenersen & Thonstad, 2017) although a handful of studies (Anderson et al., 2015; Balcombe et al., 2022; Corbin et al., 2020; Peng et al., 2020; Sommer et al., 2019; Stenersen & Thonstad, 2017; Ushakov et al., 2019; Rochussen et al. 2023) which report original research data collected during on-board measurements could be recognized. For the purposes of this study, ship owner data from 6 LPDF 2-S and 5 LPDF 4-S engines from years 2019-2022 were received to complement the data with methane slip information from recently build engines.

Majority of the found data considers methane slip from 4-stroke and 2-stroke LPDF engines, except few studies which also included measurements of LBSI engines. For HPDF engines, the results originate from engine manufacturers and no data including dependence of engine load was found, however, methane slip from HPDF engines is generally considered small due to the injection and combustion strategy of the engines (0.2-0.28 g/kWh estimated for load ranges between 25-85% (Mærsk Mc-Kinney Møller Center for Zero Carbon Shipping, 2022).

Figure 1 shows brake specific methane slip emission factors for 19 LPDF 4-S engines, 8 LPDF 2-S engines, and 8 LBSI engines for which data was available. For LPDF 4-S engines, the methane slip ranged between 2.1-10 g/kWh at 100%, 3.1-10.1 g/kWh at 75% load, 2.6-16.7 g/kWh at 50% load, 6.1-70.2 at 25% load and 12.2-123 g/kWh at 10% load. Respectively, for LBSI engines, corresponding values were 2.5-4.2 g/kWh at 100% load, 3.3-5 g/kWh at 75% load, 4.1-7.2 g/kWh at 50% load, and 6.4-42 g/kWh at 10% load. In the case of LPDF 2-S engines, methane emissions ranged between 1.9-2.5 g/kWh for operation at 100% load, 2.4-2.9 g/kWh at 75% load, 2.4-5.1 g/kWh at 50% load and 2.8-7.2 g/kWh at 25% load.

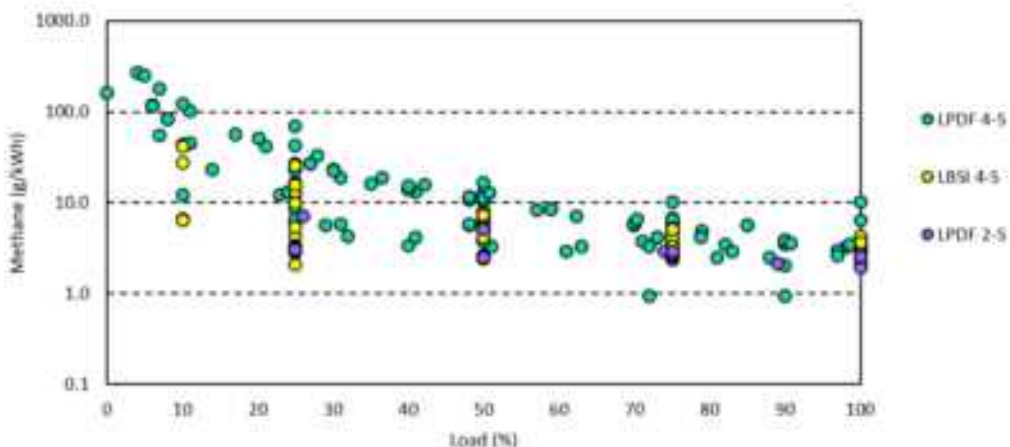


Figure 1. Break-specific emission factors as function of engine load for LPDF 4-S, LBSI 4-S, and LPDF 2-S engine. Figure includes data from reviewed literature as well as ship owner data. (Data sources: LPDF 4-S engines (Anderson et al., 2015; Balcombe et al., 2022; Corbin et al., 2020; Lehtoranta et al., 2019; Peng et al., 2020; Sommer et al., 2019; Ushakov et al., 2019; Rochussen et al. 2023; ship owner data), LBSI engines (Rolls-Royce, 2012; Ushakov et al., 2019); LPDF 2-S engines (Balcombe et al., 2022; WinGD according to Pavlenko et al., 2020; ship owner data). For details of data sources, see Kuittinen et al. (2023).

Increase in brake specific methane emissions as function of decreasing engine load could be observed for all engine types. In case of LPDF 2-S engines, the load dependency was suppressed, although it should be noted that data was limited to load conditions of 25% or above. In the case of LPDF 2-S engines all data originates from relatively new engines (~2018-2021), whereas for LBSI engines, newest published data could be found for engine from 2015. Largest amount of data was found for LPDF 4-S engines with results available for engines from 2012 until 2021. For LPDF 4-S engines, it could be noted that methane emission results for engines from 2016-2019 were equal or higher than those from engines built earlier at all engine loads. For the newest engines, emission factors obtained from ship owner data measured at test-bench show decreased values compared to engines from 2016-2019, especially at 50% load and below. For on-board studies, results from two on-board studies indicate higher values (especially below 50% load) whereas in one case (Rochussen et al. 2023) where engine from 2016 was tested with new engine control calibration, methane slip values were among the lowest and agreed with test-bed values for the new engines.

Taking a closer look to the on-board results from LPDF 4-S engines (Figure 2), 8 studies conducted on 5-6 vessels were found, covering methane and, in some cases, additional gaseous and particle emissions. These results could be complemented with recent on-board results where two engines ME4 (standard engine setup build in 2021) and ME3 (engine piloting a novel combustion concept) (see Lehtoranta et al., 2023 for details) were studied. Including the recent on-board results shows that methane slip from recently build engines can exhibit lower values than majority of the currently available literature suggests, especially at the low engine loads. At loads exceeding 25%, similar methane levels were observed for ME4 that in the case of 2016 engine fitted with new engine calibration. For the ME4 engine, methane slip varied between 3.3-3.6 g/kWh at 50-85% loads, and methane slip of 7.6 g/kWh was observed at 25% load and 12.4 g/kWh at 10% load. In the case of ME3, employing the new combustion concept, corresponding values of 1.4-1.6 g/kWh were seen at 50-85% loads, 1.5 g/kWh at 25% load, and 3.9 g/kWh at 10% load. From the previous studies, very low values of 0.9 g/kWh at 70 and 90% loads have been reported for a 7.6MW engine with larger cylinder (Anderson et al., 2015).

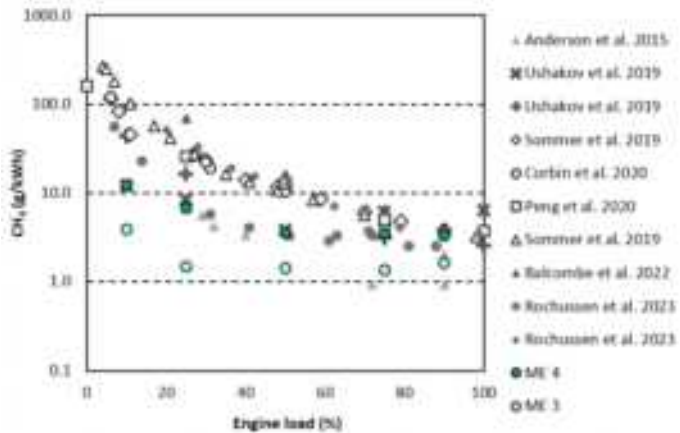


Figure 2: Methane slip emission factors for LPDF 4-S engines studied on-board from literature and recent on-board measurements (Lehtoranta et al., 2023).

Considering other gaseous emissions (Figure 3), the results obtained from the on-board study add to the current data of CO₂, nitrogen oxides (NO_x), carbon monoxide (CO), and formaldehyde (HCHO) emission factors.

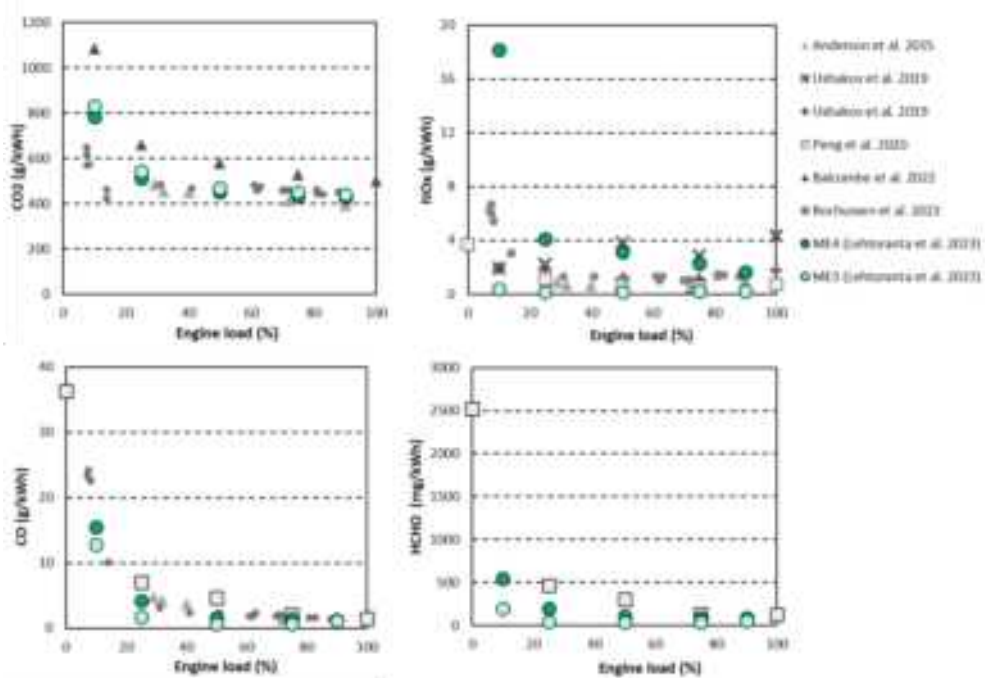


Figure 3: Emission factors of CO₂, NO_x, CO, and HCHO for LPDF 4-S engines studied on-board from literature and recent on-board measurements (Lehtoranta et al., 2023).

Together with the current literature values, it is seen that CO₂ levels observed from ME4 and ME3 somewhat align with Anderson et al. (2015) and Rochussen et al. (2023), together showing 390-550 gCO₂/kWh when load decreases from 90% to 25%. Similar trend of increased emissions at 10% load is seen as in Balcombe et al. (2022) while their study shows generally higher CO₂ level between 500-660 gCO₂/kWh (25-100% load) and 1100 g/kWh (at 10% load). NO_x emissions were covered for six different engines in the included literature, showing generally low values of 0.5-4.3 gNO_x/kWh over the load range from 25% to 100% and 1.9-6.7 gNO_x/kWh at loads below 25%. The results from ME4 mainly align with these values, except at 10% load when 18.2 gNO_x/kWh was observed. For ME3, NO_x emission factors were on a low level of 0.2-0.4 gNO_x/kWh for all load conditions between 10-100%. In case of CO, the results from ME3 (0.7-1.2 gCO/kWh) and ME4 (1.3-1.4 gCO/kWh) aligned with emission levels of 1.4-2.1 gCO/kWh at 75-100% loads from three on-board studies. At 25-50% loads, ME3 and ME4 showed somewhat lower values (0.7-1.8 gCO/kWh and 1.7-4.2 gCO/kWh) than

previous studies (2.1-7 gCO/kWh). In the literature, formaldehyde was included in one on-board study where 120-470 mgHCHO/kWh were reported at 25-100% loads and significantly increased value of 2500 mgHCHO/kWh at idle. Results from ME4 (90-550 mgHCHO/kWh) and ME3 (50-210 mgHCHO/kWh) indicate lower formaldehyde emissions from the modern engine, especially in the case of the new combustion concept.

Non-volatile particle number (PN_{nv}) has been reported earlier from two on-board studies, where $\text{PN} (>6\text{nm})$ emission factors of $1.0\text{-}3.1 \times 10^{12} 1/\text{kWh}$ (25-90% loads) together with $2.3\text{-}3.0 \times 10^{12} 1/\text{kWh}$ (53-90% loads) and $1.4 \times 10^{14}\text{-}3.0 \times 10^{15} 1/\text{kWh}$ (6-50% loads) were reported. The results from recent on-board measurements showed lower values of $0.14\text{-}3.4 \times 10^{12} 1/\text{kWh}$ ($>23\text{nm}$) and $0.39\text{-}26 \times 10^{12} 1/\text{kWh}$ ($>10\text{nm}$) for ME4 with increase towards low load conditions. For ME3, the results were $0.65\text{-}23 \times 10^{12} 1/\text{kWh}$ and $2.6\text{-}43 \times 10^{12} 1/\text{kWh}$, aligning with the previous results at high loads but remaining one to two orders of magnitude lower than the observations by Corbin et al., 2020. Different cut-points of the measurement instruments however complicate the comparison and instead of differences between engines may indicate high number of smallest particles in the exhaust.

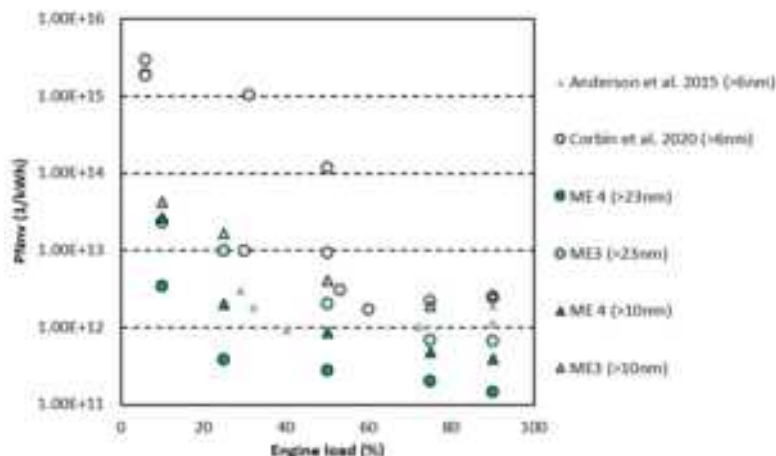


Figure 4: Non-volatile PN emission factors for LPDF 4-S engines studied on-board from literature and recent on-board measurements (Lehtoranta et al., 2023).

Conclusions

Review of literature presenting methane slip emission factors for LNG engines showed limited amount of available data for different LNG engine types. For HPDF engines, methane slip is considered low (0.2-0.3 g/kWh) and no load-dependent data was found. For other engine types, brake specific emissions increased towards low load conditions and varied between 2-26 g/kWh for LBSI, 2-70 g/kWh for LPDF 4-S, and 2-7 g/kWh for LPDF 2-S at 25-75% loads. In addition to NO_x , other gaseous and particle emissions were reported for LPDF 4-S engines. These emissions from on-board studies were complemented with recent measurements of two recently build engines on-board a modern RoPax ferry. Together they showed that reduced methane slip levels can be achieved with state-of-the-art LNG engine (3-7 g/kWh at 25-90% loads) and especially new combustion concept (1.4-1.6 g/kWh at 25-90% loads). NO_x , CO, CO_2 , formaldehyde, and PN results from on-board studies show generally low levels for LPSF 4-S engines, but increased concentrations of especially PN and formaldehyde at low loads were shown.

Acknowledgements

This work was supported by the EU HORIZON project GREEN RAY (Grant number: 101056642).

References

- Anderson, M., Salo, K., & Fridell, E. (2015). Particle- and Gaseous Emissions from an LNG Powered Ship. *Environmental Science and Technology*, 49(20), 12568–12575. <https://doi.org/10.1021/acs.est.5b02678>

- Balcombe, P., Heggo, D. A., & Harrison, M. (2022). Total Methane and CO₂ Emissions from Liquefied Natural Gas Carrier Ships: The First Primary Measurements. *Environmental Science & Technology*. <https://doi.org/10.1021/acs.est.2c01383>
- Corbin, J. C., Peng, W., Yang, J., Sommer, D. E., Trivanovic, U., Kirchen, P., Miller, J. W., Rogak, S., Cocker, D. R., Smallwood, G. J., Lobo, P., & Gagné, S. (2020). Characterization of particulate matter emitted by a marine engine operated with liquefied natural gas and diesel fuels. *Atmospheric Environment*, 220. <https://doi.org/10.1016/j.atmosenv.2019.117030>
- Kuittinen, N., Heikkilä, M., & Lehtoranta, K. (2023). Review of methane slip from LNG engines. https://greenray-project.eu/wp-content/uploads/2023/04/D1.1_Review_of_methane_slip_from_LNG_engines.pdf
- Lehtoranta, K., Aakkos-Saksa, P., Murtonen, T., Vesala, H., Ntziachristos, L., Rönkkö, T., Karjalainen, P., Kuittinen, N., & Timonen, H. (2019). Particulate Mass and Nonvolatile Particle Number Emissions from Marine Engines Using Low-Sulfur Fuels, Natural Gas, or Scrubbers. *Environmental Science and Technology*, 53(6), 3315–3322. <https://doi.org/10.1021/acs.est.8b05555>
- Lehtoranta, K., Kuittinen, N., Vesala, H., & Koponen, P. (2023). Methane emissions from a state-of-the-art LNG powered vessel. *Atmosphere*. <https://doi.org/10.3390/xxxxx>
- Lindstad, E., Eskeland, G. S., Rialland, A., & Valland, A. (2020). Decarbonizing maritime transport: The importance of engine technology and regulations for LNG to serve as a transition fuel. *Sustainability (Switzerland)*, 12(21), 1–19. <https://doi.org/10.3390/su12218793>
- Mærsk Mc-Kinney Møller Center for Zero Carbon Shipping. (2022). An overview of methane emission sources and levels onboard vessels and the technologies, solutions, and regulatory drivers that can help reduce them.
- Pavlenko, N., Comer, B., Zhou, Y., Clark, N., & Rutherford, D. (2020). The climate implications of using LNG as a marine fuel. www.theicct.org
- Peng, W., Yang, J., Corbin, J., Trivanovic, U., Lobo, P., Kirchen, P., Rogak, S., Gagné, S., Miller, J. W., & Cocker, D. (2020). Comprehensive analysis of the air quality impacts of switching a marine vessel from diesel fuel to natural gas. *Environmental Pollution*, 266. <https://doi.org/10.1016/j.envpol.2020.115404>
- Plevrakis, G., Koutsourakis, P., Stamopoulos, S., Sarvaiya, J., Soultanias, I., Vaidhyananathan, S., Seward, N., Shen, T., Zhu, A., Koliniati, R., Kalamidas, A., Barcarolo, D., Dimakopoulos, I., Zhang, A.-N., Daiyan, H., Bose, A., Bell, S., Bass, L., Crisafulli, S., & Lashbrook, J. (2022). Setting the course to low carbon shipping.
- Rochussen, J., Jaeger, N. S. B., Penner, H., Khan, A., & Kirchen, P. (2023). Development and demonstration of strategies for GHG and methane slip reduction from dual-fuel natural gas coastal vessels. *Fuel*, 349. <https://doi.org/10.1016/j.fuel.2023.128433>
- Rolls-Royce. (2012). Rolls-Royce Marine - The Environment Concept System - Low & Wide Slipping Technology
- Schuller, O., Kupferschmid, S., Hengstler, J., & Whitehouse, S. (2021). Title: 2 nd Life Cycle GHG Emission Study on the Use of LNG as Marine Fuel.
- Sommer, D. E., Yeremi, M., Son, J., Corbin, J. C., Gagné, S., Lobo, P., Miller, J. W., & Kirchen, P. (2019). Characterization and Reduction of In-Use CH₄ Emissions from a Dual Fuel Marine Engine Using Wavelength Modulation Spectroscopy. *Environmental Science and Technology*, 53(5), 2892–2899. <https://doi.org/10.1021/acs.est.8b04244>
- Stenersen, D., & Thonstad, O. (2017). SINTEF Ocean AS Maritim GHG and NO_x emissions from gas fuelled engines. www.sintef.no/ocean
- Ushakov, S., Stenersen, D., & Einang, P. M. (2019). Methane slip from gas fuelled ships: a comprehensive summary based on measurement data. *Journal of Marine Science and Technology* 24(4), 1308–1325. <https://doi.org/10.1007/s00773-018-00622-z>

Particulate and gaseous emissions from a large 2-stroke slow speed marine engine equipped with open-loop scrubber under real sailing conditions

Achilleas Grigoriadis¹, Nikolaos Kousias¹, Anastasios Raptopoulos¹, Sokratis Mamarikas¹, Anastasios Kontses¹, Zisis Toumasatos¹, Håkan Salberg², Anna Lunde-Hermansson³, Jana Moldanova², Leonidas Ntziachristos¹

¹ Department of Mechanical Engineering, Aristotle University, P.O. Box 458, 54124 Thessaloniki, Greece, *leon@auth.gr

² IVL Swedish Environmental Research Institute, PO Box 5302, SE 400 14 Goteborg, Sweden

³ Department of Mechanics and Maritime Sciences, Chalmers University of Technology, Gothenburg, SE-41296

1. Introduction

Maritime sector is responsible for transporting over 80 % of the global trade by volume (UNCTAD, 2022), but the drawback of this activity is the significant adverse contribution to air pollution, air quality degradation and human health effects. Ships emit high quantities of harmful pollutants, such as Sulphur Oxides (SO_x), Nitrogen Oxides (NO_x) (Lehtoranta et al., 2019b) and Particulate Matter (PM) (Viana et al., 2014), as well as emissions contributing to climate warming (CO_2 , BC, etc) (IMO 2020). PM properties such as particle Number (PN) concentration and Particle Size Distribution (PSD) are also of significant importance, due to severe consequences of PM on human health, since most of the emitted particles by combustion in ships are found in the ultrafine region (below 100 nm) (Kuittinen et al., 2020). Typical marine residual fuel (Heavy Fuel Oil - HFO), containing high sulphur and ash-forming components, instead of distillate (Marine Gas Oil - MGO) in high power rated engines increases energy specific PM formation (Grigoriadis et al., 2021), deterioration air pollution, especially in port areas.

The International Maritime Organization (IMO) has taken actions to reduce shipping greenhouse gas (GHG) emissions, which were projected to reach up to 17 % of global CO_2 emissions by 2050. NO_x are regulated in the context of engine certification and are subject to further geospatial restrictions in low emission areas, called Nitrogen Emission Control Areas (NECA) (IMO, 1997). IMO has regulated SO_x emissions by the introduction of fuel sulphur content (FSC) reduction from 3.5 % to 0.5 % on a mass basis at a global scale, as from 1st January 2020 (IMO, 2016). In addition, a stricter FSC limit of 0.1 % is applicable in Sulphur Emission Control Areas (SECA).

The drawback of using low sulphur fuels is the rise in fuel expenditure. An alternative enabled by IMO and often adopted is utilization of high-sulphur HFO in combination with exhaust gas cleaning systems, so-called scrubbers. Scrubbers can decrease exhaust SO_2 emissions, typically by up to 99 % (Lehtoranta et al., 2019b), so to equivalently meet low sulphur fuel criteria. Three types of scrubbers are technically feasible and most often installed in ships: open and closed loop scrubbers and hybrid. Open-loop scrubbers use the natural alkalinity of seawater to clean the exhaust, while closed-loop ones utilize fresh water with an added alkaline chemical. Hybrid scrubbers can operate on both configurations, depending on the restrictions imposed over different sailing areas. Although scrubbers are used to primarily abate SO_2 emissions, PM are indirectly affected through the reduction of sulphates (Winnes et al., 2020), organics and elemental carbon (Fridell and Salo, 2016).

Number of scrubber installations on ships have increased dramatically since the introduction of 0.5 % global sulphur cap (Comer et al., 2020), which results in increasing number of ships using high-sulphur HFO in combination with scrubber operate in ports and near populated areas. Hence, the imperative to characterize the emission performance of these emission controls is steadily rising. To evaluate emissions downstream of scrubbers, a few studies have performed on-board measurements on ships equipped with scrubbers, under real-world conditions (Winnes et al., 2020), (Fridell and Salo, 2016), (Yang et al., 2021), as well as on engines with scrubbers placed on test beds (Zhou et al., 2017), (d. Santos et al., 2022) (Jeong et al., 2023). All three types of scrubbers have been tested in literature: open-loop (Fridell and Salo, 2016), (Karjalainen et al., 2021) closed-loop (Winnes et al., 2020), (Zhou et al., 2017) and hybrid ones (Lehtoranta et al., 2019a), (Johnson et al., 2018). Exhaust was characterised for gases and particles both upstream and downstream of scrubbers in the mentioned literature studies, in order to compare emission levels and evaluate scrubber performance. Additionally, Zhou et al., (2017), Winnes et al., (2020), Karjalainen et al., (2021) and (d. Santos et al., 2022) also measured emissions at the same engine operating with a low sulphur fuel (scrubber was deactivated), to compare its emissions with those downstream of scrubber as well as to evaluate the fuel effect (high versus low sulphur fuels). Sampling has been conducted based on the ISO 8178 method in several studies (Winnes and Fridell, 2010), but this method is not applicable when FSC is greater than 0.8 % (Ntziachristos et al., 2016). Winnes et al., (2020) and Fridell and Salo, (2016) measured PN and PSDs both upstream and downstream of

the scrubber. In addition, both teams applied thermal treatment to the sample, with the application of a TD, in order to vaporize volatile particles.

Shipping exhaust particle emissions, and especially those from scrubber outlets, have not been thoroughly investigated, in comparison to particles from other sources, such as automotive. Understanding emission performance downstream of scrubbers is of importance, in order to evaluate the effect of shipping on air quality and human health, in particular near populated areas. Levels and characteristics of particle emissions in the outlet of scrubbers depend on both engine operation and scrubber performance parameters (Yang et al., 2021). Such parameters correspond to engine load (Winnes et al., 2020), engine age (Johnson et al., 2018), geographical location of cruising (ECA/other particular regional sulphur restrictions or global IMO FSC), water alkalinity (seawater or added chemical) and specific operation of scrubber by the ship crew, as well as combination of these parameters under actual sailing, however their specific contribution to emissions is not well defined.

Given the ongoing discussions on fuel change to low-sulphur or alternative fuels, and the increasing utilization of scrubber on retrofit or newbuild ships, understanding the scrubber and fuel impact on emissions and especially those of PM becomes crucial. This paper intends to present the particulate and gaseous emissions of an actual vessel equipped with a slow speed 2-stroke engine and an open loop scrubber during real-world operation over a 7-day measurement campaign. The objective is to collect real performance data in order to feed emission and air pollution modelling tools with emission factors (EF) downstream of a scrubber both for open seas operation but especially for operation near inhabited port regions.

2. Materials and methods

2.1 Measurement campaign

The on-board measurement campaign was performed on a 300 m long container vessel, between 16 and 24 November 2021, on a voyage from the port of Rotterdam, Netherlands to the port of Gebze, Turkey. The ship was built in 2002 and was equipped with a 2-stroke slow speed diesel (SSD) engine as a main engine (ME), with a nominal power of 62 MW at 98 rpm. The ship was travelling at an average speed of 18.4 knots during the cruising phase of the trip, similar to its indicated service speed, while the engine load at the same period was c.a 36.2 %. The ship is equipped with an open-loop exhaust gas cleaning system, in order to comply with the global 0.5 % FSC cap and the stricter 0.1 % FSC limit inside SECAs and ports, when fuel with high sulphur content is used. The exhaust lines of both ME and AEs enter the same scrubber and exit on a common funnel. The physical dimensions of the scrubber tower are 13.8 m in height and 4.5 m in diameter. Three pumps for seawater feeding are used to maintain the necessary seawater flow inside the scrubber. The seawater flow rate ranges from 200 to 1200 m³/h, depending on total exhaust flowrate that has to be cleaned. A dedicated software is also installed on the ship from the scrubber manufacturer to measure and monitor several parameters, including those required by regulations, i.e. SO₂/CO₂ ratio in the exhaust, pH and turbidity in the water effluent.

2.2 Fuel

~~Three types of fuels were used on the ship's ME during the on-board campaign. Two batches of HFO fuel (further called HFO1 and HFO2) were used, having FSCs of 2.64 % and 2.45 %, respectively, and one ULSFO (0.1 % FSC). Ship started its voyage by using HFO1 and after two days, on 18/11, HFO2 was inserted in the fuel system. At the final stage of the trip, on 23/11, the fuel was changed to ULSFO, while the fuel transition from HFO2 to ULSFO lasted for 5 hours.~~

2.3 Testing and sampling

The emitted particles were examined with a variety of sampling systems and conditions. Two different units of the same dilution system (Dekati eDiluter Pro) were utilized for sampling of the exhaust gas from the stack through an L-shaped probe, and its dilution. The eDiluter Pro is a two-stage dilution system operating on cleaned pressurised air, where the first stage is heated and the second stage remains at room temperature. The eDiluter was connected to the sampling probe, which was heated in case of downstream-scrubber sampling, by a heated transfer line maintained at 150 °C. The heated transfer line was insulated throughout its whole length, but heat was not applied on the section close to scrubber, due to the risk of malfunctioning the heating resistances from the major sea water leakage of scrubber. However, temperature was also maintained at this first section because of the high induced exhaust temperatures of c.a 300 °C. The diluted sample was led through a 12-

meter insulated copper line, to the instrument room, where the sample was split and fed to the individual instruments by Tygon tubing. The first eDiluter Pro (Dilution system 1) was used for collection of grabbed samples on PM filters and absorbents for off-line analyses: PM gravimetry and chemical characterisation of the exhaust. The second eDiluter (Dilution system 2) was connected to the online instrument for PN measurements.

The sampling line for the off-line characterisation used dilution with DR of c.a. 25 and temperature of 40 °C and the diluted sample was led by non-heated Tygon line of length of c.a. 5 m to a filter holder followed by a vacuum pump and gas meter. The gas flow through the filter unit was c.a. 20 l/min and the collected PM corresponded to the total suspended PM. Samples collected on polytetrafluoroethylene membrane filters (Teflo filters - Pall Corporation), with mean pore size of 2 µm, were used for PM collection for gravimetric analysis. The analysis was performed under 45-50 % relative humidity and 19-21 °C. The uncertainty for the mass determination was 20 µg with 95 % confidence interval.

PSDs and PN concentrations were measured with a Scanning Mobility Particle Sizer (TSI SMPS model 3080), comprising an impactor of 0.071 cm, a Differential Mobility Analyzer (TSI DMA model 3081) and a Condensation Particle Counter (TSI CPC model 3776), covering a particle range from 5.9 to 225 nm.

Three alternative sample conditioning schemes were studied to characterize total (volatile and non-volatile) and non-volatile particles alone, with two different thermal treatment configurations. The eDiluter Pro was used as the main dilution system for all three sampling schemes. The eDiluter has a first dilution stage, using heated dilution air that varied between 150 and 250 °C, followed by a second, non-heated (cold) dilution stage (25 °C). The total Dilution Ratio (DR) after the second stage ranged between 25 and 100, based on the measurement requirements. The DR was monitored and verified with simultaneous CO₂ concentrations measurements.

In the first sampling scheme, the diluted sample was directly fed to the instruments after the second dilution stage of the eDiluter. It is denoted as 'Raw sample'. In the second scheme a Dekati Thermomediator (TD) (Amanatidis et al., 2018) was applied after the second dilution stage of the eDiluter. The TD comprises a heating stage at 300 °C to vaporize semi-volatile particles and the vaporized material is then collected on activated carbon wall surfaces. Hence, only particles not volatile at 300 °C penetrate the TD. This is denoted as 'Thermal vaporized'. For the 'Raw' and 'Thermal vaporized' configurations the sample was taken after the second dilution. The third dilution scheme utilized a commercially custom-made Catalytic Stripper (CS) with oxidation and sulphur storage capabilities, identical to the one that was used by Amanatidis et al., (2018). The CS was designed to operate along with an Ejector Diluter (ED) providing a DR of 12. To maintain a relatively high concentration, despite the additional dilution, the sample for the CS + ED was taken from the first dilution stage of the eDiluter, at nominal DR ranging between 5 to 10. The CS + ED was heated at 350 °C, to evaporate volatile and semi-volatile particles. The scheme is denoted as 'Catalytic Stripper + Ejector Diluter'. The complete sampling scheme of the measurement campaign is demonstrated in Figure 1.

Gaseous emissions were measured in raw exhaust by a Horiba PG 350 E multi-gas analyzer and by a Bernath Atomic BA 3006 flame ionization detector (FID) for THC (Total Hydrocarbons), which both operate on 1-s time resolution. Non-dispersive infrared (NDIR) analyzer was utilized to measure SO₂, CO₂ and CO and a chemiluminescence analyzer (CLA) for NO_x in the Horiba system. The exhaust sample was extracted by a probe connected to a ceramic filter and then led to the instruments with a sampling line heated to 180 °C. The length of the heated sampling line was 15 m.

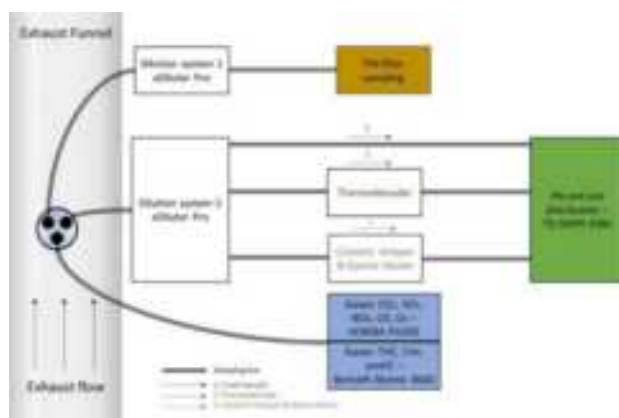


Figure 1:Layout of the measurement setup

Samples were extracted from two different locations, upstream and downstream of scrubber tower, which are designated as Sampling Point Upstream (SPU) and Downstream (SPD), respectively, illustrated in Figure 1. The sampling method followed, dilution systems and instrumentation were the same for the two sampling points with exception of some modifications of the sample extraction: The probes for PM sampling were heated in SPD to avoid condensation of the wet and cold exhaust on the probe, and the heated transfer lines, connecting the eDiluter to the sampling probe, were spanned for 2.5 m and 1 m at SPU and SPD, respectively, due to lack of suitable space and ease of accessibility in each case, without affecting the set temperature. On SPU, raw exhaust from the engine was measured, while on SPD scrubbed exhaust was collected. Therefore, the effect of scrubber from the same engine with the use of HFO can be evaluated. Measurements were also performed at ULSFO operation at SPD but with the scrubber deactivated, so, in this case, we consider this to be an equivalent sampling condition to SPU used for HFO. Thus, the effect of fuel (HFO and ULSFO) from the same engine can be assessed, as well as an emissions comparison between ULSFO and HFO combined with scrubber can also be performed.

PN concentrations and size distributions were corrected for losses, primarily occurring in the eDiluter, the rather long sampling copper transfer lines, the TD, the CS sampling lines and the CS + ED. Losses from sampling lines and the rest instruments were considered per size range, based on the SMPS size range (Figure 2). For estimating sampling line losses, a SMPS Nanoscan (TSI NanoScan SMPS model 3910) was utilized, which measured particles at various size ranges, initially at a position downstream of the eDiluter and then after the 12-meter transfer line, upstream of the SMPS. Therefore, particle losses produced into the sampling transfer lines can be assessed per size range. Losses induced from the eDiluter, TD and CS were estimated based on the manufacturer technical recommendations.

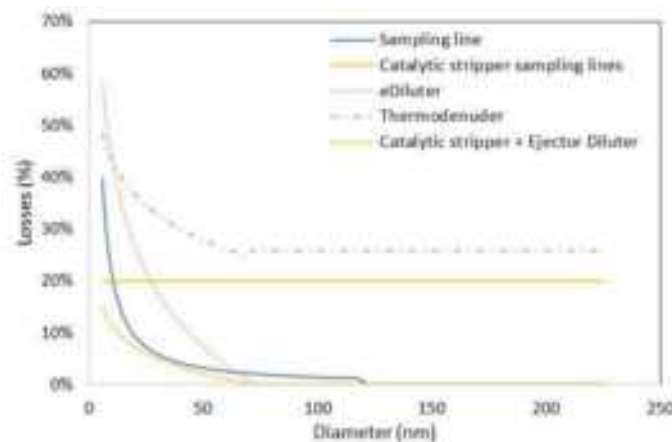


Figure 2:Dilution system, sampling copper transfer line, thermodenuder, catalytic stripper sampling lines and catalytic stripper + ejector diluter losses in relation to particle size diameter

As seen from Figure 2, losses were found to increase on smaller particles. Specifically, particle losses up to 40 % from sampling lines were observed, which were mainly attributed to diffusion, and were decreased with increase in particle diameter. In the sampling line connecting the first stage of the eDiluter to the CS and the line connecting the CS to the ED, losses were estimated to be constant at 20 % for the whole size range, which occurred due to thermophoresis, since these lines were not insulated and were exposed to room temperature, while hot exhaust was passing through. The eDiluter losses were mainly arose due to the turbulent flow and the high residence time of the sample to the system. TD losses, mainly attributed to diffusion in the adsorber section, were reduced with the increase of particle diameter and remained constant at 25 %. Losses up to 14 % were found at smaller particles on CS, due to diffusion and thermophoresis, and were minimized with diameter particle increase. In general, particle penetration losses found increased on smaller particles, due to diffusion and thermal losses (Amanatidis et al., 2018).

3. Results and discussion

3.1 Overview of gaseous emissions

The mean SO_2 , NO_x , CO and THC emission levels (in g/kgfuel) are displayed in Figure 3, where the fuel used, the sampling point and mean engine load are also depicted. The results, in Figure 3, present the mean of emission rate values, measured in 1-s resolution, for the sampling point (upstream and downstream scrubber and with ULSFO). Error bars in Figure 3 correspond to the standard deviation of the measurements per each sampling point.

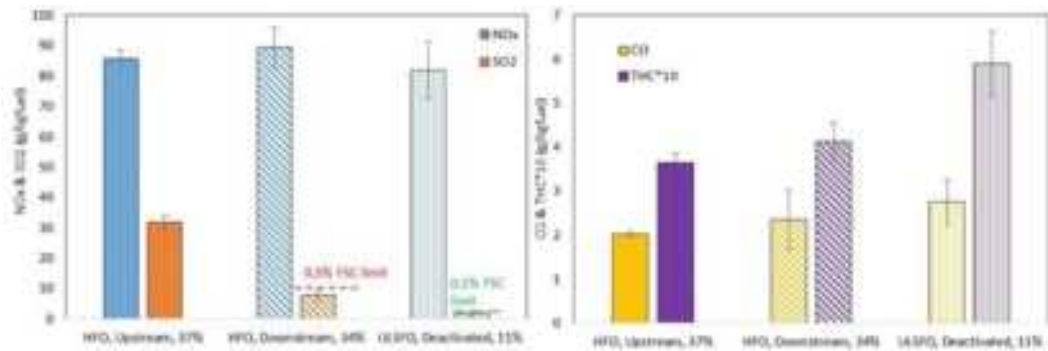


Figure 3: Emission levels (in g/kgfuel) of SO_2 , NO_x , CO and $\text{THC} \times 10$ at different sampling points (upstream and downstream the scrubber), fuel type (HFO, ULSFO) and main engine load. Error bars correspond to two standard deviations. Equivalent SO_2 for 0.5 % and 0.1 % FSC values are represented by red and green horizontal lines, respectively, on the left panel.

As expected, much higher SO_2 was measured upstream of scrubber (31.8 g/kgfuel) than downstream (7.63 g/kgfuel), which decreased SO_2 emissions by 75 %, to a level complying with the 0.5 % global sulphur limit (10 g/kgfuel equivalent – red dashed line). Scrubber was not operated on its full capacity, since the actual seawater flow rate ranged between 640 - 725 m³/h, during the cruising phase. ULSFO resulted to the lowest SO_2 levels, since this fuel actually had sulphur content similar to the stricter 0.1 % limit (2 g/kgfuel equivalent – green dashed line). Lehtoranta et al., (2019b), Winnes et al., (2020) and Fridell and Salo, (2016) reported scrubber efficiencies of approximately 99 % in SO_2 reduction. In our study, the calculated SO_2/CO_2 ratios according to MEPC (2015) were always lower than 21.5, which represents the global 0.5 % IMO FSC limit. This was also cross-checked with the scrubber monitoring equipment recordings, that were provided by the vessel crew. As a result, since regulation compliance is accomplished, there is no need for the ship operator to further increase the scrubbing performance, which would in-line increase the energy and fuel consumption.

NO_x levels vary slightly (approximately ± 4 % in average) between the different operating conditions. Specifically, based on results shown in Figure 3, scrubber operation seems to increase NO_x emission levels by 4.3 % compared to upstream, while ULSFO decrease NO_x emissions by 4.3 % compared to HFO. Grigoriadis et al., (2021) showed that lower engine load leads to higher NO_x emissions, while fuel does not play a critical role in influencing NO_x emissions, since NO_x formation is mainly determined by combustion setting parameters, rather than fuel properties for typical liquid marine fuels (residual and distillate). Winnes et al., (2020), Yang et al., (2021) and Jeong et al., (2023) observed minor or negligible differences in NO_x upstream and downstream of a scrubber, and concluded that any differences were related to the different engine loads. Fridell and Salo, (2016) observed a 12 % NO_x reduction downstream of scrubber compared to upstream, when measured on a 2-stroke SSD engine at 51 % engine load. Lehtoranta et al., (2019b) showed a 5 % decrease in NO_x emissions over the scrubber, supposing that probably NO_x are transferred into the effluent. Combining our emission observations with the existing knowledge from literature, scrubber impact on NO_x is not well established, but it is considered negligible for NO_x regulation compliance.

CO emissions upstream and downstream of scrubber and with ULSFO were found at 2.01, 2.35 and 2.75 g/kgfuel when measured at 37 %, 34 % and 11 % engine load, respectively. Similar to CO, HC emission levels upstream and downstream of scrubber and with ULSFO were observed at 0.364, 0.412, 0.588 g/kgfuel when measured at 37 %, 34 % and 11 % engine load, respectively. Our approach is that these pollutants are mainly combustion related and therefore scrubber and fuel were not affecting their emissions performance. Engine load emerges as the dominant parameter affecting these pollutants, as evidenced by a substantial increase in CO and HC emission levels. Specifically, at lower engine load (11%), CO emissions rose by 37%, and HC emissions surged by 62% compared to the levels observed at higher engine load (37%). Similar trend with

engine load for CO and THC is also observed by Grigoriadis et al., (2021). Winnes et al., (2020) and Lehtoranta et al., (2019b) reported about 20 % CO reduction downstream of scrubber on 4-stroke MSD engines, while Yang et al., (2021) did not find any statistically significant differences in CO EFs, when compared upstream and downstream of scrubber, on a 2-stroke engine. Fridell and Salo, (2016) showed a 200 % increase in CO downstream of scrubber, without providing a specific reason for that. Compared to our results, where we found 13 % increase of THC downstream scrubber, Winnes et al., (2020) measured THC reduction over scrubber of 20 % to 50 % depending on the engine load, while Fridell and Salo, (2016) only a slight decrease. In our case, scrubber seems to adversely impact CO and HC emissions, but since engine load was not remained constant between upstream and downstream of scrubber measurements, the impact of scrubber can't be fully evaluated. Literature findings in conjunction with our observations are controversial in terms of scrubber impact on CO and HC, and therefore more research is needed in this direction.

High error bars depicted in NO_x, CO and THC for measurements conducted downstream of the scrubber were most probably related to more measurements performed over different operating conditions, compared to upstream and ULSFO measurements. In total, 38 hourly downstream scrubber measurements have been performed, while this is only 5 hourly measurements upstream of the scrubber and 7 hourly ULSFO measurements, over the 7-day voyage. Since these pollutants are combustion related (Grigoriadis et al., 2021), operating conditions and mainly engine load variance, corresponds to a critical parameter that affects their performance.

3.2 Particulate emissions

3.2.1 Scrubber and fuel effects

The mean PM levels (in g/kgfuel), derived from filter-based measurements, are demonstrated in Figure 4, in relation to the fuel, sampling point and mean engine load. The results, in Figure 4, represent the average of emission rate values based on the sampling point. Error bars in Figure 4 correspond to the standard deviation of the measurements per each sampling point.

In our study, PM downstream of the scrubber was found 39 % higher compared to upstream levels, while ULSFO operation reduced PM emissions compared to HFO engine-out emissions by 68 % (Figure 4). Lehtoranta et al., (2019a) measured 21-45 % and 8-17 % PM reduction over the scrubber in high (75 %) and low (40 %) engine load conditions, respectively, from a 4-stroke MSD engine. Winnes et al., (2020) showed that PM was reduced over scrubber by 34 % and 42 % at 76 % and 49 % engine load, respectively, from a 4-stroke MSD engine. They also examined the emissions of low sulphur fuel (LSF) with 0.1 % FSC and found that PM was 59 % and 36 % lower than PM downstream of the scrubber at 75 % and 48 % engine load, respectively. Fridell and Salo, (2016) also reported reduction of PM through scrubber, with high removal efficiency (75 %). Karjalainen et al., (2022) observed 70 % decrease of PM emissions downstream of the scrubber, however the ship was also equipped with a Diesel Oxidation Catalyst (DOC) just upstream of the scrubber. They also presented 26 % PM decrease when the ship used MGO instead of using scrubber with HFO at 17 % engine load. Yang et al., (2021) tested a 2-stroke SSD engine and showed 37 % and 16 % reduction of PM over scrubber at 4 % and 70 % scrubber capacity, respectively, while no statistical changes were seen at 48 % and 85 % scrubber capacity. PM removal efficiency depends on the particle size range with smaller particles below 1 μm having the lowest efficiency (Zhou et al., 2017). They also used a LSF with 0.1 % FSC and found 90 % PM reduction of LSF compared to HFO and scrubber. Jeong et al., (2023) tested a small 4-stroke HSD engine, which was mounted on a test-bench, and reported an unclear pattern on PM scrubber removal performance, because of the inconsistent measured decreases and increases over the scrubber at different engine loads and fuel batches. Another laboratory measurement study on a small 4-stroke HSD engine designates that MGO (FSC<0.03 %) reduced PM by 21 % compared to a non-compliant to IMO FSC regulation fuel (0.86 % FSC). When a laboratory scale scrubber was used in conjunction with the non-compliant fuel, PM was reduced by 8 % to 47 %, depending on the combustion conditions variability, compared to the upstream case (d. Santos et al., 2022).

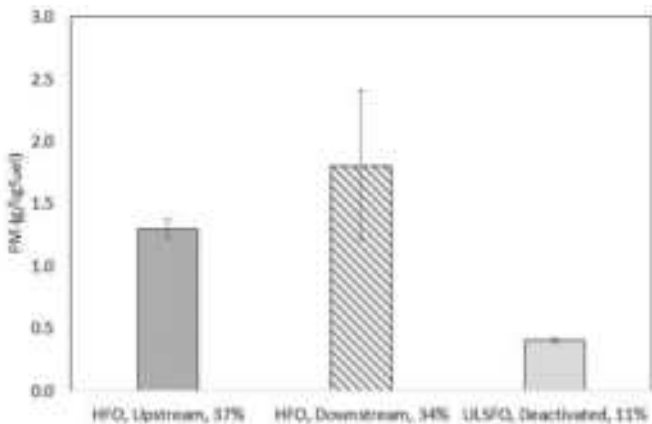


Figure 4:PM mean emission levels (in g/kgfuel) at different sampling points (upstream and downstream of the scrubber), fuel type (HFO, ULSFO) and main engine load. Error bars correspond to two standard deviations.

The effect of scrubber and fuel on the PN levels and the corresponding PSDs are demonstrated in Figure 5. These measurements were conducted on the so-called *“field sample conditions and droplet total particle”*. were obtained, including volatile and non-volatile ones. Mean PN levels and size distributions are presented in each case, together with the individual PSD along with the corresponding uncertainty range that corresponds to one standard deviation on each side of the mean value.

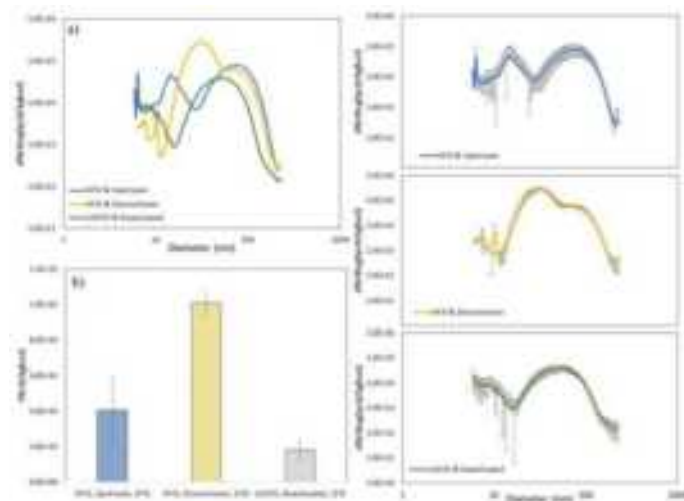


Figure 5:*Mean PN levels and size distributions (PN Number Concentration) measured upstream and downstream of the scrubber with HFO and deactivated scrubber with ULSFO. Individual mean PN size distributions per each sampling point (right panels) are depicted along with error bars that correspond to standard deviation.*

PSD upstream of scrubber appeared trimodal with one peak at 6 nm, a second at 14 nm and a third larger peak at 76 nm, while PSD downstream of scrubber was quadrimodal with the first peak at 6 nm, a second peak at 10 nm, a third one at 31 nm and the fourth one at 66 nm (Figure 5a). ULSFO led to a bimodal PSD with a first peak at 6 nm and a second higher at 53 nm. PN levels downstream of the scrubber were found higher than upstream of the scrubber by 150 %, while the lowest PN levels were observed for ULSFO use (Figure 5b). The soot mode, which represents the non-volatile carbonaceous part of particles (Amanatidis et al., 2018), was found at the same level, both in terms of PN level and PSD between upstream and downstream points. Soot emissions are mainly attributed to engine performance, combustion quality and fuel type (Ntziachristos et al., 2016). Particles downstream of the scrubber were dominated by nanoparticles in the size range between 10 and 40 nm, that were formed from nucleation of volatized fuel ash species (Kasper et al., 2007), (Ntziachristos et al., 2016), as seen in Figure 5a. Hot exhaust of c.a 300 °C, containing high amounts of SO₂ and SO₃ is inserted into the scrubber, where high humidity conditions exist, and rapidly cools down to 40 °C, due to the presence of seawater. In such conditions, SO₃ reacts with water vapour molecules to form sulphuric acid nucleating into particles in the nucleation size range (Yang et al., 2021), (d. Santos et al., 2022). These nuclei-sized sulphuric

acid particles are not captured by coalescence with the seawater droplets and therefore a new high concentration particle mode is generated downstream of scrubber. Thus, the increased PN downstream of the scrubber (Figure 5b) is probably to the enhanced nucleation mode that seems to be produced by scrubber, through nucleation or condensation on smaller particles than the measured size range upstream of the scrubber. The increased PN levels downstream of scrubber is also strengthened by the fact that scrubber was inefficient in removing soot mode particles.

On the right side of Figure 5, the mean PSDs of upstream and downstream of the scrubber, as well as with ULSFO use, of Figure 5a are separately demonstrated, along with the corresponding uncertainty ranges, expressed by one standard deviation. Deviations were emerged, due to utilization of the two HFO batches and variable DRs, for both upstream and downstream of scrubber measurements, as well as different dilution temperature upstream of scrubber and variable engine load when downstream of scrubber. On the ULSFO case, ship was cruising at slow speed (about 12 knots) and engine load was too low (10 %), which created measurement uncertainties.

Fridell and Salo, (2016) observed a bimodal PSD forming upstream of the scrubber with a first high peak at approximately 10 nm and a second lower one at about 50 nm, and a monomodal PSD downstream of the scrubber with a peak at around 50 nm. The sampling scheme comprised by dilution system that diluted the exhaust gas at a ratio of 64 to 109 and two online instruments with range of 5.6 to 560 nm and 0.3 to 10 μm , respectively. PN emission levels over scrubber were reduced by 84 % compared to engine out, when HFO with 2.3 % FSC used. Kuittinen et al., (2021) measured a bimodal PSD upstream of the scrubber, that was dominated by ultrafine particles in the size range of 20 to 40 nm and a lower in concentration soot mode between 30 and 100 nm. They also reported that the scrubber reduced particle concentration in the nucleation mode, mainly due to volatile species of smaller particles, and increased accumulation mode particles in the size range of over 50 nm. The sampling system utilized a porous tube diluter (PTD) along with an ejector diluter with nominal DR of 12 and 8, respectively, and a SMPS for PSD measurements with a size range of 10 – 414 nm. A 92 % PN reduction was observed when utilizing scrubber with 0.7 % FSC HFO. Monomodal PSD at about 50 nm was found from d. Santos et al., (2022) upstream of scrubber, while bimodal PSD with a first peak at about 20 nm and a second one at 60 nm downstream of scrubber was identified, due to the formation of a primary mode sulphuric acid particles induced by scrubber. The research team used a 2-stage dilution system at a ratio between 60 and 126 and a SMPS measuring particles at a range of 15.1 to 661.2 nm. The use of ULSFO leads to change in PSD compared to upstream scrubber and HFO, moving nucleation and soot mode to smaller particle diameters (Figure 5a). This is in contrast to the findings of Ntzachristos et al., (2016), who observed similar PSDs between a HFO and a low fuel oil (LFO) on a 4-stroke engine tested at 25 % load. Low sulphur fuels or MGO produced 70 % lower PN levels compared to downstream of scrubber under same engine conditions, as shown by Karjalainen et al., (2022). This was similar to our study, where we found 82 % decrease of PN with ULSFO, compared to the one downstream of the scrubber.

The integration of literature findings with our own experimental observations reveals a certain level of controversy regarding the impact of scrubbers on PN emissions. PN emission levels and PSDs discrepancies between our results and the existing literature findings may be attributed to a multitude of factors. These may include variations in engine types and specifications, engine load operations, engine age, the type of fuel utilized, and its respective sulfur content. Additionally, the target FSC equivalent, based on the area of sailing, can also contribute to differences. Other relevant factors encompass water alkalinity, engine and scrubber wear, as well as the specific operation of the scrubber by the crew, particularly in terms of controlling the seawater flow rate. Such a complex interplay of factors underscores the necessity for comprehensive research to ensure a holistic understanding of the scrubber influences on PN emissions and PSDs in various operating conditions. Another critical element contributing to discrepancies between research studies is the variability in sampling schemes and conditions and instrumentations employed. The choice of sampling locations, sampling lines and their length, the proper heat line application, DR and dilution temperature can significantly influence the obtained results. Additionally, variations in instrumentation sensitivity, accuracy and size range can also lead to differing measurements. To ensure more consistent and reliable data, it is crucial for future research to standardize particle sampling methodologies and adopt advanced, precise instrumentation in PN emission experiments.

The transition from HFO₂ to ULSFO took place as the ship approached the Turkish territorial waters, due to restrictions in the use of open-loop systems. PN concentrations were also measured during the fuel transition process. Mean fuel transition PN is of the same magnitude as most of the downstream scrubber PN levels, but higher than ULSFO. In Figure 6, PN emission levels at the fuel transition phase are presented over time of the $\text{t} \cdot \mu\text{s}$ along with the ship speed (in knots) and the engine load (%). On the fuel change over process, both

HFO and ULSFO were supplied to the ME, with decreasing HFO flow and increasing ULSFO, in parallel to scrubber operation, until the HFO was completely consumed from the fuel pipes. The ship decreased its speed at this stage, from 17 to 12 knots and the engine load was fluctuation between 28 % and 17 %, further contributing on the transient effect. Based on data provided from ship operator, fuel change procedure lasted for 5 hours, so this time was required for ULSFO to be stabilized for combustion in the ME. In Figure 6, only two hours of PN fuel transition time series are depicted, due to malfunction of the eDiluter heater and therefore the last three-hour measurement data was considered invalid.

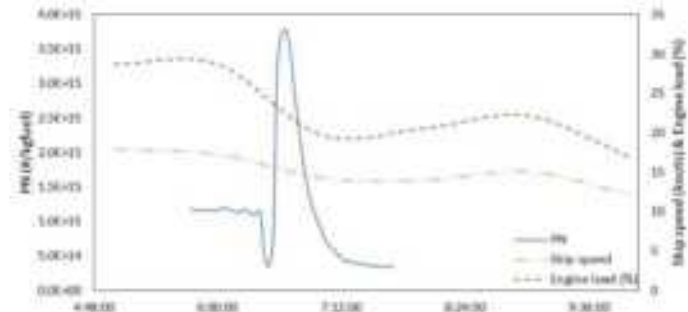


Figure 6: PN emission levels over time of the ship's trip for the fuel transition from HFO to ULSFO in relation to ship speed (knots) and engine load (%)

3.2.1 Effects of sample conditioning

Effects of sample conditioning on mean PN size distributions (left panels) and mean PN emission levels (right panels) are depicted in Figure 7. Measurements have been conducted on fresh samples taken directly from the primary eDiluter, as well as with the utilization of TD and CS + ED removing volatile part of the PM at given conditions of the respective conditioning instrument. Therefore, both total and non-volatile particles have been examined throughout the campaign, upstream and downstream of the scrubber, as well as at the ULSFO operation. According to our knowledge, our study is the first in the worldwide literature that observes the findings of non-volatile particles over scrubber with the utilization of both TD and CS + ED. Results have been grouped in relation to the sampling points, upstream (Figure 7a) and downstream (Figure 7b) of the scrubber, and with ULSFO and deactivated scrubber (Figure 7c).

The PSD of fresh sample upstream of the scrubber was trimodal with a first peak at 11 nm, a second one at 20 nm and a third peak of higher concentration at 88 nm (Figure 7a). The use of the TD, upstream of the scrubber shifted the PSD to smaller particles, but the distribution was altered to bimodal with a first mode at 10.5 nm and the second larger peak at 68.5 nm. The CS + ED completely changed the PSD to monomodal with a peak at 41 nm. The TD actually increased PN by 80 % than on fresh sample upstream of scrubber, due to the artifact formation of particles in the nucleation mode. TD soot mode remained at the same level compared to fresh, both in terms of concentration and PSD, only a slight shift was observed. This artifact creation of particles was clearly described by Amanatidis et al., (2018), who observed re-nucleation of smaller particles, starting from 5 nm, downstream of a similar TD when the temperature exceeded a certain threshold (approximately 250 °C) under high sulphur conditions (>200 ppbv). This marginal temperature is specific to the TD and depends on the TD physical dimensions, flow rate and cooling capacity of the denuding section.

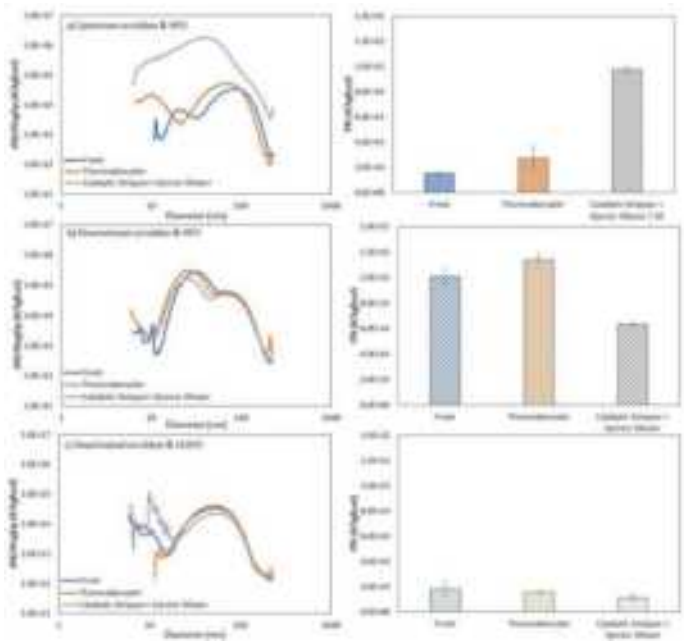


Figure 7: Mean PN size distributions (left panels) and mean PN emission levels (right panels) in (#/kgfuel) a) fresh sample with Thermoscrubber and with Catalytic Scrubber + Sootlet Diluter, downstream scrubber with HFO, b) downstream scrubber with HFO and c) deactivated scrubber with ULSFO. Error bars correspond to standard deviation. PN upstream of scrubber with Catalytic Scrubber + Sootlet Diluter is presented as PN/10.

Use of a CS + ED to isolate non-volatile particles upstream of the scrubber had the opposite effects than this intention, as the resulting PN concentration was over 65-times fold higher than in the fresh sample. Amanatidis et al., (2013) showed that in presence of oxygen and high sulphur conditions, such as combustion of marine HFO fuel, sulphur is stored in the form of sulphates in the CS solution trap. They also observed generation of sulphate particles, which grow from 5 nm to 50 nm in a short time period, when exposed to high sulphur conditions. Particle generation also depends on the CS geometry, design and storage capabilities. In our case, the increased SO₂ concentration upstream of scrubber, due to the utilization of fuels with high FSCs, accompanied by high quantities of NO_x (approximately 1500 ppm), reduced the adsorbent ability of CS and therefore sulphate and nitrate particles were generated. Specifically, we believe that the CS adsorbent material (BaO) had reached its nitrogen and sulphur storage capacity during the first CS measurement, downstream of scrubber, which lasted about 2 hours. This CS measurement was not considered valid, due to malfunction on the dilution system. We then observed that the PN concentration was increased by 2000 % on the first 5 minutes of the second CS testing, upstream of scrubber, meaning that the CS + ED configuration was creating artifact particles.

The PSD of the fresh sample downstream of the scrubber (Figure 7b) is the same to the one of Figure 5a. Use of TD downstream of the scrubber produced a trimodal PSD, similar to the fresh sample, but with a slight shift of each mode to smaller particles. The TD PN was higher than fresh sample by 12 %, mainly due to re-nucleation of particles in the size range between 10-30 nm, when exposed to high sulphur conditions (Amanatidis et al., 2018). Even downstream of scrubber, sulphur is found in increased concentrations of various sulphur-based components (SO₂, SO₃, sulphates), compared to the use of low sulphur fuels, since the scrubber cannot completely abate sulphur particle species (Yang et al., 2021). Moreover, the high operating temperature of 300 °C probably decreased the efficiency of TD and promoted the onset of re-nucleation, due to the reduction of residence time of species on low temperature, that permits adsorption in the denuding section (Amanatidis et al., 2018). CS + ED downstream scrubber PSD displayed a bimodal pattern, with a larger first peak at 20 nm and lower second peak at 70 nm, shifting the PSD to smaller particles. Initially, the CS size distribution and concentration at soot mode downstream of scrubber were found reduced by over 50 % compared to fresh ones, indicating a significant decrease of non-volatile particles at the size range of 60 nm to 100 nm. At this size range the fraction of volatiles is generally low, while CS could not effectively reduce non-volatiles. As a result, a dilution system malfunction was suspected to have occurred during the CS measurement downstream of scrubber. It is assumed that fresh soot mode PN concentration should be about equal to the CS one and thus a dilution correcting factor should be applied, which was determined to 50 %. Therefore, the corrected CS + ED PN emission level was 37 % lower compared to fresh sample one, meaning that CS + ED eliminated the majority of volatile and semi-volatile particles downstream of scrubber.

Winnes et al., (2020) used a TD, which heated the sample at 300 °C, to vaporize volatile particles, when they measured upstream and downstream scrubber with HFO. They showed that upstream of scrubber PSD was bimodal for all engine loads tested (32 %, 49 %, 76 %), with first peak at smaller than 10 nm particles and a second higher peak at 50 nm, but higher loads produced higher PN concentrations. TD seems to remove the majority of volatiles, up to 85 %, in contrast to our study, where formation of particles was observed. Downstream scrubber PSD seems bimodal and trimodal at higher (76 %) and lower (48 %) engine load, respectively, but with higher concentrations compared to upstream ones (Winnes et al., 2020). On downstream scrubber case, the effect of TD on reduction of volatiles was controversial, since concentrations were comparable before and after the TD.

Fresh sample PSD of ULSFO and deactivated scrubber is identical to the one presented in Figure 5a. TD presented bimodal PSD with a first peak 6 nm and a second one at 53 nm, while CS + ED was trimodal with a first peak at 6 nm, a second one at 10 nm and a third one at 51 nm (Figure 7c). The PN levels with TD and CS + ED were reduced by 14 % and 38 %, respectively, compared to fresh sample PN. This means that volatiles were diminished by the TD and were further eliminated by the CS + ED, due to the higher heated temperature (350 °C). High error bars that were depicted on fresh sample and CS + ED with ULSFO were related to the unstable sailing conditions of the ship, which was slow steaming (12 knots) and the engine was working at 10 % engine load during these measurements, therefore affecting the PSDs and PN emission levels.

Conclusions

This study provides the particulate and gaseous emission levels, along with the PSDs from a large 2-stroke SSD engine equipped with open-loop scrubber. These values were derived from a 7-day measurement campaign conducted on a large containership, which performed a scheduled voyage between two international ports. This is the first time in worldwide literature that real sailing conditions measurements conducted on an open-loop scrubber used to abate emissions from such a large engine with maximum power output of 62 MW. Another special and unique element of this study is the first application of both TD and CS + ED on a marine engine environment during on-board testing.

Despite the notable rise in the installation of scrubbers on newbuilding and retrofit ships worldwide, scrubber emission performance is quite controversial, since they can effectively abate SO₂ emissions but their effect on particles is still bound to uncertainty. Therefore, more research is needed on this direction to comprehensively address the remaining challenges of scrubbers emissions and effectiveness. The developed EFs downstream of scrubbers can be fed to emission and air pollution models to identify their overall effect on the environment and human health, and thus to support in promoting new effective emission control policies and regulations. This study also highlights the importance of the appropriate particle testing conditions on marine engines under various DR, temperature and thermal treatment configurations, as well as the additional complexity induced by scrubber. This should be further investigated in future publications as the necessity of creating a standardized marine measurement protocol is obvious for accurate shipping emissions estimation.

Acknowledgements

This work was conducted in the framework of EMERGE project. The EMERGE project has received funding from the European Union's Horizon 2020 research and innovation programme under grant agreement Nr.874990. This extended work will be published in Fuel journal during 2023.

References

- Amanatidis, S., Ntziachristos, L., Giechaskiel, B., Katsaounis, D., Samaras, Z., & Bergmann, A. (2013). Evaluation of an oxidant controlled catalytic stripper in cleaning up volatile material from combustion aerosol. *Journal of Aerosol Science*, 57, 144-155.
- Amanatidis, S., Ntziachristos, L., Karjalainen, P., Saukko, E., Simonen, P., Kuittinen, N., et al. (2018). Comparative performance of a thermal denuder and a catalytic stripper in sampling laboratory and marine exhaust aerosols. *Aerosol Science and Technology*, 52(4), 420-432.
- Comer, B., Georgeff, E., & Osipova, L. (2020). Air emissions and water pollution discharges from ships with scrubbers. *Consulting report, International Council on Clean Transportation*. Retrieved May, 21, 2021.

- d. Santos, L. F., Salo, K., & Thomson, E. S. (2022). Quantification and physical analysis of nanoparticle emissions from a marine engine using different fuels and a laboratory wet scrubber. *Environmental Science: Processes & Impacts*, 24(10), 1769-1781.
- Fridell, E., & Salo, K. (2016). Measurements of abatement of particles and exhaust gases in a marine gas scrubber. Proceedings of the Institution of Mechanical Engineers, Part M: *Journal of Engineering for the Maritime Environment*, 230(1), 154-162.
- Grigoriadis, A., Mamarikas, S., Ioannidis, I., Majamäki, E., Jalkanen, J. P., & Ntziachristos, L. (2021). Development of exhaust emission factors for vessels: A review and meta-analysis of available data. *Atmospheric Environment: X*, 12, 100142.
- IMO (1997). International Convention for the Prevention of Pollution from Ships (MARPOL) Annex VI.
- IMO (2016). Marpol Annex VI, Sulphur oxides (SOx) and Particulate Matter (PM) – Regulation 14, Resolution MEPC.280(70).
- IMO (2020). Fourth IMO GHG study. Full report
- Jeong, S., Bendl, J., Saraji-Bozorgzad, M., Käfer, U., Etzien, U., Schade, J., et al. (2022). Aerosol emissions from a marine diesel engine running on different fuels and effects of exhaust gas cleaning measures. *Environmental Pollution*, 120526.
- Johnson, K., Miller, W., & Yang, J. (2018). Evaluation of a modern tier 2 oceangoing vessel equipped with a scrubber. *Final report prepared for CARB*.
- Karjalainen, P., Teinilä, K., Kuittinen, N., Aakko-Saksa, P., Bloss, M., Vesala, H., et al. (2021). Real-world particle emissions and secondary particle formation from a diesel oxidation catalyst and scrubber equipped ship operating with two fuels in a SECA area. *Environmental Pollution*, 118278.
- Kasper, A., Aufdenblatten, S., Forss, A., Mohr, M., & Burtscher, H. (2007). Particulate emissions from a low-speed marine diesel engine. *Aerosol Science and Technology*, 41(1), 24-32.
- Kuittinen, N., Jalkanen, J. P., Alanen, J., Ntziachristos, L., et al. (2020). Shipping Remains a Globally Significant Source of Anthropogenic PN Emissions Even after 2020 Sulfur Regulation. *Environmental Science & Technology*, 55(1), 129-138.
- Lehtoranta, K., Aakko-Saksa, P., Murtonen, T., Vesala, H., Kuittinen, N., Rönkkö, T., et al. (2019b). Particle and Gaseous Emissions from Marine Engines Utilizing Various Fuels and Aftertreatment Systems. In *29th CIMAC World Congress on Combustion Engine* (p. 399).
- Lehtoranta, K., Aakko-Saksa, P., Murtonen, T., Vesala, H., Ntziachristos, L., Rönkkö, T., et al. (2019a). Particulate mass and nonvolatile particle number emissions from marine engines using low-sulfur fuels, natural gas, or scrubbers. *Environmental science & technology*, 53(6), 3315-3322.
- MEPC. (2015). Marine Environmental Protection Committee (MEPC). Guidelines for Exhaust Gas Cleaning Systems. IMO: London, UK.
- Ntziachristos, L., Saukko, E., Lehtoranta, K., Rönkkö, T., et al. (2016). Particle emissions characterization from a medium-speed marine diesel engine with two fuels at different sampling conditions. *Fuel*, 186, 456-465.
- UNCTAD, 2022. Review of Maritime Transport 2022.
- Viana, M., Hammingh, P., Colette, A., Querol, X., Degraeuwe, B., de Vlieger, I., & van Aardenne, J. (2014). Impact of maritime transport emissions on coastal air quality in Europe. *Atmospheric Environment*, 90, 96-105.
- Winnes, H., & Fridell, E. (2010). Emissions of NOX and particles from manoeuvring ships. *Transportation Research Part D: Transport and Environment*, 15(4), 204-211.
- Winnes, H., Fridell, E., & Moldanová, J. (2020). Effects of marine exhaust gas scrubbers on gas and particle emissions. *Journal of Marine Science and Engineering*, 8(4), 299.
- Yang, J., Tang, T., Jiang, Y., Karavalakis, G., Durbin, T. D., Miller, J. W., et al. (2021). Controlling emissions from an ocean-going container vessel with a wet scrubber system. *Fuel*, 304, 121323.
- Zhou, J., Zhou, S., & Zhu, Y. (2017). Characterization of particle and gaseous emissions from marine diesel engines with different fuels and impact of after-treatment technology. *Energies*, 10(8), 1110.

A new set of Emission Factors for ships

Achilleas Grigoriadis¹, Sokratis Mamarikas¹, Giannis Ioannidis¹, Elisa Majamäki², Jukka-Pekka Jalkanen², Leonidas Ntziachristos^{1*}

¹ Department of Mechanical Engineering, Aristotle University, P.O. Box 458, 54124 Thessaloniki, Greece, *leon@auth.gr

² Finish Meteorological Institute, P.O. Box 503, 00101 Helsinki, Finland

1. Introduction

The maritime sector remains a challenge in terms of pollutants emission reductions, compared to other transportation sectors where substantial reductions have been achieved (EEA, 2020). Shipping was responsible for 2,89% of total manmade Greenhouse Gases (GHG) in 2018 and this share is expected to increase towards 2050 (IMO, 2020). Shipping is also characterized by high emissions of harmful pollutants, such as Sulfur Oxides (SO_x), Nitrogen Oxides (NO_x) and Particulate Matter (PM), causing a significant deterioration of air quality, especially in coastal areas (Corbett et al., 2007), (Viana et al., 2014). Lehtoranta et al. (2019b) estimated that vessels produce 15% of NO_x and 5-8% of SO_x emissions of all anthropogenic activities. Viana et al. (2014) found that maritime PM contribution in European coastal areas can reach 7% of total ambient PM₁₀, and 14% of total PM_{2,5}. Moldanova et al. (2009) reported that global PM from maritime amounts 0,9-1,7 Mton annually, exposing population living in close vicinity to coastal areas to high PM concentrations. Notably, (Kuittinen et al., 2020) calculated that Particle Number (PN) emissions from vessels are at the same level with all continental anthropogenic activities together, quantified to 1,2x10²⁸ particles in 2016.

Efforts to regulate the sector have primarily focused on the reduction of sulphur oxide emissions with the IMO's most recent regulation of 0,5% fuel sulphur content limit being globally effective since January 2020 (IMO, 2016). NO_x are regulated in the context of the certification of marine diesel engines and are subject to restrictions with geospatial characteristics within low emission zones, which are currently applicable to only few parts of the world where relevant Emission Control Area (ECAs) have been established (IMO, 1997). Existing ECAs are located in the United States and in the Baltic and North Sea. CO₂ is currently being systematically monitored and reported by ship operators at EU and international levels (EC, 2013), (IMO, 2011) and energy efficient design obligations for specific ship categories have started to be applied, in the context of a detailed carbon emission reduction strategy (IMO, 2018).

As a reaction to the increasingly stringent emissions regulatory framework, the maritime sector has been strongly investing in new technology and fuels. Technological measures include vessel design and operational changes (Balcombe et al., 2019), engine optimization techniques including exhaust gas recirculation (EGR) (Raptotasis et al., 2015), and the installation and operation of exhaust aftertreatment devices such as scrubbers and selective catalytic reduction (SCR) systems (Nova and Tronconi, 2014). Fuel changes involve the use of low sulphur fuel (Sarvi et al., 2008), (Sarvi et al., 2011) and, most recently, the use of alternative fuels (i.e. LNG, methanol, NH₃) followed by all engine modifications these may require (Anderson et al., 2015), (Fridell et al., 2020), (Hansson et al., 2020).

This range of available options requires reliable and diversified Emission Factors (EFs) to calculate the contribution of shipping to current emission inventories and to project future developments under different policy scenarios. Existing EF datasets for ships, such as the IMO ship emissions toolkit (IMO, 2018), the EMEP/EEA Air Pollutant Emission Inventory Guidebook (AEIG) (Trozzi et al. 2016), the USEPA's Inventory Guidebook (EPA, 2009), and the model STEAM (Jalkanen et al., 2012), and other commercial datasets require constant maintenance and updates to be in-line with latest developments and allow users to make correct assessments related to vessel emissions.

A number of research and development activities can be used to produce new emission information from vessels, using a multitude of techniques and available tools. Measurements are conducted on marine engines in the laboratory (Ntziachristos et al., 2016) or in field campaigns on operational vessels (Winnes and Fridell, 2010). Techniques utilized range from in-funnel measurements using suitable devices (Winnes and Fridell, 2010), to airborne (Murphy et al., 2009) or coast-to-coast (Papadopoulou et al., 2014), measurement with single vessel emissions detection by satellite monitoring (Georgoulas et al., 2020), being one of the latest state-of-art techniques. Our literature review came up with more than 53 published research papers focusing on vessels emissions characterization since 2015.

In this context, the target of the present paper is to collect, analyze, process and develop EFs for various pollutants, ship engine and fuel types, based on existing datasets and latest findings available in the public domain. To offer significant resolution and versatility for use under different operation conditions, the developed EFs are expressed as a function of the ship engine load. The outputs intend to provide evidence on the existing environmental performance of ships, enhancing the overall effort to develop accurate and up-to date EFs for the sector and supporting existing models and emission inventory databases.

2. Status of emission factors and emission measurements of ships

2.1 Emission measurement methods

Emission rates, in the context of real-world measurement campaigns, can be extracted by measuring exhaust emissions in relation to fuel consumption or energy output of the vessel engines. The measurement process mainly includes the involvement of high-end pollutant analyzers or more simplified sensors, which are placed in the ship exhaust line (before or after any emission control system). For PM and PN, a dilution system is also required prior to the PM/PN measurement instrumentation, whereas particle collection in filters is also accomplished.

Emission factors can be composed in relation to specific vessel activity. Activity can be differentiated according to engine operating points or ship operating mode (i.e. maneuvering/hotel, cruising). In this process, emission factors become specific to conditions that can be quantified during the emission inventorying process. For example, one can discern the different phases of operation of a vessel in open-sea or in-port operation and assign a proper emission factor to each of the individual phases. This overall process is schematically represented in Figure 1.

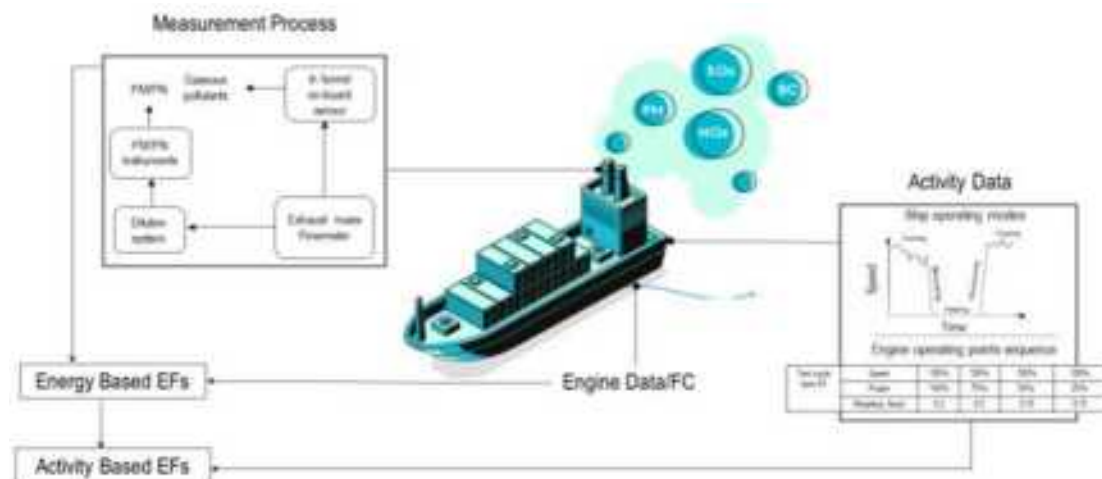


Figure 1:Schematic representation of Emission Factor development process through on-board measurements

Exhaust emission measurements can also be performed on engine test-beds in the laboratory, thus linking emission rates with specific and well-determined engine load points. In such tests, the engine is placed on the dynamometer and is operated at various constant loads at will. Engine loads are often selected from the ISO 8178 loading points. The sampling system is similar to the one used in real-world on-board emission measurements (Ntziachristos et al., 2016b). In the past few years, in-plume measurements have been conducted via remote sniffer technologies, which are installed either in fixed positions where increased ship activity exists (ports/harbor/bridges) (Ekmektizoglou et al., 2020) or on mobile means that chase ship plumes (vans, boats, aerial means) (Pirjola et al., 2014), (Murphy et al., 2009). New techniques are continuously being applied, such as drones carrying small sniffer systems that chase plumes and measure emissions.

2.2 Current study objective

Due to the recent developments in availability of emissions measurements from different vessels and the introduction of stringent environmental regulations for ships at a global level, the target of the current study is twofold. First, to develop new EFs based on literature findings through statistical processing and, second, to quantify the effect of emission control regulations in emission rates. In particular, the following questions become relevant in such an analysis:

- How do parameters such as the fuel type, nominal engine power and nominal rotational speed affect power-based EFs of gaseous pollutants and PM/PN?
- What is the effect of emission standard regulations in EF trends over time?
- How power-based EFs for gaseous pollutants vary in relation with the engine load?

3. Materials and Methods

3.1 Data collection and organization

The suitability of engine load as a variable on which to base emission factors is justified by the fact that the number of engine load points of ships during real world operation is limited, as ships spend most of their operating time at specific steady state loads. It is indicative that, on major ship classes, 94-99% (depending on vessel type) of the total operating time is on cruising or hoteling/anchoring, in which conditions the engine operates in steady state. In contrast, maneuvering is dominated by engine load changes (transient operation), but represents only 1-6% of the voyage time (Comer et al., 2017). Thus, the engine load is not a complicate explanatory variable for shipping emissions and can be easily estimated according to phase of operation.

The methodology for developing EFs is primarily based on a Literature Review (LR), which resulted in the collection of 157 papers, studies and reports focusing on vessel emissions, from which finally 59 were utilized, ~~with over 150 individual emission measurements results displaying various methods. These results comprised on-board measurements (37 measurements) and marine engine placed on test-beds (19 measurements). Also 2 identified in-plume measurements and 1 on-board and in-plume measurement were considered. For each test configuration, various emission rates, including gaseous pollutants (NO_x, CO, SO₂, THC, etc.), greenhouse gases (CO₂) and PM/PN, as well as energy consumption rates have been collected. All these data have been organized in a unique database and divided in category groups (fuel type, engine type, ship category etc.).~~

3.2 Development of load-dependent emission factors

The individual emission values collected were used to deliver an average emission performance and the dependence of emission rate with engine load. As a first step, a single engine load point had to be selected in order to use this as a reference. This reference load point per pollutant was selected to be the one most frequently observed in the available literature. Depending on engine type and pollutant, the most frequent load point encountered was found to be at 50% of engine load for the vast majority of cases or 75% for only a handful of pollutants and engine types. Average values for each pollutant (named Base EFs - BEFs) have been calculated for the three categories of marine engines (slow, medium, high speed) and for different fuel types (residual and distillate) for this reference load point.

The emission rates found in other load points than the reference one, have been normalized over the emissions rate at the reference load point. This normalization process has been separately applied for each single literature source. This produces a family of points which are centered around 1 for every single literature source. By using this method over all literature sources and combining, one obtains the relative effect of load on emissions regardless of the absolute value of emission reported in each study. A single function of load correction is then produced by means of regression over the combined set of values.

The overall process for estimating the absolute emission levels and the emission dependance with the engine load is schematically explained in Figure 2.

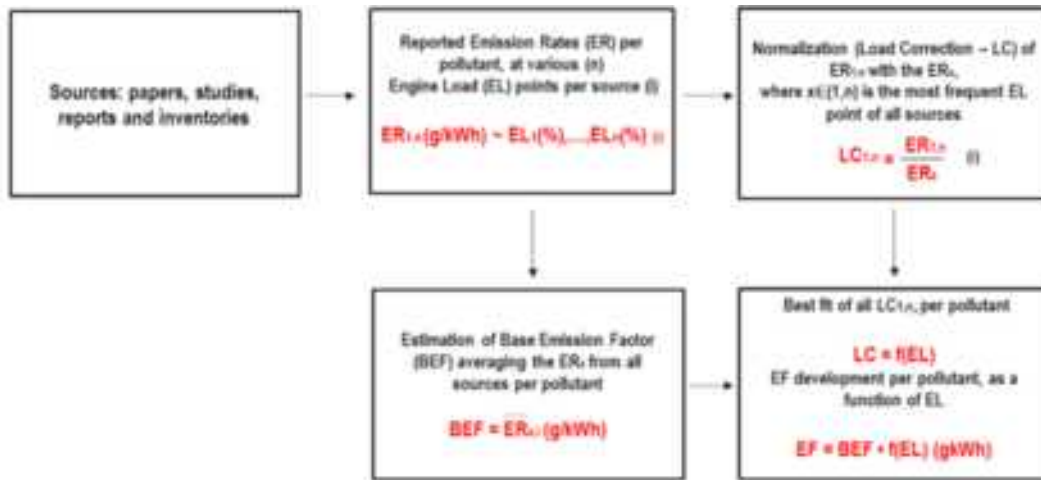


Figure 2:Schematic representation of the Emission Factor development process

4. Results

4.1 Baseline Emission factors

Averaging of emission rates from various sources over the reference engine load point led to the estimation of the baseline emission factor for various gaseous pollutants (NO_x, CO, HC) and the baseline specific fuel oil consumption factor (SFOC). Table 1 provides the absolute level of emissions and consumption depending on engine type, together with the number of measurements and the standard deviation of each value. It is reminded that these reference values correspond to 50% engine load. The same table also provides the grand average value of all measurements collected over the reference dataset under the 'Any type' column, which is suggested to be used in case the engine type is not known.

Table 1: Base Emission or Consumption Factor together with the standard deviation and the number of individual values in parenthesis per engine type at 50% engine load.

Pollutant / Consumption	Any type	SSD	MSD	HSD
NO _x (g/kWh)	13,2 ± 3,98 (35)	14,4 ± 3,60 (15)	12,4 ± 4,08 (15)	11,7 ± 3,68 (5)
CO (g/kWh)	0,898 ± 0,571 (38)	0,714 ± 0,631 (14)	0,974 ± 0,530 (18)	1,10 ± 0,361 (6)
HC (g/kWh)	0,440 ± 0,350 (20)	0,358 ± 0,234 (7)	0,405 ± 0,204 (9)	0,662 ± 0,599 (4)
SFOC (MJ/kWh)	8,83 ± 0,841 (10)	8,48 ± 0,266 (3)	8,42 ± 0,493 (4)	9,74 ± 0,891 (3)

The calculated mean values for CO and HC show that emissions are higher for high-speed engines. This is most probably the result of the fact that slow speed engines operate at higher air-to-fuel ratios and provide more time for oxidation of species after combustion than faster engines do. In terms of fuel consumption, it seems that SSD and MSD engines little differ at 50% load, while fuel efficiency drops significantly for HSD engines.

The impact of engine type on NO_x is rather opposite than CO, HC and SFOC. In this case, SSD exhibit higher NO_x emission rates, again as a result of the higher oxygen and time availability. In particular NO_x from vessels are controlled over different so-called Tier levels, depending on their date of manufacture. Hence, Table 1 values are only to be used when the vessel age or Tier level are not known. Base NO_x emission factors split according

to Tier and engine type are presented in Table 2. In all engine types, baseline emission factors drop as the Tier level advances, a finding that shows the positive impact of regulatory control on actual emission levels. In particular Tier III appears to be some 90% lower than pre-Tier levels, at least for SSD and MSD engines. In particular, all NO_x Tier III values correspond to SCR-equipped vessels. Although, in principle, Tier III can be achieved with EGR alone all the measurements found in literature were obtained on SCR-equipped engines so the actual performance of EGR on real world emission rates cannot be estimated.

Table 2: Base NO_x emission factors, standard deviation (and number of individual values in parenthesis), per engine type and TIER standards for 50% engine load.

NO _x BEF (g/kWh)	TIER 0	TIER I	TIER II	TIER III
SSD	17,7 ± 2,14 (20)	14,4 ± 2,75 (11)	11,3 ± 2,53 (14)	2,00 (1)
MSD	10,8 ± 1,60 (6)	10,5 ± 2,01 (27)	8,28 ± 0,148 (4)	1,02 ± 0,815 (9)
HSD	8,53 ± 2,71 (4)	7,41 ± 1,72 (6)	5,95 ± 1,15 (3)	1,25 ± 0,150 (2)

CO₂ and SO₂ can be calculated from SFOC values if the fuel energy content and speciation in carbon and sulphur are known. If such values are not known, the emission rates in Table 3 can be used instead. These have been derived on the basis of Table 1. SFOC values in combination with averaged fuel characteristics found in the literature. Specifically, the SO₂ calculation also takes into account the fact that part of the SO₂ is converted to SO₄ and corrects for this (more on this correction follows with the discussion around Figure 5).

Table 3: CO₂ and SO₂ Base Emission Factor, per engine and fuel type for 50% engine load

Pollutant	Fuel type	All types	SSD	MSD	HSD
CO ₂ *	Residual	678	651	646	747
(g/kWh)					
CO ₂ *	Distillate	645	619	615	711
(g/kWh)					
SO ₂ **	Residual	4,43	4,31	4,29	4,70
(g/kWh)					
SO ₂ **	Distillate	0,372	0,358	0,355	0,410
(g/kWh)					

*CO₂ has been calculated by the SFOC, considering a fuel carbon content of 86,8% and LHV of 41,5 MJ/kg for residual fuel and 86,5% and 43,4 MJ/kg for distillate. **SO₂ has been calculated by the SFOC, considering FSC of 1,42% and LHV of 41,5 MJ/kg for residual fuel and 0,0931% and 43,4 MJ/kg for distillate.

CO₂ is directly proportional to the SFOC and therefore high-speed engines produce higher emissions, due to lower efficiency, compared to medium and slow speed. The higher heating value of distillate fuels in combination with the slightly lower carbon content than residual fuels, leads to lower CO₂ emissions. For estimating SO₂ emissions, the distillate fuel that on average contains 0,09% sulphur produces significantly lower SO₂ emissions than residual, where average FSC is estimated at 1,42%. It is clarified that these values are relevant for residual fuels when no exhaust gas cleaning systems (scrubbers) are used.

For PM, the engine type was not found to have a significant impact on specific emission rate. On the contrary, PM was largely affected by the use of residual or distillate fuels that were shown to have an impact on all individual PM components (elemental carbon, organic mass, ash and sulphates). In particular for the contribution of sulphates, total PM has been calculated on the basis of hydrated sulphates (SO₄ + 6,5H₂O) or as dry PM, which includes sulphates but no addition of water. Total PM values would be relevant if one would wish to compare the calculated values in the current study with measured values collected after typical dilution ratios (e.g. 100:1). However, in plume simulation studies, the dry PM would be the starting point and then the model

would account for the partition of water between the particulate and the gaseous phases as particles age in the atmosphere. Calculated BEFs for PM (total and dry) are presented in Table 4.

Table 4: PM Base Emission Factors, per engine and fuel type for 50% engine load

Pollutant	Fuel type	All types	SSD	MSD	HSD
PM*** (g/kWh)	Residual	0,960	0,934	0,930	1,03
PM*** (g/kWh)	Distillate	0,217	0,215	0,215	0,221
Dry PM**** (g/kWh)	Residual	0,637	0,624	0,622	0,669
Dry PM**** (g/kWh)	Distillate	0,197	0,196	0,196	0,199

PM has been calculated by the sum of organic mass, elemental carbon, ash, hydrated sulphates ($\text{SO}_4 + 6,5\text{H}_2\text{O}$). *Dry PM has been calculated by the sum of organic mass, elemental carbon, ash and dry sulphates (SO_4).

Table 5 provides further speciation of PM to individual components and some average physical characteristics of particle distributions. As PM is constituted by EC and OM, a further analysis of its speciation was performed on the basis of the statistical analysis of emission rates of these two groups. For the purposes of this analysis, EC and BC were considered equivalent and were used interchangeably. Although it is well recognized that EC and BC are measured with different techniques, the range of values encountered in the literature were largely overlapping and this allowed pooling them together. Particle number (PN) distinguished to total and non-volatile (solid) particles is included in Table 5, without distinction to fuel type due to lack of data. Base EFs for OC and EC are indicated at 50% engine load, while SO_4 conversion rate, total PN and solid PN are provided at 75% load.

Table 5: OC, EC and PN Base Emission Factors, standard deviation (and number of individual values in parenthesis). OC and EC are provided for 50% engine load, while SO_4 conversion rate, PN (total and non-volatile) at 75%.

Pollutant	All types	Residual	Distillate
OC (g/kWh)	$0,232 \pm 0,158$ (14)	$0,248 \pm 0,163$ (12)	$0,138 \pm 0,0617$ (2)
EC***** (g/kWh)	$0,0182 \pm 0,0181$ (16)	$0,0206 \pm 0,0193$ (13)	$0,00827 \pm 0,00319$ (3)
SO_4 conversion rate (%)	$3,94 \pm 1,50$ (6)	$4,56 \pm 0,627$ (5)	0,827 (1)
PN (#/kWh)	$3,58\text{E}+15 \pm 1,87\text{E}+15$ (3)	N/A	N/A
PN non-volatile (#/kWh)	$6,33\text{E}+14 \pm 2,67\text{E}+14$ (2)	N/A	N/A

From Table 5, it can be observed that residual fuel leads to more OM, EC and SO_4 compared to distillate fuel use.

4.2 Load dependent functions

The dimensionless dependence of emissions rates on engine load for various pollutants (NO_x , CO, HC) and SFOC is depicted in Figure 3. As earlier explained, the most frequent engine load point for which emission rates were available in the literature was the 50% load, therefore all other emission rates have been normalized over the emission rates at this engine load. Figure 3 presents all individual normalized points together with the best-fit regression line. Emission rates from all engine types (SSD, MSD, HSD) have been included in the same pool, as our analysis could not identify specific engine type effects that would give substantially differentiated results.

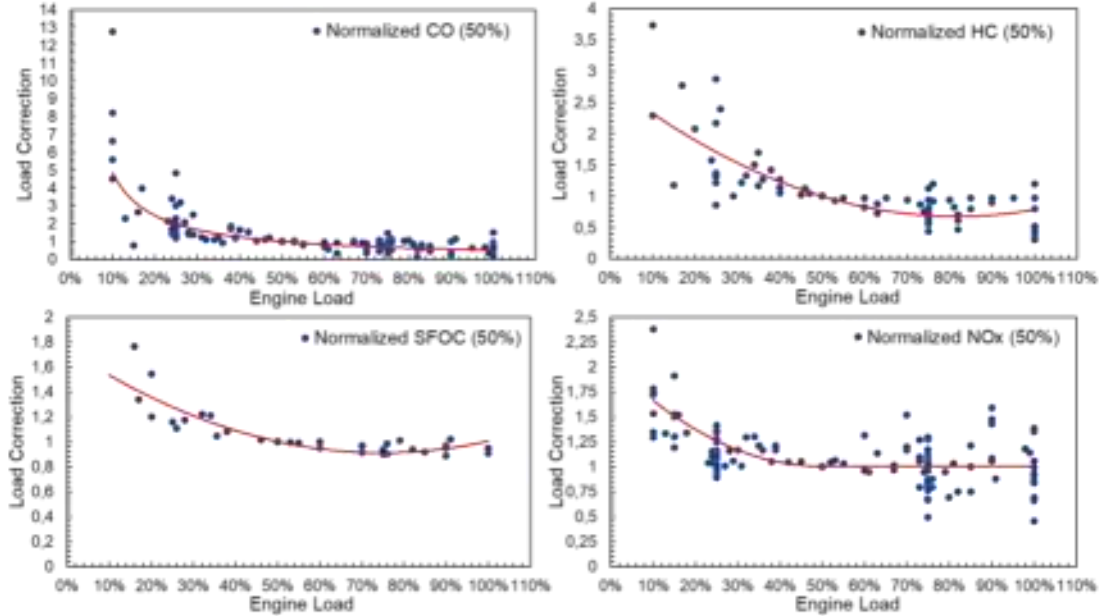


Figure 3: Engine load impact for normalized emission rates (NO_x , CO, HC) and Specific Fuel Oil Consumption at 50% load.

It is observed that the general emission trends described in section 2.2 of the current study are reflected to the shape of the regression lines derived. SFOC, which depends on the efficiency of marine engines, shows to drop as load increases towards a minimum at 75% and then this increases again. This is typical behavior for diesel engines and in particular for marine ones that are optimized for optimum fuel efficiency at cruise conditions that occur around 75% load (Yang et al., 2019).

CO emissions strongly increase as load drops below 30%. This behavior can be explained by the lower combustion temperature at low loads – the CO to CO_2 conversion is known to be very strongly linked to temperature (Sippula et al., 2014). The behavior of HC is similar to that of CO but of lesser value as the HC oxidation is not as strongly dependent on temperature as that of CO. One may also observe some slight increase in HC for 100% load. Although there is large scatter of data at this load point, slight increase of HC may be expected due to the long duration of injection at 100% load and the increased probability of hydrocarbon interaction with the piston and cylinder walls (Yang et al., 2019).

For NO_x the trend shows that emissions decrease with engine load, as this approaches 50%. For higher loads than 50%, a constant level against engine load is seen within uncertainty. At lower loads, NO_x specific emissions may increase because of leaner air fuel mixtures (Kaleder and Ergin., 2017) and the lower fuel efficiency at this engine operating area (Gysel et al., 2017) which is the denominator. Nevertheless, at higher loads (above 50%) the statistical processing verifies the contrasting findings regarding the NO_x increase or decrease with the engine load, already recognized in the literature review section. There is a respective number of emission rates either above or below the formed steady line above 50%. This behavior indicates that NO_x emissions may be influenced by parameters that counteract each other, as previously stated in the review section. The NO_x increase effect due to the temperature rise at high loads may in some cases overtake the influence of NO_x decrease, because of the enrichment of the fuel mix at high loads, while in other cases the reduction of the air to fuel ratio seems to overcome the effect of temperature. This finding leads to the consideration that parameters such as the engine age, technology maintenance and specific engine tuning further play a vital role in NO_x performance (Fridell et al., 2008). Therefore, an additional analysis has been conducted to investigate

the influence of Tier standard regulations on NO_x load dependence. Emissions are separated to three categories, according to the Tier classes I, II and to engines built before the application of Tier regulation (referred as Tier 0 - constructed before 2000). This classification is considered convenient to reflect the effect of age and technology evolution - ~~engine and aftertreatment performance that can work as drivers of modern engines NO_x performance differentiation~~. The formed trends for all three types of engines are presented in Figure 4.

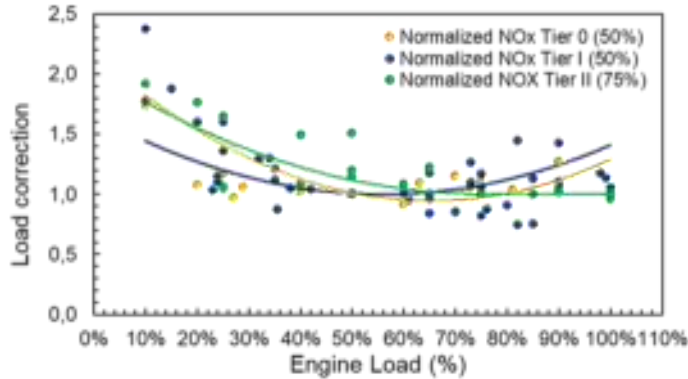


Figure 4: Engine load formed trend of pollutants for NO_x normalized emission rates for three engine technology Tier standards

The comparison of the formed trends over the emission rates for the three engine technology levels (Tiers 0, I, II) verifies the hypothesis that newer engines exhibit a different NO_x behavior at higher loads compared to the older ones. In particular, for Tiers 0 and I energy-specific emissions increase at higher engine loads, while in newer the load rise is accompanied with a reduction of emissions. The contradictory findings of literature therefore seem to be dependent on the engine type technology, while further investigation should be made in order to understand the actual mechanism that leads to the different performance, a fact which is out of the scope of the present paper.

The dependance of SO₂ on engine load is related to the respective dependencies of fuel consumption and sulphur conversion rate for the formation of SO₄. More specifically, the conversion rate to SO₄ in relation with the engine load is provided in Figure 5. The referred SO represent the total sulphur emissions. The conversion rate shows the amount of SO₄ emissions in total SO_x quantities. As evident the remaining part of sulphur found in fuel is converted to SO₂.

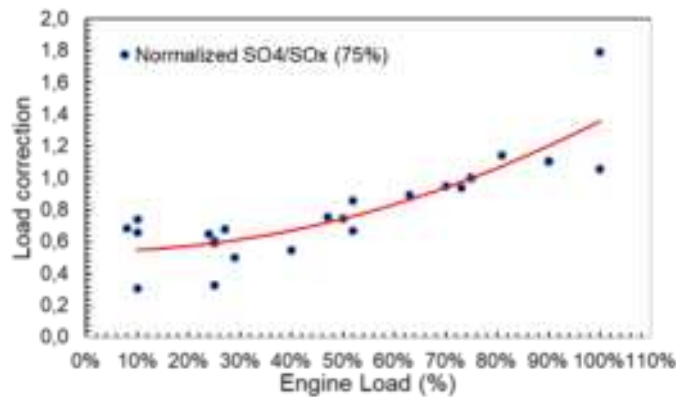


Figure 5: Normalized SO₄ conversion ratio in relation with the engine load

The expression of the conversion rate in relation to engine load shows that less SO₄ is produced at low loads, while the percentage of SO₄ in total emitted SO_x emissions increases with load. The overall contribution of SO₄ to total SO_x is estimated to be between 2-5%, depending on the engine operating condition. The SO₂ dependence on engine load is actually a combination of the dependencies of the SO₂ to SO₄ conversion rate and the SFOC. This relationship varies with fuel type (residual or distillate) as a result of different fuel properties. The trend is depicted in Figure 6, where the SO₂ and SO₄ load dependent functions have been calculated for these two main fuel categories, based on the SFOC, their % FSC and the SO₄ conversion rate.

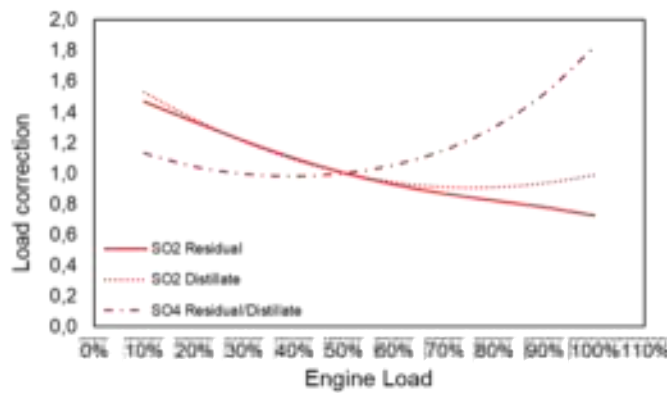


Figure 6: SO_2 & SO_4 load dependent functions for residual and distillate fuels

In particular, for the distillate fuel where the FSC is low, the SO_2 trend follows approximately the one of the SFOC. With residual fuel use, the SO_2 dependance on engine load is different than that of SFOC due to the substantial formation of SO_4 at high loads. SO_4 load dependency, also displayed in Figure 6, as expected follows the convention rate trend in combination with the SFOC. The establishment of a conversion rate dependance on engine load is not only important for the estimation of SO_2 in the emitted gaseous pollutant mix, but also for the quantification of sulphates which contribute to total PM.

PM, apart from sulphates, is also constituted by OM, EC and ash. Already the SO_4 dependency has presented in Figure 6, while the respective correlations of EC and OC are provided in Figure 7.

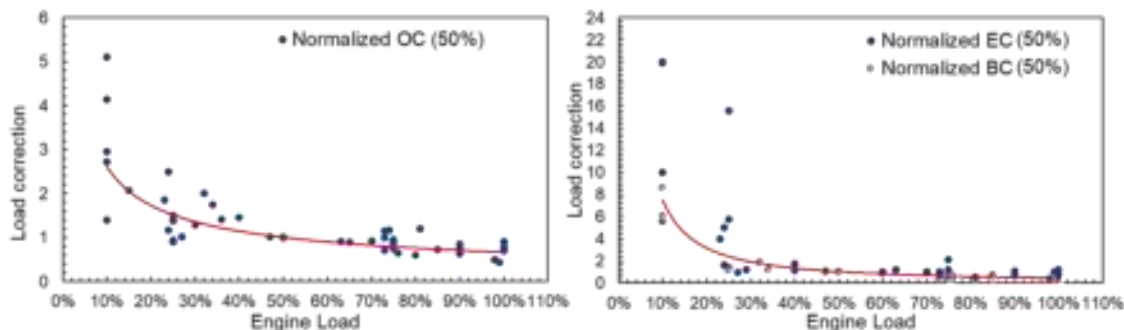


Figure 7: OC & EC engine load dependencies

The emission rates of OC and EC with the engine load are quite similar, presenting a gradual improvement of these emissions with the load increase. Thus, OC and EC are minimized at full load because of the more efficient oxidation due to high combustion temperatures at this load range. For the remaining component of PM, ash is based on the fuel ash content and SFOC. Specifically, the fuel ash content, which is a fuel property, appears to be linearly correlated with the SFOC based on literature findings (presented in Figure 8).

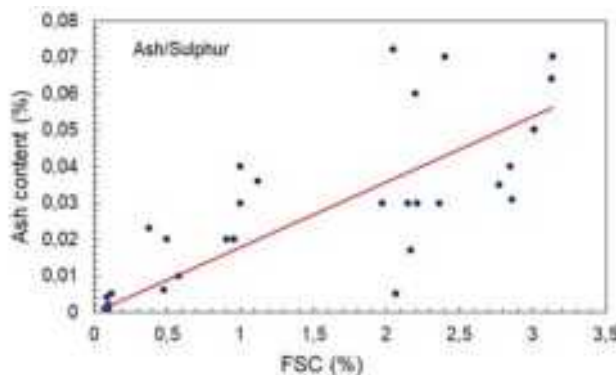


Figure 8: Ash content (%) in relation with the FSC.

The total particle mass, dry or hydrated, as already stated is calculated as the sum of species; hydrated sulphates (water and SO_4) or dry sulphates (SO_4), OM, EC and ash, at a specific engine load. Therefore, the dependency of the pollutant with the engine load is a combination of the partial dependencies of each substance (Figure 9 for residual and distillate).

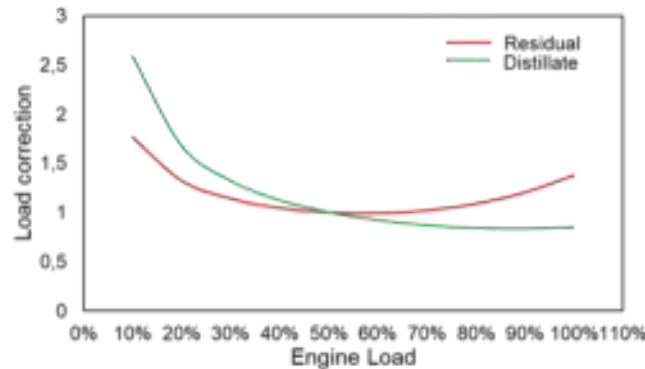


Figure 9: Hydrated PM load dependence for residual and distillate fuel types

The overall calculation for two fuel types reveals that for distillate fuel, PM is reduced with the increase of engine load due to the major contribution of the OM in the PM, while the dominant presence of hydrated sulphates at the residual fuel use leads to higher emissions at higher engine loads.

Particle emissions are also characterized by their number. The identified measurements were conducted by equipment capable of measuring particles with a diameter higher than 5nm. The dependency of the number with engine load as regards the total and the non-volatile part of particles is displayed in Figure 10.

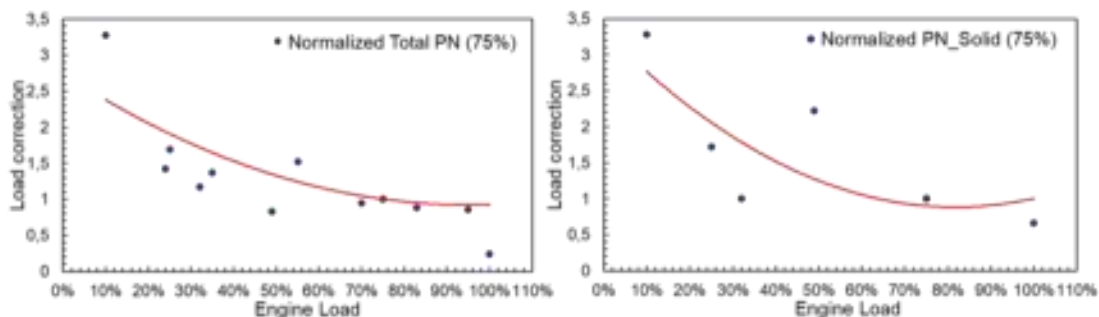


Figure 10: PN (total & solid) performance in relation with the engine load

PN is reduced at full load due to the complete combustion conditions that are being formed, while the increase of PN at low loads may be attributed to lower temperature conditions at this load area. However, the PN correlations are less strong than the respective of PM because of less available studies that examined the particle number compared to those of considering the particle mass.

PN load dependence is influenced by the OC and sulphates (SO_4). In the low load area, the existence of lower quantities of SO_4 leads to a lower PN increase, compared to the increase of OC. Also, in higher loads the decrease of PN with the load increase is lower than the respective decrease of OC as the SO_4 drastically increases at this load area.

Conclusions

The study provided mean emission rates and their engine load dependence for key pollutants produced by marine diesel engines. These values have been derived by combining information from a variety of literature sources in a consistent way. The final values and functions produced can be used in the framework of inventorying activities for shipping emissions if knowledge of engine type, fuel type and Tier standard are available. In particular for PM, emission factors were expressed as composite values of individual key PM categories (elemental carbon, organic mass, ash and sulphates) in order to retain consistency and provide values that can be proven useful to emission and air quality modelers. Emission rates for all pollutants were found to

strongly depend on engine load with g/kWh values dropping as load increased. Tier standard was found as the most significant variable for the estimation of NO_x emissions with Tier III values appearing at a fraction of 10% of pre-Tier level. Slow speed engines were also found to be higher emitters of NO_x than faster ones. PM, on the other hand, mostly depended on fuel use rather than on engine type or Tier standard.

Despite efforts to use all available engine sources and to combine those in the same pool of data, marine engines emission performance is still bound to uncertainty and more research is required to understand fuel, engine and operation mode impacts on emission profiles. In particular, this study identified some inconsistency when expressing emission factors according to their load dependence or operation mode dependence. This should be further clarified in future studies as this is potentially important for correctly estimating in-port emission contribution of vessels.

Acknowledgements

This work was supported by the SCIPPER project. The SCIPPER project has received funding from the European Union's Horizon 2020 research and innovation programme under grant agreement No 814905. This work has been published in the Atmospheric Environment X journal: doi.org/10.1016/j.aeaoa.2021.100142.

References

- Anderson, M., Salo, K., & Fridell, E. (2015). Particle-and gaseous emissions from an LNG powered ship. *Environmental science & technology*, 49(20), 12568-12575.
- Balcombe, P., Brierley, J., Lewis, C., Skatvedt, L., Speirs, J., Hawkes, A., & Staffell, I. (2019). How to decarbonise international shipping: Options for fuels, technologies and policies. *Energy conversion and management*, 182, 72-88.
- CARB. (2008). Emissions Estimation Methodology for Ocean-Going Vessels.
- Comer, B., Olmer, N., Mao, X., Roy, B., & Rutherford, D. (2017). Black carbon emissions and fuel use in global shipping, 2015. The International Council on Clean Transportation, 1225.
- Corbett, J. J., Winebrake, J. J., Green, E. H., Kasibhatla, P., Eyring, V., & Lauer, A. (2007). Mortality from ship emissions: a global assessment. *Environmental science & technology*, 41(24), 8512-8518.
- EEA. (2020). Greenhouse gas emissions from transport in Europe. <https://www.eea.europa.eu/data-and-maps/indicators/transport-emissions-of-greenhouse-gases-7/assessment>. Last accessed 13/10/2021
- Fridell, E., Kukkonen, J., Salo, K., & Stipa, T. H. (2020). Assessment of shipping emission factors through monitoring and modelling studies. *Science of the Total Environment*, 743, 140742.
- European Commission (2013). Integrating maritime transport emissions in the EU's greenhouse gas reduction policies. https://ec.europa.eu/clima/sites/default/files/transport/shipping/docs/com_2013_479_en.pdf.
- Fridell, E., Salberg, H., & Salo, K. (2020). Measurements of Emissions to Air from a Marine Engine Fueled by Methanol. *Journal of Marine Science and Application*, 1-6.
- Fridell, E., Steen, E., & Peterson, K. (2008). Primary particles in ship emissions. *Atmospheric Environment*, 42(6), 1160-1168.
- Georgoulias, A. K., Boersma, K. F., van Vliet, J., Zhang, X., Zanis, P., & de Laat, J. (2020). Detection of NO₂ pollution plumes from individual ships with the TROPOMI/S5P satellite sensor. *Environmental Research Letters*, 15(12), 124037.
- Gysel, N. R., Welch, W. A., Johnson, K., Miller, W., & Cocker III, D. R. (2017). Detailed analysis of criteria and particle emissions from a very large crude Carrier using a novel ECA fuel. *Environmental science & technology*, 51(3), 1868-1875.
- Hansson, J., Brynolf, S., Fridell, E., & Lehtveer, M. (2020). The Potential Role of Ammonia as Marine Fuel—Based on Energy Systems Modeling and Multi-Criteria Decision Analysis. *Sustainability*, 12(8), 3265.
- IMO. (1997). International Convention for the Prevention of Pollution from Ships (MARPOL) Annex VI.
- IMO. (2011). Inclusion of regulations on energy efficiency for ships in MARPOL Annex VI.
- IMO. (2016). Marpol Annex VI, Sulphur oxides (SOx) and Particulate Matter (PM) – Regulation 14, Resolution MEPC.280(70).
- IMO. (2018). GloMEEP Project Coordination Unit, Institute of Marine Engineering, Science and Technology (IMarEST). Ship Emissions Toolkit. Guide No.1: Rapid assessment of ship emissions in the national context.
- IMO. (2018). Initial IMO strategy on reduction of GHG emissions from ships.
- IMO. (2020). Fourth IMO GHG study. Full report
- Jalkanen, J. P., Johansson, L., Kukkonen, J., Brink, A., Kalli, J., & Stipa, T. (2012). Extension of an assessment model of ship traffic exhaust emissions for particulate matter and carbon monoxide. *Atmospheric Chemistry and Physics*, 12(5), 2641-2659.
- Kalender, S. S., & Ergin, S. (2017). An experimental investigation into the particulate emissions of a ferry fuelled with ultra-low sulfur diesel. *Journal of Marine Science and Technology*, 25(5), 499-507.
- Kuittinen, N., Jalkanen, J. P., Alanen, J., Ntziachristos, L., Hannuniemi, H., Johansson, L., Karjalainen, P., Saukko, E., Isotalo, M., Aakko-Saksa, P., Lehtoranta, K., Keskinen, J., Simonen, P., Saarikoski, S., Asmi, E., Laurila, T., Hillamo, R., Mylläri, F., Lihavainen, H., Timonen, H. R. J. (2020). Shipping Remains a Globally Significant Source of Anthropogenic PN Emissions Even after 2020 Sulfur Regulation. *Environmental Science & Technology*, 55(1), 129-138.
- Lehtoranta, K., Aakko-Saksa, P., Murtonen, T., Vesala, H., Kuittinen, N., Rönkkö, T., Ntziachristos, L., Karjalainen, P., Timonen, H., Teinilä, K. (2019b). Particle and Gaseous Emissions from Marine Engines Utilizing Various Fuels and Aftertreatment Systems. In 29th CIMAC World Congress on Combustion Engine (p. 399).
- Moldanová, J., Fridell, E., Popovicheva, O., Demirdjian, B., Tishkova, V., Faccinetto, A., & Focsa, C. (2009). Characterisation of particulate matter and gaseous emissions from a large ship diesel engine. *Atmospheric Environment*, 43(16), 2632-2641.
- Murphy, S. M., Agrawal, H., Sorooshian, A., Padro, L. T., Gates, H., Hersey, S., Welch, W. Jung, H. Miller, W. Cocker, D. Nenes, A. Jonsson, H. Flagan, R. Seinfeld, J. H. (2009). Comprehensive simultaneous shipboard and airborne characterization of exhaust from a modern container ship at sea. *Environmental Science & Technology*, 43(13), 4626-4640.

- Nova, I., & Tronconi, E. (Eds.). (2014). Urea-SCR technology for deNOx after treatment of diesel exhausts (Vol. 5). New York: Springer.
- Ntziachristos, L., Saukko, E., Lehtoranta, K., Rönkkö, T., Timonen, H., Simonen, P., Karjalainen, P., Keskinen, J. (2016). Particle emissions characterization from a medium-speed marine diesel engine with two fuels at different sampling conditions. *Fuel*, 186, 456-465.
- Ntziachristos, L., Saukko, E., Rönkkö, T., Lehtoranta, K., Timonen, H., Hillamo, R., & Keskinen, J. (2016b). Impact of sampling conditions and procedure on particulate matter emissions from a marine diesel engine. In *28th CIMAC World Congress* (p. 165).
- Pirjola, L., Pajunoja, A., Walden, J., Jalkanen, J. P., Rönkkö, T., Kousa, A., & Koskentalo, T. (2014). Mobile measurements of ship emissions in two harbour areas in Finland. *Atmospheric Measurement Techniques*, 7(1), 149-161.
- Raptotasis, S. I., Sakellaridis, N. F., Papagiannakis, R. G., & Hountalas, D. T. (2015). Application of a multi-zone combustion model to investigate the NOx reduction potential of two-stroke marine diesel engines using EGR. *Applied Energy*, 157, 814-823.
- Sarvi, A., Fogelholm, C. J., & Zevenhoven, R. (2008). Emissions from large-scale medium-speed diesel engines: 2. Influence of fuel type and operating mode. *Fuel processing technology*, 89(5), 520-527.
- Sarvi, A., Lyyränen, J., Jokiniemi, J., & Zevenhoven, R. (2011). Particulate emissions from large-scale medium-speed diesel engines: 1. Particle size distribution. *Fuel processing technology*, 92(10), 1855-1861.
- Sippula, O., Stengel, B., Sklorz, M., Streibel, T., Rabe, R., Orasche, J., ... & Zimmermann, R. (2014). Particle emissions from a marine engine: chemical composition and aromatic emission profiles under various operating conditions. *Environmental science & technology*, 48(19), 11721-11729.
- Trozzi, C., & De Lauretis, R. (2016). International navigation, national navigation, national fishing, *EMEP/EEA emission inventory guidebook*.
- U.S. EPA, Current Methodologies in Preparing Mobile Source Port-Related Emission Inventories, *Final Report Prepared for U.S. Environmental Protection Agency by ICF International*, April 2009
- Viana, M., Hammingh, P., Colette, A., Querol, X., Degraeuwe, B., de Vlieger, I., & van Aardenne, J. (2014). Impact of maritime transport emissions on coastal air quality in Europe. *Atmospheric Environment*, 90, 96-105.
- Winnes, H., & Fridell, E. (2010). Emissions of NO_x and particles from manoeuvring ships. *Transportation Research Part D: Transport and Environment*, 15(4), 204-211.
- Yang, Z., Tan, Q., & Geng, P. (2019). Combustion and emissions investigation on low-speed two-stroke marine diesel engine with low sulfur diesel fuel. *Polish Maritime Research*, 26(1), 153-161.

Robustness Analysis for Classification of Aerosol Particles using Machine Learning with Two Different Single-Particle Mass Spectrometry Datasets

Guanzhong Wang¹, Heinrich Ruser¹, Julian Schade^{2, 3, 5}, Johannes Passig^{3, 4, 5},

Thomas Adam^{2, 4}, Günther Dollinger¹, and Ralf Zimmermann^{3, 4, 5}

¹Institute for Applied Physics and Measurement Technology, University of the Bundeswehr Munich, Neubiberg, 85577, Germany, heinrich.ruser@unibw.de

²Institute of Chemistry and Environmental Engineering, University of the Bundeswehr Munich, Neubiberg, 85577, Germany

³Joint Mass Spectrometry Centre, Chair of Analytical Chemistry, University of Rostock, Rostock, 18059, Germany

⁴Joint Mass Spectrometry Centre, Helmholtz Zentrum München, Neuherberg, 85764, Germany

⁵Department Life, Light & Matter, Interdisciplinary Faculty, University of Rostock, Rostock, 18059, Germany

Abstract

The chemical composition of aerosol particles in the air is successfully used to determine their origins, e.g., traffic emissions, biomass burning, or ship emissions. Single-Particle Mass Spectrometry (SPMS) is a sensitive measurement technique to analyze the chemical composition in real-time. The current mainstream classification methods in the SPMS community for handling these data require intensive manual post-processing, making an online analysis impossible. A few studies have demonstrated that supervised learning can perform automated classification of SPMS data with high accuracy, enabling selective air quality monitoring in real-time. However, the generalizability and reliability of those algorithms using SPMS data from different sources (e.g., different SPMS instruments, sampling locations, or weather conditions) are still key issues to be solved. This work investigates the classification generalization capacity (or robustness) of a multilayer perceptron network using two different datasets of SPMS data. The results show that the model trained on one dataset is sensitive to the disparate characteristic features of the other dataset, causing its prediction accuracy to decrease significantly. On the contrary, the model trained with data from both datasets performs strong robustness and adaptation to both datasets, with over 96 % correct classifications. The presented results underscore the feasibility and practicability of a uniform approach for automated profiling of data from different sources.

1. Introduction

Single-particle mass spectrometry (SPMS) is a real-time measurement technique that after ionizing individual aerosol particles with a strong UV laser pulse – a process called laser ionization and desorption, LDI – reveals their chemical composition as bipolar mass spectra of the separated anions and cations (Passig *et al.*, 2021). The mass spectra represent the intensity distribution of positive and negative ions with respect to their mass-to-charge ratio (m/z) and contain important chemical information related to the origin of the particles. For example, the main source of particles rich in *Elemental Carbon* (EC) are traffic emissions (Dell'Osso and Harrison, 2006; Shields *et al.*, 2007); *Elemental Carbon and Organic Carbon* (EC-OC) and *Potassium-rich* (K-rich) classes are good trackers of biomass combustion (Toner *et al.*, 2006; Li *et al.*, 2014; Shen *et al.*, 2019); *Calcium ions* are often an important marker for additives in ship engine lubricants (Dell'Osso and Harrison, 2006; Passig *et al.*, 2021); *Vanadium ions* are the signature substance from ships using heavy oil fuels (Ault *et al.*, 2009; Passig *et al.*, 2021); *Iron ions* may come from ships using distillate fuels (Passig *et al.*, 2022); The abundance of sodium- and chloride-related ions in the spectra indicates that these particles are from sea salt (Dell'Osso and Harrison, 2006; Passig *et al.*, 2022). In Table 1, the seven aerosol particle classes used in this study and their characteristic ion markers are summarized.

Popular methods to classify the measured aerosol particles according to their bipolar mass spectra are clustering algorithms, which calculate the geometric relationships between mass spectra, such as K-means using Euclidean Distance (Healy *et al.*, 2010; Arndt *et al.*, 2021) and ART-2a using Cosine Similarity (Song *et al.*, 1990; Dell'Osso and Harrison, 2012). Clustering algorithms are relatively easy to implement and require only a low number of parameters to be set. However, to obtain meaningful results, extensive manual post-processing of their results (selecting and merging of clusters) is needed. This manual post-processing may have its significance as it allows the researcher to discover new features of particle spectra, but it cannot be automatized. Moreover, the accuracy of the obtained classification results is based on clusters rather than individual particles, and some clusters may contain thousands of particles.

In contrast, supervised machine learning algorithms can accomplish automatic pattern recognition of different mass spectra with trained models, and their accuracy is based on individual particles. However, supervised algorithms require large amounts of labeled data for training, and the process of creating labels based on expert knowledge is usually expensive and time-consuming. A few studies to automatically classify SPMS data have been published (Christopoulos *et al.*, 2018), (Wang *et al.*, 2023a, 2023b). However, these studies were performed on a single dataset and did not consider the generalizability and reliability of the trained classification models when facing data from different sources. Different measurement campaigns will differ in the settings and locations of the measurement devices, and the environments, causing significant differences among the measured mass spectra even for the same particle class. Figure 1 shows in two columns exemplary normalized mass spectra from two measurements, assigned to three different particle classes. A comparison of the two columns reveals that the mass spectra assigned to the same class show different characteristics when coming from different measurements. These disparities cause questionable robustness of supervised learning models trained on data from one campaign and used to classify data from another campaign, as those models can produce dramatically different results when facing slight perturbations in the data. This seriously affects the potential of supervised algorithms for applications in environmental studies like aerosol particle classification.

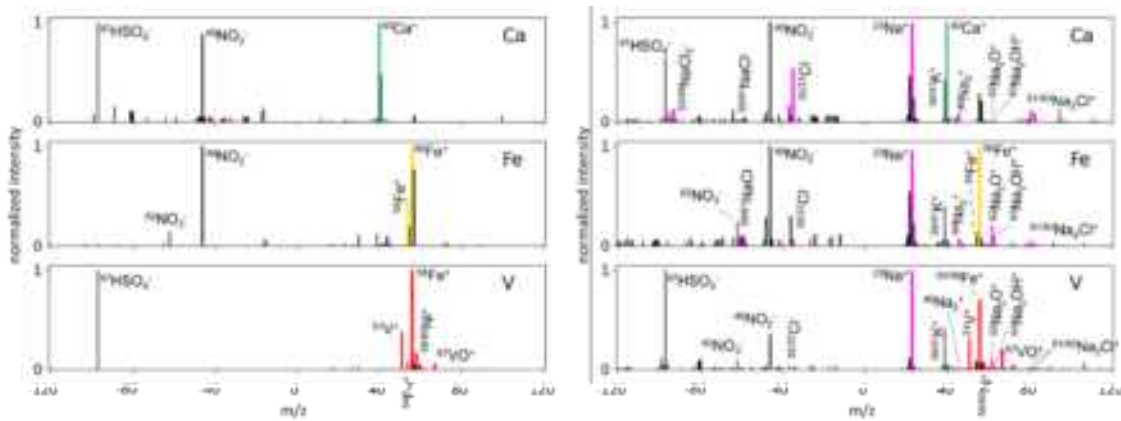


Figure 1: Examples for differences in mass spectra from two measurement campaigns, *Datasets A* (left column) and *B* (right column), assigned to the same particle class. As *Dataset B* was sampled near the coast, many particles are in mixed state with sea salt (pink signals).

In this study, to reliably classify SPMS data from different measurement campaigns, a highly adaptive Multilayer Perceptron (MLP) network architecture is proposed. Relevant strategies for the hyperparameter tuning are given and the robustness of the MLP network for the classification of seven particle classes on data from the two campaigns is compared. Finally, means to further enhance the robustness of the models are suggested.

2. Methodology

2.1 Sampling sites and equipment

To investigate the composition and possible sources of aerosol particles, two measurement campaigns were performed in the urban area of the coastal city of Rostock, Germany: Campaign 1, from which *Dataset A* was derived, was carried out from June 26 to July 2, 2018, in the southern part of the city ($54^{\circ}04'41.5''\text{N}$, $12^{\circ}06'30.6''\text{E}$, ~35 m above sea level, ~12 km south of the coast line) (Passig *et al.*, 2021); Campaign 2, from which *Dataset B* was obtained, took place from July 1 to August 3, 2022, close to the Baltic Sea ($54^{\circ}10'14.8''\text{N}$, $12^{\circ}06'24.7''\text{E}$, ~7 m above the sea level, ~1.5 km north of the port), see Figure 2. The measurement device to obtain the bipolar mass spectra from individual aerosol particles (size range approx. from 250 nm to 2.5 μm) was a Single-Particle Time-of-Flight (TOF) Mass Spectrometer with Z geometry, manufactured by Photonion, Inc., Germany. Particles are detected by a continuous wave laser and ionized with a 248 nm KrF excimer laser (laser desorption/ionization, LDI), see (Passig *et al.*, 2020, 2021) for more details.

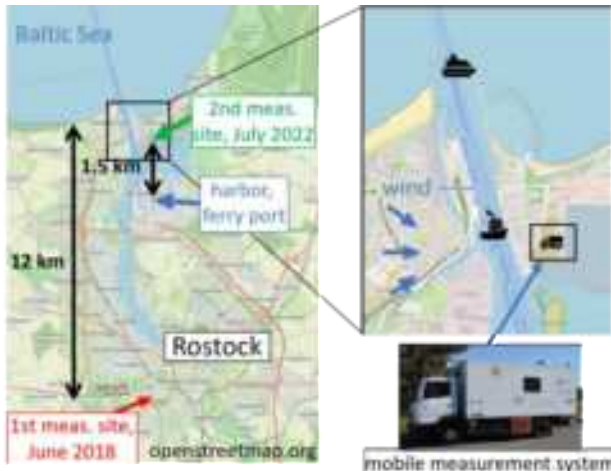


Figure 17: Maps of the locations of the two measurement campaigns (from June 2018 and July 2022) in the coastal city of Rostock, Germany, close to the Baltic Sea, where bipolar mass spectrometric data for ship emissions monitoring were measured and used for this study.

2.2 Dataset Description

Of all mass spectra measured during the two measurement campaigns mentioned above, we used selected parts to investigate the generalization capacity of several trained MLP models to reliably classify mass spectra measured during different campaigns. *Dataset A* contains approx. 24,000 mass spectra, assigned to eight different classes (Wang *et al.*, 2023a). *Dataset B* contains approx. 37,000 mass spectra classified into 13 different classes (Wang *et al.*, 2023b). Since in 2022 (*Dataset B*), the sampling site was closer to the coast than in 2018 (*Dataset A*), many more particles are in mixing state with sea salt and more particles from ship emissions were collected. In *Dataset B*, several subsets of iron-containing particles associated with ship emissions can be distinguished, based on different degrees of aging. Freshly emitted particles are in the Fe-EC class; moderately aged particles are in the Fe-Sulfate-Nitrate, Fe-EC-Nitrate and Fe-Nitrate classes and aged particles are in the Fe-dominate class.

For comparison of the applicability of a certain MLP model on two datasets, it is essential to keep the classes of both datasets identical. Therefore, we removed and merged several classes to obtain seven identical particle classes in both datasets. Table 1 details the list of the classes used in this study along with the most significant ion markers to recognize the mass spectra of the different classes and the number of samples in each class for both datasets. Although the chemical composition of the particles conforms to the rules in Table 1, the characteristic spectra of particles assigned to the same class might differ for different datasets, see Figure 1.

2.3 Training and Evaluation

Figure 3 illustrates the adaptive MLP network architecture for aerosol particle classification. To keep the data from *Datasets A* and *B* standardized, as learning features for training we used positive and negative LDI mass spectra ranging from m/z -120 to +120 and normalized according to their maximum intensity. These mass spectra are then mapped into 1×240 vectors and fed into three fully connected hidden layers (each layer consists of 512 neurons), using ReLU non-linear function for information transformation. Finally, SoftMax is used to predict the probability of classification. During training, we used cross-entropy as loss function to obtain the difference between the true and predicted labels, and Adam optimizer to minimize the loss so that the output of the model continuously approaches or reaches the optimal value. The learning rate was set to start at 0.001 and decrease by 10% every 100 epochs, for a total of 300 epochs to ensure the convergence of the network. Dropout was used to prevent overfitting during the training process.

Table 1: Overview of the particle classes used in the study with likely sources of emissions and characteristic ion markers and number of samples (#) in both datasets.

Class	Source	Ion makers	# in Dataset A	# in Dataset B
EC	traffic emissions	$EC ({}^{12n}C_n^{\pm})$: $^{12}C^{\pm}$, $^{24}C_2^{\pm}$, ..., $^{120}C_{10}^{\pm}$	4,671	816
EC-OC	biomass burning	OC : $^{27}[C_2H_3]^+$, $^{37}[C_3H]^+$, $^{39}[C_3H_3]^+$, $^{43}[C_4H_7]^+$, $^{51}[C_4H_3]^+$, $^{63}[C_5H_3]^+$, etc; EC	4,000	3,383
K-rich	biomass burning	$^{39/41}K^+$; EC ; OC ; $Sulfate$: $^{97}[HSO_4]^-$; $Nitrate$: $^{46}[NO_2]^-$, $^{62}[NO_3]^-$	3,998	3,300
Ca-rich	lubricating oil of ship engines	$^{40}Ca^+$, $^{56}[CaO]^+$; EC ; $Sulfate$; $Nitrate$	1,365	3,238
Fe-rich	ship fuel emissions	$^{54/56}Fe^+$, $^{73}[FeOH]^+$; EC ; $Sulfate$; $Nitrate$	1,729	16,222
V-rich	ship fuel emissions	$^{51}V^+$, $^{67}[VO]^+$; $^{54/56}Fe^+$, $^{60}Ni^+$; EC ; $Sulfate$; $Nitrate$	3,879	943
Na-rich	sea salt	$^{23}Na^{\pm}$, $^{39}[NaO]^\pm$, $^{46}[Na_2]^\pm$, $^{62}[Na_2O]^\pm$, $^{63}[Na_2OH]^\pm$, $^{81/83}[Na_2Cl]^\pm$, $^{35/37}Cl^-$, $^{59/61}[NaCl]^-$, $^{93/95}[NaCl_2]^-$; $Sulfate$; $Nitrate$	3,848	6,600
sum			23,490	37,406

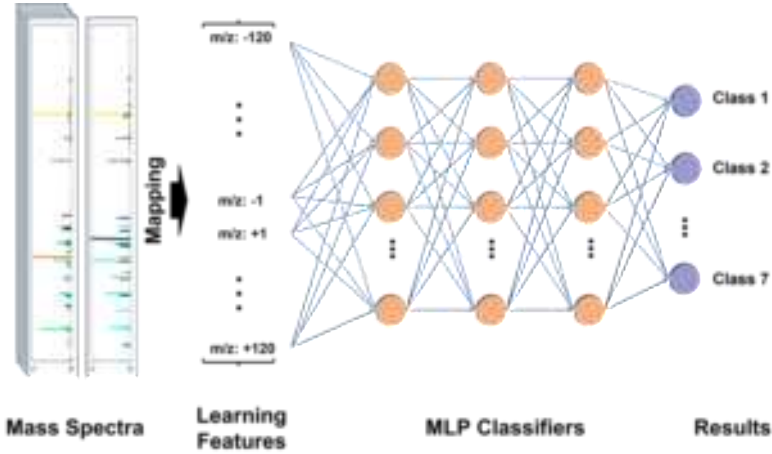


Figure 3: Schematic diagram of the used MLP architecture. The input spectra are mapped as 1×240 vectors and fed into an MLP with three hidden layers, each with 512 neurons.

3. Results and Discussion

We applied a grid search strategy to determine the hyperparameters of the MLP models and a stratified 5-fold cross-validation to evaluate the performance of the network since the number of samples in different classes in both datasets are imbalanced. Table 2 presents the experiments and their results. In all experiments, the architecture shown in Figure 3 was used. Experiments 1 and 3 give the performance of the models M_A and M_B trained separately on each single dataset, both with an accuracy of around 95 %. If the model M_A or M_B was used to predict the spectra from the other dataset (Experiments 2 and 4), the accuracy dropped significantly. Finally, in Experiment 5 model M_c was trained with the combined *Dataset A&B*, indicating the best performance. In Figure 4, the normalized confusion matrices for Experiments 2, 4, and 5 are presented.

Some observations: EC particles are often mixed with OC signals, and when the OC signals are weak, we labeled them as EC. However, the thresholds for determining the OC signal strength were more relaxed in *Dataset B* than in *Dataset A*. For example, the model M_B trained with *Dataset B* incorrectly predicts 40.7% of the EC-OC

particles from *Dataset A* as EC particles, see element (2,1) of the confusion matrix in Figure 4 (b). This is because according to the determination criteria used to create *Dataset B*, these misidentified EC-OC particles in *Dataset A* fit the criteria of EC particles in *Dataset B*.

Table 2: Classification results of five experiments. In Experiment 1, 3 and 5, 80% of the data were used for train and 20% for test. In Experiment 2 and 4, all data from the other dataset was used for test.

Experiment	Train dataset	Model	Test dataset	Accuracy in %	Recall in %	Precision in %
1	<i>A</i> (80%)	M_A	<i>A</i> (20%)	96.1 ± 3.2	96.1 ± 3.3	96.2 ± 2.0
2	<i>A</i> (80%)	M_A	<i>B</i> (100%)	80.3	76.6	78.8
3	<i>B</i> (80%)	M_B	<i>B</i> (20%)	94.0 ± 1.2	92.3 ± 2.2	90.6 ± 3.4
4	<i>B</i> (80%)	M_B	<i>A</i> (100%)	84.6	86.2	84.8
5	<i>A&B</i> (80%)	M_C	<i>A&B</i> (20%)	96.7 ± 1.5	96.5 ± 2.1	96.6 ± 2.5

In Experiment 2, a significant number of particles from *Dataset B* is incorrectly identified as sea salt (class Na-rich), see the last column of Figure 4 (a). Most of these particles are in a mixed state with sea salt (similar to the spectra in the right column of Figure 1) and exhibit strong sea salt characteristics in addition to their own signature chemical composition. This result proves that the model cannot adapt to such data discrepancies.

Experiment 5 shows that when using the merged *Dataset A&B*, the robustness can be significantly improved. The model M_C overcomes the problems encountered by the first two models and predicts very good results for all classes, see Figure 4 (c). This indicates that model M_C learned not only the internal differences of spectra from different sources but also the different criteria introduced during human annotation.

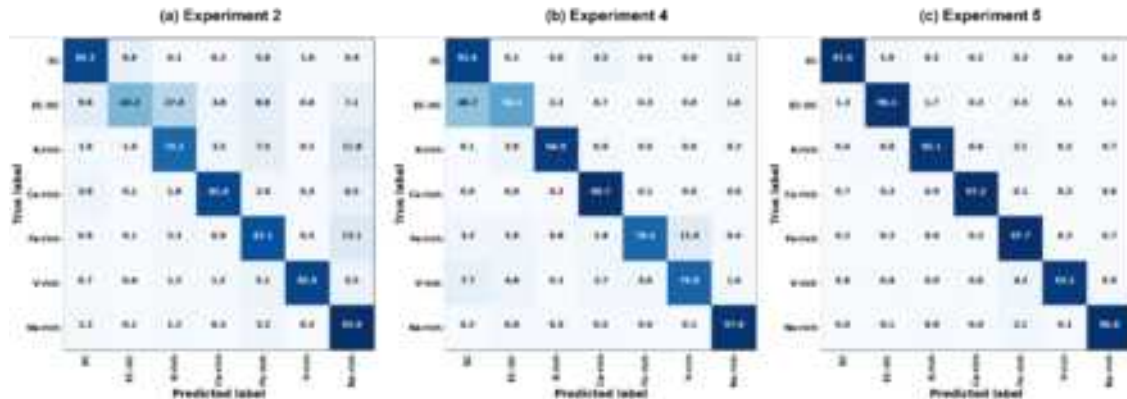


Figure 4: Normalized confusion matrix displaying the accuracy rates in % of (a) Experiment 2 (train on *Dataset A*, test on *Dataset B*), (b) Experiment 4 (train on *Dataset B*, test on *Dataset A*) and (c) Experiment 5 (train and test on the combined *Dataset A&B*). The diagonal in the matrix is the rate of correct predictions for each class; all other entries are incorrect predictions of class assignments.

4. Conclusion

For the effective detection of environmental events, e.g. for compliance monitoring of ship plumes, fast automated on-line analyzes are required. We proposed a neural-network based Multilayer Perceptron (MLP) network for the automatic classification of aerosol particles measured by Single-Particle Mass Spectrometry (SPMS). Differences in measurement campaigns (SPMS instruments, sampling locations, weather conditions, etc.) lead to differences in mass spectra from one measurement to another, even for particles of the same class. This work showed that models trained with data from a single measurement do not generalize well and are more sensitive to differences in the characteristics of data from different sources. The robustness of the model trained with merged data was substantially improved, indicating that the model exhibits high adaptability

and reliability under the condition of sufficient training data, even if there are internal differences or bias in the data.

The model learned the internal variation of data from different sources and overcame the different criteria introduced by the annotation process. However, the creation of a benchmark dataset of labeled data is expensive and time-consuming. To save time on labeling and ultimately to enhance the robustness of the model, so-called transfer learning can be used to fine-tune a pre-trained model with a small dataset. Furthermore, with data augmentation techniques more artificial SPMS data can be generated from a limited amount of measured data. This, however, is to be investigated carefully, since the discrepancy between the generated and the real data inevitably introduces noise.

Acknowledgements

This research is funded by dtec.bw – Digitalization and Technology Research Center of the Bundeswehr (project **“LERNAT”**, ~~dtec.bw is funded by the European Union~~ – NextGenerationEU).

References

- Arndt, J. *et al.* (2021). Characterization and source apportionment of single particles from metalworking activities, *Environmental Pollution*, 270, p. 116078. <https://doi.org/10.1016/j.envpol.2020.116078>.
- Ault, A.P. *et al.* (2009). Impact of Emissions from the Los Angeles Port Region on San Diego Air Quality during Regional Transport Events, *Environmental Science & Technology*, 43(10), pp. 3500–3506. <https://doi.org/10.1021/es8018918>.
- Christopoulos, C.D. *et al.* (2018). A machine learning approach to aerosol classification for single-particle mass spectrometry, *Atmospheric Measurement Techniques*, 11(10), pp. 5687–5699. <https://doi.org/10.5194/amt-11-5687-2018>.
- Ostro, M. and Harrison, R. (2006). Chemical characterisation of single airborne particles in Athens (Greece) by ATOFMS, *Atmospheric Environment*, 40(39), pp. 7614–7631. <https://doi.org/10.1016/j.atmosenv.2006.06.053>.
- ~~Harrison R M and Ostro M 2006~~ Urban organic aerosols measured by single particle mass spectrometry in the megacity of London, *Atmospheric Chemistry and Physics*, 12(9), pp. 4127–4142. <https://doi.org/10.5194/acp-12-4127-2012>.
- Healy, R.M. *et al.* (2010). Source apportionment of PM2.5 in Cork Harbour, Ireland using a combination of single particle mass spectrometry and quantitative semi-continuous measurements, *Atmospheric Chemistry and Physics*, 10(19), pp. 9593–9613. <https://doi.org/10.5194/acp-10-9593-2010>.
- Li, L. *et al.* (2014). Ambient particle characterization by single particle aerosol mass spectrometry in an urban area of Beijing, *Atmospheric Environment*, 94, pp. 323–331. <https://doi.org/10.1016/j.atmosenv.2014.03.048>.
- Passig, J. *et al.* (2020). Resonance-enhanced detection of metals in aerosols using single-particle mass spectrometry, *Atmospheric Chemistry and Physics*, 20(12), pp. 7139–7152. <https://doi.org/10.5194/acp-20-7139-2020>.
- Passig, J. *et al.* (2021). Detection of ship plumes from residual fuel operation in emission control areas using single-particle mass spectrometry, *Atmospheric Measurement Techniques*, 14(6), pp. 4171–4185. <https://doi.org/10.5194/amt-14-4171-2021>.
- Passig, J. *et al.* (2022). Single-particle characterization of polycyclic aromatic hydrocarbons in background air in northern Europe, *Atmospheric Chemistry and Physics*, 22(2), pp. 1495–1514. <https://doi.org/10.5194/acp-22-1495-2022>.
- Shen, X. *et al.* (2019). Understanding atmospheric aerosol particles with improved particle identification and quantification by single-particle mass spectrometry, *Atmospheric measurement techniques*, 12(4), pp. 2219–2240. <https://doi.org/10.5194/amt-12-2219-2019>.
- Shields, L.G., Suess, D.T. and Prather, K.A. (2007). Determination of single particle mass spectral signatures from heavy-duty diesel vehicle emissions for PM2.5 source apportionment, *Atmospheric Environment*, 41(18), pp. 3841–3852. <https://doi.org/10.1016/j.atmosenv.2007.01.025>.
- Song, X.-H. *et al.* (1999). Classification of Single Particles Analyzed by ATOFMS Using an Artificial Neural Network, ART-2A, *Analytical Chemistry*, 71(4), pp. 860–865. <https://doi.org/10.1021/ac9809682>.
- Toner, S.M., Sodeman, D.A. and Prather, K.A. (2006). Single Particle Characterization of Ultrafine and Accumulation Mode Particles from Heavy Duty Diesel Vehicles Using Aerosol Time-of-Flight Mass Spectrometry, *Environmental Science & Technology*, 40(12), pp. 3912–3921. <https://doi.org/10.1021/es051455x>.
- Wang, G. *et al.* (2023a). Machine learning approaches for automatic classification of single-particle mass spectrometry data, *EGUsphere* [preprint]. <https://doi.org/10.5194/egusphere-2023-784>.
- G. Wang et al. (2023b). 1D-CNN network based real-time aerosol particle classification with single-particle mass spectrometry, *IEEE Sensors Letters*, vol. 7, no. 10, <http://doi: 10.1109/lens.2023.3315554>.

The Association between Vessel Departures and Air Pollution at Helsinki Port Terminals 2016-2021

M. Heikkilä^{1*}

¹ Department of Atmospheric Composition, Finnish Meteorological Institute, Erik Palménin aukio 1, 00560 Helsinki, Finland, mikko.heikkila@fmi.fi

Introduction

Combustion-based ship air emissions can be divided into two categories based on their effect: (1) greenhouse gas emissions (GHG), which contribute to global warming, and (2) air pollutant emissions which contribute to air quality. The importance and urgency to decrease greenhouse gas emissions are well known, and despite committing to the Paris climate agreement, international shipping GHG emissions are found to be increasing (Faber et al., 2020). Air pollution is a major global concern to human health. Among other pollutants, there is strong evidence of the public health effects of particulate matter (PM), ozone (O_3), nitrogen dioxide (NO_2), sulphur dioxide (SO_2) and carbon monoxide (CO) (World Health Organization, 2021). The recent scientific literature shows the detrimental effect of even lower concentrations of particles than what was previously understood, and that the burden of disease caused by air pollution is somewhat equal to smoking and an unhealthy diet (World Health Organization, 2021). Both long- and short-term exposure to air pollutants have been shown to increase mortality and morbidity. A recent systematic review and meta-analysis concluded the combined risk ratio for long term exposure to $PM_{2.5}$ and natural-cause mortality to be 1.08 (95% confidence interval 1.05-1.09) per 10 g/m³ (Chen & Hoek, 2020). Another systematic review and meta-analysis found positive associations between all-cause mortality and increased 1 h maximum exposure to PM_{10} , $PM_{2.5}$, and O_3 . The same correlation was found with increased 24 h exposure to NO_2 (Orellano et al., 2020).

A recent cohort study conducted in Finland revealed that even short-term exposure to air pollutants a week before scheduled delivery raises the risk of preterm birth by 67% (95% confidence interval 14-146%) for $PM_{2.5}$ and 65% (95% confidence interval 14-137%) for NO_2 (Siddika et al., 2020). The new evidence led the World Health Organization (WHO) to update their Air Quality Guidelines (AQG) in 2021. All other revisions were made stricter except for SO_2 , which was revised upwards. The European Commission submitted a proposal for a new Air Quality Directive in October 2022 (European Commission, 2022).

Maritime transport is one the major air polluters in the world. It is estimated that shipping's share of global anthropogenic greenhouse gas emissions in 2018 was 5% and 15% of the world's air pollutants in 2018 (Englert & Losos, 2021). Multiple studies show a positive correlation between increased concentrations of pollutants and vessel traffic (Tosciano & Murena, 2019). The unequal share between GHG emissions and air pollution is because the requirements for fuel quality in shipping have not been as strict as for land-based energy production or transport. A health impact assessment made in eight Mediterranean coastal cities found that shipping contributed to 430 (95% confidence interval 220-650) annual premature deaths due to an increased exposure to $PM_{2.5}$ (Viana et al., 2020). A recent modelling study concluded that the NO_2 and $PM_{2.5}$ emissions from inland ships sailing up and down the Yangtze River should be focussed on as they carry a burden on residential areas (Huang et al., 2022).

The global sulphur cap in marine fuel was lowered from 3.5% to 0.5% only 1 January 2020. The sulphur cap in marine fuel is restricted even more to 0.1% in Sulphur Emission Control Areas (SECA), and the whole Baltic Sea has been a SECA since May 2006. A gradual reduction of the fuel sulphur content in the Baltic Sea area towards 0.1% was made over a decade. The motivation for this restriction was to reduce the impact of ship air emissions to public health, but it came with a cost as the global cooling effect of sulphur aerosol formation was also reduced (Sofiev et al., 2018), (Balkanski et al., 2010), (Tronstad Lund et al., 2012), (Fuglestvedt et al., 2009), (Capaldo et al., 1999). It is also debatable if the cost-benefit of a SECA area is positive or negative and if the focus should be on the long or the short-term impacts (Antturi et al., 2016).

Nitrogen oxide (NO_x) emissions have been restricted in specified Nitrogen Emission Control Areas (NECA) and the Baltic Sea has been included in the strictest Tier III restrictions since 1 January 2021, but the regulation

concerns only new ships. Like SO₂ restrictions, NO_x emission restrictions are driven by their impact on public health, but also to eutrophication (Gren et al., 2021). Many studies have been published that report the impact of ship emissions to the air quality around port areas (Gobbi et al., 2020), (Anastasopoulos et al., 2021), (Mousavi et al., 2018), and analyses have been run to assess the cost-benefit of connecting ships to shore power while alongside (Daniel et al., 2022), (Spengler & Tovar, 2021). Nevertheless, the European Commission has submitted a proposal, which will insist ports to have container vessels and passenger ships connected to an onshore power supply or similar system by 1 January 2030.

As with other measures to mitigate the impact from maritime air emissions, connecting ships to shore power might not work as planned. Shore power reduces only emissions caused by the auxiliary engines while alongside, but what about emissions that are caused by the main engines, when manoeuvring the ship in and out of the port? This study aims to fill that knowledge gap by first assessing what is the share of fuel combusted by passenger and container vessels that remain alongside for 2 h or more in the port of Helsinki and then analysing the effect of vessel arrivals, departures, and time at berth on port area air quality. Analyses were focused on two combustion-based engine pollutants: particulate matter (PM_{2.5}) and nitrogen dioxide (NO₂) as their recommended exposure limits were decreased most in the latest WHO update and due to their contribution to detrimental health effects and chemical smog.

Materials and methods

Ship arrival and departure data were obtained from the Finnish Transport and Communication Agency Traficom. The dataset contains information from the Porttraffic system (www.porttraffic.fi) which is publicly available. Duplicate records and errors in dates and times were corrected manually when identified. Arrivals, departures, vessel movement (arrival and departure) and vessels at berth were allocated to the hour of local time. In some of the port terminals, specific vessel movements could also be allocated to a specific berth at the terminal. In such cases, these were analysed separately. Ships were classified by type to calculate the cumulative berth times and to find out the effect of the shore power regulation.

Ship fuel consumption data were downloaded from the European Union (EU) Monitoring, Reporting and Verifying (MRV) Thetis database (mrv.emsa.europa.eu). At the time of the study, data from the years 2018–2021 were available, and the versions used were 267 for 2018, 208 for 2019, 166 for 2020 and 90 for 2021. The consumption in port was calculated based on the reported values for total annual fuel consumption, total annual CO₂ emitted, total annual CO₂ emitted while in port and time at sea.

The hourly mean concentrations data of NO₂ and PM_{2.5} were obtained from the Helsinki Region Environmental Services (HSY). Measuring was performed with the HSY mobile unit in different port areas in Helsinki. The location of the mobile unit changes once a year. The NO_x measurements were made with a Horiba AP-370 air pollution monitor and the PM measurements with a Fidas 200 instrument (Helsinki Region Environmental Services Authority, 2022). The sampling height with the mobile unit is 4 metres above ground and 6–7 metres above sea level. In 2016, the mobile unit was stationed in the Vuosaari port terminal, in 2018 the unit was at South Harbour Makasiiniterminaali, in 2019 and 2020 the unit was at West Harbour and in 2021 the unit was again at South Harbour but at the Katajanokka terminal. There are no data from 2017 as the unit was based at the airport of Helsinki. Negative values in the data were not removed based on discussions with the data provider as they compensate for measuring inaccuracies as the instruments are calibrated on 24 h mean values.

Weather data: wind direction, wind speed, air temperature, relative humidity and atmospheric pressure were downloaded from the Finnish Meteorological Institute (FMI) open data (en.ilmatieteenlaitos.fi/download-observations). The meteorological variables used were taken from the Helsinki Harmaja lighthouse observation station to minimise the effect of local pollution sources.

A multivariable linear regression was used to model the effect of vessel air emissions to the air quality data while adjusting for confounders such as meteorological factors and local time, which are associated with variation of road traffic. As the distributions of the dependent variables (measured hourly mean NO₂ and PM_{2.5}) were skewed, a natural logarithm of the values was used for the regression analysis (Formula 1).

$$\ln(Y) = b_0 + b_1x_1 + b_2x_2 + \dots + b_nx_n \quad (1)$$

where $\ln(Y)$ is the natural logarithm of the dependent variable (hourly mean NO_2 or $\text{PM}_{2.5}$), b_0 is the intercept, b_1-b_n are the regression coefficients for the chosen variables and X_1-X_n are the chosen variables.

The variables were chosen with the backward elimination method based on the statistical significance and optimum goodness of fit of the regression model (Broadhurst et al., 1997), (Suarez et al., 2017). Variables included wind direction in degrees, wind velocity in metres per second, relative humidity in percent, air temperature in degrees centigrade and time of day in hours, which was used as a proxy for road traffic.

For the sensitivity analysis, a subset of the data was used to include only weekends (Saturday and Sunday) to minimize the effect of road traffic. Additionally, when available, the effects of different vessel types were examined in detail. The statistical analyses were completed with R using the Dplyr and Openair packages (Carslaw & Ropkins, 2012). As the dependent variable was normalized by taking the natural logarithm of the measured pollutant value, the effect of the vessel movement to the hourly mean concentration in percent was calculated using Formula 2:

$$\text{Effect}(\%) = (e^{\text{Coefficient}} - 1) * 100 \quad (2)$$

Results

The vessel traffic in the port of Helsinki is dominated by passenger vessels and roll-on roll-off (ro-ro) cargo transport (Table 1). The COVID-19 pandemic resulted in a significant reduction in 2020 to ship visits (-17.4% to the mean 2018-2019) notably with passenger-carrying vessels such as the passenger ferry (Pax ferry) and the cruise ships. Ropax vessel visits however did not decrease during the pandemic.

Table 1: Ship visits to the port of Helsinki 2018-2020 by vessel type. Pax ferry: vessel that carries both roll-on roll-off cargo and passengers with the largest parts of the ship dedicated for passengers, ropax: vessel that carries both roll-on roll-off cargo with the largest parts of the ship dedicated for cargo, container: container vessel, ro-ro: cargo vessel carrying roll-on roll-off cargo, cruise: cruise ship, other: all other vessel types.

	2018		2019		2020		2021	
Type	Visits	%	Visits	%	Visits	%	Visits	%
Pax ferry	5181	64.0	5141	62.1	4259	61.1	4709	64.8
Ropax	892	11.0	1181	14.3	1340	19.2	1460	14.7
Container	766	9.5	708	8.6	660	9.5	611	8.7
Bulk	367	4.5	292	3.5	266	3.8	272	3.9
Roro	357	4.4	330	4.0	297	4.3	359	4.4
Cruise	283	3.5	300	3.6	0	0.0	15	2.5
Other	251	3.1	320	3.9	146	2.1	200	3.2
All	8097	100.0	8272	100.0	6968	100.0	7271	100.0

Passenger ferry vessels spend less time in port than cargo ships which take time discharging and loading. On the other hand, passenger vessels consume more fuel while alongside due to their larger power consumption which is required for ship hotel operations such as air conditioning, provision cooling and restaurants. The COVID-19 pandemic effect can be observed clearly in the mean time spent alongside by the passenger ferry vessels as many of them were laid up during 2020 and by the fact that there were no cruise ship calls in Helsinki in 2020 (Table 2).

Table 2: Mean time in port in hours (T_p), mean fuel consumption in port in metric tons per hour (F_p) by vessel type at port of Helsinki 2018-2020. Time in port by vessel type was calculated from the port arrival and departure data and fuel consumption in port from the MRV data.

Vessel type	2018		2019		2020	
	T_p	F_p	T_p	F_p	T_p	F_p
Pax ferry	2.48	0.43	2.46	0.35	6.39	0.23
Ropax	4.94	0.19	4.72	0.23	3.98	0.18
Container	16.87	0.26	18.65	0.12	19.67	0.12
Bulk	49.00	0.03	51.08	0.04	104.58	0.03
Roro	18.55	0.16	17.58	0.17	21.39	0.17
Cruise	8.38	0.47	8.51	0.36	0.0	0.0
All	16.1	0.34	20.5	0.28	20.1	0.20

According to the MRV data, passenger carrying vessels (pax ferry, ropax and cruise) consume around 67% (64.6-71.6) of the total fuel combusted by vessels while in port in Helsinki. The second largest consumers are container vessels: 19% (15.8-24.2). These vessel types are also mandated to be connected to shore power or a similar system while alongside by 2030 for port calls more than 2 h in EU ports as per the EU Green Deal initiative. This would lead to a 78% (74.9-80.1) reduction in fuel combusted and CO₂ emitted by ships while at berth in Helsinki.

Most of the port terminals examined in this study are situated in the urban populated area (South Harbour and West Harbour) whereas the Vuosaari terminal is at the outskirts of the city limits around 15 kilometres from the centre. The vessel traffic to Vuosaari consists mainly of cargo ships apart from ropax vessels which carry a limited number of passengers mainly to Travemünde in Germany and Muuga in Estonia. The port terminals at the city centre however are mainly operated by passenger ferry vessels with regular traffic to Mariehamn, St Petersburg, Stockholm and Tallinn and the seasonal cruise ships. Separate measuring studies have been completed in the same areas: both prior to the SECA (Pirjola et al., 2014) and after coming into force (Walden et al., 2021). Using HSY continuous measurement data, a long-term association can be established better than with short-term measuring campaigns.

Prevailing winds are from the south-west with a mean velocity of 6.75 metres per second (5.87-7.62). It is likely that the winds blow most of the air pollutants away from the port towards the urban areas.

The annual mean concentrations of NO₂ and PM_{2.5} were below the national limits (10 µg/m³ for NO₂ and 25 µg/m³ for PM_{2.5}) but above the 2021 WHO guidance limits (10 µg/m³ for NO₂ and 5 µg/m³ for PM_{2.5}) except for PM_{2.5} in 2020. Based on the annual means, port workers, ship crews, passengers and urban area populations exposed to the port emissions are affected by NO₂ and PM_{2.5} concentrations that exceed the WHO recommendations (Figure 1).

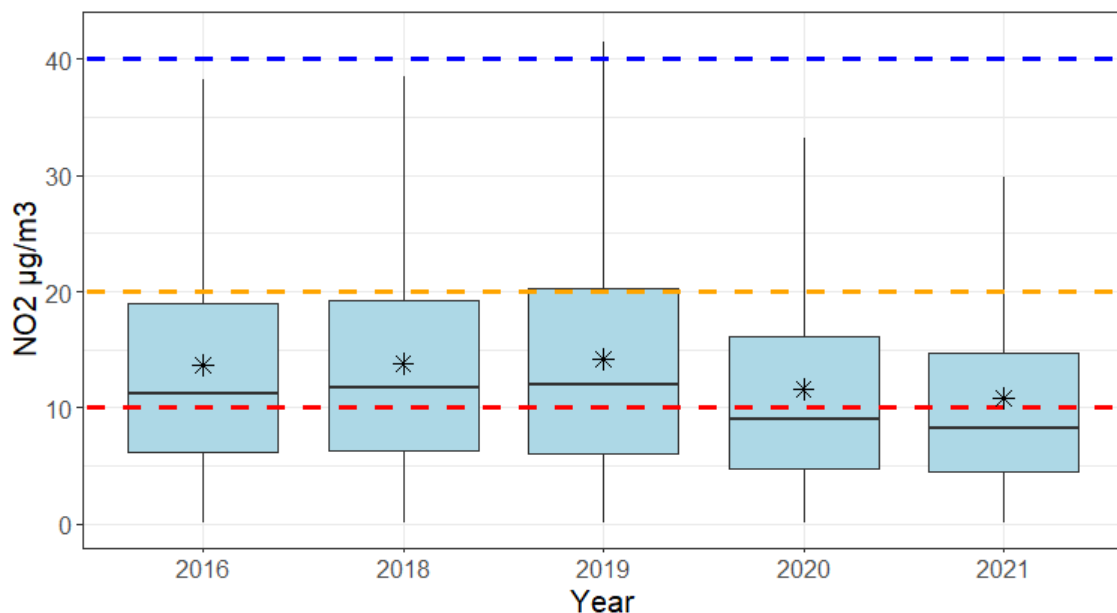


Figure 1: Boxplot of the measured annual median (black line), interquartile ranges and mean (stars) concentration of NO₂ 2016, 2018-2021 at various port terminals of Helsinki. The blue dashed line is the Finnish/EU limit of 40 µg/m³, which was in force during the studied years. The red dashed line is the WHO 2021 recommended limit of 10 µg/m³ and the orange line the EU proposal of 20 µg/m³.

Consistent results using a multivariable linear regression analysis from four different port terminals and five different years indicate that vessel departures significantly increase the hourly mean NO₂ concentrations, and the effect of arrivals is less significant or does not exist (Figure 2). The mean effect to the hourly mean NO₂ concentrations of departures for all vessels was 47.0% (95% confidence interval 41.6-53.3%) for the whole year and 38.2% (95% confidence interval 28.9-48.1%) for the weekends. These results do not directly identify if the source of the NO₂ were the ships themselves or the cargo loaded on them, but the variability between arrivals and departures suggest that emissions caused by the departures are higher than for the arrivals. A plausible explanation is the visually identifiable emission plume caused by starting the vessel's main engines prior to the departure. In general, departures consume more energy than arrivals, when vessel inertia can be utilised. Nitrogen oxide emissions have been shown to increase by 150% during the cold start of a marine engine (Chu Van et al., 2019).

The results from South Harbour in 2018, West Harbour in 2019 and South Harbour in 2021 show that the different types of ships docking at different parts of the harbour basin have a different effect size to the hourly mean NO₂ concentrations. There are multiple possible explanations for this. It seems that the closest vessel to the sampling point causes the largest effect, but the results from West Harbour in 2019 for the whole year also indicate that vessels further away but with larger engines (cruise ships compared to passenger ferry vessels) might affect the NO₂ concentrations more. In addition, combustion-based nitrogen oxide emissions are not all nitrogen dioxide, but also nitrogen monoxide, of which some will transform into NO₂. Therefore, it is likely that a close sampling point does not identify all NO₂ caused by the source. The vessel departure effect is detectable also on the hourly mean PM_{2.5} concentrations but the overall effect is much smaller indicating that sources other than port activity might be more influential.

Connecting container and passenger vessels to shore power, as required by future EU regulation, would reduce most of the emissions that all the vessels that visit Helsinki produce with the auxiliary engines while alongside. As shown in this study, this might not have a significant effect on NO₂ or PM_{2.5} concentrations as the main engines seem to have a larger effect. Hybrid electric powered ships that could manoeuvre out of the port without starting their combustion engines would probably be a better option to reduce air pollution in urban areas.

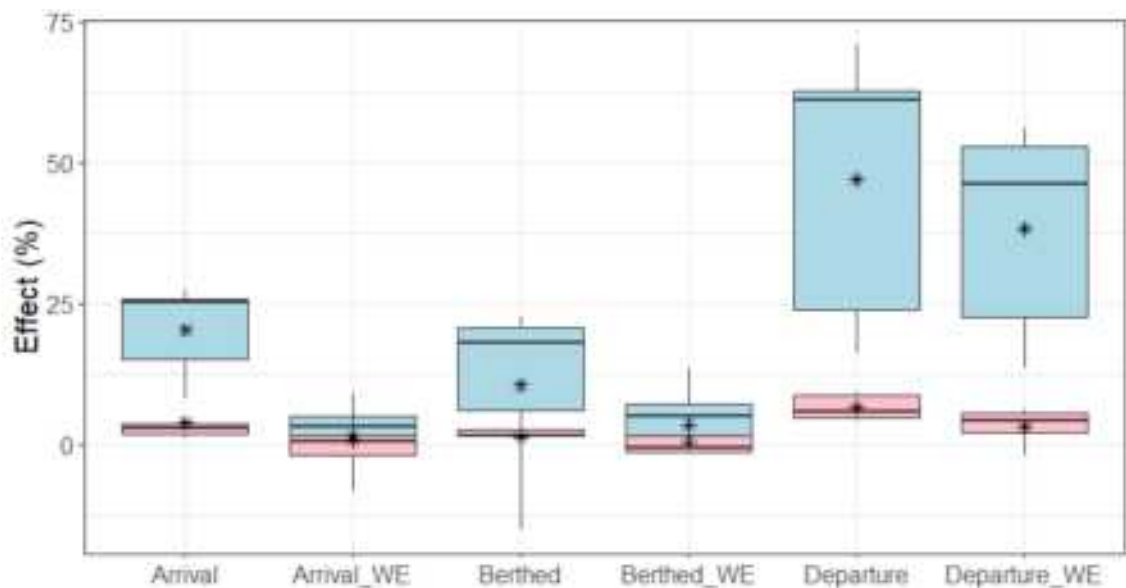


Figure 2: Boxplot of vessel movement effect in % on the hourly mean concentration of NO₂ (blue) and PM_{2.5} (pink) using the whole year data and weekends only (_WE). Boxplot showing median effect as black line with interquartile ranges and mean with star (*).

Discussion

This study aimed to calculate the effect of connecting container and passenger vessels to shore power while alongside in port for >2 h at the port of Helsinki as required by the upcoming EU regulation. The effect, 75–80%, is surprisingly large when considering that most of the ship visits are shorter than 2 h. Shore power, or cold ironing as it is often called, is a large modification to existing infrastructure of both the ports and visiting vessels with specific challenges related to retrofitting old vessels (Khersonsky et al., 2007), (Zis, 2019). To overcome this task in the most efficient way, the feasibility of both the shore power connection and energy storage on board should be considered carefully.

While at the port of Helsinki, the vessel exhaust pollutants-based air emissions are caused purely by the auxiliary engines, and during the arrivals and departures they are caused by the combination of both the main engines and the auxiliaries. On the other hand, during the port stay, additional air emissions are caused by the loading and discharging activities especially in Helsinki having a large share of roll-on/roll-off type of cargo. Based on the results, this study identified that departures seem to have the largest effect on the measured concentrations of air pollutants. The multivariable linear regression analysis shows that starting the cold main engines has a significant short-term effect on NO₂ concentration, but not on PM_{2.5}. This will probably not change by connecting the vessels to shore power, but an energy storage on board would, assuming that it has enough capacity to allow the vessel to manoeuvre besides providing the power that the auxiliary engines would for the time in port. The benefit of a hybrid system to mitigate the air pollution from ships is not limited to fuel oil powered ships, as LNG-powered vessels have been found to emit larger amounts of carbon monoxide and formaldehyde (Peng et al., 2020). An energy storage unit on board does not mean that shore power becomes obsolete, as it can be used to charge the storage unit while the ship is alongside (Kalikatzarakis et al., 2018).

The limitation of the findings is that the linear regression models could only explain 20–30% of the NO₂ variation. This can be caused by multiple factors: first, as the measuring unit was placed close to the emission source, some of the NO_x emitted by the vessel could be in the form of nitrogen monoxide (NO) and therefore not detected in the NO₂ measurement units. Second, as the ship exhaust plume and plume buoyancy may move the plume much higher than the measuring point, most of the impact may not be visible in these measurements. To have a better understanding of this, the location of the measurement site should be considered carefully if ship plumes were to be studied specifically. Third, some sources of emissions or confounding factors were possibly not identified, and the hour of day was used as a proxy to model the effect of road traffic and other urban emission sources. This is not surprising as the sampling locations were in an area that is subjected to

multiple emission sources such as powerplants using coal, natural gas and fuel oil. Lastly, hourly mean values were chosen to be used in the analyses, knowing that stronger associations and effects would have probably been observed with a shorter time resolution and including both NO and NO₂ concentrations. The scope of the study was to find whether vessel movement causes significant increases in the measured air pollution values that are subject to regulation, specifically to NO₂ and PM_{2.5} as their recommended limit values were recently lowered by the WHO.

Acknowledgements

This research was produced as part of the European Union project EMEGTE – Evaluation, control and mitigation of the environmental impacts of shipping emissions. The EMEGTE project has received funding from the European Union's Horizon 2020 – Research and Innovation Framework Programme action under grant agreement No 874990.

The author would like to thank Anu Kousa from the Helsinki Region Environmental Services and Antti Arkima from the Finnish Transport and Communications Agency for compiling the data used in this research.

References

- Anastasopoulos, A. T., Sofowote, U. M., Hopke, P. K., Rouleau, M., Shin, T., Dheri, A., Peng, H., Kulka, R., Gibson, M. D., Farah, P. M., & Sundar, N. (2021). Air quality in Canadian port cities after regulation of low-sulphur marine fuel in the North American Emissions Control Area. *Science of The Total Environment*, 791, 147949. <https://doi.org/10.1016/J.SCITOTENV.2021.147949>
- Antturi, J., Hänninen, O., Jalkanen, J. P., Johansson, L., Prank, M., Sofiev, M., & Ollikainen, M. (2016). Costs and benefits of low-sulphur fuel standard for Baltic Sea shipping. *Journal of Environmental Management*, 184, 431–440. <https://doi.org/10.1016/J.JENVMAN.2016.09.064>
- Balkanski, Y., Myhre, G., Gauss, M., Rädel, G., Highwood, E. J., & Shine, K. P. (2010). Direct radiative effect of aerosols emitted by transport: from road, shipping and aviation. *Atmospheric Chemistry and Physics*, 10(10), 4477–4489. <https://doi.org/10.5194/acp-10-4477-2010>
- Broadhurst, D., Goodacre, R., Jones, A., Rowland, J. J., & Kell, D. B. (1997). Genetic algorithms as a method for variable selection in multiple linear regression and partial least squares regression, with applications to pyrolysis mass spectrometry. *Analytica Chimica Acta*, 348(1–3), 71–86. [https://doi.org/10.1016/S0003-2670\(97\)00065-2](https://doi.org/10.1016/S0003-2670(97)00065-2)
- Capaldo, K., Corbett, J. J., Kasibhatla, P., Fischbeck, P., & Pandis, S. N. (1999). Effects of ship emissions on sulphur cycling and radiative climate forcing over the ocean. *Nature*, 400(6746), 743–746. <https://doi.org/10.1038/23438>
- Carslaw, D. C., & Ropkins, K. (2012). openair — An R package for air quality data analysis. *Environmental Modelling & Software*, 27–28, 52–61. <https://doi.org/10.1016/j.envsoft.2011.09.008>
- Chen, J., & Hoek, G. (2020). Long-term exposure to PM and all-cause and cause-specific mortality: A systematic review and meta-analysis. *Environment International*, 143, 105974. <https://doi.org/10.1016/J.ENVINT.2020.105974>
- Chu Van, T., Zare, A., Jafari, M., Bodisco, T. A., Surawski, N., Verma, P., Suara, K., Ristovski, Z., Rainey, T., Stevanovic, S., & Brown, R. J. (2019). Effect of cold start on engine performance and emissions from diesel engines using IMO-Compliant distillate fuels. *Environmental Pollution*, 255, 113260. <https://doi.org/10.1016/j.envpol.2019.113260>
- Daniel, H., Trovão, J. P. F., & Williams, D. (2022). Shore power as a first step toward shipping decarbonization and related policy impact on a dry bulk cargo carrier. *ETransportation*, 11, 100150. <https://doi.org/10.1016/J.ETRAN.2021.100150>
- Englert, D., & Losos, A. (2021). *Charting a Course for Decarbonizing Maritime Transport: Summary for Policymakers and Industry*, World Bank, Washington DC, 2021.
- European Commission. (2022). Proposal for a revision of the Ambient Air Quality Directives. In *Proposal*. European Commission: Brussel, Belgium, 2022.
- Faber, J., Hanayama, S., Zhang, S., Pereda, P., Comer, B., Hauerhof, E., Schim van der Loeff, W., Smith, T., Zhang, Y., Kosaka, H., Adachi, M., Bonello, J.-M., Bulthout, E., Chen, R., Durante, J., Klepp, A., Lee, J., Li, X., Jung, H., & Zhou, J. (2021). *Fourth IMO GHG Study*. 2021, International Maritime Organization, available online: <https://www.imo.org/en/OurWork/Environment/Pages/Fourth-IMO-Greenhouse-Gas-Study-2020.aspx>
- Fuglestvedt, J., Berntsen, T., Eyring, V., Isaksen, I., Lee, D. S., & Sausen, R. (2009). Shipping Emissions: From Cooling to Warming of Climate—and Reducing Impacts on Health. *Environmental Science & Technology*, 43(24), 9057–9062. <https://doi.org/10.1021/es901944r>
- Gobbi, G. P., Di Liberto, L., & Barnaba, F. (2020). Impact of port emissions on EU-regulated and non-regulated air quality indicators: The case of Civitavecchia (Italy). *Science of The Total Environment*, 719, 134984. <https://doi.org/10.1016/J.SCITOTENV.2019.134984>

- Gren, I. M., Brutemark, A., & Jägerbrand, A. (2021). Air pollutants from shipping: Costs of NOx emissions to the Baltic Sea. *Journal of Environmental Management*, 300, 113824. <https://doi.org/10.1016/J.JENVMAN.2021.113824>
- Helsinki Region Environmental Services Authority. (2022). *Air Quality in Helsinki regional area supplementary material*. available online: https://julkaisu.hsy.fi/material/attachments/jqzvxurqu/ilmanlaatu_paakaupunkiseudulla_2021_liiteosio.pdf
- Huang, H., Zhou, C., Huang, L., Xiao, C., Wen, Y., Li, J., & Lu, Z. (2022). Inland ship emission inventory and its impact on air quality over the middle Yangtze River, China. *Science of The Total Environment*, 843, 156770. <https://doi.org/10.1016/J.SCITOTENV.2022.156770>
- Kalikatzarakis, M., Geertsma, R. D., Boonen, E. J., Visser, K., & Negenborn, R. R. (2018). Ship energy management for hybrid propulsion and power supply with shore charging. *Control Engineering Practice*, 76, 133–154. <https://doi.org/10.1016/J.CONENGPRAC.2018.04.009>
- Khersonsky, Y., Islam, M., & Peterson, K. (2007). Challenges of Connecting Shipboard Marine Systems to Medium Voltage Shoreside Electrical Power. *IEEE Transactions on Industry Applications*, 43(3), 838–844. <https://doi.org/10.1109/TIA.2007.895810>
- Mousavi, A., Sowlat, M. H., Hasheminassab, S., Pikelnaya, O., Polidori, A., Ban-Weiss, G., & Sioutas, C. (2018). Impact of particulate matter (PM) emissions from ships, locomotives, and freeways in the communities near the ports of Los Angeles (POLA) and Long Beach (POLB) on the air quality in the Los Angeles county. *Atmospheric Environment*, 195, 159–169. <https://doi.org/10.1016/J.ATMOSENV.2018.09.044>
- Orellano, P., Reynoso, J., Quaranta, N., Bardach, A., & Ciapponi, A. (2020). Short-term exposure to particulate matter (PM10 and PM2.5), nitrogen dioxide (NO₂), and ozone (O₃) and all-cause and cause-specific mortality: Systematic review and meta-analysis. *Environment International*, 142, 105876. <https://doi.org/10.1016/J.ENVINT.2020.105876>
- Peng, W., Yang, J., Corbin, J., Trivanovic, U., Lobo, P., Kirchen, P., Rogak, S., Gagné, S., Miller, J. W., & Cocker, D. (2020). Comprehensive analysis of the air quality impacts of switching a marine vessel from diesel fuel to natural gas. *Environmental Pollution*, 266, 115404. <https://doi.org/10.1016/J.ENVPOL.2020.115404>
- Pirjola, L., Pajunoja, A., Walden, J., Jalkanen, J.-P., Rönkkö, T., Kousa, A., & Koskentalo, T. (2014). Mobile measurements of ship emissions in two harbour areas in Finland. *Atmospheric Measurement Techniques*, 7(1), 149–161. <https://doi.org/10.5194/amt-7-149-2014>
- Siddika, N., Rantala, A. K., Antikainen, H., Balogun, H., Amegah, A. K., Rytí, N. R. I., Kukkonen, J., Sofiev, M., Jaakkola, M. S., & Jaakkola, J. J. K. (2020). Short-term prenatal exposure to ambient air pollution and risk of preterm birth - A population-based cohort study in Finland. *Environmental Research*, 184, 109290. <https://doi.org/10.1016/J.ENVRES.2020.109290>
- Sofiev, M., Winebrake, J. J., Johansson, L., Carr, E. W., Prank, M., Soares, J., Vira, J., Kouznetsov, R., Jalkanen, J.-P., & Corbett, J. J. (2018). Cleaner fuels for ships provide public health benefits with climate tradeoffs. *Nature Communications*, 9(1), 406. <https://doi.org/10.1038/s41467-017-02774-9>
- Spengler, T., & Tovar, B. (2021). Potential of cold-ironing for the reduction of externalities from in-port shipping emissions: The state-owned Spanish port system case. *Journal of Environmental Management*, 279, 111807. <https://doi.org/10.1016/J.JENVMAN.2020.111807>
- Suarez, E., Perez, C. M., Rivera, R., & Martinez, M. N. (2017). Selection of Variables in a Multiple Linear Regression Model. In *Applications of Regression Models in Epidemiology* (pp. 77–86). John Wiley & Sons, Inc. <https://doi.org/10.1002/9781119212515.ch5>
- Toscano, D., & Murena, F. (2019). Atmospheric ship emissions in ports: A review. Correlation with data of ship traffic. *Atmospheric Environment: X*, 4, 100050. <https://doi.org/10.1016/J.AEAOA.2019.100050>
- Tronstad Lund, M., Eyring, V., Fuglestvedt, J., Hendricks, J., Lauer, A., Lee, D., & Righi, M. (2012). Global-Mean Temperature Change from Shipping toward 2050: Improved Representation of the Indirect Aerosol Effect in Simple Climate Models. *Environmental Science & Technology*, 46(16), 8868–8877. <https://doi.org/10.1021/es301166e>
- Viana, M., Rizza, V., Tobías, A., Carr, E., Corbett, J., Sofiev, M., Karanasiou, A., Buonanno, G., & Fann, N. (2020). Estimated health impacts from maritime transport in the Mediterranean region and benefits from the use of cleaner fuels. *Environment International*, 138, 105670. <https://doi.org/10.1016/J.ENVINT.2020.105670>
- Walden, J., Pirjola, L., Laurila, T., Hatakka, J., Pettersson, H., Walden, T., Jalkanen, J.-P., Nordlund, H., Truuts, T., Meretoja, M., & Kahma, K. K. (2021). Measurement report: Characterization of uncertainties in fluxes and fuel sulfur content from ship emissions in the Baltic Sea. *Atmospheric Chemistry and Physics*, 21(24), 18175–18194. <https://doi.org/10.5194/acp-21-18175-2021>
- World Health Organization. (2021). *WHO global air quality guidelines: particulate matter (PM_{2.5} and PM₁₀), ozone, nitrogen dioxide, sulfur dioxide and carbon monoxide*. World Health Organization: Geneva, Switzerland, 2021.
- Zis, T. P. V. (2019). Prospects of cold ironing as an emissions reduction option. *Transportation Research Part A: Policy and Practice*, 119, 82–95. <https://doi.org/10.1016/J.TRA.2018.11.003>

Maritime Greenhouse Gas Emission Reduction Scenarios – Extension of DIONE model³²

Z. Samos², J. Krause^{1**}, L. Maineri³, M. Georgakaki², G. Papadimitriou², C. Kouridis² and G. Fontaras¹

¹ European Commission Joint Research Centre, 21027, Ispra, Italy, Jette.Krause@ec.europa.eu,

Georgios.FONTARAS@ec.europa.eu

² Emisia S.A., Antoni Tritsi 21, Thessaloniki, GR-57001, Greece

³ Seidor Italy S.r.l., via Castel Morrone 24, 20125, Milano (MI), Italy

Introduction

Maritime transport plays a crucial role in the European transportation system, serving as the primary mode for global trade. In 2019, ships weighing over 1,000 gross tonnes carried about 11 billion tonnes, accounting for around 80% of the world's trade volume and 70% of its value (UNCTAD, 2019). However, this transport sector presents significant environmental challenges. In particular, maritime transportation accounted for about 4% of the EU's total greenhouse gas emissions (GhG) in 2019 (EEA, 2022), with emissions from shipping rising by about 36% over the past three decades. Additionally, the international shipping sector significantly contributes to pollutant emissions in the EU, including 15% of total nitrogen oxides (NOx), 3.6% of particulate matter with a diameter of 10 µm or less (PM10), 7% of PM2.5, and 10% of sulfur dioxide (SO₂) emissions.

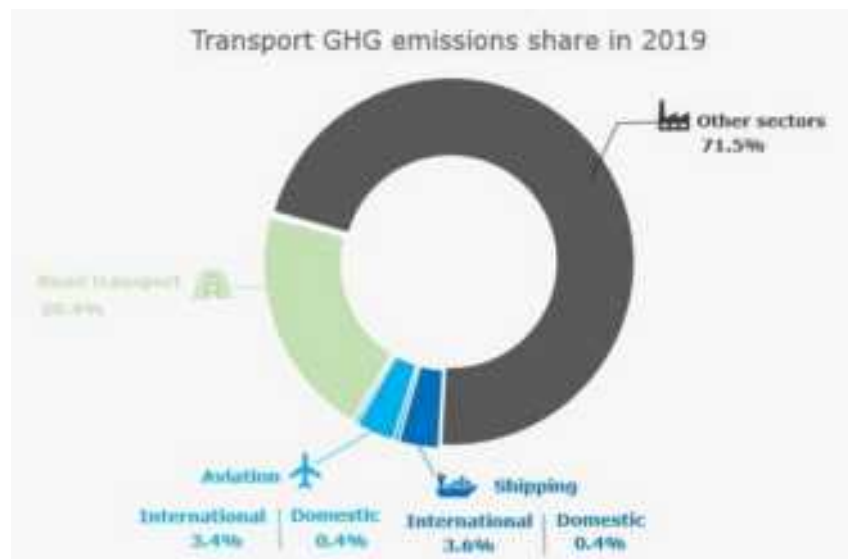


Figure 1: Transport emissions in 2019 as share of the EU's total GhG emissions.

Maritime transport is projected to experience a considerable rise in greenhouse gas emissions, with estimates ranging from 90% to 130% of 2008 levels by 2050, considering various plausible long-term economic and energy scenarios (IMO, 2020). The maritime sector must play a crucial role in curbing its emissions to align with the ambitious goal of achieving climate neutrality in Europe by 2050. To address this challenge, the European Commission has introduced the 'Fit for 55' package, which encompasses a series of legislative proposals to reduce greenhouse gas emissions by at least 55% by 2030 (versus 1990). These proposals include extending the coverage of the EU Emissions Trading System to include maritime transport, imposing limits on the greenhouse gas content of energy used by ships when calling at European ports, promoting the

³² The views expressed in this document are purely those of the authors and shall not be considered an official Commission position under any circumstance

adoption of zero-emission technology during vessel berthing, supporting the development of alternative fuel infrastructure, and revising the Renewable Energy Directive and Energy Taxation Directive.

Given the shipping industry's significant contribution to global GHG emissions, it becomes essential to quantify the potential impact of various measures and policies accurately. It is equally important to assess the effectiveness of different strategies to reduce its environmental impact. To address this, the Joint Research Centre has created a comprehensive calculation method and integrated it into a computer tool capable of evaluating future scenarios concerning vessel fleet composition, activity, and fuel mix. This tool, known as the DIONE maritime fleet emission model, has been developed in collaboration with EMISIA SA. It leverages baselines derived from Eurostat and UNFCCC National inventory data, encompassing historical information up to 2020. To project into the future, these baselines are extended based on observed trends in the EU Reference Scenario 2020 (Comission, 2020). The DIONE model thus provides a powerful tool to reliably assess and analyse the potential outcomes of various measures and policies in the shipping industry, aiding in the pursuit of environmentally responsible practices.

Methodology

The DIONE model adopts a methodology that ensures its alignment with the EMEP/EEA Guidebook (EMEP/EEA, 2019) for emission inventories when estimating emissions from maritime navigation. This approach is based on established guidelines and standards, aiming to ensure accuracy and consistency in calculating the environmental impact of waterborne transportation. There are three reporting methods known as Tiers. These Tiers vary based on the level of complexity and the quality of input data obtained. Generally, higher Tiers with increased complexity are used when more detailed input data is available.

The baseline of the model was initially implemented using the Tier 2 emission calculation level. However, the software model also incorporates a more detailed calculation methodology at the Tier 3 level, which can be utilised once all the required data becomes available. This enables the model to be flexible and adaptable, allowing for more accurate and comprehensive emission assessments when higher-quality data is accessible. Below, the steps included in the Tier2 calculation process are presented, along with the methods used to create the baseline.

The Tier 2 method follows a top-down approach, using final fuel consumption statistics as input to calculate individual pollutant emissions. The Tier 2 emission factors are based on average conditions for the entire trip and are derived as a weighted sum of EFs at different operating conditions (i.e., hoteling, manoeuvring, cruise). The equation used for the Tier 2 approach in maritime emissions is the following:

$$E_{\text{pollutant } i} = \sum_{\text{fuel type } m} (\sum_{\text{engine type } j} FC_{\text{fuel type } m, \text{ engine type } j} * EF_{\text{pollutant } i, \text{ fuel type } m, \text{ engine type } j}) \quad (1)$$

Where:

$E_{\text{pollutant } i}$: Emissions of pollutant i in kilograms

$FC_{\text{fuel type } m, \text{ engine type } j}$: Mass of fuel type m used by vessels with engine type j in tonnes (split in domestic and international fuel consumption)

$EF_{\text{pollutant } i, \text{ fuel type } m, \text{ engine type } j}$: Average emission factor for pollutant i by vessels with engine j using fuel type m in kilograms /tonnes

Fuel type m can be either Bunker Fuel Oil (BFO), Marine Diesel Oil (MDO) or Marine Gas Oil

(MGO). Concerning type of engines, there are five types of engines, namely, Slow Speed Diesel (SSD), Medium Speed Diesel (MSD), High Speed Diesel (HSD) engine, Gas Turbine (GT) and Steam Turbine (ST).

The input data needed from the model are the following:

- Total port arrivals by type of vessel
- Domestic port arrivals by type of vessel
- Fuel sold for all domestic navigation

- Fuel sold for all international navigation

The vessel types utilised in this methodology are presented in Figure 2, which also displays the corresponding default engine types and fuel types employed within this approach.

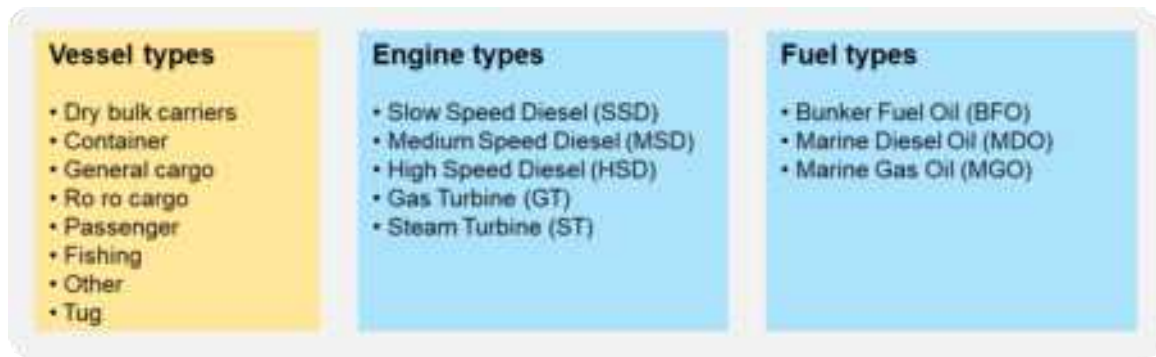


Figure 2: Default Vessel, Engine and Fuel types in the Tier 2 approach

As seen from equation 1, the emission factors used to calculate the emissions are for various combinations of engine type and fuel type, i.e., SSD MDO/MGO, SSD BFO, MSD MDO/MGO,

MSD BFO, HSD MDO/MGO, HSD BFO, GT MDO/MGO, GT BFO, ST MDO/MGO, ST BFO. The Table 1 below includes the emission factors for selected pollutants per engine type - fuel type combination.

Table 1: Emission factors for selected pollutants per engine type - fuel type combination.

EF (kg/ton of fuel)	BC	CO	NMVOC	NOx	PM10
SSD - MDO/MGO	0.05	3.24	1.64	94.30	1.07
SSD - BFO	0.09	3.10	1.56	90.20	5.20
MSD - MDO/MGO	0.05	4.45	1.86	57.90	1.07
MSD - BFO	0.09	4.25	1.78	55.30	5.21
HSD - MDO/MGO	0.04	4.34	2.64	39.60	0.96
HSD - BFO	0.08	4.15	2.52	37.90	5.01
GT - MDO/MGO	0.05	3.84	1.75	17.15	0.00
GT - BFO	0.09	3.67	1.67	17.42	0.30
ST - MDO/MGO	0.09	3.67	1.67	6.01	2.60
ST - BFO		1.75	6.01	1.00	

The model requires the total energy consumed in TJ for shipping in a country as its input. Therefore, to implement this method, it is necessary to disaggregate the user-provided total energy consumption into specific values based on engine type and fuel class combinations.

To achieve this, the following steps are followed according to the guidebook.

In particular, total power installed (in kW) for each vessel type is calculated by multiplying the total number of port arrivals with the reference estimated main engine power provided in the guidelines (Table 2). Subsequently, the total installed power for each type of vessel is distributed among different engine types / fuel classes using the reference percentage table from the guidebook (Table 3). In this way, the total installed

power is categorised by engine type and fuel class, which is the sum of the separate power of each vessel type. A direct proportionality is assumed between total fuel consumption and installed power categorised by engine type and fuel class calculated in the previous step. Consequently, based on this proportional relationship, the model allocates the statistical fuel consumption values to the different engine types and fuel classes.

Table 2: Estimated average main engine power (total power of all engines) by ship category (kW)

Liquid bulk ships	Dry bulk carriers	Container	General cargo	Ro Ro Cargo	Passenger	Fishing	Other	Tug
6,543	4,397	14,871	2,555	4,194	10,196	734	2,469	2,033

Table 3: Percentage of installed Main Engine power by engine type/fuel class (%)

Engine / Fuel type	Liquid bulk ships	Dry bulk carriers	Container	General cargo	Ro ro cargo	Passenger	Fishing	Other	Tug
SSD MDO/MGO	0.87	0.37	1.23	0.36	0.17	0.00	0.00	0.48	0.00
SSD BFO	74.08	91.63	92.98	44.59	20.09	3.81	0.00	30.14	0.00
MSD MDO/MGO	3.17	0.63	0.11	8.48	9.86	5.68	84.42	29.54	39.99
MSD BFO	20.47	7.29	5.56	41.71	59.82	76.98	3.82	19.63	6.14
HSD MDO/MGO	0.52	0.06	0.03	4.30	5.57	3.68	11.76	16.67	52.80
HSD BFO	0.75	0.02	0.09	0.45	2.23	1.76	0.00	2.96	0.78
GT MDO/MGO	0.00	0.00	0.00	0.00	2.27	4.79	0.00	0.38	0.28
GT BFO	0.14	0.00	0.00	0.10	0.00	3.29	0.00	0.20	0.00
ST MDO/MGO	0.00	0.00	0.00	0.00	0.00	0.00	0.00	0.00	0.00
ST BFO	0.00	0.00	0.00	0.00	0.20	0.00	0.00	0.00	0.00

The model's calculations are carried out independently for domestic and international navigation. The model adheres to the following criteria to differentiate between these two types of journeys: if a vessel departs

from and arrives in the same country, the voyage is labelled as domestic. Conversely, a journey is classified as international if the vessel departs from one country and arrives in a different country.

Reference baseline & Customised scenarios

Incorporated within the model is a dataset that serves as a reference baseline scenario. This dataset encompasses historical data and future projections concerning activity and emissions in the maritime navigation sector. It includes information from 27 EU member states, Norway, Turkey, the United Kingdom, and aggregated data for EU27. This selection ensures comprehensive coverage and relevant information for the model's analysis and forecasting related to the maritime navigation sector.

For developing this reference baseline scenario, Eurostat was primarily chosen as the most appropriate and reliable source for historical data up to 2020, for the required input data to the model. Additionally, the National Inventories for UNFCCC (CRF) were used as a secondary source. The inventories of countries in the UNFCCC were employed for three specific reasons. Firstly, they were used to validate the reliability of Eurostat data. Secondly, in cases where fuel consumption data was missing, inconsistent, or erroneous in Eurostat, the UNFCCC inventories were used as an alternative source for fuel consumption information. Lastly, the GhG countryspecific Emission Factors provided by the UNFCCC were used instead of the default GhG Emission Factors given in the EMEP/EEA guidebook.

In addition to historical years for which statistical data is available from 2000 (in most countries) until 2020, the reference baseline scenario includes projections for future years. These projections are based primarily on the EU Reference Scenario 2020 and extend all the way to 2050.

The EU Reference Scenario 2020 estimates the evolution of energy demand for international bunkers, inland waterways and domestic maritime up to 2050. These trends (one for domestic and one for international navigation) were applied to the evolution of the input data required for the Tier 2 methodology calculation, namely fuel consumption and port arrivals. Turkey, the United Kingdom, and Norway are not part of the EU Reference Scenario. Projection trends were derived from neighbouring or socioeconomically similar countries to account for these countries in the reference baseline scenario. For instance, the projection trend for Norway was based on trend data from Sweden. This approach allows for the inclusion of these countries in the analysis, even though the EU Reference Scenario does not directly cover them.

The model provides the flexibility to generate an alternative customised scenario, different from the reference baseline scenario. Users can specify new combinations of engines and fuel types along with their respective emission factors, thereby enabling the creation of a customised scenario. Additionally, the above-mentioned Table 3 should be modified accordingly to reallocate the percentage of installed main engine power by engine type/fuel class and include the new engine / fuel type combinations.

Results

The model's outcomes consist of a comprehensive range of data, covering both maritime greenhouse gas emissions (CO₂, CH₄, N₂O) and a variety of pollutants (NO_x, CO, non-methane volatile organic compounds (NMVOCs), SO₂, particulate matter (PM2.5, PM10), BC, and heavy metals).

The results are disaggregated into two main categories based on their scope: domestic and international. Additionally, they are further categorised by engine type and fuel type, providing a detailed breakdown that allows for a more precise analysis and understanding of the environmental impact of shipping activities.

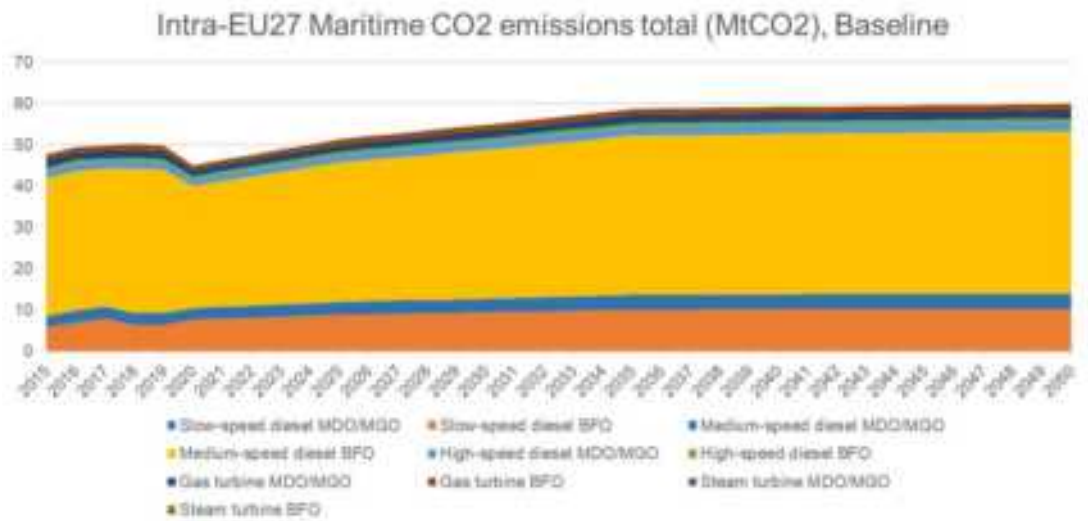


Figure 3: Baseline CO2 Emissions from Intra-EU27 Maritime Transport by engine / fuel combination

Maritime intra-EU CO2 emissions for various engine fuel type combinations up to 2050 for the reference baseline scenario are depicted in the Figure 3. As illustrated in the graph, the maritime sector is projected to gradually increase its CO2 emissions, reaching approximately 60 Mt by 2050. Moreover, a significant portion of these emissions are attributed to Medium-speed diesel BFO vessels.

References

Comission, E. (2020). Retrieved from EU Reference Scenario 2020:

https://energy.ec.europa.eu/data-and-analysis/energy-modelling/eu-reference-scenario2020_en

EEA. (2022). *EEA greenhouse gases — data viewer*. Retrieved from EEA greenhouse gases — data viewer: <https://www.eea.europa.eu/data-and-maps/data/data-viewers/greenhousegases-viewer>

EMEP/EEA. (2019). *EMEP/EEA air pollutant emission inventory guidebook 2019*. Retrieved from Technical guidance to prepare national emission inventories:

<https://www.eea.europa.eu/publications/emep-eea-guidebook-2019>

IMO. (2020). *Fourth Greenhouse Gas Study*.

UNCTAD. (2019). *Beyond Uncertainty Annual Report*. Geneva.

2.9 JS.09. Atmospheric processes and air quality impact studies: Modelling impacts of transport on air pollution, climate, health and ecosystems.

Specification of Zero-Impact Vehicle Emissions and Demonstration of Zero Impact

Ulrich Uhrner¹, Nicola Toenges-Schuller², Raphael Reifeltshammer¹, Werner Stadlhofer² and Stefan Hausberger¹

¹ Institute of Thermodynamics & Sustainable Propulsion Systems, Graz University of Technology, Austria, uhner@ivt.tugraz.at

² AVISO GmbH, 52074 Aachen, Germany

Introduction

In this work the requirements of road traffic "zero impact emission levels" have been analysed from the perspective of air quality. Therefore, aspects of atmospheric processes, road traffic, air quality and guidelines have been combined to specify **reduced emission levels of vehicles that do not affect air quality at kerbside**. In addition to regulated air pollutants such as NO₂ or PM_{2.5}, a key point of this work is particulate number (PN). Three possible definitions of "zero impact on air quality" were developed and thereafter analysed in detail.

1. The road traffic contribution to air quality concentration levels is smaller than monitored at clean rural background and untraceable related with state-of-the-art monitoring
2. The road traffic contribution at kerbside locations shall be irrelevant according to air quality directives, i.e. shall be < 3% of air quality limits (3% irrelevance criterion)
3. Concentration at the vehicle workplace + the workplace limit (960 µg/m³ for NO₂)

For the first definition, background levels at remote monitoring sites in Austria and Germany, literature as well as GAW data have been reviewed. We looked at site characteristics such as forests, settlements and roads around and the elevation of background monitoring stations. The elevation proved to be a suitable parameter to characterize a clean urban background for NO₂, PM_{2.5}, PM₁₀ and PN. Monitored PN levels were inferred from the GUAN network (Sun et al., 2019). 10 years and 5 years background trend analysis revealed that elevated stations above 900 m sea level show hardly any trend, i.e. are mainly influenced by atmospheric processes and climate.

Figure 1 summarises the results for option 1) and 2). Option 3) leads to similar emission targets as option 2) but gives different thresholds for stoichiometric and lean combustion concepts and was thus not pursued further. In the end, our zero-**impact target was the road traffic contribution to air pollutants near roads shall be irrelevant compared to the WHO 2006 air quality guidelines, i.e. lower than 3% of these ambitious air quality (AQ) targets. So far, for PN no air quality limit is defined or recommended in any AQ regulations. Therefore, the ZIV PN₂₀₋₈₀₀ criteria of 650 #/cm³ (in the size range of 20-800 nm) was derived based on conclusion by analogy using the NO₂ zero impact target related to the NO₂ clean background target (1.2 µg/m³: 3.6 µg/m³) and PN₂₀₋₈₀₀ of 2000 #/cm³ monitored at clean background sites, see Figure 1.**

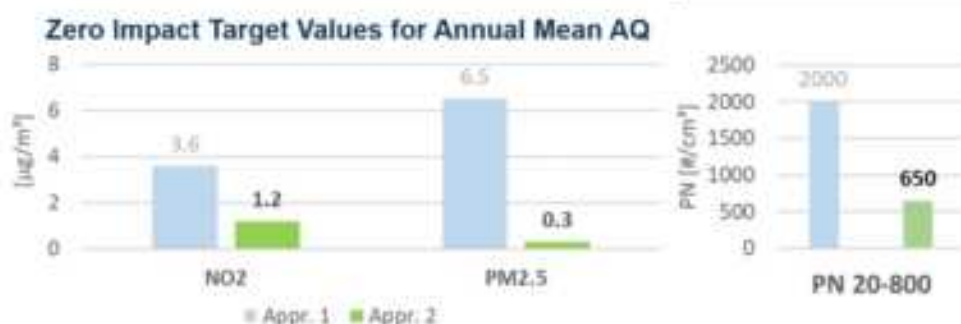


Figure 1:Comparison of zero impact targets, i.e. max kerbside traffic contribution to ambient air

Current contributions of road transport exhaust gas emissions to the air quality near roads in Europe were analysed to identify the relation between road vehicles emissions and pollutant concentrations measured next to the road. From the worst-case situation identified at "Stuttgart Neckartor" in the year 2016 we assessed the necessary traffic emission reduction rates to meet the zero impact pollutant concentrations next to the road. With these reduction rates and with the corresponding fleet average emissions, the maximum emissions per kilometer for "zero impact vehicles" were calculated as a first assessment. However, for PN source specific i.e. traffic related contributions to air quality at kerbside in Europe is rarely available. Therefore, the PM target was used and average monitored particulate numbers per emission mass were used to assess PN targets.

The resulting ZIV emission targets based on the driving situation at Stuttgart, Neckartor in 2016 are shown in Table 1.

Table 1: Specified emission targets for the ZIV fleet

Vehicle type	unit (activity)	EF NO _x (mg/unit)	EF PM2.5 (mg/unit)	EF PN ₂₀₋₈₀₀ (10 ¹¹ #/unit)
PC	km	6.7	0.4	1.2
LCV	km	7.9	0.5	1.5
	kWh	28.1	1.6	4.8

Demonstration of "Zero Impact" - Approach

The specified levels were inferred based on assumptions such as an appropriately selected monitored worst case air quality situation, and the assumption of a linear relationship between emissions and corresponding contributions to ambient concentrations, i.e. the reduction rates were transferred to zero-impact vehicle (ZIV). In order to demonstrate zero impact, local scale model calculations were carried out to validate the emission factors of a hypothetical 100% ZIV fleet to fulfil these zero impact air quality targets. In addition, latest technology fleet scenario i.e. 100 % Euro-6 d light vehicles (LV) and 100 % Euro-VI heavy vehicles (HV) have been evaluated. The basis for those two scenarios are well established validated base case simulations. The GRAMM/GRAL modelling system (Uhrner et al., 2014, Öttl 2015, Öttl 2019) was used to model detailed flow and air pollutant dispersion. Highly resolved source specific emission data have been processed for the simulations, the main dispersion set-up features are shown in Table 2. The flow around buildings impacting upon dispersion was accounted, except in the Vienna study. After validation of the base cases, the traffic exhaust related NO_x, PM and PN concentrations was assessed for the base case, Euro-6/VI and ZIV emission scenarios (see Table 2). NO_x to NO₂ conversion was computed using a simple Romberg type empirical conversion formula (Romberg et al., 1996) for the Stuttgart, Vienna and Augsburg case studies. For the Graz study, a pseudo-steady state approximation approach (Seinfeld and Pandis, 1998) using ozone and solar radiation measurements was used to compute NO to NO₂ conversion.

Table 2: Main set-up features of the case studies. ~~Study area, monitoring grid resolution~~

Case study	Domain size	Monitoring grid resolution	Air pollutant focus	# Monitoring
Stuttgart-Neckartor	1.4 x 1.7 km ²	2 m	NO _x /NO ₂	2 AQ hotspot & bg
Vienna	30 x 24 km ²	10 m	NO _x /NO ₂ , PM	17 AQ stations
	4 x 6.2 km ²	4 m	NO _x /NO ₂ , PM, PN	4 AQ stations, 2 SMPS
Augsburg CAZ	1.1 x 0.8 km ²	2 m	NO _x /NO ₂ , PN	NO _x , PN _{>4nm} , PN _{>23nm} , CO ₂
Graz Plüddemannngasse				

In Augsburg, the focus was laid on the central activity zone (CAZ). A traffic model, traffic emissions (HBEFA4.1) and residential heating emissions were established within SMARTAQNET (Uhrner et al., 2020). SMPS measurements from the GUAN network (Sun et al., 2019) were used to monitor the urban background; SMPS measurements were undertaken by TUG in the city centre at Königsplatz (KP) next to a busy road from 16.10.2020 till 12.01.2021. PN deposition was accounted, however the impact was negligible. Coagulation was neglected as a sink process.

In Graz, a detailed kerbside monitoring took place on October 20th, for details see accompanying paper Toenges et al., 2023). NO, NO₂, PN₄, PN₂₃ and CO₂ were measured at 1 m, 3 m and 5 m distance at a busy road. The monitoring interval was 10 minutes each location and the measurements were undertaken over 7 hours, on 20.10.2021. PN measurements were switched all 10 minutes to distinguish between total particle number (TPN) and solid particle number (SPN) for particles >4 nm (PN₄) and particles >23 nm (PN₂₃). However, the SPN measurement results were highly questionable and were not used. Detailed accompanying traffic monitoring was performed as well. Emissions were computed using the software PHEM (Passenger car and Heavy-duty

Emission Model) from TU Graz. These standardized PN emissions relate to solid particles >20 nm. Meteorological data for the flow field model forcing and air quality data were only available at 30-min resolution, therefore the accompanying NO_x and PN simulations were performed as 30-min means around the Plüddemanngasse street. NO_x background measurements were used from the air quality station "Graz-Nord" as well as O₃ and radiation measurements from Graz-Nord, all operated by the provincial government of Styria. The CO₂ measurements were performed in order to monitor dilution (Toenges et al., 2023). Due to the sampling strategy, available NO_x and CO₂ measurements are a factor of two higher than PN measurements. Here, these measurements were used together with the NO_x measurements to evaluate the plausibility of the (10 min) PN measurements. Therefore, at first, NO_x simulations were performed and compared with 10 minutes NO_x monitored values. Thereafter, PN₂₃ simulations were performed and compared with selected PN₂₃ monitoring. The GRAL model was run in transient mode.

Results

Stuttgart Neckartor case study NO₂

In Figure 2 the simulated and validated base case annual mean NO₂ concentrations 2019 at Stuttgart Neckartor is shown (top left). Simulated concentrations are significantly higher than the air quality standard of 40 µg/m³. Stuttgart Neckartor 2016 was identified as "worst-case" traffic related NO₂ from local contributions and background is shown for the base case 2019 (top right), the Euro-6/VI traffic NO_x Scenario (bottom left) and ZIV-scenario (bottom right). Up to 40 µg/m³ are related to traffic near kerbside with the base case, up to 20 µg/m³ with the Euro-6/VI scenario and up to 1 µg/m³ are related to the ZIV scenario, the aforementioned zero impact criteria is fulfilled.

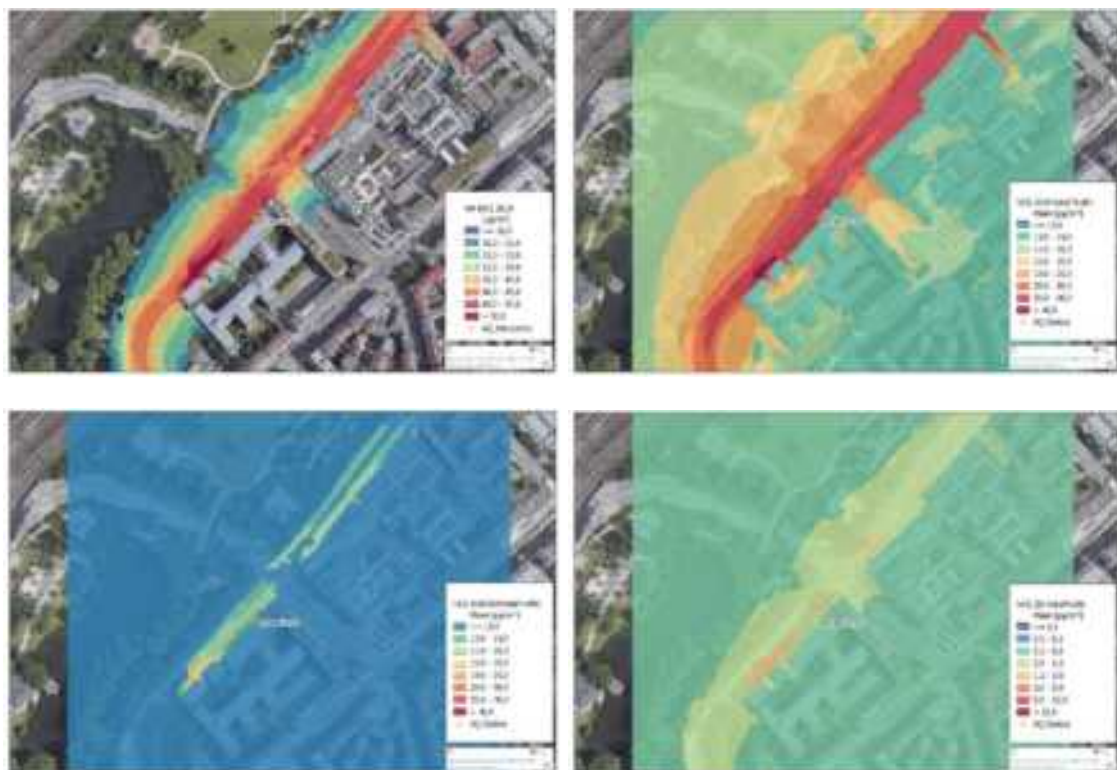


Figure 2: Base case Stuttgart Neckartor AM NO₂ simulation (top left), total base case traffic related NO₂ (top right), Euro-6/VI traffic NO_x Scenario (lower left) and ZIV-scenario (lower right)

Graz Plüddemanngasse Case Study

In Figure 5 the simulated 7 hours mean NO_x concentration on 20.10.2021 is shown. NO_x measurements were used to validate the dispersion set-up. Owing to the monitoring strategy (see accompanying paper Toenges et al., 2023) and availability of meteorological and air quality data 30-min simulated means are compared versus monitored 10-min NO_x mean concentrations (Figure 3 right). A good relation was found, the R^2 is 0.74 and the slope (0.94) is close to 1.

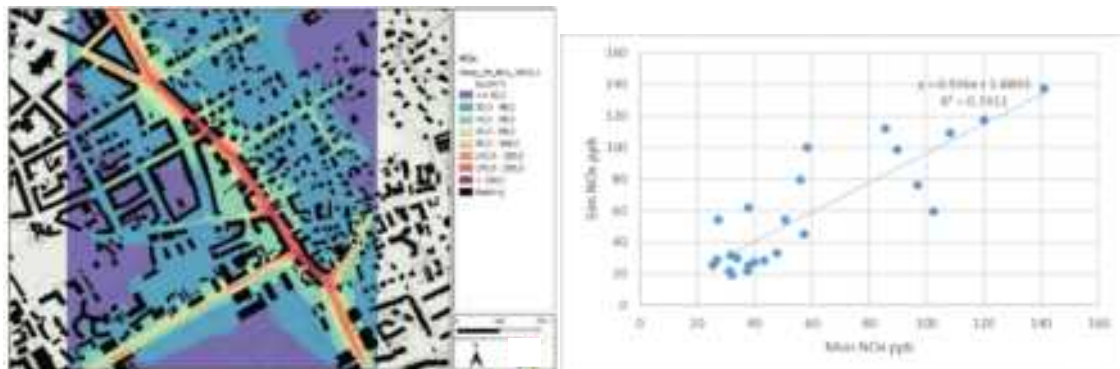


Figure 3: Graz Plüddemanngasse Mean NO_x simulation (left) and comparison mean simulated 30 min NO_x vs mean monitored 10 min NO_x (right)

Figure 4 shows the simulated spatial total PN_{23} concentration for 20.10.2021 and a comparison of simulated 30-min mean traffic related solid PN_{23} (solid PN_{23} due to emission monitoring) and monitored 10-min mean total PN_{23} concentrations. The correlation between those different measures is high ($R^2 = 0.85$). The slope of 3.89 may indicate that kerbside total PN_{23} may be composed of a large fraction of so-called delayed aerosols. These particles may be related to nucleation and rapidly growing (condensing) VOCs (Uhrner et al., 2007, Wehner et al., 2009, Ulbrunner et al., 2011). The intercept of $\sim 4000 \text{ } \mu\text{m}^{-3}$ may be attributed to the urban background and atmospheric new particle formation (Birmili et al., 2003).

Figure 5 shows the maximum traffic related solid PN_{23} for Euro-6/VI and ZIV scenario. The target value of $650 \text{ } \# \text{cm}^{-3}$ is fulfilled at kerbside with both scenarios.

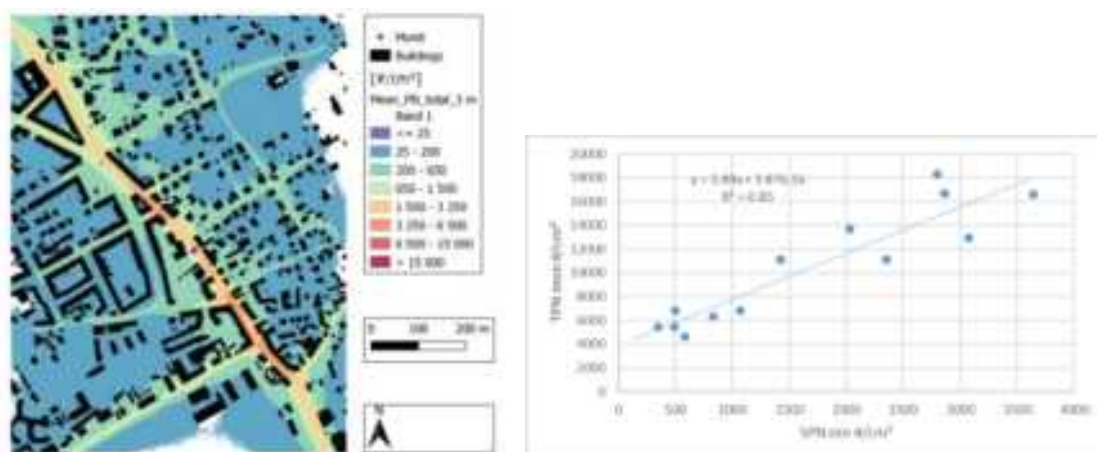


Figure 4: Graz Plüddemanngasse mean traffic related PN_{23} base case (left) and validation of the base case (right)

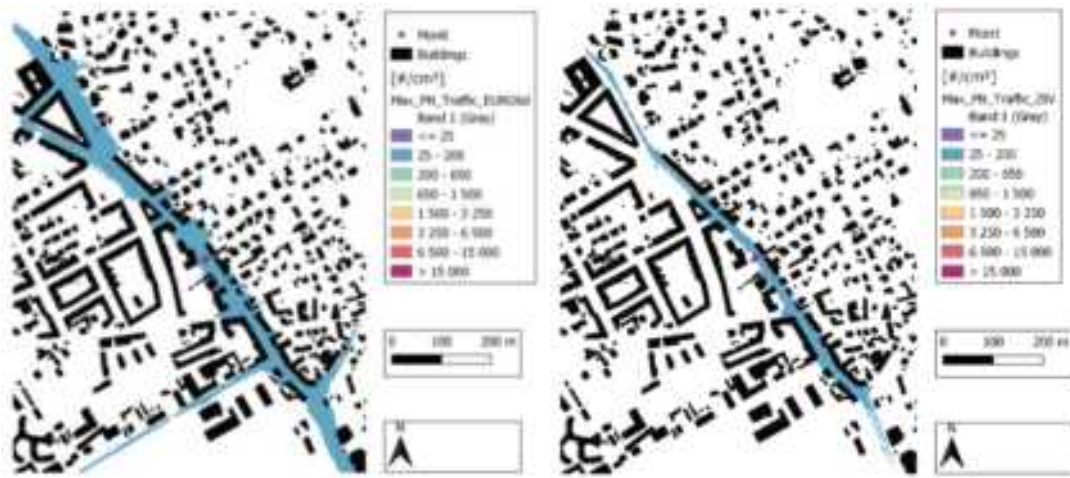


Figure 5: max. traffic related PN_{23} (Euro-6/VI) scenario (left) and ZIV scenario (right)

Augsburg central activity zone case study PN

In Figure 6 total simulated mean (16.10.20 – 12.01.21) PN concentrations is shown for the base case (top left). Residential heating and PN_{20-800} were used as urban background. The simulated increment is dominated by residential heating emissions from solid fuels. Simulated PN_{20-800} concentrations next to roads appear unrealistically low. Multiplying traffic related simulated exhaust particles by a factor of 3.8 yields the best match with the two monitoring stations and the resulting PN_{20-800} concentrations look more realistic, see Figure 6 top right. Traffic exhaust and brake wear related PN concentrations are shown for the base case (left) and the ZIV scenario (right) at the lower panel in Figure 6. The target value of $650 \text{ } \# \text{cm}^{-3}$ is fulfilled at kerbside.

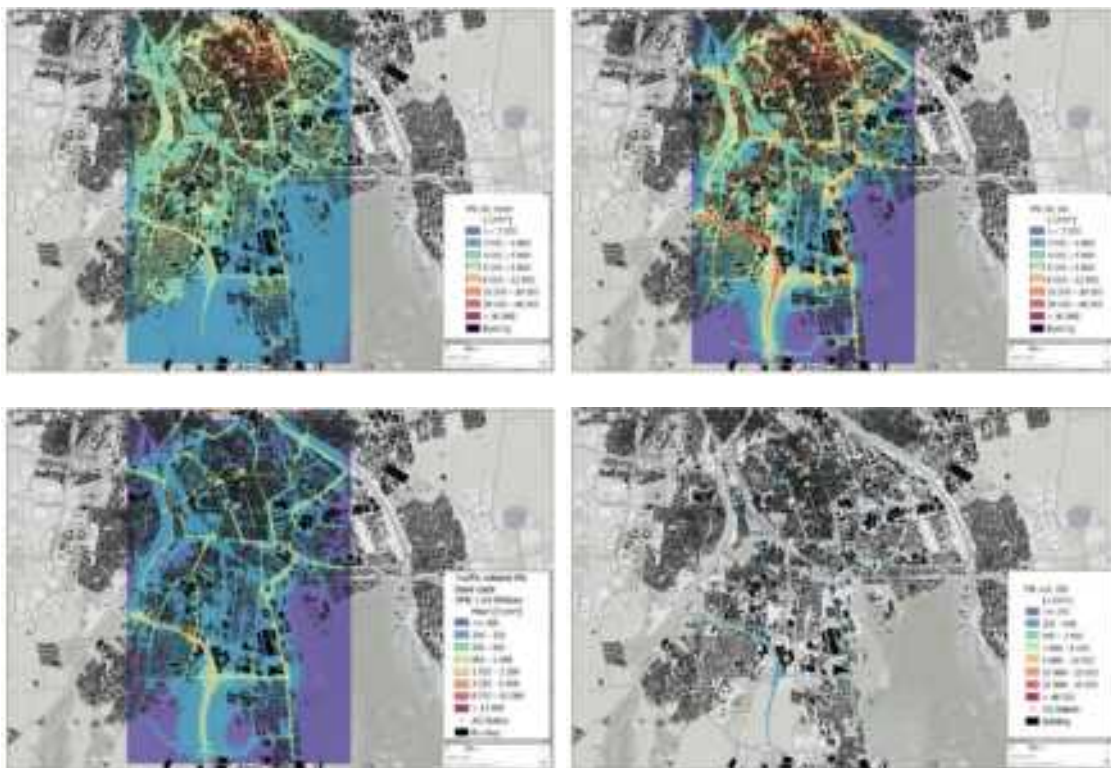


Figure 6: Base case Augsburg mean total solid $\text{PN}_{20-800\text{nm}}$ simulation (top left), base case mean total $\text{PN}_{20-800\text{nm}}$ with volatile correction (top right), base case traffic solid $\text{PN}_{20-800\text{nm}}$ (lower left) and ZIV-scenario (lower right)

Summary

In conclusion, zero-impact was demonstrated for the inferred emission targets illustrated in Table 1. A Lagrangian particle model was used to simulate the dispersion of NO_x, PM2.5 and PN in selected urban case studies and to see if the zero impact air quality targets can be generally fulfilled. Owing to the non-linearity of the NO to NO₂ conversion, to fulfil the 1.2 µg/m³ criteria for NO₂ kerbside at hot spots with high traffic volumes or extreme driving conditions seems to be most demanding zero-impact threshold. PM and PN limits for solid particles can be already fulfilled with latest Euro-6/VI exhaust technologies. However, the comparison of measured versus simulated PN concentrations indicated a clear underestimation of simulated PN predominantly in the ultra-fine particle range (<100 nm). This mismatch is most likely attributable to even dominating delayed aerosol of volatile origin. A clear relation of simulated versus unidentified secondary formed particles was found in both particle number case studies. However, accounting for the impact of volatiles in future scenarios bears large uncertainties due to complex aerosol dynamic processes within the exhaust plume of a driving car (Uhrner et al., 2011).

Acknowledgements

This work was funded by FVV (The Research Association for Combustion Engines eV) in Germany, Funding number: FVV 601407

References

- Birmili W., Berresheim H., Plass-Dülmer C., Elste T., Gilge S., Wiedensohler A., Uhrner U (2003). The Hohenpeissenberg aerosol formation experiment (HAFEX): a long-term study including size-resolved aerosol, H₂SO₄, OH, and monoterpenes measurements, *Atmos. Chem. Phys.*, 3, 361-376.
- Öttl D. (2013). *Validation of the prognostic mesoscale model GRAL against boundary-layer measurements in a street canyon*. Landesregierung, Department 15, Air Quality Control.
- Öttl D. (2015). Evaluation of the revised Lagrangian particle model GRAL against wind-tunnel and field experiments in the presence of obstacles, *Boundary-Layer Meteorol.*, No 155, pp.271-287.
- Romberg E., Bösinger R., Lohmeyer A., Runke R., Röth F. (1996). NO-NO₂ - Umwandlungsmodell für die Anwendung bei Immissionsprognosen für Kfz-Abgase. Gefahrstoffe - Reinhaltung der Luft 56 Nr. 6, S. 215-218.
- Seinfeld, J.H., Pandis S.N. (1998). From Air Pollution to Climate Change, John Wiley and Sons, New York.
- Sun J., Birmili W., Herrmann M., Tuch T., Weinhold K., Spindler G., et al. (2019). Variability of black carbon mass concentrations, sub-micrometer particle number concentrations and size distributions: results of the German Ultrafine Aerosol Network ranging from city street to High Alpine locations, *Atmos. Environ.* 202.
- Toenges-Schuller N., Hausberger S., Schneider C., Stadlhofer W., Uhrner U. (2023). Particle Number Box-Model Calculations in a Street Canyon and Comparison to Measurements. TAP&SE Göteborg 2023.
- Uhrner U., Reifeltshammer R.J., Werhahn J., Philipp A., Kunde R., Sturm, P.J., (2020). Innovative Use of Sensor Data to Improve Spatiotemporal Emission Inventories, Air Quality Conference, Thessaloniki.
- Uhrner U., Lackner B.C., Reifeltshammer R.J., Steiner M., Forkel R., Sturm P.J. (2014). Inter-Regional Air Quality Assessment, - Bridging the Gap between Regional and Kerbside PM Pollution, Results of the PMinter Project, VKM-THD Mitteilungen, Volume 98, Verlag der Technischen Universität Graz, ISBN: 978-3-85125-364-1.
- Uhrner U., von Löwis S., Zallinger M., Vehkamäki H., Wehner B., Stratmann F., Wiedensohler A. (2011). Volatile nanoparticle formation and growth within a diluting diesel car exhaust, *J. Air Waste Manag Assoc.*, 61(4), 399-408.
- Uhrner U., von Löwis S., Vehkamäki H., Wehner B., Bräsel S., Hermann M., Stratmann F., Kulmala M., Wiedensohler A. (2007). Dilution and Aerosol Dynamics within a Diesel Car Exhaust Plume – CFD Simulations of On-road Conditions. *Atmos. Environ.*, 41, 7440 – 7461.
- Wehner B., Uhrner U., von Löwis S., Zallinger M., Wiedensohler A. (2009). Aerosol number size distributions within the exhaust plume of a diesel and a gasoline passenger car under on-road conditions and determination of emission factors. *Atmos. Environ.* 43 (2009), 1235-1245
- WHO: Air Quality Guidelines; Global Update 2004; ISBN 92 890 2192 6; WHO, 2006.

The impact of shipping emissions to urban air quality in Europe – A port/city analysis

A. Megaritis^{1*}, J.S. Hullegrue², J. Tokaya², P. Coenen², and G. Valastro¹

¹ Concawe, Environmental Science for European refining, Brussels, Belgium

Corresponding author: athanasios.megaritis@concawe.eu

² Netherlands Organization for Applied Scientific Research (TNO), Utrecht, Netherlands

1. Introduction

It is well known that elevated concentrations of atmospheric pollutants can lead to adverse effects on both human health and ecosystems. Epidemiological studies have shown that the exposure to pollutants such as fine particulate matter ($PM_{2.5}$) and nitrogen dioxide (NO_2) is associated with cardiovascular and respiratory diseases, leading to increased sickness, hospital admissions and premature death (Beelen et al., 2014). Moreover, nitrogen deposition in soils and water bodies leads to eutrophication and biodiversity loss and sulphur dioxide can contribute to acidification which can harm sensitive ecosystems.

Over the past decades, legislation has been introduced to reduce emissions of these harmful pollutants. These efforts to reduce emissions in several sectors have resulted in a decrease in the atmospheric concentrations of $PM_{2.5}$, PM_{10} , NO_2 and SO_2 . The most recognized example of successful emission reduction is in SO_2 . Due to abatement measures in powerplants and desulphurization of fuels, the atmospheric SO_2 concentration in the European Union countries declined by around 70% between 2000 and 2017 (Colette & Rouil, 2020) based on aggregated observations.

The strong emissions reductions in some sectors, have inevitably shifted the focus to other less strongly contributing sources, such as shipping whose emissions relative contributions have a growing significance, in order to further reduce air pollutant concentrations (Denier van der Gon et al., 2022; Jonson et al., 2015).

In this study insights are gained with respect to the contribution of shipping emissions to the air quality in Europe and major ports and cities. Using the chemical transport model LOTOS-EUROS and its source apportionment capabilities, the contribution of international and inland shipping emissions to atmospheric air pollutant concentrations in 19 European port cities is computed and being put into context compared to the relative contribution of other sources.

An overview of the study and the main findings derived are presented in the following Chapters.

2. Methods

2.1 Model Description

LOTOS-EUROS is a 3-D chemistry transport model. The off-line Eulerian grid model simulates air pollution concentrations in the lower troposphere solving the advection-diffusion equation on a regular latitude-longitude-grid with variable resolution over Europe (Manders et al., 2017).

The vertical transport and diffusion scheme accounts for atmospheric density variations in space and time and for all vertical flux components. The vertical grid is based on terrain following vertical coordinates and when excluding stacked boundary layer on top extends to 5 km above sea level. The height of the layers on top of the 25 m surface layer is determined by heights in the meteorological input data. In the model version exploited in this study 12 model layers are used (with 7 stacked boundary layers on top), leading to a resolvent of the first km in 7 layers (depending on meteorological conditions).

Gas-phase chemistry is simulated using the TNO CBM-IV scheme, which is a condensed version of the original scheme (Whitten, 1980). LOTOS-EUROS explicitly accounts for cloud chemistry, computing sulphate formation as a function of cloud liquid water content and cloud droplet pH as described in Banzhaf et al. (2012). For aerosol chemistry the thermodynamic equilibrium module ISORROPIA2 is used (Fountoukis & Nenes, 2007). Dry Deposition fluxes are calculated using the resistance approach as implemented in the DEPAC (DEPosition of Acidifying Compounds) module (Van Zanten et al., 2010). Furthermore, a compensation point approach for ammonia is included in the dry deposition module (Wichink Kruit et al., 2012). The wet deposition module accounts for droplet saturation following Banzhaf et al. (2013).

The model is part of the Copernicus Atmospheric Monitoring Service (CAMS) regional ensemble providing operational forecasts and analyses over Europe. In this context the model is regularly updated and validated using observations from ground and satellite observations. The model performance is also subject to numerous peer-reviewed publications (Escudero et al., 2019; Skouliidou et al., 2021; Timmermans et al., 2022).

2.2 Source Apportionment

TNO has developed a system to track the impact of emission categories within a LOTOS-EUROS simulation based on a labelling technique (Kranenburg et al., 2013). This technique provides more accurate information about the source contributions than using a brute force approach with scenario runs as the chemical regime remains unchanged. Another important advantage is the reduction of computational costs with respect to the brute force approach. The source apportionment technique has extensively been used in previous studies (Pommier, 2021; Timmermans et al., 2022, Thürkow et al., 2023).

Besides the total pollutants' concentrations, the contributions of selected sources to these concentrations are calculated. The labelling routine is implemented for primary, inert aerosol tracers as well as for chemically active tracers containing a C, N (reduced and oxidized) or S atom, as these are conserved and traceable.

2.3 Emissions & Meteorology

The LOTOS-EUROS model is run with ECMWF ERA 5 reanalysis meteorological data (2018). ERA5 provides hourly estimates of a large number of atmospheric, land and oceanic climate variables, that are necessary inputs for calculations of atmospheric concentrations. Typical inputs required by LOTOS-EUROS are for example surface and air temperature, cloud cover, windspeed and direction, precipitation and relative humidity.

The CAMS-REG inventory emission data for the year 2018 version 5.1 REF2 (Kuenen et al. 2019) is used in this study for anthropogenic trace gas emissions. At the time of performing this study, this was the latest available data set, while an update with more recent data is expected to be published in 2023. The inventory uses the officially reported emission data by European countries. However, for international shipping the dataset is replaced with emissions from the Finnish Meteorological Institute (FMI) STEAM model (Jalkanen et al., 2016). This model is based on actual ship movements as registered by the AIS data and moreover they are geographical referenced. This model gives the best geographical distribution of the shipping emissions on European seas (and the Atlantic). For inland shipping the data reported in the national inventories is complemented by the spatial distribution of the emissions as calculated by the STEAM model.

2.4 Model setup

Figure 1 shows the different domains which are part of the LOTOS-EUROS simulations. A coarse resolution (circa 25 x 25 km) simulation is performed over Europe (domain shown in blue). Results from this simulation are used as boundary condition for two nested simulations over the Mediterranean and a central part of Europe (domains shown in red) at a higher resolution (circa 6 x 6 km), covering the following ports that were studied in more detail:

Sea ports:

1. Rotterdam (NL)
2. Antwerp (BE)
3. Hamburg (DE)
4. Amsterdam (NL)
5. Marseille (FR)
6. Bremerhaven (DE)
7. Barcelona (ES)
8. Le Havre (FR)
9. Genoa (IT)
10. Piraeus (GR)
11. Lisbon (PT)
12. Naples (IT)
13. Venice (IT)

Inland ports:

1. Vienna (AU)
2. Liege (BE)
3. Duisburg (DE)
4. Nijmegen (NL)
5. London (UK)
6. Cologne (DE)



Figure 1: Display of the simulation setup domains. The port/cities of interest are displayed as dots on the map (orange for sea ports and green for inland ports).

3. Results

3.1 Contribution of shipping emissions to air quality in Europe

Figure 2 shows the predicted annual average surface concentration of NO₂ in 2018 for the European domain (left panel) together with the source apportionment results of the whole domain (right panel). High NO₂ concentration values are calculated in the central part of Europe (Benelux, Germany, UK) and in the Po Valley (north of Italy) with the biggest contributions being attributed to Road Transport – exhaust and International Shipping. The relative contribution of inland shipping is < 0.5% and therefore forms a small contribution in the whole European domain.

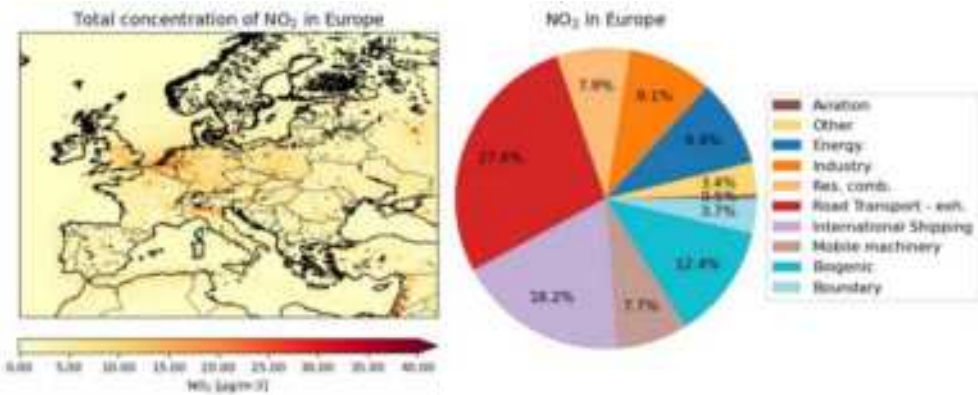


Figure 2: The annual average NO₂ surface concentration for 2018 in the simulation domain of the coarse (25x25km) resolution LOTOS-EUROS simulation (left panel). The relative contributions from the various labelled sectors to the surface concentration of NO₂ for the entire simulation domain is also shown (right panel).

For the remaining pollutants examined in the study, the predicted contribution of shipping emissions in comparison with other sectors are shown in Figure 3. From the results it is evident that shipping has the largest relative contribution for NO₂ compared to other pollutants (Figures 2, 3). For SO₂ a significant contribution from international shipping is still present (11%), while for PM the shipping contribution is relatively smaller. In addition, inland shipping is predicted to be a negligible contributor to the atmospheric pollutant concentrations on average in Europe.

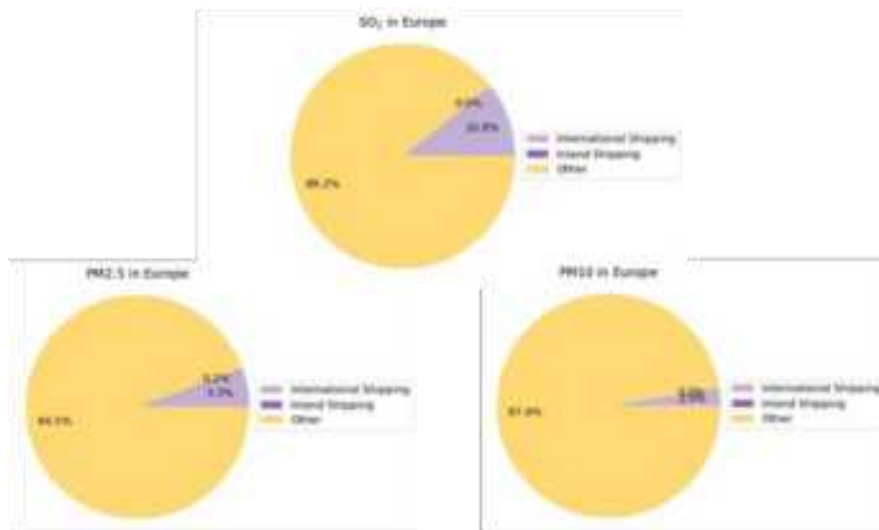


Figure 3: The predicted relative contribution from international and inland shipping to SO₂ (top), PM_{2.5} (left), and PM₁₀ (right) annual average surface concentrations over Europe in 2018.

3.2 Contribution of shipping emissions for each port

Because the highest contribution of shipping is found for NO₂, the results of the calculated shipping contribution to NO₂ levels near the ports are presented and discussed in more detail here. Illustrative examples are used for three cases: a) a port located nearby the city centre (i.e. Piraeus), b) a port located close to the city (i.e. Antwerp, ~10km distance) and c) a port located far from the city (i.e. Rotterdam, ~30km distance). Detailed results for all ports and pollutants can be found in the appendix of the Concawe study (Concawe, 2023). For the analyses, a representative central location for the port and the city centre was determined for the selected cities. The city centre locations are represented as blue dots and the port locations as green dots in Figure 4-Figure 6. For these locations of interest, the concentration fields were calculated as a weighted average of the 4 nearest grid point in the simulation domain (inversely with distance from the grid point to the coordinates of the location of interest).

3.2.1 Piraeus

In Figure 4, the absolute and relative contribution of international shipping to NO₂ annual average surface concentrations is shown. On the top left panel, it can be seen that the absolute contribution of international shipping is exceeding 5 $\mu\text{g}/\text{m}^3$ in most of the surrounding areas, and can reach up to 10 $\mu\text{g}/\text{m}^3$ or higher at the sea part. The port is located at the city centre which causes the green and blue dots in the top panels to coincide and the associated pie charts to be the same. International shipping is predicted to contribute 12 $\mu\text{g}/\text{m}^3$ (34%) to the annual average surface NO₂ concentration in Piraeus being the dominant source closely followed by exhaust emissions from the transport sector.

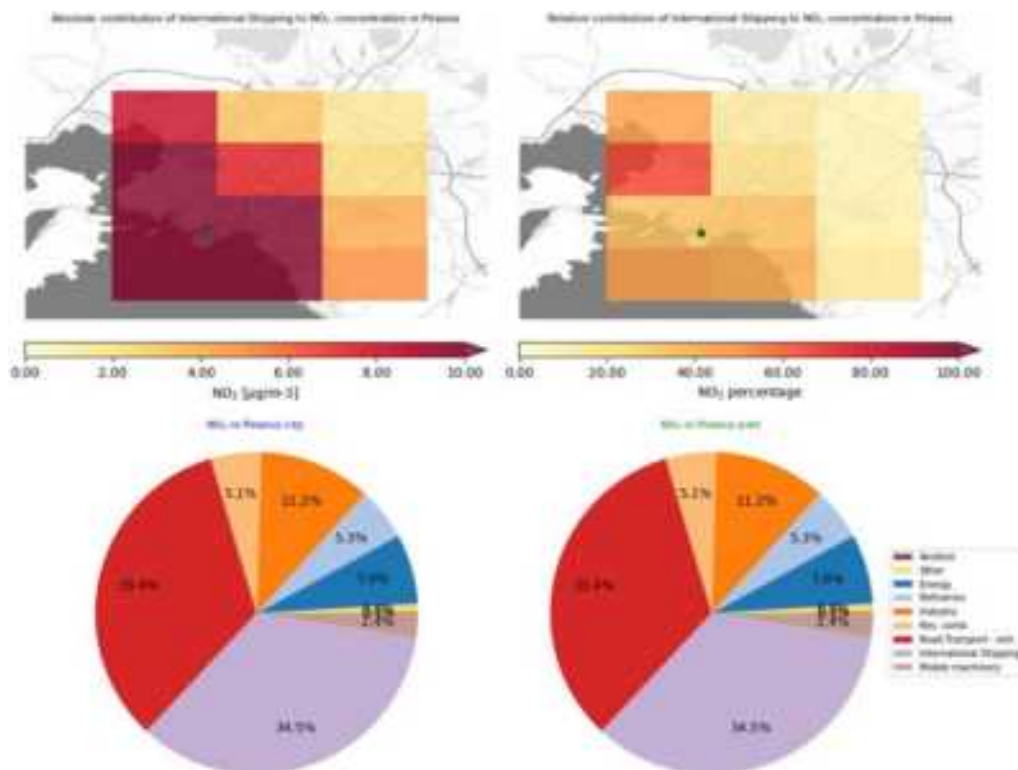


Figure 4: The calculated absolute (top left panel) and relative contributions (top right panel) of international shipping to the annual average surface NO₂ concentration in Piraeus in 2018. The pie charts for the city centre and the port are the same since the port essentially forms the city centre. Inland shipping is not shown in the pie charts as there is no contribution from this sector around Piraeus.

3.2.2 Antwerp

Antwerp is by far the biggest Belgian (sea)port, located at the river Scheldt which also features the port of Ghent closer to the sea. It plays an important role in the connection between the port of Hamburg and Le Havre in nearly all major traffic flows.

In Figure 5 the contribution of international shipping to the NO₂ concentration in Antwerp is shown. The absolute contribution of international shipping at the port of Antwerp (green dot in Figure 5) located at the delta of the Scheldt River is 16 $\mu\text{g}/\text{m}^3$ (47%). The relative contribution from international shipping can go up to 70% following the Scheldt River further downstream. The concentration in the port is predicted to receive contribution from emissions from ships at berth in the port. This also influences the air quality in the city centre of Antwerp situated to the southeast of the port (blue dot). Here international shipping contributes 5.8 $\mu\text{g}/\text{m}^3$ (24%) and inland shipping contributes 1.0 $\mu\text{g}/\text{m}^3$ (4.0%).

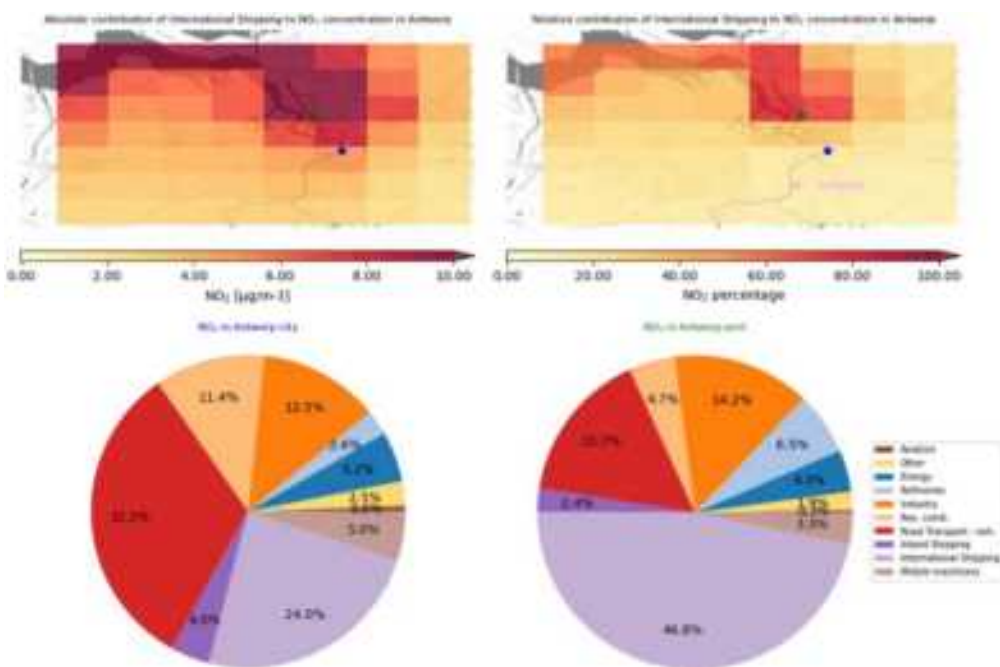


Figure 5: The calculated absolute (top left panel) and relative contributions (top right panel) of international shipping to the annual average surface NO₂ concentration in Antwerp in 2018. The relative contributions of various sectors to the NO₂ concentrations in the port (bottom right panel) and city centre (bottom left panel) of Antwerp are shown in the pie charts.

3.2.3 Rotterdam

The distribution of the contribution of international shipping to the annual average NO₂ surface concentration in the Rotterdam area for 2018 is shown in Figure 6. The pie chart is showing the relative contributions from all labelled source sectors at the main container terminal of the port (bottom right) and in the city centre of Rotterdam (bottom left).

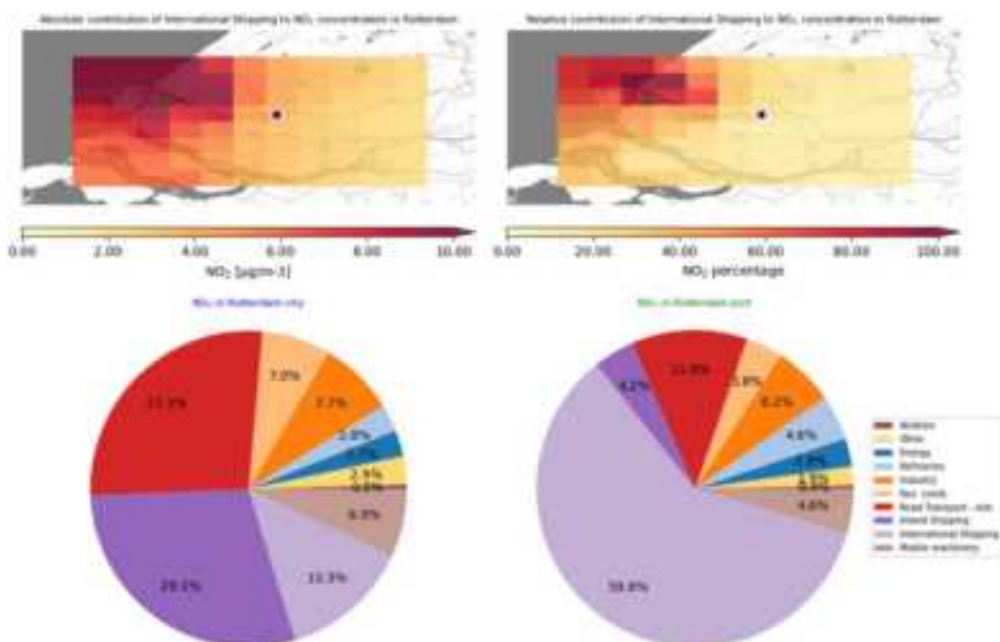


Figure 6: The calculated absolute (top left panel) and relative contributions (top right panel) of international shipping to the annual average surface NO₂ concentration in Rotterdam in 2018. The relative contributions of various sectors to the NO₂ concentrations in the port (bottom right panel) and city centre (bottom left panel) of Rotterdam are shown in the pie charts.

The average annual absolute contribution of international shipping is $16 \mu\text{g}/\text{m}^3$ (60%) at the port entrance at sea (green dot in Figure 6), while even above the city centre of Rotterdam (blue dot), considerable contributions are found of $3.7 \mu\text{g}/\text{m}^3$ (13%). The absolute contribution however, decreases between the port and the city centre due to dilution upon transport and the lifetime of NO_2 (the distance between the port and the city is approximately 30 km). On the contrary, the absolute contribution from inland shipping is larger in the city centre than at the port location (respectively 8.1 (29%) vs 1.1 (4%) $\mu\text{g}/\text{m}^3$) and inland shipping is calculated to be the most dominant source in the city centre together with exhaust emissions from the road transport sector. The river Rhine (which is the major inland waterway linking the North Sea with industrial areas in Germany and its eastern neighbours via the Rhine-Main-Danube canal) ends in Rotterdam. This leads to the significant contribution from inland shipping to the air quality in Rotterdam city.

A total overview of the absolute contributions from the labelled sectors to the city centre locations is given in Figure 7.

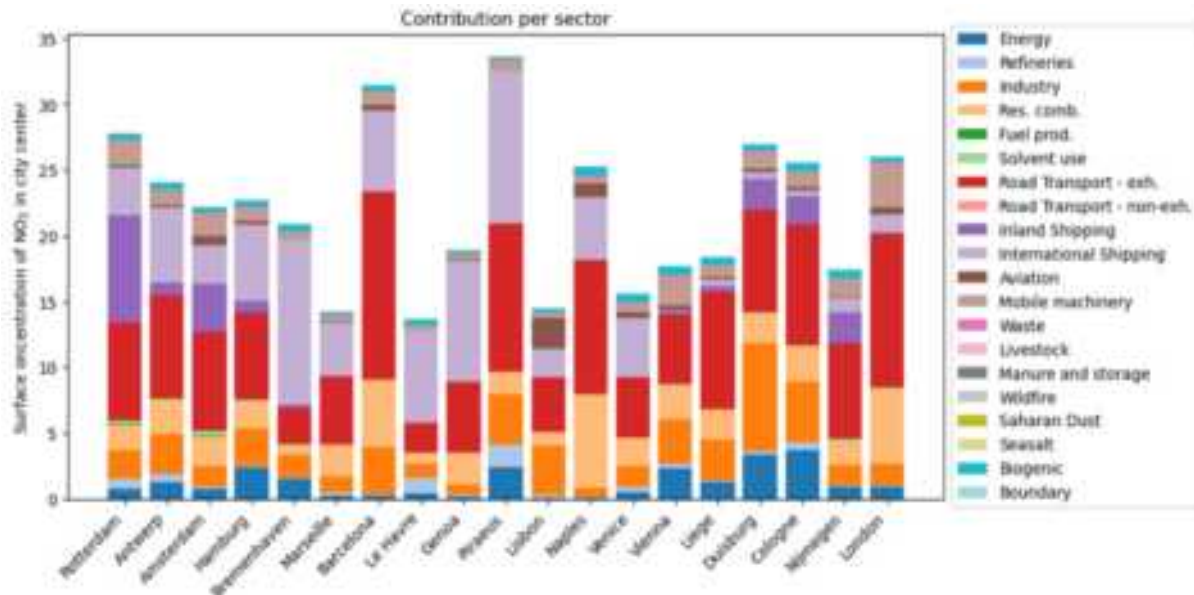


Figure 7: Stacked bar plot showing the predicted absolute contributions from the various labelled sectors to the annual average surface NO_2 in 2018 for the city centre of the port cities of interest.

4. Conclusions

The contribution of international and inland shipping to atmospheric pollutant concentrations in Europe were assessed using the chemical transport model LOTOS-EUROS and its source appointment feature that allows tracing of labelled emitted pollutants. The main findings from the study can be summarised as follows:

- International Shipping contributes significantly to NO_2 concentrations in Europe (18% on average).
- The contribution to other species is lower but still considerable (11% for SO_2 , 2.5-5% for $\text{PM}_{2.5}/\text{PM}_{10}$).
- Locally in the seaports, the influence to NO_2 concentrations is higher and reaches up to 60% (Rotterdam).
- The contribution to NO_2 remains significant in all cities located nearby the seaports, while in many cases, international shipping contribution can be the dominant source (e.g., Piraeus, Hamburg).
- Inland shipping has generally a low influence (0-4%) to NO_2 , with only a few exceptions (Rotterdam, Amsterdam).

References

- Banzhaf S. (2013). Interaction of surface water and groundwater in the hyporheic zone – application of pharmaceuticals and temperature as indicators, *Doktor Der Ingenieurwissenschaften - Dr.-Ing.*
- Banzhaf S., Schaap M., Kerschbaumer A., Reimer E., Stern R., Van Der Swaluw E., Builtjes P. (2012). Implementation and evaluation of pH-dependent cloud chemistry and wet deposition in the chemical transport model REM-Calgrid, *Atmospheric Environment*, 49, 378–390.
- Beelen R., Raaschou-nielsen O., Stafoggia M., Andersen Z. J., Weinmayr G., Hoff B., Wolf, K. (2014). Effects of long-term exposure to air pollution on natural-cause mortality: an analysis of 22 European cohorts within the multicentre ESCAPE project, *Lancet*, 383, 785–795.
- Colette A., Rouil L. (2020): Air Quality Trends in Europe: 2000-2017, Assessment for surface SO₂, NO₂, Ozone, PM₁₀ and PM_{2.5}, *Eionet Report*, ETC/ATNI 2019/16, 36 pp., 202.
- Concawe (2023). The impact of shipping emissions to urban air quality in Europe – Detailed port-city analysis, *Concawe report No. 2/23*.
- Denier van der Gon H., Kooter I., Bronsveld P., Hartendorf F., Korstanje T., Wijngaard M., Dortmans A. (2022). Particulate matter: Standard achieved, problem unsolved, TNO website, <https://www.tno.nl/en/newsroom/insights/2022/07-0/why-current-particulate-matter-standard/>
- Escudero M., Segers A., Kranenburg R., Querol X., Alastuey A., Borge R., de la Paz D., Gangoiti G., Schaap M.: Analysis of summer O₃ in the Madrid air basin with the LOTOS-EUROS chemical transport model. *Atmos. Chem. Phys.*, 19(22), 14211–14232.
- Fountoukis C., Nenes A. (2007). ISORROPIAII: A computationally efficient thermodynamic equilibrium model for K+-Ca2+-Mg2+-NH4+-Na+-SO42--NO3--Cl--H2O aerosols, *Atmos. Chem. Phys.*, 7(17), 4639–4659.
- Jalkanen J., Johansson L., Kukkonen J. (2016). A comprehensive inventory of ship traffic exhaust emissions in the European sea areas in 2011, *Atmos. Chem. Phys.*, 16, 71–84.
- Jonson J. E., Jalkanen J. P., Johansson L., Gauss M., Denier van der Gon, H. A. C. (2015). Model calculations of the effects of present and future emissions of air pollutants from shipping in the Baltic Sea and the North Sea, *Atmos. Chem. Phys.*, 15, 783–798.
- Kranenburg R., Segers A. J., Hendriks C., Schaap M. (2013). Source apportionment using LOTOS-EUROS: module description and evaluation. *Geosci. Model Dev.*, 6(3), 721–733.
- Kuenen J., Dellaert S., Visschedijk A., Jalkanen J.-P., Super I., Denier van der Gon H. A. C. (2022). Copernicus Atmosphere Monitoring Service regional emissions version 5.1 business-as-usual 2020 (CAMS-REG-v5.1 BAU 2020), Copernicus Atmosphere Monitoring Service, ECCAD [data set].
- Manders A. M. M., Builtjes P. J. H., Curier L., Denier van der Gon H. A. C., Hendriks C., et al. (2017). Curriculum Vitae of the LOTOS-EUROS (v2.0) chemistry transport model, *Geosci. Model Dev.*, 10, 4145–4173.
- Pommier M. (2021). Prediction of source contributions to urban background PM10 concentrations in European cities: A case study for an episode in December 2016 using EMEP/MSC-W rv4.15-Part 2: The city contribution, *Geosci. Model Dev.* 14, 4143–4158.
- Skoulidou I., Koukouli M.-E., Manders A., Segers A., Karagkiozidis D., Gratsia M., Balis D., Bais A., Gerasopoulos E., Stavrakou T., Van Geffen J., Eskes H. J., Richter A. (2021): Evaluation of the LOTOS-EUROS NO₂ simulations using ground-based measurements and S5P/TROPOMI observations over Greece, *Atmos. Chem. Phys.*, 21, 5269–5288.
- Thürkow M., Banzhaf S., Butler T., Pültz J., Schaap M. (2023). Source attribution of nitrogen oxides across Germany: Comparing the labelling approach and brute force technique with LOTOS-EUROS, *Atmospheric Environment*, 292, 119412.
- Timmermans R., van Pinxteren D., Kranenburg R., Hendriks C., Fomba K., Herrmann H., Schaap M. (2022). Evaluation of modelled lotos-euros with observational based pm10 source attribution, *Atmospheric Environment*, 14, 100173.
- Van Zanten M. C., Sauter F. J., Wichink Kruit R. J., Van Jaarsveld J. A., Van Pul W. A. J. (2010): Description of the DEPAC module: Dry deposition modelling with DEPAC GCN2010, *RIVM report 680180001/2010*, Bilthoven, The Netherlands, 74 pp.
- Whitten D. G. (1980). Photoinduced Electron-Transfer Reactions of Metal Complexes in Solution, *Accounts of Chemical Research*, 13(3), 83–90.
- Wichink Kruit R. J., Schaap M., Sauter F. J., Van Zanten M. C., Van Pul W. A. J. (2012). Modeling the distribution of ammonia across Europe including bi-directional surface-atmosphere exchange, *Biogeosciences*, 9(12), 5261–5277.

Potential impact of shipping on PM_{2.5} species in the Mediterranean region - a multi-model evaluation

Lea Fink^{*1}, Matthias Karl¹, Volker Matthias¹, Sonia Oppo², Richard Kranenburg³, Jeroen Kuenen³, Sara Jutterström⁴, Jana Moldanova⁴, Elisa Majamäki⁵, Jukka-Pekka Jalkanen⁵

¹Helmholtz-Zentrum Hereon, Institute of Coastal Environmental Chemistry, 21502 Geesthacht, Germany

²AtmoSud, Air Quality Observatory in the Provence-Alpes-Côte d'Azur region, 13390 Marignane, France

³TNO, Netherlands Organization for Applied Scientific Research, 3584 CB Utrecht, The Netherlands

⁴IVL, Swedish Environmental Research Institute, 411 33 Göteborg, Sweden

⁵FMI, Finnish Meteorological Institute, FI-00560 Helsinki, Finland

Introduction

Maritime transport plays an essential role in the international trade of goods of the European Union (EU) with almost 90% of the EU import and export freight trade being seaborne (Karl et al. 2019). The use of maritime transport for EU trade has increased over the last ten years. The number of active ships in 2030 is expected to be twice as high compared to 2016 (Eurostat Press Office, 2016).

With main routes for short sea and international shipping, the Mediterranean Sea is a region with dense shipping, resulting in high air pollution at coastal regions. Previous research has found that the increase in PM_{2.5} (particulate matter < 2.5 μm) concentrations induced by shipping emissions is small in Europe (Viana et al., 2009). Nonetheless, the relative ship influence on PM_{2.5} concentration in the Mediterranean area is high, accounting for 5% to 20% of total PM_{2.5} concentration (e.g., Aksoyoglu et al., 2016, Nunes et al., 2020). Especially secondary formation of inorganic aerosol contributes the largest part to ship contribution to ambient PM_{2.5}. Exposure to PM_{2.5} has been linked to the development of certain respiratory illnesses, cancer, and type 2 diabetes (Heusinkveld et al., 2016; Chen et al., 2016; Gao and Sang, 2020).

Regional air quality modeling is important to evaluate air quality. Results can be used as guidance to enhance air quality management strategies, which are important regarding the impact of air pollution on human health and the environment. A number of regional scale 3-D chemistry transport model (CTM) systems are available for the simulation of the transport, chemical transformation and fate of atmospheric pollutants. Although these models are steadily improved, intercomparison studies have shown that they often underestimate the PM_{2.5} concentration. Im et al. (2015) reported an underestimation of particulate matter in their intercomparison study with largest underestimations observed in the Mediterranean region.

In the present study, five different chemistry transport models (CAMx, CHIMERE, CMAQ, EMEP, LOTOS-EUROS) are used to evaluate and compare modelled concentrations of air pollutants in the Mediterranean Sea. The main focus was to compare the output of the models regarding the concentration of PM_{2.5} and to calculate the potential ship impact to total air pollution concentration. The model performance was quantified by comparing modelled data against data measured at background stations in coastal areas of the Mediterranean Sea. As ships contribute mainly to the formation of inorganic particle species, focus was laid on NH₄⁺, SO₄²⁻, NO₃⁻ as well as their precursors.

Model Setup & Methods

Emission part of the set-up was the same for all five models: ship emissions were calculated with the Ship Traffic Emission Assessment Model (STEAM, version 3.3.0; Jalkanen et al. 2012) and land-based emissions were taken from the CAMS-REG v2.2.1 dataset (further development of the inventory described in Kuenen et al. 2022) for a domain comprising the Mediterranean Sea on a resolution of 12x12 km² (or 0.1° x 0.1°). Meteorological data as well as boundary and initial conditions differed among the model runs as all CTMs used their standard set-up. This was done because a change of the meteorological driver of a CTM is often very difficult and might be connected with unwanted errors in the simulations. With all models a reference run for the current air quality situation was performed including all run options: base case, and one run without the emissions from shipping

In each port case the zero-out method was used to determine the potential ship impact. The modelled year was 2015.

The models used in the intercomparison are CAMx v6.50 (Ramboll Environ., 2016), CHIMERE 2017r4 (Menut et al., 2013), CMAQ v5.2 (Byun and Schere, 2006; Appel et al., 2017), EMEP MSC-W (Simpson et al., 2012; Simpson et al., 2020), LOTOS-EUROS v2.0 (Manders et al., 2017).

Based on the daily files, the annual averaged ensemble mean is derived from the results of all models. All of the model run outputs included PM_{2.5} in µg/m³ at a daily resolution on a 2D grid from the lowest layer and were given as a netcdf file in accordance with CF standards. For the intercomparison, concentrations in the lowest layer closest to the ground were employed. Depending on the major physical and chemical mechanisms used, the CTM systems computed PM_{2.5} concentrations in various ways.

Model results for total surface concentrations of PM_{2.5} from the five CTM simulations are evaluated against available measurements of the air quality monitoring network from the European Environment Agency (EEA, 2021).

Results & Discussion

The current work examines and analyses the predictions of five different CTM systems for the dispersal and transformation of PM_{2.5} and inorganic particles (NH₄⁺, SO₄²⁻, NO₃⁻) in the Mediterranean region. In addition to the total concentration, the potential ship impact is taken into account. The results show that four of the five models underestimated the actually measured PM_{2.5} concentrations at stations near the European coast (Table 1). Considering the spatial distribution, the potential impacts of PM_{2.5} from ships simulated by CAMx, LOTOS-EUROS and EMEP have the largest ranges with values up to 25% along the main shipping routes in the Mediterranean Sea. CMAQ and CHIMERE simulated potential ship impacts of 15% along major shipping lanes near the African coast. These impacts are within the range of ship impacts determined in other studies (Figure 1).

Table 1: Correlation (R), normalized mean bias (NMB), root mean square error (RMSE) for daily PM_{2.5} values for 2015 over all 28 stations.

	Correlation	NMB	RMSE
CAMx	0.19	-0.33	11.5
CHIMERE	0.02	0.06	11.1
CMAQ	0.50	-0.42	10.7
EMEP	0.17	-0.33	12.2
LOTOS-EUROS	0.54	-0.53	10.9

Various reasons for underestimation of PM_{2.5} in regional CTM systems could be attributed to model-specific calculations. Studies have shown that these might be linked to meteorological parameters and to the overestimate of vertical mixing in the lower atmosphere. In addition, the mechanisms for calculating the equilibrium between the gas and aerosol phases can differ among the CTM systems and lead to underestimations. One other reason for underestimations of PM_{2.5} by CTMs might be the missing descriptions of secondary organic aerosol processes in the model.

A number of reasons and combinations of reasons can lead to underestimations of PM_{2.5} in the CTM systems used in the present study.

For a better understanding, the inorganic particle species are considered, since inorganic aerosols account for a higher percentage of ship-related PM_{2.5} concentrations emissions compared to organic aerosols.

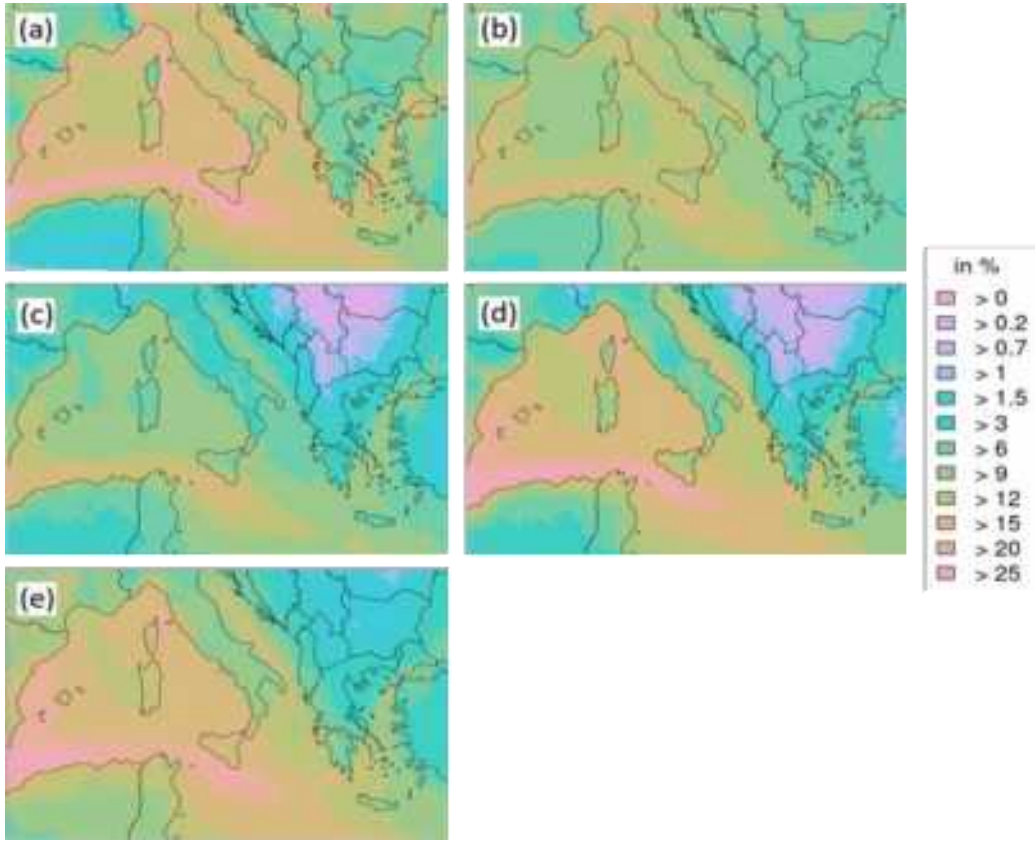


Figure 1: Annual mean PM_{2.5} relative potential ship impact. (a) = CAMx, (b) = CHIMERE, (c) = CMAQ, (d) = EMEP, (e) = LOTOS-EUROS

Sulfate is the main contributor to the total PM_{2.5} concentration related to ship emissions. For the median of model ensemble mean for absolute ship concentration, SO₄²⁻ accounts for about the half of PM_{2.5} (Median SO₄²⁻ ~0.4 µg/m³; Median PM_{2.5}: ~0.8 µg/m³; Figure 2). With regard to the absolute ship impact on SO₄²⁻, the model simulations show similar concentrations and are to a certain degree lower for CMAQ and LOTOS-EUROS.

Ammonium in atmospheric aerosols preferentially binds to SO₄²⁻ to form (NH₄)₂SO₄, thus less NH₄NO₃ is formed in areas above water. Higher concentrations over land than over water are expected due to NH₄NO₃ formation in areas characterized by high NH₃ and HNO₃ conditions and low SO₄²⁻ conditions. This explains the high values for sulfate in the present study, since the domain mainly covers the water areas of the Mediterranean area.

The potential impacts of ships on NO₃⁻ differ between models. CAMx and CMAQ results are similar high (~ 0.1 µg/m³) whereas for CHIMERE and EMEP absolute potential ship impact is rather low (~ 0.05 µg/m³). Low nitrate levels can be explained by the preferential formation of (NH₄)₂SO₄, which keeps nitrate in the gas phase or converts it to the coarse mode. These low values for SO₄²⁻ and NO₃⁻ in CMAQ, but relatively high values for EMEP, CAMx and LOTOS are reflected in the PM_{2.5} ship impacts and partially explain the variation in PM_{2.5} between the models.

The preference of NH₄⁺ to bind to SO₄²⁻ to form (NH₄)₂SO₄ in atmospheric aerosols explains why in some models NO₃⁻ shows relatively low values when the SO₄²⁻ concentration is high. For example, CHIMERE has an NO₃⁻ annual median of about 0.05 µg/m³ and for SO₄²⁻ an annual median of about 0.4 µg/m³, while in the CAMx results NO₃⁻ is about 0.1 µg/m³ but for SO₄²⁻ around 0.25 µg/m³.

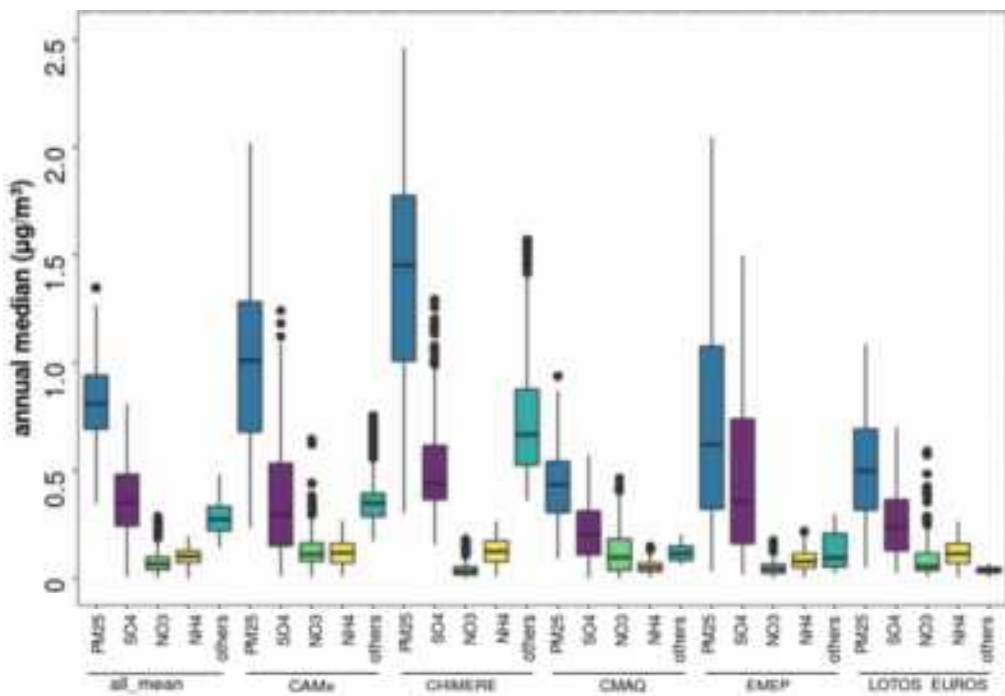


Figure 2: Boxplots for potential ships impact concentrations of $\text{PM}_{2.5}$, and the $\text{PM}_{2.5}$ components SO_4^{2-} , NO_3^- , NH_4^+ and "others" as simulated by the five CMs. The variable "others" is full median $\text{PM}_{2.5}$ calculated as $\text{PM}_{2.5}$ minus the sum of SO_4^{2-} , NO_3^- and NH_4^+ .

Acknowledgements

This work supported by SCIPER project which has received funding from the European Union's Horizon 2020 research and innovation programme under grant agreement Nr.814893. AtmoSud acknowledges the continuous support of CAMx by RAMBOLL and CHIMERE by LMD. The Community Multiscale Air Quality Modelling System (CMAQ) is developed and maintained by the USEPA. Its use is gratefully acknowledged. Ronny Petrik from Helmholtz-Zentrum Hereon (now at Marinekommando Deutsche Marine, Rostock) is acknowledged for providing meteorology and boundary conditions for CMAQ runs.

The computations for the regional modeling using the EMEP-model was enabled by resources provided by the Swedish National Infrastructure for Computing (SNIC), partially funded by the Swedish Research Council through grant agreement no. 2018-05973.

Support from Meteorological Synthesizing Center – West of EMEP at Norwegian Meteorological Institute, especially Peter Wind and David Simpson, in implementation of emissions and meteorological fields used in this paper into EMEP Open Source model is gratefully acknowledged.

References

- Aksoyoglu, S., Baltensperger, U., and Prévôt, A. S. H. (2016). Contribution of ship emissions to the concentration and deposition of air pollutants in Europe, *Atmos. Chem. Phys.*, 16, 1895–1906, <https://doi.org/10.5194/acp-16-1895-2016>.
- Appel, K. W., Napelenok, S. L., Foley, K. M., Pye, H. O. T., Hogrefe, C., Luecken, D. J., Bash, J. O., Roselle, S. J., Pleim, J. E., Foroutan, H., Hutzell, W. T., Pouliot, G. A., Sarwar, G., Fahey, K. M., Gantt, B., Gilliam, R. C., Heath, N. K., Kang, D., Mathur, R., Schwede, D. B., Spero, T. L., Wong, D. C., and Young, J. O. (2017). Description and evaluation of the Community Multiscale Air Quality (CMAQ) modeling system version 5.1, *Geosci. Model Dev.*, 10, 1703–1732, <https://doi.org/10.5194/gmd-10-1703-2017>.
- Byun, D. and Schere, K. L. (2006). Review of the Governing Equations, Computational Algorithms, and Other Components of the Models-3 Community Multiscale Air Quality (CMAQ) Modeling System, *Appl. Mech. Rev.*, 2, <https://doi.org/10.1115/1.2128636>.
- Chen, R., Hu, B., Liu, Y., Xu, J., Yang, G., Xu, D., and Chen, C.: Beyond PM_{2.5}: The role of ultrafine particles on adverse health effects of air pollution, *Biochim Biophys Acta*, 1860(12), 2844-2855, <https://doi.org/10.1016/j.bbagen.2016.03.019>, 2016. European Environment Agency EEA (2021). Download service: <https://discomap.eea.europa.eu/map/fme/AirQualityExport.htm>. Access 16.03.2021.
- Eurostat (2021): Maritime transport statistics - short sea shipping of goods. https://ec.europa.eu/eurostat/statistics-explained/index.php?title=Maritime_transport_statistics_-_short_sea_shipping_of_goods#Italy_and_the_Netherlands_accounted_for_almost_30.25_of_EU_short_sea_shipping_in_2019. ISSN 2443-8219. Access 15.06.2021.
- Eurostat Press Office (2016). World Maritime Day. Half of EU trade in goods is carried by sea, *Eurostat Press Office*, News Release 184/2016, <https://ec.europa.eu/eurostat/documents/2995521/7667714/6-28092016-AP-EN.pdf>. Access 20 January 2023.
- Eyring, V., Isaksen, I., Berntsen, T. et al. (2009). Transport impacts on atmosphere and cli-mate: Shipping, *Atmos. Environ.*, 44, 4735–4771. <https://doi.org/10.1016/j.atmosenv.2009.04.059>.
- Gao, R. and Sang, N.: Quasi-ultrafine particles promote cell metastasis via HMGB1-mediated cancer cell adhesion, *Environ. Pollut.*, 256, 113390, <https://doi.org/10.1016/j.envpol.2019.113390>, 2020.
- Heusinkveld, H. J., Wahle, T., Campbell, A., Westerink, R. H. S., Tran, L., Johnston, H., Stone, V., Cassee, F. R., and Schins, R. P. F.: Neurodegenerative and neurological disorders by small inhaled particles, *NeuroToxicology*, 56, 94-106, <https://doi.org/10.1016/j.neuro.2016.07.007>, 2016.
- Im, U., Bianconi, R., Solazzo, E., Kioutsoukis, I., Badia, A., Balzarini, A., Baró, R., Bellasio, R., Brunner, D., Chemel, C., Curci, G., van der Denier Gon, H., Flemming, J., Forkel, R., Giordano, L., Jiménez-Guerrero, P., Hirtl, M., Hodzic, A., Honzak, L., Jorba, O., Knoté, C., Makar, P. A., Manders-Groot, A., Neal, L., Pérez, J. L., Pirovano, G., Pouliot, G., San Jose, R., Savage, N., Schroder, W., Sokhi, R. S., Syrakov, D., Torian, A., Tuccella, P., Wang, K., Werhahn, J., Wolke, R., Zabkar, R., Zhang, Y., Zhang, J., Hogrefe, C., and Galmarini, S. (2015). Evaluation of operational online-coupled regional air quality models over Europe and North America in the context of AQMEII phase 2. Part II: Particulate matter, *Atmos. Environ.*, 115, 421-441, <https://doi.org/10.1016/j.atmosenv.2014.08.072>.
- Jalkanen, J.-P., Johansson, L., Kukkonen, J., Brink, A., Kalli, J., and Stipa, T. (2012). Extension of an assessment model of ship traffic exhaust emissions for particulate matter and carbon monoxide, *Atmos. Chem. Phys.*, 12, 2641–2659, <https://doi.org/10.5194/acp-12-2641-2012>.
- Karl, M., Bieser, J., Geyer, B., Matthias, V., Jalkanen, J.-P., Johansson, L., and Fridell, E. (2019). Impact of a nitrogen emission control area (NECA) on the future air quality and nitrogen deposition to seawater in the Baltic Sea region, *Atmos. Chem. Phys.*, 19, 1721–1752, <https://doi.org/10.5194/acp-19-1721-2019>.
- Kuenen, J., Dellaert, S., Visschedijk, A., Jalkanen, J.-P., Super, I., and Denier van der Gon, H.: CAMS-REG-v4: a state-of-the-art high-resolution European emission inventory for air quality modelling, *Earth Syst. Sci. Data*, 14, 491–515, <https://doi.org/10.5194/essd-14-491-2022>, 2022.
- Manders, A. M. M., Builtjes, P. J. H., Curier, L., van der Denier Gon, H. A. C., Hendriks, C., Jonkers, S., Kranenburg, R., Kuenen, J. J. P., Segers, A. J., Timmermans, R. M. A., Visschedijk, A. J. H., Wichink Kruit, R. J., van Pul, W. A. J., Sauter, F. J., van der Swaluw, E., Swart, D. P. J., Douros, J., Eskes, H., van Meijgaard, E., van Ulft, B., van Velthoven, P., Banzhaf, S., Mues, A. C., Stern, R., Fu, G., Lu, S., Heemink, A., van Velzen, N., and Schaap, M. (2017). Curriculum vitae of the LOTOS-EUROS (v2.0) chemistry transport model, *Geosci. Model Dev.*, 10, 4145–4173, <https://doi.org/10.5194/gmd-10-4145-2017>.
- Menut, L., Bessagnet, B., Khvorostyanov, D., Beekmann, M., Blond, N., Colette, A., Coll, I., Curci, G., Foret, G., Hodzic, A., Mailler, S., Meleux, F., Monge, J.-L., Pison, I., Siour, G., Turquety, S., Valari, M., Vautard, R., and Vivanco, M. G. (2013). CHIMERE 2013: A model for regional atmospheric composition modelling, *Geosci. Model Dev.*, 6, 981–1028, <https://doi.org/10.5194/gmd-6-981-2013>.

Nunes, R. A. O., Alvim-Ferraz, M. C. M., Martins, F. G., Calderay-Cayetano, F., Durán-Grados, V., Moreno-Gutiérrez, J., Jalkanen, J.-P., Hannunniemi, H., and Sousa, S. I. V. (2020). Shipping emissions in the Iberian Peninsula and the impacts on air quality, *Atmos. Chem. Phys.*, 20, 9473–9489, <https://doi.org/10.5194/acp-20-9473-2020>.

Ramified Environment and Health User Guide EMISSIONS AND AIR QUALITY MODEL WITH EMISSIONS FROM SHIPS, https://camx-wp.azurewebsites.net/Files/CAMxUsersGuide_v7.10.pdf.

Simpson, D., Benedictow, A., Berge, H., Bergström, R., Emberson, L. D., Fagerli, H., Flechard, C. R., Hayman, G. D., Gauss, M., Jonson, J. E., Jenkin, M. E., Nyíri, A., Richter, C., Semeena, V. S., Tsyro, S., Tuovinen, J.-P., Valdebenito, Á., and Wind, P. (2012). The EMEP MSC-W chemical transport model – technical description, *Atmos. Chem. Phys.*, 12, 7825–7865, <https://doi.org/10.5194/acp-12-7825-2012>.

Simpson, D., Bergström, R., Briolat, A., Imhof, H., Johansson, J., Priestley, M., and Valdebenito, A. (2020). GenChem v1.0 – a chemical pre-processing and testing system for atmospheric modelling, *Geosci. Model Dev.*, 13, 6447–6465, <https://doi.org/10.5194/gmd-13-6447-2020>.

Smith, T. W. P., Jalkanen, J. P., Anderson, B. A. et al. (2014). Third IMO GHG Study 2014. *Tech. rep. International Maritime Organization (IMO)*. London. UK.

Viana, M., Amato, F., Alastuey, A., Querol, X., Moreno, T., Dos Santos, S. G., Herce, M. D., and Fernández-Patier, R. (2009). Chemical tracers of particulate emissions from commercial shipping, *Environ. Sci. Technol.*, 43(19), 7472–7477, <https://doi.org/10.1021/es901558t>.

A numerical CFD model to quantify traffic-related pollutant concentrations in urban scale.

G. Ioannidis¹, T. Riedel², C. Li², P. Tremper², L. Ntziachristos¹

¹ Laboratory of Applied Thermodynamics, Department of Mechanical Engineering, Aristotle

University of Thessaloniki, Thessaloniki, 54124, Greece

² Institute for Telematics, TECO, Karlsruhe Institute of Technology, Karlsruhe, 76131, Germany

Introduction

Urban environments face significant challenges in terms of atmospheric pollution. The residents of these areas are directly impacted by anthropogenic emissions, leading to their daily exposure to harmful gaseous and particulate pollutants. Consequently, poor air quality is associated with health issues and respiratory diseases (Zhang & Batterman, 2013). Specifically, in urban regions like Augsburg, pollutants such as CO, NO_x, and Particulate Matter are prevalent, primarily originating from vehicular activity. Slemr et al. (2002) revealed that traffic activity accounts for 54% of NO_x concentrations and 88.5% of CO concentrations in the broader Augsburg area. Qadir et al. (2014) conducted a source apportionment study in Augsburg, highlighting that 28% of PM₁₀ concentrations can be attributed to vehicular activity. Therefore, monitoring the concentrations of these three pollutants is crucial for accurately assessing the levels of hazardous contaminants present in the environment.

The assessment of air quality in urban areas has always been a challenging task. To assess pollution levels of different contaminants, Air Quality monitoring stations are positioned throughout cities. These stations have limitations as they only measure what enters their path of deduction, thus failing to fully capture the overall pollution condition of the wider area. To overcome this limitation, Air Quality models are employed to represent and predict pollution in urban regions, considering various pollution sources that contribute to the deterioration of the atmosphere. In this study, a CFD model has been developed offering a high spatial resolution compared to measuring stations. This model has the capability to construct reliable 3D pollution maps based on meteorological and emission scenarios.

The objective of this study is to employ Computational Fluid Dynamics to predict pollutant concentrations at a micro scale and validate the model using measurement data. Additionally, the simulated concentrations are utilized to evaluate the extent to which the Air Quality stations accurately represent the pollution levels in the broader area where they are located. The model uses traffic-related emissions of CO, NO_x that were calculated using COPERT and PM₁₀ that were estimated using emission factors of that period. All the emission are based on traffic activity levels observed in September 2018.

Digital model and CFD setup

The study focuses on a specific area measuring 1.6 km x 2 km, which encompasses a significant portion of Augsburg's city center in Germany. Within this area, two official Air Quality stations, operated by the Bavarian State Office of Environment, monitor various pollutants such as PM₁₀, CO, NO and NO₂. Figure 1 illustrates the positioning of these stations, with the Karlstraße (KS) station situated in the northern part of the domain and the Königsplatz (KP) station positioned at the center. The KS station is placed at a height of 2.5m above the ground, while the KP station is elevated at 4m. The measurements provided by these stations offer hourly

levels measured in $\mu\text{g m}^{-3}$.

The geometric characteristics of the area under investigation were extracted from the

OpenStreetMap open-source platform. To create a computational mesh on the building surfaces, a pre-processing procedure was implemented to clean and smooth the geometry. This process involved correcting any flawed points in the acquired geometry. Blocken (2015) suggests that the design of the computational domain should have a minimum height of 6H and an upstream distance of 5H, where H represents the height of the tallest building in the area. Emission sources were then established along the main arterial roads. These sources were represented as rectangular elements within the computational domain, corresponding to sections of the

road where vehicles travel. The width of these sources was set at 8m, which aligns with the typical road width. The developed CFD model employed a tetrahedral unstructured mesh with a growth rate of 1.2. The mesh resolution on the buildings was set to 2m, while it was 0.5m for the emission sources and 20m for the boundaries of the domain. In total, the volume mesh comprised of 54 million elements.

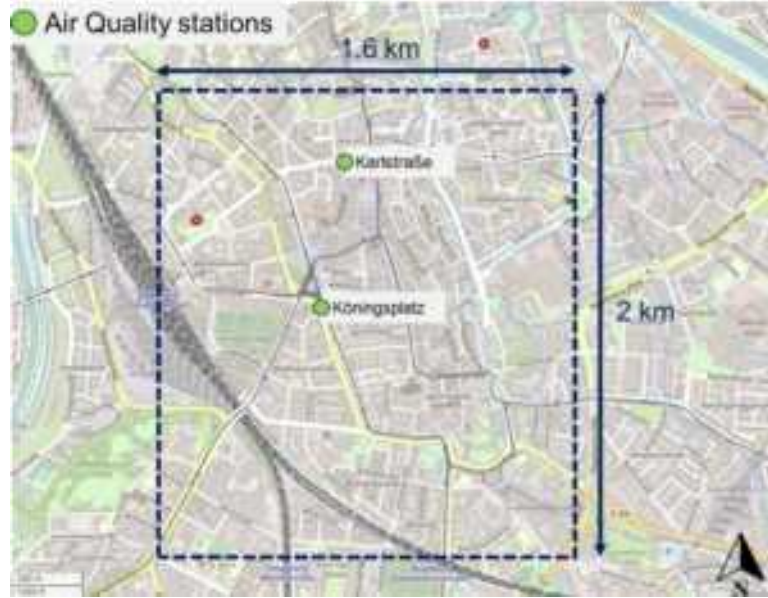


Figure 1. Area of interest containing two official AQ stations

Figure 2 presents the areas where the Air Quality (AQ) stations are located, shown in the left column, and their corresponding representation in the digital model, depicted in the right column. The comparison of the modelled concentrations with the measured values is conducted at the exact height and coordinates as the real location. This represents a notable advantage of utilizing a CFD model, as it enables the generation of representative concentrations, considering the surrounding geometrical characteristics of the area.

The pollutant dispersion modelling is carried out using the open-source CFD code OpenFOAM. The numerical solver utilized in this study is simpleFoam, which employs the RANS equations to solve for the velocity field (Peralta et al., 2014). To account for the dispersion of pollutants, the passive scalar transport equation (Eq. 1) is incorporated into the modified solver, and the code is compiled into the system accordingly. This approach allows for the simulation of passive pollutant dispersion (Elfversson & Lejon, 2021; Miao et al., 2014).

$$\frac{\partial C}{\partial t} + \frac{\partial(\bar{u}_j C)}{\partial x_j} - \frac{\partial}{\partial x_j} \left((D_t + D_m) \frac{\partial C}{\partial x} \right) = 0 \quad (1)$$

j

$$U(z) = \frac{u^*}{\kappa} \ln \left(\frac{z + z_0}{z} \right) \quad (2)$$

In equation (1), the term D_t represents the turbulent diffusion coefficient, while D_m represents the molecular diffusion coefficient. For CO, the molecular diffusion coefficient at a temperature of 20°C is reported to be 2.08e-5 m²/s (Cleary et al., 2015). In the case of NO_x traffic emissions, which predominantly consist of NO, a portion of it is oxidized in the atmosphere to form NO₂ (Rivas et al., 2019). For simulation purposes, the NO_x mixture is simulated as NO₂, with a diffusion coefficient of 1.56e-5 m²/s (Cape, 2005). For the RANS simulations, the standard k-ε turbulence model is employed, as it has been demonstrated to be the most suitable model for urban pollutant dispersion modelling with CFD in various studies (Amorim et al., 2013; Santiago et al., 2013).

Pantusheva et al. (2022) specifically highlighted that 38% of the examined cases favoured the standard k-ε model.

Regarding the atmospheric velocity profile, equation (2) defines the profile applied at the inlets for each simulation case. U_{inlet} represents the friction velocity, K denotes the Von Karman constant (set to 0.41), and z_0 corresponds to the aerodynamic roughness length at a height of 2m, specifically for urban environments (Irwan Ramli et al., 2009). The simulations were conducted considering the prevailing wind direction during September 2018, which was determined to be a south-western wind direction. As a test case, the period between 13:00 and 14:00 on September 18, 2018, was selected due to its wind direction of 260 degrees.

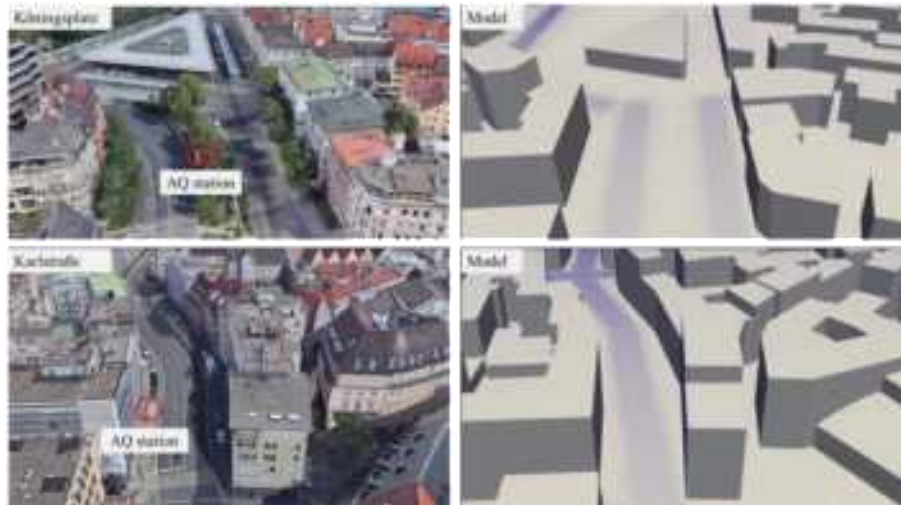


Figure 2. AQ station's location and corresponding area of the model.

Results

The converged simulations of pollutant dispersion provided final concentration values across the entire domain. To directly compare these simulated concentrations with measurements, background concentrations obtained from a background station during the corresponding hour were subtracted from the indications of the AQ stations. This approach helps isolate the urban increment by excluding pollutant concentrations unaffected by the urban area (Jeanjean et al., 2017). The background station, located 5km outside the city, remains unaffected by urban emissions.

Figure 3 illustrates the comparison between simulated and observed values. In Figure 3a, the comparison is shown for the Karlstraße Air Quality station. The deviation between the measured and simulated values is 29% for CO, 31% for NO_x , and close to zero for PM_{10} . Figure 3b demonstrates the comparison at the location of the sensor for the Königsplatz station. The simulated concentration of CO deviates by 27% from the measurement, while NO_x deviates by 41%. For PM_{10} , the modelled concentration shows a deviation of 62%. It is important to highlight that the simulated values consistently fall within the same range as the observed values, and also indicating that the model results are highly accurate with a precision of two decimal places. However, it should be acknowledged that the CFD values consistently underestimate the measurements. This difference could be attributed to the fact that the dispersion model solely considers traffic emissions, neglecting other urban sources like heating, cooking, construction, and waste management, which could potentially contribute to the overall concentration levels. Considering that all the values are within the same range and the average deviation across all cases is approximately 30%, the model results are considered acceptable for the intended purpose. It can be concluded that the model provides correct estimates of traffic-related pollutant concentrations for the entire domain.

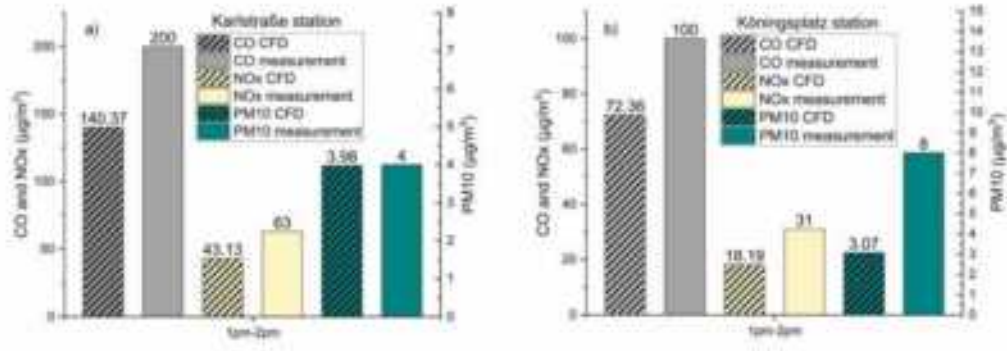


Figure 3. Comparison between simulated and observed values for CO, NO_x and PM₁₀ for Karlstraße station (a) and Königsplatz station (b)

One of the notable advantages of using a CFD model as a dispersion model is its high spatial accuracy, which sets it apart from other mesoscale models. In this study, we aim to leverage this advantage by utilizing the numerous data points available in the vicinity of the sensor location, at a height of 1.5m, representing the average exposure height of the urban population. To evaluate the representativeness of the Air Quality (AQ) station's indication, we consider an area with a radius of 100m centred around the two sensors, as shown in Figure 4 specifically for the case of CO. The criterion employed to assess the representativeness of the simulated concentration within this area is whether it deviates by 20% from the observed indication (Santiago et al., 2021). This criterion provides a measure of agreement between the simulated and observed values, enabling a thorough evaluation of the model's performance in capturing the pollutant concentrations within the immediate vicinity of the AQ station.

The spatial representativeness of the Air Quality (AQ) stations is calculated for the three pollutants, CO, NO_x, and PM₁₀, within the constrained area around the sensor's location. Based on the criteria established, the representativeness of the Karlstraße station indication is found to be 15% for CO and 10% for NO_x, while the Königsplatz station demonstrates a representativeness of 14% for CO and 16% for NO_x. As for PM₁₀, the representativeness is 21% for Karlstraße and 7% for Königsplatz. Rivas et al. (2019) examined the spatial representativeness of AQ stations in the city of Pamplona using CFD for NO₂. They found that for a traffic monitoring station, the representativeness percentage was 17%, indicating that the findings of the work do not deviate greatly from similar studies in literature. It is worth noting that the relatively low representativeness values in this study can be attributed to a significant portion of the wider area around the two sensors consisting of pedestrian roads. The inclusion of traffic emissions as the only source considered in this study could also be a reason of the underestimation of the concentrations.

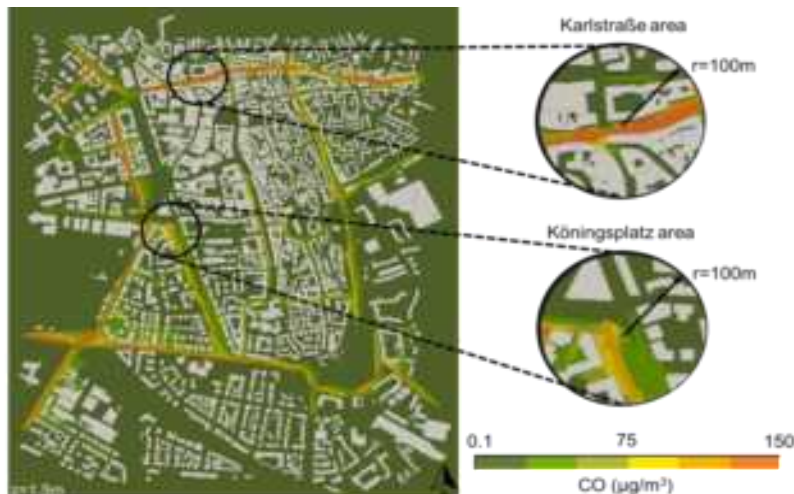


Figure 4. Modelled CO concentration from traffic at $z=1.5\text{m}$. Closeup to the wider area of the two official AQ stations.

Conclusions

This study successfully developed and applied a CFD model to assess air quality, specifically focusing on traffic emissions. Two official measuring stations are located within a 1.6 km x 2 km area, and the model's performance was validated against the indications provided by these sensors. The average deviation between the modelled and measured values for both stations was 28% for CO, 36% for NO_x and 31% for PM₁₀. All the simulated values lie within the same range as the measurements. The criterion set for representativeness was a maximum deviation of 20% from the measured value, within an area of a radius of 100m. The Karlstraße station demonstrated a representativeness of 16% for all three pollutants, while the Königsplatz station showed a representativeness of 13%. This difference in representativeness may be attributed to the presence of more roads within the area surrounding the Karlstraße station, whereas the Königsplatz area includes a tram line. By assessing the spatial representativeness of AQ stations within a constrained area close to the sensor location, it is possible to determine if the stations are correctly placed and whether their indications accurately reflected the pollution situation of the area.

Acknowledgments

This work is supported by GRANT and is part of the ALFA project concerning the "Air Quality in Smart Cities" topic. The University of GRAZ, specifically Ulrich Uhrner and Raphael Reifelshammer, is recognized for their contribution of traffic activity data. Finally, the open-source software OPENFOAM® is a registered trademark of OpenCFD Limited, producer and distributor of the OpenFOAM software via www.openfoam.com.

References

- Amorim, J. H., Rodrigues, V., Tavares, R., Valente, J., & Borrego, C. (2013). CFD modelling of the aerodynamic effect of trees on urban air pollution dispersion. *Science of the Total Environment*, 461–462, 541–551. <https://doi.org/10.1016/j.scitotenv.2013.05.031>
- Blocken, B. (2015). Computational Fluid Dynamics for urban physics: Importance, scales, possibilities, limitations and ten tips and tricks towards accurate and reliable simulations. *Building and Environment*, 91, 219–245. <https://doi.org/10.1016/j.buildenv.2015.02.015>
- Cape, J. N. (2005). Review of the use of passive diffusion tubes for measuring concentrations of nitrogen dioxide in air.
- Cleary, T., Yang, J., & Fernandez, M. (2015). *New Research on Diffusion of Carbon Monoxide through Gypsum Wallboard*.
- Elfversson, D., & Lejon, C. (2021). Use and scalability of openfoam for wind fields and pollution dispersion with building-and ground-resolving topography. *Atmosphere*, 12(9). <https://doi.org/10.3390/atmos12091124>
- Irwan Ramli, N., Idris Ali, M., & Saad, H. (2009). *Estimation of the Roughness Length (z o) in Malaysia using Satellite Image Earthquake View project EVALUATION OF ECONOMICAL ASPECTS TO IMPLEMENT SEISMIC DESIGN FOR NEW REINFORCED CONCRETE BUILDINGS IN MALAYSIA View project*. <https://www.researchgate.net/publication/267769103>
- Jeanjean, A., Buccolieri, R., Eddy, J., Monks, P., & Leigh, R. (2017). Air quality affected by trees in real street canyons: The case of Marylebone neighbourhood in central London. *Urban Forestry and Urban Greening*, 22, 41–53. <https://doi.org/10.1016/j.ufug.2017.01.009>
- Miao, Y., Liu, S., Zheng, Y., Wang, S., & Li, Y. (2014). Numerical study of traffic pollutant dispersion within different street canyon configurations. *Advances in Meteorology*, 2014. <https://doi.org/10.1155/2014/458671>
- Pantusheva, M., Mitkov, R., Hristov, P. O., & Petrova-Antanova, D. (2022). Air Pollution Dispersion Modelling in Urban Environment Using CFD: A Systematic Review. *Atmosphere*, 13(10). <https://doi.org/10.3390/atmos13101640>
- Peralta, C., Nugusse, H., Kokilavani, S. P., Schmidt, J., & Stoevesandt, B. (2014). Validation of the simpleFoam (RANS) solver for the atmospheric boundary layer in complex terrain. *ITM Web of Conferences*, 2, 01002. <https://doi.org/10.1051/itmconf/20140201002>

- Qadir, R. M., Schnelle-Kreis, J., Abbaszade, G., Arteaga-Salas, J. M., Diemer, J., & Zimmermann, R. (2014). Spatial and temporal variability of source contributions to ambient PM10 during winter in Augsburg, Germany using organic and inorganic tracers. *Chemosphere*, 103, 263–273. <https://doi.org/10.1016/j.chemosphere.2013.12.015>
- Rivas, E., Santiago, J. L., Lechón, Y., Martín, F., Ariño, A., Pons, J. J., & Santamaría, J. M. (2019). CFD modelling of air quality in Pamplona City (Spain): Assessment, stations spatial representativeness and health impacts valuation. *Science of the Total Environment*, 649, 1362–1380. <https://doi.org/10.1016/j.scitotenv.2018.08.315>
- Santiago, J. L., Borge, R., Sanchez, B., Quaassdorff, C., de la Paz, D., Martilli, A., Rivas, E., & Martín, F. (2021). Estimates of pedestrian exposure to atmospheric pollution using highresolution modelling in a real traffic hot-spot. *Science of the Total Environment*, 755. <https://doi.org/10.1016/j.scitotenv.2020.142475>
- Santiago, J. L., Martín, F., & Martilli, A. (2013). A computational fluid dynamic modelling approach to assess the representativeness of urban monitoring stations. *Science of the Total Environment*, 454–455, 61–72. <https://doi.org/10.1016/j.scitotenv.2013.02.068>
- Slemr, F., Baumbach, G., Blank, P., Corsmeier, U., Fiedler, F., Friedrich, R., Habram, M., Kalthoff, N., Klemp, D., Kühlwein, J., Mannschreck, K., Möllmann-Coers, M., Nester, K., Panitz, H. J., Rabl, P., Slemr, J., Vogt, U., & Wickert, B. (2002). Evaluation of modeled spatially and temporally highly resolved emission inventories of photosmog precursors for the city of Augsburg: The experiment EVA and its major results. *Journal of Atmospheric Chemistry*, 42(1), 207–233. <https://doi.org/10.1023/A:1015712611966>
- Zhang, K., & Batterman, S. (2013). Air pollution and health risks due to vehicle traffic. *Science of the Total Environment*, 450–451, 307–316. <https://doi.org/10.1016/j.scitotenv.2013.01.074>

Estimate of health benefits if air pollution goals are achieved along highways

L. Broman¹, B. Lövenheim¹, H. Kriit³ and C. Johansson^{1,2}

¹Environment and health administration, SLB-analys, 104 20 Stockholm, Sweden

²Department of Environmental Science, Stockholm University, 10691 Stockholm, Sweden

³Department of Public Health and Clinical Medicine, Umeå University, Umeå, Sweden

Presenting author email: lina.broman@slb.nu

Introduction

Road traffic emissions are among the most important sources of many air pollutants like NO₂ and PM10 and it is the most important source of exposure to many pollutants in densely trafficked cities. In Sweden, the road authorities are responsible for taking action to reduce air pollution exposure of people living close to roads. PM10 is the most problematic air pollutant in comparison to the limit values and objective. Concentrations of PM10 exceed EU air quality directives along large parts of the highways in the county of Stockholm. Also exceeded is the environmental quality objective for PM10. The objectives aim to ensure that concentrations of air pollutants do not exceed low-risk levels for cancer or target values for protection against diseases or impacts on plants, animals, materials, and cultural objects. The most important actions to achieve limit values and national objectives include reducing the use of studded winter tyres, reducing speed limits, and actions to reduce road traffic.

The project aims to estimate the health benefits for the population if the limit values and objectives were achieved along the highways in the Stockholm region.

Methodology

We have calculated

1. the concentrations of PM10 within 200 m along the highways
2. the concentration reductions required to achieve the annual and daily limit values and goals
3. the corresponding reduction in population exposure of the population
4. the health benefits
5. the benefits in terms of reduced societal costs associated with the exposure.

A Gaussian air quality dispersion model (<https://www.airviro.com/airviro/>) is used to calculate concentrations of PM10 within 200 m along the highways and the concentration reductions required to achieve the annual and daily limit values, upper assessment threshold, and the national goal 2020 and 2030. Concentrations within the road area are not considered – road width is obtained from the National Road database. Exposure of drivers along roads is not included. Geographic resolution in the calculations varies depending on the emissions from 35 m by 35 m to 500 m by 500 m. Contributions to the concentrations from sources outside of the domain are taken from measurements at a rural location where local source contributions are negligible.

Wear of the road asphalt is the most important emission of PM10 and this is taken into account using the Nortrip model (Denby et al., 2013). The Nortrip model calculates emissions of PM10 from the wear of roads, brakes, and tyres and the suspension of road dust depending on dust load, type of tyres, vehicle speed, road surface moisture, and sanding/salting. The model has been validated by comparison with measurements at different sites including Hornsgatan in Stockholm. Traffic amounts, speed limits, number of lanes, etc. on highways are obtained from the National Road Database (<https://www.nvdb.se/sv/about-nvdb/>).

Meteorological conditions were based on a climatology created from 21 years of meteorological measurements (15 min averages) in a 50 m high mast located in the southern part of Stockholm. A deterministic wind model is used to generate a wind field over the whole calculation domain. This model considers variations in surface roughness, land use, topography, etc. Concentrations are calculated at 2 m above the surface. Individual buildings and street canyons were not resolved but treated using a roughness parameter.

Population-weighted exposure is estimated based on concentrations at residential addresses in the whole county of Stockholm. Total number of people in every 100 x 100 m grid is obtained from Statistics Sweden and represents the situation 2020-12-31.

Health benefits and societal costs are based on estimated PM2.5 exposure according to a recent evaluation for Swedish road traffic emissions based on a review of epidemiological studies (Forsberg et al., 2021). The change in the population health outcomes is calculated as:

$$\Delta Y = Y_0 [1 - e^{(-\beta \Delta C)}]$$

where

~~ΔY is the change in the health outcome~~

Y_0 is the baseline health incidence of the outcome

β is the dose-response factor (equal to the logarithm of relative risk) per $\mu\text{g}/\text{m}^3$,

~~ΔC is the change in population exposure ($\mu\text{g}/\text{m}^3$)~~

Baseline incidence for different outcomes is taken from national health registers. The cost of health is calculated according to the REVSEK project based on typical national population exposure modeling. The cost is 8163 SEK per $\mu\text{g}/\text{m}^3$ persons) (Forsberg et al. (2021)). This refers to 2017 and it includes costs associated with e.g mortality, stroke, diabetes, and childhood asthma. Premature mortality constitutes the highest cost (61% of the total costs) and is calculated considering the value of quality-adjusted life years.

Population data

The total number of people living within 200 m of the state highways is ca 393 500, which is 16% of the total population in Stockholm (2 386 632).

Table 1 shows that 335 and 390 people living within this zone were exposed to concentrations above the limit value during 2020 and 2030 respectively. Corresponding number of people living in areas with concentrations above the national PM10 goal was 16 435 and 22 460 for 2020 and 2030, respectively.

Table 1: Number of people exposed above the limit value, the upper assessment threshold, and the Swedish environmental quality objective in 2020 and 2030.

	2020	2030
AQ daily limit value ($50 \mu\text{g}/\text{m}^3$) ¹	335	390
Upper assessment threshold, daily ($35 \mu\text{g}/\text{m}^3$) ¹	3545	4950
Environmental quality objective, annual mean ($15 \mu\text{g}/\text{m}^3$)	16 435	22 460

¹ Not to be exceeded more than 35 days.

Required reductions in emissions and concentrations

Calculations have been performed for Stockholm's entire state road network, divided into smaller road sections (between traffic junctions). Figure 1 shows the reduction of the PM10 concentration that is necessary to reach limit values along a part of the E4 highway in northern Stockholm (Tpl Bredden -Tpl Rotebro and Tpl Rotebro-Tpl Häggvik).

The calculations show that large reductions in studded winter tyre share and/or vehicle speed are required to achieve the PM10 limit values in 2030:

- The maximum studded tyre share needs to be reduced from today's values of 60% to 11% and 16% for the two highway stretches respectively.
- The needed reduction in PM10 can also be achieved by reducing the traffic speed by 41 km/h and 37 km/h respectively.

Up to 20 $\mu\text{g}/\text{m}^3$ lower PM10 concentration is needed to achieve the environmental quality goals for the same highway section (Figure 2).

As a single measure, neither a reduction of the traffic speed nor a reduction of the studded tyre share is estimated to be effective enough to reduce the PM10 level to the environmental quality goal. Rather, a combination of measures such as limitation traffic volumes, traffic speed, and reduction of studded tyre share could be effective to reach the air quality goals.

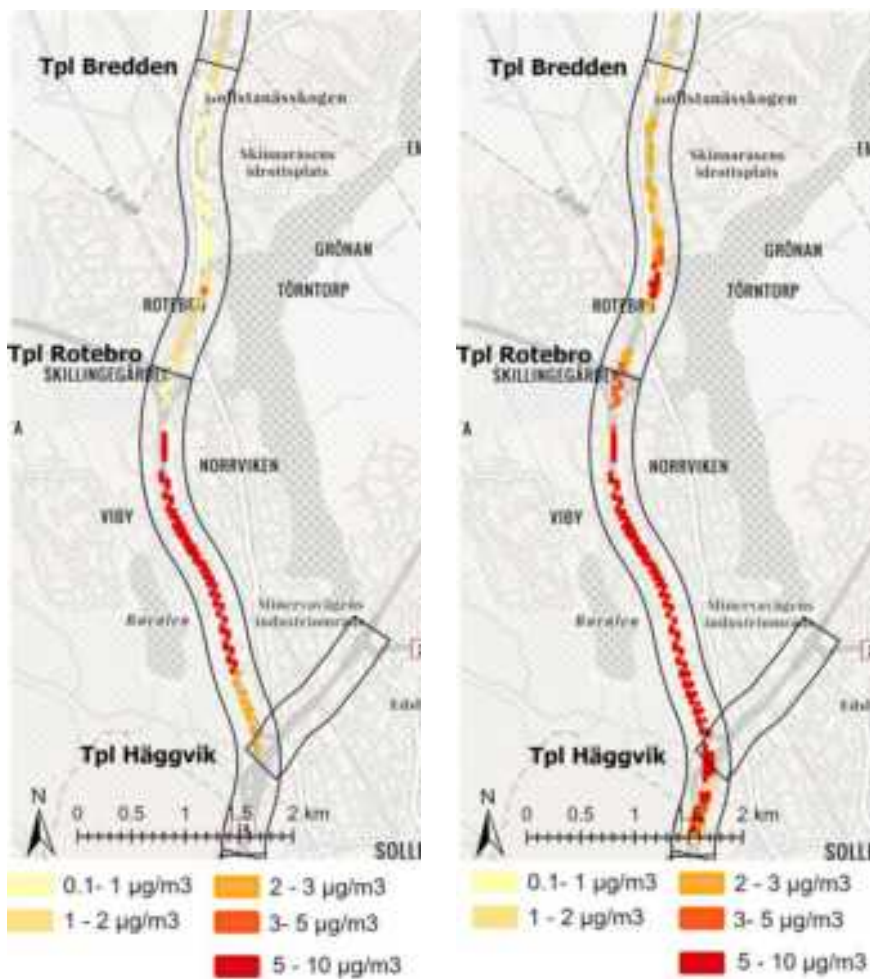


Figure 1: Concentration reductions needed within 200 m along part of the E4 highway to achieve environmental air quality limits of annual PM10 concentration 2020 (left) and 2030 (right).

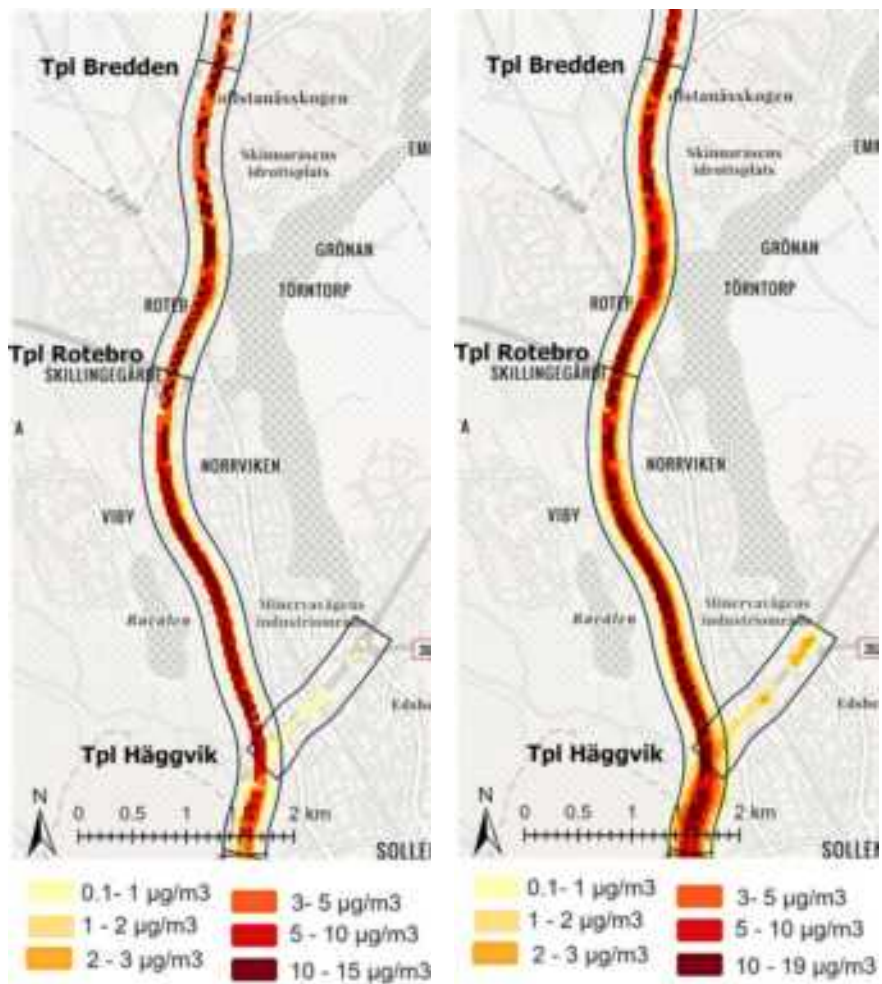


Figure 2. Concentration reductions needed within 200 m along part of the E4 highway to achieve the environmental quality goal of annual PM10 concentration in 2020 (left) and 2030 (right).

Health benefits and reduction in societal costs

If the PM10 goal ($15 \mu\text{g}/\text{m}^3$ as an annual mean value) would be achieved along the highways, it is estimated that 15 or 20 years of life would be saved in 2020 and 2030, respectively (Table 2). Achieving the PM10 daily mean limit value would only save 0.4 and 0.5 life years in 2020 and 2030, respectively. Achieving the upper assessment threshold would save 5 years of life in 2020. Considering both effects on mortality as well as morbidity (including stroke, diabetes, and childhood asthma) the corresponding reduction in societal costs if goals were achieved is estimated to be 36 and 52 million SEK per year in 2020 and 2030 respectively.

Table 2: Calculated reductions in population exposure to PM2.5 and associated health costs (2017) and saved life years for different scenarios.

PM10 scenario	Population-weighted exposure of PM2.5*	Reduced health costs (million SEK)	Saved years for the population	life
	($\mu\text{g}/\text{m}^3$)			
Year 2020	0.3735	0.84	0.4	
PM10 limit ($50 \mu\text{g}/\text{m}^3$ day) achieved				
Year 2020	0.3729	11	5	
PM10 upper assessment threshold ($35 \mu\text{g}/\text{m}^3$ day) achieved				
Year 2020	0.3716	36	15	
PM10 goal ($15 \mu\text{g}/\text{m}^3$ year) achieved				
Year 2030	0.4035	1.1	0.5	
PM10 limit ($50 \mu\text{g}/\text{m}^3$ day) achieved				
Year 2030	0.4009	52	22	
PM10 goal ($15 \mu\text{g}/\text{m}^3$ year) achieved				

*Difference compared to baseline with exceedances of limit values, upper assessment threshold, and goal.

Discussion

It should be noted that the calculations include the effects of actions taken on the highways with no influence of emissions on other roads. In reality, reducing studded tyres on highways will also lead to reduced use of studded tyres on other roads, which will contribute to reducing concentrations along the highways. The consequences of studded tyre reductions are thus underestimated.

On the other hand, we have not considered that road wear is higher from electric cars compared to conventional cars, due to the higher weight of electric cars compared to conventional cars. According to vehicle fleet statistics for 2022 average electric cars weigh around 400 kg more than average mix of diesel and petrol cars. Extrapolating the trend to 2030, this could mean that wear of roads is 50% larger if the share of electric cars increases by 2030. Then the reductions in emissions by speed restrictions or restrictions in studded winter tyres will not have the same effect as if electric cars had the same wear as conventional cars.

It is important to note that in the above calculations, it is assumed that the proportion of studded tyres is the same for electric cars as for other passenger cars. Now surveys in Trondheim, Helsinki, and Stockholm show that the proportion of studded tyres is significantly lower among electric cars. A recent survey of the city of Helsinki in the spring of 2023, for example, shows that the studded tyre share of electric cars was 16% compared to the share of petrol cars of 69% (Ana Stojilovic, Finnish Environmental Centre, SYKE, personal contact). In that case, it could mean that PM10 emissions actually decrease rather than increase with an increasing proportion of electric cars, even if one expects that the electric cars are heavier.

Conclusions

Achieving the PM10 environmental quality objective along densely trafficked highways could have substantial health benefits as it would reduce the exposure not only of people living close to the roads but also the exposure of people in the whole county. Reductions of emissions along highways can be achieved by reducing the use of studded winter tyres, reducing the speeds of vehicles, or reducing the amount of traffic. It is uncertain if the objectives can be achieved by 2030, but if they would, we estimate that up to 20 years of life could be saved associated with the reduced exposure to PM2.5 in Stockholm County with more than 2 million inhabitants.

Acknowledgements

The project was funded by the Swedish Transport Administration.

References

Denby, B. R., Sundvor, I., Johansson, C., Pirjola, L., Ketzel, M., Norman, M., Kupiainen, K., Gustafsson, M., Blomqvist, G., Omstedt, G. (2013). A coupled road dust and surface moisture model to predict non-exhaust road traffic induced particle emissions (NORTRIP). Part 1: road dust loading and suspension modelling *Atmos. Environ.*, 77, 283-300.

Forsberg et al., 2021. Report in Swedish only Swedish Transport Administration, 2021:253. ISBN: 978-91-7725-988-6.

Assessing the Impact of Car Cabin Filters mileage on In-Vehicle Air Quality: Results from Controlled Environment

N. Hafs¹, A. Mehel¹, G. Fokoua¹, H. Er-Rbib² and P. Chevrier³

¹Department of Mechanical and Environmental Engineering, Air Quality group, ESTACA, Paris Saclay Campus, 78180, Montigny-le-Bretonneux, France

²UTAC, av Georges Boillot, 91310 Linas,

³ARIAMIS Engineering, 18-22 rue de la Marne, 92800 Nanterre

Introduction

Air quality has become a crucial issue both from a public health and economic perspective. According to the World Health Organization (2014), air pollution caused the premature deaths of over 7 million people each year (OMS, 2014). The associated health expenses and income losses are estimated at 225 billion annually. The transportation domain is a major source of various pollutants, leading to exposure for individuals in transit. Studies have shown that exposure to pollutants remains significant regardless of the mode of transportation used, including cars, bicycles, trains, and walking (Knibbs et al., 2011). Recent investigations (Silverman et al. 2012; Valentino et al. 2016) have shown that air pollution is responsible for respiratory and cardiovascular problems and an increased risk of cancer, with even the placental barrier unable to provide a healthy environment. In the case of an enclosed space, such as the cabin of a car, exposure can, in some cases, be more significant due to the temporary accumulation of pollutants. Consequently, numerous studies have focused on characterizing the air quality inside car cabins (Hudda et al. 2012). These studies have shown that key parameters such as ventilation rates and the age of the vehicle can significantly affect the quality of air inside the cars (Mehel et al., 2019). In France, the average commuting duration by car is 50 minutes, with residents of the Paris region having twice the travel time of those in smaller urban areas (68 minutes versus 35 minutes) (INSEE, 2015). Given the amount of time people spend in their cars, it is crucial to control the parameters that affect the pollution rate in the car cabin to improve air quality and limit passenger exposure to pollutants. Due to the increasing harmful effects of air pollution, various studies have investigated the health risks associated with population exposure to vehicle-emitted pollutants. Initially, the research focused on measuring gaseous pollutants and their effects on health (McAdam et al., 2011). Later, due to the particularly harmful effects of observed particulate pollutants, especially after smog caused a large number of deaths (Bell, Samet, and Dominici 2004). Many studies have characterized several personal exposure in the Netherlands, Belgium, and Sydney and have demonstrated that the time spent in traffic significantly contributes to the daily average exposure to PM₁₀, PM_{2.5} and ultrafine particles (Wichmann et al. 2005; Van Roosbroeck et al. 2008; Knibbs et al. 2010; Int Panis et al. 2010). According to a study made by (Miao et al. 2015), the rush hour commuting leads to increased exposure to the air pollution, regardless the transportation mode. Add to that studies made in London (Briggs et al. 2008; Kaur, Nieuwenhuijsen, and Colvile 2005), found that while walking, the average pollution in the air was significantly higher than those experienced while driving inside the car cabin. Also, these studies found that the transportation type used, route taken, and the commuting duration all had an important impact on the exposure of the PM_{2.5}, ultrafine particles, and CO.

All knowledge gained during this period contributed to the establishment of European standards, which set emission limits for gaseous and particulate pollutants in terms of mass concentration. With the Euro 5 standard, it is the first time that a limit of number concentrations was set for the emissions of particulate matter in gasoline and diesel vehicles. This first threshold was set at 10¹¹ particles/km for diesel engines and 10¹² particles/km for gasoline engines. The problem of air quality inside the cabin is also heightened by the existence of a diverse fleet of vehicles, not only in terms of technology but also in age and use. In addition to pollutant emissions from exhaust gases from combustion, other sources of toxic emissions related to the braking system or wear of tires by friction with the road surface are added. This increases the heterogeneity of pollutants (Kam et al. 2012; Pant and Harrison 2013). These pollutants, which are both particulate and gaseous, infiltrate the cabins of moving vehicles, exposing passengers to high concentrations, have attracted the attention of many scientists.

The most comprehensive in this area is the study by (Hudda et al. 2012) which developed a model to predict ultrafine particle concentrations inside vehicle cabins, while knowing concentration values at the roadside. This model depends on vehicle characteristics (age and speed), ventilation parameters, and driving conditions. The study involved measuring ultrafine particle concentrations inside 73 vehicles while varying ventilation parameters and driving speed. It emerged from the study by (Hudda et al. 2012) that the air exchange ratio ~~value is the value of the cabin's volume that is changed every hour~~ is the most dominant and important parameter in determining the ratios between internal and external particle concentrations (I/O Inside-tooutside). This ratio is influenced by ventilation parameters (recirculation or external air intake), which include the fan speed, but also on other parameters such as the age or mileage of the vehicle. The other reference study regarding IAQ is the one conducted by (Zhu et al. 2007), who defined the different ventilation parameters to minimize the ultrafine particle concentration rate inside vehicle cabins. One of the experiments performed by these authors showed that the particle rate inside the cabin changed (decreased) (30-60s) after activating the fans. This shows an air exchange rate (AER) of 60 to 120/h, and the highest recorded protection rate is around 85% when the fans are activated with the recirculation mode. The same study showed that the size distribution of particles [7.5-217] nm inside the cabin was bimodal: two peaks were recorded; the primary peak appears for particles of size (10-30) nm, and the secondary peak for particles of size (30-70nm). Furthermore, the installation of cabin filters at vehicle air inlets reduces particles of size [5-70] nm by about 50% and particles of size [20-200] nm by 20 to 30%.

The characterization of car cabin air quality is an essential aspect of understanding the exposure of vehicle occupants to airborne pollutants, including particulate matter, volatile organic compounds, and gases. However, the most common approach to measuring car cabin air quality involves conducting on-road measurements (Szczerk and Maciejewska 2016; Lim et al. 2021; Lohani and Acharya 2016). This approach presents several limitations that could impact the accuracy of the results (Franco et al. 2013). One of the main limitations of on-road measurements is that external parameters, such as weather conditions, traffic congestion, and the distance between vehicles, are beyond our control (Mehel et al., 2023). These parameters can significantly affect the local on-road concentration of pollutants and hence the representativity of the measurements. For example, driving in heavy traffic or in congested urban areas increase the local on-road concentrations with a rapid change that depend on the inter-vehicle distance and also on the type of the front vehicle. This influences the process of pollutants infiltration. On the other hand, mobile measurements induce airflow around the probe that could influence the accuracy of measurements. Therefore, to overcome these limitations and to develop a better understanding of car cabin air quality, there is a need for more controlled and standardized measurement techniques. This would involve the use of controlled environments, such as laboratory test chambers, where the concentration of pollutants and other parameters can be precisely controlled and monitored (Hafs, 2023).

In this study, we are engaged in the characterization of fine and ultrafine particle infiltration rates within the vehicle cabin, operating within a controlled polluted atmosphere with a homogeneous particle concentration environment. In the present investigation we use three distinct cabin filters, each representing different mileage intervals: initial (0 km), intermediate (2800 km), and extended use (28000 km). The primary aim of this study is to elucidate the impact of filter age on the air quality within vehicular cabins in a controlled environment. This comprehensive characterization entails evaluations under both outdoor air intake (OA) and recirculation (RC) ventilation modes, across a spectrum of three distinct ventilation flow rates: no flow, medium flow (50%), and full flow (100%). All three filters under investigation are of the identical activated carbon type, and this characterization is meticulously conducted on the very same vehicle and platform.

This approach allows the significant advantage of studying the influence of filter aging without the influence of variable external parameters such as ambient outdoor pollution levels and meteorological conditions. The precision of our measurement setup allows us to meticulously use a controlled polluted environment, in which the distribution of pollutants remains consistently uniform. Consequently, between filter age and the air quality inside vehicle interiors, eliminating the influence of external factors.

Methodology:

The study focuses on characterizing the impact of cabin filter age and mileage on air quality within a controlled environment, carefully designed to minimize the influence of external variables. This controlled setup involves an enclosed chamber where the vehicle is positioned, allowing the creation of a simulated polluted environment

surrounding the vehicle. The testing bench is meticulously controlled to replicate real-world on-road pollution concentrations, providing a precise platform for assessing cabin filter efficiency. Importantly, the bench setup allows for filter assessment when it is mounted in the vehicle HVAC as for its standard operation. This enables the evaluation of pollutant infiltration and the assessment of internal (I) to external (O) pollutant concentrations ratios.

- The measurement bench and the vehicle:

The measurement bubble is a dedicated structure designed to investigate the air quality within a car cabin. It is a large, closed enclosure. It allows a vehicle with different sizes to be characterized. Its main objective is the ability to generate a polluted and controlled environment while we can control the pollution levels and types and also the temperature. This original platform, that we called the bubble, it uses seals to maintain stable pollutant concentrations, while allowing various gases and particulate pollutants to be generated at different concentration levels. The structure has two doors located in the front and a fan, which is used to distribute pollutants evenly throughout the enclosure. To obtain a homogeneous distribution of the particles injected in the bubble we use a fan which is positioned in the centre of the bubble. To ensure that the concentration of ~~pollutants is not affected by vehicle's engine but~~ an exhaust extractor is connected directly to the car's exhaust when the vehicle's engine is On. And lastly an air conditioning system is used to maintain a stable temperature inside the measurement bubble during the characterization of the car cabin.

The vehicle used is a SUV-type with a mileage of 28000 km.



Figure 1: The measurement platform (the bubble)

- Instrumentation

The instrumentation that we used in our study is the TSI Dust track, it is used for measuring the particulate matter mass concentrations in real-time. It uses the optical diffraction technique to detect and quantify the mass concentration of particulate matter in the air. The instrument operates by drawing air through a sample inlet, which passes through a laser beam, and the scattered light is then detected and analysed to determine the particle size and concentration. The TSI dust track can detect particles in the range of 0.1 to 10 micrometres with an acquisition rate of one measurement per second. This instrument is widely used for monitoring indoor and outdoor air quality, occupational health, and environmental studies.

- The protocol of the measurements:

The protocol for characterizing the car cabin involves several steps. First, the car is introduced into the ~~measurement car bubble and the exhaust gas extractor is connected to the car's exhaust. The fan is then activated to ensure a homogenous distribution of particles. Next, measurement instruments are placed both~~ measurement car bubble and the exhaust gas extractor is connected to the car's exhaust. The fan is then activated to ensure a homogenous distribution of particles. Next, measurement instruments are placed both

inside the car cabin and within the measurement bubble to determine the particle concentration levels.. Then particles are injected until a concentration of 1 mg/m³ is achieved inside the measurement bubble, which simulates external car pollution. The AGK2800 valve is used to regulate the particle injection and attain the desired concentration. Once the pollution concentration is stabilized, the car engine is turned on, and the concentration of particles infiltrating the car cabin is measured for different ventilation modes, Recycled (RC) and Outdoor Air (OA), and ventilation flow rate (0%, 50%, and 100%). The indoor/outdoor concentration ratio is calculated for different ventilation modes and flow rates, to characterize the infiltration of the particles. This protocol allows for the characterization of the car cabin air quality in relation to external pollution and different ventilation modes and flow rates. This characterization process is applied to all three cabin filters of the vehicle: the 0 km filter, the 2800 km filter, and the 28000 km filter. Furthermore, for each individual filter, the characterization procedure is replicated five times. The filter characterization takes place under consistent conditions within a polluted environment, maintaining a stable pollution level of 1 mg/m³.

Results:

In this section, we present the time-evolution of particle concentrations: the one generated within the measurement bubble (blue curve) and the one in the car cabin (Orange curve) across various ventilation modes and ventilation flow rates. Figures 2 to 4 provide visual depictions of particle concentrations within the air quality testing environment, as well as the particles infiltrating the vehicle cabin. These visualizations are based on different ventilation modes and varying ventilation flow rates. Notably, it becomes evident that the pollution levels within the controlled environment remain relatively consistent throughout the duration of the measurements. However, intriguing disparities arise when examining the particle concentration levels within the vehicle cabin, which are notably influenced by the distinct ventilation modes employed. It seems that less fine particles infiltrate within the cabin when the ventilation mode is set to the recycled (RC).

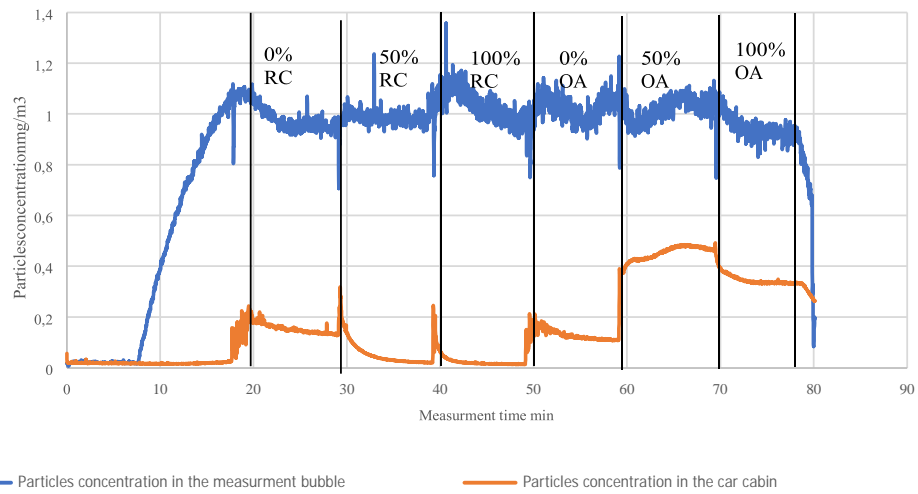


Figure 2 : Particles concentration in the measurement bubble and in the car cabin (for 0 km cabin filter)

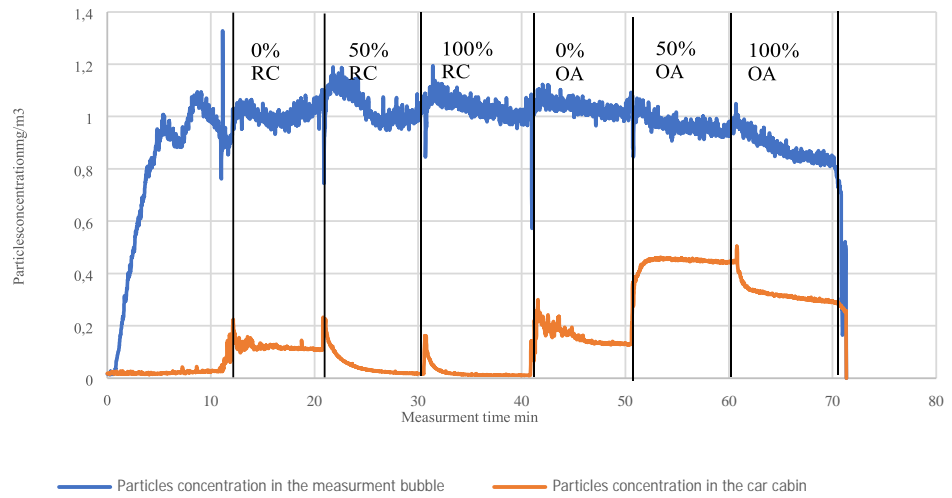


Figure 3 : Particles concentration in the measurement bubble and in the car cabin (for 2800 km cabin filter)

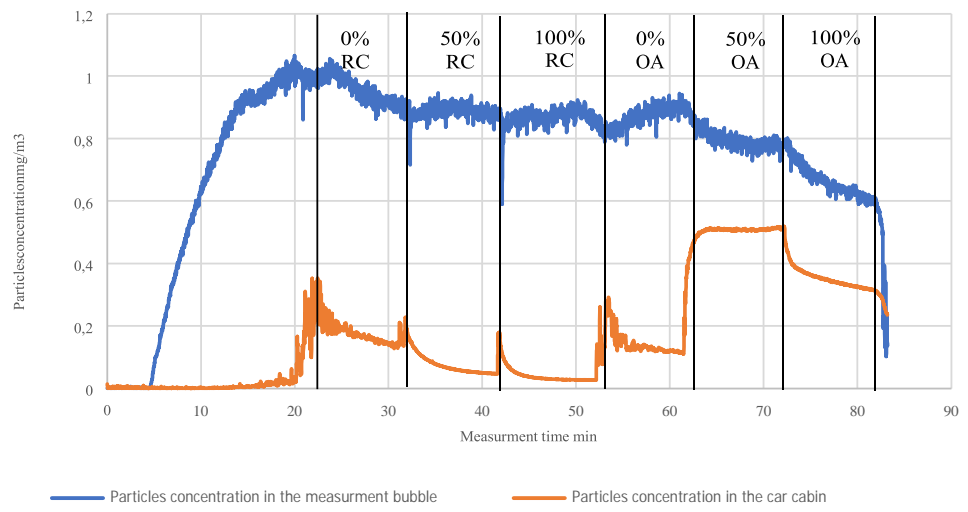


Figure 4 : Particles concentration in the measurement bubble and in the car cabin (for 28800 km cabin filter)

To delve deeper into the implications of these varying ventilation modes on particle concentration levels within the cabin, a crucial metric known as the indoor/outdoor (I/O) infiltration ratio is meticulously calculated for each unique ventilation configuration (Figure 5-7). This calculation has the objective to quantify the extent to which external particles penetrate the cabin space relative to the surrounding external atmosphere. By elucidating this I/O infiltration ratio across diverse ventilation settings, we can discern the nuanced interplay between ventilation modes and the resultant cabin air particle dynamics. Such insights not only elucidate the mechanics of air exchange within vehicular interiors but also contribute to a more comprehensive understanding of the factors influencing cabin air quality in such controlled environment.

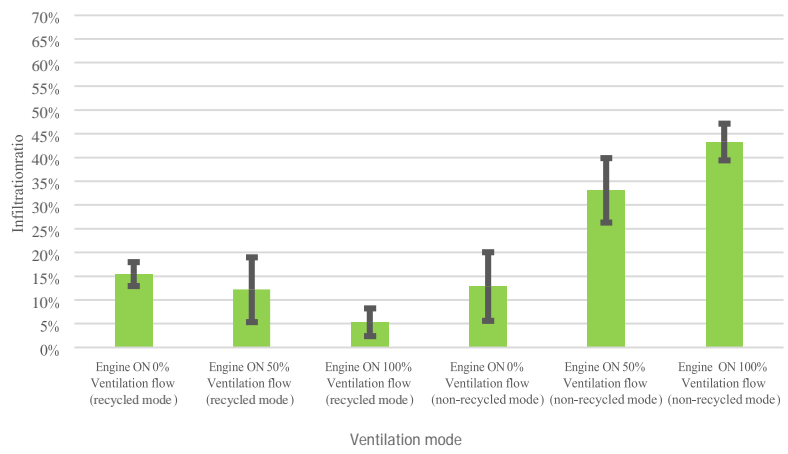


Figure 5 : Particles infiltration rate (I/O) for 0 km filter

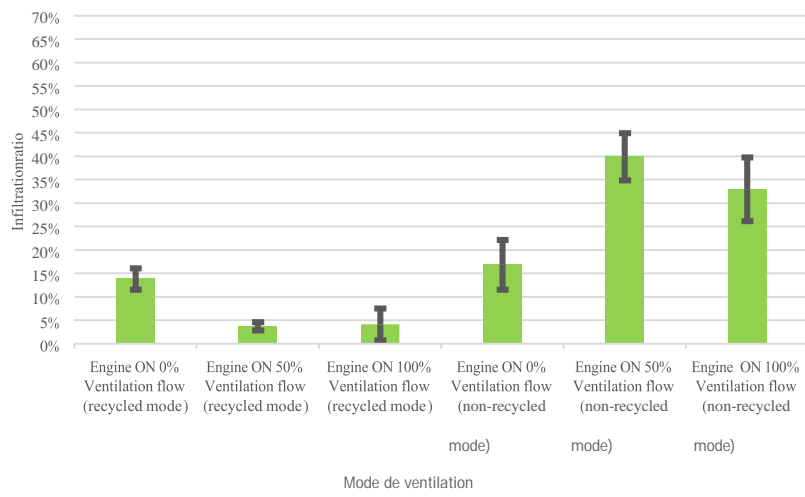


Figure 6 : Particles infiltration rate (I/O) for 2800km filter

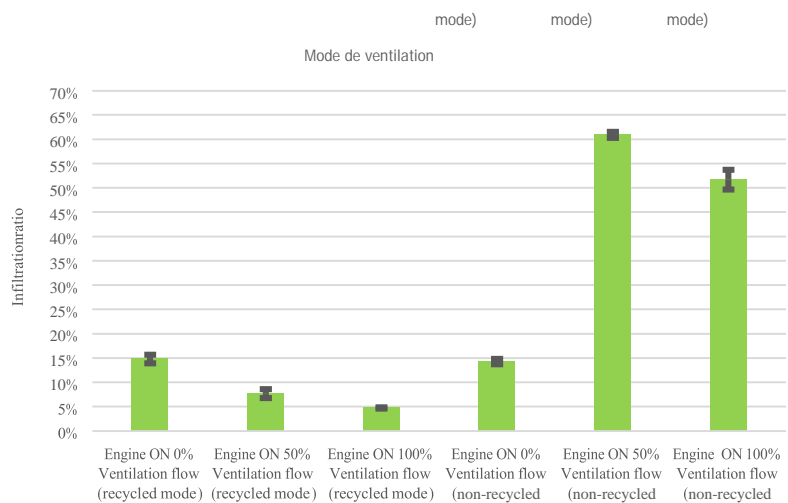


Figure 7 : Particles infiltration rate (I/O) for 28800km filter

Figures 5 to 7 depict the rates of particle infiltration into the vehicle cabin for various ventilation configurations using the three different filters. It is evident that, across all three filters, the outside air (OA) mode unfortunately promotes a higher degree of particle infiltration into the cabin. Moreover, it is noteworthy that the filter with a moderate age of 2800 km exhibits superior air filtration capabilities, thereby contributing to enhanced air quality. This is a known results from numerous previous studies (Knibbs et al., 2010; Hudda et al., 2012; Mehel et al., 2023).

A discernible pattern emerges wherein the filter having undergone 2800 km of use effectively restrains particle infiltration. This is evidenced by comparatively lower particle concentrations within the cabin, indicating a more efficient filtration process. Significantly, this advantageous outcome becomes evident when comparing results with both the pristine (0 km) and well-traveled (28000 km) filters. These findings underscore the potential of a moderately aged filter, specifically one with 2800 km of usage, to significantly contribute to an improved cabin environment. For a more comprehensive understanding of the filter age's impact, we have collated the consolidated data all the results into a single histogram. This approach will facilitate a more effective and meaningful comparison. Figure 8 illustrates the particle infiltration rates into the vehicle cabin across various cabin ventilation configurations and three distinct filter ages. The characterization of these three filters was conducted under identical conditions, with a particle concentration of 1 mg/m³ in the same vehicle model. The results reveal compelling insights. When considering the recirculation mode, the new filter exhibits the highest particle infiltration rates, reaching levels of up to 15%. Intriguingly, the filter with 2800 km of usage displays significantly lower infiltration rates, dropping to less than 5% under the same recirculation mode and a ventilation flow rate of 50%.

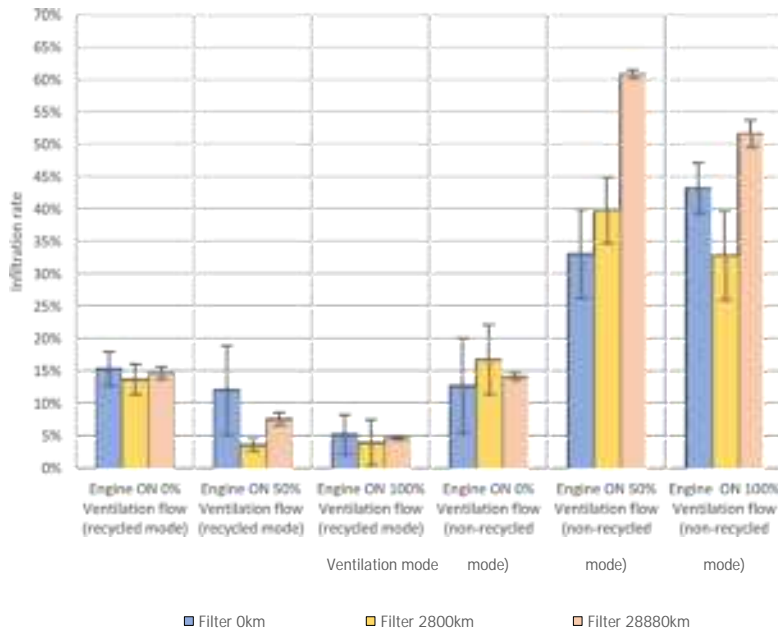


Figure 8 : Comparison of the infiltration rates between the 3 filters and for different ventilation settings

Shifting the focus to the external air mode (OA), the oldest filter exhibits remarkably elevated particle infiltration rates, surpassing 60% for non-recirculated ventilation and a flow rate of 50%, while the I/O is about 40% for the 2800 km filter and 33% for the new filter. For the highest fan speed (100%), the I/O are 52%, 33% and 44% respectively for the 28000 km, 2800 km and 0 km filter mileage respectively. The oldest filter is the one that has the greater I/O ratios as the findings of Xu et al. (2011) when filters have been characterised in a dedicated bench.

The filter behaviour that could explain this is that the new filter has the greatest porosity allowing for a higher infiltration rate as the fan speed is greater. While the 28000km filter, since it is more clogged, the pressure drop is higher which favours infiltration from different leakages.

Overall, the filter with 2800 km of usage demonstrates the most favourable performance in terms of particle infiltration rates among the three filters across various ventilation scenarios.

These results clearly emphasize the impact of filter age on the air quality within the vehicle cabin. The findings also highlight that optimal air quality is not solely dependent on the installation of a new filter.

Conclusion

In summary, this study highlights a key factor in the discussion concerning indoor air quality within vehicles: the age of the cabin filter. Observations reveal that the effectiveness of this filter extends beyond its initial installation. Through controlled testing methods, we were able to isolate the direct impact of filter age, eliminating external factors such as background pollution levels, traffic and weather fluctuations.

These conclusions emphasize the significance of a comprehensive approach to maintaining clean air inside the cabin. By considering the age of the filter along with other factors, we can optimize maintenance and ventilation practices, enhancing the driving experience by ensuring greater safety and comfort.

In the ongoing quest for continuous improvement in vehicle air quality, these findings urge us to consider filter efficiency holistically. By accounting for the various influences on cabin air quality, we can design vehicles that prioritize the well-being of passengers and drivers. This research thus contributes to the ongoing discourse on achieving optimal air quality standards in vehicles, ultimately enhancing the overall driving experience while ensuring the health and comfort of all occupants.

Acknowledgements

The authors would like to express their gratitude to ESTACA LAB and AULME for the funding of this project.

References:

- Hill, M., Belli, J., Jonathan M. Sartor, and Francisco Domingo. 2004. "Impacts on Indoor Particulate Matter." *Annual Review of Public Health* 25 (1): 247–80.
<https://doi.org/10.1146/annurev.publhealth.25.102802.124329>.
- Hoppe, Axel, E. van de Hooghe, Chloe Morris, and Joeri De Geyter. 2008. "Effects of Traffic: Study on Exposure to Particulate Air Pollution." *Environment International* 34 (1): 12–22.
<https://doi.org/10.1016/j.envint.2007.06.011>.
- Franco, Vicente, Marina Kousoulidou, Marilena Muntean, Leonidas Ntziachristos, Stefan Hausberger, and Panagiota Dilara. 2013. "Road Vehicle Emissions: Evaluation, Development, A Review." *Atmospheric Environment* 70 (May): 84–97.
<https://doi.org/10.1016/j.atmosenv.2013.01.006>.
- Hudda, Neelakshi, Sandra P. Eckel, Luke D. Knibbs, Constantinos Sioutas, Ralph J. Delfino, and Scott A. Brunekreef. 1994. "On-Road Ultrafine Particle Exposures to On-Road Concentrations." *Atmospheric Environment* (Oxford, England: 1994) 59 (November): 578–86.
<https://doi.org/10.1016/j.atmosenv.2012.05.021>.
- Hafs, N.M.; Mehel, A.; Fokoua, G.; Chevrier, P. and Er-Rbib, H. 2023. 'Generation of a Controlled Polluted Atmosphere for Vehicles Cabins Air Quality Characterization' *Journal of Mechanical Engineering and Automation* 13(2):17-31.
<https://DOI:10.17265/2159-5275/2023.02.001>
- Int Panis, Luc, Bas De Geus, Grégory Vandenbulcke, Hanny Willems, Bart Degraeuwe, Nico Bleux, Vinit Mehra, Isabelle Cormier, and Karin M. Mikkelsen. 2010. "Exposure to Particulate Matter in Traffic: A Comparison of Drivers and Car Passengers." *Atmospheric Environment* 44 (June): 2263–70.
<https://doi.org/10.1016/j.atmosenv.2010.04.028>.
- Kam, William, James W. Jacob, James L. Schauer, Ralph J. Delfino, and Constantinos Sioutas. 2012. "On-Road - Off-Road Factors of PM Pollutants for Light-Duty Vehicles (LDVs) Based on Urban Street Driving Conditions." *Atmospheric Environment* 61 (December): 378–86.
<https://doi.org/10.1016/j.atmosenv.2012.07.072>.

- Knibbs, Luke D., M. E. Nieuwstraeten, and R. N. Colb. 2005. "Predicting Exposure to Air Pollution along a Major Road in Central London, UK." *Atmospheric Environment* 39 (38): 7307–20.
[https://doi.org/10.1016/j.atmosenv.2005.09.008.](https://doi.org/10.1016/j.atmosenv.2005.09.008)

Knibbs, Luke D., Tom Cole-Hamner, and Edoor Mortazavi. 2011. "A Review of Personal Exposure to Ultrafine Particles and its Health Effects." *Atmospheric Environment* 45 (16): 2611–22.
[https://doi.org/10.1016/j.atmosenv.2011.02.065.](https://doi.org/10.1016/j.atmosenv.2011.02.065)

Knibbs, Luke D., and Richard J. de Dear. 2010. "Exposure to Ultrafine Particles and PM2.5 in Four Sydney Transport Modes." *Atmospheric Environment* 44 (26): 3224–27.
[https://doi.org/10.1016/j.atmosenv.2010.05.026.](https://doi.org/10.1016/j.atmosenv.2010.05.026)

Liu, Lianzhen, Christopher Buratti, Jon Chidley, Linda L. Griffiths, and Tim J. Munday. 2021. "Characterizing Personal, On-Car, Exposure to Traffic-Related Air Pollution: Evidence for Reduction Strategies from in-Vehicle Personal Exposure Monitoring." *Environmental International* 155 (August): 106532.
[https://doi.org/10.1016/j.envint.2021.106532.](https://doi.org/10.1016/j.envint.2021.106532)

Lohar, Deekshith, and Jayaram Acharya. 2016. "Real-time In-Vehicle Air Quality Monitoring using Mobile Sensing." In 2016 IEEE Annual India Conference (INDICON), 1–6.
[https://doi.org/10.1109/INDICON.2016.7839099.](https://doi.org/10.1109/INDICON.2016.7839099)

McAdam, Kim, Peter Steer, and Kim Perrotta. 2011. "On-road Continuous Sampling to Examine the Distribution of Traffic-Related Air Pollution in Proximity to a Major Road." *Atmospheric Environment* 45 (12): 2080–86.
[https://doi.org/10.1016/j.atmosenv.2011.01.050.](https://doi.org/10.1016/j.atmosenv.2011.01.050)

Mehel, A., Murzyn, F., Cuvelier, P., Deville Cavellin, L., Baudic, A., Joly, F., Patte Rouland, B., Varea, E., and Sioutas, C. 2014. "Evaluation et Analyse des Pollution Routière, Transport Automobile à l'Intérieur des Habitacles des Véhicules, Final report, CAPTHIV Project, ADEME, 136 pages".

Mehel, A., Deville Cavellin, L., Joly, F., Sioutas, C., Murzyn, F., Cuvelier, P., Baudic, A., 2023. « On-board measurements using two successive vehicles to assess in-cabin concentrations of on-road pollutants ». *Atmospheric Pollution Research* 14 (6): 101673

Moss, D., M. Michele Richard, Jennifer Chen, Mark W. Rosenberg, and Kristan T. Anderson. 2013. "Controlling Residential and Exposure to Air Pollution in Montreal, Canada." *Science of the Total Environment* 464 (March): 184–98.
[https://doi.org/10.1016/j.scitotenv.2013.11.078.](https://doi.org/10.1016/j.scitotenv.2013.11.078)

WHO. 2014. "2.9 Billion Premature Deaths are Linked to Air Pollution Every year." 2014. WHO World Health Organization. 2014.
[https://apps.who.int/mediacentre/news/releases/2014/airpollution/fr/index.html.](https://apps.who.int/mediacentre/news/releases/2014/airpollution/fr/index.html)

Patterson, J., and Roy M. Martens. 2013. "Estimation of the Contribution of Road Traffic Emissions to Particulate Matter Concentrations from Field Measurements: A review." *Atmospheric Environment* 77 (October): 28–97.
[https://doi.org/10.1016/j.atmosenv.2013.04.028.](https://doi.org/10.1016/j.atmosenv.2013.04.028)

Silverman, Debra T., Claudine M. Samanic, Jay H. Lubin, Aaron E. Blair, Patricia A. Stewart, Roel Vermeulen, Joseph B. Coble, et al. 2012. "The Diesel Exhaust in Miners Study: A Nested Case–Control Study of Lung Cancer and Diesel Exhaust." *Cancer Journal of the National Cancer Institute* 104 (11–12): 671–68.
[https://doi.org/10.1093/jnci/djs034.](https://doi.org/10.1093/jnci/djs034)

Szyszkowicz, Agnieszka, and Monika M. Krajewska. 2016. "Categorization for Air Quality Assessment in Land Transport." *Transportation Research Part D: Transport and Environment* 48 (October): 161–70.
[https://doi.org/10.1016/j.trd.2016.08.015.](https://doi.org/10.1016/j.trd.2016.08.015)

"The Cost of Air Pollution: Strengthening the Economic Case for Action". n.d. Accessed 22 February 2023.
[https://openknowledge.worldbank.org/handle/10986/25013.](https://openknowledge.worldbank.org/handle/10986/25013)

Valentino, Sarah A., Anne Tarrade, Josiane Aioun, Eve Mourier, Christophe Richard, Michèle Dahirel, Delphine Rousseau-Richard, et al. 2016. "Maternal Exposure to Diesel Engine Exhaust Alters Pulmonary Function and Induces Intergenerational Effects in Ratios: Particles and Endotoxins." *Toxicology* 351: 59–69.
[https://doi.org/10.1186/s12989-016-0151-7.](https://doi.org/10.1186/s12989-016-0151-7)

Van Hoornbeek, Sofie, Sander Lefebvre, Tom Van der Velde, and Bruno Desmet, and Dennis Naegelen. 2008. "Traffic-Related Outdoor Air Pollution and Respiratory Symptoms in Children: The Impact of Adjustment for Exposure Measurement Error." *Toxicology* 191 (3): 409–16.

Wijnen, Esther, Koenraad A. H. G. Lambrechts, Markel van der Zee, and Bert Brunekreef. 2005. "Traffic-Related Differences in Indoor and Personal Absorption Coefficients Measured in Amsterdam, the Netherlands." *Atmospheric Environment* 39 (38): 7384–92.

<https://doi.org/10.1016/j.atmosenv.2005.09.015>.

Xu, B., Liu, S., Liu, J. and Zhu, Y. Effects of cabin filter on in-cabin to on-roadway ultrafine particle ratios. *Aerosol Science and Technology*, *Aerosol Science and Technology*, 45, pp. 215–224, 2010.

Zhu, Yifang, Arantzazu Eiguren-Fernández, William C. Linds, and Antonio I. Miquel. 2007. In-Cabin Commuter Exposure to Ultrafine Particles on Long-Distance Travel. *Environmental Science & Technology* 41 (7): 2138–45.
<https://doi.org/10.1021/es0618797>.

A numerical study of particle dispersion in the wake of a static and rotating cylinder

K. Chekrouba^{1*}, A. Benabed¹ and A. Mehel¹

¹ INSTITUT NATIONAL DE LA PHYSIQUE ET DE LA CHIMIE DES SOLIDES – Paris-Saclay, F-78180 Montigny-le-Bretonneux, France

*khaled.chekrouba@estaca.fr

Introduction

Particulate matter emissions from road traffic have been linked to numerous adverse health effects, including respiratory and cardiovascular diseases, and can also impact ecosystems and the climate (Ostro et al., 2015). The ground vehicles, from their rotating wheels are responsible of particles resuspension which has become an important source of dust emissions and dispersion in the air. Therefore, their contribution to air pollution requires our understanding of the mechanisms responsible for their dispersion in the wake of a rotating wheel. The aerodynamic behavior of the airflow around an isolated rotating wheel is complex to study experimentally which led to a lack of data to validate numerical simulations (Gerardin, 2014). In this case, the flow around a rotating cylinder could be an interesting alternative configuration, as a first step, to understand the flow topology impact on particles dispersion given the geometrical similarity with a rotating wheel of a specific aspect ratio i.e., cylinder length to its diameter.

Extensive studies have been carried out on the aerodynamics of static 3D cylinders in the sub-critical regime ($Re < 3 \times 10^5$). However, there remains a notable gap in our understanding concerning the complex interactions between cylinder rotation and flow patterns. This also concerns their possible impact on particle transport in the cylinder wake. Although a few studies have addressed particle dispersion behind a static 2D cylinder (Huang et al., 2014; Keita et al., 2019), there is no comprehensive study of these dynamics. To fill this gap, the present study uses numerical method to investigate how cylinder rotation influences flow structures and, subsequently, particle dispersion in its wake. This research aims to make a significant contribution to the ongoing effort to understand these phenomena.

The flow in the wake of bluff bodies, particularly circular cylinder, is characterized by the development of vortex shedding patterns. The process of dispersion is mainly driven by particles-vortex interactions which make it very important to correctly predict the flow topology (Keita et al., 2019). Within this context, Unsteady Reynolds Averaged Navier Stokes (URANS) numerical simulations were performed in this work to study the wake flow ~~topology of a 3D cylinder with two counter-rotating vortices rotating velocity to air flow velocity~~ at $\alpha = 0$ and 1 and at $Re = 5000$. Solutions of three different URANS turbulence models Shear Stress Transport (SST), Local Correlation-based Transition Model (LCTM), and Reynolds Stress Model_BSL (RSM) were compared with available experimental and numerical data. Following that, the study investigates the impact of rotation on the configuration of flow and its subsequent impact on particle dispersion within the near and far wake of both static and rotating cylinder.

Numerical approach

Flow field simulations

3D numerical simulations of the flow around a cylinder are conducted using Ansys CFX using coupled solver, second order upwind scheme for advection term, Second Order Backward Euler implicit scheme for the transient term and a coupled algorithm for pressure-velocity coupling. This study is focused on URANS solutions, as this remains by far the most common approach in air quality applications. The system of equations consists of momentum equations (Eq 1) and continuity equation (Eq 2):

$$\frac{\partial \bar{u}_i}{\partial t} + \bar{u}_j \frac{\partial \bar{u}_i}{\partial x_j} = - \frac{1}{\rho_f} \frac{\partial p}{\partial x_i} + \frac{\mu}{\rho_f} \frac{\partial^2 \bar{u}_i}{\partial x_j^2} + \frac{\partial}{\partial x_j} (-\bar{u}'_i \bar{u}'_j) \quad (1)$$

$$\frac{\partial \bar{u}_i}{\partial x_i} = 0 \quad (2)$$

$\bar{u}'_i \bar{u}'_j$ denotes the Reynolds shear stress tensor terms arising from turbulent fluctuations.

ρ_f : fluid density (kg/m^3)

\bar{u}_i : mean velocity components (m/s)

$$\begin{aligned}
\mathbf{u}'_t &: \text{fluctuating velocity components (m/s)} \\
p^- &: \text{mean pressure (N/m}^2\text{)} \\
\mu &: \text{fluid dynamic viscosity (kg/m s)} \\
\mu_t &: \text{turbulent viscosity (kg/m s)} \\
k = \frac{1}{2} \overline{\mathbf{u}'_t \mathbf{u}'_t} &: \text{turbulent kinetic energy (m}^2/\text{s}^2\text{)} \\
\delta_{ij} &: \text{Kronecker delta}
\end{aligned}$$

To close this system of equations, three different models were chosen in this study:

- The SST model, developed by (Menter, 1994), it is a two-equation eddy-viscosity model that combines the advantages of the $k-\omega$ and $k-\epsilon$ models. It effectively captures physics in the near-wall region and the far field. However, like all eddy-viscosity models, the SST model cannot accurately capture anisotropic effects of turbulence.
- The LCTM is a modification of the standard SST model, developed to better predict laminar-turbulent transition (Menter, Langtry and Völker, 2006). It is based on local correlations and handles the intermittency function and transition onset criteria using additional equations. This model offers improved accuracy in predicting the transition from laminar to turbulent flow (Menter, Langtry and Völker, 2006), crucial in our case study. However, it does come with an increase of 30 % in computational effort.
- The RSM is a seven-equation model that solves transport equations for each Reynolds stress component and the turbulent dissipation rate. Unlike the eddy-viscosity models, the RSM is a second order closing formulation that can capture the anisotropic behavior of turbulence. However, the complexity of the model leads to a higher computational cost. The Reynolds stress model chosen is RSM BSL (Baseline Reynolds stress model) (Launder, Reece and Rodi, 1975). In this model the transport equation of dissipation is modeled as in the BSL k - ω model (similar to k - ω SST model) (D. C. Wilcox et al, 1998).

Case study description

The geometry to be considered is a cylinder with diameter D facing in a uniform air flow. The computational domain is a 3D cylindrical volume with a diameter of $40D$ (a proper extension according to Breuer (1999) and a spanwise thickness of $1D$ (see Figure 1)). This extension was carefully chosen to be $Z = D$ based on the study of Breuer (1999). The center of the cylinder is positioned at the center of this domain, maintaining a distance of $20D$ from the inlet, outlet, and other boundaries.

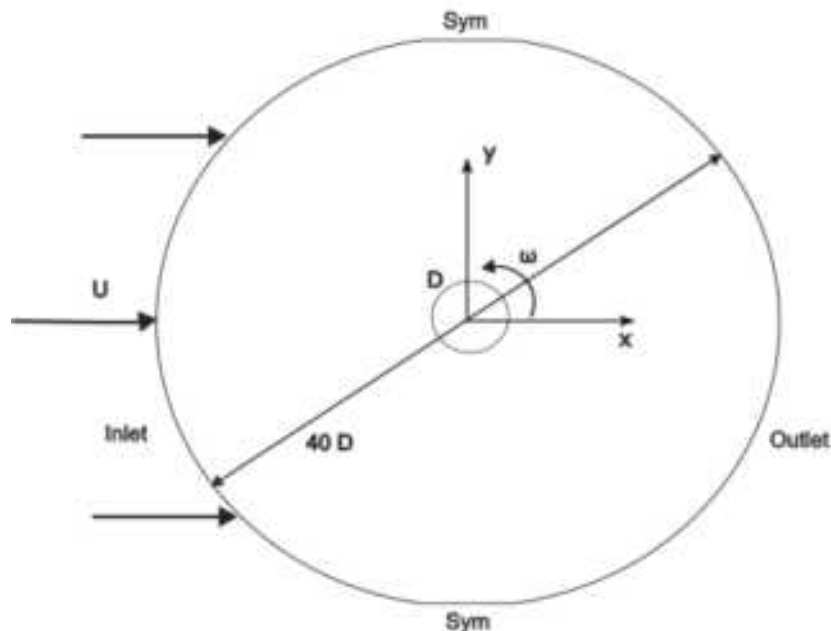


Figure 1: Computational domain and boundary limits

The simulations are conducted for Reynolds number $Re = 5000$ based on the cylinder diameter D and the free stream velocity U . The choice of this Reynolds number is motivated by the availability of data from the literature for simulations validation purposes. Two case studies are considered: static cylinder, and a rotating cylinder (Figure 2). In the rotating cylinder case, a rotation ratio of $\alpha = 1$ is employed. This later is defined as $\alpha = (\omega/r)/U$, where ω represents the rotational speed of the cylinder around its axis, and r is the radius of the cylinder. Velocity inlet condition is considered for each case, a non-slip condition is applied on the cylinder surface. Two symmetrical conditions on domain walls up and down the cylinder (Figure 1) to separate the inlet from the outlet. An atmospheric pressure condition is applied to the outlet of the domain. Symmetry boundaries are applied to the spanwise walls of the domain. For the rotative cylinder case wall rotation boundary condition is imposed on the cylinder surface in the counterclockwise direction (Breuer, 2000).

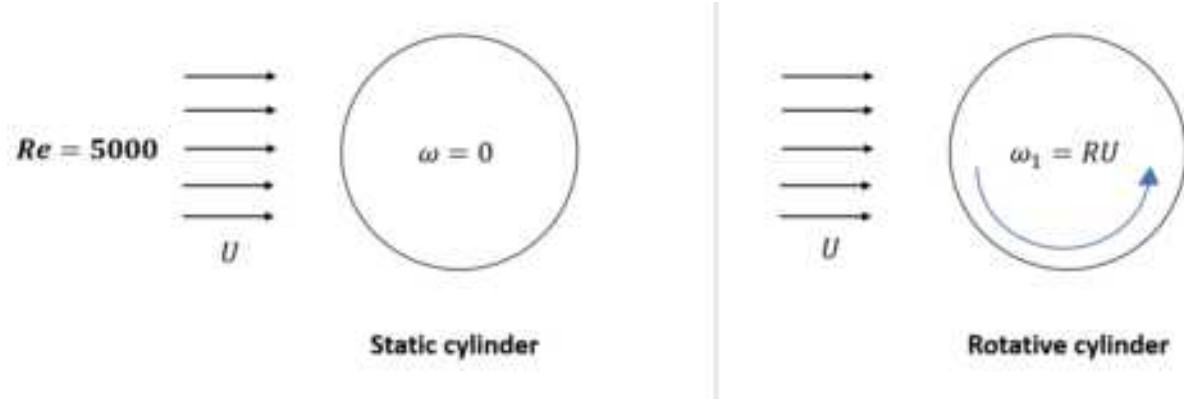


Figure 2: Simulation case studies

A single curvilinear body fitted with O-type grid type mesh was generated based on the studies of (Breuer, 2000; Karabelas, 2010). In the cross-sectional plane (x, y), 152×152 points are used, while in the spanwise direction 64 points are distributed on the 1D extension. The generated mesh comprising a total of 1.7 M elements. Fine grids are considered in the near-wall region to be able to capture the thinnest boundary layer and respect the constraints of the three models (Figure 3).

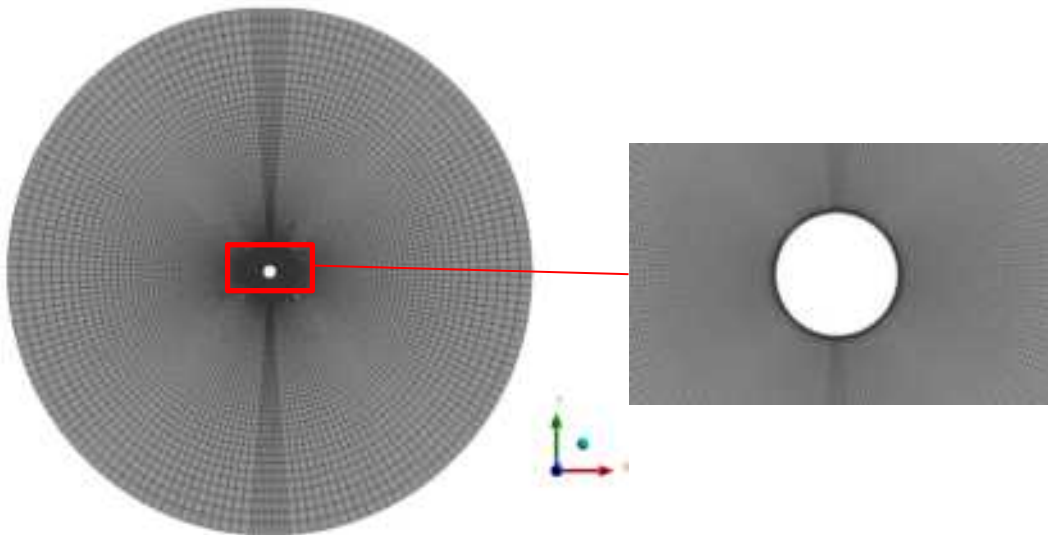


Figure 3: Mesh of the computational domain

The generated mesh respects the constraints of turbulence models used in all cases ($y^+ < 5$) for the automatic wall treatment to resolve the viscous sublayer. The wall normal distance can be evaluated as $y^+ = u_\tau y/\nu$, where u_τ is the friction velocity defined as $u_\tau = \sqrt{\tau_w/\rho}$ and τ_w is the wall shear stress. This will guarantee accurate prediction of turbulent flow dynamics near the wall, which is crucial for the prediction of flow separation as the most important feature of the studied cases (Aljure *et al.*, 2015; Pereira *et al.*, 2019). Three meshes are used to conduct the mesh independence study: the original mesh and two other meshes with 0.75 M

and $5.2 M$ elements. The latter were generated by changing only the resolution of the cross-sectional plane (x, y) and maintaining the resolution for the near wall elements. Three dimensionless time steps $\Delta t^+ = \Delta t U/D$ are considered to study the influence of time step.

Unsteady simulations of all cases are run till convergence of the results. After that the results obtained from each case are compared in terms of, the main mean flow characteristics: Strouhal number St , separation angle θ_s , normalized recirculation length L_r / D , drag coefficient C_D , lift coefficient C_L , back pressure coefficient C_{pb} were compared with different literature results.

Particle phase simulation

Particles dispersion study was achieved using the Lagrangian approach (Zhang and Ahmadi, 2005) in which particles trajectories are calculated (see Eq 3) based on the flow solution and taking accounting for the external forces acting on particles. Some assumptions have been made for the present simulation:

- The volumetric fraction of particles present in the air is sufficiently low $< 1\%$. This allows the use of a one way coupling where the effect of particles on the flow is neglected, as well as the potential for collisions between particles.
- Particles are supposed to be spherical with a density $\rho_p = 3950 \text{ kg/m}^3$ corresponding to that of Alumina particles, which is much larger than that of the air. Alumina particles have physical properties that mimic those of many naturally occurring particulates. Their density can be similar to dust and other airborne particulates.
- ~~The orientation of each solid particle is governed by Newton's second law of motion (see Eq 4)~~ (Ansys, 2021):

$$\frac{d\mathbf{x}_p}{dt} = \mathbf{u}_p \quad (3)$$

$$m_p \frac{d\mathbf{u}_p}{dt} = F_D(\mathbf{u} - \mathbf{u}_p) + \left(\frac{\rho_p - \rho_f}{\rho_p} \right) \mathbf{g} + \mathbf{F}_S + \mathbf{F}_B \quad (4)$$

where \mathbf{u} is the velocity of the fluid phase, \mathbf{u}_p is the particle velocity, ρ_f is the fluid density, ρ_p is the particle density. $F_D(\mathbf{u} - \mathbf{u}_p)$ represents the drag force per unit mass of the particle, defined as:

$$F_D = m_p \left(\frac{1}{\tau_p} \right) \left(\frac{C_D Re_p}{24} \right) \quad (5)$$

where Re_p is the particle Reynolds number, defined as:

$$Re_p = \frac{\rho_f d_p |\mathbf{u}_p - \mathbf{u}|}{\mu} \quad (6)$$

C_D represents the drag coefficient and is calculated by CFX based on Re_p using the Schiller Naumann model:

$$C_D = \max \left(\frac{24}{Re_p} (1 + 0.15 Re_p^{0.687}), 0.44 \right)$$

τ_p is the particle relaxation time defined as the ratio of the particle-to-fluid relative velocity to its acceleration under the effect of the Stokes drag force, given by the expression:

$$\tau_p = \frac{\rho_p d_p^2 C_c}{18 \rho_f \nu} \quad (7)$$

where ν is the kinematic viscosity of the fluid, and d_p is the particle diameter, respectively, and C_c is the Stokes-Cunningham slip correction factor which depends on the ratio of air molecular mean free path λ to particle diameter.

$$C_c = 1 + \frac{2\lambda}{d_p} \left(1.257 + 0.4e^{-\left(\frac{1.1d_p}{2\lambda}\right)} \right) \quad (8)$$

\mathbf{F}_B represents the Brownian force (Eq 9) and was included to consider the Brownian motion particularly for small particles. This force is modeled as proposed by (Li and Ahmadi, 1992) as a Gaussian white noise random process in every direction:

$$\mathbf{F}_B = m_p \mathbf{G} \sqrt{\frac{\pi S_0}{\Delta t}} \quad (9)$$

where the \mathbf{G} are zero-mean, unit-variance, independent Gaussian random numbers and Δt is the time step used in the calculation. S_0 is the spectral intensity given by:

$$S_0 = \frac{216\rho_f v k_b T}{\pi \rho_p^2 d_p^5 C_c} \quad (10)$$

where T is the absolute temperature of the fluid (K) and $k_b = 1.38 \times 10^{-23} \text{ J K}^{-1}$ is the Boltzmann constant.

\mathbf{F}_s represents the Saffman lift force (Eq 11) which is also considered to include the lift effect on large particles in shear regions. Its components are calculated with the following expression:

$$\mathbf{F}_s = m_p \frac{2\rho_f K v^{\frac{1}{2}} S_{ij}}{\rho_p d_p (S_{lk} S_{kl})^{\frac{1}{4}}} (\mathbf{u} - \mathbf{u}_p) \quad (11)$$

where $K = 2.594$ and S_{ij} are the components of the mean strain tensor.

The instantaneous fluid velocity \mathbf{u} is decomposed into mean and fluctuating components $\mathbf{u} = \bar{\mathbf{u}} + \mathbf{u}'$. In this approach, the averaged component is given by the URANS computation. The fluctuating component is modeled along each particle trajectory using a stochastic dispersion model EIM (Eddy Interaction Model) (Gosman and Ioannides, 1983). A wide range of particle sizes including ultrafine, fine and large particles ($d_p = 0.01, 0.1, 2.5, 10, 50 \mu\text{m}$) were injected at 7 positions close to the cylinder, on the symmetry plane, as illustrated in Figure 4. A single injection of 28000 particles of each size was carried out at time $t = 0 \text{ s}$. All particles were subsequently tracked in the wake of the cylinder over a dimensionless duration of $T = t \times U/D = 20$, equivalent to the convective time up to the exit of the domain. This approach was used by Huang et al., (2014) to better understand the dynamics of particles from the release instants until the outlet of the domain. Since symmetry conditions are applied to the lateral walls of the domain, particle exiting from one side of the domain will re-enter from the opposite side. A rebound condition is applied to the cylinder wall with a restitution coefficient of 1. This implies that a particle will rebound off the wall while maintaining its original speed.

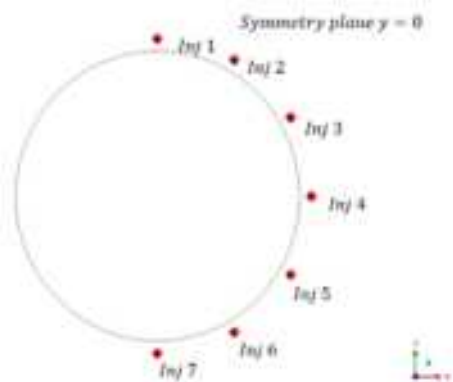


Figure 4: Injection points downstream the cylinder

Results and discussions

Fluid phase

In this section, flow characteristics are compared with literature results to validate the numerical approach and choose the most suitable turbulence model for this specific regime. The simulations of the flow around a static and rotating cylinder, ran for a duration of $T = 200D/U$ which corresponds to 50 cycles of vortex shedding. The flow variables were then time-averaged over the last 10 vortex release cycles ($T = 40D/U$). Finally, these variables were averaged in the Z direction, corresponding to the cylinder length direction, to obtain a mean 2D solution (Karabelas, 2010; Aljure et al., 2015). This approach is necessary to compare with existing data for the validation procedure of the numerical method. Flow topology is important to accurately simulate the particle dynamics.

Figure 5 shows the averaged velocity streamlines of the three different turbulent models obtained. Accordingly, all chosen turbulence models capture the symmetrical topology of the wake as predicted in the literature (Aljure et al., 2015) i.e., the two upper and lower separations followed by two shear layers with equal length. Both stagnation (S) and (SP) saddle points lie within the horizontal line of symmetry. However, SST and LCTM models show two additional tiny vortices in proximity of cylinder wall. This observation was made previously by (Young and Ooi, 2007) numerical study at $Re = 3900$. On the other hand, the solution obtained with the RSM model shows only two vortical structures and a wider recirculation zone.

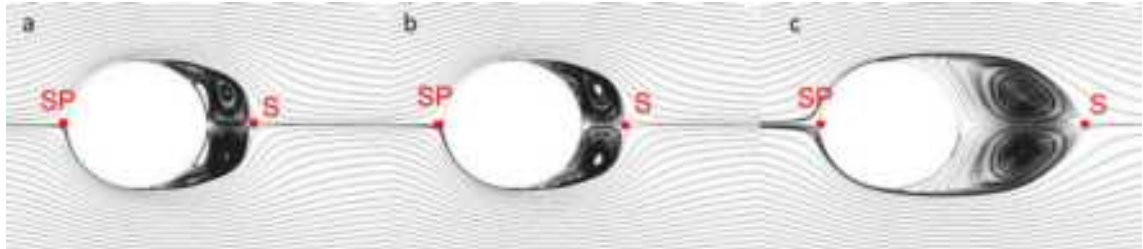


Figure 5: Time averaged of the mean streamlines around the static cylinder at $Re = 5000$ for: a) SST, b) LCTM, c) RSM; SP: stagnation point, S: saddle point

Table 1 presents the computed global parameters of the flow compared to the experimental results from Norberg (1993, 1994, 1998) and DNS results from Aljure et al., (2015). The table shows that both SST and LCTM models overestimate all indicators except the Strouhal number. In addition, for these two models, relative difference of the recirculation length L_r / D with respect to experimental result, exceeds 50 %. These discrepancies are due to premature transition to turbulence in the boundary layer which is marked by the large values of separation angle and the appearance of the two additional tiny structures in the wake of the cylinder (see Figure 5, a). On the other hand, the RSM model shows an acceptable separation angle, with a relative difference around 7 % compared with experimental separation position, which leads to a better estimation of recirculation length.

Table 1: Integral mean quantities for static cylinder computed at $Re = 5000$, compared to literature experimental and numerical results

Model	St	C_D	L_r / D	$\theta_s [^\circ]$	C_{pb}
SST	0.224	1.457	0.79	95.51	1.41
LCTM	0.219	1.475	0.79	95.97	1.43
RSM	0.233	1.160	1.33	88.92	1.08
DNS Aljure et al., (2015)	0.210	1.050	1.76	82.20	0.94
EXP Norberg (1993, 1994, 1998)	0.209	1.020	1.80	-	0.93

Figure 6 shows the averaged streamlines of the three models in the case of the rotative cylinder. It can be observed that the three models predict the same overall topology with minor differences in the two vortex sizes. Moreover, the cylinder rotation breaks the symmetry of the flow. Therefore, the recirculation zone shrinks and deflects in the direction of rotation leading to a larger upper vortex and a smaller lower one. Consequently, the stagnation and saddle points move up and get closer to each other.

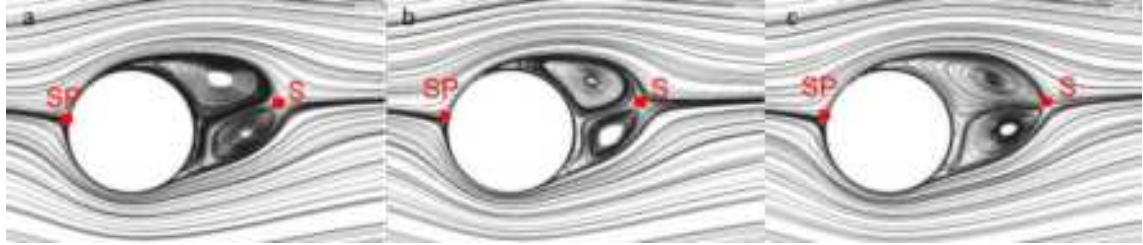


Figure 6: Time averaged of the mean streamlines around the rotative cylinder at $Re = 5000$ for: a) SST
b) LCTM, c) RSM; SP: stagnation point, S: saddle point

Table 2 compare the mean flow characteristics of the three models compared to that of DNS simulations of Aljure et al., (2015) for the rotating cylinder case. Similar to the static case, the SST and LCTM models underestimate the recirculation length, while the RSM model predicts accurately this parameter. Nevertheless, drag coefficient is well estimated by the LCTM model with an error of 2 %. Both RSM and SST models predicted with lower accuracy the drag coefficient with a relative difference of approximately 10 %. The lift coefficient is underestimated by the three models with an error of 19%, 24%, and 21% for SST, LCTM, and RSM respectively. Additionally, the Strouhal number is well predicted by the three models with a max relative difference of 9 %. It can be concluded that all flow main characteristics are reasonably predicted by the three models in the rotating cylinder case.

Table 2: Integral mean quantities for the rotative cylinder computed at $Re = 5000$, compared to experimental and other numerical results.

Model	St	C_D	L_r /D	C_L	C_{pb}
SST	0.231	0.802	0.67	-1.667	1.16
LCTM	0.218	0.883	0.53	-1.732	1.25
RSM	0.243	0.810	0.78	-1.698	1.16
DNS Aljure et al (2015)	0.223	0.900	0.79	-1.400	0.99

To conclude this validation section, by considering both rotating and static cylinder cases, the global quality of results is improved with RSM model. This model was chosen to conduct all the particle-laden simulations.

Particles Phase

In this work, the Lagrangian approach is employed to track particles. In the model we take into account different forces that were mentioned in section 2.3, among them turbulent and Brownian diffusions which consider random processes in their formulations. Consequently, different samples of the same particles number can yield distinct outcomes. This approach is statistical, and according to (Graham and Moyeed, 2002), the variability of computed results diminishes with the increase of both number of repetitions and particles. The CFX solver ensures the convergence of particle trajectories through iterative resolution of the equation of motion (Eq 3 and 4). Through multiple iterations, the solver calculates the average of all the solutions. To obtain reliable outcomes, we investigated the impact of sample size on statistical quantities. It was found that a number of particles of 28000 particle for each particle size was sufficient to guarantee the convergence of concentration of particles (results were not shown here to respect the number of pages).

Figure 7 shows instantaneous particles distributions at $T = 20$ in the wake of static cylinder (left) and rotative cylinder (right) for the different particle sizes. Firstly, for static cylinder case it can be noted that except for $50 \mu m$ particles, distributions of different particle sizes are symmetrical irrespective the fact that it is periodical. This is due to the symmetrical nature of the flow in the wake considering the fact that this symmetry is time-shifted. Particles of sizes ranging from $0.01 \mu m$ to $10 \mu m$ which have a stokes number $Stk < 0.1$ which exhibit the same behavior. They diffuse in the vortex cores with a uniformly distributed pattern as well as the thin region connecting the vortices. This behavior is associated with the relatively low relaxation time of these particles (Yao et al., 2009; Keita et al., 2019). Although, $50 \mu m$ particles have a stokes number close to that of the less inertial particles ($Stk = 0.22$), they present a different pattern. These particles interact less with eddies and sediment under the effect of gravity. Secondly, for rotative cylinder case (Figure 7, right) it can be noticed that independently of Reynolds number and particle size, all distributions are inclined to the direction of rotation ($y > 0$). This is due to the asymmetric nature of the wake as discussed in the fluid phase section. Subsequently, particles exhibit less dispersion in the y direction in the wake of the rotating cylinder compared to the static cylinder case.

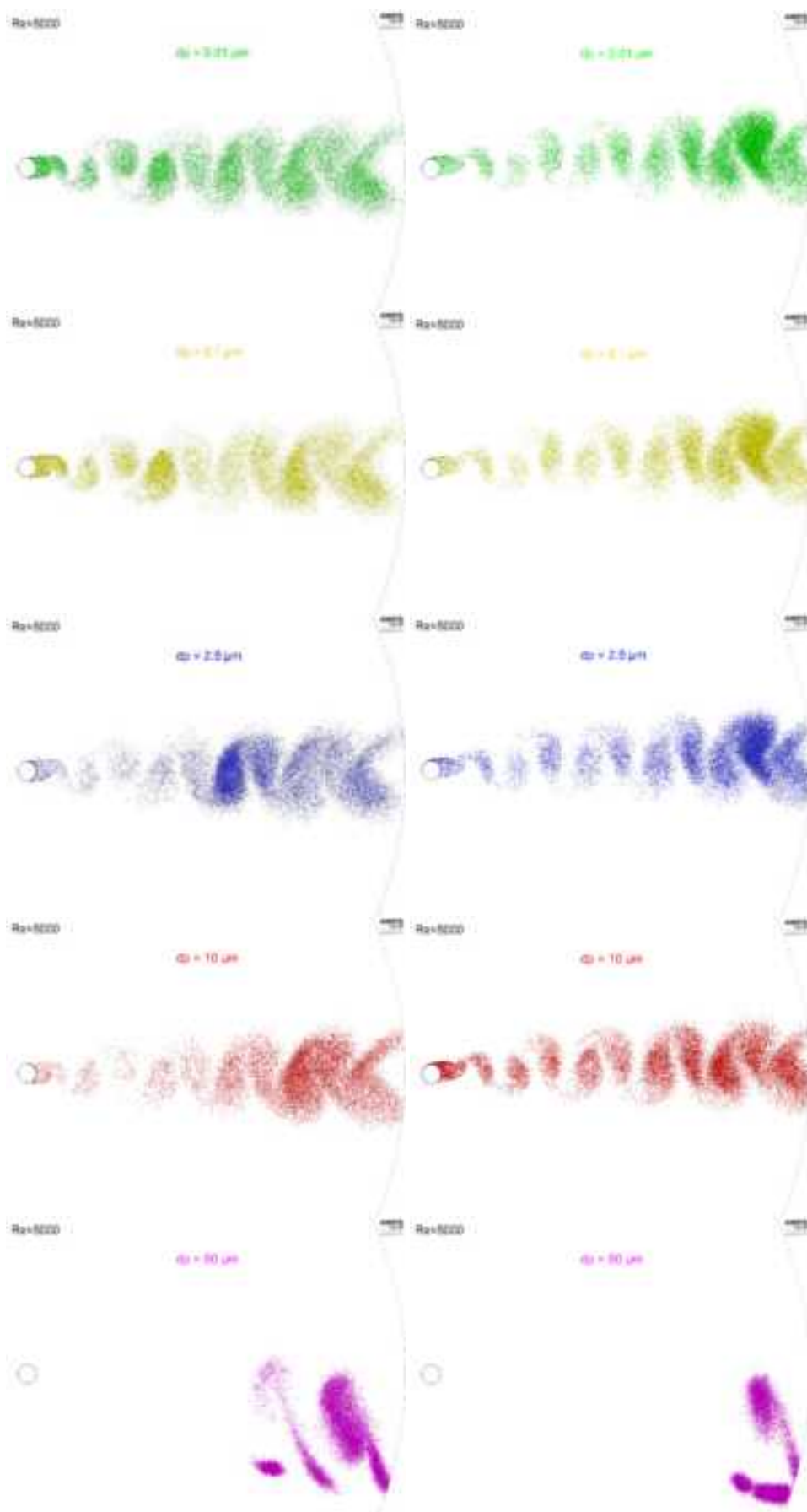


Figure 7: Distribution of different size particles at $T = 20$ in the wake of a: static cylinder (left), rotative cylinder (Right)

Conclusion

Particle-laden flow around a static and rotative cylinder was investigated using CFD simulations, based on URANS approach. Comparison between numerical results of flow main characteristics and literature results showed that RSM model is the most suitable for accurately reproducing the flow topology.

Visualizations of particle distributions of different sizes in the cylinder's wake revealed distinct behaviors
Particles with sizes $< 50 \mu\text{m}$ diffuse within vortices due to their low relaxation time. Conversely, particles of $50 \mu\text{m}$ interact less with the vortical structures owing to their relatively higher relaxation time, leading to sedimentation under gravity. Furthermore, cylinder rotation has two noticeable effects on particle distributions: a decrease in particle dispersion in the normal direction y , and an inclination of particle distributions in the direction of rotation $y > 0$.

As a next step, further studies involve considering additional scenarios of particle simulations under various turbulent regimes and different spin ratios to enhance our understanding of the effect of rotation on particle dispersion in general.

Acknowledgements

All simulations data used in this paper was elaborated within ESTACA lab.

References

- Aljure, D.E. et al. (2015). Influence of rotation on the flow around a cylinder at $Re = 16000$. *International Journal of Heat and Fluid Flow*, 55, pp. 76–90. Available at: <https://doi.org/10.1016/j.ijheatfluidflow.2015.07.015>.
- Bauer, M. (1999). Large-eddy simulation of a shear-layer transition in the circular cylinder flow. In S. H. Ho et al. (eds.), *Industrial and Environmental Applications of Direct and Large-Eddy Simulation*. Springer Berlin Heidelberg (Lecture Notes in Physics), pp. 176–189. Available at: <https://doi.org/10.1007/BFb0106102>.
- Bauer, M. (2005). A challenging test case for large-eddy simulation at high Reynolds number: cylinder wake flow. *International Journal of Heat and Fluid Flow*, 21(5), pp. 648–654. Available at: [https://doi.org/10.1016/S0142-727X\(00\)00056-4](https://doi.org/10.1016/S0142-727X(00)00056-4).
- Gerardin, E. (undated). *Étude expérimentale et numérique de la dispersion et déposition dans le sillage d'une roue de cyclone*. p. 239.
- Gutman, B.I. and Moyeed, R.A. (2002). *Breakaway particles for the Langmuir circulation*. *Powder Technology*, 125(2–3), pp. 179–186. Available at: [https://doi.org/10.1016/S0032-5910\(01\)00504-6](https://doi.org/10.1016/S0032-5910(01)00504-6).
- Huang, Y. et al. (2014). A numerical study on dispersion of particles from the surface of a circular cylinder placed in a gas flow using discrete vortex method. *Journal of Hydrodynamics*, 26(3), pp. 384–393. Available at: [https://doi.org/10.1016/S1001-6058\(14\)60043-3](https://doi.org/10.1016/S1001-6058(14)60043-3).
- Karadzhov, G. (2010). Large-eddy simulation of a high-Reynolds-number flow past a rotating cylinder. *International Journal of Heat and Fluid Flow*, 31(4), pp. 518–527. Available at: <https://doi.org/10.1016/j.ijheatfluidflow.2010.02.010>.
- Keita, N.S. et al. (2018). Numerical study of ultrafine particle deposition in the wake of a cylinder. *Atmospheric Pollution Research*, 10(1), pp. 294–302. Available at: <https://doi.org/10.1016/j.apr.2018.08.006>.
- Lindner, B.F., Rieneck, F. and Seidl, W. (1970). Progress in the development of a Reynolds-stress turbulence closure. *Journal of Fluid Mechanics*, 68(3), pp. 537–566. Available at: <https://doi.org/10.1017/S0022112075001814>.
- Li, A. and Ahmadi, G. (1992). Dispersion and deposition of spherical particles from point sources in a turbulent plume. *Aerosol Science and Technology*, 16(4), pp. 209–226. Available at: <https://doi.org/10.1080/02786829208959550>.
- Menter, F.R. (1994). Two-equation eddy-viscosity turbulence models for engineering applications. *AIAA Journal*, 32(8), pp. 1598–1605. Available at: <https://doi.org/10.2514/3.12149>.
- Menter, F.R., Lai, C. and Walker, S. (2002). Transition Modeling for General Purpose CFD Codes. *Flow, Turbulence and Combustion*, 77(1–4), pp. 277–303. Available at: <https://doi.org/10.1007/s10494-006-9047-1>.
- Ostro, B., Hu, J., Goldberg, D., Reynolds, P., Hertz, A., Bernstein, L., & Kleeman, M. J. (2015). Associations of mortality with long-term exposures to fine and ultrafine particles, species, and sources: results from the California Teachers Study Cohort. *Environmental health perspectives*, 123(6), 549–556.
- Pereira, F.S. et al. (2019). On the simulation of the flow around a flat cylinder at $Re = 16000$. *International Journal of Heat and Fluid Flow*, 76, pp. 40–56. Available at: <https://doi.org/10.1016/j.ijheatfluidflow.2019.01.007>.

Yao, J. et al. (2006) Numerical Simulation of Particle Dispersion in the Wake of a Circular Cylinder. *Aerosol Science and Technology*, 43(2), pp. 174–187. Available at: <https://doi.org/10.1080/02786820802549441>.

Young MF and Ono A (1996) Comparative Assessment of LES and DRAG for Flow over a Cylinder at a Reynolds Number of 3000. p 8.

Zhang S and Ahmad S (2005) CFD—Lagrangian simulations of liquid–gas–solid flows in three-phase fluidized beds. *Chemical Engineering Science*, 60(18), pp. 5089–5104. Available at: <https://doi.org/10.1016/j.ces.2005.04.033>.

The assessment of a Zero Emission Zone: air quality and human health impacts in the metropolitan city of Milan

A. Piccoli^{1,2*}, V. Agresti², M. Bedogni³, G. Lonati¹ and G. Pirovano².

¹ Department of Civil and Environmental Engineering, Politecnico di Milano, Milan, Italy

² Sustainable Development and Energy Sources, RSE S.P.A., Milan, Italy andrea.piccoli@rse-web.it

³ Agenzia Mobilità Ambiente e Territorio (AMAT), Milan, Italy

Introduction

The Po Valley is one of the most polluted regions in Europe (Pernigotti et al., 2012), where the air quality standards imposed by the European Union are often not respected. The city of Milan stands is the most populated city in the Po Valley. A recent study conducted by the Institute for Global Health (ISGlobal) has ranked the Milan metropolitan area as the fifth-worst European city in terms of NO₂-related mortality and the 13th worst in terms of PM_{2.5} (Khomenko et al., 2021). Among the policies to mitigate the impact of air pollution on human health in urban areas, several European cities have planned and implemented Zero Emission Zones (ZEZ) (Cui et al., 2020). ZEZs are areas where only electric vehicles, pedestrians, and cyclists are allowed unrestricted access. Assessing the potential air quality benefits of ZEZs can be done using atmospheric models. In this work, we developed a modelling chain composed of a road traffic, an emission, and an air quality model to simulate the impacts of mobility scenarios. The modelling chain was applied to assess the potential impact of a ZEZ scenario in the city centre of Milan on air quality.

Methods

HERMESv3 (Guevara et al., 2020) in the bottom-up version was used to estimate road traffic emissions in Milan, starting from road traffic data. HERMESv3 allows to simulate both exhaust and non-exhaust emissions, including the contribution of PM resuspension due to vehicle transit. Accurate modelling of non-exhaust emissions is crucial in electric mobility scenario studies, as this PM component also affects electric vehicles. For the private traffic sector, we used a macroscopic traffic simulation of a typical working day as the starting point for the road traffic emission modelling. Milan's environment and mobility agency (AMAT) provided the traffic simulation. Daily traffic count indices for 2017, developed by AMAT, were used to achieve weekly and monthly temporal disaggregation. Area specific profiles for the fleet composition were employed to differentiate the circulating fleet within the city, thus reproducing the effect of the enforced congestion charging scheme. Open data on bus lines geometry and bus trip frequency, available on the Milan's municipality open data portal, were used to simulate emissions from the public transport sector. The contribution of all the other emission sources necessary for the air quality model was estimated using the classical top-down approach.

The core of the modelling system is the Comprehensive Air Quality Model with Extensions (CAMx) version 7.1 (Ramboll, 2020). CAMx was applied over two nested domains (Figure 1). The external domain covers Italy (ITA) and a portion of the neighbouring countries with a horizontal resolution of 4 km and an extent of 284x364 cells. The nested domain (MIL) is centred over the city of Milan, with 70x70 cells and a horizontal resolution of 1 km. Both domains share the same vertical layers set-up, consisting in 14 terrain following levels of increasing depth. The meteorological simulation used to drive the air quality simulation was performed using the Weather Research and Forecasting (WRF) model version 3.9 (Skamarock et al., 2008) employing a similar configuration of nested domains. The WRF domains are slightly larger than the CAMx ones to limit the influence of border effects on air quality simulations. For the top-down emission estimation, we used the Sparse Matrix Operator Kernel Emissions (SMOKE) model version 3.5 (UNC, 2013). Over the ITA domain the national Italian emission inventory ISPRA 2015 (ISPRA, 2020) was used for Italy and the EMEP 2010 emission inventory was used for Europe and North Africa. In the MIL domain, we employed the regional emission inventory INEMAR (ARPA Lombardia, 2017) developed by the Lombardy region environmental protection Agency (ARPA). Biogenic and sea salt emission were estimated using the MEGAN model (Guenther et al., 2006) and the SEASALT model (Gong, 2005). Finally, the boundary conditions were derived from the C-IMERL module using MERRA-2 Pre-Atmos (Raouil et al., 2009).

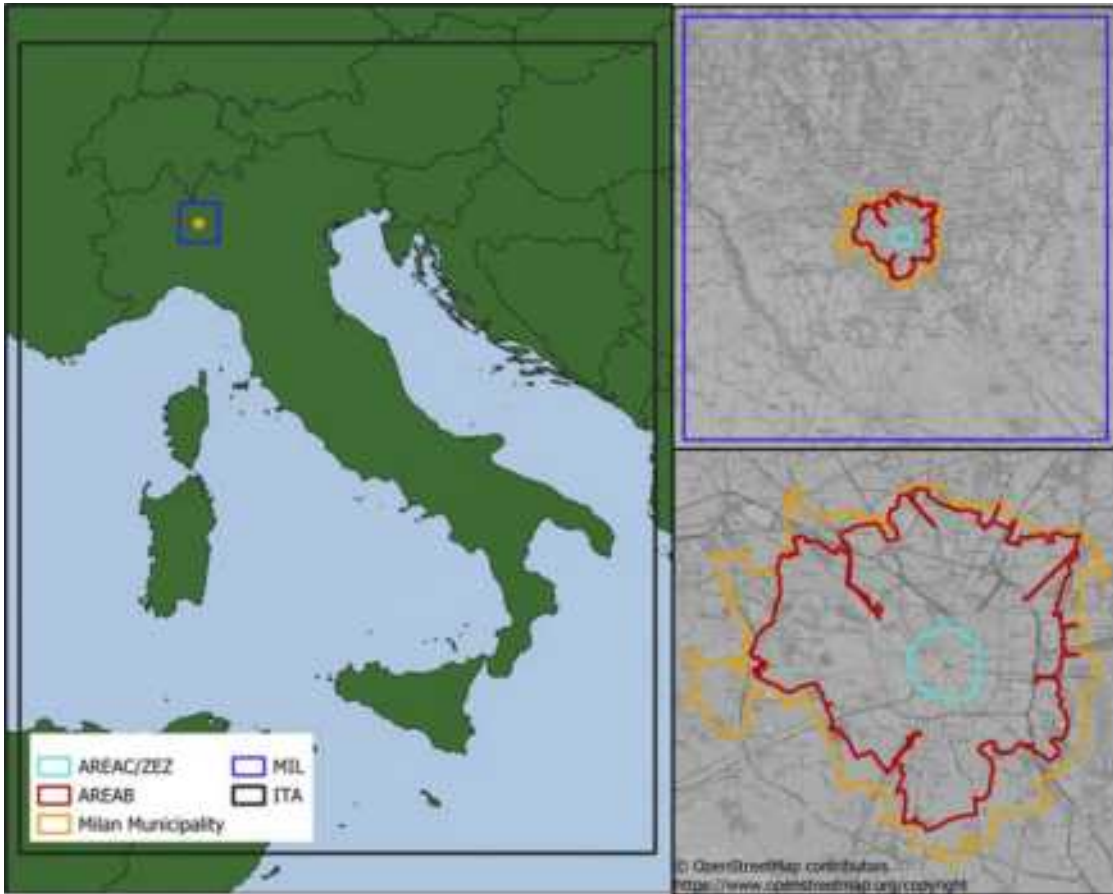


Figure 1: Maps of the study area. Left: ITA and MIL Domain. Upper right: MIL domain and the city of Milan with the Low Emission Zones. Bottom right: Milan and the LEZ.

The modelling chain is completed by a module that starting from Concentration Response Functions (CRFs) and pollutant atmospheric concentration change (between BASE and ZEZ scenario) allows estimating the impact on human health of the mobility scenario in terms of avoided mortality and avoided Years of Life Lost (YLL). The CRFs employed in this study are based on the most recent Relative Risk (RR) guideline values from the World Health Organization (World Health Organization, 2021). Both PM2.5 and NO₂ are considered for long-term effects. Additionally, we estimated morbidity indicators, specifically the number of hospital admissions and the total hospitalization days attributed to NO₂ and PM2.5. For these indicators, we used the CRFs developed within the European project HRAPIE (World Health Organization, 2013).

Definition of the Zero Emission Zone scenario

The ZEZ scenario implements objectives stated in Milan's municipality's Air Quality and Climate Plan (Piano Aria Clima or PAC) intended to improve air quality and combat climate change. The PAC, adopted by the city council in 2020, includes the establishment of a Zero Emission Zone (ZEZ) as one of its objectives for 2030. This ZEZ is intended to replace the existing Low Emission Zone AREAC in the city centre (Figure 1). In 2019 Milan introduced AREAB, that covers most of the municipal area and imposes some restriction to highly polluting vehicles. Furthermore, the ZEZ scenario implements the Full Electric plan proposed by the local transport agency for the public transport vehicle fleet. Compared to the BASE scenario, the ZEZ scenario considers:

- Creation of a ZEZ in place of AREAC.
- Conversion of resident passenger cars in AREAC and already admitted vehicles to electric vehicles (EV).
- Removal of remaining internal combustion engine vehicles (ICEVs) from the ZEZ.
- Conversion of light-duty vehicles and mopeds/motorcycles in the ZEZ to EVs.
- Conversion of the Public Transport to EVs.
- Implementation of AREAB

The fraction of cars circulating in AREAC that is removed amounts to 46%.

Results

Firstly, we evaluated the reduction in road traffic emissions in ZEZ scenario with respect to the base case 2017 (BASE). The most significant benefit is the reduction of NOx emissions, with a 19.3% decrease of the annual road traffic emissions in Milan (Table 1). Conversely, the reductions for particulate matter fractions are relatively smaller, in the order of 10% for PM2.5 and of only 6% for PM10. The lower reduction for PM10 is primarily due to higher contribution of non-exhaust emissions of coarse particles from electric cars (Timmers and Achten, 2016). As the ZEZ scenario mainly affects a specific area of the city, the emission reductions are more pronounced in the model domain cells covering the city centre compared to the city-wide average. For NOx, a 100% emission reduction is expected for the cells totally included in the ZEZ, because all the vehicles still circulating in the area in the ZEZ Scenario will be electric. Similarly, for PM10 and PM2.5 the highest reduction levels are expected within the ZEZ, with maximum values of 37% and 48% respectively.

Table 1: Road traffic emissions (Mg year^{-1}) and relative reductions between base case 2017 and ZEZ scenario for Milan Municipality.

Pollutant	Scenario		Relative reduction
	BASE	ZEZ	
NOX	4348.32	3506.76	19.3%
PM10	448.50	423.24	5.6%
PM2.5	271.82	245.94	9.5%

Figure 2 shows the annual reduction in yearly mean concentration for NO2 and PM2.5 in the ZEZ scenario. Due to the similarity between PM fractions in terms of both spatial pattern and reduction values, we have chosen to display PM2.5 only. Both pollutants exhibit maximum concentration reductions within the ZEZ, with significant values also observed within the borders of the newly implemented AREAB. The effects of the scenario measures outside of AREAB are close to negligible. As expected, NO2 is the pollutant that benefits the most from the ZEZ scenario, with reduction values ranging from 8% to 9% for all the model cells within the ZEZ.

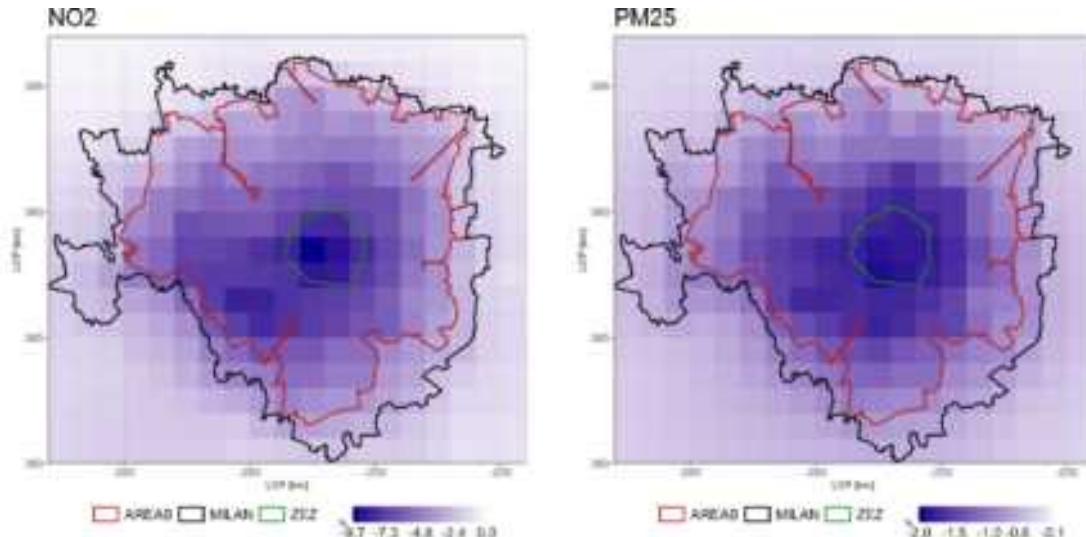


Figure 2: Spatial distribution of the relative reduction of NO2 and PM2.5 yearly mean concentration in the ZEZ scenario compared with BASE scenario.

The impact of these expected reductions in concentrations levels on the compliance with current and prospected EU air quality standards and WHO guidelines has been evaluated at the 8 Air Quality Monitoring Sites (AQMS) in Milan, both for long- (i.e. annual) and short-term (i.e. daily and hourly average) reference parameters. As for the annual average concentrations, the improvements in air quality allow reaching compliance with the current $40 \mu\text{g m}^{-3}$ limit for NO2 only at one site and with the $25 \mu\text{g m}^{-3}$ limit for PM2.5 at two more sites (from four to six). For PM10, as compliance with the $40 \mu\text{g m}^{-3}$ limit was already achieved in the BASE scenario, the small reductions expected will have no effect. However, when comparing the annual average values estimated for the ZEZ scenario with the prospected EU limits for 2030 ($20 \mu\text{g m}^{-3}$ for NO2, $10 \mu\text{g m}^{-3}$ for PM2.5, $20 \mu\text{g m}^{-3}$ for PM10) and with the WHO guidelines ($10 \mu\text{g m}^{-3}$, $5 \mu\text{g m}^{-3}$ and $15 \mu\text{g m}^{-3}$, respectively), non-compliance is expected at all AQMS for both all pollutants.

Regarding the daily average concentrations, the estimated reductions do not impact limit compliance. In both the BASE and ZEZ scenarios, the limits are not respected. For PM10, the current $50 \mu\text{g m}^{-3}$ threshold is exceeded on more than 35 days at all the monitoring sites, with an average number of days (54 for BASE, 52 for ZEZ scenario) practically unchanged. The limit proposed for 2030 and the WHO guideline value, both stricter in terms of concentration threshold and number of annual exceedances, are not attained in both scenarios, with about 3.5 and 20 time higher exceedances, respectively. Despite the very high number of exceedances, small reductions of non-compliant days are estimated in the ZEZ scenario with (-10% with respect to the EU proposal limit, -5% to WHO guideline)

Finally, the hourly limit for NO2 ($200 \mu\text{g m}^{-3}$). The average number of exceedances for the NO2 hourly limit, which is consistent across all regulations and guidelines, decreases from 1.88 to 0.25. With the new scenario, all AQMS will comply with the allowed one exceedance for calendar year of the proposed standard for 2030.

Table 2: Average number of exceedances of the current EU daily limits, of the 2030 EU proposed standards for 2030, and of the WHO guideline values calculated across all air quality monitoring stations in the city of Milan (PM2.5 and NO2 have no daily limit in the current EU regulation).

Pollutant	EU current limit		EU proposal 2030		WHO guideline		
	BASE	ZEZ	BASE	ZEZ	BASE	ZEZ	
NO2	-		18 exc. $50 \mu\text{g m}^{-3}$		3 exc. $25 \mu\text{g m}^{-3}$		
	156		142		257		
PM2.5	-		18 exc. $25 \mu\text{g m}^{-3}$		3 exc. $15 \mu\text{g m}^{-3}$		
	143		140		228		
PM10	35 exc. $50 \mu\text{g m}^{-3}$		18 exc. $45 \mu\text{g m}^{-3}$		3 exc. $45 \mu\text{g m}^{-3}$		
	54		52		66		
						63	

A comprehensive evaluation of the impact on air quality of the actions implemented in ZEZ scenario was developed based on the European Air Quality Index (AQI) (EEA, 2023) computed at two traffic exposed AQMS, located inside and outside the proposed ZEZ (Figure 3). The AQI gives information on the potential impacts of air quality on human health, and is calculated using daily concentrations of NO2, PM10, and PM2.5. The overall daily index is based on the highest score among the three pollutants.

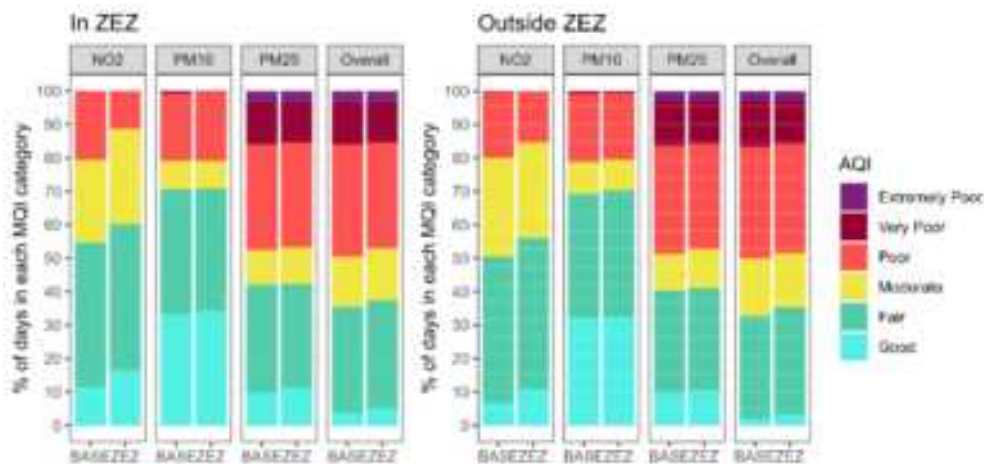


Figure 3: Comparison of the annual frequencies of the European Air Quality Index estimated at two AQMS located inside and outside the proposed ZEZ.

Inside the ZEZ, there is a 10% increase (from 80% to 90%) in the number of days with acceptable (i.e. moderate or better) air quality when considering NO₂ only, but overall, the improvement is only 2.7% due to AQI being mainly influenced by PM2.5 and PM10. Outside the ZEZ, the impact of the interventions on mobility is lower, but a small improvement is still expected: the number of "acceptable" days improve on 4.7% for NO₂ and 1.4% for the overall AQI. However, in both scenarios 50% of the year is characterized by poor or even worse air quality and the implementation of the ZEZ scenario is expected to provide very limited improvements.

The air quality benefits estimated in the ZEZ scenario have been also analysed in terms of the impacts on human health through mortality and morbidity indicators computed for the city of Milan (Table 3).

Table 3: Mortality and morbidity indicators: avoided mortality (number of deaths) and Years of Life Lost (YLL), avoided number of Hospital Admissions and Hospital Stay days for the ZEZ scenario with respect to the BASE scenario. (95% confidence interval reported in brackets).

	Avoided Mortality	Avoided YLL	Avoided Hospital Admission	Avoided Hospital Stay
PM2.5	38 (28-42)	391 (296-438)	14 (0-28)	145 (-2-300)
NO ₂	42 (21-83)	427 (214-847)	72 (46-98)	804 (514-1092)

For NO₂ the positive impacts of the new scenario amounts to 8.5% circa of the estimated total of the base case for both mortality and morbidity indicators, while for PM2.5 this value is only 1.9%.

Conclusions

In this work we estimated the potential impact of a ZEZ scenario in the city centre of Milan on both air quality and related impacts on human health, thanks to bottom-up a modelling chain. We present results for road traffic emissions, air quality, and human health impacts under the ZEZ scenario, in comparison with the baseline case of 2017. The mobility containment measure improves air quality in terms of NO₂ atmospheric concentration, but it is less effective for reducing particulate matter pollution. Within the ZEZ boundaries, the complete transition to electric mobility effectively eliminates NO_x emissions, resulting in an overall reduction of 19.35% in traffic-related NO_x emissions. Thus, we estimated concentration reductions ranging from 8% to 9% for NO₂ within the ZEZ, while the reductions for PM2.5 are less than 2%. The ZEZ implementation is expected to only marginally aid in complying with annual and daily air quality standards set or prospected by the European Union. To meet the proposed EU air quality standards for 2030 or the more stringent WHO guidelines, further efforts are necessary. Finally, we analysed the effects of the concentration reductions on human health, specifically on mortality and morbidity. The expected reduction in mortality and hospitalization in Milan due to NO₂ concentrations is estimated to be 8.5%, while for PM2.5 is 1.9%.

Despite the measures on mobility implemented in the ZEZ scenario, the air quality estimated for Milan remains poor for almost half of the year. While significant positive impacts can be achieved for NO₂, the effects on PM10 and PM2.5 are limited. In our base case estimation, only around 20% of total primary PM10 emissions are attributed to exhaust, with non-exhaust and resuspension accounting for the remaining 80%. As noted by Timmers and Achten, the total non-exhaust emissions of electric vehicles are higher due to the increased weight of such vehicles (Timmers and Achten, 2016), while resuspension is expected to be the same. Therefore, solely changing the vehicle fleet without reducing the amounts of circulating vehicles will only marginally affect PM concentrations. Moreover, although local traffic emissions likely contribute to a significant portion of NO₂ concentrations in Milan (Pepe et al., 2019), both modelling and experimental studies suggest that traffic directly contributes to less than 20% of PM concentration in the city (Amato et al., 2016; Pepe et al., 2019). Consequently, a more comprehensive approach to air quality management is needed to significantly improve PM concentrations in Milan. This approach should extend beyond a single emission sector or a restricted area, encompassing measures that transcend city borders. However, it is important to note that the planned ZEZ will have positive benefits in other environmental fields not modelled in this work, such as urban noise reduction and city's carbon footprint reduction.

Acknowledgements

This work has been financed by the Research Fund for the Italian Electrical System under the Three-Year Research Plan 2022-2024 (DM MITE n. 337, 15.09.2022), in compliance with the Decree of April 16th, 2018.

References

- Amato, F., Alastuey, A., Karanasiou, A., Lucarelli, F., Nava, S., Calzolai, G., Severi, M., Becagli, S., Gianelle, V.L., Colombi, C., Alves, C., Custódio, D., Nunes, T., Cerqueira, M., Pio, C., Eleftheriadis, K., Diapouli, E., Reche, C., Minguillón, M.C., Manousakas, M.-I., Maggos, T., Vratolis, S., Harrison, R.M., Querol, X., 2016. AIRUSE-LIFE+: a harmonized PM speciation and source apportionment in five southern European cities. *Atmospheric Chemistry and Physics* 16, 3289–3309.
- ARPA Lombardia, 2017. Inemar. <https://www.inemar.eu/xwiki/bin/view/Inemar/HomeLombardia>
- Cui H., Gode P., and Wesselhorst S. (2021) A global overview of zero-emission zones in cities and their development progress. *ICCT Briefing, International Council On Clean Transportation*
- EEA, 2023. European Air Quality Index. European Air Quality Index (europa.eu) (Last access 2023/07/01)
- Gong, S.L., 2003. A parameterization of sea-salt aerosol source function for sub- and super-micron particles. *Global Biogeochemical Cycles* 17, 1097.
- Guenther, A., Karl, T., Harley, P., Wiedinmyer, C., Palmer, P.I., Geron, C., 2006. Estimates of global terrestrial isoprene emissions using MEGAN (Model of Emissions of Gases and Aerosols from Nature). *Atmospheric Chemistry and Physics* 6, 3181–3210.
- Guevara, M., Tena, C., Porquet, M., Jorba, O., Pérez García-Pando, C., 2020. HERMESv3, a stand-alone multi-scale atmospheric emission modelling framework-Part 2: The bottom-up module. *Geoscientific Model Development* 13, 873–903.
- ISPRA, 2020. Italian Emission Inventory 1990-2018. Informative Inventory Report 2020. Istituto Superiore per la Protezione e la Ricerca Ambientale.
- Khomenko, S., Cirach, M., Pereira-Barboza, E., Mueller, N., Barrera-Gómez, J., Rojas-Rueda, D., Hoogh, K. de, Hoek, G., Nieuwenhuijsen, M., 2021. Premature mortality due to air pollution in European cities: a health impact assessment. *The Lancet Planetary Health* 5, e121–e134.
- Pepe, N., Pirovano, G., Balzarini, A., Toppetti, A., Riva, G.M., Amato, F., Lonati, G., 2019. Enhanced CAMx source apportionment analysis at an urban receptor in Milan based on source categories and emission regions. *Atmospheric Environment: X* 2, 100020.
- Pernigotti, D., Georgieva, E., Thunis, P., Bessagnet, B., 2012. Impact of meteorology on air quality modeling over the Po valley in northern Italy. *Atmospheric Environment* 51, 303–310.
- Rouil, L., Honoré, C., Vautard, R., Beekman, M., Bessagnet, B., Malherbe, L., Meleux, F., Dufour, A., Elichegaray, C., Flaud, J.M., Menut, L., Martínez Prado, J., Pichot, M., 2007. Present An Operational Forecasting and Mapping System for Air Quality in Europe. *Bulletin of the American Meteorological Society* 90, 73–84.
- Skamarock, W.C., Klemp, J.B., Dudhia, J., Gill, D.O., Barker, D.M., Duda, M.G., Huang, X.-Y., Wang, W., Powers, J.G., 2008. A Description of the Advanced Research WRF Version 3.
- Timmers, V.R.J.H., Achten, P.A.J., 2016. Non-exhaust PM emissions from electric vehicles. *Atmospheric Environment* 134, 10–17.
- UNC, 2013. *AMAP User's Manual*
- World Health Organization, 2021. WHO global air quality guidelines: particulate matter (PM_{2.5} and PM₁₀), ozone, nitrogen dioxide, sulfur dioxide and carbon monoxide. *World Health Organization*.
- World Health Organization, 2013. Health risks of air pollution in Europe – HRAPIE project. Recommendations for concentration-response functions for cost-benefit analysis of particulate matter, ozone and nitrogen dioxide. *WHO Regional Office for Europe*.

Improving 3-day deterministic air pollution forecasts using machine learning algorithms

C. Johansson^{1,3}, Z. Zhang², M. Engardt^{3*}, M. Stafoggia⁴ and X. Ma²

¹Department of Environmental Science, Stockholm University, 10691 Stockholm, Sweden

²KTH Royal Institute of Technology, Dept. of Civil and Architectural Engineering, 100 44 Stockholm, Sweden

³Environment and health administration, SLB-analys, 104 20 Stockholm, Sweden

⁴Department of Epidemiology, Lazio Region Health Service, Rome, Italy

Presenting author email: magnuz.engardt@slb.nu

Introduction

Air quality forecasts can be based on deterministic dispersion modelling, but to be accurate this requires process-oriented dispersion models and detailed information on future emissions and meteorological conditions. Application of machine learning (ML) models to predict outdoor air quality is getting more and more popular. Studies have used ML to predict both hourly and daily average concentrations of particulate matter (PM) as well as gaseous air pollutants using meteorological and traffic data (e.g. Thongthammachart et al., 2021; Kurniawita 2019; Chakravarthi et al. 2021; Sareenwary et al. 2020; Shteing et al., 2020). In addition, a combination of ML, land-use data, dispersion modelling, ground-based and satellite measurements have been used to obtain temporally and spatially distributed concentrations (Shteing et al., 2020). Although good prediction results have been achieved using ML, the challenges of forecasting air pollution concentrations in a longer-term horizon such as a day or even several days have not been investigated and only few studies have combined deterministic models and ML in forecasting air pollution levels several days into the future.

In this paper we demonstrate how ML can help improve the accuracy of 1-, 2- and 3-day deterministic forecasts of particulate matter (PM10, particles with diameter less than 10 µm), nitrogen oxides (NOx) and ozone (O₃) for urban background and street canyon sites in Stockholm, Sweden. The deterministic forecast utilises the CAMS ensemble model to account for non-local sources (long-range transport). A Gaussian model is applied over the urban area of Stockholm accounting for local emissions and a street canyon model (OSPM) to account for the effect of buildings on the dispersion of local traffic emissions along the roads in the central area of the city. We compare three different machine learning algorithms; two based on decision trees (random forest (RF) and XG Boost (XGB)) and one neural network model (LSTM). Important questions addressed are also if there are systematic differences in performance depending on different pollutants and different sites. A more detailed presentation of the results from this study is presented by Johansson et al. (2023).

Air pollution measurements

Input data (in situ observations) for ML modelling are taken from four monitoring stations in central Stockholm, including one urban background site (Torkel Knutssonsgatan, hereafter called UB or urban) and 3 street canyon sites (Hornsgatan HO, Folkungagatan FO and Sveavägen SV). They are all located in central Stockholm (Figure 1).



Figure 1. Map of central Stockholm showing locations of the urban background site (Torkel Knutssonsgatan) and the street canyons traffic sites.

The Stockholm air quality forecast system

A system of three nested dispersion models is used to forecast concentrations of air pollution in Stockholm. The CAMS ensemble model, part of the Copernicus program (Peuch et al., 2022) is used to obtain forecasts of long-range transported air pollution from outside of the Greater Stockholm. CAMS forecasted concentrations representative of background air, hour by hour, are extracted from a location outside the greater Stockholm domain. The contributions to concentrations due to local emissions in the metropolitan area were performed on a 100 m resolution using a Gaussian dispersion model part of the Airviro system (<https://www.airviro.com/airviro/>), modelling domain (Greater Stockholm, 35 by 35 km). The Gaussian model is fed with meteorological forecasts from the Swedish Meteorological and Hydrological Institute (SMHI). A diagnostic wind model is used to account for influences of variations in topography and land-use on the dispersion parameters input to the Gaussian model. Finally, the Operational Street Pollution Model (OSPM, Berkowicz, 2000), driven by forecasted meteorology from SMHI is applied for the street canyon sites. NO_x and PM₁₀ are modelled on all scales, whereas O₃ is only forecasted by the CAMS ensemble model.

Meteorological forecasts

As an integral part of the Stockholm air quality forecast system, meteorological forecasts for a point in central Stockholm are downloaded every morning from SMHI (<https://www.smhi.se/data/oppna-data>) and MET Norway (<https://docs.api.met.no/doc/>). The meteorological forecasts extend over 10 days and are a combination of output from a number of regional and global numerical weather prediction models. The combination is based on statistical adjustments as well as manual edits. The meteorology is initially used to drive the models of weather-dependent PM emissions and the urban- and street canyon air quality modelling. The forecasted meteorological data are, finally, also used as predictors in the ML algorithms as detailed below.

Machine learning models

Two decision tree based ML models, RF and XGB, and one deep learning model, LSTM are applied. In addition, an ensemble learning approach based on a General Additive Model (GAM), aggregating the above three models, is also applied to further optimise the results. Figure 2 provides an overview of input and output data and the processing of the data using the MLs for the four sites with separate training data for 1-, 2- and 3-day forecasts for each site and pollutant (PM₁₀, NO_x and O₃). Note that the input includes the deterministic forecasts of PM₁₀, NO_x and O₃, in order to evaluate how much the deterministic forecasts can be improved by the ML algorithms. Several common performance metrics have been selected for comparing the prediction results of different machine learning models including Pearson correlation (r) and error measures: normalised mean average error (nMAE), mean absolute percentage error (MAPE) and normalised root mean squared error (nRMSE). For details on the methods and definition of the statistical performance indicators used, see Johansson et al. (2023).

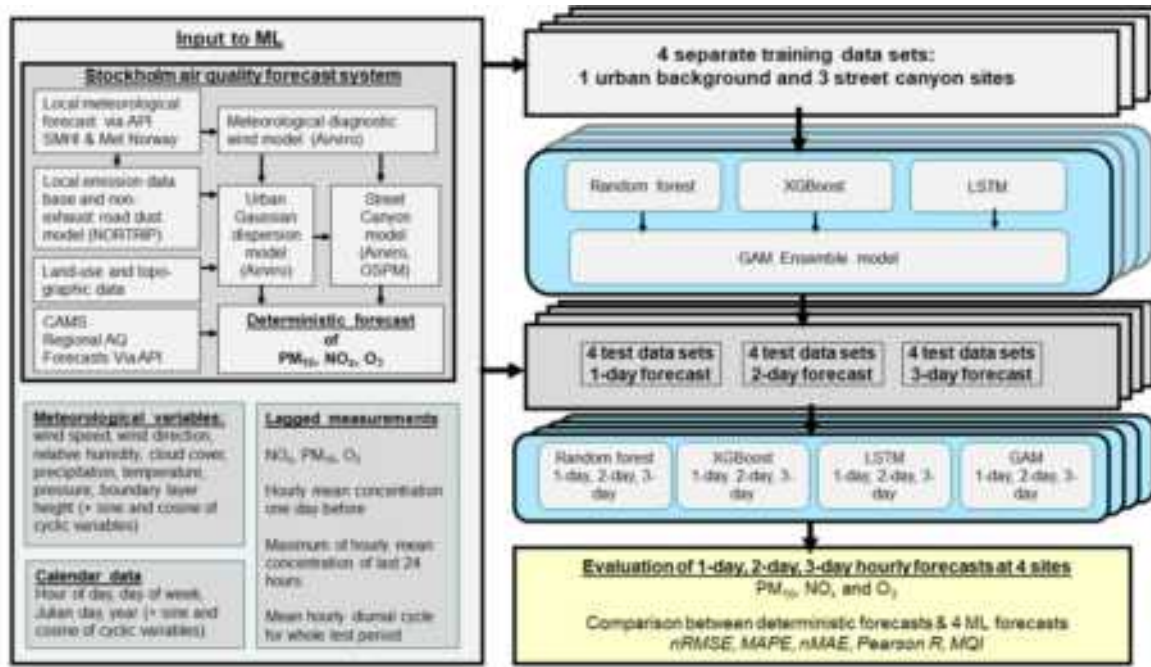


Figure 2. Schematic showing input data and division between training data sets for the different models, sites and pollutants.

Comparison between deterministic forecasts and ML - urban background

Figure 3 shows an example of the temporal variations in September 2021 in the forecasts with deterministic modelling and GAM in comparison to the observations. For all pollutants the ML tend to improve the variability in the observed concentrations compared to the deterministic forecasts, but there are significant deviations. For O₃ the minimum concentrations observed are often not forecasted so well and for PM₁₀ the highest concentrations are not captured by the models.

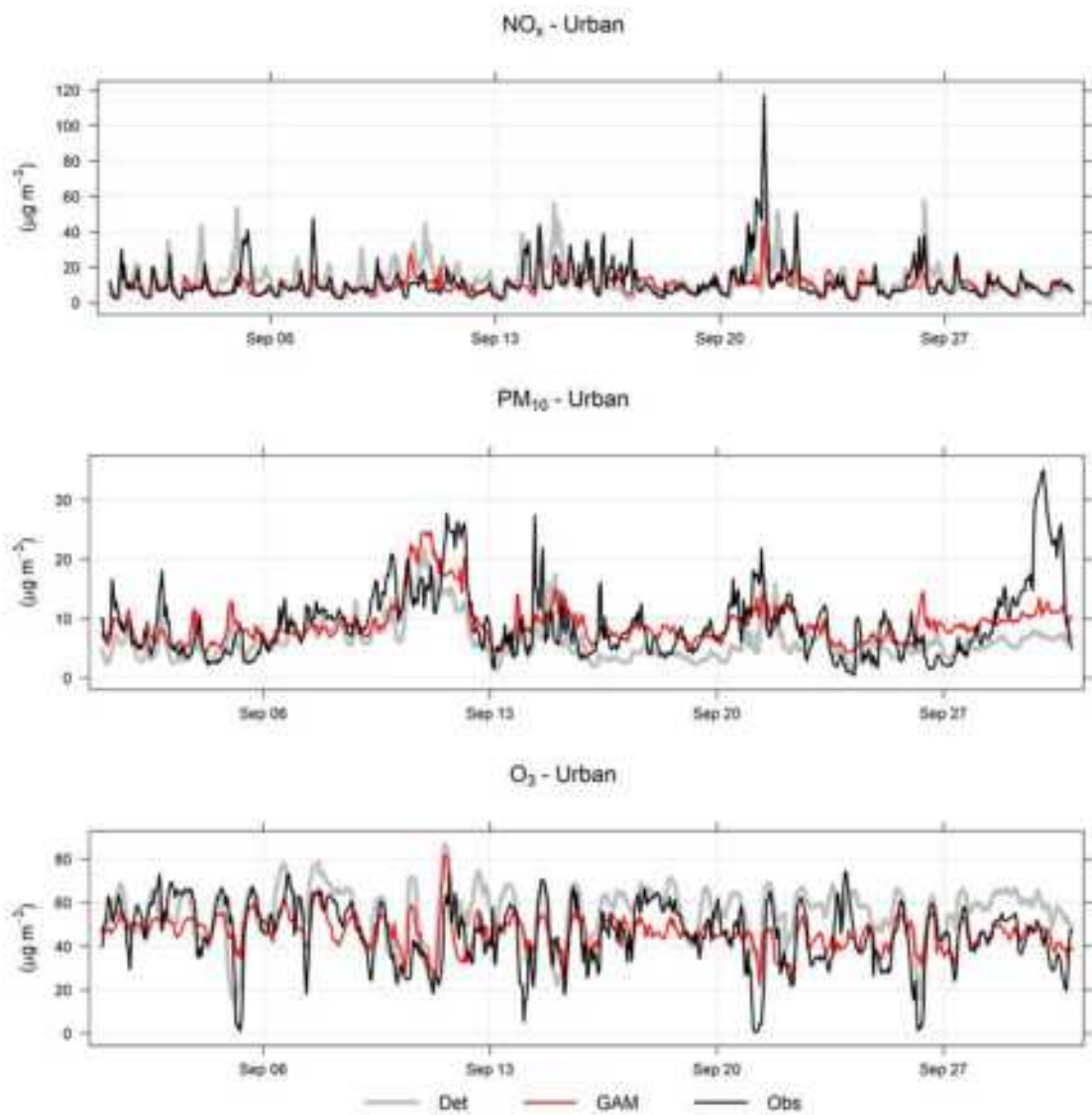


Figure 3. Temporal variations in hourly mean NO_x, PM10 and O₃ concentrations at the urban background site during September 2021 based on observations, deterministic forecasts and GAM. Mean of 1-, 2- and 3-day forecasts.

Figure 4 presents mean of 1-day, 2-day and 3-day statistical performances as ratios of ML to deterministic forecasts. This shows that NO_x is consistently improved using whatever ML model for all statistical performance indexes, whereas for PM10 and O₃ there are improvements in nRMSE and nMAE, but MAPE. Overall, the difference in performance between different models is small, less than 30%, but larger when comparing different pollutants.

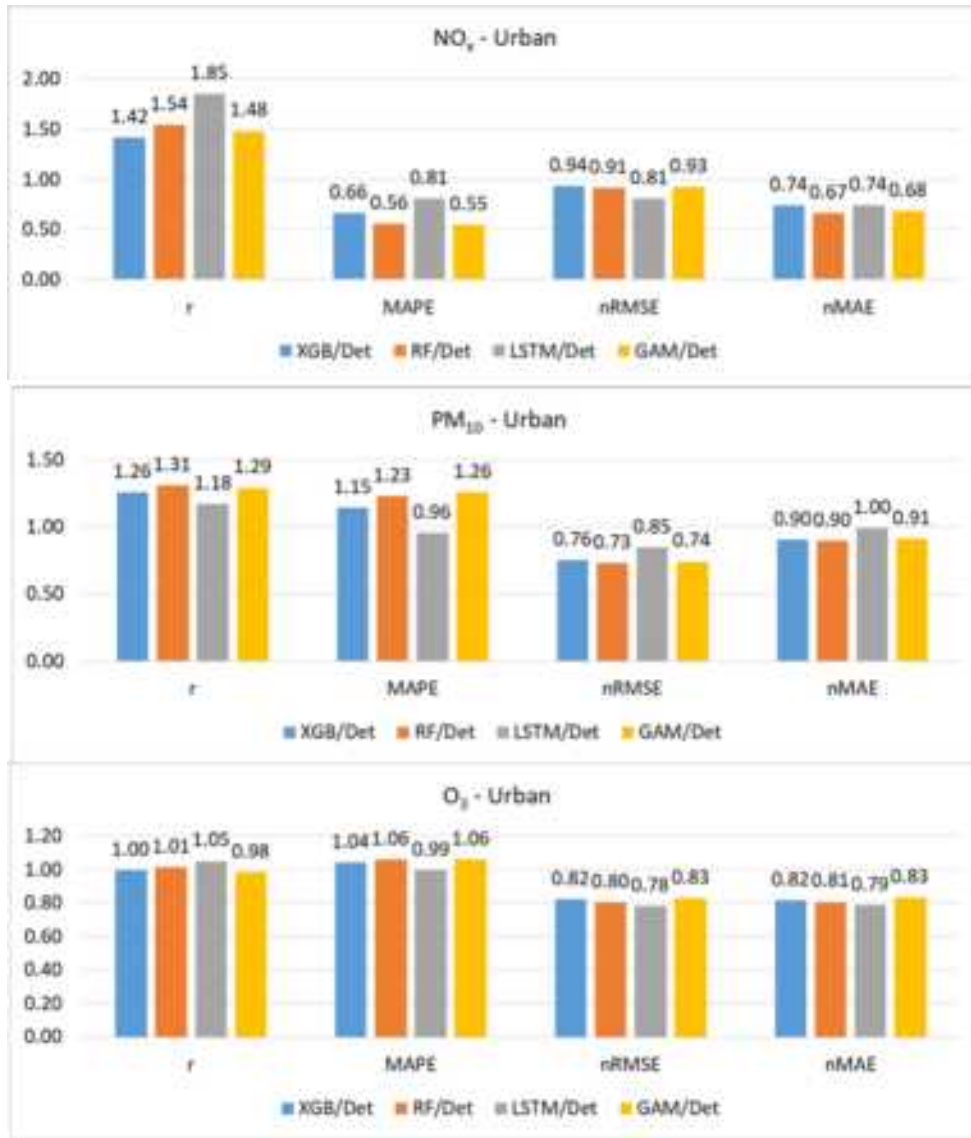


Figure 4. Ratios of statistical performances for ML versus the deterministic hourly forecasts for the urban site. Mean of 1-day, 2-day and 3-day forecasts.

Importance of features - urban background

The relative importance of different features depending on model (RF or XGB), pollutant (PM10, NOx, O₃) and forecast period (1-day, 2-day and 3-day) indicates the processes not captured by the deterministic models. In summary regarding importance of features for urban background:

- NOx. Lagged 24-hour mean concentrations, calendar data, wind speed and local deterministic forecasts are among the top-10 most important variables using RF and XGB, but it can be noted that the deterministic forecast is not the most important feature for any model. Of the calendar features hour is most important reflecting the importance of regular, diurnal variations in traffic emissions.
- PM10. The regional deterministic forecast is the most important feature for PM10 forecasts, both for RF and XGB and for all forecast days. Also lagged measurements, both average, minimum and maximum concentrations is important. Of the calendar features the seasonal variation is reflected in the importance of the Julian day.
- O₃. For O₃ RF and XGB shows very similar characteristics when comparing relative importance of different features. The regional deterministic forecast is the dominant feature both for RF and XGB, and for all forecast days. Also lagged measured maximum concentrations is of some importance. The

relative humidity is important, likely reflecting that O₃ concentrations are typically higher during dry, clear sky conditions, which may not be completely captured by the deterministic forecasts.

Discussion

The performances of the ML models are quite similar for the different sites and forecast days. But there are large differences in improvements for different pollutants. In general, our results indicate that ML is more effective in improving NOx than PM10 and O₃. For PM10 the ML show slight improvement in r but not much improvements in relative errors. This difference in improvement is likely associated with the different processes controlling the concentrations, such as different sources: NOx concentrations being mainly due to vehicle exhaust emissions which shows regular variations from one day to the next depending on day of the week and time of day, while PM10 is mainly due to road dust emissions controlled by a combination of variations in vehicle volumes and meteorological conditions that affect suspension of coarse particles from street surfaces (e.g Denby et al., 2013). Road dust is accumulated on the road surfaces during wet road surface conditions and suspended by vehicle induced turbulence during dry conditions.

The improvement of the forecasts of NOx with ML is partly driven by the calendar, hour, day of the week and to some degree also Julian day, and different features are similarly important for RF and XGB. For PM10 the seasonal variation described by Julian day is the most important feature at the street canyon sites, both for RF and XGB. This indicates that the deterministic forecasts are not capable at describing impacts of meteorology and road dust emissions on PM10, even though parameterisations of these processes are included in the deterministic modelling system. The total mass generated by road wear is a key factor for PM10 emissions and these emissions are strongly controlled by surface moisture conditions and this is taken into account by the NORTRIP model. But there are periods where surface wetness is not well modelled and it is not known if this is the result of input data, e.g. precipitation, or of the model formulation itself.

The deterministic forecast of O₃ underestimates concentrations at the urban site due to the fact that the local emissions of NOx influencing the photochemistry is not properly considered by the CAMS model, but this is corrected using the MLs. Despite this the deterministic forecast is the most important feature for both RF and XGB but also lagged measured mean and maximum O₃ concentrations improve the deterministic forecasts.

Conclusions

We have applied different machine learning algorithms to improve 1-, 2- and 3-day deterministic forecasts of NOx, PM10 and O₃ concentrations for a number of locations in Stockholm, Sweden. It is shown that degree of improvement of deterministic forecasts depend more on pollutant and monitoring site than on what ML algorithm is applied. Deterministic forecasts of NOx are improved at all sites, using all models. Pearson correlations increase by up to 80% and errors are reduced by up to 60%. For PM10 more variable results are seen, likely reflecting the more complicated processes controlling the road wear emissions which constitute a large fraction of PM10. For O₃ at the urban background site deviation between deterministically modelled absolute level is correct using ML; nRMSE and nMAE is reduced by on average around 20%, but there is almost no improvement in the correlation and MAPE.

Acknowledgements

The project was funded by ICT – The next generation and Digital future at KTH Royal Institute of Technology (contract VF 2021-0082).

References

- Denby, B. R., Sundvor, I., Johansson, C., Pirjola, L., Ketzel, M., Norman, M., Kupiainen, K., Gustafsson, M., Blomqvist, G., Omstedt, G. (2013). A coupled road dust and surface moisture model to predict non-exhaust road traffic induced particle emissions (NORTRIP). Part 1: road dust loading and suspension modelling *Atmos. Environ.*, 77, 283-300.
- Berkowicz, R. (2020). OSPM - A parameterised street pollution model, *Environmental Monitoring and Assessment*, 65, 323-331.
- Chuluunsaikhan, T., Heak, M., Nasridinov, A., Choi, S. (2021). Comparative Analysis of Predictive Models for Fine Particulate Matter in Daejeon, South Korea. *Atmosphere*, 12, 1295. <https://doi.org/10.3390/atmos12101295>.
- Doreswamy, Harishkumar K S., Yogesh, K.M., Gad, I. (2020). Forecasting Air Pollution Particulate Matter (PM2.5) Using Machine Learning Regression Models. *Procedia Computer Science* 171, 2057–2066.
- Johansson, C., Zhang, Z., Engardt, M., Stafoggia, M., and Ma, X. (2023). Improving 3-day deterministic air pollution forecasts using machine learning algorithms. *Atmos. Chem. Phys. Discuss.* [preprint], <https://doi.org/10.5194/acp-2023-38>, in review.
- Kamal, I. A. (2017). A random forest partition model for predicting NO₂ concentrations from traffic flow and meteorological conditions. *Science of the Total Environment* 651, 475–483.
- Krecl et al., 2021. Road dust is accumulated on the road surfaces during wet road surface conditions and suspended by vehicle induced turbulence during dry conditions
- Peuch, V.-H. et al. (2022). The Copernicus Atmosphere Monitoring Service: From Research to operations. *BAMS* 103, E2650–E2668.
- Stafoggia, M., Johansson, C., Glantz, P., Renzi, M., Shtein, A., de Hoogh, K., Kloog, I., Davoli, M., Michelozzi, P., Bellander, T. (2020). A Random Forest Approach to Estimate Daily Particulate Matter, Nitrogen Dioxide, and Ozone at Fine Spatial Resolution in Sweden. *Atmosphere*, 11, 239, 1-19.
- Shtein, A. Kloog, I., Schwartz, J., Silibello, C., Michelozzi, P., Gariazzo, C., Viegi, G., Forastiere, F., Karnieli, A., Just, A.C., Stafoggia, M. (2020). Estimating daily PM2.5 and PM10 over Italy using an ensemble model. *Environ. Monit. Assess.* 122
- Thongthammachart, T., Araki, S., Shimadera, H., Eto, S., Matsuo, T. and Kondo, A. (2021) An integrated model combining random forests and WRF/CMAQ model for high accuracy spatiotemporal PM2.5 predictions in the Kansai region of Japan. *Atmospheric Environment* 262, 118620.

Effects of noise barriers on population exposure to and health impacts of air pollutants downwind of highways

D. Schlesinger^{1*} and C. Johansson^{1,2}

¹ SLB-analys, Environment and Health Administration, City of Stockholm, 104 20 Stockholm, Sweden

² Department of Environmental Science (ACES), Stockholm University, 10691 Stockholm, Sweden

*correspondence: daniel.schlesinger@slb.nu

Introduction

Road traffic emissions are among the most important sources of many air pollutants like nitrogen oxides (NOx) and particulate matter (PM10) and it is the most important source of human exposure to many pollutants and noise in densely trafficked cities. Noise barriers are commonly used along highways passing close to populated areas to reduce impacts of noise exposure on residents. Previous studies show that air pollutant concentrations can be significantly reduced behind noise barriers placed along busy highways depending on, for example, the height of the barrier, the distance between the receptor and the barrier, and meteorological conditions.

In this study we use the Line source implementation RLINEXT of the U.S. EPA AERMOD dispersion model to estimate air pollutant concentrations in populated areas downwind of highways with noise barriers. Varying geometric and meteorological parameters, sensitivity of the concentration changes on those parameters is investigated. The model results are then combined with spatial population data to calculate population-weighted concentrations and the associated health effects, assuming an established dose-response function. Changes in pollutant concentrations due to the presence of noise barriers and their geometry are in this way used to estimate corresponding health benefits.

Methods

For the description of barriers in dispersion simulations we use the RLINEXT source type (Research Line Source model (RLINE)-Extended) as part of the line source option of the U.S. EPA regulatory air dispersion model AERMOD (AMS/EPA Regulatory Model, AERMOD, 2021; Snyder et al, 2013). The AERMOD/RLINEXT model (in the following referred to as RLINE model) is a semi-empirical dispersion model that provides good descriptions of concentrations measured in wind tunnel and tracer field studies in geometries that include a barrier between a line source and the receptor (Francisco et al., 2022).

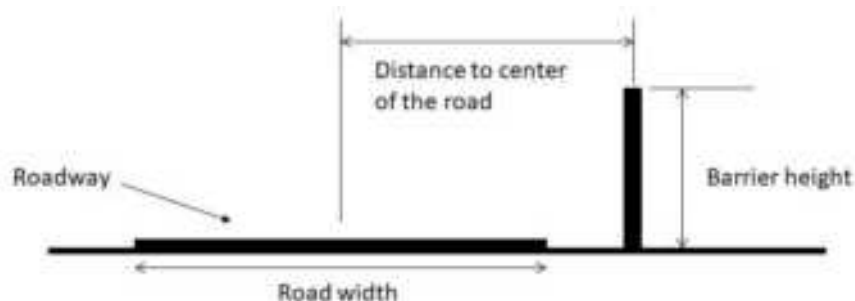


Figure 1: Parameters to be specified to run the RLINE model: distance to center of the road, road width and barrier height.

We ran sensitivity tests of the RLINE model to identify parameters that affect the results most and to compare to those of Computational Fluid Dynamics (CFD) simulations and expected behavior. All sensitivity tests were run for an idealized geometry of a long (ca 2.5 km), straight road extending in east – west direction on flat and open terrain. A noise barrier of height 2, 4, 6 and 8 m was placed north of the road in a distance of 8, 12 and 16 m from the center of the road, respectively. Apart from the geometric parameters, sensitivity to meteorological conditions, i.e. atmospheric stability and windspeed, was investigated. The computational

domain extended 100 m along the road, 300 m from the center of the road in perpendicular direction and 16 m in height with a computational grid of 1 m resolution in all three spatial dimensions.

For evaluating the potential health benefit of noise barriers we calculated NOx concentrations with and without barriers along highway E20 passing through a 4.5 km x 4.7 km densely populated area (15 325 inhabitants per km²) in southern Stockholm. Barriers of 2, 4, 6 and 8 m height were simulated on the northern side, barriers of 4 and 8 m height on both sides along the roughly 5 km long highway section. The horizontal resolution was set to 50 m (91 x 94 grid cells) and we used a climatology with 360 weather cases based on 18 years of meteorological measurements from a meteorological mast in Stockholm. The total population exposure was calculated as population-weighted concentrations based on annual mean concentrations at 2 m above ground and residential address (not accounting for people living at different floors). The change in total exposure was used to estimate an expected health impact (Martenies et al., 2015; Oudin et al., 2022):

$$\Delta N = \Gamma_{BLI} \times \left(1 - \exp\left(-\frac{\ln(RR)}{10} \Delta C\right) \right)$$

where ΔN is the change in death rate, RR is the relative risk per 10 µg/m³ and ΔC is the change in annual mean population-weighted concentration. We calculated the change in annual mortality applying a RR for NOx of 1.08 (CI: 1.06-1.11) (Nafstad et al., 2004). The baseline incidence rate, Γ_{BLI} , was set to 1329 deaths per 100 000 persons per year.

Sensitivity tests of the RLINE model

Generally, the concentrations behind barriers are well mixed over a height roughly proportional to the barrier height, and this persists over several barrier heights downwind. The barrier causes increased turbulence that spreads the plume and vertically lifts pollutants above the top of the barrier.

We investigate the sensitivity of the RLINE results for concentration changes on meteorological conditions, i.e. atmospheric stability and windspeed, the noise barrier's height and the distance between the barrier and the center of the road. The results are presented as concentration change relative to a situation without noise barrier, see Figure 2.

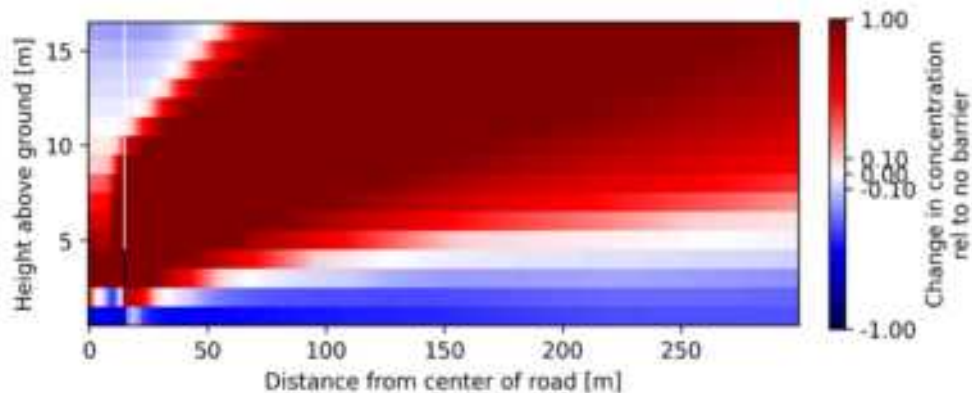


Figure 2: Concentration changes relative to concentrations without barrier. The vertical axis indicates the height above ground, the horizontal axis the distance from the center of the road. The above example shows results for a barrier located 16 m from the center of the road, a barrier height of 4 m and southerly (i.e. left to right) wind at speed 6 m/s.

The results for the example presented in Figure 2 show the expected uplift of the polluted air volume over the barrier and simultaneous dilution with significantly decreased concentration downwind and close to the ground and increased concentration higher up. Concentration changes on 2 m height above ground are assumed to be most relevant to the exposure of the population and we therefore focus on concentration changes at this height, see Figure 3. The calculated concentrations are enhanced just behind the barrier (< 30 m) to rapidly decrease

below those without barrier for longer distances downwind. Some unstable meteorological conditions can lead to slightly enhanced concentrations even at intermediate distances (~100 m) of the barrier, an effect known as "building downwash".

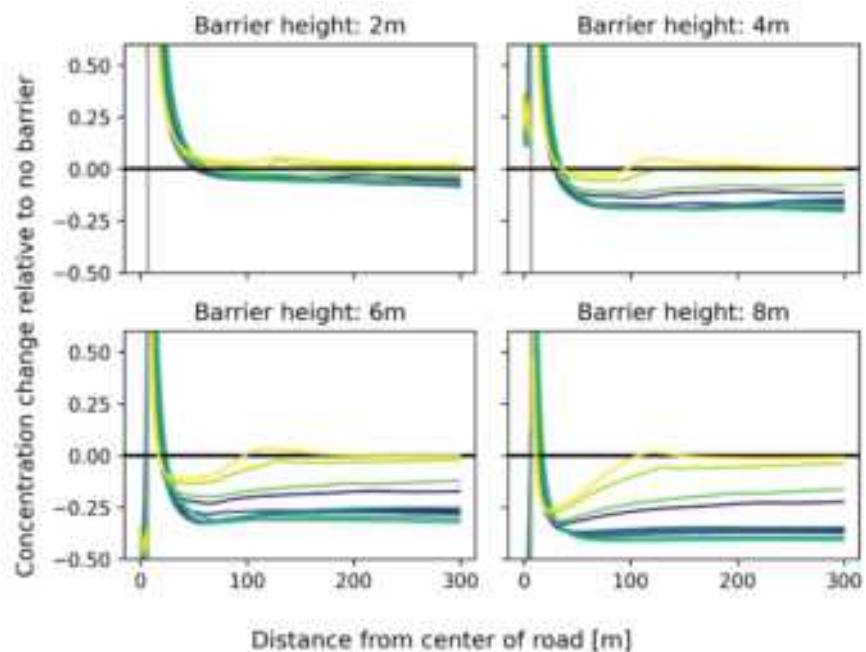


Figure 3: Variation of concentration changes at 2 m height above ground for different meteorological conditions and barrier heights. Meteorological scenarios change from darker colors for stable, to lighter colors for unstable stratification.

Concentrations downwind of the barrier generally decrease with increasing barrier height while the magnitude of this decrease strongly depends on the meteorological conditions.

Sensitivity tests with noise barriers placed at different distances to the center of the road show that the concentration change profiles are essentially shifted with the barrier's position which is thus insignificant for the concentration change at longer distances.

Potential changes in pollutant exposure and associated health impacts due to noise barriers

Using the RLINE model, we aim to estimate the effect of noise barriers on population-weighted air pollutant concentrations and the associated health impacts. In this theoretical scenario, the changes due to noise barriers along highway E20 in southern Stockholm are modelled.

With barriers, annual mean concentrations are found to be higher close to the highway (< 30 m) but lower by up to roughly 12 % than without barrier at longer distances (Figure 4).

Population-weighted concentrations are found to be lower for all barrier heights (Figure 5). Using a relative risk of mortality of 8 % per $10 \mu\text{g}/\text{m}^3$ we estimate the change of mortality due to the decrease in population-weighted concentrations that is caused by the presence of noise barriers. Depending on the height of the barrier, we estimate that 1 to 13 premature deaths may be saved per year per 100 000 inhabitants with barriers compared to the scenario without barrier.

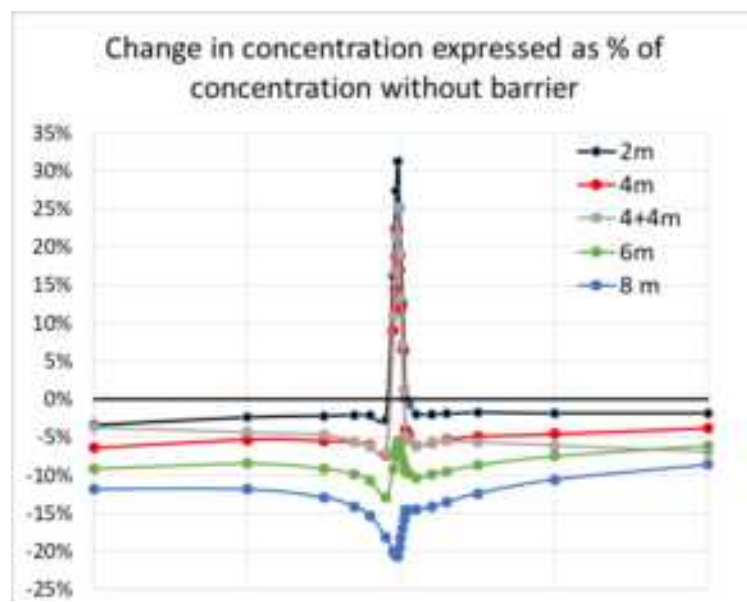


Figure 1: Percentage change in annual mean concentrations with distance from the center of the highway depending on barrier height (4-4 m means 4 m barriers on both sides of highway; otherwise barriers on one side of the highway).

Barriers on both sides of the highway can further reduce the concentrations significantly compared to barriers on one side of the highway. It should be noted that we have not considered if it is actually practically possible to install barriers everywhere along the highway and that the calculations do not consider any topographic or building effects. More detailed calculations considering these aspects would require CFD modelling.

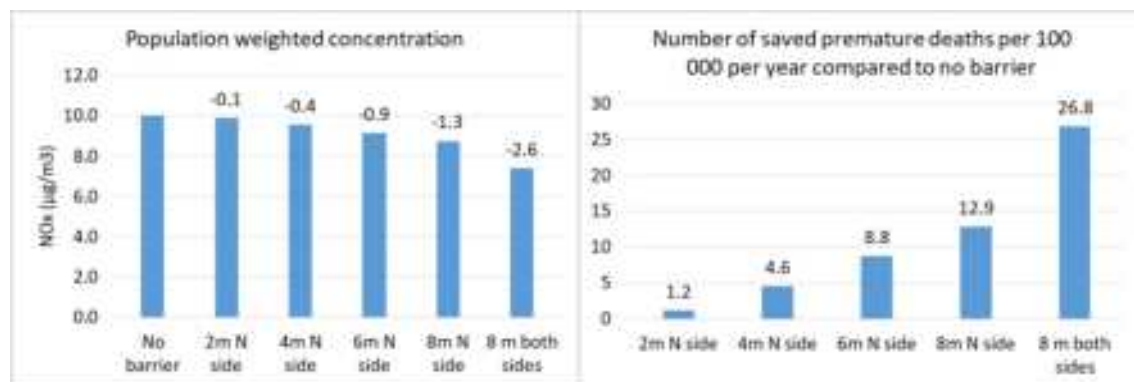


Figure 2: Variation of NO_x concentrations with the distance from the highway E20 (left diagram) and number of saved premature deaths per year per 100 000 inhabitants with barriers compared to without barrier (right diagram).

Summary

In this work we use the RLINEXT line source implementation of AERMOD to calculate air pollutant concentrations downwind of highways with noise barriers. We run sensitivity tests of the model for different barrier heights, distance of the barriers to the center of the road, and for different meteorological scenarios.

The model is found to generate high concentrations close (< ca 30 m) to the barrier and generally lower concentrations at larger distances from the barrier than without barrier. Concentrations at longer distances downwind generally decrease with increasing barrier height with the magnitude of this decrease strongly depending on the meteorological conditions.

The results on concentration changes due to the presence of a noise barrier are further used to estimate the potential mean changes in the population exposure to air pollutants and associated health impacts in a case study for highway E20 in southern Stockholm. The results of this case study show that, depending on the ~~barrier height~~, between 1 and 13 premature deaths per year per 100 000 inhabitants could be prevented using noise barriers.

Acknowledgements

This work was funded by the Swedish Transport Administration (Trafikverket) as part of the research and innovation portfolio *Bygga*.

References

- AERMOD (2021). User's Guide for the AMS/EPA Regulatory Model (AERMOD) U.S. Environmental Protection Agency, Office of Air Quality Planning and Standards, Research Triangle Park, NC (2021) Report No. EPA-454/B-21-001.
<https://www.epa.gov/scram/air-quality-dispersion-modeling-preferred-and-recommended-models#aermod>
- Amini S., Enayati Ahangar F., Schulte N., & Venkatram A. (2016). Using models to interpret the impact of roadside barriers on near-road air quality, *Atmospheric Environment*, 138(2016), 55–64. <http://dx.doi.org/10.1016/j.atmosenv.2016.05.001>
- Francisco D. M., Heist D. K., Venkatram A., Brouwer L. H., Perry S. G. (2022). Observations and parameterization of the effects of barrier height and source-to-barrier distance on concentrations downwind of a roadway, *Atmospheric pollution research*, 13(4), 101385. <https://doi.org/10.1016/j.apr.2022.101385>
- Martenies S. E., Wilkins D., Batterman S. A. (2015). Health impact metrics for air pollution management strategies. *Environment International* 85, pp 84-95. <https://doi.org/10.1016/j.envint.2015.08.013>
- Nafstad, P., Håheim, L.L., Wisloff, T., Gram, F., Oftedal, B., Holme, I., Hjermann, I. and Leren, P. (2004). Urban air pollution and mortality in a cohort of Norwegian men, *Environmental health perspectives*, 112(5), pp.610-615. <https://doi.org/10.1289/ehp.6684>
- Oudin A., Forsberg B., Malmqvist E. (2022). Hälsovinster med att uppnå miljömålet frisk luft, Umeå universitet, Institutionen för folkhälsa och kliniskmedicin, Avdelningen för hållbar hälsa. ISSN-nr 2003-3281 *Folkhälsa och klinisk medicin i Umeå rapporterar*.
- Schulte N., Snyder M., Isakov V., Heist D., Venkatram A. (2014). Effects of solid barriers on dispersion of roadway emissions, *Atmospheric Environment*, 97(2014), 286–295. <http://dx.doi.org/10.1016/j.atmosenv.2014.08.026>

Transition to Cleaner and Carbon-free Marine Fuels and their Potential Impacts on Air Quality in the North and Baltic Seas in the Future

D. A. Schwarzkopf¹, J. Hahn¹, R. Petrik¹, V. Matthias^{1*}, L. Ntziachristos².

¹ Helmholtz-Zentrum Hereon, Geesthacht, Germany, volker.matthias@hereon.de

² Aristotle University of Thessaloniki, Thessaloniki, Greece

Introduction

With a share of approximately 3 % to global greenhouse gas (GHG) emissions, the shipping sector is a significant contributor to global warming (IMO, 2020). To tackle this problem, the International Maritime Organization (IMO) announced in 2018 to limit NO_x emissions with the reduction of GHG emissions by 2050 with the goal to reduce ship-related GHG emissions by at least 50 % until 2050 compared to 2008. The precise pathway to achieve this goal is not yet clear but a transition to cleaner and carbon-free fuels, such as liquefied natural gas (LNG) or ammonia is an essential component.

The present study utilizes a novel methodology for constructing ship emission scenarios that is based on a virtual ship fleet using the Modular Ship Emission Modeling System (MoSES, Schwarzkopf et al., 2021, 2023). A future ship emission inventory for 2050 calculated with this method, focusing on the application of marine ammonia fuel, was used in a chemistry transport model (CTM). The results of this simulation allow an assessment of the potential future impacts of shipping on air quality in northern Europe, including the effects of ship-related ammonia emissions.

Emissions Data

The expected distribution of ship energy consumption on marine fuels is based on projections described in the *Maritime Trends 2050* (DNV-GL, 2020). The predictions for the increase in ship numbers and fleet capacity are based on the SHEBA Deliverable 1.4 (Fridell, 2016). The basis for the generated scenario shipping fleets was a reference fleet created from automatic identification system (AIS) ship position data for 2015. Temporally and spatially resolved scenario ship emissions data were calculated on the basis of these future shipping fleets using the MoSES model (Schwarzkopf et al. 2021). Applied emission factors for new fuels as well as for traditional fuel oils are based on recent literature. For marine ammonia engines, an ambitious technological development was assumed (Schwarzkopf et al., 2023).

The total gas and aerosol emissions from ships, calculated with the MoSES model show that CO₂ equivalent emissions decrease by 44% and NO_x by 61% until 2050 compared to 2015. Furthermore, emissions of primary aerosols decrease significantly.

Future projections of land based emission were calculated with the integrated assessment model REMIND (Baumstark et al. 2021). They were consistent with the middle-of-the-road SSP2 scenario (Riahi et al. 2017) and assume socio-economic developments and additional climate policy targets. Subsequently, all land-based emissions were mapped to GNFR emission sectors and spatially and temporally distributed with the internally available Highly Modular Emission Model (HiMEMO).

Emissions from biogenic sources were calculated using the Model of Emissions of Gases and Aerosols from Nature (MEGAN, version 3, Guenther et al. 2012, 2020).

Chemistry Transport Modeling

Pollutant concentrations and the impact of shipping on air quality were simulated with the chemistry transport model CMAQ v5.3 (Byun, 1999, 2006) for a domain that includes the North and Baltic Seas, as well as northern Europe gridded to 12 x 12 km² cells. The CMAQ model was built with the carbon bond 5 photochemical mechanism and the AE6 aerosol mechanism (Yarwood et al., 2005; Whitten et al., 2010; Sarwar et al., 2011).

Meteorological forcing data for the year 2015, calculated with the community model COSMO-CLM (version 5.0-clm15) (Rockel et al., 2008), which is embedded into the COSMO model for numerical weather prediction (Doms and Schättler, 2002; Doms et al., 2011; Baldauf et al., 2011), were used for CMAQ simulations.

Results and Discussion

Air pollutants from ship emissions can be transported atmospherically into populated regions and impact the air quality. To gain insight into potential future changes in air quality impacts of a major switch from marine fossil fuel oils to ammonia fuel, a respective emission scenario for 2050 was developed and used as input to the CMAQ chemistry transport model. The absolute impact of ships to air quality was calculated using the zero-out method. Percentage changes from a reference run for 2015 were calculated according to the relative growth.

The CTM results for 2050 show that ship-related NO₂ concentrations may decrease to less than $2 \mu\text{g m}^{-3}$ along the major shipping routes in the North and Baltic Seas. However, in hot spot regions, such as the Rotterdam-Antwerp port cluster, NO₂ concentrations remain high, up to $4-5 \mu\text{g m}^{-3}$ (Figure 1, left). In general, ship-related NO₂ concentrations are decreasing by 50 % or more (Figure 1, right), mainly due to the effect of the Nitrogen Emission Control Area (NECA), which applies to all vessels sailing in the North and Baltic Seas and that were laid-keel in 2021 or later.

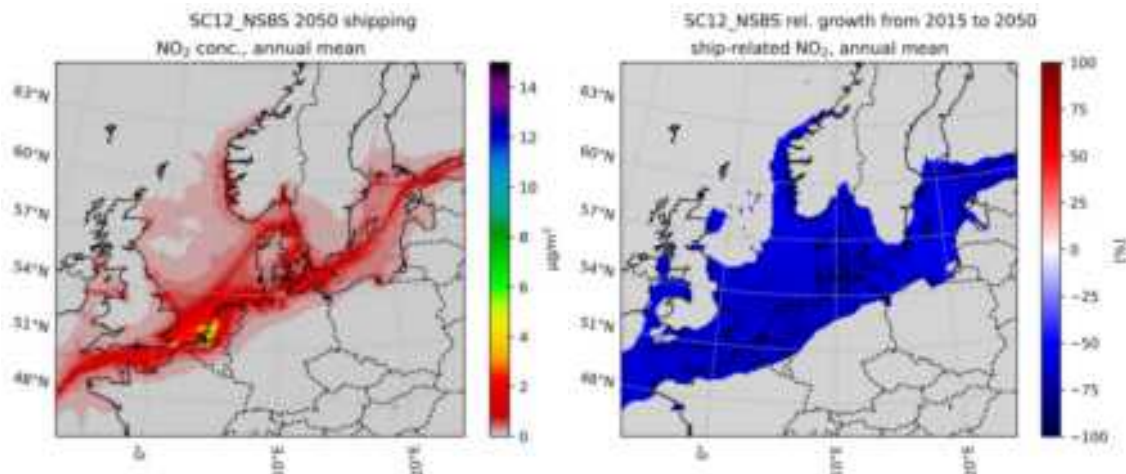


Figure 1: Annual averages of ship-related NO₂ concentrations [$\mu\text{g m}^{-3}$] in northern Europe and the North and Baltic Seas are shown in the left figure. The relative growth [%] from 2015 to 2050 for ship-related NO₂ is shown in the right figure.

Absolute ship-related PM_{2.5} concentrations in 2050 were simulated at 0.5 to $0.75 \mu\text{g m}^{-3}$ in coastal regions of the southern United Kingdom and Sweden, northern France and Germany and the Benelux countries. In the vicinity of the Rotterdam-Antwerp port cluster concentrations are higher at approximately $1 \mu\text{g m}^{-3}$ (Figure 2, left). Compared to 2015, ship-related PM_{2.5} concentrations decrease strongly by 50 to 75 %. Particularly over land (Figure 2, right). Over the sea, this decrease is less pronounced, due to additional secondary particulate matter that can form from the new ammonia emissions from shipping in combination with nitrogen or sulfur oxides. In front of the Rotterdam-Antwerp port cluster this even results in a slight increase of PM_{2.5} by approximately 10 %.

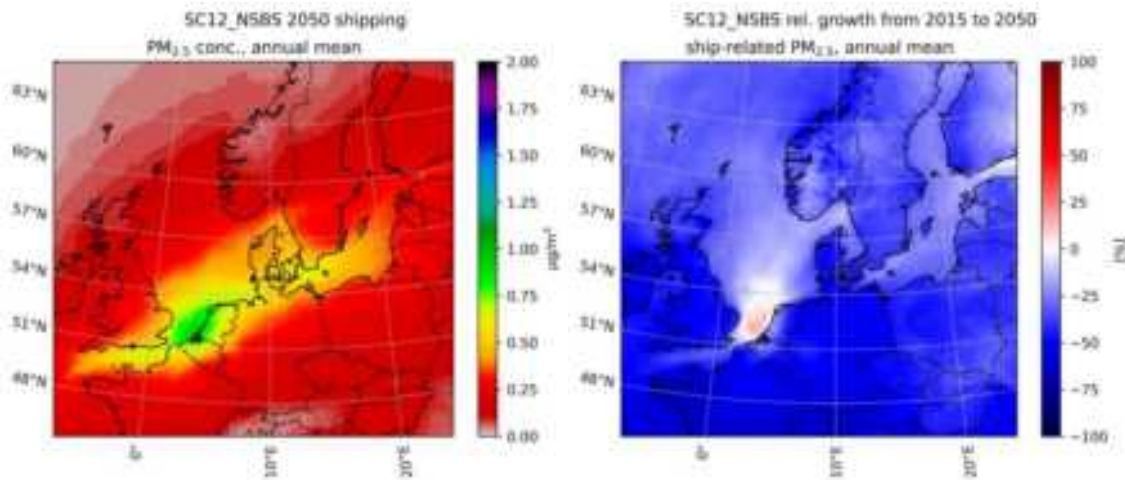


Figure 2: Annual averages of ship-related PM_{2.5} concentrations [$\mu\text{g m}^{-3}$] in northern Europe and the North and Baltic Seas are shown in the left figure. The relative growth [%] from 2015 to 2050 for ship-related PM_{2.5} is shown in the right figure.

The observations described for PM_{2.5} are even more pronounced for ammonium. Absolute ship-related NH₄⁺ concentrations in 2050 are in the range of 0.05 to 0.1 $\mu\text{g m}^{-3}$ in the affected coastal regions and up to 0.175 $\mu\text{g m}^{-3}$ close to Rotterdam/Antwerp (Figure 3, left). Compared to 2015, a decrease of 25 to 50 % can be observed over land. However, in most marine regions, however, ammonium concentrations increase by 25 to 75 % due to the newly emerging ship-related ammonia emissions (Figure 3, right).

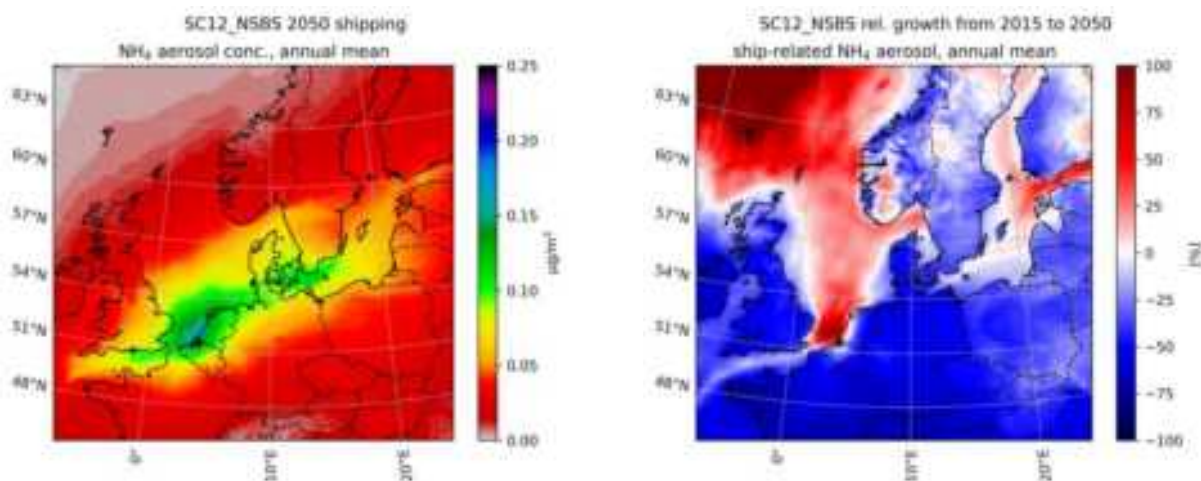


Figure 3: Annual averages of ship-related NH₄⁺ concentrations [$\mu\text{g m}^{-3}$] in northern Europe and the North and Baltic Seas are shown in the left figure. The relative growth [%] from 2015 to 2050 for ship-related NH₄⁺ is shown in the right figure.

The impact of ship emissions on ozone formation changes from an ozone-reducing effect of up to 15 along the major shipping routes and ports (Figure 4, left) to a promoting effect by up to 5 $\mu\text{g m}^{-3}$ (Figure 4, right). This is due to the reduced NO_x emissions from the designated NECA.

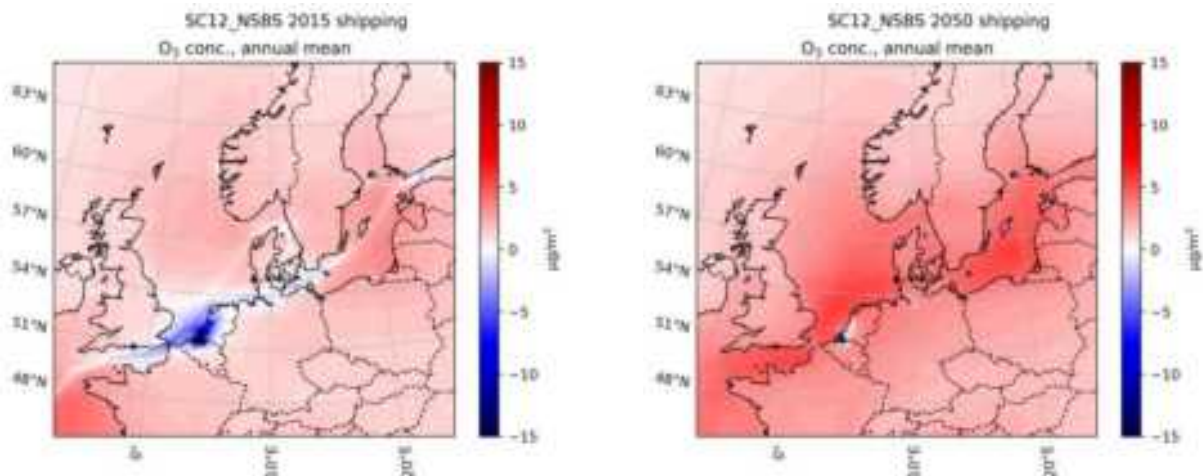


Figure 4: Annual averages of ship-related O_3 concentrations [$\mu\text{g m}^{-3}$] in northern Europe and the North and Baltic Seas are shown in the left figure. The relative growth [%] from 2015 to 2050 for ship-related O_3 is shown in the right figure.

Acknowledgements

This research were funded by the German Federal Maritime and Hydrographic Agency (BSH) in the framework of the BSH project BSH contract code 10042529 (Horizon contract code 130 2018) and the EU Horizon 2020 project SCAMPEX (No. 814805).

References

- Baumstark L., et al. (2021). REMIND2.1: transformation and innovation dynamics of the energy-economic system within climate and sustainability limits, *Geosci. Model Dev.*, 14.10, 6571–6603.
- DNV-GL (2020). Maritime forecast to 2050 - Energy transition outlook 2020 Ed, *Technical report*.
- Fridell E., Parsmo R., Boteler B., Troeltzsch J., Kowalczyk U., Piotrowicz J., Jalkanen J.P., Johansson L., Matthias V., Ytreberg E. (2016). Sustainable Shipping and Environment of the Baltic Sea Region (SHEBA) Deliverable 1.4, type RE, *Technical report*, IVL.
- Guenther A. B., Jiang X., Heald C. L., Sakulyanontvittaya T., Duhl T., Emmons L. K., Wang X. (2012). The model of emissions of gases and aerosols from nature version 2.1 (MEGAN2.1): An extended and updated framework for modeling biogenic emissions. *Geosci. Model Dev.*, 5(6), 1471–1492.
- Guenther A., Jiang X., Shah T., Huang L., Kemball-Cook S., Yarwood G. (2020). Model of Emissions of Gases and Aerosol from Nature Version 3 (MEGAN3) for Estimating Biogenic Emissions, *Air Pollution Modeling and its Application XXVI*, 187–192.
- International Maritime Organisation (2020). Fourth IMO GHG Study, *Technical report*.
- Riahi K., et al. (2017). The Shared Socioeconomic Pathways and their energy, land use, and greenhouse gas emissions implications: An overview, *Glob. Environ. Change*, 42, 153–168.
- Sarwar G., Appel K. W., Carlton A. G., Mathur R., Schere K., Zhang R., Majeed M. A. (2011). Impact of a new condensed toluene mechanism on air quality model predictions in the US, *Geosci. Model Dev.*, 4, 183–193.
- Schwarzkopf D.A., Petrik R., Matthias V., Quante M., Majamäki E., Jalkanen, J.P. (2021). A ship emission modeling system with scenario capabilities, *Atmos. Environ.*: X, 12, 100132.
- Schwarzkopf D. A., Petrik R., Hahn J., Ntziachristos L., Matthias V., Quante M. (2023). Future ship emission scenarios with a focus on ammonia fuel, *Atmosphere*, 14, 5.
- Whitten G. Z., Heo G., Kimura Y., McDonald-Buller E., Allen D. T., Carter W. P., Yarwood G. (2010). A new condensed toluene mechanism for carbon bond: CB05-TU, *Atmos. Environ.*, 44, 5346–5355.
- Yarwood G., Rao S., Yocke M., Whitten G (2005). Updates to the carbon bond mechanism: CB05, *Technical report*.

The impact of data splitting in air quality modelling on the possibilities of interpretation of the results

J. Kajewska¹, J. Kajewska-Szkudlarek²

¹Department of Applied Mathematics, Wroclaw University of Environmental and Life Sciences, Grunwaldzka Street 53, 50-357 Wroclaw, Poland; ORCID 0000-0002-0157-516X

² Institute of Environmental Engineering, Wroclaw University of Environmental and Life Sciences, Grunwaldzki Square 24, 50-363 Wroclaw, Poland; ORCID 0000-0002-0253-8133

Introduction

The issue of air quality modelling is widely discussed in the literature. One of the trends is the analysis of the relationship/influence of environmental factors on the concentration of pollutants in the air using various (supervised and unsupervised) machine learning methods. The main problem of these models is their poor fit and interpretation potential. A key issue in pollutant concentration modelling is to determine explanatory variables. The most common predictors are traffic intensity and meteorological conditions (Kamińska 2018; Shang et al., 2019; Sahu et al., 2020; Xie et al., 2020; Gu, Li and Meng, 2022) or additionally air pollution factors (Gu et al., 2020; Menares et al., 2021; Xing et al., 2021). Implemented alone, these provide predictions with unsatisfactory accuracy: Larkin et al. (2017) obtained a 52% fit, Sayegh et al. (2016) a 54% fit, Kamińska (2018) a 58%, Kajewska & Turek (2020) 69% fit between observed and predicted values (yellow part in Fig.1.).

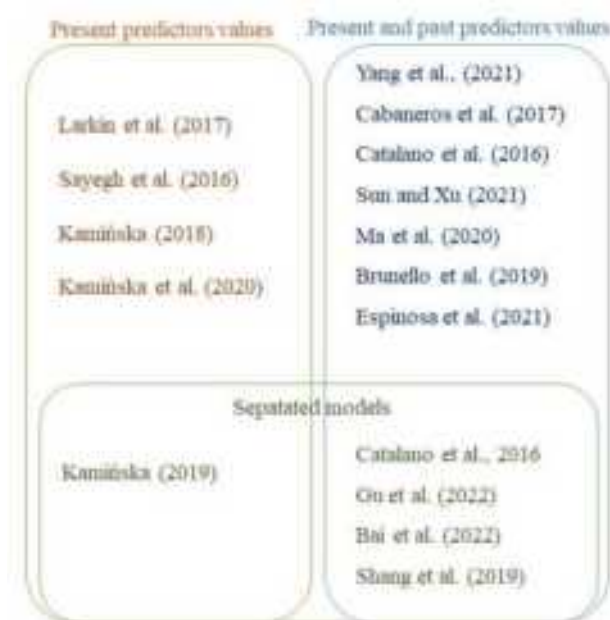


Figure 1: Examples of work using only current or also past predictor values and split models in air pollution modelling

To improve the quality of the model, researchers began to introduce the past values of the dependent variables (blue part in Fig.1.) Such models gain in accuracy because history carries essential information, which computational intelligence is able to use in forecasting (Yang et al., 2021). Cabaneros et al. (2017) used lagged air pollution and meteorological data to predict roadside NO₂ concentration using Multilayer Perceptron (MLP) alone and combined with Classification and Regression Trees (C&RT), stepwise regression, and principal component analysis (PCA). Catalano et al. (2016) created ARIMAX model by considering previous values of NO₂ concentrations, as well as traffic and meteorological data. Sun and Xu (2021) used historical data describing weather and pollution conditions to forecast hourly PM_{2.5}. Ma et al. (2020) used lagged time series of meteorological and pollution factors in the PM_{2.5} model (Lag layer-LSTM-Fully Connected network). Researchers analysed pollution concentration as a time series also and considered the impact of number of lagged values on the air quality modelling (Brunello et al., 2019; Espinosa et al., 2021).

A further way to obtain high accuracy is to split the whole database into subsets and create separate models for each subset. However, this strategy requires a large data set to provide enough data sets to train and test each of the component models. The use of optimized partitioning even for models without past values has improved the quality of modelling (Kaminska and Gurowska-Szkudlarek 2019). Multi-model approach allows one to estimate well also peak concentrations (Catalano *et al.*, 2016). Gu *et al.* (2022) proposed a hybrid interpretable model combining a deep neural network and a Nonlinear Auto Regressive Moving Average with Exogenous Input (NARMAX) for actual PM_{2.5} prediction. They included historical PM_{2.5}, weather, and seasonal variables, as well as their time lags, and built two submodels for typical and peak PM_{2.5} concentrations. Bai *et al.* (2022) also used a hybrid machine learning technique (extreme learning machine, ELM) based on PM_{2.5} outlier detection and splitting of the database into subseries with different characteristics. Shang *et al.* (2019) similarly implemented split models for PM_{2.5} concentration prediction using classification and regression tree (C&RT) and ensemble extreme learning machine (EELM) techniques.

The aim of the present research was to create an hourly prediction of NO_x levels for the urban area taking into account the splitting of the data set into subsets of characteristics due to some feature or set of features. We combines C&RT and CA (cluster analysis) to divide the data set into subsets with similar conditions and machine learning methods such as RF, MLP, and SVR for NO_x modelling. The research was conducted based on measurement data from 2015 to 2021 in Warsaw, Poland (GPS coordinates 19.80741-17.17594 E; 51.04278-51.20996 N).

Methods

The scheme of these research is as follows:

- 1) selection of predictors for NO_x modelling using RF;
- 2) splitting the database into subsets in two different ways, using Classification and Regression Tree (C&RT) and Cluster Analysis (CA);
- 3) creation of Random Forest (RF), multilayer perceptron (MLP), and Support Vector Regression (SVR) predictive models for NO_x hourly concentrations.

All details of methods one can find in (Kaminska and Gurowska-Szkudlarek, 2023).

Results

We proposed a splitting of the data, which grouped the moments in time in a given way. The 13 variables used in the modelling ($ws_{t-2}, ws_{t-1}, tr_{t-2}, tr_{t-1}, tr_t, t_t, rh_{t-1}, rh_t, NOx_{t-2}, NOx_{t-1}, NO2_{t-2}, NO2_{t-1}, h_t$)³³ were selected from 23 available by the iterative method using Random Forest (RF).

We considered two splitting methods: decision tree (DT) and cluster analysis (using C&RT algorithm). In the decision tree method, only one variable proved crucial in making the splitting - NOx_{t-1} . This means that in this method, the only splitting criterion is the last measured concentration of NO_x. This method produced eight NOx_{t-1} intervals covering \mathbb{R}_+ , with boundary points at 47.04, 82.1, 117.3, 162.5, 242.6, 355.4, and 526.8 μgm^{-3} (Fig.2.)

As a result of the cluster analysis, 8 clusters were also obtained. In this method, all variables played a role in creating subsets. Each cluster describes different ambient conditions that most strongly influence the current concentration of NO_x, taking into account traffic volume, meteorological conditions, and time of day (Fig.3.).

³³ ws - wind speed, tr – traffic flow, t – air temperature, rh - relative humidity, h - hour in 24h system (the lower subscript indicates the delay in time (t - actual, t-1 from the previous hour, etc.).

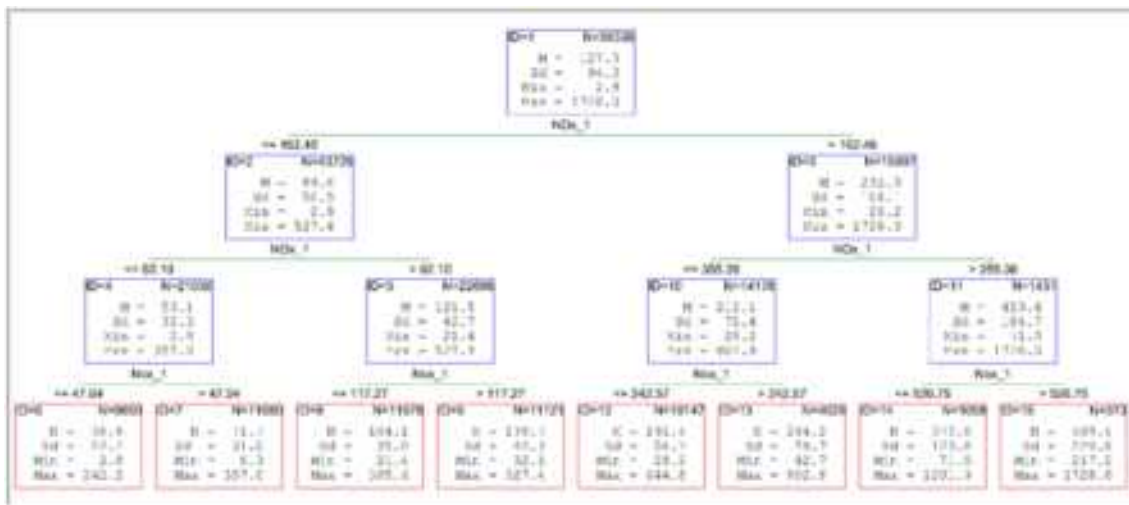


Figure 2:C&RT regression decision tree, where M – mean, Sd – standard deviation source: Karmyska and Kajewska-Szkudlarek, 2023)

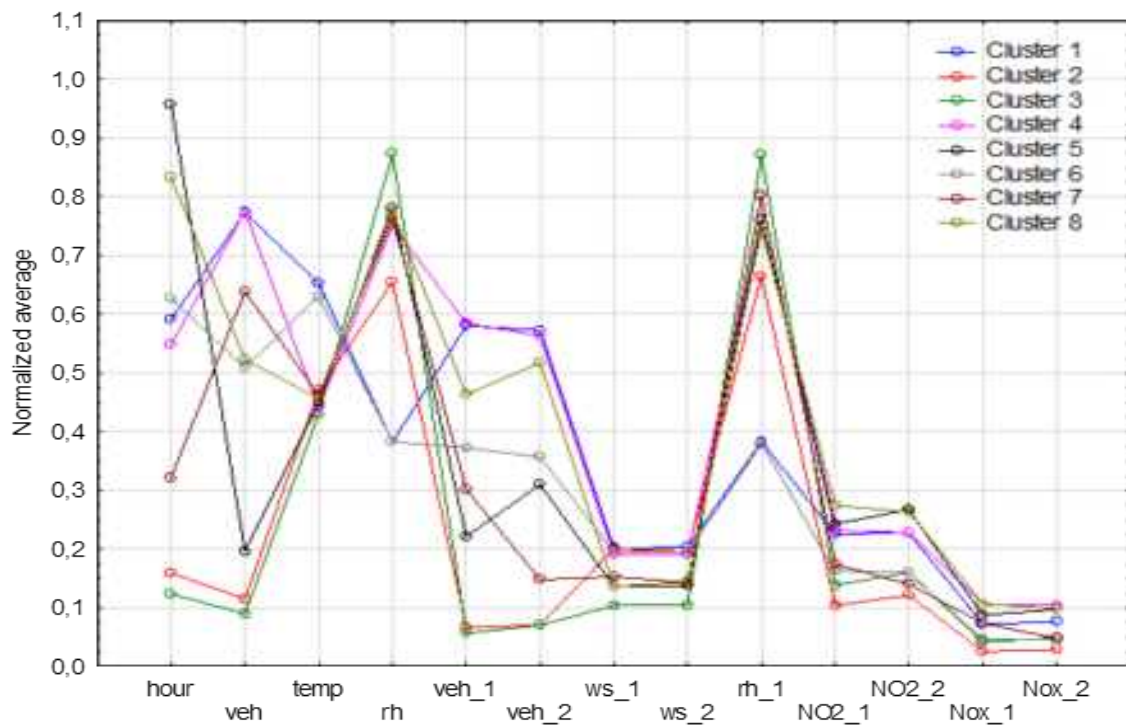


Figure 3:Mean values of predictors in clusters source: Karmyska and Kajewska-Szkudlarek, 2023)

Clusters 1 and 4 are one of the most numerous (10215 and 10374 samples, respectively) and contain the peak traffic periods in the afternoon with the highest traffic flow and high concentrations of NO_x and NO_2 from the previous hours. They differ in terms of weather conditions. Cluster 1 represents high-pressure summer conditions: high air temperature and low humidity, both current and past. Cluster 4 represents low temperature and very high humidity – wet spring-autumn weather. In both cases, the wind conditions favour the evacuation of pollutants.

Clusters 2 and 3 contain night times with the lowest traffic flow and current and previous concentrations of NO_x and NO_2 , but the periods in cluster 2 are characterized by favourable wind conditions for pollutants evacuation. Cluster 3 is the most numerous, with 11395 samples.

Cluster 5 contains evening and night hours with relatively low traffic flow that continues to decrease hour by hour, as well as relatively high concentrations of NO_x and NO_2 from preceding hours and average weather conditions.

Cluster 6 also contains mainly afternoon peak periods, but with significantly lower traffic flows, suggesting weekends and holidays, where the volumes are lower than on working days but higher than during the night.

Cluster 7 contains morning peak traffic hours, with increasing traffic flow and NO_x and NO₂ concentrations, and average weather conditions.

Cluster 8 consists of late afternoon and early evening hours, with comparable current and previous traffic levels (one and two hours ago) and relatively low wind speeds. The accumulation in the hours preceding the pollutants and unfavourable weather conditions for the evacuation of the pollutants lead to the highest average concentration of NOx equal to 190.9 μgm^{-3} .

For each of the two received divisions (each time into 8 subsets), we created models using machine learning: Random Forest (RF), Artificial Neural Network (ANN) and Support Vector Regression (SVR). For comparison purposes, we also built models for a full dataset without splitting for each modelling methods. The goodness of model fit was measured by 4 popular measures summarized in Tab.1. In each case, the model based on the SVR technique was the weakest fit. ANN and RF methods show a similar level of fit. Interesting conclusions can be drawn from the analysis of the fit of individual models for each of the subsets.

Table 1. Goodness of fit measures for analysed models.

	Goodness of fit measures	RF	ANN	SVR
C&RT	R^2	0.869	0.872	0.840
	$MADE [\mu\text{gm}^{-3}]$	21.0	20.6	24.8
	$MAPE [\%]$	17.2	16.8	23.7
	$RMSE [\mu\text{gm}^{-3}]$	33.9	34.0	38.1
CA	R^2	0.842	0.878	0.836
	$MADE [\mu\text{gm}^{-3}]$	21.7	21.5	27.4
	$MAPE [\%]$	17.3	17.3	34.7
	$RMSE [\mu\text{gm}^{-3}]$	40.4	34.3	39.7
Full dataset	R^2	0.852	0.856	0.678
	$MADE [\mu\text{gm}^{-3}]$	21.8	22.2	42.0
	$MAPE [\%]$	17.5	18.9	91.6
	$RMSE [\mu\text{gm}^{-3}]$	36.5	35.8	53.5

Model fit for individual leaves (in DT splitting method) and clusters (in CA splitting method) varied (Fig. 2).

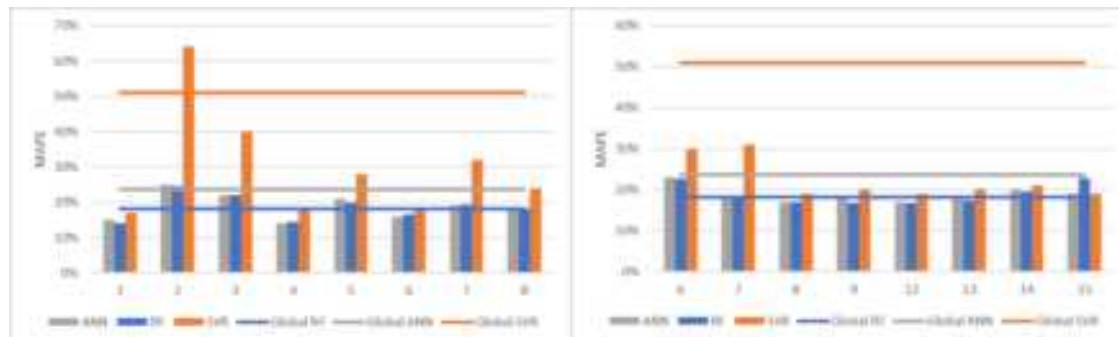


Figure 4: Mean Average Percentage Errors for each subset separately in CA (left) and C&RT (right)
source: Karmaska and Kajiwoda-Szkudlarek, 2023)

We recorded the most uniform fit for C&RT partitioning, with the model predicting the lowest and low concentrations the weakest (leaves 6 and 7 in Fig.4.). In contrast, partitioning by complex environmental conditions resulted in a more varied quality of fit for individual clusters. All models obtained the best fit (MAPE between 14% and 18%) for afternoon peak traffic periods under different ambient conditions: clusters 1, 4, and 6 (Fig. 4.). A much worse fit was recorded for the RF and ANN models constructed for night-time conditions (clusters 2 and 3), which featured low NO_{xt-1} values. The least fit models were all for cluster 2, which described night hours with favourable conditions for the evacuation of pollutants, which gave the lowest pollution concentrations.

Conclusions

The results show that both approaches to model specification may be effectively used to improve the quality of modelling of NO_x concentrations in urban areas. The choice of approach should be determined by the purpose of the analysis. If the forecast is to be used only to provide instantaneous information, for example, to provide public warnings, then methods based on C&RT will be sufficient. However, if the goal of the analysis is to identify particular ambient conditions that favour the achievement of a particular level of air quality, with an analysis of the influence of individual factors, and the creation of scenarios for development planning or other city management actions, then models based on CA provide the possibility of obtaining such information.

Acknowledgements

This work was supported by Department of Applied Mathematics and Institute of Environmental Engineering of Wroclaw University of Environmental and Life Sciences (Poland). Traffic data are provided by the Department of Traffic and Public Transport Management of the Roads and City Maintenance Board in Wroclaw. Meteorological data are provided by Institute of Meteorology and Water Management - National Research Institute (PIB). The source of the meteorological data is IMGW (PIB). Data from IMGW (PIB) have been processed. Data are publicly available on the portal <https://danepubliczne.imgw.pl/>. Air pollution data was collected by the Provincial Environment Protection Inspectorate in Wroclaw.

References

- Han, F., Li, Z. and Wang, L. (2022) Novel hybrid extreme learning machine and multi-objective optimization algorithm for air pollution prediction. *Applied Mathematical Modelling*, 106, pp. 177–198. doi:10.1016/J.APM.2022.01.023.
- Brunello, A. et al. (2019) Assessing the Role of Temporal Information in Modelling Short-Term Air Pollution Effects Based on Traffic and Meteorological Conditions: A Case Study in Wroclaw. *Communications in Computer and Information Science*. doi:10.1007/978-3-030-30278-8_45.
- Caballero, J.M., Gómez, I.B. and Leal, R.R. (2017) Traffic And Visual Network Models for Effective Prediction and Mitigation of Odor in Roadside NOx Pollution. *Energy Procedia*, 142, pp. 3524–3530. doi:10.1016/J.EGYPRO.2017.12.240.
- Catalano, M. et al. (2016) Impacting the prediction of air pollution peaks episodes generated by urban transport networks. *Environmental Science & Policy*, 60, pp. 69–83. doi:10.1016/J.ENVSCI.2016.03.008.
- Espinosa, R. et al. (2021) A time series forecasting-based multi-criteria methodology for air quality prediction. *Applied Soft Computing*, 113, p. 107850. doi:10.1016/J.ASOC.2021.107850.
- Gu, Y. et al. (2020) Assessing outdoor air quality and public health impacts: attributing air to residential areas based on air monitoring. *Resources, Conservation and Recycling*, 159, p. 104812. doi:10.1016/J.RESCONREC.2020.104812.
- Gu, Y., Li, H. and Meng, Q. (2021) Hybrid interpretable predictive machine learning model for air pollution prediction. *Neurocomputing*, 468, pp. 123–136. doi:10.1016/J.NEUCOM.2021.09.051.
- Karmaska, T. (2018) The use of random forests in modelling short-term air pollution effects based on traffic and meteorological conditions: A case study in Wroclaw. *Journal of Environmental Management*, 217. doi:10.1016/j.jenvman.2018.03.094.
- Karmaska, T. and Kajiwoda-Szkudlarek, J. (2023) The importance of data splitting in estimating NO_x concentration

- Pradhan, S. *Science of The Total Environment*, 868, p. 161744. doi:10.1016/J.SCITOTENV.2023.161744.
- Ramakrishna, T. A. and Durdle, J. 2020. Exploratory spatial description of the traffic impact on the NO₂ concentrations in the traffic corridor. *Archives of Environmental Protection*, 46(1), pp. 93–99. doi:10.24425/aep.2020.132530.
- Ramakrishna, T. A. 2018. A random forest partition model for predicting NO₂ concentrations from traffic flow and meteorological conditions. *Science of The Total Environment*, 651(1), pp. 475–483. doi:10.1016/j.scitotenv.2018.09.196.
- Larkin, A. et al. 2017. Global Land Use Regression Model for Nitrogen Oxide Air Pollution. *Environmental Science & Technology*, 51(12), pp. 6957–6964. doi:10.1021/acs.est.7b01148.
- Ma, J. et al. 2020. LSTM-FLSTM deep learning network based on Bayesian Optimization for multi-sequential-variant PM2.5 prediction. *Sustainable Cities and Society*, 60, p. 102237. doi:10.1016/J.SCS.2020.102237.
- Menares, C. et al. 2021. Investigating PM2.5 levels in Mexico City using deep learning neural networks. *Urban Climate*, 38, p. 100906. doi:10.1016/J.UCLIM.2021.100906.
- Sahu, S.K. et al. 2020. Estimating ground-level PM2.5 concentrations and associated health risk in India using satellite-based SO₂ and WRF simulated meteorological parameters. *Chemosphere*, 255, p. 126969. doi:10.1016/J.CHEMOSPHERE.2020.126969.
- Sayegh, A., Latte, J. E., and Ropponen, E. 2015. Understanding how roadside concentrations of NO₂ are influenced by the background levels, traffic density, and meteorological conditions using Bounded Regression Trees. *Atmospheric Environment*, 127, pp. 163–175. doi:10.1016/j.atmosenv.2015.12.024.
- Shang, Z. et al. 2018. A novel model for monthly PM2.5 concentration prediction based on GARCH and EEMD. *Science of The Total Environment*, 651, pp. 3043–3052. doi:10.1016/J.SCITOTENV.2018.10.193.
- Xie, W. and Xie, Z. 2021. A novel monthly PM2.5 concentration prediction model based on feature selection, training set screening, and mode decomposition-marginalization. *Sustainable Cities and Society*, 75, p. 103348. doi:10.1016/J.SCS.2021.103348.
- Xie, M. et al. 2019. A novel hybrid multi-variate time series model for forecasting the traffic-related air pollution. *Applied Mathematical Modelling*, 77, pp. 1242–1254. doi:10.1016/J.APM.2019.09.013.
- Xing, H. et al. 2020. PM_{2.5} concentration modeling and prediction by using temperature-based deep neural network. *Neural Networks*, 133, pp. 157–165. doi:10.1016/J.NEUNET.2020.10.013.
- Yang, Z. et al. 2021. Nonlinear and adaptive meteorological effects on daily levels of ambient PM_{2.5} and O₃: Evidence from ZH41000000. *Journal of Cleaner Production*, 278, p. 123931. doi:10.1016/J.JCLEPRO.2020.123931.

Particle Number Box-Model Calculations in a Street Canyon and Comparison to Measurements

Nicola Toenges-Schuller^{1*}, Stefan Hausberger², Christiane Schneider¹, Werner Stadlhofer², Ulrich Uhrner²

¹ AVISO GmbH, 52074 Aachen, Germany, nicola.toenges-schuller@avisogmbh.de, ² Institute of Thermodynamics & Sustainable Propulsion Systems, Graz University of Technology, Austria

Introduction

Directly at the tailpipe, motor-related exhaust particles are mostly solid (elemental carbon, organics of very low volatility, ash components). Due to increasing use and improvements of filters as part of the exhaust aftertreatment systems of cars and other motor vehicles, solid exhaust particles lose importance compared to other road traffic emission processes such as abrasion processes, and the formation of secondary particles. The latter are formed by nucleation and/or condensation of exhaust compounds, that are in the gas-phase at the time of emission, and by cooling, dilution, and oxidation end up in the particle-phase (water, sulfuric acid, other volatile organic compounds of intermediate volatility). The time scale for this lies between a few seconds (cooling, dilution) and minutes to days (oxidation of VOCs). Some of these newly formed very small particles vanish again quickly by dry deposition or evaporation, as, e.g., can be seen by the measurements of Wehner et al. (2009), who measured PN at the rear of a passenger car (inlets of the instruments mounted on a modified bicycle rack).

The limit value for PN emissions at the tailpipe in type approval and in-service testing of vehicles refers to solid particles, PN air quality measurements usually include also volatile particles. It is therefore desirable to link solid particles emitted from the tailpipe of vehicles to all traffic-induced particles in the street. Giechaskiel et al. (2022) give an overview of existing vehicle exhaust emissions regulations and possible adaptations/extensions how volatile particles can be accounted for.

To better understand the underlying particle dynamics and chemistry mechanism in AQ modelling, a measurement and simulation campaign was performed as part of a project funded by FVV. In addition to the box modelling approach described in the following, dispersion calculations of solid particles were performed by Uhrner et al. (2023) using the GRAL model.

Measurements

The measurements took place 2021 on October 20th, between 10:15 am and 05:15 pm in Plüddemanngasse in Graz, which was chosen because of busy traffic and the street canyon situation there. NO_x, NO, and PN were measured at three different distances from the road (1m, 3m, 5m). Solid particles (using a thermodenuder) and total particles at these distances were measured at alternating time intervals. The schematic measurement setup is shown in Figure 1.

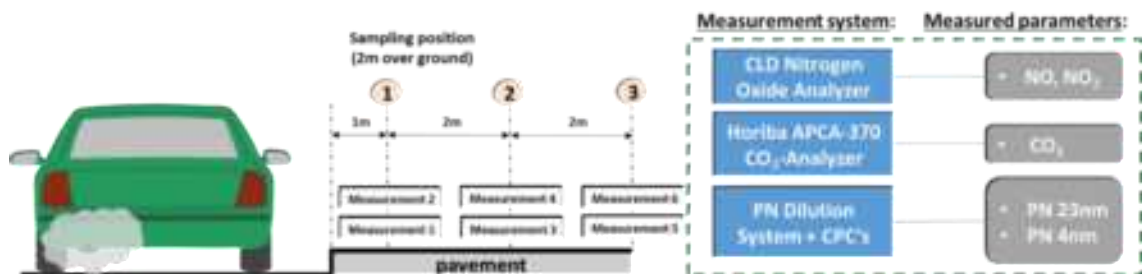


Figure 1: Schematic measurement setup and arrangement of the different measuring positions

During the measurement period traffic counts were done at Plüddemanngasse, the traffic flow (level of service) was determined by measurement runs.

In Figure 2, for the measurements in Plüddemanngasse on 20.10.2021, hourly mean values for NO and NO_x, PN_{4nm} and PN_{23nm} (all particles, and solid particles (measured after denuder), respectively), during the measurement period are shown.

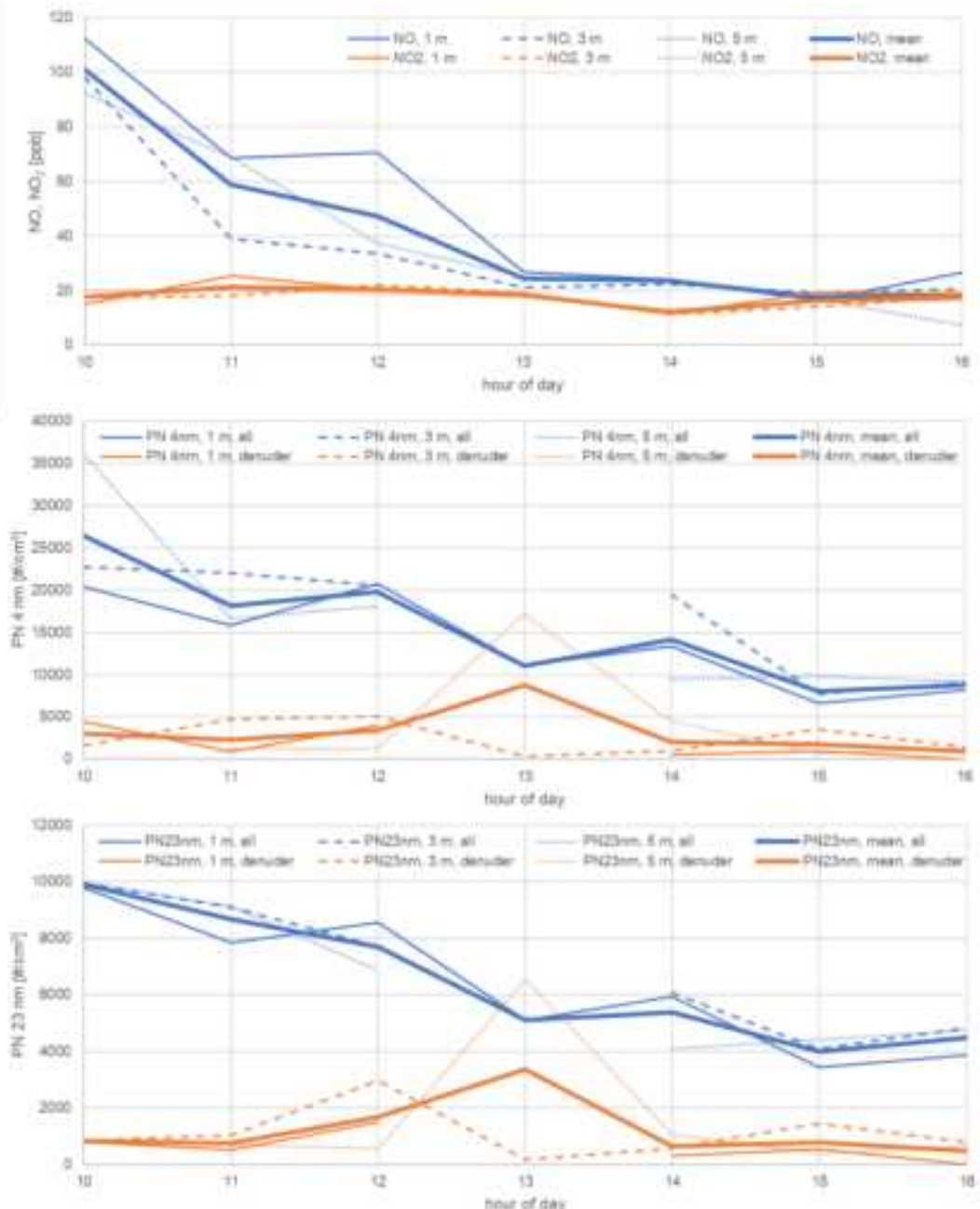


Figure 2: Measurements in Plüddemanngasse, 20.10.2021: hourly mean values for NO and NO₂ (top), PN_{4nm} (all particles and solid particles measured after denuder, middle), and PN_{23nm} (all particles and solid particles measured after denuder, bottom) during measurement period, each at one, three and five m distance from the road and for the spatial average (bold lines)

Since the spatial concentration gradient with respect to distance from the road is not constant over time (possible reasons: vehicle induced turbulence, mixing in of air parcels of varying origin and composition, effects of single and possibly higher than average emitting vehicles in the fleet, measurement uncertainty), for comparison with model results, measured concentrations were averaged (bold lines in Figure 2).

Box model calculations

Box model calculations of particle number (PN) concentrations in a street canyon were done by a coupled aerosol (MADE, modal aerosol dynamics model for Europe, Ackermann et al., 1998) and gas-phase chemistry model

(Memmesheimer et al., 2007). Emission, nucleation, and aerosol aging processes are accounted for. Dilution is parameterised by a simple two-stage process.

MADE is a simplified parametrisation of the very complex processes of particle dynamics, aerosols are represented by three particle modes (nucleation mode, accumulation mode and coarse particles) based on lognormal size distributions. The coarse mode is not evaluated here, since exhaust particles completely fall into the size range of the finer modes. MADE distinguishes aerosol particles from primary sources (elemental and organic carbon, sand dust, sea salt, and anthropogenic particles of other origin (e.g., from abrasion processes)), and secondary particles (formed by oxidation/condensation of gas-phase precursors (SO_2 , NH_3 , HNO_3 , 17 organic compounds)). Aerosol dynamics in MADE includes nucleation (initiated in the $\text{H}_2\text{SO}_4\text{-H}_2\text{O}$ system), coagulation, condensation, evaporation, and dry deposition. This model was applied to PN in a generic street canyon by Toenges-Schuller et al. (2015), but not compared to actual PN measurements before.

Local road traffic emissions were calculated

- based on HBEFA4.1,
- using traffic counts during the measurement period,
- using traffic flow (level of service) derived from measurement runs,
- using extrapolations for the whole day outside the measurement period based on typical diurnal variation curves,
- for the average urban fleet composition for Austria 2021,
- for a fleet consisting of 100% Euro 6d/Euro VI vehicles.

Compared to the average urban 2021 fleet, in a 100% Euro 6d/Euro VI fleet solid exhaust PN emissions are reduced by 99%.

Hourly values for traffic volume, mean trip speed, and NO_x emissions from the 2021 fleet for the day of the measurements are shown in Figure 3.

Further model input data are hourly values of meteorological parameters and background concentrations of NO , NO_2 , O_3 and $\text{PM}_{2.5}$, which were taken from urban background measurement stations in Graz.

Even "sulphur free" fuels contain traces of sulphur. In HBEFA, corresponding emission factors are given as SO_2 . In the atmosphere, SO_2 is oxidised to SO_3 and further to sulphuric acid, causing particle nucleation. Atmospheric SO_2 oxidation is a slow process, and relevant on larger spatial and temporal scales, not in the vicinity of the street. However, for vehicles equipped with oxidation catalysts, part of the SO_2 is already oxidised in the catalyst. For various emission concepts, Toenges-Schuller et al. (2015) compiled an overview of SO_3 fractions of the emitted SO_2 . For the urban Austrian fleet 2021 and the traffic shares in Plüddemannngasse, this results in an overall SO_3 fraction of SO_2 of ~3%.

Since the box model is well established to model NO and NO_2 (Toenges-Schuller et al., 2016), NO and NO_2 measurements were used for model calibration, see Figure 4. To be compatible with the measurements, five boxes were coupled in a row perpendicular to the street. However, the measured concentrations didn't show a clear gradient with the distance from kerbside over time, possibly due to vehicle induced turbulence, variable emission contributions of individual vehicles and the mixing-in of air parcels of varying origin during the alternating time intervals of the measurements. Therefore, modelled concentrations were averaged over box 2-5 and compared to measured averages over the distances 1m, 3m and 5m from kerbside. Model box 1 corresponds to the street itself, closer to the emissions than the measurements, and is therefore treated separately.

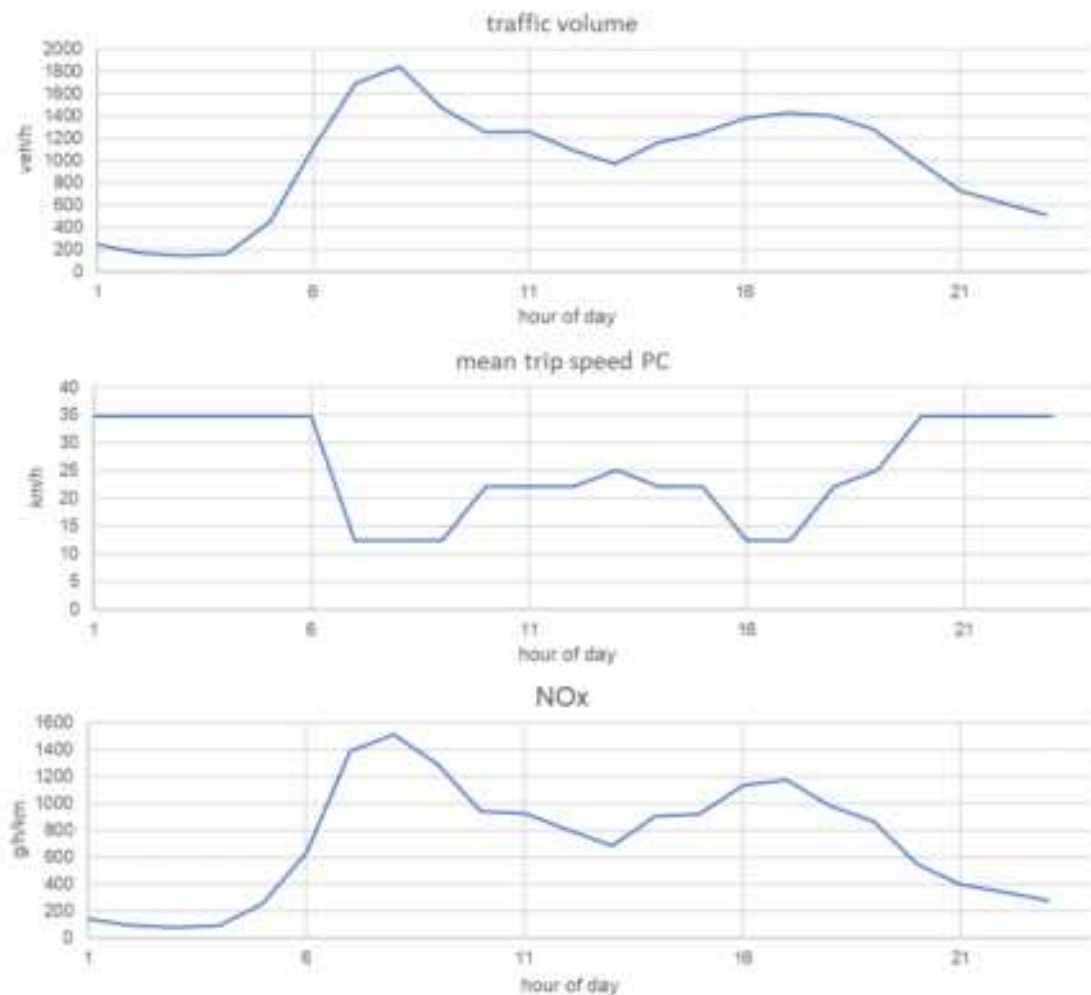


Figure 3: Plüddemanngasse, 20.10.2021: Traffic volume (top), mean trip speed (middle), and NO_x emissions from the 2021 fleet (bottom).

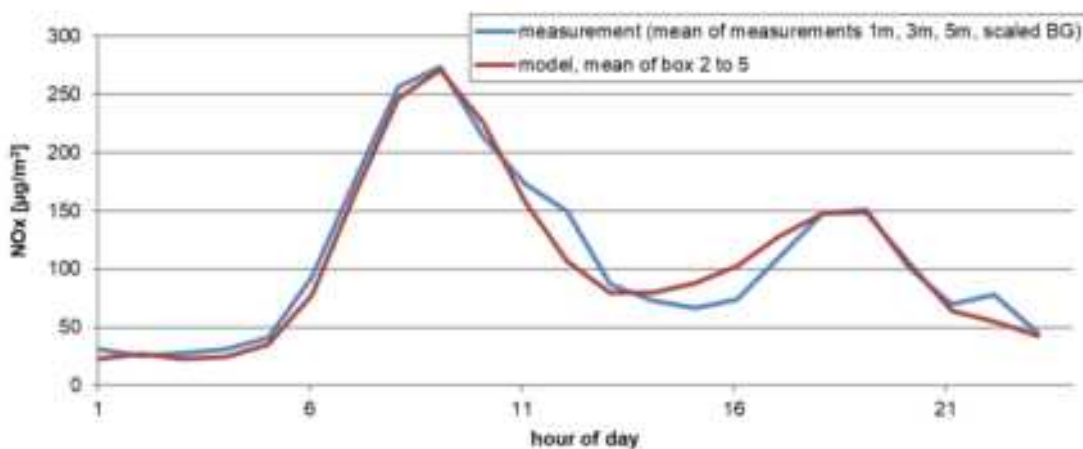


Figure 4: Box model calibration: modelled and measured NO_x at Plüddemanngasse, 20.10.2021

In Figure 5, hourly mean measured and modelled total PN concentrations during the measurement period are shown. The following can be seen:

1. The model captures both the order of magnitude and the trend of the measurements, which is a fairly good agreement a first comparison of a model to measurements.

2. Modelled PN concentrations are significantly higher right in the street (box 1) than at kerbside (box 2-5).
3. A high reduction of solid exhaust PN emissions (99%) results in a much lower reduction of modelled total PN due to contributions of the background, of secondary particle formation (mostly sulfuric acid, water, organic carbon), and of abrasion particles. Because of the simplicity of the approach, this is not intended as a quantitative forecast, but to show the conditions qualitatively.

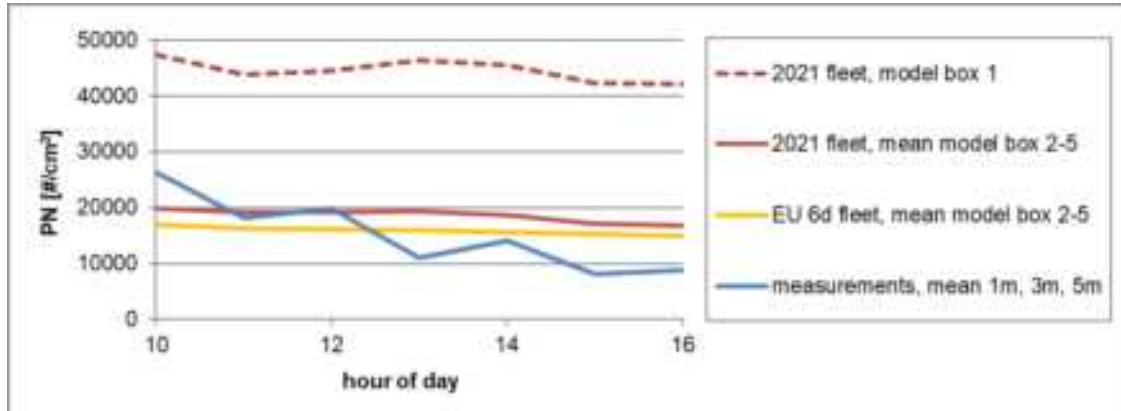


Figure 5: Modelled hourly PN concentrations in box one and mean of box two to five in comparison with measurements (all particles, mean of 1m, 3m, 5m) at Plüddemanngasse during measurement period for the fleets 2021and Euro 6d/VI.

Acknowledgements

This work was funded by FVV (The Research Association for Combustion Engines eV) in Germany, Funding number: FVV 601407

References

- Ackermann I. J. Hass H., Memmesheimer M., Ebel A., Binkowski F. S., Shankar U. (1998). Modal aerosol dynamics model for Europe: Development and first applications, *Atmospheric Environment* vol. 32, No. 17, 1998
- Giechaskiel B., Melas A., Martini G., Dilara P., Ntziachristos L. (2022): Revisiting Total Particle Number Measurements for Vehicle Exhaust Regulations. In: *Atmosphere* 2022, 13, 155. <https://doi.org/10.3390/atmos13020155>
- Memmesheimer M., Wurzler S. Friese E., Jakobs H. (2007). Long-term simulations of photo-oxidants and particulate matter over Europe with emphasis on North Rhine-Westphalia. *Developments in Environmental Sciences*, Chapter 2.8, Elsevier
- Toenges-Schuller N., Schneider C., Niederau A., Vogt R., Birmili W. (2015). Modelling particle number concentrations in a typical street canyon in Germany and analysis of future trends. *Atmospheric Environment*. 111. 127-135. 10.1016/j.atmosenv.2015.04.006.
- Toenges-Schuller N., Schneider C., Niederau A., Vogt R., Hausberger S. (2016). Modelling the effect on air quality of Euro 6 emission factor scenarios, *Journal of Earth Sciences and Geotechnical Engineering*, vol.6
- Uhrner U., Toenges-Schuller N., Reifelthammer R., Stadlhofer W., Hausberger S. (2023). Specification of Zero-Impact Vehicle Emissions & Demonstration of Zero Impact. Oral presentation TAP&SE Göteborg 2023
- Wehner B., Uhrner U., von Löwis S., Zallinger M., Wiedensohler A.(2009). Aerosol number size distributions within the exhaust plume of a diesel and a gasoline passenger car under on-road conditions and determination of emission factors. *Atmos. Environ.* 43 (2009), 1235-1245

Temporal distribution of national emission data for dispersion calculations with chemical transport models

Nicola Toenges-Schuller^{1*}, Stefan Feigenspan², Stephan Nordmann², Michael Pelzer¹, Christiane Schneider¹

¹ AVISO GmbH, 52074 Aachen, Germany, nicola.toenges-schuller@avisogmbh.de, ² German Environment Agency, Department Air, Wörlitzer Platz 1, 06844 Dessau-Roßlau, Germany

Introduction

As all European member states, Germany reports annual emissions based on national, European, and international agreements (Gothenburg Protocol of the Convention on Long-range Transboundary Air Pollution (CLRTAP)) to the EU. This reporting is executed by the German Environment Agency (UBA-DE). The reported emissions are also essential input data for chemical transport models (CTM), which, on the one hand, are used to simulate air pollutant concentrations over Germany, and, on the other hand, are used to model scenarios for strategies and measures to reduce pollution. The latter are required to be able to assess the potential of individual measures to achieve compliance with air quality limit values. They are also a basis for the national air pollution control program (NAPCP) within the framework of the NEC Directive 2016/2284/EU.

Spatially and temporally distributed emission data are required for dispersion calculations with chemical transport models. The CTM REM-CALGRID (RCG, see Stern, 2009) currently operated at UBA-DE, but also other CTMs, work with static time profiles (annual, weekly, and daily cycles) for emissions at SNAP Level 1 (Selected Nomenclature for Air Pollution) category level.

For use in CTMs, the emissions recorded as annual national totals must be distributed spatially to the corresponding model grid and temporally to all hourly values of the year. The quality of the model results, especially for scenario calculations, is largely determined by the quality of the incoming emission data - quantity, spatial and temporal distribution.

The "Gridding Emission Tool for ArcGIS" (GRETA) was developed for the spatial distribution of emission data (Schneider et al., 2016). The sectoral annual emissions of the Central Emissions System (ZSE) are spatially distributed using distribution parameters. With GRETA, it is possible to regionally quantify the contributions of individual sectors to air pollution.

Currently, static time profiles are used for the temporal distribution in RCG, and in many other CTMs established in Europe. These are fixed daily, weekly, and annual profiles for each source group (usually: SNAP Level 1 level) that do not show any spatial or temporal variance. For example, the annual profiles for emissions from small combustion installations in the Alpine region currently do not differ from those in the Rhine Valley, even if heating is required in the Alps for longer. The static time profiles are also identical for all years: Special events, such as the corona-related lockdowns in 2020 or the flood disaster in 2021, during which, for example, road traffic volume fell significantly, cannot be considered.

Therefore, the tool TeResE (Temporal Resolution of Emission data) was developed for the dynamic temporal distribution of emissions, in which spatial and/or temporal dependencies of the time profiles are considered using local and year-specific input data.

TeResE

This tool generates dynamic, regionalized time profiles for the emissions of nitrogen oxides (NO_x), particulate matter (PM_{10} , $\text{PM}_{2.5}$), ammonia (NH_3), non-methane volatile organic compounds (NMVOC), sulphur dioxide (SO_2) and carbon monoxide (CO), called splitting factors (SF). These splitting factors contain the share of the respective emission for each grid box and each source category per hour. The SF depend dynamically on the respective spatial and/or temporal conditions, e.g., different years differ in terms of meteorology: the type, characteristics and times of the weather conditions that occur vary both spatially and from year to year. This directly influences the temporal emission profiles of source groups such as agriculture or small combustion installations. In the case of road transport, local conditions and special temporal situations can be considered by using hourly data for the traffic volume from the automatic continuous counting stations of the BASt (Federal Highway Research Institute).

The SF are initially generated for each NFR sector. For this purpose, representative time profiles for annual, weekly, and diurnal emissions are derived, based on an hourly resolution if possible. Regional aspects are

considered, i.e., the splitting factors are provided regionalized according to regions or grid cells. TeResE can output the regionalized temporal distribution of emissions at both NFR and SNAP level.

Temporal dependencies

The meteorological and other dependencies to be considered for the SF and the data sources to be used were compiled for all NFR sectors. The most important are:

- Power plants: Large power plants are included in the spatial distribution of emissions by GRETA as point sources. Time series of hourly energy deliveries are available from ENTSO-E (European Network of Transmission System Operators for Electricity) for blocks of large power plants. The corresponding time profiles are used directly for the point sources in the PRTR (Pollutant Release and Transfer Register), which are used in the spatial distribution by GRETA and can be assigned in ENTSO-E³⁴. Mean values from the transmission system operators are used for all unassigned point sources and for the power plant emissions available as area sources.
- Residential stationary Combustion: Degree Day figures are used for the time profiles of building heating. On heating days, i.e., on days when the outside temperature falls below a certain value, degree day figures correspond to the difference between the desired inside temperature and the outside temperature. The outside temperatures are calculated based on the COSMO-DE meteorology³⁵ for different climate regions, which also serves as a model driver for the RCG.
- NFR sectors of the source groups industry, commerce, energy excluding power plants and transport excluding road transport: Data from the Federal Statistical Office³⁶ is used for the annual variation at monthly level (production indices, transport services, number of take-offs and landings at major airports, etc.). Weekly and daily cycles are each taken from the static default time profiles of RCG.
- Road transport: The time behaviour of the emissions from road transport is essentially given by the time profile of the traffic volume. The BAST's automatic continuous counting stations³⁷ are used as the data source. A distinction is made between light- and heavy-duty transport as well as between motorways, federal roads, and inner-city roads. The time profiles of the motorways and federal roads are spatially averaged over the regions defined for the road traffic census. The time profiles for road traffic on urban roads are averaged nationwide. In addition, a dependency on the temperature is considered for the evaporative emissions and for the nitrogen oxide emissions from light duty vehicles.
- Agriculture: Functions for the temporal distribution of NH₃ emissions according to Skjøth et al. (2004) and Gyldenkærne et al. (2005) are used. These were originally derived for Denmark, but the parameters can be adjusted. For the temporal distribution of emissions from those NFR sectors of agriculture, that cannot be related to NH₃, the static default profiles of the RCG are used.
- Other product applications: This sector is particularly relevant because it includes fireworks, among other things. Separate time profiles were created for the relevant sub-sectors, for example the fine dust emissions from the New Year's Eve fireworks were placed in the first hour of the year.

Input and output data

The following input data is required:

- Configuration files that contain information and data or boundary conditions for the calculation.
- Data on the meteorology of the model year (currently used: temperature at 2 m above ground level and wind speed at 10 m above ground level), specifically in the form of the COSMO-DE meteorology, which is also used in the RCG model calculation for evaluation. As part of this project, the years 2016

³⁴https://transparency.entsoe.eu/content/static_content/Static%20content/knowledge%20base/SFTP-Transparency_Docs.html

³⁵https://www.dwd.de/DE/forschung/wettervorhersage/num_modellierung/_01_num_vorhersagemodele/regionalmodell_cosmo_d2.html

³⁶https://www.destatis.de/DE/Home/_inhalt.html

³⁷<https://www.bast.de/DE/Verkehrstechnik/Fachthemen/v2-verkehrszaehlung/Verkehrszaehlung.html>

and 2017 were evaluated; as long as the structure of the data remains unchanged, any year can be processed.

- Input data on the spatial location of the climatic regions, the road and rail network, the waterways, the point sources, etc. must be available as feature layer files.
- Other important year-specific input data are the counting data from the BAST permanent counting stations, ENTSO-E data, production indices, etc.

During the calculation process, first, the calculation grids are set up, then all geometric data are projected onto these grids and the quantities derived from the meteorological data are calculated. The splitting factors are then calculated for all groups, and finally, output files are written at NFR and SNAP Level 1 level. The currently available version of TeResE generates splitting factors for the Nest-2 grid (approx. 2 km x 2 km resolution over Germany) of the chemical transport model REM-CALGRID (RCG) currently operated at UBA-DE.

Evaluation

To evaluate the SF, two model calculations for 2016 were done with the REM-CALGRID (RCG) chemical transport model (Stern, 2009) currently operated by UBA-DE (German Environment Agency). ~~The model running RCG using static default values provides "static" and one model run using the dynamic SF generated by TeResE "dynamical".~~ The spatial distribution of emissions for the evaluation was done by the tool GRETA.

The evaluation was carried out ~~by comparing both the "static" and the "dynamical" model calculation with measurement data.~~ Eight air quality monitoring stations were selected for this comparison, five from the urban background and three from unpolluted rural background.

In Figure 1 (A), the annual mean NO₂ concentration 2016 modelled by RCG using static SF (default) is shown. The white circles mark the positions of the eight measurement stations selected for evaluation; the colour values inside correspond to the measured annual mean concentrations. The spatial distribution of the NO₂ concentrations visible on the map corresponds to expectation: It is increased in conurbations, large cities and along traffic axes such as the Kiel Canal, the Rhine, and the motorways.

For most of the monitoring stations selected for evaluation, the comparison of the measured annual mean concentration with the RCG model calculation shows good agreement. Within the resolution of the colour scale, there are visible deviations for NO₂ at only one station (Emsland, on the map: red-filled white circle in the north-west); here, the model underestimates the measurement (surroundings of the circle: coloured yellow). A possible explanation for the higher NO₂ measurement at the Emsland station (classified as urban background) is, that this value is partly influenced by emissions from the bypass and the nearby A31. The motorway can be seen on the map as a thin line with increased NO₂ concentrations, but at the 2 km x 2 km resolution it only stands out faintly against the background.

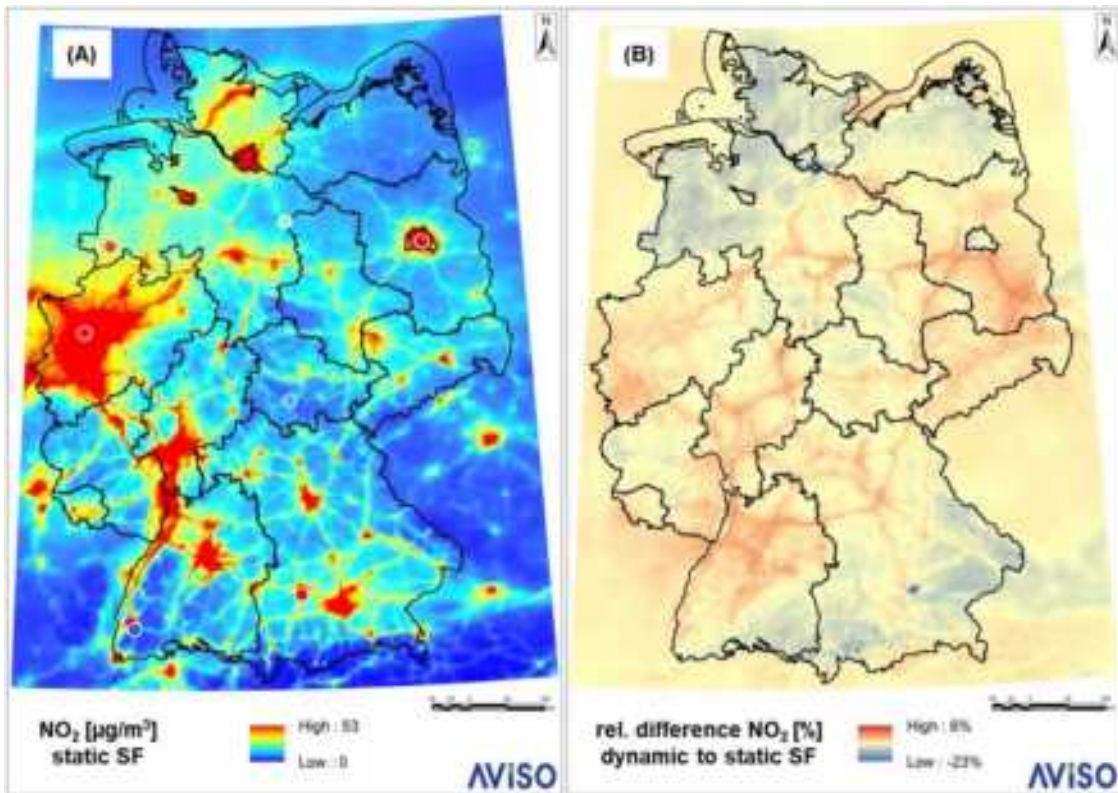


Figure 1: (A): Modelled annual mean NO₂ concentration 2016 (RCG model run using static splitting factors (default); the white circles mark the positions of the measurement stations considered, the colour values inside correspond to the measured annual mean concentrations there. (B): Relative difference between the annual mean NO₂ concentration 2016 modelled by RCG using dynamic SF to the default.

In Figure 1 (B), the relative difference between the annual mean NO₂ concentration 2016 modelled by RCG using dynamic splitting factors to the default is shown. Although the total amount of emissions does not change for the year, the change in time distribution due to the dynamic SF also leads to changes in the annual mean concentrations, which for NO₂ range between -23% and +6%. The difference map for annual NO₂ shows:

- decreases in agricultural areas with low absolute emissions
(In sparsely populated areas with little traffic and industry, agriculture is the dominating source for NO_x, mostly emitting NO. By using dynamic SF, the spring maximum of agriculture emissions is moved forward by about one month into a time with lower ambient ozone concentrations. Consequently, a lower fraction of NO reacts with ozone to NO₂.)
- decreases for some isolated grid cells
(Most of them contain point sources as airports and power stations emitting into higher model layers where concentrations are particularly dependent on the meteorological conditions prevailing at the time the emissions are released),
- increases along the motorways
(By using dynamic SF, road transport emissions are partly shifted from summer to winter, since ~~verstärkte Abgasemissionen durch Emissionen direkt unterhalb der Umgebungstemperatur (thermische Wirkung)~~. The NO₂/NO_x ratio for road transport emissions is higher than for agriculture emissions, so in this case, a shift of NO₂ emissions into a time period with lower photolysis rates result in higher annual mean NO₂ concentrations.)

For the grid cells in which the eight measuring stations selected for the evaluation are located, time series of averaged concentration values were examined. The goal is the best possible match between model calculation and measurement for the entire period under consideration (year) and the smallest available averaging interval (hour). This time series of annual changes from hourly mean values contains all temporal influences (diurnal changes, weekly changes, annual changes). However, it is difficult to isolate possible causes for discrepancies between model calculation and measurement using this time series. Therefore, in addition to the annual course of the hourly mean values, the following time series were examined to be able to consider diurnal courses, weekly courses, and seasonal behaviour separately:

- annual cycle from hourly averages, daily averages, and monthly averages,
- weekly cycle from daily mean values,
- different diurnal cycles (all days, Sundays including public holidays) from hourly averages

This allows conclusions to be drawn about source groups, whose emissions vary particularly strongly on the respective time scales.

These time series were analysed quantitatively using the statistical parameter R^2 (R^2 (Pearson's correlation coefficient) shows, how strong two variables are linearly related, R^2 can be interpreted as the proportion of the variance in one variable that can be explained by the other variable).

If the ratio $R^2_{\text{dynamic}}/R^2_{\text{static}}$ is larger than one, the model behaviour is improved by using dynamic SF. For NO₂, NO_x, O₃ and PM₁₀, these ratios are shown as an example for the stations Berlin-Neukölln (urban background) and Schauinsland (remote rural background) in Figure 2 in the form of two hexagonal network diagrams.

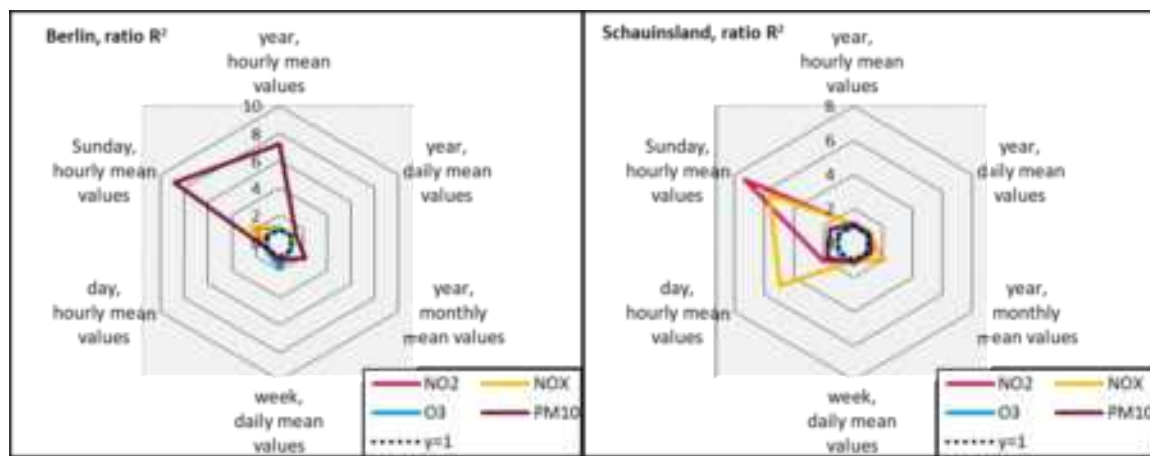


Figure 2: Dynamic to static ratios for the statistical parameter R^2 (values > 1 mean an improvement) for the considered species at the stations Berlin-Neukölln (urban background, left figure) and Schauinsland (remote rural background, right figure) in 2016.

In both diagrams, the ratios $R^2_{\text{dynamic}}/R^2_{\text{static}}$ for the time series of the annual variation from hourly mean values are plotted in the direction of the upper corner. The other five corners correspond, clockwise, to the following time series: annual variation from daily mean values, annual variation from monthly mean values, weekly variation from daily mean values, diurnal variation from hourly mean values and diurnal variation on Sundays including public holidays from hourly mean values. The black dotted hexagon corresponds to the "y=1" line: values outside this hexagon mean an improvement in the model calculation by using dynamic time profiles.

For the Berlin Neukölln station (urban background), the largest improvements occur for PM₁₀ for the time series "year, hourly mean values" and "Sundays, hourly mean values", essentially due to two things: the consideration of the New Year's Eve fireworks, and the omission of the morning peak of the traffic diurnal profile on Sundays. (In the static default profiles, road traffic emissions are lower on Sundays due to the weekly cycle, but there is no special diurnal cycle for each day of the week. So, the profile on Sundays exhibits a morning and an evening peak just as on working days, only on a lower level. In the dynamic profiles, working days show a traffic peak in the morning and in the evening, Saturdays, and Sundays show only one peak.)

At the Schauinsland station (remote rural background on a mountain in the Black Forest), correlations between model and measurements are generally lower than at the other stations considered, because this station is lying temporarily in the free troposphere. However, the changes in R^2 are similar to those at the other stations, with improvements in nitrogen oxides occurring in particular on Sundays and public holidays (hourly mean values).

In addition to the detailed evaluation at selected stations, both model runs were evaluated with the FAIRMODE DELTA-Tool (Thunis et Cuvelier, 2022), using measurement data from all valid background stations in Germany 2016 (243 stations for NO₂, 212 for PM₁₀ and 241 for O₃). This evaluation showed a slight improvement of R for PM₁₀ and NO₂ at urban background stations and hardly any change of R for O₃.

Overall, it can be concluded that the concentrations modelled using dynamic SF match the measured concentrations better than the concentrations modelled using static time profiles for most stations, pollutants, and time scales.

Acknowledgements

This work was funded by UBA-DE within the framework of the Departmental research plan of the Federal Ministry for the Environment, Nature Conservation and Nuclear Safety, Forschungskennzahl 3718 52 208 0

References

- Gyldenkærne S., Skjøth C. A., Hertel O., Ellermann T. (2005). A dynamical ammonia emission parameterization for use in air pollution models., *Journal of Geophysical Research* vol. 110, D07108, doi:10.1029/2004JD005459
- Schneider C., Pelzer M., Toenges-Schuller N., Nacken N., Niederau A. (2016). ArcGIS basierte Lösung zur detaillierten, deutschlandweiten Verteilung (Gridding) nationaler Emissionsjahreswerte auf Basis des Inventars zur Emissionsberichterstattung, *UBA Texte* 71/2016
- Skjøth C. A., Hertel O., Gyldenkærne S., Ellermann T. (2004). Implementing a dynamical ammonia emission parameterization in the large-scale air pollution model ACDEP, *Journal of Geophysical Research*, vol. 109, D06306, doi:10.1029/2003JD003895
- Stern R. (2009). Das chemische Transportmodell REM-CALGRID, Modellbeschreibung. Freie Universität Berlin, Institut für Meteorologie, Troposphärische Umweltforschung, Januar 2009
- Thunis P, Cuvelier C. (2022). [The REM-CALGRID Concept: One Step Closer](#)

Transport emission footprint in the Slovak economy

J. Horváth^{1,2}, J. Šimonek¹ and J. Szemesová¹

¹ Department of Emissions and Biofuels, Slovak Hydrometeorological Institute, Jeséniova 17, Bratislava, Slovakia, jan.horvath@shmu.sk

² Faculty of Ecology and Environmental Science, Technical University in Zvolen, Ul. T. G. Masaryka 24, Zvolen, Slovakia

Introduction

Enhancing the methodology for allocating emissions arising from road transport bears significant implications for the accuracy and robustness of Environmental Air Emissions Accounts (AEA) reporting, as stipulated by Regulation 691/2011 on European environmental economic accounts (European Parliament and Council, 2022). The allocation of emissions to NACE rev.2 categories enables meticulous analysis, unravelling the major contributors to air emissions among various economic activities. NACE rev.2, a standardized classification system with 6 characters within the European industry, holds binding significance within the EU (European Parliament and Council, 2006; SK NACE, 2022). Through comprehensive analyses, potential enhancements in policies and measures can be identified, facilitating targeted interventions in relevant economic sectors.

In relation to the first paragraph, along the AEA reporting, PEFA accounts serve as a pivotal platform for recording the flow of energy between the environment and the economy, encompassing natural inputs, products within the economy, and residues back to the environment. PEFA accounts are closely linked to the AEA reporting by providing valuable data on the energy-related emissions that contribute to the carbon footprint of economic activities. Furthermore, PEFA accounts aid in identifying energy inefficiencies, emission hotspots, and potential areas for improving resource management within the economy. The integrated framework enables holistic analyses, encompassing environmental, energy, and economic dimensions. By analysing the data from PEFA accounts in conjunction with the AEA reporting, stakeholders can identify opportunities to reduce the carbon footprint and enhance energy efficiency across different economic sectors. This integration of data helps in formulating strategies and initiatives aimed at transitioning towards a greener and more environmentally responsible economy.

The research objectives outlined herein arise from the statistical reporting obligations of the Slovak Republic to Eurostat, with a focus on improving the allocation of emissions from road transport within the AEA module to NACE rev.2 categories and household categories. These objectives constitute an independent section of the questionnaire and align with the National Action Plan, fulfilling the obligations of the Slovak Republic (Horváth, et al., 2021). A previous contribution, titled "Allocation of Emissions from Road Transport According to Economic Activities (NACE rev.2) and Coherence between AEA and PEFA Modules" (Horváth et al., 2023), communicated the action plan in 2021. Rodríguez et al. (2016) in their study on air pollution and urban structure linkages utilized national air emission accounts alongside their findings to reinforce the hypothesis that urban structure has substantial impacts on pollution concentration. The research demonstrated the importance of considering both local and national-level data to better understand the relationship between urban characteristics and air pollution levels, providing valuable insights for environmental policy and urban planning.

The second objective concerns on refining the coherence between the AEA and PEFA modules, particularly focusing on fuels for road transport. The methodologies derived from the primary objective are instrumental in correctly allocating fuels in road transport to NACE rev.2 categories and households.

Methodology and Software

The original methodology for allocating greenhouse gas emissions (GHG) and pollutants (AP) relied on four key parameters: vehicle category (passenger, light commercial vehicle, heavy-duty, and motorcycles), total annual mileage, quantity of transported goods (tonne-kilometres), and gross value added (GVA). The resultant matrix, while straightforward, neglected the actual number of vehicles in individual NACE rev.2 categories, leading to imprecise environmental impact assessments.

In contrast, the new methodology is grounded in a more detailed analysis of input data (Chapter 2.1). A prototype database system and software tool (Horváth, et al., 2021) were developed, enabling data storage and processing with output verification.

2.1 First phase: methodology and software development

The initial phase entailed data collection from diverse sources, including the IS EVO vehicle database, the Technical Control Database, and the Register of Organizations (RO) (Figure 1). IS EVO as the information system for vehicle registration, provides essential data on registered vehicles in Slovakia, such as VIN numbers, fuel types, engine capacity, and relevant information. The Technical Control Database contributes crucial data on technical inspections, and the RO offers organizational data for NACE rev.2 allocation.

2.2 Second phase: methodology and software development

Subsequently, the second phase integrated outputs from the COPERT emission model, ton-kilometres according to NACE rev.2 categories, and annual mileage according to the COPERT model (EMISIA, 2022). The COPERT model, partly funded by the European Environment Agency (EEA), estimates greenhouse gas and pollutant emissions in road transport, considering various parameters like vehicle type, fuel used, and EURO emission standards.

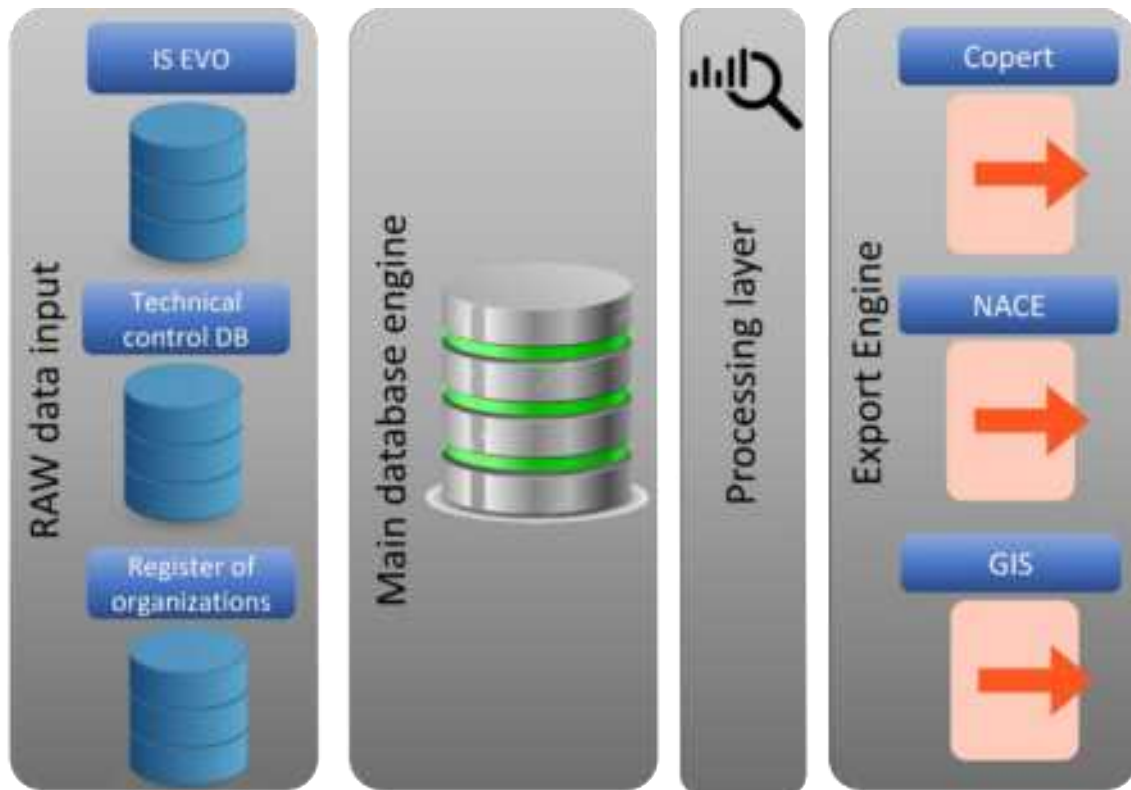


Figure 1: Schema of the software tool

2.3 Matrix for AEA and PEFA

The development of the allocation matrix necessitated the integration of data from two phases of the process: the number of vehicles in each NACE rev.2 category and the data related to the number of kilometres driven and emissions for the given year. The division of the total number of kilometres driven for each vehicle category and fuel type yielded a ratio as follows:

$$KM_x \div V_x = km_x \text{ (eq.1)}$$

$$km_x \times V_{NACE} = km_{NACE} \text{ (eq. 2)}$$

$$km_{NACE} \div KM_x = R \text{ (eq.3)}$$

Where:

- KM_x represents the total number of kilometres driven in the specified vehicle category and fuel type.
- V_x denotes the total number of vehicles in the specified category and fuel type.
- km_x stands for the average number of kilometres per vehicle in the specified category and fuel type.
- V_{NACE} represents the vehicles of the specified category and fuel type in the NACE rev.2 category.

- km_{NACE} corresponds to the total number of kilometres driven in the NACE rev.2 category for each vehicle category and fuel type.
- R represents the ratio for the matrix.

The resulting allocation matrix features emissions ratios from each economic activity based on the NACE rev.2 categorization in the rows, with each column representing a vehicle category with a specific fuel type. This matrix offers a comprehensive breakdown of the vehicle fleet for a specific year, along with detailed disaggregated information for each NACE rev.2 category. It is an integral part of the software tool and, once populated with estimated GHG and pollutant emissions, can be exported to AEA (Figure 2).



Figure 2: Process diagram for completing the AEA questionnaire

Distinguishing the AEA and PEFA matrices lies in their respective levels of data aggregation concerning the number of vehicles and, for PEFA, the volume of transported goods, which directly influences fuel consumption. PEFA requires aggregation at the EURO emission standard level, while AEA necessitates division into individual vehicle segments at a higher level of aggregation.

Results

The original methodology allocated emissions to the AEA account primarily based on gross value added and expert estimates. In this allocation, the most significant category within NACE rev.2 was category H (Transportation and Storage).

With the new methodology, emissions from road transport are no longer allocated based on this parameter. This means that the new methodology enables the fulfilment of Slovakia's commitments and improves reporting for two inadequate elements, as identified in the self-assessment of the road transport methodology in 2018 (Horváth, et al., 2021).

The change in the allocation of GHG and pollutant emissions introduced in the new methodology is significant. Household emissions have increased significantly, rising by 76% in 2013 in comparison to the previous allocation method. This increase is mainly attributed to the separation of gross value added from emissions production, relying solely on precise data and the number of vehicles used and registered for economic activities within NACE rev.2. The increase in household emissions is also due to the inclusion of a large number of buses and their emissions within households. This is because buses do not have their own identification numbers (ICO) assigned in the IS EVO database, making it impossible to allocate them correctly to NACE rev.2.

Wholesale and Retail Trade; Repair of Motor Vehicles (category G) has also experienced a significant increase in emissions, with a rise of 230% in 2019 as indicated by the new allocation method. The overall results and changes in emission allocations are available in the interim report on the EUROSTAT project grant (Horváth, et al., 2023).

The new methodology extensively disaggregates emissions and provides higher accuracy through various databases acquired to achieve the objectives.

In addition to significant changes in Households (HH) and category H (Figures 3, 4, 5), there have been substantial changes in emissions within categories C (Manufacturing) and G. In the case of industrial production allocated in category C, emissions have significantly decreased (up to fourfold) since the implementation of the new methodology. The initially high share of allocated emissions in this category was due to the high proportion of industrial production in total gross value added. By separating emissions from gross value added, emissions have shifted and relocated to other parts of the national economy or households. Category G is one of these categories.

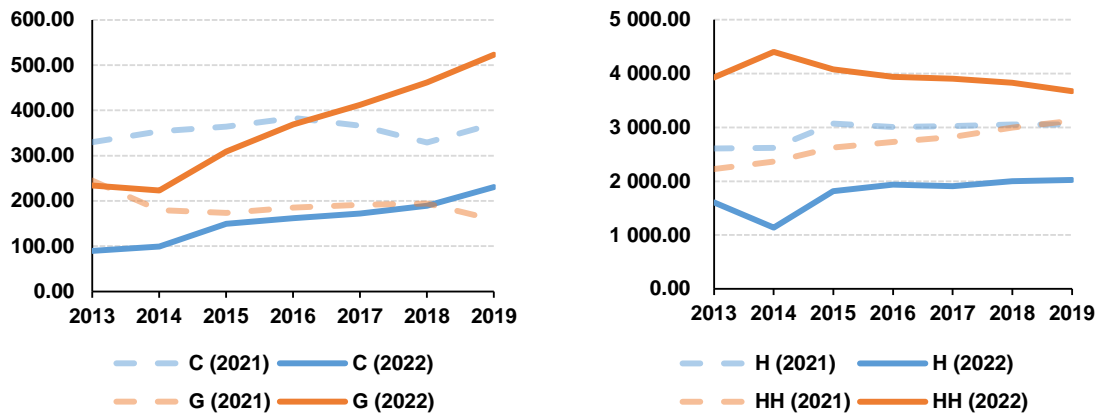


Figure 3: Changes in CO₂ emissions allocation in kt for the dominant NACE rev.2 categories

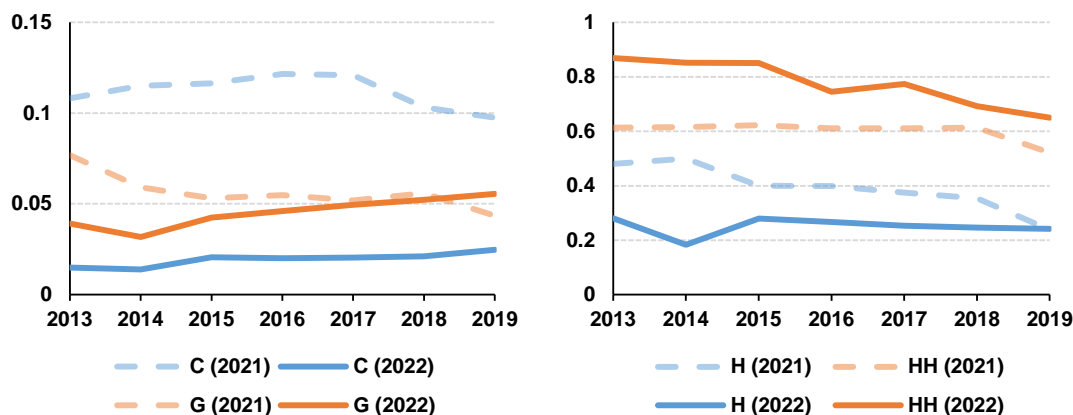


Figure 4: Changes in PM_{2.5} emissions allocation in kt for the dominant NACE rev.2 categories

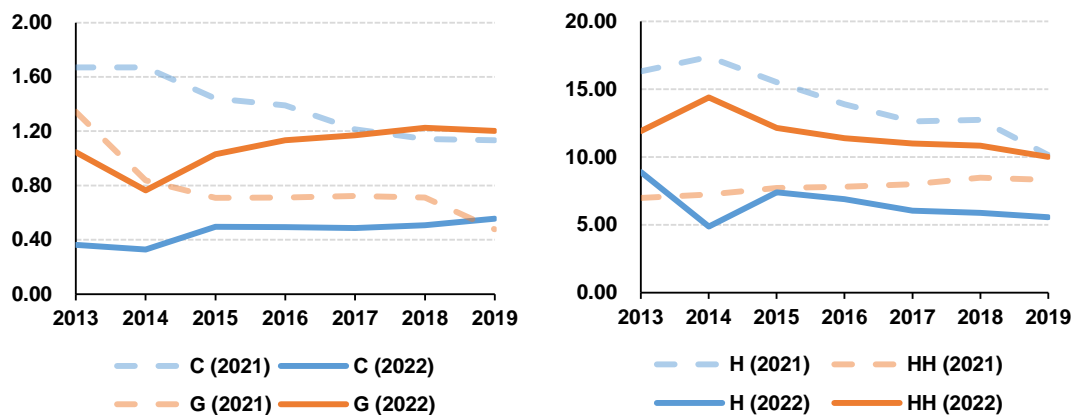


Figure 5: Changes in NO_x emissions allocation in kt for the dominant NACE rev.2 categories

Furthermore, the implementation of the new methodology in AFA has not only resulted in substantial changes in emissions, but has also provided valuable insights into shifts in gasoline and diesel usage across economic activities. The result of the new matrix for the allocation of physical energy flows in PEFA not only provides a new distribution of gasoline and diesel usage in economic activities but also offers insights into likely changes within the economy itself. In 2013, the largest consumers of gasoline were categories G, H, and M (Professional, Scientific, and Technical Activities), which together accounted for 54% of the total gasoline consumption in the national economy. By 2019, the significance of category H had decreased, and it was replaced by category N (Administrative and Support Services). In 2019, these three categories (G, H, and N) accounted for 47% of gasoline consumption.

When analysing diesel consumption, categories C, G, and H emerged as the largest consumers in 2013. Together, they accounted for up to 87% of diesel consumption in road transport. In 2019, change happened, category C losing importance and either deliberately or otherwise reducing its diesel consumption, while category N surpassed it in terms of consumption among the top three diesel consumers. There was also a decrease in the share of the top three categories in total diesel consumption, reaching 77%.

These changes and declines suggest that there have been slight shifts in the dynamics of economic sectors and even diversification, considering the decrease in the share of the top three consumers between 2013 and 2019, whether in gasoline or diesel (Figure 6).

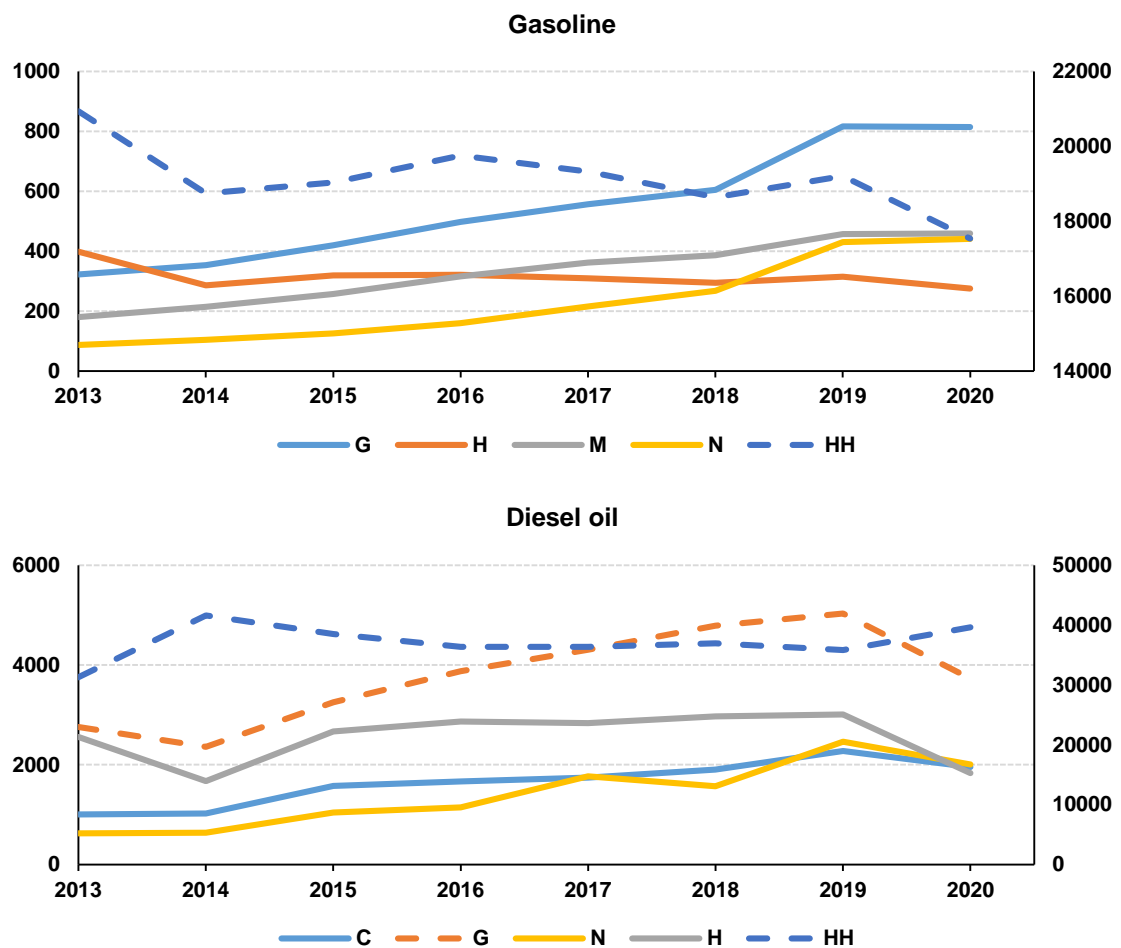


Figure 6: Fuel allocation and their changes in TJ (dotted line with vertical axis on the right)

A more realistic and accurate allocation of emissions and fuels from road transport according to economic activities and households in Slovakia is the result of the project. By improving the allocation and separating it from gross value added, it is possible to conduct deeper and more precise analyses. These analyses identify economically productive areas with relatively low emissions as well as high-emission areas with low added value.

The information obtainable through the analysis of AEA and PEFA accounts is a valuable basis for policymakers and decision-makers at both the EU and Slovak levels. It helps to properly target supportive and incentive mechanisms for activities with higher added value, while discouraging activities and economic practices with negative environmental impact and low added value.

Acknowledgements

This project was funded by EUROSTAT scheme ESTAT-2020-PA8-E-ENVACC.

References

EMISIA S.A. (2022). COPER model.

Regulation (EC) No 1893/2006 of the European Parliament and of the Council of 20 December 2006 establishing the statistical classification of economic activities NACE Revision 2 and amending Council Regulation (EEC) No 3037/90 as well as certain EC Regula [Online], Accessed August 4 2023, <https://eur-lex.europa.eu/legal-content/EN/TXT/?uri=CELEX:32006R1893>

Regulation (EU) No 691/2011 of the European Parliament and of the Council of 6 July 2011 on European environmental economic accounts (Text with EEA relevance)Text with EEA relevance [Online], Accessed August 4 2023, <https://eur-lex.europa.eu/legal-content/EN/TXT/?uri=CELEX%3A02011R0691-20220220>

Horváth L, Luhovský J, Černík Z, Vranačová I, Želochová I. (2021) Improving the Allocation of road transport emissions in AEA module and coherence between AEA and PEFA modules [Conference], *Zborník príspevkov z konferencia Ochrana ovzdušia 2021*. - Bratislava : Kongres Studio

Horváth L, Luhovský J, Černík Z, Vranačová I. (2021) Improving the Allocation of Road Transport Emissions in AEA Module and Coherence between AEA and PEFA Modules. *Deliverable 1.1: Methodology for Allocation of Road Transport Emissions* [Report]. - [s.l.] : Slovenský hydrometeorologický ústav

Rodríguez Miguel Cárdenas, Dupont-Courtade Laura and Oueslati Walid (2016) Air pollution and urban structure linkages: Evidence from European cities, *Renewable and Sustainable Energy Reviews*, Vol. 53, 1-9.

SK NACE [Online] (2023), <http://www.nace.sk/> (accesed on 2 August 2023)

2.10 JS.10. Compliance monitoring technological and legal frameworks; experimental studies; theoretical impact studies.

Shipping emissions monitoring with on-board and remote techniques and impacts on air quality: The SCIPPER project summary and results

L. Ntziachristos^{1*}, S. Mamarikas¹, V. Matthias², M. Karl², L. Fink², P. Simonen³, J. Keskinen³, M.D. Maso³, E. Fridell⁴, J. Moldanova⁴, Å. Hallquist⁴, J. Mellqvist⁵, V. Conde⁵, R. Verbeek⁶, J. Duyzer⁶, D. van Dinther⁶, H. Timonen⁷, J.-P. Jalkanen⁷, A.-M. Sundström⁷, E. Majamäki⁷, A. Stylogiannis^{8,9}, V. Ntziachristos^{8,9}, T. Smyth¹⁰, M. Yang¹⁰, A. Deakin¹¹, R. Proud¹¹, J. Oeffner¹², J. Weisheit¹², J. Beecken^{13,16}, A. Weigelt¹³, S. Griesel¹³, H. Schoppmann¹³, S. Oppo¹⁴, A. Armengaud¹⁴, B. D'Anna¹⁵, G.-M. Lanzafame¹⁵, B. Temime-Roussel¹⁵, B. Knudsen¹⁶, J. Knudsen¹⁶, M. Irjala¹⁷, A. Somero¹⁷, T. Rantala¹⁷, L. Buckers¹⁸, J. van Vliet¹⁸

¹AUTH *(leon@auth.gr), ²HEREON, ³TAU, ⁴IVL, ⁵CHALMERS, ⁶TNO, ⁷FMI, ⁸TUM, ⁹HMGU, ¹⁰PML, ¹¹eEE, ¹²CML, ¹³BSH, ¹⁴ATMOSUD, ¹⁵AMU-CNRS, ¹⁶EXPLICIT, ¹⁷AEROMON, ¹⁸ILT

Introduction

While vessels exhibit comparatively low fuel consumption per unit of cargo-distance, they still produce high specific emissions of nitrogen oxides (NOx), sulphur oxides (SOx) and particulate matter (PM). In an effort to decisively reduce the environmental footprint of shipping, new stricter regulations were established by the IMO and further adopted by member states (IMO 2016). These primarily target to reduce SOx globally, while impose NOx limits when ships sail to specific areas (IMO 2008). To comply with the new status quo in the legislation, ship owners and operators have to prominently act, by either using cleaner fuels or equipping their ships with appropriate emission control technology. Therefore, any type of environmental regulation applied in maritime sector, currently and in the future, can be only effective when ships are regularly checked for compliance.

In this context, a main research question is related on how authorities will verify that correct fuels or proper aftertreatment technology are utilized. SCIPPER (Shipping Contributions to Inland Pollution Push for the Enforcement of Regulations) was a Horizon 2020 research project that sought to answer this question, addressing the overall need for: a) compliance check of environmental regulations, and b) more evidence on monitoring possibilities for low sulphur levels, new pollutants, as well as implications of non-compliant ships to air pollution. So, the main objectives of SCIPPER were a) to provide evidence on the performance and capacity of different techniques for shipping emissions monitoring and regulations enforcement including quality in measurements and cost efficiency in monitoring, and b) to assess the impacts of shipping emissions on air quality, under different regulatory enforcement scenarios.

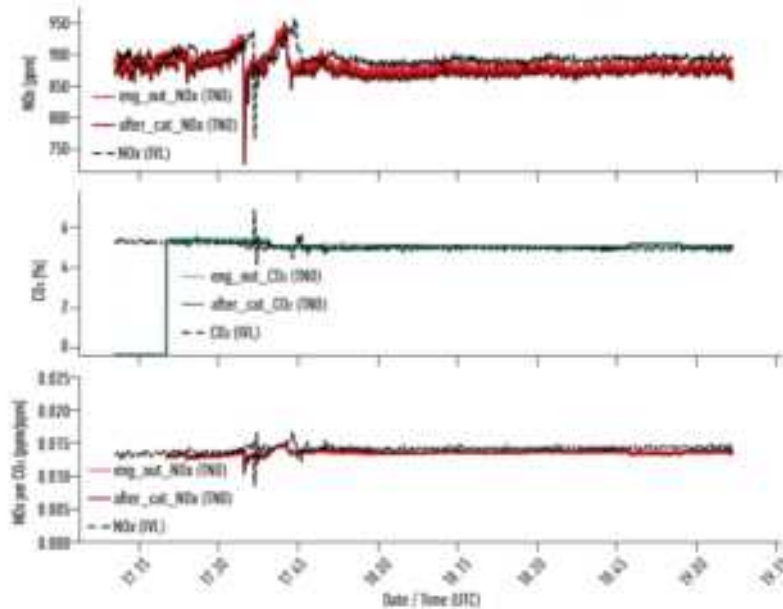
To address these challenges in checking and enforcing new emission limits, SCIPPER deployed state-of-art and next-generation measurement techniques to monitor emissions of vessels under their normal operation. Techniques applied include many on-board sensors and a wide spectrum of remote instruments (sniffers, mini sniffers on drones, optical remote, satellites). All this instrumentation was implemented in five real-world campaigns in critical European shipping areas (ports of Marseille & Hamburg, shipping line from Gothenburg to Kiel, English Channel), where more than a thousand of ship plumes were measured. Together with SOx and NOx, which are the current legislative priorities, techniques also characterized PM as a candidate pollutant for future regulations. In addition, other emissions of interest were considered. Experimental information from the campaigns was combined with advanced plume dispersion and chemical transport models (CTMs) to estimate current ship-induced air pollution and predict the impact of various degrees of compliance to major port areas in Europe. The present paper highlights main outcomes and results of SCIPPER, both in deploying the abovementioned techniques and in assessing the effect of new regulations in improving air quality.

On board Sensors

Within SCIPPER, innovative cost-effective sensors were considered and tested for conducting continuous on-board emissions monitoring. Some sensors are being developed by SCIPPER partners and others are packaged to be used as complete monitoring devices for on-board applications. The market of such systems is currently primitive and the ones existing were known to still have durability and sensitivity issues. Moreover, the precise censoring, data processing and reporting format has to be standardised. However, the arrival of Tier III and the new global sulphur regulations significantly grows the need of adopting such cost-effective systems for emissions monitoring, on a ship constant operation basis.

So, SCIPPER has successfully tested, during the two on-board experimental campaigns (Line Gothenburg to Kiel and English Channel), five innovative low-cost sensor packages, capable of monitoring NO_x, NH₃, SO_x, CO₂, BC, PM and PN concentrations. Refer to Verbeek (2023) and SCIPPER D1.6 (2022). Innovative sensors sensitivity was defined by comparing their exhaust measurements with the reference ones provided by high-end instrumentation, the accuracy of which is well-proven from their long-term application in the automotive sector. Results of the low-cost emissions monitoring for gaseous pollutants showed good agreement with the reference instrumentation, especially for NO_x, CO₂ and CO. This is indicatively depicted in Figure 1, where low-cost sensor measurements, presented with solid lines, are compared with the reference ones that appear with dashed, for a two-hour continuous monitoring period.

Figure 1. Cost-effective (solid lines) vs high-end (dashed lines) emissions monitoring performance



The sensors application for measuring NH₃, SO₂ was less reliable, showing issues of fast decay, attributed to specific sampling conditions. For particles, all sensors operated sufficiently during the measurements, including detecting BC, and no fouling or loading issues were noticed.

Experiments also focused on the durability of the sensors, a criterion that will reveal their potential for continuous unmanned monitoring. Based on tests over a 6-month period, the lifetime of gaseous sensors for NO_x constant monitoring is expected to range between 2.000 to 4.000 annual operating hours, while adjustments to the sampling systems for controlling sensors exhaust gasses exposure can extend their operational lifetime from one to two years. For particles, the long-term uninterrupted monitoring appears to be feasible, but existing aspects of contamination limit their unmanned functioning.

The overall demonstration of on-board sensors within SCIPPER has led to the following findings:

- there is a promising potential of sensors to be used for onboard monitoring,
- protection against fouling, in the form of intermittent sampling or air shield, is needed to protect sensors - once a year maintenance, including replacement of sensors, will probably be necessary,
- NO_x can be measured in raw exhaust, but for most components; SO_x, PM, PN, BC, a dilution system is needed - some advice would be to develop a simple mechanical dilution system which is adjusted once during installation,
- use of S-AIS as a real-time data transmission pipeline was demonstrated successfully.

Remote Sensors

Techniques were deployed by SCIPPER for the remote monitoring of shipping emissions, including sniffers and optical remote sensors. These sensors were placed on fixed stations for checking ships that operate closed to ports and were also carried by various means as patrol vessels, drones and satellites, with the ability to extend measurements in ships sailing outside of port areas. On a period where stricter SO_x mitigation regulations are globally enforced, remote techniques can become a valuable and cost-effective tool for authorities to massively

check ships compliance, in addition to the existing regulatory provision of fuel sampling. Similar challenges also arise for NOx within NECAAs, as well as for the pollutants that will be regulated in the future.

So within SCIPPER experimental campaigns, standard and high sensitive sniffers equipped fixed stations and patrol vessels, while mini sniffers were mounted on drones. Optical solutions (DOAS and satellites) were supplementary evaluated as they are less mature than the sniffer systems. The remote systems measured pollutants such as NOx, CO₂, SO₂, PN, PM, BC, as well as identified the fuel sulphur content (FSC) of ships. Accuracy of these techniques was then evaluated; quality assurance and harmonization reporting aspects were addressed, and their operational particularities in the field were highlighted.

The level accuracy of remote sniffer instrumentation in identifying the FSC of ships was mainly evaluated in relation to fuel samples that were taken from on-board inspections in the port of Hamburg. Results, presented in Figure 2, revealed the sniffers ability to capture the content of sulphur in fuel. However, a slight underestimation is depicted, compared to the actual values recorded in the reference sampling, primarily attributed to ambient and calibration conditions, but with further research investigation to be required for safe conclusions. The total uncertainties for the different systems were found to be varying between 0.03 and 0.14 % S m/m at an FSC level of 0.1 % S m/m considering a 95 % confidence interval.

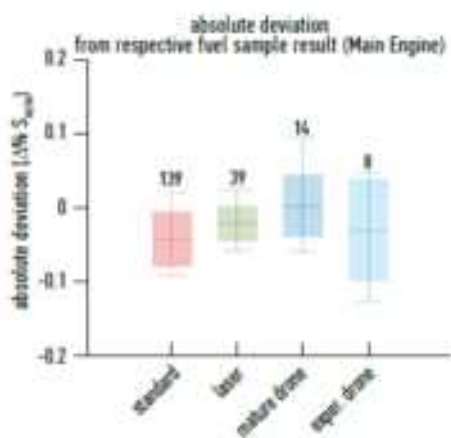


Figure 2. Sniffer systems FSC detections in relation to fuel sampling results

SCIPPER examined the potential of checking ship compliance through satellites, using TROPOMI observations. So single ships NOx and SO₂ emission footprints were tried to be detected. Findings for NOx show that single ship plumes are visible in TROPOMI observations. However, more investigation is needed for exploiting satellite observations for compliance check, but global monitoring seems to be feasible for NO₂. On the other hand, existing TROPOMI SO₂ retrieval algorithms are not sufficient to make emissions in shipping lanes observable. SO₂ signal from shipping appears to be below the detection limit of TROPOMI.

The overall remote techniques deployment and evaluation led to the elaboration of recommendations on how to conduct remote measurements of gas-pollutant emissions from ships, including data validation procedures, uncertainty calculation and reporting. So SCIPPER proposes that:

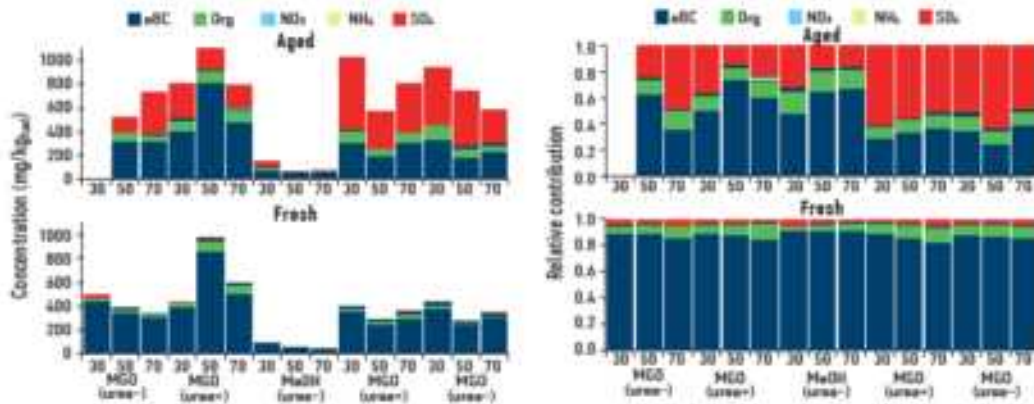
- validation is needed that the measurement with remote instrumentation is correctly conducted,
- quality scoring system per technique could be applied, with criteria of weather, signal to noise ratio and traceability - scoring should not be part of the reporting, but part of the uncertainty analysis,
- uncertainty needs to be subtracted from measurement results when focus comes to compliance monitoring.

Plume ageing & air quality

Shipping induced pollutants, after emitted, may spend a considerable time in the atmosphere and undergo significant transformation before reaching coastal and urban areas. Therefore, SCIPPER linked the atmospheric evolution of the fresh emissions with the air quality final impacts imposed by the aged emissions, when these reach the shore. The assessment of ageing transformation phenomena was conducted at two stages. The first one concerns the period when the plume exits the ship funnel, while the second stage considers the evolution in distances far from ships till the shore.

Reference exhaust sampling measurements vs ageing experiments were made during the on-board campaign to understand the exact differences between fresh and aged plume synthesis. The tested ship operation under different fuels (Marine Gas Oil - MGO, Methanol-MeOH) and aftertreatment technology activation phases (Selective Catalytic Reduction – SCR: on/off), provided additionally the opportunity to study plume synthesis and ageing phenomena when popular emission reduction options are applied. A snapshot of this assessment is provided in Figure 3, where fresh and aged PM concentration results are presented, along with the absolute and relative speciation synthesis.

Figure 3. Fresh vs aged plume PM concentration together with speciation analysis, for MGO and MeOH fuels, as



well as for SCR on-off status, at different engine loads.

Overall, PM increases as the plume ages. For fresh emission, BC dominates PM chemical composition for all tested conditions, followed by organics and sulphate. For aged samples, sulphate contributed more to PM mass, followed by organic compounds, likely due to oxidation of SO_2 and organic compounds. The load or catalyst urea injection did not have major impact on composition of particulate emissions or relative concentrations of major species. For MeOH, the emissions of all major species were significantly lower. Furthermore, in the aging analysis for the particles size distribution, the contribution of nucleation particles increased in the plume, whereas the soot mode concentrations were stable. Experiments were repeated during the port of Marseille campaign, with plumes sampled remotely close to ships and onshore. Results also here showed an important increase of the total PM mass in aged plumes.

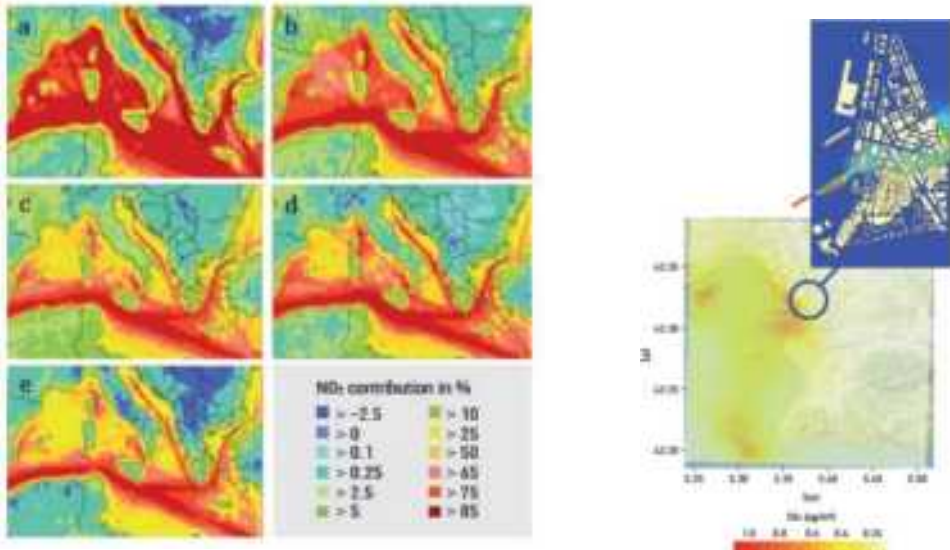
The main conclusions of the plume ageing characterization activities of SCIPPER are:

- besides decreasing the NOx emissions, the SCR system significantly also decreased THC and fresh aerosol mass emissions,
- MeOH fuel significantly decreased BC and PM emissions, as well as the secondary aerosol formation potential,
- ship plumes are a source of secondary aerosol precursors - the secondary aerosol mass is generally higher than the fresh aerosol mass,
- on gaussian plume scales, secondary aerosol formation is low enough to be insignificant in the initial dispersion phase.

The impact of shipping on air quality was evaluated on two different scales. Macroscale assessments, conducted for the areas of Mediterranean Sea, the North and Baltic Seas. These targeted to cover the contribution of shipping to air pollution in a spatially wide and temporally long-term perspective. Several air quality models of macroscopic type were used for this purpose, after cross-validated on a specific domain in the Mediterranean. Results for the Mediterranean area showed that shipping impacts on NO_2 concentrations are highest in short distance (less than approx. 100 km) to the shipping lanes, as indicatively depicted in Figure 4 (right), and $\text{PM}_{2.5}$ concentrations increase by 10-15% because of shipping emissions in many coastal areas. Similar results were observed for North and Baltic Seas. Overall, European coastal areas along the Mediterranean Sea are most significantly affected by air pollution from shipping in southern Spain, southern Italy and along the Greek and

Turkish coastline. In general, the southern North Sea region and the English Channel experience the highest pollution from shipping in Europe.

Figure 4. Right: Impact of shipping on the annual mean NO₂ concentration in the Mediterranean Sea in 2015 estimated by various models (a = CAMx, b = Chimere, c = CMAQ, d = EMEP, e= LOTOS-EUROS); Left: Shipping air quality impacts for the port of Marseille, assessed with local-scale (down) and microscale (up) models



More detailed shipping impacts and precise pollutants distribution in harbour areas were revealed through local and microscopic models. Assessments were conducted for the port areas of Marseille, Hamburg, Gothenburg, Rotterdam, Kiel, and Thessaloniki. A characteristic example of the application of detailed models for the Marseille port is provided in Figure 4 (right), where NO₂ concentrations were calculated for the port area (down) and further analyzed in more detail (up) to better understand more local phenomena.

The overall air-quality work conducted in SCIPPER also led to the production of Improved air-quality models for coastal areas and harbour-scale modelling, including secondary aerosol processes. The main conclusions can be summarized in the following points:

- ship emission model systems were improved with new emission factors,
- regional chemistry transport model systems are well suited tools for quantifying the impacts of shipping emissions on air pollution,
- shipping has a large impact on NO₂ concentrations with highest values along the main shipping routes - shipping has impacts on O₃ leading to increased concentrations on average and in larger distances from shipping lanes,
- through complex interactions with pollutants from other sources shipping emissions also lead to increased secondary PM_{2.5} concentrations,
- impacts of shipping emissions on air quality in harbour cities can be quantified with city scale model systems,
- NO₂ concentrations in harbour cities increase as a results of shipping emissions while O₃ concentrations decrease. Among the investigated cities, largest effects take place in Rotterdam and Hamburg,
- a wide application of ammonia as a shipping fuel in the future will cause significant particle formation, unless emissions will be regulated,
- air-quality model systems were improved with respect to their representation of ship plumes, the treatment of organic emissions and the formation of secondary particles.

Conclusions

SCIPPER assessed several shipping measurement techniques, through the real-world demonstration of several emission measurement systems in five experimental campaigns. The following conclusions can be drawn based on this evidence:

- emission measurement systems that incorporate mature technology, already applied in other fields (automotive, air quality), can be used to effectively check if ships operate under the established limits,

- on-board systems gather several operational advantages in revealing the actual emission profile of ships both to the authorities and ship owners, but standard remote systems also appear particularly attractive for authorities as an independent system under a regulatory perspective,
- remote systems mounted in aerial means or in patrol vessels can supplement the standard fixed-station ones, expanding the monitoring capacity of authorities outside of port areas,
- optical systems (fixed station and satellites) present an alternative to the sniffer-based remote monitoring; however, technology maturity parameters and operational aspects reduce their applicability today,
- cost per ship for on-board monitoring is higher than the respective one of any of the remote systems, however on-board sensors in all vessels mean that all vessels can be monitored.

SCIPPER further synthesized its outputs to provide policy recommendations on next steps in shipping emission monitoring, and in achieving future effective regulations. Refer to SCIPPER D5.5 (2023). Main concluding recommendations are summarized in the following points:

- all ships to install sensor systems for on-board monitoring of NOx, SOx and BC - data should be automatically transferred to a monitoring center, using encrypted format,
- establish a not-to-exceed (NTE) limit, suitable for NOx compliance monitoring using remote sensing measurements,
- mandate minimum deployment of remote sensing stations to detect when fuel with too high sulphur content is used. Use remote sensing to identify ships with non-functioning NOx abatement systems, especially in ECA environment,
- develop routines for remote sensing measurements and legal actions,
- establish more NOx Emission Control Areas and establish an emission test cycle for NOx certification that also reflects operation at low loads, and require in-use measurements or sensors to verify that abatement equipment works,
- develop emission limits and measurement procedures for particle related properties (e.g., PN, PM, BC), for NH₃ – both for SCR systems and when ammonia is used as fuel, for methane - most relevant for LNG as fuel, and for N₂O - most relevant for ammonia fuel.

Acknowledgements

The SCIPPER project has received funding from the European Union's Horizon 2020 research and innovation programme under grant agreement Nr.814893

References

- IMO (2008): IMO Resolution MEPC 177(58), Amendments to the technological code on control of emission of nitrogen oxides from marine diesel engines, NOx Technical Code 2008, 10 October 2008.
- IMO. (2016). Marpol Annex VI, Sulphur oxides (SOx) and Particulate Matter (PM) – Regulation 14, Resolution MEPC.280(70)
- SCIPPER D1.6 (2022) Weisheit, J., Verbeek, R., Paschinger, P., Verhagen, V., Irjala, M., Simonen, P., Kousias, N., Moldanova, J., Mellqvist, J., Fridell, E., Verbeek, R., et al. A compilation of technical deliverables of enhanced sensor monitoring. SCIPPER Deliverable D1.6. September 2022. EU Horizon 2020 project No. 814893. <https://www.scipper-project.eu/library/>.
- SCIPPER D5.5 (2023) Erik Fridell, Ruud Verbeek, Volker Matthias, Johan Mellqvist: Policy recommendations related to regulations, monitoring and enforcement. SCIPPER deliverable D5.5, February 2023. EU Horizon 2020 project No. 814893. <https://www.scipper-project.eu/library/>.
- Verbeek (2023). Experiences with sensor based continuous emission monitoring for demonstration of maritime emissions compliance. R. Verbeek, et.al.. TAP & SE conference Gothenburg, September 2023.

Application of a 24-hour ship plume forecasting system

R. Badeke¹ and V. Matthias¹

Institute of Coastal Environmental Chemistry, Helmholtz-Zentrum Hereon, Geesthacht, Germany, Ronny.Badeke@hereon.de

Introduction

Shipping emissions represent a significant source of air pollutants, primarily including oxides of nitrogen (NO_x), particulate matter (PM), secondary ozone (O_3), sulphur oxides (SO_x), carbon monoxide (CO) and volatile organic compounds (VOCs). Exposure to these pollutants is associated with respiratory and cardiovascular diseases, and the deposition of nitrogen and sulfur compounds can lead to the acidification and eutrophication of water bodies.

The Baltic Sea has been a focal point for air quality research for decades, driven by the economic importance of ship traffic and the large population residing in nearby coastal cities. Adverse health effects have been quantified in exposure studies (Barregard et al., 2019, Ramacher et al., 2019). Ship impact on air quality in the Baltic Sea region has been modeled using various approaches, including CAMx (Aksoyoglu et al., 2016), CMAQ, EMEP/MSC-W and SILAM (all in Karl et al., 2019a) on the regional scale, or EPISODE-CityChem on the city scale (Ramacher et al., 2019).

The effectiveness of designating the Baltic Sea as an emission control area has been assessed in terms of air quality and deposition (e.g., Jonson et al., 2015, Karl et al., 2019b) and has shown significant pollution reduction, particularly with the ongoing fleet modernization. However, ensuring compliance with emission regulations is essential, and in light of the new air quality recommendations from the World Health Organization (WHO, 2021), monitoring coastal air quality is of crucial importance. To further mitigate health issues for individuals residing in coastal areas, the implementation of a precise forecasting system for ship pollution, similar to weather or pollen forecasts, can be a valuable tool. This study presents and evaluates the initial outcomes of a new local-scale ship pollution forecasting system, based on the setup of the urban air quality forecast system in Hamburg (AQF, 2023).

Methods

The focus of this study is the German coast in the Southern Baltic Sea region, specifically the Kadestrinne, a heavily trafficked channel between the city Rostock and the islands of Fehmarn and Bornholm (Fig. 1). Shipping activity in this area significantly contributes to coastal pollution, particularly during north and west wind conditions.

Air quality simulations are conducted using the Eulerian model EPISODE-CityChem v1.8 (Karl et al., 2019c). An overview of the model setup is provided in Fig. 2.

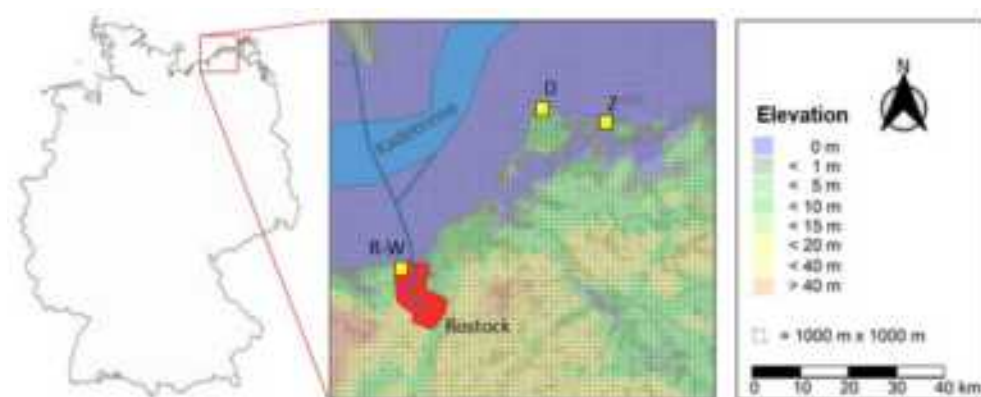


Figure 1: Depiction of the research domain. D = Darßer Ort, R-W = Rostock-Warnemünde, Z = Zingst.

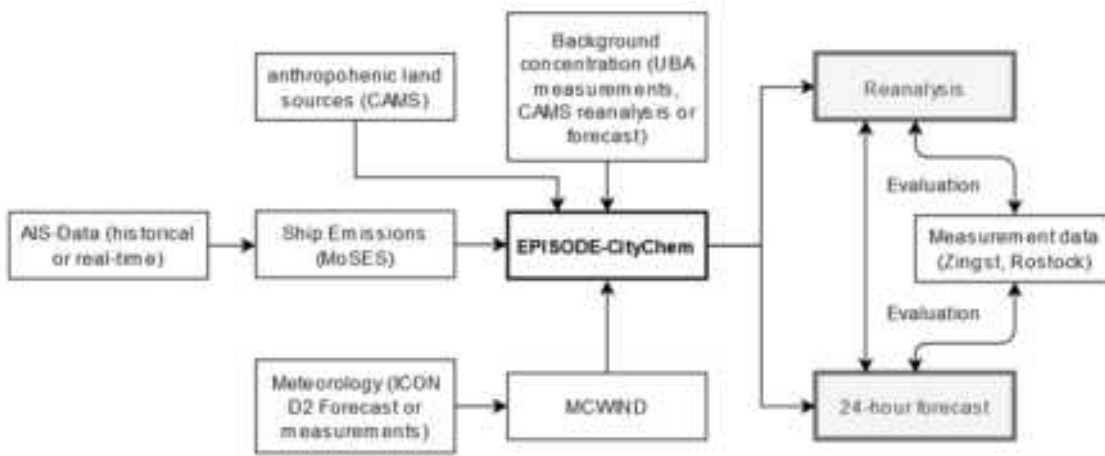


Figure 2: Overview of the numerical model system employed in this study.

The model's performance is assessed in two stages. First, its ability to represent actual quality conditions based on reanalyzed data is examined. In the second stage, the forecast itself is evaluated.

The meteorological data are obtained from either measurements taken at the German Weather Service (DWD) station located at Rostock-Warnemünde (see Fig. 1) or forecasts based on ICON D2 data up to 24 hours (DWD, 2023). The key meteorological parameters in this setup include wind speed, wind direction, temperature and atmospheric stability. These parameters undergo preprocessing with the MCWIND v1.3 preprocessor (Hamer et al., 2020). Ship numbers and movement information are derived from AIS (Automatic Identification System) statistics. Shipping emission data are calculated using the Modular Ship Emission modeling System MoSES (Schwarzkopf et al., 2021). Background concentration data from the German Environment Agency's measurement station Zingst (see Fig. 1) and from the Copernicus Atmospheric Monitoring Service (CAMS, 2023) are utilized. CAMS data are also incorporated for land-based emissions. The calculated concentrations for NO₂, O₃ and PM₁₀ are compared against measurements from the German Environment Agency.

Results and Discussion

Figure 3 presents NO₂ and O₃ modeling (reanalysis) compared to measurement results for two exemplary weeks in July 2018 at the Zingst measurement station. Corresponding statistical evaluations of the model quality, including PM₁₀ results, are presented in Table. The biases are small, particularly for NO₂, and the Pearson correlation coefficient indicates a strong agreement between modeled and measured values.

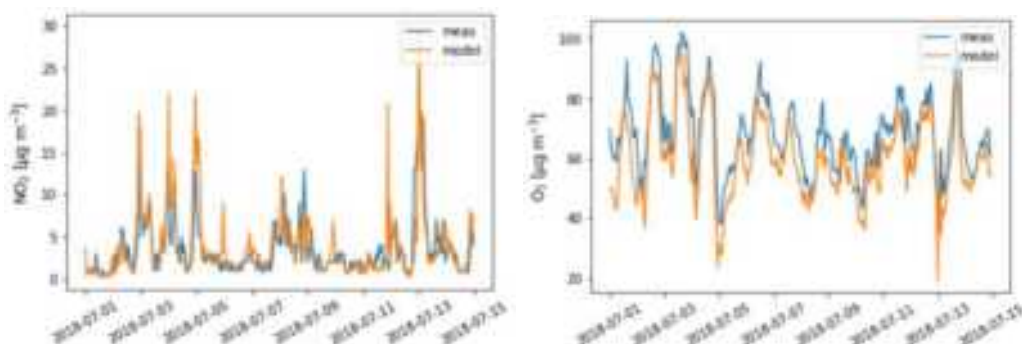


Figure 3: Comparison between modeled and measured NO₂ concentrations at the measurement location Zingst.

Table 1: Statistical performance of the model performance (reanalysis).

	NO_2	O_3	PM_{10}
BIAS	$0.35 \mu\text{g m}^{-3}$	$-7.9 \mu\text{g m}^{-3}$	$0.1 \mu\text{g m}^{-3}$
NMB	10 %	-12 %	1 %
R	0.72	0.89	0.96

To assess the impact of ship emissions at a coastal background position (Darßer Ort, Fig. 1) a zero-out method was employed, calculating differences between a model run with and without ship emissions. Figure 4 and Table 2 provide an overview of these results. While the overall average relative ship effect on O_3 and PM_{10} over the two-week period is relatively low, it is more significant for NO_2 . A relative impact of 81.28 % is attainable, but this should be cautiously interpreted, as these high percentages mainly occur when comparing already low concentrations. Therefore, evaluating the mean relative difference, which stands at 22.77 % with a mean absolute difference of $0.92 \mu\text{g m}^{-3}$, is more meaningful. During hours of heavy ship traffic, the maximum absolute NO_2 impact reaches nearly $8 \mu\text{g m}^{-3}$, simultaneously causing the most pronounced reduction of O_3 , approximately $9 \mu\text{g m}^{-3}$. Ozone formation in the Baltic Sea occurs can occur under hot summer day conditions, primarily during strong radiation, high temperatures and low wind speed (Aksoyoglu et al., 2016, Badeke et al., 2023).

The results are comparable to a study by Ramacher et al. (2019), which also utilized the EPISODE-CityChem model, focusing mainly on concentrations within coastal cities, including Rostock. They found a local shipping impact on NO_2 concentrations of 11 % annually averaged for Rostock and a low impact on PM concentrations, similar to the findings of this study.

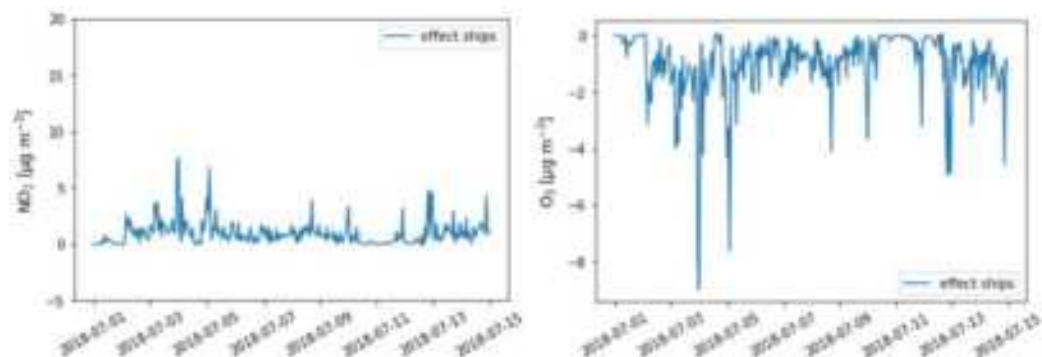


Figure 4: Ship effect on NO_2 and O_3 concentrations at the station Darßer Ort for a two week simulation in July, 2018.

Table 2: Ship effects at the position Darßer Ort for a two week simulation in July, 2018.

	NO_2	O_3	PM_{10}
mean diff	$0.92 \mu\text{g m}^{-3}$	$-0.97 \mu\text{g m}^{-3}$	$0.02 \mu\text{g m}^{-3}$
max diff	$7.69 \mu\text{g m}^{-3}$	$0.08 \mu\text{g m}^{-3}$	$0.33 \mu\text{g m}^{-3}$
min diff	$-0.07 \mu\text{g m}^{-3}$	$-8.97 \mu\text{g m}^{-3}$	$0 \mu\text{g m}^{-3}$
mean rel diff	22.77 %	-1.75 %	0.37 %
max rel diff	81.28 %	0.26 %	5.17 %
min rel diff	-25.95 %	-24.02 %	0 %

Based on these results, the setup is deemed to have sufficient performance to calculate representative air quality results using reanalyzed data. However, achieving a good forecast necessitates accurate predictions for several input parameters presented in Fig. 2, particularly meteorology, ship movement, and background chemistry.

In the current stage of this study, only the effect of the meteorological forecast on the resulting concentration fields is evaluated. Due to limited data for July, the forecast results are calculated for another period - the first week of October 2018. Figure 5 illustrates wind speed and wind direction forecast performance and includes modeled results from the July reanalysis for comparison.

The meteorological preprocessor MCWIND is driven by a single meteorological measurement station, specifically the measurements or forecasts at the Rostock-Warnemünde station. Statistical parameters for wind speed in the reanalysis setup shows a BIAS of 1.1 m s^{-1} (model overestimation), NMB = 18 %, and R = 0.98, indicating a good performance consistent with the model results in Figure 3.

During the forecast period, wind speed exhibits a variable pattern with changing high and low wind conditions as well as short peaks of high wind speed. The wind direction primarily lies between southwest and north, including a rapid change on October 7, 2018. The model captures the wind direction well, but the wind speed forecast demonstrates lower quality. Statistical parameters for the wind speed forecast are BIAS = -0.63 m s^{-1} , NMB = -10 % and R = 0.48. Overall, the current status of the forecast underestimates wind speed and requires further improvement, particularly regarding the correlation coefficient. This enhancement will involve including a larger number of weather stations into the forecast, improving the model's representation of wind dynamics. Differences from real measurements can also arise due to differences in the model layer reference height (lowest layer height of 17.5 m) and the instrument measurement height (10 m). The results herein provide a solid baseline for future improvements.

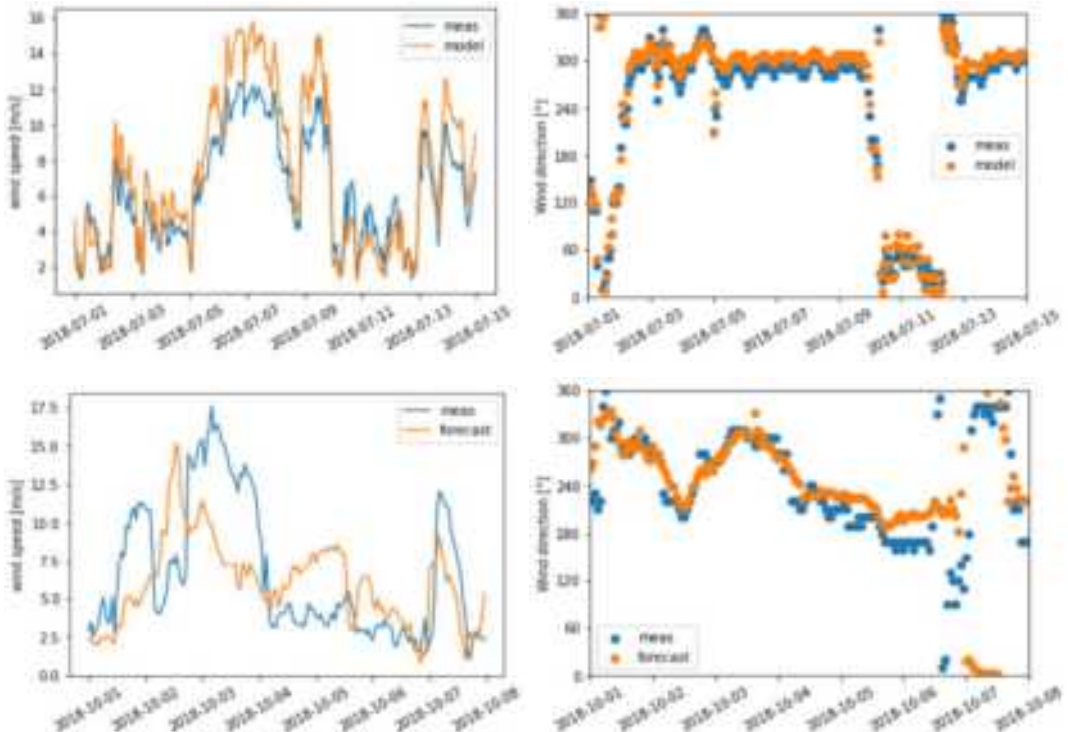


Figure 5: Comparison of wind speed (left) and wind direction (right) for measured and modeled values at the position Rostock-Warnemünde. The upper row are results from the July period (reanalysis) and the lower row are results from the October period (forecast).

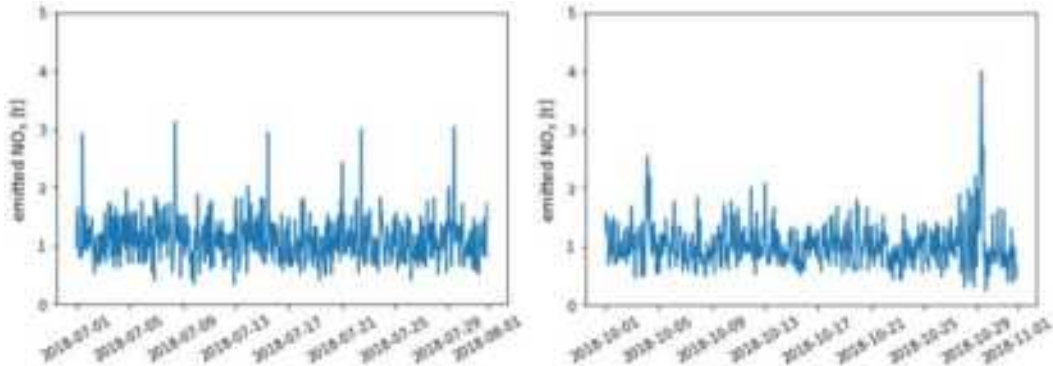


Figure 6: Sum of emitted NO_x from ships inside the research area. Emission values are given on an hourly resolution.

An individual ship movement prognosis has not yet been incorporated into the model. However, overall emission for both periods has been investigated in Figure 6, illustrating ship activity in the entire research area based on total NO_x emission values. Emissions mostly range from 0.5 to 1.5 tons per hour. Regular spikes in July correspond to Sundays and may be linked to cruise ship activities. The effect of variable ship movement on forecast quality is anticipated to be significant during individual averaging hours. For daily average pollution, it is assumed to exhibit similar behavior from day to day, therefore, thus allowing the application of a daily average profile to represent ship emission.

A CAMS forecast for background concentration exists but not yet been applied in this study yet. Nevertheless, to demonstrate the potential impact of different background concentration sources on the results, Figure 7 presents forecast results for NO_2 and O_3 with the forecasted wind field, as well as with and with both measured background values and reanalyzed CAMS background values. The statistical comparison is provided in Table 3.

The NO_2 forecast shows overall good results when using measured background data. Stronger deviations occur at times when the wind forecast is also showing lower performance (days 5 and 7), which is expected. The NO_2

forecast with CAMS background data shows a lower performance. For O_3 , the forecast with measured background data is sufficient and shows an underestimation similar to the reanalysis. CAMS background give a better agreement for the BIAS of O_3 . The PM forecast is good but not strongly affected by ship emissions.

Conclusion

The setup has the potential to be employed as a real-time early warning system, primarily contingent on a high-quality weather. It will undergo further improvement and investigation, especially for periods after the Baltic Sea became a nitrogen emission control area in 2021.

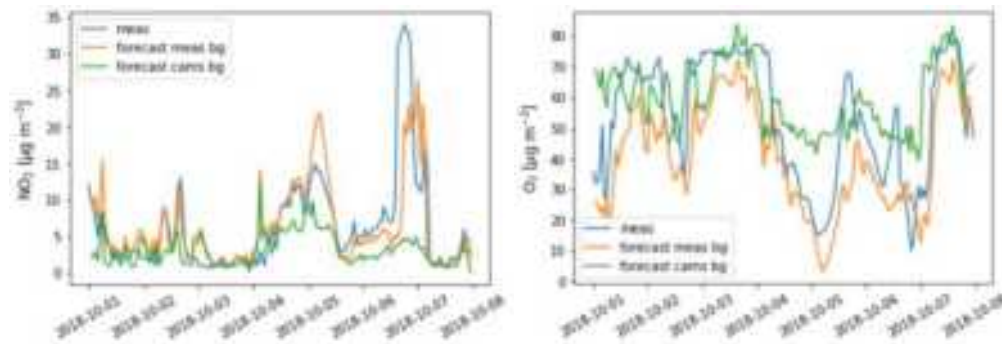


Figure 7: Measured and forecasted values of NO_2 and O_3 in the first week of October 2018. Two different runs with background data from measurement (meas bg) and CAMS (cams bg) are shown.

Table 3: Statistical performance of the model forecast for the measurement position Zingst. Different results are achieved with measured and CAMS background concentration.

	NO_2 meas	NO_2 cams	O_3 meas	O_3 cams	PM_{10} meas	PM_{10} cams
BIAS	0.18	-3.17	-12.37	6.75	-0.21	0.51
NMB	3 %	-50 %	-23 %	13 %	-2 %	4 %
R	0.70	0.35	0.85	0.56	0.96	0.69

Acknowledgements

This research is funded by dtec.bw – Digitalization and Technology Research Center of the Bundeswehr. dtec.bw is funded by the European Union – NextGenerationEU.

References

- Aksoyoglu, S., Baltensperger, U., and Prévôt, A. S. H. (2016). Contribution of ship emissions to the concentration and deposition of air pollutants in Europe, *Atmos. Chem. Phys.*, 16, 1895–1906.
- AQF (2023). Urban air quality forecast, <https://urbanaqforecast.coastalpollutiontoolbox.org>.
- Badeke, R., Schneider, K., and Matthias, V. (2023). Analyzing ozone formation conditions for aged ship plumes in a local scale chemistry transport modeling study, EGU General Assembly 2023, Vienna, Austria, 24–28 Apr 2023, EGU23-5758.
- Barregard, L., Molnár, P., Jonson, J. E. and Stockfelt, L. (2019). Impact on population health of baltic shipping emissions, *Int. J. Environ. Res. Public Health*, 16, 1954.
- CAMS (2023). Cams-europe-air-quality-reanalyses, <https://www.copernicus.eu/en/access-data/copernicus-services-catalogue/cams-europe-air-quality-reanalyses>.
- DWD (2023). NWP forecast data, https://www.dwd.de/EN/ourservices/nwp_forecast_data/nwp_forecast_data.html.

Hamer, P. D., Walker, S.-E., Sousa-Santos, G., Vogt, M., Vo-Thanh, D., Lopez-Aparicio, S., Schneider, P., Ramacher, M. O. P., and Karl, M. (2020). The urban dispersion model EPISODE v10.0 - Part 1: An Eulerian and sub-grid-scale air quality model and its application in Nordic winter conditions, *Geosci. Model Dev.*, 13, 4323–4353.

Jonson, J. E., Jalkanen, J. P., Johansson, L., Gauss, M., and Denier van der Gon, H. A. C. (2015). Model calculations of the effects of present and future emissions of air pollutants from shipping in the Baltic Sea and the North Sea, *Atmos. Chem. Phys.*, 15, 783–798.

Karl, M., Jonson, J. E., Uppstu, A., Aulinger, A., Prank, M., Sofiev, M., Jalkanen, J.-P., Johansson, L., Quante, M., and Matthias, V. (2019a). Effects of ship emissions on air quality in the Baltic Sea region simulated with three different chemistry transport models, *Atmos. Chem. Phys.*, 19, 7019–7053.

Karl, M., Bieser, J., Geyer, B., Matthias, V., Jalkanen, J.-P., Johansson, L., and Fridell, E. (2019b). Impact of a nitrogen emission control area (NECA) on the future air quality and nitrogen deposition to seawater in the Baltic Sea region, *Atmos. Chem. Phys.*, 19, 1721–1752.

Karl, M., Walker, S.-E., Solberg, S., and Ramacher, M. O. P. (2019c). The Eulerian urban dispersion model EPISODE - Part 2: Extensions to the source dispersion and photochemistry for EPISODE-CityChem v1.2 and its application to the city of Hamburg, *Geosci. Model Dev.*, 12, 3357–3399.

Ramacher, M. O. P., Karl, M., Bieser, J., Jalkanen, J.-P., and Johansson, L. (2019). Urban population exposure to NOx emissions from local shipping in three Baltic Sea harbour cities - a generic approach, *Atmos. Chem. Phys.*, 19, 9153–9179.

Schwarzkopf, D. A., Petrik, R., Matthias, V., Quante, M., Majamäki, E., & Jalkanen, J. P. (2021). A ship emission modeling system with scenario capabilities. *Atm. Environment: X*, 12, 100132.

Umweltbundesamt (2023). Air data, <https://www.umweltbundesamt.de/en/data/air/air-data/stations/>.

World Health Organization (2021). WHO global air quality guidelines: particulate matter (PM_{2.5} and PM₁₀), ozone, nitrogen dioxide, sulfur dioxide and carbon monoxide, <https://apps.who.int/iris/bitstream/handle/10665/345329/9789240034228eng.pdf?sequence=1&isAllowed=y>.

SEICOR – Ship Emission Inspection with Calibration-free Optical Remote sensing

M. Rieker^{1*}, A. Daubinet¹, K. Krause², F. Wittrock², A. Richter², S. Schmitt³, D. Pöhler³, C. Haisch⁴

¹ HORIBA Europe GmbH, D-61440, Oberursel, Germany, Marcus.Rieker@horiba.com

² Institute of Environmental Physics, University of Bremen, D-28359, Bremen, Germany

³ Airyx GmbH, D-69214, Eppelheim, Germany

⁴ Technische Universität München, D-81377, Munich, Germany

Introduction

Ship emissions of particles, SO₂ and NO_x (the sum of NO and NO₂) are a significant source of air pollution in coastal areas and close to busy in-land shipping routes. National and international regulations have been put in place to limit emissions and minimize the impact of shipping on air quality. Monitoring of ship emissions is challenging and so far, no automated system is operational for systematic surveillance of the compliance with regulations.

Most of the time in-situ instruments, which rely on the wind to transport the emissions towards the measurement site, are used to monitor the emissions of ships. However, in times with low wind speeds or an unfavourable wind direction the emissions cannot be measured. Additionally, regular calibration is needed to ensure the quality of the measurements.

Active Optical Remote Sensing, such as Differential Optical Absorption Spectroscopy (DOAS), allows to measure ship emissions without being dependent on wind and almost every passing ship plume can be measured. Another advantage is that calibration gases are not required at all which enables long term autonomous operation without frequent on-site maintenance or calibration procedures.

Briefly, an active Optical Remote Sensing system consists of a light source on one side of the river or port, and a reflector on the other side (typically in a distance of a few hundred meters to kilometres). The system is set up in such a way that the emitted light passes through the plume of passing ships. Using spectroscopic methods, the concentrations of pollutants in the plume can be determined. In conjunction with an Automated Identification System (AIS), the plumes can be assigned to individual ships and their emissions can be analysed in the context of regulations. The capabilities of such an active Optical Remote Sensing system have been demonstrated already (Krause, et al., 2021)(Krause, et al., 2021) and will be briefly presented in the following.

The results from this study will serve as a base for the development of a new Open Path system for the operational monitoring of ship emissions (NO₂, NO, SO₂, CO₂) in the framework of the SEICOR project.

Measurements of ship emissions using LP-DOAS

To measure ship emissions on the river Elbe, a long-path Differential Optical Absorption Spectroscopy (LP-DOAS) system has been set up in Wedel, Germany, 10 km downriver of the port of Hamburg, Germany. The Elbe serves as the entrance route to the port of Hamburg and sea and inland ships pass the measurement site regularly. The measurement site is part of the ship exhaust gas measurement network of the Federal Maritime and Hydrographic Agency of Germany (Bundesamt für Seeschifffahrt und Hydrographie, BSH) and is equipped with weather station, in-situ instruments to measure pollutants emitted by passing ships (e.g., NO_x, SO₂ and particles) and an AIS receiver. A detailed description of the instruments can be found in Kattner, et al., 2015.

The characteristics of the used LP-DOAS system are shown in Table 1. The system was set up on the northern riverbank and the retroreflector was installed on the southern riverbank. The measurement geometry is shown in Figure 1.

Table 2: Characteristics of the LP-DOAS system

Component	Details
Light source	Laser-driven light source Energetiy EO99
Optical fibres	200, 800 μm
Telescope mirror	Diameter 30 cm, focal length 150 cm
Spectrometer	Acton SpectraPro 300i
CCD	2048 x 512 pixel Roper scientific back illuminated
Measured wavelengths	280 – 362 nm, 0.53 nm resolution

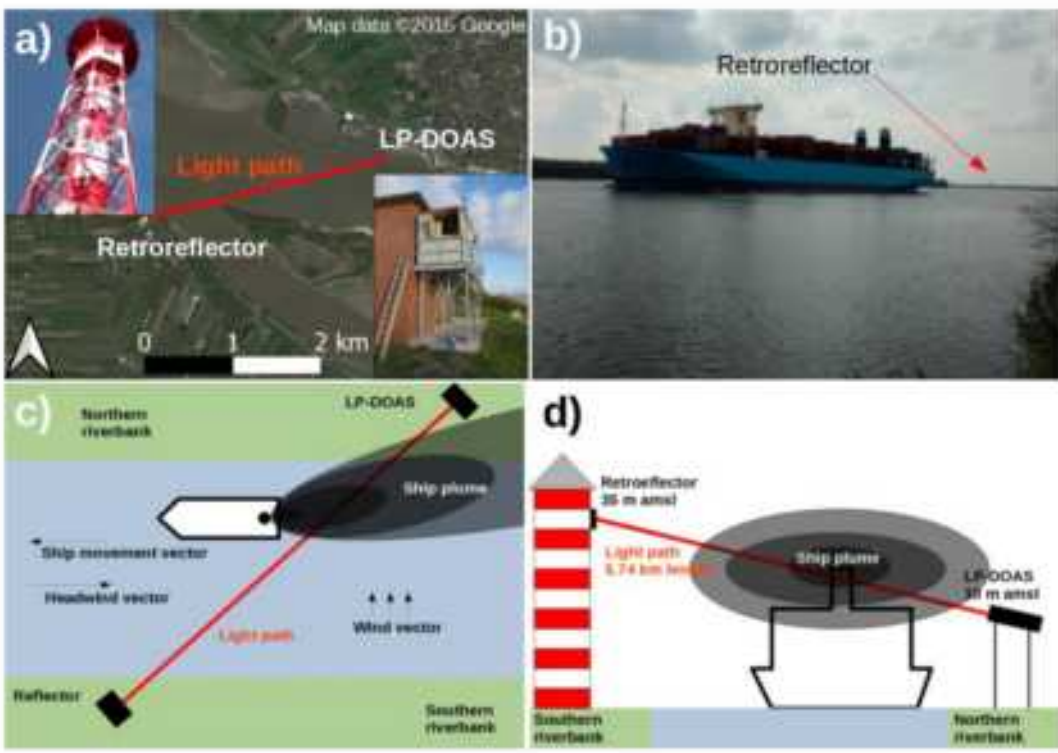


Figure 18: a) Satellite image of instrument location, with the LP-DOAS marked as a red dot on the northern riverbank and the retroreflector position marked as a yellow dot on the southern riverbank. (b) Image of a passing container ship next to the measurement site. (c) Schematic overview of the measurement geometry of the LP-DOAS for a passing ship leaving Hamburg towards the North Sea, seen from above. (d) Same as panel (c) but seen from the port of Hamburg. Note that panels (c) and (d) are not to scale. Adapted from Krause, et al., 2021.

The system sends out a beam of light across the river which is reflected by the retroreflector and measures the received spectra. The total length of the light path through the atmosphere is about 5.74 km. The measured

spectra contain absorption features according to Lambert-Beer's Law. In conjunction with reference spectra of the light source, which did not pass through the atmosphere and therefore do not show absorption features, the measured spectra can be evaluated for trace gases using the DOAS method.

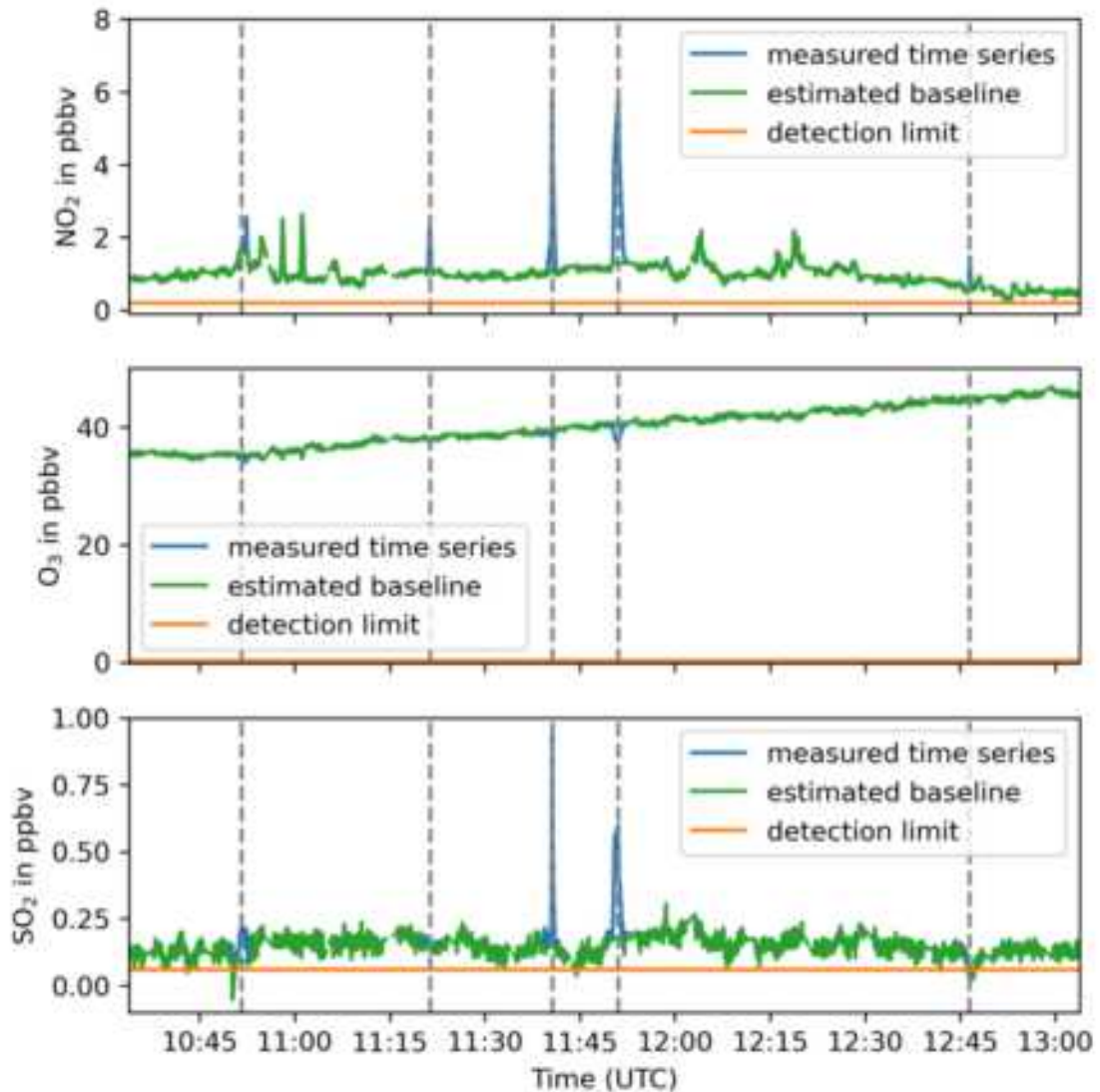


Figure 19: Example time series of the fitted trace gases from 19 August 2018 between 10:30 and 13:00 UTC. In each plot the blue line shows the fitted time series of the respective trace gas, and the orange line shows the respective median detection limit. The grey dashed lines mark passing ships that have been assigned to a peak in the time series. The green line shows the calculated background. Adapted from Krause, et al., 2021.

Being restricted to the wavelength range between 280 and 360 nm, the LP-DOAS only measures NO_2 , while the ship emits NO_x . Only a portion of the measured NO_2 is produced during the combustion process directly, while the rest is formed after emission by reaction with ozone. Therefore, the total NO_x emissions must be estimated from the measured NO_2 concentrations. The NO_2/NO_x -ratio can be obtained by summing the NO_2 enhancements and the O_3 decreases and plotting them against measured NO_x increases. NO_2 , NO_x and O_3 can be measured by the in-situ instruments on site. Using these measurements, a mean NO_2/NO_x ratio of 0.138 ± 0.006 was found (see Figure 3), which agrees with previous studies. Using this ratio and the O_3 and NO_2 measured by the LP-DOAS allows to estimate the increase in NO_x originating from the passing ship.

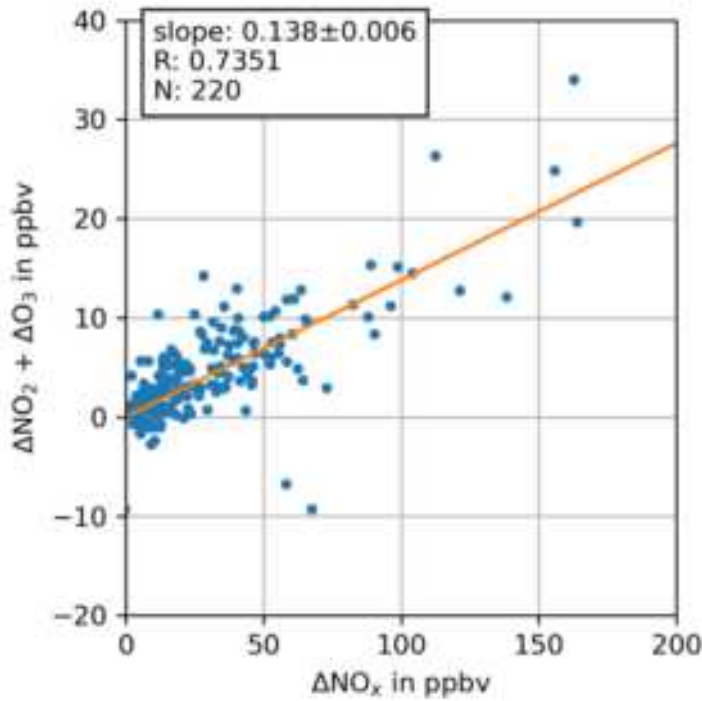


Figure 20: Plot of $\Delta NO_2 + \Delta O_3$ against ΔNO_x from peaks measured with the in-situ instruments between April 2018 and May 2019. All concentrations have been corrected for background concentrations. For this analysis, 220 manually quality-checked peaks were used. This results in a slope (a NO_2/NO_x ratio) of 0.138 with a respective standard error of 0.006.

Adapted from Krause, et al., 2021.

An example time series of the measured trace gases can be seen in Figure 2. The time series of the measured trace gases show peaks (SO_2 and NO_2) and dips (O_3) when a ship plume passes through the light path. These peaks and dips can be assigned to their respective source ships using AIS data. The assignment is based on the position and the time of the passing ship.

The LP-DOAS measures the enhancement of trace gases in the light path and not directly at the stack of the ship. To gain absolute emission rates from the measured NOx data, a model has to be applied to estimate how the plume evolves in the atmosphere. Generally, a ship is a point source and a simple model to describe the plume of a point source is the Gaussian plume model (Pasquill, 1968) (Pasquill, 1968):

$$C(x, y, z) = \frac{Q}{2\pi U \sigma_z \sigma_y} \exp\left(\frac{-y^2}{2\sigma_y^2}\right) \left[\exp\left(\frac{-(z-H)^2}{2\sigma_z^2}\right) + \exp\left(\frac{-(z+H)^2}{2\sigma_z^2}\right) \right]$$

Where Q is the emission rate, U is the wind speed along the main wind direction (along x), σ_z and σ_y are the dispersion parameters in horizontal and vertical direction and H is the height of the plume centreline. The dispersion parameters depend on x , the atmospheric stability, and the surrounding environment. To calculate the emission rate of a ship, the model is evaluated with an arbitrary but constant emission rate (Q_{model}), using the ship's position as the starting point of the plume. This model run then gives insight into the dispersion of the plume in the atmosphere and the concentration measured by the LP-DOAS instrument (C_{meas}) is compared to the concentration of a virtual light path through the model (C_{model}). Finally, the emission rate can be calculated as:

$$Q_{meas} = \frac{C_{meas}}{C_{model}} Q_{model}$$

In total more than 7400 ships have been identified and evaluated by applying the plume model described above. Each evaluated ship passed has been quality controlled and cases where simple Gaussian plume model is not able to reflect the real plume were removed from the dataset before further analysis. The resulting emission rates were then evaluated with respect to size, speed, and type of ships. An example of repeated measurements of several ships is shown in Figure 4.

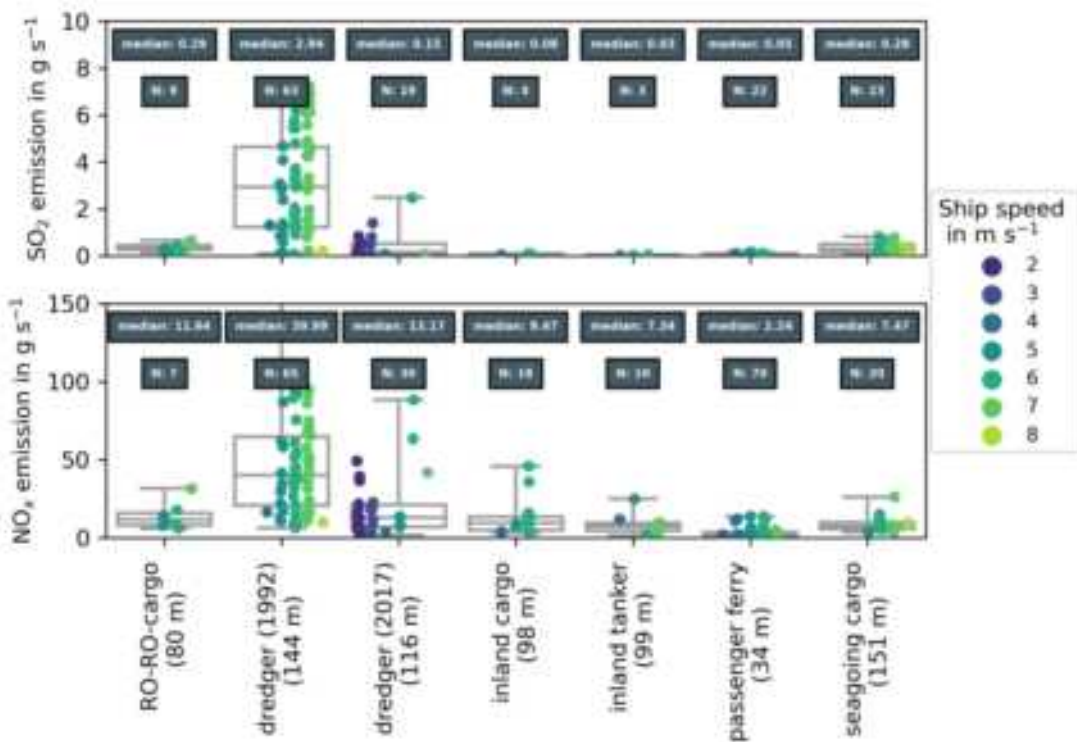


Figure 21: Box plot of SO_2 and NO_x emission rates in grams per second for individual ships; their respective length is given in brackets. Boxes indicate the 25th and 75th percentile, the line in the middle is the median, and the bars show minimum and maximum values. Dots show individual measurements and are colour coded by corresponding ship speed. Dark grey boxes show the median emission rate and total number of observations for this ship. Adapted from Krause, et al., 2021.

Aims of the SEICOR project

The SEICOR project aims to improve the presented method and to develop a system for automated long-term surveillance of emissions from ships and other, similar sources. It will be based on the experiences and tools from the study described above. The new system will cover measurements of all necessary gas species (NO_2 , NO , SO_2 , CO_2), data analysis of the emission factors to direct generation of warnings in case of high emissions as well as automated reporting to the authorities, port operators and / or ship owners.

The new Open Path instrument developed in SEICOR will be a combination of a UV/vis system (for NO_2 and SO_2 measurements) and an IR system to enable measurements of CO_2 and NO . The CO_2 can then be used as a proxy for the amount of burnt fuel, and thereby also of the ship's current energy consumption. The additional CO_2 measurements would then enable to calculate emission factors, e.g., for SO_2 where the regulations are based on limits for the fuel sulphur content. In combination with the direct measurement of NO , the system will directly

quantify NO_x and Sulphur emission factors from ratios of SO₂/CO₂ and NO_x/CO₂, respectively, without the uncertainties induced by plume dispersion models.

Acknowledgements

This work was supported by the University of Bremen, by the German Federal Maritime and Hydrographic Agency and the Federal Ministry for economic affairs and climate action.

Bibliography

Kattner, L., Mathieu-Üffing, B., Burrows, J. P., Richter, A., Schmolke, S., Seyler, A., & Wittrock, F. (2015). Monitoring compliance with sulfur content regulations of shipping fuel by in situ measurements of ship emissions. *Atmospheric Chemistry and Physics*, 15, 10087–10092. doi:10.5194/acp-15-10087-2015

Krause, K., Wittrock, F., Richter, A., Schmitt, S., Pöhler, D., Weigelt, A., & Burrows, J. P. (2021). Estimation of ship emission rates at a major shipping lane by long-path DOAS measurements. *Atmospheric Measurement Techniques*, 14, 5791–5807. doi:10.5194/amt-14-5791-2021

Pasquill, F. (1968). Atmospheric diffusion: The dispersion of windborne material from industrial and other sources (1. publ., reprint ed.). D. Van Nostrand.

Experiences with sensor based continuous emission monitoring for demonstration of maritime emissions compliance

Ruud Verbeek¹, Pauli Simonen⁸, Jana Moldanova⁷, Tim Smyth², Anthony Deakin³, Richard Proud³, Nikos Kousias⁴, Sokratis Mamarikas⁴, Leonidas Ntziachristos⁴, Matti Irlala⁵, Jonathan Weisheit⁶, Andy Chink Nok⁶, Vincent Verhagen¹, Pierre Paschinger¹, Linda Haedrich⁹, Antti Rostedt⁸, Hilkka Timonen¹⁰,

¹TNO, ²PML, ³exactEarth Europe, ⁴AUTH, ⁵Aeromon Oy, ⁶CML, ⁷IVL, ⁸TAU, ⁹HMGU, ¹⁰FMI

Keywords: shipping emissions, maritime transport, enforcement, monitoring

Abstract

Exhaust emissions of maritime vessels are important due to their growing contribution in air quality problems on land and coastal areas, with reduction of other emission sources and the increase in maritime traffic. For this reason, Emission Control Areas (ECA) were introduced in Europe to reduce SOx emissions. This has been ~~expanded to more stringent Tier III NOx regulation – NECAI for new vessels from land in 2021 onwards.~~

The EU H2020 SCIPPER project was set-up to study various possibilities for monitoring and enforcement of pollutant emissions regulations on vessels. Reported here are sensor-based, onboard monitoring results for two vessels: a conventional survey vessel and a ferry RoPax vessel with SCR. Particular good results were achieved with NOx, PM and BC monitoring. Nevertheless, periodic maintenance and intermittent sampling or an air shield, is needed to protect sensors and secure sufficient lifetime. It is also concluded that continuous onboard monitoring gives much more insight in real sailing emissions than the legislative E2/E3 test cycle. Apart from the sensor results, this paper also describes the overall system setup with satellite data transmission and simple reporting formats to judge emissions performance over longer periods.

Introduction

The EU Horizon 2020 project SCIPPER³⁸ was set-up to study the various possibilities for monitoring and enforcement of pollutant emissions from vessels, and how this would contribute to the air quality in coastal and port areas. This included continuous monitoring onboard of vessels (in the exhaust stack) and several types of remote sensing options (onshore, via drones and satellite). SCIPPER was aimed to develop solutions for ~~regulatory and enforcement gaps – Report to EC D5.1 (2019) and SCIPPER D5.5 (2023)~~. The gaps addressed in this publication include primarily; the lack of monitoring procedures for NOx abatement equipment for Tier III, including procedures to discover SCR deactivation. Moreover, the fact that the simple legislative test cycle (E2, E3, etc.) allows for substantial differences between test cycle emissions and Real Sailing Emissions (RSE) and the limited robustness of the emission control technologies.

System description

In the SCIPPER project, six sensor systems for continuous onboard monitoring were tested. The emphasis in this publication is on automotive sensors and NOx monitoring. For a full overview, refer to SCIPPER D1.6 (2022). The SCIPPER strategy for onboard monitoring is built around the following principles:

- Reducing the number of monitoring parameters to the bare minimum. This makes simple validation, and third party checks possible.
- Increase transparency by continuous monitoring and by publishing average performance.
- Monitoring of Real Sailing Emissions (RSE), rather than mimicking the formal test cycles (E3, E2, D2), with stationary operation at specific engine load points.

The (continuous) onboard monitoring concepts investigated in the SCIPPER project, includes satellite data transmission and collecting this data within a web-based monitoring centre. Refer to figure 1.

³⁸ EU H2020 project No. 814893. <https://www.scipper-project.eu>. SCIPPER stands for “Shipping Contributions to Inland Pollution Push for ~~Regulatory and enforcement gaps – Report to EC D5.1 (2019) and SCIPPER D5.5 (2023)~~.

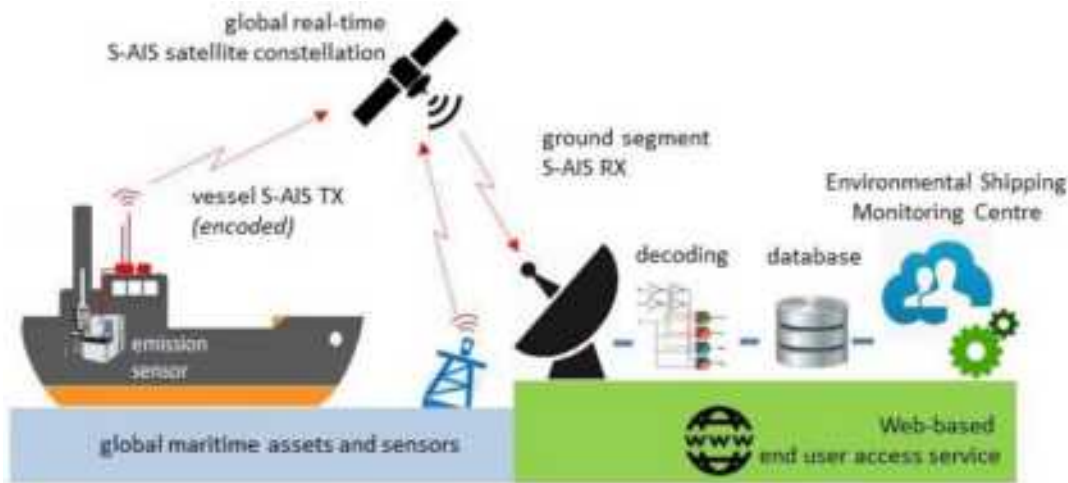


Figure 1. A schematic showing the end-to-end emissions reporting service from ship-to-shore and then to the cloud-based user access services.

For onboard monitoring, it is proposed to express the NOx and other emissions primarily in mass ratios with CO₂ and/or with fuel. This is a simple and robust calculation for which fuel flow and engine power are not needed. The only parameters needed are exhaust concentrations (in ppm) and specific CO₂ emissions of the fuel type used (kg CO₂ per kg fuel). These emissions can also simply be converted to approximate g/kWh values by multiplying the g/kg fuel values with a load dependent or constant Specific Fuel Consumption (SFC) value at sufficient engine load. For further explanation see SCIPPER D1.6 (2023) and also Verbeek (2021).

Results

Table 1 provides an overview of the two campaigns with onboard monitoring. The first one was in the English Channel, the second one in the Baltic Sea. In both campaigns satellite data transmission was tested.

Table 1. Overview of campaigns CX and C2 for onboard sensor monitoring

	CX English Channel	C2 Baltic Sea
Ship	Plymouth Quest - Research Vessel	Stena Germanica - RoPax Ferry
Sensors	automotive sensors – SEMS	All sensor systems
Monitoring period	2021: May – Aug.	2021: September to 2022: January

English Channel

In the English channel, the monitoring took place with automotive sensors and s-AIS data transmission on the Plymouth Quest research vessel. Refer to figure 2 below.



Figure 2: Sensors attached to the exhaust funnel of the RV Plymouth Quest from the TNO SEMS system (Oxygen, NO_x, NH₃ and temperature probes).

The instrumentation onboard of the Plymouth Quest was simple: the exhaust gas concentrations with the automotive NO_x and O₂ sensor and NH₃ sensor were monitored with 1 Hz, and additionally the engine speed (RPM) and Speed-Over-Ground (SOG) with a GPS module. Each minute the data was also sent to a webserver via satellite data transmission. The engine power was calculated according to the propeller law and engine speed, and a SFC curve was fitted based on engine data. The SFC was used to calculate g/kWh emissions based on NO_x/CO₂ ratios. Engine power and air or exhaust flow are not needed with this approximation.

In figure 3, NOx emissions data is shown based on the onboard monitoring during vessel trip #26. This is based on the 1 Hz data. The figure shows the NO_x/CO₂ ratio, NO_x in g/kWh, engine speed and engine power. The figure shows two periods of around 50 minutes with an engine speed just over 1600 rpm. At this speed, the NO_x/CO₂ concentration ratio is around 0.014 and the NO_x is just over 10 g/kWh. In this case, we see also a period with an engine speed just over 800 rpm. The NO_x/CO₂ ratio is then about 30% lower, but due to the lower engine efficiency at the lower power level, the NO_x in g/kWh drops only a bit to just below 10 g/kWh.

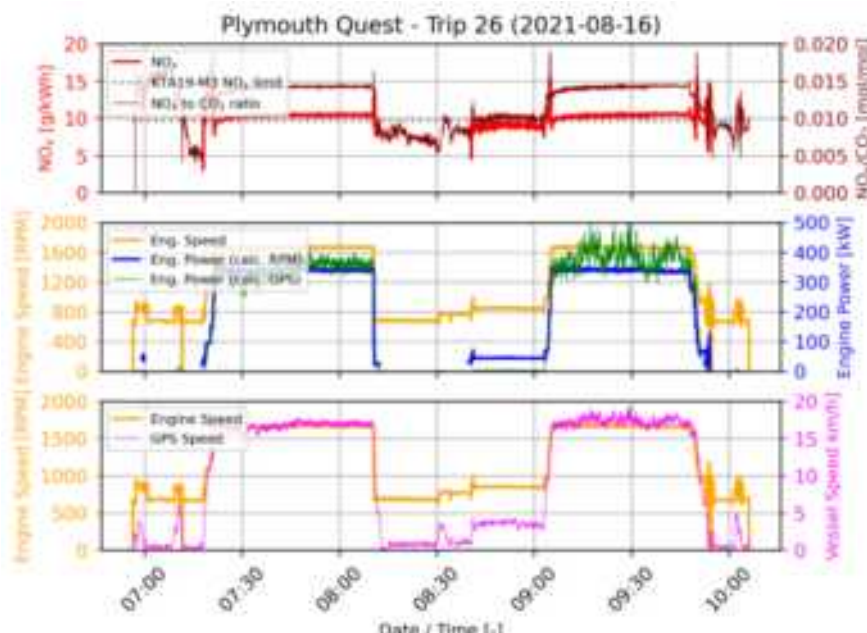


Figure 3 Emission data and ship parameters from Plymouth Quest Trip 26. Source SCIPPER D1.1. Only based on exhaust sensor, engine speed and GPS

Baltic Sea – RoPax ferry

Monitoring with NOx and other sensors in the exhaust stack was carried out on the STENA Germanica sailing from Gothenburg to Kiel. Automotive NO_x/O₂ and NH₃ sensors were installed both in the engine room, before the catalyst, and downstream of the catalyst. Two types of fixtures were tested. The first fixture is a simple tube of about 10 cm diameter, which brings the sensors (NO_x, NH₃ and temperature) about 10cm within the exhaust pipe (shown in Figure 4). This fixture was used during the entire testing period (4 months). In a second fixture, a sample tube branched some exhaust gas to just outside of the main exhaust pipe lead along the sensor and fed back into the exhaust pipe. This was tested during some 2 months.

The sensors were not excessively fouled after 4 months of running. It should however be noted, that the NO_x and NH₃ sensors mounted at the engine-out position showed some technical problems (respectively after 4 months and after 2-3 months). For the automotive NOx sensor a lifetime of at least 6000 hours is estimated for the electronics parts based on ambient temperatures in the funnel or engine room of the vessel. The sensor itself may be affected by SO_x, PM and other impurities due to the fuel composition, uncommon in automotive applications. For that reason, it is advised to limit the exposure time to exhaust gases, e.g. by intermittent exposure. Exposure can be limited by installing the sensor in a bypass duct with a valve, or by an air shield system.



Figure 4. Stena Germanica with sensor fixture in exhaust pipe (right): NH₃, NOx and temperature sensor.

The emission measurements of the automotive NOx sensor were compared in detail to the emission measurements of the reference measurements (Moldanova, 2022). The difference between the automotive NOx sensor and the Horiba analyser was generally in the range of 1% to 6%. This is considered as more than sufficiently accurate given the objective of onboard monitoring, i.e., real-world effectiveness of emission control systems.

The SCIPPER objective was also to produce simple overviews which give direct insight in the overall emissions period during a longer period and also to be able to compare that with the legislative requirements. Three options studied by SCIPPER are: a) emission maps, b) daily averages and c) location specific emissions. Two maps of NOx emissions over a longer period are presented in figure 5 below. These same figures can also be drafted as a function of engine power.

The satellite data transmission used in SCIPPER has a relatively small bandwidth and low frequency (e.g. about 10 data transmissions per hour). Additionally, also 1 Hz data is recorded and transmitted via cellular (when close to land). For more details on the satellite data transmissions refer to Smyth (2023) and SCIPPER D1.5 (2021).

Figure 6 shows an overview with simple daily average NOx emission. This is only based on exhaust gas concentrations of NOx and CO₂. The NOx/CO₂ ratio (linear proportional with g/kg fuel emissions) is averaged. No weighing is applied with respect to engine power or exhaust mass flow. The main advantage of this simple average are transparency and robustness. Onboard verification can simply be done by sticking an analyzer probe in the exhaust gas. This figure also shows the Tier II and Tier III limit values (based on a SFC of 200 g/kWh and a maximum engine speed of 600rpm).

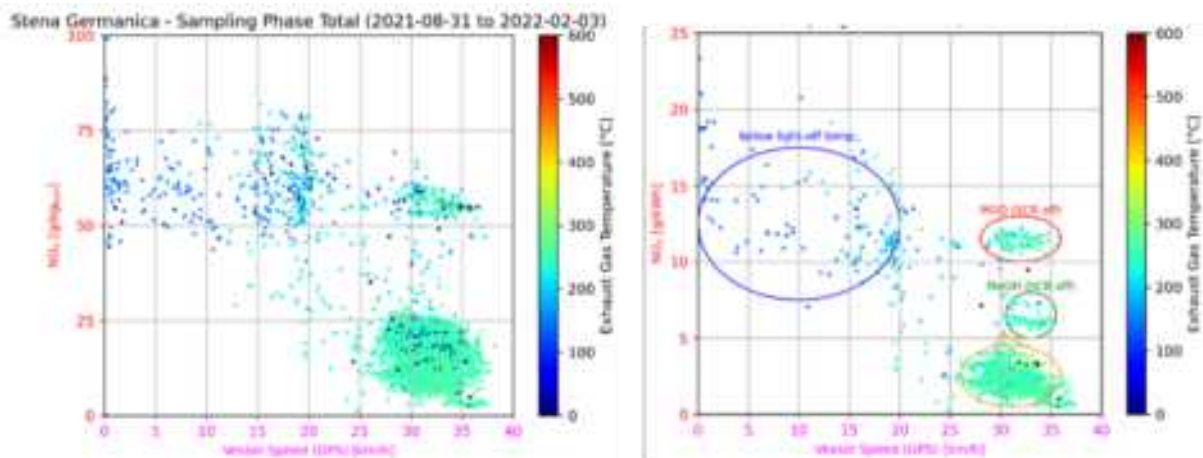


Figure 5. NOx emission maps of Stena Germanica ferry: NOx in g/kg fuel (left) and in g/kWh (right)

Figure 6 also shows the correlation of the daily average between the 1 Hz data (line) and the data transmitted via satellite. In most cases (days) they are almost identical, however on 5 and 10 October there were some differences. It is concluded that, in this case, the daily averages are in line with the Tier III limit value. The successful satellite data transmission for the Stena Germanica averaged around 6 messages per hour. For the English channel (Plymouth Quest), the average transmission rate was about 18 messages per hour, Refer to Smyth (2023) and SCIPP D1.5 (2021). This demonstrates the capability for using s-AIS binary messaging to report emissions data via satellite in real-time. In principle this should work from any location globally.

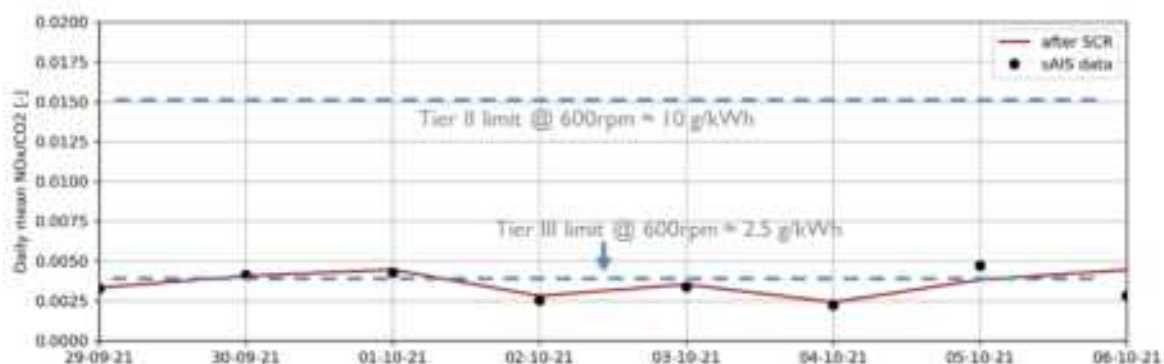


Figure 6. Stena Germanica. Comparison of daily average NOx bases on continuous monitoring (red line) and low frequency data via s-AIS satellite transmission (black dots).

Black Carbon and PN monitoring

A total of five particulate matter sensors were tested: two PN sensors, two standard optical black carbon sensors (ObservAir) and one prototype opto-acoustic BC sensor (AUTH/HMGU). All PN sensors were sampling from an eDiluter (Dekati Ltd) connected downstream of the SCR catalyst. Optical sensors report BC mass concentration based on light attenuation caused by particles deposited on a filter. With the eDiluter intermittent sampling was applied. In this way the exposure time of the particulate sensors was limited to extend the lifetime of the sensors.

Contrary to the NOx sensors, the particulate matter sensors were only tested for a relatively short period (1-2 weeks). During this period, all particulate matter sensors operated well and no fouling or loading issues were noticed. The PN sensors appear as quite feasible for unsupervised monitoring of the number concentration in the exhaust line. The optical BC sensors also operated well, but as these require periodic filter media changes, they are less feasible for unsupervised use. During the campaign, one filter change per day was required even with intermittent sampling used. The opto-acoustic BC sensor showed good potential for unsupervised monitoring, although is still in an early stage of development.

Conclusions

The SCIPPER program demonstrated the full chain of sensor-based onboard monitoring, satellite data transmission and centralized reporting of emissions performance. Standards for data formats and simple reporting formats were proposed. The best results were achieved with NOx and PM/BC monitoring. Furthermore the following conclusions were made:

- There is a good potential of sensors to be used for onboard monitoring. Automotive NOx sensors in combination with build in O₂ measurement provide a good bases to calculate NOx in g/kg fuel and g/kWh.
- Protection against fouling, in the form of intermittent sampling or air shield, is needed to protect sensors. Once a year maintenance, including replacement of sensors, will probably be necessary.
- NOx can be measured in raw exhaust, but for most components; SOx, PM, PN, BC, a dilution system is needed. An advice is to develop a simple mechanical dilution system which is adjusted once during installation.
- The PN sensors appear as quite feasible for unsupervised monitoring of the number concentration in the exhaust line, although the possible fouling may limit the operation time.
- Several simple reporting formats for NOx emissions were demonstrated. The optimum reporting format for NOx, NH₃ and PM is dependent on the purpose of the monitoring results:
 - Emissions modelling: emissions as function of geographical location (g/kg fuel, g/h)
 - Vessel emissions in normal operation: daily averaged emissions (g/kg fuel, g/kWh)
 - Engine compliance with legislation: plot of emissions as function of engine power or vessel speed (g/kWh, g/kg fuel).
- Both experiments on the Quest and the Stena Germanica demonstrated the capability for using s-AIS binary messaging to report emissions data via satellite IoT in real-time and independent of a vessel's location (i.e. globally).

References

Moldanova (2022)

Jana Moldanova et.al.: Measurement campaign for characterising and monitoring of emissions from vessel with alternative fuels and NOx emission control. IAC 2022, Athens, Greece 5/9-2022.

SCIPPER D1.5 (2021)

Compliance pipeline from ship to shore to web enabled secure data delivery. Tim Smyth, Anthony Deakin, Richard Proud. SCIPPER deliverable D1.5, 20 October 2021. EU Horizon 2020 project No. 814893. <https://www.scipper-project.eu/library/>.

SCIPPER D1.6 (2022)

Weisheit, J., Verbeek, R., Paschinger, P., Verhagen, V., Irljala, M., Simonen, P., Kousias, N., Moldanova, J., Merelli, L., Smyth, T., Deakin, A., Proud, R. *Cost-effectiveness of technical, policy and economic approaches for onboard sensors in monitoring NOx EPLR*. Deliverable D1.6. September 2022. EU Horizon 2020 project No. 814893. <https://www.scipper-project.eu/library/>.

SCIPPER D5.1 (2019)

Hulda Winnes, Erik Fridell, Ruud Verbeek, Jan Duyzer, Andreas Weigelt, Sokratis Mamarikas, Leonidas Ntziachristos: Gaps in current emission enforcement regulations and impacts to real-world emissions. EU Horizon 2020 project No. 814893. <https://www.scipper-project.eu/library/>.

SCIPPER D5.3 (2022)

Ruud Verbeek, Daniëlle van Dinther, Sokratis Mamarik, Achilleas Grigoriadis, Andreas Weigelt, Jasper van Vliet, Tim Smyth, Anthony Deakin, Matti Irljala. Cost-effectiveness of different approaches for compliance Monitoring. EU Horizon 2020 project No. 814893. <https://www.scipper-project.eu/library/>.

SCIPPER D5.5 (2023)

Erik Fridell, Ruud Verbeek, Volker Matthias, Johan Mellqvist: Policy recommendations related to regulations, monitoring and enforcement. SCIPPER deliverable D5.5, February 2023. EU Horizon 2020 project No. 814893. <https://www.scipper-project.eu/library/>.

Smyth (2023).

Tim Smyth, et.al.: Faster, Better, Cheaper: Solutions to the Atmospheric Shipping

Emission Compliance and Attribution Conundrum. *Atmosphere* 2023, 14, 500.
<https://doi.org/10.3390/atmos14030500>.

Verbeek (2021)

~~I. Verbeek et al. 'What scaling choices are best for monitoring vessels using sensors and satellite data? A review' on 24th TAP conference, online, <https://www.tapconference.org/>. 30 March – 1 April 2021~~

2.11 JS.11. Reduction measures for GHG emissions – alternative fuels, electrification, energy use and optimization; inner-disciplinary and cross-sector studies.

Active traffic management for improved air quality and reduced climate impact

M. Norman^{1*}, M. Benyamine-Remah², J. Archer,² C. Johansson^{1,3}, M. Elmgren¹, L. Burman¹ and M. Engardt¹

¹SLB-analys, Environment and health Administration, City of Stockholm, S-104 20, Sweden

²Swedish Road Administration, Sundbyberg, S-172 90, Sweden

³ Department of Environmental Science, Stockholm University, S-106 91 Stockholm, Sweden

Introduction

The traffic manager unit measure vehicle speed limits (VSL) has been used internationally for many years, but rarely in Sweden. VSL is primarily a traffic safety measure and rarely targets air quality improvement or reductions regarding environmental and health impacts. In the autumn of 2019, the research and innovation project: "Active traffic management for improved air quality and reduced climate impact along the state road network" began. The main purpose of this project was to investigate whether traffic control in the form of variable speed limits (VSL) could reduce the impact of traffic on air quality and climate related emissions.

Study area and Method

The road section studied is located on E4/E20 between the Hallunda intersection and Fittja intersection on the outskirts of Greater Stockholm in the Botkyrka municipality, south of Stockholm, Figure 1. The E4/E20 is the major road towards Stockholm from the south. The 2.7 km stretch of motorway has a considerable flow of traffic that passes a densely populated area. The roadway has known problems with environmental quality standards for outdoor air. Accessibility and traffic safety are generally good, but some congestion occurs during rush hours. The posted speed limit before the introduction of VSL was 80 km/h.



Figure 1: The area along E4/E20 south of Stockholm where the VSL has been in use.

VSL was introduced in March 2021 on the road section in Figure 1. Two air quality monitoring stations have been measuring on both sides of the road since 2019. In addition to air quality measurements, detailed monitoring of the traffic, including vehicle counts, vehicle speed and fleet composition through license plate identification, has also been conducted. During periods with high traffic intensity the speed limit was lowered to 60 km/h. Due to some technical problems the VSL only showed 60 km/h about half of the time that the algorithm proposed that is should.

Results traffic

The average traffic and speed during weekdays during 2021 are shown in Figure 2. The average speed was ~84 km/h but varies during the day with higher speed during nighttime. The average daily traffic flow was ~100 000 vehicles per day but with significant peaks in morning and afternoon (rush hours). The major traffic flow is northwards towards Stockholm in the morning and southwards in the afternoon.

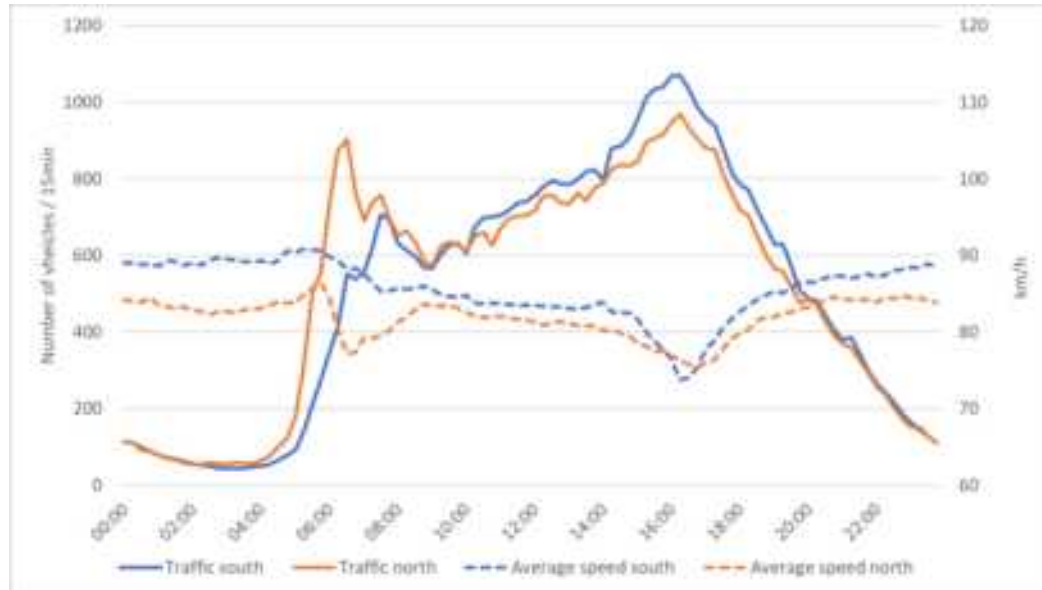


Figure 2. Average traffic flow and speed during weekdays during 2021 at the site. Data presented as 15-minute values and divided into north and south.

The detailed vehicle composition was analyzed using license plate detection (ANPR) and is shown in Figure 3. The vehicle composition was used when analyzing the emissions from HBEFA (HBEFA, 2019). As shown in Figure 3 there is almost equal fraction of petrol and diesel cars. However, the Euro classes shows that the diesel cars to a much larger extent are newer with only small fraction of Euro 3 and older. In contrast a significant part of the petrol cars were Euro 3 and older. The major part of the heavy trucks were Euro 6 vehicles.

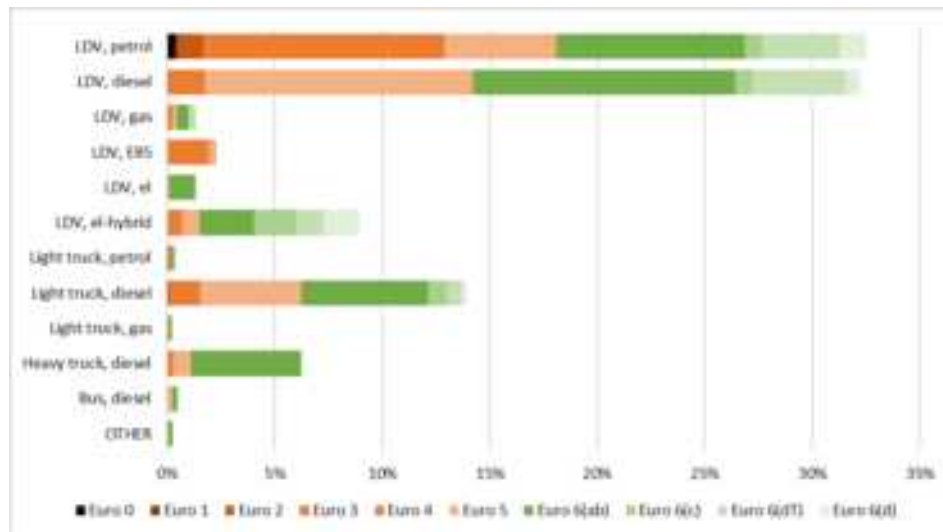


Figure 3. The average vehicle composition at the site.

The effect from VSL was studied from March until Dec 2021. In Figure 4 is the occurrence of hours with displayed 60 km/h shown. Since the VSL was based on traffic density it is not surprising that most of the VSL with 60 km/h are found for northbound traffic in the morning and southbound traffic in the afternoon. In total

were ~2.5 million vehicle passages affected by the VSL 60 km/h, which corresponds to 6.8% of the vehicle passages during March to December 2021.

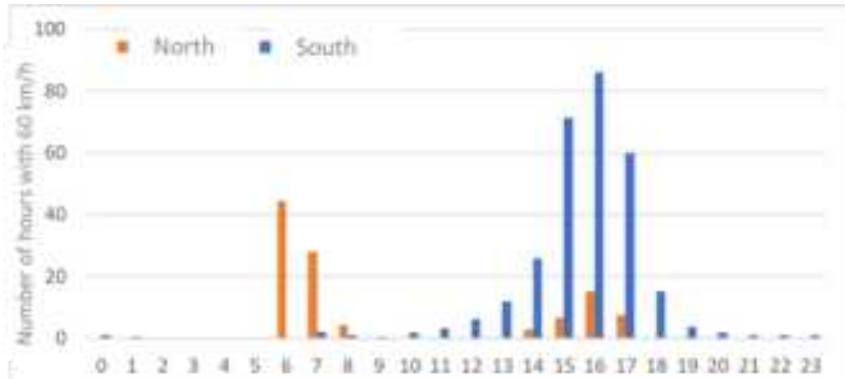


Figure 4. Number of hours when the VSL has shown 60 km/h. Data dived into north/south and time during the day.

The effect of the VSL60-activations on average speed were determined by comparing similar periods of dense traffic where VSL60 was activated and where it should have been activated but was missed due to technical problems. From this comparison it could be determined that average speed was reduced by approximately 6.0 km/h for the northbound and 5.5 km/h for the southbound direction, respectively. The low level of speed-compliance reflects, an unwillingness on the part of drivers to adapt their speed to the speed limit and as well as lack of speed-enforcement measures.

Results air quality

High levels of air pollutant occurred at the two measuring sites next to the road. The number of hours with NO₂ concentration >60 µg/m³ are shown in Figure 5 and number of hours with PM10 50 µg/m³ in Figure 6. The levels of 60 µg/m³ NO₂ and 50 µg/m³ PM10 were chosen because of those are the daily average air quality limit values in Sweden.

High concentration of NO₂ mainly occurs during morning and evening traffic peaks (compare with Figure 2). But high NO₂ concentration are more likely to occur in the late evening although the traffic numbers then are low. This is caused by the more stable meteorological conditions and lower windspeed in evenings and during nights in comparison to daytime.

The PM10 depicts a different feature with high concentrations mostly occurring in the afternoon and early evening. High PM10 in Scandinavia and Sweden are mainly caused by road dust from studded tyres wear on the road and winter road maintenance as salt and sand (Norman et al., 2016). The road dust is only emitted into the air when the road surface is dry, while it stays on the road surface during wet conditions. Dry road surface more commonly occurs during the afternoon causing the- high PM10 concentrations mostly in the afternoon.

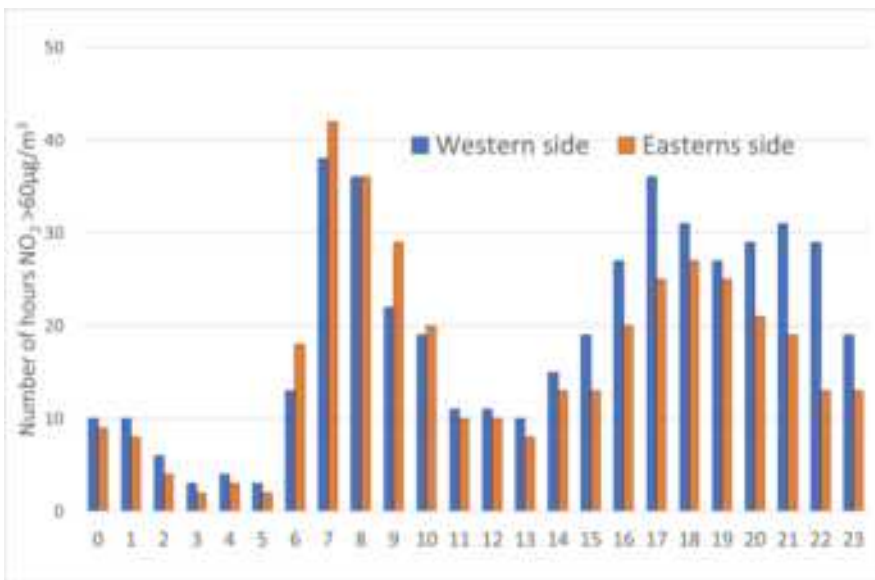


Figure 5. Number of hours when the NO₂ >60 µg/m³. Data presented from both western and eastern measurement station.

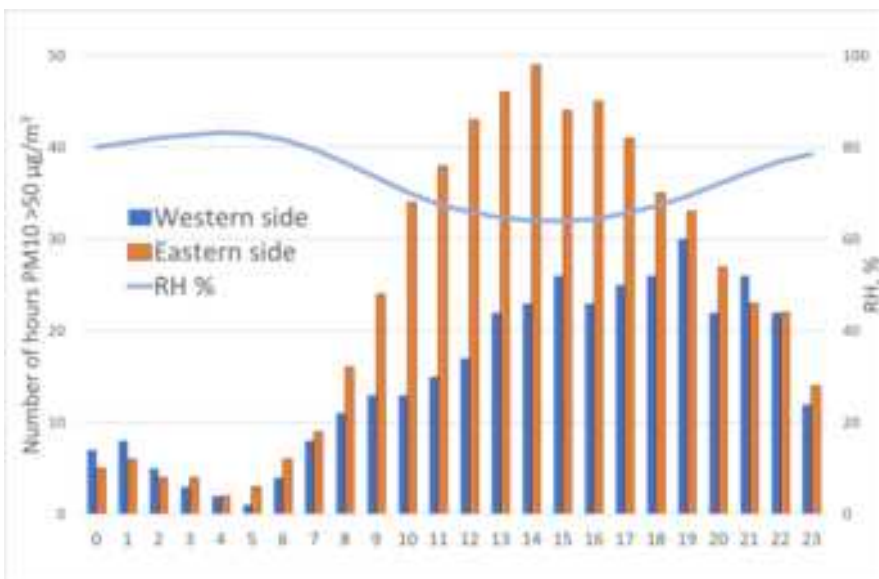


Figure 6. Number of hours when the PM10 >50 µg/m³. Data presented from both western and eastern measurement station.

Effect from Variable Speed Limits, VSL

The effect from the VSL on emissions of CO₂, NOx and PM10 as well as concentrations of NO₂ and PM10 were calculated and analyzed using three different scenarios for the period of March to December 2021, Table 1

- VSL observed: This scenario corresponds to the reality. In the analysis were the speed reduced with 6 km/h during the periods when the VSL displayed 60 km/h.
- VSL full function: As for "VSL observed" but in addition were the speed reduced also with 6 km/h also during those periods when the VSL system should have displayed 60 km/h, but did not due to technical problems.
- VSL controlled track: The same periods as for "VSL full function" but the speed was lowered to 60km/h during active VSL, meaning that all vehicles followed the speed regulation.

The reduced emissions of NO_x and CO₂ with VSL was calculated using detailed vehicle composition in combination with HBEFA 4.1 (HBEFA 2019). The reduced emissions and concentrations for PM10 were calculated using the NORTRIP model (Denby et al., 2013). The effect on air quality was calculated using the same scenarios and applied to the observed air quality at the monitoring sites.

The reduced emissions with the VSL scenarios are presented in Table 1. The VSL observed caused a reduction in CO₂ emissions with 24 ton, which corresponds to ~59 000 fewer vehicle passages during March – December 2021 or ~200 fewer per day. With fully active VSL and all vehicles driving 60 km/h the CO₂ emission reduction would be 113 tons which equal 280 000 less vehicle passages or ~940 per day.

Table 1: The three scenarios used for the analysis and the reduced amount of CO₂- NO_x and PM10-emissions due to different scenarios of the VSL for Mar – Dec 2021.

	VSL obs.	VSL full realistic	VSL theoretical max
Speed (km/h)	-6*	-6*	60
Vehicle passages affected (millions)	2.5	3.5	3.5
Reduced CO ₂ emission (tons)	24	38	113
Reduced NO _x emissions (kg)	42	66	227
Reduced PM10 emissions (kg)	90	129	191

The positive effect on air quality was limited, Figure 7. During the period March – December 2021 was 272 and 280 hours with NO₂ concentration above 60 µg/m³ (Swedish Environmental Goals) observed at the eastern and western site respectively. Only two less hours with NO₂-concentrations >60 µg/m³ was calculated with the observed VSL. With the maximal theoretical scenario up to 10 less hours with maximum effect scenario. For PM10 daily average above 30 µg/m³ (Swedish environmental goals) was there no fewer days for any of the scenarios compared to the measured.

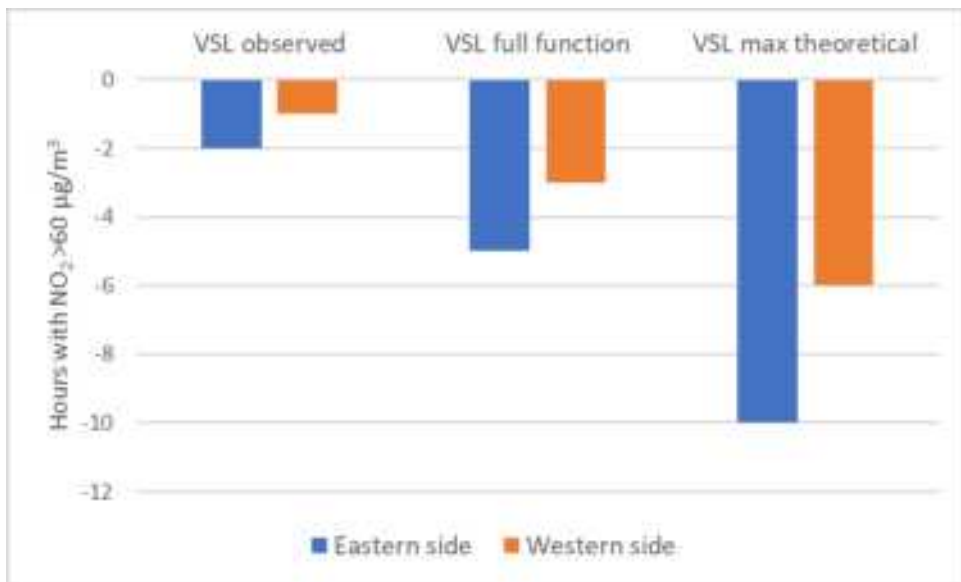


Figure 7: Change in number of hours with $\text{NO}_2 > 60 \mu\text{g}/\text{m}^3$ for the different scenarios of VSL Mar – Dec 2021.

Before VSL was introduced additional scenarios were used to calculate the potential effect of VSL if it was active also during periods with high concentrations of pollutants and not only dense traffic. When comparing the occasions with VSL based on traffic (Figure 4) with the occasions of high NO_2 and PM10 concentrations (Figure 5 and Figure 6) there is some discrepancy, especially for PM10 . Calculations for 2019 and 2020 showed that the number of occasions with high PM10 - and NO_2 concentrations would be significantly reduced if VSL (60 km/h) was triggered at times with high concentrations of PM10 and/or NO_2 , (full compliance of speed limits). VSL based on air quality would lower the risk of exceeding the EU guidelines along the road. The calculations showed that using VSL based on air quality and dense traffic would be much more effective than using VSL only for dense traffic.

Some conclusions

- VSL has the potential in improving air quality along major road and to reduce the CO_2 emissions.
- The actual speed reduction was low (~6km/h) although the signed speed was reduced from 80 to 60 km/h.
- In total 2.5 million vehicle passages were affected by the VSL with 60 km/h during the test period March – Dec 2021. This corresponds to 6.8 % of all vehicle passages at the test site.
- The effect on air quality would improve significantly if the VSL showed lower speed also at times with bad air quality and not only during dense traffic situations

Acknowledgements

This project was funded by the Swedish Transport Administration.

References

HBEFA 4.1., Handbook for Emission Factors 4.1, 2019, www.hbefa.net

Denby B.R., Sundvor I., Johansson C., Pirjola L., Ketzel M., Norman M., Kupiainen K., Gustafsson M., Blomqvist G., Omstedt G. (2013). A coupled road dust and surface moisture model to predict non-exhaust road traffic induced particle emissions (NORTrip). Part 1: Road dust loading and suspension modelling <http://dx.doi.org/10.1016/j.atmosenv.2013.04.069>

Norman M., Sundvor I., Denby B.R., Johansson C., Gustafsson M., Blomqvist G., Janhäll S. (2016). Modelling road dust emission abatement measures using the NORTrip model: Vehicle speed and studded tyre reduction. <http://dx.doi.org/10.1016/j.atmosenv.2016.03.035>

2.12 JS.12. Scenarios and policy options for sustainable transport

Solid Oxide Fuel Cells for Reduced Health and Climate Impact of Ship Emissions – Emission Analysis

J. Pagels¹, A. Oudin², R. Rittner², S. Ansar³, V. Malmborg¹, J. Rex¹ and A. Kristensson⁴

1. Department of Design Sciences, Ergonomics & Aerosol Technology, Lund University, LTH, Lund, SE 22100 Sweden

2. Department of Laboratory Medicine, Lund University, Lund, SE 22100 Sweden

3. Department of Clinical Sciences, Lund University, Lund, SE 22100 Sweden

4. Department of Physics, Lund University, Lund, SE 22100 Sweden

Introduction

Air pollution from the shipping sector is responsible for substantial adverse health impact. Brandt et al. (2013) estimated that the contribution from international ship traffic was 7 % of the total health-related economical external costs in Northern Europe in the year 2000, and increase to 12 % for the year 2020. PM emissions from ships are estimated to be responsible for around 600 000 premature deaths annually from cardiopulmonary disease and lung cancer in coastal areas of Europe, East Asia and South Asia (Maragkogianni et al. 2016). Viana et al. (2020), furthermore also showed substantial health impacts by air pollution from shipping, and also showed clearly that the more stringent global sulphur reduction IMO standards from 2020 would reduce the number of premature deaths attributable to PM2.5 by 15%. Shipping is contributing to around 3% of the global anthropogenic CO₂ emissions. Shipping also emits several other climate warming pollutants such as Methane and Black Carbon (Aakko-Saksa et al. 2023). The greenhouse gas (GHG) strategy by the International Maritime Organisation (IMO) aims to cut the shipping sector's carbon intensity by up to 40% by 2030 and 70% by 2050 compared to 2008.

There are several new technologies developed to reduce both the climate and health impact of shipping. This includes the use of new cleaner fuels in ICEs and the introduction of exhaust aftertreatment systems as has previously been done for road transport (Aakko-Saksa et al. 2023). The H2020-project NAUTILUS (Nautical Integrated Hybrid Energy System for Long-haul Cruise Ships) evaluates solid oxide fuel cells (SOFCs) operating in hybrid with batteries as future clean propulsion technology for passenger shipping. The new technology will be implemented using a modular strategy to gradually replace existing Internal Combustion Engine (ICE) generators. The short-term goal of the NAUTILUS project is to reach IMO targets for 2030

(10% increase in energy efficiency, 40% CO₂ reduction by using LNG as a fuel) and to reduce Nitrogen Dioxides (NO_x), PM (particulate matter) and Sulphur Dioxide (SO₂) by >99% compared to a baseline case using HFO with no exhaust after treatment. Due to their high operating temperature SOFCs offer higher fuel flexibility compared to other fuel cell technologies. This opens up possibilities for use of low carbon intensity or carbon neutral fuels (van Veldhuizen et al. 2023a, 2023b). A Techno-economic analysis for a range of fuels used in the system have been carried out (Pina et al. 2023). Although the potential to reduce air pollutants such as PM, NO_x, SO_x and BC are high for the SOFC concept, there is a lack of direct experimental data to fully confirm this. A recent study of a biogas fueled SOFC plant for heat generation showed experimental evidence of low emissions (Gandiglio et al. 2020). For some pollutants the emissions were below the detection limit of the applied emission analysers. This highlights the need for more sensitive methods for example from ambient monitoring to quantify the emissions.

Here we report on the progress of the emission analysis task of the project where the following activities are carried out: Literature survey of ship emissions based on ambient, on-board and laboratory investigations and of the toxicity of transport emissions including shipping. A measurement strategy is currently designed and tested to allow detailed emission measurements of the SOFC - post combustor system. Direct emission measurements will later in the project be carried out at a demonstrator unit (60 kW_e) that will be constructed in the project. PM_{2.5}, NO_x, Black Carbon, SO₂ and select emerging pollutants will be measured. Combining baseline emissions from the literature survey with measurements of SOFC emissions will allow quantification of the emission reduction potential of the new technology for the key pollutants.

Finally, a health impact assessment will be carried out for different scenarios of implementation of the new technology.

Literature Survey: Emissions and Exposure to Air Pollution from Shipping

The emission survey within Nautilus serves the purpose to evaluate the emission reduction potential of SOFC system. The survey is based on laboratory, on-board (L/O) and ambient studies (A). Many of these papers can be found in the reviews by Aako-Saksa and Lehtoranta (2019), Di Natale and Caratonuto (2015), Aako-Saksa et al. (2023) and Grigoriadis et al. (2021). The L/O studies allow studies of individual ship engines and consequences of engine load, fuel switches and exhaust aftertreatment devices on measured emissions expressed as grams emitted pollutants per kg fuel consumption – emission factor (EF). Ambient studies normally have the benefit of representing an entire fleet sailing along a ship route, but can also be calculated for individual ships. Mainly data on gaseous pollutants SO₂, NO_x, formaldehyde, ammonia, methane, CO, hydrocarbons, particle number (PN), particulate matter (PM) and BC are available. For the L/O studies, quite extensive data is available on use of HFO, MDO/MGO and LNG fuels and some exhaust aftertreatment systems, while LNG data is not yet available for ambient studies.

With the introduction of SOFC technology, a few preliminary studies in the literature show that there is a large reduction potential for the emission factors shown for many pollutants, for example SO_x, NO_x, and PM, being several orders of magnitude lower than even ships sailing on LNG fuel.

Currently a number of emission scenarios are being finalised that will be used for the Life-Cycle Assessment carried out in the project to deduce the total environmental benefit of the SOFC technology. Air pollutant exposure analysis is also underway in Nautilus. The exposure takes place in harbours or at coastal areas downwind of shipping routes. It can be estimated from dispersion air pollution modelling or from measured exposure plus source/receptor models or quantification of the impact of individually measured ship plumes. The modelled exposure is usually overestimated compared to measured, and the reason for this is at present unclear (Karl et al., 2019). The exposure analysis will be used as input to the health impact assessment task in the project.

Literature Survey: Toxicity of PM Air Pollution from Transport Sources

An integrative systematic review of the literature was performed. Literature between 2018-2023 that included the toxic and cellular mechanism behind the effects of particulate matter emissions from transportation was collected from the databases Embase, PubMed and Web of Science. Toxic effects of PM emission include oxidative damage, cytotoxicity, genotoxicity and mutagenicity. The particles toxicity depends on their chemical composition and size which is dependent on the emission sources. Smaller size particles are considered of particular importance for health since they exert greater toxicity due to their large reactive surface area and the ability to be inhaled deeply in the alveoli of the lungs and translocate into vital organs. Airways are lined with an epithelial cell layer, which constitutes the barrier between the environment and the organism. Pollution penetrating through these barriers reaches the bloodstream and can be transported throughout the body. Endothelial cells line the blood vessels and constitute a second barrier between the circulation and the organs. Alterations in barrier function are early predictors of disease including diseases associated with PM air pollution exposure such as respiratory, cardiovascular, (thrombosis, ischemic risk, atherosclerosis, and hypertension), neurodegenerative, metabolic diseases and cancer. High and long-term exposure to PM2.5 and ultrafine particles have been correlated with endothelial and epithelial dysfunction. The reviewed studies demonstrate that PM exposure induces oxidative stress leading to gene transcription and activation of a stress response, including the release of pro-inflammatory cytokines, chemokines, adhesion molecules, and vasoconstrictors causing endothelial and epithelial dysfunction and impairment of the barrier. This may explain the widespread effects of these particles around the body cause. Taken together, the reviewed studies demonstrate that PM exposure leads to barrier dysfunction and altered homeostasis, which in turn contribute to the increased risk of respiratory, cardiovascular, neurodegenerative, and metabolic diseases as well as cancer. As the toxicity depends on emission sources studies have demonstrated that emission from shipping is more toxic compared to vehicle transportation. As of June 2023, more than 40% of cruise ship orders are LNG powered globally. There are currently also rapid investments into Methanol and Ammonia as ship-fuels. However, the effect on health and the underlying pathophysiological mechanisms that emissions from these new fuels may cause are still unknown.

NAUTILUS SOFC Technology

The Nautilus proof-of-concept utilises a 32 kWe SOFC module, coupled with a lithium-ion battery to allow for high power transients that are characteristic for ship operation. It represents a conceptional genset that is

evaluated to gradually replace conventional ICE gensets on cruise ships, considering its transient behaviour and scalability. A simplified schematic of the SOFC system is given in Figure 1, using methane as fuel. The main components of relevance for pollutant formation and removal are the following: 1) A pre-reformer (steam reformer) with the aim to partly convert the natural gas fuel to hydrogen. 2) A large stack module that consists of several SOFC stack towers and 3) A post-combustor system. Other auxiliary components, referred to as "balance of plant" are used for temperature and flow control of the different components. A fraction of the anode and/or cathode off-gas leaving the LSM/SOFC unit may be recirculated. The anode off-gas from the SOFC consists of water vapor, unreacted hydrogen, carbon monoxide, carbon dioxide and traces of other gases. The role of the post-combustor unit is to oxidise carbon monoxide, non-reacted hydrogen and other trace pollutants to enable low emissions from the system. As in any combustion process new pollutants may form, for example trace levels of NOx.

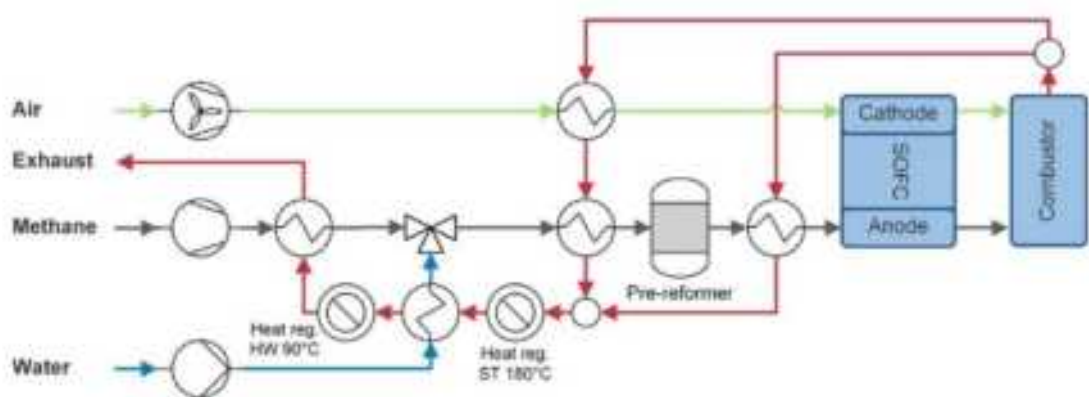


Figure 1. Schematic of SOFC system using methane as fuel. Reproduced from van Veldhuizen et al. 2023a under CC BY 4.0.

Emission Measurement Strategy for SOFC – Post-combustor Systems

A set-up has been designed with the purpose to analyse the emissions from SOFC – postcombustor systems (Figure 2). The system includes the following measurement techniques, an FTIR Spectrometer using a 180 C heated sampling head for analysis of a large number of organic and inorganic gases (model atmosFIRt, Protea Ltd.). A separate sample was diluted 1:10 using an ejector diluter followed by a set of instruments with high sensitivity commonly used for ambient monitoring. This includes a chemiluminescence analyser for NO and NO₂ (model CLD 700, Eco Physics), an aethalometer for Black Carbon emissions (AE33, Magee Sci.) and a condensation particle counter for particle number emissions (CPC 3775, TSI Inc.).

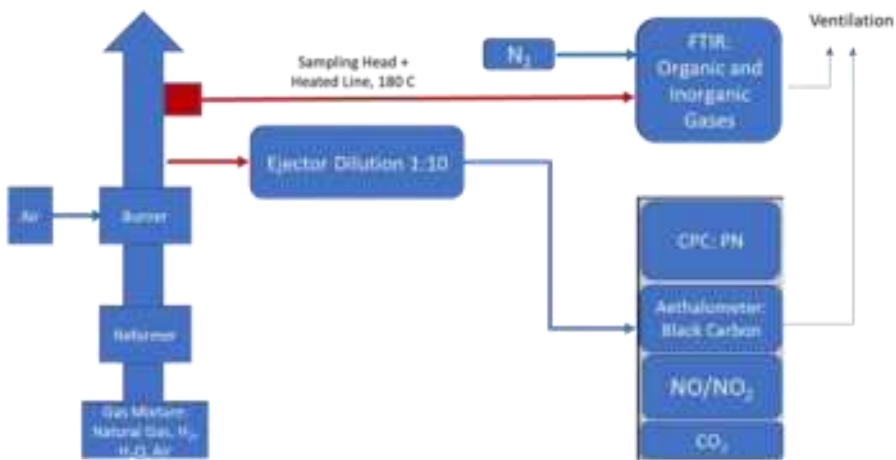


Figure 2. Set-up to analyse emissions (right) connected to the simplified reformer-burner system (left) to generate SOFClike emissions.

A first experimental test of the suitability of the sampling and emission characterisation techniques for expected SOFC emissions was recently carried out at the SolydEra site in Switzerland. Gas compositions of relevance for measurements downstream the burner in SOFC systems were generated using a synthetic gas-mixture that was passed through a reformer before being fed directly into the postcombustor/burner. The SOFC was in this first test bypassed because of practical limitations. A number of operating points were investigated by varying the fuel (natural gas) flow rate, the steam flow rate (and thereby the steam to carbon ratio) and the pre-reforming ratio. The aim was to investigate the suitability of the emission measurement set-up for SOFC-like conditions. Another aim was as to investigate the limits of the post-combustor in terms of formation of pollutants or break-through of fuel. The data are currently being analysed.

Health Impact Assessment of Air Pollution from Shipping - Preliminary Results

In the Nautilus project, we will estimate premature deaths attributable to ship emissions in the study areas Skåne, Southern Sweden, and the Hamburg urban area. We present specific case studies to illustrate the local effects of shipping emissions in selected areas of Europe. In Skåne, despite an overall decrease in particle and soot/BC emissions from shipping between 2000 and 2011, certain port cities, like Trelleborg, still experience significant air pollution from shipping activities. Similarly, in the Hamburg urban area, shipping contributes a substantial percentage to NO₂ and PM2.5 exposure. We employ the concept of an air pollution health impact assessment (HIA), which estimates mortality rates and disease incidence resulting from changes in air pollution concentrations. The traditional assumption is that concentration-response functions for PM2.5 are the same for long-range transported and locally produced particles but recent research indicates a potentially steeper concentration-response curve for locally emitted PM2.5. This distinction is particularly relevant in countries like Sweden, where in-transported PM2.5 plays a significant role.

Our preliminary results show that when looking at the study area Skåne, Southern Sweden, we found that fine particulate air pollution (PM2.5) in total was estimated to be a contributing cause of 699 deaths annually. Of these, 7 (1%) were estimated to come from emissions from shipping. In comparison, the corresponding numbers from road traffic was 63 (9%), for small-scale residential heating was 49 (7%), and for PM2.5 from long-range transport was 580 (83%). Overall, the preliminary results emphasize the urgent need for international regulation of shipping emissions due to their substantial contribution to climate change, air pollution, and associated health burdens. The results furthermore provide insights into the specific impacts of shipping emissions in European coastal regions, highlighting the importance of addressing this issue at both global and local levels.

Outlook

In 2024 direct emission measurements will be carried out at a 60 kW demonstrator unit that is currently being constructed in the project. We aim to add additional emission instrumentation for this part of the project, including size distributions of ultrafine particles. Using the baseline emissions and different scenarios from the literature review the emission reduction potential of the new technology will be quantified for the key pollutants.

Future health impact assessment analysis will focus on the port cities of Trelleborg and Hamburg urban area. We will furthermore investigate different assumptions regarding the concentration-response curve. We aim to investigate the health benefit of different scenarios of introduction of the novel SOFC technology. The reduction of exposure will be based on the direct emission measurements at the demonstrator.

Acknowledgements: We acknowledge funding from EU (H2020-NAUTILUS, GA-861647).

Patrik Nilsson, Stefan Diethelm, Florian Waeber and Zacharie Wuillemin are acknowledged for contributing to the experimental tests using SOFC relevant gas-mixtures.

References

- Aakko-Saksa, P., and Lehtoranta, K. (2019). Ship emissions in the future: Review. VTT Technical Research Centre of Finland. VTT Research Report No. VTT-R-00335-19.
- Aakko-Saksa, P. T., Lehtoranta, K., Kuittinen, N., Järvinen, A., Jalkanen, J.-P., Johnson, K., Jung, H., Ntziachristos, L., Gagne, S., Takahashi, C., Karjalainen, P., Rönkkö, T., & Timonen, H. (2023). Reduction in greenhouse gas and other emissions from ship engines: Current trends and future options. *Progress in Energy and Combustion Science*, 94, 101055.

- Brandt, J., Silver, J. D., Christensen, J. H., Andersen, M. S., Bønløkke, J. H., Sigsgaard, T., ... & Frohn, L. M. (2013). Assessment of past, present and future health-cost externalities of air pollution in Europe and the contribution from international ship traffic using the EVA model system. *Atmospheric Chemistry and Physics*, 13(15), 7747-7764.
- Di Natale, F., & Caratonuto, C. (2015). Particulate matter in marine diesel engine exhausts: Emissions and control strategies. *Transportation Research, Part D*, 40, 166-191.
- Gandiglio, M., Lanzini, A., Santarelli, M., Acri, M., Hakala, T., & Rautanen, M. (2020). Results from an industrial size biogas-fed SOFC plant (the DEMOSOFC project). *International Journal of Hydrogen Energy*, 45(8), 5449-5464.
- Grigoriadis, A., Mamarikas, S., Ioannidis, I., Majamäki, E., Jalkanen, J. P., & Ntziachristos, L. (2021). Development of exhaust emission factors for vessels: A review and meta-analysis of available data. *Atmospheric Environment*: X, 12, 100142.
- Karl, M., Jonson, J. A., Uppstu, A., Aulinger, A., Prank, M., Sofiev, M., Jalkanen, J.-P., Johansson, L., Quante, M., & Matthias, V. (2019). Effects of ship emissions on air quality in the Baltic Sea region simulated with three different chemistry models. *Atmospheric Chemistry and Physics*, 19, 7019-7053.
- Maragkogianni, A., Papaefthimiou, S., & Zopounidis, C. (2016). Mitigating shipping emissions in European ports: Social and environmental benefits (pp. 1-9). Berlin: Springer.
- Nutilus Project: <https://nutilus-project.eu/>
- Pina, E. A., van Veldhuizen, B., & Marechal, F. (2023). A Comparative Techno-Economic Assessment of Alternative Fuels in SOFC Systems for Cruise Ships. *ECS Transactions*, 111(6), 2459.
- van Veldhuizen, B. N., van Biert, L., Amladi, A., Woudstra, T., Visser, K., & Aravind, P. V. (2023a). The effects of fuel type and cathode off-gas recirculation on combined heat and power generation of marine SOFC systems. *Energy Conversion and Management*, 276, 116498.
- van Veldhuizen, B., van Biert, L., Aravind, P. V., & Visser, K. (2023b). Solid Oxide Fuel Cells for Marine Applications. *International Journal of Energy Research*, 2023.
- Viana, M., Rizza, V., Tobías, A., Carr, E., Corbett, J., Sofiev, M., ... & Fann, N. (2020). Estimated health impacts from maritime transport in the Mediterranean region and benefits from the use of cleaner fuels. *Environment international*, 138, 105670.

2.13 SE.13. Marine processes – fate of pollution from shipping in the marine environment impact studies on ecotoxicology, eutrophication and acidification, energy pollution including underwater noise & induced mixing experimental work, modelling studies of dispersion, transport, and chemical and biological processes in marine waters.

Ecotoxicological Effects of Exhaust Gas Cleaning System (EGCS) Discharge Water on Marine Copepods

M. Picone^{1*}, E. Giubilato¹, K. Magnusson², M. Granberg², A. Volpi Ghirardini¹, and A. Marcomini¹

¹ Department of Environmental Sciences, Informatics, and Statistics (La Sies) Research University Center - SIES, Italy
marco.picone@unive.it

² Swedish Environmental Research Institute (IVL), Kristineberg Marine Research Station, Kristineberg, 45178, Sweden

Introduction

Exhaust Gas Cleaning Systems (EGCS) operating in open-loop mode continuously release in marine waters acidic effluents (scrubber waters) containing metals, alkylated and non-alkylated polycyclic aromatic hydrocarbons (PAHs), other polycyclic aromatic compounds (PACs), and particulate matter (Lunde Hermansson et al. 2021). These effluents can affect the planktonic community in the receiving waters, including bacteria, algae, and invertebrates at the adult and larval stages (Ytreberg et al 2021).

Copepods dominate the zooplankton biomass in marine and estuarine environments and occupy a crucial food resource in the aquatic food webs because they graze on the phytoplankton and serve as a food reservoir for consumers of higher trophic levels (Turner, 2004). Copepods primarily graze in surface waters, exposing them to the potentially toxic effects of scrubber water since organisms in the surface waters are exposed to less diluted EGCS discharges and hence to higher concentrations of the scrubber water than, e.g., bottom-living ones. Furthermore, since the productivity of aquatic ecosystems is often highly dependent on the lower trophic levels, according to bottom-up ecosystem regulations (Irigoin et al. 2004), adverse effects towards copepods might have detrimental effects also on the whole marine and coastal ecosystem.

To assess the adverse effects of scrubber waters on copepods, we exposed laboratory-cultured specimens of the calanoid copepod *Acartia tonsa* to two different scrubber waters: 1) an artificial EGCS discharge water produced by the engine lab at the Chalmers University of Technology; 2) a real scrubber water collected on board the LEO C vessel in the Mediterranean Sea ($36^{\circ}26'21.86''N$, $17^{\circ}34'53.21''E$) on the journey from Antwerp (Belgium) to Gebse (Turkey).

Copepod culturing and toxicity tests

Copepods used for testing derived from in-house laboratory cultures maintained at the Ca' Foscari University of Venice originated from adult copepods obtained from Guernsey Sea Farms (Port Vale, Guernsey, UK). Copepods (600-800 individuals) were cultured in 2-L glass beakers using a 20% *salinaria* culture medium prepared according to ISO 16778 (ISO, 2015). The cultures were kept at $20 \pm 1^{\circ}\text{C}$, under continuous aeration, 16-h light and 8-h dark photoperiod, and were fed *ad libitum* with a mixture of *Tetraselmis suecica*, *Pavlova lutheri*, and *Tisochrysis lutea* (Picone et al. 2021). The food was administered four times per day using a timer-controlled peristaltic pump.

The toxicity tests included acute exposures, larval development tests, and long-term exposures aiming to detect ~~acute, reproduction, and offspring effects~~. All tests used the 20% *salinaria* culture medium as control and dilution water and were performed according to the CRED (Criteria for Reporting and Evaluating ecotoxicity Data) evaluation method for the reliability and relevance of toxicity data (Moermann et al. 2016).

The acute test was performed according to the ISO 14669 standard method (ISO, 1999) using adult copepods and copepodite stage V (C-V) individuals exposed for 48-h to different scrubber water dilutions, covering the range of 0.01% to 40% scrubber water. The acute test was run in 4 replicates, using a sample volume of 20 mL in 30 mL crystallising dishes. Copepod mortality was used as the endpoint.

The larval development test was performed according to the ISO 16778 standard method (ISO, 2015), modified as reported by Picone et al. (2021). Freshly released eggs from the in-house culture were exposed for 5 days to different dilutions of test solution covering the range of 0.01% to 40% scrubber water. The larval development test was run in 6 replicates, using a sample volume of 30 mL in 100 mL glass beakers. On day 2, the test solution was refreshed by adding 30 mL of scrubber water dilution. The exposure ended on day 5, when approximately 40 % of the larvae in controls should have completed the metamorphosis to the copepodite-I stage (C-I). Egg hatching, larval mortality, and the ratio of larvae that reached the C-I stage were used as endpoints.

The long-term exposure was performed according to the procedure outlined in Picone et al. (2022). The test started by adding 400–600 newly released eggs to each test solution (0.001%, 0.01%, 0.1% and 1% scrubber water) in 1L glass bottles (F_0 exposure). The bottles were then kept at $20 \pm 1^\circ\text{C}$, with a 16-h light 8-h dark photoperiod for 21 days. The food was provided thrice weekly during the renewal of test solutions. On day 13, twelve mature females were collected from each test bottle and individually placed into 15 mL glass vials filled with 10 mL of 20‰ salinity medium and 100 µL of the algae mix at 10^4 cells mL $^{-1}$. Their egg production was checked daily for three days.

In addition to the ship-derived and artificially produced scrubber water samples, ambient seawater collected in the North Adriatic Sea (NSW) was also tested to identify possible background effects in the receiving water offshore the Port of Venice.

The no-observed effect concentration (NOEC) and the lowest observed effect concentration (LOECs) were estimated using the one-way ANOVA and Tukey's HSD post hoc test ($p < 0.05$). Before ANOVA data normality and homoscedasticity were verified using the Kolmogorov-Smirnov and Levene's tests, respectively. Effective concentrations 50 % (EC $_{50}$ s) were calculated using a statistical program for continuous response developed at the Technical University of Denmark (Christensen et al., 2009) by assuming a log-normal distribution of the observed effects. All statistical analyses were performed using the IBM SPSS statistical software V.2.

Results and discussion

The ship-derived scrubber water affected adult survivals starting from the 10% treatment (5d-LOEC = 10%; EC $_{50}$ = 11%), while effects on hatching and larval survival in the larval development tests were significantly inhibited at 20% scrubber water (Picone et al., 2023). The larval development to the C-I stage was a more sensitive endpoint than hatching and mortality, being significantly inhibited at a lower concentration (5d-LOEC at 2% scrubber water) than hatching and early-life stages mortality (Picone et al., 2023). The reproduction after the long-term exposure was also affected by scrubber water, with egg production lower than the control (8.2 ± 1.4 eggs female $^{-1}$ d $^{-1}$) in all the tested concentrations. However, a U-shaped trend was observed, with the lowest egg production obtained at 0.01% scrubber water (2.9 ± 0.7 eggs female $^{-1}$ d $^{-1}$) and then an increase at 0.1% and 1% scrubber water (4.2 ± 0.9 eggs female $^{-1}$ d $^{-1}$ and 6.2 ± 1.0 eggs female $^{-1}$ d $^{-1}$, respectively).

The results obtained with the artificially produced scrubber water were similar but denoted a slightly higher toxicity of the ship-derived scrubber water than the artificial one (Table 1). The artificially produced scrubber water affected adult survival only at the 40% treatment (one-way ANOVA: $F = 2.59$, $p = 0.031$), which showed a 33% mortality compared to the control. Similarly, in the larval development test, the hatching rate was significantly inhibited at 40% scrubber water (one-way ANOVA: $F = 8.92$, $p < 0.001$). The early-life stage mortality was slightly more sensitive than hatching and adult mortality, providing a 5d-NOEC at 10% scrubber water and a 5d-EC $_{10}$ at 9% scrubber water. The larval development from egg to the C-I stage was confirmed as the more sensitive endpoint and was also significantly inhibited at the 0.01% scrubber water concentration (Table 1). Egg production in the long-term exposure was significantly lower than the control (7.1 ± 1.5 eggs female $^{-1}$ d $^{-1}$) in all the tested concentrations. However, also in this case, it showed a U-shaped trend, with a higher daily egg release at 1% scrubber water (3.1 ± 0.8 eggs female $^{-1}$ d $^{-1}$), than at 0.01% and 0.1% scrubber water (2.3 ± 0.9 eggs female $^{-1}$ d $^{-1}$ and 2.2 ± 1.5 eggs female $^{-1}$ d $^{-1}$, respectively).

Toxic effects in NSW were negligible. Adult survival in NSW was comparable to that observed in control (Tukey's HSD test: $p = 0.999$; Picone et al., 2023). Similarly, in the larval development test, no differences were observed for hatching (Tukey's HSD test: $p = 0.406$), larval survival (Tukey's HSD test: $p = 0.481$), and larval development rates (Tukey's HSD test: $p = 0.991$) between the control and NSW (Picone et al., 2023). The egg production was lower in NSW (4.0 ± 1.5 eggs female $^{-1}$ d $^{-1}$) compared to the control (7.1 ± 1.5 eggs female $^{-1}$ d $^{-1}$), but the difference was not statistically significant (Tukey's HSD test: $p = 0.219$).

Table 1: Summary of the toxicity data for the scrubber water samples. Data for the ship-derived scrubber water were obtained from Picone et al. (2023).

Toxicity test	Endpoint	Artificial scrubber water			Ship-derived scrubber water		
		NOEC	LOEC	EC ₅₀	NOEC	LOEC	EC ₅₀
Acute test	Mortality	20%	40%	n.c.	5%	10%	11%
Larval development test	Hatching	20%	40%	n.c.	10%	20%	25%
	Larval survival	10%	20%	9%	10%	20%	13%
	Larval development	<0.01%	0.01%	0.009%	1%	2%	1.5%
Long-term exposure	Egg production	<i>parameters not calculable due to the U-shaped curve. Lowest egg production at 0.01% scrubber water</i>					

Contaminant concentrations (metals and PAHs) varied relevantly between the scrubber water samples, especially V, Cr, Fe, Cu, and PAHs (Table 2), confirming that different engines and fuels have a significant impact on the chemistry of the EGCS discharge water (Teuchies et al., 2020), which in turn might affect the plankton community in different ways. Metal concentrations in the undiluted scrubber waters were generally below literature data on adverse effect levels for mortality and larval development. However, a few exceptions to this trend were observed, including Cu in the artificially produced scrubber water ($155 \mu\text{g L}^{-1}$), which concentration was higher than the 48h-LC₂₀ ($111 \mu\text{g L}^{-1}$) and the 5d-NOEC for the larval development ratio ($150 \mu\text{g L}^{-1}$). Thus, the toxicity of both scrubber waters was likely due to the synergistic effects of the chemical mixture and physicochemical properties of the scrubber water.

The different effects exerted by artificially produced and ship-derived scrubber water on *A. tonsa* in the acute and larval development test are probably due to the different chemical compositions of the two samples, with ship-derived scrubber water being more enriched in PAHs and artificially produced one in metals. In particular, both trace metals and PAH are known to affect different traits in copepods, which may lead to retarded development, both through increasing costs for detoxification (Han et al., 2014; Lee et al. 2008) and limiting feeding and assimilation (Saiz et al., 2009; Xu et al., 2001).

Different hypotheses were formulated about reduced egg production after exposure to low concentrations of scrubber water, including impairment of gonad development and maturation and oxidative stress. Indeed, contaminants in the scrubber water might have damaged the tissues of the gonads, impaired their maturation, or disrupted the oogenesis (Hook and Fisher 2001; Jensen et al., 2008). Similarly, reactive oxygen species generated by exposure to contaminants might have damaged the gonadal tissues and increased the costs for antioxidant defences, including antioxidant enzyme synthesis (Han et al., 2014).

Due to the complex mixture of chemicals and particles in scrubber water samples, identifying the potential toxicity pathways is very complex. Anyhow, since tests with single substances evidenced a significant and positive correlation between egg production and feeding (Figure 1; Picone et al., unpublished data), we hypothesised that disruption of feeding might be at least one explanation for the observed effects. The mechanisms underlying the inhibition of feeding need to be further studied.

Table 2: Summary of the chemical analyses in the undiluted scrubber water and NSW samples. Data for the ship-derived scrubber water and NSW were obtained from Picone et al. (2023).

Contaminant	Unit	Analysed sample		
		Artificially produced scrubber water	Ship-derived scrubber water	NSW
V	$\mu\text{g L}^{-1}$	1.40	348.28	0.73
Cr	$\mu\text{g L}^{-1}$	63.00	7.50	0.16
Mn	$\mu\text{g L}^{-1}$	12.0	3.1	2.8
Fe	$\mu\text{g L}^{-1}$	611	109	4
Co	$\mu\text{g L}^{-1}$	1.400	0.474	0.026
Ni	$\mu\text{g L}^{-1}$	74.0	99.46	0.35
Cu	$\mu\text{g L}^{-1}$	55.0	5.3	4.8
Zn	$\mu\text{g L}^{-1}$	66	49	49
As	$\mu\text{g L}^{-1}$	1.70	2.02	0.94
Cd	$\mu\text{g L}^{-1}$	0.057	0.032	0.007
Hg	$\mu\text{g L}^{-1}$	0.0004	0.0018	0.0003
Pb	$\mu\text{g L}^{-1}$	1.30	0.35	0.65
U	$\mu\text{g L}^{-1}$	3.3	6.9	1.7
PAHs	ng L^{-1}	1,440	15,400	38

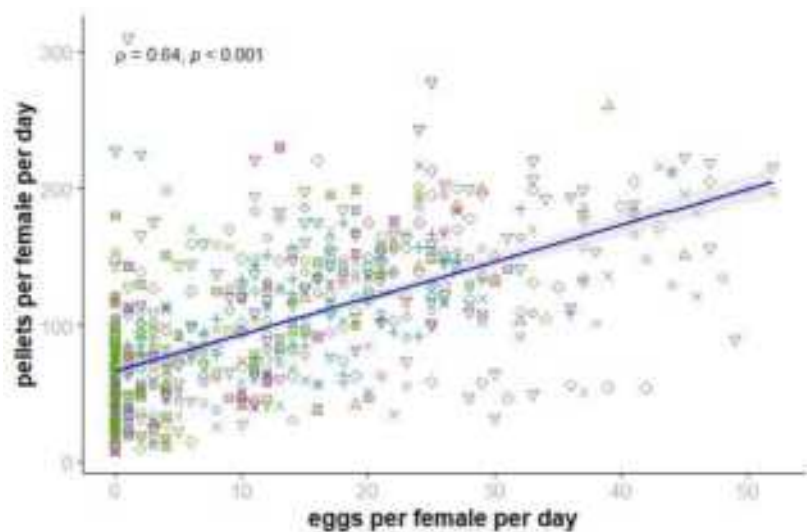


Figure 1: Scatterplot showing the relation between reproduction (using egg production as a proxy) and feeding (using pellet production as a proxy) in testing organic chemicals with *A. tonsa*. Colours identify different test substances; shapes indicate different test concentrations. The grey area identifies the 95% confidence limits for the regression line.

Conclusions

The scrubbing process generates acidic effluents characterized by high concentrations of metals (V, Ni, Cr, Cu, and Fe in particular), PAHs, alkylated PAHs, and possibly other contaminants not measured here, with the potential to exert adverse effects on the copepod assemblage of the receiving water.

The data highlight that exposure to scrubber water significantly affected *A. tonsa* at low concentrations, mainly by reducing reproductive success and retarding larval development. These adverse effects may have detrimental consequences at the population level with possible impacts at higher levels of the aquatic food webs. The results of this work stress the relevance of long-term exposure to comprehensively assess the impact of scrubber water on the marine ecosystem and, in general, contribute to the evaluation of new technologies for emission control in maritime shipping. Nevertheless, for many contaminants of concern in scrubber water samples (i.e., V and alkylated PAHs), there is a need to increase the dataset of adverse effects levels for individual chemicals since such information is not available for many relevant sublethal endpoints, including larval development and egg production.

Acknowledgements

This work has received funding from the European Union's Horizon 2020 research and innovation program under Grant Agreement No 874990 (EMERGE project). The authors are deeply grateful to Leonidas Ntziachristos (Aristotle University of Thessaloniki, Greece), Andreas Gondikas (Creative Nano, Greece), Jana Moldanova (IVL, Sweden) and the whole team planning and allowing the realisation of the field campaign on the Leo C and to Erik Ytreberg, Ida-Maja Hassellöv, Kent Salo for providing the artificial scrubber water using the engine lab at the Chalmers University of Technology. Without their contribution, it would not have been possible to have any sample of scrubber water for the testing and evaluation of effects. The authors are also grateful to Anna Lunde Hermansson and all people that make feasible the on-board sampling of scrubber water, the storage of the samples, and finally their delivery in Venice, and to Mira Petrovic, Elisa Garcia, and Meritxell Gross for managing and analysing such an amount of samples during the Project. The authors also thank all partners in Task 2.3 of the EMERGE Project for the proficient discussions concerning the test species and methods used in the other project case studies.

References

- Barata C., Calbet A., Saiz E., Ortiz L., Bayona J.M. (2005). Predicting single and mixture toxicity of petrogenic polycyclic aromatic hydrocarbons to the copepod *Oithona davisae*. *Environ Toxicol Chem*, 24, 2992–2999.
- Christensen E.R., Kusk K.O., Nyholm N. (2009). Dose-response regressions for algal growth and similar continuous endpoints: Calculation of effective concentrations, *Environ Toxicol Chem*, 28, 826–835.
- Han J., Won E.J., Hwang D.S., Shin K.H., Lee Y.S., Leung K.M.Y., Lee S.J., Lee J.S. (2014). Crude oil exposure results in oxidative stress-mediated dysfunctional development and reproduction in the copepod *Tigriopus japonicus* and modulates expression of cytochrome P450 (CYP) genes, *Aquat Toxicol*, 152, 308–317.
- Hook S.E., Fisher N.S. (2001). Reproductive toxicity of metals in calanoid copepods, *Mar Biol*, 138, 1131–1140.
- Irigoién X., Hulsman J., Harris R.P., (2004). Global biodiversity patterns of marine phytoplankton and zooplankton, *Nat*, 429, 863–867.
- ISO (1999). Water Quality — Determination of acute lethal toxicity to marine copepods (Copepoda, Crustacea). ISO 14669:1999.
- ISO (2015). Water Quality — Calanoid Copepod Early-life Stage Test with *Acartia tonsa*. ISO 16778:2015.
- Jensen M.H., Nielsen T.G., Dahllöf I. (2008). Effects of pyrene on grazing and reproduction of *Calanus finmarchicus* and *Calanus glacialis* from Disko Bay, West Greenland, *Aquat Toxicol*, 87, 99–107.
- Lee K.W., Raisuddin S., Rhee J.S., Hwang D.S., Yu I.T., Lee Y.M., Park H.G., Lee J.S. (2008). Expression of glutathione S-transferase (GST) genes in the marine copepod *Tigriopus japonicus* exposed to trace metals, *Aquat Toxicol*, 89, 158–166.
- Lunde Hermansson A., Hassellöv I.-M., Moldanova J., Ytreberg E. (2021). Comparing emissions of polyaromatic hydrocarbons and metals from marine fuels and scrubbers, *Transp Res Part D Transp Environ*, 97, 102912.
- Moermond C.T.A., Kase R., Korkaric M., Ågerstrand M. (2016). CRED: Criteria for reporting and evaluating ecotoxicity data, *Environ Toxicol Chem*, 35, 1297–1309.

Picone M., Distefano G.G., Marchetto D., Russo M., Vecchiato M., Gambaro A., Barbante C., Volpi Ghirardini A. (2021). Fragrance materials (FMs) affect the larval development of the copepod *Acartia tonsa*: An emerging issue for marine ecosystems, *Ecotoxicol Environ Saf*, 215, 112146.

Picone M., Distefano G.G., Marchetto D., Russo M., Baccichet M., Brusò L., Zangrando R., Gambaro A., Volpi Ghirardini A. (2022). Long-term effects of neonicotinoids on reproduction and offspring development in the copepod *Acartia tonsa*, *Mar Environ Res*, 181, 105761.

Picone M., Russo M., Distefano G.G., Baccichet M., Marchetto D., Volpi Ghirardini A., Lunde Hermansson A., Petrovic M., Gros M., Garcia E., Giubilato E., Calgaro L., Magnusson K., Granberg M., Marcomini A. (2023). Impacts of exhaust gas cleaning systems (EGCS) discharge waters on planktonic biological indicators, *Mar Pollut Bull*, 190, 114846.

Saiz E., Movilla J., Yebra L., Barata C., Calbet A. (2009). Lethal and sublethal effects of naphthalene and 1,2-dimethylnaphthalene on naupliar and adult stages of the marine cyclopoid copepod *Oithona davisae*, *Environ Pollut*, 157, 1219–1226.

Teuchies J., Cox T.J.S., Van Itterbeeck K., Meysman F.J.R., Blust R. (2020). The impact of scrubber discharge on the water quality in estuaries and ports, *Environ Sci Eur*, 32, 1–11.

Turner J. (2004). The importance of small planktonic copepods and their roles in pelagic marine food webs, *Zool Stud*, 43, 255–266.

Xu Y., Wang W.X., Hsieh D.P.H. (2001). Influences of metal concentration in phytoplankton and seawater on metal assimilation and elimination in marine copepods, *Environ Toxicol Chem*, 20, 1067–1077.

Ytreberg E., Karlberg M., Hassellöv I-M., Hedblom M., Nylund A.T., Salo K., Imber, H., Turner D., Tripp L., Yong J., Wulff, A. (2021). Effects of seawater scrubbing on a microplanktonic community during a summer-bloom in the Baltic Sea, *Environ Pollut*, 291, 118251.

2.14 SE.14. Holistic assessment of shipping impacts on the environment, shipping in the marine spatial planning.

Financial incentives for ship underwater noise mitigation

A. T. Johansson^{*1}, S. Sköld², Carl Andersson¹, Cecilia Andersson¹, and H. Winnes²

¹ IVL Swedish Environmental Research Institute, Gothenburg, Sweden. torbjorn.johansson@ivl.se

² Swedish Maritime Administration, Norrköping, Sweden.

Introduction

When a ship arrives at a port, the ship owner is typically charged a port fee. In Sweden and Finland, ship owners are also levied with fairway dues. In Sweden, these dues are payable to the Swedish Maritime Administration. The dues are differentiated based on the ship's environmental performance which provides a financial incentive for ship owners to improve their environmental performance. Ports are free to structure their fees as they see fit and may choose to implement financial incentives for improved environmental performance. Port and fairway dues can be based on ship environmental indexes such as the Clean Shipping Index (CSI) or the Environmental Shipping Index (ESI). Here, we consider how ship underwater noise could be included in the Clean Shipping Index.

The function of the Clean Shipping Index

Ship owners who have registered and verified the ship's environmental performance within the Clean Shipping Index (CSI) system are eligible for a rebate on the Swedish national fairway dues. In the beginning of 2023, Clean Shipping Index evaluates a ship's environmental performance in categories (Clean Shipping Index, 2022). These are

- Carbon dioxide emissions
- Nitrous oxides emissions
- Sulphur oxides and particulate matter emissions
- Use of chemicals
- Water and waste management

CSI scores the environmental performance on a scale from 0 to 150. Each category is assigned a maximum of 30 points (Figure 1). A ship owner wishing to certify a ship answers a questionnaire to determine the environmental performance. The CSI is structured in such a way that emission measurements are not required, placing emphasis on the low financial effort required of the ship owner to obtain the certification. However, a validation by a third party is sometimes required to obtain specific economic incentives, e.g., by the Swedish Maritime Administration.

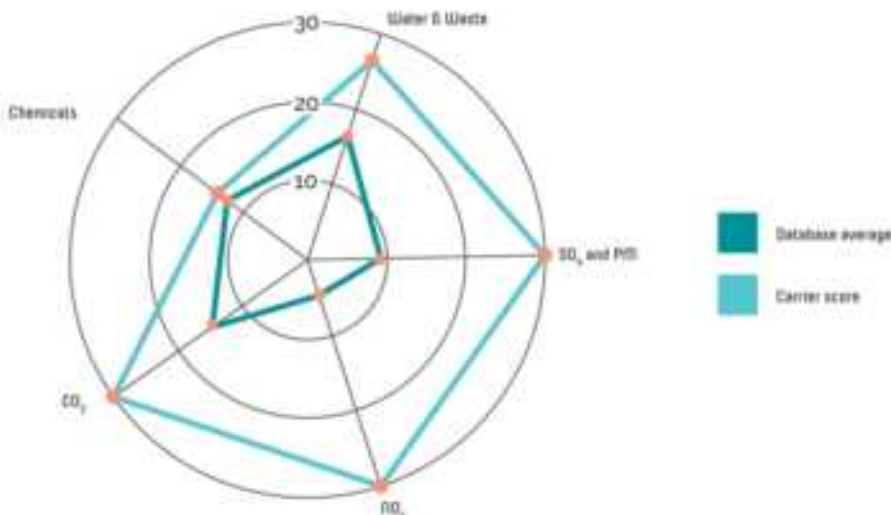


Figure 1: Category scoring by the Clean Shipping Index.

Introducing underwater noise into the Clean Shipping Index

Introducing an underwater noise category in the Clean Shipping Index would be a way of implementing a financial incentive for the reduction of ship underwater noise. It is therefore of interest to investigate how this could be done. Note that there are several other systems for evaluating a ship's environmental performance, e.g. the Environmental Ship Index (ESI) and Green Marine. Each index has its own way of operating and scoring. While the focus here is on Clean Shipping Index, we will also attempt to draw general conclusions on introducing ship underwater noise into an environmental scoring system for ships.

Basing an incentive on dedicated measurement of the underwater radiated noise of a ship is not appropriate. First, Clean Shipping Index does not require measurement of any other environmental category. Second, performing an accurate measurement of ship underwater radiated noise requires specialised equipment and skills and is costly. There are few actors who offer this service to ship owners.

This study has evaluated six different ways of developing an environmental score for the underwater noise radiated by a ship. These are

- Predicting the radiated noise of a ship based on its characteristics
- Rewarding speed reductions
- Rewarding technical measures for noise mitigation
- Basing the score on silent notations from classification societies
- Performing a noise investigation (without direct measurement)
- Establishing bespoke measurement stations that measure the ship underwater noise with sufficient accuracy to establish a score

We will now discuss each of these alternatives in turn.

Predicting the radiated noise of a ship

Ship noise levels in the environment can be modelled by combining data from measurements of ship source spectra and models for the noise propagation. One important component in this is estimating the source spectrum of ships without requiring an acoustical measurement of each individual ship, i.e., using some predictive model.

Physically informed models, e.g. (Wittekind, 2014) and (Arveson and Vendittis, 2000), attempt to model the noise spectrum of a ship as accurately as possible, based on knowledge of the properties of the ship. These models are difficult to obtain since they require thorough acoustical measurements of ships as well as a detailed description of the ships in question. This makes these models able to predict how noise levels would change if the physical properties or operative conditions of a ship is changed, although only with certainty for the specific parameters and ships that were included in the study. If this behaviour, often derived from a small sample of ships, generalizes over an entire fleet, it can be used to predict how fleet-wide actions can impact the overall noise level. However, such a generalization is a source of uncertainty and possible errors. It can also be difficult to apply physical models in practice since they may rely on ship properties which are not easily available.

Statistical ensemble models, e.g. (Wales and Heitmeyer, 2002) and (MacGillivray and de Jong, 2021), on the other hand are by design meant to represent an entire fleet and can as such accurately predict the average noise levels present due to a large number of ships. Most statistical models do not, however, attempt to describe anything but the current ensemble of ships. This means that they are not good predictors of the effects of any changes to ship design or operating conditions that are not represented in the current ensemble of ships. E.g., if a statistical model is derived from measurements of ships at cruise speed, it cannot be used to estimate the effect of operating the ships at speeds lower than their respective cruise speeds.

Neither physically informed models or statistical ensemble models are currently not accurate enough to use for incentives. They can produce reasonably correct averages across a large fleet of ships of different types and characteristics and are useful for noise mapping. They can also inform operative measures such as speed reduction by predicting the effect of a potential speed reduction, as long as the intended speed reduction is not

outside the range of the data that was used to develop the model(s). However, the predictions for individual vessels may be quite inaccurate. Moreover, the models do not consider the propeller or hull design or any technical measures that may affect the underwater radiated noise performance. As such, they will not stimulate mitigation of underwater radiated noise.

Rewarding speed reductions

An incentive may reward vessel speed reductions. Large scale trials in Vancouver and off the coast of California (MacGillivray et al., 2019; ZoBell et al., 2022) found that on average, speed reductions led to underwater noise reductions. A vessel's average or peak speed when travelling through an area can be determined from AIS data without the need for external verification. An incentive could then be based on giving rebates to those ships that have performed a speed reduction. Speed reductions are generally also beneficial for fuel efficiency and carbon footprint, thus may yield multiple benefits. It would not be sufficient to apply the same speed limit for all ship types, as some ships are designed to travel at slower speeds and may otherwise be granted the rebate despite not having changed their operations.

It is not certain that a speed reduction will lead to a noise reduction; for some ships, there may be no noise reduction or even an increase in radiated noise levels. This depends on the ship's design and propeller. Ships are typically designed to operate at one or a few speeds e.g. the cruise speed. Lowering the speed slightly from this cruise speed puts the ship outside its designed mode of operation which may result in noise and efficiency drawbacks.

A large enough speed reduction that the speed drops below the cavitation inception speed (CIS) will make the propeller significantly quieter than what it is above the CIS, which will probably have a large positive effect on the overall levels of underwater radiated noise. However, such large speed reductions may not be feasible; transit times will increase significantly which will affect the financial situation of ship owners. During interviews and workshops, several ship owners have expressed that significant speed reductions are only feasible in small areas, so that the average transit times are not greatly affected.

In Swedish and European waters, controllable pitch propellers (CPP) are common. This is not the case in North American waters. It is more difficult to describe the noise radiation of a CPP propeller across its different operation modes because not only the speed but also the pitch of the propeller blades is variable. The combination of speed and pitch is known as the combinator curve. This curve is typically optimized for fuel efficiency, and it is not clear how levels of radiated noise are affected by speed reductions for ships equipped with CPP propellers.

Rewarding technical measures for noise mitigation

Several technical noise mitigation measures have been proposed and are in operation, including fins and rudders, special propeller designs and resilient engine mounts, see e.g. (Vard Marine Inc., 2019). The port of Vancouver rewards a number of such measures with port fee rebates, and it would be straightforward to apply a similar rebate system in Sweden. To secure the quality of such a system, it would be vital to obtain independent scientific results on typical noise reductions that result when using a specific technology. Such results are missing at the time of this study's publication. It appears likely that noise reductions that can be obtained with a certain technology depend on ship characteristics, and it may be that certain technologies are only applicable to ships that fulfil certain requirements. According to interviews with technical ship design experts, there is also room for improvements on propeller design. It would be difficult to reward such efforts since it is difficult to define quantitative propeller requirements for low noise radiation. Nevertheless, the efforts of the port of Vancouver stimulate the adoption of technical measures that can be expected to reduce the radiated noise and should be commended. Basing an incentive on technical measures for noise mitigation rewards effort on the part of the ship owner, which in turn may drive a positive development in terms of ship underwater noise.

Using silent notations

Currently, six ship classification societies have issued guidelines on underwater radiated noise, including measurement principles. These guidelines all prescribe one or two spectral limit curves. If the noise radiation of a ship under test is below the limit curve in all frequency bands, some form of silent notation is awarded. An incentive for underwater noise reduction could reward ships that have such silent notations. This would be a straightforward way to introduce an incentive and it would also be cost effective for the incentive organization. Classification societies perform independent investigations so there would be no need for external third-party verification. However, silent notations are not commonly issued. A representative of one of the classification societies stated that less than 100 ships had obtained their silent notation. The scarcity of silent notations is probably due to the lack of incentives or regulations that could motivate obtaining such a notation. Contracting a classification society to perform the detailed measurements that are required will cost at least a few hundred thousand SEK, equivalent to at least 20-~~50~~ ~~SEK~~ ~~or the ship cannot be measured in port, it will need to be taken~~ out of operation for the noise measurements, which may incur an even larger loss of income to the ship owner.

For a level playing field, all silent notations should be given the same score within an incentive. It is however worth noting that classification societies have different limit curves for ship underwater noise.

When a silent notation is issued, the classification society may report the noise levels of the vessels. If societies ~~are willing to do so and provide this information, the measurement of a ship's noise may be based on the actual radiated noise levels.~~ If not, a simple pass/pass/failure is what is available, and only two different scores can be awarded.

Performing a noise inquiry

A noise inquiry may be performed to determine likely noise sources onboard a ship and identify relevant mitigations for reduced underwater radiated noise. This inquiry should be performed by an external party and may list recommended mitigations considering mitigation and cost efficiency as well as operational constraints. A lower level of incentive may be awarded at completion of such an inquiry. Upon fulfilment of one or several recommended mitigations, a higher level of incentive may be awarded. An advantage of this approach is that measurements are not needed. A drawback is that it may not be clear from the inquiry what the dominant noise sources are.

Establishing bespoke measurement stations

There is really no alternative to direct measurement if one wants to know how much noise a certain vessel radiates. Thus, if one desires to base an incentive on the actual levels of radiated noise, these must be measured. Classification societies measure underwater noise for their silent notations, and we have seen that using silent notations issued by classification societies is an alternative. However, these notations are not ~~commonly awarded~~ ~~are costly to obtain and societies may not disclose full information on a ship's noise radiation.~~

Given that ships typically travel in specific fairways, underwater noise fingerprints may potentially be obtained by deploying autonomous measurement stations at certain points where many ships pass. Such measurements have been performed e.g., near the port of Vancouver. The data has been used to investigate average effects of speed reduction and to develop prediction models, but not to set incentives. An example of an opportunistic measurement station is given in Figure 2. It was placed at Böttö in the inlet to the port of Gothenburg, Sweden, and recorded underwater and airborne noise of passing vessels. Due to a limited number of hydrophones and insufficient knowledge of sound propagation conditions, the accuracy was however not sufficient for use in an incentive.



Figure 2: A ship noise measurement station deployed at the island of Böttö, Sweden, adjacent to the main fairway into the port of Gothenburg. The upper arrow indicates the position of a microphone, while the lower arrow indicates the position of a hydrophone at 13 m depth.

Opportunistic measurements typically suffer from poor accuracy due to e.g., a lack of control of the studied ships and uncertain noise propagation conditions. The type of studies performed in Vancouver can still achieve their goals, but to set incentives on individual vessels the accuracy may need to be better. If the accuracy can indeed be improved, measurement stations could be placed at or near inlets to major ports and collect noise fingerprints on which an incentive could be based.

Summary and conclusions

Six different ways of designing a financial incentive for ship underwater noise reduction have been described, each having its benefits and drawbacks. Rewarding speed reductions or technical measures for noise mitigation is feasible but the scientific basis is not clear. An incentive may be based on a silent ship notation from a classification society, but these are not commonly issued. A noise inquiry may be performed, but it may be difficult to identify the most relevant mitigations without underwater noise measurement. Bespoke measurement stations at or near port inlets may be a cost-effective way to collect measurement data, but the accuracy of such opportunistic measurements would need to be improved if the data is to be used for a financial incentive.

Acknowledgements

This work was funded by Formas, a Swedish research council for sustainable development, under grant no 2021-02660.

References

- Clean Shipping Index (2022). Methodology and Reporting Guidelines 2022. Clean Shipping Index, Gothenburg, Sweden.
- Arveson, P. T., Venditti D. J. (2000). Radiated noise characteristics of a modern cargo ship. *The Journal of the Acoustical Society of America*, 107, 118-129.
- Wittekind, D. K. (2014). A Simple Model for the Underwater Noise Source Level of Ships. *Journal of Ship Production and Design*, 30, 7-14. doi:10.5957/jspd.30.1.120052

- Wales, S. C., Heitmeyer, R. M. (2002). An ensemble source spectra model for merchant ship-radiated noise. *The Journal of the Acoustical Society of America*, 111, 1211-1231. doi:10.1121/1.1427355
- MacGillivray, A., & de Jong, C. (2021). A Reference Spectrum Model for Estimating Source Levels of Marine Shipping Based on Automated Identification System Data. *Journal of Marine Science and Engineering*, 9. doi:10.3390/jmse9040369
- ZoBell V. M., Frasier K. E., Hildebrand J. A. (2022). Sound Levels of Participating Vessels during the 2021 Vessel Speed Reduction Program in the Santa Barbara Channel. Final Report. *Marine Physical Laboratory Technical Memorandum 659*.
- MacGillivray, A. O., Zizheng L., Hannay D. E., Trounce K. B., Robinson O. M. (2019). Slowing Deep-Sea Commercial Vessels Reduces Underwater Radiated Noise. *The Journal of the Acoustical Society of America* 146,340–51. doi:10.1121/1.5116140.

3 Conference Proceedings – Short abstracts

This volume of ~~the conference report proceedings complements the full-text collection of the conference papers with short one-page abstracts for those, which have not been submitted as an extended abstract.~~

Papers of this section are:

- structured based on the thematic sessions of the TAP&SE 2023, as defined in the final program of the conference,
- listed in the order that were presented during the conference,
- ~~included in the version that was submitted by authors to the conference's website before the implementation dates of TAP&SE 2023.~~

Table 1 lists the short abstracts by session/topic of TAP&SE 2023.

Table 1. List of short abstracts presented in Volume 2 by session/topic of TAP&SE 2023.
TAP denotes poster presentation

Session/Paper ID	Corresponding author, Title	
TAP.02	On-board monitoring and diagnostics, emission tampering and deterioration	
TAP.02.1	Pöhler, D.	Identification of Manipulated & Defective Truck NOx Emission Reduction Systems with Plume Chasing for Authority Inspections
TAP.02.2	Wang, H.	Strong impact of ambient temperature on nitrogen oxides emissions from heavy-duty diesel trucks based on plume chasing tests
TAP.03	In-service conformity and new concepts for enhanced emission testing <small>in PTI'</small>	
TAP.03.2	Leblanc, M.	Extended evaluation of the emissions of top-selling Euro 6 cars depending on powertrain and exhaust after-treatment technologies
TAP.04	Remote sensing of vehicle emissions	
TAP.04.1	Imtiaz, H.	A Gas Schlieren Imaging Sensor System for Locating and Examining Automotive Exhaust Plumes for Remote Emission Sensing Applications
TAP.04.3	Schmidt, C.	Optimisation and Validation of Plume Chasing for Particle and NOx High Emitter Identification
TAP.04.4	Sjödin, Å.	A method for deriving characteristic emission polygons for engine families based on large datasets from remote sensing measurements
TAP.04.5	Knoll, M.	Intercomparison of Remote Emission Sensing Methods and Validation with PEMS Measurements
TAP.05	Vehicle greenhouse gas emissions, energy consumption, vehicle and fuel life cycle analysis	
TAP.05.4	Mamarikas, S.	Electric and conventional vehicles energy consumption under various traffic conditions
TAP.06	Vehicle emission modelling and measurements and impact assessment of emission regulations	
TAP.06.1	Wen, Y.	Updated vehicle emission inventory in China.
TAP.06.2	Sanna, S.	Long-term trends of black carbon and particle number concentrations and vehicle emission factors in Stockholm
TAP.07	Non-road emissions	
TAP.07.1	Tu, M.	Train type effect on nanoparticles on an underground metro platform in Stockholm

TAP.07.2	Juárez-Facio, A.	Toxicity of particle emissions from car and train brake materials
TAP.07.5	Vroom, Q.	Brake wear ultrafine particle emissions from a light duty vehicle under real driving conditions
TAP.07.6	Landl, L.	A Novel Simulation Approach for Non-Exhaust Particle Emissions
JS.08	Air pollutant and GHG emissions, water contaminants, ambient and underwater noise and vessel-induced mixing	
JS.08.1	Schade, J.	Remote detection of ship exhaust plumes from different marine fuels on board a research vessel in the Baltic Sea region using single-particle mass spectrometry
JS.08.4	Voniati, G.	Ammonia as a Marine Fuel Towards Decarbonization: Emission Control Challenges
JS.08.5	Moldanova, J.	Characterisation of emissions from marine vessel with E-methanol fuel and NOx emission control
JS.08.6	Grönholm, T.	Discharges from exhaust gas cleaning systems in the OSPAR marine area
JS.08.7	Hallquist, Å.	Characterisation of fresh and aged ship emissions in the Port of Marsei
JS.08.8	Lunde Hermansson, A.	Distribution of PAHs and metals between exhaust and scrubber water discharge from a large 2-stroke slow speed marine engine equipped with open loop scrubber
JS.09	Atmospheric processes and air quality impact studies: Modelling impacts of transport on air pollution, climate, health and ecosystems	
JS.09.2	Jutterström, S.	Impacts of shipping emissions on air pollution in 2040: effects of NECA and non-compliance
JS.09.3	Maragkidou, A.	Direct evidence of the substantial effect of SECA in the Baltic Sea
JS.09.5	Russo, M.	Future impact of shipping emissions on air quality in Europe under climate change scenarios
JS.09.9	Dal Maso, M.	On the determination of ship exhaust aerosol volatility in the SCIPPER project
JS.10	Compliance monitoring: technological and legal frameworks; experimental studies; theoretical impact studies	
JS.10.2	Van Dinter, D.	Comparison of particle emission factors from shipping using different instruments
JS.10.3	Beecken, J.	Performance assessment of state-of-the-art and novel methods for remote compliance monitoring of sulphur emissions from shipping
JS.10.4	Mellqvist, J.	Remote monitoring of NOx from shipping- validation and long term results
JS.12	Scenarios and policy options for sustainable transport	
JS.12.1	Parsmo, R.	Potential impact on emissions of an introduction of hydrogen and fuel cell based propulsion in Nordic shipping
JS.12.2	Malik Kanchiralla, F.	Environmental and economic assessment of green and blue fuels for shipping
JS.12.3	Fridell, E.	Policy scenarios for analysing use of scrubbers in shipping
JS.12.4	Majamäki, E.	Projections of shipping emissions in Europe in 2040 and 2050
JS.12.5	Matthias, V.	Climate friendly and pollution-free? Scenarios for air pollution from shipping in Europe in 2050
SE.13	Marine processes - fate of pollution from shipping in the marine environment: impact studies on ecotoxicology, eutrophication and acidification, energy pollution including underwater noise & induced	

		mixing; experimental work, modelling studies of dispersion, transport, and chemical and biological processes in marine waters
SE.13.1	Granberg, M.	A multi species and multi system evaluation of the ecotoxicological effects of scrubber water – a synopsis of results from the EMERGE project
SE.13.3	Mujingni, J.	Sampling strategies and characterization of greywater from ships
SE.13.4	Nylund, A.	Turbulent ship wakes: extent, intensity, and interaction with stratification
SE.13.5	Egardt, J.	Response in the marine diatom <i>Nitzschia</i> sp., following exposure to bilge water from different ships
SE.13.6	Chen, C.	Scrubber water impairs fertilization and development in the green sea urchin (<i>Strongylocentrotus droebachiensis</i>) at very low concentrations
SE.13.7	Bensow, R.	The possibilities and effects of ship speed reduction on underwater noise – a case study
SE.13.8	Booge, D.	Influence of scrubber effluent on biogenic trace gas production
SE.14		Holistic assessment of shipping impacts on the environment, shipping in marine spatial planning
SE.14.1	Guéret, S.	Impact assessment of shipping activities: Applying the critical load concept to both the atmosphere and marine environment
SE.14.2	Elliott, M.	Managing Marine Resources Sustainably: a transdisciplinary approach to the causes, consequences and responses to environmental problems of shipping and navigation
SE.14.3	Francis, F.	Impacts of expanding commercial anchoring on the Pacific Coast of Canada
SE.14.4	Sakellariadou, F.	Reducing particulate contribution to climate change
PS1		Poster session 1
PS.1.1	Kupper, M.	Measurement and Analysis of Brake and Tyre Particle Emissions for High-Load Driving Scenarios on a Test Bed
PS.1.2	Aletras, N.	Predictive energy management for a plug-in hybrid electric truck
PS.1.3	Mehlig, D.	The EVolution of non-exhaust emissions
PS.1.7	Svensson, N.	The effect of a porous pavement on air quality in comparison to a dense pavement
PS.1.8	Suarez-Corujo, J.	CO2 emissions targets, revisiting the transition from 2020 NEDC to 2021 WLTP
PS.1.11	Elihn, K.	Development of a mobile ALI exposure system for toxicity testing of emissions from different transportation modes
PS.1.14	Rossi, T.	Fuel consumption, regulated and unregulated exhaust emission tests on three Euro 6d bi-fuel LPG passenger cars, fed by an innovative LPG/DME 80/20 (V/V) blend
PS.1.16	Gómez Vilchez, J.	Future SUV fleet and CO2 emissions projections in Australia and the European Union
PS.1.17	Introna, M.	Toxicity of real-world road tunnel emissions in an ALI exposure model.
PS.1.21	Coulson, G.	Non-Exhaust Emissions in Aotearoa New Zealand
PS.1.25	Rausch, J.	Characterization & quantification of traffic-derived non-exhaust particles (TWP/TRWP, brake & road wear) in airborne dust
PS.1.29	Unterschütz, L.	Data protection in remote sensing through profiling high-emitting vehicles

PS.1.32	Priestley, M.	Lubrication oil as a potential source of traffic originated secondary particulate mass
PS.1.37	Krasa, H.	A simplified in-Field Calibration method for Periodical Technical Inspections Particle Counters with atomized NaI
PS.1.54	Qin, X.	Roadway diesel vehicle emission measurement by PEMS and its dispersion at on-road conditions captured by plume chasing
PS.1.55	Molden, N.	Comparative chemical composition of US and European tyres VOC profile, potential environmental impact, including 6PPD
PS.1.56	Thomas, D.	Incorporating NOx into the Periodic Technical Inspection vehicle emission test procedures
PS.2	Poster session 2	
PS.2.3	Mao, W.	AIS data mining to identify tank cleaning operations at sea
PS.2.4	Prignon, M.	DOAS applied to shipping emission monitoring: compliance assessment and comparison to satellite measurements
PS.2.5	Beecken, J.	FUGitive Methane Emissions from Ships (FUMES): Characterizing methane emissions from LNG-fueled ships using drones, helicopters, and on-board measurements
PS.2.7	Jalkanen, J.	Discharges from ships to the sea in European sea regions
PS.2.9	Kousias, N.	A Low-Cost Optoacoustic Sensor for Black Carbon monitoring of Ships
PS.2.10	Conde, V.	Remote monitoring of sulphur emissions from shipping with a novel high sensitive laser system.
PS.2.11	Eger, P.	Measurement of NOx and ultrafine particles from inland shipping in Germany
PS.2.12	Hundt, M.	A single instrument for simultaneous monitoring of greenhouse gases and air pollutants
PS.2.14	Lunde	Monetary return on scrubber installations at the expense of environmental damage
PS.2.15	Hermansson, A.	VOC emissions from ships
PS.2.16	Salo, K.	The actor perspective on reaching a low emitting shipping sector
PS.2.24	Malmgren, E.	Legal barriers to transporting CO2 streams by ships
PS.2.25	Argüello, G.	High-resolution air quality mapping via massive mobile monitoring and land use random forest models
PS.2.26	Zheng, T.	Is post-exposure feeding inhibition of Artemia sp. and Mytilus galloprovincialis impaired by exposure to scrubber-waters?
PS.2.27	Abrantes, N.	Air quality assessment at the street level: sensitivity analysis of a road traffic-emissions-CTM model chain for the Paris region
PS.2.28	Lannes, M.	Environmental fate modelling of organic pollutants from land-based and shipping emissions in the Northern Adriatic Sea coastal areas
PS.2.30	Calgaro, L.	Deposition quantification of gaseous emissions at the air-water interface during a single vessel travel
PS.2.32	Rapkos, N.	Variation in responses of microalgae, <i>Nitzchia</i> sp. exposed to grey water from ships.
PS.2.34	Rathnamali, M.	Holistic environmental impact assessment from shipping: A decision support tool for stakeholder engagement
PS.2.35	Winiwarter, W.	CFD dispersion modelling for the reproduction of real shipping emission conditions in a port area
PS.2.36	Boikos, C.	Cumulative effects of commercial anchoring on the Pacific Coast of Canada: Ecological and Socio-Economic Effects
PS.2.37	Hannah, L.	The impact of maritime activities on air quality in three European ports
Ramacher, M.		

PS.2.38	Parsmo, R.	Assessing the impact of environmental policy instruments for ships in Europe with a modelling tool
PS.2.40	Hassellöv, I.	LNG feeder vessel environmental pressures, partially decoupled from transport demand
PS.2.42	Hassellöv, I.	The Poseidon Principles: Designing and implementing a regulatory framework to create ecosystem sustainability
PS.2.44	Rutgersson, A.	ShipTRASE, Global shipping: Linking policy and economics to biogeochemical cycling and air-sea interaction
PS.2.46	Gondikas, A.	Identification and quantification of contaminant particles from scrubber water effluents in a high-intensity shipping area
PS.2.51	Yang, S.	Optimization of Drone-based Sensor Sniffing System for Monitoring Fuel Sulphur Content in Ocean-going Vessel Based on Field Measurements in Hong Kong Waters
PS.2.52	Santos, L.	Changes in cloud activity of ship exhaust particles: Potential effects on Arctic mixed-phase clouds

3.1 TAP.02. On-board monitoring and diagnostics, emission tampering and deterioration.

Identification of Manipulated & Defective Truck NOx Emission Reduction Systems with Plume Chasing for Authority Inspections

D. Pöhler^{1,2}, C. Schmidt^{1,2}, S. Schmitt¹, J.P. Lolinga³, T. Frateur³, N. E. Ligterink³, M. Vojtíšek⁴, J. Borken-Kleefeld⁵, Y. Bernard⁶, Å. Sjödin⁷

¹ Airyx GmbH, Justus-von-Liebig-Straße 14, Eppelheim, 69214, Germany

² Institute of Environmental Physics, University of Heidelberg, INF 229, Heidelberg, 69120, Germany

³TNO, Anna van Buerenplein 1, 2595, The Hague, Netherlands

⁴CVUT, Czech Technical University Prague, Technická 4, 166 07, Praha, Czech Republic

⁵Institute of Transport Planning and Road Traffic, TU Dresden, Hettnerstraße 1, 01069 Dresden, Germany

⁶ICCT International Council on Clean Transportation, Berlin, 10178, Germany

⁷IVL Swedish Environmental Research Institute, Goteborg, 411 33, Sweden

Keywords: Plume Chasing; SCR manipulation, emulator, CARES, NOx emissions, high emitter, heavy duty.

Presenting author email: denis.poehler@airyx.de

EURO V and VI trucks (heavy duty vehicles) achieve required low NOx (nitrogen oxides) emissions using Selective Catalytic Reduction (SCR) systems consuming AdBlue®. The operation and maintenance of the SCR system is costly. There are illegal manipulations of the emission system typical with emulators which turn down the SCR system while the engine electronics is not identifying the deactivation. Additionally, there are also defective systems which are not repaired or not properly maintained according to regulations. Manipulations and defects increase the emissions, harm environment and citizens and create an unfair advantage with respect to correctly operated and maintained vehicles. Thus, identification and punishment of illegal cost saving manipulations or avoided maintenance is important.

To detect these manipulations or defects in an inspection is difficult and time consuming. The Plume Chasing (PC) method is a remote measurement method to identify these high emitting vehicles. A system from Airyx was developed for this purpose with the support of the CARES project. It is designed to measure emissions from trucks in real traffic and identify the high emitters. It pre-selects vehicles that should be investigated in further inspection, which significantly increase the effectiveness of authorities (Pöhler, 2021). The accuracy of this PC system for NOx emission measurements was demonstrated in several studies, e.g., Janssen and Hagberg (2020).

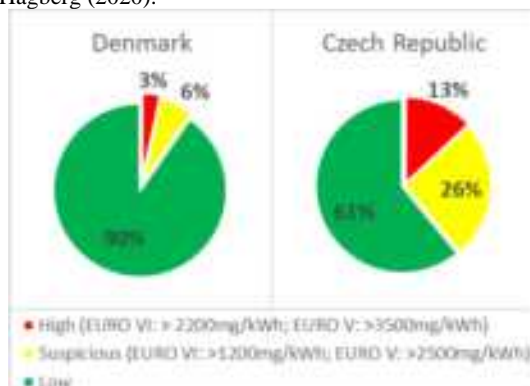


Figure 1. Rates of high and suspicious emitting trucks.

First authorities in Europe start to use Airyx PC as a standard tool for their daily inspection work. We here report on extensive PC studies in Denmark, Belgium, the Czech Republic and. Figure 1 shows the measured truck emission classification in Denmark (n=480) and the Czech Republic (n=986). While in Denmark less than 10% of trucks displayed suspicious or high emissions, these are about 40% in Czech Republic.

Several of the suspicious and high emitting trucks were stopped for detailed inspections by authorities (Figure 2). A reason for high emissions was found in all (0% "No Error"), confirming the effectiveness of the PC for high-emitter detection. Most trucks had defects, also manipulation was clearly proven on many vehicles. Some trucks had a cold SCR due to warm up problems (mainly EURO V, and suspicious emitters) and a few had missed emission software updates.

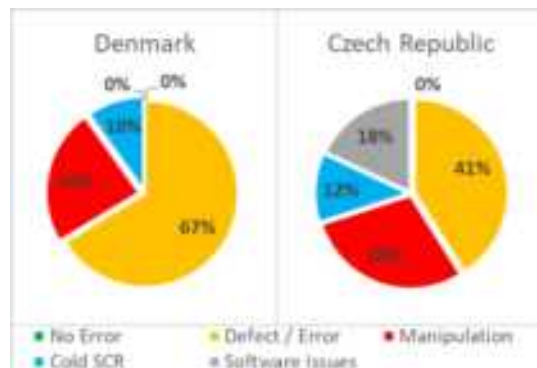


Figure 2. Results of inspection.

This work was supported by the EU H2020 CARES Project No. 814966.

Pöhler, D. (2021), *Heavy Duty Vehicle (HDV) NOx emission measurement with mobile remote sensing (Plume Chasing) and subsequent inspection of high emitters*, Final Report, Airyx GmbH, Germany.

Strong impact of ambient temperature on nitrogen oxides emissions from heavy-duty diesel trucks based on plume chasing tests

Hui Wang¹, Shaojun Zhang¹, Xiaomeng Wu¹, and Ye Wu¹

¹ School of Environment, Tsinghua University, Beijing, 100084, China.

Keywords: heavy-duty diesel trucks, nitrogen oxides, ambient temperature

Presenting author email: hui-wang1992@tsinghua.edu.cn

Controlling the emissions from heavy-duty diesel trucks (HDDTs) is one of the prioritized tasks to further improve air quality in China. Nitrogen oxides (NO_x) emitted by HDDTs is a key precursor of ozone pollution and the precursor of ammonium salt for haze episodes. It is essential to accurately evaluate real-world emission levels. Previous studies have focused on the leading drivers, such as emission standards and driving speed affecting NO_x emissions from HDDTs. However, few studies have explored the influence of environmental conditions, such as ambient temperature on NO_x emissions, which is important for exactly evaluating seasonal emission differences for HDDTs. In this study, we conducted large-size plume chasing tests for on-road HDDTs across several seasons in China to explore the NO_x emission trends caused by ambient temperature.

In this study, we dispatched the well-verified mobile platform (Wang, 2020) to conduct plume chasing tests for HDDTs across several major regions in China. This campaign measured more than two thousand HDDTs (gross vehicle weight over 4.5 tons) with NO_x emissions between 2017 and 2020. Real-world NO_x emissions trends for HDDTs affected by ambient temperature were thus analyzed. Generalized additive models (GAMs) with advantages in nonlinear fitting were used to predict the sensitivity of ambient temperature on NO_x emissions for different emission standards and vehicle types based on the plume chasing test dataset (see Figure 1). HDDTs NO_x emissions were found to be highly dependent on ambient temperature with low temperatures resulting in higher NO_x emissions. For example, the low temperature (-3°C) would lead to a 137% increase in NO_x emissions for China V HDDTs (gross vehicle weight between 4.5-31 tons) compared to under the high temperature (35°C).

The ambient temperature corrections module that can characterize the seasonal and regional difference of NO_x emission prediction for HDDTs was developed based on the large-size data. Figure 2 illustrates the NO_x emission variation in wintertime and summertime compared to regional annual temperature in several regions of China in 2019 when considering the ambient temperature corrections module. Affected by the “low-temperature NO_x emission penalty”, the seasonal variation between wintertime and summertime of NO_x EFs for HDDTs is estimated to be 9%-33% for eight regions in China. This variation would be especially important for northern regions located in the high latitudes with greater seasonal temperature differences. This trend highlights the importance of accounting for the effect of ambient temperature in NO_x emission modelling and prediction. The results revealed the high impact of

ambient temperature dependency on NO_x emissions from HDDTs and this is important for accurately assessing the spatial-temporal variation in on-road NO_x emissions for HDDTs.

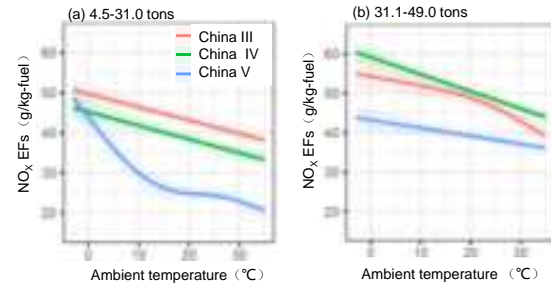


Figure 1. Generalized addition models (GAMs) of fuel-specific NO_x emissions based on ambient temperature for China III to China V HDTs. (a) 4.5-31.0 tons HDDTs; (b) 31.1-49.0 tons HDDTs. The shaded zones represent the GAMs' standard error for the prediction.

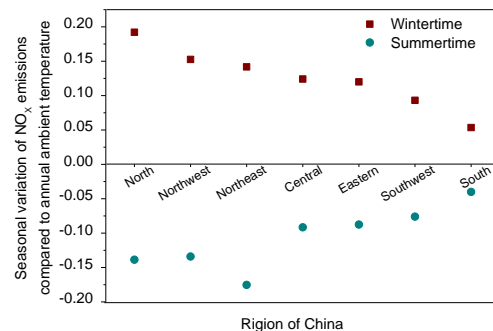


Figure 2. The NO_x emission variation for HDDTs in wintertime and summertime compared to regional annual temperature in major regions of China in 2019.

This work was supported by the Ministry of Science and Technology of China's International Science and Technology Cooperation Program (2018YFE0106800, MOST of China and European Union Horizon 2020 collaborative project).

Wang, H., Wu, Y., Zhang, K. M. et al. (2020) Evaluating mobile monitoring of on-road emission factors by comparing concurrent PEMS measurements. *Science of the Total Environment*, 2020, 736: 139507.

3.2 TAP.03. In-service conformity and new concepts for enhanced emission testing in PTI.

Extended evaluation of the emissions of top-selling Euro 6 cars depending on powertrain and exhaust after-treatment technologies

M. Leblanc¹, A. Albinet² and S. Raux¹

¹ IFP Energies nouvelles, Rond-point de l'échangeur de Solaize, BP3, 69360 Solaize, France ; Institut Carnot IFPEN Transports Energie

² INERIS - Parc technologique Alata, BP 2, 60550 Verneuil-en-Halatte, FRANCE

Keywords: Euro 6, Euro 7, exhaust, Diesel, gasoline, regeneration, WLTC, RDE, NH₃, N₂O, PN, PAH

Presenting author email: mickael.leblanc@ifpen.fr

While from 2035, all new cars sold on the European market should be zero-emission to ensure the transport sector to become carbon-neutral by 2050, vehicles equipped with a thermal engine still should represent up to 55 % of new registrations in 2030 (Ntziachristos, 2022). Of these, 61 % should be Diesel, 39 % gasoline, including 45 to 50 % hybrids (plug-in or not) for each.

For this reason and to further reduce pollutant emissions from new motor vehicles sold meanwhile, the European Commission recently published Euro 7 standards proposal (European commission, 2022). The current Euro 6d standard considers distinct fuel-dependent emission limits while Euro 7 proposal finally introduces fuel neutral ones. Other improvements of the test procedures are proposed to better reflect the normal conditions of use. This includes Diesel particulate filter [DPF] active regenerations that still need to be taken into account to better evaluate the total exhaust emissions, as well as their possible impacts.

Objectives

This work provides a comprehensive evaluation of regulated and unregulated emissions of a Euro 6 car, among the most sold in France, equipped with different engine types and exhaust after-treatment systems [EATS].

Experimental setup

The RHAPSODIE project studied the exhaust emissions of three models of the same top-selling European sedan (Table 1), under various driving (WLTC, CADC and RDE) and starting (ambient/hot) conditions.

Table 1. Vehicle main characteristics.

Engine	Standard	EATS
Gasoline	6b	3WC
Gasoline	6d-TEMP	3WC+GPF
Diesel	6d-TEMP	DOC+SCR+SCRF

A wide panel of online and laboratory protocols have been used to extensively analyse the regulated and unregulated pollutants present in the gaseous and particulate phases of the exhaust emissions, including ammonia [NH₃], methane [CH₄] and solid particle number [PN], above and below 23 nm, proposed to be limited for future Euro 7 cars.

Other species were monitored, still not regulated for cars, including nitrous oxide [N₂O], formaldehyde [CH₂O], non-methane organic gases [NMOG], expected

to be regulated only for heavy-duty vehicles, and polycyclic aromatic hydrocarbons and their nitrated and oxygenated derivatives [PAHs, nitro- and oxy-PAHs] quantified in both gaseous and particulate phases.

Results

Thanks to the distance covered during the campaign (around 6,500 km), an extensive comparison of the emissions (regulated or not) of the two gasoline and Diesel versions of a same Euro 6 model car is proposed. The results (Figure 1) highlight that the two Euro 6d vehicles comply with their respective emission limits, with particularly low particle emissions. The results also allow to quantify the specific contribution of DPF regenerations to the gaseous and particulate emissions of the Diesel version. Finally, the results are compared to the proposed Euro 7 targets regarding WLTC and RDE-like trip, this latter being not strictly compliant with official Real Driving Emissions [RDE] conditions for Euro 6, particularly due to its lower distance and duration.

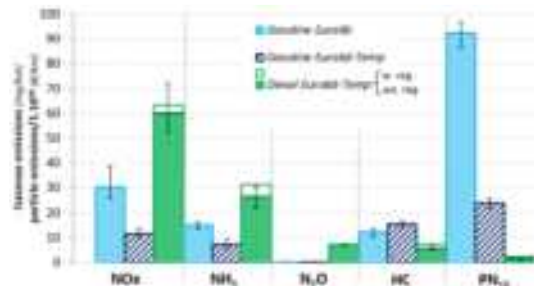


Figure 1. Emission factors of the vehicles under RDE-like (homothetic) trip

This study has been performed within the framework of the RHAPSODIE project funded by the French Environment and Energy Management Agency (Agreement 1766C0003) and supported by the French Ministry of Environment.

European Commission, Ntziachristos, L., Papadopoulos, G., Samos, Z. et al., *Euro 7 impact assessment study*, 2022, <https://data.europa.eu/doi/10.2873/249061>

European Commission, *Proposal for a regulation of the European Parliament and of the council*, 2022 https://ec.europa.eu/commission/presscorner/detail/en/ip_22_6495

3.3 TAP.04. Remote sensing of vehicle emissions.

A Gas Schlieren Imaging Sensor System for Locating and Examining Automotive Exhaust Plumes for Remote Emission Sensing Applications

Hafiz Hashim Imtiaz¹, Paul Schaffer¹, Martin Kupper¹ and Alexander Bergmann¹

¹Institute of Electrical Measurement and Sensor Systems, Graz University of Technology, Graz, 8010, Austria

Keywords: schlieren imaging, gas imaging, refractive index, vehicle exhaust, remote emission sensing

Presenting author email: hafiz.imtiaz@tugraz.at

Synthetic Schlieren (or Background Oriented Schlieren) is an established method to visualize differences of the refractive index in a fluid and can thus be used to picture flows, (Sutherland, 1999). Changes of the refractive index can be caused e.g. by temperature, humidity or concentration changes. In this work, we present a Gas Schlieren Imaging Sensor System (GSIS) for imaging exhaust gas plumes for remote emission sensing (RES). The GSIS is a cost-effective way to detect plume sizes, spreading directions and velocity. Analysis is made possible by advanced image processing techniques and deep learning algorithms.

The setup consists of a digital camera with a frame rate of 30 fps (target moving speed of vehicles ~ 50 km/h) and a uniformly structured (white and black checker pattern), illuminated background board. The principle is shown in fig. 1. With a disturbance between the pattern board and the camera, the light is deflected from the straight path. By comparison of two images, differences can be identified as movements of the gas - the resulting schlieren image.

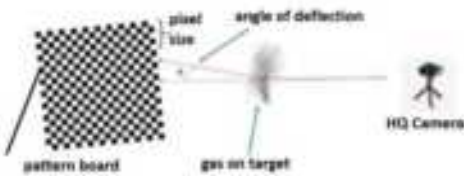


Figure 1. Principle of synthetic schlieren.

Automated image processing steps are applied (contrasting, blurring, thresholding, erosion and dilation) to carve out the plume in schlieren image. The plume is then detected by a trained neural network. The plume size in mm is calculated from the image by considering the camera sensor size in mm and in pixels, distance to the gas plume and the focal length of the camera.

The feasibility of the GSIS for imaging of exhaust plumes was proven by capturing the exhaust plume of bypassing cars with 30 km/h, see fig. 2a for an exemplary visualization. Data from vehicle measurements for an evaluation are gathered.

Lab experiments were started to identify the actual influences of the exhaust (gas compounds, temperature, humidity) to the visibility. For first identification of influences on the GSIS, a defined gas mixture was led through a glass pipe (diameter 3 cm) in a tube furnace with 6 l/min and the outflow in air was captured by the GSIS, as shown in fig. 2b and 2c. Humidity, temperature, volume flow and concentrations of gas mixtures can be varied in a controlled manner.

Preliminary results from the experiments can be seen in fig. 3. The relation between relative visibility of

CO₂, air, N₂ and CO₂-air mixtures at different temperatures is shown. The visibility is assessed by the number of pixels associated to the plume, normalized to the respective maximum acquired value. The identified dependencies suggest a dominant influence of CO₂, what makes an application in RES under environmental conditions seem feasible. A direct relation between visibility and temperature can still be seen from air and N₂ data, while CO₂ and CO₂-air mixture curves show opposite trends, here visibility decreased with the increase in temperature. For mixtures an overlay of both trends can be observed. A description of the observed behaviour via density changes of the gas components is pursued.

The characterization of the GSIS in the lab is currently in progress. It aims to quantify the influences of the varied parameters on the visibility in the schlieren images and find limit values. A well-founded statement will be presented at the conference.

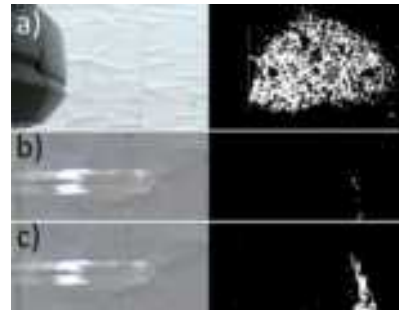


Figure 2. Photographs and the corresponding schlieren images. a) automotive exhaust, b) 20% CO₂ in synthetic air 200 °C, c) 20% CO₂ in synthetic air 25 °C.

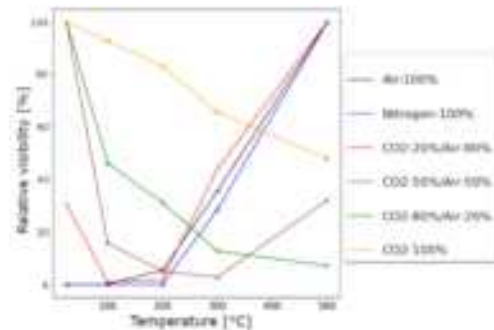


Figure 3. Selected preliminary characterization results. Dots indicate measured values. Relative visibility is not comparable in-between datasets yet.

This work is funded by FFG Project 888105 “LASERS”

Sutherland, B.R., Dalziel, S.B., Hughes, G.O. and Linden, P.F. (1999) *Journal of Fluid Mechanics*, Cambridge University Press.

Optimisation and Validation of Plume Chasing for Particle and NO_x High Emitter Identification

C. Schmidt^{1,2}, D. Pöhler^{1,2}, S. Schmitt², M. Knoll³, T. Frateur⁴, J. P. Lollinga⁵, N. E. Ligterink⁴, M. Vojtíšek⁶, N. J. Farren⁷, D. C. Carslaw⁷, Y. Bernard⁸, U. Platt^{1,2}

¹Institute of Environmental Physics, University of Heidelberg, Heidelberg, 69120, Germany

²Airyx GmbH, Eppelheim, 69214, Germany

³Institute of Electrical Measurement and Sensor Systems, Graz University of Technology, Graz, 8010, Austria

⁴Department of Sustainable Transport and Logistics, TNO, The Hague, 2595 DA, NL

⁵Department of Environmental Modelling, Sensing & Analysis, TNO, Utrecht, 3584 CB, NL

⁶CVUT, Czech Technical University Prague, Praha, 166 07, Czech Republic

⁷Wolfson Atmospheric Chemistry Laboratories, University of York, YO10 5DD, United Kingdom

⁸ICCT International Council on Clean Transportation, Berlin, 10178, Germany

Keywords: air quality, plume chasing, remote sensing, particle emissions, CARES

Presenting author email: cschmidt@iup.uni-heidelberg.de

Besides Nitrogen Oxides (NO_x), particle emissions from vehicles are a major cause of bad air quality in urban areas. Over their lifetime vehicles are often not properly maintained or tampered which leads to substantially higher emissions. In several studies it has been shown that those high emitters are responsible for the major share of emissions. It is therefore crucial to monitor and identify such high emitters to significantly improve the overall air quality. Plume Chasing (PC) is a remote emission sensing (RES) technique which is perfectly suitable for high emitter identification (e.g. Pöhler, 2021). Currently, it has mainly been applied for the detection of high NO_x emitters. PC was further developed in the framework of the EU project CARES (City Air Remote Emission Sensing, <https://cares-project.eu/>). The project included test studies to optimize and validate the PC method in terms of hardware and data analysis algorithms. As one part of this study particle instruments were compared for their usage in PC and their applicability in high emitter identification.

The PC method uses a measurement vehicle equipped with different instruments to chase the emission plume of investigated vehicles. The sampled air from the emitted plume is analysed in real-time by instruments that allow fast (1 s time resolution) and simple measurements with high accuracy and wide measurement range. During a two weeks measurement campaign in Czech Republic (12.09.-24.09.22) 1.835 vehicles were measured with PC and several particle instruments were evaluated for their usage in PC. Several particle metrics exist, where especially particle number concentration (PN) and black carbon (BC) are of particular interest. PN is of increasing interest nowadays due to the introduced emission limits. BC is a selective marker for detecting diesel particulate filter (DPF) failures. In the campaign, two diffusion chargers (particle counter, TEN AEM; counter, AVL DiTest) for measuring PN and one photoacoustic instrument (Black Carbon Tracker (BCT), TUG) for measuring BC were compared. We used as reference instrument an SMPS (Electrostatic Classifier 3082 and TSI 3775 CPC) measuring 80 nm particles, which showed very good performance in detecting a DPF tampered vehicle in a validation study in the CARES project (Farren

et al., 2022). All instruments were installed in a measurement vehicle from TNO (Utrecht, Netherlands).

The AVL DiTest counter showed a very good correlation ($R^2=0.94$) with the SMPS (see Fig. 2). A good agreement could also be found for the BCT ($R^2=0.71$). The performance of the TEN AEM particle counter could be improved compared to the validation study. Nevertheless, it still has a significantly higher, likely false positive, identification of high particle emitters compared to the SMPS. This evaluation shows the applicability of the individual instruments for their usage in PC and shows the great potential of high particle emitter identification with the PC method.

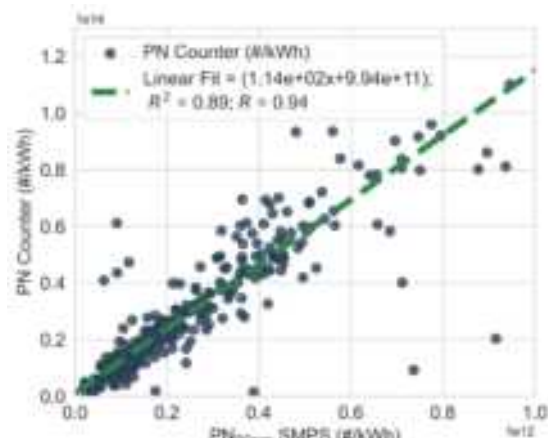


Figure 2. Particle number measured by AVL DiTest Counter versus SMPS (80nm) for 327 HDVs.

This work was supported by the EU H2020 CARES Project No. 814966.

Farren, N. et al (2022) *DI.1 – Measurement technology intercomparison and evaluation, Public Report, CARES Project*.

Pöhler, D. (2021) *Heavy Duty Vehicle (HDV) NO_x emission measurement with mobile remote sensing*

A method for deriving characteristic emission polygons for engine families based on large datasets from remote sensing measurements

Å. Sjödin¹, S. Hausberger², M. Jerksjö¹ and Y. Cha¹

¹IVL Swedish Environmental Research Institute, Gothenburg, SE-400 14, Sweden

² Institute for Thermodynamics & Sustainable Propulsion Systems, Graz University of Technology, Graz, A-8010, Austria

Keywords: remote sensing, emission characteristics, light-duty vehicles, engine families
Presenting author email: ake.sjodin@ivl.se

Vehicle emission measurements are crucial for a comprehensive understanding of road traffic related air pollution and for effectively controlling the emissions through various policies - from the local to the international level. In the case of diesel vehicles, the strategies applied in Europe to control emissions of nitrogen oxides in the past have largely failed, probably best exemplified by the dieselgate scandal revealed in 2015 (Thompson *et al.*, 2014).

The possibility of vehicle manufacturers to cheat with the legislative emission tests, and the often-observed discrepancies between emissions measured in the laboratory over a standardized driving cycle and emissions encountered in real-world driving, have substantially increased the interest during the last 5-10 years to apply various methods that measure emissions on the road in real drive operation, e.g., PEMS (Baldino *et al.*, 2017) and remote sensing - RS (Davison *et al.*, 2020).

Whereas PEMS can measure the emission performance of an individual vehicle in very large detail but at a rather high cost, and therefore relatively few vehicles are measured, remote sensing catches only an "emission snapshot" of each vehicle, but on the other hand can measure thousands of vehicles in one day, able to provide good statistics and fleet representativity.

We have developed a method that utilizes large datasets from remote sensing measurements to derive characteristic emission polygons for engine families, building on the engine family taxonomy developed in the H2020 uCARe project (https://www.project-ucae.eu/wp-content/uploads/2019/11/uCARe_D1.1_taxonomy.pdf).

The method also builds on a set of equations for estimates of VSP and of fuel flows developed from simulations with the TU Graz PHEM model and HBEFA data for vehicle and engine technologies, see Figure 1 (example for a Euro 6d-temp diesel car).

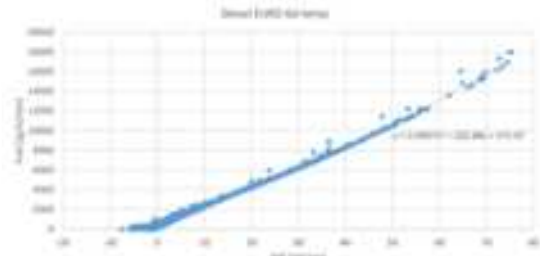


Figure 1. Fuel consumption vs VSP for an average Euro 6d-temp diesel car according to PHEM simulations.

The PHEM and HBEFA derived equations are designed to be applied to convert remote sensing results from [g/kg fuel or CO₂] into [g/s or g/km]. The derived remote sensing-based emission factors can then be plotted against vehicle speed over a large speed range. An example is given by Figure 2, in which average absolute NO_x emissions (in g/s) by 5 km/h speed bins are plotted against vehicle speed for a very common engine family in Europe – the Volkswagen AG Euro 6b diesel engine with engine displacement 1598 cm³ and rated power 81 kW.

The method allows comparing the emission performance of different engine families that are the most common on the European market. Such comparisons will be presented based on the large datasets that are present in the older CONOX and the newer CARES RS database.

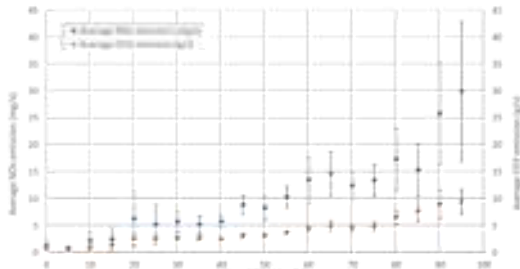


Figure 2. NO_x (and CO₂) emissions derived with the method as a function of speed, derived from remote sensing measurements on ~1700 cars equipped with the VAG 1598 cm³, 81 kW, Euro 6b diesel engine.

This work was supported by the H2020 projects uCARe (No. 815002) and CARES (No. 814966).

Thompson, G. J., Daniel, D. K., Carder, C., Marc C., Besch, M. C. and Thiruvengadam A. (2014) In-use emissions testing of light-duty diesel vehicles in the U.S. Final report prepared on behalf of International Council on Clean Transportation, May 15, 2014.

Baldino, C., Tietge, U., Muncrief, R., Bernard, Y. and Mock, P. (2017) Road tested: Comparative overview of real-world versus type-approval NO_x and CO₂ emissions from diesel cars in Europe. ICCT White Paper, September 2017.

Davison, J., Bernard, Y., Borken-Kleefeld, J., Farren, N. J., Hausberger, S., Sjödin Å., Tate, J. E., Vaughan, A.

Intercomparison of Remote Emission Sensing Methods and Validation with PEMS Measurements

M. Knoll¹, M. Penz¹, T. Rossi², H. Juchem³, C. Schmidt^{3,4}, D. Pöhler^{3,4}, S. Casadei², Y. Bernard⁵, A. Bergmann¹ and Å. Sjödin⁶

¹Institute of Electrical Measurement and Sensor Systems, Graz University of Technology, Graz, 8010, Austria

²Innovhub SSI, Stazioni Sperimentali per l'Industria, Milan, 20133, Italy

³Institute of Environmental Physics, Heidelberg University, Heidelberg, 69120, Germany

⁴Airyx GmbH, Eppelheim, 69214, Germany

⁵ICCT International Council on Clean Transportation, Berlin, 10178, Germany

⁶IVL Swedish Environmental Research Institute, Goteborg, 411 33, Sweden

Keywords: Remote emission sensing, point sampling, PEMS, validation study, CARES

Presenting author email: markus.knoll@tugraz.at

Emissions from internal combustion engine vehicles are currently not properly monitored during their lifetime. In specific, NO_x and particulate matter (PM) emissions of a small share of poorly maintained or tampered vehicles are responsible for the vast amount of emissions (Park et al., 2011, Bainschab et al., 2020). Remote emission sensing (RES) is one potential method of screening in-use vehicles bringing along the potential capability of high emitter identification. Different RES concepts exist, such as open-path RES or extractive point sampling (PS). So far, validation studies comparing these technologies are rare, especially under real-world conditions. As a part of the EU H2020 project CARES (City air remote emission sensing - <https://cares-project.eu/>) a detailed validation study was conducted during the city demonstration campaign in Milan (September-October 2021) which compares and evaluates the different methods.

A newly developed PS system was co-located alongside a commercial open-path RES system (EDAR, Hager Environmental & Atmospheric Technologies (HEAT)) during 8 days of the measurement campaign. Emission factors (EF) for several thousand vehicles could be derived using both systems. The PS system features the determination of black carbon (BC), particle number (PN) concentration and NO_x EFs with high-grade equipment such as a newly developed black carbon tracker, a custom-developed diffusion charger (Schriefl et al., 2020) and an ICAD (Airyx GmbH). In addition to the co-location, validation measurements with a portable emission measurement system (PEMS) (AVL Move) were conducted to compare the performance of the RES methods. More than 100 test drives were performed with several test vehicles equipped with PEMS.

A good agreement was found for average NO_x emissions of the overall measured fleet between PS and HEAT with mean values of 4.63 and 4.44 g/kg fuel (median: 1.11 and 1.04 g/kg fuel), respectively. In case of PM emissions, BC EFs from PS and PM EFs from HEAT were compared. Comparable average values (115.46 and 85.77 mg/kg fuel) were determined. In contrast, median values (16.25 and 0.46 mg/kg fuel) show a high deviation between the two systems with a factor of 35 between them. A more detailed view of individual measurements was performed with PEMS test drives. In case of NO_x emissions, mean and median EFs determined by PS and

HEAT agree very well with the PEMS result. Looking at the measurement precision, the PS system delivers a better performance for individual measurements compared to the HEAT system (Figure 1). For PN, a high correlation ($R^2 = 0.8$, excluding outliers) between PEMS and PS EFs was found (with median values of 0.09 and $0.10 \cdot 10^{15}$ particles/kg fuel). The outcome of the investigations provides more insights into the capabilities of the different systems for real world emission screening and the potential identification of high emitter.

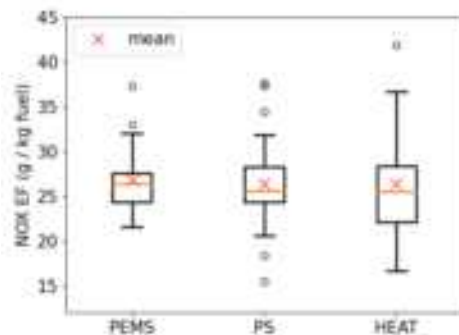


Figure 1. Boxplot of NO_x EFs of the PEMS equipped test vehicles and the two RES systems (PS, HEAT).

This work is conducted in the framework of the H2020 project CARES with grant agreement No. 814966.

Park, S. S., Kozawa, K., Fruin, S., Mara, S., Hsu, Y.K., Jakober, C., Winer, A., and Herner, J. (2011) *Emission Factors for High-Emitting Vehicles Based on On-Road Measurements of Individual Vehicle Exhaust with a Mobile Measurement Platform*. Journal of the Air and Waste Management Association.

Bainschab, M., Schriefl, M. A., and Bergmann, A. (2020) *Particle number measurements within periodic technical inspections: A first quantitative assessment of the influence of size distributions and the fleet emission reduction*. Atmospheric Environment: X.

Schriefl, M.A., Nishida, R.T., Knoll, M., Boies, A.M., Bergmann, A. (2020) *Characterization of particle number counters based on pulsed-mode diffusion charging*. Aerosol Science and Technology.

3.4 TAP.05. Vehicle greenhouse gas emissions, energy consumption, vehicle and fuel life-cycle analysis.

Electric and conventional vehicles energy consumption under various traffic conditions

S. Mamarikas¹, S. Doulgeris¹, Z. Samaras¹ and L. Ntziachristos¹

¹Department of Mechanical Engineering, Aristotle University, P.O. Box 458, 54124 Thessaloniki, Greece

Keywords: Battery Electric Vehicles, energy consumption, driving cycles, average speed approach
Presenting author email: samarik@meng.auth.gr

As more Battery Electric Vehicles (BEVs) start to penetrate traffic streams (EEA 2020), a main research question is whether the traffic conditions that used to be considered as optimum, in energy consumption terms, for Internal Combustion Vehicles (ICEVs) continue to be so for BEVs. BEVs in principle seem to exhibit a different energy consumption pattern compared to ICEVs, while they are being driven under various traffic conditions. Main differentiation factors appear to be the regenerative braking and the efficiency characteristics of their powertrain (Gao et al., 2007, Huynh & Hsieh, 2018).

In this context, the target of the present paper is to evaluate the energy performance of BEVs under many traffic states and to identify those traffic patterns that result into optimum energy behaviour. The specific effect of congestion and traffic measures on the energy consumption of BEVs is also approached. The overall analysis is conducted comparatively to the according performance of ICEVs.

BEVs and ICEVs energy performance was revealed through a simulation process, in which validated instantaneous power-based models were used to characterize their consumption over more than 100 driving cycles. Then, consumption estimates of the current study became suitable for expressing the performance of powertrains at a macroscopic traffic level, with consideration of the average speed as the explanatory variable.

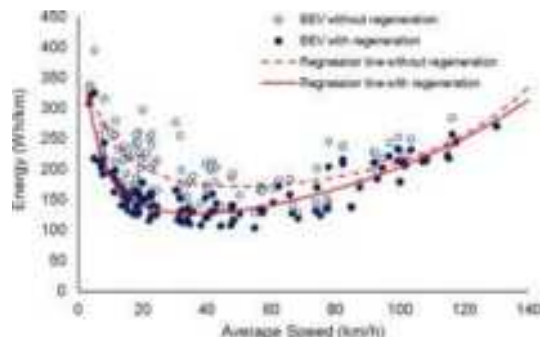


Figure 1. BEVs energy consumption as a function of average speed. The effect of braking regeneration on consumption is highlighted.

The impact of a range of traffic conditions on the energy consumption of BEVs is shown in Figure 1. Similar figures were reproduced for ICEVs. BEVs minimum consumption is identified at low-speed urban traffic, mainly because of regenerative braking and high

part-load powertrain efficiency. This differs to ICEVs that exhibit their optimum fuel consumption at higher speeds, mostly experienced in suburban and rural environments.

Focusing more on traffic conditions, congestion mitigation at urban speeds brings minimal energy gains for BEVs as depicted in Figure 2. But, the gain becomes significant at higher speed regions, where the overall influence of regeneration is reduced.

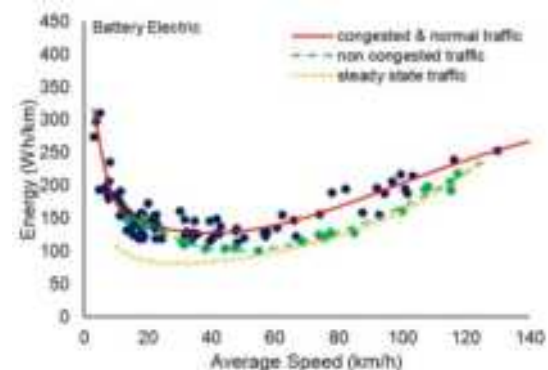


Figure 2. BEVs energy consumption over various speeds for congested & normal, non-congested and steady-state traffic

Finally, traffic measures, such as Urban Traffic Control, roundabouts and other traffic calming interventions are beneficial for BEVs energy consumption, but the achieved relative gains are lower than ICEVs.

This research was supported by the Hellenic Foundation for Research and Innovation (HFRI) under the HFRI PhD Fellowship grants (Fellowship Number:1041). This work has been published in the Transportation Research Part D: Transport and Environment. doi.org/10.1016/j.trd.2022.103231

- EEA, 2020. New registrations of electric vehicles in Europe. last accessed 27/1/2022 European Environmental Agency Data
Gao, Y., Chu, L., & Ehsani, M. (2007). Design and control principles of hybrid braking system for EV, HEV and FCV. In 2007 IEEE Vehicle Power and Propulsion Conference (pp. 384-391). IEEE.
Huynh, T. A., & Hsieh, M. F. (2018). Performance analysis of permanent magnet motors for electric vehicles (EV) traction considering driving cycles. Energies, 11(6), 1385.

3.5 TAP.06. Vehicle-emission modelling and measurements and impact assessment of emission regulations.

Updated vehicle emission inventory in China

Yifan Wen, Min Liu, Xiaomeng Wu, Shaojun Zhang, Ye Wu

School of Environment, State Key Joint Laboratory of Environment Simulation and Pollution Control, Tsinghua University, Beijing, 100084, China

Keywords: nitrogen oxide (NO_x), emission factors, emission inventory, temperature impacts, localization.
Presenting author email: wenyf@mail.tsinghua.edu.cn

China's total vehicle population (excluding motorcycles) increased from 15 million in 2000 to 273 million in 2020, and have created substantial concerns regarding the adverse impacts on air quality, public health and energy systems. Vehicle emission model serves as an important tool to estimate emission factors (EF) of various vehicle categories and quantify on-road emissions. However, recent field measurements and modeling studies conducted in various countries have noted discrepancies in annual and seasonal trends between the real-world vehicle emissions and model estimates. Ambient conditions (e.g., temperatures) have recently been identified as an important source of the large variability in real-world emissions for both light-duty gasoline vehicles (LDGVs) and heavy-duty diesel trucks (HDDTs) vehicles (Grange et al., 2019). Also, several studies deduced that the real-world emissions from in-use HDDTs exceed emission limits due to the failures in aftertreatment and unideal driving conditions, thus, rendering the traditional supervision methods ineffective.

EMBEV model is the archetype of the on-road transportation chapter of China National Emission Inventory Guidebook. In the latest update of EMBEV model (V2.0), we introduced the start emission sub-model and modified temperature correction modules utilizing localized measurement data and longitudinal trip-chain profiles to improve the territorial and seasonal resolutions of EFs and inventory modelling in China (Wen et al., 2021). Typically, we collected a large sample of real-world plume chasing data from more than 6000 vehicles to better represent the emission levels of in-use HDDTs and cover a wide range of ambient and driving conditions.

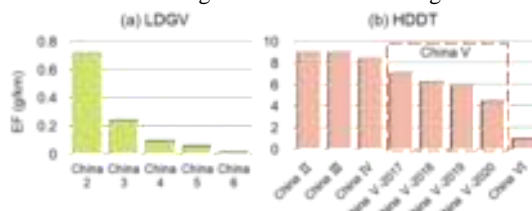


Figure 1. NO_x emission factors by emission standard and model year for LDGV and HDDT fleet

As shown in Fig 1, NO_x EFs of LDGVs declined significantly with the updates of emission standards, while NO_x EFs from China II to China IV HDDTs were not significantly improved even with the widely application of selective catalytic reduction (SCR) systems since China IV. This phenomenon was primarily due to the unsatisfactory SCR working performance caused by low exhaust temperature, which is rather frequent for low-speed urban driving conditions. Moreover, we witnessed

an obvious decreasing trend in NO_x EFs of China V HDDTs with model year, reflecting the improved in-use compliance for HDDT fleet in China.

EFs of key fleets in China show significant regional and seasonal variations affected by ambient temperature (Fig 2). The temperature dependence of LDGVs is mainly dominated by cold start emissions, while HDDTs are mainly affected by aftertreatment performance. The annual average NO_x EFs of LDGVs and HDDTs in Heilongjiang province are 1.3 and 1.9 times as large as those in Hainan province, respectively. In total, the ratio of vehicular NO_x emissions in Jan and July, 2019 varies from 1.1 (Hainan) to 2.0 (Hebei) among various provinces in China.

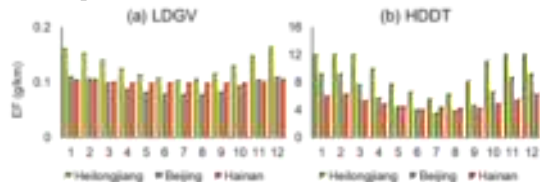


Figure 2. Monthly fleet average NO_x emission factors of key fleets in three typical provinces in China

Fig 3 shows the total vehicle NO_x emissions in China estimated by the old and latest version of EMBEV model (i.e., V1.0 and V2.0) and COPERT model. The gaps between estimations of various models enlarge with the phase-in of Euro IV and V HDDTs, revealing the importance of real-world supervision for in-use vehicles and the timely update of vehicle emission models based on localized vehicle measurements.

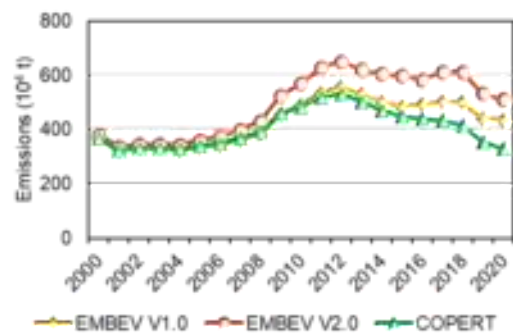


Figure 3. Estimated total vehicle NO_x emissions in China based on EMBEV and COPERT model

- Grange, S., Farren, N., Vaughan, A., et al. (2019) *Environmental science technology*, 53, 6587-6596.
Wen, Y., Zhang, S., He, L., et al. (2021) *Atmospheric Environment*, 245, 118040.

Long-term trends of black carbon and particle number concentrations and vehicle emission factors in Stockholm

P. Krecl¹, C. Johansson^{2,3}, M. Norman³, S. Silvergren³ and L. Burman³

¹Graduate Program in Environmental Engineering, Federal University of Technology, Londrina, 86036-370, Brazil

²Department of Environmental Science, Stockholm University, Stockholm, 10691, Sweden

³Stockholm Environment and Health Administration, Stockholm, 10420, Sweden

Keywords: ultrafine particles, nanoparticles, on-road emissions, air pollution.

Presenting author email: patriciaak@utfpr.edu.br

Given the detrimental effect on human health, the World Health Organization has recommended to systematically measure black carbon (BC) and ultrafine particle number (PN) concentrations (WHO, 2021). These concentrations are typically high in traffic environments (e.g., Krecl *et al.*, 2017) and, thus, curbing vehicle emissions is of outmost importance to reduce population exposure.

We analyzed the trends of BC and PN concentrations and vehicle emission factors (EF) in Stockholm, Sweden. Hourly measurements were conducted at Hornsgatan (SHO, street canyon) and Torkel (STK, urban background) sites in the periods 2013-2019 (BC) and 2009-2019 (PN). Hourly meteorological variables were measured at Högdalen station.

Pollutant concentrations were meteorologically normalized (*rmweather* package), and used to estimate the linear trends by the non-parametric Theil-Sen method (Krecl *et al.*, 2021). EF were determined based on the street increment of ambient concentrations (curbside minus urban background concentrations), traffic volume and dilution rate. The latter was calculated by inverse modeling with the Operational Street Pollution model (OSPM).

As expected, the street canyon was more polluted than the urban background site (mean values of BC and PN in 2019: 0.75 vs. 0.35 $\mu\text{g m}^{-3}$ and 1.37×10^4 vs. $6.31 \times 10^3 \text{ cm}^{-3}$). A decreasing trend in BC and PN concentrations was found for all cases (Table 1). In 2013-2019, the reduction was higher for BC than for PN. The small PN reduction at STK suggests other sources than traffic contributing to PN at the urban background site.

Table 1. Trends in BC and PN concentrations (% yr⁻¹) and 95% confidence intervals (in parentheses).

Site	BC [2013-2019]	PN [2013-2019]	PN [2009-2019]
SHO	-9.4 (-9.5, -9.3)	-4.9 (-7.5, -4.0)	-5.0 (-5.7, -5.2)
STK	-7.2 (-8.1, -5.9)	-0.5 (-1.0, 0.3)	-0.8 (-1.0, -0.6)
Str. inc.	-10.8 (-10.9, -10.7)	-6.7 (-8.6, -5.8)	-7.2 (-7.4, -6.4)

Table 2 displays mean EF for the fleet calculated with inverse modelling (real-word) and based on the HBEFA 4.2.2 database.

Table 2. Annual mean EF for the vehicle fleet.

Year	EF _{BC} [mg veh ⁻¹ km ⁻¹]	EF _{PN} [10^{12} veh ⁻¹ km ⁻¹]	^a HBEFA	^b Real-world
2009	16.0	-	24.4	424.3
2010	14.6	-	22.4	418.8
2011	13.1	-	20.4	351.7
2012	11.0	-	17.2	336.6
2013	9.7	24.4	15.1	369.1
2014	8.3	24.4	13.0	379.1
2015	6.9	23.0	10.7	219.4
2016	5.7	14.7	8.7	222.8
2017	4.9	14.6	7.4	182.3
2018	4.1	15.8	6.2	182.3
2019	3.5	8.4	5.1	166.5

^aNon-volatile particles, diameter $d_p \geq 23 \text{ nm}$. ^b $d_p \geq 4 \text{ nm}$.

There was a decreasing trend in EF due to the progressively stringent Euro emission standards, especially when diesel particulate filters (DPF) were fitted in Euro 5, 6 and VI vehicles. Real-world EF_{BC} were a factor of 2.4-4.8 higher than the HBEFA-derived EF_{BC} (Table 2). Direct comparison between real-world and HBEFA EF_{PN} is difficult due to different lower cut-off sizes and measurement protocols. In 2013-2019, the reduction was similar for all EF (64-66%), except real-world EF_{PN} (55%). This difference could be explained by DPF being less efficient for small d_p (Krecl *et al.*, 2017).

Thus, EF from the HBEFA database should be revised for BC and PN since they are used to compile official national inventories for the road transport and assess their associated health impacts.

The BC monitoring was partly financed by the Swedish EPA. The work was funded by CNPq Brazil (grant 305145/2020-7) for PK, and the European Union's Horizon 2020 programme (nPETs, grant 954377) for her co-authors.

Krecl, P., Johansson, C., Targino, A.C., Burman, L. and Ström, J. (2017) *Atmos. Env.* **165**, 155-168.

Krecl, P., Harrison, R.M., Johansson, C., Targino, A.C., Beddows, D.C., Ellermann, T., Lara, C. and Ketzel, M. (2021) *Env. Poll.* **290**, 118105.

WHO (2021) *WHO Global Air Quality Guidelines*.

3.6 TAP.07. Non-road emissions.

Train type effect on nanoparticles on an underground metro platform in Stockholm

M. Tu¹, L. Bard¹, and U. Olofsson¹

¹Department of Machine Design, KTH Royal Institute of Technology, S-100 44 Stockholm, Sweden

Keywords: nanoparticles, metro, emission, nPETS

Presenting author email: minghuit@kth.se

Nanoparticles or ultrafine particles are airborne particles whose aerodynamic diameters are not larger than 100 nm. They have been frequently mentioned due to their adverse effects on human health (Donaldson et al., 2001). However, there are rare nanoparticle studies in multi-transport environments because of their complex environmental conditions.

As a part of the nPETS project, the present work focused on nanoparticle concentration and size distribution based on field measurement on the underground metro platform. The field measurement was performed on the Tekniska Högskolan underground metro platform in Stockholm, and the measurement period was between September 2021 and March to June 2022.

The TSI FMPS 3091 (TSI, 2023) was used during the measurement. Its measurement range is between 5.6 and 560 nm with 1Hz time resolution. The mean value and standard deviation region of the measurement results is shown in Figure 1.

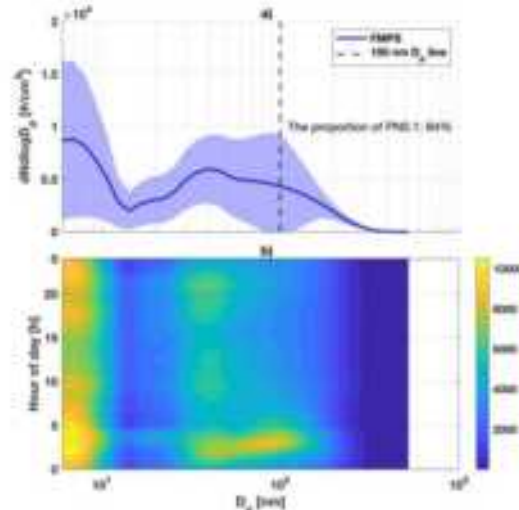


Figure 1. Sub-fig a shows the particle number size distribution. The shaded area is the standard deviation region; sub-fig b shows the average particle size distribution during the day.

The distribution of the nanoparticle emission over the hour of the day has also been investigated, as shown in Figure 1. It indicates that the maximum concentration appeared between hours zero and four. As mentioned in previous work, a possible explanation can be the night maintenance work (Tu and Olofsson, 2021).

The other main finding is the effect of the C30 train fraction of the total hourly train frequency on particle

emissions. Currently, three types of metro trains are operating in the Stockholm metro system: CX, C20 and C30 from old to new. The CX and C30 train fraction effects have been studied using a mixed linear model. As shown in Figure 2, with the increase in the train frequency, the PN0.1 level would decrease if having a higher CX fraction or lower C30 fraction.

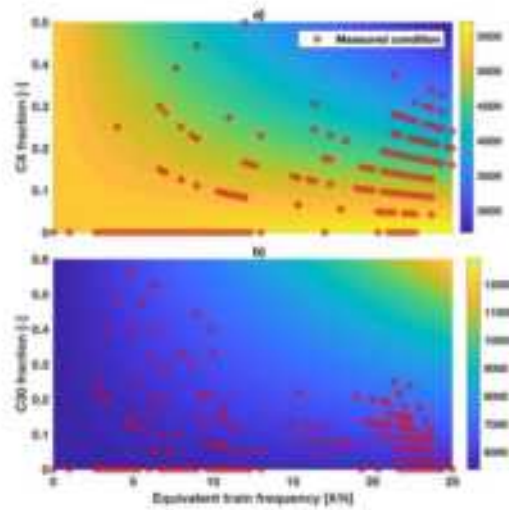


Figure 2. Based on the mixed linear model results, sub-fig a and b show the variation of PN0.1 levels under different conditions of train frequency, CX train fraction, and C30 train fraction. The red points show the actual conditions that happened during the measurement.

The nPETS project is funded by the European Union's Horizon 2020 programme under grant No 954377.

Donaldson, K., Stone, V., Clouter, A., Renwick, L., MacNee, W., 2001. Ultrafine particles. Occup. Environ. Med. 58, 211–216. <https://doi.org/10.1136/oem.58.3.211>
TSI, 2023. Fast Mobility Particle Sizer (FMPS) 3091 [WWW Document]. TSI.com. URL [https://tsi.com/Products/Particle-Sizers/Fast-Particle-Sizer-Spectrometers/Fast-Mobility-Particle-Sizer-\(FMPS\)-3091](https://tsi.com/Products/Particle-Sizers/Fast-Particle-Sizer-Spectrometers/Fast-Mobility-Particle-Sizer-(FMPS)-3091) (accessed 2.22.23).

Tu, M., Olofsson, U., 2021. PM levels on an underground metro platform: A study of the train, passenger flow, urban background, ventilation, and night maintenance effects. Atmospheric Environ. X 12, 100134. <https://doi.org/10.1016/j.aeaoa.2021.100134>

Toxicity of particle emissions from car and train brake materials

A.T. Juárez-Facio¹, M. Intronà¹, L. Bard², M.H. Tu², S.S. Steimer¹, U. Olofsson² and K. Elihn¹

¹Department of Environmental Science, Stockholm University, 10691 Stockholm, Sweden

²KTH Royal Institute of Technology, Stockholm, Sweden

Keywords: Air-Liquid Interface exposure, airborne particles, brake wear, non-exhaust emissions.

Presenting author email: ana.juarez@aces.su.se

Road traffic is one of the main emitters of air pollution in cities. An important part of these emissions comes from non-exhaust sources like brakes, tires, road wear, and road dust resuspension (Amato, 2018).

Brake particles represent an important part of non-exhaust emissions. Their characteristics depend on the speed, load, temperature, and friction pair materials. The metallic components of the brakes may cause their toxic effects (Karlsson et al., 2005; Puisney et al., 2018). Trains are also known to emit airborne particles during braking. Studies have found high particle concentrations at underground stations (Tu et al., 2019) and inside train cabins (Cha et al., 2018).

This work aimed to evaluate the toxicity (*in vitro*) of fresh airborne particles from 4 car brake materials and 2 train brake materials using an alveolar cell line (A549) exposed at the air-liquid interface (ALI).

The particle generator (a tribometer using contact pressure 0.9 MPa, velocity 4 m/s) was connected to the ALI exposure system, as shown in Figure 1. Cells were exposed to airborne particles for 2h, and were then incubated for 24h before measuring the cell viability (Alamar Blue™ assay).



Figure 1. ALI system used to test the toxicity of airborne brake particles in the tribology laboratory.

Results

Brake particles decreased cell viability more than the gaseous emissions (control) in three of the car brakes (FM2, FM3, and FM4) and one of the rail brakes (C6), as shown in Figure 2. The brakes have different metal compositions: FM1 and FM2 have a low metal content and are Cu-free, FM3 is Cu-enriched, and FM4 is non asbestos organic (NAO) and Cu-free. In the train brakes, there is mainly Ca in C6, and Fe in C20. Moreover, the estimated exposure dose of the cells was around 4-6 $\mu\text{g}/\text{cm}^2$. Further analyses will be done to better understand

the toxicity of these materials by testing different particle fractions using submerged exposures.

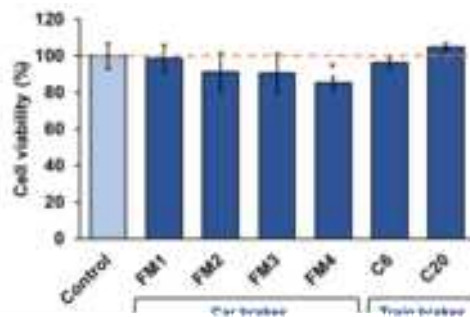


Figure 2. Cell viability of A549 cells exposed to PM_{2.5} from different car and train brake materials for 2h and incubated for 24h. Results are expressed as mean \pm SD of at least 3 independent experiments.

Acknowledgments

This work was supported by the European Commission's Horizon 2020 research and innovation program: nPETS (grant agreement No 954377, <https://www.npets-project.eu/>), aimed at studying the sub-100 nm particles emitted from transport.

References

- Abbasi, S., Jansson, A., Sellgren, U., Olofsson, U., 2013. Particle Emissions From Rail Traffic: A Literature Review. *Crit. Rev. Environ. Sci. Technol.* 43, 2511–2544.
- Amato, F., 2018. Non-Exhaust Emissions - 1st Edition URL <https://www.elsevier.com/books/non-exhaust-emissions/amato/978-0-12-811770-5>.
- Cha, Y., Tu, M., Elmgren, M., Silvergren, S., Olofsson, U., 2018. Factors affecting the exposure of passengers, service staff and train drivers inside trains to airborne particles. *Environ. Res.* 166, 16–24.
- Karlsson, H.L., Nilsson, L., Möller, L., 2005. Subway particles are more genotoxic than street particles and induce oxidative stress in cultured human lung cells. *Chem. Res. Toxicol.* 18, 19–23.
- Puisney, C., Baeza-Squiban, A., Boland, S., 2018. Mechanisms of Uptake and Translocation of Nanomaterials in the Lung. *Adv. Exp. Med. Biol.* 1048, 21–36.
- Tu, M., Cha, Y., Wahlström, J., Olofsson, U., 2019. Towards a two-part train traffic emissions factor model for airborne wear particles. *Transp. Res. Part Transp. Environ.* 67, 67–76.

Brake wear ultrafine particle emissions from a light duty vehicle under real driving conditions

G.Q. Vroom¹, N.E. Ligterink¹

¹Department of Sustainable Transport and Logistics, TNO, The Hague, South Holland, 2595 DA, the Netherlands

Keywords: non-exhaust emissions, ultrafine particle emissions, brake wear, real-world conditions.
Presenting author email: quinn.vroom@tno.nl

Tailpipe emissions have been reducing significantly due to stringent particle number emission limits, while non-exhaust emissions such as brake wear have not yet been regulated. Currently, the majority of small air-borne road side particles, relevant for health, are from wear. Laboratory setups, like in current Euro 7 proposal addresses brakes and tyres particle emissions, but do not fully reflect the real world impact. The magnitude of the brake wear emissions depends on the temperature of braking system, and thus on cooling, and most work found in literature applies a methodology involving either laboratory testing (Chasapidis, 2018) with artificial cooling wind conditions or on-road testing with an (semi) enclosed setup (Hagen, 2019) pumping air through the system at a constant rate, thereby influencing the temperature behaviour of the system. At the same time health studies show that there are strong indicators that exposure to ultrafine particles, particles up to 100nm in size, causes negative effects on the cardiovascular system and the respiratory tract (Health Council, 2021). On road temperature and cooling need to be included.

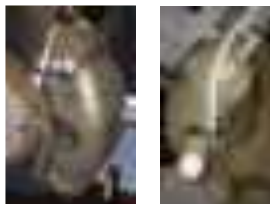


Figure 1. Thermocouple inserted in the brake pad (left) and particle sampling point on the bottom of the calliper (right).

A passenger vehicle was equipped with a K-type thermocouple (brake pad, figure 1), a TEN AEM broadband particle counter (calibrated for 50-80nm particles) and OBD logging. This simple and fully open test setup allowed for real world measurements, without influencing the heat transfer of the braking system.

The test campaign involved multiple sessions in various conditions, ranging from slow urban to fast highway driving in the Netherlands. The time-based data showed indications of a rising trend in brake wear particle number concentration peaks with rising brake system temperature during similar braking events, see figure 2. Further analysis into this dependency was done by extracting the peaks in the calculated braking power, link them to the corresponding peaks in the particle number concentration and the brake system temperature. In four temperature bins, the particle number concentration was

plotted against the braking power and a quadratic curve was fitted (in red), see figure 3.

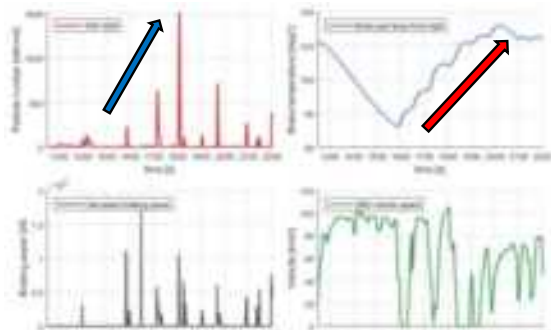


Figure 2. Brake PN (red), brake temperature (blue), braking power (black) and vehicle speed (green) plotted over time.

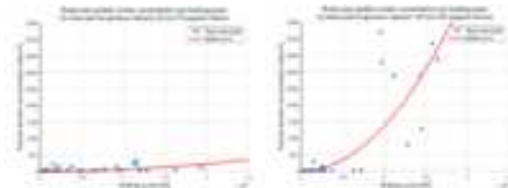


Figure 3. Brake PN vs. braking power for the lowest (left) and the highest (right) temperature bin.

The results show a clear increase in ultrafine particle concentration when the brake pad temperature increases and even a strong indication for a direct link between brake system temperature, applied braking power and ultrafine brake particle emissions, all under real driving conditions. However, for a statistically strong direct dependency further research is needed. Future steps involve measuring background particles and estimating total ultrafine particle number emissions.

This work was funded internally by TNO.

Health Council of the Netherlands (2021) *Risks of ultrafine particles in the outside air*, No. 2021/38, The Hague, September 15, 2021.

Chasapidis, L. et al (2018) *Study of brake wear particle emissions of a minivan on a chassis dynamometer*, Emission Control Science and Technology, 4, 271-278.

zum Hagen, F.H.F. et al (2019) *On-road vehicle measurements of brake wear particle emissions*, Atmospheric Environment, 217, 116943.

A Novel Simulation Approach for Non-Exhaust Particle Emissions

L. Landl¹, S. Hausberger¹

¹Institute for Sustainable Propulsion Systems, University of Technology, Graz, Styria, 8010, Austria

Keywords: Non-Exhaust Emissions, PM, PN, Road Traffic, Simulation

Presenting author email: landl@ivt.tugraz.at

Particle emissions from brake-, tyre- and road-wear have increased with traffic volumes while exhaust particle emissions have decreased considerably due to the introduction of strict exhaust standards requiring particle filters for most new vehicle categories.

Thus, the share of the "non-exhaust particles" (NEP) in traffic emissions is increasing sharply. In addition to the increasing share, the composition of NEP is relevant for the environmental impact. Tyre-wear produces e.g. large quantities of micro plastics, which are also mixed with additives from the tyre rubber. In the case of brake wear, ultra-fine particles are produced from binding agents, especially at high temperatures in the brake system, and abrasion of brake pads and discs generally occurs during every braking process.

Due to the increasing importance of NEP emissions, a novel method was developed at TU Graz for data collection and simulation of emission factors of tire-, road- and brake wear PM and PN emissions.

The new simulation method was developed in a Horizon 2020 project called uCARe (<https://www.project-ucae.eu/>) and further optimised in a project for BAFU (Hausberger, 2023). The method is integrated in the vehicle emission model PHEM from TU Graz, which is inter alia used to calculate all base emission factors for exhaust emissions for the HBEFA (www.hbefa.net).

The model PHEM calculates the power at the wheels and at the mechanical brakes as well as corresponding rotational speeds for vehicles using the equations of longitudinal dynamics. The brake wear emissions are interpolated from characteristic polygons which define the emission flow over the product of mechanical brake power (P) and disc speed (Ω)^{0.5}, as shown in Figure 1 for PN₂₃.

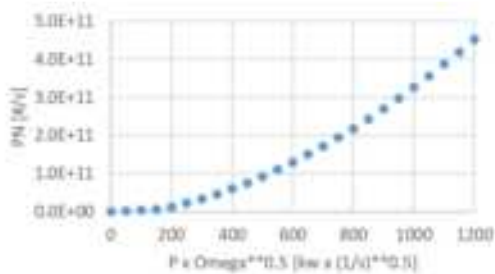


Figure 1. Characteristic polygon for LDV brake wear PN₂₃ emissions

The PM and PN emissions from tire-wear are interpolated from characteristic polygons defining the emission flow over transmitted power between wheel and road. Due to the limited data, the road wear emissions are calculated

with a constant factor from tire wear results. All calculations run in 1 Hz resolution.

The characteristic polygons are obtained from measured emission data by averaging the data for each section of the x-axis. This allows the use of a broad range of data sources, such as the WLTP brake test data and thus a systematic data collection and model update in future. The inclusion of more explaining parameters in the model, such as brake temperatures and tire slip is planned when sufficient test data is available.

The equations of longitudinal dynamics are general valid and allow the simulations of any combination of vehicle, loading, speed trajectory and road gradients. Thus, the model PHEM offers a much higher resolution compared to other approaches.

Figure 2 shows e.g. results for motorway free-flow compared to dense urban driving, each for flat road and for +2% and -2% gradient respectively. Not surprising, brake wear emissions are almost zero on the free highway but dominate PM10 NEP emissions in dense urban traffic. Brake power and emissions are lower when driving uphill than when driving downhill. Thus, in dense urban traffic the total NEP emissions are lower in uphill than in downhill driving. On the motorway, more power is needed at the wheels when driving uphill than when driving downhill, so that the total NEP emissions there are higher for positive gradients.

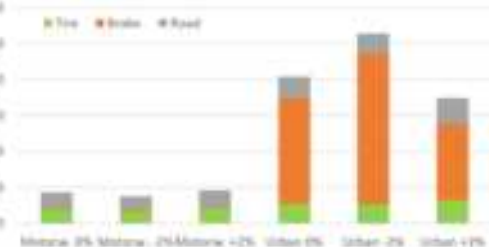


Figure 2. Non-Exhaust emissions simulated for a passenger car for three different traffic situations

In the paper, we present the approach and the corresponding data base and vehicle tests performed. We show model results for pure electric, hybrid and conventional vehicles including also exhaust particle emissions for comparison.

This work was supported by H2020 and BAFU.

Hausberger S., Landl L.: Simulation of Non-Exhaust Particle Emissions; funded by BAFU; TU Graz 2023

3.7 JS.08. Air pollutant and GHG emissions, water contaminants, ambient and underwater noise and vessel-induced mixing.

Remote detection of ship exhaust plumes from different marine fuels on board a research vessel in the Baltic Sea region using single-particle mass spectrometry

J. Schade^{1,2}, J. Passig^{2,3}, E.I. Rosewig², H. Osterholz⁴, J. Hovorka⁵, D. Schulz-Bull⁴, R. Zimmermann^{2,3} and T.W. Adam^{1,3}

¹Faculty of Mechanical Engineering, Institute of Chemistry and Environmental Engineering, University of the Bundeswehr Munich, Neubiberg, 85577, Germany

²Joint Mass Spectrometry Center/Analytical Chemistry, University of Rostock, Rostock, 18059, Germany

³Joint Mass Spectrometry Center/Cooperation Group “Comprehensive Molecular Analytics” (CMA), Helmholtz Zentrum München, Neuherberg, 85764, Germany

⁴Leibniz-Institute for Baltic Sea Research Warnemünde (IOW), Rostock, 18119, Germany

⁵Faculty of Science, Institute for Environmental Studies, Charles University, Prague, 128 01, Czech Republic

Keywords: single-particle mass spectrometry, ship emissions, sulphur emission control area (SECA), ambient air measurement.

Presenting author email: julian.schade@unibw.de

Ship emissions are a major cause of global air pollution and have a significant impact on climate and human health. To reduce emissions and improve air quality, several sulphur emission control areas (SECAs) have been established worldwide to further improve air quality in densely populated coastal areas and preserve vulnerable ecosystems. Consequently, ships in SECAs are only authorized to operate on low-sulphur fuels or use exhaust after-treatment devices such as exhaust gas scrubbers. To comply with these regulations at sea, sophisticated measurement systems are needed. In this paper an approach to remotely detect and characterize ship exhaust plumes through on-board measurements from a research vessel in the Baltic Sea is presented.

The ship exhaust plumes are detected by particle number concentration and their size distribution through CPC and SMPS+CPC measurements and qualitatively analysed by on-line single-particle mass spectrometer (SPMS). Passig *et al* (2020) showed that the ionization method using KrF excimer laser with 248 nm wavelength, also used in this study, exhibits high sensitivity especially for iron but also for other transition metals. In particular, this high sensitivity of the measurement method to health-relevant metals, which are contained in PM from ships with exhaust gas scrubbers and thus serve to distinguish the fuels used, is exploited.

The method of SPMS and the device used here are described in more detail in the work of Li *et al* (2011) and Passig *et al* (2021). Essentially, single particles in a size range of 0.2 - 2.5 μm can be detected and analysed. In contrast to gas phase measurements, a measurement by SPMS can easily be performed from several kilometres distance in land-based measuring stations, but these measurements are strongly dependent on wind direction (Passig *et al*, 2021). To overcome the dependency on wind direction, the measurements for this study were performed on board the German research vessel *Elisabeth Mann Borgese*. The plumes of passing ships could be recorded and analysed from a distance of several kilometres. As an example, a single event is listed in Fig. 1, which suggests the use of HFO in conjunction with an exhaust gas scrubber. These measurements show that SPMS can be a powerful tool for ship exhaust monitoring.

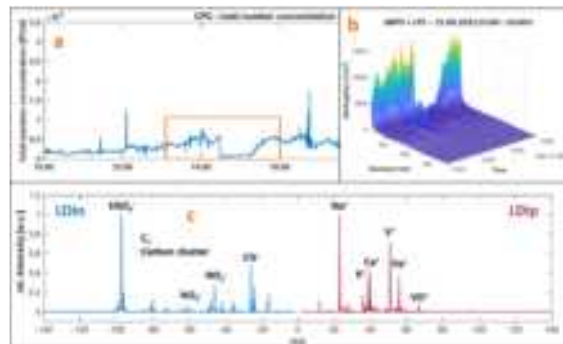


Figure 1. (a) Total number concentration from CPC measurements showing single pollution events from ship exhaust plumes over time/a day. (b) Size distribution from SMPS+CPC in the marked time frame showing a single ship exhaust plume with an additional mode at around 100 nm at 14:00 h. (c) Average mass spectrum from the ship exhaust plume indicating the use of HFO due to signals of V/Fe/Ni in the positive mass spectrum as well as sulphate in the negative mass spectrum.

This work was funded by the DFG (German Research Foundation) – 471841824 (project “PlumeBaSe”), Czech Science Foundation (22-03426L), and by dtec.bw – Digitalization and Technology Research Center of the Bundeswehr (project LUKAS). dtec.bw is funded by the European Union – NextGenerationEU.

Passig, J., Schade, J., Rosewig, E.I., Irsig, R., Kröger-Badge, T., Czech, H., Sklorz, M., Streibel, T., Li, L., Li, X., Zhou, Z., Fallgren, H., Moldanova, J. and Zimmermann, R. (2020) *Atmos. Chem. Phys.* **20**, 7139-7152.

Li, L., Huang, Z., Dong, J., Li, M., Gao, W., Nian, H., Fu, Z., Zhang, G., Bi, X., Cheng, P., Zhou, Z., (2011) *Int. J. Mass Spectrom.* **303**, 118-124.

Passig, J., Schade, J., Irsig, R., Li, L., Li, X., Zhou, Z., Adam, T. and Zimmermann, R. (2021) *Atmos. Meas. Tech.*, **14**, 4171-4185

Ammonia as a Marine Fuel Towards Decarbonization: Emission Control Challenges

G. Voniati, A. Dimaratos, G. Koltsakis, L. Ntziachristos

Laboratory of Applied Thermodynamics, Department of Mechanical Engineering, Aristotle University of Thessaloniki, 54124 Thessaloniki, Greece

Keywords: shipping, decarbonization, GHG, ammonia, emission control, NO_x, N₂O
gk111@auth.gr (G. Koltsakis), adimaratos@auth.gr (A. Dimaratos)

Maritime transport emitted 1,056 million tons of Carbon Dioxide (CO₂) in 2018 and is responsible for almost 3% of global Greenhouse Gas (GHG) emissions (IMO, 2020). In addition, it accounts for 24% of Nitrogen Oxides (NO_x), 24% of Sulphur Oxides (SO_x) and 9% of Particulate Matter (PM) emissions in the European Union (EU) (EMSA, 2021).

According to the initial IMO strategy, GHG emissions shall be reduced by at least 50% by 2050 (compared to 2008), aiming at complete decarbonization of the maritime sector by 2100 (IMO, 2018). Latest meetings of the IMO's Marine Environment Protection Committee (MEPC) have revised the targets, setting the complete decarbonization goal for 2050 (IMO 2023). Moreover, the global sulphur cap limits the fuel sulphur content to 0.5%, with a separate 0.1% limit in Sulphur Emission Control Areas (SECAs). In parallel, NO_x emissions shall comply with Tier III requirements in Emission Control Areas (ECAs) and Tier II globally.

Among alternative fuels with low or zero carbon content (LNG, LPG, methanol, biofuels and hydrogen), ammonia (NH₃) is a promising solution to limit carbon emissions from the maritime sector due to several advantages such as high energy density and relatively easy storage (Rodriguez et al., 2022).

Ammonia combustion produces three main emission species: unburned NH₃, NO_x and Nitrous Oxide (N₂O) (Rodriguez et al., 2022). The latter is a GHG with Global Warming Potential (GWP) almost 300 times higher compared to CO₂ (Chai et al., 2021), therefore even small concentrations of N₂O may counterbalance the benefit of CO₂ reduction.

In the present study, commercial catalytic devices are examined, studying the potential reduction of NO_x and NH₃, as well as the formation of N₂O in the catalytic system. However, the trial-and-error approach to design emission control systems is cost-prohibitive, particularly for a large 2-stroke engine. Therefore, it is crucial to develop accurate predictive models of aftertreatment systems that can guide optimal design in the early stages, which is the primary objective of this study.

In this work, experiments are first conducted to derive the chemical kinetics information for two relevant catalyst technologies, which are then incorporated into physico-chemical models. The model is subsequently utilized to examine two potential scenarios regarding the proportion of NH₃ and NO_x emissions during ammonia combustion: (1) engine-out NH₃ lower than NO_x (NH₃/NO_x<1), requiring additional NH₃ injection upstream of a Vanadium-based SCR (V-SCR) catalyst to

achieve NO_x levels below Tier III limits, and (2) excess of engine-out ammonia (NH₃/NO_x>1), where a platinum-based ammonia oxidation catalyst (AOC) is integrated into the aftertreatment system to address ammonia slip. Particular attention is given to the formation of N₂O through catalytic reduction of NO_x and oxidation of NH₃.

The outcomes of the simulations demonstrate that in both scenarios it is possible to optimize NO_x conversion to meet the strictest IMO limits with minimal NH₃ slip. Concerning N₂O, it is produced in very low levels in the case of shortage of NH₃ in the exhaust gas, while excess of NH₃ tends to selectively promote the formation of N₂O, particularly at higher NH₃ concentrations. In such cases, the CO₂ equivalent emissions are comparable to the levels of LNG engines (Pavlenko et al., 2020). Furthermore, N₂O emissions from ammonia in-cylinder combustion are expected to increase the total N₂O emissions. Thus, both sources need to be considered for the successful control of N₂O emissions, eventually via a separate additional catalyst.

Acknowledgement

This work has been funded by the ENGIMMONIA project which has received funding from the European Union's Horizon 2020 research and innovation programme under grant agreement Nr. 955413

- Chai, W. S., Bao, Y., Jin, P., Tang, G., & Zhou, L. (2021). A review on ammonia, ammonia-hydrogen and ammonia-methane fuels. In Renewable and Sustainable Energy Reviews (Vol. 147). Elsevier Ltd.
EMSA. European Maritime Transport Environmental Report 2021.
International Maritime Organization – IMO(MEPC72). Resolution MEPC.304(72), Initial IMO Strategy on Reduction of GHG Emissions from Ships, 2018.
International Maritime Organization – IMO. Fourth IMO GHG study Full report, 2020.
International Maritime Organization – IMO, Marine Environment Protection Committee (MEPC 80), 3-7 July 2023.
Pavlenko, N.; Comer, B.; Zhou, Y.; Clark, N.; Rutherford, D. The climate implications of using LNG as a marine fuel. International Council on Clean Transportation 2020.
Rodríguez, C. G., Lamas, M. I., Rodríguez, J. de D., & Abbas, A. (2022). Possibilities of Ammonia as Both Fuel and NO_x Reductant in Marine Engines: A Numerical Study. Journal of Marine Science and Engineering, 10(1).

Characterisation of emissions from marine vessel with E-methanol fuel and NOx emission control

J. Moldanova¹, H. Timonen², P. Simonen³, G. M. Lanzafame⁴, R. Verbeek⁵, H. Salberg¹, L. Barreira², K. Teinilä², S. Saarikoski², L. Markkula³, J. Kalliokoski³, B. D'Anna⁴, B. Temime-Roussel⁴, H. Hellen², L. Ntziachristos^{3,6}

¹ IVL, Swedish Environmental Research Institute, Gothenburg, Sweden

² Atmospheric Composition Research, Finnish Meteorological Institute, Helsinki, 00101, Finland

³ Aerosol Physics Laboratory, Physics Unit, Tampere University, Tampere, 33014, Finland

⁴ Aix Marseille University, CNRS, LCE, Marseille, France

⁵ Department of Sustainable Transport and Logistics, TNO, Den Haag, Netherlands

⁶ Laboratory of Applied Thermodynamics, Aristotle University of Thessaloniki, Thessaloniki, Greece

Keywords: Ship exhaust emissions, abatement measures, chemical composition

Presenting author email: jana.moldanova@ivl.se

During the last decade the International Maritime Organization's (IMO) tightened the limits for emissions of SOx and NOx from the shipping sector, targeting reduction of contributions of shipping to air pollution with both NOx, SOx and particulate matter (PM). At the same time IMO has set a target to reduce the greenhouse gas emissions from shipping by 50% by 2050. Significant part of this decrease is expected to come from increasing energy efficiency of the shipping sector, however, to achieve such high reduction under simultaneous growth of the whole sector will require significant decarbonisation. One of the promising alternative fuels is synthetic methanol (e-methanol). To assess effectiveness and secondary impacts of the regulations, impacts of the shipping emissions on air quality under different regulatory scenarios need to be investigated and this requires good knowledge of impact of the deployed abatement measures on emissions of both the targeted pollutants and of other emitted species. In this paper, we present characterisation of emissions of gases and particles from a vessel equipped with a 4-stroke medium-speed marine engine equipped with SCR and operating on 2 different fuels, e-methanol and marine gasoil (MGO). The measurements were performed during a one-week measurement campaign onboard a RoPax ferry, when emissions from the two investigated fuels and impact of selective catalytic reduction (SCR) system were characterized with an array of high-end instrumentation and onboard sensors under different operational conditions. The in-stack measurements were performed both in the engine room directly after the engine and close to the exhaust funnel outlet, downstream of the catalyst, and gave information about chemical and physical properties of the exhaust and its changes with the different fuels, with and without urea injection downstream of the catalyst and over the catalyst.

The exhaust characterisation included both gaseous (SO₂, NOx, NO, NO₂, CO₂, CO, O₂, CH₄, total HC, NMVOCs, PAHs) and particulate (PM, EC, OC, ions and elemental composition) pollutants measured both upstream and downstream of the catalyst. In addition, two mobile laboratories carried state-of-the-art instrumentation for online analyses of detailed chemical composition and physical properties of gases and particles in the exhaust downstream the catalyst, including size-resolved composition of PM, characterisation of organic

matter, secondary PM formation potential determined by a Potential Aerosol Mass (PAM) chamber and measurements of BC.

The measurements showed that the SCR with urea injection reduced NOx emissions but also significantly reduced emissions of organic matter, both volatile and in particulate phase. Reduction of the organic matter over the catalyst was observed both with and without urea injection. Total hydrocarbon emissions were reduced with 80%, OC with 60% and different PAHs with 70% to 95%. Emissions of EC were not affected by the SCR but total PM emissions were reduced with 40%. Emissions from combustion of the methanol fuel (including 6-13% MGO), when compared to MGO, reduced emissions of NOx with ~30%, emissions of EC with ~70%, OC with ~40% while PAH emissions remained unchanged. Characterisation of organic species with several analytical methods gave new information on chemical composition and volatility profile of the exhaust.

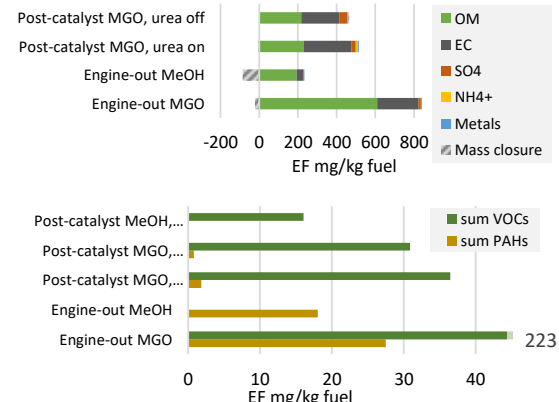


Figure 1. Emissions of PM species (upper panel) and sum of VOCs and PAHs (lower panel) for measurements upstream (engine-out) and downstream (post-catalyst) the catalyst with and without urea injection for MGO and Methanol fuel. Mass closure = PM mass - Sum of PM species

The SCIPPER project has received funding from the European Union's Horizon 2020 research and innovation programme under grant agreement Nr.814893. Stena Line and engine crew of Stena Germanica are gratefully acknowledged for their great support of the measurement campaign.

Discharges from exhaust gas cleaning systems in the OSPAR marine area

T. Grönholm¹, J.-P. Jalkanen¹, J. Kukkonen¹, and I.-M. Hassellöv²

¹Finnish Meteorological Institute, Helsinki, FI-00560, Finland

²Mechanics and Maritime Sciences, Chalmers University of Technology, Gothenburg, SE-41296, Sweden

Keywords: scrubber, shipping, discharge water, contaminant load.

Presenting author email: tia.gronholm@fmi.fi

Since stricter global regulation of maximum allowed sulphur in marine fuels entered into force in 2020, an increasing number of ships are using scrubbers to enable continued use of heavy fuel oil. Scrubbers wash out sulphur oxides and other contaminants from the exhausts and produce large volumes of heavily polluted wash water. Depending on the system, the used scrubber water is discharged back into the ocean (open loop) or recirculated, treated (closed loop) and the sludge is disposed of in the port.

The Ship Traffic Emissions Assessment Model (STEAM v3.5, Jalkanen et al., 2021 and references therein) utilizing ship position data from Automatic Identification System was used to calculate the amount of discharged scrubber water from open and closed loop scrubbers. Combining the modelled water volume with the concentration results obtained from water sampling and laboratory analyses, it was possible to give the estimations for the mass fluxes of various pollutants to the sea.

In 2020, the total effluent release volume from scrubbers in all OSPAR areas was about 620 million tonnes. Of this, more than 99% was from open loop scrubbers. About half of this discharge water was released in the North Sea and the English Channel. The most (84%) of the scrubber effluent in the OSPAR domain was released inside the 200 nautical mile zone. Close to the coast, inside the 12 nautical mile zone about 20% of the total effluent volume was discharged. The volumes of produced water from the oil and gas extraction was estimated to be the individual largest industrial waste stream into the OSPAR area $300 \times 10^6 \text{ m}^3$ (e.g. Beyer et al., 2020).

Most contributing ship types were containerships, Roll-On/Roll-Off cargo ships, bulk cargo carriers, and crude oil tankers. About half of the effluent was released from vessels carrying an EU flag. Most of the scrubbers in the OSPAR area were of open loop type.

Contaminant loads from open loop scrubbers in the OSPAR area were dominated by vanadium (110 tonnes) and nickel (29 tonnes) which both may originate from heavy fuel oil. Nickel may also originate from piping material in the scrubber, which, together with marine growth protection systems, is the hypothesized primary source of zinc (69 tonnes) and copper (24 tonnes) in open loop discharge water.

The closed loop contaminant loads are in the order of 10^3 - 10^4 times lower than the open loop loads. Nickel constitutes the largest calculated closed loop load (190 kg), almost twice the load of vanadium (100

kg) and chromium (90 kg), while the estimated loads of copper and nickel are lower, 40 and 30 kg, respectively.

The estimated PAH loads in OSPAR region are dominated by phenanthrene (940 kg), followed by fluorene, pyrene acenaphthene, chrysene and fluoranthene (between 100-290 kg). The estimated total load of PAH:s is almost 2.5 times higher than the mass of the 16 high priority PAH pollutants (16 PAH, EPA), suggesting that for example alkylated PAHs should also be considered. The closed loop PAH load is in the order of 10^5 - 10^6 times lower compared to open loop PAH load, since closed loop scrubber technology are generally more efficient in removing PAHs (than metals) during the recirculating scrubber process.

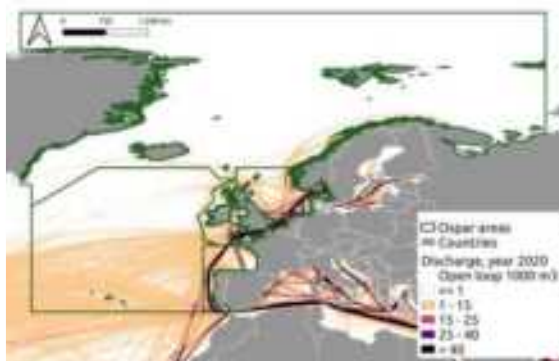


Figure 1. A map showing amount of discharged water from open loop scrubbers in Ospar regions (green polygons) in 2020.

This project has received funding from the European Union's Horizon2020 research and innovation programme under grant agreement #874990 (EMERGE project). This work reflects only the authors' view and CINEA is not responsible for any use that may be made of the information it contains.

Beyer, J., Goksøyr, D., et al. (2020). Environmental effects of offshore produced water discharges: A review focused on the Norwegian continental shelf. *Marine Environmental Research*, 162: 105155.

Jalkanen, J.-P., Johansson, L., et al. (2021). Modelling of discharges from Baltic Sea shipping. *Ocean Science*, 17(3), 699–728. <https://doi.org/10.5194/os-17-699-2021>.

Characterisation of fresh and aged ship emissions in the Port of Marseille

Å. M. Hallquist¹, G. M. Lanzafame², B. Temime-Roussel², P. Simonen³, M. Dal Maso³, H. Salberg¹, J. Kalliokoski³, J. Mellqvist⁴, V. Conde⁴, J. Keskinen³, L. Ntzachristos^{3,5} and B. D'Anna²

¹IVL Swedish Environmental Research Institute, Gothenburg, Sweden

²Aix Marseille University, CNRS, LCE, Marseille, France

³Aerosol Physics Laboratory, Physics Unit, Tampere University, Tampere, Finland

⁴Department of Earth, Space and Environment, Chalmers University of Technology, Gothenburg, Sweden

⁵Aristotle University of Thessaloniki, Thessaloniki, Greece

Keywords: ship emissions, secondary particle mass, Go:PAM, OFR

Presenting author email: asa.hallquist@ivl.se

Shipping contributes to emissions of gaseous and particulate pollutants that can affect climate and health. In the atmosphere the primary emissions can further oxidise leading to the formation of secondary pollution, e.g., secondary organic aerosol (SOA), which is very important on a regional and global scale (Hallquist et al., 2009).

As part of the EU H2020 project SCIPPER (Shipping contribution to Inland Pollution Push for the Enforcement of Regulations) detailed characterisation of the fresh and aged ship emissions was conducted in the Port of Marseille from 11 to 23 July in 2021. The measurements were done at the Phares at Balises (PHB) site [N43.3353, E5.3393] using the stationary ship plume measurement technique, including continuous extractive sampling of the ambient air (Jonsson et al., 2011). The experiments were set-up in order to enable simultaneous characterisation of the freshly emitted emissions and the oxidised emissions utilising an oxidation flow reactor (OFR), specially designed for these types of measurements, i.e., Go:PAM (Watne et al., 2018) (Fig. 1).

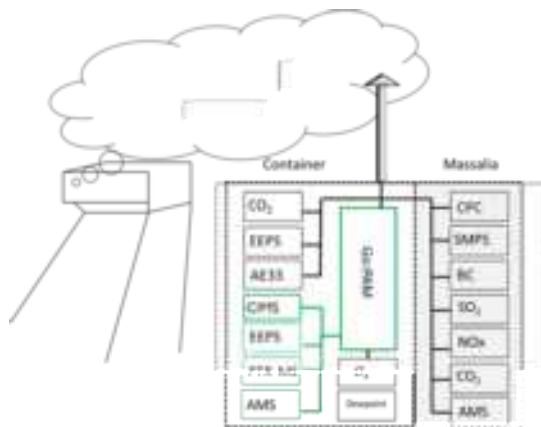


Figure 1. Schematic of the experimental set-up and instrumentation used.

Emission factors (EF) of individual ships were calculated using the carbon balance method, assuming complete combustion and an EF_{CO_2} of 3.2 kg per kg fuel burnt (Jonsson et al., 2011). The identification of the plumes was done using AIS (automatic identification

system) data, giving e.g., the identity, position and speed of the ship; and meteorological data (wind speed and wind direction) (Hallquist et al., 2023). In total 102 ship plumes have been identified and characterised.

Results will be presented with focus on the particle emissions (particle number, mass, size and chemical composition) (Fig. 2).

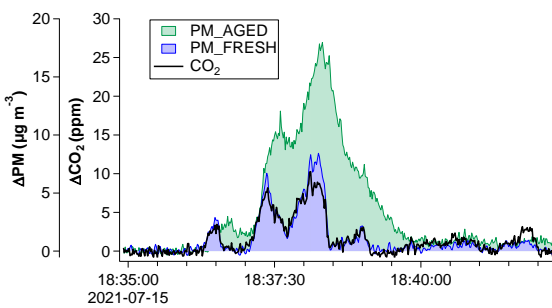


Figure 2. Example of a ship plume measured in Marseille harbour utilising Go:PAM. PM_{AGED} and PM_{FRESH} are the particle mass measured with and without oxidation of the emissions in the OFR.

This work was financed by the European Union's Horizon 2020 research and innovation programme under grant agreement No 814893.

Hallquist M. et al., (2009) *The formation, properties and impact of secondary organic aerosol: current and emerging issues*, Atmos. Chem. Phys., 9, 5155–5236.

Hallquist Å. M., et al., (2023) *Characterization of Ship Emissions 2010-2015: Impact of International Maritime Organization Regulations in a Sulfur Emission Control Area (SECA)*, Manuscript in preparation

Jonsson, Å. M., Westerlund, J., Hallquist, M. (2011) *Size-resolved particle emission factors for individual ships*, Geophys Res. Lett, 38, L13809

Watne et al., (2018) *Fresh and Oxidized Emissions from In-Use Transit Buses Running on Diesel, Biodiesel, and CNG*, Environ. Sci. & Tech., 52 (14), 7720-7728

Distribution of PAHs and metals between exhaust and scrubber water discharge from a large 2-stroke slow speed marine engine equipped with open loop scrubber

A. Lunde Hermansson¹, J. Moldanova², B. Strandberg³, E. Garcia-Gómez^{4,5}, M. Gros^{4,5}, M. Petrović^{4,6}, S. Rodríguez-Mozaz^{4,5}, I.-M. Hassellöv¹ and E. Ytreberg¹

¹ Department of Mechanics and Maritime Sciences, Chalmers University of Technology, Gothenburg, SE-41296

² IVL, Swedish Environmental Research Institute, P.O. Box 53021, 400 14 Gothenburg, Sweden

³ Division of Occupational and Environmental Medicine, Lund University, 22100 Lund, Sweden

⁴ Catalan Institute for Water Research (ICRA), C. Emili Grahit 101, 17003 Girona, Spain

⁵ Universitat de Girona (UdG), Girona, Spain

⁶ Catalan Institution for Research and Advanced Studies (ICREA), Passeig Lluís Companys 23, Barcelona, Spain

Keywords : scrubber, pollution, emission factors, mass balance

Presenting author email: anna.lunde.hermansson@chalmers.se

To comply with IMO regulations, aiming at reducing negative impact of sulphur oxides (SO_x) and particulate matter (PM) on air quality, shipowners are required to switch to compliant fuels, of lower sulphur content, or to install a scrubber, allowing for continued use of cheaper high sulphur heavy fuel oils (HSHFOs). The 2020 reduction of the maximum sulphur (S) content in marine fuels from 3.5% to 0.5% m/m S led to massive increase in number of scrubber installations.

Previous studies show that scrubber discharge water contains high concentrations of e.g. metals and polycyclic aromatic hydrocarbons (PAHs), proving that contaminants are being scavenged by the scrubber water and discharged to the marine environment. It is however unknown in what extent these contaminants are being scavenged in the scrubber and discharged to the marine environment and how much is emitted through the exhaust. Few studies have compiled emission factors from ships equipped with scrubbers to include both the atmospheric and marine perspective, but there is a lack in simultaneous measurements on-board ships. The objective of this study was to assess emissions of contaminants to the marine environment, and to evaluate the mass balance between air emissions and water discharges downstream the scrubber.

During the fall of 2021, an on-board campaign was carried out, where sampling of metals and PAHs (including alkylated species) in exhaust gas and scrubber discharge water were done simultaneously together with characterisation of number of other pollutants, such as emissions of NO_x, SO_x, VOCs, PM and its composition. The container vessel, equipped with an open loop scrubber, was sailing through different marine domains, from the North Sea to the Eastern Mediterranean. To the knowledge of the authors, this is the first published mass balance assessment and the results from the analysis provide information on the distribution of contaminants between exhaust emissions and scrubber water discharge.

Metal and PAH content were characterized in the tested fuels (two batches of HSHFO and ultra-low S fuel oil, ULFSO), the exhaust and the scrubber discharge water. The exhaust was sampled before and after the scrubbing process, and in case of ULFSO, only after a deactivated scrubber. Exhaust PAH samples were pumped through combined samplers consisting of a particle filter and XAD absorbent tube.

Metal concentrations of the exhaust were obtained from ED-XRF analysis on the PM filter samples. Scrubber discharge water was sampled on-board and the particulate and dissolved fractions of metals and PAHs were differentiated in the lab.

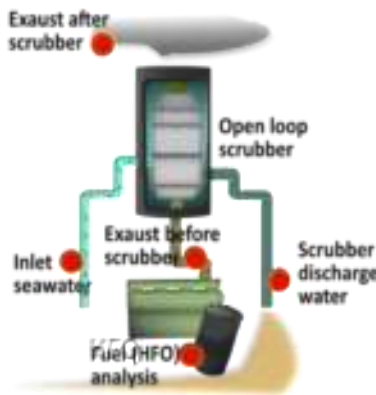


Figure 1. Schematic over the sampling setup (red dots indicate sampling points) during the onboard campaign

Results suggest that the scrubber is scavenging a substantial fraction of PAHs (also alkylated and dibenzothiophenes (DBTs)). Air emissions were largely dominated by naphthalene and alkylated naphthalenes. In scrubber discharge water, naphthalene and phenanthrene represented the highest concentrations of the parent PAHs. The alkylated PAHs were also prevalent in scrubber water. Known tracers of HFO combustions, such as nickel and vanadium, are found in the exhaust gas before and after the scrubber as well as in elevated levels in the scrubber discharge water, indicating that the contaminants will be distributed between the different sources and that both the atmosphere and marine environment will act as primary recipients when a scrubber is used.

Acknowledgement

This work was funded by the European Union's Horizon 2020 research and innovation programme Evaluation, control and Mitigation of the Environmental impacts of shipping Emissions (EMERGE) [grant agreement No 874990].

3.8 JS.09. Atmospheric processes and air quality impact studies: Modelling impacts of transport on air pollution, climate, health and ecosystems.

Impacts of shipping emissions on air quality in 2040: effects of nitrogen emission control areas and non-compliance

S. Jutterström¹, J. Moldanova¹, E. Majamäki², J.-P. Jalkanen², J. Kuenen³, and V. Matthias⁴

¹IVL Swedish Environmental Research Institute, Gothenburg, SE-400 14, Sweden

² Finnish Meteorological Institute, Helsinki, FIN-00101, Finland

³ TNO, Netherlands Organization for Applied Scientific Research, Utrecht, 3584, The Netherlands

⁴ Helmholtz-Centre Hereon, Institute of Coastal Environmental Chemistry, Geesthacht, 21502, Germany

Keywords: shipping, nitrogen oxide emissions, air pollution, future scenarios

Presenting author email: sara.jutterstrom@ivl.se

Shipping contributes significantly to the emissions of air pollutants such as SOx, NOx, and particulate matter (PM), especially in coastal areas, as well as to the emissions of the greenhouse gasses. As maritime transport is projected to continue to grow in the future, there are increasing efforts to reduce emissions. While emissions of SOx and associated PM sulphate are targeted by regulation of the fuel S content with immediate impact after implementation of the legislation, emissions of NOx are targeted by NOx Tiers in Nitrogen Emission Control Areas (NECAs) applying for new-build ships key laid after the date of implementation of the legislation, which leads to a slow, gradual reduction of emissions. Further, the International Maritime Organization (IMO) has set a target to reduce the greenhouse gas emissions from shipping by 50% by 2050 compared to emissions in 2008 where important tool is gradual increase of energy efficiency of the new-build vessels which also brings reduction of emissions of air pollutants. More stringent regulations can lead to for instance use of cleaner fuels, increased use of scrubbers, use of exhaust gas aftertreatment targeting NOx emissions, use of alternative fuels and improvements in fuel efficiency.

As a part of the SCIPPER project, the effects of shipping emissions on air quality in coastal regions in Europe were investigated for year 2015 and for three ship emission scenarios for year 2040 focusing on the effects of an implementation of a European NECA and a related possibility of partial failure of its implementation through partial non-compliance and the exhaust aftertreatment not operating at low engine loads. To highlight the impact of shipping emissions in the scenarios, these were compared to a scenario excluding the shipping emissions in the 2 investigated years.

Three regions with high impact of shipping emissions were investigated in more detail.

The regional model simulations were done with a combination of the STEAM ship emission model with the EMEP-MSC-W regional chemistry transport model (open-source version rv3.34 on a $0.1^\circ \times 0.1^\circ$ resolution). The land emissions were derived from the ECLIPSE v6b global emission scenarios with an MFR (Maximum Feasible Reduction) scenario selected.

In this contribution, the results from the year-2015 and the investigated year-2040 scenario simulations for

concentration levels of NO₂, O₃ and PM_{2.5}, as well as deposition of nitrogen and their shipping shares are compared and discussed (Figure 1).

The results clearly show that the implementation of a European-wide NECA will reduce NO₂ and PM_{2.5} concentrations as well as nitrogen deposition. O₃ concentrations are also expected to decrease in most areas. However, in regions with formerly very high NOx emissions ozone concentrations will increase because of reduced ozone titration through reactions with NO. The effects of non-compliance on air pollution from shipping are visible but they are much smaller than the gains through the NECA implementation.

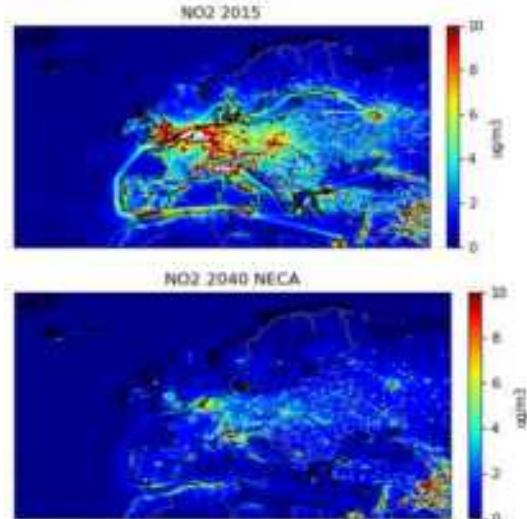


Figure 1. Annual mean NO₂ concentrations in Europe in 2015 (top) and for a NECA shipping scenario in 2040 (bottom).

Acknowledgments:

This work was carried out in the SCIPPER project: Shipping Contributions to Inland Pollution Push for the Enforcement of Regulations, EU Horizon 2020 No. 814893.

Direct evidence of the substantial effect of SECA in the Baltic Sea

A. Maragkidou¹, T. Grönholm¹, L. Rautiainen¹, T. Mäkelä¹, L. Laakso¹ and J. Kukkonen^{1,2}

¹Finnish Meteorological Institute, Helsinki, Uusimaa, FI-00101, Finland

²Centre for Atmospheric and Climate Physics Research, and Centre for Climate Change Research, University of Hertfordshire, College Lane, Hatfield, AL10 9AB, UK

Keywords: SO₂, shipping, emissions, SECA.

Presenting author email: androniki.maragkidou@fmi.fi

From 1st of July 2010 and onwards, the International Maritime Organization (IMO) implemented a rule that required ships sailing in SECA regions (including the Baltic Sea) to use fuel with a sulfur content no higher than 1.0%. This rule was further tightened in 2015, reducing the sulfur limit to 0.1%. Ships are therefore required either to use low-sulfur fuel or install scrubbers to remove sulfur from their exhaust.

The Air Quality Station of Utö is located on a small island in the Archipelago Sea of the Baltic Sea. The island has a long history of meteorological, marine, and air quality measurements. Air quality measurements have been carried out for SO₂ since 1980 and for NO₂ since 1986. Concentrations have been measured according to the EU standards using UV-fluorescence and chemiluminescence gas analyzers. The island's location makes it an optimal place for plume tracking, as the regional background levels of NO_x and SO₂ are very low, and it is near a busy sea route (Grönholm *et al.*, 2021).

The results (Figure 1) evidenced a clear decrease of the measured concentrations of SO₂ since 2015. This provides direct evidence that shipping in the nearby route has complied with the Annex VI of the IMO MARPOL Convention. An example of SO₂ and NO_x concentrations originating from shipping are presented in Figure 2, before and after the passing of a ship. Based on an analysis of the various timeseries of concentrations, and analyses of individual ship bypasses, we have compiled extensive evidence regarding the effect of the introduction of SECA in this region.

This study presents for the first time decadal long-term data (since the early 1980's) from a remote station in the open sea in the Baltic. The measured data and their analysis provide conclusive evidence of the substantial effect of the introduction of SECA since 2015 regarding the concentrations of SO₂.

In addition, compared to previous studies in the field, our work presents novel features in terms of analysis of shipping plumes of SO₂, NO_x and PM measured at a remote station close to a shipping lane. However, further analysis of plumes is still under progress and more results are expected.

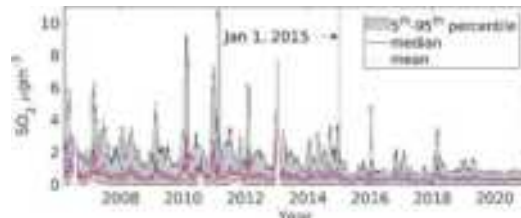


Figure 1. Timeseries of the SO₂ concentrations during 2006-2020 at Utö. The results highlight a substantial decrease of concentrations since 2015.

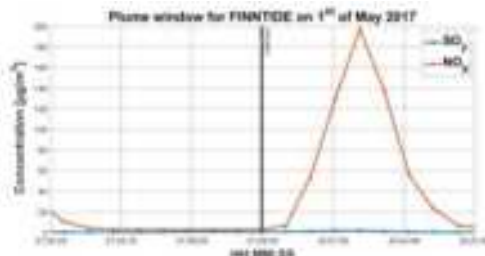


Figure 2. An example of our results concerning the measured concentrations of SO₂ and NO_x at Utö, before and after the passing of a ship called "FINNTIDE" on the 1st of May 2017.

This work has received funding from the European Union's Horizon 2020 research and innovation program under grant agreement No 874990 (EMERGE project). This work reflects only the authors' view and the Innovation and European Climate, Infrastructure and Environment Executive Agency (CINEA) is not responsible for any use that may be made of the information it contains.

Grönholm, T., Mäkelä, T., Hatakka, J., Jalkanen, J.-P., Kuula, J., Laurila, T., Laakso, L. and Kukkonen, J. (2021) *Environ. Sci. Technol.* **55**, 13677–13686.

Future impact of shipping emissions on air quality in Europe under climate change scenarios

A. Monteiro¹, M. Russo¹, D. Carvalho² and J. Jukka-Peka³

¹CESAM, Department of Environment and Planning, University of Aveiro, Portugal

²Department of Chemical Engineering, University of Elsewhere, City, Region, Postcode, Country

³Finnish Meteorological Institute, Helsinki, Finland

Keywords: shipping, atmospheric emissions, numerical modelling, air quality, climate change scenario.

Presenting author email: alexandra.monteiro@ua.pt

Ship engine combustion emits several atmospheric pollutants, such as particulate matter (PM), sulphur oxides (SO_x), and nitrogen oxides (NO_x), which can have adverse health effects and are significant contributors to decreased air quality (Viana *et al*, 2014; Aksoyoglu *et al*, 2016). Due to the distribution of maritime transport activity routes in the EU, a large portion of the population is exposed to shipping emissions throughout Europe (Sofiev *et al*, 2018). Therefore, in light of the European Commission long-term objective of “zero-waste, zero-emission” for maritime transport, the focus of this study is to quantify the impact of shipping emissions in 2050, considering both emissions projection for the shipping sector and climate change scenarios. The WRF-CHIMERE modelling system domain covers the entirety of Europe and main shipping routes throughout the continent.

To obtain future contributions of maritime transport to total pollutant concentrations, simulations were divided into a present and two future scenarios for 2050, one which only includes shipping projections, and another that include climate change (RCP8.5 worst-case scenario) and shipping emission projections.

The results obtained in terms of the impact of the emissions projection for NO_x are (Figure 1) show that shipping has a large impact on coastal air quality and a non-negligible impact in areas < 50 km inland. The seasonal analysis indicates higher concentrations and differences during warm months.

The results indicate that the signal from climate change can be higher than the future impact of shipping emissions, mostly in the Mediterranean, but this effect is also noticeable in the North and Baltic seas (Figure 2). Climate change alone accounts for differences of over 25 µg·m⁻³ for NO_x and Ozone (O₃) concentrations throughout Europe, which is equivalent and even higher than the differences caused by the changes in shipping emissions.

Besides the shipping sector, climate change has significant impacts in large urban areas where NO_x emissions are highest, registering differences of over 10 µg·m⁻³. SO₂ concentrations are overall low at inland locations and northern Europe, with the only notable differences occurring in eastern Europe and the Mediterranean (mainly due to shipping and fossil fuelled energy production), with values below 10 µg·m⁻³.

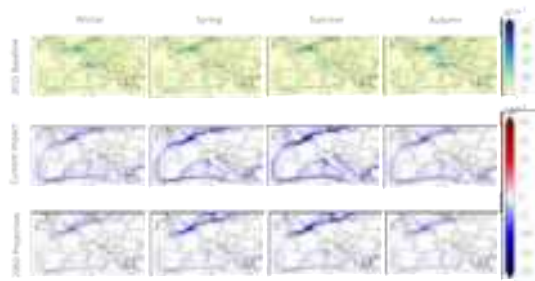


Figure 1. Impact of shipping emissions projections (2050), per season, for NO_x pollutant.

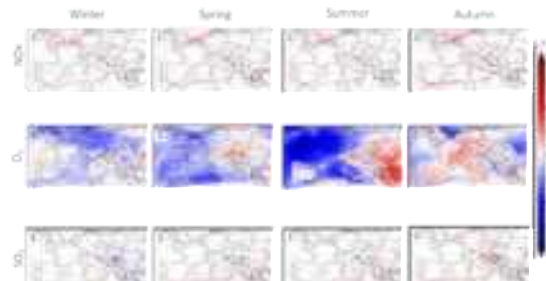


Figure 2. Impact of shipping emission projections and climate change scenario, per season, for NO_x, O₃ and SO₂ pollutants.

This research has been supported by the EU H2020 project EMERGE, which has received funding from the European Union's Horizon 2020 research and innovation programme under grant agreement n°874990. Thanks are also due for the financial support to CESAM (UIDP/50017/2020+UIDB/50017/2020+LA/P/0094/2020).

- Aksoyoglu, S., Baltensperger, U., Prévôt, A. (2016) Contribution of ship emissions to the concentration and deposition of air pollutants in Europe. *Atmos. Chem. Phys.* **16**, 1895–1906.
Sofiev, M., Winebrake, J., Johansson, L., Carr, E., Prank, M., Soares, J., Vira, J., Kouznetsov, R., Jalkanen, J.-P., Corbett, J. (2018) Cleaner fuels for ships provide public health benefits with climate tradeoffs. *Nature Communications* **9**, 406
Viana, M., Hamming, P., Colette, A., Querol, X., Degraeuwe, B., Vlieger, I., van Aardenn, J. (2014) Impact of maritime transport emissions on coastal air quality in Europe. *Atmos. Environ.* **90**, 96–105.

On the determination of ship exhaust aerosol volatility in the SCIPPER project

M. Dal Maso¹, P. Simonen¹, O. Kangasniemi, J. Kalliokoski., A. Wagner., L. Markkula¹, H. Timonen², L. Barreira², J. Moldanova³, B. D'Anna⁴, B. Temime-Roussel⁴, G. M. Lanzafame⁴, K. Teinilä², S. Saarikoski², H. Salberg³, J.-P. Jalkanen², E. Majamäki², L. Ntzachristos^{1,5}, J. Keskinen¹

¹Aerosol Physics Laboratory, Physics Unit, Tampere University, Tampere, 33720, Finland

²Atmospheric Composition Research, Finnish Meteorological Institute, Helsinki, 00101, Finland

³Swedish Environmental Research Institute, Gothenburg, Sweden

⁴Aix Marseille Univ, CNRS, LCE, Marseille, France

⁵Aristotle University of Thessaloniki, Thessaloniki, Greece

Keywords: Ship exhaust emissions, volatility, aerosol composition

Presenting author email: miikka.dalmaso@tuni.fi

Particulate and gaseous emissions from ship engines have both climatic and health effects, which depend in various manners on the physical and chemical properties of the emitted aerosol. In order to understand, model, and finally efficiently regulate such emissions, these properties need to be accurately determined. One of the properties highlighted by research is particle volatility (Donahue et al., 2006) and its dependence on aerosol composition, on engine parameters, evolution during dilution and atmospheric aging.

Here, we report the results of a comprehensive set of measurements of ship exhaust with state-of-the-art instrumentation both on-board and from atmospheric conditions both from the shore and while chasing during the SCIPPER project. In the on-board and chasing measurements, the particle volatility was inspected with thermodenuder measurements, where the sample is led through heated tubing, and the fraction of mass remaining in particle phase was studied as a function of temperature. Another method was isothermal dilution, in which the sample was diluted and allowed to equilibrate for a longer time than in a thermodenuder.

The evaporation of individual chemical species was studied with a FIGAERO-CIMS (Lopez-Hilfiker et al., 2014) setup, where particles are first collected onto a filter, and then desorbed with heated nitrogen. The nitrogen temperature was ramped up to obtain thermograms of different particle-phase molecules. The evaporated compounds were then detected with chemical ionization mass spectrometry using iodide ions creating the necessary charges, in order to target semivolatile organic compounds. FIGAERO thermograms can be deconvoluted using positive matrix factorization to retrieve grouped volatility information (Buchholz et al., 2020)

In addition, the chemical composition of the particulate and gas phases was studied using an SP-AMS aerosol mass spectrometer as well as a time-of-flight proton transfer mass spectrometer for volatile organic compounds. Simulated aging of exhaust was performed by exposing the sample to high concentrations of oxidants in an Aerodyne Potential Aerosol Mass reactor (PAM). Even in the case of detailed characterization, determination of the volatility distribution of the primary aerosol is not straightforward (Riipinen et al., 2010). We applied a detailed microphysical multicomponent aerosol

evaporation together with a genetic optimization algorithm (Tikkanen et al., 2019) to find the best estimate of volatility distributions.

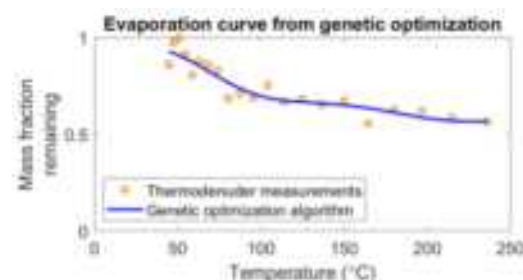


Figure 1: Evaporation curve obtained by genetic optimization to thermodenuder measurements

The focus of our presentation is on the results of the volatility determination for ship emission, and the implications for the determination and modelling of both primary and secondary OA from shipping. We present a comparison of our results to existing literature and the STEAM emission model (Jalkanen et al., 2009), and also present the methodology the modification of existing emission data to include updated volatility information.

The SCIPPER project has received funding from the European Union's Horizon 2020 research and innovation programme under grant agreement Nr.814893.

Buchholz, A., et al. *Atmos. Chem. Phys.*, **20**, 7693–7716
Donahue, N. M. et al (2006) *Environ. Sci. Technol.* **40**, 2635–2643.

Lopez-Hilfiker, et al. (2014) *Atmos. Meas. Tech.*, **7**, 983–1001.

Jalkanen, J.-P. et al (2009) *Atmos. Chem. Phys.* **9**, 9209–9223.

Riipinen, I. et al (2010) *Atmos. Environ.* **44**, 597–607.

Tikkanen, O.P. et al (2019) *Atmos. Chem. Phys.* **19**, 9333–9350.

3.9 JS.10. Compliance monitoring technological and legal frameworks; experimental studies; theoretical impact studies.

Comparison of particle emission factors from shipping using different instruments

D. van Dinther¹, A. Weigelt², J. Beecken^{2,3}, J. Mellqvist⁴, V. Conde Jacobo⁴, M. Blom¹, and J. Duyzer¹

¹ Netherlands Organisation for Applied Scientific Research (TNO), Petten, the Netherlands

² Federal Maritime and Hydrographic Agency (BSH), Hamburg, Germany

³now at Explicit ApS, Copenhagen, Denmark

⁴Chalmers University of Technology, Gothenburg, Sweden

Keywords: emission factors, shipping, aerosol, particles, particle size distribution, emission factor.

Presenting author email: danielle.vandinther@tno.nl

Air quality in cities with large ports can significantly be impacted by shipping. For example, Visschedijk and Denier van der Gon (2022) showed that, in the Rotterdam area (the Netherlands), sea shipping is the largest source of ultra-fine particles (UFP) with a contribution of 56% to total UFP emissions. In the EU-project SCIPPER (Shipping Contributions to Inland Pollution Push for the Enforcement of Regulations; www-scipper-project.eu) a six week measurement campaign was undertaken at the river Elbe about 10 km downstream of the port of Hamburg (Germany) in 2020. Sea going vessels pass the measurement site at a distance of 400 to 800 m. Three different groups measured side-by side different gaseous compounds, aerosols and the meteorology conditions on-shore. The BSH and Chalmers University each measured the particle size distribution between 5.6 and 10 000 nm with combined EEPS and OPS systems. Next to their permanent installed aerosol- and trace gas monitoring system, BSH additionally operated a mobile system consisting of identical equipment. TNO used a LAS (type 3340A of TSI) to measure particles with sizes between 90 and 10 000 nm. Black carbon (BC) was measured by two groups using aethalometers (Magee AE33). However, the BC set-ups were different (dried vs non-dried and different size cut-offs). The emission factors (EF) of the different ships were calculated in #/kg_{fuel} as well as mg/kg_{fuel} with the simultaneously measured carbon dioxide concentrations. This provides a unique dataset to better understand comparability of particle emission factors measured by different devices. This comparability is important if, in the future, legislation to decrease aerosol emissions of shipping is applied and needs to be enforced. The standard BSH system operational on the site since 2020 and was used as the reference system. Note, this was an arbitrary choice as no true reference of particle emissions exist. Results showed the relatively large contribution of mainly UFP, with 90% of the total amount of particles being smaller than 80 nm and 75% of the total particle mass originate from particles smaller than 200 nm. A total of 1299

plumes where measured during the complete campaign. However, not all instruments were operated at the same times. Comparison of the EF were made for instances where all systems were operated and a plume was measured by all of them, which left around 60 plumes. Table 1 shows the regression statistics for EF of particle number (PN). The comparison showed very promising results when the same equipment was tested side-by-side. For the two BSH (EEPS/OPS) systems R² is at least 0.79 over the entire size range. Results also showed that data treatment to retrieve EF influences the results. For example, the Chalmers system compared less well to the BSH standard system, though the same equipment was used. The EF of the TNO systems compared fairly well to BSH standard system for PN ($R^2 \geq 0.68$). Comparability of the different devices to measure EF of particle numbers, where in general somewhat better than those at of particle mass. For particle mass the TNO LAS system misses a too large fraction of the smaller particles below 90 nm to give reliable EF. If only the EF of particles larger than 90 nm are used, the comparison of EF up to PM1 (particle diameter up to 1 μm) of the LAS system with the BSH standard system is fairly good with R² values between 0.65 and 0.82. The difference in the experimental set-up for black carbon used by the different groups, proved to have a too large impact on the results to give comparable emission factors. In conclusion, the data agrees reasonably well between the used systems. Hence, in the future, it should be possible to use on-shore measurements to monitor aerosol emissions from shipping even when different equipment is used.

The SCIPPER project has received funding from the European Union's Horizon 2020 research and innovation programme under grant agreement Nr.814893.

Visschedijk, A., Denier van der Gon, H. (2022). UFP emissie in de Rijnmond regio in 2019 (in Dutch). Utrecht: TNO-report R10616.

Table 1: Regression statistics of EF_{PN} of BSH mobile system (BSH_{MMS}),TNO and Chalmers system against BSH standard system.

Size range [nm]	BSH _{MMS}			TNO			Chalmers		
	Slope	Offset	R ²	Slope	Offset	R ²	Slope	Offset	R ²
<100	0.83	1.2x10 ¹⁵	0.79	NA	NA	NA	0.62	2.1x10 ¹⁵	0.49
90-300	0.86	3.4x10 ¹³	0.88	0.66	8.4x10 ¹³	0.69	0.99	1.7x10 ¹⁴	0.55
300-10000	1.1	-2.3x10 ¹¹	0.98	1.3	1.7x10 ¹²	0.68	0.82	8.1x10 ¹¹	0.83

Performance assessment of state-of-the-art and novel methods for remote compliance monitoring of sulphur emissions from shipping

J. Beecken^{1,4}, A. Weigelt¹, S. Griesel¹, J. Mellqvist², A.V. Conde Jacobo², D. van Dinther³, J. Duyzer³, B. Knudsen⁴, J. Knudsen⁴, L. Ntziachristos⁵

¹Federal Maritime and Hydrographic Agency (BSH), Hamburg, Germany

²Chalmers University of Technology, Gothenburg, Sweden

³Netherlands Organisation for Applied Scientific Research (TNO), Petten, the Netherlands

⁴Explicit ApS, Copenhagen, Denmark

⁵Aristotle University Thessaloniki, Thessaloniki, Greece

Keywords: ship exhaust, sulphur emission, emission monitoring, remote measurements, fuel sulphur content, MARPOL Annex VI, compliance monitoring

Presenting author email: jbe@explicit.dk

Sulphur emissions to the air from sea-going and inland vessels were measured simultaneously by eight different, state-of-the-art and novel, monitoring systems during a six-week campaign at the Elbe River, at about 90 km upstream the river's mouth to the North Sea and 10 km distance downstream of the port of Hamburg, Germany. The comparison was conducted as part of EU project SCIPPER: Shipping Contributions to Inland Pollution Push for the Enforcement of Regulations (www.scipper-project.eu/). Stationary, and airborne systems on unmanned aerial vehicles (UAV), were operated by four participating partners in a side-by-side measurement setup to observe the emissions from individual ships under real-world conditions. The measurement site is located in the Northern European SO_x emission control area (SECA) where the allowed fuel sulphur content (FSC) is limited to 0.10 %Sm/m.

In total, 966 plumes that originated from 436 different vessels were analysed. At the same time, fuel samples, obtained from 34 different vessels, and bunker delivery notes from five additional vessels were used as references. The results are summarized in Figure 1.

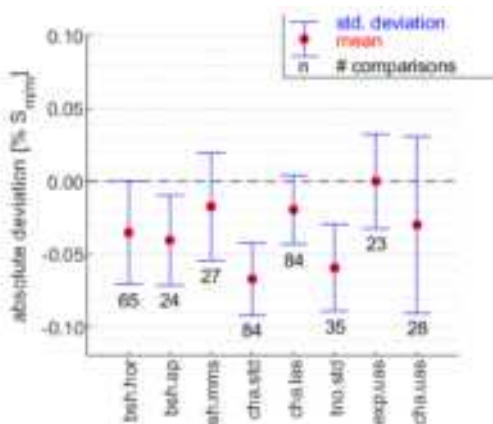


Figure 1. Difference between reported FSC results and reference data from fuel analysis and bunker delivery notes for each remote sensing system.

The stations bsh.hor, bsh.ap, bsh.mms, cha.std, and tno.std are stationary sniffer systems that are operated from land-based sites near shipping lanes by BSH, Chalmers, and TNO, respectively. A novel stationary sniffer system with a more sensitive SO₂ monitor, cha.las, was demonstrated for the first time. Airborne sniffers onboard UAV were applied by Explicit (exp.uas) and Chalmers (cha.uas), whereof the latter was an experimental prototype setup.

All systems except the UAV-borne exp.uas showed a significant negative bias of the remotely assessed FSC. Correlation plots indicate a possible dependence on relative humidity.

Total uncertainties were calculated for each system for a 95 % confidence interval as shown in Table 1

Table 1. Re-calculated uncertainties corresponding to a confidence level of 95 % for the systems.

system	bias (%Sm/m)	uncertainty (%Sm/m)	total uncertainty (%Sm/m)
bsh.hor	-0.035	0.071	0.082
bsh.ap	-0.040	0.064	0.080
bsh.mms	-0.017	0.076	0.079
cha.std	-0.067	0.049	0.092
cha.las	-0.020	0.047	0.052
tno.std	-0.059	0.060	0.092
exp.uas	0.000	0.067	0.067
cha.uas*	-0.030	0.124	0.129

*experimental

It was found that the systems can detect non-compliances with a confidence of 95 % if the actual FSC of the combusted fuel of the monitored vessel exceeds 0.15 to 0.19 %Sm/m.

The SCIPPER project has received funding from the European Union's Horizon 2020 research and innovation programme under grant agreement Nr.814893.

Remote monitoring of NO_x from shipping- validation and long-term results

J. Mellqvist¹, J. Beecken^{2,4}, A. Weigelt², S. Griesel², A.V. Conde Jacobo¹, D. van Dinther³, J. Duyzer³, B. Knudsen⁴, J. Knudsen⁴, M. Irljala⁵, L. Ntziachristos⁶

¹Chalmers University of Technology, Gothenburg, Sweden

²Federal Maritime and Hydrographic Agency (BSH), Hamburg, Germany

³Netherlands Organisation for Applied Scientific Research (TNO), Petten, the Netherlands

⁴Explicit ApS, Copenhagen, Denmark

⁵Aeromon Oy, Helsinki, Finland

⁶Aristotle University Thessaloniki, Thessaloniki, Greece

Keywords: ship exhaust, NO_x emission, emission monitoring, remote measurements, NECA

Presenting author email: johan.mellqvist@chalmers.se

A NO_x emission control area (NECA) is established in Northern Europe since 2021, requiring ~75 % NO_x reduction of new ships (Tier III) compared to the earlier requirement for ships built during 2011 and 2020 (Tier II). The emission value limit to be controlled is the brake specific emission (g·NO_x/kWh), corresponding to a weighted average of emissions at multiple engine loads, and this value is heavily weighted towards engine loads above 50 %. It is however not possible to take on board samples of NO_x and use for legal proof, like for Fuel Sulfur content, since it is produced from the combustion air itself when running the engines. Port state controls authorities instead inspect that the installed engine and the exhaust gas aftertreatment system is certified to meet the limits. In the EU project SCIPPER (www.scipper-project.eu/) it has been investigated if remote measurements can be used to indicate whether ships follow the NECA limits. Several sensor systems for remote sniffer measurements of fuel-mass specific emissions of NO_x have been compared in side-by-side measurements in campaigns in Hamburg, Kiel and Marseille. The studied sensors include standard sniffers at fixed locations (BSH, Chalmers, TNO), mobile manned platforms (Chalmers), and compact mini-sniffers used on drones (Explicit and Aeromon). Several of the sensors have been operated over long periods on different sites. The standard sensor for CO₂ is based on infrared absorption while for NO_x it is based on chemiluminescence. In the drone-based system the NO_x is measured by several electrochemical sensors while CO₂ is measured by the same principle as for the standard sniffers. From the NO_x-to-CO₂ ratio in the flue gas the fuel-mass specific emission (g NO_x/kg_{fuel}) is obtained. The comparison in the different field campaigns shows that the fuel-mass specific emission of NO_x (g/kg_{fuel}) of by-passing ships had a measurement uncertainty (CI 95 %) of 8 - 17 g/kg_{fuel} (17 % - 40 % relative uncertainty), varying for different campaigns

and slightly for different sensors. These uncertainties were derived from the difference between more than 100 individual measurements and the ensemble average of all the individual side-by-side measurements. The fuel-mass specific emission of NO_x obtained by the remote measurements are converted to the brake specific emission by multiplying with the specific fuel oil consumption (g_{fuel}/kWh). This value depends on ship and engine type and typically varies within 25 % from an average of 200 g/kWh, with generally increasing values at lower engine loads. When taking this variability into account as a contribution to the total uncertainty, the latter ranges between 30 % and 47 % for the remotely measured brake specific emissions (g/kWh), for the different campaigns. The data in SCIPPER shows that the fuel-mass specific NO_x emission, and the brake specific one, varies relatively little above 50 % engine load. Since the emission value limit in the NO_x technical code is heavily weighted towards higher engine loads this means that the remote measurements can be used to assess and control this value. For engine loads below 50 % more care must be taken when using such data. For Tier III ships, when doing type approval of engines, there already exists Not-To-Exceed limits (NTE) which are not allowed to be exceeded by more than 50 % at any engine load point. Here we show that the measurement errors are small enough to make it useful to implement NTE limits to facilitate compliance monitoring using remote measurements. In addition, long term NO_x measurements by the individual groups participating in SCIPPER show that the NO_x emissions of Tier III ships during 2021 were exceedingly high for more than 50 % of 65 Tier III vessel measurements at several locations. This should be studied further, since if continued it will hamper the success of NECA.

The SCIPPER project has received funding from the European Union's Horizon 2020 research and innovation programme under grant agreement Nr.814893.

3.10 JS.12. Scenarios and policy options for sustainable transport.

Potential impact on emissions of an introduction of hydrogen and fuel cell-based propulsion in Nordic shipping

R. Parsmo^{1,2}, H. Lundström¹, J. Hansson^{1,2}, E. Fridell^{1,2}, and K. Jivén¹

¹IVL Swedish Environmental Research Institute, Box 530 21, 400 14 Gothenburg, Sweden

²Department of Mechanics and Maritime Sciences, Chalmers University of Technology, Gothenburg, Sweden

Keywords: hydrogen, fuel cell, emissions, alternative marine fuels.

Presenting author email: rasmus.parsmo@ivl.se

One way of reducing harmful emissions from ships and at the same time reduce greenhouse gas (GHG) emissions is to utilize alternative fuels. This can be hydrogen or ammonia as a hydrogen carrier, methanol, or any biofuel or synthetic fuels with low GHG footprint.

The purpose of this study is to estimate the potential impact on selected emissions of an introduction of hydrogen and fuel cell-based propulsion in Nordic shipping. Besides direct and indirect GHG emissions (including carbon dioxide, CO₂, methane, CH₄, and nitrous oxide – N₂O), also direct emissions of nitrogen oxides (NO_x) and particles are included.

First, Nordic shipping and associated current CO₂ emissions were investigated starting by identification of vessel movement patterns in the Nordic region using historical port call data for Nordic ports from Marine Traffic. This was followed by a mapping of the distance between Nordic ports using statistics from Sea routes. Vessels below 5 000 gross tonnage (GT) and fishing and service vessels were excluded from the data. Then, official data reported to European Union via the Monitoring, Reporting and Verification (MRV) system was used to compile average fuel consumption for each individual ship and CO₂-emissions per nautical mile (THETIS-MRV, 2022). This resulted in estimations of the CO₂ emissions that can be attributed to Nordic shipping on voyages to/from and between ports in the Nordic region. The direct emissions of CH₄ and N₂O are estimated based on estimated fuel used and emissions factors from Fourth IMO GHG study by IMO.

Two cases for the development of Nordic shipping by 2030 and 2050 was then outlined, a high a low growth case. Four factors were considered: 1) transport development based on DNV (2020), 2) ship size, 3) energy efficiency improvements, and 4) improved utilization.

A few possible deployment trajectories for hydrogen and fuel cells in Nordic shipping has been outlined. In the first scenario hydrogen and fuel cells are assumed to be implemented on all relevant vessels identified as Nordic shipping by this study. Relevant is here assumed to depend on the length of the routes for the vessels. Up to 600 NM are considered potentially possible for hydrogen and fuel cell propulsion as a rough estimate. In the second scenario, hydrogen and fuel cells are assumed to be implemented only on board all relevant RoPax vessels (ferries) in or between the Nordic countries (representing a considerable share of Nordic shipping).

The CO₂ emission reduction potential in the two scenarios is presented in Table 1.

Table 1. Estimated potential emission reduction of CO₂, in 2030 and 2050 from an implementation of hydrogen in fuel cells for (i) all vessels with voyages up to 600 NM (All ships) and (ii) for all ferries in and between the Nordic countries (Only Nordic ferries), for a high and low growth transport scenario respectively.

			(Mtonnes)
Low	2030	Only Nordic ferries	1.9
		All ships	8.2
	2050	Only Nordic ferries	2.6
		All ships	10.2
High	2030	Only Nordic ferries	2.1
		All ships	9.5
	2050	Only Nordic ferries	3.7
		All ships	17.1

The study finds that an introduction of hydrogen-based solutions may considerably reduce the emissions of GHG as well as other air pollution from Nordic shipping. Introducing hydrogen in other ship categories besides RoPax vessels such as cruise ship and cargo vessels will also reduce the GHG emissions but not to the same extent. A significant benefit on air quality can also be expected due to reductions also of other emissions. The quantitative impact is explored in more detail in Jivén et al (2023).

However, hydrogen-based solutions do not seem to be the lowest cost option for regional shipping, e.g., electrification has advantages on certain routes. Policies are crucial for the transition in the shipping sector and details in the policy design can be crucial for the prerequisites also for hydrogen solutions.

This work is supported by Swedish Transport Administration, Nordic Energy Research and other Nordic funders via the HOPE project.

THETIS-MRV. 2022. CO₂ Emission Report. European Commission, EMSA.

DNV. 2020. Maritime Forecast to 2050 - Energy Transition Outlook 2020.

Jivén K et al. 2023. Concept design and scenario and impact analysis in HOPE - Report of WP3 and WP5 in the HOPE project.

Environmental and economic assessment of green and blue fuels for shipping

Fayas Malik Kanchiralla¹, Elin Malmgren¹, Maria Grahn¹ and Selma Brynolf¹

¹ Department of Mechanics and Maritime Sciences, Chalmers University of Technology, SE-412 96, Gothenburg, Sweden

Keywords: alternate fuels, ship, green fuels, blue fuels, battery, and e-fuels.

Presenting author email: fayas.kanchiralla@chalmers.se

Transitioning to fuels with zero or very low greenhouse gas (GHG) emissions throughout their life cycle is necessary in the shipping sector to address the climate challenge. There are three types of energy sources that are considered to be potential climate-neutral solutions 1) biomass, 2) renewable electricity, and 3) fossil fuel with CCS. In this study, several energy carriers either based on renewable electricity or fossil fuels with CCS are assessed from a life cycle perspective. The purpose of this study is to compare the climate impact and cost assessment from cradle to grave for selected blue fuels, green fuels, and battery-electric for a case study vessel.

Prospective life cycle assessment is used to evaluate the climate impact, and life cycle costing is used to evaluate the cost considering a time horizon of 2030. Blue fuels considered are liquid hydrogen (blueLH2) and ammonia (blueNH3), which are assumed to be produced from natural gas with carbon capture and storage. The green fuels considered are electro-liquid hydrogen (greenLH2), electro-ammonia (greenNH3), and electro-methanol (greenMeOH) which are assumed to be produced from renewable electricity. In this particular investigation, the propulsion system is based on internal combustion engines, fuel cells for blue fuels and green fuels, and the utilization of renewable electricity as battery-electric. The results are compared with marine gas oil (MGO) used in an internal combustion engine (ICE).

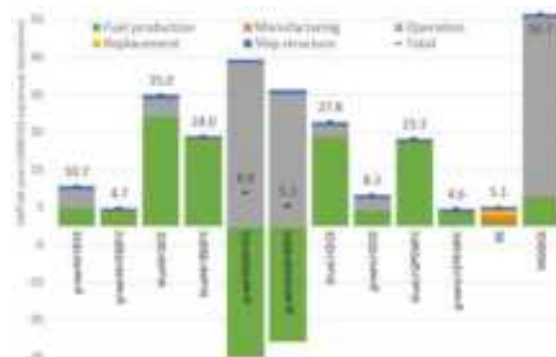


Figure 1. GWP100 results of different fuels assessed from cradle to grave. ICE: internal combustion engine, SOFC-solid oxide fuel cell, PEMFC: proton exchange membrane fuel cell, BE: battery electric.

Figure 1 shows the global warming potential over 100 years for the assessed options. Compared to the marine gas oil used in shipping, all options could reduce GHG emissions by 2030. Blue fuels (from natural gas with carbon capture and storage) have a reduction potential of around 40% to 60%, whereas green fuels

(from offshore wind electricity) have a reduction potential of around 80% to 95%, compared to MGOICE. Compared to engines, fuel cells have higher GHG reduction potential for the same energy carrier. The emissions of GHGs for engines is primarily related to the use of fossil fuels as pilot fuel in ICE and their higher consumption of fuel compared to fuel cells. The result shows that greenLH2PEMFC has the highest GHG reduction potential for the case vessel followed by greenNH3SOFC. The impact from ship structure is not significant compared to impacts from other phases.

Figure 2 shows the life cycle costs and carbon abatement costs of the assessed options. The life cycle cost of blue fuels in engines are lower compared to the cost of green fuels. Blue ammonia is found to have the lowest life cycle cost as the main cost of the options is related to fuel cost. Options based on blue fuels have 1.5 to 2 times the cost of marine gas oil option whereas options based on green fuels have 2 to 3 times the cost of marine gas oil option. Among green fuels, electro-ammonia, followed by electro-methanol, has the lowest cost when used in the ICE. Distribution cost is high for the hydrogen option and battery electric as the infrastructure for the bunkering is complex for these energy carriers. Despite lower fuel consumption compared to engines, fuel cell options tend to have relatively high costs for all ship types due to higher investment costs and the lower operation life of the fuel cell.

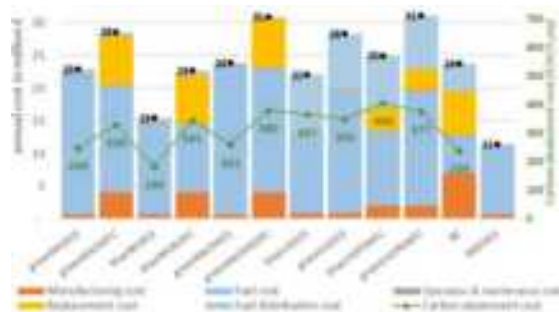


Figure 2. Life cycle cost results of different fuels assessed.

In summary, there is a potential to decarbonize the shipping industry by changing fuels. For the short term, blue fuels seem to be a solution that has only limited global warming reduction potential, however, they come with a lower cost. For the longer term, only the transition towards green fuels can meet the requirement of the GHG reduction targets as per the IMO's GHG strategy.

Policy scenarios for analysing use of scrubbers in shipping

Erik Fridell¹, Rasmus Parsmo¹, Elisa Majamäki² and Jukka-Pekka Jalkanen²

¹IVL Swedish Environmental Research Institute, Gothenburg, Sweden

²FMI, Helsinki, Finland

Keywords: scrubber, shipping, scenarios, emissions.

Presenting author email: erik.fridell@ivl.se

The future impact of shipping on the environment and climate is analysed in a set of scenarios. The aim is to describe that different policy measures will lead to different outcomes in the future. Special focus is on the use of scrubbers and the effects on air quality and emission of scrubber water.

The emissions of sulphur oxides and particles from shipping is regulated through the fuel sulphur content. However, it is also allowed to use high sulphur fuel if the emissions of sulphur oxides is reduced by the use of scrubbers, in turn leading to emissions to sea of polluted scrubber water. In the EMERGE project we have constructed eight scenarios where the development of the ship traffic is based on scenarios constructed by DNV (2020). The scenarios investigates the use of abatement equipment, different fuel mixes and different development of ship traffic. Following the assumptions made, the emissions to air and water are modelled with the STEAM-model, divided on different ship types and different sea areas.

Scenario 1 (S1) is a high-pressure scenario. The maritime transport development is high, there are no further measures to reduce the use of fossil fuels in shipping other than those already decided today, there is high use of scrubbers. In this scenario there is thus a significant pressure on the environment from scrubber water.

Scenario 2 (S2) is the same as Scenario 1 but instead of open-loop scrubbers the same ships are assumed to use closed-loop scrubbers.

In **Scenario 3** (S3) we use the same assumptions as in S1 and also that SECA and NECA are introduced in all European sea areas.

In **Scenario 4** (S4) there is low development of ship traffic and more use of LNG for short-sea shipping but otherwise identical to S1.

Scenario 5 (S5) is a low-pressure scenario. There is low development of ship traffic, measures are assumed to be in place for shipping to reach the IMO objective of a 50% reduction in the emissions of green-house gases by 2050 (with 2008 as base year), there is no use of scrubbers.

For **Scenario 6** (S6) we assume high development in ship traffic, measures in place to reach the IMO 50% goal, high use of scrubbers. When comparing with S1 this will show the effect of the IMO 50% goal.

Scenario 7 (S7) is similar to S6 but with low use of scrubbers.

Scenario 8 (S8) is an LNG scenario. It has the same assumptions as S7 but with an extensive use of LNG in Europe.

The use of scrubbers is modelled with an economic model assuming that ships will install and use scrubbers when profitable, i.e. in principle when the investment cost is lower than the cost difference between high sulphur and low sulphur fuel. The costs for installing and using scrubbers are taken from EMERGE D1.1 (2020). The annual fuel use for individual ships is taken from the global STEAM model.

Figure 1 shows the cost-savings for individual ships in Europe vs annual fuel consumption; for ships above zero it is economically beneficial to use scrubbers. Figure 2 shows as an example the emission of scrubber water in Europe in 2050 in the scenarios, split on ship type.

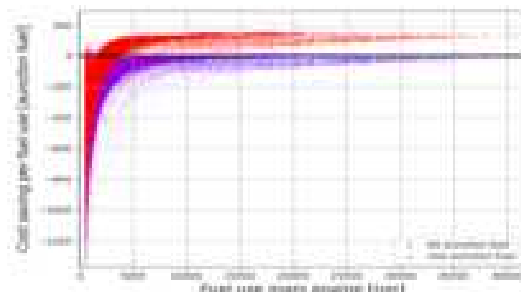


Figure 1 Cost savings vs fuel use for all ships in Europe when using open-loop scrubbers rather than VLSFO.

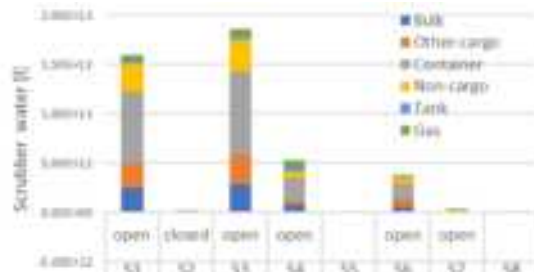


Figure 2. The volumes of emitted scrubber water in Europe in the different scenarios split on ship type. Note that S2 assumes closed-loop scrubbers.

This presentation is based on results from the EU project EMERGE, (2020 – 2024; <https://emerge-h2020.eu/>). DNV, Energy Transition Outlook 2020. A global and regional forecast of the energy transition to 2050, DNV GL 2020,

Winnes et al., 2020. Summary and analysis of available abatement methods for SO_x, NO_x and PM, together with data on emissions, waste EMERGE D1.1

Projections of shipping emissions in Europe in 2040 and 2050

E. Majamäki¹, J.-P. Jalkanen¹, V. Matthias², J. Moldanova³, L. Johansson¹

¹Finnish Meteorological Institute, Helsinki, 00560 Finland

²Helmholtz-Zentrum Hereon, Geesthacht, 21502 Germany

³IVL Swedish Environmental Research Institute, Gothenburg, 40014 Sweden

Presenting author email: elisa.majamaki@fmi.fi

The International Maritime Organization (IMO) has set a target to reduce the greenhouse gas emissions from shipping by 50% by 2050 compared to emissions in 2008. To achieve this, shipping sector must find new energy sources to replace traditionally used fossil fuels. In addition, there are goals to reduce the impacts of shipping on air quality. One important tool for this is the implementation of emission control areas for sulphur (SECA) and nitrogen compounds (NECA). Estimations of the ship emissions in the future and the emission reduction potential of new regulations are needed for supporting policy makers in deciding the best pathways for reducing emissions from shipping. Aim of this study is to develop shipping emission inventories for Europe in 2040 and 2050 under different future scenarios.

In this study, several different projections of the future of shipping sector were considered. Emission scenarios for 2040 focus on different regulatory scenarios. Shipping emissions with and without an implementation of a new NECA within 200nm from the coastline is studied. In addition, scenarios of non-compliance and reduced efficiency of Selective Catalytic Reactors (SCRs) in low engine loads have been investigated. Scenarios for 2050 focus on impact of different energy sources on shipping emissions. Four different cases with different dominant fuels, such as traditional marine fuels, Liquified natural gas (LNG), ammonia and methanol, have been simulated.

Ship emission inventories have been produced using Ship Traffic Emission Assessment Model (STEAM) (Johansson et al. 2017). Shipping activity is based on Automatic Identification System (AIS) data from year 2015 and the development of the shipping fleet, transportation work and shipping fuel mix from 2015 to the target years 2040 and 2050 are based on projections by DNV-GL (2020). When defining the fuel type used by different vessels, it was assumed that short-sea shipping will move to alternative fuels, such as methanol and ammonia, first while ships that mainly sail on intercontinental routes will prefer more traditional fuels. Ship emission inventories for 2040 and 2050 were generated for European domain (lat: lon: 23.0 ... 70.0; -30.0 ... 38.0) with a resolution of 10km x 10km and an hourly temporal resolution.

Results for 2040 show that implementing a European wide NECA could reduce NOx emission by nearly 50% in comparison to a situation without implication of new NECAs in Europe by 2040. However, possible non-compliance or reduced efficiency of SCRs would weaken the benefits of the new NECA. Projections for 2050 show significant reduction e.g., in emissions of

particulate matter and sulphur oxides regardless of the increase in ship traffic. However, results indicate that emissions of some currently unregulated pollutants, such as ammonia (NH_3), methane (CH_4) and nitrous oxide (N_2O), can increase in the future if emissions of these pollutants remain uncontrolled. *Figure 1* shows an example of the gridded results of the study: total emissions of NH_3 in 2050 under a scenario with high fraction of energy (>40%) in shipping coming from combustion of ammonia.



Figure 1. Total predicted ammonia (NH_3) emissions from shipping in Europe in 2050

This study has received funding from the European Union's Horizon 2020 Programme Research and Innovation action under grant agreement No 814893 (SCIPPER project).

Johansson, L., Jalkanen, J.-P. and Kukkonen, J. (2017) *Global assessment of shipping emissions in 2015 on a high spatial and temporal resolution*, *Atmos. Environ.*, **167**, 403–415

DNV-GL. (2020) *Maritime forecast to 2050, Energy transition outlook 2020*.

Climate friendly and pollution-free? Scenarios for air pollution from shipping in Europe in 2050

Volker Matthias¹, Lea Fink¹, Achilleas Grigoriadis³, Josefine Hahn¹, Jukka-Pekka Jalkanen², Jereon Kuenen⁴, Elisa Majamäki², Leonidas Ntziachristos³, Ronny Petrik¹, Daniel Schwarzkopf¹

¹Helmholtz-Zentrum Hereon, Geesthacht, Germany

²Finnish Meteorological Institute, Helsinki, Finland

³Aristotle University of Thessaloniki, Thessaloniki, Greece

⁴TNO, Utrecht, The Netherlands

Keywords: ship emissions, air quality, future scenarios, chemistry transport modelling

Presenting author email: volker.matthias@hereon.de

Shipping contributes significantly to emissions of air pollutants and green house gases. The International Maritime Organisation (IMO) aims at reducing these emissions and adopted a strategy with the goal of a 50% reduction of greenhouse gas emissions in 2050 compared to 2008. This goal can only be reached through the introduction of new fuels. Among the most promising ones are liquefied natural gas (LNG) and ammonia (NH_3). Possible effects on air quality through significantly modified emissions from ships were investigated through the construction of ship emissions scenarios for 2050 and subsequent chemistry transport model simulations for meteorological conditions in 2015.

The scenarios were developed within the HORIZON 2020 project SCIPPER and the German SeAir project. They are based on projections of expected fuel use and transported cargo volumes given by the ship classification company DNV-GL in their report “Maritime Forecast 2050” (DNV-GL, 2020). We investigated a fuel use scenario with relatively high fraction of ammonia and LNG use and calculated spatially resolved emission maps for 2050 with the STEAM ship emission model (Johansson et al, 2017). Emission factors for new fuels were taken from recent literature and they were varied according to the installed engine technology (Majamäki et al., 2023). Impacts on air quality were simulated for entire Europe with the chemistry transport model CMAQ v5.3. Land based emissions included significant emission reductions until 2050, according to a current legislation scenario developed based on CAMS-REG inventory.

The STEAM results showed that NOx emissions per ton mile decrease drastically until 2050. However, the relative impact of shipping on atmospheric NO_2 increases compared to 2015 because of lower land based emissions and increased ship traffic. Shipping emissions will still cause increased ozone concentrations with potential impacts in the order of 10% on annual average in the Mediterranean region. In a case with high ammonia emissions from shipping, HNO_3 concentrations were drastically reduced because of ammonium nitrate particle formation close to the shipping lanes. The model simulations show ammonium concentrations of 0.4 – 0.6 $\mu\text{g}/\text{m}^3$ and nitrate concentrations of 1-2 $\mu\text{g}/\text{m}^3$ that can be attributed to shipping (Figure 1). The CMAQ results also show a considerable increase in ammonia concentrations over sea, indicating that only part of the emitted ammonia will be consumed in new particle formation processes.

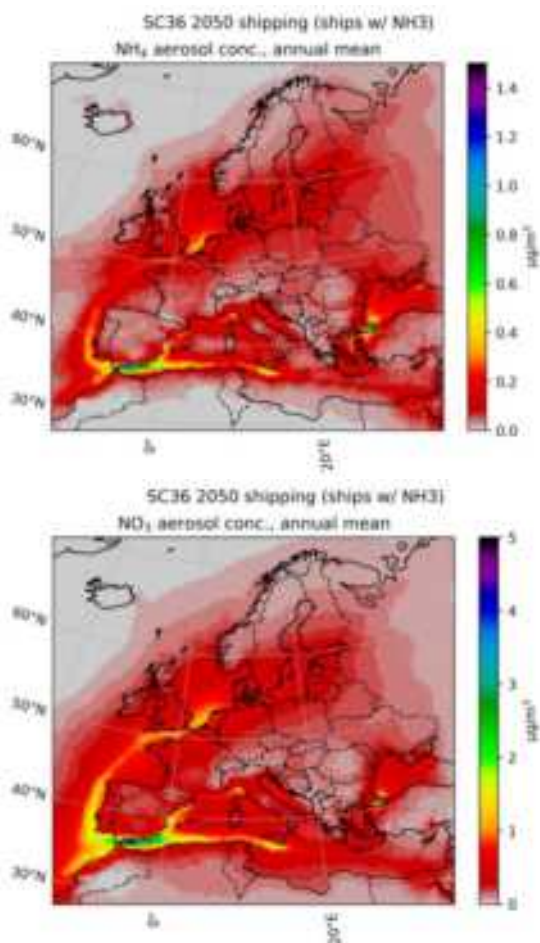


Figure 1: Impact of shipping emissions on particulate ammonium (top) and nitrate (bottom) concentrations for the case of high ammonia emissions from shipping in 2050.

DNV-GL (2020). Maritime forecast to 2050 - Energy transition outlook 2020

Johansson, L., Jalkanen, J.-P. and Kukkonen, J. (2017). Atmos. Environ., 167, 403–415

Majamäki, E., Jalkanen, J.P., Matthias, V., Moldanova, J., Johansson, L. (2023). TAP and S&E Conference 2023

3.11 SE.13 Marine processes – fate of pollutions from shipping in the marine environment: impact studies on ecotoxicology, eutrophication and acidification, energy pollution including underwater noise & induced mixing, experimental work, modelling studies of dispersion, transport, and chemical and biological processes in marine waters.

A multi species and multi system evaluation of the ecotoxicological effects of scrubber water – a synopsis of results from the EMERGE project

M.E. Granberg¹, K. Magnusson¹, N. Abrantes², M. Baccichet, L. Calgaro³, C.Y. Chen¹, G. G. Distefano³, S. Dupont⁴, E Garcia², S Genitsaris⁵, A. Volpi Ghirardini⁵, E. Giubilato³, M. Gros^{6,7}, I.-M. Hassellöv⁸, A. Lunde Hermansson⁸, M.D. Hudson⁹, D. Marchetto³, Antonio Marcomini³, A.A. Monteiro³, M. Moustaka-Gouni⁵, L. Ntziachristos⁵, P. Osborne⁹, M. Petrovic^{6,10}, M. Picone³, A. Ré¹¹, M. Russo³, K. Salo⁸, N. Stefanidou⁵, I. Williams⁹, L. M. Zapata-Restrepo⁹ & E. Ytreberg⁸

¹IVL Swedish Environmental Research Institute, Kristineberg Center, Fiskebäckskil, 45178, Sweden

²Dept. Of Biology & CESAM, University of Aveiro, Aveiro, 3810-193, Portuga.

³Environmental Sciences, Informatics and Statistics, University Ca' Foscari Venice, 30172, Italy

⁴BIOENV, University of Gothenburg, Kristineberg Center, Fiskebäckskil, 45178, Sweden

⁵Biology, Aristotle University of Thessaloniki, Thessaloniki, 54124, Greece

⁶Catalan Institute for Water Research, Girona, 17003, Spain

⁷Universitat de Girona (UdG), Girona, Spain

⁸Mechanics and Maritime Sciences, Chalmers University of Technology, Gothenburg, 412 96, Sweden.

⁹Engineering and Physical Sciences, University of Southampton, Southampton, SO17 1BJ, United Kingdom

¹⁰Catalan Institute for Research and Advanced Studies (ICREA), Barcelona, Spain

¹¹Dept. of Environmental planning & CESAM, University of Aveiro, Aveiro, 3810-193, Portugal

Keywords: Scrubber water, ecotoxicology, marine, effects

Presenting author email: maria.granberg@ivl.se

Allowing for installation of exhaust gas cleaning systems (scrubbers) as an alternative to using a cleaner fuel, to comply with the IMO 2020 Sulphur cap, has been done without appropriate consideration of negative impacts on marine life. The toxic and acidic cocktail of scrubber water may pose a serious threat to marine organisms and ecosystems, with consequences for commercial fish stocks (Koski *et al* 2017, Thor *et al* 2021).

Ecotoxicological experiments were carried out on endemic species at five European research laboratories within the research project EMERGE (EC-Horizon 2020), aiming to investigate effects of scrubber water on marine life. Different life stages, species and microbial plankton communities were investigated. Scrubber water was obtained from open loop systems onboard operating ships (DANAOS Shipping co. LTD) and from a pilot system at Chalmers University of Technology, Sweden. A range of scrubber water concentrations (0.0001 to 40% v/v sea water) were tested. Protocols for collection, storage and handling of scrubber water were developed in order not to alter chemical characteristics. All laboratories used CRED methodology (Moermond *et al*, 2016).

Toxic effects were detected at much lower concentrations (0.0001-0.001%) than previously reported. Invertebrate fertilization and larval development were the most sensitive endpoints. These endpoints were not included in previous studies on scrubber water toxicity but are vital for species recruitment and thus for maintaining sustainable marine food webs. Microalgal growth rate of and invertebrate mortality are endpoints commonly used in standardized ecotoxicity tests; however, these parameters were found to be less sensitive. Marine microbial communities showed high resilience with effects detected at 10% scrubber water. Bacterial community change towards pollution resistant and PAH degrading strains was observed.

We conclude that there is an apparent risk that scrubber water may have a serious impact on populations of key species of marine food webs. This risk must be considered in the continued debate about the future use of scrubbers in shipping.

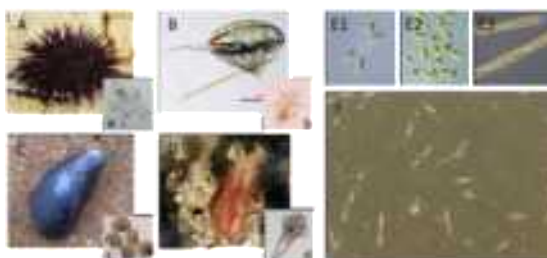


Figure 1. Species, larvae and planktonic communities investigated. A: Sea urchin (*Paracentrotus lividus*, Echinodermata) & pluteus larva (a), B: Copepod (*Calanus sp.*, Crustacea) & nauplius larva (b), C: Blue mussel (*Mytilus sp.*, Mollusca) & veliger larva (c), D: Polychaete (*Sabellaria alveolata*, Annelida) & trochophore larva (d), E: Microalgae, *Phaeodactylum tricornutum* (E1), *Dunaliella tertiolecta* (E2) and *Pseudo-nitzschia sp.* (E3), F: Phytoplankton community.

This work was supported by the EC Horizon 2020 EMERGE project (Grant Agreement No. 874990).

Koski, M., C. Stedmon, and S. Trapp (2017) *Marine Environmental Research* **129**, 374-385.

Moermond, C. T. A., R. Kase, M. Korkaric, and M. Ågerstrand (2016) *Environmental toxicology and chemistry* **35**, 1297-1309.

Thor, P., M. E. Granberg, H. Winnes, and K. Magnusson (2021) *Environmental Science & Technology* **55**, 5826-5835.

Sampling strategies and characterization of greywater from ships

J.T. Mujingni¹, G.B.M Rathnamali², I-M Hassellöv¹, E. Ytreberg¹ and K. Salo¹

¹Department of Mechanics and Maritime Sciences, Chalmers University of Technology, Gothenburg, 412 96, Sweden

²Department of Marine Sciences, Gothenburg University, Gothenburg, 405 30, Sweden

Keywords: greywater, characterization, sampling, ships, emissions.

Presenting author email: mujingni@chalmers.se

Greywater is not regulated by the International Convention for the prevention of pollution from ships, the MARPOL Convention (IMO, 2019), as such ships are currently discharging this sanitary liquid stream into the sea in various forms; sometimes untreated, treated together with sewage before discharge, delivered to port reception facilities (PRF) or mixed and discharged with food waste. Recent studies have revealed that over 5.5 million m³ of grey water is discharged into the Baltic Sea annually but there is a lack of knowledge about the quantity of all the greywater sub-flows, their chemical composition as well as the generated and discharged volumes from various ship segments (Ytreberg *et al.*, 2020).

The composition of greywater makes it hazardous when discharged untreated, hence, it presents a risk to the Baltic Sea environment due to lack of international and regional conventions governing its discharge. Ship-generated greywater originates from accommodation (sinks and showers), laundry facilities, and drains in the galley (kitchen area) and contains various contaminants (Folbert *et al.*, 2022; US-EPA, 2011). However, there's limited knowledge about the contributions from specific products (e.g., cleaning products) used on board and their chemical composition, as well as their individual contribution to the contaminant loads from various greywater sources. Moreover, there is, no standardized strategy to sample greywater from ships, given a variation in systems structure and configuration on different ship types. This makes it difficult to assess the magnitude and impact of greywater discharge on the marine environment, and for stakeholders to suggest relevant management strategies with respect to greywater discharges in the Baltic Region. This also illuminates the need for detailed prior planning and pre-sampling visits on board the ships.

This paper presents a structured strategy for sampling, and characterization of greywater from a set of ships operating in the Baltic Region. This includes investigation of the presence and concentrations of nutrients, metals, TSS, pH, BOD7, Coliform Bacteria, TIC, TOC, PMOC, PFAS, Phthalates, pharmaceuticals and microplastics in greywater from the ships.

A literature review was carried out to ascertain the pollutant types detected in greywater from prior research. Next, 9 shipping companies were invited to participate in the study, and 10 ships from 4 shipping lines expressed their intent to participate. Planned visits on board were organized, firstly, to map sampling points, and secondly, to carry out sampling of greywater on the ships. The sampling points were noted, and an

assessment was made whether to sample from the holding tank or the discharge pipe. A consideration of the sampling of sub-flows from the accommodations, laundry and galley was also made. Sampling was done on high-flow days when the ships were at almost full occupancy. On each ship, a main sample was first collected using a 10L glass bottle which served as an initial sampling container where the sample was mixed to ensure homogeneity before distributing into smaller, pre-cleaned plastic and glass bottles according to the laboratory instructions. The 10L sampling bottles were prepared by treating with methanol and milli-Q water, while the smaller bottles were heated in an oven overnight at 400 degrees. Sampling bottles from ALS arrived already sterilized. Representative samples were obtained from the 10 ships and sent to the laboratories for analysis. The various parameters were analyzed by different laboratories according to their areas of expertise (ALS Scandinavia AB, ICRA and the University of Gothenburg).

The results will present a sampling strategy that is replicable in the industry, as well as a database containing the detectable concentrations of pollutants in the studied categories; ascertaining the need greywater environmental management strategies on board ships, mitigate their impact on the Baltic Sea. The novelty of this study lies in its sampling strategy and the provision of detailed primary ship-generated greywater characterization data within the Baltic Region, which is currently nonexistent. It is also a potential contributor to the amendment of MARPOL Annex IV at IMO.

This work is funded by the Swedish Transport Agency and the Swedish Agency for Marine and Water Management, as part of the project by "Gråvatten i Östersjön" HaV Dnr 865-22.

Folbert, M. E. F., Corbin, C., & Löhr, A. J. (2022). *Sources and Leakages of Microplastics in Cruise Ship Wastewater*. Frontiers in Marine Science, 9. <https://doi.org/10.3389/fmars.2022.900047>

US-EPA (2011). Graywater Discharges from Vessels. EPA - 800-R-11-001, United States Environment Protection Agency, Office of Wastewater Management, Washington, DC 20460.

Ytreberg, E., Eriksson, M., Maljutenko, I., Jalkanen, J.-P., Johansson, L., Hassellöv, I.-M., & Granhag, L. (2020). *Environmental impacts of grey water discharge from ships in the Baltic Sea*. Marine Pollution Bulletin, 152, 110891. <https://doi.org/10.1016/j.marpolbul.2020.110891>

Turbulent ship wakes: extent, intensity, and interaction with stratification

Amanda T. Nylund¹, Ida-Maja Hassellöv¹, Anders Tengberg^{1,2}, Rickard Bensow¹, Göran Broström², Martin Hassellöv², and Lars Arneborg³

¹ Department of Mechanics and Maritime Sciences, Chalmers University of Technology, 412 96 Gothenburg, Sweden.

²Department of marine sciences, University of Gothenburg, 413 19 Gothenburg, Sweden.

³Department of Research and Development, Swedish Meteorological and Hydrological Institute (SMHI), Gothenburg, 426 71 Västra Frölunda, Sweden.

Keywords: Turbulent ship wake, stratification, contaminant dispersion, energy pollution.

Presenting author email: amanda.nylund@chalmers.se

Turbulent ship wakes are a form of ship-induced energy pollution that has previously been overlooked (Nylund et al., 2021). In intensively trafficked shipping lanes, ships pass up to every 10-15 min, resulting in a frequent input of intense turbulent mixing in the shipping lane surface layer. Frequent and intense turbulence has the potential to impact local hydrography, air-sea gas exchange, and mortality in plankton. In addition to the direct impact of the turbulence, understanding the development and intensity of the turbulent wake is also needed to correctly model and monitor the dispersion of contaminants in shipping lanes. Therefore, a characterisation of the turbulent wake development in natural conditions is important.

The turbulent wake and its impact occur on spatiotemporal scales that are challenging to observe and model and are therefore easily overlooked. There is currently a lack of suitable methodologies to capture the entire turbulent wake extent from the hull and propeller to the total wake length of several km (Nylund et al., 2021). Field observations do not allow for observations in the region closest to the ship, and, on the contrary, resolution requirements in the numerical models are too high to normally extend over the entire wake with sufficient resolution to capture the spatial scales of the wake.

In this work we have characterised the entire turbulent wake development, with respect to spatiotemporal scales and turbulence intensity, by combining *in situ* observations and high-resolution modelling. The interaction between turbulent wake development and stratification has been investigated. The presented work is based on a unique and extensive dataset of turbulent ship wakes, their spatiotemporal extent and input of turbulent energy.

Two field campaigns were conducted in shipping lanes on the Swedish west coast, where bottom-mounted Acoustic Doppler Current Profilers (ADCP) were used to observe the spatiotemporal extent and intensity of turbulent wakes. Turbulent kinetic energy dissipation rate (ϵ) was calculated from the observed current velocities and was used as an estimate of the turbulent intensity. Automatic Identification System (AIS) records were used to identify the wake-inducing ships and stratification was observed using conductivity, temperature, depth (CTD) measurements. Two ship-designs similar to ships present in the *in situ* dataset, were used in a high resolution Reynolds Average Navier Stokes (RANS) model, to compare the modelled wake

distribution to the wake observed in the field. The model was run for 40 s (at 300 m aft of the ship) in both stratified and non-stratified conditions.

The field observations showed turbulent wake durations of 5-10 min and depth extents of up to 30 m. However, the detected wake depths varied greatly between locations and ships, with similar ships inducing wakes of depths from 10-30 m. One explaining factor for this variance in wake depth, was the presence of stratification, as it was found to clearly limit the vertical extent of the wake and cause the wake to distribute horizontally along the stratification instead. However, vertical mixing across the stratification was also observed, in the field as well as in the model results.

The ship-induced ϵ observed in the wake were well above previously reported values shown to cause increased mortality in zooplankton. The modelled and observed ϵ were in the same order of magnitude in the small region of overlap, about 300 m after the propeller. This indicates that the model and observations are consistent with each other with respect to turbulent kinetic energy and its dissipation rate. Moreover, most of the turbulent kinetic energy dissipated within the first 40 s of the wake, hence relying only on ADCP observations would greatly underestimate the turbulent energy input. On the other hand, the deepest part of the wakes generally occurred after the first 40 s, hence the RANS modelling, performed up to 40 s, underestimates the vertical extent of the turbulent wake.

The results of this work show that stratification impacts the turbulent wake development and should be considered when sampling and modelling contaminant dispersion in shipping lanes. They also show that ship-induced turbulence is an overlooked source of vertical mixing across stratification in areas with intense ship traffic.

This work was funded by Chalmers Area of Advance Transport, Swedish Agency for Marine and Water Management (Dnr 796-20) and the European Union's Horizon 2020 research and innovation programme Evaluation, control and Mitigation of the Environmental impacts of shipping Emissions (EMERGE) [grant agreement No 874990].

Nylund, A. T., Arneborg, L., Tengberg, A., Mallast, U. and Hassellöv, I. M. (2021) *In situ* observations of turbulent ship wakes and their spatiotemporal extent, *Ocean Sci.*, **17**, 1285-1302.

Response in the marine diatom *Nitzschia* sp., following exposure to bilge water from different ships

J. Egardt¹, I.-M. Hassellöv², I. Dahllöf¹

¹Department of Biological & Environmental Sciences Gothenburg University, 405 30 Gothenburg, Sweden

²Department of Mechanics and Maritime Sciences, Chalmers University of Technology, 412 96 Gothenburg, Sweden

Keywords: bilge water, toxicity, marine environment, *Nitzschia*
Presenting author email: jenny.egardt@bioenv.gu.se

The bilge is the lowest point in marine vessels, and the water collected here originates from several different on-board areas, primarily condense water from the engine room. Bilge water contains residues of fuel, hydraulic and lubricating oils, metals, detergents, degreasers etc. (US EPA, 2008, Tiselius & Magnusson, 2017).

Discharge of bilge water en route is allowed if compliant with IMO regulations. The main target is that oil content is below 15 ppm (MARPOL (73/78) Annex I) and to achieve that, prior to discharge the bilge water is treated in an oily water separator (OWS).

Reducing the total oil content below 15 ppm may, however, not make it environmentally safe to discharge. It has for example been shown in analysis of treated bilge water that although the total content of organic substances was below 15 ppm, individual PAH:s were above their predicted no effect levels (PNEC) (Isaksson & Möller, 2021). The same study showed that metals and surfactants remained after treatment in the OWS. When exposing the marine copepod *Acartia tonsa* to 1-10 % dilutions of treated bilge water, Tiselius & Magusson (2017) found significant negative effects already at 1-5 % of bilgewater content, and that effects differed markedly between bilge waters from different ships.

The amount of produced bilge water depends on a vessel's engine capacity, and for passenger ships and RoPax vessels with engine powers ranging between 5287-62901 kW the daily production is between 70-10900 L (Det Norske Veritas, 2009, Magnusson et al. 2018). Considering the number of vessels of the global fleet trafficking our seas there is therefore potential for a negative impact on the marine environment.

In our study, we will show results from exposure of the diatom *Nitzschia* sp. to bilge water from six different vessels to assess toxicity to a common primary producer in the Baltic Sea, and compare difference in toxicity between bilge waters with known content. As effects of bilge water is not yet well studied and results from studies vary depending on the ship (Tiselius & Magusson, 2017), it has not been ascertained if it is specific compounds or the mixture itself that is driving the toxicity.

By comparing effects of bilge waters with known contents we can start narrowing down potential suspects that cause harm to marine organisms and aid in getting regulations in place to protect the marine environment.

Acknowledgment: Projects is funded by FRAM (Future Risk Assessment and Management) at Gothenburg University.

- Det Norske Veritas. (2009). *Study on Discharge Factors for Legal Operational Discharge to Sea from Vessels in Norwegian Waters*. Report No. 2009-0284, 47pp.
Isaksson, M., and Möller, M. (2021). *Chemical pollutants released in treated bilge water. BSc thesis*. Chalmers University of Technology. 124pp.
Magnusson, K., Jalkanen, J. P., Johansson, L., Smailys, V., Telemo, P., & Winnes, H. (2018). *Mar Poll Bull*, 126, 575-584.
Tiselius, P., and Magnusson, K. (2017). *Mar Poll Bull*, 114(2), 860-866.
US EPA (2008). *Cruise Ship Discharge Assessment Report*. Report no. 842-R-07-005, pp. 1-21

Scrubber water impairs fertilization and development in the green sea urchin (*Strongylocentrotus droebachiensis*) at very low concentrations

C.Y. Chen¹, K. Magnusson¹, S. Dupont², R. Pfeiffer¹ & M.E. Granberg¹

¹IVL Swedish Environmental Institute, Kristineberg Center, Kristineberg 566, 45178 Fiskebäckskil, Sweden

²Department of Marine Ecology, Kristineberg Center, Kristineberg 566, 45178 Fiskebäckskil, Sweden

Keywords: Scrubber effluent, sea urchin, larvae development, PAH

Presenting author email: chiau.yu.chen@ivl.se

Fertilization and larval development of the green sea urchin (*Strongylocentrotus droebachiensis*) are susceptible to environmental stressors, especially during the planktonic (pelagic) larval stage, which in turn directly affects recruitment rates. Scrubber water generated from exhaust gas cleaning systems, intended to reduce sulphur emission from large commercial ships, have been shown to be one of these stressors. Scrubber water effluent is usually acidic and contains a complex mixture concentrated heavy metals and polycyclic aromatic hydrocarbons (PAHs) (Thor *et al.*, 2021; Petrović *et al.*, 2022). We investigated the effects of scrubber water (collected onboard a vessel in the English Channel on route from Belgium to Turkey) on the fertilization and larval development of the green sea urchin. Severe toxic effects were observed across the concentration gradient. Fertilization was affected at the lowest tested concentration of 0.0001% and a no-effect concentration could thus not be determined. Deformation of larvae severely increased across the concentration gradient, from $23\% \pm 10$ (average \pm SD) in the controls to $97\% \pm 6.6$ (average \pm SD) at a treatment concentration of 10% of scrubber water, as shown in Figures 1 and 2. Skeletal formation was absent at treatment concentrations from 5% and higher. Larvae exposed to 10% of scrubber water were not able to enter the pluteus stage. Growth in body length was decreased with increasing scrubber water concentration, with a total collapse at 10%. At Day 6 when larval feeding would normally begin, individuals in the 10% treatment exhibited negative growth. We hypothesize that lack of arm development due to inhibited skeletal formation hindered feeding activity. We conclude that scrubber water exposure already at very low concentrations may severely disrupt recruitment of green sea urchin larvae by affecting development of key life stages.

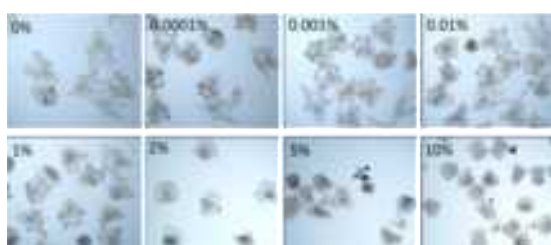


Figure 1. Increasing deformation of larvae across treatment concentrations. Skeletal formation was absent at 5% scrubber water and higher, and development is hampered at 10% scrubber water.

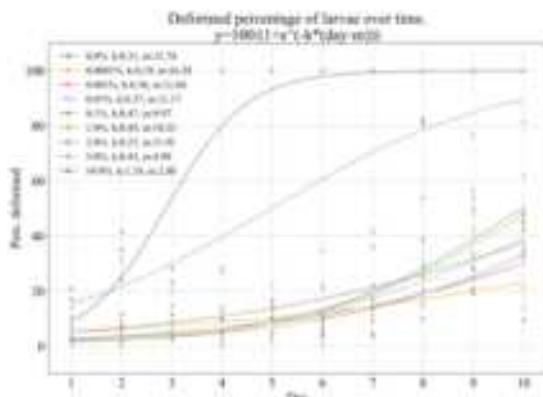


Figure 2. Percentage of deformed larvae across scrubber effluent concentration and time post-fertilization.

This work was supported by the EMERGE project funded under the European Union's Horizon 2020 research and innovation programme (Grant Agreement No. 874990).

Petrović, M., Gros, M., García, E., Hassellöv, M., Gondikas, A. (2022). *Report on measurements of dissolved and particulate contaminants in case study regions*, Deliverable 2.2, EMERGE Project.
Thor, P., Granberg, M. E., Winnes, H. and Magnusson, (2021). *Environ. Sci. Technol.* **55**, 5826-5835.

The possibilities and effects of ship speed reduction on underwater noise – a case study

R.E. Bensow¹, D. Glebe², M. Andersson³, L.-G. Malmberg⁴, E. Lalander³, D. Langlet,⁵ K. Larsson⁶, M. Svedendahl³, I.-M. Hassellöv¹, E.-L. Sundblad⁷

¹Department of Mechanics and Maritime Sciences, Chalmers University of Technology, Gothenburg, Sweden

²Department of Process Modelling and Digitalisation, IVL Swedish Env. Research Inst., Gothenburg, Sweden

³Department of Defence Technology, Swedish Defence Research Agency, Stockholm, Sweden

⁴Department of Law, School of Business, Economics and Law, Gothenburg University, Sweden

⁵Department of Law, Uppsala University, Uppsala, Sweden

⁶Kalmar Maritime Academy, Linnaeus University, Kalmar, Sweden

⁷Swedish Institute for the Marine Environment, Gothenburg, Sweden

Keywords: underwater noise, ship speed reduction, Automatic Identification System, regulation

Presenting author email: rickard.bensow@chalmers.se

Underwater radiated noise (URN) by ships and its effect on the marine wildlife is receiving increased attention. Energy input, such as sound, to the ocean was acknowledged as a pollutant by the EU in the MSFD 2008/56/EC. Recently, an assessment framework, including threshold values for URN, was adopted by EU, forming a basis for future national regulations (Borsani et al., 2022).

The current status of and the means to achieve good environmental status with respect to URN from shipping are however not clear. There are no technical solutions for all or any vessel that reduces URN without risk of increasing other shipping pressures, such as CO₂-emissions, and modifying ship routes to protect certain areas may be difficult for business and judicial reasons. One possible option, though, may be to reduce the ship speed. In 2017, within the ECHO program, ships passing the Haro Strait outside Vancouver voluntarily reduced speed to 11 knots and the noise was measured before and after the trial period. Depending on ship type, measured noise levels were reduced by 3-12 dB by slowing down (MacGillivray et al., 2019).

Here, we investigate the possibilities to enforce a speed reduction in the southern Kattegat and the potential this may have in reducing ship URN. An area between Sweden and Denmark was selected, where there are major shipping lanes, ferry traffic, fishing areas, protected wildlife area, and important populations of cod, harbour porpoise and seabirds. The area is thus important for the protection of marine wildlife while including various types of ship traffic as well as some judicial complications as the economic zone is divided between the two states.

We have analysed the AIS data for ships passing the region for one year (2021) and classified these based on ship type, speed, and length. The traffic in this area is considerably different from the one studied in the ECHO program thus the experiences may not be directly transferable. A simulation model was set up, using the available AIS data and based on the JOMOPANS-ECHO source level (SL) model (MacGillivray and de Jong, 2021) to simulate the effect of speed reduction measured in the area. Different traffic regulation scenarios were assessed with respect to, e.g., number of ships affected by different general speed limitations, or noise reduction effect of limiting only certain types of traffic.

Further, we investigated the applicability of the JOMOPANS-ECHO SL-model, which is based on the

data from the ECHO program, for the ships in our scenario. To do this, data from a hydrophone station outside Gothenburg, collected by Swedish Defence Research Agency, FOI, within the JOMOPANS project, were compared to the SL-model. This concerns, e.g., smaller tankers and RoRo vessels, rather common in our dataset and not present in the ECHO dataset.

Preliminary results indicate that a speed reduction to 11 knots is likely to influence URN levels in the area; preliminary results indicate a reduction by up to 5 dB. The effect is somewhat limited as some ships with higher design speed, like container ships, anyway slow down due to heavy traffic. With this strict speed limitation, almost all vessels in the area are affected; other, less restrictive, scenarios will also be presented at the conference. The simulations also indicate that single vessels have a minor impact on average equivalent sound levels but may be responsible for peak levels. The variations in sound level over time are in general minor, since the traffic in the area is heavy and loud single ship passages are averaged out some distance away from the routes.



Figure 1. The area studied; black lines mark shipping routes and the green area is a protected wildlife area

Borsani et al. (2022). *Setting of EU Threshold Values for continuous underwater sound, TG Noise Recommendations* (TG Noise Deliverable 4). Editorial coordination: Maud Casier, DG Environment, EC

MacGillivray et al. (2019). *Slowing deep-sea commercial vessels reduces underwater radiated noise*. J. of the Acoustical Society of America 146, 340

MacGillivray and de Jong (2021) *Reference Spectrum Model for Estimating Source Levels of Marine Shipping Based on Automated Identification System Data*. J. Mar. Sci. Eng., 9, 369

Influence of scrubber effluent on biogenic trace gas production

D. Booge¹, A. J. Paul¹, J.F. Tavares², S.C. Yang³, K. Salo⁴, K.R.M. Mackey², S.G. John³ and C. Marandino¹

¹GEOMAR Helmholtz Centre for Ocean Research Kiel, 24105, Germany

²Department of Earth System Science, University of California, Irvine, 92697, United States

³Department of Earth Sciences, University of Southern California, Los Angeles, 90089, United States

⁴Maritime Environmental Sciences, Maritime Studies, Chalmers Univ. of Tech., Gothenburg, 41296, Sweden

Keywords: climate active trace gases, open-loop scrubber, closed-loop scrubber, incubation experiments

Presenting author email: dbooge@geomar.de

Transport of international goods by ships is the most carbon-efficient method and its use is projected to increase significantly in the future (Sardain et al. 2019). It is known, that emissions of exhaust gases and particles into the marine boundary layer from ships contribute significantly to the total emissions from the transportation sector (Dalsoren et al. 2009). Based upon IMO framework standards, shipbuilding and operational standards have been introduced to regulate the amount of certain emissions to the atmosphere. These regulations result in use of alternative fuels as well as in increased use of wet scrubbers. Ships can still run with cheaper high sulphur containing fuel and still fulfil atmospheric emission regulations by scrubbing the exhaust gas with seawater. Scrubber effluent is pumped over board, but the effects of this effluent on seawater could potentially cause problems for marine ecosystems (Endres et al. 2018, Ytreberg et al. 2019). Some research has been done to investigate the potential toxic effect of scrubber effluent on marine organisms, including phytoplankton (Ytreberg et al. 2019) or zooplankton communities (Thor et al. 2021). However, no research has been done to date to study the cycling of marine biogenic trace gases which are impacted by changes in biological activity. These climate-active trace gases reach the atmosphere where they are readily oxidized and form oxidation products leading to particles and clouds (e.g. Liss and Johnson 2014). Hence, it is critical to understand how anthropogenic perturbations will affect climate-relevant trace gases formed in the ocean.

In this study, we present incubation experiment results about the influence of scrubber effluent on the climate active biogenic trace gases isoprene and dimethyl sulphide (DMS). Baltic Sea water was spiked with different amounts of either open-loop or closed-loop scrubber, in addition to the control treatment with pure seawater. Besides trace gas concentrations we measured a variety of other parameters which could explain changes in trace gas production during the experiment.

Our results clearly show that closed-loop scrubber effluent drastically influences biology and led to either reduced or no further trace gas production (Figure 1), dependent on the amount of scrubber addition, which was mainly due to incorporation of soot particles into phytoplankton cells and a consequent die off. However, open-loop scrubber effluent did not significantly influence the net trace gas production during the experiment (Figure 1). Scrubber effluent addition sometimes initially stunted phytoplankton growth but the system could recover after a few days with increasing cell

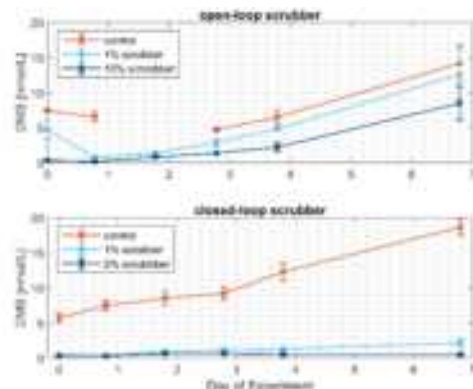


Figure 1. DMS concentrations in incubation treatments with different amounts of scrubber effluent compared to the control run (red) over a period of 7 days

counts and consequent trace gas production.

Although the net trace gas production was not significantly influenced by open-loop scrubber addition, the initial trace gas concentration in the incubation bottles was drastically reduced. Addition of open-loop and closed-loop scrubber caused an initial decrease of DMS and isoprene concentrations within 24 hours of up to 90% and 64%, respectively, compared to the control treatment (Figure 1, T0). These results clearly show that scrubber effluent directly decreases the apparent trace gas concentration when entering the ocean.

Climate relevant trace gases in the ocean will decrease through anthropogenic perturbation, as will atmospheric mixing ratios, likely leading to less aerosols and clouds and ultimately could facilitate climate change.

This work was conducted within the Belmont Ocean Sustainability joint research project ShipTRASE and was financed by the BMBF through grant 03F0843A.

Dalsoren, S. B., et al. (2009). *Atmospheric Chemistry and Physics* **9**, 2171-2194.

Endres, S., et al. (2018). *Frontiers in Marine Science* **5**

Liss, P. S. and M. T. Johnson (2014). *Ocean-atmosphere interactions of gases and particles*.

Sardain, A., et al. (2019). *Nature Sustainability* **2**, 274-282.

Thor, P., et al. (2021). *Environmental Science & Technology* **55**, 5826-5835.

Ytreberg, E., et al. (2019). *Marine Pollution Bulletin* **145**, 316-324.

3.12 SE.14. Holistic assessment of shipping impacts on the environment, shipping in marine spatial planning.

Impact assessment of shipping activities: Applying the critical load concept to both the atmosphere and marine environment

S. Guéret¹, W. Winiwarter^{1,2} A. Lunde Hermansson³, J. Borken-Kleefeld^{1,4}, I.M. Hassellöv³ and E. Ytreberg³

¹International Institute for Applied Systems Analysis (IIASA), 2361 Laxenburg, Austria

²Institute of Environmental Engineering, University of Zielona Góra, 65-417 Zielona Góra, Poland

³Department of Mechanics and Maritime Sciences, Chalmers University of Technology, Horselgången 4, 41756 Göteborg, Sweden

⁴Technische Universität Dresden, Chair of Transportation Ecology, 01069 Dresden, Germany

Keywords: Critical Load, Shipping emissions, Environmental Impact assessment, Scrubbers

Presenting author email: gueret@iiasa.ac.at

The IMO global sulphur cap regulation allows the use of scrubbers for controlling sulphur dioxide emissions while keeping up the use of cheap heavy fuel oil with high sulphur contents. However, discharge water from scrubbers contains high concentrations of metals, polycyclic aromatic hydrocarbons (PAHs), and acidifying compounds, threatening marine habitats and biota as well as the buffering capacity of the ocean. Thus, there is a trade-off between pollution of the atmosphere and the marine environment as the total pollutant load with scrubbers may be higher compared to combustion of low sulphur fuels (*e.g.*, MGO). As a widely used concept to devise emission control strategies and policies as a target for atmospheric depositions (De Vries *et al.*, 2015), critical loads are relevant tools to develop impact indicators and assess this trade-off.

Here we propose the critical levels of metals and PAHs, as well as the calcite saturation state, as new marine indicators for marine biota toxicity and ocean acidification, respectively. These can be quantified in three steps: (i) the characterization of the area and the derivation of maximum permissible concentration/load per grid cell, (ii) determination of the loads here specifically from ship discharges (taken from the ship emission model STEAM – Jalkanen *et al.*, 2021 – being distributed according to the ocean model Chemical Drift – Aghito *et al.*, 2022) to estimate concentrations per grid cell, and (iii) estimation of potential exceedances of critical levels.

The new marine indicators are combined with an established air pollution assessment scheme, also applying the concept of critical loads, and here extended to the marine environment. We apply this new approach to assess the impact on water and air, and subsequent marine and terrestrial biota, based on a set of shipping scenarios covering open and closed loop scrubber systems as well as alternative fuels. In a first application to a shipping lane in the Baltic Sea, scrubbers are identified as contributing to local exceedance of benzo[a]pyrene critical levels (Figure 1) and increase of calcite-under-saturated areas. Our research serves as groundwork for cost-effectiveness analyses of the given scenarios, as well as the development of a decision-support tool allowing stakeholders to identify trade-offs or co-benefits connected to measures imposed on shipping (Winiwarter *et al.*, this conference).

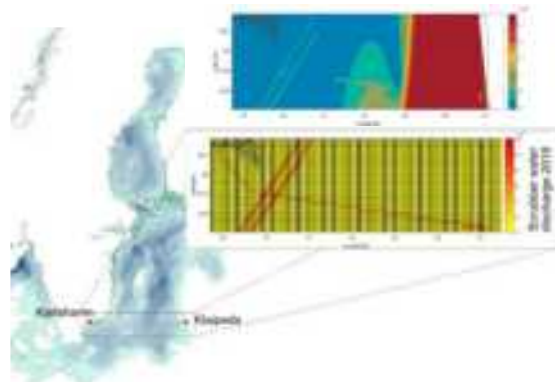


Figure 1. Map of the Baltic Sea area showing bathymetry (depth) and the Karlshamn-Klaipeda study area (red dashed lines). Enlarged is shown the exceedance of critical levels of benzo[a]pyrene ($\mu\text{g/L}$) derived from monitoring data (ICES Dome Data Portal) and open-loop scrubber discharges data (L) based on ship activity data from the year of 2018 (Jalkanen *et al* (2021)).

This work was supported by EU H2020 project EMERGE, which has received funding from the European Union's Horizon 2020 research and innovation programme under grant agreement no. 874990 (EMERGE project).

Aghito, M., Calgaro, L., Dagestad, K.-F., Ferrarin, C., Marcomini, A., Breivik, Ø., and Hole, L. R. (2022) ChemicalDrift 1.0: an open-source Lagrangian chemical fate and transport model for organic aquatic pollutants. *Geosci. Model Dev. Discuss* [preprint].

ICES Dome Data Portal: <https://www.ices.dk/data/data-portals/Pages/DOME.aspx>

Jalkanen, J., Johansson, L., Wilewska-Bien, M., Granhag, L., Ytreberg, E., Eriksson, K., Yngsell, D., Hassellöv, I., Magnusson, K., Raudsepp, U., Maljutenko, I., Styhre, L., Winnes, H., Moldanova, 004A. (2020). Modelling of discharges from Baltic Sea shipping. *Ocean Science* **17**, 699-728.

De Vries, W., Hettelingh, J.-P., Posch, M. (2015). *Critical Loads and Dynamic Risk Assessments: Nitrogen, Acidity and Metals in Terrestrial and Aquatic Ecosystems*. Environmental Pollution Series. vol. 25. Springer, Dordrecht.

Managing Marine Resources Sustainably: a transdisciplinary approach to the causes, consequences and responses to environmental problems of shipping and navigation

M. Elliott^{1,2}, I.-M. Hassellöv³

¹ International Estuarine & Coastal Specialists (IECS) Ltd., Leven, HU17 5LQ, UK

² School of Environmental Sciences, University of Hull, Hull, HU6 7RX, UK

³Department of Mechanics and Maritime Sciences, Chalmers University of Technology, Gothenburg, SE-41296, Sweden

Keywords: DAPSI(W)R(M), shipping, environmental management, activity-footprints,
Presenting author email: mike.elliott@hull.ac.uk

Ships compare to floating industries with a range of onboard systems giving rise to marine pollution (Jalkanen et al. 2021, Nylund et al. 2021). However, ship activities are not included in industrial regulatory frameworks e.g. the European Industrial Emission Directive (2010/75/EU), but rather that ship pollution prevention are often regulated through global conventions e.g. IMO MARPOL, and use of type approval of individual onboard systems. This implies a gap in relation to marine management which needs to consider the cumulative pressure from all ships operating in the marine area of interest.

By merging concepts and approaches from the natural and social sciences, this paper considers all aspects of the causes of environmental changes due to shipping and navigation. It focuses on the DAPSI(W)R(M) problem-defining framework (Elliott et al. 2017), in which the Drivers (the basic needs for shipping), leading to Activities (ship movement patterns, including operation/functioning of onboard systems such as antifouling paint, scrubber wash water and ballast water) and their Pressures as mechanisms of effects (chemical, biological, physical and energy pollution). In turn, we identify the State Changes on the natural system and Impacts (on human welfare) which then require Responses (using management Measures). The latter will be presented using the so-called 10-tenets problem-solving framework, relating the solutions both inside and outside national waters. These encompass covering the ecological, technological, economic, societal, legislative, administrative, political, ethical/moral, cultural and communication aspects. This includes the identification of the activity-, pressures-, effects- and management response-footprints including the spatio-temporal characteristics. The spatio-temporal variations between activity-, pressures- and effects-footprints add complexity in the ability to adequately assess and eventually manage shipping environmental impacts; for example, the intermittent shipping activity sewage discharge may be considered a point source, but can result in a delayed organic-enrichment effect, not limited to the immediate point of discharge in the shipping lane. The effects of shipping will especially depend on the characteristics of

the receiving environment; for example, the more organically-rich and hydrodynamically-enclosed Baltic Sea is more susceptible to eutrophication compared to the oligotrophic Mediterranean Sea or the open waters of the North Sea. Hence, the footprint analyses indicate both the problems and solutions especially given the challenge of 'intermittent and mobile/moving activity-footprints' typified by shipping. In this way, shipping and navigation are treated as creating both endogenic and exogenic pressures (pressures emanating inside and outside a particular management area) which then dictate where the management responses (the so-called Programmes of Measures) should lie. The analysis here has consequences for cumulative effects assessments and the bodies responsible for monitoring, assessment and management.

Jalkanen, J. P., Johansson, L., Wilewska-Bien, M., Granhag, L., Ytreberg, E., Eriksson, K. M., Yngsell, D., Hassellöv, I.-M., Magnusson, K., Raudsepp, U., Maljutenko, I., Winnes, H., & Moldanova, J. (2021). *Modelling of discharges from Baltic Sea shipping*. Ocean Sci., 17(3), 699-728.

<https://doi.org/10.5194/os-17-699-2021>

Nylund, A. T., Arneborg, L., Tengberg, A., Mallast, U., & Hassellöv, I. M. (2021). *In situ observations of turbulent ship wakes and their spatiotemporal extent*. Ocean Sci., 17(5), 1285-1302.

<https://doi.org/10.5194/os-17-1285-2021>

Elliott, M., Burdon, D., Atkins, J. P., Borja, A., Cormier, R., de Jonge, V. N., & Turner, R. K. (2017). "And DPSIR begat DAPSI(W)R(M)!" - A unifying framework for marine environmental management. Mar Poll Bull, 118(1), 27-40.

<https://doi.org/https://doi.org/10.1016/j.marpolbul.2017.03.049>

Impacts of expanding commercial anchoring on the Pacific Coast of Canada

F.T. Francis¹, K. Douglas², L.C. Hannah¹, S. Agbayani¹, K. Berry¹, S. Dudas¹, R. Enkin², D. Havens¹, T. Norgard¹, C. Robb¹, E. Rubidge¹, S. Verrin¹, and C. Murray¹

¹Institute of Ocean Sciences, Fisheries and Oceans Canada, Sidney, British Columbia, V8L 5T5, Canada

²Geological Survey of Canada Pacific, Natural Resources Canada, Sidney, British Columbia, V8L 4B2, Canada

Keywords: anchorages, benthic impacts, scours, multiple stressors.

Presenting author email: fiona.francis@dfo-mpo.gc.ca

Vessels at anchor can have ecological and socio-economic effects in coastal areas, yet the impacts of large scale commercial anchoring are poorly understood. Anchorages are often sited in deep water soft sediment areas; understudied ecosystems with high diversity which play an important role in ecosystem function. First Nations and local communities have expressed concerns for anchorage stressor impacts in Pacific Canada (DFO, 2018). Building on a Pathways of Effects conceptual model for shipping (Hannah *et al* 2020) we identified three sub-activities of concern from anchoring, 1) discharges and emissions, 2) vessel movement and presence, and 3) anchor movement and presence. To date, few scientific studies have attempted to examine the effects and impacts of these anchoring activities, especially on the benthic ecosystem, and none have looked at these effects over a broad geographic scale.

In this study we provide novel baseline data to examine patterns of anchorage occupancy and anchoring events from usage data for 154 commercial anchorages along the entire Pacific Coast of Canada over a 15-year time period to identify how evenly anchorages are used and highlight areas where effects from both discharges and emissions and vessel movement are likely highest. We further examine a subset of these anchorages to determine how the potential effects from chain and anchor presence as well as patterns of repositioning, where ships

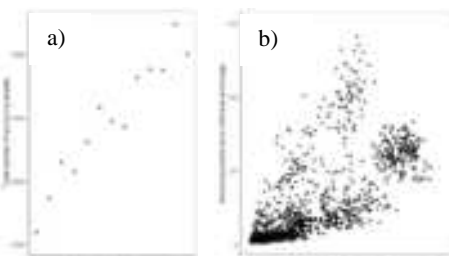


Figure 1. a) Total anchoring events across commercial anchorages in Pacific Canada have increased 60% over time
b) Anchoring events at an individual anchorage in relation to % of the year that anchorage is occupied

are required to retrieve and redeploy the anchor because of dragging, impact measures of seabed ruggedness (Sappington *et al* 1997) and numbers of presumed anchor scour marks identified from multibeam surveys to provide an estimate of benthic disturbance around anchorages along an entire coast.

Overall, anchoring events steadily increased over time from 2008-2022 (Fig. 1a) and were positively correlated with anchorage occupancy times (Fig. 1b) but

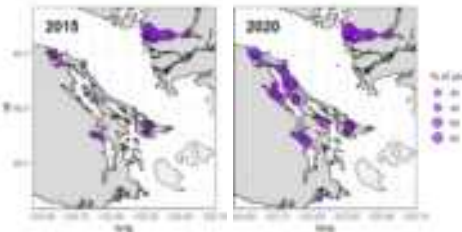


Figure 2. Anchorage occupancy in 2015 and 2020 in the southern region of Pacific Canada

were highly spatially variable (Fig. 2). Ships occupied individual anchorages from 0-89% of the year in some years, and this high spatial variation suggests the impacts of anchoring are not evenly distributed across the coast.

Anchorage repositioning events were infrequent and occurred in 1.85% of total anchoring events in the time series. A mixed-effects model showed that repositioning varied strongly between years but that there was a weak effect of both total number of anchoring events and region on repositioning. This suggests that factors other than usage, such as environmental variables like storms or currents may have a stronger effect on anchor dragging. We quantified 5,410 anchor scour marks at a subset of 117 anchorages and found that they were generally most prevalent in areas of high anchorage use but did not appear related to occurrence of repositioning events.



Figure 3. Multibeam images showing ruggedness within a 200m radius buffer around two commercial anchorages (A and B) compared to an adjacent control area (C).

Reducing ports' contribution to climate change

F. Sakellariadou¹, I.-M. Hassellöv², C.F. Wooldridge³ and D. Kitsiou⁴

¹Dept of Maritime Studies, University of Piraeus, Piraeus 18534, Greece.

²Dept of Mechanics and Maritime Sciences, Chalmers University of Technology, SE-412 96 Gothenburg, Sweden.

³ Science Coordinator, EcoPorts EcoSLC.

⁴Dept of Marine Sciences, University of the Aegean, Greece.

Keywords: first, second, third, fourth.

Presenting author email: fsakelar@unipi.gr

Seaports play a crucial role for maritime shipping and international trade, as the ports are vital hubs of the global supply chain. Located in coastal areas, port activities will contribute to the cumulative environmental pressure from various anthropogenic activities, such as industry, tourism, fisheries, and human settlements. The resulting multiple environmental stressors will degrade the fragile coastal ecosystems and have several socioeconomic impacts.

Port activities give rise to pressures on all environmental compartments; air, water, and soil. The most commonly addressed pressures from port operations are Green House Gas (GHG) emissions contributing to global climate change (e.g. Winnes et al 2015; Styhre et al. 2017), and air pollutants (e.g. Tzannatos 2010) like sulphur and nitrogen oxides contributing to local and regional effects of acidification and eutrophication, as well as human health impacts. Ships are the single largest source of port-related air pollution.

Less attention has been paid to water pollution in port areas, although these pollutants will also contribute to degradation of coastal ecosystems through acidification, eutrophication and ecotoxicological effects. The exemption is dredging of contaminated port sediments, which is a well-recognized challenge in environmental management. The degradation of the marine environment will indirectly impact climate change as the capacity of the ocean to withstand, and hamper, climate change will decrease. In some regions, like the Baltic Sea, shipping is responsible for a significant share of the contaminant loads to the marine environment. The IMO has set ambitious targets to achieve lower GHG emissions from shipping. However, to reduce contribution of shipping to climate change, both direct and indirect impacts need to be addressed.

Ports can play an important role in guiding shipping companies towards reduced contribution to climate change. Port authorities should facilitate increased supply of alternative fuels, extend shore-side power supply, and apply environmentally differentiated port fees for ships. Relevant Environmental Management System (EMS) Quality Standards require port authorities to set their own targets for GHG reduction, air emissions and to set low emission zones or berth standards. The sector recognizes that these issues require an integrated approach to monitoring, reporting and management due to cross-boundary considerations of multi-stakeholder involvement from quayside to the port area, and further to hinterland connections included in the logistics chain. The

identification and application of related Environmental Performance Indicators (EPI) are vital to achieve sustainable development.

Another, strong, incentive for ports to reduce contribution to climate change is their own susceptibility to climate change related effects. Coastal areas are particularly vulnerable with respect to sea level rise and intense storms, while estuaries and coastal cities are at risk from flooding hazards. The severity of the potential climate change related impacts on ports creates an urgent need to strengthen the ports' resilience and adaptation to projected future changes of e.g. sea level rise. To enable such a development, collaboration of a broad range of experts and stakeholders is required. Further, more systematic approaches and technological considerations are essential for the construction of new resilient infrastructure, as well as use of soft and hard adaptation measures, to increase the resilience of existing infrastructure.

This study is part of the #2021-026-3-600 project sponsored by IUPAC Division VI.

Alamoush, A.S. et al. (2022) *CLSCN*, 3, 100021.

Styhre, L. et al. (2017) *Transp Res D Transp Environ.* 54, 212-224.

Tzannatos, E. (2010) *Atmos Environ.* 44(3), 400-407.

Winnes, H. et al. (2015) *Res. Transp. Bus. Manag.* 17, 73–82.

Projected climate change, potential impacts and associated risks strengthen the global response in the context of sustainable development. All industrial sectors, including shipping, are facing the sustainability challenge.

3.13 PS.1. Poster session 1 (TAP sessions)

Measurement and Analysis of Brake and Tyre Particle Emissions from Automotive Series Components for High-Load Driving Tests on a Wheel and Suspension Test Bed

M. Kupper¹, L. Schubert², M. Nachtnebel³, H. Schrottner^{3,4}, M. Huber², A. Bergmann¹ and P. Fischer²

¹ Institute of Electrical Measurement and Sensor Systems, Graz University of Technology, Graz, 8010, Austria

²Institute of Automotive Engineering, Graz University of Technology, Graz, 8010, Austria

³Austrian Centre for Electron Microscopy, Graz, 8010, Austria

⁴Institute of Electron Microscopy and Nanoanalysis, Graz University of Technology, Graz, 8010, Austria

Keywords: Tyre Wear, Brake Wear, Non-Exhaust Emissions, Measurement, Nanoanalysis.

Presenting author email: martin.kupper@tugraz.at

The next challenge towards clean road and rail transport is non-exhaust emissions. Important advances regarding measurement systems including well defined characterization techniques as well as regulation will happen in the next few years (Grigoratos et al. 2023).

In this work, we present detailed results of particle emissions from a test bed for wheel suspension and brakes (see fig. 1), consisting of aerosol (size distribution, particle number (PN) and mass (PM)) and electron microscopy (EM) measurements under different load conditions.

Standard tires and brakes from series production (Continental ContiSportContact 5 255/45 R22 107Y XL tyres and SUV brake discs) were tested with a high-load driving cycle over a wide, well-defined range of operating parameters. The test cycle was repeated 1100 times (11 days, 100 cycles per day). The test cycle was carried out fully automated and is reproducible in terms of speed profile, force on wheel and tire, brake pressure as well as skew angle. The brake temperature was measured throughout.

Particle measurements were conducted by gravimetric measurements and with a TSI SMPS, a TSI APS and a GRIMM OPS at three sampling positions in the supply and exhaust air of the test bed, as well as directly inside the test bed (see fig. 1). A custom developed electrostatic sampler with four precipitator stages was used to collect electron microscopy (EM) samples, operated at Voltages from 800 V to 200 V in steps of 200V and 0 V as for the reference plate.



Figure 1. Left: CAD representation of the ventilation system of the test bed and the sampling positions. Right: Photography from the test bed.

In fig. 2 exemplary PM measurement results from 20 cycles from the GRIMM OPS are shown. The measurements were highly repeatable once the brake pad temperature levelled after the first two runs. Our results suggest, in agreement with previously published literature (Asbach et al. 2019), that particulate emissions are related to brake disc temperature and occur in significant amounts above a threshold temperature.

A bimodal particle size distribution was obtained with the SMPS, with peaks at 20 nm and 400 nm with the majority of PN below 50 nm. The OPS showed a trimodal distribution with peaks at 400 nm, 3 µm and 41 µm. EM analysis of >1400 single particles from the electrostatic sampler matches these results. The measured PM values were between 300 and 400 µg/m³ with maximum values around 450 µg/m³ and PN concentrations between 2000 and 2500 #/cm³ with the OPS. Particle emission can clearly be associated to brake events. EM characterization of filter samples revealed mostly particles of diameters between 100 nm - 4.5 µm (mean 0.82 µm), the largest size was 22.3 µm. Results from the electrostatic sampler show ultrafine particles, mainly from O, Fe, Si, Ba, Mg and S and also fractal particles with high C fractions, possibly from combustions at the brake disk surface.



Figure 2. Measurement data from GRIMM OPS measurements of the test bed exhaust air.



Figure 3. Exemplary High-Resolution EM image

This work received no funding.

Asbach, Christof, et.al. 2019. "Entstehung Und Möglichkeiten Zur Messung von Fein- Und Ultrafeinstaub Beim Bremsen." XXXVII. Internationales µ-Symposium 2018, 45–67. https://doi.org/10.1007/978-3-662-58024-0_4

Grigoratos, Theodoros, et al. 2023. "Characterization of Particle Number Setups for Measuring Brake Particle Emissions and Comparison with Exhaust

Predictive energy management for a plug-in hybrid electric truck

Aletras¹ N., Broekaert² S., Bitsanis² E., Fontaras² G., Samaras¹ Z., Ntziachristos¹ L.*

¹Mechanical Engineering Department, Aristotle University of Thessaloniki,
GR 54124, Thessaloniki, Greece

²European Commission, Joint Research Centre, Directorate for Energy, Transport and Climate, Via Enrico Fermi 2749, 21027 Ispra, Italy

Keywords: energy management, plug-in hybrid, heavy duty vehicles
Presenting author email: nealetra@auth.gr

This research work examines the potential fuel consumption (FC) benefits through predictive equivalent minimization strategy (ECMS) for hybrid heavy duty vehicles (HDVs).

Global warming is one of the major environmental problems and is directly related to carbon dioxide (CO₂) emissions. In the transportation sector, HDVs are important contributors of CO₂ emissions, indicating the importance of reducing emissions from those vehicles. Electrified vehicles have already emerged as one of the options for reducing CO₂ emissions from transportation sector. Plug-in hybrid electric vehicles (PHEVs) have the potential to reduce CO₂ emissions in the HDVs sector (Gao et al., 2017).

The FC – and thus CO₂ emissions - of PHEVs is strongly dependent on the performance of the on-board energy management system (EMS). EMS chooses the share between battery and engine power (Onori et al., 2016). One possible way to improve the performance of an EMS algorithm – in terms of FC – is to include power demand prediction (Tianheng et al., 2015). If the EMS algorithm utilizes both current and predicted future states of the vehicle – e.g., power demand for propulsion – then the algorithm can achieve solutions that are closer to the global optimum and lower FC (Tianheng et al., 2015). Recent technological developments in intelligent transportation systems (ITS) and 5G will enable prediction of vehicle speed and associated power demand (Zhang et al., 2019). Therefore, it is important to quantify the potential benefits in FC reduction - and corresponding reduction in CO₂ emissions - by incorporating the predicted power demand into the EMS algorithm.

To quantify the potential FC benefits through predictive ECMS, a parallel P2 PHET model has been implemented. Figure 1 shows the layout of the PHET model which has been built in the AVL Cruise simulation platform. The applied EMS algorithm is a version of an ECMS adapted to the Vehicle Energy Consumption Calculation Tool's (VECTO) equations for the cost function (*Vecto User Manual*). The PHET model has been validated with experimental data provided by the Joint Research Center (JRC).

After model validation, the cost function of the validated EMS algorithm has been extended with terms that take into consideration the predicted power demand. The extended and the validated versions of

the EMS algorithm are compared over the different regulatory mission profiles for different HDV group categories.

The outcomes of the study could be used to quantify the FC benefits for hybrid HDVs due to future technologies - such as intelligent transportation systems and 5G.

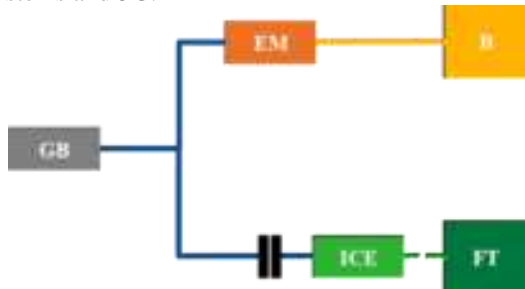


Figure 1. Layout of the examined vehicle configuration. ICE: Internal Combustion Engine, EM: Electric Motor, B: Battery and GB: Gearbox, FT: Fuel tank.

The research work was supported by the Hellenic Foundation for Research and Innovation (HFRI) under the 3rd Call for HFRI PhD Fellowships (Fellowship Number: 6653).

Gao, Z., Lin, Z. & Franzese, O. (2017). Energy Consumption and Cost Savings of Truck Electrification for Heavy-Duty Vehicle Applications. *Transportation Research Record: Journal of the Transportation Research Board*, 2628(1), 99–109. <https://doi.org/10.3141/2628-11>

Onori, S., Serrao, L. & Rizzoni, G. (2016). *Hybrid Electric Vehicles*. Springer London. <https://doi.org/10.1007/978-1-4471-6781-5>

Tianheng, F., Lin, Y., Qing, G., Yanqing, H., Ting, Y. & Bin, Y. (2015). A Supervisory Control Strategy for Plug-In Hybrid Electric Vehicles Based on Energy Demand Prediction and Route Preview. *IEEE Transactions on Vehicular Technology*, 64(5), 1691–1700. <https://doi.org/10.1109/TVT.2014.2336378>

Vecto User Manual.

Zhang, F., Hu, X., Langari, R. & Cao, D. (2019). Energy management strategies of connected HEVs and PHEVs: Recent progress and outlook. *Progress in Energy and Combustion Science*, 73, 235–256. <https://doi.org/10.1016/j.pecs.2019.04.002>

The EV-olution of non-exhaust emissions

D. Mehlig¹, H. ApSimon¹

¹Centre for Environmental Policy, Imperial College London, London, SW7 1NE, UK

Keywords: Non-Exhaust Emissions, Electric Vehicle, PM2.5, Air Quality.

Presenting author email: d.mehlig18@imperial.ac.uk

Non-exhaust emissions (NEEs) from tyres, brakes, and the road surface, are now the major source of primary particulate matter from road transport in many countries and have grown in importance over the past decade due to the introduction of successful exhaust emission control technologies. NEEs are produced by all vehicles and so electric vehicles have fallen into the NEE spotlight with many asking will EVs increase or reduce these emissions? This study addresses this question using state-of-art modelling, the latest NEE emission factors, and a scenario of EV uptake.

There has been a recent increase in the number of studies modelling NEEs and estimating their emission factors. These models account for the EVs where there may be NEE increases due to heavier vehicles and decreases due to regenerative braking. These new emission factors need to be compared against one another to evaluate which is most appropriate today and in the future, where there will be an increasingly diverse fleet stock with various vehicle technologies affecting NEEs.

This study applies seven of these recent NEE emission factor sets with a fleet turnover and emission model (Mehlig, 2022; Mehlig et al. 2023), using the UK passenger car fleet as a case study, to simulate the emissions of NEEs today and how these emissions change over time as the fleet evolves through the adoption of EVs.

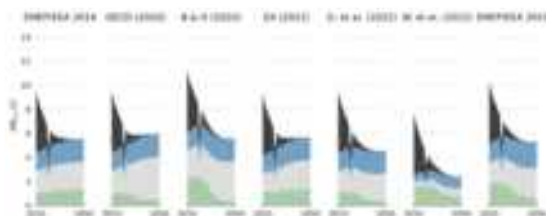


Figure 1. Car NEEs by source (given in colour) for each of the different seven NEE models from 2010 to 2050.

The results show, when using the standard emissions factors from the EMEP/EEA emission inventory guidebook (Ntziachristos and Boulter, 2016), that in the UK over the past decade for passenger cars exhaust PM_{2.5} has reduced by almost an order of magnitude, whereas NEEs have continued to increase in line with growth in vehicle kilometres. In the future, with the oldest most polluting vehicles leaving the fleet and clean ICEVs and zero-exhaust emission BEVs entering the fleet, exhaust PM_{2.5} will be far be outweighed by NEEs. The left-hand panel of Figure 1 shows for cars that by 2030 PM_{2.5} from NEEs will be 16 times greater than PM_{2.5} from exhaust, and by 2040 exhaust emissions will be negligible.

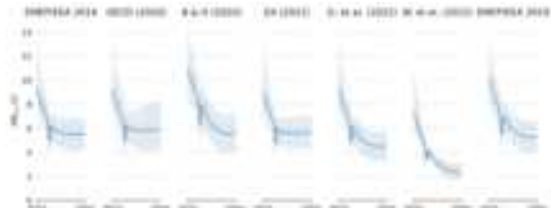


Figure 2. Total car NEEs from 2010 to 2050, where the blue line gives the mean emissions and coloured areas give 95% confidence intervals.

When using the latest NEE emission factors that account for the difference in emission rates depending on the vehicle technology and vehicle curb mass, emissions from tyre wear increase and brake wear decreases as more EVs enter the fleet. Despite these changes, Figure 2 shows that the overall amount of NEEs does not significantly change with the uptake of EVs. This result is consistent across each of the different NEE models. For models that are functions of vehicle curb mass there was added uncertainty in these results.

Overall, these results show the introduction of EVs alone will not substantially change the total amount of NEEs for passenger cars, instead changing the ratio between tyre wear and brake wear. This suggests that further technological solutions addressing vehicle emission components or policies aimed to reduce vehicle kilometres driven are still needed to mitigate NEEs.

This work was supported by the UK's Department for Transport and the Natural Environment Research Council Grant NE/S013350/1.

Mehlig, D (2022) *Electricity: powering vehicles & reducing pollution*, Imperial College London.

Mehlig et al. (2023) *The rapid uptake of electric vehicles: Vehicle and power station emissions*, Manuscript submitted for publication.

Ntziachristos, L, and P. Boulter (2016) "I.A.3.b.vi-vii Road tyre and brake wear 2016", EMEP/EEA emission inventory guidebook.

The effect of a porous pavement on air quality in comparison to a dense pavement

N. Svensson¹, J. Lundberg², M. Gustafsson¹, S. Janhäll³ and S. Kulovuori⁴

¹Swedish National Road and Transport Research Institute (VTI), Linköping, 58195, Sweden

²Transport and Roads, Lund University, Lund, 22363, Sweden

³Research Institutes of Sweden (RISE), Borås, 50462, Sweden

⁴Automotive and Mechanical Engineering, Metropolia University of applied Sciences, Vantaa, 01600, Finland

Keywords: stone mastic asphalt, double layered porous asphalt concrete, PM10, road dust suspension

Presenting author email: nina.svensson@vti.se

Porous pavements are used because of their ability to remove water from the road surface, thus reducing the risk of aquaplaning, as well as reducing road traffic noise from the road/tyre interaction. Previous studies (e.g. Norman et al. 2017) have shown that porous pavements also can have positive effects on air quality. This study aims to investigate this effect and its causes further.

Air quality measurements (PM₁₀ and NO_x) were performed for 7 months (November to May) near two different asphalt pavements located along the same road link in Linköping, Sweden. Meteorological conditions were recorded and road moisture conditions were visually observed. The reference pavement was a dense SMA (Stone Mastic Asphalt) which is commonly used in Sweden. The porous pavement was a new DLPAC (Double Layered Porous Asphalt Concrete).

In addition, measurements of particle emissions behind the tyre of a moving light vehicle were performed with summer, studless and studded winter tyres. The car was driving back and forth along the road stretch for five laps for each tyre type.

The results from the air quality measurements showed that the average ratio of PM₁₀/NO_x was distinctly lower at the porous pavement during all meteorological conditions (Figure 1a), indicating that the porous pavement reduces traffic-induced suspension.

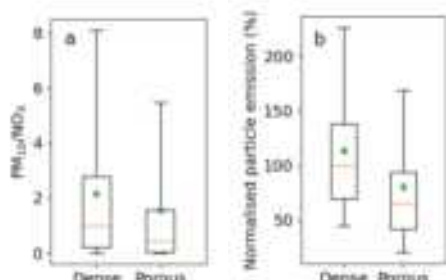


Figure 1: a) The ratio of PM₁₀/NO_x at the two surfaces for the whole measurement period and b) Normalised particle emissions measured behind the wheel of a moving vehicle from four different tyres at the two road surfaces.

Two processes could be related to the lower suspension. Firstly, the visual observations of road moisture showed that the porous pavement was more often moist and less often wet or dry than the dense pavement (Figure 2). The longer the road stays moist after rain, the longer the dust suspension will be suppressed.

This indicates that the porous pavement's void system retains moisture which contributes to its ability to retain road dust.

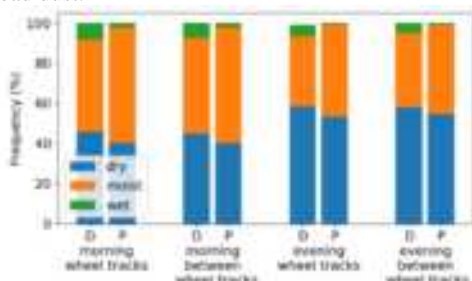


Figure 2: Visually observed road moisture conditions on the two surfaces. D: dense, P: porous.

Secondly, the mobile emission measurements made on dry road surface, showed that the emissions of road dust were lower on the porous pavement compared to the dense for all investigated tyres (Figure 1b). This is suggested to be an effect of dust being less available for suspension due to the air voids of the porous pavement. This is also mentioned as a possible explanation in Norman et al. (2017) and Rasmussen et al. (2023). Previous measurements of the dust load on the road surface (Lundberg et al, 2020) at the same site corroborate these findings.

The results from this study imply that porous pavements can reduce the PM₁₀ suspension from the roads and therefore reduce the concentration of PM₁₀.

This work was funded by The Swedish Transport Administration (2015/9482) and the foundation Fredrik Bachmans minnesfond (2019035).

Lundberg, J., Gustafsson, M., Janhäll, S., Eriksson, O., Blomqvist, G., Erlingsson, S. (2020) Temporal variation of road dust load and its size distribution – A comparative study of a porous and a dense pavement. *Water, air and soil pollution* 231:561

Norman, M., Elmgren, M. and Johansson, C. (2017) Emissions of PM10 and coarse particles from “silent” asphalt. Proceeding of abstracts 11th International Conference on Air Quality Science and Application

Rasmussen, L.A., Lykkemark, J., Andersen, T.R., Vollertsen, J., 2023. Permeable pavements: A possible sink for tyre wear particles and other microplastics? *Science of the Total Environment* 869, 10.1016/j.scitotenv.2023.161770.

CO₂ emissions targets: revisiting the transition from 2020 NEDC to 2021 WLTP

J. Suarez¹, D. Komnos², M.A. Ktistakis² and G. Fontaras¹

¹European Commission, Joint Research Centre (JRC), Ispra, 21027, Italy

²FINCONS Group, Vimercate, 20871, Italy

Keywords: CO₂ emissions, FC gap, WLTP, EU targets.

Presenting author email: jaimie.suarez-corujo@ec.europa.eu

Road transport forms the highest proportion of transport emissions, with passenger cars and vans contributing almost 15% of the European Union (EU) total emissions of carbon dioxide (CO₂). Hence, they constitute one of the main focuses of the regulators.

To progressively decarbonise the fleet, the EU establishes a general CO₂ reference target for the whole fleet of vehicles. Annual specific targets for each manufacturer or pool of manufacturers are adjusted from the EU fleet-wide target based on the average mass of the manufacturers' new registrations. Mandatory targets were first adopted in 2009, setting an EU fleet-wide target of 130 g/km from 2015 to 2019. In 2020 the EU fleet target was redefined to 95 g/km. The 2020 target compliance was determined after applying several flexible mechanisms, such as excluding a percentile of the highest emitting vehicles of the manufacturers and incentivising electrified vehicles.

To monitor compliance with the targets, starting from 2011 the EC gathers annually the technical characteristics, including the CO₂ emissions, of all new cars registered in the Member States. These official values are used to calculate the specific average CO₂ emissions at a fleet and at a manufacturer level, which are assessed against the corresponding standards established by the EC.

Up to 2020, target compliance was based on emissions obtained from the New European Driving Cycle (NEDC). The outdated conditions and flexibilities set out in the NEDC have been identified as one of the main causes of the gap between real-world and official CO₂ emissions (and fuel consumption) – known as the fuel consumption gap. Starting in 2017, the EC introduced the Worldwide harmonised Light vehicles Procedure (WLTP), a more stringent testing procedure which is therefore expected to narrow down the gap. As of 2021, the WLTP totally replaced the NEDC, and compliance is assessed solely based on WLTP measurements.

From 2021 to 2024, the 2020 NEDC-based EU fleet-wide target of 95 g/km is adjusted to a WLTP equivalent. This is done by renormalising each manufacturer's target by a factor that reflects the respective CO₂ average difference between the WLTP and NEDC emissions in 2020. 2020 and 2021 are two years of vital importance concerning the targets. This is not only because of the transition to the WLTP, but also due to the fact that new reduction targets of 15% and 37.5% will apply for the years 2025 and 2030, respectively. These reductions are calculated based on measured 2020

emissions, the 2021 masses, and the number of registrations.

This study uses the final 2020 and 2021 datasets of all EU passenger car registrations published by the European Environment Agency to examine the factors determining target compliance. An in-depth analysis is performed on an EU fleet-wide and on a manufacturer level. 2020 and 2021 compliance are compared, and the reasons why in 2020 the pools, without utilising the provisions, are so far from their respective targets (Figure 1A), while in 2021 the flexible mechanisms are almost redundant (Figure 1B), is examined.

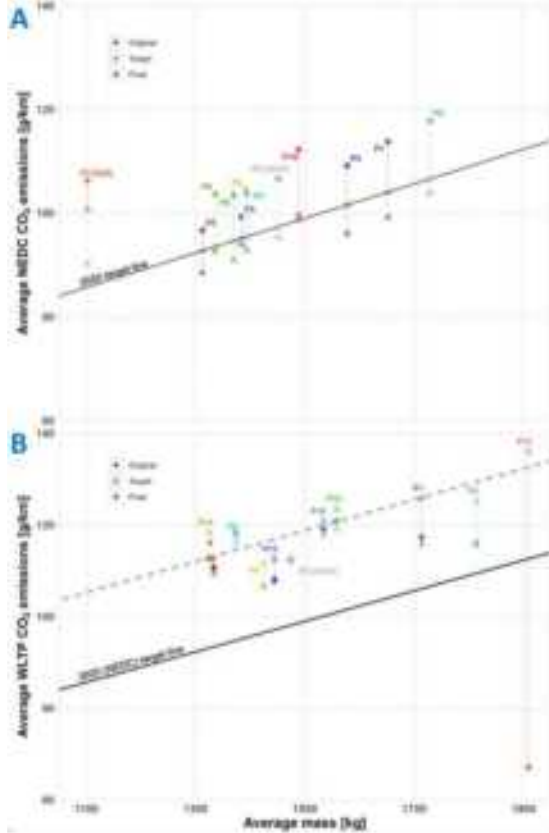


Figure 1. A: 2020 targets; B: 2021 targets; ND: niche derogation; dashed line: linear regression of 2021 targets

Development of a mobile ALI exposure system for toxicity testing of emissions from different transportation modes

M. Introná¹, A.T. Juárez-Facio¹, S.S. Steimer¹ and K. Elihn¹

¹Department of Environmental Science, Stockholm University, 10691 Stockholm, Sweden

Keywords: ALI system, transportation modes, airborne particles, nanoparticle toxicity.

Presenting author email: Karine.Elihn@aces.su.se

Emissions from different transports cause several human health effects. An Air Liquid Interface (ALI) exposure system can examine the toxicity of airborne particles (Elihn *et al.*, 2017), and be used to assess their effects on humans. ALI systems use human lung cells, and can be regarded as a model of the human lung. In our current project, we have developed the ALI system into a mobile unit, see Fig. 1, for outdoor usage to examine the toxicity of real-world particles, such as transportation emissions from cars, trains, ships, and aeroplanes.

Our ALI system has several advantages that enable toxicity testing of airborne nanoparticles and gases at outdoor locations:

1. The ALI system can test the toxicity of a flow of airborne nanoparticles directly from a particle source. Therefore, particles that deposit onto cells are unchanged and look exactly as in the air, i.e., they have the same size, shape, and chemical composition as particles inhaled by humans.

2. Our ALI system is designed to facilitate the deposition of nanoparticles. Nanoparticles can easily follow an airstream and may therefore be difficult to deposit in the cell chambers of an ALI system. An electrostatic field and charging of the particles enable efficient deposition of nanoparticles onto the cell cultures.

3) Our ALI system contains separate cell chambers. Therefore, different exposure scenarios can be examined at the same time, without the risk of cross-contamination between chambers. Simultaneously, we can separately study aerosols and gases (by using filters for particle removal). In this way, reference samples can be created at exactly the same conditions as exposed samples, with no need for separate gas exposure experiments (to see the effect of the flowing gas or gaseous air pollutants).

4) Our ALI system has a controlled temperature and humidity to resemble the conditions in a human lung, and to keep the cells alive in a flow of clean air (non-exposure conditions).

5) A Scanning mobility particle sizer (SMPS) is attached prior to and after our ALI system to enable online characterization of the particle size distribution and, subsequently, to determine the particle dose on cells.

6) Our mobile ALI unit makes it possible to perform exposure measurements at any out-of-the-lab location, e.g., in road tunnels and chassis dynos, which has not been possible before. This new design opens up the possibility to examine the toxicity of a great variety of aerosols/ emissions, and to judge their effects on human health.

7) A concentrator can be used prior to the ALI system to facilitate toxicity testing at outdoor locations with low particle concentrations. Alternatively, a longer exposure time may be used in case it is possible to keep the cell survival high at non-exposure conditions.

Our ALI system can examine the toxicity of fresh unchanged airborne nanoparticles (and larger particles and gases) at any out-of-the-lab location. The parameters of the ALI system have been optimized for best cell survival (aerosol flow, temperature, humidity, voltage), and particle deposition and toxicity testing have been validated (Juárez-Facio *et al.*, 2023). Two mobile systems have so far successfully tested the toxicity of emissions in a road tunnel (Introná *et al.*, 2023), subway station, tribology laboratory, chassis dyno, harbour, and an outdoor background location. We expect mobile ALI systems to become a widely used tool for future assessments of aerosol's effects on human health.



Figure 1. A mobile ALI system to examine the toxicity of airborne particles at outdoor locations.

This research was supported by the European Commission's Horizon 2020 research and innovation programme: nPETS (grant agreement No 954377, <https://www.npets-project.eu/>) aimed at studying the sub-100 nm particles emitted from transport.

Latvala, S., Vare, D., Karlsson, H.L. and Elihn, K. (2017) *J. Appl. Tox.* doi: 10.1002/jat.3510

Juarez, A., Introná, M., Steimer, S.S., and Elihn, K. (2023) Submit to *Nanotoxicology* Feb 2023.

Introná, M., Juarez, A., Steimer, S.S., Karlsson, H.L., Vallabani, S., Tu, M.H., Olofsson, U. and Elihn, K. (2023) Submit to *Int. J. Environ. Res. Public Health* April 2023.

Fuel consumption, regulated and unregulated exhaust emission tests on three Euro 6d bi-fuel LPG passenger cars, fed by an innovative LPG/DME 80/20 (V/V) blend

T. Rossi*, S. Casadei, S. Lixi, M. Martini and D. Faedo

Innovhub - Stazioni Sperimentali per l'Industria, Sustainable Mobility Team, Via G. Galilei 1, 20097, San Donato Milanese, Milano, Italy

Keywords: exhaust emissions, alternative fuel, LPG/DME.

Presenting author email: tommaso.rossi@mi.camcom.it

The use of Dimethyl ether (DME) as a blend component in spark-ignition engines fuelled by liquefied petroleum gas (LPG) is a relatively new application compared to diesel engines [1]. DME can be produced by biomass and it has been considered by the EU as a part of its biofuel energy mix of 2030, and also by renewable feedstocks (e.g. landfill, municipal waste). In this respect, DME is also mentioned in the Renewable Energy Directive (RED) II [2].

In this research, in order to investigate a new potentially fully renewable fuel blend, DME was mixed with LPG and used to fuel LPG/gasoline bi-fuel passenger cars equipped with spark-ignition engines. Both DME and propane can be obtained from renewable sources, which makes this blend promising as an alternative sustainable fuel. Initially, several octane tests using CFR engines (both RON and MON) were carried out to find the suitable fuel blend that would allow to meet the European LPG specification (EN 589) and not to damage the engine components. The fuel blend chosen was made by 80% LPG (commercial propane) and 20% DME.

Three Euro 6d bi-fuel passenger cars of both small and medium segments (two PFI, one TGDI) were tested, both running on gasoline and on LPG/DME fuels, in order to verify if the innovative blend could affect the testing vehicles' gaseous and particulate exhaust emissions.

The testing cars were driven in laboratory over the homologation WLTC (Worldwide harmonized Light duty driving Test Cycle) and over the hot-start CADC (Common Artemis Driving Cycle), as well as on road, following the EU RDE testing procedure.

On WLTC, all Euro 6 standards were well met both running on gasoline and on LPG/DME. Switching from gasoline to LPG/DME fuelling, the gaseous emission results point out an increase of CO and NO_x (two PCs), whereas THC and NMHC were found to decrease (two PCs); the particulate emission results point out a reduction of solid particles (two PCs).

Generally, due to the role of the three-way catalyst, much lower gaseous emissions were detected running the testing vehicles on the CADC: except for one PC, switching from gasoline to LPG/DME fuelling, the emission behaviour reflects the one of the testing PCs run on the WLTC.

Also PCs' particulate unregulated emissions (solid and volatile ones) detected over both testing cycles basically reflect what was detected for the regulated ones.

All the regulated emissions were found to meet the latest Euro 7 standards proposed by the European Commission, except for PN10, which could not be

measured. Interestingly, although NH₃ emitted over the WLTC was found over its Euro 7 limit in PC 3 fuelled by gasoline, this emission was well lowered in the same PC fuelled by LPG/DME. With the LPG/DME fuelling, NH₃ decreased for all testing PCs and cycles.

All emissions detected over the RDE tests were found to fully meet the RDE limits as well.

LPG/DME fuelling turned out to a systematic decrease of CO₂ for all testing PCs and cycles, both in laboratory (Figure 1) and even on road.

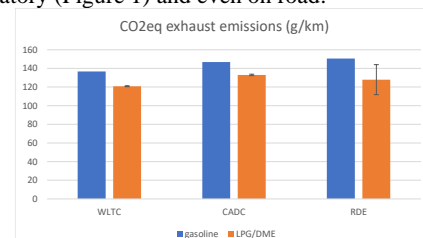


Figure 1. CO₂ equivalent emission over all cycles.

A final focus was dedicated to the energy consumption, a decreasing of which was found in two PCs and detected both in laboratory (Figure 2) and on road.

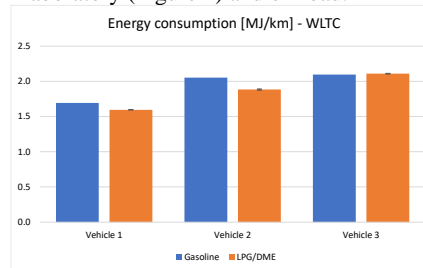


Figure 2. Energy consumption over WLTC.

All of these results identify the innovative LPG/DME 80/20 (V/V) blend not only as potentially convenient in terms of GHG emissions reduction, as long as both propane and DME are made from renewable sources, but even compliant with EN 589 and both Euro 6 and part of the Euro 7 exhaust emission standards.

This work was funded by Liquigas S.p.a.

- [1] Arcoumanis C., Bae C., Crookes R., Kinoshita E. (2008). *The potential of di-methyl ether (DME) as an alternative fuel for compression-ignition engines: A review*. Fuel, 87(7), pp. 1014-1030.
[2] Directive (EU) 2018/2001

Future SUV fleet and CO₂ emissions projections in Australia and the European Union

J.J. Gómez Vilchez¹, R. Smit², D. Komnos¹ and G. Fontaras^{1*}

¹European Commission, Joint Research Centre (JRC), Ispra, Italy

²Transport Energy/Emission Research (TER), Launceston, Tasmania, 7249, Australia

Keywords: CO₂ emissions, fleet modelling, simulation, sport utility vehicle.

Presenting author email: Jonatan.gomez-vilchez@ec.europa.eu

Background

Two vehicle markets where heavier cars have gained importance over the past years are Australia and the European Union (EU). According to the European Environment Agency (EEA), “the increase in emissions between 2017 and 2019 was mostly due to the increase in the share of sport utility vehicles (SUVs) and other larger and heavier cars” (EEA, 2022) (p. 47). This abstract complements the work by Komnos et al (2023) by focusing on the car fleet in these two markets.

The specific goal of this study is to model the potential implications of possible future SUV fleets, in terms of energy demand and CO₂ emissions. Electric SUVs are beyond the scope of this work (see (Gómez Vilchez, Pasqualino, & Hernandez, 2023)).

Methodology

A simulation model was built to calculate the car fleet, disaggregated into SUVs and nonSUVs, as influenced by the annual registration and deregistration rates. An overview of the model, following the system dynamics modelling approach ((Forrester, 1961), (Sterman, 2000)), is provided in Figure 1.

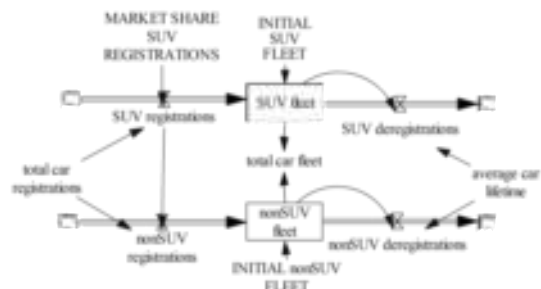


Figure 1. Fleet model. Rectangles and valves with pipes represent stock and flow variables, respectively.

The model is informed with data from ACEA (2022), EEA (2020) and TER. Two scenarios are reported: ‘SUV decline’ and ‘SUV growth’. The difference between them lies in the assumed future market share of SUV registrations, which is higher for the latter. The simulations run from 2005 to 2030, with a year resolution and a time step of 0.25 years. The solution is provided via Euler integration with Vensim.

Results and conclusion

Figure 2 shows the simulated evolution of SUV fleets in Australia and the EU in the two scenarios.

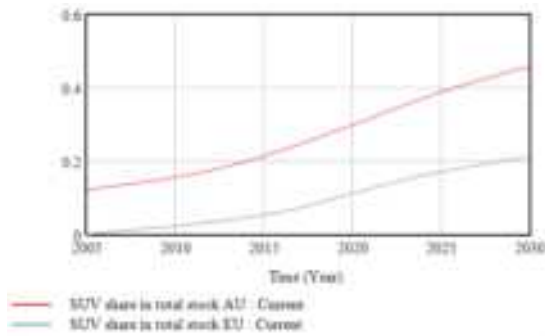


Figure 2. Simulated SUV fleet and CO₂ emissions.

Figure 2 also shows the simulated level of CO₂ emissions. The extended abstract reports the corresponding energy demand and driver costs resulting from fuel prices, comparing Australia and the EU.

We conclude that the SUV fleets in the two regions will become larger over time following the high share in SUV registrations in recent years. This will hamper decarbonisation, unless other measures are adopted.

Further research

The work presented here is limited by the fact that the current version of the model captures the car fleet at a rather aggregated level. In future work, this limitation may be overcome by introducing one-year age cohorts and a more detailed categorisation of nonSUVs.

There is no funding for this work.

- ACEA. (2022). New passenger cars by segment in the EU. European Automobile Manufacturers’ Association (ACEA). Various years.
EEA. (2020). Monitoring of CO₂ emissions from passenger cars – Regulation (EU) 2019/631. European Environment Agency (EEA).
EEA. (2022). *Decarbonising road transport — the role of vehicles, fuels and transport demand. Transport and environment report 2021*. EEA Report No 02/2022. European Environment Agency (EEA).
Forrester, J. W. (1961). *Industrial Dynamics*. MIT Press.
Gómez Vilchez, J. J., Pasqualino, R., & Hernandez, Y. (2023). The new electric SUV market under battery supply constraints: Might they increase CO₂ emissions? *Journal of Cleaner Production*, 383, 135294.
Sterman, J. D. (2000). *Business Dynamics: Systems Thinking and Modeling for a Complex World*. Boston: McGraw-Hill/Irwin.

Toxicity of real-world road tunnel emissions in an ALI exposure model

M. Introna¹, A.T. Juárez-Facio¹, S.S. Steimer¹, M.H. Tu², U. Olofsson², H.L. Karlsson³, N.V.S. Vallabani³, and K. Elihn¹.

¹Department of Environmental Science, Stockholm University, 10691 Stockholm, Sweden

²KTH Royal Institute of Technology, Stockholm, Sweden

³Institute of Environmental Medicine, Karolinska Institute, SE-171 77, Stockholm, Sweden

Keywords: Air-Liquid Interface, real-world exposure, airborne particles, PM2.5, exhaust emissions, road tunnel.

Presenting author email: nicol.introna@aces.su.se

Urban areas are a hotspot for air pollution because of the intensive presence of human activities and traffic. Since the late 90s, high pollution levels have proven to be responsible for reducing the quality of life, causing diseases and premature deaths. (Dockery et al., 1993).

Pollution can be composed of fine particle matter (PM2.5) generated by fuel combustion (Harrison, 2020). PM2.5 become harmful when inhaled because these particles are small enough to reach the deepest part of the lungs, where they can deposit and accumulate (Lv et al., 2021). Different studies investigated their toxicity in humans, but few studied their deposition in a real-world environment.

In this study, lung cells were exposed in real time to fresh fine particles emitted from vehicles driving in an urban road tunnel (Söderledstunneln) in the city centre of Stockholm. About 30.000 vehicles per direction use this tunnel weekly to cross the city.

A mobile air-liquid interface system (ALI) with human lung cells (A549) was used to mimic particle deposition in the lungs (Juárez-Facio et al. 2023). The ALI system was placed behind the wall next to the single-carriageway road of the tunnel (Fig.1). Cells were exposed for two hours during week days to road tunnel emissions, that were concentrated 5 times (Heikkilä et al., 2022). Afterwards, cells were investigated for cytotoxicity and inflammatory response (cytokine release) after 24h incubation.

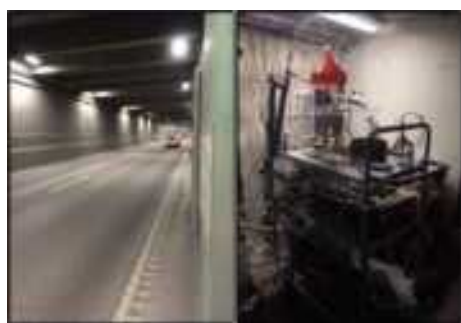


Figure 1. Left: inside of the Söderledstunneln during a week day; right: ALI system behind the road tunnel wall.

Results

Cell viability was tested in human lung cells exposed to road tunnel particles. Cell viability was not affected in any of the groups (A: road tunnel air without particles, E: exposure to particle emissions, and LPS)

compared to negative control. A biological increase of inflammatory markers IL-1 β , IL-8 and IL-6 was observed in cells exposed to road tunnel emissions compared to filtered tunnel air and negative controls (Fig 2). No statistical significance was observed for any of the measured cytokine due to the variation of exposure dose between experiments in a real-world environment.

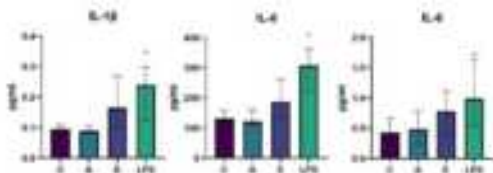


Figure 2. Cytokine release from cells exposed to road tunnel emissions, based on ≥ 4 experiments. LPS (1 $\mu\text{g/mL}$) was our positive control. C: neg. control, A: air without particles, E: exposure to particle emissions.

Acknowledgments

I acknowledge P. Heikkilä and J. Keskinen from Tampere University in Finland for borrowing the concentrator. This work was supported by the European Commission's Horizon 2020 research and innovation programme: nPETS (grant agreement No 954377, <https://www.npets-project.eu/>) aimed at studying the sub-100 nm particles emitted from transport.

References

- Dockery, D. W., Pope, C. A., Xu, X., Spengler, J. D., Ware, J. H., Fay, M. E., Ferris Jr, B. G., & Speizer, F. E. 1993. An association between air pollution and mortality in six US cities. NEJM 329, 1753–1759.
- Harrison, R. M. 2020. Airborne particulate matter. Philos. Trans. Royal Soc., 378(2183), 20190319.
- Heikkilä, P., Rostedt, A., Toivonen, J., & Keskinen, J. 2022. Elemental analysis of single ambient aerosol particles using laser-induced breakdown spectroscopy. Sci. Rep. 12.
- Lv, H., Li, H., Qiu, Z., Zhang, F., & Song, J., 2021. Assessment of pedestrian exposure and deposition of PM10, PM2.5 and ultrafine particles at an urban roadside: A case study of Xi'an, China. Atmos. Pollut. Res., 12, 112–121.
- Juarez-Facio, A.T., Introna, M., Steimer, S.S., and Elihn, K., 2023, Submit to Nanotoxicology Feb 2023.

Non-Exhaust Emissions in Aotearoa New Zealand

G.F.J. Coulson¹, P.K. Davy², E.R. Somervell¹, G. A. Olivares¹, A. Semadeni-Davies¹ and I. D. Longley¹

¹ National Institute of Water and Atmospheric Research, 41 Market Place, Auckland 1010, New Zealand

²GNS Science, PO Box 31312, Lower Hutt 5040, New Zealand

Keywords: traffic emissions, non-exhaust, New Zealand

Presenting author email: guy.coulson@niwa.co.nz

As exhaust emissions from combustion engines fall and BEVs become more prevalent, emissions of particles from non-exhaust traffic sources (Non-Exhaust Emissions, NEE) are expected to become increasingly important.

Few studies have been carried out in Aotearoa New Zealand explicitly to isolate the non-exhaust traffic signal from the bulk PM. EFs used in New Zealand are mostly derived from overseas studies. A road dust resuspension study carried out in Auckland by NIWA in 2008 was unable to conclusively quantify resuspended road dust but was able to conclude that it was consistent with then current literature (NIWA unpublished data). Source apportionment by Davy and Trompeter (2019) in Auckland indicates that NEE and exhaust emissions crossed over in 2016 with NEE becoming more important (Figure 1).

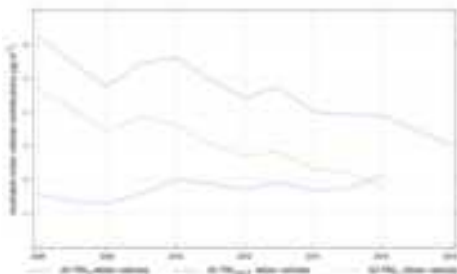


Figure 1. The contribution of fine and coarse fractions to road derived PM10 in Auckland - from Semadeni-Davies et al (2021)

A study is underway to develop New Zealand specific NEE EFs. The first part, a review by Semadeni-Davies et al (2021) concluded that there are numerous gaps in understanding NEEs that make it difficult to determine the most appropriate Emission Factors (EFs) for use in New Zealand – including that New Zealand’s vehicle fleet is significantly older than those in other countries. The review recommended a two-part approach to improving NEE EFs in NZ; 1) sensitivity analysis using current EFs to determine how choice of EF determines the outcome, and 2) reanalysis of existing air quality data to apportion airborne PM from traffic to vehicles. Based on the outcomes of these analyses, a decision could then be made to either retain the current EFs or undertake new monitoring and modelling to develop and test a new set of EFs for New Zealand. The second part is underway to carry out these recommendations. It will assess existing air quality data to derive New Zealand specific NEE EFs

which will be used as part of a sensitivity study compared with existing EFs and establishing requirements for future measurement and modelling to reduce uncertainties in modelling impacts of air quality. Air quality modelling in New Zealand relies on a suite of homegrown and international models including emission, dispersion and meteorological, each bringing its own errors to the calculation. However, analysis of the sensitivity to errors of any of the models has never been conducted.

GNS Science holds an archive of filter-based, time-integrated particulate matter samples that have been analysed by ion beam analysis (IBA), X-ray fluorescence analysis (XRF) and light reflectance to provide elemental composition data (e.g., Trompeter et al 2014). PM samples have been collected from approximately 40 sites across New Zealand using National Environmental Standard (NES) compliant methods. In addition, several studies have targeted source specific particulate matter composition, these include motor vehicle tunnels in order to better understand emission source characteristics and composition (Ancelet et al 2011, Davy et al 2011).

This work was supported by Waka Kotahi, NIWA and GNS

Ancelet T, Davy PK, Trompeter WJ, Markwitz A & Weatherburn DC (2011). Carbonaceous aerosols in an urban tunnel. *Atmospheric Environment*, 45, 4463-4469.

Davy PK, Trompeter WJ & Markwitz A (2011). Concentration, composition and sources of particulate matter in the Johnstone's Hill Tunnel, Auckland. GNS Science consultancy report 2010/296.

Davy PK & Trompeter WJ (2019). Composition, sources and long-term trends for Auckland air particulate matter: Summary Report. GNS Science Consultancy Report 2019/151. Institute of Geological and Nuclear Sciences.

Semadeni-Davies, A.F., Coulson, G., Gadd, J., Somervell, E., Longley, I. and Olivares G (2021). Non-exhaust emissions from vehicles: literature review and recommendations for developing new emission factors for New Zealand (Waka Kotahi NZ Transport Agency research report)

Trompeter WJ, Davy PK, Barry B & Kennedy J (2014). Influence of filter thickness on PESA calibration. *Nuclear Instruments and Methods in Physics Research, Section B: Beam Interactions with Materials and Atoms*, 332, 445-448.

Characterization & quantification of traffic-derived non-exhaust particles (TWP/TRWP, brake & road wear) in airborne dust

J. Rausch¹, D. Jaramillo-Vogel¹ and S. Perseguers²

¹Particle Vision Ltd., Passage du Cardinal 13B, Fribourg, 1700, Switzerland

² Gradiom Ltd., Avenue de Tivoli 4, 1700 Fribourg, Switzerland

Keywords: non-exhaust, tire wear, brake wear, road wear, road marking (paint), SEM/EDX single particle analysis, source apportionment, machine-learning
Presenting author email: juanita.rausch@particle-vision.ch

The link between particle pollution and health issues has been widely demonstrated during the last decades. This is the reason why the WHO set ambitious targets by drastically lowering the recommended limit values for particulate matter PM10 and PM2.5 in the newest Global air quality guidelines from September 2021. In view of these new recommendations, it can be expected that many measuring stations (and therefore, inhabited areas) are affected by PM10 and PM2.5 exceedances. Therefore, authorities have more than ever the need of seeking lowering PM values.

To achieve lower PM10 and PM2.5 concentrations we need first to obtain a better understanding on the fine dust constituents. This is crucial to implement targeted dust mitigation measures. Unfortunately, there is no one single method that can characterize the totality of PM10 and PM2.5. Owing to the intrinsic different characteristics of particles, and hence, stability and detectability with the various available methods, a combination of techniques needs to be applied. Here, a set of classical bulk analyses (e.g. TOT, IC) and a newly developed morpho-chemical single particle analysis method is applied to achieve an in-depth PM10 characterization and differentiation.

Due to the increasing share of traffic-derived non-exhaust particles in airborne dust a need for a reliable, and cost-effective method to quantify and differentiate particles like tire, brake, road and road marking wear becomes evident. However, the differentiation of such primary particles is not always straightforward based on bulk analysis. Here, we present a powerful approach to perform the differentiation of primary particles (e.g., traffic-derived non-exhaust). The method is based on single-particle analysis by Scanning Electron Microscopy (SEM) and Energy Dispersive X-ray Spectroscopy (EDX) coupled to a machine learning-based algorithm that classifies and quantifies the concentration of the different particle types (for methodological details see Rausch et al., 2022). The algorithm considers not only the elemental composition of single particles but also their size, morphology, and degree of heterogeneity (mixing), as they occur in real-world environmental samples.

Thanks to the detailed particle characterization, and the source-differentiated results (Figs. 1 & 2), the influence of specific human-induced activities (e.g., traffic, quarrying/mining, industry) on air quality can be monitored, allowing targeted measures to be taken by decision makers. In addition, a verification and quantification of the effectiveness of the implemented

dust mitigation measures can be performed (e.g. determination of the contribution of non-exhaust particles emitted by combustion engine vehicles vs. electric vehicles).

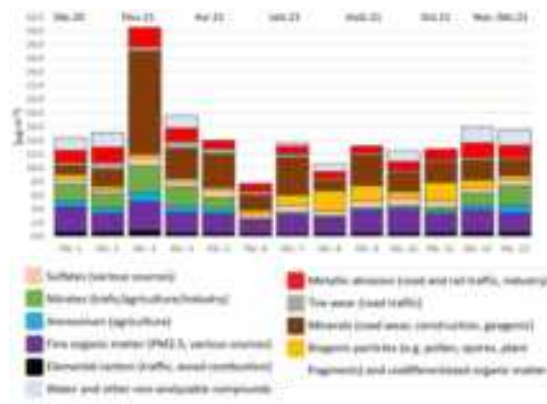


Figure 1. Stacked plot showing the concentration and temporal variability over 1 year at an urban traffic site (Canton of Vaud, Switzerland) of the different constituents of PM10 (including non-exhaust particles).

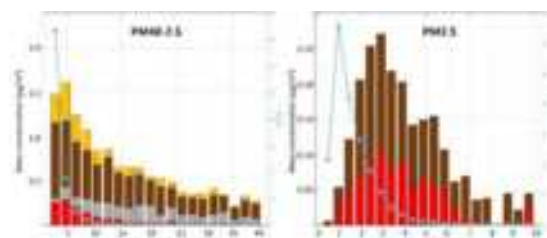


Figure 2. Size-resolved mass concentration of the main primary particle types in PM40-2.5 and PM2.5 (annual mean of the above case study).

The Swiss Federal Office for the Environment (FOEN) and the Canton of Vaud (Switzerland) are thanked for funding the one-year measurement campaigns.

Rausch, J., Jaramillo-Vogel, D., Perseguers, S., Schnidrig, N., Grobety, B., & Yajan, P. (2022). Automated identification and quantification of tire wear particles (TWP) in airborne dust: SEM/EDX single particle analysis coupled to a machine learning classifier. *Science of The Total Environment*, 803, 149832.

Data protection in remote sensing through profiling high-emitting vehicles

Lukas Unterschütz, Pascal Kerschke, Jens Borken-Kleefeld

“Friedrich List” Faculty of Transportation and Traffic Sciences, Technische Universität Dresden Dresden, Sachsen, 01069, Germany

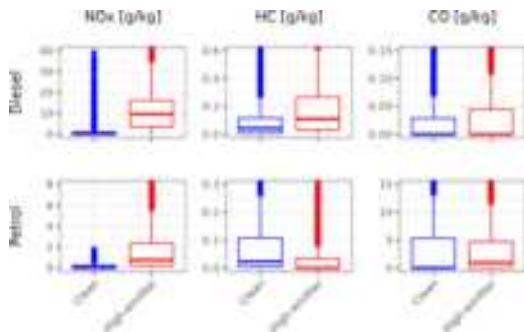
Keywords: Euro 5, Euro 6, CADC, PEMS, real world
Presenting author email: lukas.felix.unterschuetz@tu-dresden.de

Remote sensing (RS) is a powerful method to quickly scan the exhaust emissions from thousands of vehicles passing by a monitoring site. However, proper analysis currently requires number plate photographing, storing and reading in order to match measured emissions with the technical specifications of the vehicle retrieved from the registration data. This causes concerns for data protection and could be a road-block to a more widespread application. In particular, when searching for the potentially few high-emitting vehicles, the number plate processing could be considered unduly intruding the privacy of many drivers with well functioning exhaust emission controls. How can the emission standard of a passing vehicle be determined based on instantaneous emissions readings?

Qiu and Borken-Kleefeld (2022) developed a scheme focusing on NO_x emissions from diesel cars to differentiate high-emitting from clean vehicles. Building on this idea, we here introduce a multivariate machine learning approach using all the pollutants measured to detect high-emitting cars based only on their emission profile, in particular without recourse to technical data retrieved through number plate reading. For this, first, typical emission profiles are derived, differentiated by fuel type, emission standard and whether a car is high-emitting. This is done using data from chassis dynamometer and PEMS tests. These profiles are then used to classify instantaneous RS observations into clean and high-emitting vehicles.

In this work, we focus on petrol and diesel Euro 5 and 6 passenger cars and convert emissions from chassis and PEMS tests to gram pollutant per kilogram fuel, to be immediately compatible with RS results. To classify a vehicle as clean, emission data is taken from controlled experiments and compared to the applicable emission standard. If the measurements remain within a 20%-margin of the threshold for all relevant pollutants, a vehicle is classified as clean. This information is then used to derive a typical emission profile per Euro norm and fuel type.

To check the feasibility of creating such profiles, the average emission of clean and high-emitting Euro 6 petrol and diesel vehicles is displayed in Figure 1. The data is obtained from controlled experiments and observations comparable to RS measurements are



selected, i.e., for positive engine loads as well as acceleration and speeds of more than 5 kilometers per hour. Each pollutant is displayed as the ratio of the

Lubrication oil as a potential source of traffic originated secondary particulate mass

M. Priestley^{1,2}, A. A. Hammoud^{2*}, E. Tsiliogianni, M. Hallquist², Å. M. Hallquist¹

¹IVL Swedish Environmental Research Institute, Gothenburg, Sweden

²Department of Chemistry and Molecular Biology, University of Gothenburg, Gothenburg, Sweden

* Now at: LazeraH ab, Erik Dahlbergsgatan 11A, Gothenburg, Sweden

Keywords: Lubrication oil, oxidation, aerosol, secondary particulate mass

Presenting author email: michael.priestley@ivl.se

It is well known that traffic is a large contributor to gaseous and particulate pollutants in the urban environment. In the atmosphere primary vehicle emissions can further oxidise forming secondary pollution. Previous work has shown that the formation of secondary particulate mass (PM) from atmospheric oxidation of exhaust can be significant and much larger than the primary emitted PM (Robinson et al. 2007, Watne et al., 2018) and based on our recent findings, attributed to an important non-fuel dependent source that we hypothesize can be lubrication oil (LO) (Le Breton et al. 2018).

LOs are a complex mixture of organic compounds that can evaporate and contribute to fugitive volatile organic compound (VOC) emissions. Once in the atmosphere these VOCs can oxidise to form oxygenated VOCs with reduced volatilities contributing to the formation of secondary organic aerosol (SOA). The extent to which these LOs can contribute to PM is currently not well known.

Here, results from a laboratory study aiming to identify tracers of lubrication oil oxidation products and quantify their contribution to the formation of PM are presented. We atomized LOs used by CNG and RME-fuelled buses. The produced aerosol was heated to 200°C and passed through an oxidation flow reactor (Go:PAM) after which it was sampled by a Scanning Mobility Particle Sizer (SMPS), to measure particle size distributions and mass concentrations, and a Time-of-Flight Chemical Ionisation Mass Spectrometer (ToF-CIMS) with a Filter Inlet for Gas and AEROsols (FIGAERO) to measure gaseous and chemical composition. A measurement cycle included fresh sampling followed by OH/O₃ oxidation to simulate their atmospheric ageing. These cycles were repeated with and without the addition of NO_x.

The FIGAERO-ToF-CIMS measured a large suite of gaseous and particle phase organics from both the fresh and aged emissions (e.g., Figure 1). Ageing the emissions produced a greater quantity of lower mass gas phase compounds and a large number of secondary particle phase compounds, of which the composition was different between the CNG and RME LOs. The impact of ageing and the presence of NO_x on particle mass concentrations for the CNG and RME LO will also be presented.

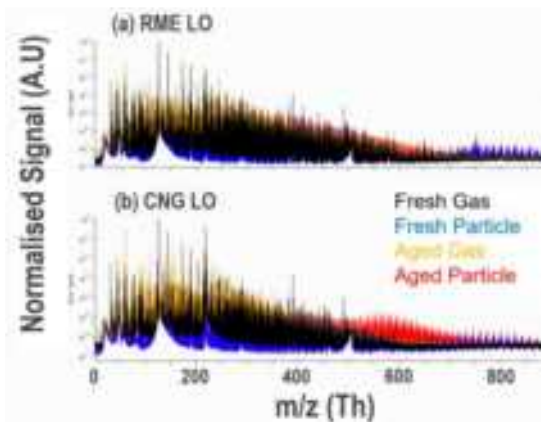


Figure 1. Fresh and aged gas and particle phase mass spectra of (a) RME and (b) CNG lubrication oil (LO).

This work was financed by Formas (2020-1907).

Le Breton M., Psichoudaki M., Hallquist M., Watne Å. K., Lutz A., Hallquist Å. M. 2019 *Application of a FIGAERO ToF CIMS for on-line characterization of real-world fresh and aged particle emissions from buses*, AS&T, 53, 244

Robinson A. L. et al. 2007 *Rethinking organic aerosols: Semivolatile emissions and photochemical aging*, Science, 315, 1259

Watne Å. K., Psichoudaki M., Ljungström E., Le Breton M., Hallquist M., Jerksjö M., Fallgren H., Jutterström S. and Hallquist Å. M. 2018, *Fresh and Oxidized Emissions from In-Use Transit Buses Running on Diesel, RME and CNG*, ES&T 52, 7720

A simplified in-Field Calibration method for Periodical Technical Inspections Particle Counters with atomized NaI

Helmut Krasa¹, Martin Kupper¹, Mario A. Schriefl^{1,2}, Alexander Bergmann¹

¹Institute of Electrical Measurement and Sensor Systems, Graz University of Technology, Graz, 8010, Austria,

²Emission Measurement Department, AVL DiTEST GmbH, Graz, 8010, Austria

Keywords: Periodical Technical Inspections, Particle Number, Calibration, Natrium Iodide

Presenting author email: helmut.krasa@tugraz.at

Starting with 2023, Germany included particle number (PN) measurement as part of periodical technical inspections (PTI) of registered vehicles. As PN instruments were previously limited to homologation measurements and laboratories, the number of distributed PN counters increased significantly and therewith the demand for regular calibrations. With an estimated number of 35 000 PN counters in Germany alone, a fast and high-throughput calibration procedure is required.

Calibration of PTI PN counters involves two measurements, (i) counting efficiency (CE) and (ii) linearity. The CE is defined as the ratio of the PN counted by the instrument to the PN counted by a traceable calibrated reference instrument. The CE decreases with smaller sizes and must be within a certain range for several sizes (e.g. 20 to 60 % at 23 nm (BMDV, 2021)). In addition, the CE is evaluated in the plateau region for larger particles. Furthermore, a linear response over a specified PN concentration range has to be fulfilled.

We present a mobile calibration method that allows for simultaneous calibration of the plateau efficiency parameter and linearity using atomized NaI.

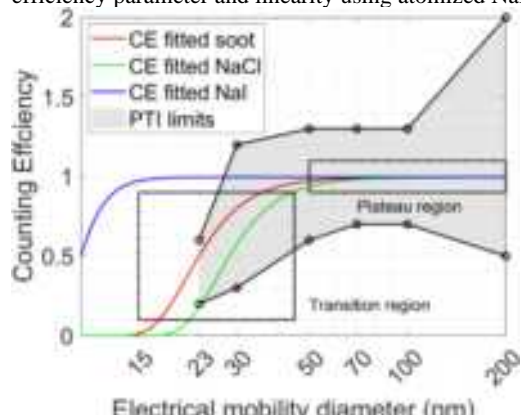


Figure 1: Graph of fitted CE curves for different particle types of a PN counter curve and the required limits

In our proposed method, particles are generated with an atomizer containing a NaI salt solution. The atomizer requires pressurized air and is otherwise fully portable. It has been shown that NaI particles are fully counted down to less than 20 nm with butanol-based condensation particle counters (CPC) with $d_{0.5}$ value calibrated to 23 nm from factory calibration (Krasa, 2023). A NaI concentration of 1.2 % was used in solution, resulting in a mean particle diameter of 46.8 nm and a geometric standard deviation of 1.7. The CE for NaI is in

the plateau for the relevant size regime for 23 nm CPCs and particle concentrations for sizes below full detection are negligible. This allows the plateau efficiency to be assessed using a polydisperse aerosol. Typically, the plateau efficiency is evaluated with monodisperse aerosol, using a differential mobility analyzer, what is to be avoided for on-site calibrations. Using polydisperse aerosol also allows for simultaneous evaluation of the linearity, as polydisperse aerosol provides sufficiently high PN concentrations - two to three order of magnitudes higher compared to monodisperse distributions.

A TSI 3790 ($CE_{0.5} = 23$ nm) CPC was calibrated with a TSI 3775 ($CE_{0.5} = 4$ nm) as a reference using mono- and polydisperse aerosol for comparison. In the monodisperse case the CE was 1.085, evaluated for four sizes of 30, 50, 75 and 100 nm. In the polydisperse case, the concentration response was highly linear ($R^2 > 0.99$) and the CE was 1.079. See figure 2 for the measurement data. The CE deviated less than 1% between the calibration methods, thus proving a precise calibration using polydisperse atomized NaI.

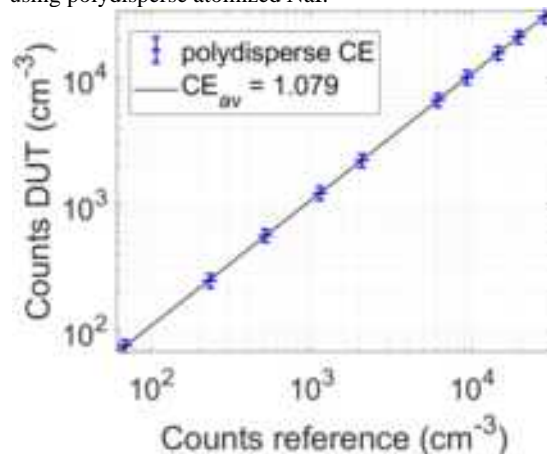


Figure 2. Linearity test with polydisperse NaI. The CE for monodisperse aerosol was 1.085 on average

Krasa H, Kupper, M. A. Schriefl & A. Bergmann (2023), *Aerosol Science and Technology, Toward a simplified calibration method for 23 nm automotive particle counters using atomized inorganic salt particles* DOI: 10.1080/02786826.2023.2174410.

BMDV (2021). *Anlage VIIIa Straßenverkehrs-Zulassungs-Ordnung (StVZO)*. VkBl. Nr. 8, 404

Roadway diesel vehicle emission measurement by PEMS and its dispersion at on-road conditions captured by OPCAS

Xiaoliang, Qin¹; Anand, Abhishek¹; Nirmal Kumar Gali¹; Zhi, Ning¹

¹Division of Environment and Sustainability, The Hong Kong University of Science and Technology, Hong Kong

Keywords: Mobile emission, Driving style, Plume chasing, PEMS, Emission factors

Presenting author email: xqinaf@connect.ust.hk

Diesel commercial vehicles (DCVs) have long been a major source of particulate matter (PM), BC and nitrogen oxide (NOx) emissions. During the period from September 2013 to April 2014, Lau et al. (2015) collected a large dataset of on-road vehicle emission in Hong Kong by plume chasing methods. The results showed that individual diesel goods vehicles and buses exhibited varying emission factors (EFs), and high-emitting vehicles were not solely limited to older Euro emission standards. The study revealed that the high emitters were not all vehicles of older Euro emission standards. Additionally, there is clear evidence that the high-emitters of one pollutant may not be the high-emitter of another pollutant. Gini coefficients for fleet emissions have been established to give a quantitative measure of the emission disproportionality to prioritize the removal of high emitters.

To tackle emissions from DCVs, the Hong Kong Government has been phasing out pre-Euro IV DCVs progressively since Feb 2014 with the completion date set to the end of 2019. Meanwhile, starting from 2014, franchised bus companies were reimbursed the full cost of retrofitting Euro II and Euro III franchised buses (FBs) with selective catalytic reduction devices (SCRs) to upgrade the NOx emission performance to Euro IV or above by the end of 2017. The DCV emission control programmes have been implemented for over four years and a significant reduction in primary emissions is expected.

Portable emissions measurement systems (PEMS) are widely recognized internationally as the most effective method for measuring vehicle emissions (Vlachos et al., 2014). However, PEMS still require modifications to the exhaust system and installation of equipment on the target vehicle. This study aims to compare on-road plume chasing and analysis system (OPCAS) with the PEMS under different driving conditions for applicability evaluation. A medium goods vehicle (MGV) and a heavy goods vehicle (HGV) were observed based on the real driving emissions regulation (RDE). The results demonstrate that plume chasing devices can be used as a screening tool to detect both low- and high-emitting vehicles during driving. The probability of producing high instantaneous NOx emissions increases with rapid changes in vehicle speed. When the ratio of acceleration to deceleration is greater than 0.6, the concentration of CO₂ and NOx increases rapidly. The ratio of NO to NOx can be used as an indicator to define the plume. The measured emissions are in good correlation with the results from PEMS measurements. The study also establishes the limitations of plume pursuit in certain road

layouts, traffic conditions, and speed variations. These findings are significant for designing high-emission vehicle regulation policies and provide a reference for future research on real-time monitoring of on-road emissions.

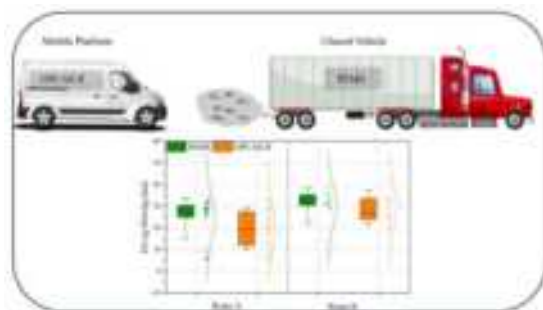


Figure 1. A schematic diagram of on-road experiments by using OPCAS and PEMS.

This research is funded by the [Hong Kong Environment and Conservation Fund \(ECF/21/2021\)](#).

Lau, C. F., Rakowska, A., Townsend, T., Brimblecombe, P., Chan, T. L., Yam, Y. S., ... & Ning, Z. (2015). Evaluation of diesel fleet emissions and control policies from plume chasing measurements of on-road vehicles. *Atmospheric Environment*, 122, 171-182.

Vlachos, T. G., Bonnel, P., Perujo, A., Weiss, M., Villafuerte, P. M., & Riccobono, F. (2014). In-use emissions testing with portable emissions measurement systems (PEMS) in the current and future European vehicle emissions legislation: overview, underlying principles and expected benefits. *SAE International Journal of Commercial Vehicles*, 7(2014-01-1549), 199-215.

Comparative chemical composition of US and European tyres VOC profile, potential environmental impact, including 6PPD

Nick Molden, Ime Usen

Emissions Analytics Ltd. Stokenchurch, Buckinghamshire, HP14 3PD, United Kingdom
Presenting author email: Nick@emissionsanalytics.com

Tires are complex products, with sophisticated physical design and chemical composition. They must deliver a range of often conflicting performances including slow wear (for maximum life), low rolling resistance (to reduce carbon dioxide emissions and fuel consumption), wet grip and low noise. There exist regulatory and labelling requirements around these. Where information is currently lacking is in the wear rates and chemical composition of the tires. This is relevant to the amount material released into the environment, where it goes and what damage it does to human and animal health, and the environment more widely.

This presentation will focus on the chemical composition of hundreds of different models of tires sold, drawn from both the US and European markets. Commonalities and differences will be analyzed. A hypothesis will be considered that US tires contain different chemical components as the market focuses more on durability, compared to the European market that tends to value lower rolling resistance more highly. It will draw on Emissions Analytics' tire material database, which typically identifies over 400 organic compounds in each tire, using its optimized process of thermal desorption and pyrolysis, coupled with two-dimensional gas chromatography and time-of-flight mass spectrometry.

Organic species that will be specifically analyzed are 6PPD and their substitutes. These are preservatives that are added to tires to prevent ageing and cracking, especially under sunlight. Recently, 6PPD has been linked to the death of a significant proportion of coho salmon and trout on the West Coast of the US. The concentration of 6PPD will be shown to vary significantly between different models of tire. The method will be shown to be the potential basis for enhanced product labelling.

Incorporating NOx into the Periodic Technical Inspection vehicle emission test procedures

D. Thomas¹ and G.S. Sandhu²

¹3DATX Corporation, 3600 Genk, Belgium

²3DATX Corporation, Buffalo, NY, 14228, USA

Keywords: Passenger vehicle, emissions, NOx, PTI.

Presenting author email: daisythomas@3datx.com

NOx pollution is one of the greatest air quality issues that urban areas face today, particularly within the European Union (EU), yet currently this pollutant is only controlled through the homologation process. There is no periodic technical inspection (PTI) process for NOx emissions within the EU, leaving a weakness in the legislation that is currently allowing gross polluters to negatively impact air quality (CITA, 2022). Work needs to be done to incorporate a simple, quick, inexpensive and representative test to accurately identify these high emitters within the on-road vehicle fleet.

In this project, vehicle and tailpipe emissions data was collected using the parSYNC® iPEMS and a HEM OBD data logger from over 600 light passenger vehicles simulating an enhanced PTI emissions test. The tested vehicles were a random sample of passenger cars passing through a Swedish PTI test centre, so are broadly representative of the fleet in Sweden. These vehicles ranged from model years 1979 to 2019, with vehicles covering the European emission standards Euro 1 to Euro 6, and including both gasoline and diesel fuel types of various engine powers and sizes.

The enhanced PTI emission test performed on each vehicle consisted of an idle test, one of two types of high idle test, and a dynamic acceleration test. The repeatability of all three test types was good. Options for the meaningful incorporation of the dynamic acceleration test are investigated, such as the use of VSP methods to characterise the dynamic properties of such tests. The NOx concentrations have strong correlations to the mass emissions for each test type, with the use of mean values being deemed more representative than the use of maximum values. The mean results across the tested fleet are calculated and used to define pass/fail thresholds for different vehicle types as suggested by CITA (Buekenhoudt, 2019). These are outlined in table 1.

Table 1. Suggested NOx (ppm) thresholds for each test type, for different vehicle types.

Fuel Type	Emission Standard	Idle	High Idle ¹	High Idle ²	Acceleration
Diesel	Euro 4	298	228	240	445
	Euro 5	306	312	234	400
	Euro 6	226	186	228	362
Petrol	Euro 4	130	392	NA	163
	Euro 5	138	220	NA	387
	Euro 6	74	138	NA	132

¹ Mean NOx value from a ~5s hold at 2500 rpm

² Mean NOx value from a free acceleration test

An investigation into the trends in emissions from the tested vehicle fleet is also performed using this dataset. The NOx concentrations resulting from the different test types (low idle, high idle, free acceleration and a range of dynamic acceleration tests) are compared against vehicle age, odometer reading, Euro standard, and other vehicle characteristics such as emissions abatement technology and fuel injection type. By comparing the average results from Euro 4, Euro 5, and Euro 6 vehicles as well as those Euro standards, Figure 1 shows that the NOx from EURO-6 vehicles reverse the increase seen in EURO-5, but still fail to deliver the level of reductions in real-world emissions as per the emission standards.

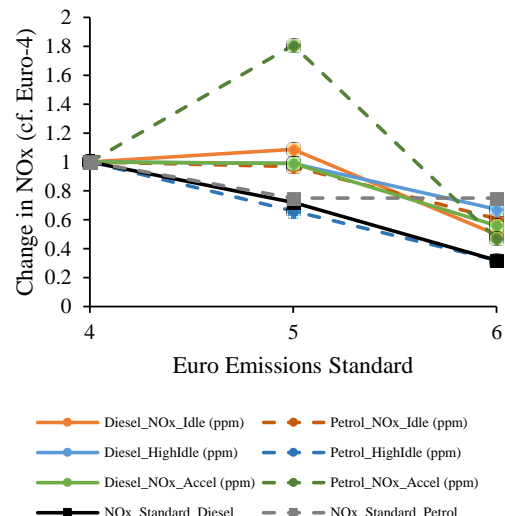


Figure 1. Mean NOx concentration values for different test types and NOx limits relative to Euro4 vehicles.

The ability of the above NOx test methods to identify high emitting vehicles from the test fleet is analysed, and indicates that a loaded test is required for NOx emitter detection, with a dynamic acceleration test performing well. The impact of engine and vehicle conditioning and ambient weather conditions on the results is investigated. Availability and assimilation into enhanced PTI of important ECU/OBD parameters is evaluated. Other challenges of doing such a program are also discussed.

Buekenhoudt, P.; Müller, G.; Mäurer, H.-J et al. SET II Project - Sustainable Emission Test for Diesel Vehicles Involving NOx Measurements; CITA: Brussels, Belgium, 2019.
CITA Monitoring of NOx Emissions as Part of the PTI; International Motor Vehicle Inspection Committee (CITA); Brussels, Belgium, 2022.

3.14 PS.2. Poster session 2 (Joint and S&E sessions)

AIS data mining to identify tank cleaning operations at sea

W. Mao¹, S. Wang² and I.-M. Hassellöv¹

¹Department of Mechanics and Maritime Sciences, Chalmers University of Technology, Gothenburg, 41296, Sweden

²Department of Navigation, Dalian Maritime University, Dalian, Liaoning, 111404, China

Keywords: AIS, data missing, abnormal trajectories, tank cleaning.

Presenting author email: wengang.mao@chalmers.se

Following increased transport by chemical tankers of products classified as IMO MARPOL Annex II substances, such as biofuels, the Swedish Coast Guard are detecting an increasing number of chemical pollution events in Swedish waters and the Baltic Sea. The regulation of tank cleaning is complex and leaves room for different interpretation, yet also legal tank cleaning operations may pose a threat to the marine environment. To carry out environmental risk assessment there is a need to know when and where tank cleaning operations are carried out (in addition to what type of substance, cleaning agents and volume discharged). Currently, chemical tankers are not obliged to report such information. One possible way to get information about when and where tank cleaning operations are carried out is then to analyse the ship activities through their navigation data including ship position, speed, course, etc., collected and transmitted among ships and shore-based stations by the AIS (Automatic Identification System). The AIS is a mandatory instrument for ships sailing at sea to aid ship navigation safety (IMO 2015). It is also an effective means of maritime monitoring (Lensu and Goerlandt 2019, Yang et al. 2019).

In this study, the AIS information from chemical tankers sailing in Swedish waters and the Baltic Sea is used to investigate if there are some navigation patterns that can indicate a possible/suspected tank cleaning operation. In addition, detected pollution events confirmed by the Swedish Coast Guard and hypothesised to originate from tank cleaning operations, were matched to some of the patterns related to abnormal sailing trajectories during tank cleaning operations. Analysis of AIS data around those detected marine chemical pollution spots help to reveal certain sailing patterns for designing data mining techniques, for example, sharp turning, unnecessarily sailing to open sea (outside of Swedish Economic Zone), normal sailing speeds, ballast loading conditions, etc.

Three data mining techniques are implemented to fast search the big AIS database, find and analyse: 1) abnormal AIS signal missing that with a high probability is not caused by AIS transmission technical problems, 2) abnormal sailing trajectories (e.g., unnecessary sharp turning, unnecessary long-distance sailing, etc.) by the machine learning DBSCAN algorithm and direct filtering algorithms, 3) hotspot areas around the Swedish waters with large amount of abnormal AIS data transmission and sailing characteristics. By automatic identification of those abnormal sailing behaviours of chemical tankers by analysing both real-time and historical AIS data, the

implemented data mining methods are expected to be able to provide data support for maritime regulatory authorities.

Based on the big data analysis of AIS signals collected around Swedish waters, this study shows that missing AIS data signals are more frequent for the investigated chemical tankers compared to cargo ships. Even though it is not possible to judge how many of those AIS signals missing scenarios are related to tank cleaning operations, serious AIS signal loss, i.e., more than 30-50 minutes data while the ship is sailing faster than 5 knots, may be interpreted as suspicion of tank cleaning. A follow up check of their trajectories before and after the AIS signal loss may give more confidence about the suspicion of tank cleaning operations. Furthermore, for chemical tankers granted prewash exemption, much fewer AIS missing data were observed (no serious AIS signal missing was observed).

In addition to those analysed sailing characteristics, further data mining analysis and discussions with domain experts on tank cleaning operations should be able to cluster more patterns to design machine learning algorithms to automatically searching potential tank cleaning operations based on the AIS data.

This work was supported by the Havs- och vattenmyndigheten, anslag 1:11.

IMO (2015). Resolution A.1106 (29) Revised guidelines for the onboard operational use of shipborne automatic identification systems (AIS). *Assembly 19th session*, adopted on 2 December 2015.

Lensu, M. and Goerlandt, F. (2019). Big maritime data for the Baltic Sea with a focus on the winter navigation system. *Marine Policy*, **104**, 53-65.

Yang, D., Wu, L. X., Wang, S. A., Jia, H. Y. and Li, K. X. (2019). How big data enriches maritime research - a critical review of Automatic Identification System (AIS) data applications. *Transport Reviews*, **39**(6), 755-773.

DOAS applied to shipping emission monitoring: compliance assessment and comparison to satellite measurements

M. Prignon¹, V. Conde¹, T. J. Smyth², A.-M. Sundström³, J. van Vliet⁴, and J. Mellqvist¹

¹Chalmers University of Technology, Department of Space, Earth and Environment, Göteborg, Sweden

²Plymouth Marine Laboratory, Plymouth, UK

³Space and Earth Observation Centre, Finnish Meteorological Institute, Helsinki, Finland

⁴Netherlands Human Environment and Transport Inspectorate, Den Haag, The Netherlands

Keywords: shipping emission monitoring, remote sensing, DOAS, satellite observation.

Presenting author email: maxime.prignon@chalmers.se

The intensive activity of the shipping transport mode (80 % to 90 % of global merchandise trade volume), coupled with high specific emissions of nitrogen oxides (NO_x), sulphur oxides (SO_x) and particulate matter (PM) has significant impact on the environment and the human health. Today, NO_x and SO_x emissions are regulated under the International Maritime Organization (IMO) MARPOL Convention Annex VI (adopted in 1997 and entered into force on 19 May 2005). SO_x emissions are regulated through the limitation of fuel sulphur content (FSC), which must be lower than 0.5% globally since 2020. FSC is further limited in emission control areas (ECAs). Since 2015, the European ECA (English Channel, North Sea and Baltic Sea) requires FSC to be lower than 0.1%.

Compliance monitoring for FSC is usually done by the collection and analyse of fuel samples by competent authorities for ships at berth. The complexity and the cost of the method results in very few ships being formally controlled. Facing this, remote measurement techniques of individual exhaust ship plumes have been developed and applied for more than a decade. The state-of-the-art technique, the sniffer technique, usually implies a remote sample extraction of the ship exhaust plume followed by an analysis with analyser instruments (e.g., UV fluorescence-based, chemiluminescence-based, small electrochemical, or small-sized non-dispersion infrared instruments). FSC is then estimated by computing the ratio between the integrated SO_2 and CO_2 concentrations measured inside the ship plumes, with the assumption that most of the fuel carbon is converted to CO_2 and that most of the fuel sulphur is converted to SO_2 .

Well-known optical remote sensing techniques, as the ultraviolet/visible differential optical absorption spectroscopy (DOAS), have also been applied to ship emission monitoring in the past years. As sniffer measurements, the DOAS technique can be used from different platforms (e.g., ground-based, aircraft-based, ship-based, satellite-based) and is therefore well suited for the measurement of single ship plumes.

In the framework of the SCIPPER European project (<https://www.scipper-project.eu/>, last access 23rd February 2023), we have performed DOAS observations, together with standard sniffer measurements, of single ship plumes during the two days of an observation campaign in the English Channel in May 2022. In between ship plume crossings, we also performed multi-axis DOAS observations (MAX-DOAS) to retrieve NO_2

vertical columns with the objective of a comparison of the NO_2 background abundance with the TROPOMI (Tropospheric Monitoring Instrument) space-based instrument.

Our DOAS results show that almost all sampled plumes are detectable in the recorded NO_2 spectra (33 over 34 sampled ships). For SO_2 , we could detect it in three plumes (e.g., ships #2 and #9 in Fig.1). When looking at the highly sensitive sniffer results, we see that 2 of these ships were actually running with FSCs above 0.1% (i.e., non-compliant). The sniffer system could detect one more ship that was about the legal limit (0.1%). All other ships sampled by the sniffer were complying to the FSC regulation (3 over 38 ships above 0.1%). These results suggest that the ship-based DOAS technique could be used to discriminate non-complying ships from complying one in a qualitative way, i.e., if SO_2 can be detected from the measured spectra. In that way, the relatively simple DOAS method could be used as a first screening of passing ships, the flagged ships could be then reported to the competent authorities to proceed to a formal and legal control.

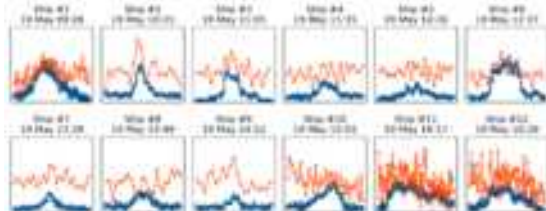


Figure 1. Example of DOAS results. On the vertical axis are the NO_2 (blue) and SO_2 (red) slant column densities measured while crossing the plumes (constant scale among the different ships). The horizontal axis is the time (varying from ship to ship).

The comparison between the ship-based and the TROPOMI -for which the plumes are detected following a deep-learning method- observations show encouraging results. Both instruments recorded higher background columns for the second day of observation, with a comparable absolute increase in comparison to the first day. The comparison of in-plume values is more challenging and is, at the moment, inconclusive. An effort is underway to determine a more relevant emission proxy from the DOAS and the satellite measurements.

FUGitive Methane Emissions from Ships (FUMES): Characterizing methane emissions from LNG-fueled ships using drones, helicopters, and on-board measurements

Bryan Comer¹, Liudmila Osipova¹, Elise Sturup¹, Jörg Beecken², Bettina Knudsen², Jon Knudsen², Robin Vermeulen³, Pierre Paschinger³, Ann Delahaye³, and Ruud Verbeek³

¹The International Council on Clean Transportation, Washington DC, USA

²Explicit ApS, Copenhagen, Denmark

³Netherlands Organisation for Applied Scientific Research (TNO), The Hague, the Netherlands

Keywords: methane emission, methane slip, Liquefied Natural Gas (LNG), marine fuel.

Presenting author email: jbe@explicit.dk

The fleet of vessels which are propelled by Liquefied Natural Gas (LNG) is rapidly increasing, and as such the emissions of methane (CH_4) in the maritime sector. Between 2012 and 2018, the use of LNG increased by 30 %, leading to an estimated increase of 150 % in methane emissions from international shipping over this period according to IMO's Fourth Greenhouse Gas Study 2020. Methane contributes to global warming and its global warming potential is around 30 times stronger as compared to carbon dioxide (CO_2) after a residence time of 100 years in the atmosphere and even around 82 times stronger after 20 years (IPCC, 2021).

Current estimates of CH_4 emissions are based on limited on-board and laboratory measurements leaving a high uncertainty related to these findings. There are several sources for possible methane emissions on LNG propelled vessels, e.g. the methane slip in the marine engines, and fugitive emissions from the fuel and cargo tanks. These emissions are dependent on parameters such as engine type and engine load. But currently, there are not much data available on the real-sailing emissions of LNG propelled vessels.

Hence, the FUgitive Methane Emissions from Ships (FUMES) project, a collaboration between the International Council on Clean Transportation (ICCT), the emissions monitoring company Explicit ApS, and the Netherlands Organization for Applied Scientific Research (TNO), was established in 2022 to collect a comprehensive dataset of real-sailing emissions of methane in conjunction with nitrogen oxides (NO_x).

One particular objective of the FUMES project is to gain a better understanding of the dependence of methane emissions on different engine types but also other engine factors such as age under consideration of different engine load conditions.

Data are collected by drone, helicopter, and on-board measurements. The drone and helicopter measurements are aiming to retrieve emissions data from high number of vessels, representing a broad spectrum of engine configurations while on-board measurements are focusing on emissions of specific engine types under different operational conditions.

The emission rates of fugitive CH_4 from LNG carriers are assessed using the Drone Flux Measurement (DFM) method (Knudsen and De Rossi, 2022), while loading/unloading operations were ongoing at an LNG terminal, see Figure 1.



Figure 1. Visualization of emission rates of fugitive CH_4 of an LNG carrier at a terminal using the DFM method.

The data collection is now, February 2023, still ongoing until summer this year. But until now emissions of more than 30 different vessels were measured, some of them repeatedly, with abundant CH_4 emissions. First observations show a large spread of methane slip, which relates the mass of uncombusted CH_4 to the mass of the LNG supplied to the engine, from below 1 % up to double-digit percentages. Overall, the current results indicate a higher methane slip than estimated in ship emissions inventories or assumed in the regulations, e.g. FuelEU maritime.

IPCC: Climate Change 2021: *The Physical Science Basis. Contribution of Working Group I to the Sixth Assessment Report of the Intergovernmental Panel on Climate Change*, Cambridge University Press, Cambridge, United Kingdom and New York, NY, USA, 2391 pp, <https://doi.org/10.1017/9781009157896>, 2021.

Knudsen, J. and De Rossi, L.: *The Plane Project: Mapping and quantification of GHGs from diffuse emission sources using drone technology and vertical measuring walls*, The Danish Environmental Protection Agency, 2022.

Discharges from ships to the sea in European sea regions

J.-P. Jalkanen¹, E. Majamäki¹, L. Johansson¹, T. Grönholm¹, A. Maragkidou¹ and Jaakko Kukkonen

¹Atmospheric Composition Research, P.O. Box 503, FI-00101, Helsinki, Finland

Keywords: Ship emissions, discharges, SOx, scrubbers
Presenting author email: jukka-pekka.jalkanen@fmi.fi

The introduction of SOx Emission Control Areas (ECA) for marine fuel sulfur content has led to an increased use of alternative means to comply with the new regulation, which avoids the use of more expensive low sulfur liquid fuels. These include Exhaust Gas Cleaning Systems (EGCS) and a large-scale adoption of Liquid Natural Gas (LNG) as a fuel. However, both alternatives have their drawbacks. Use of LNG has increased the methane emissions from ships because unburnt methane escapes from combustion engines of ships. While cleaning the air with an EGCS, ships have created a new pollution stream to the sea, with increased concentrations of various Polyaromatic Hydrocarbons (PAH) and heavy metals.

In this paper, we present ship discharge modeling results for the EU domain. The work is based on global Automatic Identification System (AIS) data and was made with the Ship Traffic Emission Assessment Model (STEAM) of the FMI (Jalkanen et al., 2009; Jalkanen et al., 2012; Johansson et al., 2013; Johansson et al., 2017; Jalkanen et al., 2021). During 2018, over 447 million tonnes of EGCS effluent was discharged to the sea from 287 vessels, and over 99.9% of that was from open loop systems. From that, over 28% was discharged to the Baltic Sea. Since the 0.1% sulfur limit became effective in SOx ECAs, also global sulfur cap of 0.5% on Jan 1st, 2020, increased the number of vessels using EGCS significantly. In 2021, over 4300 ships operated EGCS globally and estimated effluent releases exceeded 15 000 million tonnes. With the current high price premium of low sulfur fuels, it is expected that the number of ships with EGCS will increase significantly in the near future.



Figure 1. Discharge from Open Loop EGCS in the EU domain during 2018.

The STEAM emission and discharge data generated are used as input to atmospheric and ocean models. These enable large scale studies to understand the shipping contributions to impacts concerning humans and the marine environment.

This project has received funding from the European Union's Horizon2020 research and innovation programme under grant agreement #874990 (EMERGE project). This work reflects only the authors' view and CINEA is not responsible for any use that may be made of the information it contains.

- Jalkanen, J.-P., Johansson, L., Wilewska-Bien, M., Granhag, L., Ytreberg, E., Eriksson, K. M., ... Moldanova, J. (2021). *Ocean Science*, **17**(3), 699–728.
- Jalkanen, J.-P., Johansson, L., Kukkonen, J., Brink, A., Kalli, J., and Stipa, T. (2012). *Atmospheric Chemistry and Physics*, **12**(5), 2641–2659.
- Jalkanen, J. P., Brink, A., Kalli, J., Pettersson, H., Kukkonen, J., and Stipa, T. (2009). *Atmospheric Chemistry and Physics*, **9**(23), 9209–9223.
- Johansson, L., Jalkanen, J.-P., and Kukkonen, J. (2017). *Atmospheric Environment*, **167**, 403–415.
- Johansson, L., Jalkanen, J.-P. P., Kalli, J. and Kukkonen, J. (2013). *Atmospheric Chemistry and Physics*, **13**(22), 11375–11389.

A Low-Cost Optoacoustic Sensor for Black Carbon monitoring of Ships

N. Kousias¹, L. Haedrich², A. Stylogiannis², I. Raptis¹, V. Ntziachristos², L. Ntziachristos¹

¹Department of Mechanical Engineering, Aristotle University of Thessaloniki, Thessaloniki, GR54124, Greece

²Chair of Biomedical Imaging, Technical University of Munich, Munich, Bavaria, D-81675, Germany

Keywords: opto-acoustic, sensing, black carbon, ships, low-cost, monitoring

Presenting author email: nkousias@meng.auth.gr

Black Carbon (BC) is a significant pollutant that has strong contribution to climate change (Bond et al. 2013) while it also has negative effects on human health (World Health Organization 2012). The shipping sector is a key emitter of BC particles due to their emissions in the arctic. BC absorption is enhanced in the arctic, while it also accelerates snow melting due to deposition (Kühn et al. 2020). Monitoring of BC emissions from ships is considered by the IMO (5th meeting of the Sub-Committee on Pollution Prevention and Response (PPR 5)). Optoacoustics is a viable technology, but current systems are expensive for implementation on-board vessels where often multiple instruments, one for each exhaust line, are required. We have developed a sensor that is suitable for on-board monitoring and tested it on two ships under real conditions.

The main innovation of the sensor (Stylogiannis et al. 2021) is the geometry of the measuring cell, which is an ellipsoid. An ellipse has two focal spots. The sample flow and the light beam intersect at the first focal spot, where a sound source is created. The sound is then refocused to the second focal spot due to the ellipsoid geometry. A sensitive sound transducer (QTF) is positioned at the second focal spot where all the acoustic energy is refocused. The distance between the contaminating sample flow and the QTF is several centimetres, thus protecting the QTF from particle contamination. The chamber's acoustic properties, in combination with the high sensitivity of the QTF, allow the use of a low-cost laser diode. The design is shown in Figure 1.

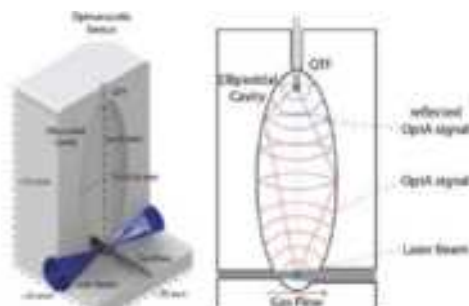


Figure 1. Design of the Optoacoustic sensor

The first implementation of the sensor was on a RoRo ferry that was transporting passengers and cargo in the Baltic. The ship was powered by four 4-stroke medium speed main engines equipped with SCR catalysts for NOx reduction. The fuel used during the campaign was MGO. Exhaust from one of the main engines of the

ship was sampled with an eDiluter Pro (Dekati, eDiluter Pro). An aethalometer (ObservAir) is used as a reference.

The second implementation was on a large container ship, travelling from Netherlands to Turkey. The ship was equipped with one 2-stroke low-speed engine and an open-loop Scrubber for SOx reduction. The fuel used was HFO. In addition, measurements were performed both before (Upstream-US) and after (Downstream - DS) the scrubber. An eDiluter Pro was used for sampling and an optoacoustic instrument (AVL MSS) was used as a reference.

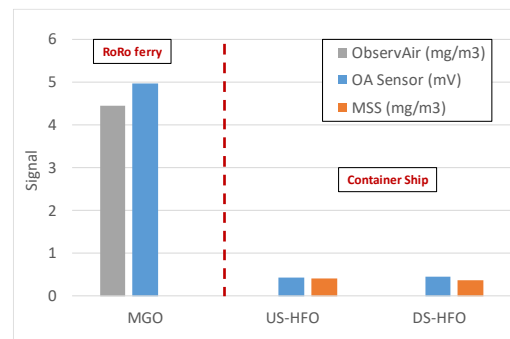


Figure 2: Comparison of the sensor's signal with BC concentration for both ships

Figure 2 shows the average BC emission levels of the undiluted ship's exhaust for both ships and for different conditions. The signal from our sensor agrees very well with the concentration that is measured from the reference instruments for both ships. We observe that the RoRo ferry has significantly higher concentration compared to the container ship. In the case of the container ship, the Scrubber does not have a significant effect on the emitted BC.

This work was supported by the European Union's Horizon 2020 research and innovation programmes under grant agreement No 814893 (SCIPPER) and No 874990 (EMEGRE).

- Bond, T. C. et al. 2013. *Journal of Geophysical Research Atmospheres* 118(11): 5380–5552.
Kühn, Thomas et al. 2020. *Atmospheric Chemistry and Physics* 20(9): 5527–46.
Stylogiannis, Antonios et al. 2021. *Sensors (Switzerland)* 21(4): 1–14.
World Health Organization. 2012. Available at: <http://hdl.handle.net/20.500.11822/8699> (Accessed: 8 March 2022)

Remote monitoring of sulphur emissions from shipping with a novel high sensitive laser system.

V. Conde Jacobo¹, J. Mellqvist¹, T. Smyth², J. Beecken^{3,4}, A. Weigelt³

¹ Chalmers University of Technology, Gothenburg, Sweden

² Plymouth Marine Laboratory, Plymouth, UK

³ Federal Maritime and Hydrographic Agency (BSH), Hamburg, Germany

⁴Explicit ApS, Copenhagen, Denmark

Keywords: sulphur emission control area (SECA), fuel sulphur content, compliance monitoring, Laser spectroscopy.

Presenting author email: vladimir.conde@chalmers.se

Sulphur emissions have a major impact on nature, climate and human health. Aiming to reduce their environmental impact; organizations like the International Marine Organization (IMO) in coordination with policy makers have agreed on regulations for reducing the global emissions of SO₂ due to marine traffic.

The implementation of these policies have effectively lead to a new global cap of 0.5% mass Fuel Sulphur Content (FSC) on marine traffic, since 2020, from the previous global FSC limit of 3.5%. At sulphur Emission Control Areas (SECA), the FSC cap is even lower (0.1%).

In view of the current marine traffic emission policies, several remote measurement techniques have been developed and implemented. Stationary systems near shipping lanes are used to analyze the chemical composition of exhaust plume of by-passing ships. These systems, positioned up to a few kilometres downwind of the ship lanes, can run continuously and autonomously.

However, as the new regulations are pushing to lower sulphur emissions, they come with the drawback that the remote monitoring of the emissions compliance has become more challenging. This situation is particularly noticeable when SO₂ measurements are carried out in SECA areas.

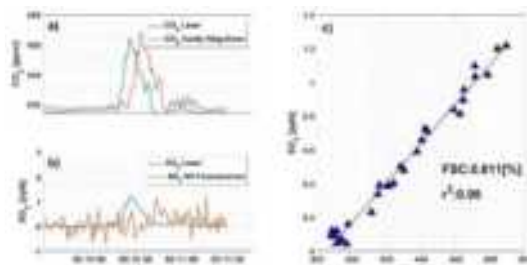


Figure 1. CO₂ and SO₂ measurements for a passing vessel by four different instruments in a Sulphur Emission Controlled Area. a) CO₂: Laser and cavity ring-down instruments. b) SO₂: Laser and UV-fluorescence. c) FSC estimation with the Laser system.

In the frame of the EU project SCIPPER: Shipping Contributions to Inland Pollution Push for the Enforcement of Regulations (www.scipper-project.eu/), a novel gas sniffer technique based on laser spectroscopy was introduced. Several FSC measurement campaigns, using this technique, were carried out at different locations, including the English Channel (Figure 2), the Port of Marseille (France), the Elbe River (Germany), PeberHolm (Sweden-Denmark) and the port of Gothenburg.

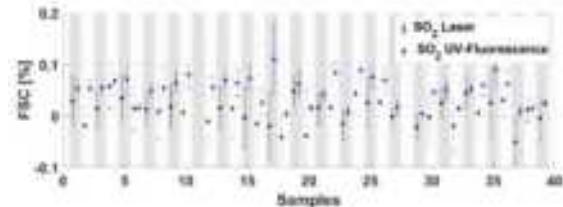


Figure 2. Individual ships FSC measurements at the English Channel (May-2022) by two different systems: UV-Fluorescence with Cavity Ring-Down and the Laser System.

From field results and experiments, the performance and limitations of this system against other widely used methods for FSC monitoring will be presented and discussed in this study. Overall, an enhanced signal-to noise-ratio has been observed along the different measurement scenarios, including two different FSC limits of 0.1% and 0.5% respectively.

The SCIPPER project has received funding from the European Union's Horizon 2020 research and innovation program under the grant agreement Nr.814893.

Beecken, J., Mellqvist, J., Salo, K., Ekholm, J., and Jalkanen, J.-P.: *Airborne emission measurements of SO₂, NO_x and particles from individual ships using sniffer technique*, Atmos. Meas. Tech., 7, 1957–1968, 2014.

Mellqvist, J., Beecken, J., Conde, V., and Ekholm, J.: *Surveillance of Sulphur Emissions from Ships in Danish Waters*, <https://doi.org/10.17196/DEPA.001>, 2017.

Measurement of NO_x and ultrafine particles from inland shipping in Germany

P. Eger¹, T. Mathes¹, A. Zavarsky¹ and L. Duester¹

¹Federal Institute of Hydrology, Qualitative Hydrology, Koblenz, Germany
Presenting author email: eger@bafg.de

Inland shipping is a potential contributor to air pollution in cities along European rivers and canals, on which a large number of goods is transported. These waterways often run through densely populated areas, where the quantification of ship emissions is of major interest but the separation from other sources like road transport remains a difficult task. Literature studies often focus on sea-going ships in coastal and harbour areas, from which the findings cannot easily be transferred to inland vessels due to differences in ship dimensions, operating conditions and fuel composition (especially the sulfur content). With regard to inland vessels, there is a critical lack of representative measurements under real-world driving conditions. We show that this gap can be closed by the continuous monitoring of nitrogen oxides (NO_x = NO + NO₂), particulate matter (PM), particle number concentration (PNC), ultrafine particles (UFP) and black carbon (BC) along waterways with high traffic density. From the observations the additional contribution of inland vessels to local background concentrations can be calculated and specific emission factors can be derived for the use in emission inventories and transport models.



Figure 1. Measurement setup at (a) Rhine and (b) canal.

We present data from two long-term field studies at the river Rhine in Worms (see Fig. 1a) and at the Dortmund-Ems canal (Fig. 1b) in Germany, conducted as part of the RAUCH project. CO₂, NO, NO₂, BC and PM₁ as well as particle number and size distribution from 5 nm to 10 μm were measured with high temporal resolution (1–3 s) for more than one year. A typical time series observed at the canal is presented in Fig. 2, with distinct spikes visible in all measured parameters when ships passed the station. Emission plumes were generally characterised by a large NO-to-NO₂ ratio of about 10 and the dominance of UFP with observed geometric mean particle diameters varying from 20 to 100 nm.

Combining a peak analysis algorithm with automatic identification system (AIS) and technical ship data, the additional burden from individual ships was calculated for each analyte. From this, monthly average contributions for each location were derived, resulting in an NO₂ increase of approximately 5–10 % due to inland vessels close to the shipping lanes at Rhine and canal. A

similar contribution was observed for UFP and BC. Given their adverse health effects, this underlines the importance of considering them in ship-related studies and integrating them into existing air pollution monitoring networks.

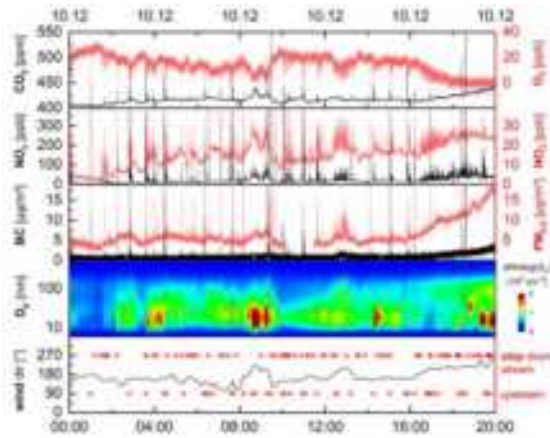


Figure 2. Typical time series derived for the Rhine.

Average emission factors relative to the amount of fuel used were determined for both locations (Table 1), revealing a large ship-to-ship variability. The influence of different ship parameters, operating conditions and engine characteristics was examined, with the latter turning out to have the largest effect on NO_x and particle emissions. These results stress the need to overcome limitations in data accessibility (engine-specific data is currently not sent via AIS) to improve the quantification of the contribution from inland shipping in emission inventories and modeling studies.

Table 1. Comparison of calculated emission factors (EF).

EF (g kg ⁻¹)	Rhine	Canal
NO _x	37 ± 16	46 ± 22
NO ₂	2.6 ± 1.1	4.1 ± 2.0
BC	0.5 ± 0.3	0.9 ± 0.7
PM ₁	1.7 ± 1.1	1.9 ± 1.5

The comparison of emission factors under real-world driving conditions with existing emission regulation limits by the EU revealed the potential to monitor the effect of fleet modernization measures like exhaust gas aftertreatment and diesel particulate filters.

A single instrument for simultaneous monitoring of greenhouse gases and air pollutants

Jonas Bruckhuisen¹, Marco Brunner¹, Oleg Aseev¹, Morten Hundt¹

¹MIRO Analytical AG, Widenholzstrasse 1, CH-8304 Wallisellen, Switzerland

Keywords: GHG monitoring, multi-compound gas analyzer, air quality monitoring
Presenting author email: morten.hundt@miro-analytical.com

Air pollution and greenhouse gas emissions are two closely linked problems. They can be attributed to a variety of sources, where transportation is always a main contributor. Monitoring several different air pollutants and GHG simultaneously with high selectivity and sensitivity helps to gain critical insights on the different sources as different sources contain specific ratios of certain gases providing characteristic emission fingerprints. Additionally, plume-measurements to observe compliance of shipping companies with legislation regarding e.g. the fuel-sulfur content need multi-species measurements including CO₂, NO, NO₂, SO₂ and NH₃.

Solutions to monitor these air pollutants or GHG with high precision and temporal resolution were commonly offered as “one-species-one-instrument”, leading to large, immobile measurement setups with high energy consumption. We provide a new compact laser absorption spectrometer that combines several mid-IR lasers. Our solution allows simultaneous high-precision measurements of the greenhouse gases CO₂, N₂O, H₂O and CH₄, and the pollutants CO, NO, NO₂, O₃, SO₂ and NH₃ within a single instrument and is therefore well suited to detect the relations of the co-emitted pollutants and GHGs.

In our contribution, we will demonstrate examples of our instruments’ applications for mobile monitoring of 10 GHGs and air pollutants in urban areas and airborne measurements with airships (Tillmann, 2022; Schuldt, 2023). Furthermore, we will present the results of parallel monitoring with our instrument and standard conventional gas analysers used for GHG and air pollutant measurements. It demonstrates the ability of our instrument to serve as an all-in-one solution and to replace up to 7 standard gas analysers opening a wide range of new mobile multi-compound gas monitoring applications, for example, in airplanes, ships or cars.

References:

Tillmann, R., Gkatzelis, G. I., Rohrer, F., Winter, B., Wesolek, C., Schuldt, T., Lange, A. C., Franke, P., Friese, E., Decker, M., Wegener, R., Hundt, M., Aseev, O., and Kiendler-Scharr, A. (2022): *Air quality observations onboard commercial and targeted Zeppelin flights in Germany – a platform for high-resolution trace-gas and aerosol measurements within the planetary boundary layer*, Atmos. Meas. Tech., 15, 3827–3842, <https://doi.org/10.5194/amt-15-3827-2022>.

Schuldt, T., Gkatzelis, G. I., Wesolek, C., Rohrer, F., Winter, B., Kuhlbusch, T. A. J., Kiendler-Scharr, A., and Tillmann, R. (2023): *Electrochemical sensors on board a Zeppelin NT: in-flight evaluation of low-cost trace gas measurements*, Atmos. Meas. Tech., 16, 373–386, <https://doi.org/10.5194/amt-16-373-2023>.

Monetary return on scrubber installations at the expense of environmental damage

A. Lunde Hermansson¹, I.-M. Hassellöv¹, J.-P. Jalkanen², J. Hassellöv¹ and E. Ytreberg¹

¹Department of Mechanics and Maritime Sciences, Chalmers University of Technology, Gothenburg, SE-41296

²Finnish Meteorological Institute, Erik Palmenin aukio 1, 00101 Helsinki, Finland

Keywords: scrubbers, impact assessment, payback time, external costs.

Presenting author email: anna.lunde.hermansson@chalmers.se

Since the introduction of stricter regulations of sulphur content in marine fuels, more ships use exhaust gas cleaning systems (EGCS), often called scrubbers, as an alternative compliant method. In 2022, approximately 25% of the global marine bunker fuel demand was represented by heavy fuel oils (HFO) which can only be used on ships equipped with scrubbers. When the scrubber removes sulphur oxides (SO_x) from the exhaust, other contaminants such as metals and polycyclic aromatic hydrocarbons (PAHs) are also scavenged by the scrubber water and discharged to the marine environment. There is an increasing concern regarding the contaminant loads from the scrubber fleet, and studies show that large quantities of metals (e.g. vanadium, chromium and nickel) and PAHs (e.g. anthracene and fluoranthene) are being discharged directly to the marine environment.



Figure 1. Assessment of Good Environmental Status in European waters aggregated over all descriptors.

The necessity of guidelines for scrubbers was acknowledged already at the forty-first session of the MEPC meeting in 1998. Since then, many States have commissioned research and literature reviews of the potential impact of scrubbers and stricter regulations and control are expected to be implemented. During the 78th Marine Environment Protection Committee (MEPC) meeting, new guidelines on how to assess risk and impact from scrubber water discharge were approved.

The impact assessment is described in section 7 of the guidelines where paragraph 7.4 stipulates criteria that, if fulfilled, motivates the adoption of restrictions or a ban on discharge of scrubber water. For example, if the environmental objectives in the area of concern are not met (e.g. Good Environmental Status (GES) according to the Marine Strategy Framework Directive (MSFD)), this could motivate stricter regulations or ban on scrubber

water. From an EU perspective, most water bodies already fail to achieve GES (Figure 1) which motivate stricter regulations on scrubber-use within European waters.

During the latest MEPC meeting (MEPC 79), questions were raised regarding the use of scrubbers as appropriate means of compliance (i.e., *Equivalents*) and while several delegations expressed their support to restrict the use of scrubbers, other delegations raised their concern regarding the *(economic) uncertainty for the industry, which has in good faith invested in EGCS technology in accordance with the provisions of MARPOL Annex VI*.

The overall aim of this study was therefore to investigate all aspects of the discussion on the restriction of scrubbers by performing an impact assessment according to the MEPC guidelines (paragraph 7.4) and to evaluate the costs, both in terms of payback time for the ship owner and in terms of damage costs on the marine environment.

To accomplish this, results from EU Member States' 2018 reporting on the extent to which they have achieved GES were collected from WISE-Marine (Water Information System for Europe). All descriptors were assessed but extra focus was directed towards Descriptor 8, *Concentration of contaminants*. The payback period of scrubber investments was calculated for all vessels known to be equipped with scrubbers from 2014 to 2022. The calculations were based on installation date, scrubber type and fuel consumption collected from the Ship Traffic Emission Assessment Model (STEAM) and high-resolution data covering fluctuations in fuel price of HFO, MGO and VLSFO was provided by Ship & Bunker. As a Baltic Sea case study, the monetary gain of the scrubber fleet, by not having to switch to more expensive fuels (MGO and VLSFO), was then compared to the damage costs for the marine environment, resulting from scrubber emissions of PAHs and metals.

The results show that most ship owners have already gotten return on their scrubber investments and that the comparative damage cost can be substantial. This study will thus provide important input to the discussion on restricting the use of scrubbers and prohibiting the discharge of scrubber water.

The project has received funding from the Swedish Agency for Marine and Water management [grant agreement No 2911-22], The Swedish Transport Administration, [grant agreement TRV 2021/12071] and by the European Union's Horizon 2020 research and innovation programme Evaluation, control and Mitigation of the EnviRonmental impacts of shippinG Emissions (EMERGE) [grant agreement No 874990].

VOC emissions from Ships

K.Salo¹, J. Mellqvist² and A. V. Conde²

¹Department of Mechanics and Maritime Sciences, Chalmers University of Technology, Gothenburg, 412 96, Sweden

²Department of Space, Earth and Environment, Chalmers University of Technology, Gothenburg, 412 96, Sweden

Keywords: shipping, hydrocarbons, VOC, UV-fluorescence, cross-sensitivity.
Presenting author kent.salo@chalmers.se

Introduction

Research studies using advanced instrumentation show that ships emit significant amounts of organic compounds and that these can dominate the total particle emissions in the exhaust (Zhang et al. 2020). The particulate emissions are presently not being removed by abatement technology and there is little discussion about their adverse impact on environment and health. This contrasts with the land-based sector in which all new diesel vehicles are obliged to utilize abatement technology which removes a considerable portion of these particles. Some studies propose that these particles mainly consist of volatile material originating from lubrication oil, and it is very difficult to measure these with simple instrumentation (Eichler et al. 2017). In this project several techniques to measure and quantify these emissions have been investigated, including a new unique way of combining two types of UV fluorescence measurements. Results are presented from studies in a test engine and on a passenger ferry that was running different fuels, including methanol.

Methods

Three type of measurement techniques were compared, i.e. FTIR and a temperature controlled multireflection cell measuring a wide range of hydrocarbons, UV-fluorescence measuring SO₂ and a Flame Ionization Detector (FID) measuring the Total Hydrocarbons (THC).

Two fluorescence systems designed for SO₂ monitoring have been used in parallel, one using a hydrocarbon denuder and one without. The latter one is cross-sensitive to VOCs and hence the difference between the two systems could, with appropriate calibration, be used for cost effective quantification of volatile hydrocarbons.

Results

Several different VOC were identified with the FTIR, including methane, higher alkanes, alkenes and aldehydes. These data are presently being compared with the fluorescence system and the FID. In figure 1 is shown an example FTIR spectrum of exhaust gases sampled from the exhaust gas channel of the passenger ferry running on methanol showing a clear signal of formaldehyde.



Fig.1 Formaldehyde spectrum measured in the exhaust funnel when using methanol as a fuel on passenger ferry.

It was also clearly seen that the difference in signal from the two UV-fluorescence instruments were dependent on the concentrations of hydrocarbons in the exhaust gas. Implying that it is possible to use the cross-sensitivity for hydrocarbons as, at least, an indicator of hydrocarbon during exhaust characterisation. In figure 2 a comparison is shown between the signal from the FID and the tandem fluorescence system during different engine loads is displayed.

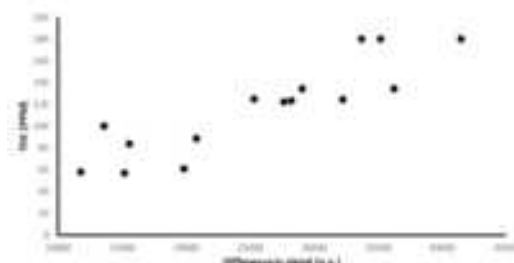


Fig 2. THC measured with FID signal compared with the difference in signals from the tandem fluorescence system.

This work was funded by the Chalmers Area of Advance Transport and measurements on board the passenger ferry was carried out as part of the EU Horizon 2020 SCIPPER-project.

References

- Eichler, P et al. (2017) Environ. Sci. Technol. Lett. 2017, 4, 2, 54–58
Zhang, Y., et al. (2020) Atmos. Chem. Phys., 20, 1887–1900.

The actor perspective on reaching a low emitting shipping sector

E. Malmgren¹, S. Brynolf² and L. Styknes¹

¹Department of Mechanics and Maritime Sciences, Chalmers University of Technology, Gothenburg, 412 96, Sweden

²IVL Swedish Environmental Research Institute, Gothenburg, 411 33, Sweden

Keywords: emission reduction, alternative fuel, future fuels, shipping.

Presenting author email: elin.malmgren@chalmers.se

The transitioning of the shipping sector to low-emission fuels is currently slow and the uptake of alternative fuel is low. To meet the international goal set by the International Maritime Organization to reduce the climate impact from shipping by 50% by 2050 the transition must accelerate fast. Barriers hindering the sector from moving to fossil-free fuels, such as cost and technical feasibility, is discussed in the literature today, but there is a lack of studies that involve perspectives of the actors and how they interact and collaborate to reduce ship emissions. This study aims at clarifying the criteria considered when actors make and influence the choice of shipping fuel. This is done by looking at barriers and the driving forces for the usage of alternative fuels.

The primary data sources were 17 semi-structured interviews held with key representatives of companies within the shipping industry (see Table 1). Five different actor types were interviewed: Cargo owners, freight forwarders, shipping companies, charter brokers and ports. The interviews focused on actors' view of the transition towards a sustainable shipping sector, what activities and measures are currently taking place to counter environmental issues of shipping, and what is needed for alternative fuels to be utilized to a higher degree.

Table 1. Summary of types of actors interviewed and number of interviews.

Actor types	Number of interviews
Cargo owner	4
Forwarder	3
Shipping companies	5
Charter brokers	3
Ports	2

The main countermasures to reduce emissions brought up by the interviewees were i) increase energy efficiency ii) onshore power supply, and iii) alternative fuels. Shifting goods from road to sea was also mentioned by many respondents as a measure to reduce transport emissions, but this is not directly related to transitioning the shipping sector.

Cargo owners raised the complex relationship between different stakeholders as one of the main barriers when procuring sea transport. Charter brokers and some forwarders also highlighted this as one of their main functions – guiding buyers in the decision making. However, sustainability performance was primarily brought up by shipping companies and cargo owners in procurement rather than presented by forwarders. The

decision makers and influential actors in the fuel choice for a voyage, as viewed by the interviewees, is depicted in Figure 1.



Figure 1. Key interactions between actors.

The barriers brought up differed between actors and within the actor types. The main perceived barriers found were:

1. Increased cost
2. Investment risks
 - a. Uncertain future legislation
 - b. Uncertain future fuel supply
3. Lack of interest in environmental performance
 - a. From other actors
 - i. Different time frames when making decisions
 - ii. Communication issues
 - b. Internally
4. Lack of decision support due to missing environmental data

Cases when alternative fuels were used have been identified. The cases were primarily of four types: governmental procurements, long-term fleet investments driven by the shipping company, green corridors, and direct collaborations between cargo owners and shipping companies. The main highlighted driving forces differed greatly between actors, with shipping companies raising the longevity of the fleet, the willingness-to-pay of the cargo owner, and secured fuel supply as some of the main aspects. The cargo owners primarily raised set environmental targets for the company or product as the main driver to mitigate emissions from sea transport. There was a clear difference between liner and spot shipping, with customer having a far less perceived influence on the fuel choice in liner shipping when the cargo space onboard is divided between a great number of customers. All interviewees highlighted well-developed legislative requirement as an effective tool to drive change.

This work was supported by the Swedish Energy Agency.

Transporting CO₂ streams by ships: another threat for the marine environment?

O. Bokareva¹, G. Argüello²

¹ Faculty of Law, Lund University, Lund, 223 62, Sweden

² Department of Law, Gothenburg University, Gothenburg, 405 30, Sweden

Keywords: CO₂ transport, ships, dumping, policy, legal and regulatory issues

Presenting author email: gabriela.arguello@law.gu.se

The ocean is progressively transforming into the last frontier to pursue ambitious climate objectives. While climate action is often presented positively, it does not always lead to win-win scenarios. In fact, climate action can often cause social, environmental, and economic conflicts (Bogojević 2023). A case in point is carbon capture and storage (CCS). Over the years, CCS has been recognized as an integral part of the portfolio of measures to mitigate climate change (IPCC, 2022). At European Union (EU) level, CCS has a crucial role in climate policy, especially in decreasing CO₂ emissions of energy-intensive industries (European Commission, 2021). Yet, important questions remain unanswered, including the liability for discharges in the marine environment occurring during the transportation of CO₂ by ships and for long-term stewardship of sub-seabed storing sites.

It must be noted that the transport of captured CO₂ presents an important element in the whole chain and links the capture places with the storage sites. The new projects in Europe and worldwide indicate that ship transportation can become a viable solution to transport CO₂ over longer distances and when pipeline transport is unavailable or not feasible (Mittler 2023, Weber 2021).

Notably, this type of transportation is relatively new and suitable ships need to be built to transport the CO₂ in a safe and sustainable manner subject to the International Maritime Dangerous Goods Code (IMDG Code) and the International Gas Carrier Code (IGC Code). Several projects are underway and the new ships will be ready for service by 2024 (Northern Lights, 2022). Thus, it is evident that such emerging technologies require an adequate legal framework in light of the current legal regime or adoption of new suitable legislation at international, EU or national levels.

Against this background, the authors assess the barriers that CO₂ transportation by ships faces and the available mechanisms to govern the environmental risks of this transportation. Considering that ship transport of CO₂ will most likely have transboundary implications, we investigate existing legal limitations and risks related to the export of CO₂ streams for disposal.

Particularly relevant is the 2009 amendment of Article 6 of the 1996 London Protocol to the 1972 London Convention on dumping, which allows the export of carbon dioxide streams for disposal. Despite the efforts to facilitate the deployment of CCS, the amendment is yet to

enter into force. As an interim solution, in 2019, the Conference of the Parties (COP) to the London Protocol decided to allow “for the provisional application of the 2009 amendment (COP to the London Protocol 2019).” Based on this decision, several contracting parties are planning to enter into arrangements to facilitate the export of CO₂ in accordance with Article 6 of the London Protocol. Sweden, for example, intends to negotiate such an agreement with Norway, the United Kingdom and the Netherlands (Swedish Energy Agency 2022). This paper discusses whether this provisional application is a viable legal alternative in light of the Vienna Convention on the Law of Treaties. Furthermore, the authors analyze the operational liabilities that may occur in CCS operations from an international and EU law perspective considering for example, the Carriage of Hazardous and Noxious by Sea Convention (HNS Convention), its 2010 Protocol and Directive 2009/31/EC (CCS Directive).

References:

- Bogojević, S. (2023). Legal Dilemmas of Climate Action. *Journal of Environmental Law* 35, 1-9. <https://doi.org/https://doi.org/10.1093/jel/eqad007>
- Council Directive 2009/31/EC of 23 April 2009 on the geological storage of CO₂ [2009] OJ L140/114 (CCS Directive)
- COP to the London Protocol. (2019). Resolution LP.5(14) on the provisional application of the 2009 amendment to Article 6 of the London Protocol.
- European Commission. (2021). *Sustainable Carbon Cycles* (Communication from the Commission to the European Parliament and the Council Issue).
- IPCC. (2022). Summary for Policymakers. In H.-O. Pörtner, D. C. Roberts, E. S. Poloczanska, K. Mintenbeck, M. Tignor, A. Alegria, M. Craig, S. Langsdorf, S. Löschke, V. Möller, A. Okem, & B. Rama (Eds.), *Climate Change 2022: Impacts, Adaptation and Vulnerability. Contribution of Working Group II to the Sixth Assessment Report of the Intergovernmental Panel on Climate Change* (pp. 3-330). Cambridge University Press. <https://doi.org/doi:10.1017/9781009325844.001>
- Northern Lights. (2022). Northern Lights awards ship management contract to “K LINE.”
- Mittler, Cea. "The Carbon Voyage – Emissions Liability in Transporting Sea for CCS." *NUS Centre for Maritime Law Working Paper* 5 (2023): 1-33. <https://ssrn.com/abstract=4492441> or <http://dx.doi.org/10.2139/ssrn.4492441>.
- Swedish Energy Agency. (2022). *National Centre for CCS*. <https://www.energimyndigheten.se/en/sustainability/carbon-capture-and-storage/national-centre-for-ccs/>
- Weber, V. (2021). Are we ready for the ship transport of CO₂ for CCS? Crude solutions from international and European law. *RECIEL, Review of European, Comparative & International Environmental Law*(30), 387-395. <https://doi.org/10.1111/reciel.12399>

High-resolution air quality mapping via massive mobile monitoring and land use random forest models

Tie Zheng¹, Shaojun Zhang^{1,2}, Yifan Wen¹, Ye Wu^{1,2}, Sheng Xiang¹

¹ School of Environment, Tsinghua University, Beijing, 100084, China

² Beijing Laboratory of Environmental Frontier Technologies, Beijing 100084, China

Keywords: Traffic-related air pollutants, Big data, Machine learning, Land use regression

Presenting author email: tiezhengsitu@gmail.com

Introducion. High-resolution air quality maps can provide important implications in the management and assessment of air pollutants. Now, the hyperlocal scale (< 100 m) and high-quality air quality maps were often obtained by massive mobile monitoring with fast response instruments (Apte et al., 2017). However, this method is costly and requires a large investment of manpower and time, thus, being difficult to scale larger areas. The costly measurement also limited the wider application of this method and the present studies were mainly conducted in developed and resourceful regions. This is a pioneer study in China that performed massive mobile monitoring using fast response instruments, producing hyperlocal air quality maps at 100 m. Over 4.6 million 1-s data of multiple traffic-related air pollutants were collected on major roadways in Shen Zhen in 2020~2021. Land use random forest (LURF) models were used to predict pollutant concentrations at locations without measurements. Then, the air quality of the full coverage road network in the interested area was revealed. This study provides important information on air quality maps in China and could address some of the major challenges in producing high-resolution air quality maps worldwide.

Method and Results. The measured air pollutants include particle number and mass concentration (PN and PM), black carbon (BC), etc. All involved roads were discretized into 100-m road segments. Then, data were cleaned and snapped to the nearest road segment. The data-snapping technology is similar to that of Messier et al., (2018) which we used “median of drive day median” as the core metric. The road segments with less than 5 visiting days were discarded in the analysis. In total, 227 land use variables were extracted in ArcGISPro 3.0, including the area of different land use types, road type and length, mean elevation, population, vegetation index, GDP, etc. Then, five-fold cross validation was used to assess the performance of the LURF model.

Fig. 1 shows the data-only map of PN_{0.001-1}. Fig. 2 shows the results of model cross validation. Fig. 3 shows the predicted PN concentration at 100 m resolution in the interested area. Overall, the developed machine learning model can well predict the PN concentration at locations without measurements ($R^2 = 0.801$) and the full coverage of road network PN concentration is presented (Fig. 3). The PN concentration is a lot higher on the highways and in the southwest part of the area, offering important implications for better management of air quality in the city. With the LURF model, the experimental investment could be greatly reduced to produce high-resolution air quality maps, making it easier to scale larger areas.



Figure 1. Data-only map of PN_{0.001-1} at 100 m resolution. The dashed line shows the selected area for PN prediction.

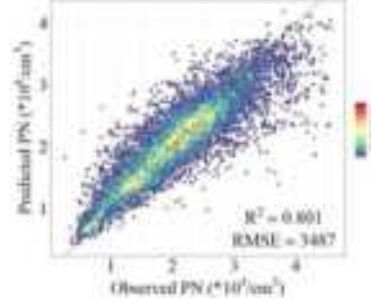


Figure 2. Cross validation results of the LURF model.



Figure 3. PN predictions at 100 m resolution.

Apte et al., (2017). High-resolution air pollution mapping with Google Street View cars: exploiting big data. *EST*, 51(12), 6999-7008.

Messier et al., (2018). Mapping air pollution with Google Street View cars: Efficient approaches with mobile monitoring and land use regression. *EST*, 52(21), 12563-12572.

Is post-exposure feeding inhibition of *Artemia sp.* and *Mytilus galloprovincialis* impaired by exposure to scrubber-waters?

A. Ré¹, A.T. Rocha², A. Monteiro¹, M. Granberg³ and N. Abrantes²

¹Department of Environment and Planning & Centre for Environmental and Marine Studies (CESAM), University of Aveiro, 3810-193 Aveiro, Portugal.

²Department of Biology & Centre for Environmental and Marine Studies (CESAM), University of Aveiro, 3810-193 Aveiro, Portugal.

³IVL Swedish Environmental Research Institute, Kristineberg Marine Research Station, Kristineberg 566, 45178 Fiskebäckskil, Sweden.

Keywords: Scrubber-water, post-exposure feeding inhibition, Saltwater ecosystems, Invertebrates
Presenting author email: njabrantes@ua.pt

In response to the sulphur regulation rules approved and adopted by the International Maritime Organization, many shipping companies have invested in scrubber-water systems instead of using fuels with a lower sulphur percentage, transferring atmospheric pollutants (SO_x, NO_x and CO_x, PAHs, metals and particles) to the seawater. This decision was made without any risk assessment on scrubber-water effects in marine and coastal ecosystems. Within the research project EMERGE (EC-Horizon 2020), the present work aimed to assess the ecotoxicological effects of scrubber-waters on the feeding behaviour of two seawater organisms.

Post-exposure feeding inhibition bioassays were carried out with the filter crustacean, *Artemia sp.* and the mussel *Mytilus galloprovincialis*. Both species play important roles in marine ecosystems: *Artemia sp.* cysts and nauplii provide food to many marine organisms being crucial to the success of the fish, crustaceans and cephalopod mollusks larval development and the mussel as a very powerful filter feeder, tend to accumulate for long periods waterborne contaminants of multiple types, being also used as human food. The feeding behaviour has been considered as a good indicator of toxic effects in suspension-feeding macroinvertebrates because it can be systematically linked to ecosystem functions, representing an ecologically relevant response.

In this bioassay, three types of scrubber-water produced with Atlantic seawater were used: scrubber-water A (SWA) artificially produced, and Scrubber-water B and C (SWB, SWC) produced on board of two different ships. The scrubber-waters were tested at distinct concentrations: control; 0.001; 0.1; 1.0; and 10.0%. The three scrubber-waters were analysed, showing very low pH values and an enrichment of PAHs and alkylated-PAHs, as well as trace metals. *Artemia sp.* organisms showed low mortality when exposed to scrubber water dilutions below 50%. In the post-exposure feeding inhibition bioassay, artemia showed higher sensitivity to scrubber-water, with NOEC (No Observed Effects Concentration) values of 0.1% for SWA and 0.001% for SWB and SWC (Figure 1A). The mussel revealed a decrease in the amount of ingested algae with the increase of the percentage of scrubber-waters (Figure 2B). For the SWA and SWB the NOEC values were 0.1% and 1.0%

for the SWA and SWB respectively. For SWC, the NOEC was <0.001%, but the proportionality ratio between scrubber-water percentage and feeding rate was not verified, with an increase in feeding for 0.1 and 1.0% scrubber-water dilutions (Figure 1B). These responses seem to be related to the metals, PAHs and alkylated-PAHs concentrations of the scrubber-waters. The present results showed that scrubber-waters are highly toxic to the two tested species. Furthermore, the artemia and the mussel post-exposure feeding inhibition bioassay showed to be suitable to assess the risk of scrubber-waters on marine aquatic species.

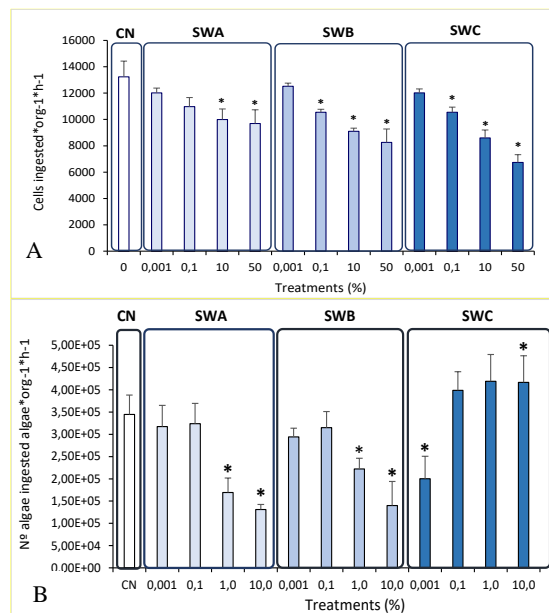


Figure 1 – Post-exposure feeding inhibition results, A–*Artemia sp.* and B–*Mytilus galloprovincialis* (CN – control, SW(ABC) – scrubber-waters).

This work was supported by the EMERGE project – “Evaluation, control and Mitigation of the Environmental impacts of shipping Emissions”, with a postdoctoral fellowship BPD/UI88/2741/2021.

Air quality assessment at the street level: sensitivity analysis of a road traffic-emissions-CTM model chain for the Paris region

Marjolaine Lannes^{1,2}, Yelva Roustan¹ and Nicolas Coulombel²

¹ CEREA, École des Ponts, EDF R&D, Marne-la-Vallée, France

² LVMT, École des Ponts, Université Gustave Eiffel, Marne-la-Vallée, France

Keywords: street-scale air quality, vehicle emissions, agent-based simulation, sensitivity analysis

Presenting author email: marjolaine.lannes@enpc.fr

Introduction

The Paris region is a densely populated metropolitan area that regularly experiences overrunning regulatory thresholds for nitrogen dioxide (NO₂) and particulate matter (PM_{2.5} and PM₁₀). In order to assess the effect of transport policies on air quality and exposure, integrated mobility – emissions – air quality modelling chains have been developed (Gurram, Stuart, and Pinjari 2019; Vallamsundar et al. 2016). However, little is known regarding the uncertainties associated with these modelling chains. This study thus aims (a) to develop a street-level modelling chain for air quality assessment based on an agent-based mobility model coupled with an emissions model and an air quality model, and (b) to perform a sensitivity analysis on the calculation of air pollutants concentrations. The developed modelling chain will also allow to evaluate air pollution exposure for the simulated population in future works.

Methodology

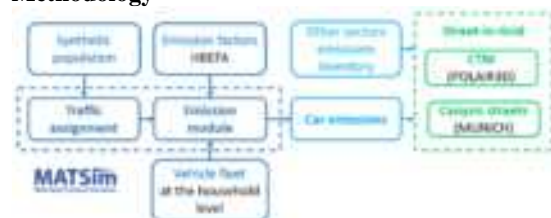


Figure 1. An integrated modelling framework for ambient air pollution modelling

We develop a mobility-emissions-air quality modelling chain. Mobility and road traffic are simulated using the travel demand agent-based model, MATSim. We then use the outputs of the dynamic traffic assignment to estimate private car emissions at the street level and vehicle level, considering its fuel type and Euro standard. We complete these emissions with emissions inventories for other sectors. Road traffic emissions are assigned to streets in which air quality is simulated with the MUNICH street-network model (Kim et al. 2022). The urban background concentrations are simulated with the Polair3D Eulerian chemical transport model (CTM).

In order to study the modelling chain sensitivity, we compare concentrations when using a disaggregate vehicle fleet versus an average vehicle in the emissions model. Another sensitivity test compares the use of the background CTM model alone (Polair3D) and the combined CTM and street air quality model.

Results

Regarding the disaggregated vehicle fleet model, comparing the performance of ten AI models, the number of cars per household was predicted with 76.6% accuracy, 58.7% for fuel type, and 28.2% for emission standards. This model provides inputs for the agent-based mobility model to compute traffic-related daily emission profiles based on a synthetic population and synthetic vehicle fleet. The considered street network is created using OpenStreetMap's road network. The emissions of passenger cars were then modelled based on HBEFA emission factors. The results showed that although petrol cars accounted for almost three-quarters of the car fleet, they were responsible for less than half of PM_{2.5} emissions. Finally, these emissions will be used as inputs for the air quality models.

Conclusions and perspectives

This sensitivity analysis will highlight the concentration uncertainty resulting from averaging vehicular emissions, along with the uncertainty related to the use of background pollution concentrations instead of pollution levels in the streets. By combining individual travel patterns and street-level pollution concentrations from this modelling framework, future research will focus on the assessment of personal exposure to air pollution for the region's population.

This work is supported by Paris Region in the framework of DIM Qi2.

Gurram, Sashikanth, Amy Lynette Stuart, and Abdul Rawoof Pinjari. 2019. ‘Agent-Based Modeling to Estimate Exposures to Urban Air Pollution from Transportation: Exposure Disparities and Impacts of High-Resolution Data’. *Computers, Environment and Urban Systems* 75: 22–34.

Kim, Youngseob et al. 2022. ‘MUNICH v2.0: A Street-Network Model Coupled with SSH-Aerosol (v1.2) for Multi-Pollutant Modelling’. *Geoscientific Model Development* 15(19): 7371–96.

Vallamsundar, Suriya et al. 2016. ‘A Comprehensive Modeling Framework for Transportation-Induced Population Exposure Assessment’. *Transportation Research Part D: Transport and Environment* 46: 94–113.

Environmental fate modelling of organic pollutants from land-based and shipping emissions in the Northern Adriatic Sea coastal areas

Calgaro L.¹, Giubilato E.¹, Aghito M.², Jalkanen J.P.³, Ferrarin C.⁴, Semenzin E.¹, and Marcomini A.¹

¹ Dept. of Environmental Sciences, Informatics and Statistics, University Ca' Foscari Venice, Via Torino 155, 30172 Mestre, Venice (Italy)

² Norwegian Meteorological Institute, Allégaten 70, 5007 Bergen, (Norway)

³ Finnish Meteorological Institute, Erik Palménin aukio 1, FI-00560 Helsinki, (Finland)

⁴ CNR-ISMAR, Arsenale Castello, 2737/F, 30122 Venice (Italy)

Keywords: water modelling, chemical fate, shipping emissions, exposure assessment

Presenting author email: loris.calgaro@unive.it

Coastal and marine ecosystems are threatened by diverse anthropogenic pollutants, both from land-based sources (e.g., industrial and agricultural activities) and direct discharges (e.g., shipping emissions). Recently, the adoption of the global limits on sulfur content for marine fuels increased the use of shipping emission abatement technologies like exhaust gas cleaning system (scrubbers) as an alternative to the use of cleaner but more expensive fuel types, whose acidic exhaust discharge water contain different chemical contaminants. Considering scrubber water and other shipping emissions to water, the presence of shipping lanes and ports may significantly contribute to the exposure of chemical pollutants in coastal areas, potentially increasing risks posed to aquatic ecosystems and human health.

In this context, fate and transport modelling offers an effective way to estimate the contribution of shipping emissions to the overall chemical exposure in coastal and marine waters.

In this work an exposure assessment for benzo(a)pyrene and fluoranthene accounting for both land-based sources and shipping emissions was carried out for the Northern Adriatic Sea. The modelling effort, realized within the H2020 “EMERGE” project, focused on the integration of high-resolution predictive models to help exploring the implications of different abatement emissions techniques in managing environmental risks under current and future scenarios.

In detail, shipping-related emissions of pollutants were simulated with the STEAM (Ship Traffic Emission Assessment Model) model (Maljutenko et al., 2021), based on Automatic Identification System data, while land-based emissions were quantified by combining daily river flow measurements with water concentrations from routinely monitoring of each tributary. The newly developed ChemicalDrift model, a chemical transport module included in the open-source Lagrangian framework OpenDrift, was applied for a baseline scenario using 2018 data. Forcing data for the case study area were obtained from the SHYFEM model (ocean currents, temperature, and salinity) (Ferrarin et al., 2019) and Copernicus Marine Services (mixed layer depth and winds).

Preliminary results showed that shipping emissions can contribute significantly to the exposure to

the selected contaminants, especially during the summer period when water flow from the tributaries reaches its minimum values and the number of cruise ships equipped with open-loop scrubbers increases.

This work has received funding from the European Union’s Horizon 2020 research and innovation program under Grant agreement No 874990 (EMERGE project).

Ferrarin C., Davolio, S., Bellafiore, D., Ghezzo, M., Maicu, F., Mc Kiver, W., Drofa, O., Umgiesser, G., et al. (2019) *J. Oper. Oceanogr.* 12, 86–103
Maljutenko, I., Hassellöv, I.M., Eriksson, M., Ytreberg, E., Yngsell, D., Johansson, L., Jalkanen, J.P., et al., (2021). *Mar. Pollut. Bull.*, 173, 112985.

Deposition quantification of gaseous emissions at the air-water interface during a single vessel travel

N. Rapkos and L. Ntziachristos

Department of Mechanical Engineering, Aristotle University, P.O. Box 458, 54124, Thessaloniki, Greece
Presenting author email: nikorapk@auth.gr

The objective of this study is to assess the quantification of gaseous pollutants that are emitted during a single vessel travel and deposited at the air-water interface. Gaseous emissions from ships are indirectly related to water quality degradation, as the dry and wet deposition of pollutants cause problems such as acidification and the deterioration of ecosystems (Doney et al., 2007, Grennfelt et al., 2020, Wu and Zhang, 2018).

The study utilizes AIS data for a small container ship that departs from the Piraeus port and is moving to Hellespont through the Aegean (Figure 1). Regarding the meteorological conditions, the wind is assumed as north with an intensity of 20 knots and considered constant for the total ship's travel. The gaseous pollutants that were studied are sulphur dioxide (SO_2) and nitrogen oxides (NO_x).

The results of this study demonstrate the quantity that is deposited at the air-water interface during the total ship's travel. The quantification considers, as a first step, the ship's load factor estimation from the AIS data. Next, the load factor results are applied to the emission factor formulas that were introduced by Grigoriadis et. al (2021) for the emission rate calculation of SO_2 and NO_x . The deposited SO_2 and NO_x quantity is being predicted by the in-house quantification model of gaseous pollutants at the air-water interface which utilizes the emission rate data for the ship's total travel.



Figure 1: Location points of the container ship during its travel in Aegean. The ship departs from the Piraeus port and attends Hellespont. Map source: Bing

Acknowledgements

The work has been supported by EU HORIZON 2020 Project EMERGE (Grant agreement ID: 874990). AIS data was provided by 'exactEarth Europe LTD'.

References

Doney, S. C., Mahowald, N., Lima, I., Feely, R. A., Mackenzie, F. T., Lamarque, J.-F., & Rasch, P. J. (2007). Impact of anthropogenic atmospheric nitrogen and sulfur deposition on ocean acidification and the inorganic carbon system. www.pnas.org/cgi/doi/10.1073/pnas.0702218104

Grennfelt, P., Engleryd, A., Forsius, M., Hov, Ø., Rodhe, H., & Cowling, E. (2020). Acid rain and air pollution: 50 years of progress in environmental science and policy. In Ambio (Vol. 49, Issue 4, pp. 849–864). Springer. <https://doi.org/10.1007/s13280-019-01244-4>

Grigoriadis, A., Mamarikas, S., Ioannidis, I., Majamäki, E., Jalkanen, J.-P., & Ntziachristos, L. (2021). Development of exhaust emission factors for vessels: A review and meta-analysis of available data. Atmospheric Environment: X, 12, 100142. <https://doi.org/10.1016/j.aeaoa.2021.100142>

Wu, W., & Zhang, Y. (2018). Effects of particulate matter ($\text{PM}_{2.5}$) and associated acidity on ecosystem functioning: response of leaf litter breakdown. Environmental Science and Pollution Research, 25(30), 30720–30727. <https://doi.org/10.1007/s11356-018-2922-1>

Variation in responses of microalgae, *Nitzchia* sp. exposed to grey water from ships.

G. B. M. Rathnamali¹, J.T. Mujingni², J. Egardt³, I. Dahllöf³, I.-M. Hassellöv², E. Ytreberg², and K. Salo²

¹Department of Marine Sciences, Gothenburg University, 405 30 Gothenburg, Sweden

²Department of Mechanics and Maritime Sciences, Chalmers University of Technology, 412 96 Gothenburg, Sweden

³Department of Biological & Environmental Sciences Gothenburg University, 405 30 Gothenburg, Sweden

Keywords: grey water, toxicity, *Nitzchia* sp
Presenting author email: rathnamali.mekhala@gmail.com

Grey water originates from three primary sources onboard a ship, the accommodation area (showers, bath, and sinks), the galley (kitchen) area, and laundry practices. Thus, greywater contains different groups of pollutants such as bacteria, organic matter, metals, nutrients, pharmaceuticals, and microplastics (Ytreberg et al. 2020). The average greywater generation from a ship differs from 130 L per person·day⁻¹ (Furstenberg et al. 2009 cited in Holmberg, 2021) to 160 L per person·day⁻¹ (Vicente-Cera et al. 2019a). But cruise ships (254 L per person·day⁻¹) account for the highest greywater generation (EPA842-R-07-005, 2008) while oil and gas tanker ships represent the lowest greywater generation, 105 L per person·day⁻¹ (Ytreberg et al., 2020). Counting the high generation loads and pollutants in greywater, there is an increased interest in assessments of the environmental impact of grey water from ships. Respectively, greywater is hypothesized to have ecotoxicological effects. Yet, there is a complete lack of toxicity studies on ship-generated grey water.

In this study, the marine diatom *Nitzchia* sp. will be measured for its growth as the response parameter and monitored with chlorophyll a fluorescence, and optical density. The unicellular algae, *Nitzchia* genus has been used extensively in ecotoxicological evaluations. Additionally, their ability to grow in milliliter volumes in test wells within short test durations makes them ideal test organisms for toxicity evaluations.

The *Nitzchia* sp culture for the study was obtained from the algae bank at the University of Gothenburg (Algbank - GUMACC | Department of Marine Sciences, University of Gothenburg). An onboard sampling of grey water was carried out on ships operating in the Baltic Sea during spring 2023. In total, 3 ferries, 3 cruise ships, and one coast guard ship were sampled. 10 L glass bottles rinsed with 70% ethanol and milli-q water were used for initial onboard sampling on the ships, and after mixing thoroughly, the subsamples were transferred to a set of bottles suited for the respective analysis of different pollutant groups, including nutrients, metals,

pharmaceuticals, phthalates, and microplastics. One liter, precleaned bottles, were used to collect grey water samples for use in the toxicity tests.

For the toxicity tests, each grey water sample was prepared as follows: 10 mL volume of greywater was diluted with 10 mL of 20 psu (Practical Salinity Units) solution to test a 10psu, 50% diluted grey water from the different ships. Equal volumes of *Nitzchia* sp. culture and the nutrition media were added to each solution. Four replicates of each solution and positive control with the same physicochemical conditions except the grey water were arranged into five 48-well cell culture plates. The plates were run in a plate reader to record chlorophyll a fluorescence and optical density at specific time intervals of the algal growth phase.

The software Statistical Package for the Social Sciences (SPSS 28.0) was used for the data analysis. The correlation of selected contaminant concentrations in the 7 samples and the growth rate of *Nitzchia* sp. in each sample will be discussed to evaluate the variations in toxicity between the different greywater samples.

This study will conclude the toxicity of ship-generated greywater according to the presence of different pollutants and their levels. Moreover, it will provide a comparison between different ships and their strategy for handling grey water.

Acknowledgment: This study is part of the “Gråvatten I Östersjön” project, Ref. nr. TSA 2022-170, funded by the Swedish transportation agency.

Furstenberg S., Mohn H., Sverud T., 2009. Study on discharge factors for legal operational discharges to sea from vessels in Norwegian waters, DNV report NO. 2009-0284, Hovik, Norway.

Holmberg, J. (2021). (rep.). Study of grey water samples from cargo and passenger ships and an assessment of the impacts of wastewater on the marine environment (Ser. ISSN 2670-2185).

<https://dec.alaska.gov>

Vicente-Cera, I., Moreno-Andrés, J., Amaya-Vías, D., Biel-Maeso, M., Pintado-Herrera, M., & Lara, Martín, P.

Holistic environmental impact assessment from shipping: A decision support tool for stakeholder engagement

W. Winiwarter^{1,2} and S. Guéret¹

¹International Institute for Applied Systems Analysis (IIASA), 2361 Laxenburg, Austria

²Institute of Environmental Engineering, University of Zielona Góra, 65-417 Zielona Góra, Poland

Keywords: Shipping emissions, Environmental Impact assessment, Scrubbers, Decision Support Tool

Presenting author email: winiwarter@iiasa.ac.at

The shipping industry is a major cause of environmental harm, affecting both atmosphere and hydrosphere, and climate. The implementation of the Global Sulphur Cap in January 2020 focusses on removal of Sulphur Dioxide only, while the release of other compounds discharged into the air or sea and their environmental effects remains untouched. Environmental impact assessments are essential tools to evaluate the effects of operational shipping compared to other sources of pollution and to fill regulatory gaps. (Moldanová *et al.*, 2022). Port authorities, policy makers, and other stakeholders, however, require more readily accessible tools to develop science-based decisions to uphold environmental quality relevant for their specific situation.

Here we present a decision support tool allowing stakeholders to evaluate the future impacts of scrubbers and other scenarios of future shipping to very different environmental aspects, which allows identification of co-benefits or trade-offs connected to measures imposed on shipping. The tool translates scientific insights into results useful for decision makers in practice and is being codesigned between scientists and stakeholders.

We use established impact assessment methodology in combination with newly developed features for the marine system to evaluate impacts leaning on the categories established as the U.N. Sustainable Development Goals:

1. Human Health (SDG3): using Years of Life Lost and ozone related health damage as parameters, impacts are taken from the GAINS model (Amann *et al.*, 2011)
2. Life on land (SDG 15): ecosystem impacts of acidification and eutrophication are quantified via a critical loads approach, and photochemically caused damage is parameterized as phytotoxic ozone dose (POD), again from GAINS
3. Life below sea (SDG 14): differentiating between pelagic and benthic marine ecosystems, we take advantage of a newly developed impact assessment scheme presented by Guéret *et al* (this conference). In this scheme, critical loads of heavy metals and persistent organic pollutants – specifically, Polycyclic Aromatic Hydrocarbons (PAHs) – as well as the calcite saturation state characterize ecosystem impacts.

We use results from the ship emission model STEAM (Jalkanen *et al.*, 2021), the atmospheric model SILAM (Sofiev *et al.*, 2015), and the ocean model

Chemical Drift (Aghito *et al.*, 2022) to quantify ship emissions and their discharges to air and water, respectively. Scenarios are taken from Fridell *et al.* (EMERGE D1/4) and reflect a general understanding of possible future shipping developments over Europe in 2030 and 2050.

The decision support tool allows users to understand the impact of different shipping scenarios to the respective local environment of any given grid cell (representing 20x20 km grids) in the European seas and adjacent shorelines. Adjustment of the scenarios allows to account for local conditions, to mimic change in ship movements as well as local restrictions regarding the release of certain compounds to air and sea and their respective altered impacts to the environmental endpoints.

This work was supported by EU H2020 project EMERGE, which has received funding from the European Union's Horizon 2020 research and innovation programme under grant agreement no. 874990 (EMERGE project).

Aghito, M., Calgaro, L., Dagestad, K.-F., Ferrarin, C., Marcomini, A., Breivik, Ø., and Hole, L. R. (2022) ChemicalDrift 1.0: an open-source Lagrangian chemical fate and transport model for organic aquatic pollutants. *Geosci. Model Dev. Discuss* [preprint].

Amann, M., Bertok, I., Borken-Kleefeld, J., Cofala, J., Heyes, C., Höglund-Isaksson, L., Klimont, Z., Nguyen, B., Posch, M., Rafaj, P., Sandler, R., Schöpp, W., Wagner, F., Winiwarter, W. (2011). Cost-effective control of air quality and greenhouse gases in Europe: modeling and policy applications. *Environmental Modelling and Software* **26**, 1489-1501.

Jalkanen, J., Johansson, L., Wilewska-Bien, M., Granhag, L., Ytreberg, E., Eriksson, K., Yngsell, D., Hassellöv, I., Magnusson, K., Raudsepp, U., Maljutenko, I., Styhre, L., Winnes, H., Moldanova, J. (2020). Modelling of discharges from Baltic Sea shipping. *Ocean Science* **17**, 699-728.

Moldanová, J., Hassellöv, IM., Matthias, V. et al. (2022) Framework for the environmental impact assessment of operational shipping. *Ambio* **51**, 754–769.

Sofiev, M., Vira, J., Kouznetsov, R., Prank, M., Soares, J., Genikhovich, E. (2015). Construction of the SILAM Eulerian atmospheric dispersion model based on the advection algorithm of Michael Galperin. *Geoscientific Model Development* **8**, 3497-3522.

CFD dispersion modelling for the reproduction of real shipping emission conditions in a port area

C. Boikos¹, L. Ntziachristos^{1,*}, S. Oppo², A. Armengaud²

¹ Mechanical Engineering Department, Aristotle University of Thessaloniki, GR 54124, Thessaloniki, Greece

² AtmoSud, Air Quality Observatory in the Provence-Alpes-Côte d'Azur region, FR 13006, Marseille, France

Keywords: RANS-CFD, air quality modelling, port, shipping emissions.

Presenting author email: mpoikosc@auth.gr

This research work studies the impact of shipping emissions on the air quality of a port area using a CFD model for the dispersion of pollutants.

Transport sector, including shipping, is one of the major contributors regarding emissions of hazardous pollutants such as nitrogen oxides (NO_x), carbon monoxide (CO), and particulate matter (PM_{10}) (EEA, 2022). Recently, scientific community (Karl et al., 2019; Matthias et al., 2010) has been trying to quantify shipping emissions in coastal areas. In addition, the International Maritime Organization (IMO) has established new set of regulations to mitigate air pollution of shipping emission in the aforementioned areas.

Air quality models are often used to estimate concentration of pollutants in urban areas originated from various emission sources. These models can be classified in regional scale, local scale, and microscale ones, depending on their temporal and spatial resolution. Regional and local scale models are widely used for air quality studies. However, for city scale studies, microscale models can provide the spatial distribution of pollutant concentrations in higher resolution compared to local and regional scale ones.

For the purposes of this work, a Computational Fluid Dynamics (CFD) software was used for the modelling of plume dispersion. Port of Marseille was selected as case study, including detailed geometric representation of ships, their exhaust stacks as well as of the buildings in the surrounding area. No chemical reactions were included, meaning that pollutants were treated as inert gases. Pollutants concentration was quantified and depicted on a high-resolution grid (~3m) within urban canopy, providing detailed information about spatial distribution of pollutants, level of exposure on them, and possible hotspots in the city where pollutants can be trapped. Compared with in-port observations, predicted concentrations presented 33.9% average absolute deviation, which is considered within the acceptable range.

The main objective of this study is to provide a more holistic view of shipping emissions impact on the air pollution of port areas, giving useful information about plume evolution on them. A model like this can constitute an advisory tool for port authorities and policy makers, targeting to reduce the imprint of shipping emissions in urban environments.

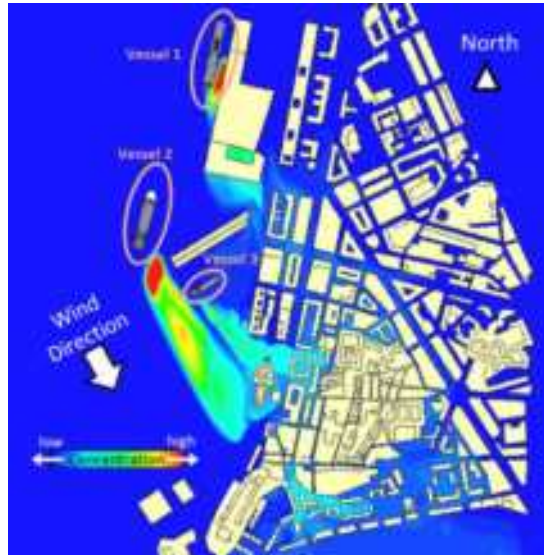


Figure 1. Concentration field of a test case with three vessels in the port of Marseille, predicted with CFD model.

The research work was supported by the Hellenic Foundation for Research and Innovation (HFRI) under the 3rd Call for HFRI PhD Fellowships (Fellowship Number: 6316).

European Environmental Agency. (2022). *Air quality in Europe 2022*.

International Maritime Organization. (2016). Marpol Annex VI, Sulphur Oxides (SO_x) and Particulate Matter (PM) – regulation 14. *Resolution MEPC, 280 (70)*.

Karl, M., Bieser, J., Geyer, B., Matthias, V., Jalkanen, J. P., Johansson, L., & Fridell, E. (2019). Impact of a nitrogen emission control area (NECA) on the future air quality and nitrogen deposition to seawater in the Baltic Sea region. *Atmospheric Chemistry and Physics, 19*(3), 1721–1752.
<https://doi.org/10.5194/acp-19-1721-2019>

Matthias, V., Bewersdorff, I., Aulinger, A., & Quante, M. (2010). The contribution of ship emissions to air pollution in the North Sea regions. *Environmental Pollution, 158*(6), 2241–2250.
<https://doi.org/10.1016/j.envpol.2010.02.013>

Cumulative effects of commercial anchoring on the Pacific coast of Canada: ecological and socio-economic effects

L.C. Hannah¹, F.T. Francis¹, K. Douglas², E. Rubidge¹, T. Norgard¹, S. Dudas¹, K. Berry¹, S. Agbayani¹, C. Robb¹, R. Enkin², S. Verrin¹, D. Havens¹, and C.C. Murray¹

¹Institute of Ocean Sciences, Fisheries and Oceans Canada, Sidney, British Columbia, V8L 5T5, Canada

²Geological Survey of Canada Pacific, Natural Resources Canada, Sidney, British Columbia, V8L 4B2, Canada

Keywords: anchorages, anchoring, pathways of effects, multiple stressors, cumulative effects

Presenting author email: lucie.hannah@dfo-mpo.gc.ca

Commercial anchorages on Canada's Pacific coast are located near the major Ports of Vancouver and Prince Rupert, and many are also in areas of natural beauty and within sight of local communities. Recent increases in anchorage use in these areas has heightened First Nations and local community concerns about potential ecological and socio-economic effects (Clear Seas, 2021) (Fig 1.). Few studies have examined the ecological effects of commercial anchoring together, and to our knowledge, none have considered socio-economic effects.



Figure 1. Artistic depiction of anchorage effects on environment and coastal communities.

To examine the cumulative effects of commercial anchoring, we developed an anchoring-specific Pathways of Effects (PoE) conceptual model that included both ecological and socio-economic components. To establish the structure of the PoE, we divided anchoring into three sub-activities: 1) discharges and emissions, 2) vessel movement and presence, and 3) anchor movement and presence, and identified the stressors associated with each.

Using this structure, we next identified the effects and endpoints for the ecological and socio-economic components of the model. For the ecological components, we built upon previous work (Hannah et al 2020) that used literature review and expert elicitation to identify potential effects of stressors to marine organism and habitat endpoints. For the socio-economic component, we identified the effects and endpoints through the examination of official information submitted by Indigenous First Nations, coastal communities and special interest groups concerned about increases in commercial anchoring. These included documents relating to development projects (e.g., submissions in relation to proposed shipping terminal expansion and a pipeline expansion), as well as from local concern groups, and

from submissions to Transport Canada from community members. Anchorage-related concerns were linked to the relevant stressor, effect and endpoint to create pathway linkages for the socio-economic component. PoE conceptual models are notoriously hard to represent visually given the numerous and complex linkages. To facilitate understanding and clarity we developed a new method to visually represent this information that is intuitive to understand and can be used for both ecological and socio-economic components (Fig 2).

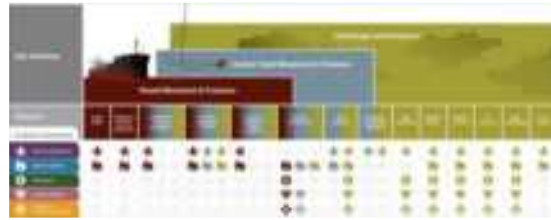


Figure 2. Pathways of Effects conceptual model visualisation showing an overview of effects of commercial anchoring on endpoint categories

The visualisations of the diverse effects of commercial anchoring, combined with the database of supporting evidence for linkages, provides a way to understand the cumulative effects of commercial anchoring from different perspectives, as well as providing the structure and knowledge required for future assessments.

Individual linkage chains identified in this work can help inform decision-makers, as each can be used as a potential management lever to help to mitigate or manage effects of commercial anchoring on the environment and local communities.

This work was supported by a CSRF grant from Fisheries and Oceans Canada.

Clear Seas (2021). Anchors Away: Understanding the issues about ships at anchor. Date modified: 2022-02-22. <https://clearseas.org/en/blog/anchors-away-understanding-the-issues-about-ships-at-anchor/>

Hannah, L., Thornborough, K., Murray, C., et. al. (2020) Pathways of Effects Conceptual Models for Marine Commercial Shipping in Canada:

The impact of maritime activities on air quality in three European ports

M. Karl¹, M.O.P. Ramacher¹, R. Badeke¹, A. Aulinger¹

¹Department of Chemistry Transport Modelling, Institute of Coastal Environmental Chemistry, Helmholtz-Zentrum Hereon, Geesthacht, 21502, Germany

Keywords: shipping emissions, port cities, urban-scale air quality, EPISODE-CityChem.

Presenting author email: martin.ramacher@hereon.de

Ships are significant sources of air pollution, particularly in port cities and coastal areas. Emissions from ships include particulate matter, nitrogen oxides, and sulphur oxides, which can have negative impacts on human health and the environment. Accurate modelling of these emissions, their transport and transformation can help policymakers and regulators to develop effective strategies to reduce pollution and to protect public health. Additionally, modelling can also be used to evaluate the effectiveness of existing policies and regulations, and to identify areas where further action is needed.

Consequently, in the EU Horizon 2020 project SCIPPER (Shipping Contributions to Inland Pollution Push for the Enforcement of Regulations) the impact of shipping emissions on air quality in the Mediterranean Sea and the North and Baltic Sea regions was investigated and compared. In this abstract, we present results that describe the air quality in three European port-cities: Hamburg (Germany), Kiel (Germany), and Marseille (France). The objective is to evaluate the local impacts of the emissions in order to estimate an average contribution of the port on the city's air quality.

For all city-scale simulations in this study, the urban-scale Chemistry Transport Model EPISODE-CityChem (Karl et al., 2019; Ramacher et al., 2019) was applied in a coupled setup with regional-scale simulations using the Community Multiscale Air Quality Modelling System (CMAQ). EPISODE-CityChem used the time-varying 3-D concentration field from CMAQ at the lateral and vertical boundaries as initial and boundary conditions.

In EPISODE-CityChem, emission sources are defined as gridded area sources, linear sources and point sources. The emission inventories for the local shipping around Hamburg, Kiel and Marseille and in its ports consist of hourly emissions from ships on 250m × 250m grid resolution calculated with STEAM-3 (Johansson et al. 2017) provided by the Finnish Meteorological Institute (FMI). The STEAM-3 emissions are processed as input for EPISODE-CityChem, which calculates the vertical distribution of ship emissions individually at every x-y position of the surface grid and generates individual exponential Gauss distributions (Badeke et al., 2022) in dependence of the current wind speed and stability.

Road traffic emissions from CAMS-REG-AP v5.1 gridded emission inventory for BAU (business as usual) in year 2020 were combined with lockdown correction factors for 2020 (Matthias et al. 2021) and downscaled to line sources for city-wide road traffic emissions applying the UrbEm framework (Ramacher et al., 2021).

The modelled simulations were all compared with measurements (SCIPPER field campaigns and data from local air quality networks) and the contribution of ships was assessed using the zero-out method.

Our study shows a strong impact of maritime activities along the ship trajectories to and from the ports, in port areas, and even in the city centre. Indeed, ship manoeuvres in port areas but also their stay at the quay are connected with gaseous and particulate emissions, which affect the air quality in the port cities.

Table 1. Modelled shipping impact

City	Modelled shipping impact		
	NO ₂ [µg/m ³]	SO ₂ [µg/m ³]	PM _{2.5} [µg/m ³]
Hamburg	10 (51%)	0.8 (14%)	0.6 (6%)
Kiel	5 (73%)	0.2 (33%)	0.15 (2%)
Marseille	5 (31%)	0.9 (34%)	0.4 (3%)

The highest concentrations of PM_{2.5} and NO₂ due to shipping activities were simulated in Hamburg, which is the 3rd most important port in Europe in terms of freight transport and the port is close to the city centre. In general, the simulated NO₂ and PM_{2.5} concentrations in each port are correlated with the importance of the port. However, for SO₂, the highest concentrations were modelled in the harbour of Marseille because it is a Mediterranean port, which is not in a sulphur emission control area (SECA), unlike other Northern European ports. Depending on the activities of the city, the contribution of the port to the degradation of the air quality varies. In Kiel, for example, ships impact NO₂ concentrations by up to 73% in summer while in Marseille the impact is at most 31% (Table 1).

This project has received funding from the European Union's Horizon 2020 research and innovation program under grant agreement Nr.814893.

- Badeke, R., Matthias, V., Karl, M., and Grawe, D. (2022) *Geosci. Model Dev.* **15**, 4077–4103.
Johansson, L., Jalkanen, J.-P., Kukkonen, J. (2017) *Atmospheric Environment* **167**, 403–1415.
Karl, M., Walker, S.-E., Solberg, S. and Ramacher M.O.P. (2019) *Geosci. Model Dev.* **12**, 3357–3399.
Matthias, V., Quante, M., Arndt, J.A., Badeke, R., Fink, L., Petrik, R., Feldner, J., Schwarzkopf, D., Link, E.-M., Ramacher, M.O.P., and Wedemann, R. (2021) *Atmos. Chem. Phys.* **21**, 13931–13971.
Ramacher, M.O.P., Karl, M., Bieser, J., Jalkanen, J.-P., and Johansson, L. (2019) *Atmos. Chem. Phys.* **19** 9153–9179.
Ramacher, M.O.P., Kakouri, A., Speyer, O., Feldner, J., Karl, M., Timmermans, R., Denier van der Gon, H., Kuenen, J., Gerasopoulos, E., and Athanasopoulou, E. (2021) *Atmosphere* **12**, 1404.

Assessing the impact of environmental policy instruments for ships in Europe with a modelling tool

R. Parsmo^{1,2}, J. Hansson^{1,2}, E. Ytreberg², E. Fridell^{1,2}, and S. Brynolf²

¹IVL Swedish Environmental Research Institute, Box 530 21, 400 14 Gothenburg, Sweden

²Department of Mechanics and Maritime Sciences, Chalmers University of Technology, Gothenburg, Sweden

Keywords: Environmental policy instruments, Cost of abatement, Abatement measures

Presenting author email: rasmus.parsmo@ivl.se

There are several policies in place, or being considered, to address environmental issues related to shipping at different levels:

1. Global policies include market-based incentives such as a proposed CO₂ levy, and regulations like the MARPOL (SECA and NECA) and AFS Conventions.
2. Regional policies include the inclusion of shipping in EU-ETS, and the proposed Fuel EU Maritime initiative.
3. National policies include the NOX fund and public procurement in Norway, as well as port- and fairway discounts adopted in Sweden.

The total number of environmental policies being introduced or proposed is increasing, which makes it essential to systematically assess their impact on both the environment and the shipping industry. In this study, we propose and test a model (Figure 1) for evaluating the impact on seven different environmental policy instruments linked to shipping in Europe based on MRV data. Our model intends to assess policies from both the social planner and shipping industry perspectives by comparing their respective costs and benefits. The social planner perspective compares the damage cost (i.e., the cost pollution) with all other costs and benefits to society, while the industry perspective focuses on whether the policy is effective in encouraging change by considering only the costs and benefits relevant to the industry's decision-making.

The model uses various types of input data related to: 1) individual ships (red) such as fuel consumption, engine size, and distance/time to the sea, 2) emission factors to air and water (yellow), and 3) the costs of abatement measures (blue). The model also includes scenario analysis (purple) to examine possible future outcomes. The results produced by the model depend on the policy (green) or measure (grey) being assessed. Some policies are of command-and-control type, and the industry must comply (such as requirements for reduced NO_x emissions or a ban on scrubbers), while in other cases, the industry can choose not to implement measures (such as economic incentives like the EU ETS, where it is possible to buy emission allowances). The results can include potential absolute emission reductions, costs per emission, or absolute costs, depending on the policy instrument or abatement strategy's that is assessed.

For example, Figure 2 illustrates the annual abatement cost per ship if all ships in the EU were forced to use electro-methanol in 2030. In this case, the annual abatement costs have been applied to the theoretical

European fleet in 2030, with each bar representing an individual ship. The scenario presented in Figure 2 can be analyzed in several ways for different purposes. For example, a decision-maker may want to determine whether the introduction of the EU ETS would prompt ships to install and use electro-methanol in 2030. If Figure 2 presents costs from the industry perspective, the result suggests that the CO₂ price would need to be at least €350/tonneCO₂ for any ship to be willing to invest in methanol propulsion, or approximately €500/tonnesCO₂ to achieve a total emission reduction from shipping from this measure of 80 Mtonnes CO₂. The current EU ETS price of around €90/tonnesCO₂ and expected future levels indicate the need for additional policies. In addition, potential emissions reductions of NO_x or SO_x can be assessed in a similar way with the model.

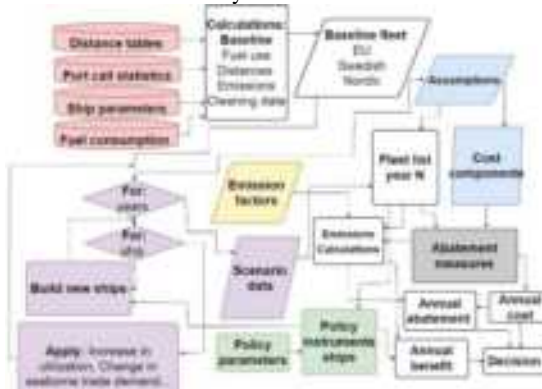


Figure 1. Proposed model for assessing policy instruments for shipping.

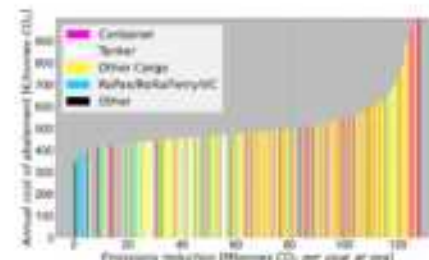


Figure 2. Example results: Comparing abatement cost of introducing electro-methanol with total annual abatement calculated the European ship fleet (2030).

This work was supported by the Swedish Transport Administration and the Swedish Foundation for Strategic Research (SSF)

LNG feeder vessel environmental pressures, partially decoupled from transport demand

I.-M. Hassellöv¹ and A. Hörteborn^{1,2}

¹ Dept of Mechanics and Maritime Sciences, Chalmers University of Technology, SE-412 96 Gothenburg, Sweden

² RISE Research Institutes of Sweden, SE-412 96 Gothenburg, Sweden

Keywords: LNG, gas, energy system, shipping, marine environment, environmental assessment.

Presenting author email: idamaja@chalmers.se

Liquified Natural Gas (LNG), is proposed to play a role in the transition to sustainable shipping. LNG can reduce emissions of sulphur and nitrogen oxides, and particulate matter. However, LNG is a fossil fuel and will thereby contribute to global climate change. The ongoing discussion on the methane slip from ships operating on LNG is further challenging the assumptions of LNG as a sustainable solution (Grönholm et al. 2022). In addition, LNG vessels give rise to other types of environmental pressures, such as leakage of biocides from antifouling paint, sewage, grey water and bilge water. Environmental assessments or life cycle assessment of LNG vessels should encompass all the different types of operational emissions and discharges. Finally, spending time at sea, implies an increased navigational risk and resulting maritime accidents, which should also be included in such analysis.

Another aspect to consider in the environmental assessment of shipping is the goods that are transported (Liu et al. 2019). Here we show that LNG feeder vessels may spend as much as 25% of their time at sea just running the ship burning Boil Off Gas (BOG), to ensure the pressure in the tanks are not exceeded. This behaviour is not directly attributed to the shipment of gas from one port or ship, to another (Figure 1), which means, the economic incentives are currently allowing for roughly one third's increase of the ships' operational emissions and discharges and increased navigational risks.

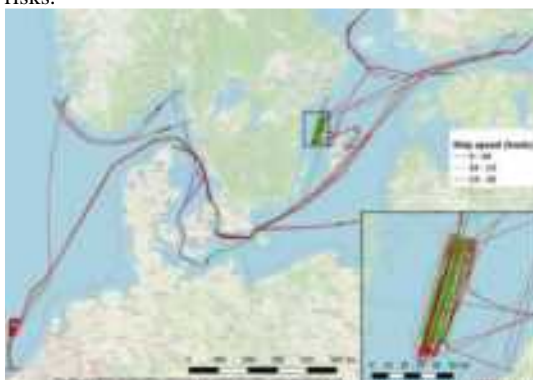


Figure 1. Sailing paths of the LNG feeder between June 1st 2022 and Aug 31st 2022. The ship's speed over ground is illustrated with three different colours. The inset shows a zoomed in view of the sailing path of the LNG feeder in the area between the Swedish Island Gotland and Swedish coast during the same period which corresponds to 130 hours spent on burning BOG.

This behaviour can be put in the context of IMO GHG reduction strategy, to reduce the total annual GHG emissions from international shipping by at least 50 percent by 2050. Analogously, in the light of national and international work (e.g., the EU marine strategy framework directive, (2008/56/EC)), avoiding BOG at sea should be a low hanging fruit to reduce loads of hazardous substances and nutrients on the marine environment. Most coastal areas are heavily affected by anthropogenic activities and e.g., in the Baltic Sea shipping is recognized as a significant source of metals and PAHs (Ytreberg et al 2022).

Even if the LNG feeder vessels are currently few, this study highlights the importance to distinguish the economic and technological drivers of vessels activity patterns. During the fall 2022, LNG tanker vessels were reported to spend time at sea awaiting higher prices on the gas market. Identifying the vessel activity decoupled from transport demand, and including it in e.g. life cycle assessment, is the first step towards policy action. The possibility to reduce the environmental impact of vessels by up to 32% should be an attractive opportunity for future policy measures and investigation of technological solutions of the problem.

This work was supported by the Hugo Hammar Foundation (Grant no. HHS-297 and ML 112). The authors acknowledge the maintainers of the open-source GIS platform, QGIS.

Grönholm, T., Mäkelä, T., Hatakka, J., Jalkanen, J.-P., Kuula, J., Laurila, T., Laakso, L., & Kukkonen, J. (2021). *ES&T*, 55(20), 13677-13686.

Liu, H., Meng, Z.-H., Lv, Z.-F., Wang, X.-T., Deng, F.-Y., Liu, Y., Zhang, Y.-N., Shi, M.-S., Zhang, Q., & He, K.-B. (2019). *Nature Sustainability*, 2(11), 1027-1033.

Ytreberg, E., Hansson, K., Hermansson, A. L., Parsmo, R., Lagerström, M., Jalkanen, J.-P., & Hassellöv, I.-M. (2022). *Mar Poll Bull*, 182, 113904.

The Poseidon Principles: Designing and implementing a regulatory framework to create ecosystem sustainability

I.-M. Hassellöv¹, L. Huemer², and C. Martinson²

¹ Dept of Mechanics and Maritime Sciences, Chalmers University of Technology, SE-412 96 Gothenburg, Sweden.

² Dept of Strategy and Entrepreneurship, BI Norwegian Business School, N-0442 Oslo, Norway.

³ Dept of Law, School of Business, Economics and Law, University of Gothenburg, SE-405 30, Gothenburg, Sweden.

Keywords: Poseidon Principles, ship emissions, shipping regulatory framework, decarbonization
Presenting author email: [ida-maja@chalmers.se](mailto:idamaja@chalmers.se)

The demand for regulation of international shipping has since long been high for many different reasons, equal treatment in competition being one of them. Climate sustainability has taken this demand to a higher level. Regulation of international shipping is however difficult because of the relative lack of regulatory power. Regulations are primarily made through consensus decisions within the International Maritime Organization, implying rather slow processes. The strive for global regulatory frameworks as base for sustainable development of the shipping industry is complemented by voluntary initiatives. For example, the Clean Shipping Index promotes sustainable technologies onboard ships through reduced fairway dues, yet the economic incentives of these instruments are rather limited compared to the shipping companies' finances.

The initiative Poseidon Principles, launched in 2019, advances the idea of industry sectorial responsibility and enables stronger economic incentives by "integrating climate considerations into lending decisions to promote international shipping's decarbonization" (Poseidon Principles, 2022). The Poseidon Principles are a framework for assessing and disclosing the climate alignment of ship finance portfolios. They create common global baselines that are consistent with and supportive of society's goals to better enable financial institutions to align their portfolios with responsible climatic impacts. Today 30 financial institutions are Signatories to the Poseidon Principles, and together they represent a bank loan portfolio covering over 70% of the global ship finance portfolio. With the combination of stakeholders from different branches, and the possibilities to involve also other bodies with regulatory interests, the Poseidon Principles show an interesting regulatory model where different kinds of analyses can indicate the potential.

This multidisciplinary study combines insights from cooperative strategy, maritime and transport law, and maritime environmental science. Based on a mixed methods design, we study the potential impact of the Poseidon Principles on sustainable value creation in the shipping industry. We demonstrate that regulatory frameworks represent resource bundles that extend (i) the resource-based view's firm level focus on competitive advantage; (ii) the relational view's emphasis on interorganizational competitive advantage, which, if based on rare and inimitable relationship, can lead to supranormal profits, and; (iii) recent research on resource

bundles which maintain the conventional focus on rareness and imitability. A well-designed regulatory framework does not create a firm level competitive advantage as stressed by the resource-based view, or an interorganizational competitive advantage based on relational rents which result in supranormal profits if relationships are rare and inimitable. Regulatory frameworks provide ecosystem sustainability (primarily the economic ecosystem, but in this study extended to include natural marine ecosystem) when they provide match with other resources in the ecosystem, and when they increase the value of those resources. The conventional emphasis on rareness and inimitability are counterproductive with respect to ecosystem sustainability and what we label the creation of a planetary advantage.

Today the Poseidon Principles are focused on decarbonization, but we foresee possible development towards integration of other types of environmental impacts of shipping. In some areas, typically estuarine or semi-enclosed environments with intensive shipping, like the Baltic Sea, shipping is a significant contributor to pollution of hazardous substances, e.g. close to 40% of the copper load and 8-9% of individual organic pollutants, to the Baltic Sea (Ytreberg et al. 2022). Integrating other pressures than CO₂ emissions, stimulating internalization of the associated external costs, could realise the transformative ambition and assumed potential of the Poseidon Principles.

This work was supported by University of Gothenburg and Chalmers University of Technology's Area of Advance Transport.

Poseidon Principles. (2022). A global framework for responsible ship finance. Version 4.1. 61pp.

Ytreberg, E., Hansson, K., Hermansson, A. L., Parsmo, R., Lagerström, M., Jalkanen, J.-P., & Hassellöv, I.-M. (2022) *Mar Poll Bull*, 182, 113904.

ShipTRASE, Global shipping: Linking policy and economics to biogeochemical cycling and air-sea interaction

A. Rutgersson¹, C. Marandino², D. Booge², S. Hajjaji³, R. Kumar¹, N. Matz-Luck³, L. Recuero-Virto⁴, K Salo⁵, M. Sebe⁴, and F. Yao⁴

¹Department of Earth Sciences, Uppsala University, Uppsala, 752 32, Sweden

²GEOMAR Helmholtz Centre for Ocean Research Kiel, 24105, Germany

³The Walther Schücking Institute for International Law, University of Kiel, Kiel, 24118 Germany

⁴Polytechnic School of Paris, and European Institute for Marine Studies, France

⁵Chalmers University of Technology, Göteborg, Sweden

Keywords: scenarios, green shipping, scrubbers

Presenting author email: anna.rutgersson@met.uu.se

The shipping sector is presently going through a transitional phase with enhanced focus on green shipping, this includes implementation of control areas (ECAs) to reduce the shipping emissions of Nitrogen oxides, Sulphur oxides and Particulate matter, as well as targets for reduction of greenhouse gas (GHG) emissions. Switching to Liquefied Natural Gas (LNG) or installing exhaust gas cleaning systems (as scrubbers) have previously been identified as the most suitable solutions for shipping companies. However, some concerns have arisen for the use of those technologies. Open-loop scrubbers release chemicals in seawater, and LNG releases unburned methane (so-called "*methane slip*").

There is a need for a holistic evaluation of new fuels and cleaning technologies. This includes understanding of climate and environmental impacts, economic implications, regulatory requirements and technical possibilities. Within the ShipTRASE project we evaluate short- and long-term possibilities for cleaning technologies and alternative fuels from a multidisciplinary perspective.

Short-term perspective

Regulations have led to increased use of low-sulphur fuels, but also allows abatement technologies such as scrubbers, which require a separate legal framework. In 2022, guidelines for risk and impact assessments of the discharge water from scrubbers was adopted. Although the guidelines have been stepwise improved, they are still only recommendatory in nature (Shi et al., 2023).

Since January 1, 2020, only 0.50% fuel oil sulphur content for non-emission control areas (ECAs) and 0.1% for ECAs and their corresponding SO₂/CO₂ are relevant. Although the scrubber's air emissions are consistent with the limits set in the guidelines, there is a major uncertainty regarding national regulations on the scrubbers' wash water (discharge) in the sea.

Results from incubation experiments show that the addition of scrubber effluent impacts the production of climate relevant biogenic trace gases (i.e. dimethyl sulfide and isoprene). The trace gas concentration is indirectly influenced as the toxicity of the scrubber effluent influences the growth of phytoplankton communities. Constituents of scrubber effluent directly react with dissolved trace gases leading to a significant decrease in the ocean concentration and therefore dampen the air-sea gas exchange.

Long-term perspective

In a prospective approach to assess the development of shipping fuel for the Baltic Sea, we have defined scenarios considering legal (national and international regulations), environmental and economic aspects (investment costs and fuel prices) including multidisciplinary consultations with stakeholders. Figure 1 presents the share of fuel used in the Baltic Sea Region in 2050 in each scenario, and reveals the projected long-term decline of fossil fuels. The availability of alternative fuels is limited, consideration taken to LNG (concerns of methane slips), methanol (concerns with bunkering), hydrogen and ammonia. From the legal part, different scenarios will help to adopt the best legal and institutional model to achieve climate neutrality by 2050. The European Climate Law 2021 imposes a mandate to reach zero emission by 2050. However, it is not clear on what is the expected legal model that the EU, or its institutions, will employ to achieve that target regarding the shipping industry.

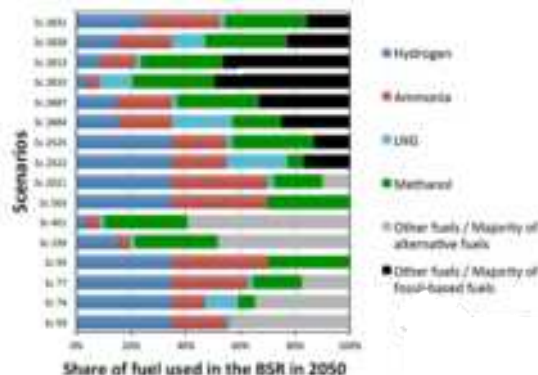


Figure 1. Share of fuel used in the Baltic Sea region in 2050 from Kumar et al. (2023).

This work was supported by the Belmont Forum with national funding agencies.

Kumar, R et al (2023). Assessment of Shipping fuel pathways in changing climates.

Shi, Z, S. et al. (2023). Perspectives from ship stacks: air pollutant emissions and their impacts on the surface ocean and lower atmosphere. Elementa

Identification and quantification of contaminant particles from scrubber water effluents in a high-intensity shipping area

A. Gondikas^{1,2}, M. Hassellöv³, S. Chen⁴, I-M. Hassellöv⁵

¹Creative nano, PC, Metamorfosi, 14451 Athens, Greece

²Department of Geology and Geoenvironment, National and Kapodistrian University of Athens, Panepistimiopolis Zografou, 15771 Athens, Greece

³Department of Marine Sciences, University of Gothenburg, BOX 461, SE-405 30 Gothenburg, Sweden

⁴State Environmental Protection Key Laboratory of Environmental Risk Assessment and Control on Chemical Process, School of Resources and Environmental Engineering, East China University of Science and Technology, Shanghai 200237, PR China

⁵Department of Mechanics and Maritime Science, Chalmers University of Technology, SE-412 96 Gothenburg, Sweden

Keywords: scrubber, washwater, particles, monitoring.

Presenting author email: a.gondikas@creativenano.gr

Shipping has been traditionally considered an environmentally friendly means of transportation of goods and people, a perspective that is challenged by scientific evidence on air quality impacts; as a result, the International Maritime Organization has put regulations in place to limit atmospheric pollution from shipping. Scrubbers are highly efficient in capturing sulphur species from ship exhaust gas and are currently the most popular sulphur abatement technology in large ships. In short, seawater is fed in the scrubber and brought in contact with the exhaust gas, allowing mass transfer of components from the gaseous into the water phase; the resulting washwater is returned to the sea with or without pre-treatment. In addition to sulphur, scrubbers are highly efficient in removing particulate matter from the exhaust gas, which is likely to contain hazardous elements, such as metallic and organic pollutants (Turner *et al* 2017) (Ytreberg *et al* 2022). It is therefore imperative to determine the fate and transport of particles from scrubber effluents into the marine environment. The determination of physical and chemical properties of these particles is a crucial step, prior to testing toxicological effects on marine organisms and applying models to predict their transport in the ocean. These properties may then be used in monitoring efforts to identify pollution from ships operating with scrubbers. In this study, we apply automated microscopy and spectroscopy methods to characterize particle populations in seawater from marine areas with high shipping intensity.

International ports attract large numbers of cargo and passenger ships and are susceptible to shipping pollution. We therefore collected samples across the shipping lanes off of Piraeus port, which is the 5th largest port of the EU in terms of volume of good transferred (TEU). In addition, narrow crossings form a natural barrier for shipping routes, forcing ships to pass through small water bodies, making them susceptible to shipping pollution. We collected samples from the Öresund strait, which is one of the busiest crossings in the northern hemisphere. Samples were filtered and analysed with automated methods of scanning electron microscopy with energy dispersive spectroscopy (SEM-EDS). The applied procedure allows

for the determination of physical characteristics, such as size and shape and chemical characteristics, such as partial elemental composition. The automated methods tackle all issues related to operator bias in electron microscopy and produce large datasets that are representative of the particle populations in the sample. The analytical procedure is limited to the pore size and material of membranes used. Seawater passing through the filter was analyzed with single-particle inductively coupled plasma mass spectroscopy (spICPMS) for a selection of elements. This procedure allows counting particles containing the target element, thus shedding some light on the smaller particle population and is limited by the instrument detection limits for each element and the acquisition of partial composition data.

Due to the large number of particulate matter from natural and non-scrubber anthropogenic activities, combinations of properties of particle populations is necessary. The challenge increases with decreasing particles size, due to the overwhelming number of non-scrubber particles. Our study demonstrates the applicability of analytical techniques and remaining challenges in the detection of particles from scrubber washwater in the marine environment and highlights properties of particles that may be used for source allocation in monitoring efforts.

This work has received funding from the European Union's Horizon 2020 research and innovation program under grant agreement No 874,990 (EMERGE project). This work reflects only the authors' view and CINEA is not responsible for any use that may be made of the information it contains.

Turner, D. R., Hassellöv, I.-M., Ytreberg, E., and Rutgersson, A. (2017) *Elem Sci Anth*, 5: 45
Ytreberg, E., Hansson, K., Hermassnon, A. L., Parsmo R., Lagerström M., Jalkanen, J.-K. and Hassellöv, I.-M.. (2022) *Mar. Pollut. Bull.* vol. 182, 113904.

Optimization of Drone-based Sensor Sniffing System for Monitoring Fuel Sulphur Content in Ocean-going Vessel Based on Field Measurements in Hong Kong Waters

Shiyi Yang¹, Ghadikolaei, Meisam Ahmadi¹, Mengyuan Chu¹, Xiaoliang Qin¹, Zhi Ning¹

¹Division of Environment and Sustainability, The Hong Kong University of Science and Technology, Hong Kong

Keywords: Sulfur dioxide; Ocean going vessels; Fuel sulfur content; Unmanned aerial vehicle; microsensor sniffing system

Presenting author email: syangct@connect.ust.hk

Like most coastal cities with huge port activities, pollution from marine vessel emissions is one of the key contributors to the emission inventories in Hong Kong. The utilization of high fuel sulfur content (FSC) bunker oil makes ocean-going vessels (OGVs) as the primary anthropogenic source of sulfur dioxide (SO_2) emissions. To regulate SO_2 emissions from marine transportation, the Hong Kong government implemented regulations in 2019 that required OGVs operating in Hong Kong waters to adhere to an FSC limit of no more than 0.5% (HKEPD, 2018).

Nevertheless, the need for an efficient tool for obtaining emission data from moving OGVs remains a major obstacle in enforcing air regulation policies for most emission control regions. Traditionally the fuel samples are collected from the bunker inside an OGV to measure its FSC. Though portable emission measurement systems (PEMs) have been developed and installed near the plume of a source to gather pollutant data under the actual operating conditions of OGVs, it can only be applied in individual vessel measurement and is not practical for regulating ship emissions on a large scale. In the last few years, microsensor technology integrated with unmanned aerial vehicles (UAV) have shown to exhibit potential ability in ship emission measurement, but there still lacks an optimum systematic operation protocol.

From our previous study (Anand et al, 2020), a UAV-based microsensor sniffing system (MSS) has been developed and evaluated for measuring OGVs plume SO_2 , NO_2 , NO , CO_2 , and CO in real time. In this study, we further applied the UAV-based MSS in the practical field in Hong Kong waters and around Kwai Tsing Container Terminals (Figure 1). During the study period, 12 successful field trips were conducted to achieve 100 valid OGV samples (out of 151 measured) from April 2022 to December 2022. Out of the total 100 valid samples, 18 were collected using land-based measurement methods, while 82 were collected using sea-based measurement methods. According to the carbon balance method, the FSC value can be calculated by the ratio of SO_2 and CO_2 concentration excess in the plume compared with the background value. Furthermore, the crest, regression and area methods were applied in FSC calculations to further optimize the protocol such as sharp peak and wide plume area, respectively. Further the performance of UAV-MSS is evaluated by comparing the Bunker Delivery Note (BDN) in this study.

Preliminary results indicated that the crest method exhibited the smallest absolute error (13.2%) and relative error (13.2%) compared to the area method and regression

method. Moreover, the sea-based measurement method has the advantage of not being limited by LoRa link distance, making it easier to obtain multi-peak samples, which greatly reduces measurement uncertainty and results in less error (12.3%) than land-based measurement data. Additionally, correlation analysis of the 100 valid samples in this study with OGV characteristics revealed a significant relationship with the built year, while no clear relationship was found with the gross tonnage and area.

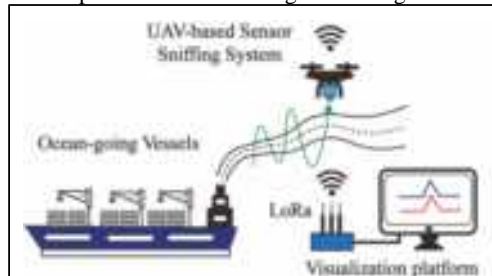


Figure 1. Operation process of UAV-based microsensor sniffing system

This study will continue to optimize the systematic protocols, including sensor calibration methods, field operation procedures, and data analysis, to facilitate the efficient application of UAV-based MSS in real-world ship FSC monitoring. Additionally, based on the VIS database, the correlation between FSC values and characteristic factors of vessels will be analyzed to reveal potential patterns.

This research is funded by the Environmental Protection Department of Hong Kong (Reference: 17-04647), the Science and Technology Commission of Shanghai Municipality of China (Projects No. 17DZ1203101, 17DZ1203105).

References:

HKEPD, 2018. Hong Kong air pollutant emission inventory - navigation. Retrieved May 9, 2020, from Environmental Protection Department. <https://www.epd.gov.hk>.

Anand, A., Wei, P., Gali, N. K., Sun, L., Yang, F., Westerdahl, D., ... & Ning, Z. (2020). Protocol development for real-time ship fuel sulfur content determination using drone based plume sniffing microsensor system. *Science of The Total Environment*, 744, 140885.

Changes in cloud activity of ship exhaust particles: Potential effects on Arctic mixed-phase clouds

Luis Santos,¹ Kent Salo,² Hannah Frostenberg,³ Xiangrui Kong,¹ Jun Noda,⁴ Thomas B. Kristensen,⁵ Takuji Ohigashi,⁶ Annica Ekman,⁷ Luisa Ickes³ and Erik S. Thomson¹

¹Department of Chemistry and Molecular Biology, University of Gothenburg, Gothenburg, Sweden;

²Department of Mechanics and Maritime Sciences, Chalmers University of Technology, Gothenburg, Sweden

³Department of Space, Earth and Environment, Chalmers University of Technology, Gothenburg, Sweden

⁴School of Veterinary Medicine, Rakuno Gakuen University, Ebetsu, Japan

⁵FORCE Technology, Brøndby, Denmark

⁶UVSOR Synchrotron, Institute for Molecular Science, Okazaki, Japan

⁷Department of Meteorology, Stockholm University, Stockholm, Sweden

Keywords: Ships, aerosol, clouds, Arctic.

Presenting author email: luis.santos@cmb.gu.se

Maritime shipping remains a large source of anthropogenic airborne pollutants, including exhaust particles that can act as cloud condensation nuclei (CCN). The International Maritime Organization (IMO) imposed global fuel sulfur content (FSC) limits on marine fuels in order to target ship exhaust sulfur oxides and particulate matter emissions, but has allowed competing pathways to regulatory compliance; i.e., low FSC fuels versus exhaust after-treatment. Laboratory experiments revealed that these compliance measures have secondary effects on physicochemical properties of exhaust particles, affecting their CCN activity (Santos *et al.*, 2022; 2023). We observe that combustion of low FSC fuels results in emissions of highly hydrophobic particles, causing significant reductions in CCN emissions, whereas wet scrubbing leads to an increase in CCN activity.

One area of focus is the Arctic region, which has been shown to be particularly susceptible to the effects of climate warming. A steady decrease in observed sea ice cover amplifies the regional warming (Screen and Simmonds, 2010), but also opens the region to increased ship traffic which may result in further climate feedbacks (Stephenson *et al.*, 2018). It is of particular interest to identify how increased ship exhaust particle emissions may affect cloud processes; for example, by facilitating liquid droplet formation and thus, potentially changing the radiative properties of the aerosol and clouds.

Here, we investigate how increased shipping activity potentially influences the properties of Arctic mixed-phase clouds. In our study the experimentally observed characteristics of marine particle emissions and their liquid droplet forming potential have been implemented in large eddy simulations. We use the MIMICA model (MISU/MIT Cloud-Aerosol model) (Savre *et al.*, 2014) to simulate a stable stratiform mixed-phase cloud based on the Arctic Summer Cloud Ocean Study (ASCOS) (Tjernström *et al.*, 2014). A range of

input parameters for ship aerosol, including size distributions, number concentrations, vertical distributions and hygroscopicities, has been studied to assess the potential impact on cloud properties and regional climate.

This work was supported by the Swedish Research Councils FORMAS and VR.

Santos, L., Salo, K. and Thomson, E. (2022). *Environ. Sci.: Processes Impacts*, 24:1769-1781

Santos, L., Salo, K., Kong, X., Noda, J., Kristensen, T., Ohigashi, T. and Thomson, E. (2023). *Environ. Sci.: Atmos.*, 3:182-195

Savre, J., Ekman, A. and Svensson, G. (2014). *J. Adv. Model. Earth Syst.*, 6:630-649

Screen, J. and Simmonds, I. (2010). *Nature*, 464(7293):1334–1337

Stephenson, S., Wang, W., Zender, C., Wang, H., Davis, S. and Rasch, P. (2018). *Geophys. Res. Lett.*, 45:9898–9908

Tjernström *et al.* (2014). *Atmos. Chem. Phys.*, 14:2823-2869

GETTING IN TOUCH WITH THE EU

In person

You can find your nearest representation of the European Union or one of its agencies at [europa.eu/contact-us/representations-and-agencies](#).

On the phone or in writing

The European Commission has a range of channels for you to contact it:

- [EU institutions and agencies](#) — [EU institutions and agencies](#)
- [EU law and related documents](#)
- [Open data from the EU](#)

FINDING INFORMATION ABOUT THE EU

Online

For a quick look at what's new on the EU website, visit the homepage of the European Commission at [europa.eu](#).

EU publications

EU publications are freely available online at [europa.eu/europa-publications](#). Most copies of these publications can be obtained free of charge by visiting the website of the relevant [europa.eu/europa-publications](#).

EU law and related documents

EU law is freely available online at [europa.eu/eu-law](#). You can also search for EU law by topic at [europa.eu/eu-law-search](#).

Open data from the EU

The portal [europa.eu/open-data](#) provides access to the data of the European Union and its agencies. This includes data which is released under the EU's Freedom of Information Act, as well as data published by the public sector under the EU's Open Data Directive.

Science for policy

The Joint Research Centre (JRC) provides independent, evidence-based knowledge and science, supporting EU policies to positively impact society



EU Science Hub

joint-research-centre.ec.europa.eu



Publications Office
of the European Union